International Journal of Geographic Information System
Vol. 4, No. 1, April 2017, pp.1-519
Available Online at http://acascipub.com/Journals.php

Research article

Lexicographically cartesian-ordered differential calculi for spectrotemporally extracting vertical foliage profiles from raw moderate resolution waveform in-situ near infra fluorescence quantum sub-surface spectroscopic discontinuous geodesic fluxions in a metaheursitic chorophyll-*a* translucent emissivity map of eco-georeferenceable sporadically canopied narrow agro-village riverine tributary *Simulium damnosum* s.l. oviposition sites employing bio-optical multivariate Gaussian prior covariances and a spline within a reproducing non-frequentist diagonalization of amalgamized positive definite kernels in Hilbert space: Implementation of a 'Slash and Clear' control intervention in two agro-village complexes in northern Uganda

Benjamin G. Jacob[1], Denis Loun[2]Peter Alinda[3], Denis Munu[4], Moses N. Katabarwa[5], Thomas Lakwo[2], Peace Habomugish[4] Thomas R. Unnasch[1]

[1]Global Health Infectious Disease Research Program, Department of Global Health, University of South Florida, Tampa, Florida, United States of America

[2] Vector Control Division, Ministry of Health, Kampala, Uganda

[3] Nwoya District Health
Office, Gulu, Northern Uganda

[4] The Carter Center, Kampala, Uganda

[5]Emory University and The Carter Center, Atlanta, Georgia, United States of America

Corresponding Author: E-mail: bjacob1@health.usf.edu

International Journal of Geographic Information System
Vol. 4, No. 1, April 2017, pp.1-519
Available Online at http://acascipub.com/Journals.php

RUNNING HEAD: Implementing an onchocerciasis control strategy

Abstract

A smoothness regularization algorithm was employed in ArcGIS for parsimoniously constructing a forecast, vulnerability endmember, 5 meter (m), chlorophyll (Chl-*a*), RapidEye™, trailing vegetation, turbid water, capture point, black fly, vector, *Similium damnosum* s.l., geometric, endmember, signature, stochastic interpolator for implementing onchocerciasis larval control strategies (i.e., 'Slash and Clear') in two agro-village complexes in the Goma district in northern Uganda. The study sites were geolocated 1 kilometer (km) or less from the river Ayago, and were separated by approximately 15km from one another. Interventions were conducted in the Gongcoyo and Adibuk villages, while larval control monitoring with no interventions were conducted in the Ayago-Nile and Laminlatoo villages. A line transect delineating a plot of 15km × 15km was measured onto a 128km x 128km, RapidEye^{TM}, 5m polygon employing four, differentially corrected, cardinal points to calculate the frequency of occurrence of the dominant flora encompassing the oviposition capture points at the agro-village, eco-epidemiological, study sites. Canopy plants associated with larval breeding attachments at the study sites were *Oryza barthii, Pterocarpus santalinoides, Andropogon gayanus* and *Lawsonia inermis.* Colored dissolved organic matter (CDOM) absorption was deduced at a mean of 440nm for the study sites, which were measured between 0.30 to 2.10m^{-1}. Secchi disk transparency ranged from 0.21m to 1.3m. An interpretive, three-band, signature model was tuned to select the 5m spectral bands for iterative interpolation of the endmember, Chl-*a,* canopy foliage. The spatial non-randomness in the oviposition, canopy gap pixel reflectance was tabulated in ENVI employing visible and near infra-red (NIR), RapidEye^{TM} waveband data. Canopy leaf, eigenvector emittance was measured by the adaxial, sparsely shaded, leaf surfaces specifically where light passed through the leaf into the integrating, wavelength, 5m sphere. Linear models were constructed between the intervention, agro-village complexes and log-normalized, multivariate, satellite data. The residual prediction deviation (RPD) endmember scores were derived based on model performance. The coefficient of determination (R^2) and the root mean squares error (RMSE) of calibration sets, and the RPD were used to evaluate the model forecasts. VNIR calibration obtained accounted for at least 65% of the variance in log Chl-*a* wavelengths employing only VNIR spectra.The high RPD of 2.81 obtained suggested that the final model derived was suitable to prognosticate Chl-*a,* canopy concentrations. The three-band, model forecasts included 675 and 755 nm (R_{675} and R_{755}) and reflectance of Red Edge center wavelength at 731nm (R_{718}), with the equation RES = (R_{718}-R_{675})/(R_{755}- R_{675}) where R was λ. A differential equation was generated where *F* was written as a linear combination of the forecast, oviposition, endmember derivatives of *y*: $y^{(n)} = \sum_{i=0}^{n-1} a_i(x)y^{(i)} + r(x)$ where $a_i(x)$ and $r(x)$ were continuous functions in *x.* The articulated regression, proxy, uncoalesced, signature, land use land cover (LULC) explanators accounted for an average of 83.7% of variation in Chl-*a,* capture point, canopy, concentration values with a RMSE of less than 7.14%. The background landscape emittance rendered from the Chl-*a,* canopy material, sample material was linked to its optical depth (*τ*) and to the capture point, synthetic, orthogonal surfaces. Absorbance rates were quantitated, employing $\frac{\Phi_e^t}{\Phi_e^i} = e^{-\tau} = 10^{-A}$, where Φ_e^t was the radiant flux transmitted by the uncoalesced canopy pigment, sample. Φ_e^i illustrated the radiant flux emitted by the sample. An *n* attenuating species in the discontinuous canopy sample via $e^{\sum_{i=1}^{N} \sigma_i \int_0^{\ell} n_i(s)ds} = 10^{\sum_{i=1}^{N} \varepsilon_i \int_0^{\ell} c_i(s)ds}$ was synthesized. By developing a tool in ArcGIS based

on simultaneous diagonalization of positive definite kernels, minimax rates of convergence were achieved for forecasts rendered from an iterative stochastic interpolator which revealed that the optimal rate of convergence for the regularized estimator (i.e., f_{nX}) was $n^{-2(1-a)}(r+s)^{/(}(r^{s}+^{1)}$. An eigenfunction decompostion algorithm revealed that smoothness, regularized, CDOM-specific, time series descriptors could achieve optimal RMSE (< 11.3 %) with quantizable rates of convergence for unbiasedly prognosticating seasonal hyperproductive, *S. damnosum* s.l., Chl-*a* endmember, oviposition, eigenvector ensembles. New properties in the model arose due to the orthogonal eigen-decomposition of the Hilbert space, including projections, over the unit interval of one dimension and angles between functions, particularly between those which were non-zero constant mulitples of each other whenst A^2 ʊ and (D[$W_0^{1,2}$ (ʊ)] were exposed.Numerical results were formulated to elucidate the merits of the the targeted, immature habitat, removal technique (i.e., "Slash and Clear") based on the the Chl-*a* canopy, capture point, iteratively quantitively interpolated, proxy, endmember, vulnerability, signature maps of the intervention villages. In Gonycogo, the mean daily collection during the last three days of the 31 day study was 32.66, representing an 89.10% reduction in biting density from the mean collection in the baseline collection of 292.4 adults. In contrast, the mean daily collection in the paired control village of Ayago/Nile was essentially unchanged from the baseline collection during the last three days of the study (352.7 baseline versus 348.6 at the end of the study). Similar results were seen in the other village pair. An 81.21% reduction in biting rate was observed in the intervention village (Adbuk), while the biting rate in the control village (Laminlato) at the end of the study was 98.11% of that seen in the baseline evaluation.

Keywords; Chlorophyll, trailing vegetation, 'Slash and Clear, RapidEye™, *S. damnosum* s.l., canopy, onchocerciasis, ArcGIS.

Introduction

Onchocerciasis, or river blindness, is historically one of the most important causes of blindness worldwide [1]. The disease is caused by the filarial parasite *Onchocerca volvulus*. Approximately 37 million individuals in Africa alone are believed to be infected with this parasite [2]. Several characteristics of onchocerciasis combine to make it a particularly severe public health problem. The major pathogenic manifestation of the infection, ocular damage leading to blindness, commonly affects individuals beginning in the second decade of life. This has the effect of disabling individuals just as they are entering the most productive period of their lives. Further, although blindness associated with onchocerciasis has been shown to lead to a fourfold increase in mortality [3], the majority of the afflicted individuals survive and require long term care by the community. In areas where blinding onchocerciasis is hyperendemic, the care of blinded individuals places a severe stress on the community. Historically, this has often led to the dissolution of entire communities as a result of the infection [4]. Finally, the parasite is transmitted by black flies (*Simulium damnosum s.l.*) that breed in fast running rivers and streams. Thus, transmission of the parasite is most intense in the river basins, rendering many such areas uninhabitable [4]. Unfortunately, the river basins contain much of the fertile land found in the sub-Saharan African savanna. By preventing the agricultural use of the most fertile lands, onchocerciasis has had a significant negative impact on the economic growth of many of the poorest countries of Africa.

In the 1980s, ivermectin was first shown to be a potent microfilaricide against *O. volvulus* [5]. Early studies also demonstrated that mass treatment of an afflicted population with ivermectin could reduce transmission of the parasite [6, 7]. Based upon the dramatic effect of ivermectin on both *O. volvulus* and its ability to reduce or eliminate the symptoms of the infection in afflicted individuals, Merck, the manufacturer of ivermectin, announced that

they would provide the drug free of charge for the treatment of onchocerciasis, "as much as needed for as long as needed" [8]. As a result of this generous donation, several large international programs were begun to either control or eliminate onchocerciasis, employing a strategy of mass drug administration (MDA) of ivermectin to the afflicted communities. Most notably, these included the African Programme for Onchocerciasis Control (APOC) in Africa and the Onchocerciasis Elimination Program of the Americas (OEPA). OEPA, employing a strategy of semi-annual distribution of ivermectin with high coverage rates, has succeeded in eliminating onchocerciasis in three of the six formerly endemic countries in Latin America (Colombia, Ecuador, and Mexico), and has interrupted transmission in all but two foci in the region [9]. In Africa, studies conducted in Mali and Senegal [10] and Nigeria [11] have suggested that long term annual community directed treatment with ivermectin (CDTI) resulted in the elimination of onchocerciasis from some isolated foci in West Africa. These successes have resulted in a change in strategic focus from a goal of disease control of onchocerciasis to a goal of complete elimination. This goal was enshrined in the London Declaration on Neglected Tropical Diseases in 2010, where the international community set a goal of eliminating onchocerciasis from Africa by 2020 [12].

Despite the successes documented in both Africa and in Latin America that demonstrate that mass distribution of ivermectin can eliminate onchocerciasis in some situations, it is clear that ivermectin alone is not likely to be a panacea. For example, in many areas of Africa where vector populations are high, eco-epidemiological, vulnerability, forecasting, risk models indicate that ivermectin MDA alone will probably not be sufficient to interrupt transmission. This is due to the fact that transmission intensity is driven by the amount of exposure to the vector, as measured by the annual biting rate (ABR), or the average number of bites from the vector experienced over one year by an individual living in the endemic area. Thus, in areas where the vector density is very high, annual MDA alone may not be sufficient to interrupt transmission [13].

Vector control, as a tactic to combat onchocerciasis in Africa, has a long and storied history. The use of larvicides to eliminate adult flies and to block transmission of *O. volvulus* was first implemented in Kenya from 1946-1955 [14] using DDT to eliminate populations of the local vector *Simulium neavei* in the six Kenyan foci of onchocerciasis. Elimination of the vector was successful in interrupting transmission in Kenya, and follow-up studies conducted in 1964 confirmed that the parasite had been eliminated from these foci [15]. The Kenyan success of targeting the vector population was used as a model for the first international onchocerciasis control program in Africa. The Onchocerciasis Control Programme of West Africa, or OCP, was a large-scale, vertically integrated program whose aim was to eliminate blinding onchocerciasis as a public health problem throughout eleven countries in West Africa, where the disease was a significant public health problem. The OCP began operations in 1975, and relied primarily upon a strategy of source reduction, (i.e., aerial spraying of *Simulium damnosum sensu lato* larval breeding sites, the major vector of *O. volvulus* throughout Africa). The OCP was a disease control program and not an elimination program; thus, while elimination of the parasite did not occur over the entire area under control by the OCP, elimination of severe ocular disease was achieved in its core transmission areas that were formerly hyperendemic in Burkina Faso, Ghana and Togo after 14 years of vector control [16]. A great deal of public health value was accomplished by this landmark effort throughout the region. Skin disease was significantly reduced, more than 200,000 cases of blindness were prevented and the size and distribution of the *O. volvulus* population in the

regions was substantially decreased [17]. The OCP successfully completed its operations in 2002.

More recently, Uganda has demonstrated the power of utilizing a combination of vector control and ivermectin MDA. The first evidence for this came from western Uganda, where it was found that combining vector control (larviciding small streams supporting populations of *Simulium neavei*) with ivermectin MDA resulted in a rapid decline in transmission and in the prevalence of infection in the human population [18]. In 2007, this observation was incorporated into the strategic plan of the newly formed Uganda Onchocerciasis Elimination Program (UOEP). Since beginning operations in 2007, the UOEP has used a strategy that combines the use of vector control (local larviciding of vector breeding sites) with semi-annual MDA. This has resulted in the apparent interruption of transmission of onchocerciasis in 9 of the 17 foci in Uganda, a finding that has been confirmed in the Wadelai, Itwara and Mt. Elgon foci [19-21]. These data support the hypothesis that vector control, used in combination with ivermectin MDA, is a powerful strategy to eliminate onchocerciasis, an approach that has the potential of bringing the goals of the London declaration within reach.

The vector control measures that have been used to assist in onchocerciasis control and elimination have traditionally relied upon insecticide treatment of breeding sites to kill larvae. This approach is expensive and logistically difficult to accomplish, as it relies upon expensive insecticides and trained entomologists to implement. Here, we evaluated a different cost-effective approach for the control of the black fly vectors of *O. volvulus*. Our approach utilizes an accurate mathematical model constructed in an ArcGIS cyberenvironment employing object-based technology (i.e., ENVI) and geospectral, geosampled eco-georeferenceable, capture point**,** narrow, African, riverine, tributary, agro-village, trailing vegetation, Precambrian rock, *S***.** *damnosum* s.l., oviposition site, uncoalesced, proxy, biosignature, landscape, explanators iteratively interpolated to identify hyperproductive, sparsely shaded,unknown, un-geosampled, breeding sites for the black fly vectors of this parasite while utilizing local residents to destroy the breeding habitats containing larvae at these sites (i.e., “Slash and Clear”). This approach is in keeping with the approach of Community Directed Treatment with Ivermectin (CDTI), which is the approach currently used to conduct MDA with ivermectin throughout Africa. CDTI relies upon volunteer drug administrators, chosen by the communities themselves, to distribute ivermectin to targeted villages based on adult catching rates.

Medical, entomological-related, stochastic, land use land cover (LULC) endmember, biosignature, endemic models constructed from moderate resolution [e.g., visible and near infra-red (NIR), RapidEye^{TM}, 5m wavelengths], log-transformed, normalized, explanators in literature has revealed that unknown, infrequently canopied, seasonal, hyperproductive, trailing vegetation, capture point, Precambrian rock, *S. damnosum* s.l., endemic, turbid water, geosampled in oviposition sites in narrow, African, riverine, agro-village tributaries may be precisely prognosticated for mapping geolocations within multitemporal, ArcGIS, vector libraries. *Simulium* larvae is limited to fluvial ecosystem and its ecology have been recorded in watercourses which run through quaternary sediments, large pebbles and coarse, sharp, sand bed with earth stones or from bedrocks of tertiary volcanic and or Precambrian origin [6]. Larvae are attached to sun exposed substrata near the surface of water while some are found in completely shaded areas. The breeding sites of *Simulium* species are well aerated clean streams with rocky rapids [7].

An uncoalesced dataset of hyperspectral, seasonal, oviposition, *S. damnosum* s.l., Precambrian rock, trailing vegetation, inhomogeneously canopied, image endmembers may be defined as "pure" land use land cover (LULC) attributes extracted under idealized in situ or laboratory conditions whenst discontinuous, capture point, frequency, wavelength, reflectance, derivative spectra are acquired employing a portable spectroradiometer[1]. Alternatively, discontinuity in a dataset of seasonal, hyperproductive, *S. damnosum* s.l., capture points, sparsely canopied, mixed pixel ("mixel") endmembers may be discernible from imagery employing object-based "classifers [e.g., Spectral Angle Mapper in ENVI^{TM}] which may be stored in a variety of sources (ASCII spectra, spectral libraries, spectral plots, statistics files, ROIs). Geostatistical, algorithmic, endmember, LULC, biosignature, forecast, vulnerability models may regress orthogonally eigen-decomposable, moderate resolution, geoclassifiable, stochastic, endogeneous descriptors which may identify eco-georeferenceable, oviposition, seasonal, hyperproductive, *S. damnosum* s.l., capture points based on grid-stratifiable, eigenvalues. Black fly, time series grid-stratifiable, endmember, biosignature, explicative, ecological forecasts values in a raster format optimally derived from a limited number of geo-spatiotemporal or geo-spatiotemporal, geosampled geoclassifiable, sub-mixel, LULC, narrow, African, riverine, hyperproductive, capture points may be optimally employable to determine unknown un-geosample, values of eco-geographic, geomorphological, capture point, immature habitat, data points such as elevation, rainfall, soil chemical concentrations[1].

Unfortunately, signal viewing detection problems may arise when binary hypothesis testing explicatively, iterable, trailing vegetation, Precambrian rock, *S. damnosum* s.l., endemic, oviposition, proxy, geometric, orthogonal, endmember, moderate resolution, LULC biosignatures with unquantitated, frequency, wavelength, white noise. In signal processing, white noise is a random signal with a constant power spectral density [2]. The term is used in many scientific and technical disciplines, including physics, acoustic engineering, telecommunications, statistical forecasting, and many more. White noise refers to a statistical model for signals and signal sources, rather than to any specific signal [www.esri.com].

In an inhomogeneously canopied, hyperproductive, endemic, oviposition, capture point, trailing vegetation, Precambrian rock, *S. damnosum* s.l., eco-epidemiologically forecastable, moderate resolution, uncoalesced, mixed pixel ("mixel"), unquantitated white noise could be a geoclassifiable, oviposition foci, discrete signal whose samples may be regarded as a sequence of serially uncorrelated LULC, random variables with zero mean and finite variance in a hierachical regression-oriented framework. Two geosampled, moderate resolution, geoclassfiable, unmixed, *S. damnosum* s.l., oviposition, capture point, LULC, explanatorial, regressable, random variables, X,Y, are said to be uncorrelated if their covariance, $\mathrm{E}(XY) - \mathrm{E}(X)\mathrm{E}(Y)$, is zero[2]. If two variables are uncorrelated, there is no linear relationship between them[24].Uncorrelated, oviposition, *S. damnosum* s.l., endmember, LULC, capture point, probabilistic, random variables may be optimized employing a Pearson correlation coefficient of zero, except in the trivial case when sub-mixel, immature habitat geosampled variables reveal zero variance [1].

Jacob et al. [1] managed to show that if an empirical, optimizable, eco-epidemiological, dataset of empirical,

uncoalesced. geosampled, trailing vegetation, Precambrian rock, seasonal hyperproductive, *S. damnosum* s.l. oviposition, moderate resolution, endmember, random

variable is constant : P(X=μ)=1P(X=μ)=1, then the variance in the summary statement is zero:E[X2]=∑ki=1piX2i=>E[X2]=∑i=1kpiXi2=> (given X_i is constant)=>X2∑ki=1pi=X2=>X2∑i=1kpi=X2E[X]2=(∑ki=1piXi)2=(X∑ki=1pi)2=X2E[X]2 =(∑i=1kpiXi)2=(X∑i=1kpi)2=X2. This is relatively straight forward to computate in an unmixed, eco-epidemiological, black fly, forecast, vulnerability model predictive equation for targeting geoclassifiable seasonal, hypeproductive, geosampled, moderate resolution, geometric endmember dataset since the variance may be optiamlly computated employing E[X2]−E[X]2.

The question an arbovirologist or onchocerciasis researchist may want to resolve however, is that does a zero variance necessarily imply a constant oviposition, time series, random variable in an capture point, *S. damnosum* s.l. endmember forecast, vulnerability, LULC remotely sensed, eco-epidemiological, entomological model? Jacob et al. [1] managed to show that if an empirical dataset of uncoalesced, trailing vegetation, Precambrian rock, seasonal hyperprproductive, endmember, *S. damnosum* s.l. moderate resolution, oviposition, random variables is constant : P(X=μ)=1P(X=μ)=1 then the variance is zero in the geosampled dataset whenst E[X2]=∑ki=1piX2i=>E[X2]=∑i=1kpiXi2=> (given X_i is constant)=>X2∑ki=1pi=X2=>X2∑i=1kpi=X2E[X]2=(∑ki=1piXi)2=(X∑ki=1pi)2=X2E[X]2 =(∑i=1kpiXi)2=(X∑i=1kpi)2=X2. This is relatively straight forward to computate for determining seasonal, hyperproductive, black fly foci geolocation from an uncoalesced explanatory, capture point, time series, eco-epidemiological forecast, vulnerability, LULC model for optimally remotely targeting geoclassifiable seasonal, geo-spectrotemporal or geo-spatiotemporal geosampled, moderate resolution, biosignature endmembers since the variance in the model may be computatable employing E[X2]−E[X]2.

The question an arbovirologist or onchocerciasis researchist may want to resolve however, in an eco-epidemiological, oviposition, capture point, *S. damnosum* s.l. endmember LULC, remotely sensed, forecast, vulnerability entomological model is that does a zero variance necessarily imply a constant random variable? Although the probability a geo-spectrotemporal or geo-spatiotemporal, geosampled, grid-stratifiable, moderate resolution, black fly model sub-mixel,time series, to take on a different endmember, LULC eco-epidemiological estimator value is 0, no constant random variable process would be present in the prognosticated eco-georeferenceable, remotey targeted oviposition dataset.

There also may be examples where the converse is false in the capture point, endmember, biosignature, LULC model. For example, if an arbovirologist or onchocerciasis researcher chooses U uniformly in [0,1] whenst constructing the entomological model and lets X=2 then U would be rational and X would equal 3. In such circumstances the variance of X is zero in the model output since the Lebesgue measure of Q is 0

In measure theory, the Lebesgue measure is the standard way of assigning a measure to subsets of n dimensional Euclidean space[44]. For $n = 1$, 2, or 3, it coincides with the standard measure of length, area, or volume. In general, it is also called n-dimensional volume, n-volume, or simply volume. It is employed throughout eco-entomological, vector arthropod-related time series regression LULC , biosignature endmember analysis, in particular to define Lebesgue integration.

The integral of a non-negative function of a single explanatory geo-spectrotemporal or geo-spatiotemporal geosampled, moderate resolution, *S. damnosum* s.l., oviposition

optimizable, geometric,endmember, LULC, variable can be regarded, in the simplest case, as the area between the graph of that function and the *x*-axis. The Lebesgue integral will extends the integral to a larger class of functions [24]. It may also extends the domains on which geoclassifiable, LULC, *S. damnosum* functions can be defined.

It had long been understood that for non-negative functions with a smooth enough graph—such as continuous functions on closed bounded intervals—the *area under the curve* could be defined as the integral, and computed using approximation techniques on the region by polygons. However, as the need to consider more irregular functions arises—(e.g., quantiating the limiting processes of a seasonal, geosampled, *S. damnosum* s.l., eco-epidemiological, oviposition, moderate resolution, geometric, endmember analysis) —it became clear that more careful approximation techniques are needed to define a suitable integral for remotely targeting seasonal hyperproductive, immature habitat, capture points. Also, an arbovirologist or onchocerciasis researcher might wish to integrate on spaces more general than the real line whenst constructing a robust, prognosticative, sub-mixel, eco-epidemiological, oviposition, trailing vegetation, Precambrian rock, capture point, *S. damnosum* s.l. endemic, LULC moderate resolution, eco-georeferenceable, risk model . The Lebesgue integral would provide the right abstractions needed for the model to render optimal eco-diagnostic, explicative, field verifiable forecasts (e.g., seasonal geolocations of high density immature foci). The Lebesgue integral plays an important role in probability theory, in the branch of mathematics called real analysis and in many other fields in the mathematical sciences. It is also a pivotal part of the axiomatic theory of probability.

Regardless a non-negative, geo-spectrotemporal or geo-spatiotemporal , eco-epidemiolgical, geosampled, forecast-oriented, seasonal, hypeproductive, *S. damnosum* s.l. eco-georeferenceable, capture point, moderate resolution, endmember, optimizable,prognosticative ovispoition, uncoalesced, biosignature, random variable with a zero expected value is almost surely equal to 0. This may be ascertained from the properties of the integral in the entomological model .If an arbovirologist or onchocerciasis researcher applies this perspective to the geosampled eco-epidemiological, immature habitat black fly, oviposition, optimizable, moderate resolution, LULC random, ecogeorferenceable, explanatory variables employing (X−E(X))2(X−E(X))2, which is non-negative, then V(X)=E[(X−E(X))2]=0V(X)=E[(X−E(X))2]=0 would imply that (X−E(X))2=0(X−E(X))2=0 whenst X=E(X)X=E(X).In so doing, seasonal hyperproductive foci of *S. damnosum* s.l. ovispoition sites may be identifiable on moderate resolution, grid-stratified, satellite data

In general, uncorrelatedness in an eco-epidemiological, eco-georeferenceable, black fly, forecast, vulnerability, habitat, biosignature, oviposition model is not the same as orthogonality, except in the special case where either X or Y has an expected value of 0. In this case, the covariance in the endmember, biosignature LULC, prognosticative model would be the expectation of the product, and X and Y would be uncorrelated if and only if E(XY) = 0.If X and Y are independent, with finite second moments, then the grid-stratifiable, moderate resolution, entomological, vector arthropod, parameterizable, uncoalesced, immature habitat, capture point, orthogonal, LULC geosampled covariates would be uncorrelated. In mathematics, the second moment method is a technique employable in probability theory and analysis to show that a random variable has positive probability of being positive[24]. More generally, in a robust black fly, moderate resolution, endmember, geo-spectrotemporal or geo-spatiotemporal, eco-epidemiological LULC, model the "moment

method" would consist of bounding the probability that a random variable fluctuates far from its mean, by using its moments.

Quantitating first moments in a seasonal, hyperproductive, trailing vegetation, Precambrian rock, *S. damnosum* s.l., oviposition, moderate resolution, capture point, eco-epidemiological model may deduce a lower bound based on the probability that a quantitative, orthogonal, random endmember, grid-stratfiable, orthogonal LULC, prognosticative variable is larger than some constant times its expectation. The method would involve comparing the second moment of random variables to the square of the first moment.

The 2nd moment of an ecogeoreferenecable, eco-epidemiological, seasonal, trailing vegetation, Precambrian rock, *S. damnosum* s.l. capture point, hyperproductive, endemic foci may be optimally defined as a gemeterical property of an immature black fly habitat based on uncoalesced, moderate resolution, wavelength frequency irradiant incanopy, geoclassified, endmember LULCs distributed with an arbitrary axis.The second moment of an area is typically denoted with either 1 for an axis that lies in the plane of J for an axis perpendicular to the plane [24]. For a capture point, eco-epidemiological,black fly, geo-spectrotemporal or geo-spatiotemporal, forecast, vulnerability model the 2nd moment may be optimally calculable with a multiple integral over the capture point, eco-georeferenceable, oviposition geolocation.This integral may have its unit of dimensions when working with the International System of Units which is meters to the fourth (m^4). The first moment method is a simple application of Markov's inequality for integer-valued variables[24]. In probability theory, Markov's inequality may render an upper bound for the probability that a non-negative function of a random uncoalesced, endmember, gridded, stratfiied, moderate resolution, LULC , *S. damnosum* s.l., capture point, ovipsoition, signature variable which may be greater than or equal to some positive constant.

Markov’s inequality: for any nonnegative, geo-spectrotemporal or geo-spatiotemporal, geosampled, *S. damnosum* s.l., explanatory, random, moderate resolution, endmember, LULC variable X, may be quantitated employing y t > 0, Pr[X ≥ t] ≤ E[X] t . For example, X may take on a geoclassifiable, grid-stratifiable, moderate resolution, geosampled, sub-meter resolution , geoclassifiable, eigendecomposable, endmember LULC values x1 < x2 < . . . < xj = t < . . . < xn in an eco-epidemiological, forecast, vulnerability, orthogonal, oviposition, *S. damnosum* s.l., risk model. First, however, an arbovirologist or onchocerciasis researcher must prove the inequality in the grid-stratifiable, eigenvector, biosignature paradigm. By employing E[X] = Xn i=1 xi ∗ Pr[X = xi] ≥ Xn i=j xi ∗ Pr[X = xi] ≥ Xn i=j t ∗ Pr[X = xi] the equivalence to a more useful form, for s > 0 may tabulated whenst s may represent immature *Similium*, seasonal, larval count, iteratively interpolative, eigenvalues. Then Pr[X ≥ s · E[X]] ≤ 1 would be rendered in the forecasts for optimally targeting seasonal, hypeporductive foci. Alternatively, let t = sE[X] in the *S. damnosum* s.l., oviposition,eco-epidemioloigical, entomological, parameter estimator, geoclassified, LULC dataset.Then by, inventing a random optimizable, LULC variable and a moderate resolution, unbiased estimator distribution such that, Pr[X ≥ 1,whenst E[X]] , a robust dataset may be generated of eco-georeferenceable, hyperproductive, seasonal black fly foci geolocations.

However, not all uncorrelated, geo-spectrotemporal or geo-spatiotemporal geosampled, endmember, explanative, *S. damnosum* s.l., moderate resolution, geoclassifiable, LULC ovipositon variables are independent. For example, if X is a continuous sub-mixel,

LULC random variable uniformly distributed on $[-1, 1]$ and $Y = X^2$ in a seasonal, hyperproductive, eco-epidemiological, eigendecomposable, trailing vegetation, Precambrian rock, black fly, endmember model whose covariates were geosampled in narrow African, riverine, tributary, agro-village, capture point, then X and Y would be uncorrelated even though X could determine Y. In so doing, a particular seasonal, endmember, LULC, immature habitat, capture point geosampled value of Y may be optimally rendered by only one or two values of X.

Depending on the context an eco-epidemiological, eco-georeferenecable seasonal, hypeproductive, capture point, immature, black fly, unmixed, optimally regresseable frequency, wavelength,moderate resolution, mixel samples may be independent and have the same probability distribution [in other words independently and identically distributed (i.i.d) would be a simplest representative of the capture point, white noise]. Eco-epidemioligical, capture point LULC samples of a white noise signal may be sequential in time, or arranged along one or more spatial dimensions [1]. In digital image processing of eco-entomological, optimizable, grid-stratifiable, endmember, eigen-decmposable. LULC datasets, the mixels of a white noise image are typically arranged in a rectangular, orthgonal matrix and are assumed to be independent random variables with uniform probability distribution over some interval [3].

Most of the studies of inhomogeneous, uncoalesced, LULC, eco-entomological, vector arthropod, capture point, reference biosignature, canopy endmember, noise-induced phenomena in the literature assume that the noise source is Gaussian because of the possibility of obtaining some analytical results when working with Gaussian noises. In particular, if each discontinuous, eco-georeferenceable, Precambrian rock, trailing vegetation, seasonal, hyperproductive, uncoalesced, capture point, endmember, moderate resolution, geoclassifiable, *S. damnosoum* s.l., frequency, wavelength, LULC, capture point, foci sample has a normal distribution with zero mean, the signal would contain Gaussian white noise. The quantitation of latent endmember, non-Gaussian, propogagtional noises is rare in any geo-spectrotemporal or geo-spatiotemporal, geosampled, eco-georeferenecable, eco-epidemiological, capture point, vector, arthropod-related, eco-entomological, forecast-oriented, eigen-decomposable, inhomogeneously canopied, geometric, LULC reference biosignature, mainly because of the difficulties in handling them in cyberplatforms. Experimental sub-mixel, cartographic and geostatistical algorithmic evidence indicates that moderate resolution, grid-stratifiable, trailing vegetation, Precambrian rock, capture point, seasonal hypeproductive, *S. damnosum* s.l., oviposition-related phenomena noise sources, can be non-Gaussian [3]. "Non-gaussianity" in an eco-georeferenecable, seasonal, hyperproductive, eco-epidemiological, trailing vegetation, Precambrian rock, *S. damnosum* s.l., geo-spectrotemporally or geo-spatiotemporally geosampled in a narrow, African, river, tributary agro-village foci does not mean "non-existence of moments", rather it refers to the existence of non-symmetry and/or skewness/excess kurtosis in the residual explanatory dataset of eigendecomposable forecasts (e.g., geolocations of seasonal black fly, eco-georeferenceable, hypeproductive, foci based on an iteratively quantitatively interpolated, moderate resolution, oviposition, reference LULC, biosignature).

Poissonian, sub-mixel, eco-entomological, oviposition, *S. damnosum* s.l., capture point, seasonal, immature data counts[4] and sparsely corrupted, geosampled, immature habitat, endmember data[5] can induce non-playkurotic distribution[1].The methods for image and signal processing are different when different types of non-Gaussian noise are considered [www.esri.com].In probability theory and statistics, the Poisson distribution is

a discrete probability distribution that expresses the probability of a given number of events (e.g., geosampling *S. damnosum* s.l. capture points) occurring in a fixed interval of time and/or space if these events occur with a known average rate and independently of the time since the last event [11]. The Poisson distribution can also be used for the number of events in other specified intervals such as distance, area or volume.

Analyses of causal, uncoalesced, regressed, moderate reosolution, orthogonal synthetic, endmember, LULC quantitated effects between in-canopied, trailing vegatation, Precambrian rock, *S. damnosum* s.l.,eco-epidemiological, capture point foci or between geosampled, categorical or continuous-valued predictor variables of the immature habitat may require uasage of an autoregressive probabilistic paradigm or structural model with instaneous quantizable, LULC effects. Estimation of unmixed, Gaussian moderate resolution, wavelength frequencies within linear, structural, prognosticative, regression equation frameworks may have serious identifiability problems including non-quantitability of spectroradiometeric, propogagtional heteroskedastic uncertainites. In statistics, identifiability is a property which a model must satisfy in order for precise inference to be possible. Hence a robust iteratively stochastic or detremintsic seasonal hypeporductive, trailing vegetation, Precambrian rock, S. damnosum s.l. immature habitat, capture point, may be identifiable if it is theoretically possible to learn the true LULC values of the model's underlying parameters after obtaining an infinite number of geo-spectrotemporal or geo-spatiotemrpoal observations from it. A non-Gaussian, endmember, LULC model may be optimally employable to differentiate unmixed, moderate resolution, wavelength, frequency, irradiance properties emitted from a black fly, hyperproductive, seasonal, foci. In so doing, an onchoncerciasis researcher or other experimenter may be able to combine non-Gaussian, geoclassifiable, LULC endmember models with other autorgressive probabilistic, wavelength, frequency unmixing models to determine geolocations of hyperproduuctive foci in narrow, African, riverine tributaries. In effect this combination of model paradigms could be referred to as a structural, endmember, vector, autogression model. Such an instanteous, forecast, vulnerability model could render an identifiable iteratively qualitatively, eco-epidemiological,uncoalesced, interpolative, endmember, LULC bisignature, eco-georeferenecable, eco-epidemiological, forecast (e.g., geolocation of an capture point, black fly, seasonal, hyperproductive foci). The non-Gaussian may reveal structural vector autoregression estimates without prior knowledge of network structures. An arbrovrirologist or other onchocerciasis experimenter may propose computationally efficient geometric, endmember eigen-decomposition algorithmic, orthogonal, iterative, biosignature, unmixing methods for estimating the model as well as methods to assess the significance of the causal LULC influences .

Two classes of algorithms: expectation maximization (EM)-Type algorithms may deal with a weighted Poissonian and an adaptive outlier pursuit for endmember image and signal reconstruction for optimally quantitating non-Gaussian, sparsely corrupted, trailing vegetation, Precambrian rock,seasonal, hyperproductive, *S. damnosum* s.l., eco-epidemiological, capture points. In statistics, an expectation–maximization (EM) algorithm is an iterative method for finding maximum likelihood or maximum a posteriori (MAP) estimates of parameters in statistical models, where the model depends on unobserved, diagnostic, latent explanators[11]. The EM procedure for quantiating eco-epidemiological, uncoalesced, eco-georeferenceable, capture point of geosampled narrow, African riverine, tributary, agro-village, uncoalesced, moderate resolution, endmember, *S. damnosum* s.l., oviposition, wavelength frequencies would consist of two alternating steps: first, the expectation (E) step, which would compute an expectation of the likelihood by including the

latent extracted, moderate resolution, sub-mixel, inhomogeneously canopied, noisy, sub-mixel, LULC variables as if they were observed; second, the maximization (M) step, would compute the Maxiumum Likehood Estimation (MLE) of the oviposition, black fly, eigen-decomposable, grid-stratfiable, empirical, frequency, wavelength, parameterical orthogonal, LULC, paramterizable covariate estimator datasets by maximizing the expected likelihood found in the E step. In so doing, a reference dataset of uncoalesced, wavelength. biosignature, ecogeoreferenceable, imaged, seasonal, hyperproductive, *S. damnosum* s.l., sub-mixel, LULC, feature attributes estimators found in the M step may be parsimoniously employed for the next E step, and the iteration process may be repeatable until convergence. These eigen-forecasted, unbiased, optimally regressable, grid-stratifiable, eco-georeferenceable, endmember, LULC, black fly, seasonal, hyperproductive, oviposition, immature estimates may then be optimally employable as a respone variable to determine the distribution of the explanative, latent, discontinuous, canopy, wavelength, frequency, moderate resolution, endmembers in the next E step. The EM algorithm is used to find (locally) ML parameters of a statistical model in cases where the equations cannot be solved directly [4]. For example, in a time series, mixture, an eco-epidemiological uncoalesced, endmember, optimizable dataset of moderate resolution, imaged, capture point, eco-georeferenceable, trailing vegetation, Precambrian rock, discontinuously canopied, *S. damnosum* s.l. orthogonally, parameterizable, LULC, biosignature, interrogative, optimizable descriptors may be geo-spectrotemporally or geo-spatiotemporally identifiable more simply by assuming that each capture point has a corresponding unobserved point. In so doing, any black fly, geosampled, geo-spectrotemporal, latent explanatory, variable may specify the precise endmember, LULC, component that each prognosticated, seasonal, hypeproductive foci belongs to.

Finding a ML endmember, solution in an orthogonal, uncoalesced, endmember, forecasting, eigen-decomposable, geo-spectrotemporal, geosampled, moderate resolution, eigenvector, *S. damnosoum* s.l., capture point, predictive, oviposition, would require seperating the trailing vegetation, Precambrian rock and turbid water sub-mixel data in an unmixing paradigm which may require quantitating the derivatives of the likelihood function with respect to all the un-geosampled, uncoalesced, iteratively, quantitatively, interpolative, LULC, oviposition, biosignature. The endmember dataset would require eigen-decomposable LULC eigenvalues,their parameters and theire latent variables for optimally solving the resulting endmember, uncertainty, frequency equations. In moderate resolution, discontinuously canopied, forecasting, vulnerability, vector, medical entomological, grid-stratifiable, LULC, orthogonal, endmember, signature models with latent heteroskedastic, moderate resolution, wavelength, frequency, transmittance variables, this usually is not possible. Instead, the result is typically a set of interlocking equations in which the endmember LULC solution to the geosampled, *S. damnosum* s.l., wavelength, frequency, orthogonal, parameter estimator dataset requires synthesization of the inhomogeneously canopied, diagnostic, sub-mixel eigenvalues of the regressed, latent, variables and vice versa, but substituting one set of equations into the other in the endmember vulnerability, forecast analyses would render an unsolvable uncertainty equation.

In general there may be multiple maxima, but there is no guarantee that the global maximum will be found in a moderate resolution, imaged, trailing vegetation, Precambrian rock, *S. damnosum* s.l. inhomogeneously canopied, seasonal, hypeproductive, eco-epidemiological, Precambrian rock, African, narrow, riverine tributary, ecosystem, oviposition, eco-epidemiological, seasonal, hyperproductive foci. Some quantitative endmember likelihoods also have singularities in them, (i.e. nonsensical maxima)[2]. For

example, one of the targeting capture point, moderate resolution, grid-stratifiable, eco-georeferenceable, LULC, biosignature endmember solutions that may be found by EM for a mixture of, discontinuous, trailing vegetation, Precambrian rock, *S. damnosum* s.l.,moderate resolution, immature, eco-epidemiological, forecast, vulnerability, probabilistic, geo-spectrotemporal geosampled, uncoalesced, model estimators may involve setting one of the iteratively interpolative, sub-mixel extracted components to have zero variance and the mean parameter for the same habitat component to be equal to one of the capture point, frequency, wavelength prognosticators. Unfortunately, EM algorithm has several limitations for endmember LULC modeling moderate resolution unmixed capture point, *S. damnosum* s.l. immature habitat data such that as:(i) the number of the endmember discontinuous explanative clusters has to be pre-determined; (ii) the initial parameter estimators of EM influences the performance of the algorithm;(iii) it does not work as well for the concave clusters[24]. Probabilistically autoregressively quantitating, uncoalesced, explicative, residual,time series, discrete signal, geo-spectrotemporal, moderate resolution, eco-georeferenceable, discontinuously canopied, trailing vegetation, Precambrian rock, *S. damnosum* s.l., oviposition, trailing vegetation, narrow, riverine tributary, white noise in an covariance matrix employing optimizable, eigen-decomposable, agro-village, proxy, endmember, LULC biosignature signature geoclassifiable, variables for orthogonally optimally iteratively, quantiatively, interpolating discontinuously canopied, capture point, samples may require regarding sequences of serially uncorrelated, diagnostic,endmember variables with zero mean and finite variance in an ArcGIS cyberenvironment.

Depending on the context, a medical entomologist or ochocerciasis experimenter may require that an uncoalesced, endmember, LULC geo-spectrotemporal or geo-spatiotemporal, geosampled, dataset of elucidatively optimizable, trailing vegetation, Precambrian rock, *S. damnosum* s.l., seasonal, hyperproductive, capture point, oviposition, forecast-oriented, explanatorial,eco-georeferenceable, ,parameterizable, covariate coefficient, grid-stratifiable, regression values be independent and have the same probability distribution. In so doing, the i.i.d, moderate resolution, sub-mixel,wavelength, frequency, transmittance, emissivity transluscent,diagnostic covariance, LULC regressors would be the simplest representative of the immature habitat, forecast, vulnerability, stochastic, iterative, discontinuous canopied, endmember,proxy biosignature, quantizable, residual, wavelength, frequency, white noise. In probability theory and statistics, a sequence or other collection of random variables is i.i.d. if each explanatorial orthogonal random variable has the same probability distribution as the others and all are mutually independent [http://mathworld.wolfram.com]. In particular, if each, orthogonal, eigen-decomposable, discontinuously canopied, moderate resolution, capture point, endmember, trailing vegetation, Precambrian rock, hyperproductive, seasonal, *S. damnosum* s.l., geo-spectrotemporal, geo-sampled, moderate resolution optimally parameterizable, unmixed, capture point, explanatorial, frequency-related, wavelength, predictor, covariate, LULC coefficient has a normal distribution with zero mean, the signal would be classified as Gaussian white noise.

An infinite-bandwidth white noise signal is a purely theoretical construction [2]. The bandwidth of white noise is limited in practice by the mechanism of non-continuous, orthogonal, synthetic, endmember, noise generation, by the transmission medium and by finite observation capabilities [3]. A random, moderate resolution, LULC, oviposition, endmember, inhomogeneously canopied, discontinuous signal emitted from an eco-georeferenceable, hyperproductive, seasonal, trailing vegetation, Precambrian rock, *S. damnosum* s.l., capture point, oviposition, LULC site eco-cartographically mosaiked into a geoclassified, LULC, grid-stratifiable, eco-georeferenceable polygon in an ArcGIS

cyberenvironment may be be considered "white noise" if it is observed to have a flat spectrum over a range of orthogonally eigen-decomposable, wavelength frequencies. This diagnostic, bidirectional, irradiance endmember quantification would be relevant to endemic,vulnerability modelling the topographic and bathymetric geomorphological context of the discontinuously canopied, *S. damnosum* s.l. capture point, moderate resolution image. White noise draws its name from white light, although light that appears white generally does not have a flat spectral power density over the visible band [4].The term white noise may be also employable in non-technical discontinuous canopied, endmember, LULC contexts, in the metaphoric sense of "random talk without meaningful sub-mixel explanatorial contents for example, for optimally autoregressively quantitating an empirical, operational, eco-gereferenceable, uncoalesced, siganture dataset of moderate resolution, trailing vegetation, seasonally hyperproductive,narrow, African, agro-village, riverine tributary, trailing vegetation, Precambrian rock *S. damnosum* s.l., eco-epidemiological, capture point, geo-spectrotemporal, oviposition wavelength frequencies as synthesized from ArcGIS-derived, grid-stratifiable, geo-spatially geoclassifiable, LULC polygons.

In digital image processing, in ArcGIS, the mixels of a seasonal, hyperproductive, eco-epidemiological, capture point, trailing vegetation, Precambrian rock, *S. damnosum* s.l., oviposition, residual, moderate resolution, white noise image would be typically arranged in a rectangular grid, and assumed to be independent orthogonal, explanatorial, random variables with uniform probability distribution over some interval. *S. damnosum* s.l., digital images are prone to a variety of types of endmember noise[1]. Noise is an error which is superimposed on top of a true signal (www.esri.com). Noise may be random or systematic in an eco-georferenecable, capture point, trailing vegetation, seasonal, hyperproductive,narrow, African, agro-village, riverine tributary, *S. damnosum* s.l., eco-epidemiological, geo-spectrotemporal, oviposition, capture point, moderate resolution, breeding foci image. Noise in these images may be the result of errors in the image acquisition process that result in eigen-decomposable, mixel values that do not reflect the true intensities of the geoclassified, trailing vegetation, capture point, endemic, black-fly, LULC, oviposition site on moderate resolution partially shaded, discontinuous, canopy (“gap”) backgrounds.

A Canopy Height Profile (CHP) procedure presented in Harding et al. (2001) for large footprint LiDAR data was tested in a closed canopy environment as a way of extracting vertical foliage profiles from LiDAR raw-waveform. In this study, an adaptation to small-footprint signature LULC, moderate resolution data was shown, tested and validated in an Australian sparse canopy forest at plot- and site-level. Further, the methodology itself has been enhanced by implementing a endmember dataset-adjusted reflectance ratio calculation according to Armston et al. (2013) in the processing chain, and tested against a fixed ratio of 0.5 estimated for the laser wavelength of 1550 nm. As a by-product of the methodology, effective leaf area index (LAIe) estimates were derived and compared to hemispherical photography values. To assess the influence of LiDAR aggregation area size on the estimates in a sparse canopy environment, LiDAR CHPs and LAIes were generated by aggregating waveforms to plot- and site-level footprints (plot/site-aggregated) as well as in 5 m grid-stratified processes. LiDAR profiles were then compared to field biomass profiles generated based on field tree measurements. The correlation between field and LiDAR profiles was very high, with a mean R^2 of 0.75 at plot-level and 0.86 at site-level for 55 plots and the corresponding 11 sites. Gridding had almost no impact on the correlation between LiDAR and field profiles (only marginally improvement), nor did the dataset-adjusted reflectance ratio. However, gridding and the dataset-adjusted reflectance ratio were found to improve the correlation between raw-waveform LiDAR and hemispherical photography LAIe estimates,

yielding the highest correlations of 0.61 at plot-level and of 0.83 at site-level. This proved the validity of the approach and superiority of dataset-adjusted reflectance ratio of Armston et al. (2013) over a fixed ratio of 0.5 for LAIe estimation, as well as showed the adequacy of small-footprint LULC signature, wavelength, frequency data for LAIe estimation in discontinuous canopy forests.A trailing vegetation, moderate resolution, capture point, moderate resolution, imaged, *S. damnosum* s.l., eco-epidemiological, diagnostic, endmember, forecastable, vulnerability, uncoalesced, proxy, LULC, inhomogeneously canopied, endmember biosignature may be an dependent variable in an quantitatively, geo-spectrotemporal,geosampled, stochatistic interpolator constructed in an ArcGIS cyberenvironment. Employing the gap probability of a discontinuous vegetation canopy, such as narrow, African, riverine forest, savanna, or agro-village, tributary shrubland, a robust, black fly, oviposition, seasonal, predictive risk moderate resolution, LULC, endmember signature model may be optimally constructable in ArcGIS. If negative exponential attenuation of light within individual, geo-spectrotemporal, geosampled immature, eco-georeferenceable, eco-epidemiological, capture point, trailing vegetation, Precambrian rock, *Similium* habitat canopies is assumed, then the problem of modeling the gap probability must be resolved in the remotely retrieved, endmember LULC datasets prior to forecasting any orthogonal, grid-stratifiable, African, riverine tributary geolocations for optimally field verifying (i.e., ground truthing) unknown, hyperproductive, black fly, capture points, employing moderate resolution, satellite datasets. The problem of estimating the distribution for quantitating Euclidean distances within various discontiuous canopy “hot spots” can be addressed in geostatistical gridded algorithms (e.g., evidential, hierarchical, Bayes posterior predicted endmember probability) in SAS/GIS . These geostatistically derived orthogonal localities may be where a photon emitted by the source of illumination may pass more efficiently that other, black fly, discontinuously canopied, seasonal, hyperproductive, capture point, geo-spectrotemporally geoclassifiable. iteratively, quantitatively, interpolative, moderate resolution, endmember, LULC, uncoalesced, wavelength frequencies .

The diffuse, diagnostic, uncoalesced, discontinuously canopied, hyperproductive, immature,capture point, habitat endmember, bi-directional reflection of radiation emitted from an eco-georeferenceable, oviposition, seasonal hyperproductie, trailing vegetation, Precambrian rock, narrow ,African, riverine tributary, trailing vegetation, Precambrian rock, *S. damnosum* s.l., eco-epidemiological, geo-spectrotemporal, geosampled, eco-georeferenceable, moderate resolution, LULC, eco-epidemiological, capture point, moderate resolution, discontinuously canopied. endmember, proxy, signature, probabilistic, wavelength frequency paridigm may have a sharp maximum in the backward direction. This phenomenon is known as heiligenschein in meteorology, the opposition effect in astronomy, and the hot spot effect in aerial photography and optical remote sensing. These three effects are caused by the same bio-geophysical mechanisms, and hence are essentially equivalent. If an empricial dataset of fractionalized, inhomogeneously canopied seasonal, hyperproductive, black fly, capture point, moderate resolution, geoclassified, LULC,oviposition foci endmembers of the reflecting/scattering medium cast shadows, then the shadows cannot be seen looking along the incident rays since they would be screened by the particles themselves. With a change in the view direction a medical entomologist or an onchcerciasis experimenter may be able to recognize some geoclassifiable, oviposition, trailing discontinuous canopy shadows on moderate resolution, eco-georeferenceable, grid-stratifiable, sub-mixel, LULC polygons in an ArcGIS cyberenvironment. Generally, the prolific, immature habitat, *S. damnosum* s.l., capture point radiance of the reflecting medium should decrease with increasing angle α between the view direction and incident rays

transmitted from the foci due to the decreased probability of the illuminative, orthogonal, eigen-decomposeable, moderate resolution, LULC eigenvectors. This phenomenon would be easily computable in an eigenfunction decompositiom algorithm in AUTOREG using the mean radiance of the geo-spectrotemporal geosampled, uncoalesced, discontinuously, canopied endmember, wavelength, frequency, LULC, endmember reflection dataset.

In AUTOREG an eigenfunction of a linear operator *D* defined on some function space is any non-zero function *f* in that space that, when acted upon by *D*, is only multipliable by some scaling factor of an eigenvalue.(www.sas.edu). In linear algebra, an eigenvector or characteristic vector of a linear transformation *T* from a vector space *V* over a field *F* into itself is a non-zero vector that does not change its direction when that linear transformation is applied to it. In other words, if v is a vector in an eco-epidemiological,seasonal, hyperproductive, inhomogeneously canopied, orthogonal, moderate resolution, LULC, endmember eigenvector, trailing vegetation, Precambrian rock, *S. damnosum* s.l.,capture point, quantitatively, uncoalesed, endmeber, wavelength, LULC biosignature, iterative, stochastic, frequency interpolator that is not the zero vector, then it is an eigenvalue of a linear transformation *T,* but only maybe if *T*(v) is a scalar multiple of v in the forecast, vulnerability, sub-mixel model. In mathematics, a zero element is one of several generalizations of the number zero to other algebraic structures [2].

Iteratively, diagnostically optimally interpolating a grid-stratifiable, eco-epidmeiological, ecogeoreferenceable, dataset of orthogonally eigen-decomposable, discontinuously canopied, trailing vegetation, Precambrian rock, *S. damnosum* s.l.,capture point, fractionalized orthogonal endmembers rendered from an empirical geo-spectrotemrpoal, geosampled dataset of hyperproductive, seasonal, eco-georefernceable, narrow, African, riverine tributary, trailing vegetation, eco-epidemiological, capture point, proxy LULC biosignature is not difficult if the distribution of individual oviposition canopy sizes and shapes on moderate resolution geoclassified polygons is known and the individual immature, habitat canopies are randomly distributed. If the canopies do intersect and/or overlap such that discontinuously canopied, foliage, endmember, LULC density remains constant within the overlap area, the mixel spectral extraction problem may be more difficult. An object-based diagnostic, geo-classification, approximation, unmixing algorithm in object based technology (ENVI) may be employable for time series, sub-mixel mapping inhomogenous canopy cover of a eco-epidemiological, capture point, seasonal, hyperproductive, trailing vegetation, Precambrian rock, *S. damnosum* s.l. immature, African, narrow, riverine tributary, capture point.

Spectral Angle Mapper (SAM) is a geophysically-based geospectral geoclassification algorithm that employs an *n*-qD angle to match mixels to reference LULC spectra. The algorithm may determine the spectral similarity between two derivative, endmember, trailing vegetation, Precambrian rock *S. damnosum* s.l., eco-epidemiological, capture point, LULC spectra by calculating the angle between the spectra and treating them as vectors in a space with dimensionality equal to the number of bands. This technique, when employed on calibrated immature, black fly capture point, eco-epidemiological, oviposition, discontinuously canopied, moderate resolution, fractionalized, endmember, uncoalesced, geoclassifiable, immature habitat, bidirectional reflectance, LULC data, may be relatively sensitive to illumination and albedo effects. Endmember, orthogonal, geometric, *S. damnosum* s.l., capture point spectra employed by SAM can come from ASCII files or spectral libraries, or can be extracted directly from an image as ROI averaged spectra. SAM will compare the angle between the inhomogenous canopied endmember, moderate

resolution, grid-stratfiable, LULC, spectrum vector and each mixel vector in *n*-D space of the geo-specrotemporal, geosampled, hyperproductive, *S. damnosum* s.l., capture point.

In the trailing vegetation, Precambrian rock, eco-georeferenceable, sub-mixel, *S. damnosum* s.l., capture point, eco-epidemiological, endmember LULC model, smaller angles would represent closer matches to the immature habitat reference spectrum. Uncoalesced, oviposition, geoclassified, LULC mixels further away than the specified maximum angle threshold in radians would not be geoclassifiable. SAM classification assumes reflectance edata(www.harrisgeospatial.com/Products). However, if a medical entomologist or experimenter employs geo-spectrotemporally uncoalesced, moderate resolution, trailing vegetation, discontinuously canopied, seasonally hyperproductive, *S. damnosum* s.l. capture point, immature habitat, moderate resolution, LULC irradiance, wavelength, frequencies the error would not be significant because the origin would still be near zero. Spectral Information Divergence (SID) is a spectral classification method that uses a divergence measure to match mixels to reference spectra. The smaller the divergence, the more likely the mixels are similar. Biosignature, landscape, capture point, *S. damnosum* s.l., grid-stratifiable, orthogonal mixels with a measurement greater than the specified maximum divergence threshold would not be geoclassifiable. Endmember spectra used by SID can come from ASCII files or spectral libraries, or can be extractable directly from an image as ROI average spectra. (https://www.harrisgeospatial.com/docs/spectralinformationdivergence.html)

A comparison of modeled gap probabilities with observed, moderate resolution, geoclassifiable, LULC quantizable, discontinuous, canopy gap probabilities for remotely optimally prioritizing, eco-gereferenceable, hyperproductive, seasonal, *S. damnosum* s.l., capture point, trailing vegetation, turbid water, narrow, African, riverine tributary, agro-village complex, endemic, oviposition sites overlaid onto a moderate resolution geoclassified , gridded, stratified LULC polygons may show good agreement for zenith angles of illumination up to about 45**".** Above 45**",** the fit may worsen, presumably due to the the horizontal branch structure of the oviposition, black fly, immature habitat canopy which may be less attenuating as the illumination angle approaches the horizon. A medical entomologist or experimenter may derive simple indexes that are functions of an uncoalesced empirical dataset of endmember, LULC, riverine ,tributary, agro-village habitat, regressors specifically, leaf area index, leaf angle distribution, count density (number per square unit of area) and size (base radius and height) of the immature habitat canopies(which may be assumed to be either spherical or ellipsoidal). These indexes may be parsimoniously usable to assess quantitatively the difference between continuous and discontinuous, seasonal, hyperproductive, trailing vegetation, Precambrian rock, oviposition sites along discontinuously canopied, LULC geolocations. Robustly iteratively quantitatively, geo-spectrotemporally interpolating eco-georeferenceable, elucidative, geospatial, forecasting, vulnerability, time series probabilistic, endmember, proxy LULC signatures in ArcGIS may reveal robust, iterative stochastic interpolators endproducts thatmay optimally target hyperproductive, immature, *S. damnosum* s.l., capture point, seasonal habitats on a polgonized, gridded, stratified, geoclassified LULC,vulnerability, eco-epidemiological, real-time map, but sub-mixel,probabilistic noise must be quantized.

An explanative, diagnostic, noise-robust, geospatial preprocessing module in ArcGIS may be used prior to spectral unmixing moderate resolution, remotely sensed, hyperspectral narrow, African agro-village, riverine tributary images. The method first would optimally derive a spatial homogeneity index which would be relatively insensitive to the noise present in the original, hyperspectral, *S. damnosum* s.l., capture point, immature habitat,eco-

epidemiological datasets. Then, it would fuse this index with a geospectral-based, diagnostic classification. In so doing, a set of pure endmeber LULC regions may be employable to guide the unmixing process. An experimental comparison of the proposed method with other geospatial-geospectral unmixing algorithmic approaches in an ArcGIS cyberenvironment may optimally use both synthetic and real hyperspectral explanatorial data collected by some moderate resolution (e.g., Rapid Eye 5m ^{TM}) satellite dataset. The LULC experiments may indicate that spectral unmixing of an explanative, geo-spectrotemporally geosampled, hyerproductive, trailing vegetation, discontinuously canopied, seasonal, *S. damnoum* s.l. eco-georeferenceable, immature, oviposition site on a geoclassifiable moderate resolution LULC, grid-stratified polygon can benefit from the proposed pre-processing algorithmic approach in ArcGIS, in particular, when the noise level present in the original hyperspectral narrow, African agro-village, riverine tributary scene is relatively high.

Geospectral–geospatial preprocessing in ArcGIS using multihypothesis prediction may be proposed for improving accuracy of hyperspectral image geoclassification of an unmixed datasets of hyerproductive, endmember, trailing vegetation, discontinuously canopied, seasonal, *S. damnoum* s.l. eco-georeferenceable, immature, LULC, oviposition sites on a geoclassified moderate resolution, grid-stratified polygons. Specifically, multiple geospatially geolocated, LULC oviposition, mixel vectors may be used as a hypothesis set from which a prediction for each hyerproductive, seasonal, immature habitat mixel vector of interest may be generated. Additionally, a spectral-band partitioning strategy based on inter-band correlation coefficients may be proposed in an ArcGIS geodatbase cyberenvironment to improve the geo-representational power of the hypothesis set. To calculate an optimal explanatory, linear combination of the hypothesis endmember, moderate resolution, LULC geo-spectrotemporal, elucidative grid-stratifiable, endmember signature predictions, a distance-weighted Tikhonov regularization to an illposed, least-squares optimization may be employable in ArcGIS

In statistics, Tikhonov regularization is known as ridge regression, which may be usable for optimally diagnostically quantitating multiple, independent explanative, time series, constrained, linear inversions for predicting,seasonal, hypeproductive, eco-georeferenecable,capture point, *S. damnosum* s.l. narrow, riverine tributary, trailing vegetation, Precambrian rock, ovispoition sites on geoclassified moderate resolution, grid-stratified data. It may be related to the Levenberg–Marquardt algorithm (LMA) for non-linear, least-squares, computation problems. In mathematics, computing, the LMA, also known as the damped least-squares (DLS) method, is employed to solve non-linear least squares problems. These minimization problems arise especially in least squares curve fitting.The LMA is used in many software applications for solving generic curve-fitting problems. However, as for many fitting algorithms, the LMA finds only a local minimum, which is not necessarily the global minimum especially in an uncoalesced dataset of iteratively interpolative, moderate resolution, endmember, capture point, discontinuously canopied, *S. damnsoum* s.l. trailing vegetation, geoclassified, LULC, orthogonal habitat, decomposeable wavelength frequencies. The LMA interpolates between the Gauss–Newton algorithm (GNA) and the method of gradient descent. The LMA is more robust than the GNA, which means that in many cases it finds a solution even if it starts very far off the final minimum [23]. For well-behaved functions and reasonable starting , black fly, ovisposition, LULC, geo-spectrotemporal, endmember parameters, the LMA tends to be a bit slower than the GNA. LMA can also be viewed as Gauss–Newton using a trust region approach [25].The resulting iteratively quantitatively iteratively interpolatable uncoalesced, biosignature LULC predictions of hyperproductive, seasonal, ecogeoreferenecable, trailing vegetation, *S.*

damnosum s.l. oviposition sistes on a moderate resolution geoclassified, grid-stratified polygon may effectively integrate discontinuously canopied,geospectral and geospatial LULC information during geoclassification in lieu of the original mixel vectors. This processed hyperspectral image dataset would have less intraclass variability and more geospatial regularity as compared to the original uncoalesced, sub-mixel, LULC eco-epidemiological, endmember, ovispositiondataset. Geoclassification results for two, seasonal, hyperspectral imaged, eco-georeferenceable, *S. damnosum* s.l. optimizable, moderate resolution, endmember eigenvector datasets in ArcGIS may demonstrate that the proposed method can enhance the geoclassification accuracy of both maximum-likelihood and support vector LULC geoclassifiers,especially under small, sample size, immature, capture point, constraints and noise corruption .

There are some noise that can be introduced into an eco-gereferenceable, geo-spectrotemporally uncoalesced, trailing vegetation, discontinuously canopied, hyperproductive,narrow, African, agro-village, riverine tributaries seasonally hypeproductive, *S. damnosum* s.l., endemic, oviposition geolocation, moderate resolution, LULC scene, depending on how the moderate resolution, image is created. For example, if the grid-stratified, orthogonally polgonized, eco-georeferenceable, immature habitat image is acquired directly in a digital format, the mechanism for gathering the data (such as a CCD detector) can introduce noise.

The CCD is a major piece of technology in digital imaging. In a CCD image sensor, mixels are represented by p-doped MOS capacitors. These capacitors are biased above the threshold for inversion when image acquisition begins, allowing the conversion of incoming photons into electron charges at the semiconductor-oxide interface; the CCD is then used to read out these charges. Although CCDs are not the only technology to allow for light detection, CCD image sensors are widely used in professional, medical, and scientific applications where high-quality image LULC data is required.

Seasonal, hyperproductive, narrow, African, riverine tributary, agro-village, *S. damnosum* s.l., endemic, oviposition, geo-spectrotemporally geoclassified on moderate resolution, grid-stratified, satellite data can exhibit endmember noise which can be greatly reduced in an eco-georeferenceable, trailing vegetation, discontinuously canopied, uncoalesced, diagnostic, geoclassifiable, LULC, proxy, endmember, moderate resolution, biosignature, probabilistic signature, orthogonal, eigenvector paradigm in an ArcGIS iteratively, quantaitive, interpolative cyberenvironment by transmitting signals digitally instead of in analog form. Since each piece of information is allowed only diagnostic, discrete values which are spaced farther apart than the contribution the noise linear filtering algorithms in ArcGIS can remove remove certain types of LULC noise. Certain filters in ArcGIS such as averaging or Gaussian filters, are appropriate for this purpose. Because each geosampled, geoclassified, moderate resolution, uncoalesced, seasonal,capture point, *S. damnosum* s.l., hypeproductive, geo-spectrotemporally extracted, immature, habitat mixel gets set to the average of the mixels in its neighborhood, precise geo-specifications in localational, polygonial, gridded, quantized, endmember, LULC variations may optimally reduce noise in a capture point, trailing vegetation, discontinuously canopied, hyperproductive, narrow, African, agro-village, riverine tributary, vulnerability, proxy, eco-georeferenceable, endmember biosignature, probabilistic, stochastic or determintsic, iterative, quantitative, interpolator in ArcGIS.

The noise in Differential, GPS (DGPS) coordinate time series is known to follow a power-law, explanative, endmember, geometric, noise model with different components(e.g., white noise, flicker noise, random-walk). A medical entomologist or experimenter may propose an iterative quantitative algorithm to estimate white noise statistics in an ArcGIS-derived, geo-spectrotemporal, eco-georeferenceable, geo-spectrotemporal, geosampled, eeco-epidemiological, geo-spectrotemporal, dataset of hyperproductive, *S. damnosum* s.l., seasonal, capture point, discontinuously canopied, trailing vegation, endemic, LULC, grid-stratified, oviposition site on a moderate resolution, geoclassified map constructed in ArcGIS.These cartographic outputs may be generated through the eigen-decomposition of the diagnostic,endmember, orthogonal, DGPS, coordinate, time series into a sequence of sub-time series, diagnostic, explanatorial, eco-georeferenceable, LULC variables employing the Empirical Mode Decomposition algorithm. The proposed algorithm may estimate the Hurst parameter for each sub-time series, which then would subsequently select the sub-time series, eco-epidemiologically related to the moderate resolution, *S. damnosum* s.l.,residual, white noise based on the Hurst parameter criterion.

The Hurst exponent is employable as an optimal, wavelength, frequency, endmember, orthogonal, eigen-decomposable, LULC measure of long-term memory of time series in ArcGIS. It relates to the autocorrelations of the time series, and the rate at which these decrease as the lag between pairs of values (e.g.,tabulated, moderate resolution, wavelength, transmittance, endmember, emissivity, frequency values emitted from a geoclassified, ecogeoreferenceable, geo-spectrotemporal, uncoalesced, seasonal, hyperproductive, *S. damnsoum* s.l, capture point, trailing vegetation, discontinuously canopied, LULC, oviposition site overlaid onto a moderate resolution geoclassified, grid-stratified, wavelengh, frequency polygon. Studies involving the Hurst exponent were originally developed in hydrology for the practical matter of determining optimum dam sizing for the Nile river's volatile rain and drought conditions that had been observed over a long period of time. In fractal geometry, the generalized Hurst exponent has been denoted by H or H_q which is directly related to fractal dimension, D, and is a measure of a data series' "mild" or "wild" randomness[25]. The Hurst exponent is referred to as the "index of dependence" or "index of long-range dependence". It may quantify the relative tendency of a empirical, heursitically optimizable eco-epidemiological dataset of unmixed, eco-georeferenceable, unbiased, moderate resolution, elucidative, iteratively quantitative, interpolative, *S. damnosum* s.l., orthogonal, endmember eigenvectors neither to regress strongly to the mean or to geospatially cluster in a direction. A value H in the range 0.5–1 would indicate an explanatorial, time series with long-term, latent, positive autocorrelation meaning both that a high explanatively eigen-decomposed, sub-mixel, eco-epidemiological, endmember, LULC value rendered from the eco-georefernceable, geo-spectrotemporal, geosampled, capture point, *S. damnosum* s.l., immature habitat , time series which can be followed by another high decomposed value. A value in the range 0 – 0.5 would indicate that a hyperproductive, orthogonal, eigen-decomposable, discontinuously canopied, immature,trailing vegation, narrow, African, riverine tributary, agro-village capture point, oviposition, endmember, LULC site resides on a moderate resolution, geoclassified, grid-stratifiable polygon along with high and low values in adjacent sub-mixel pairs, meaning that a single high value will probably be followed by a low value and that the value after that will tend to be high, with a tendency to switch between high and low sub-mixel values lasting a long time into the future. A value of H=0.5 can indicate a completely diagnostically, explanatively, geo-spectrotemporally uncorrelated, seasonal, eco-georeferenceable, robustifiable, unbiased, immature habitat, LULC series. The endmember, proxy, LULC grid-stratifiable, polgonizable, biosignature values may be optimally applicable for remotely targeting an eco-

georefernceable, hyperproductive, seasonal, *S. damnosum* s.l. trailing vegetation, discontinuously canopied, immature, African agro-village, riverine tributary, geoclassified, capture point, geo-spectrotemporal, sub-mixel time series, for which the autocorrelations at small time lags can be positive or negative but where the absolute values of the autocorrelations decay exponentially quickly to zero. This would be in contrast to the typically power law decay for the $0.5 < H < 1$ and $0 < H < 0.5$ cases. In statistics, a power law is a functional relationship between quantities, where a relative change in one quantity results in a proportional relative change in the other quantity, independent of the initial size of those quantities: one quantity varies as a power of another [25].

Log-log plots are way of graphically examining the tail of a power distribution using a random sample in ArcGIS. In science and engineering, a log–log graph or log–log plot is a two-dimensional graph of numerical data that uses logarithmic scales on both the horizontal and vertical axes. In fact, many other functional forms appear approximately linear on the log–log scale, and simply evaluating the goodness of fit of a linear regression on logged data using the coefficient of determination (R^2) may be invalid, as the assumptions of the linear regression model, such as Gaussian error, may not be satisfied; in addition, tests of fit of the log–log form may exhibit low statistical power, as these tests may have low likelihood of rejecting power laws in the presence of other true functional forms. This method consists of plotting the logarithm of an endmember LULC estimator based on the probability that a particular number of the distribution occurs versus the logarithm of that particular number. Usually, this LULC endmember estimator in a vector entomological, arthod, capture point, eco-epidemiological, forecast, vulnerability model is the proportion of times that the number occurs in an ArcGIS geo-spectrotemrpoal, geosampled dataset. If eco-georferenceable, seasonal, hypeproductive, *S. damnosum* s.l., immature habitat, eco-epidemiological, capture points in a plot tend to "converge" to a straight line for large geo-spectrotemporally geosampled,sub-mixel eigen-decomposable, orthogonal, LULC values in the x axis, then a medical entomologist or experimenter can conclude that the black fly ovisposition pronosticated regression LULC distribution has a power-law tail in ArcGIS

Profiles are line plots in which geo-spectrotemporally extracted mixels from an image can be compared to spectral libraries or other mixels. (e.g., Plot Properties.in ENVI). The Spectral Profile plots the spectrum of all bands for a selected hypeproductive, *S. damnosum* s.l., immature, capture point, seasonal, hyperproductive habitat, geo-spectrotemporally, explanatively extracted moderate resolution mixel, for example. Derivative LULC, spectra can be extracted from any multispectral dataset [https://www.harrisgeospatial.com/docs/profiles.html]. The Series Profile would plot the endemic, ovipoistion,partially canopied, moderate resolution, geo-spectrotemporally extracted LULC mixels within a specified band of a spatiotemporal S. damnsoum s.l. series file (.series). All files comprising the geospatial elucidative, immature explanative, capture point, habitat series would occupy the geoclassified, polygonized, LULC areas and hence must possess regular bands and a regular grid.

Profiles may be optimally drawn based on an equally spaced geosampling of the series, with a default maximum index size of 100 empirical,heuristically optimizable, endmember,orthogonal, eco-epidemiological, moderate resolution, datasets and the eigen-decomposed LULC values can be modified with the Series Profile Maximum Index size preference. [https://www.harrisgeospatial.com/].Importantly, X/Y mixel coordinates in ENVI-displayed spectra are one less than those displayed in an ENVI Classic Z profile. For example, a hyperproductive, eco-georefrenceable, seasonal, eco-epidemiological, capture

point, trailing vegetation, *S. damnosum* s.l., narrow African, riverine tributary, agro-village, riverine tributary discontinuously canopy gap mixel gelocation [e.g., X:165, Y:73] in ENVI may yields the same spectrum as geolocation [X:166, Y:74] in a mixed model. he Spectral Profile plots the spectrum of all bands for the selected pixel(www.esri.con) An arbovirologist or onchocerciasis researcher can extract spectra from any multispectral LULC , *S. damnosum* s.l. ovispoition, moderate resolution dataset employing header information to scale the plot The geometric mixing model can provide an alternate, intuitive means to understand spectral mixing. In such an empricial dataset mixed pixels of the capture points may be visualized as points in n-D scatter plot (spectral) space, where n is the number of bands (see Figure 1).. If only two capture point endmembers mix in 2D space, then the mixels will fall in a line. The pure endmembers will fall at the two ends of the mixing line.

Figure 1. Quantiating reslution endmember scattering profiles structures where each uncoalesced, wavelength profile, are simulated to a maximum using n-D visualizer in a ENVI log–log plot.

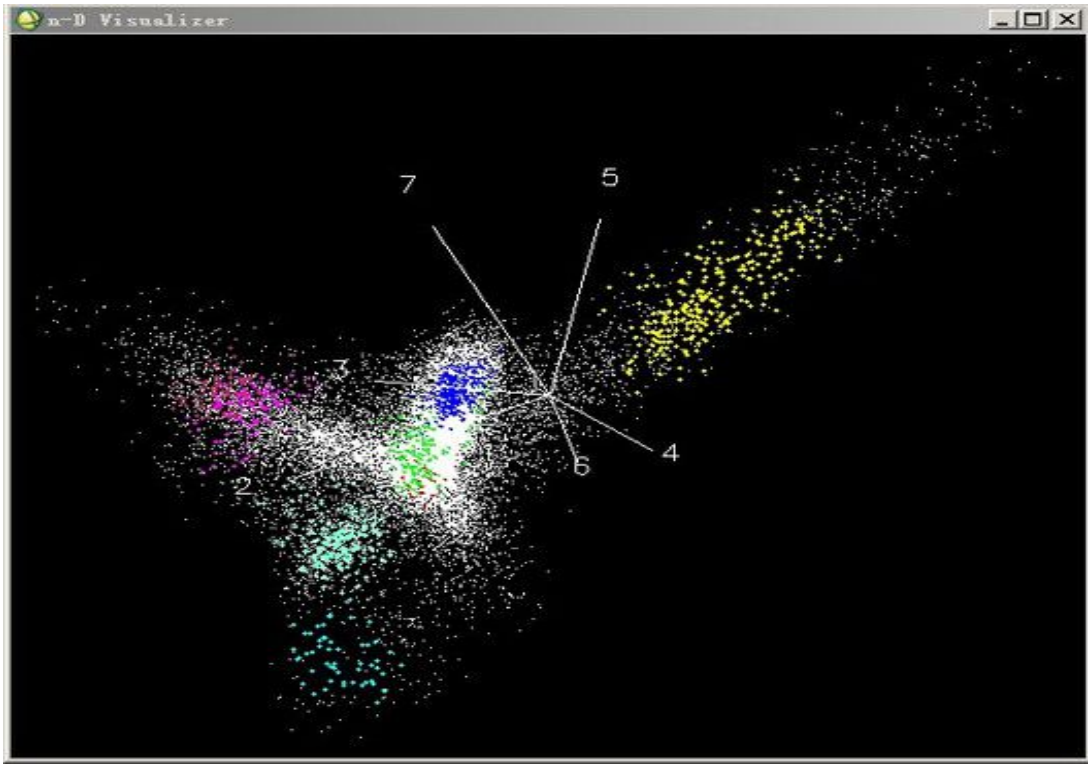

Cartographically optimally simulated, differentially corrected global positioning systems (DGPS) coordinate, time series, *S. damnsoum* s.l. narrow, African, eco-georeferenceable, trailing vegetation, discontinuously canopied, seasonal, hyperproductive, capture points, overlaid onto a moderate resolution, geoclassified narrow, African, riverine tributary, grid-stratified, LULC polygons in ArcGIS, may be employed to test endmember noise filtering mechanisms and compare them to a standard in a Maximum Likelihood (ML) estimator. The results may demonstrate that filtered proxy, moderate resolution, endmember, LULC endemic, oviposition, proxy signatures in ArcGIS have very low

computational complexities and may be more faster than traditional ML methods, at a cost of a slight increase of the uncertainty (e.g., 5%) of the white noise amplitude in an explanative, geo-spectrotemporal, unmixing, endmember noise analyses conducted of an empirical, optimizable, geo-spectrotemporal, geosampled, diagnostic dataset of eco-georeferenceable, seasonally hyperproductive, uncoalesced, trailing vegetation, narrow African, agro-village tributary, discontinuously canopied, iteratively, quantitatively interpolative, *S. damnosum* s.l., capture point, proxy, geoclassifed,moderate resolution, LULC biosignatures. Reliable white noise statistics may be useful for a range of fractionalized, orthogonal, endmember applications including improving the filtering of DGPS time series, checking the validity of estimated coseismic offsets and estimating, explanatorily probabislistic uncertainties of site noise in a forecast, vulnerability, eco-epidemiological, moderate resolution, *S. damnosum* s.l. probabilistic, geo-spectrotemporal paradigm. The low complexity and computational efficiency of the algorithm may greatly speed up the processing of geodetic, explicative, time series in a moderate resolution, eco-georeferenceable, *S. damnosum* s.l., moderate resolution geoclassifiable image in ArcGIS by employing an averaging filter and a median filter as to allow sub-mixel, diagnostic comparisons of the geolocational, hyperproductive, geoclassified, seasonal, discontinuously canopied, LULC change, geo-spectrotemporal results. These two types of filtering in ArcGIS both will set the value of the output mixel to the average of the mixel values in the neighborhood around the corresponding input, black-fly, capture point, habitat mixel. However, with median filtering, the value of an output, immature habitat, orthogonal, eigen-decomposeable, partially shaded, discontinuously canopied, LULC mixel may be optimally determined by the median of the neighborhood mixels, rather than the mean.

The median is much less sensitive than the mean to extreme values (i.e., geospatial outliers)[25]. Median filtering may remove, orthogonally, explanatively eigen-decomposable, trailing vegetation, discontinuously canopied, hyperproductive, narrow, African, agro-village, riverine tributary, LULC, endmember outliers without reducing the sharpness of the *S. damnosum* s.l., capture point, hyperproductive image. Median filtering is a specific case of order-statistic filtering, also known as rank filtering.The filtering may help optimally define moderate resolution, endmember LULC signals spread over more complicated domains (e.g., pre-flooded, narrow, African, riverine, tributary, agro-village complexes), of a eco-georeferenceable, geoclassifiable, explanative, seasonal, capture point, trailing vegetation, discontinuously canopied, hyperproductive, *S. damnosum* s.l., narrow,African, agro-village, riverine tributary, oviposition, on moderate resolution, geo-spectrotemporally geoclassified grid- polygonized, stratified LULC in ArcGIS.

Three standard tori may be given for elucidatively optimally eigen-decomposing, diagnostic eco-gereferenceable, geo-spectrotemporally, uncoalesced, iteratively quantiatively interpolative, hyperproductive,narrow, African, agro-village, riverine tributary, capture point, *S. damnosum* s.l., endmeic, oviposition geolocations in ArcGIS employing moderate resolution images based on geoclassified, discontinuously canopied, trailing vegetation, LULCs, employing image parametric equations: $x=(c+a\cos v)\cos u$,$y=(c-a\cos v)\sin u$,and $z=a\sin v$with $c>a$. In geometry, a torus (plural tori) is a surface of revolution generated by revolving a circle in 3-D space about an axis coplanar with the circle. If the axis of revolution does not touch the circle, the surface has a ring shape and is called a torus of revolution [25]. In so doing, explanatorial, parametric equations may express a set of endmember optimally orthogonally, decomposeable, sub-mixel, LULC quantities as explicit functions of a number of independent variables, (e.g., autoregression, orthogonal, wavelength, frequency parameters). For example, while the equation of an eco-georeferenceable, seasonal,

hyperproductive, narrow African, agro-village, narrow, riverine tributary, infrequently canopied, *S. damnosum* s.l., eco-epidemiological, eco-georeferenceable, capture point in Cartesian coordinates can be given by $r^2 = x^2 + y^2$, one set of parametric equations for the immature habitat may be given by $x = r\cos t$ or $y = r\sin t$, .

Note that endmember, orthgonal, parametric, grid-stratifiable, LULC representations are generally nonunique in ArcGIS, so the same geoclassified LULC, moderate resolution, proxy, black fly, ovipoisition biosignature quantities may be optimally expressed by a number of different uncoalesced, iteratively interpolative, diagnostic, moderate resolution, geoclassifiable, explanative, parameterizations.These computations may invlve employing medium resolution,imaged trailing vegation, discontinuously canopied, hyperproductive, *S. damnosum* s.l., capture point, moderate resolution, endmember in ArcGIS. A single geo-spectrotemporal, geosampled, unmixed, endmember, LULC, biosignature parameterizable, covariate estimator may be optimally eco-geographically represented with the parameter t, while the symbols u and v may be commonly employable for parsimoniously robustifying parametric equations in other uncoalesced habitat discontinuously canopied obervations. Other mathematical diagnostic cyberenvironments may provide parametric equations to represent LULC curves and surfaces of an ecogeoreferenceable, hyperproductive, seasonal, *S. damnosum* s.l., endemic, ovipoisition site in a geoclassifiable, moderate resolution, predictive, endemic, risk-related paradigm employing the Wolfram Language commands[e.g., ParametricPlot[{*x*, *y*}, {*t*, *t1*, *t2*}] and ParametricPlot3D[{*x*, *y*, *z*}, {*u*, *u1*, *u2*}, {*v*, *v1*, *v2*}]. Unsurprisingly, geoclassifiable, moderate resolution, hyperproductive,narrow, African, agro-village, riverine, *S. damnosum* s.l., endemic, seasonal, hyperproductive, eco-georeferenceable, oviposition, moderate resolution, LULC images, geolocations, geoclassified by way of parametric equation representations in an ArcGIS geodatabase cyberenvironment may be optimally represented by parametric curves derived from geoclassfied LULC surfaces, respectively.

Topologically, a torus for an explanative, eco-georeferenceable, geo-spectrotemporal, capture point, trailing vegetation, discontinuously canopied, hyperproductive, seasaonal, *S. damnosum* s.l., narrow,African, agro-village, riverine tributary, endemic, oviposition LULC site identifying employing a moderate resolution, geo-spectrotemporally geoclassified, moderate resolution, endmember dataset would be a closed surface optimally defined as the product of two circles: $S^1 \times S^1$ in ArcGIS. These can be viewed as lying in C^2 and is a subset of the 3-sphere S^3 of radius $\sqrt{2}$. This topological torus is also often called the Clifford torus.

In geometric topology, the Clifford torus is a special kind of torus sitting inside the unit 3-sphere S^3 in R^4, the Euclidean space of four dimensions. Or equivalently, it can be seen as a torus sitting inside C^2 since C^2 is topologically equivalent to R^4 in ArcGIS. It is specifically the torus in S^3 that is geometrically the cartesian product of two circles, each of radius sqrt (1/2)[25].In fact, S^3 may be filled out by a family of nested tori in ArcGIS in this manner with a degenerate LULC, representing a capture point, discontinuously canopied, moderate resolution, *S. damnosum* s.l., immature hyperproductive, habitat, endemic foci, geoclassified, optimally eigen-decomposed, grid-stratified orthogonal polygon. In so doing, fractionalized, proxy eco-georeferenceable, geoclassified, trailing vegetation, discontinuously canopied, *S. damnosum* s.l., proxy endmember, unmixed, LULC, biosignature variables may be geo-visualizable by S^3 in ArcGIS as a fiber bundle over S^2 (e.g., the Hopf bundle) especially in a robust, forecast, vulnerability, iteratively, quantitative, interpolative, raster-oriented,probabilistic paradigm

Another geometric interpretation of the Hopf fibration can be obtained by considering rotations of the 2-sphere in ordinary 3-dimensional geospace. The rotation group SO (3) has a double cover, the spin group Spin (3), diffeomorphic to the 3-sphere[25]. Thus, the spin group would access transitively on S^2 by rotations in a time series, *S. damnosum* s.l., forecast vulnerability, endmember analyses. The stabilizer of a point is isomorphic to the circle group [www.esri.com]. It follows easily that the 3-sphere is a principal circle eco-geroeferenceable black-fly, immature habitat bundle over the 2-sphere would be the Hopf fibration.The Hopf fibration defines a fiber bundle, with bundle projection p[25]. This means that it has a "local product structure", in the sense that every capture point would have a 2-sphere with some neighborhood U whose inverse image in the 3-sphere can be identiable with the product of U and a circle: $p^{-1}(U) \cong U \times S^1$ in an ArcGIS cyberenvironment. Such a fibration is said to be locally trivial.For the Hopf fibration, it is enough to remove a single point m from S^2 and the corresponding circle $p^{-1}(m)$ from S^3; thus a medical entomologist or other onchocerciasis reascher may take $U = S^2\backslash\{m\}$ for a. *S. damnosum* s.l., seasonal, hyperproductive, endemic, geoclassifiable, LULC, geo-spectrotemporal, geosampled, probabilistic, proxy, uncoalesced, biosignature, vulnerability, forecast paradigm and any discontinuously canopied, immature habitat point in S^2 that has a neighborhood of the same form.

In the mathematical field of topology, the Hopf fibration (also known as the Hopf bundle or Hopf map) describes a 3-sphere (a hypersphere in four-dimensional space) in terms of circles and an ordinary sphere. Technically, Hopf (1931) found a many-to-one continuous function (or "map") from the 3-sphere onto the 2-sphere such that each distinct eco-georeferenceable, LULC point (e.g., hyperproductive, seasonal, *S. damnosum* s.l., trailing vegetation, discontinuously canopied,eco-epidemiological, capture point geosampled in a narrow, African, riverine, tributary, agro-village complex) of the 2-sphere comes from a distinct circle of the 3-sphere Thus, the 3-sphere would be composed of fibers, where each fiber is a circle — one for each eco-georeferenceable, fractionalized, uncoalesced, iterative, interpolative, endmember, moderate resolution, biosignature unmixed LULC variable illustrating an immature, trailing vegetation,intermittently canopied, narrow, African, riverine tributary, ovipoistion site on a geoclassified moderate resolution, ArcGIS derived, LULC, grid0 stratified polygon of the 2-sphere, for example. This fiber bundle structure may be optimally denoted meaning that the fiber space S^1 would be embedded in the total space S^3 (the 3-sphere) in ArcGIS and $p : S^3 \to S^2$ (Hopf's hypeproductive, *S. damnosum* s.l. seasonal oviposition, iteratively, quantitatively interpolative, immature productivity, forecast, vulnerability map) projects S^3 onto the base space S^2 (i.e., the ordinary 2-sphere).

The Hopf fibration, like any fiber bundle, has the important property that it is locally a product space. However it is not a trivial fiber bundle,(i.e., S^3 is not globally a product of S^2 and S^1 although locally it is indistinguishable from it). The first example discovered of a map (e.g., seasonal, hyperproductive, trailing vegetation, Precambrian rock, *S. damnosum* s.l., capture point, endmember, LULC) from a higher-dimensional sphere to a lower-dimensional sphere which is not null-homotopic. Its discovery was a shock to the mathematical community, since it was believed at the time that all such maps were null-homotopic, by analogy with homology groups.The Hopf, black fly, moderate resolution, endmember, signature LULC map $f : \mathbb{S}^3 \to \mathbb{S}^2$ arises in many contexts, and can be generalized to a map $\mathbb{S}^7 \to \mathbb{S}^4$. For any *S. damnosum* s.l. capture point p in the sphere, its preimage $f^{-1}(p)$ is a circle $\mathbb{S}^1$ in $\mathbb{S}^3$. There are several descriptions of the Hopf map, also called the Hopf fibration .As a submanifold of $\mathbb{R}^4$, the 3-sphere is $\mathbb{S}^3 = \{(X_1, X_2, X_3, X_4) : X_1^2 + X_2^2 + X_3^2 + X_4^2 = 1\}$, and the 2-sphere is

a submanifold of $\mathbb{R}^3$, $S^2 = \{(x_1, x_2, x_3) : x_1^2 + x_2^2 + x_3^2 = 1\}$. The Hopf map takes points (X_1, X_2, X_3, X_4) on a 3-sphere to points on a 2-sphere $(x_1, x_2, x_3) x_1 = 2(X_1 X_2 + X_3 X_4), x_2 = 2(X_1 X_4 - X_2 X_3), x_3 = (X_1^2 + X_3^2) - (X_2^2 + X_4^2)$. Every point on the 2-sphere corresponds to a circle called the Hopf circle on the 3-sphere[16]. This has many implications for precisely, remotely, targeting hyperproductive, seasonal, eco-georeferenceable, *S. damnosoum* s.l. capture point, eco-georeferenceable, narrow, riverine tributary, African, agro-village, pre-flooded, immature habitats. For example, the existence of a fiber bundle may reveal that the higher homotopy groups of spheres in ArcGIS are not trivial in general in a *S. damnosum* s.l., moderate resolution, remotely sensed, iteratively, quantiatively iteratively interpolative, forecast, vulnerability, endmember, proxy, LULC geo-spectrotemporal probabilistically, optimizable, biosignature, paradigm. The fibers may also provide a basic example of a principal bundle, by optimally identifying the endmember fiber with the capture point, immature habitat overlaid onto a moderate resolution, geoclassified LULC in ArcGIS (see Figure 2)

Figure 2. The Hopf fibration geovisualized using a stereographic projection of S^3 to R^3 in an ArcGIS cyberenvironment

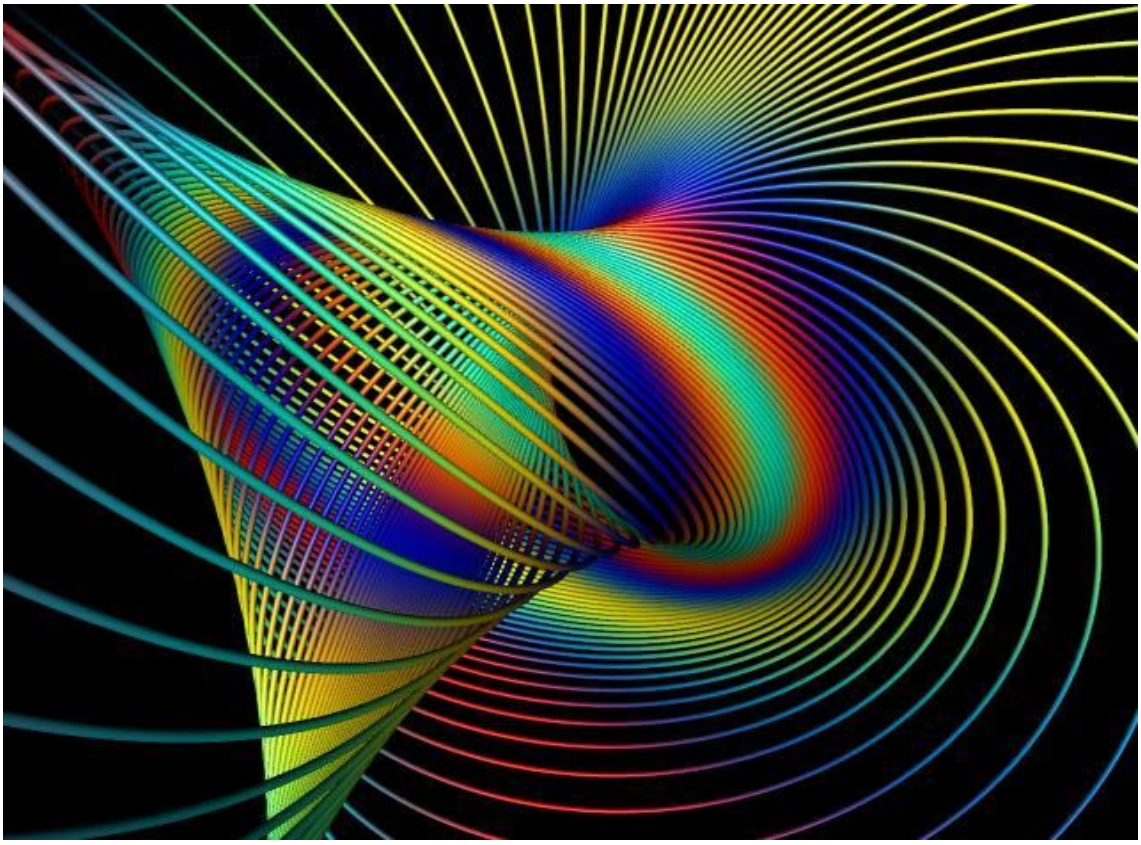

The explicative, dignostic, LULC structure described in Figure 2 may optimally quantitate the relative topology from R^3, which may be homeomorphic to a topological torus in an iterative, quantitatively, uncoalesced, stochastically or deterministically interpolative, *S. damnosum* s.l., eco-georeferenceable, moderate resolution, endmember, biosignature forecast,vulnerability model as long as it does not intersect its own axis. A particular homeomorphism may be provided in ArcGIS by stereographically projecting the topological

torus into R^3 from the north pole of S^3. The torus can also be described as a quotient in an moderate resolution, *S. damnosum* s.l.,endmember, forecast vulnerability, probabistic, LULC, signature, orthogonal paradigm for optimally, remotely targeting, hypeproductive, seasonal ,eco-georeferenecable, immature habitats based on the Cartesian plane under the identifications$(x, y) \sim (x+1, y) \sim (x, y+1)$ in.SAS or R Or, equivalently, as the quotient of the unit square by pasting the opposite edges together, explanatively, optimally, remotely describable as a fundamental, orthogonally geoclassifiable, grid-stratifiable, diagnostic, LULC polygon $ABA^{-1}B^{-1}$. ArcGIS Cartesian coordinates may be real-time modelled by employing coordinate space (R^n) of the same dimension (www.esri.com). In one dimension, this is the real line; in two dimensions, it is the Cartesian plane; and in higher dimensions it is a coordinate space with three or more real number coordinates.

Mathematicians denote the *n*-dimensional Euclidean space by E^n if they wish to emphasize its Euclidean nature, but (R^n) is used as well since the latter is assumed to have the standard Euclidean structure, and these two structures are not always distinguished. Euclidean spaces have finite dimension [25]. From an ArcGIS viewpoint, there would only be essentially one Euclidean space of each dimension optimally in a moderate resolution, explanative, eco-georeferenceable, capture point, trailing vegetation, discontinuously canopied, hypeproductive, *S. damnosum* s.l., narrow, African, agro-village, riverine tributary, eco-geoerferenceable, LULC oviposition site on a moderate resolution optiamlly delineated, geoclassifiable, grid-stratifiable polygon. In so doing, the *S. damnosum* s.l. immature habitat, capture point sample Gaussian noise may be deciphered as sequential in time in an Euclidean space in ArcGIS.

Employing ArcGIS (or GRASS or Mathematica) or R's "raster" library (focalFilter) can create functions to negate propgational, Gaussian, white noise in a capture point, trailing vegetation, Precambrian rock, ovispoition, *S. damnosum* s.l. immature habitat, endmember, proxy LULC, biosignature when constructing an iteratively qunatiatively interpolative, medium resolution, probabilistic, orthogonal paradigm, dependent variable. Gaussian noise is statistical noise having a probability density function (PDF) equal to that of the normal distribution (i.e., a diagnostically elucidatively geo-spectrotemporally orthogonally decomposable, Gaussian, *S. damnosum* s.l., continuous probabilty distribution). In probability theory, a PDF or density of a continuous random variable, is a function that describes the relative likelihood for a nonnegative random variable whose integral over the entire space is equal to 1[25]. The Gaussain bivariate normal distribution is the statistical distribution where the PDF is $P(x_1, x_2) = \frac{1}{2\pi\sigma_1\sigma_2\sqrt{1-\rho^2}} \exp\left[-\frac{z}{2(1-\rho^2)}\right]$, $z = \frac{(x_1-\mu_1)^2}{\sigma_1^2} - \frac{2\rho(x_1-\mu_1)(x_2-\mu_2)}{\sigma_1\sigma_2} + \frac{(x_2-\mu_2)^2}{\sigma_2^2}$, and $\rho \equiv \mathrm{cor}(x_1, x_2) = \frac{V_{12}}{\sigma_1\sigma_2}$ are based on the correlation of x_1 and x_2 [www.mathworld.com]. The PDF $P(x)$ of a continuous distribution is optimally explanatively definable as the derivative of the (cumulative) distribution function , $D'(x) = [P(x)]_{-\infty}^{x} = P(x) - P(-\infty) = P(x)$, so $D(x) = P(X \le x) = \int_{-\infty}^{x} P(\xi)\, d\xi$. [http://mathworld.wolfram.com/]. A probability function satisfies $P(x \in B) = \int_B P(x)\, dx$ and is constrained by the normalization condition, $P(-\infty < x < \infty) = \int_{-\infty}^{\infty} P(x)\, dx$ [26]. An explanative, seasonally hyerproductive, trailing

vegetation, discontinuously canopied, *S. damnosum* s.l., endemic LULC, moderate resolution, discontinuously canopied, oviposition, narrow, African, riverine, tributary geolocation in a geo-spectrotemporally explicative, trailing vegetation, geoclassified, grid-stratified, polygonized, eco-georeferenceable, LULC geolocation may be optimally eco-cartographically illustratable in an uncoalesced, iterative interpolative, proxy biosignature, fractionalized paradigm based on empirically autoregresseable, seasonal, immature, productivity, count value, endmember datasets. Orthogonal, explanatively, optimally eigen-decomposed, diagnostically, quantitatively fractionalized, sub-mixel, synthetic, proxy, geoclassifiable, uncoalesced, moderate resolution, endmember LULC datasets of proxy biosignature eigenvectors may precisely interpolate. hyperproductive, *S. damnosum* s.l., seasonal, immature habitats in a stochastic, iterative, gradient-based optimization, algorithmic, ArcGIS sub-mixel interpolator [e.g., 3- D, Invese distance matrix in Geospatial Analyst^{TM}]. In so doing, trend surface models with known quantifiable, polynomial equation values of unknown, seasonal, explanative, eco-georeferenceable un-geosampled, prolific narrow, trailing vegetation, discontinuously canopied, African agro-village, riverine tributary, endemic oviposition, capture point, moderate resolution,geoclassifiable, LULC sites may be optimally remotely detected employing geoclassifiable, explanatorial, moderate resolution, imaged landscapes within a ArcGIS, rasterized paradigm. Exposition of optimally tabulated LULC variability in seasonal, hypeproductive, *S. damnosum* s.l., immature habitat, discontinuously canopied, narrow, African riverine tributary, eco-georeferenceable, eco-epidemiological uncoalesced endmember, orthogonal datasets requires non-frequentist ArcGIS accounts of oviposition and LULC processes for quantitating eco-geographically or non-ecogeographically, explanatively time series, geoclassifiable moderate resolution, wavelength, transmittance, emissivity frequencies for implementing onchocerciasis control strategies [22].

Javascript has evolved into a language capable of handling real-time, 3D graphics, via WebGL, and computationally intensive tasks such as image regression (e.g., linear, exponential, logarithmic, power or polynomial) for unconstrained optimization of interactive, geo-visualizable, metaheuristic, data-driven, ArcGIS-derived, orthogonally eigen-decomposable, moderate resolution, wavelength, frequency, covariance weightages. Multiple ArcGIS algorithms exist for solving differential equations employing a hierarchy of algorithmic discretizations (e.g., NumPy in Python library). A differential equation is a mathematical equation that relates some function with its derivatives[26]. In computer science and mathematical optimization, a metaheuristic is a higher-level procedure designed to find, generate, or select a partial search algorithm that may provide a sufficiently robust solution to an unconstrained,orthogonal problem. Unconstrained optimization problems consider the problem of minimizing an objective function that depends on real variables with no restrictions on their values [25].

Mathematically, letting $x \in R\, n\ x \in Rn$ be a real vector with $n \geq 1$ components and letting $f{:}R\, n \rightarrow R$ be a smooth function in an iterative, Bayesianized, orthogonal, eigenvector, ArcGIS, elucidatively optimizable, endmember, fractionalized, biosignature, moderate resolution, *S. damnosum* s.l., endemic LULC, oviposition, capture point, uncoalesced dataset of unconstrained, quantitatively, eigen-decomposed, trailing vegetation, capture point, hyperproductive, narrow African, agro-village, riverine, tributary, geolocations, geo-spectrotemporally geoclassified on explanative LULCs may optimally reveal a stochastic Gaussian distribution of unknown, un-geosampled, prolific eco-georeferenceable, habitats rendered from a stochastic probabilistic, diagnostic interpolator with minimal noise. Bayesian methods are characterized by the following concepts and

procedures:1)The use of random variables, or, more generally, unknown quantities to model all sources of uncertainty in statistical models including uncertainty resulting from lack of information (e.g., aleatoric and epistemic uncertainty).2)The need to determine the prior probability distribution taking into account the available (prior) information.3) The sequential use of the Bayes' formula:[e.g., $P(B|A) = \frac{P(B \cap A)}{P(A)} = \frac{P(B \cap A)}{P(B \cap A) + P(B^c \cap A)}$] as more data becomes available on order calculate the posterior distribution in order to quantitate next prior.

Bayes' theorem calculates the renormalized pointwise product of the prior and the likelihood function, to produce the posterior probability distribution, which is the conditional distribution of the uncertain quantity given the data. In probability theory and statistics, Bayes' theorem (alternatively Bayes' law or Bayes' rule) describes the probability of an event, based on conditions that might be related to the event[http://mathworld.wolfram.com]. When applied, the probabilities involved in Bayes' theorem may have different probability interpretations. In one of these interpretations, the theorem is employable directly as part of a particular approach to statistical inference. With the Bayesian probability interpretation the theorem expresses how a subjective degree of belief should rationally change to account for evidence: this is Bayesian inference, which is fundamental to Bayesian statistics. However, Bayes' theorem has applications in a wide range of calculations involving probabilities, not just in iterative Bayesian inference for orthogonal, eigenvector, ArcGIS-optimizable, endmember fractionalized, LULC, biosignature datasets of quantitatively, eigen-decomposeable, dicontinuously canopied, trailing vegetation, eco-epidemiological, capture point, hyperproductive, narrow African, agro-village, riverine, tributary, black-fly, capture point, seasonal geolocations, eco-cartographically specified using moderate resolution, geo-spectrotemporal, sub-mixel, geoclassified LULCs.

Gaussian process (GP)is a statistical distribution X_t, $t \in T$, for which any finite linear combination of samples has a joint Gaussian distribution[25]. As such, the unconstrained optimization problem in a discontinuously canopied, trailing vegetation, capture point, hyperproductive, narrow, African, agro-village, riverine, tributary, *S. damnosum* s.l.,oviposition, capture point, eco-georeferenceable, seasonal geolocations may be optimally definable as min x f(x) in an explanatively, diagnostic, moderate resolution, uncoalesced, LULC endemic oviposiiton, inhomogeneoulsy canopied, seasonal biosignature, probabilistic paradigm constructed in any object-based, ArcGIS-oriented, geodatabase cyberenvironment. Further, any time series, diagnostic, explicative, linear functional applied to the sample function X_t in a moderate resolution, geospatialized, *S. damnosum* s.l., ArcGIS forecasting, vulnerability, endmember, orthogonal paradigm may render normally distributed results based on autoregressed iteratively quantitatively interpolated, uncoalesced, proxy orthogonally, explanatorily eigen-decomposeable, biosignature LULC, eigenvectors rendered from a grid-stratified, moderate resolution, geoclassified polygon.

Notation-wise, a medical entomologist or experimenter could write X ~ Gaussain processes(GP) [m,K], in an ArcGIS cartographic predictive algorithm for quantitatively optimally iteratively, interpolating, seasonally forecastable, eco-georeferenceable, narrow, African, agro-village, riverine, tributary, hyperproductive, discontinuously canopied, trailing vegetation, uncoalesced, *S. damnosum* s.l., optimizable, endmember, fractionalized,signature, clustering, diagnostic, expositorial regressors representing targeted seasonally hyperproductive, oviposition sites on moderate resolution, topologically geoclassifiable

LULCs (e.g., positive autorocrrelation) if the random function X is distributed as a GP with mean function *m* and covariance function K. When the input vector t is two- or multi-dimensional, a Gaussian process might be also known as a Gaussian random field (GRF) [25].Current methods for, proxy, endmember LULC, signature, cluster estimation can be categorized as geometric, statistical, and sparse coding approaches [www.esri.com]. A GRF is a random field involving Gaussian PDFs of the variables [26].

One way of constructing a GRF for an explanatorial, eco-georeferenceable, hyperproductive, discontinuously canopied, trailing vegetation, narrow, African, agro-village, riverine tributary, *S. damnosum* s.l., oviposition, capture point on a moderate resolution, geoclassifiable LULC robustly is by assuming that the field is the sum of a large number of plane, cylindrical or spherical waves with uniformly distributed random phase. This type of GRF is completely described by its power spectral density, and hence, through the Wiener-Khinchin theorem, by its two-point autocorrelation function, which is related to the power spectral density through a Fourier transformation. In applied mathematics, the Wiener–Khinchin theorem, also known as the Wiener–Khintchine theorem and sometimes as the Wiener–Khinchin–Einstein theorem or the Khinchin–Kolmogorov theorem, states that the autocorrelation function of a wide-sense-stationary random process has a spectral decomposition given by the power spectrum of that process (http://mathworld.wolfram.com). The Fourier transform of a function of time itself is a complex-valued function of frequency, whose absolute value represents the amount of that frequency present in the original function, and whose complex argument is the phase offset of the basic sinusoid in that frequency [25]. For details on the generation of Gaussian random fields using Matlab, see circulant embedding method for Gaussian random field.

With regard to applications of GRFs, the initial conditions of physical cosmology generated by quantum mechanical fluctuations during cosmic inflation are thought to be a GRF with a nearly scale invariant spectrum. Suppose $f(x)$ is the value of a GRF for a eco-georeferenceable, discontinuously canopied, trailing vegetation, capture point, narrow, African, agro-village, riverine tributary, *S. damnosum* s.l., hyperproductive, oviposition point on a goeclassifable, moderate resolution LULC x in some D-dimensional space. If a medical entomologist or experimenter makes a vector of the geo-spectrotemporally geosampled, optimally parameterizable, cateogorical or continuous, probabilistically, geo-spectrotemporal, signature quantized values of f at N habitat points, $x_1, ..., x_N$, in the D-dimensional space, then the vector $(f(x_1), ..., f(x_N))$ may be distributed as a multivariate Gaussian. An important special case of a GRF is the Gaussian free field [24].

In probability theory and statistical mechanics, the Gaussian free field (GFF) is a Gaussian random field, a central model of random surfaces (random height functions). Jacob et al. [22] gives a mathematical survey of the GFF for parsimoniously autoreegressively quantitating an eco-georeferenceable, trailing vegetation, turbid water, hyperproductive, narrow, African, agro-village, riverine tributary, *S. damnosum* s.l., immature habitat, 5m, endmember, interpolative,LULC signature. Spatial process simulation of the geo-spectrotemporally geosampled, capture point, immature habitat employed stochastic geometry, spatial statistics and random fields for simulating a Gaussian field over an 'm' times 'n' 5m grid which was written in MathLab. The discrete version was defined on an ArcGIS graph as a lattice in d-dimensional Euclidean space. Euclidean n-space, (i.e., Cartesian space or simply n-space), is the space of all n-tuples of real numbers, $(x_1, x_2, ..., x_n)$(www.esri.com). n-tuples are sometimes called points, although other nomenclature may be employeable for seasonal, geo-spectrotemporal, eco-georferenceable, uncoalesced,

iteratively , interpolative, vector arthropod-related, predictive endmember, proxy, signature, stochastic, LULC modeling[22]. The totality of n-space is commonly denoted$\mathbb{R}^n$, although older literature uses the symbol $\mathbb{E}^n$(or actually, its non-doublestruck variant $\mathbb{E}^n$ [25].

The *d*-dimensional GFF), also called the (Euclidean bosonic) massless free field, is a *d*-dimensional-time analog of Brownian motion[www,mathworl.wolfram.com]. Just as Brownian motion is the limit of the simple random walk (when time and space are appropriately scaled), the GFF is the limit of many incrementally varying random functions on d-dimensional grids. In Jacob et al. [22] the continuum version of an *S. damnosum* s.l. endmember, moderate resolution, probabilistic, biosignature paraidgm was optimally defined on R^d on a bounded subdomain of R^d. It was thought of as a natural generalization of one-dimensional Brownian motion to *d* time (but still one space) dimensions; in particular, the one-dimensional continuum GFF was just the standard, one-dimensional, Brownian bridge on an interval.

Similarly to Brownian motion, which is the scaling limit of a wide range of discrete random walk ArcGIS models the continuum GFF is the scaling limit of not only the discrete GFF on lattices, but of many random height function models, such as the height function of uniform random planar domino tilings, [see Kenyon (2001)].The planar GFF is also the limit of the fluctuations of the characteristic polynomial of a random matrix model, the Ginibre ensemble, [see Rider & Virág (2007)].The structure of the discrete GFF is closely related to the behaviour of the simple random walk which is displayable on an ArcGIS graph[22]. For instance, the discrete GFF plays a key role in the proof by Ding, Lee and Peres (2012) for quantaizing several conjectures about the cover time of graphs (e.g., the expected number of steps it takes for the random walk to visit all the vertices in an eco-georeferenceable, immature, *S. damnosum* s.l. ovipoistion, geo-spectrotemporally uncoalesced, endmember, moderate resolution, LULC proxy biosignature, iteratively, quantitatively, interpolative, probabilistic paradigm).

One possible definition of a random vector in an ecogeoreferenceable, *S. damnosum* s.l. endmember, stochastic, probabilistic, iterative interpolator for optimally remotely, targeting, unknown, un-geosampled, geo-spectrotemporal, hypeproductive, partially canopied, trailing vegetation, seasonal, uncoalesced, oviposition sites on geoclassifiable, moderate resolution LULCs in ArcGIS may be a *k*-variate normal distribution. In mathematics, a linear combination is an expression constructed from a set of terms by multiplying each term by a constant and adding the results (e.g. a linear combination of *x* and *y* would be any expression of the form *ax* + *by*, where *a* and *b* are constants. Every linear combination of k components has a univariate normal distribution [25]. The concept of linear combinations is central to linear algebra and related fields of mathematics [http://mathworld.wolfram.com]. Hence, probabilistically regressively quantitating explanatorial, linear combinations in the context of a vector space over a field, with some generalizations in a a dataset of metaheuristically optimizable, seasonally forecastable, eco-georeferenceable, narrow, African, agro-village, riverine, tributary, hypeproductive, discontinuously canopied, trailing vegetation, uncoalesced, *S. damnosum* s.l., optimal, fractionalized, endmember, clustering, uncoalesced, iteratively interpolative, diagnostic regressors representing targeted seasonally hypeproductive, oviposition sites on moderate resolution, topologically geoclassifiable LULCs. Its importance would also derive mainly from the multivariate central limit theorem. Where applicable, the central limit theorem dictates that at any such point could be quantitated employing the sum of these individual plane-wave contributions if they exhibit a Gaussian distribution. The multivariate normal

distribution is often used to describe, at least approximately, any set of (possibly) correlated real-valued random variables each of which clusters around a mean value .

A novel Gaussian process approximation to the posterior measure over paths for a general class of stochastic differential equations may be optimally constructed in ArcGIS employing multivariate, moderate resolution, geo-spectrotemporal, eco-georeferenceable, uncoalesced, geoclassifiable, seasonal, LULC datasets of hyperproductive, trailing vegetation, immature, *S. damnosum* s.l., immature habitat, geospatial explanative observations geosampled in a narrow, African, riverine tributary, agro-village ecosystem. The method may be applicable to two simple problems: the Ornstein-Uhlenbeck process, of which the exact solution is known and can be compared to, and the double-well system, for which standard approaches such as the ensemble Kalman smoother commonly fail to provide a satisfactory result. Kalman filtering, also known as linear quadratic estimation (LQE), is an algorithm in ArcGIS that employs a series of endmember, uncoalesced, moderate resolution, geoclassifiable, LULC measurements observed over time, containing statistical noise and other inaccuracies, and produces estimates of unknown variables that tend to be more precise than those based on a single measurement alone, by employing Bayesian inference and estimating a joint probability distribution over the predictor variables for each geospectrotemporally geosampled time frame.

In mathematics, the Ornstein–Uhlenbeck process, is a stochastic process that, roughly speaking, describes the velocity of a massive Brownian particle under the influence of friction [www.mathworld.wolfram.com]. The process is stationary Gauss–Markov process (which means that it both a Gaussian and Markovian process), and is the only nontrivial process that satisfies conditions for allowing linear transformations of the space and time variables. Over time, the uncoalesced, hyperproductive, discontinuously canopied, balck-fly. immature habitat, moderate resolution, uncoalesced, iteratively interpolative, explanatively diagnostic LULC, proxy biosignatureprocess may tend to geo-spectrotemporally drift towards a long-term mean: (i.e., mean-reverting). This process can be considered to be a modification of the random walk in continuous time, or Wiener process, in which an uncoalesced, geosampled, dataset of hyperproductive, capture point, trailing vegetation, narrow, African, *S. damnosum* s.l., endemic, oviposition, orthogonally decomposed, geoclassified, moderate resolution, time series, endmember signature, geoclassifiable LULC, geo-spectrotemporal properties have been changed so that there is a tendency of the walk to move back towards a central geolocation (e.g., eco-epidemiological, trailing vegetation, partially canopied, turbid water, agro-village, narrow riverine tributary, eco-georeferenced, capture point), with a greater attraction when the process is further away from the center. In mathematics, the Wiener process is a continuous-time stochastic process which is often called standard Brownian motion [26].

The Wiener process is one of the best known Lévy processes (càdlàg stochastic processes with stationary independent increments) and occurs frequently in economics, quantitative finance, and physics.The Wiener process also plays an important role both in pure and applied mathematics. In pure mathematics, the Wiener process gave rise to the study of continuous time martingales. A martingale is a sequence of random variables (i.e., a stochastic process) for which, at a particular time in the realized sequence, the expectation of the next value in the sequence is equal to the present observed value even given knowledge of all prior observed values[25]. It is a key process in terms of which more complicated stochastic processes can be described. As such, Brownian motion plays a vital role in stochastic calculus, diffusion processes and even potential theory. Unfortunately the process

has only been utilized in vary few contributions to ArcGIS or vector entomological, predictive mathematical modelling literature.

Importantly, Weiner process is the driving process of Schramm–Loewner evolution.In probability theory, the Schramm–Loewner evolution with parameter κ, also known as stochastic Loewner evolution (SLE_κ), is a family of random planar curves that have been proven to be the scaling limit of a variety of two-dimensional lattice models in statistical mechanics. Given a parameter κ and a domain in the complex plane U in a moderate resolution, *S. damnosum* s.l., endrmic, oviposition, probabilistic, moderate resolution, endmember LULC, signature paradigm would render a family of random curves in U, with κ controlling how much the curve turns in the habitat distribution data

There are two main variants of SLE, chordal SLE which gives a family of random curves from two fixed eco-georeferenceable, boundary points, and radial SLE, which gives a family of random curves from a fixed boundary point to a fixed interior point. These curves are defined to satisfy conformal invariance and a domain Markov property.

Stochastic process has the Markov property if the conditional probability distribution of future states of the process (i.e., conditional on both past and present states) depends only upon the present state, not on the sequence of events that preceded it. A. In probability theory and statistics, given two jointly distributed random variables X and Y, the conditional probability distribution of Y given X is the probability distribution of Y when X is known to be a particular value; in some cases the conditional probabilities may be expressed as functions containing the unspecified value x of X as a parameter [25]. In case that both "X" and "Y" are categorical variables like in moderate resolution, *S. damnosum* s.l. seasonal, eco-epidemiological, forecast vulnerability, immature habitat, regression model a conditional probability table is typically employeable to represent the conditional probability in the diagnostic, residual forecasts (e.g., eco-georeferenceable, targeted, hypeproductive, capture point, *S. damnosum* s.l., endemic, oviposition geolocation). The conditional distribution contrasts with the marginal distribution of a random variable, which is its distribution without reference to the value of the other variable (http://mathworld.wolfram.com). The term strong Markov property is similar to the Markov property, except that the meaning of "present" is optimally definable in terms of a random variable known as a stopping time. Both the terms "Markov property" and "strong Markov property" have been used in connection with a particular "memoryless" property of the exponential distribution [25].

According to Jacob et al. [22], an explicative Poissonized, processed, optimal, eco-epidemiological, forecast, vulnerability, geo-spectrotemporal, *S. damnosum* s.l., immature, habitat, fractionalized endmember, iteratively, interpolative, biosignature ,probabilistic,paradigm can remotely target, seasonally hyperproductive, geo-spectrotemporally uncoalesced, eco-georeferenced, capture point, oviposition sites on moderate resolution, geoclassifed LULCs employing iteratively interpolative diagnostic statistics. Possion is a particular case of the gamma distribution [http://mathworld.wolfram.com]. A gamma distribution is a general type of statistical distribution that is related to the beta distribution and arises naturally in processes for which the waiting times between Poisson distributed events are relevant [25]. It is the continuous analogue of the geometric distribution, and it has the key property of being memoryless. In probability, statistics and related fields, a Poisson point process or Poisson process (also called a Poisson random measure, Poisson random point field or Poisson point field) is a type of random mathematical object that consists of points randomly located on a mathematical

space[http://mathworld.wolfram.com]. The exponential distribution is not the same as the class of exponential families of distributions, which is a large class of probability distributions that includes the exponential distribution as one of its members, but also includes the normal distribution, binomial distribution, gamma distribution, Poisson, and many others which may be displayed in ArcGIS. In such paradigms the exponential distribution (a.k.a. negative exponential distribution) would be the probability distribution that would optimally describe the time between sampling events in an *S. damnosum* s.l., habitat, uncoalesced, moderate resolution, wavelength, trasnmittance, parameterizable, frequency, covariate estimator dataset [i.e. a process in which events occur continuously and independently at a constant average rate].

Interestingly, the Ornstein–Uhlenbeck process can also be considered as the continuous-time analogue of the discrete-time autoregressive [AR] (1) process in ArcGIS. An (AR) model is a representation of a type of random process; as such, it describes certain explanatorial, time-varying, multivariate, moderate resolution, geoclassifiable, LULC, explanatively, residually diagnostic, endmember, proxy signature, predictive, vulnerability, modelling exercises. The autoregressive model in ArcGIS specifies that the output variable which may depend linearly on its own previous values and on a stochastic term (an imperfectly predictable geo-spectrotemporally geosampled, eco-georeferenceable, hyperproductive, immature, *S. damnosum* s.l., seasonal, oviposition eco-georeferenceable, moderate resolution, imaged geolocation, covariate term); thus, the model would in the form of a stochastic difference equation in ArcGIS.Together with the Moving-Average (MA) model, it is a special case and key component of the more general ARMA and ARIMA models of time series in ArcGIS, which may have a more complicated stochastic structure; it may have a special case of the vector autoregressive model (VAR), which consists of a system of more than one stochastic difference equation.Contrary to the MA model, the AR model in ArcGIS is not always stationary as it may contain a unit root(www.esri.com).

A unit root is a feature of processes that evolve through time that can cause problems in statistical inference involving time series, moderate resolution, bio-ecological explanative,LULC processes (e.g., probabilistic, endmember, proxy, signature paradigms representing uncoalesced, *S. damnosum* s.l. iterative, interpolative, forecasting vulnerability, oviposition estimators as a response (dependent variable). A linear stochastic process has a unit root if 1 is a root of the process's characteristic equation [25]. Such a process is non-stationary, but does not always have a trend. If the other roots of the characteristic equation lie inside the unit circle in an explanative, metaheuristically optimizable, *S. damnosum* s.l., predictive, eco-epidemiological, moderate resolution, risk model—that is, if the paradigm has a modulus (i.e., absolute value) less than one—then the first difference of the process will be stationary; otherwise, the process will need to be differenced multiple times to become stationary. Due to this characteristic, unit root processes are also called difference stationary [25]. Unit root processes may sometimes be confused with trend-stationary model processes; while they share many properties, they are different in many aspects. It is possible for a time series, trailing vegetation, turbid water, narrow, African, riverine, tributary, ecosystem, moderate resolution, eco-epidemiological, forecast, vulnerability, endmember, LULC,proxy biosignature, discontinuously canopied, *S. damnosum* s.l., eco-georeferenceable, habitat model to be non-stationary, have no unit-root yet be trend-stationary. In both unit root and trend-stationary processes, the mean can be growing or decreasing over time; however, in the presence of a shock, trend-stationary processes are mean-reverting (i.e. transitory, the time series, optimally parameterizable, moderate resolution, *S. damnosum* s.l., elucidative, endmember, uncoalesced LULC, proxy biosignature, uncoalesced, paramterizable covariates

will converge again towards the growing mean, which may not be affected by the shock) while unit-root processes may have a permanent impact on the mean (i.e. no convergence over time). If a root of the process's characteristic equation is larger than 1, then it is called an explosive process, even though such processes are often inaccurately called unit roots processes[25].The presence of a unit root in a seasonal, hyerproductive, trailing vegetation, narrow, African, riverine tributray, agro-village, *S. damnosum* s.l., eco-georeferenced, oviposition, geoclassified capture point on a moderate resolution, ArcGIS-derived, LULC can be tested employing a unit root test. In statistics, a unit root test tests whether a time series, predictor variable is non-stationary and possesses a unit root where the null hypothesis is generally definable as the presence of a unit root and the alternative hypothesis is either stationarity, trend stationarity or explosive root depending on the test used [26].

SAS/GIS software may reveal variational approximation is optimally feasible in a geo-spectrotemporal, moderate resolution, eco-georeferenceable, geospatial, explanative, diagnostic, hyperproductive, seasonal, trailing vegetation, turbid water, agro-village complex, *S. damnosum* s.l., endemic, oviposition, targeting, probabilistic paradigm. The results may be very promising as the variational approximate solution may outperform standard Gaussian process regression for non-Gaussian Markov processes. To every Markov process with a symmetric transition density, there corresponds two random fields over the state space: a Gaussian field (the free field) φ and the occupation field which describes the amount of time the object spends at each state [25]. A relation between these two explicative diagnostic, time series, random fields in a orthogonally decomposable, moderate resolution, eco-georeferenceable, seasonally hyperproductive, trailing vegetation, *S. damnosum* s.l., oviposition, forecast, vulnerability, geoclassifiable LULC, proxy, endmember, signature model may be established which would be useful both for optimally quantitating, geo-spectrotemporal, derivative, endmember, Markovian processes. A Markov process can be thought of as 'memoryless': loosely speaking, a process satisfies the Markov property if one can make predictions for the future of the process based solely on its present state [25].

Every Gauss–Markov process X(t) possesses the three following properties:1)If h(t) is a non-zero scalar function of t, then Z(t) = h(t)X(t) is also a Gauss–Markov process,2) If f(t) is a non-decreasing scalar function of t, then Z(t) = X(f(t)) is also a Gauss–Markov process and and, 3) if there exists a non-zero scalar function h(t) and a non-decreasing scalar function f(t) such that X(t) = h(t)W(f(t)), where W(t) is the standard Wiener process. Any continuous stochastic process with the Markov property, e.g. the Wiener process.

In applied mathematics, the Wiener process is used to represent the integral of a white noise Gaussian process, random vector (that is, a partially indeterminate process that produces vectors of real discrete explanatorial integers such as geo-spectrotemporally geosampled, *S. damnosum* s.l. seasonal, trailing vegetation, narrow, African, riverine tributary, agro-village, complex, decomposed, immature habitat, regression, wavelength, trasmittance, emissivity, uncoalesced, covariate coefficients) is said to be a white noise vector or white random vector if its components each have a probability distribution with zero mean and finite variance, and are statistically independent: that is, their joint probability distribution must be the product of the distributions of the individual components.

A necessary (but, in general, not sufficient) condition for statistical independence of two, elucidative, trailing vegetation, eco-georeferenceable, *S. damnosum* s.l. seasonal, immature habitat, autoregressive, geo-spectrotemporal variables, geosampled in a narrow, African, riverine, agro-village, sparsely canopied, tributary is that they be statistically

uncorrelated; that is, their covariance is zero[22]. S such, the covariance matrix R of the components of a white noise vector w with n elements must be an n by n diagonal matrix, where each diagonal element R_{ii} is the variance of component w_i; and the correlation matrix must be the *n* by *n* identity matrix. In particular, if in addition to being independent every geo-spectrotemporally geosampled endmember LULC biosignature, uncoalesced, explicatively, geoclassified, moderate resolution, orthogonally decomposed, predctor variable (e.g., hyperproductive, *S. damnosum* s.l. partially canopied, seasonal, eco-georefernceable, narrow, African, agro-village, riverine tributary, immature, trailing vegetation, turbid water, capture point, discontinuously canopied covariate) in w also has a normal distribution with zero mean and the same variance, w is said to be a Gaussian white noise vector. In that case, the joint distribution of w is a multivariate normal distribution; the independence between the hyperproductive, capture point, endemic, oviposition, eco-georeferenceable, heursitically optimizable, predictor variables then implies that the distribution has spherical symmetry in *n*-dimensional space. Therefore, any orthogonal transformation of the vector will result in a Gaussian white random vector in the forecasting vulnerability model. In particular, under most types of discrete Fourier transform (DFT), such as FFT and Hartley, the transform W of w will be a Gaussian white noise vector, too; that is, the *n* Fourier coefficients of w will be independent Gaussian variables with zero mean and the same variance .

In mathematics, the DFT converts a finite sequence of equally spaced samples of a function into the list of coefficients of a finite combination of complex sinusoids, ordered by their frequencies, that has those same sample values. It can be said to convert the sampled function from its original domain (often time or position along a line) to the frequency domain.The input samples are complex numbers (in practice, usually discrete variables (endmember, geosampled, *S. damnosum* s.l., uncoalesced, moderate resolution, waveband values), and the output coefficients are complex as well. The frequencies of the output sinusoids are integer multiples of a fundamental frequency, whose corresponding period is the length of the sampling interval. The combination of sinusoids obtained through the DFT is therefore periodic with that same period. The DFT differs from the discrete-time Fourier transform (DTFT) in that its input and output sequences are both finite; it is therefore said to be the Fourier analysis of finite-domain (or periodic) discrete-time functions.

The DFT is the most important discrete transform, used to perform Fourier analysis in many practical applications. In digital signal processing, the function is any quantity or signal that varies over time, such as the pressure of a sound wave, a radio signal, or daily temperature readings, sampled over a finite time interval (often defined by a window function) [25].In image processing, the samples can be the values of mixels along a row or column of a raster image. The DFT is also used to efficiently solve partial differential equations, and to perform other operations such as convolutions or multiplying large discrete integers. The FFT is commonly used to transform an image between the spatial and frequency domain (www.esri.com). Unlike other domains such as Hough and Radon, the FFT method preserves all original data. Plus, FFT fully transforms images into the frequency domain, unlike time-frequency or wavelet transforms. The FFT can decompose a trailing vegetation, hypeproductive, discontinuously canopied, eco-georeferenced, *S. damnosum* s.l., immature, LULC, capture point, oviposition site on a moderate resolution geoclassified image into sines and cosines of varying amplitudes and phases, which can reveals repeating endmember pattern within a narrow African, riverine, tributray, agro-village ecosystem seasaonl image.

The displacement between two seasonal, hyperpoductive, eco-georeferenced, *S. damnosum* s.l., habitat, proxy signature images may be determined by computing the ratioF_1 conj(F_2)=[F_1F_2}; and then applying the inverse Fourier transform in ArcGIS. The result may be an impulse-like function, which may be approximately zero everywhere except at the displaceent that is necessary to optimally register moderate resolution, geoclassifiable, endmember, LULC images. Converting from rectangular coordinates to log-polar coordinates, shifts representing rotation and scaling can also determined to complete the georectification process of the images. A FFT-based algorithm has been successfully implemented in Interactive DataLanguage (IDL) and added as two user functions to an image processing software package—Environment for Visualizing Images (ENVI) interface. ENVI handles all pre- and post-processing works such as input/output, display, filter, analysis, and file management. (www.harrisgeospatial.com).

Nonhomogeneous, seasonal, moderate resolution, trailing vegetation, turbid water, narrow, African, agro-village, complex ecosystem, eco-georeferenceable, seasonally hyperproductive, discontinuously canopied, *S. damnosum* s.l. immature habitat, capture point geo-spectrotemporal, endmember, forecasting, endmember signature-oriented, ordinary differential equations may be solved in Python. Python was introduced to the ArcGIS community at 9.0 and since then, it has been accepted as the scripting language of choice for ArcGIS users (www.esri.com). PyDSTool is platform independent, written primarily in Python with some underlying C and Fortran legacy code for fast solving. NumPy is the fundamental package for scientific computing with Python which contains among other things:a powerful N-dimensional array, object-oriented, sophisticated, broadcasting, functions tools for integrating C/C++ and Fortran code useful for linear algebra, Fourier transform, and random number capabilities The SciPy library is one of the core packages that make up the SciPy stack. It provides many user-friendly and efficient numerical routines such as routines for numerical integration and optimization (http://scipy.org/scipylib/). PyDSTool is a sophisticated and integrated simulation and analysis environment for dynamical systems models of bio-geophysical systems (ODEs, DAEs, maps, and hybrid systems) such as fractionalized endmember iteratively interpolative, *S. damnosum* s.l., ecogeoreferenceable, capture points. The platform can make use extensive use of the numpy and scipy libraries. PyDSTool van may support symbolic math, optimization, phase plane analysis, continuation and bifurcation analysis, data analysis, and other tools for optimal, forecast vulnerability seasonal, *S. damnosum* s.l., endemic, transmission-oriented, regression modeling for remotely targeting, hyperproductive, narrow, African , riverine tributary, endemic, oviposition sites using a geo-spectrotemporally uncoalesced, moderate resolution, geoclassifiable, proxy LULC, fractionalized endmember biosignature as a dependent varable in a stochastic iterative interpolator.

Suppose the general solution to the homogenous version is known, in an elucidatively empirical Bayesian, iteratively interpolative, undetermined, explantive dataset of probabilistically quantitatively geo-spectrotemporal, eco-geoereferenceable, endmember, *S. damnosum* s.l. capture point, moderate resolution, sub-optimally parameterizable, geoclassified, orthogonally decomposed, seasonal LULC, optimizable, biosignature covariate.In such circumstances, equations dy/dx=f(x,y). may be assumed to be homogeneous if the function f(x,y) is homogeneous, that is f (tx,ty)= f(x,y) for any geo-spectrotemporal, geosampled, seasonally, explantive, hyerproductive, eco-georeferenceable, *S. damnosum* s.l., oviposition, endemic,sites on a moderate resolution, geoclassified, ArcGIS-derived, LULC, [trailing vegetation, turbid water, discontinuously canopied, agro-village, flooded habitat). By substitution, a medical entomologist or experimenter may consider the

new functionz=y/x in PROC MODEL which would be equivalent to y-xz.The new differential equation satisfied by z would be x dz/dx+z=f(1,z) which is a separable equation. The solutions are the constant ones f(1,z) - z =0 and the non-constant ones would then be given by $\ln|x| = \int \frac{dz}{f(1,z)-z} + C$ In so doing, moderate resolution, wavelength transmittance emissivity, variant and invariant, metaheursitcially optimizable parameters can be parsimoniously tabulated to resolve residual frequency distribution non-normalities in krigeable uncoalesced biased, prolific,immature black-fly, habitat, frequency estimators on geoclassified ArcGIS moderate resolution LULC s (e.g., partially canopied, trailing vegetation, agro-village, riverine tributray meandering corridor).

The Bayesian approach to endmember regularization and model-comparison may be demonstrated by studying the inference problem of interpolating noisy, moderate resolution, *S. damnosum* s.l, orthogonally decomposed, eco-georeferenceable, seasonal,LULC, endemic, oviposition data in ArcGIS. The concepts and methods described may be applicable to many other data modeling problems. Regularizing constants may be set by examining the posterior probability distribution. Alternative regularizers (priors) and alternative basis sets amay be objectively compared by evaluating the evidence for them. “Occam's razor” may be automatically embodied by this process. One justification of Occam's razor is a direct result of basic probability theory which by definition explicity states that all assumptions introduce possibilities for error; if an assumption does not improve the accuracy of a theory, its only effect is to increase the probability that the overall theory is wrong [Hawking, Stephen (2003). On the Shoulders of Giants. Running Press. p. 731. ISBN 0-7624-1698-X. Retrieved 2016-03-24]. The way in which Bayes infers the values of regularizing constants and noise levels may have an elegant interpretation for constructing an eco-georeferenced, trailing vegation, discontinuously canopied, endemic, oviposition dataset of empricial , eco-georferenecable, LULC, eco-epidemiological,capture points, geo-spectrotemporally geosampled in narrow, African, riverine, tributary,agro-village ecosystems in terms of the effective number of parameters determined by the data for targeting seasonal, hyperproductive,immature, seasonal, habitats.

In Bayesian statistics, one does not "test normality" per se, but rather computes the likelihood that the data come from a normal distribution with given parameters μ,σ (for all μ,σ), and compares that with the likelihood that the data come from other distributions under consideration, most simply using a Bayes factor (giving the relative likelihood of seeing the data given different models), or more finely taking a prior distribution on possible models and parameters and computing a posterior distribution given the computed likelihoods. Bayesian approach to interpolation of spatial processes can provide a general methodology for taking into account the uncertainty about geoclassifiable LULC parameters on subsequent predictions. Empirical Bayesian kriging (EBK) is a geostatistical interpolation method that automates the most difficult aspects of building a valid kriging model.

The basic idea of kriging is to predict the value of a function at a given point by computing a weighted average of the known values of the function in the neighborhood of the point. The method is mathematically closely related to regression analysis. Both theories derive a best linear unbiased estimator, based on assumptions on covariances, make use of Gauss-Markov theorem to prove independence of the estimate and error, and make use of very similar formulae. In statistics, the Gauss–Markov theorem, states that in a linear regression model in which the errors have expectation zero and are uncorrelated and have equal variances, the best linear unbiased estimator (BLUE) of the coefficients is given by the

ordinary least squares (OLS) estimator Even so, they are useful in different frameworks (e.g., interpolating a geo-spectrotemporally, geospatially uncoalesced datset of moderate resolution *S. damnosum* s.l. endmembers).Kriging is made for estimation of a single realization of a random field, while regression models are based on multiple observations of a multivariate data set[25].

Kriging starts with a prior distribution over functions. This prior takes the form of a Gaussian process wherebysamples from a function will be normally distributed, andthe covariance between any two samples is the covariance function (or kernel) of the Gaussian process evaluated at the spatial location of two points. In a Gaussian process, every point in some continuous input space is associated with a normally distributed random variable (www.esri.com). A set of decomposed, values (e.g., interpolatable, moderate resolution, partially canopied, trailing vegetation, partially canopied, trailing vegetaion, turbid water, endmember eigenvectors) is then observed, each value associated with a spatial location (e.g., eco-georeferenceable, hyperproductive, *S. damnosum* s.l. habitat). Now, a new value can be predicted at any new spatial geolocation, by combining the Gaussian prior with a Gaussian likelihood function for each of the observed values. The resulting posterior distribution is also Gaussian, with a mean and covariance that can be simply computed from the observed values in ArcGIS or SAS, where the variance, and the kernel matrix is derivable from the prior. In mathematics, and more specifically in linear algebra and functional analysis, the kernel (also known as null space or nullspace) of a linear map $L : V \rightarrow W$ between two vector spaces V and W, is the set of all elements v of V for which $L(v) = 0$, where 0 denotes the zero vector in W.

The kriging estimation of an orthogonally decomposed, trailing vegetation, discontinuously canopied, *S. damnsoum* s.l., narrow, African, riverine tributary agro-village, immature habitat, moderate resolution, orthogonally decomposed, endmember,geoclassified, LULC, oviposition signature may also be seen as a spline in a reproducing kernel Hilbert space, with the reproducing kernel given by the covariance function. In In probability theory and statistics, covariance is a measure of how much two variables change together, and the covariance function, or kernel, describes the spatial covariance of a random variable process or field [25]. In functional analysis (a branch of mathematics), a reproducing kernel Hilbert space (RKHS) is a Hilbert space of functions in which point evaluation is a continuous linear functional. Roughly speaking, this means that if two functions f and g in the RKHS are close in norm, i.e., ||f-g|| is small, then f and g are also pointwise close,(i.e., |f(x)-g(x)| is small for all x). The reverse need not be true. It is not entirely straightforward to construct a Hilbert space of functions which is not an RKHS [26]. Note that L^2 spaces are not Hilbert spaces of functions (and hence not RKHSs), but rather Hilbert spaces of equivalence classes of functions (e.g., the functions f and g defined by f(x)=0 and g(x)=1 may be equivalent in a forecast vulnerability, moderate resolution, hypeproductive, seasonal, eco-epidemiological, capture point, eco-georeferenceable, trailing vegetation, turbid water, narrow, African, riverine tributary, agro-village, partially canopied, *S. damnosum* s.l., probabilistic, endmember paradigm based on L^2). A square-integrable function, also called a quadratically integrable function, is a real- or complex-valued measurable function for which the integral of the square of the absolute value is finite[http://mathworld.wolfram.com].

Many differential equations can be solved exactly in the Wolfram Language using DSolve[eqn, y, x], and numerically using NDSolve[eqn, y, {x, xmin, xmax}]. The Wolfram Language introduces a full Geographic Information System (GIS) which integrates the powerful new GeoGraphics function for map constuction. In so doing, the new Entity

framework can access the large corpus of geo-spectrotemporally geosampled, *S. damnosum* s.l. seasonal information in Wolfram|Alpha, and improve functionality for geodetic computations. An ordinary differential equation (frequently called an "ODE," "diff eq," or "diffy Q") as an equality involving a function and its derivatives. An ODE of order n is an equation of the form. In general, an n th-order ODE has *n* linearly independent solutions. Furthermore, any linear combination of linearly independent functions solutions would also be a solution in a robust, *S. damnosum* s.l., predictor model for targeting seasonal, hyperproductive, trailing vegetation, discontinuously canopied, immature, riverine agro-village, tributary habitats

Simple theories exist for first-order (integrating factor) and second-order (Sturm-Liouville theory)ODEs , and arbitrary ODEs with linear constant coefficients which can be solved when they are of certain factorable forms. Integral transforms such as the Laplace transform can also be used tosolve classes of linear ODEs. Sturm-Liouville equation $\frac{d}{dx}[p(x)y'] + [\lambda w(x) - q(x)]y = 0.$ Morse and Feshbach (1953, pp. 667-674) give canonical forms and solutions for second-order ordinary differential equations.

While there are many general techniques for analytically solving classes of ODEs for optimal, *S. damnosum* s.l., forecast, vulnerability-oriented, fractionalized, endmember LULC biosignature, iterative, interpolative modeling the only practical solution technique for useage of such complicated equations in ArcGIS is to employ numerical methods. The most popular of these is the Runge-Kutta method, but many others have been developed, including the collocation method and Galerkin method. In numerical analysis, the Runge–Kutta methods are a family of implicit and explicit iterative methods, which includes the well-known routine called the Euler Methods, used in temporal discretization for the approximate solutions of ordinary differential equations[26].The Euler method is a first-order method, which means that the local error (error per step) is proportional to the square of the step size, and the global error (error at a given time) is proportional to the step size. The Euler method often serves as the basis to construct more complex methods, [e.g., Predictor–corrector method. (http://mathworld.wolfram.com) Temporal discretization involves the integration of every term in different equations over a time step (Δt)] [25]. The spatial domain in a *S. damnosum* s.l., endmember, probabilsic paradigm may be discretized to produce a semi-discrete form.

Semi discrete discontinuous Galerkin methods andstage-exceeding-order, strong-stability-preservingRunge–Kutta time discretizations may probabilistically quantitate moderate resolution, orthogonally decomposed, endmember *S. damnosum* s.l. propagational noise. the use of a special class of strong-stability-preserving (SSP) Runge–Kutta time discretization methods in ArcGIS in conjunction with discontinuous Galerkin (DG) finite element spatial discretizatons may aid in precision traghteing hypeproductive, seasonal, *S. damnosum* s.l. , oviposition, eco-epidemioloigical, eco-georferenceable, capture points, in narrow , African riverine , tributary ecosystems, The class of SSP methods investigated here would be defined by the property that the number of stages s is greater than the order k of the method. From analysis, Courant–Friedrichs–Lewy (CFL) conditions for the linear (L^2) stability of the methods defined using the s > k SSP schemes are obtained that
are less restrictive than those of the ‘‘standard’’ so-called RKDG methods that use s = k SSP Runge–Kutta schemes. In mathematics, the CFL condition is a necessary condition for convergence while solving certain partial differential equations (usually hyperbolic PDEs) numerically by the method of finite differences[26]. The improvement in the CFL conditions for linear stability of the methods may more than offset the additional work introduced by the

increased number of stages. Given that the CFL conditions for linear stability in a robust, *S. damnosum* s.l., predictive, risk model are what must be respected in practice in order to maintain high-order accuracy in the residual forecasts targeting the prolific narrow African riverine tributary, partially canopied, trailing vegetated, immature habitats, the use of the s > k SSP schemes in ArcGIS may results in RKDG methods that are more efficientthan those previously defined. Furthermore, with the application of a slope limiter, the nonlinear explanative, stability properties of the forward Euler method and the DG spatial discretization in the *S. damnosum* s.l. oviposition, forecasting vulnerability, probabilistic paradigm may be preserved with these methods under less restrictive CFL conditions than those required for linear stability. Thus, more efficient RKDG methods that possess the same favorable accuracy and stability properties of the ‘‘standard’’ RKDG methods may obtained for the model. Numerical validation results may verify the CFL conditions for stability obtained from the *S. damnosum* s.l. immature habitat analysis and demonstrate the efficiency advantages of these new RKDG methods in ArcGIS. The resulting RKDG methods may provide stable, high-order accurate,and highly parallelizable schemes that may easily handle complicated geometries and boundary conditions of moderate resolution imaged eco-georferenced *S. damnosum* s.l. immature habitats. The theoretical and algorithmic aspects of these methods in ArcGIS may show several alternative model applications including, the compressible and incompressible Hamilton-Jacobi-like equations for predictinf hypeproductive habiatts of this vector arthropod.

In mathematics, the Hamilton–Jacobi equation (HJE) is a necessary condition describing extremal geometry in generalizations of problems from the calculus of variations, and is a special case of the Hamilton–Jacobi–Bellman equation[26]. The Hamilton-Jacobi Equation is a first-order nonlinear partial differential equation of the form H(x,u x (x,α,t),t)+u t (x,α,t)=K(α,t) with independent variables (x,t)∈R n ×R and parameters α∈R n . The equations defined by $q = -\frac{\partial H}{\partial q}$, where $\dot{p} = dp/dt$ and $\dot{q} = dq/dt$ is fluxion notation and H is the so-called Hamiltonian, are called Hamilton's equations. These equations frequently arise in problems of celestial mechanics. The vector form of these equations is $\dot{q}_i = H_{p_i}(t, \mathbf{q}, \mathbf{p})$ and $\dot{p}_i = -H_{q_i}(t, \mathbf{q}, \mathbf{p})$[26]. Another formulation related to Hamilton's equation is $p = \frac{\partial L}{\partial \dot{q}}$, where L is Lagrangian. [http://mathworld.wolfram.com].

It has wide applications in optics, mechanics, and semi-classical quantum theory. Its solutions determine infinite families of solutions of Hamilton's ordinary differential equations, which are the equations of motion of a mechanical system or an optical system in the ray approximation. In physics, it is a formulation of classical mechanics, equivalent to other formulations such as Newton's laws of motion. Lagrangian mechanics and Hamiltonian mechanics. The Hamilton–Jacobi equation is particularly useful in identifying conserved quantities for mechanical systems, which may be possible even when the mechanical prblem itself cannot be solved completely.

The Hamilton-Jacobi equation may be employed in order to derive analytical formulae for a motion of acapture point, trailing vegetation, narrow, African, agro-village complex, hypeproductive, seasaonl *S. damnosum* s.l., oviposition, eco-georferenceable, model in the central Newtonian M/r potential. The derived formulae can then be used to compare an approximate numerical solution against an analytical,(i.e., exact solution to the problem of geolocating, un-geosampled, prolific habitats in a narrow, African, riverine

tributray, agro-village complex). The problem may be easiest to describe in spherical coordinates, r, $\theta$and ϕin ArcGIS. In these coordinates the Hamiltonian would assume the following form: $H = \frac{p_r^2}{2} + \frac{p_\theta^2}{2r^2} + \frac{p_\phi^2}{2r^2 \sin^2\theta} - \frac{M}{r}$ where the gravitational constant G = 1, and the mass of the material point m = 1 too. The Hamilton-Jacobi equation that corresponds to that Hamiltonian is $\frac{1}{2}\left(\frac{\partial S}{\partial r}\right)^2 + \frac{1}{2r^2}\left(\frac{\partial S}{\partial \theta}\right)^2 + \frac{1}{2r^2 \sin^2\theta}\left(\frac{\partial S}{\partial \phi}\right)^2 - \frac{M}{r} + \frac{\partial S}{\partial t} = 0$[26].The method that is commonly use here is called the separation of variables. The Hamiltonian does not depend explicitly on time, t and angle ϕTherefore, an optimal solution may be sought for seasonal, *S. damnosum* s.l. model fitting in the following form: $S = -Et + p_\phi \phi + S_r(r) + S_\theta(\theta) + C$,where C is a constant. Substituting this into the Hamilton-Jacobi equation would yield$\frac{1}{2}\left(\frac{dS_r}{dr}\right)^2 + \frac{1}{2r^2}\left(\frac{dS_\theta}{d\theta}\right)^2 + \frac{p_\phi^2}{2r^2 \sin^2\theta} - \frac{M}{r} - E = 0$.

Multiplying this equation by 2 r^2.in ArcGIS may allow rewriting this equation placing all terms that depend on θon the left hand side and all terms that depend on r on the right hand side: $\left(\frac{dS_\theta}{d\theta}\right)^2 + \frac{p_\phi^2}{\sin^2\theta} = 2Mr + 2Er^2 - r^2\left(\frac{dS_r}{dr}\right)^2$ Because expressions on both sides of this equation depend on different LULC variables, the equality can hold in the *S. damnosum* s.l. forecast, vulnerability probabilisc paradigm only if they are equal to the same constant, L^2: $\left(\frac{dS_\theta}{d\theta}\right)^2 + \frac{p_\phi^2}{\sin^2\theta} = L^2 = 2Mr + 2Er^2 - r^2\left(\frac{dS_r}{dr}\right)^2$ And this implies that: $\frac{dS_r}{dr} = \sqrt{2\left(\frac{M}{r} + E - \frac{L^2}{2r^2}\right)}$ and $\frac{dS_\theta}{d\theta} = \sqrt{L^2 - \frac{p_\phi^2}{\sin^2\theta}}$ These, in turn, are first order ODE which can be readily integrated..into a moderate resolution *S. damnosum* s.l., stochastic endmember signature interpolatior in ArcGIS.

The solutions to an ODE satisfy existence and uniqueness properties. These can be formally established by Picard's existence theorem for certain classes of ODEs. Let a system of first-order ODE be given by $\frac{dx_i}{dt} = f_i(x_1, \ldots, x_n, t),$ for $i = 1, \ldots, n$and let the functions $f_i(x_1, \ldots, x_n, t)$, where $i = 1, \ldots, n$, all be defined in a domain $D$of the $(n+1)$-dimensional space of the variables $x_1, \ldots, x_n, t$. Let these functions be continuous in $D$and have continuous first partial derivatives $\partial f_i / \partial x_j$for $i = 1, \ldots, n$and $j = 1, \ldots, n$in D. Let $(x_1^0, \ldots, x_n^0)$be in$D$. Then there exists a solution of (4) given by $x_1 = x_1(t), \ldots, x_n = x_n(t)$for $t_0 - \delta < t < t_0 - \delta$(where$\delta > 0$) satisfying the initial conditions $x_1(t_0) = x_1^0, \ldots, x_n(t_0) = x_n^0$.

Furthermore, the solution is unique, so that if $x_1 = x_1^*(t), \ldots, x_n = x_n^*(t)$is a second solution of (◇) for $t_0 - \delta < t < t_0 + \delta$satisfying (◇), then $x_i(t) \equiv x_i^*(t)$for $t_0 - \delta < t < t_0 + \delta$. Because every nth-order ODE can be expressed as a system of $n$first-order ODEs, this theorem also applies to the single nth-order ODE. An exact first-order ordinary differential equation is one of the form $p(x, y)\,dx + q(x, y)\,dy = 0$,where $\frac{\partial p}{\partial y} = \frac{\partial q}{\partial x}$. An equation of the form

($\diamondsuit$) with $\frac{\partial p}{\partial y} \neq \frac{\partial q}{\partial x}$ is said to be nonexact. If $\frac{\frac{\partial p}{\partial y} - \frac{\partial q}{\partial x}}{q} = f(x)$ in ($\diamondsuit$), it has an x-dependent integrating factor. If $\frac{\frac{\partial q}{\partial x} - \frac{\partial p}{\partial y}}{x p - y q} = f(x y)$ in ($\diamondsuit$), it has an $x y$-dependent integrating factor. If $\frac{\frac{\partial q}{\partial x} - \frac{\partial p}{\partial y}}{p} = f(y)$ in ($\diamondsuit$), it has a y-dependent integrating factor. Other special first-order types include cross multiple equations $y f(x y) dx + x g(x y) dy = 0$, homogeneous equations $y' = f\left(\frac{y}{x}\right)$, linear equations $y' + p(x) y = q(x)$, and separable equations $y' = X(x) Y(y)$.

Special classes of second-order ordinary differential equations include $y'' = f(y, y')$ (x missing) and $y'' = f(x, y')$ (y missing). A second-order linear homogeneous ODE $y'' + P(x) y' + Q(x) y = 0$ for which $\frac{Q'(x) + 2P(x)Q(x)}{2[Q(x)]^{3/2}} = [\text{constant}]$ can be transformed to one with uncoalesced, moderate resolution, geoclassifiable, diagnostic, LULC, constant coefficients. The equation is called homogeneous if f(t)=0. Otherwise, it is called non-homogeneous [25].A second-order differential equation is accompanied by initial conditions or boundary conditions. Initial conditions are in the form y(t_0)=y_0 and y'(t_0)=y'_0. Boundary conditions might be of the form: y(t_0)=a and y(t_1)=b.For the initial value problem, the existence and uniqueness theorem states that if p(t), q(t) and f(t) are continuous on some interval (a,b) containing t_0, then there exists a unique solution y(t) to the ode in the whole interval (a,b).

The procedure for solving linear second-order ODE in an ArcGIS geodtabase cyberenvironment has two steps for finding the general solution of the homogeneous problem: $y'' + p(t)y' + q(t)y = 0$. According to the theory for linear differential equations, the general solution of the homogeneous problem is $y_H(t) = C_1 y_1(t) + C_2 y_2(t)$ where C_1 and C_2 are constants and y_1 and y_2 are any two explanatively, linearly independent solutions to the homogeneous equation. For finding a particular solution of the non-homogeneous problem in a S. damnosum s.l.model may require $y'' + p(t)y' + q(t)y = f(t)$. The particular solution is any solution of the non-homogeneous problem and is denoted y_p(t).The general solution of the full non-homogeneous problem in the vector arthropod model may be conducted parsimoniously by $y(t) = C_1 y_1(t) + C_2 y_2(t) + y_p(t)$.

The key point to note is that all possible solutions to a linear second-order ODE can be obtained from two linearly independent solutions to the homogeneous problem in a *S. damnosum* s.l. forecast, vulnerability model and any particular solution. Here is an example. Consider the ODE $y'' + 3y' + 2y = 6e^t$ The homogeneous equation is $y'' + 3y' + 2y = 0$. It can be shown that y_1=exp(-t) and y_2=exp(-2t) are solutions to the homogeneous equation. A particular solution of the non-homogeneous equation for the model may be exp(t). Hence,the general solution of the ODE would be $y(t) = C_1 e^{-t} + C_2 e^{-2t} + e^t$ where C_1 and C_2 are constants.

The following are examples of important ODEs which may help target highly productive seasonal S. damnosum s.l., trailing vegetation, narrow African, riverine tributray, trailing vegetation, discontinously canopied, Abel's differential equation $y' = f_0(x) + f_1(x) y + f_2(x) y^2 + f_3(x) y^3 + \ldots$

$[g_0(x)+g_1(x)y]\,y' = f_0(x)+f_1(x)y+f_2(x)y^2+f_3(x)y^3$.Airy differential equation $y''-x\,y=0$.,Anger differential equation $y''+\frac{y'}{x}+\left(1-\frac{\nu^2}{x^2}\right)y=\frac{x-\nu}{\pi x^2}\sin(\nu\pi)$.,Baer differential equations $(x-a_1)(x-a_2)\,y''+\frac{1}{2}[2x-(a_1+a_2)]\,y'-(p^2x+q^2)y=0$and $(x-a_1)(x-a_2)\,y''+\frac{1}{2}[2x-(a_1+a_2)]\,y'-(k^2x^2-p^2x+q^2)y=0$.Bernoulli differential equation $y'+p(x)y=q(x)y^n$.Bessel differential equation $x^2y''+xy'+(\lambda^2x^2-n^2)y=0$.Binomial differential equation $(y')^m=f(x,y)$.Bôcher equation $y''+\frac{1}{2}\left[\frac{m_1}{x-a_1}+\ldots+\frac{m_{n-1}}{x-a_{n-1}}\right]y' +\frac{1}{4}\left[\frac{A_0+A_1x+\ldots+A_lx^l}{(x-a_1)^{m_1}(x-a_2)^{m_2}\cdots(x-a_{n-1})^{m_{n-1}}}\right]y=0.$ Briot-Bouquet equation $x^m y'=f(x,y)$.Chebyshev differential equation $(1-x^2)y''-xy'+\alpha^2y=0$.,Clairaut's differential equation $y=xy'+f(y')$.,Confluent hypergeometric differential equation $xy''+(c-x)y'-ay=0$.,d'Alembert's equation $y=xf(y')+g(y')$.Duffing differential equation $y''+\omega_0^2y+\beta y^3=0$.,Eckart differential equation $y''+\left[\frac{\alpha\eta}{1+\eta}+\frac{\beta\eta}{(1+\eta)^2}+\gamma\right]y=0$, where $\eta=e^{\delta x}$. Emden-Fowler differential equation $(x^\theta y')'\pm x^\sigma y^n=0$.Euler differential equation $x^2y''+axy'+by=S(x)$.Halm's differential equation $(1+x^2)^2+y''+\lambda y=0$.Hermite differential equation $y''-2xy'+\lambda y=0$.Heun's differential equation $w''+\left(\frac{\gamma}{x}+\frac{\delta}{x-1}+\frac{\epsilon}{x-a}\right)w'+\frac{\alpha\beta x-q}{x(x-1)(x-a)}w=0$, where $w'=dw/dx$. is Hill's differential equation $y''+\left[\theta_0+2\sum_{n=1}^{\infty}\theta_n\cos(2nz)\right]y=0$.

Furthermore, geo-spectrotemporally uncoalesced datsets of moderate resolution, endmember eigenvectors from a hypergeometric, *S. damnosum* s.l., differential equation $x(x-1)y''+[(1+\alpha+\beta)x-\gamma]\,y'+\alpha\beta y=0$.may be robustly constructed in ArcGIS. Other differncial equations for targeting seasonally hypeproductive, eco-georeferenceable parameterizable oviposition, trailing vegetation, narrow African, agro-village, hypeproductive *S. damnosum* s.l. sites on geoclassifiable moderate resolution, LULCs (e.g., partially canopied, trailing vegetation, narrow, riverine tributary, flooded habitats) include Jacobi differential equation $(1-x^2)y''+[\beta-\alpha-(\alpha+\beta+2)x]\,y'+n(n+\alpha+\beta+1)y=0$. and the Laguerre differential equation $xy''+(1-x)y'+\lambda y=0$.Other differential equations for aiding in remotely targeting hyperproductive, seasonal, eco-georferenceable, *S. damnosum* s.l. paramterizable covariates include $(x^2-b^2)(x^2-c^2)z''+x(x^2-b^2+x^2-c^2)z'-[m(m+1)x^2-(b^2+c^2)p]z=0$, where $z'=dz/dx$ may also be a Lane-Emden differential equation $\frac{1}{\xi^2}\frac{d}{d\xi}\left(\xi^2\frac{d\theta}{d\xi}\right)+\theta^n=0$. Also Legendre differential equation $(1-x^2)y''-2xy'+\alpha(\alpha+1)y=0$., Linear constant coefficients $a_0y^{(n)}+\ldots+a_{n-1}y'+a_ny=p(x)$. a Lommel differential equation $x^2y''+xy'-(x^2-\nu^2)y=kx^{\mu+1}$.,Löwner's differential equation $y'=-y\frac{1+\kappa(x)y}{1-\kappa(x)y}$. Malmstén's differential equation $y''+\frac{r}{z}y'=\left(Az^m+\frac{s}{z^2}\right)y$.,Mathieu's differential equation $V''+[a-2q\cos(2v)]\,V=0$,where$V'=dV/dv$., and a,Modified spherical Bessel differential

equation $r^2 R'' + 2rR' - [k^2 r^2 + n(n+1)] R = 0$, where $R' = dR/dr$ andRayleigh differential equation $y'' - \mu\left(1 - \frac{1}{3}y'^2\right)y' + y = 0.$ may be applicable to mapping geo-spectrotemporally geosampled, orthogonally decomposed endmembers of eco-georefrenceable, hyperproductive, trailing vegetation, S. damnosum s.l. ovipoistion sites on moderate resolution, geoclassified LULCs.Systems with constant coefficients are of the form $\frac{d\mathbf{x}}{dt} = \mathbf{A}\mathbf{x}(t) + \mathbf{p}(t).$ [26].

The electromagnetic spectrum is divided into a number of arbitrary wavebands depending on either the source of the photons (e.g., solar or terrestrial thermal radiation), or their interaction with living material (e.g., ultraviolet, visible, photosynthetically active, etc.)]. Coupling, non-frequentistic, explanatorily uncoalesced, quantitatively interpolative, moderate resolution, web-related, cartographic, iterative applications with elucidatively uncoalesced, eco-georeferenceable, discontinuously canopied, log-transformed, log-normalized, illuminative, radation flux, descriptive, proxy endmember, fractionalized, signature covariates of seasonal narrow, riverine, African, tributary, agro-village, capture point, habitat, suitability structures within customizable, layered subclasses (e.g., esri.layers.GraphicsLayer) in ArcGIS (e.g., API for JavaScript) may also aid in optimally forecasting un-geosampled, seasonally hyperproductive, trailing vegetation, turbid water, partially shaded, *S. damnosum* s.l., oviposition geolocations. Distinct signatures without redundant endmembers and errors of moderate resolution, unmixed, land use land cover (LULC), wavelength, transmittance, frequency emissivities in a multivariate, stochastic interpolator can remotely distinguish a seasonally hyerprproductive, *S. damnosum* s.l. trailing vegetation, narrow, African, riverine tributary, eco-georefernceable, capture point, ovipoistion site on a moderate resolution, expositorily uncoalesced, goclassified, LULC signature [see 22]. This would allows construction of a very large variety of maps—in any cartographic projection and including the representation of results of arbitrary computations—with any type of geoclassifiable , moderate resolution, LULC dataset.

A simulation algorithm may be proposed in ArcGIS (e.g, Geospatial Analyst™) to generate sample functions of a stationary, multivariate, stochastic process as devised from an uncoalesced, proxy, endmember, moderate resolution, signature dataset aggregated from an eco-georeferenced, seasonally hyperproductive, trailing vegetation, turbid water, discontinously canopied, *S. damnosum* s.l., capture point, according to a prescribed cross-spectral density matrix. If the components of the vector process correspond to different, prolific, oviposition, landscape geolocations in geospace, then the process would be nonhomogeneous in any geospace [e.g., 5 kilometer (km) grid cell of a moderate resolution, imaged, narrow, African, riverine tributray, agro-village complex]. The ensemble cross-correlation matrix of the generated sample functions would be identical to the corresponding target (e.g., hyperproductive, explanative, capture point, ovipoistion site on a geoclassified, ArcGIS-derived, LULC signature). The simulation algorithm in ArcGIS could generate ergodic sample functions in the sense that the temporal cross-correlation matrix of each and every generated sample function would be identical to the corresponding target, when the length of the sample function is equal to one period. The generated sample functions would be periodic. The proposed ArcGIS algorithm may be based on an extension of the geo-spectrotemporal representation algorithmic method which may be very efficient computationally since it could take advantage of specific techniques embedded in the geodatabase (e.g., Fast Fourier transform). The generated sample functions would be Gaussian in the limit as the quantizable number of terms in the frequency discretization of the

cross-spectral density matrix in ArcGIS approaches infinity. An example involving simulation of turbulent, African, riverine tributray pathway fluctuations and seasaonal meaderings may be optimally cartographically presented in ArcGIS in order to demonstrate the capabilities and efficiency of the proposed algorithm for identifying unknown, un-geosampled , iteratively interpolated, hyperproductive, trailing vegetation, eco-georferenceable, *S. damnosum* s.l., narrow agro-village complex sentinel sites and capture points for optimally developing and implementing seasonal, onchocerciasis, control strategies.

Many seasonal, control applications require knowledge of the state vector at intermediate, eco-epidemiological, sample, time frames that are commonly initially unavailable. One way to approximate these land use land cover (LULC) intermediate states of endmember transitions in an explanatively, orthogonally, quantitatively, decomposeable, uncoalesced, moderate resolution, dataset of eco-georeferenceable, hypeproductive, *S. damnosum* s.l. trailing vegetation, turbid water, infrequently canopied, oviposition, moderate resolution, proxy signatures optimally rendered from a, geoclassifiable, narrow, African, riverine tributary, agro-village LULC, (e.g., partially canopied, trailing vegetation) forecast vulnerability map in ArcGIS may be by performing a time series, deterministic interpolation.

Deterministic interpolation techniques in ArcGIS create surfaces from measured points(e.g., eco-georefereceable geo-coordinates of seasonally hyperproductive, narrow, African riverine, tributary, oviposition sites on an geoclassified LULCs based on either the extent of similarity (inverse distance weighted) or the degree of smoothing (radial basis functions).Geostatistical interpolation techniques (kriging) utilize the statistical properties of the measured points(www.esri.com). Geostatistical techniques in ArcGIS can quantitate the spatial autocorrelation among measured, geo-spectrotemporally geosampled, parameterized, seasonally, hyperproductive, capture point, *S. damnosum* s.l., endmember, oviposition points while accounting for the configuration of the sample points around the ecogeoreferenced, oviposition, habitat geolocations [22]

Deterministic interpolation techniques can be divided into two groups, global and local. Global techniques calculate predictions employing the entire dataset. Local techniques calculate predictions from the measured points within neighborhoods, which are smaller spatial areas within the larger study area. Geostatistical Analyst provides global polynomial as a global interpolator and inverse distance weighted, local polynomial, radial basis functions, kernel smoothing, and diffusion kernel as local interpolators (www.esri.com).

An iterative, ArcGIS-derived, deterministic, explanatorial, geo-spectrotemporal interpolation can either force the resulting surface to pass through the geosampled, eco-georeferenceable dataset of iterative, uncoalesced sub-mixel values or not. An interpolation technique that optimally explanatorily forecasts a sub-mixel value that is identical to the measured value at a geosampled geolocation (e.g., eco-georeferenceable, turbid water, sparsely canopied, hyperproductive, *S. damnosum* s.l. oviposition site at an ArcGIS-geoclassified, 1 kilometer (km) moderate resolution, gridded, irrigated, riceland, agro-village, riverine tributary, seasonally imaged, LULC, centroid geolocatio) would be known as an exact interpolator. An inexact interpolator predicts a value that is different from the measured value. The latter can be used to avoid sharp peaks or troughs in a seasonal, African, riverine tributray, agro-village output surface (e.g., agro-village tributary, discontinuously canopied, flooded, LULC). Inverse distance weighted and radial basis functions are exact interpolators,

while global polynomial, local polynomial, kernel interpolation with barriers, and diffusion interpolation with barriers are inexact(https://www.arcgis.com).However, deterministic interpolation techniques may fail to capture correct probability time series, distribution of intermediate seasonally geoclassified moderate resolution, partially canopied, endmember LULC signatures. Brownian interpolation captures the correct joint distribution by sampling from a conditional Gaussian distribution. This sampling technique is referred to as a Brownian Bridge.

A Brownian bridge is a stochastic process $X=\{X\,t:t\in[0,1]\}$ $X=\{Xt:t\in[0,1]\}$ with state space R that satisfies the following properties:1)$X\,0=0$ and $X\,1=0$ (each with probability), 2)X is a Gaussian process,3)$E(X\,t)=0$ for $t\in[0,1]$ 4)$\mathrm{cov}(X\,s,X\,t)=\min\{s,t\}-st$ for $s,t\in[0,1]$: and, 5) probability 1, $t\mapsto X\,t$ $t\mapsto Xt$ is continuous on [0,1]. According to Einstein, (1956) a Brownian bridge is a continuous Gaussian process with $X\,0=X\,1=0$ with mean and covariance functions respectively. There are several ways of constructing a Brownian bridge from a standard Brownian motion for an uncoalesced, forecast vulnerability, iterative, interpolative, diagnostically probabilistc, moderate resolution, signature paradigm for remotely targeting partially canopied, trailing vegetation, turbid water, eco-georeferenceable, seasonally hyperproductive, *S. damnosum* s.l., seasonal, oviposition geolocations on geoclassified LULCs.

Brownian motion process$Z=\{Z\,t:t\in[0,\infty)\}$ $Z=\{Zt:t\in[0,\infty)\}$ is a continuous, explanative, Gaussian process with $Z\,0=0$ Z0=0, $E(Z\,t)=0$ E(Zt)=0 for $t\in[0,\infty)$ $t\in[0,\infty)$ and $\mathrm{cov}(Z\,s,Z\,t)=\min\{s,t\}$ $\mathrm{cov}(Zs,Zt)=\min\{s,t\}$ for $s,t\in[0,\infty)$ $s,t\in[0,\infty)$. Thus, suppose that $Z=\{Z\,t:t\in[0,\infty)\}$ $Z=\{Zt:t\in[0,\infty)\}$ is a standard Brownian motion in a forecast, vulnerability, geo-spectrotemporal, trailing vegation, turbid water, narrow African riverine, agro-village complex, probabilistic paradigm for trageting seasaonl, hypeproductive, *S. damnosum* s.l.,immature habitats, and $X\,t=Z\,t-tZ\,1$ $Xt=Zt-tZ1$ for $t\in[0,1]$ $t\in[0,1]$ occurs . Then $X=\{X\,t:t\in[0,1]\}$ $X=\{Xt:t\in[0,1]\}$ is a Brownian bridge in the remotely sensed, predictive, optimizable, risk model. Note that $X\,0=Z\,0=0$ and $X\,1=Z\,1-Z\,1=0$. Linear combinations of the geosampled, eco-georeferenceable, uncoalesced, iteratively, interpolative, moderate resolution, decomposed, sub-mixel, signature, predictor variables in X would optimally reduce to linear combinations of the variables in Z and hence would have normal distributions of the endmember, residual forecasts for targeting unknown, un-geosampled, hyperproductive, ovipoistion *S.damnosum* s.l., geolocations and their respective LULC sites. Thus, X in a *S. damnosum* s.l. iterative, Bayesian, probabilistic, interpolative estimation matrix i would be a Gaussian process. Further $.E(X\,t)=E(Z\,t)-tE(Z\,1)=0$ may be optimally parsimonioulsy quantitated and solved for $t\in[0,1]$ Additionally $\mathrm{cov}(X\,s,X\,t)=\mathrm{cov}(Z\,s-sZ\,1,Z\,t-tZ\,1)=\mathrm{cov}(Z\,s,Z\,t)-t\mathrm{cov}(Z\,s,Z\,1)-s\mathrm{cov}(Z\,1,Z\,t)+st\mathrm{cov}(Z\,1,Z\,1)=\min\{s,t\}-st-st+st$ $\mathrm{cov}(Xs,Xt)=\mathrm{cov}(Zs-sZ1,Zt-tZ1)=\mathrm{cov}(Zs,Zt)-t\mathrm{cov}(Zs,Z1)-s\mathrm{cov}(Z1,Zt)+st\mathrm{cov}(Z1,Z1)=\min\{s,t\}-st-st+st$ for $s,t\in[0,1]$. Finally, $t\mapsto X\,t$ $t\mapsto Xt$ would be continuous on [0,1] in the eco-epidemiological, time series, explanatorial, *S. damnosum* s.l., predictive model.since $t\mapsto Z\,t$ $t\mapsto Zt$ is continuous on [0,1] .

Jacob et al. [26] conducted an experiment consisting of running the Brownian bridge process $Y=\{Y\,t:t\in[0,1]\}$, which was obtained from the standard Brownian motion process $X=\{X\,t:t\in[0,1]\}$ $X=\{Xt:t\in[0,1]\}$ by periodically conditioning a eco-georeferenceable, seasonal, *S. damnosum* s.l., sample event as $X(1)=0$ $X(1)=0$. Using a Phillips-Perron unit root A unit root is a feature of processes that evolve through time that can cause problems in statistical inference involving time series models. The authors in Jacob et al. [3] quantitates the endmember non-Gaussain noise in the moderate resolution dataset of geo-

spectrotemporally uncoalesced, *S. damnosum* s.l. trailing vegetation, narrow, riverine tributray, agro-village complex, eco-georeferenecable signature varaibles. The Phillips-Perron cointeration test is *non-parametric*, (i.e. it does not require to select the level of serial correlation). The authors uses the same estimation scheme as in DF test, but corrected the statistic to conduct for autocorrelations and heteroscedasticity (ii.e, HAC type corrections).which was based on asymptotic theory**.** Fortunately the test did not require a priori information regarding the functional form of the geosampled *S. damnosum* s.l. sub-mixel residuals

Jacob et al. [26] quanatized the random walk process as $y_t = y_{t-1} + u_t$ where the disturbances were serially correlated in SAS (i.e., FORECAST procedure) with possible heteroscedasticity. Phillips and Perron (1988) proposed the unit root test of the OLS regression model, $y_t = \rho y_{t-1} + u_t$[24]. The authros then let $s^2 = \frac{1}{T-k}\sum_{t=1}^{T}\hat{u}_t^2$and let $\hat{\sigma}^2$be the variance estimate of the regression estimator $\hat{\rho}$, where $\hat{u}_t$ was the residual optimally forecasted unbiased explanator. .The authors estimate sthe asymptotic variance of $\frac{1}{T}\sum_{t=1}^{T}\hat{u}_t^2$by employing the truncation lag *l*. $\hat{\lambda} = \sum_{j=0}^{l}\kappa_j[1-j/(l+1)]\hat{\gamma}_j$ where $\kappa_0 = 1$, $\kappa_j = 2$for $j > 0$, and $\hat{\gamma}_j = \frac{1}{T}\sum_{t=j+1}^{T}\hat{u}_t\hat{u}_{t-j}$.. A truncated sample can be thought of as being equivalent to an underlying sample with all values outside the bounds entirely omitted, with not even a count of those omitted being kept[24].. With statistical censoring, a note would be recorded documenting which bound (upper or lower) had been exceeded and the value of that bound.

Then the Phillips-Perron $\hat{Z}_\alpha$(defined here as $\hat{Z}_\rho$) tested the zero mean case which was written $\hat{Z}_\rho = T(\hat{\rho}-1) - \frac{1}{2}T^2\hat{\sigma}^2(\hat{\lambda}-\hat{\gamma}_0)/s^2$ which resdiaully left the following limiting $\frac{\frac{1}{2}\{B(1)^2-1\}}{\int_0^1[B(x)]^2dx}$ distribution: where *B*(.) was a standard Brownian motion. Note that the realization $B(x)$from the stochastic process $B(x)$was distributed as $N(0,x)$and thus $B(1)^2 \sim \chi_1^2$. The authors deteremined that $P(\hat{\rho}<1)\approx 0.68$as $T\to\infty$, revealed that the limiting distribution was skewed to the left.

The authors in Jacob et al. [3] then let $\tau_\rho$be the τstatistic for $\hat{\rho}$. The Phillips-Perron $\hat{Z}_t$defined has $\hat{Z}_\tau$ test iwas then written as $\hat{Z}_\tau = (\hat{\gamma}_0/\hat{\lambda})^{1/2}t_{\hat{\rho}} - \frac{1}{2}T\hat{\sigma}(\hat{\lambda}-\hat{\gamma}_0)/(s\hat{\lambda}^{1/2})$and its limiting distribution was optimally derived as $\frac{\frac{1}{2}\{[B(1)]^2-1\}}{\{\int_0^1[B(x)]^2dx\}^{1/2}}$. Each run, on the path was shown on a distribution graph in ArcGIS.The random variable of interest was the position Y t at time t∈[0,1] which was the normal distribution with mean 0 and standard deviation t(1−t) in the eco-epidemiological, trailing vegation, turbid water, narrow African riverine, agro-village complex, *S. damnosoum* s.l. probabilistic paradigm. On each run, the value of a geoclassified LULC variable was recorded in a table, where point (t,Y t) (t,Yt) was shown as a red dot in a path graph in ArcGIS. The probability density function and moments, and the empirical density function and moments were shown in the distribution graph and in a distribution table. The parameter t varied with the input control.

ArcGIS Generates Brownian Bridge Movement Models and different home range estimates. Input files can be either .txt or ESRI shapefiles while outputs must be .txt files (which can be later uploaded to GIS software) .Unfortunately the pardigms works with

Cartesian system not latitude-longitude geo-coordinates. Home range estimators include exponential power, 1 mode Bivariate Normal, 2 Mode Bivariate Circle Mix, 2 Mode Bivariate Normal Mix and Kernel (fixed and adaptive). ArcGIS allows comparison between two or more models using Information Theoretic Criteria (www.esri.com). ArcGIS also can use different smoothing parameters, including: Likelihood cross-validation (CVh), Least squares cross-validation (LSCVh)and optimal smoothing parameter (h_ref) . In so doing, user-specified value endmember *S. damnosum* s.l. trailing vegation, heyproductive, eco-georference moderate resolution Output: .txt with X,Y coordinates and probability values of grid cells may be formally forecasted.Brownian Bridge Movement ModelInput requires: Easting (x) and Northing (Y) – in meters, for predicting location and location error (www.esri.com).

A Brownian bridge movement model (BBMM) is a relatively new concept that estimates the path ofan animal's movement probabilistically from data recorded at brief intervals. A BBMM assumes that locations arenot independent, whereas the "classical" kernel-density estimator (KDE) assumes they are. Fischer et al. (2013) estimated BBMM home ranges for 11 Black Vultures (*Coragyps atratus*) and 7 Turkey Vultures (*Cathartes aura*) equipped with satellitetransmitters near Marine Corps Air Station Beaufort, South Carolina, from October 2006 to November 2008.The 95% BBMM home ranges (95% BBMM) of the two Black Vultures that traveled >100 km from the capturesite were 833 and 2111 km2; of the nine that did not travel as far, 95% BBMM ranged from 33 to 778 km2 and averaged(± SE) 243 ± 76 km2. The majority of Turkey Vultures (n = 6) traveled >100 km from the capture site with95% BBMM ranging from 923 to 7058 km2 and averaging 3173 ± 1109 km2. We also estimated KDE home ranges,using newer satellite technology for comparison with previous studies. Overall 95% KDE ranged from 17 to 16066km2 for the Black Vulture and 988 to 36257 km2 for the Turkey Vulture. The concept of an animal's home range hasevolved over time, as have home-range, explanative, estimators. With increasing use of satellite telemetry, application of BBMMcan greatly enhance our understanding of home ranges, migration routes, seasonal movements, and habitat-use LULC patterns of wild birds over large and often remote areas.

For the Brownian bridge X X , the authors in Jacob et al. [3] noted in particular that X t was normally distributed with mean 0 and variance t(1−t) for t∈[0,1] for a robust moderate resolution. forecasting vulnerability, ArcGIS-derived probabilistic, endmember, *S.damnosum* s.l. signature paradigm. . Thus, the variance increased and then decreased on [0,1] reaching a maximum of 1/4 at t=1/2 t. Of course, the variance was 0 at t=0 and t=1 , since X 0 =X 1 =0 was quanatiated deterministically. Opening the simulation of the Brownian bridge process, the authors noted the change in the probability density function and moments in the uncoalesced, moderate resolution, iterative, hypeproductive, endmember, *S. damnsoum* s.l., trailing vegation, turbid water, eco-georferenceable, oviposition dataset. For various values of t , the authors ran the simulation 10,000 times and compared the emprical density function and moments to the true density function and momens.They then built a standard Brownian motion on the time interval [0,1]] from the Brownian bridge. In so doing, the multivariate, stochatic interpolated, prolific habitats along a flooded riverine corridor in northern Uganda (Achwa basin) [see 22].

There may be another way to construct a Brownian bridge from a standard Brownian motion for targeting seasonally hyperproductive, unknown, un-geosampled, *S. damnsoum* s.l., trailing vegetation, turbid water, eco-georeferenceable, seasonal, explanative, oviposition

signature on geoclassified moderate resoltuion LULCs. Suppose that Z={Z t :t∈[0,∞)} is a standard Brownian motion. A medical entomologist or experimenter may define X 1 =0 and X t =(1−t)Z(t1−t),t∈[0,1) in ArcGIS. Then X={X t :t∈[0,1]} would be a Brownian bridge. Note that X 0 =Z 0 =0 by definition would occur in this bridge .Linear combinations of geosampled, geo-spectrotemporal, uncoalesced, moderate reoslution, geoclassifiable LULC variables geospatially asscoiated to a capture point, hypeproductive habitat in X may reduce to linear combinations of other endmember variables in Z may reveal normal distributions in a multivariate, probabilistic, regression paradigm in ArcGIS. Thus, X would be a Gaussian process.For t∈[0,1] ,E(X t)=(1−t)E[Z(t1−t)]=0 .If s,t∈[0,1) with s<t then s/(1−s)<t/(1−t) so cov(X s ,X t)=cov[(1−s)Z(s1−s),(1−t)Z(t1−t)]=(1−s)(1−t)s1−s =s(1−t). In so doing, t↦X t may be continuous with probability 1 on [0,1) with probability 1, X t =(1−t)Z[t/(1−t)]→0 as t↑1 .

When constructing a spectrotemporally geosampled, hyerproductive, capture point, *S. damnsoum* s.l.,regression , forecasting vulnerability, estimation model $y_t = \mu + \rho y_{t-1} + u_t$for the true random walk process (i.e., single mean case), the limiting distribution of the statistic $\hat{Z}_\rho$ may be written $\frac{\frac{1}{2}\{[B(1)]^2 - 1\} - B(1)\int_0^1 B(x)dx}{\int_0^1 [B(x)]^2 dx - \left[\int_0^1 B(x)dx\right]^2}$ in FORECAST while the limiting distribution of the statistic $\hat{Z}_\tau$ may be optimally rendered by $\frac{\frac{1}{2}\{[B(1)]^2 - 1\} - B(1)\int_0^1 B(x)dx}{\{\int_0^1 [B(x)]^2 dx - \left[\int_0^1 B(x)dx\right]^2\}^{1/2}}$.In so doing, the limiting distribution of the Phillips-Perron test for the random walk with drift process $y_t = \mu + y_{t-1} + u_t$(i.e., trend case) may be derived as $\begin{bmatrix} 0 & c & 0 \end{bmatrix} V^{-1} \begin{bmatrix} B(1) \\ \frac{B(1)^2 - 1}{2} \\ B(1) - \int_0^1 B(x)dx \end{bmatrix}$where $c = 1$for $\hat{Z}_\rho$and $c = \frac{1}{\sqrt{Q}}$for $\hat{Z}_\tau$, $V = \begin{bmatrix} 1 & \int_0^1 B(x)dx & \frac{1}{2} \\ \int_0^1 B(x)dx & \int_0^1 B(x)^2 dx & \int_0^1 xB(x)dx \\ \frac{1}{2} & \int_0^1 xB(x)dx & \frac{1}{3} \end{bmatrix} Q = \begin{bmatrix} 0 & c & 0 \end{bmatrix} V^{-1} \begin{bmatrix} 0 \\ c \\ 0 \end{bmatrix}$ in ArcGIS When several endmmeber variables $\mathbf{z}_t = (z_{1t}, \cdots, z_{kt})'$are cointegrated, there exists a $(k \times 1)$cointegrating vector $\mathbf{c}$such that $\mathbf{c}'\mathbf{z}_t$is stationary and $\mathbf{c}$is a nonzero vector[24]. The residual based cointegration test may assume the following regression model: $y_t = \beta_1 + \mathbf{x}_t'\beta + u_t$where $y_t = z_{1t}$, $\mathbf{x}_t = (z_{2t}, \cdots, z_{kt})'$, and $\beta = (\beta_2, \ldots, \beta_k)'$ In so doing, a medcal entomologiist or experimenter may parsimoniously estimate the consistent cointegrating vector by employing regression if all the endmember variables are difference stationary — that is, I(1). The Phillips-Ouliaris test performs the test for the null hypothesis of no cointegration (https://en.wikipedia.org/wiki/MathWorld). The estimated cointegrating vector for an iteratively interapolative *S. damnsoum* s.l. probabilistic, predictive, signature-oriented, decomposed paradigm for targeting seasonally hyperproductive, *S. damnsoum* s.l., African, riverine, agro-village ecosystem, oviposition geolocations on geoclassifiable LULCs (e.g., trailing vegetation, discontinuously canopied) may be optiamlly written in SAS/GIS cyberenvironment employing $\hat{\mathbf{c}} = (1, -\hat{\beta}_2, \cdots, -\hat{\beta}_k)'$.

Further, suppose that X={X t :t∈[0,1]} is a Brownian bridge. in a geo-spectrotemporal, eco-epidemiological, moderate resoltuion, *S. damnosum* s.l. forecast,vulnerability model in SAS/GIS. Then by defining Z t =(1+t)X(t1+t),t∈[0,∞) where Z={Z t :t∈[0,∞)} a standard Brownian motion process could be elaborated for a *S.*

damnosum s.l. habitat , risk model.Note that in this instance, $Z_0 = X_0 = 0$. Linear combinations of the geo-spectrotemporal, geosampled, eco-georeferenceable, immature, decomposed, *Similium* habitat explanatorial, endmember variables in Z may reduce to linear combinations of the variables in X , and hence would have have normal distributions. Thus, Z would be a Gaussian process where for $t \in [0,\infty)$, $E(Z_t) = (1+t)E[X(t_1+t)] = 0$, If $s,t \in [0,1]$ with $s<t$,=thens/$(1+s)<t/(1+t)$ socov$(Z_s, Z_t) = \text{cov}[(1+s)X(s_1+s),(1+t)X(t_1+t)] = (1+s)(1+t)[s_1+s - s_1+s\ t_1+t] = s$ .Since $t \mapsto X_t$ again may be continuous, $t \mapsto Z_t$ would also be continuous in the remotely sensed probabilistic, paradigm.

Suppose that $X = \{X_t : t \in [0,\infty)\}$ is a standard Brownian motion in a geo-spectrotemporal, *S. damnosum* s.l. moderate resolution, iteratively interpolatable, signature-oriented, geoclassifiable LULC, vulnerability, eco-epidemiological, forecast model. Then conditioned on $X_1 = 0$, would be the explicative process $\{X_t : t \in [0,1]\}$ which then would be the Brownian bridge process Part of the argument here would be based based on properties of the multivariate normal distribution. The conditioned process would still be continuous and would still be a Gaussian process. In particular, suppose that $s,t \in [0,1]$ with $s<t$ in the forecasting equation in the *S. damnosum* s.l. model. Then (X_t, X_1) would have a joint normal distribution with geosampled parameters specified by the mean and covariance functions of X . By standard computations, the conditional distribution of X_t would be given by $X_1 = 0$ which would be normal with mean 0 and variance $t(1-t)$. Similarly, the joint distribution of (X_s, X_t, X_1) would be normal with parameters specified by the mean and covariance functions of X. Again, by standard computations, the conditional distribution of (X_s, X_t) in the *S. damnosoum* s.l. habitat model would be given $X_1 = 0$ would be bivariate normal with 0 means and with $\text{cov}(X_s, X_t | X_1 = 0) = s(1-t)$.

Perhaps the Brownian bridge may be optimally defined in terms a stochastic integral when constructing a eco-georeferenceable, explanatorial, diagnostic, forecast vulnerability endmember , moderate resolution prpobabilsic pardigmn for targeting hyperproductive, eco-georeferenceable *S. damnsoum* s.l., trailing vegetation, turbid water, partially, infrequently canopied, immature, seasoanl habitats in a narrow African, riverine , agro-village, tributary ecosystem, Stochastic calculus is a branch of mathematics that operates on stochastic processes. In so doing, a consistent theory of integration may be used to define integrals with respect to stochastic processes. In so doing, model systems that behave randomly may be quantitated.

The best-known stochastic process to which stochastic calculus is applied is the Wiener process which is used for modeling Brownian motion as described by Louis Bachelier in 1900 and by Albert Einstein in 1905 and other physical diffusion processes in space of particles subject to random forces. In pure mathematics, the Wiener process gave rise to the study of continuous time martingales. , a martingale is a sequence of random variables (i.e., a stochastic process) for which, at a particular time in the realized sequence, the expectation of the next value in the sequence is equal to the present observed value even given knowledge of all prior observed values.A basic definition of a discrete-time martingale for a geo-spectrotemporally uncoalesced, eco-georeferenced, hyeprproductive, immature , capture point is a discrete-time stochastic process (i.e., a sequence of random variables) $X_1, X_2, X_3, \ldots$ that satisfies for any time n, Since the 1970s, the Wiener process has been widely applied in financial mathematics and economics to model the evolution in time of stock prices and bond interest rates)http://mathworld.wolfram.com/). A continuous-time, explanative, diagnostic, *S. damnosum* s.l. habitat , moderate resolution, stochastic process

$W(t)$for $t \geq 0$with $W(0) = 0$ may be constructed such that the increment $W(t) - W(s)$is Gaussian with mean 0 and variance $t - s$for any $0 \leq s < t$, where the increments for nonoverlapping time intervals are independent.

The issue of giving an explicit description of the flow of information concerning the time of sampled S. damnsoum s.l. habitats in narrow African riverine tributray ecosystems may be tackled by defining a bridge process starting from zero and conditioned to be equal to zero when the default occurs. I so doing some empirical facts on the behavior of seasonally hyperproductive oviposition sites on moderate resolution LULCs: when the bridge process is away from zero. However, when the information process is close to zero, in the *S. damnosum* s.l. forecasting vulnerability model the risk of an imminent default is highre . In this sense the bridge process leaks information concerning the default before it occurs. Brownian bridges on stochastic intervals imay to provide the basic properties to quanatiate such processes.

Brownian bridges can be constructed in QuantLib. QuantLib is an open-source software library which provides tools for software developers interested in financial instrument valuation and related subjects. QuantLib is written in C++. ++ is a general-purpose programming language. It has imperative, object-oriented and generic programming features, while also providing facilities for low-level memory manipulation. The QuantLib project is aimed at providing a comprehensive software framework for quantitative finance. QuantLib is a free/open-source library for modeling, trading, and risk management in real-life.QuantLib is written in C++ with a clean object model, and is then exported to different languages such as C#, Objective Caml, Java, Perl, Python, GNU R, Ruby, and Scheme. An AAD-enabled version is also available. The reposit project facilitates deployment of object libraries to end user platforms and is used to generate QuantLibXL, an Excel addin for QuantLib, and QuantLibAddin, QuantLib addins for other platforms such as LibreOffice Calc. Bindings to other languages and porting to Gnumeric, Matlab/Octave, S-PLUS/R, Mathematica, COM/CORBA/SOAP architectures, FpML, are under consideration. QuantLib can be downloaded from http://quantlib.org/download.shtml; installation instructions are available at http://quantlib.org/install.shtml for most platforms.Documentation for the usage and the design of the QuantLib library is available from http://quantlib.org/docs.shtml (See Table 1) .A list of changes for each past versions of the library can be browsed at http://quantlib.org/reference/history.html

Table 1. Output a realization of a Brownian Bridge from QuantLib

```
*/

#include <iostream>
```

```
#include <time.h>
#include <boost/random/normal_distribution.hpp>
#include <boost/random/mersenne_twister.hpp>
#include <boost/random/variate_generator.hpp>


#include <ql/quantlib.hpp>

/// Prints the bridge, including the cumulative sum of the variations
/// which is the actual path of the underlying
void printBridge(const std::vector<double> &b)
{
 double cumsum=0;
 for(size_t i=0; i<b.size(); ++i)
 {
  cumsum+=b[i];
  std::cout<<i+1
       <<","
       <<b[i]
       <<","
       <<cumsum
       <<std::endl;
 }
}


void bbridgeout(void)
{
 const size_t n=500;

 QuantLib::BrownianBridge bridge(n);

 std::vector<double> inp(n);

 //
 inp[0]=0.0;

 // Generate the rest of the variates as standard Gaussian random
 // values
 boost::variate_generator<boost::mt19937, boost::normal_distribution<> >
  generator(boost::mt19937(time(0)),
       boost::normal_distribution<>());

 for(size_t i=1; i<inp.size(); ++i)
  inp[i]=generator();

 std::vector<double> out(n);
 bridge.transform(inp.begin(),
            inp.end(),
            out.begin());
```

```
 printBridge(out);
}

int main(void)
{
 bbridgeout();

 return 0;
```

The expected value of the bridge is zero, with variance $t(T - t)$, implying that the most uncertainty is in the middle of the bridge, with zero uncertainty at the nodes. The covariance of $B(s)$ and $B(t)$ is $s(T - t)$ if $s < t$. The increments in a Brownian bridge are not independent. Covariance provides a measure of the strength of the correlation between two or more sets of random variates. The covariance for two random variates X and Y, each with sample size N, is defined by the expectation value $\operatorname{cov}(X, Y) = \langle (X - \mu_X)(Y - \mu_Y) \rangle = \langle X Y \rangle - \mu_X \mu_Y$ where $\mu_x = \langle X \rangle$ and $\mu_y = \langle Y \rangle$ are the respective means, which can be written out explicitly as $\operatorname{cov}(X, Y) = \sum_{i=1}^{N} \frac{(x_i - \bar{x})(y_i - \bar{y})}{N}$. For uncorrelated variates, $\operatorname{cov}(X, Y) = \langle X Y \rangle - \mu_X \mu_Y = \langle X \rangle \langle Y \rangle - \mu_X \mu_Y = 0$, so the covariance is zero. However, if the variables are correlated in some way, then their covariance will benonzero. In fact, if $\operatorname{cov}(X, Y) > 0$, then Y tends to increase as X increases, and if $\operatorname{cov}(X, Y) < 0$, then Y tends to decrease as X increases. Note that while statistically independent variables are always uncorrelated, the converse is not necessarily true.The covariance is especially useful when looking at the variance of the sum of two random variates, since $\operatorname{var}(X + Y) = \operatorname{var}(X) + \operatorname{var}(Y) + 2 \operatorname{cov}(X, Y)$. The covariance is symmetric by definition since $\operatorname{cov}(X, Y) = \operatorname{cov}(Y, X)$. Given n random variates denoted X_1, ..., X_n, the covariance $\sigma_{ij} = \operatorname{cov}(X_i, X_j)$ of X_i and X_j is defined by $\operatorname{cov}(X_i, X_j) = \langle (X_i - \mu_i)(X_j - \mu_j) \rangle = \langle X_i X_j \rangle - \mu_i \mu_j$, where $\mu_i = \langle X_i \rangle$ and $\mu_j = \langle X_j \rangle$ are the means of X_i and X_j, respectively. The matrix (V_{ij}) of the quantities $V_{ij} = \operatorname{cov}(X_i, X_j)$ is called the covariance matrix[25].

A variance-covariance matrix is a square matrix that contains the variances and covariances associated with several variables. The diagonal elements of the matrix contain the variances of the variables and the off-diagonal elements contain the covariances between all possible pairs of variables. The variance-covariance matrix is symmetric because the covariance between X and Y is the same as the covariance between Y and X. Therefore, the covariance for each pair of variables is displayed twice in the matrix: the covariance between the ith and jth variables is displayed at positions (i, j) and (j, i). Many statistical applications calculate the variance-covariance matrix for the estimators of parameters in a statistical model. It is often used to calculate standard errors of estimators or functions of estimators. For example, s logistic *S. damnosum* s.l. forecast vulnerability regression model would create amatrix for the estimated uncoalesced, trailing vegetation, endmember covariate coefficients for robustly quanatiting the variances of the geosampled, geo-spectrotemporal, explanative,coefficients and the covariances between all possible pairs of coefficients.

A Brownian bridge, or a functional of a Brownian bridge may be constructed for

creating a signature, moderate reosolution, decomposed trailing vegation, narrow Africanm, riverine tributary oviposition, eco-georefernced, *S. damnoum* s.l. model if performance is measured in the expected value sense. To describe a problem of this type, let X be a Brownian bridge with Xq = X\ =0, and define the value V= sup EXT. (1.1) 0<r<l in AUTOREG Here the supremum may be optimally taken over all random times that are stopping times with respect to the filtration generated by X In a Brownian bridge process for an interpolative, interpolative, uncoalesced geo-spectrotemporal, moderate resolution, target reference signature on the other hand, not only is $B(0) = 0$ but $B(1) = 0$, mya be required in the forecast, vulneranility, endmember model where processes would be "tied down" at $t = 1$ as well. Just as a literal bridge is supported by pylons at both ends, a Brownian Bridge is required to satisfy conditions at both ends of the interval [0,1][26].

Consider the random walk process $y_t = y_{t-1} + u_t$ in a *S. damnosum* s.l. habitat, forecast, vulnerability probabilistic, distribution paradigm where the disturbances might be serially correlated with possible heteroscedasticity. Phillips and Perron (1988) proposed the unit root test of the regression model, $y_t - \rho y_{t-1} + u_t$ Let $s^2 = \frac{1}{T-k}\sum_{t=1}^{T}\hat{u}_t^2$ and let $\hat{\sigma}^2$ be the variance estimate of the estimator $\hat{\rho}$, where $\hat{u}_t$ is the residual. A medical entomologist or experimenter may optimally estimate the asymptotic variance of $\frac{1}{T}\sum_{t=1}^{T}\hat{u}_t^2$ by using the truncation lag l. $\hat{\lambda} = \sum_{j=0}^{l}\kappa_j[1 - j/(l+1)]\hat{\gamma}_j$ where $\kappa_0 = 1$, $\kappa_j = 2$ for $j > 0$, and $\hat{\gamma}_j = \frac{1}{T}\sum_{t=j+1}^{T}\hat{u}_t\hat{u}_{t-j}$ in a Similium iteratively interpolative model, Then the Phillips-Perron $\hat{Z}_\alpha$ (defined here as $\hat{Z}_\rho$) test (zero mean case) may be written $\hat{Z}_\rho = T(\hat{\rho} - 1) - \frac{1}{2}T^2\hat{\sigma}^2(\hat{\lambda} - \gamma_0)/s^2$ which would reveal the following limiting distribution: $\frac{\frac{1}{2}\{B(1)^2 - 1\}}{\int_0^1 [B(x)]^2 dx}$ where $B(.)$ is a standard Brownian motion. Note that the realization z from the stochastic process $B(x)$ would eb distributed as $N(0,x)$ and thus $B(1)^2 \sim \chi_1^2$. Note that $P(\hat{\rho} < 1) \approx 0.68$ as $T \to \infty$, which may show that the limiting distribution is skewed to the left. Let τ_ρ be the τ statistic for $\hat{\rho}$ in the mdoel The Phillips-Perron $\hat{Z}_t$ (defined here as $\hat{Z}_\tau$) test then could written $\hat{Z}_\tau = (\gamma_0/\hat{\lambda})^{1/2}\tau_{\hat{\rho}} - \frac{1}{2}T\hat{\sigma}(\hat{\lambda} - \gamma_0)/(s\hat{\lambda}^{1/2})$ and its limiting distribution would eb derivable as $\frac{\frac{1}{2}\{[B(1)]^2 - 1\}}{\{\int_0^1 [B(x)]^2 dx\}^{1/2}}$

Suppose we have generated a number of points $W(0)$, $W(1)$, $W(2)$, $W(3)$, etc. of a Wiener process path by computer simulation *S. damnsoum* s.l. model. It may be desireable to fill in additional points in the interval [0,1], that is to interpolate between the already generated points $W(0)$ and $W(1)$. The solution is to use a Brownian bridge that is required to go through the values $W(0)$ and $W(1)$. Let B be a standard Brownian motion in *a S. damnosum* s.l. model. A medical entomologist or experimenter may then define a Brownian bridge b by b t =B t −tB 1 .The standard Wiener process would satisfy $W(0) = 0$ and would therefore be "tied down" to the origin, may other geosampled, *S. damnsoum* s.l trailing vegetation, African, narrow , riverine tributary, points ,may be less interpolatively restricted (see Figure 3).

Figure 3. Browinan bride where expected value of the bridge is zero, with variance $t(1 - t)$, for quantiating uncertainty with zero uncertainty at the nodes. with a

covariance of $B(s)$ and $B(t)$ is $s(1-t)$ if $s < t$.

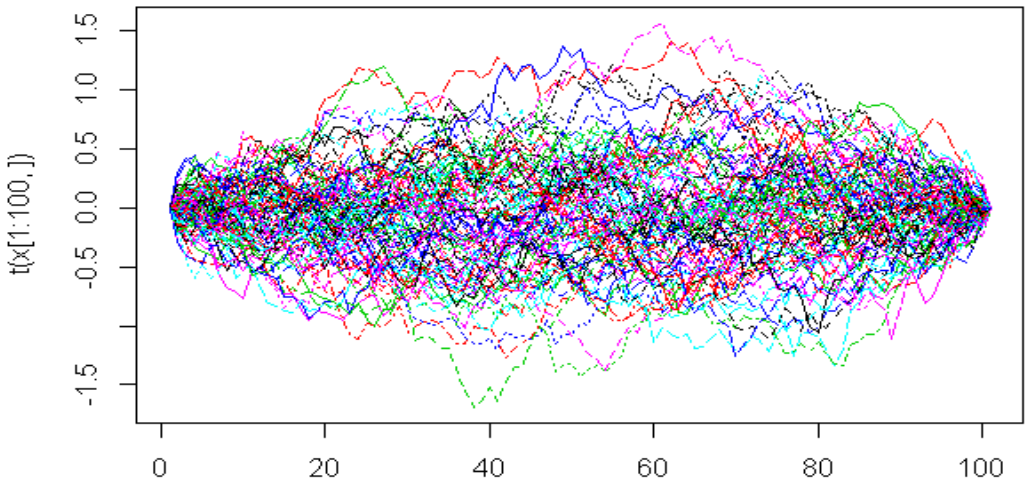

Brownian bridge is the result of Donsker's theorem in the area of empirical processes which is also employed in the Kolmogorov–Smirnov test in the area of statistical inference In statistics, the Kolmogorov–Smirnov test (K–S test or KS test) is a nonparametric test of the equality of continuous, one-dimensional probability distributions that can be used to compare a sample with a reference probability distribution (one-sample K–S test), or to compare two samples (two-sample K–S test)[24]. In probability theory, Donsker's theorem (also known as Donsker's invariance principle, or the functional central limit theorem), is a functional extension of the central limit theorem.

In probability theory, the central limit theorem (CLT) states that, given certain conditions, the arithmetic mean of a sufficiently large number of iterates of independent random variables, each with a well-defined (finite) expected value and finite variance, will be approximately normally distributed, regardless of the underlying distribution[24]. To illustrate what this means, suppose that a eco-georeferenced, hypeproductive*, S. damnsoum* s.l., geoclassifiable,moderate resolution, ArcGIS-derived , LULC sample is obtained containing a large number of ovipoistion observations, each observation being randomly generated in a way that does not depend on the values of the other observations, and that the arithmetic average of the observed values is computed. If this procedure is performed many times, the central limit theorem says that the computed values of the average will be distributed according to the normal distribution (commonly known as a "bell curve"). The central limit theorem has a number of variants [24]. In its common form, the decompose,, elucidative diagnostic, endmember, random variables must be identically distributed. In variants, convergence of the mean to the normal distribution also occurs for non-identical distributions or for non-independent observations, given that they comply with certain conditions.

In more general usage, a central limit theorem is any of a set of weak-convergence theorems in probability theory. They all express the fact that a sum of many independent and identically distributed (i.i.d.) random variables, or alternatively, random variables with specific types of dependence, will tend to be distributed according to one of a small set of attractor distributions. When the variance of the *S. damnsoum* s.l., immature habitat, eco-georeferenceable, expositorial i.i.d. variables is finite, the attractor distribution is the normal distribution. In contrast, the sum of a number of i.i.d. random variables with power law tail distributions decreasing as $|x|^{-\alpha-1}$ where $0 < \alpha < 2$ (and therefore having infinite variance) will tend to an alpha-stable distribution with stability parameter (or index of stability) of α as the number of variables grows

Let X1, X2, X3, . . . be a sequence of i.i.d. geo-spectrotemporal, random variables with mean 0 and variance 1. Let Sn := ∑n i=1 Xi . The stochastic process S := (Sn)n∈N is known as a random walk. Define the diffusively rescaled random walk by W(n) (t) := S⌊nt⌋ √ n , t ∈ [0, 1]. The central limit theorem would then assert that W(n) (1) converges in distribution to a standard Gaussian random variable W(1) as n → ∞ . Donsker's invariance principl extends this convergence to the whole function W(n) := (W(n) (t))t∈[0,1] . More precisely, in its modern form, Donsker's invariance principle states that: As random variables taking values in the Skorokhod space D[0, 1] , the random function W(n) converges in distribution to a standard Brownian motion W := (W(t))t∈[0,1] as n → ∞. 1

The Skorokhod space D = D([0, 1] : R1) consists of functions x : [0, 1] ! R1 which admit limit x(t−) from the left at each point t ∈ (0, 1] and limit x(t+) from the right at each point t ∈ [0, 1). After regularization by taking the right-continuous version, such functions are often called "cadlag", In mathematics, a càdlàg (French "continue à droite, limite à gauche"), RCLL ("right continuous with left limits"), or corlol ("continuous on (the) right, limit on (the) left") function is a function defined on the real numbers (or a subset of them) that is everywhere right-continuous and has left limits everywhere. Càdlàg functions are important in the study of stochastic processes that admit (or even require) jumps, unlike Brownian motion, which has continuous sample paths[25].

The Skorokhod space may provide a natural andconvenient formalimalized for description of trajectories of stochastic processes admitting jumps in a seasonal , epidemiological dataset of eco-georeferenceable, uncoalesced, explanatorial, diagnostic, forecast vulnerability endmember , moderate resolution probabilistic , unbiased model estimaors for targeting hyperproductive, trailing vegetation, turbid water, partially, infrequently canopied, *S. damnosum* s.l. immature habitats site in a narrow African tributary, ecosystem. .In particular: trajectories of Poisson process, L´evy processes,martingales and semimartingales, empirical distribution functions, trajectories of discretizations of stochastic processes may be robustly parsimoniously quantitated. The supremum norm would convert the Skorokhod space into a nonseparable Banach space, which may be disadvantageous in geolocalizing seasaonlly, eco-georferenceable, prolific, capture, *S. damnsoum* s.l. canopied, immature, oviposition sites on geoclassifiable ArcGIS-derived , moderate resolution LULCs(e.g., trailing vegetation, sparsely canopied, pre-flooded agro-village)

In mathematics, more specifically in functional analysis, a Banach space is a complete normed vector space Let V be a complex vector space in a *S. damnosum* s.l. forecast, vulnerability model/. A norm on V is a function|| · || : V → R may satisfy the following three conditions:(i) $||v|| \geq 0$, ∀ v ∈ V, and $||v|| = 0 \Leftrightarrow v = 0$;(ii) $||\alpha v|| = |\alpha|\,||v||$, ∀ v ∈ V, α ∈

C;(iii) ||v + w|| ≤ ||v|| + ||w||, ∀ v,w ∈ V.A vector space equipped with a norm is called a normed vector space[25]. Then based on the Reverse triangle inequality, V may be a normed vector space in the a eco-georeferenceable, diagnostic, forecast vulnerability endmember , moderate resolution probabilistic, vector arthropod, probabilistic paridigm.In so doing, ||v − w|| ≥ | ||v|| − ||w|| | , ∀ v,w ∈ V may occur in the expsoitorial, diagnostic, normalized, residual wavelength, transmittance frequency forecasts for for enabling optimal targeting of hyperproductive, eco-georeferenceable, *S. damnsoum* s.l., trailing vegetation, turbid water, discontinuously canopied, immature, seasonal oviposition sites in narrow, African riverine, tributary compex ecosystems Suppose a medical entomologist or experimenter lets v,w ∈ V in the risk model. Then ||v − w|| ≥ ||v|| − ||w|| or ||v − w|| ≥ ||w|| − ||v|| and ||v|| = ||(v − w) + w|| ≤ ||v − w|| + ||w|| may diagnostic, quanatiate, explanatorial, paramterizable covariates of these prolific habitats,Proof of the Reverse triangle inequality suggests without loss of generality that ||*x*|| is no smaller than ||*y*||. Thus, it is imperative to show $\|x\| - \|y\| \leq \|x - y\|$ in a iterative, forecast, vulnerability, *S. damnosum* s.l., probabilistic, seasoanl paradigm. .This follows directly from the triangle inequality itself if a medical entomologist or experimenter writes *x* as *x=x-y+y* and assumes that it is*x=(x-y) + y*. Taking norms and applying the triangle inequality then would render $\|x\| = \|x - y + y\| \leq \|x - y\| + \|y\|$ which implies (*). Moreove,for optimal synthesization of discontinuous elements of D in the vector arthropod paradigm, simple and natural approximation procedures like discretizations may be optimally convergent uniformly.

Let (*M*, *d*) be a metric space, in an elucidative, time series, orthogonally decomposed, moderate resolution, geo-spectrotemporally uncoalesced, fractionalized, moderate resolution, signature, metaheursitically optimizable,epidemiological,optimizable, dataset of *S. damnosum* s.l., quantitative, endmember, interpolative, explanatorily, paramterizable, wavelength, trasnmittance signature, geoclassifiableLULC frequencies and let $E \subseteq \mathrm{R}$. A function $f\colon E \to M$ (a càdlàg function).Then , for every $t \in E$, in the , residual eco-epidemiological, eco-georeferenceable forecasts, the left limit $f(t-) := \lim_{s \uparrow t} f(s)$ may exist and the right limit $f(t+) := \lim_{s \downarrow t} f(s)$ may exist and equal $f(t)$. That is,the model output may reval f is right-continuous with left limits

Certain path properties of a symmetric α-stable process X(t) = ∫Sh(t, s) dM(s), t ∈ T, may be studied in terms of the kernel. in geo-spectrotemrpoal, geosampled, moderate reasolution uncoalesced, *S. damnossum* s.l., forecast, vulnerability, epidemiological, endmember, simulation model for targeting, , hyerpproductive, trailing vegtaion, turbid water, African, narrow, agro-village complex, capture point, eco-georefereneceable oviposition LULC sites, The function $K(\alpha, t)$in an integral or integral transform $g(\alpha) = \int_a^b f(t) K(\alpha, t)\, dt.$ [www.mathworld.com].The existence of an appropriate modification of the kernel may enable a medical entomologist or experimenter to employ results from stable measures on Banach spaces in these predictive paradigms in SAS/GIS for precision, seasonal, habitat targeting prolific *Simium* capture points in a narrow riverine, tributary, African ecosystem agro-village complex. Bounds for the moments of the norm of sample paths may be optimally obtained in the diagnostic, model residual, explantive, forecasts. The yields would be definite bounds for the moments of a double α-stable integral. Also, necessary and sufficient conditions for the absolute continuity of sample paths in the model , endmember, moderate resolution, uncoalesed,proxy, endmember, signaturare variables may

be rendered . Along with the above stochastic integral representation of stable processes, the representation of stable random vectors due to R. LePage, M. Woodroofe, and J. Zinn (1981, Ann. Probab.9, 624–632) may be optimally usable to quantaite the relationship between these two geo-representations of simulated *S. damnosum* s.l., hypeproductive , eco-georeferenced, seasaonal geolocations.

Let Fn be the empirical distribution function of the sequence of independently distributed dataset of uncoalesced, geo-spectrotemporal, moderate resolution, hypeproductive, trailing vegation, partially shaded, narrow, African riverine tributray, *S. damnosum* s.l. oviposition, capture point, eco-georferenceable, random variables X1, X2, X3, . . . with distribution function Fn . Defining the centered and scaled version of Fn by $Gn(x) = \sqrt{n}(Fn(x) - F(x))$ indexed by $x \in R$ may then aid in precision targeting geolocations of eco-georeferenceable , prolific seasonal habitats. By the classical central limit theorem, for fixed x, the random variable Gn(x) would convergs in distribution to a Gaussian (normal) random variable G(x) with zero mean and variance $F(x)(1 - F(x))$ as the sample size n grows. In probability theory, the central limit theorem (CLT) states that, given certain conditions, the arithmetic mean of a sufficiently large number of iterates of independent random variables, each with a well-defined expected value and well-defined variance, will be approximately normally distributed, regardless of the underlying distribution.The sequence of Gn(x), as random elements of the Skorokhod space D converges in distribution to a Gaussian process G with zero mean and covariancemay be given by $cov[G(s), G(t)] = E[G(s)G(t)] = \min\{F(s), F(t)\} - F(s)F(t)$ in the probabilisc predictive pardigm. The process G(x) can be written as B(F(x)) where B is a standard Brownian bridge on the unit interval in SAS/GIS. Kolmogorov (1933) showed that when F is continuous, the supremum supt Gn(t) and supremum of absolute value, supt |Gn(t)| converges in distribution to the laws of the same functionals of the Brownian bridge B(t), see the Kolmogorov–Smirnov test. In 1949 Doob asked whether the convergence in distribution held for more general functionals, thus formulating a problem of weak convergence of random functions in a suitable function space. [25] Donsker stated and proved (not quite correctly)a general extension for the Doob-Kolmogorov heuristic approach.

Asymptotic theorems on the difference between the (empirical) distribution function calculated from a sample and the true distribution function governing the sampling process are well known. Simple proofs of an elementary nature have been obtained for the basic theorems of Komogorov and Smirnov by Feller, but even these proofs conceal to some extent, in their emphasis on elementary methodology, the naturalness of the results (qualitatively at least), and their mutual relations. Feller suggested that the author publish his own approach which does not have these disadvantages, although rather deep analysis would be necessary for its rigorous justification of these distributions in a geo-spectrotemparolly geosampled, itarative interpolative, diagnostic, proxy signture-related, iterative interpolative, uncoalesed, capture point, trailing vegation, narrow, African , riverine tributray, agro-village tributray *S. damnosum* s.l. seasonal, epidemiological model. The approach may therefore be presented at one critical point (e.g., hyeprpoductiove seasoanal, eco-georferenceable oviposition site on an ArcGIS geoclassified LULC) as heuristic reasoning which leads to results in investigations of this kind, even though the easiest proofs may use entirely different methods. No calculations would be required to obtain the qualitative results, based on the existence of limiting distributions for large geo-spectrotemporally geosamped, optimizable datasets of various measures of *georferenced, Similium* habitats and of the qunatized discrepancy between empirical and true distribution functions psot regression. The numerical evaluation of these limiting distributions may require certain results concerning the Brownian

movement stochastic process and its relation to other Gaussian processes in the probabilistic oviposition paradigm.

In the original paper, Donsker proved that the convergence in law ofGn to the Brownian bridge holds for Uniform[0,1] distributions with respect to uniform convergence in t over the interval [0,1].[2] However Donsker's formulation was not quite correct because of the problem of measurability of the functionals of discontinuous processes. In 1956 Skorokhod and Kolmogorov defined a separable metric d, called the Skorokhod metric, on the space of cadlag functions on [0,1], such that convergence for d to a continuous function would be equivalent to convergence for the sup norm, and showed that Gn converges in law in D[0, 1] to the Brownian bridge. Later Dudley reformulated Donsker's result to avoid the problem of measurability and the need of the Skorokhod metric. Thus a medical entomologist or experimenter may prove that there exist Xi, independently uniform in [0,1] and a sequence of sample-continuous Brownian bridges Bn, such that $\|Gn - Bn\|\infty$ is measurable and converges in probability to 0. An improved version of this result, in SAS/GIS may provide more detail on the rate of convergence, is the Komlós–Major–Tusnády approximations in the geo-spectrotemporal, moderate resolution, iterative , quantitatively, explantive, capture point, S. damnosum s.l ., trailing vegtaion, narrow African, riverine, tributary ecosystem, oviposition model when precision targeting a uncoalesced, diagnostically interpolative unbiased, ArcGIS-derived, LULC estimators of hypeproductive seasonal , eco-georeferenceable habitats. In theory of probability, the Komlós–Major–Tusnády approximation (also known as the KMT approximation, the KMT embedding, or the Hungarian embedding) is an approximation of the empirical process by a Gaussian process constructed on the same probability space.

Any order-invariant function of a sequence of geospectrotemrporally uncoalesced, eco-geoeerferenceable modearte resolution, *S. damnosum* s.l., capture point , oviposition, explanatorial LULC diagnostic , iterative interpolative diagnostic, trailing vegation, sparsely canopied, signature-related, fractionalized , discontinuous decomposed values may be expressed as a functional of the sample's empirical distribution function. In so doing, a very general approach to the theory of functions of sample values can be based on the empiric distribution function for targeting seasaonlly hypeproductive habitats in narrow African, riverine tributray , agro-village complex ecosystems. The KMT) approximation may provide a remarkable, mathematically tractable representation for the empiric distribution function of a random, eco-epidmiological, capture point, oviposition sample. Hence, one of the aims of the probabilistic, vector arthropod-related , forecast, vulnerability model construction processwould be to optimally describe the KMT approximation, particularly as it relates to other forms of uncoalesced, geoclassifiable, LULC approximations in ArcGIS, and to survey some of its many applications.(e..g, iterative interpolation of a dataset of moderate resolution orthogonally, elucidatively, orthogonally decomposed, *S. damnosum* s.l. habitat,proxy LULC signature, eigenvectors in Geospatial Analyst ^{TM}).

An uncoalesced, eco-geoereferenceable modearte resolution, *S. damnosum* s.l., capture point ,hypeproductive, oviposition, site on an ArcGIS-goclassifiable partially canopied, LULC diagnostic , iterative interpolative diagnostic, trailing vegetation, signature-related, fractionalized , discontinuous decomposed explanative, random variable X may be also described well by its distribution function FX. This is a real-valued function defined as $FX(s) = P[X \leq s]$ on R, where $\{X \leq s\}$ is the event of all experiments ω satisfying $X(\omega) \leq s$. The distribution function will not encode the internal structure of the random variable X; it does not reveal the structure of the probability space, for example. But the function FX would

allows the construction of a probability space in the predictive paradigm with exactly this distribution function. There are two important types of distributions, continuous distributions with a probability density function fX = F′X and discrete distributions for which F is piecewise constant[www.mathworld.com]. An example of a continuous distribution in a residiual forecast targeting a prolific, eco-georeferenceable, *S. damnosum* s.l. habitat may be the standard normal distribution, where fX(x) = e−x2/2/√2π. A medical entomologist or experimenter can characterize it as the distributionwith maximal entropy I(f) = −Rlog(f(x))f(x) dx among all distributions which may have zero mean and variance 1. An example of a discrete distributionis the Poisson distribution P[X = k] = e−λ λk k! on N = {0, 1, 2, . . . } as in Jacob et al[22]. The authors in that contribution described a datset of geo-spectrotemporally uncoalesced *S. damnosusm* s.l. hypeproductive, trailing vegetation, turbid, narrow, riverine, tributary, log-normalized, explanatorial, seasonal,geosampled, proxy signature, random variables by their moment generating functions MX(t) = E[eXt] and by their characteristic function φX(t) = E[eiXt]. The later models were construced in an ArcGIS cyberenvironment employimng the Fourier transform of the law μX = F′X which was a measure onthe real line R.

The law μX of the random variable is a probability measure on the real line satisfying μX((a, b]) = FX(b)−FX(a) (https://en.wikipedia.org/wiki/MathWorld). By the Lebesgue decomposition theorem, a medical entomologist or experimenter can decompose any measure μ into a discrete part μpp, an absolutely continuous part μac and a singular continuous part μsc. Random variables X for which μX is a discrete measure are called discrete random variables, random variables with a continuous law are called continuous random variables [25]. Traditionally, these two type of random variables are the most important ones for qunatiating probability spaces in forecast vulnerability paradigms. But singular continuous random variables appeartoo: in spectral theory, dynamical systems or fractal geometry.

The Chebychev inequality P[|X − E[X]| ≥ c] ≤ Var[X] c2 may be optimally employed for precsion targeting, hyperproductive, trailing vegetation, turbid water, narrow, African, riverine, tributary ecosystem, oviposition sites on ArcGIS-derived, moderate resolution, multivariate LULCs In probability theory, Chebyshev's inequality guarantees that in any probability distribution, "nearly all" values are close to the mean—the precise statement being that no more than $1/k^2$ of the distribution's values can be more than k standard deviations away from the mean (or equivalently, at least $1-1/k^2$ of the distribution's values are within k standard deviations of the mean) [24]. A random, iteratively interpolative, explanative diagnostically, orthogonally decomposed, moderate resolution, endmember variable can be mixed discrete and continuous in a forecast vulnerability, geo-spectrotemporal, *S. damnosum* s.l., wavelength, transmittance, frequency model [22]. Inequalities play an important role in probability theory [25]. A special case of the Chebychev-Markov inequality h(c) · P[X ≥ c] ≤ E[h(X)] for quantitating habitat monotone nonnegative functions may be applicable when iteratively interpolating a S. *damnosum* s.l. uncoalesced, iteratively quantitatively, interpolative, moderate resolution, proxy signature. In mathematics, a monotonic function (or monotone function) is a function between ordered sets that preserves or reverses the given order. This concept first arose in calculus, and was later generalized to the more abstract setting of order theory. Other inequalities are the Jenseninequality E[h(X)] ≥ h(E[X]) for convex functions h, the Minkowski inequality ||X + Y ||p ≤ ||X||p + ||Y ||p or the H¨older inequality ||XY ||1 ≤||X||p||Y ||q, 1/p + 1/q = 1 for random variables, X, Y , for which ||X||p =E[|X|p], ||Y ||q = E[|Y |q] are finite. Any inequality which appears in analysiscan be useful in the toolbox of probability theory [25].

Independence is a central notion in probability theory. Two events A,B are called independent, if P[A ∩ B] = P[A] · P[B]. An arbitrary set ofevents Ai is called independent, if for any finite subset of them, the probability of their intersection is the product of their probabilities. Two σ-algebras A, B are called independent, if for any pair A ∈ A,B ∈ B, the events A,B are independent. Two random variables X, Y are independent, if they generate independent σ-algebras. It is enough to check that the events A = {X ∈ (a, b)} and B = {Y ∈ (c, d)} are independent for all intervals (a, b) and (c, d). A medical entomologist or experimenter should think of independent *S. damnosum* s.l. agro-village complex narrow riverine, tributary, eco-georeferenceable, immature habitat, random variables as two aspects of the field laboratory which do not influence each other. Each event A = {a < X(ω) < b } would then be independent of the event B = {c < Y (ω) < d }. While the distribution function FX+Y of the sum of two independent random variables is a convolution RR FX(t−s) dFY (s), themoment generating functions and characteristic functions satisfy the formulas MX+Y (t) = MX(t)MY (t) and φX+Y (t) = φX(t)φY (t) (https://en.wikipedia.org/wiki/MathWorld). These identities makeMX, φX may be valuable tools to compute the distribution of an arbitrary finite sum of independent random variables. For an uncoalesced, iterative, explanative, diagnostic, interpolative, moderate resolution, eco-georeferenceable, geo-spectrotemporal, fractionalized endmember, seasonally hyperproductive, *S. damnosum* s.l. oviposition LULC site.

Independence can also be explained in a forecast, vulnerability, eco-georeferenceable, *S. damnosum* s.l. ,predictive, optimizable, geo-spectrotemporal, geospatial, proabilistic paradigm employing conditional probability with respect to an event B of positive probability: the conditional probability P[A|B] = P[A ∩ B]/P[B] of A is the probability that A happens when we know that B takes place[25]. If B is independent of A in the oviposition, moderate resolution, uncolaesced, LULC model, then P[A|B] = P[A] but in general, the conditional probability would be larger. The notion of conditional probability leads to the important notion of conditional expectation E[X|B] of a random variable X with respect to some sub-σ-algebra B of the σ algebra**).** A; it is a new random variable which is B-measurable. (https://en.wikipedia.org/wiki/MathWorld). For B = A, it is the random variable itself, for the trivial algebra B = {∅, }, which may be optimally obtainable by quantiating the usual expectation E[X] = E[X|{∅, }]. If B is generated by a finite partition B1, . . . ,Bn of of pairwise disjoint setsin the eco-epidemiological, *S. damnosum* s.l. habitat model, then E[X|B] is piecewise constant on the sets Bi and the value on Bi is the average value of X on Bi. If B is the σ-algebra of an independent random variable Y , then E[X|Y] = E[X|B] = E[X].

In general, the conditional expectation with respect to B is a new random diagnostic, explanator obtained by averaging on the elements of B. One has E[X|Y] = h(Y) for some function h, extreme cases being E[X|1] = E[X],E[X|X] = X. An illustrative example is the situation where X(x, y) is a continuous function on the unit square with P = dxdyas a probability measure and where Y (x, y) = x. In that case, E[X|Y] is a function of x alone, given by E[X|Y](x) =R 10 f(x, y) dy. This function may be an conditional integral in an iterative , interpolative, moderate resolution, geo-spectrotemrpoal, *S. damnosum* s.l., forecasting vulnerability, epidemiological, probabilistic paradigm for targeting seasonally hyperproductive, *S. damnosum* s.l., trailing vegetation, eco-georeferenceable, oviposition sites on a ArcGIS geoclassified LULC in a narrow, African, riverine tributary ecosystems.A set {Xt}t∈T of random variables defines a stochastic process. The variablet ∈ T is a parameter called ”time”.

Stochastic processes are to probabilitytheory what differential equations are to calculus. An example is afamily Xn of uncoalesced, geospectrotemrpoal, fractionalized endmeber eigenvectors rendered from an orthogonal decomposition of a dataset of eco-georeferenceable, *S. damnosum* s.l., diagnostic explanative, time series, trailing vegetation, narrow, African riverine, agro-village complex, elucidative, random variables which evolve with discrete time n ∈ N. Deterministic dynamical system theory branches into discrete time systems,the iteration of maps and continuous time systems, the theory of ordinaryand partial differential equations(https://en.wikipedia.org/wiki/MathWorld). Similarly, in probability theory, one distinguishesbetween discrete time stochastic processes and continuous timestochastic processes. A discrete time stochastic process is a sequence of randomvariables Xn with certain properties[25]. An important example is when Xn are independent, identically distributed *S. damnosum* s.l. random variables that eco-geographically represent hyppeorductive seasaonl geolocations. A continuoustime stochastic process in such a probabilistic, endmember, iterative interpolative paradigm may be rendered by a family of *S. damnosum* s.l. random variables Xt, where t is real time. An example is a solution of a stochastic differential equation [SDE].With more general time like Zd or Rd random variables are called random fields which play a role in statistical physics. Unfortunately SDE they have not beed employed for any vector arthropod-related, forecast, vulnerability, iterative analyses for targeting prolific seasaonl, eco-georferenceable habitats.

The main flavours of stochastic calculus are the Itô calculus and its variational relative the Malliavin calculus. In probability theory and related fields, Malliavin calculus is a set of mathematical techniques and ideas that extend the mathematical field of calculus of variations from deterministic functions to stochastic processes (e.g., iterative interpolation of fractionalized Rapid Eye TM visibl and NIR wavelength, transmittance , bidirectional frequencies from LULC signature surfaces). For technical reasons the Itô integral is the most useful for general classes of processes but the related Stratonovich integral is frequently useful in problem formulation (particularly in remote engineering disciplines.)

In stochastic processes, the Stratonovich integral is a stochastic integral. The main benefit of the Stratonovich integral for *Similim* habitat, forecast, vulnerability modelling is that it obeys the usual chain rule and therefore does not require Itô's lemma. In some circumstances, integrals in the Stratonovich definition are easier to manipulate. In mathematics, Itô's lemma is an identity used in Itô calculus to find the differential of a time-dependent function of a stochastic process which serves as the stochastic calculus counterpart of the chain rule http://mathworld.wolfram.com). Unlike the Itô calculus, Stratonovich integrals are defined such that the chain rule of ordinary calculus holds.In calculus, the chain rule is a formula for computing the derivative of the composition of two or more functions (e.g., , if f and g are geo-spectrotemporal, uncoalesced, seasonal, *S. damnsoum* s.l. hypeproductive, oviposition functions, then the chain rule would express the derivative of their composition $f \circ g$ where the function maps x to $f(g(x))$ occurs in terms of the derivatives of f and g and the product of functions). These intergrals can be heuristically derived by forming the Taylor series expansion of the function up to its second derivatives and retaining terms up to first order in the time increment and second order in the Wiener process increment. In pure mathematics, the Wiener process gave rise to the study of continuous time martingales. (^ Forum,"Variance of integrated Wiener process", 2009). A martingale is a sequence of random variables (i.e., a stochastic process) for which, at a particular time in the realized sequence, the expectation of the next value in the sequence is equal to the present observed value even given knowledge of all prior observed values (www.sas.edu).

Perhaps the most common situation in which these are encountered is as the solution to Stratonovich stochastic differential equations. A stochastic differential equation (SDE) is a differential equation in which one or more of the terms is a stochastic process, resulting in a solution which is also a stochastic process. SDEs are used to model various phenomena such as unstable stock prices or physical systems subject to thermal fluctuations. (http://mathworld.wolfram.com). Typically, SDEs contain a variable which represents random white noise calculated as the derivative of Brownian motion or the Wiener process. However, other types of random behaviour are possible, such as jump processes. These processes may enable efficient targeting of eco-georeferenceable, geo-spectrotemporally uncoalesced, iteratively interpolative, explanatively, quantitative moderate resolution, trailing vegation, sparsely canopied, turbid, narrow, African riverine, agro-village, seasaonally productivity *S. damnosum* s.l. data to be expressed in a coordinate system invariant form, which would be invaluable when developing stochastic calculus on manifolds other than R^n.

The dominated convergence theorem does not hold for the Stratonovich integral, consequently it is very difficult to prove results without re-expressing the integrals in Itô form. In measure theory, Lebesgue's dominated convergence theorem provides sufficient conditions under which almost everywhere convergence of a sequence of functions implies convergence in the L^1 norm. Its power and utility are two of the primary theoretical advantages of Lebesgue integration over Riemann integration.In mathematics, the integral of a non-negative function of a single variable can be regarded, in the simplest case, as the area between the graph of that function and the *x*-axis. http://mathworld.wolfram.com). The Lebesgue integral extends the integral to a larger class of functions. It also extends the domains on which these functions can be defined which may be applicable to remote targeting hypeproductive iterative interpolative, moderate resolution sparsely canopied, eco-georeferenceable *S. damnosum* s.l. capture points. In the branch of mathematics known as real analysis, the Riemann integral, was the first rigorous definition of the integral of a function on an interval

Suppose that T is a real-valued explanative, random, geosampled, trailing vegetation, turbid water, eco-georeferenceable, partially canopied, medium resolution, LULC, endmember, predictor variable of a *S. damnosum* s.l. hyperproductive, trailing vegation, turbid water, oviposition sits geosampled in a narrow African, riverine tributary ecosystem with an unknown distribution. Let F denote the distribution function of T so that $F(t)=P(T\leq t)$ for $t\in R$. The objective then would be to construct an unbiased estimator of F ,so naturally the first step would be to sample from the distribution of T This would generate a sequence $T=(T_1, T_2, \ldots)$ of independent riverine agro-village, predictor variables, each with the distribution of T and with distribution function F . Think of T as a sequence of independent copies of T . For $n\in N_+$ and $t\in R$, the natural estimator of F(t) would then be based on the first n sample values is $F_n(t)=1n\sum_{i=1}^{n} 1(T_i\leq t)$ which would be simply the proportion of the first n sample values that fall in the interval $(-\infty,t]$. Appropriately enough, Fn is known as the *empirical distribution function* corresponding to the sample of size n (www.mathworld.com). Note that $(1(T_1\leq t),1(T_2\leq t),\ldots)$ would be a sequence of independent, identically distributed indicator variables (and hence is a sequence of Bernoulli trials), and would correspond to sampling from the distribution of $1(T\leq t)$ in the probabilistic paradigm . The estimator $F_n(t)$ would simply employ the sample mean of the first n of these variables. The numerator would be a number of the original geo-sampled, hypeproductive, capture point, eco-georeferenceable, geo-spectrotemporally uncoalesced, seasoanl, *S. damnosum* s.l., oviposition LULC variables with values such as $(-\infty,t]$, which would then have a binomial distribution with parameters n and F(t) . Like all sample means

from independent, identically distributed samples, $F_n(t)$ may satisfy some basic and important properties of an interatively, quantitatively interpolated, geo-spectrotemporally, geosampled, eco-georefernceable, uncoalesced, moderate resolution, endmember signture of a hyperproductiuve, seasonally, imaged, *S. damnsoum* s.l., oviposition site, on a geoclassifiable, LULC geolocation.

Suppose that T has the standard uniform distribution, that is, the continuous uniform distribution on the interval [0,1] in a geo-spectrotemporal, forecasting, *S. damnsoum* s.l., vulnerability, probabilistic paradigm. In this case the distribution function would be simply $F(t)=t$ for $t\in[0,1]$, and as such the sequence of stochastic processes $X_n=\{X_n(t):t\in[0,1]\}$ for $n\in N+$, where $X_n(t)=n\sqrt{}[F_n(t)-t]$ may be quantitatble.As such, the process X_n in the vector arthropod, eco-epidemiological, risk model would have a mean function 0, variance function $t\mapsto t(1-t)$ with a fixed $t\in[0,1]$. The distribution $X_n(t)$ would converge to the corresponding normal distribution as $n\to\infty$. Interestingly, the covariance function of X_n in the *S. damnsoum* s.l. signature interpolator would be the same as that of the Brownian bridge. In probability theory and statistics, the continuous uniform distribution or rectangular distribution is a family of symmetric probability distributions such that for each member of the family, all intervals of the same length on the distribution's support are equally probable (www. mathworld.com). The support would be optimally defined by two eco-georeferenceable,time series, explanatory parameters, *a* and *b*, in the predictive, riverine habitat vulnerability paradigm which would be its minimum and maximum values. The distribution would be abbreviated $U(a,b)$. This support would eco-georgraphically represent maximum entropy probability distribution for a random, explanatively geosampled *Similium* oviposition variate X under no constraint other than that it is contained in the distribution's support.

If $\mathrm{cov}[X_n(s),X_n(t)]=\min\{s,t\}-st$ for $s,t\in[0,1]$ exists in a geo-spectrotemporal, geospatial, *S. damnsoum* s.l. oviposition probabilistic, moderate resolution, iteratively interpolative, eco-epidemiological, trailing, vegetation, turbid water, discontinuously canopied, forecast, vulnerability model. Then $s\leq t$ would be revealed in the eco-georeferenceable residual, time series explanatorial forecasts, From basic properties of covariance, the model would reveal $\mathrm{cov}[X_n(s),X_n(t)]=n\mathrm{cov}[F_n(s),F_n(t)]$.Further, $\mathrm{cov}(\sum_{i=1}^{n}1(T_i\leq s),\sum_{j=1}^{n}1(T_j\leq t))=1n\sum_{i=1}^{n}\sum_{j=1}^{n}\mathrm{cov}[1(T_i\leq s)1(T_j\leq t)]$. But if $i\neq j$ in the dataset of the epidemiological, geo-spectrotemporally geosampled, oviposition, seasonal explanators, then $(T_i\leq s)$ and $1(T_j\leq t)$ would be independent, and hence have covariance. On the other hand, if a moderate resolution, iterative interpolative explanative, moderate resolution, uncoalesced, signature of a hypeproductive, *S. damnosum* s.l., moderate resolution, imaged, immature, seasonal habitat is employed as a dependent variable in a spatiotemporal, iterative, probabilistic, Bayesian iterative matrix then $\mathrm{cov}[1(T_i\leq s),1(T_i\leq t)]=P(T_i\leq s,T_i\leq t)-P(T_i\leq s)P(T_i\leq t)=P(T_i\leq s)-P(T_i\leq s)P(T_i\leq t)=s-st$ hence,$\mathrm{cov}[X_n(s),X_n(t)]=1n\sum_{i=1}^{n}\mathrm{cov}[1(T_i\leq s),1(T_i\leq t)]=s-st$

Bayesian statistics in WinBUGSio® and spatial filter eigenvectors from SAS/GIS® (http://ftp.sas.com) were employed in Jacob et al. [2] for constructing a series of robust, endemic ,multivariate, explanatorial, transmission-oriented, field-operational , forecasting, agro-village capture point, seasonally hyperproductive *S. damnosum* s.l. , oviposition sites on moderate resolution, gridded, geo-spectrotemporal, moderate resolution, predictive risk maps based on a Browinan bridge. The authors developed a framework for a remote habitat-based surveillance system employing PROC NL MIXED, SAS/GIS, WinBUGSio and satellite-derived, landscape-oriented, unbiased, endemic, transmission-related, forecasting ,

explanative, vulnerability models.The authors decomposed the Wishart probability distribution of the sample covariance matrix by employing models generated in PROC NL MIXED and SAS/GIS into probability distributions of eigenvalues and eigenvectors in order to calculate multiple seasonal probabilistic, Bayesian, error estimation, orthogonal matrices employing a datset of eco-georeferenced, geo-spectrotemporally geosampled, uncoalesced, iteratively interpolative, hyperproductive, seasonal, moderate resolution, *S. damnosum* s.l.,endemic, transmission-oriented parameterized covariates. Generalizations of the multivariate inverse gamma densities include Wishart distributions [www.sas.edu]. An important use of the Wishart distribution is as a conjugate prior for multivariate normal sampling [1]. In Jacob et al. [2] these models combined to generate a semiparametric spatial filtering eigenvector approach in AUTOREG to deal explicitlywith uncertainty in the eco-georferenceable, trailing vegation, partially canopied, turbid water, capture point, *S. damnosum* s.l., larval habitat, eco-epidemiological, forecast, vulnerability distribution, probabilistic paradigm by reducing the number of data parameters employing spatially laggedautoregressive models and simultaneous autoregressive spatial models.

Residual estimates from the off-diagonal elements of a covariance matrix were then generated from the spatial filter eigenevector analysis prior to support exporting the geosampled data into a Bayesian estimation matrix. For the fixed, *S. damnosum* s.l. regression parameters, a suitable choice the authors assumed was the diffuse prior, (i.e., $p(\gamma)$ *const*.) but a weakly informative Gaussian prior was also employed. In so doing, second-order Gaussian random walk prior allowed enough flexibility in the iteration process while penalizing abrupt changes in the function. The second-order random walk model is commonly used for smoothing data and for modelling response functions (www.sas.edu). In Jacob et al. [2] the algorithm computationally was efficient which the authors deemed to be due to the Markov properties of the joint (intrinsic) Gaussian density.

The second order random walk (RW2) model is commonly used for smoothing data and for modelling response functions. It is computationally efficient due to the Markov properties of the joint (intrinsic) Gaussian density. For evenly spaced the RW2 model is well established, whereas for irregularly spaced geolocations (e.g., eco-georeferenceable, trailing vegetation, turbid water, *S. damnosum* s.l. African, riceland agro-village, riverine, tributary habitat geolocations) there is no well established construction in the literature. By considering the RW2 model as the solution of a SDE, a discretely observed integrated Wiener process may derive the density preserving the Markov properties in an iterative interpolatve Bayesian inferencial paradigm by augmenting the state-space with the velocities. In so doing, a computationally more efficient RW2 *S. damnosum* s.l., moderate resolution, eco-epidemiological, forecast, vulnerability model for irregular hyperproductive oviposition geolocations using a Galerkin approximation to the solution of the SDE without the need of augmenting the state-space. In mathematics, in the area of numerical analysis, Galerkin methods are a class of methods for converting a continuous operator problem (such as a differential equation) to a discrete problem. Numerical comparison with the exact solution may demonstrate that the error in the Galerkin approximation is small and negligible in optimizable, epidemiological, predictive risk model applications for targeting eco-georeferenceable, hypeproductive *S. damnosum* s.l. immature, trailing vegation, turbid water, immature oviposition sites on geoclassified, moderate resolution LULCs.

Jacob et al. [2] employed WinBUGSio, an SAS macro program, which facilitates remote execution of WinBUGS from within SAS. This is an SAS macro, which does the data handling and input/output from WinBUGS® via SAS®. The program produced a column

format data file based on the geo-spatiotemporally geosampled eco-georeferenced, clinically, field and remote specified *S. damnosum* s.l. riverine, tributray, agro-village irrigated riceland, larval habitat, multivariate, endemic, transmission-oriented, explanatory,paramterizable, time series, interpolatable, predictor, covariate, coefficient estimates and also wrote a list format data file for constants. The macro program then wrote a script file to the WinBUGS directory referencing the appropriate datafile, model file, init file, and log file names. The script then ran WinBUGS in batch mode which read in the node statistics block from the log file. Although there was a requirement to specify the input and output file names and directory path as well as the statistics to be monitored in WinBUGS, the code checked for optimal convergence diagnostics within the geodatabase cyberenvironment. The authors checked for non-normal distributed random errors in the regression equation. Methods for regressing geo-spectrotemporal, geosampled, explanative, vector, arthropod-related, larval habitat, eco-georeferenecable, data rely on the assumption of normality and the use of linear estimation methods (e.g., least squares) to make probabilistic inferences [2].

In the iterative, Bayesian, *S. damnosum* s.l. model, the authors considered the inverse-Wishart distribution which is a proper conjugate prior for an unknown covariance matrix in a multivariate normal model. Some specific analytical results for the inverse-Wishart have been derived; for example, the marginal distribution of a diagonal block submatrix of draws from an inverse- Wishart distribution [www.sas.edu]. In statistics, the inverse Wishart distribution, also called the inverted Wishart distribution, is a probability distribution defined on real-valued positive-definite matrices. In Bayesian statistics it is used as the conjugate prior in a *S. damnsoum* s.l. habitat model for the covariance matrix of a multivariate normal distribution [2].

Thereafter, the authors performed a non-smooth optimization by stabilizing the steepest descent in the riverine, tributary, risk model by exploiting gradient and subgradient information in the regressands. The authors then investigated the behaviour of quasi-Newton (i.e., variable metric) methods, specifically,the well-known Broyden-Fletcher-Goldfarb-Shannon (BFGS) method, to minimize non-smooth functions, both convex and nonconvex in the *S. damnosum* s.l. riverine tributary, geo-spectrotemporally imaged, larval habitat, epidemiological models.

In numerical optimization, the Broyden–Fletcher–Goldfarb–Shanno (BFGS) algorithm is an iterative method for solving unconstrained nonlinear optimization problems.The BFGS method approximates Newton's method, a class of hill-climbing optimization techniques that seeks a stationary point of a (preferably twice continuously differentiable) function. For such problems, a necessary condition for optimality is that the gradient be zero. Newton's method and the BFGS methods are not guaranteed to converge unless the function has a quadratic Taylor expansion near an optimum. These methods use both the first and second derivatives of the function. However, BFGS has proven to have good performance even for non-smooth optimizations.

In quasi-Newton methods, the Hessian matrix of second derivatives does not need to be evaluated directly. Instead, the Hessian matrix is approximated using rank-one updates specified by gradient evaluations (or approximate gradient evaluations).Quasi-Newton methods are generalizations of the secant method to find the root of the first derivative for multidimensional problems. In multi-dimensional problems, the secant equation does not specify a unique solution, and quasi-Newton methods differ in how they constrain the solution. The BFGS method is one of the most popular members of this class.[2] Also in

common use is L-BFGS, which is a limited-memory version of BFGS that is particularly suited to problems with very large numbers of variables (e.g., >1000).

In optimization, quasi Newton methods (a special case of variable metric methods) a real algorithms for finding local maxima and minima of functions [www.mathworld.com]. Quasi-Newton methods are also a generalization of the secant method to find the root of the first derivative for multi-dimensional problem solving [www.sas.edu].In multiple dimensions, the secant equation is underdetermined for Quasi-Newton methods, which were used to find the stationary point of a function in the *S. damnosum* s.l. habitat model when the gradient is 0. Any locally Lipschitz non-smooth function f was viewed as a limit of increasingly ill-conditioned differentiable functions in the geo-spectrotermpoal, moderate resolution, explanatory, time series, dependent, endemic, transmission-oriented, forecast, vulnerability, *S. damnosum* s.l. eco-epidemiological, risk model via “mollifiers”,

In mathematics, mollifiers (also known as approximations to the identity) are smooth functions with special properties, used for example in distribution theory to create sequences of smooth functions approximating nonsmooth (generalized) functions, via convolution. Intuitively, given a function which is rather irregular, by convolving it with a mollifier the function gets "mollified", that is, its sharp features are smoothed, while still remaining close to the original nonsmooth (generalized) function [1]. Unfortunately most of them may have noconsequence for asymptotic convergence behaviour when f is notdifferentiable at its minimizer. These are commonly seen in smooth functions with special properties employed in distribution theory to create sequences of smooth functions approximating non-smooth (i.e., generalized) functions, via convolution however, they have never been applied for seasonal, predictive, vector, arthropod-related, endemic, transmission-oriented, risk modeling.

Lipschitz continuity is an important concept in mathematical analysis. In modern variational analysis, it has been generalized for set-valued mappings. Among many extensions, the pseudo-Lipschitzian property has been recognized as a natural and useful for determining the inverse of a piecewise affine function around a sample point. It is nowcalled by different names, such as the Aubin property or the Lipschitzlike property [www.mathworld.com]. The concept has been also used extensively in the study of sensitivity analysis of optimization problems and variational inequalities. The pseudo-Lipschitzian property also plays an important role in developing generalized differentiation calculi for non-smooth functions and set-valued mappings. Accordingly, for a set-valued mapping rendered from a regressed georeferenced empirical dataset of seasonal, clinical, field and remote, geo-spectrotemporally geosampled, explanatory, *S. damnosum* s.l., endemic transmission-oriented, parameterizable estimators employing$F : Rm \rightarrow\!\!\!\!\rightarrow Rn$, for instance, the Aubin property around$(-x, -y) \in \text{gph } F := \{(x, y) \in Rm \times Rn \mid y \in F(x)\}$ may be efficiently.

Considering multiple classes of error distributions in a geo-spectrotemporal, moderate resolution, *S. damnosum* s.l., larval habitat, immature capture point, eco-epidemiological, African narrow tributary, eco-georeferenceable, riverine, agro-village, larval habitat multivariate, seasonal, endemic transmission-oriented, predictive risk model may be a useful alternative to the normal distribution: t-distributions, generalized error distributions, and Tukey’s contaminated normal distribution. It may be assumed that these probabilistic distributions are robust in the sense that any outliers in a seasonal geosampled *S.*

damnosum s.l. riverine larval habitat empirical ecological dataset logically would have less of an effect on the estimated mean (i.e., regression) function than on the residual forecasts targeting the statistically significant endemic transmission-oriented basednormal/non-normal distributions. At an intuitive non-mathematical level, the use of heavy tailed *S. damnosum* s.l. habitat distributions in a seasonal infectious disease model may allow for a small number of large error residuals to be quantitated.

Further, it may be assumed that since a normal distribution would force the predicted residuals to be within a few standard deviations of the mean, the *S. damnosum* s.l. larval habitat outliers could adversely affect the estimated mean, biasing the estimate in a time series explanatory, clinical, field and remote specified risk-related endemic transmission-oriented, predictive model by greatly inflating the estimated standard error of the mean. It also may be assumed that these outliers would cause loss of predictability power in the residually geo-spectrotemporally regressed derivatives increasing the width of confidence intervals in the risk model outputs. Therefore, PROC NL MIXED SAS/GIS, WinBUGSio, and moderate resolution -derived regression-based, forecast, vulnerability , probabilistic paradigms can account for any multivariate predicted variability in a eco-georeferenced, seasonal, geosampled empirical dataset of clinical, field and remote, geo-spectrotemporally geosampled, explanatory covariate coefficients for statistically representing larval habitat productivity of *S. damnosum* s.l. in a riverine tributary, ecosystem agro-village, study site.

Constructing robust, ecological-weighted, regression equations and global autocorrelation statistics to identify linear and non-linear based elucidative predictors associated to hyperproductive, seasonal, *S.damnosum* s.l., trailing vegation, turbid water,capture point, immature habitats and the quantitate latent autocorrelation uncertainty coefficients in the model residual forecasts using a covariance matrix rendered from an eigenfunction decomposition spatial filter algorithm may reveal parameterizable covariates associated with hypeproductive oviposition sites on geoclassifiable, moderate resolution LULCs. Further, generate inverse-Wishart priors within a Bayesian probabilistic estimation framework for forecasting regression-based distribution of multiple clinical, field and remote-sampled endemic transmission-oriented, *S. damnosum* s.l. riverine, agro-village complex, unmixed, larval habitat explanatory, signature-related, iteratively interpolatable, covariate coefficients geo-spectrotemporally geoampled in an narrow riverine tributary African agro-ecosystem may forecast precisely unknown, un-geosampled, hypeproductive, seasonal habitats.

Due to the usage of multivariate spectral channels in various wavelengths, an image mixed pixel (“mixel”) is actually a mixel vector, of which each expositorily fractionalized, endmember component is a single mixel in an image (e.g., moderate resolution, seasonally, geo-spectrotemporally geosampled, discontinuously canopied, eco-georeferenceable, *S. damnosum* s.l., immature, capture point,oviposition site) acquired by a particular spectral channel. As a result, different elucidative, geoclassifiable, multi-resolutionary,geo-spectrotemporal, endmember, seasonally explanative datset of LULC substances (e.g., eco-georefereneable, foliar height diversity) may accurately regressively delineate discontinuous, canopied, uncoalesced elements essential for iteratively interpolating seasonal, *Similium,* hyperproductive, oviposition signatures at the landscape, riverine, tributary, agro-village scale. This scale can be also measured by explicatively iteratively, quantitatively interpolated, orthogonally decomposed, fractionalized, endmember signature in a single mixel vector. Such proxy, illuminative, bidirectionally reflective, optimally explanatorily geoclassifiable,

moderate resolution, LULC substances may appear either as sub-mixel, explanative, parameterizable, covariate weightage of a eco-georeferenceable, eco-epidemiological, study site, capture point scale or a form mixed by other proxy substances in a mixel vector.

Linear spectral mixture analysis is a common acceptable approach for optimizing hierarchically-oriented, frequentistic, algorithmic, geoclassification, sub-mixel optimization routines in ArcGIS, for optimally defining unique signatures of pure ground components (i.e., endmembers) and linear combinations of endmember materials (i.e, eigenvectors). In the simplest case, a radiance endmember optimization problem consists of maximizing or minimizing a real function by systematically choosing fractionalized, orthogonal, spatial filter, endmember and eigenvector, input, wavelength, unmixed transmittance values from within an empirically, optimally parameterizable, dataset of time series, frequentistic-oriented, probabilistically regressable, moderate resolution, expositively forecastable, uncoalesced, emissivity values of a function. According to Jacob et al [22], geo-spectrotemporally geoclassified seasonally prolific, eco-georeferenceable, *S. damnosum* s.l., geospatially uncoalesced datsets of capture point, time series, regressed, uncoalesced, LULC patterns vector libraries is cartographically illustratable via an eigenfunction decomposition algorithm employing a particular spatial correlation, weighted, grid matrix in ArcGIS (e.g., Geostatistical Analyst ^{TM}).This data may be projected onto a orthogonal complement of a dominant baseline subspace. More generally, time series, explanatorial, LULC optimization in ArcGIS can render robust, unmixed, regressively synthesiziable, sub-mixel, orthogonal, eigenvector values for vulnerability mapping eco-georeferncable, hyperproductive, seasonal, trailing vegetation, turbid water, partially shaded, *S. damnosum* s.l., immature, capture point, ecosystem complex, iterative interpolative, forecastable, objective functions given a defined domain, or a set of fractionalized sub-mixel constraints. These geo-spectrotemporal, endmember data points could include a variety of different types of unmixed, objective, proxy, eco-geophysiological, iteratively, quantitatively interpolative, time series, frequentistic, LULC signature, functions [e.g., vertical foliage of discontinuous, forest canopy (i.e., gaps) during dry season, nitrogen distribution in an irrigated, narrow, tributary, agro-village, complex, peripheral, flooded habitat) which would be cartographically optimally delineated employing multiple, geoclasssifiable, stratified polygons in ArcGIS. The method would consist of aggregating seasonal, eco-geographical, coordinates of, explanative, proxy, polgonized, endmember LULC, time series, stratifiable regions of a discontinuous, sparsely shaded, seasonal hyperproductive, optimally parameterizable, *S. damnosum* s.l., geo-spectrotemporal, georeferenceable, capture point, in ArcGIS based on an eigenanalyses employing moderate resolution-derived, fractionalized, Euclideanized, sub-mixel, distance-related, categorical variables. Fractionalized orthogonalized, explanative endmembers can be identified by maximizing a simplex volume, or finding maximal distances in subsequent subspace projections, while unmixing may consider a simple projection problem in the riverine tributary, vulnerability probabilistic paradigm. Since many of these algorithms may be written in terms of distance geometry in ArcGIS, where mutual distances are the properties of interest instead of Euclidean coordinates, an unmixing chain may be optimistically quantitated using robustly, parsimoniously uncoalesced, iteratively interpolative, discontinuous, sparsely shaded, geo-spectrotemporal, partially canopied, distance metrics. In so doing, preprocessing steps such as nonlinear, dimensionality reduction or data whitening, and several nonlinear unmixing models such as the Hapke and bilinear models, may be optimally constructed in ArcGIS employing a subset of proxy, orthogonalized, explanatively geoclassifiable, eco-georeferenecable, LULC signature, spatial filters for expressing surface spatial structural discontinuity variables in partially canopied, trailing vegetation, seasonally, hypeproductive, narrow, African, riverine tributary, agro-

village complex, capture point, oviposition site vulnerability, forecast models, which may be deemed mappable at different spatial scales. If so, transformations may be conducted in data spaces where the endmember data may optimally depicit simulations of hyperprobabilistic, hyperendemic geolocations of eco-georeferenceable, iteratively interpolated, seasonal, hyperproductive habitats, positively autocorrelated along a riverine tributary corridor employing abundance and distrubtion collection points in ArcGIS based on time series, immature, productivity, count data, predictor variables with a corresponding metric (i.e., Morans *i* coefficient).

Different metrics in geometry-based, moderate resolution, immature, *S. damnosum* s.l., capture point, geo-spectrotemporal algorithmic extraction processes in ArcGIS may demonstrate the results for some well-known metrics, such as the Mahalanobis distance. Further, for intimate mixing, a polynomial, post-nonlinear, model estimators and graph-geodesic distance, endmember measurements may be regressively or cartograpically quantitated from a field-operational, eco-epidemiological, empirical dataset of eco-georeferenceable, uncoalesced, moderate resolution, parameterizable, wavelength transmittance, endmember frequencies.

The Mahalanobis distance is a measure of the distance between a point P and a distribution D which is a multi-dimensional generalization of the idea of measuring how many standard deviations away P is from the mean of D. This distance is zero if P is at the mean of D, and grows as P moves away from the mean: along each principal component axis, it measures the number of standard deviations from P to the mean of D. If each of these axes is rescaled to have unit variance, then Mahalanobis distances computed of seasonally hypeproductive, eco-georeferenceable geolocations of multiple, iteratively interpolative, eco-epidemiological, capture point, *S. damnosum* s.l. oviposition, geo-spectrotemporal, geoclassifiable, LULC sites in a geo-classifiable, ArcGIS, stratifiable, moderate resolution, polygon may correspond to standard Euclidean distance in the transformed space (Figure 4). Mahalanobis distance is unitless and scale-invariant, and takes into account the correlations of the data set (www.esri.com). The canonical Mahalanobis distance is defined as the empirical multivariate location and scatter, respectively[26]. This defination excludes the intercept. For Gaussian distributed *S. damnosum* s.l. habitat data, the distance of an observation $x_i$to the mode of the distribution can be computed using its Mahalanobis distance: $d_{(\mu,\Sigma)}(x_i)^2 = (x_i - \mu)'\Sigma^{-1}(x_i - \mu)$where $\mu$and $\Sigma$are the habitat geolocation and the covariance of the underlying Gaussian distribution.In practice, $\mu$and $\Sigma$are replaced by some estimates. The usual covariance maximum likelihood estimate is very sensitive to the presence of outliers in the data set and therefor, the corresponding Mahalanobis distances are. In statistics, an outlier is an observation point that is distant from other observations.[1][2] An outlier may be due to variability in the measurement or it may indicate experimental error; the latter are sometimes excluded from the data set[25]. Outliers can occur by chance in any distribution, but they often indicate either measurement error or that the population has a heavy-tailed distribution One would better have to use a robust estimator of covariance to guarantee that the estimation is resistant to “erroneous” observations in the data set and that the associated Mahalanobis distances accurately reflect the true organisation of the observations.The relation between the Mahalanobis distance and the hat matrix may be quantized as: $H = (h_{ij}) = X(X^TX)^{-1}X^T h_{ii} = \frac{1}{n-1}MD_i^2 + \frac{1}{n}$ under certain assumptions, where the distribution of th ML estimator of a vector of S. damnsoum s.l. moderate resolution LULC parameters can be approximated by a multivariate normal distribution with mean and covariance matrix . In this model the log-likelihood of one capture point observation from the

sample, evaluated at the true parameter would be the gradient where the vector of first derivatives of the log-likelihood is unknown .Because the habitat variable is unknown, also this covariance matrix is unknown.. Under these assumptions we also have that the information equality holds, so thatwhere the Hessian matrix is the matrix of second-order partial derivatives of the log-likelihood function.(see Figure 4)

Figure 4 A flexible ArcGIS processing chain, within a Hessian matrix of proper Mahalanobis distance functions

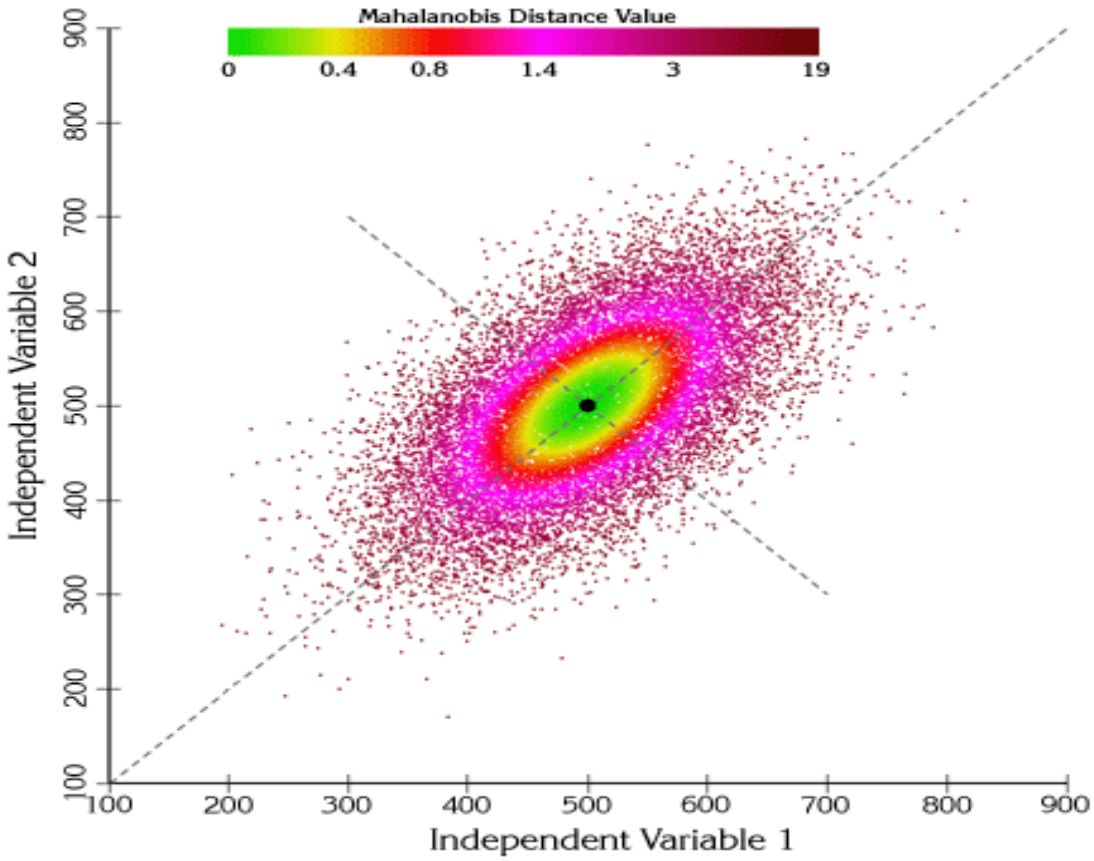

For multivariate, explicity diagnosable, fractionalized, moderate resolution, geo-spectrotemporal,eco-georefernceable, empirical, hyperproductive, *S. damnosum* s.l. oviposition, eco-epidemiological, seasonal, capture point, uncoalesced, proxy signature endmember datasets, the classical, nonrobust, estimate of a geolocation of interest (e.g., seasonally hyperproductive, trailing vegetation, turbid water, discontinuously canopied, riverine tributary, agro-village, flooded habitat) would be the vector mean which in ArcGIS could be simply tabulated as the explanative vector whose *i*th component is the mean of the *i*th geosampled, explanatorial, iterative, quantitative interpolative, variable. The classical, nonrobust estimate of scatter for a forecast vulnerability, moderate resolution, wavelength, emissivity, frequency, probabilistic, *S. damnosum* s.l. paradigm may be the covariance matrix. In a seasonal, vector arthropod-related, eco-epidemiological, risk analyses, a covariance matrix (also known as dispersion matrix or variance–covariance matrix) would be a matrix whose element in the *i*, *j* position (e.g., habitat capture point, covariate and

endmember, uncoalesced probabilistic regressable, coefficient value) would be the covariance between the i^{th} and j^{th} elements of a random vector. An uncoalesced, trailing vegation, turbid water, partially canopied, hyperproductive, seasonal, eco-georeferenceable multivariate, *S. damnsoum* s.l. oviposition, capture point, sub-mixel, random variable or random vector may be revealed as a list of mathematical variables in ArcGIS whose value is unknown, either because the value has not yet occurred or because there is imperfect knowledge of its value. These individual riverine, explanatorial, endmember, oviposition, seasonal, habitat variables in a random vector could be grouped together in ArcGIS since there would be correlations among them Correlation is any of a broad class of statistical relationships involving dependence, though in common usage it most often refers to the extent to which two variables have a linear relationship with each other[25]. These sub-mixel habitat estimators may represent different properties of an individual statistical unit in a *S. damnosum* s.l., oviposition, targeting model. For example, while a given *Similium* oviposition LULC site has an ArcGIS quantifiable, specific canopy age and height, the representation of any eco-georeferenceable, hyerproductive, seasonal habitat may be revealed employing a regression equation whereby a within group random vector could be a response variable. Normally each element of a random vector is a real number [25]. Random vectors are often employed as the underlying implementation of various types of aggregate, random, geo-spectrotemporal, LULC variables within ArcGIS cyberenvironments , (e.g. a random matrix, random tree, random sequence, stochastic process, etc)

An outlier in a forecast, vulnerability, seasonal, moderate resolution, geo-spectrotemporal, *S. damnosum* s.l., hyperproductive, oviposition, explanatorial, diagnostic, probabilistic endmember, paradigm, may be optimally definable observation whose Mahalanobis distance from is greater than some cutoff value generated in ArcGIS. In statistics, an outlier is an observation point that is distant from other observations [25]. An outlier in a forecast, *S. damnosum* s.l. eco-epidemiological, eco-georefrenceable, geo-spectrotemporal, vulnerability model may be may be due to variability in the measurement or it may indicate experimental error; the latter are sometimes excluded from the data set [22] Outliers in empiricial, vector, arthropod-related, entomological, forecasting datasets can occur by chance in any distribution, but they often indicate either measurement error or that the population has a heavy-tailed distribution. In the former case an expeimenter or medical entomologist may wish to discard the residual predicted regressands or use statistics that are robust to outliers, while in the latter case the targeted hyperproductive, eco-georeferenceable, prolific, seasonal, ovipoisition sites on geoclassifiable, moderate resolution, stratified LULCs can indicate that the distribution has high skewness. According to Jacob et al. [22]any assumption of a normal distribution would be violated. If assumptions are violated in a forecasting, trailing vegation, seasonally hyyperproductive, eco-georeferenceable, agro-village, *S. damnosum* s.l. seasonal capture point, regresssion equation then the model findings will be misspecified (e.g., in a Possionian probabilistic paradigm if the varaince in not equivalent to the mean). A frequent cause of outliers is a mixture of two distributions, which may be two distinct sub-populations, or may indicate 'correct trial' versus 'measurement error'; this is modeled by a mixture model.

In most larger samplings of data, some data points will be further away from the sample mean than what is deemed reasonable [24]. This can be due to incidental systematic error or flaws in the theory that generated an assumed family of probability distributions, or it may be that some observations (remotely targeted, hyperproductive, *S. damnosum* s.l., seasonal, prolific, oviposition sites on geoclassifiable LULCs) are far from the center of the data. Outlier points can therefore indicate faulty data, erroneous procedures, or areas where a

certain theory might not be valid in a riverine, narrow, tributary trailing vegetation, turbid water, partially or dense canopied, seasaonal hyperproductive *S. damnosoum* s.l. habitat. However, in large samples, a small number of outliers is to be expected (and not due to any anomalous condition) [25].

As in the univariate case, both classical estimators are sensitive to outliers in seasonal *Simiulum* habitat, geosampled, eco-georeferenceable, empirical datasets. Consequently, medical entomologists and experimenters may create robust estimates (prolific, seasonal, iteratively, quantitatively interpolated, *S. damnosum* s.l., ovipoisition sites on geoclassifiable LULCs employing the center and the scatter (covariance) matrix.

Tradtionally difference between a scatter matrix and the covariance may be probabilistically regressively quantited in an ArcGIS cyberenvironment. Some distributions, such as elliptical, time series, *S. damnosum* s.l. geo-spectrotemporally uncoalesced, iteratively interpolative, endmember distributions, may not have a covariance matrix but most definitively will always have a "scatter" matrix (see Jacob et al. [22]. Thus, the covariance and scatter matrix may not coincide in a regression cartographic geodatabase. The scatter matrix is a function of a sample set that estimates the covariance matrix [25]. There are distributions for which the covariance is undefinable (e.g., a kriged, *S. damnosum* s.l. trailing vegation, turbid water, moderate resolution, habitat, proxy LULC signature) , but if an experimenter or medical entomologist restricts him or herself to some finite set of sample, explanatorial, diagnostic, normalized, eco-georeferenceable, hyperproductive, riverine, tributary, ovipoistion, capture point, geospatial, geoclassifiable, moderate resolution, stratifiable, expositorial, LULC data points, these Universal Transverse Mercator (UTM) points and other imaging geocoordinates may mechanically form the scatter matrix based on an estimate of the the mean of a 1-variable distribution by taking the average of a sample. The Universal Transverse Mercator (UTM) and Universal Polar Stereographic (UPS) coordinate systems both use a metric-based cartesian grid laid out on a conformally projected surface to locate positions on the surface of the Earth which is not a single map projection but a series of sixty, each covering 6-degree bands of longitude(www.esri.com) In so doing, the two matrices may coincide in ArcGIS (assuming the covariance is definable.

In probability theory, the law of large numbers (LLN) is a theorem that describes the result of performing the same experiment a large number of times. According to the law, the average of the results obtained from a large number of trials should be close to the expected value, and will tend to become closer as more trials are performed. The LLN is important for geo-spectrotemporal, predictive, endmember modelling, uncoalesced, moderate resolution, iteratively interpolative signatures of eco-georeferenceable, explanatorial, trailing vegetation, narrow, riverine tributary, *S. damnosum,* s.l., unbiased model estimators as it would stablize long-term results for the averages of some random geosampling seasonal events. For example, while a hyperproductive, capture point, oviposition, LULC site may lose some immature productivity throughout an eco-epidemiological, sample frame its immature values will tend towards a predictable percentage over a large number geosampled habitats. It is important to remember that the LLN only applies (as the name indicates) when a large number of observations are considered [25]. There is no principle that a small number of capture point, *S. damnosum* s.l., habitat observations will coincide with the expected value or that a streak of one geosampled oviposition, capture point value will immediately be "balanced" by the other values (e.g., gambler's fallacy). A form of the law of large numbers would thus explicity state that under certain conditions (which may be stronger in the *S. damnosum* s.l. habitat forecast vulnertability paradigm than just the existence of the

covariance matrix) the limit for large *n* would be explantively quantitatable as the scatter matrix approaches the covariance matrix in ArcGIS .

For robustifiable estimation of an uncoalesced, explanative, geo-spectrotemporal, moderate resolution, endmember dataset of eco-georeferenceable, trailing vegetation, turbid water, partially canopied, hyperproductive, *S. damnosum* s.l. ovipoisition, capture point, parameterizable, wavelength, transmittance frequencies, a Minimum Covariance Determinant (MCD) in ArcGIS may be algorithmically employable. The main idea of this matrix is due to Rousseeuw (1985), but the algorithm that is commonly used for predictive endmember modeling was developed by Rousseeuw and Van Driessen (1999). The MCD algorithm for a forecast, vulnerability,sub-mixel, probabilistic paradigm for cartographically and regressively revealing geolocations of eco-georeferenceable seasonal, S. *damnosum* s.l., hyperproductive, oviposition sites on geoclassifiable, moderate resolution LULC would work by sampling *h* observations from the data over and over again, where *h* is typically in the range $n/2 < h < 3n/4$. The "winning" subset would be the *h* points whose covariance matrix has the smallest determinant. Points far from the center of this subset would be optimally excluded in the sub-mixel geo-spectrotemporal analyses in ArcGIS and the center and scatter of the remaining points would be parsimoniously employed as the robust estimates of the prolific geolocations and scatter. Recently, Hubert, Rousseeuw, and Verdonck (2010) have published a deterministic algorithm for the MCD. The SAS/IML language includes the MCD function for robust estimation of multivariate location and scatter

The ROBUSTREG procedure can also compute MCD estimates. Usually, the ROBUSTREG procedure is used as a regression procedure, but you can also use it to obtain the MCD estimates by "inventing" a response variable. The MCD estimates are produced for the explanatory variables, so the choice of a response variable is unimportant [www.sas.edu]. In contrast, the ROBUSTREG procedure uses the MCD algorithm to identify influential observations in the space of explanatory (that is, X) variables These are also called high-leverage points. They are observations that are far from the center of the X variables. High-leverage points of seasonally hyperporoductive *S. damnosum* s.l., oviposition, capture points are very influential in ordinary least squares regression, and that is why it is important to identify them. s are the robust distances[22]. The "leverage" variable is an indicator variable that tells you which observations are far from the center of the explanatory variables [25]. There may be are multivariate, explanatively diagnostic, elucidatively uncoalesced, moderate resolution, inconspicuous, LULC "outliers" in the space of the X variables in a forecast, vulnerability, *S. damnosum* s.l., probabilistic, targeting , geo-spectrotemporal, paradigm although they may not be necessarily outliers for the response (Y) variable.

Elucidatively uncoalesced, proxy geo-spectrotemporal, signature-oriented, expositively fractionalized, radiance, synthetic orthogonal, eigenvectors may also be employable as optimal unbiased, eco-physiological, bio-geophysical georeference markers in forecasting vulnerability time series paradigms constructed in ArcGIS (e.g., Geostatistical Analyst ™). Both discrete-return and non-diffuse, moderate resolution, metaheuristically, expositorily optimizable waveforms may also be quantitatively employable to identify unknown, un-geosampled, narrow, tributary, hyperproductive, seasonal, *S. damnosum* s.l., immature capture points in an African, agro-village, riverine ecosystem, empirical, eco-georeferenceable, regressed dataset of iteratively explanatorily, interpolatable, uncoalesced, hyperproductive, habitat proxy, LULC signature covariates. Whilest so doing, the algorithm would retrieve the fractionalized, endmember, discontinuous, photosynthetic and non-

photosynthetic elements of the oviposition, capture point including canopy height, biomass, vertical distribution of leaves and branches, canopy closure, Leaf Area Index (LAI) canopy height profile and vertical foliar diversity. Leaf area index is a dimensionless quantity that characterizes plant canopies which is definable in ArcGIS as the one-sided green leaf area per unit ground surface area (LAI = leaf area / ground area, m^2 / m^2) in broadleaf canopies. (www.esri.com). Employing multiple and partial,time series, regression analyses in ArcGIS (e.g., Geostatistical Analyst ^{TM}) employing an eigenfunction decomposition, orthogonal, spatial filter algorithm, thereafter, the moderate resolution, endmember variables may be manipulated in geospace so as to take into account latent autocorrelation coefficients which can reveal wavelength, transmittance, clustering, moderate resolution,coefficient emissivity, frequencies at a "hot spot"(hyperproductive, seasonal, agro-village, narrow, riverine tributary, *S. damnsoum* s.l. oviposition, moderate resolution, imaged LULC site). Autocorrelation in filters and in the regression residuals can be used as stopping rules to define which filters will be used in an endmember probabilistic analyses[24].

A Rapid Eye ^{TM} unbiased, seasonal, geo-spectrotemporal, vertical, canopy height, diagnostic, sub-mixel, profile model was constructed in a ArcGIS cyberenvironment in Jacob et et al. [22] for obtaining a footprint of a eco-georeferenceable, hyperproductive, seasonal, *S. damnosum* s.l., eco-georferenceable, capture point in a geosampled, narrow tributary, African agro-village, ecosystem complex (Chutes Dienkoa) in Burkina Faso. Initially, the geosampled data was tested in a closed canopy environment as a way of optimally extracting robustifiable, iteratively interpolative, explicative, eco-georeferenceable, seasonal, vertical foliage profiles from Rapid Eye ^{TM} raw-waveform. The small-footprint, uncoalesced, interpolated data was validated in an neighboring, sparsely shaded, discontinuously canopied, immature, capture point, hyperproductive, habitat plot employing estimates rendered from a stochastic iterative interpolator [e.g., Ordinary krige-based algorithm) in Geospatial Analyst ^{TM} which revealed a optimum rate (92.1%) in field-verification ("ground truthing") exercises.The methodology itself was enhanced by implementing a dataset-adjusted, reflectance, ratio calculation in ArcGIS which allowed a capture point signal, to be calibrated against a fixed, mixel, geo-spectrotemporally extracted up to a wavelength of 1,250 nm. As a by-product of the methodology, effective, quantifiable, decomposed, LAI estimates were optimally derived and compared to hemispherically reterived, discontinuous, canopied values.

The canopy height profile procedure presented in Jacob et al. [22] for the geo-spectrotemporally uncoalesced, footprint Rapid Eye ^{TM} data was tested in a canopy environment as a way of extracting vertical foliage profiles from raw-waveform of the datasets. An adaptation of this method to small-footprint data was validated in a sparse canopy forest, plot and agro-village riverine tributary site in Burkina Faso and northern Uganda. The methodology itself was enhanced by implementing a dataset-adjusted reflectance ratio calculation according in the processing chain, and tested against a fixed ratio of 0.5 estimated for the Rapid Eye wavelength data (nm). As a by-product of the methodology, effective LAI estimates were derived and compared to hemispherical, shade canopied, decomposed, endmember values. To assess the influence of the Rapid Eye^{TM} aggregation area size based on the remotely diagnosed estimates in the sparse canopy, riverine, seasaonl, LULC agroecosystem environment, multiple LAIs were generated in ArcGIS by aggregating waveforms to plot- and site-level footprints (e.g., *Similium* habitat plot/site-aggregated) as well as in 5m processed grids. Rapid Eye^{TM} profiles were then compared to field biomass profiles generated based on field canopy discontinuous gap measurements. The correlation between field and Rapid Eye ^{TM} profiles was very high, with a

mean R^2 of 0.77 at plot-level and 0.81 at site-level for 52 *S. damnosum* s.l. trailing vegetation, Precambrian rock, turbid water, riverine plots. Gridding had impact on the correlation between Rapid Eye ™ field elucidative profiles and on the optimally quantitated, adjusted, reflectance ratio. Gridding and the dataset-adjusted, reflectance ratio were found to improve the correlation between raw-waveform Rapid Eye™ and hemispherical LAI estimates, yielding the highest correlations of 0.64 at plot-level and of 0.87 at the oviposition site-level. This proved the validity of the approach and superiority of endmember dataset-adjusted reflectance ratio over a fixed ratio of 0.5 for LAI estimation for revealing the adequacy of iteratively, quantitatively, interpolating, uncoalesced, small-footprint, Rapid Eye ™ signatures for LAI and LULC estimation in explicative, discontinuously canopied, narrow, African, riverine tributaries for remotely targeting, hyperproductive, trailing vegetation, sparsely canopied, eco-georeferenceable, *S. damnosum* s.l. seasonal geolocations. Treatment of habitat pertubations should be based on abundance and distribution of immature, seasonally quanatitaive, productivity counts [25].

To assess the influence of the Rapid Eye ™ aggregation, seasonal, hypeproductive, explanatorial, capture point, LULC area size on the probabilistically regressable estimates geosampled in a sparse, narrow tributary, African, agro-village complex, geo-spectrotemporally geosampled, moderate resolution, eco-epidemiological, elucidatively decomposed dataset of discontinuously canopied, height profiles and LAIs generated by aggregating waveforms to immature habitat- and site-level may metaheuristically optimally render 5m, eco-georeferenceable, proxy, LULC footprints (habitat/site-aggregated) in 5 km processed, ArcGIS, stratified, geo-spectrotemporally weighted, grid matrix. Rapid Eye ™ profiles may then be then comparablable to iteratively quantitatively, explanatorily geospectrotemporally interpolative, uncoalesced, field biomass profiles optimally generated based on unbiased, signature-related, moderate resolution, ArcGIS-derived, decomposed, wavelength, radiance measurements. The correlation between field and Rapid Eye ™ profiles may be very high, with a mean for seasonally hypeproductive, discontinuous, immature, infrequently canopied, sparsely shaded, hyperproductive, seasonal, eco-georeferenceable, immature habitats and corresponding validation sites. Gridding and employing a dataset-adjusted reflectance canopy ratio may improve the correlation between raw-waveform, Rapid Eye™ and hemispherical LAI estimates in ArcGIS. The residual regression tabulations may optimally yield elucidative, time series correlations at the eco-georeferenceable, capture point-level with a computatable mean for robustly parsimoniously iteratively, quantitatively interpolating uncoalesced, explanatorily forecastable geo-spectrotemporally, vertical canopied, hyperproductive, immature, narrow riverine tributary, agro-ecosystem habitat, LULC signatures. The validity of the approach and its regressability may reveal superiority of Rapid Eye ™ fractionalized, endmember dataset-adjusted reflectance ratio over a mixel fixed ratio for LAI estimation which may unveiled the adequacy of 5m, proxy, Rapid Eye signal for LAI estimation for optimally identifying, sub-mixel, discontinuous canopied, sparsely shaded, trailing vegetation, eco-georefernceable, turbid water, geo-spectrotemporally explanative, hyperproductive, seasonal, S. *damnosum* s.l., immature habitat, geospatial aggregations in narrow tributary, African, agro-village, ecosystem complexes.

Spectral unmixing is an important technique for hyperspectral data exploitation, in which a mixed spectral signature is decomposed into a collection of spectrally pure constituent, derivative spectra which may represent a set of correspondent fractions,or *abundances*, that indicate the proportion of each endmemberpresent in the mixture[25]. Over

the last years, several algorithmshave been developed for automatic or semiautomatic endmember extraction. Some available approaches assume that the input dataset contains at least one pure spectral signature for each distinct material (e.g., decoposed endmember of a moderate resolution, seasonal ecogeoreferenceable, trailing vegetation, hyperproductive, *S. damnosum* s.l., partially canopied, turbid water, agro-village complex, narrow tributray, oviposition LULC site) and further conduct a search for the most geo-spectrally pure signatures in the high-dimensional space spanned by the hyperspectral data. Among these approaches, those aimed at maximizing the volume of the simplex that can be formed using available signatures have found wide acceptance in literature. However, the presence of spectrally pure constituents is unlikely in remotely sensed hyperspectral scenes due to spatial resolution, mixing phenomena, and other considerations (e.g., looding of a hyperproductive, riverine, *S. damnosum* s.l. habitat). In order to address this issue, other available algorithms have been developed to generate *virtual*endmembers (not necessarily present among the input data samples) by finding the simplex with minimum volume that encloses all available observations. Jacob et al. [3] discussed maximum-volumeversus minimum-volume enclosing solutions and further develop a novel algorithm in the latter category which incorporated the fractional abundance, sub-mixel estimation as an internal step of the endmember searching process (i.e., it did not require an external method to produce endmember fractional abundances). The authros so for aiding in iteratively quantitatively, geo-spectrotmporally interpolating an uncoalesced, 5m, *S. damnosum* s.l.. trailing vegetation, Precambrian rock, turbid water, LULC signature . The method was based on iteratively enclosing the geo-spectrotemporally geosampled, endmber observations in a lower dimensional space and removing observations that were most likely not to be enclosed by the simplex of the endmembers to be estimated. The performance of the algorithm was investigated and compared to that of other algorithms (with and without the pure mixel assumption)employing synthetic and moderate resolution data sets collected by Rapid Eye ^{TM} imaging instruments

Many algorithms have been developed in Linear Spectral Mixing Algoirthms (LSMA), for conducting, decomposeable, sub-mixel, explanatively fractionalized, time series, radiance analysis and sub-mixel geo-classification. However, a constrained LSMA may actually produce better results than unconstrained LSMA especially in a probabilistically regressable, time series, dependent, decomposeable datasets of eco-georeferenceable, empirically uncoalesced, moderate resolution, discontinuously canopied, iteratively, fractionalized endmember abundance and signature estimations rendered from a seasonally, hyperproductive, trailing vegetation, turbid water, sparsely shaded, discontinuously canopied, narrow tributary, African agro-village complex, geo-spectrotemporally geosampled, *S. damnosum* s.l. capture point. The LSMA is generally preferred and implemented in unconstrained spectral unmixing paradigms [24]. This is because the constrained LSMA cannot be solved analytically and must rely on numerical solutions, compared to the unconstrained LSMA that has closed-form solutions, such as least squares based LSMA approaches, signal-to-noise ratio (SNR)-based orthogonal subspace projection (OSP), and Mahalanobis distance-based Gaussain maximum likelihood estimation (GMLE). These approaches for optimally obtaining unconstrained, diagnostic, metaheuristically explicatively, eco-georeferenceable, moderate resolution, trailing vegetation, turbid water, discontinuously canopied, narrow tributary, African complex ecosystem, seasonal, *S.damnsoum* s.l capture points, may employ second-order, sub-mixel, decompositional, statistics-based techniques in ArcGIS and arrive at the same matched filter. Consequently, they can be considered least square error (LSE)-based approaches.However, individually the LSE may not necessarily be the optimal criterion to measure classification error in a seasonal, *S. damnosum* s.l. forecast vulnerabilityparadigm.

The method of least squares is a standard approach in regression analysis to the approximate solution of overdetermined systems,(i.e., sets of equations in which there are more equations than unknowns). "Least squares" means that the overall solution minimizes the sum of the squares of the errors made in the results of every single equation.The most important application is in data fitting. The best fit in the least-squares sense can minimize the sum of squared residuals, a residual being the difference between an observed *S. damnosum* s.l. decomposed endmember value and the fitted value provided by a model [25].

It may be interesting to employ the squared residuals in a forecast, vulnerability, diagnostic, geo-spectrotemrpoal, eco-georeferenceable, explanatorial, geospatial, seasonally hypeproductive, trailing vegetation, turbid water, capture point, *S. damnosum* s.l. model instead of the absolute residuals in OLS estimation of a datset of empirically , orthogonally decomposed , moderate resolution, endmember, wavelength, transmittance emissivity frequencies.Actually in the definition of standard deviation, it may not be necessitated to square the difference from the mean to get the mean (E) and take the square root back at the end. It may be more strategic to quantitate the absolute value of the difference instead in a *S. damnosum* s.l. capture point model and tabulate the expected value (mean) of those time series, habitat endmember regressands that show the variation of the geosampled habitat data. The number is going to be different from square method (i.e., the absolute-value method will be smaller), but it may still show the spread of the decomposed S. damnosum .sl. oviposition data.

The definition of standard deviation: $\sigma=E[(X-\mu)\ 2\ \sigma=E[(X-\mu)2]$[25]. It may be more important for an explicative, iterative, quantitative, interpolative, orthogonally decomposed, moderate resolution, *S. damnosum* s.l. LULC signature, forecast, vulnerability probabistic paradigm to diagnostically elucidatively quantiate the absolute value instead in the residual endmember , epidemiological forecasts which may be a good measurement rendered from $\sigma=E[|X-\mu|]\ \sigma=E[|X-\mu|]$.The idea would be firstly to use the square of the error values, so that forecasts below the fitted line (which are then negative), would still have to be able to be added up to the positive errors. Otherwise, there would be an error of 0 simply because a huge positive error would cancel with a huge negative error.

So why square the oviposition LULC estimate instead of just taking the absolute value in a moderate resolution, iteratively interpolative, *S. damnosum* s.l., capture point signature model the extra penalty for higher errors would be easily quantizable (e.g., instead of 2 being 2 times the error of 1, it would 4 times the error of 1 when it is squared). In a way, the measurement proposed is widely used in case of error (model quality) analysis -- then it is called MAE, "mean absolute error".

The MAE measures the average magnitude of the errors in a set of forecasts, without considering their direction. It measures *accuracy* for continuous variables. The equation is given in the library references. Expressed in words, the MAE is the average over the verification sample of the absolute values of the differences between forecast and the corresponding observation. The MAE is a linear score which means that all the individual differences are weighted equally in the average.

The RMSE is a quadratic scoring rule which measures the average magnitude of the probabilistic error (progagational non-normal, non-homoskedastic paramters) in a iteratively quantitatively, explanatively interpolative, uncoalesced, geo-spectrotemporal, *S. damnosum* s.l., forecast vulnerability endmeber signature, probabilic, decomposeable algorithmic

paradigm. The equation for the RMSE is given in both of the references. Expressing the formula in words, the difference between forecast and corresponding observed values are each squared and then averaged over the sample. Finally, the square root of the average is taken. Since the errors are squared before they are averaged, the RMSE gives a relatively high weight to large errors. This means the RMSE is most useful when large errors are particularly undesirable.The MAE and the RMSE can be used together to diagnose the variation in the errors in a set of forecasts. The RMSE will always be larger or equal to the MAE; the greater difference between them, the greater the *variance* in the individual errors in the sample. If the RMSE=MAE, then all the errors are of the same magnitude Both the MAE and RMSE can range from 0 to ∞. They are negatively-oriented scores: Lower values are better.

Unfortunately, when a moderate resolution, *S. damnosum* s.l., vulnerability, endmember, probabilistic paradigm has substantial uncertainties in the independent variable (the *x* variable), then simple regression and least squares methods may have problems in forecasting seasonally hyperproductive ovipositions golocation LULC sites ; in such cases, the methodology required for fitting errors-in-variables models may be considered instead of that for least squares in SAS.Least squares problems fall into two categories: linear or ordinary least squares and non-linear least squares, depending on whether or not the residuals are linear in all unknowns[25]. The linear least-squares problem occurs in statistical regression analysis; it has a closed-form solution. The non-linear problem is usually solved by iterative refinement; at each iteration the system is approximated by a linear one, and thus the core calculation is similar in both cases.

Polynomial least squares in PROC GLM may describe the variance in a prediction of the dependent variable in an *S. damnosoum* s.l. eco-epidemiological, moderate resolution model as a function of the independent variable and the deviations from the fitted curve. Polynomial model such as $y = b_0 + b_1x + b_2x^2 + e$ appears curved when y is plotted against x. It is, however, not a nonlinear model. In order to geo-visualize an endmember dataset of geo-spectrotemporally uncoalesced, modertate resolution, geosampled, unbiased, *S. damnosum* s.l., hypeproductive, oviposition estimators , an experimenter may quanatiate derivatives of y with respect to the parameters b_0, b_1, and b_2: $dy/db_0 = 1$, $dy/db_1 = x$, $dy/db_2 = x^2$ None of these derivatives would depend on a model parameter.

In contrast, an expeimenter may consider the log-logistic model $y = d + (a - d)/(1 + \exp\{b \log(x/g)\}) + e$ Take derivatives with respect to d, for example: $dy/dd = 1 - 1/(1 + \exp\{b \log(x/g)\})$. In probability and statistics, the log-logistic distribution (known as the Fisk distribution in economics) is a continuous probability distribution for a non-negative random variable. It is commonly used in survival analysis as a parametric model for events whose rate increases initially and decreases later, for example blindness rates from onchocerciasis following diagnosis or treatment. It has also been used in hydrology to model stream flow and precipitation, and in economics as a simple model of the distribution of wealth or income. Thus, a geo-spectrotemporal, uncoalesced, regressed endmember, iterative, log-logistic distribution of explanatively hypeproudtcive seasoanl *S. damnosum* s.l., oviposition, LULC, moderate resolution , agro-village complex sites is the probability distribution of a random variable whose logarithm has a logistic distribution. It would be similar in shape to the log-normal distribution but has heavier tails. Unlike the log-normal, its cumulative distribution function can be written in closed form. In probability theory and statistics, the cumulative distribution function (CDF) of a real-valued random variable *X*, or just distribution function of *X*, evaluated at *x*, is the probability that *X* will take a value less than

or equal to *x*[25]. When the observations come from an exponential family and mild conditions are satisfied, least-squares estimates and maximum-likelihood estimates are identical [3]. The method of least squares can also be derived as a method of moments estimator..

A new and alternative approach to LSMA, called Fisher's LSMA (FLSMA) in ArcGIS extends the well-known pure-mixel-based Fisher's linear discriminant analysis to LSMA. Interestingly, what can be done for the LSMA can be also developed for the FLSMA in ArcGIS. Of particular interest are two types of constraints imposed on the LSMA, target signature-constrained LSMA and target abundance-constrained LSMA, which may be retrievable in parallel for the FLSMA. Hence, a feature-vector constrained FLSMA (FVC-FLSMA) or a abundance-constrained, FLSMA (AC-FLSMA), respectively may unbiasedly develop a metaheuristically optimizable, eco-georeferenceable, iteratively interpolative, explicatively geoclassifiable, narrow riverine, tributary, African, agro-village complex, eco-georeferenceable, *S. damnosum* s.l., hyperproductive, capture point, proxy, moderate resolution, LULC signature for robustly identifying unknown un-geosampled, seasonal,trailing vegation, turbid water, sparsely shaded, infrequently, discontinuously canopied, capture points parsimoniously in a stochastic or deterministic, iterative interpolator. Further, since Fisher's ratio employed by the FLSMA is a more appropriate classification criterion than the LSE or SNR used for the LSMA, the FVC-FLSMA may improve classical least squares based LSMA and SNR-based OSP in a dataset of sub-mixel, moderate resolution, quantitative, *S. damnosum* s.l., immature habitat, proxy LULC eco-geophysiological, bio-geophysical, orthogonally decomposable, metaheuristic, probabilistic signature, geo-classifiers. Similarly, the AC-FLSMA may also improve abundance-constrained, least squares based LSMA for optimally extraploating uncoalesceable proxy, LULC, iteratively interpolative, endmember, moderate resolution, decomposable, signature, abundance fractions.

Given an empirically probabilistically regressable, optimizable, fractionalized, moderate resolution, endmember dataset of explicatively eco-georeferenceable, mixed, multispectral or hyperspectral vectors, FVC-FLSMA may metheursitically optimally estimate the number of reference, seasonally hyperproductive,eco-georeferenceable, trailing vegetation, turbid water, infrequently shaded, discontinuously canopied, narrow tributary, African. riverine, agro-village complex, *S. damnosum* s.l., immature, capture point, substances (i.e., endmembers), their spectral proxy, LULC signatures, and their orthogonalized, spatial filter, eigenvector, abundance fractions. The LSMA assumes that an image pixel [i.e., digital number (DN)] is linearly mixed by materials with relative abundance fractions present in the image [24]. In order for an FVC LSMA to optimally uncoalesce a discontinuous dataset of expositively fractionalized, eco-geophysiological, eco-georeferenceable, explicative, bio-physical, moderate resolution, infrequently canopied, sparsely shaded, expositively fractionalized, endmember, trailing vegetation, turbid water, geo-spectrotemporal endogenous regressors for optimally identifying unknown, un-geosampled, iteratively interpolative, seasonal, hyperproductive, narrow, African, riverine tributary, agro-village complex, geoclassifiable, parameterizable,*S. damnosum* s.l., capture points, using proxy, LULC signature wavelength eigenevectors, two constraints must be imposed by the decompositonal algorithm: the abundance sum-to-one constraint and the abundance nonnegativity constraint.

An empirical, metaheursitically optimizable, geo-spectrotemporally probabilistically autoregressable eco-georeferenceable, optimizable eco-georeferenceable, uncoalesced

dataset of explicatively orthogonally fractionalizable, constant-sum constrained, unmixed, non-arbitrarily, pre-determined, proxy, LULC signature, covariance weightages in ArcGIS may allow a disjoint partitioning of a sub-mixel fractionalized subset to robustly eco-cartographically delineate, moderate, spatial resolution, geosampled, *S. damnosum* s.l., iteratively lagged, static and dynamic, web–based explanators (e.g., Euclideanized distance from a hyperproductive, partially canopied, eco-epidemiological, capture point to a hyperendemic, narrow, riverine tributary, agro-village, complex centroid). Static web pages are view only without animation or interactivity(www.esri.com). These elucidatively regressively, optimally mappable, forecastable, vulnerability-oriented, fractionalized, parameterizable, endmember regressors, and their unmixed graphical, wavelength frequency-oriented, moderate resolution, irradiance, covariate coefficients may be subsumed by global maximum likelihood (ML) estimators over one or more diffuse, multiscattered, transmittance, eigenvector emissivities whence eco-cartographically illustrating multinomial, discontinuous, geo-spectrotemporalized, geosampled, moderate resolution, imaged, uncoalesced, *S. damnosum* s.l., capture point, proxy LULC, iteratively interpolative signatures. When several roots to the likelihood equation exist, the root corresponding to the global maximizer of the likelihood is generally retainable, but this procedure supposes that all possible roots are identifiable linear predictor functions [24].

Since, in many cases, the global maximizer is the only consistent root in a discontinuous datatset of empirically geo-spectrotemporally, metaheursitically optimizable, infrequently canopied, trailing vegation, turbid water, hypeproductive, capture point, *S. damnosum* s.l., explicatively binomialized, optimizable, time series, datasets of geoclassifiable, explanatively uncoalesced, moderate resolution, proxy LULC signature, radiance, endmember regressors for exemplifying eco-georeferenceable, conditional probability distributions from expostively fractionalized, 2-D, times series, illuminatively forecastable, wavelength, vulnerability paridigms, first sum-to-one constraint may not efficiently decorrelate disproportionately heterogeneous, sparsely shaded, explicative, intermittently canopied, covariance weightages rendered from quantiatively uncoalesceable, diffuse, wavelength, frequency-oriented, tranmittance emissivities. In statistics, binomial regression is a technique in which the response (often referred to as Y) is the result of a series of Bernoulli trials, or a series of one of two possible disjoint outcomes (traditionally denoted "success" or 1, and "failure" or 0)[24]. In probability and statistics, a Bernoulli process is a finite or infinite sequence of binarizable explicative random variables, so it is a discrete-time stochastic process that takes only two values, canonically 0 and 1.

Whilest the standard method to moderate resolution geo-spectrotemporally, optimally extractable, weighted Least Square, non-orthogonalizable, expositively fractionalized, unmixed trailing vegetation, turbid water, sparsely shaded, eco-georeferenceable, non-parameterizable, *S. damnsoum* s.l., capture point, moderate resolution, wavelength, frequency-oriented, transmittance, emissivity estimates have very appealing theoretical and numerical properties, rendered fractionalized, radiance endmember estimates are often unstable in the presence of extreme observations (i.e., geospatial outliers) which are rather common in eco-epidemiological, forecast vulnerability analyses of hyperproductive, seasonal, imature habitats of this black-fly species. One approach to deal with such extreme covariate radiance, observations is the application of robust or resistant unbiased, estimators in ArcGIS, like Least Quantile of Squares estimators. Unfortunately, for many such alternative approaches, the estimation is much more difficult than in the Least Squares case, as the objective function in a proxy LULC, biosignature forecasting, vulnerability, paradigm often contain diffuse sparsely shaded, discontinuously canopied, trailing vegation,

convex/concave, explicative, sub-mixel, reflectance variables which has subsequently many local optim.

When a moderate resolution, wavelength, frequency-oriented, unmixed trailing vegation, turbid water, sparsely shaded, eco-georeferenceable, non-parameterizable, *S. damnsoum* s.l., capture point, transmittance, emissivity function to be optimized is continuous, it may be possible to employ calculus to find local optima. In applied mathematics and computer science, a local optimum of an optimization problem is a solution that is optimal (either maximal or minimal) within a neighboring set of candidate solutions (http://mathworld.wolfram.com/html). In mathematics, a function is a relation between a set of inputs and a set of permissible outputs with the property that each input is related to exactly one output(e.g., the function that relates each real number x to its square x^2) [24].

Hence, in an elucidative, eco-georeferenceable, seasonally hyperproductive, trailing vegetation, turbid water, explanative, *S. damnosum* s.l., immature, capture point, fractionalized, uncoalesced, forecasting,vulnerability analysis, moderate resolution, optimally imaged, geo-spectrotemporally proxy LULC signature, geoclassifiable, endmember datasets may optimally identify unknown, un-geosampled, infrequently shaded, discontinuously canopied, immature habitats when the footprint is iteratively quantitatively interpolated in narrow tributary, African, riverine, agro-village complexes. The maxima and minima (the respective plurals of maximum and minimum) of a function, known collectively as extrema (the plural of extremum), are the largest and smallest value of the function, either within a given range (the local or relative extrema) or on the entire domain of a function (the global or absolute extrema) [24].

In contrast to a global optimum, which is the optimal solution amongst all possible solutions, not just those in a particular geospatialized neighborhood of elucidative orthogonally decomposed,fractionalized, endmember values (e.g., positively autocorrelated, geo-spectrotemporal, geosampled, *S. damnosum* s.l., iteratively lagged, static and dynamic, web–based narrow, African, riverine tributary, agro-village complex, trailing vegation, turbid water, discontinuous, concave, sparsely shaded, canopied,fractionalized iteratively interpolated endmember explanators). If the first derivative exists in a metaheursitic, forecasting vulnerability paradigm everywhere it can be equated to zero; if the function has an unbounded domain, for a point (e.g., seasonally explicatively, geosampled, *S. damnosum* s.l., immature, hypeproductive, narrow tributary, a African, agro-village complex ecosystem seasonal, immature habitat, capture point). In mathematical analysis and related areas of mathematics, a set is called bounded, if it is, in a certain sense, of finite size; conversely, a set which is not bounded is unbounded [24]. A second derivative test can also provide a sufficient condition for the capture point to be differentially geometerically geoclassified as local maxima and maximum or local minima.

In calculus, a derivative test uses the derivatives of a function to locate the critical points of a function and determine whether each point is a local maximum, a local minimum, or a saddle point [24]. Derivative tests may also give information about the concavity/convexity of a function for optimally identifying a dataset of iteratively quantiative geo-spectrotemporally uncoalesced, moderate reosolution, interpolative, proxy, LULC signature, fractionalized, endmember eigenvectors representing a seasonal, eco-georeferenceable, hyperproductive, capture point, trailing vegetation, turbid water, infrequently *S. damnosum* s.l., immature, habitat. A function of a single variable is concave if every line segment joining two points on its graph does not lie above the graph at any

point. Symmetrically, a function of a single variable is convex if every line segment joining two points on its graph does not lie below the graph at any point [24].

Local search or hill climbing methods for solving optimization problems start from an initial configuration and repeatedly moves to an improving geo-spatializable, eco-georeferenceable, neighboring configuration. In computer science, hillclimbing is a metaheuristic method for solving computationally hard optimization problems. Local search can be used on problems that can be formulated as finding a solution maximizing a criterion among a number of candidate solutions[24]. Hill climbing is good for finding a local optimum (i.e., a proxy, geo-spectrotemporal, geoclassifiable,uncoalesced, iteratively interpolative proxy, LULC, signature solution, *S. damnosum* s.l. that can forecast a neighbouring eco-georeferenceable, configuration of capture point, immature habitats) but it may not necessarily guarantee to find the best possible solution (i.e., the global non-seasonal optimum) out of all possible solutions in the search space. Regardless, in convex/concave discontinuous, sporadic, moderate resolution, canopy, endmember, uncoalesced, wavelength, frequency-oriented, transmittance emissivity problems, hill-climbing may be optimal. Examples of algorithms that solve convex/concave, explanative, discontinuously canopied, bidirectional optimizable, quantization problems include include the simplex algorithm for linear programming and binary search in the hill-climbing algorithm[24].The characteristic that only local optima are guaranteed can be cured by using restarts (repeated local search), or more complex schemes based on iterations, like iterated local search, on memory, like reactive search optimization and tabu search, or memory-less stochastic modifications, like simulated annealing in a Local search algorithm.Local search algorithms are widely applied to numerous hard computational problems, including problems from computer science (particularly artificial intelligence), mathematics, operations research, engineering, and bioinformatics. Examples of local search algorithms are WalkSAT and the 2-opt algorithm [http://www.ncsa.illinois.edu/].

A trajectory in search space may be created for an eco-georeferenceable, *S. damnosum* s.l., seasoanl hypeproductive, narrow tributary, African, agro-village complex, trailing vegetation, discontinuous, infrequently canopied, hypeporductive, turbid water, sparsely shaded, seasoanl, *S. damnosum* s.l., eco-georeferenceable, capture points in an ArcGIS-derived, forecast, vulnerability map employing an initial eco-georeferenceable, explanative point (e.g., uncoalesced elevated, geo-spectral, wavelength intensity index) to a local optimum. The search space may be subdivided into basins of specific wavelength attractions, in ArcGIS each consisting of proxy, LULC, endmember, iteratively, quantitatively interpolated, uncoalesced, signature, moderate resolution, capture points which may have a given local optimum as the final point of the local search, wavelength, frequency-oriented, emissivity trajectory. A local optimum can be isolated surrounded by non-locally-optimal points or part of a plateau (e.g., a geolocally optimal region of a pre-flooded, eco-georeferenceable, narrow tributary, agro-village, African, ecosystem complex with more than one *S. damnosum* s.l., seasonal, capture point of equal decompositional endmember or orthogonalized spatial filter eigenvector value).If the problem to be solved has all locally metahueristic, seasonal, hyperproductive, eco-georeferenceable, capture points with the same geospectral values of the function to be optimized, local search effectively solves the global problem: finding a local optimum delivers a globally optimal solution[24]. The locality of the optimum, *S. damnosum* s.l., forecasting, vulnerability paradigm may be dependent on the neighborhood narrow tributary, African, agro-village, ecosystem complex, geo-spectrotemporal, geospatial, structure as defined by the local search method that is used for optimizing the function.

Subsequently quantitating local optima may deliver moderate resolution discontinuous fractionalized endmember and eigenvector optimal solutions for unbiasing, non-explicative, non-parameterizable, sub-mixel, non-residual, regressional, non-metaheursitically optimizable, uncoalesceable,noisy, *S. damnosum* s.l., capture point, eco-epidmiological residual, wavelength, frequency-oriented, forecasts which may subsequently ideally render quantitative, expostively fractionalized, geo-spectrotemporal, capture point, space–time, explicit, unobserved, random, orthogonalizable, irradance, transmittance, emissivity estimators. Further, their contributions would firmly non-nullify robustification of canopy porosity rasters and the per-mixel supervised classification geolocations regions narrow, riverine tributary, agro-village, complex, moderate resolution geo-predictive maps) of any irradiance, transmittance, frequency-oriented, misspecified, decomposed, radiance covariate coefficients. Explanatively geoclasssifiable, moderate resolution, discontinuous, infrequently canopied, sparsely unquantitated iteratively, interpolative, mixed, proxy, LULC, randomized, geo-spectrotemporally, geoclassifiable, LULC biosignature, disturbance terms in sub-mixel moderate resolution, eco-geophysiological or bio-physical,cateogorical varables may generate, flux-weighted, input regressand endmembers, which can render markedly varying inferences from normalized, eigenvector, data streams.

Jacob et al. [22] analyzed explicative, discontinuity in an emprically probabilistically regressed, eco-georferenceable, dataset of geoclassifiable, *S. damnosum* s.l., capture point, canopy gap areas, main orientation, gap shape-complexity index and a quantitative assessment index using the matching with reference gaps in Poissonized polygons for estimating elucidatively, iteratively intepolated geo-spectrotemporally, uncoalesced, moderate reosolution,(Rapid Eye ^{TM} visible and NIR data) for identiyfing seasonally hyperproductive,, sparsely shaded, trailing vegetation, turbid water, standardizable , geo-spectrotemporal, proxy, LULC biosignature beta coefficients igeosampled in a narrow, African, riverine tributary, agro-village complex, in northern Uganda (Achwa riverine basin). In statistics, Poisson regression is a form of regression analysis used to model count data and contingency tables. Poisson regression assumes the response variable Y has a Poisson distribution, and assumes the logarithm of its expected value can be modeled by a linear combination of unknown parameters [24]. During the regression exercise, discontinuous, infrequently canopied sub-mixel, was homogenized so that the variances of dependent and independent variables were 1. A Logistic regression Pseudo R^2 was also rendered which tended to be underinflated as compared with Poissionized outcome since in the latter actual count variables were employed as regressands whilest the explicatively dichotomous model employed log-transmformed, binarized, dependent variables.

Expostorily fractionalized, metaheuristically optimizable, explanatively eco-georeferenceable 5m, wavelength, tranmsittance, frequency-oriented, vulnerability coefficients were robustly linearly and then quantized based on how many standard deviations the dependent variable (e.g., total immature prouctivity count at a capture point) transitioned as per standard deviation increase in the exogenous, trasnmittance emissivity regressands. For univariate seasonal, *S. damnosum* s.l., capture point, endmember paradigms, the absolute value of the standardizable coefficient would equal the correlation coefficient [24]. Note, in Jacob et al. [22] the quantitated interative explanatorial correlations took the place of the corresponding variances and covariances in the forecast vulnerability model estimators. In probability theory and statistics, covariance is a measure of how much two random variables change together [25]. Standardization of the explicative, discontinuous, non-randomized, infrequently canopied, parameterizable, geo-spectrotemporal, covariate coefficients rendered from a stochastic interpolator (i.e., Ordinary kriged algorthm) revealed

unbiased lineraizable estimators eco-cartographically illustrating exogenously residual, metaheuristically optimizable, eco-epidemiological forecasts of un-geosampled, independent vulnerability illuminative, prolific, immature habitat variables which had a greater effect on the dependent variable in the analysis when the variables were measured in different units of proxy, uncoalesced, geoclassified, LULC biosignature, moderate resolution orthogonally decomposable, fractionalized endmember and orthogonalized spatial filter synthetic, measurements (e.g., immature pre-flooded, productivity, counts of narrow, African, riverine tributary, agro-village complex, sparsely shaded, trailing vegetation, turbid water, *S. damnosum* s.l.,capture point measured in measured in discontinuous canopy gap) in ArcGIS.

Renderings from a non-fractionalized, non-expositive, non-optimizable, non-orthogonalizable, eco-geophysiologically, endmember, explanative, moderate resolution, non-metaheursitic, elucidative, bio-physical, criterion variable, in an geo-spectrotemporally uncoalesceable, explicatively probabilistic image regression, equation in ArcGIS where covariace weightages are geoclassfiable, geosampled, eco-georeferenceable, explanative, hyperproductive, seasonal, eco-epidemiological, infrequently canopied, sparsely shaded, *S. damnosum* s.l., narrow tributary, African, riverine agro-village, ecosystem complex, capture point, wavelength, eigenvector, frequencies, the discontinuous, canopied, sparsely shaded, illuminative, irradiance, may be geospatially recified. For example, a continuity of solutions rendered from Calculus Methode/MapServer™ may resolve perturbation and constrained, semi-infinite, vector optimization problems of non-quantitable, *S. damnosum* s.l., fractionalized, capture point, space–time, endmember, orthogonalized, synthetic, eigenvector, forecast-oriented, vulnerability coefficients (e.g., geospatial outiers) in moderate resolution, eco-geographical, regression space. In so doing, the expositively decomposed, moderate resolution, wavelength, transmittance, emissivity forecasts of unknown, un-geosampled, seasonally trailing vegetation, turbid water, sparsely shaded, discontinuously canopied, immature capture point, hyperproductive habitats would be would be optimally identified,.

Calculus Methode/Map Server ™ is a powerful 2D GIS application system for networking systems. With specific algorithm, it has advantages of quick image demonstration, rapid geometry processing and accuracy GIS analysis. Map Server makes it possible to display image data (e.g., explicatively uncoalesced, eco-georeferenceable, *S. damnosum* s.l., capture point endogenous explanators) instantly. With 3D displaying function of Map Server, an ecologist, entomologist or other researcher may specify the range and resolution for a 3D, narrow, tributary, African, agro-village, geomorphological, complex ecosystem, terrain-related, probabilistic, regression, forecast, vulnerability model on a given range at same time in an seasonally hypeproductive, trailing vegetation, turbid water, discontinuous, infrequently canopied, sparsely shaded, eco-georeferenceable, capture point. Modifications can be made on geo-spectrotemporally extracted, immature, *S. damnosum* s.l., habitat mixels by API with temporary storage layers provided by 2D and 3D of Map Server. This system has a high efficiency macro image imbedding ability. In a remote sensing cyberenvironment, this module may have high viewing technology with optimizing compression for high efficiency modelling hyperproductive, trailing vegation, turbid water, discontinuous, sporadically canopied, *S. damnosum* s.l., immature, seasonal ecogeoreferenceable, caprture points, geo-spectrotemporally geosampled in narrow tributary, African, construction Cooperating with the specifically designed transmission protocol and high-efficiency cache mechanism, an ecologist, entomologist or other researcher can browse the macro embedded image in the internet without setting up other software when attempting to resolve extractable, geometrically differential, moderate resolution, iteratively

quantitatively, interpolated, expositively fractionalized, decomposed, endmember, eigenvector contributions of seasonally hypeproductive, trailing vegetation, turbid water, discontinuous, infrequently canopied, sparsely shaded, capture points in stochastic equations. A differential equation is a mathematical equation that relates some function with its derivatives [24] A cache is a component that stores data so future requests for that data can be served faster; the data stored in a cache might be the result of an earlier computation, or the duplicate of data stored elsewhere(www.esri.com)

A stochastic differential equation (SDE) is a differential equation in which one or more of the terms is a stochastic process, resulting in a solution which is also a stochastic process In applications, the functions usually represent physical quantities [e.g., iteratively interpolated geo-spectrotemporally geosampled, dataset of fractionalized, *S. damnsoum* s.l., proxy, uncoalesced LULC biosignature, endmember eigenvector independent random variables] whilest the derivatives represent their rates of change. Apart from describing the explicative, sub-mixel, eco-epidemiological, properties of each geoclassified proxy LULC biosignature, orthogonally explanatively decomposable, exogenous regressor in the forecast equation itself, these classes of differential equations can help in identification of unknown, un-geosampled, iteratively quantitatively interpolative, seasonally hyperproductive, discontinuous, trailing vegetation, sparsely shaded, turbid water, *S. damnsoum* s.l., capture points by geometerically differentiating, discontinuously canopied, wavelength, frequnecy-oriented, transmittance in a moderate resolution spectrum. In so doing, exact contributions may be qualitatively quantiated for unbiasedly kriging, geo-spectrotemporalized, geospatialized, discontinuous, sparsely shaded, canopy foliage, endmember distributions. Commonly employed distinctions in Calculus Methode/Map Server include Ordinary/Partial, Linear/Non-linear, and Homogeneous/Inhomogeneous equations. This list is far from exhaustive; there are many other properties and subclasses of differential equations in Calculus Methode/Map Server which may be very useful for creating robust geo-predictive autocorrelation, ArcGIS maps identifying seasonally hypeproductive, eco-georeferenceable *S. damnosum* s.l., immature, capture points in narrow, African tributary, agro-village complexes.

Theorectically a differential geo-predictive, *S. damnosum* s.l. capture point equation is linear if the unknown function and its derivatives have a degree >1 and nonlinear otherwise. The characteristic property of linear equations is that their solutions form an affine subspace of an appropriate function space, which results in much more developed theory of linear differential equations. In mathematics, an affine space is a geometric structure that generalizes the properties of Euclidean spaces that are independent of the concepts of distance and measure of angles, keeping only the properties related to parallelism and ratio of lengths for parallel line segments [24]. A dataset of homogeneous, seasonal, geo-spectrotemporal, explicatively, uncoalesced, expositively fractionalized, sub-mixel, spatial filter, orthogonal, eigenvector, moderate resolution, *S. damnosum* s.l. capture point, linear differential equations can be formulated in Calculus Methode/Map Server as a subclass of linear differential equations for which the space of solutions is a linear subspace (i.e., the sum of any set of solutions or multiples of solutions is also a solution). The extrapolated vulnerability coefficients of the unknown function and its derivatives in a linearizable, hyperproductive,eco-georeferenceable, trailing vegetation, turbid water, discontinuous, infrequently canopied, sparsely shaded, eco-georefernceable, agro-village, narrow, riverine tributary, *S. damnosum* s.l. seasonal, elucidative, capture point differential equation can be explanative functions of the unmixed, moderate resolution, heursitically optimizable, wavelength, frequency-oriented, emissivity, independent random variables. If these radiance coefficients are constants then a constant coefficient, linear, capture point, differential

equation may be robustly parsimoniously constructed in Calculus Methode/Map Server. This model may suggest some distribution-free methods for testing hypothesis of parallelism and concurrence in mutliple, eco-georeferenceable, seasaonlly hypeproductive, elucidatively, geo-spectrotemporally uncoalesced, trailing vegetation, turbid water, discontinuous, infrequnetly canopied, speardely shaded, narrow tributary, African riverine linear regressions. It may be assumed that the independent variable in these geo-predictive models are equally spaced. The proposed procedures may be compared with nonparametric competitors and the normal theory t-test.

Given a differential equation $F\left(x, y, y', \cdots, y^{(n)}\right) = 0$ a function u: $I \subset \mathrm{R} \rightarrow \mathrm{R}$ is called the solution or integral curve for F, if u is n-times differentiable on I, and $F(x, u, u', \ \cdots, \ u^{(n)}) = 0 \quad x \in I.$ (http://mathworld.wolfram.com/) In mathematics, an integral curve is a parametric curve (e.g., $x = \cos t$ where t is an geo-spectrotemporally uncoalesced, explanative, hyperproductive, seasonal, trailing vegetation, discontinuous, turbid water, sparsely shaded, infrequently canopied, narrow, riverine tributary, agro-village complex ecosystem, geosampled, seasonal parameter) that can represent a specific solution or system of equations. If the differential equation is represented as a vector field or slope field in Calculus Methode/Map Server, then the corresponding integral curves would be tangent to the field at each ecogeoreferenceable, iteratively quantiative, exptrapolative, interpolative, eco-geographic, eco-epidemiological, seasonal hyperproductive, *S. damnossm* s.l. capture point.Given two solutions u: $J \subset \mathrm{R} \rightarrow \mathrm{R}$ and v: $I \subset \mathrm{R} \rightarrow \mathrm{R}$, u is an extension of v if $I \subset J$ and $u(x) = v(x) \quad x \in I.$ In vector calculus, a vector field is an assignment of a vector to each point in a subset of space[24].

In Calculus Methode/Map Server, a nonlinear, elucidative, geospectrotemporally geosampled, *S. damnosum* s.l, geometerically differential expositively fractionalized, moderate resolution, endmember uncoalesced, eigenvector, capture point, proxy LULC, eco-georeferenceable, explicatively, forecasting simultaneous biosignature equation in which the unknowns (or the unknown functions in the case of differential equations) can appear as variables of a polynomial of degree higher than 1. The unknown or un-geosampled, *S. damnosum* s.l, capture point, eco-epidemiological, model functions may also occur in the argument of a function which is not a polynomial of degree one. In other words, in a nonlinear system of forecasting geo-spectrotemporally geosampled, uncoalesced, hypeproductive, trailing vegetation, discontinuous, infrequently canopied, sparsely shaded, agro-village, narrow, riverine tributary, seasonal parameter equations, the equation(s) to be solved cannot be written as a linear combination of the unknown, proxy LULC biosignature variables or functions that appear in them. In Calculus Methode/Map Server it does not matter if explanative, non-linearizable, known functions appear in the equations, a vulnerability paradigm can be parsimonioulsy constructed regardless. In particular, a differential equation is linear if it is linear in terms of the unknown function and its derivatives, even if nonlinear in terms of the other variables appearing in it[24].

As nonlinear equations are difficult to solve, nonlinear systems are commonly approximated by linear equations (linearization)(http://mathworld.wolfram.com/). This works well up to some accuracy and some range for input *S. damnsoum* s.l. geospectrotemporally uncoalesced sub-mixel, explanatorial, discontinuous, uncoalesced, sparsely shaded, canopied values, but some interesting phenomena such as quantitable singularities which may be inconspiciuous by linearization may still exist in the forecast post-quantization residuals.

Some aspects of the behavior of the fractonalized, sub-mixel, nonlinear system may be unpredictable or counterintuitive. Although such unruly behavior may resemble random behavior, it may not be random in nonlinear, geo-spectrotemporal, geo-spatialized, *S. damnosum* s.l, geometerically differential, expositively fractionalized, endmember eigenvector, capture point, uncoalesced, eco-georeferenceable, iteratively interpolated, forecasting proxy, LULC biosignature explanators. There may be only few methods of solving, nonlinear, sub-mixel, *S. damnosum* s.l, capture point, differential equations exactly; those that are known may typically depend on the equation having particular symmetries. Maybe one of the regressors can be a non-linear function of another regressor in the capture point, forecasting vulnerability model or of the data in the model may be efficiently delineated in polynomial regression and/or segmented regression framewworks. However these regressions equations may lead to the same estimation procedures; however, different approaches to the asymptotic analysis may be employable in these two model situations. Both interpretations may be appropriate in different cases of decompositionally fractionalized, moderate reosolution, endmember eigenvector iterative interpolation for optimally identifiying unknown, un-geosampled seasonal, *S. damnsoum* s.l. hyperproductive, capture points.

However an elucidative, nonlinear, geo-spectrotemporally uncoalesced, explanative, geometerical, differential ,capture point, forecasting, vulnerability, iterative, interpolative equation can exhibit very complicated behavior over extended time intervals employing multiple, chaotic, eco-geophysiological, biogeophysical, expostively fractionalized, moderate resolution, fractionalized, proxy, biosignature LULC, endmember, eigenvector characteristics. Chaos theory is the field of study in mathematics that studies the behavior and condition of dynamical systems that are highly sensitive to initial conditions [24]. Small differences in initial conditions (such as those due to rounding errors in numerically uncoalesced, sub-mixel, hyperproductive, *S. damnsoum* s.l., capture point, iterative interpolative computations) may yield widely diverging outcomes when optimally forecasting, geo-spectrotemporally eco-georeferenceable, narrow, tributary, African agro-village, seasonal, immature, capture point, hyperproductive habitats making long-term forecasting impossible in general. This happens even though these systems are deterministic, meaning that their future behavior is fully determined by their initial conditions, with no random elements involved.

The deterministic nature of eco-georeferenceable, uncoalesced, sub-mixel, hyperproductive, *S. damnsoum* s.l., capture point, iterative interpolative capture points systems does not make them conducive to eco-geographically geo-prediction. Such determinitsic occurrences may be unquantitable using simple unmixing algorithms in most software packages for identying unknown, un-geosampled, moderate reoslution, imaged, seasoanally hyperproductive, eco-georeferenceable, geospectrotemporally uncoalesced,moderate reosolution, trailing vegetaion, turbid water, discontinuous, infrequnetly canopied, sparsely shaded, *S. damnsoum* s.l. capture points with precision in an iterative interpolator. Chaotic behavior exists in many natural systems, such as weather and climate [24[. This behavior may be studied through fractional endmember analysis of a chaotic mathematical model, or through analytical techniques such as recurrence plots in Calculus Methode/Map Server. In descriptive statistics and chaos theory, a recurrence plot is a plot showing, for a given moment in time, the times at which a phase space trajectory visits roughly the same area in the phase space. In other words, it is a graph of $\vec{x}(i) \approx \vec{x}(j)$, showing i on a horizontal axis and j on a vertical axis, where $\vec{x}$ is a phase space trajectory.

Tests have confirmed that the speed of processing the macro image in Calculus Methode/Map Server is fast comparable with other mathematical GIS internet server products. (www.esri.com). The product can transform geo-spectrotemporally geospatialized, explanatorial, *S. damnosum* s.l., capture point. 3D maps from 2D, Planar maps. In graph theory, a planar graph is a graph that can be embedded in the plane,(i.e., it can be drawn on the plane in such a way that its edges intersect only at their endpoints) (www.esri.com).The Geometric Calculus Map Server uses Buffering Tools and Best Path tools which are designed especially with both efficiency and accuracy thus, ecogeoreferencable, elucidative geometrically differentiatiable, hyperproductive, trailing vegetation, turbid water, discontinuous, sporadically canopied, sparsely shaded, *S. damnosum* s.l., geo-spectrotemporally uncoalesced, moderate resolution, capture point, bidirectional, wavelength, frequency-oriented, transmittance may be differentially geometrically mapped.

In calculus a differentiable function of one real variable is a function whose derivative exists at each point in its domain. As a result, a graph of a expositively differentiable forecasting geo-spectrotemporally uncoalesced, eco-georeferenceable, hypeproductive, trailing vegetation, discontinuous, infrequently canopied, sparsely shaded, seasonal parameter function must have a (non-vertical) tangent line at each point in its domain, be relatively smooth, and cannot contain any breaks, bends, or cusps. In mathematics a cusp, sometimes called spinode in old texts, is a point on a curve where a moving point on the curve must start to move backward [24]. More generally, if x_0 is a geo-spectrotemporally geosampled hypeporductive, *S. damnsoum* s.l., seasonal, capture point in the domain of a function f, then f is said to be differentiable at x_0 if the derivative $f'(x_0)$ exists. This means that the graph of f has a non-vertical tangent line at the point $(x_0, f(x_0))$. The function f may b elocally linear at x_0, as it may be well approximated by a linear function tabulated near this agro-village, narrow, riverine tributary, immature, capture point, hyperproductive, agro-village complex, habitat

Sub-differential, nonsmooth, optimization techniques for conducting endmember eiegenvetcor moderate reoslution, deompositional variational analysis may be stablized in Calculus Methode/Map Server for parsimoniously, qualitatively quantitating Lipschitz behavior of archived robustifiable, Pareto solutions rendered from logistically regressed, capture point, *S. damnosum* s.l., sub-mixel, geo-spectrotemporal, moderate resolution, dichotomized exogenous covariates iterated in parametric, nonconvex, semi-infinite algorithms in Calculus Methode/MapServer™. Logistic regression measures the relationship between the categorical dependent variable and one or more independent variables by estimating probabilities using a logistic function, which is the cumulative logistic distribution. probability theory and statistics, the CDF of a real-valued random variable X, or just distribution function of X, evaluated at x, is the probability that X will take a value less than or equal to x[http://mathworld.wolfram.com/.html]. A continuous *S. damnsoum* s.l., fractionalized endmember eigenvector distribution, may render the area under the probability density function (PDF) from minus infinity to x. Cumulative distribution functions may be used to specify the distribution of multivariate random variables[24].

Thus, this explanatorial, linear paradigm would treats the same set of uncoalesced *S. damnosum* s.l., sub-mixel, fractionalized, moderate resolution data variables as probit regression using similar techniques, with the latter using a cumulative normalized distribution curve instead. Lipschitz continuity, is a strong form of uniform continuity for functions [24]. Equivalently, in the latent variable interpretations of these methods, ecologists, entomologists and other researchers may employ a binarized regressand dataset of fractionalized moderate

resolution, geo-spectrotemporal, unmixed *S. damnsoum* s.l. trailing vegetation, turbid water, ecogeoreferenceable, sparsely shaded, immature, seasonal hyperproductive, capture point, forecast, vulnerability model estimator with a standard logistic normalized distribution of errors.

The use of binary variable regressions in the analysis of qualitative endmember moderate resolution variables (is not confined to the dicho tomeous variable case when quantiating a continuous, eco-georeferenceable, narrow tributray, African, agro-village complex, seasonal, capture point, trailing vegetation, turbid water, discontinuous, sparsely shaded, sporadically canopied, *S. damnsoum* s.l., fractionalized endmember eigenvector distribution. It is evident that a orthogonalizable regressor which can take more than two different seasonal geo-spectrotemporally, values, can be redefined in terms of a set of binary variables. It is perhaps less obvious, however, that this also applies to the regressand. The principle was pointed out by Theil (1969) for the linear logistic model. A similar device is used for contingency tables.

Let B1, B2, ..., Bm be a set of mutually exclusive geo-spectrotemporally geospatialized, geosampled, eco-georeferenceable, trailing vegetation, turbid water, discontinuous, sporadically canopied, S. damnsoum s.l., moderate resolution, fractionalized endmember and orthogonalized, spatial filter eigenvector, characteristics of a sample unit, say m alternative classes of a classification scheme. Let A1, A2, .. Ak be k uncoalesced capture point characteristics which may or may not occur for each frequency-oriented, , wavelength, sample unit (*S. damnosum* s.l., agro-village , narrow tributary immature hypeporductive , seasonal, habitats). Then an experimenter, or medical entomologist or other researcher may draw transmittance emissivity inferences on the set of quantitated conditional probabilities of B1, B2, ...,Bm respectively, given the various possible endmeber eigenvector combinations of the A-characteristics. One way of doing this is by means of m regression equations (one of which is redundant) in ArcGIS. To represent B1, B2, ..., Bi,, a set of moderate resolution, binarized expositive, unmixed, *S. damnosum* s.l. geo-spectrotemporal, geosampled, illuminative, immature capture point, variables may quantitateY1, Y2, ..., Ym. For each of these variables the regression on the set of binary variables X1, X2, ..., Xk, representing A1, A2, ..., Ak, and their products up to the kth order may then be computated in ArcGIS (e.g., Geostatistical Analyst ™).

If any explanative, geo-spectrotemporal, fractionalized endmember, *S. damnsoum* s.l. trailing vegetation, turbid water, ecogeoreferenceable, sparsely shaded, immature, seasonal hyperproductive, capture point, regression assumptions is violated (i.e., if there are nonlinear inconspicuous, undected, non-quantitative relationships between explicative, dependent and independent, discontinuous, non-homogenous, geo-spectrotemporally uncoalesced, sparsely shaded, trailing vegetation, turbid water, endmember, orthogonalized eigenvectors or the errors exhibit wavelength, frequency-oriented, non-decomposeable transmittance, emissivity correlation non-normalities such endmember heteroscedasticity) in a geoclassifiable, eco-georeferenceable, narrow, African, riverine tributary, agro-village complex, hyperproductive, capture point reflectance-oriented, regression map then the eco-epidemiological forecasts (e.g., unbiased iteratively interpolated, proxy, LULC biosignature, covariate coefficients of eco-cartographically unknown, un-geosampled *S. damnosum* s.l., seasona,l capture points), rendered from the confidence intervals, and scientific insights yielded by the *S. damnosum* s.l regression model may be (at best) inefficient or (at worst) seriously biased or misleading. Ideally, a statistical software will automatically provide charts and statistics that test whether these assumptions are satisfied for such a forecast, vulnerability model. Unfortunately, many

software packages do not provide such output by default (e.g., additional menu commands must be executed or codes must be written) and some such as Excel's built-in regression add-in offer only limited options. RegressIt does provide such output and in graphic detail but many non-heuristic, non-optimizable, sub-mixel, fractionalized, canopy structural, endmember models generated have violated many linear assumptions (e.g., the expected value of the moderate resolution, uncoalesced, wavelength dependent variable is a straight-line function of each orthogonalized independent variable whenst holding the others fixed, or the slope of the regression line does not depend on the explanatorial regressor values of the other capture point geosampled variables).

Unfortunately, many of geo-spectrotemporally fractionalized, endmember eigenvector moderate resolution regression, forecastable, *S. damnosum* s.l. and other medical entomological vector capture point, eco-georefernceable, vulnerability paradigms are accepted by a naïve user on the basis of a large value of R-squared. A regression (e.g., Poisson, Negative binomial with a non-homogenous distributed mean) geo-predictive, *S. damnosum* s.l. time series dependent, vulnerability equations that does not satisfy the assumptions reasonably well may be repaired employing nonlinear transformation of variables in ArcGIS. The normal quantile plots from those models may reveal robustifiable, ArcGIS Online web maps, or a basemap and operational layers revealing geolocations of unknown, un-geosampled *S. damnosum* s.l., iteratively interpolative, hyperproductive, seasonal .habitats).

An ecologist, entomologist or other researcher may establish sufficient conditions in Calculus Methode/Map Server for the Aubin Lipschitz-like property of the Pareto solution which may map under *seasonal, S. damnosum* s.l., habitat perturbations of both the objective function and constraints. Among many extensions, the pseudo-Lipschitzian property introduced by Aubin [1] the Aubin property or the Lipschitz-like property has been used extensively in the study of endmember sensitivity analysis of optimization problems and variational inequalities. It also plays an important role on developing generalized differentiation calculi for nonsmooth functions and set-valued mappings; introduce a notion of Levitin-Polyak well-posedness for generalized semi-infinite multiobjective programming problems in terms of weakly efficient solutions. A obtain some metric characterizations of Levitin-Polyak well-posednessfor this problem. We derive the relations between the Levitin-Polyak well-posedness and the upper semi-continuity of approximate solution maps for generalized semi-infinite multiobjective programming problems.

Multi-objective error optimization (also known as multi-objective programming, vector optimization, multicriteria optimization, multiattribute optimization or Pareto optimization) is an area of multiple criteria decision making that is concerned with mathematical optimization problems involving more than one augmented objective function (www.esri.com). The elements of this parameter vector may enable geometerically, differnentially correcting, hyperproductive, trailing vegetation, seasonal, infrequently canopied, turbid water, *S. damnosum* s.l.,narrow tributary, eco-georefernceable, African, riverine agro-village, ecosystem complex, discontinuous, infrequently canopied, sparsely shaded, capture point may be thereafter re-computated in Calculus Methode/MapServer^{TM} and interpreted as the partial derivatives of the response variable [e.g., uncoalesced, red, green and blue (RGB) corresponding to the ‘‘standard moderate resolution, model’’ of additive color reproduction] employing fractionalized, proxy, LULC eco-geophysiological, bio-geophysical, endmember biosignature contributions) in the forecast vulnearbility paradigm.

International Journal of Geographic Information System
Vol. 4, No. 1, April 2017, pp.1-519
Available Online at http://acascipub.com/Journals.php

In mathematics, a partial derivative of a function of several variables is its derivative with respect to one of those variables, with the others held constant, as opposed to the total derivative, in which all variables are allowed to vary. Partial derivatives are used in vector calculus. Vector calculus (or vector analysis) is a branch of mathematics concerned with differentiation and integration of vector fields, primarily in 3-dimensional Euclidean space.The partial derivative of a function $f(x, y, ...)$ with respect to the variable x is variously denoted by $f'_x,\ f_x,\ \partial_x f, \frac{\partial}{\partial x} f,$ or $\frac{\partial f}{\partial x}$ [24]. Since in general a partial derivative is a function of the same arguments as in the original function, this functional dependence is sometimes explicitly included in the notation, as in $f_x(x, y, ...),\ \frac{\partial f}{\partial x}(x, y, ...).$ Partial derivatives are used in vector calculus and differential geometry.. Differential geometry is a mathematical discipline that uses the techniques of differential calculus, integral calculus, linear algebra and multilinear algebra to study problems in geometry. Partial derivatives are key to target-aware image resizing algorithms. Widely known as seam carving, these algorithms require each mixel in an image to be assigned a numerical 'energy' to describe their dissimilarity against orthogonal adjacent mixels [25]. The algorithm then progressively removes rows or columns with the lowest energy. The formula established to determine a mixel's energy (magnitude of gradient at a pixel) depends heavily on the constructs of partial derivatives.

Suppose that $f(x, y)$ is a differentiable real function of two variables whose second partial derivatives exist. The Hessian matrix H of f is the 2 × 2 matrix of partial derivatives of f: Hence, suppose that f is a function of more than one fractionalized, geo-spectrotemporal, geosampled, seasonal, explanatorial, moderate resolution, optimally imaged, hyperproductive, discontinuous, infrequently canopied, turbid water, sparsely shaded, *S. damnosum* s.l., trailing vegetation or turbid water, decomposable, input variable in an eco-georeferenceable, narrow tributary,African, riverine agro-village, ecosystem complex within a moderate resolution uncoalesced spectrum, In such circumstances an unbiased geospatialized, moderate resolution, eco-epidemiolgical, capture point, fractionalized, endmember eigenvector, forecast-oriented, parameterizable estimator dataset may be optimizable by $z = f(x, y) = x^2 + xy + y^2$ (See Figure 3). As such, accurate endmember comparisons of moderate resolution, ground-based measurements of the fractionialized photosynthetically active radiation intercepted by seasonal, discontinuous, *S. damnosum* s.l. proxy, LULC biosignature may be reviwed in Geospatial Analyst [TM]. In so doing , exact eco-geophysiological, biophysical and biochemical substance measurmenets may be revealed and thus iteratively interpolated (e.g., Chorophyll (Chl)-a) In mathematics, the Hessian matrix or Hessian is a square matrix of second-order partial derivatives of a scalar-valued function, or scalar field. It describes the local curvature of a function of many variables. Specifically, suppose $f : \mathbb{R}^n \to \mathbb{R}$ is a function taking as input a vector $\mathbf{x} \in \mathbb{R}^n$ and outputting a scalar $f(\mathbf{x}) \in \mathbb{R}$; if all second partial derivatives of f exist and are continuous over the domain of the function, then the Hessian matrix $\mathbf{H}$ of f is a square $n \times n$ matrix, usually defined.

The Jacobian matrix of the derivatives $\partial f/\partial x_1$, $\partial f/\partial x_2$, ..., $\partial f/\partial x_n$ of a function $f(x_1, x_2, ..., x_n)$ with respect to x_1, x_2, ..., x_n is called the Hessian H of f, i.e.,

$$H f(x_1, x_2, ..., x_n) = \begin{bmatrix} \frac{\partial^2 f}{\partial x_1^2} & \frac{\partial^2 f}{\partial x_1 \partial x_2} & \frac{\partial^2 f}{\partial x_1 \partial x_3} & \cdots & \frac{\partial^2 f}{\partial x_1 \partial x_n} \\ \frac{\partial^2 f}{\partial x_2 \partial x_1} & \frac{\partial^2 f}{\partial x_2^2} & \frac{\partial^2 f}{\partial x_2 \partial x_3} & \cdots & \frac{\partial^2 f}{\partial x_2 \partial x_n} \\ \vdots & \vdots & \vdots & \ddots & \vdots \\ \frac{\partial^2 f}{\partial x_n \partial x_1} & \frac{\partial^2 f}{\partial x_n \partial x_2} & \frac{\partial^2 f}{\partial x_n \partial x_3} & \cdots & \frac{\partial^2 f}{\partial x_n^2} \end{bmatrix}.$$

[25]. As in the case of the Jacobian, the

term "Hessian" unfortunately appears to be used both to refer to this matrix and to the determinant of this matrix (Gradshteyn and Ryzhik 2000, p. 1069). In the second derivative test for determining extrema of a function $f(x, y)$, the discriminant $D$is given by $H f(x, y) = \begin{vmatrix} \frac{\partial^2 f}{\partial x^2} & \frac{\partial^2 f}{\partial x \partial y} \\ \frac{\partial^2 f}{\partial y \partial x} & \frac{\partial^2 f}{\partial y^2} \end{vmatrix}$. The Hessian can be implemented in the Wolfram Language as HessianH[f_, x_List?VectorQ] := D[f, {x, 2}] (http://mathworld.wolfram.com).

Taking the differential $d\mathbf{y} = \mathbf{y_x}\, d\mathbf{x}$ may shows that $J$is the determinant of the matrix $\mathbf{y_x}$, in a *S. damnosum* s.l. forecast, vulnerability probabilisc paradigm, and therefore would render the ratios of n-dimensional volumes (contents) in $y$and x, $dy_1 \cdots dy_n = \left|\frac{\partial(y_1, \ldots, y_n)}{\partial(x_1, \ldots, x_n)}\right| dx_1 \cdots dx_n$. The use of determinants in calculus includes the Jacobian determinant in the change of variables rule for integrals of functions of several variables. The differentials therefore appears, for example, in the change of variables theorem.

The theorem which effectively describes how lengths, areas, volumes, and generalized n-dimensional volumes (contents) are distorted by differentiable functions. In particular, the change of variables theorem reduces the whole problem of figuring out the distortion of the content to understanding the infinitesimal distortion, i.e., the distortion of the derivative (a linear *S. damnosum* s.l. map), which is given by the linear map's determinant. So $f : \mathbb{R}^n \to \mathbb{R}^n$is an area-preserving linear transformation iff $|\det(f')| = 1$, and in more generality, if $S$is any subset of $\mathbb{R}^n$, the content of its image is given by $|\det(f')|$times the content of the original. The change of variables theorem takes this infinitesimal knowledge, and applies calculus by breaking up the domain into small pieces and adds up the change in area, bit by bit. The change of variable formula persists to the generality of differential k-forms on manifolds, giving the formula $\int_M (f^* \omega) = \int_W (\omega)$ under the conditions that $M$and $W$are compact connected oriented manifolds with nonempty boundaries, $f : M \to W$is a smooth map which is an orientation-preserving diffeomorphism of the boundaries. In one dimension, the explicit statement of the theorem for fa continuous function of $y$is $\int_S f(\phi(x)) \frac{d\phi}{dx} dx = \int_T f(y) dy$, where $y = \phi(x)$is a differential mapping on the interval $[c, d]$and $T$is the interval $[a, b]$with $\phi(c) = a$and $\phi(d) = b$(Lax 1999). In two dimensions, the explicit statement of the theorem is $\int_R f(x, y)\, dx\, dy = \int_{R^*} f[x(u, v), y(u, v)] \left|\frac{\partial(x, y)}{\partial(u, v)}\right| du\, dv$ and in three dimensions, it is $\int_R f(x, y, z)\, dx\, dy\, dz = \int_{R^*} f[x(u, v, w), y(u, v, w), z(u, v, w)] \left|\frac{\partial(x, y, z)}{\partial(u, v, w)}\right| du\, dv\, dw$, where $R = f(R^*)$is the image of the original region R^*, $\left|\frac{\partial(x, y, z)}{\partial(u, v, w)}\right|$is the Jacobian, and $f$is a global orientation-preserving diffeomorphism of $R$and R^*(which are open subsets of $\mathbb{R}^n$). The concept of the Jacobian can also be applied to $n$functions in more than $n$variables. For example, considering $f(u, v, w)$and $g(u, v, w)$, the Jacobians $\frac{\partial(f, g)}{\partial(u, v)} = \begin{vmatrix} f_u & f_v \\ g_u & g_v \end{vmatrix}$, $\frac{\partial(f, g)}{\partial(u, w)} = \begin{vmatrix} f_u & f_w \\ g_u & g_w \end{vmatrix}$can be optimally defined [25]. For the case of geo-spectrotemporal explanative uncoalesced,

moderate resolution, trailing vegation, discontinuously canopied, eco-georeferenceable, immature *S. damnosum* s.l. datset of quanatized endmember variables, the Jacobian takes the special form $J f(x_1, x_2, x_3) = \left| \frac{\partial \mathbf{y}}{\partial x_1} \cdot \frac{\partial \mathbf{y}}{\partial x_2} \times \frac{\partial \mathbf{y}}{\partial x_3} \right|$, where $\mathbf{a} \cdot \mathbf{b}$ is the dot product and $\mathbf{b} \times \mathbf{c}$ is the cross product, which can be expanded by $\left| \frac{\partial(y_1, y_2, y_3)}{\partial(x_1, x_2, x_3)} \right| = \begin{vmatrix} \frac{\partial y_1}{\partial x_1} & \frac{\partial y_1}{\partial x_2} & \frac{\partial y_1}{\partial x_3} \\ \frac{\partial y_2}{\partial x_1} & \frac{\partial y_2}{\partial x_2} & \frac{\partial y_2}{\partial x_3} \\ \frac{\partial y_3}{\partial x_1} & \frac{\partial y_3}{\partial x_2} & \frac{\partial y_3}{\partial x_3} \end{vmatrix}$. to give targeted, iteratively interpolated, eco-georeferenced, hypeproductive habitats.

The dot product can be defined for two vectors $\mathbf{X}$ and $\mathbf{Y}$ by $\mathbf{X} \cdot \mathbf{Y} = |\mathbf{X}| \, |\mathbf{Y}| \cos\theta$, where θ is the angle between the vectors and $|\mathbf{X}$ is the norm. It follows immediately that $\mathbf{X} \cdot \mathbf{Y} = 0$ if $\mathbf{X}$ is perpendicular to $\mathbf{Y}$. The dot product therefore has the geometric interpretation as the length of the projection of $\mathbf{X}$ onto the unit vector $\hat{\mathbf{Y}}$ when the two vectors are placed so that their tails coincide. By writing $A_x = A \cos\theta_A \quad B_x = B \cos\theta_B$ and $A_y = A \sin\theta_A \quad B_y = B \sin\theta_B$, it follows that (1) yields
$\mathbf{A} \cdot \mathbf{B} = A\,B \cos(\theta_A - \theta_B) = A\,B(\cos\theta_A \cos\theta_B + \sin\theta_A \sin\theta_B) = A \cos\theta_A \, B \cos\theta_B + A \sin\theta_A \, B \sin\theta_B =$
$A_x B_x + A_y B_y$. So, in general, $\mathbf{X} \cdot \mathbf{Y} = \sum_{i=1}^{n} x_i \, y_i = x_1 \, y_1 + \ldots + x_n \, y_n$. This can be written very succinctly using Einstein summation notation as $\mathbf{X} \cdot \mathbf{Y} = x_i \, y_i$. Einstein summation is a notational convention for simplifying expressions including summations of vectors, matrices, and general tensors.[25]. The dot product is implemented in the Wolfram Language as Dot[*a*, *b*], or simply by using a period, *a* . *b*. The dot product is commutative $\mathbf{X} \cdot \mathbf{Y} = \mathbf{Y} \cdot \mathbf{X}$, and distributive $\mathbf{X} \cdot (\mathbf{Y} + \mathbf{Z}) = \mathbf{X} \cdot \mathbf{Y} + \mathbf{X} \cdot \mathbf{Z}$. The associative property is meaningless for the dot product because $(\mathbf{a} \cdot \mathbf{b}) \cdot \mathbf{c}$ is not defined since $\mathbf{a} \cdot \mathbf{b}$ is a scalar and therefore cannot itself be dotted. However, it does satisfy the property $(r\,\mathbf{X}) \cdot \mathbf{Y} = r\,(\mathbf{X} \cdot \mathbf{Y})$ for r a scalar. The derivative of a dot product of vectors is $\frac{d}{dt}[\mathbf{r}_1(t) \cdot \mathbf{r}_2(t)] = \mathbf{r}_1(t) \cdot \frac{d\mathbf{r}_2}{dt} + \frac{d\mathbf{r}_1}{dt} \cdot \mathbf{r}_2(t)$. The dot product is also called the scalar product and inner product. In the latter context, it is usually written $\langle a, b \rangle$. The dot product is also defined for tensors A and B by $A \cdot B \equiv A^{\alpha} B_{\alpha}$. So for four- geo-spectrotemporal explanative uncoalesced, moderate resolution, trailing vegation, discontinuously canopied, eco-georeferenceable, immature *S. damnosum* s.l. datset of quanatized endmember vectors a_μ and b_μ, may be defined by $a_\mu \cdot b_\mu = a_\mu \, b^\mu = a^0 \, b^0 - a^1 \, b^1 - a^2 \, b^2 - a^3 \, b^3 = a^0 \, b^0 - \mathbf{a} \cdot \mathbf{b}$, where $\mathbf{a} \cdot \mathbf{b}$ is the usual 3-D dot product. The dot product is invariant under rotations $\mathbf{A}' \cdot \mathbf{B}' = A'_i \, B'_i = a_{ij} \, A_j \, a_{ik} \, B_k = (a_{ij} \, a_{ik}) A_j \, B_k = \delta_{jk} \, A_j \, B_k = A_j \, B_j = \mathbf{A} \cdot \mathbf{B}$, where Einstein summation has been used.

In mathematics, especially in applications of linear algebra to physics, the Einstein notation or Einstein summation convention is a notational convention that implies summation over a set of indexed terms in a formula, thus achieving notational brevity. The first item on the above list can be employed to greatly simplify and shorten equations involving tensors. For example, using Einstein summation, $a_i \, a_i \equiv \sum_i a_i \, a_i$ and $a_{ik} \, a_{ij} = \sum_i a_{ik} \, a_{ij}$. The second and third items on the list indicate that the expression $M_{ij} \, v_j \equiv \sum_j M_{ij} \, v_j$ is valid, whereas the

expressions $M_{ij}\ u_j\ v_j + w_i$ and $T_{i\ j,\ k}\ u_k + M_{i\ p}$ are invalid because the index j appears three times in the first term of (), while the non-repeated index j in the first term of () doesn't match the non-repeated p of the second term. The convention was introduced by Einstein (1916, sec. 5), who later jested to a friend, "I have made a great discovery in mathematics; I have suppressed the summation sign every time that the summation must be made over an index which occurs twice..." (Kollros 1956; Pais 1982, p. 216). In practice, the convention tends to occur alongside both the Kronecker delta and permutation symbol. Moreover, the Einstein summation convention easily accommodates both superscripts and subscripts for contravariant and covariant tensors, respectively. As part of mathematics it is a notational subset of Ricci calculus; however, it is often used in applications in physics that do not distinguish between tangent and cotangentspaces.

If $m = n$, the Jacobian matrix is a square matrix, and its determinant, a function of x_1, …, x_n, is the Jacobian determinant of f in a trailing vegation, narrow African, riverinme tributray, hypeporductive, eco-georeferenceable, *S. damnsoum* s.l., capture point, moderate resolution, geo-spectrotemporal, forecast vulnerability probabilsitic paradigm. It may provide LULC important information about the local behavior of f (e.g., immature productivity count on a moderate resolution, geoclassifieable LULC) In particular, the function f would have locally in the neighborhood of a hyperproductive , seasaonl ecpoi-georefrenceable, explanative, point x an inverse function that is differentiable if and only if the Jacobian determinant is nonzero at x (see the Jacobian conjecture in Figure 5). The Jacobian determinant occurs also when changing the variables in multiple integrals (see substitution rule for multiple variables)[25]. If $m = 1$, f is a scalar field and the Jacobian matrix is reduced to a row vector of partial derivatives of f—i.e. the gradient of

Figure 5. A differential geometrical graph of $z = x^2 + xy + y^2$ forecast endmember *S. damnsoum* s.l., vulnerability paradigm derivative as the best affine approximation to a function at a hypeproductive habitat point, calculated via a m=n Jacobian matrix. where the partial derivative at (1, 1) leaves y constant and where the corresponding tangent line is parallel to the xz-plane for estimatimating incident solar radiation in a discontinuous canopy surface sample

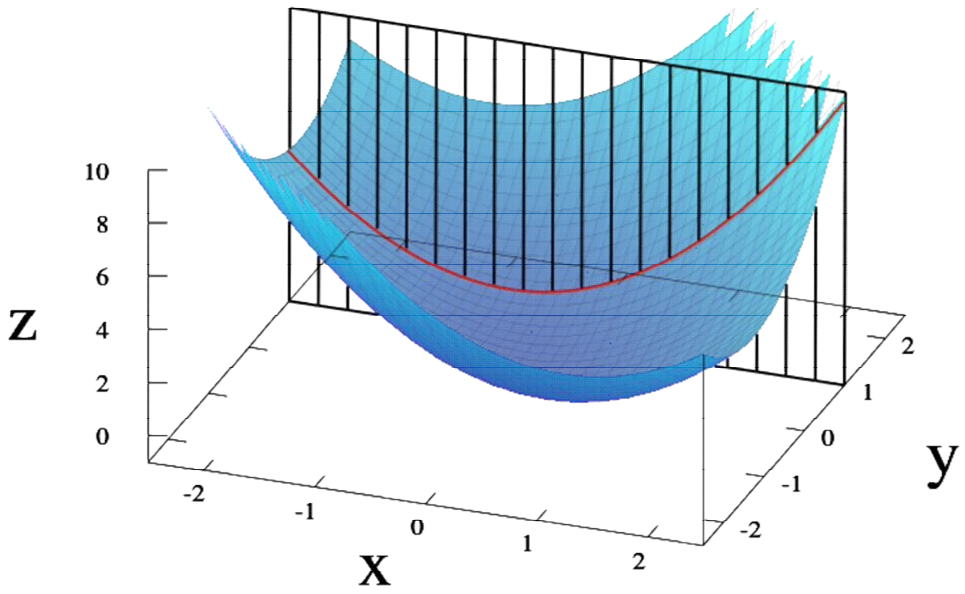

A trailing vegetation, hyperproductive, seasonal, turbid water, eco-georeferenceable,explanative, *S. damnosum* s.l., narrow tributary,African, riverine agro-village, ecosystem complex, discontinuous, infrequently canopied, sparsely shaded, forecast, vulnerability geo-spectrotemporal, geosampled, graph function in Calculus Methode/MapServer™ may optimally define an eco-epidemiological, capture point, immature habitat surface in Euclidean space. In geometry, Euclidean space encompasses the 2-D Euclidean plane and the 3-D space of Euclidean geometry (http://mathworld.wolfram.com/CauchySequence.html). For example, for every eco-georeferenceable, capture point on a infrequently canopied, immature, discontinuous, *S. damnosum* s.l.habitat surface sample, there would be an finite number of tangent lines (e.g., wide range of scatter when quantiating seasonal reflectance/canopy height relationships for determining layering information such canopy layer structure or foliage profile layering).In geometry, the tangent line (or simply tangent) to a plane curve at a given point is the straight line that "just touches" the curve at that point[24]. More precisely, a straight line is said to be a tangent of a curve $y = f(x)$ at a point $x = c$ on the curve if the line passes through the point $(c, f(c))$ on the curve and has slope $f'(c)$ where f' is the derivative of f. A similar definition applies to space curves and curves in n-dimensional Euclidean space in Calculus Methode/MapServer™.

Partial differentiation in an explanatorial, seasonally hyperproductive, explicative, eco-georeferenceable, capture point, forecast, vulnerability model, residual output in in Calculus Methode/MapServer™ may determine *S. damnosum* s.l.,exogenous catchment 3-D, slope covariate coefficients. The difference of the canopy elevation and underlying terrain elevation yields a canopy height modelthat can eco-cartographically represents a spatially-explicit

description of canopy structure (i.e. volume, height, biomass, etc.) over a given area [www.esri.com] Usually, the lines of most interest are those that are parallel to the *xz*-plane, and those that are parallel to the *yz*-plane which result from holding either y or x constant, respectively. To find the slope of the line tangent to the function at P(1, 1) that is parallel to the *xz*-plane, the *y* variable should treated as constant in the capture point model . In so doing, a differential graph can determine if iteratively interpolated , eco-georeferenceable, *S. damnosum* s.l. capture point geospectrotemporally uncoalesced, discontinuous canopy visible wavelength reflectance is negatively correlated to canopy height due to chlorophyll absorption and structural shadowing effects, for example, while optimally quantiating whether near-IR reflectance is positively correlated due to the light scattering properties of leaf internal structure. ArcGIS provides a simulation, at a moderate spectral resolution, of quasiinfinite leaf reflectance (as represented by stacked leaves) and single leaf reflectance(www.esri.com). Single leaf reflectance and transmittance are important input variables to vegetation canopy reflectance models[24].

Partial derivatives are defined as derivatives of a function of multiple variables when all but the variable of interest are held fixed during the differentiation. $\frac{\partial f}{\partial x_m} = \lim_{h \to 0} \frac{f(x_1, \ldots, x_m + h, \ldots, x_n) - f(x_1, \ldots, x_m, \ldots, x_n)}{h}$ [26].The above partial derivative is sometimes denoted f_{x_m} for brevity. Partial derivatives can also be taken with respect to multiple variables, as denoted for examples $\frac{\partial^2 f}{\partial x^2} = f_{xx}$, $\frac{\partial^2 f}{\partial x \partial y} = f_{xy}$ and $\frac{\partial^3 f}{\partial x^2 \partial y} = f_{xxy}$.Such partial derivatives involving more than one variable are called mixed partial derivatives. For a "nice" two-dimensional function $f(x, y)$(i.e., one for which f, f_x, f_y, f_{xy}, f_{yx}exist and are continuous in a neighborhood (a, b)), then $f_{xy}(a, b) = f_{yx}(a, b)$.[http://mathworld.wolfram.com/] More generally, for "nice" functions, mixed partial derivatives must be equal regardless of the order in which the differentiation is performed, so it also is true that $f_{xxy} = f_{xyx} = f_{yxx}$.

On the graph in Figure 3 the *S. damnsoum* s.l., forecast vulnerability quantiated explanative function looks on the plane $y = 1$. By finding the derivative of the equation while assuming that y is a constant, in the model's latent forecasts, the slope of f at the point (x, y) may be found by optimally employing $\frac{\partial z}{\partial x} = 2x + y$. So at (1, 1), by substitution, the slope of a geo-spectrotemporally iteratively plotted, explanatorial, seasonal, discontinuous canopy patterns of gross primary productivity, inferred from eddy covariance measurements of surface–atmosphere CO2 exchange surface may be determined (i.e., 3). The derivative of a function $f(x)$ of a variable x is a measure of the rate at which the value of the function changes with respect to the change of the variable [26]. It is called the derivative of f with respect to x. If x and y are real numbers,(e.g., dataset of uncoalesced *S. damnosum* s.l., moderate resolution wavelength, transmittance emissivty frequencies) and if the graph of f is plotted against x, the derivative is the slope of this graph at each point.The simplest case, apart from the trivial case of a constant function, is when y is a linear function of x, meaning that the graph of y divided by x is a line. Therefore,$\frac{\partial z}{\partial x} = 3$at the geosampled, geospatialized, moderate resolution, trailing vegetation, hyperproductive, seasonal, turbid water, *S. damnosum* s.l.narrow tributary,African, riverine agro-village, eco-georeferenceable, ecosystem complex, capture point (1, 1). That is, the partial derivative of z with respect to x

at (1, 1) is 3, as shown in the graph in Figure 6.

Figure 6. A differential graph of a hypothetical, capture point, geo-spectrotemporally uncoalesced, proxy *S. damnsoum* s.l.,biosignature revealing the function in the *xz*-plane at *y*= 1 where two axes are optimally forecastable with different scales and the slope of the tangent line is 3.

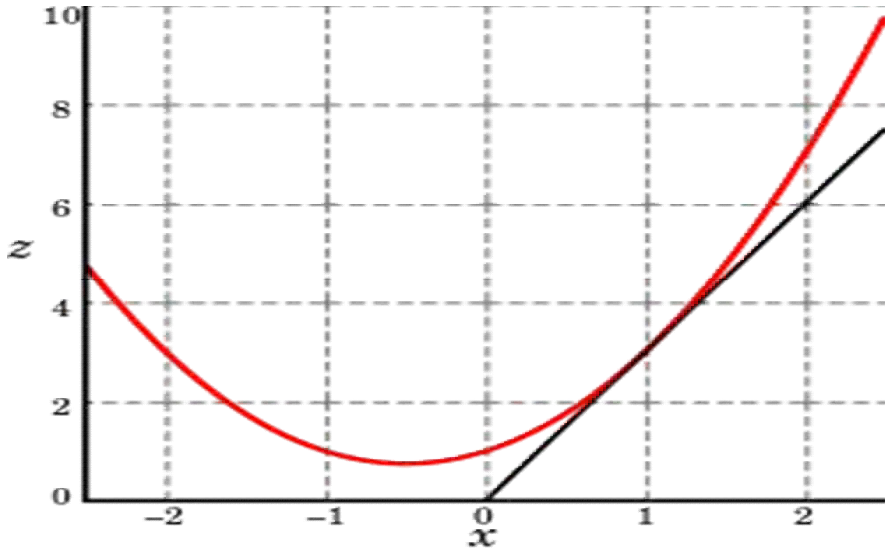

Currently, there does not exist a single solution that can simultaneously heuristically optimize each log-transformed, *S. damnosum* .s.l., seasonal, geo-spectrotemporal porxy LULC biosignature endmember, eigenvector forecastor, for resolving diffuse, nontrivial, multi-objective, irradiance optimization problems in discontinuous canopy leaves (e.g., broadly related moderate resolution ,vegetation geoclassifiable LULCs amount and vigor that are not sensitive to canopy structure). Leaves are an important component of trailing vegetation, hyperproductive, seasonal, turbid water, eco-georeferenceable,explanative, *S. damnosum* s.l., narrow tributary,African, riverine agro-village, ecosystem complex, discontinuous, infrequently, sparsely shaded canopies, and it is the concentration of their biochemical constituents, namely, pigments, water, nitrogen, cellulose, and lignin, together with canopy structure that shapes the absorption features of a capture point's reflectance endmember spectra. Absorption features in the NIR region of the spectrum (1000–2500 nm) in a *S. damnosum* s.l., seasonally hypeproductive, immature habitat may be a function of the bending and stretching vibrations of biochemical bonds between, for example, hydrogen–carbon and nitrogen–oxygen atoms, together with their harmonics and overtones. In the visible region, chlorophyll and carotenoid pigments have strong absorption due to electron energy transitions [24].

Moderate spectral resolution remotely sensed data can be statistically analyzed to estimate the concentration of biochemicals in canopies (www.esri.com). Such information has been used to drive ecosystem, simulation,n proxy LULC biosignature models for estimating photosynthetic efficiency, the rate of nutrient cycling, and the degree of vegetation stress. Strong correlations between leaf biochemical concentrations and specific wavebands of measured spectra quantitated from eco-epidemiolgical, *S. damnosum* s.l. forecasting vulnerability paradigms. However, heuristically optimizable, wavebands selected by multiple linear regression using biochemical assay data are often not consistent with the absorption

features of the biochemicals within canopy leaves. Even when known causal wavebands are selected in the regression equation, geo-spectrotermpoal correlations with explicative, biochemical concentrations are not always strong [24]. To investigate this further, a physical modeling approach may be required to describe and quantify the reflectance, scattering, and absorption of trailing vegetation, hyperproductive, seasonal unquantiated, turbid water, eco-georeferenceable,explanative, *S. damnosum* s.l., narrow tributary,African, riverine agro-village, ecosystem complex, discontinuous, infrequently ,sparsely shaded, canopy leaves as a function of their biochemical and physical properties.

Thus, qualitaively quantitating geo-spectrotemporal, eco-georeferenceable, aggregations of expositively uncoalesced, moderate resolution, proxy, geoclassfiable LULC, biophysical, iteratively interpolative,fractionalized,endmember,biosignature, probabilistic uncertainties (e.g., low reflectance saturation values for visible and NIR bands, perhaps caused by smaller canopies being shadowed by adjacent discontinuous trailing vegation). Hence, eco-epidemiological, frequentistic or non-frequentistic, fractionalized, endmember, heursitically optimiazable datasets of iteratived, geospatialized, eco-georeferenceable, seasonally hyperproductive, *S. damnsoum* s.l., capture point, geo-spectrotemporalized geosampled capture points in narrow tributary, African, agro-village, complex ecosystem with sub-optimally moderate resolution, wavelength, frequency-oriented, transmittance, emissivity estimators may reveal defective interpolated orthogonal eigenvectors which may not quantiate sparsely shaded, discontinuous canopy, narrow tributary, African, agro-village complex ecosystem-level phenological responses to climate change.

As such, identification of a kriged (i.e., Gaussian process regression) iteratively interpolated dataset of un-geosampled,seasonally hyperproductive, *S. damnosum* s.l. capture points may be hindered as the objective functions for the forecasting paradigms may be geospatially conflicting, and there may exist possibly infinite number of Pareto optimal solutions. By yielding all of the potentially optimal endmember solutions in, Calculus Methode/MapServer^{TM} an ecologist, entomologist or other researcher can make focused tradeoffs within a constrained set of parameterizable, sub-mixel, moderate resolution, time series dependent datasets of hueristically oprimizable, *S. damnosum* .s.l., seasonal, endmember, orthogonalized, eigenvector forecastors rather than needing to consider the full ranges of parameters in a Pareto frontier, $P(Y)$. For example , consider an eco-georeferenceable, seasaonlly hyperproductive, *S. damnsoum* s.l., capture point, optimally parameterizable geo-spectrotemporal, moderate resolution, uncoalesced, wavelength, frequency-oriented, transmittance, emissivity estimator dataset with function $f : \mathbb{R}^n \rightarrow \mathbb{R}^m$, where X is a compact set of feasible decisions in the metric space $\mathbb{R}^n$, and Y is the feasible set of criterion vectors in $\mathbb{R}^m$, such that $Y = \{y \in \mathbb{R}^n : y = f(x), x \in X\}$. An ecologist, entomologist or other researcher may assume that the preferred directions of criteria values in Calculus Methode/MapServer^{TM} are known. A geospectrotemporal, *Similium*, seasonal, immature habitat, $y'' \in \mathbb{R}^m$ may be preferred to another eco-georferenceable, immature habitat point $y' \in \mathbb{R}^m$, which may be optimally written as $y'' \succ y'$ in Calculus Methode/MapServer^{TM} The Pareto frontier may then be written as: $P(Y) = \{y' \in Y : \{y'' \in Y : y'' \succ y', y'' \neq y'\} = \emptyset\}$. for capturing near-surface, spatial and temporal variation in *S. damnsoum* s.l., capture point, discontinuous, canopy phenology.

The canopy-absorbed photosynthetically active radiation $APAR_{CAN}$ is the solar energy consumed in the canopy photosynthetic process [25]. Due to the difficulty of acquiring extensive ground-based observations trailing vegetation, hyperproductive, seasonal, turbid

water, eco-georeferenceable,explanative, *S. damnosum* s.l., narrow tributary,African, riverine agro-village, ecosystem complex, discontinuous, infrequently canopied, sparsely shaded, forecast, vulnerability geo-spectrotemporal, geosampled, increasing efforts are being devoted to estimate $APAR_{CAN}$ from optical satellite measurements[22]. So far, $APAR_{CAN}$ has been obtained from the downwelling PAR at the surface (SFC), $PAR_{SFC}\downarrow$, and the fraction of PAR absorbed by a canopy, FPAR for eco-georeferenceable, capture point, seasonally hyperproductive, *S. damnosum* s.l. immature habitats. A new approach Calculus Methode/MapServer^{TM} may define $APAR_{CAN}$ as the product of $APAR_{SFC}$ and RPAR in a iterative interpolative, moderan resolution, forecast, vulnerability model. $APAR_{SFC}$ is the total PAR absorbed by all surface materials including canopy, soil, litter, etc., while RPAR is the ratio of the PAR absorbed by the green canopy only, to $APAR_{SFC}$. [24]. The advantage of this differential approach is that $APAR_{SFC}$ and $PAR_{SFC}\downarrow$, can be optimally determined more accurately. The determination of seasonal, RPAR may be found to be aws accurate as that of FPAR in a *S. damnosum* s.l. habitat model.. The whole approach may be introduced in two parts in a difeferential geometrical forecasting vulnerability model. Part I, may be presented in Calculus Methode/MapServer^{TM}, dealing with the exact retrieval of $APAR_{SFC}$. Using a complex atmospheric radiative transfer model, $APAR_{SFC}$ may then be found to be related to the upwelling PAR reflected at the top of the atmosphere (TOA),(e.g., $PAR_{TOA}\uparrow$.). The relationship may be independent of cloud parameters and surface conditions, and moderately dependent on ozone amount and aerosol optical properties. A parameterization may be developed to estimate $APAR_{SFC}$ from $PAR_{TOA}\uparrow$ inferred from satellite measurements (e.g., iteratively interpolated, geospectrotemrpoally uncoalesced S. damnosum s.l.capture point, proxy LULC biosignatrures) which may be more pronounced in the visible bands. Error analyses may be also conducted in Calculus Methode/MapServer^{TM} using data from both model simulations and field observations. In Jacob et al. [22] performed elucidative parameterizations and found estimating absorbed photosynthesis radiation and leaf area index from spectral reflectance estimator may be valid to within 5 W m^{-2} compared to the results of detailed discontinuous gap, radiation model simulations. A preliminary comparison against (First ISLSCP Field Experiment) FIFE ground observations may revealed a bias error of −2.3 W m^{-2} and a standard error of 23.7 W m^{-2} for the instantaneous estimates of $APAR_{SFC}$.

It would be invalid to treat Pareto efficiency as equivalent to optimality when constructing a trailing vegetation, hyperproductive, seasonal, turbid water, eco-georeferenceable,explanative, *S. damnosum* s.l., narrow tributary,African, riverine agro-village, ecosystem complex, discontinuous, infrequently canopied, sparsely shaded, *S. damnsoum* s.l., forecasting vulnerability paradigm since the latter is a normative concept that is a matter of opinion but typically would take into account the degree of inequality of an eco-epidemiological, frequentistic or non-frequentistic, endmember dataset of iteratively interpolative, explicatively geospatialized, eco-georeferenceable, seasonally hyperproductive, *S. damnsoum* s.l., capture point, seasonal distributions.Pareto efficiency does not require an equitable distribution of data. This possibility is inherent in the definition of Pareto efficiency; often the status quo is Pareto efficient regardless of the degree to which data (e.g., un-geosampled,seasonally hyperproductive, forecasted *S. damnosum* s.l. defective narrow tributary, African, agro-village, complex ecosystem, trailing vegetation, discontinuous, infrequently canopied,sparsely shaded, turbid water, capture points) is equitably distributed.

The Remez penalty and smoothing algorithm (RPSALG) is a unified framework for penalty and smoothing methods for solving min-max, convex, semi-infinite, programing

problems, whose convergence may be plotted in Calculus Methode/MapServer^{TM}. The min-max-problem is a convex problem, as the functionf(x) = maxi2V fi(x) is convex since point-wise maximum of convex functions preserves convexity. For a min-max problem in the form of min$x_{\in}X$ max$t_{\in}T$ {$ft(x)$}, the nondifferentiability of the max function $F(x) \equiv$ max$t_{\in}T$ {$ft(x)$} may present special difficulty in finding optimizable solutions in most software packages or cyberenvironments for forecasting geo-spectrotemporally uncoalesceable, moderate resolution explanative seasonally, eco-georeferenceable, unknown, un-geosampled, eco-geophysiosological biophysical, hyperproductive, *S. damnsoum* s.l., narrow tributary, African, agro-village complex, ecosystem, capture point, trailing vegetation, discontinuous, infrequently canopied,sparsely shaded, turbid water, eco-epidemiological, capture points and theire uncoalesced datasets of frequentistic or non-frequentistic, explicatively iteratively interpolative, optimally imaged, orthogonally decomposable, iteratively interpolative fractionalized, endmember eigenvectors.

It may be shown in Calculus Methode/MapServer^{TM} that an entropic regularization procedure can provide a smooth approximation $Fp(x)$ that uniformly converges to $F(x)$ over X, in an explanatorial eco-georeferenceable, prolific, *S. damnsoum* s.l. seasonal, geo-spectrotemporal, geosampled, capture point, as p tends to infinity. Entropy regularization is a straightforward and successful method of semi-supervised learning that augments the traditional, conditional likelihood, objective function with an additional term that aims to minimize the geo-predicted label entropy on unlabeled data[24]. In this fashion, an empirical regressable dataset of unknown, ungeosampled,trailing vegation, disconstinuous, infrequently canopied, sparsely shaded, turbid water, seasonal, hyperproductive, narrow tributary, African, agro-village complex, eco-georeferenceable, *S. damnsoum* s.l. ecosystem, capture point, may be optimally mapped. Additionally, elucidatively residualized, optimizable eco-geophysiosological biophysical, elucidative forecastors may be rendered in Calculus Methode/MapServer^{TM} with p being sufficiently large, minimizing the smooth function $Fp(x)$ over X. In so doing, a very accurate approximate solution to the min-max problem in a robustly fractionalized, geo-spectrotemporal, geo-spatial, endmember eigenvector iteratively, quantitative, interpolative, uncoalesced, moderate resolution, wavelength, transmittance, frequency-oriented, emissivity, eco-epidemiological, forecast, vulnerability model may be devised. This approach may be applicable for solving linearizable semi-infinite programming problems such as quantitating biased, constrained, convexical eco-georeferenceable, hyperproductive, *S. damnosum* s.l. seasonal, capture point, forecasting moderate resolution, fractionalized, endmember, eigenvector misspecified contributions.

Each iteration of RPSALG in an Calculus Methode/MapServer^{TM} cyberenvironment involves two types of auxiliary optimization problems: the first one consists of obtaining an approximate solution of some discretized convex problem, while the second one requires solving a non-convex optimization problem involving the parametric constraints as objective function with a endmember, forecastable regressional, explanatorial seasonally geosampled variable (e.g., Percent of discontinuous, sporadically canopied, trailing vegetation at a hyerproductive, *S. damnosum* s.l., capture point). The latter problem may be optimally quantitated with a variant of the cutting angle method for parsimoniously implementing a heursitic deterministic technique for resolving different moderate resolution, proxy, uncoalesced LULC biosignature uncertainties (waveband diffuse multiscattering) in sub-mixel, optimally parameterized, *S. damnosum* s.l. noisy datasets especially those that may exhibit equifinality. Equifinality is the principle that in open systems a given end state can be reached by many potential means [24].

By increasing positive homogeneous (IPH) functions over the unit simplex in Calculus Methode/MapServer^{TM}, Lipschitz problems may be optimally qualitatively quantated in an uncoalesced dataset of fractionalized moderate resolution, orthogonalized synthetic, spatial filter, trailing vegation, discontinuous, infrequently canopied, sparsely shaded, turbid water, seasonal, hyperproductive, narrow tributary, African, agro-village complex, eco-georeferenceable, ecosystem, *S. damnsoum* s.l. capture point, immature habitats eco-geophysiosological biophysical seasonal, endmember eigenvectors rendered from any iterative interpolator . A function f such that $|f(x) - f(y)| \leq C|x - y|$ for all x and y, where $C$is a constant independent of x and y , is called a Lipschitz function[24]. Any seasonally hyperproductive, *S. damnsoum* s.l., moderate resolution, imaged, immature habitat, capture point, function with a bounded first derivative must be Lipschitz[22]. In so doing, the reflectance of a seasonal, hyperproductive, narrow tributary, African, agro-village complex, eco-georeferenceable, *S. damnsoum* s.l. ecosystem, capture point discontinuous canopy may be similar, but may be seasaonlly modified by the nonuniformity of incident solar radiation, specific plant structureal (e.g., relationships leaf reflectance and chlorophyll fluorescence), leaf areas, shadows, and background reflectivities

An ecologist, entomologist or other research may also derive the Lipschitz dependence of the set of solutions of a convex minimization or other problems and its Lagrange multipliers in a Calculus Methode/MapServer^{TM} cyberenvironment. In mathematical optimization, the method of Lagrange multiplier is a strategy for finding the local maxima and minima of a function subject to equality constraints. Optimally tabulating geo-spectrotemporally, explanative, robust geospatially, optimally geoclassifiable elucidative datasets of heursitically parameterizable, quantitatable, proxy, LULC biosignature, eco-geophysiosological, biophysical, fractionalized fractionalized, endmember eigenvector, estimator, moderate resolution, proxy datasets may enable iteratively interpolation of uncoalesced, eco-georeferenceable, eco-epidemiological, seasonally hyperproductive, *S. damnsoum* s.l., narrow tributary, African, agro-village complex, ecosystem, capture point, trailing vegetation, discontinuous, infrequently canopied,sparsely shaded, turbid water, immature habitat, wavelength, tranmittance, emissivities in Calculus Methode/MapServer^{TM} may aid in revealing geolocations of unknown, ungeosampled hyperproductive, seasonal habitats employing priciples rendered from the inverse function theorem.

In mathematics, specifically differential calculus, the inverse function theorem gives sufficient conditions for a function to be invertible in a neighborhood of a point (e.g., a seasonally hyperproductive, narrow tributary, African, agro-village, trailing vegetation, discontinuous, infrequently canopied, turbid water *S. damnsoum* s.l. eco-georeferenceable, capture points) in its domain. The theorem also gives a formula for the derivative of the inverse function. In multivariable calculus this theorem can be generalized to any continuously differentiable, elucidative vector-valued function whose Jacobian determinant is nonzero at a point in its domain. In Calculus Methode/MapServer^{TM},the Jacobian matrix is the matrix of all first-order partial derivatives of a vector-valued function(www.esri.com).

Suppose $f : \mathbb{R}^n \to \mathbb{R}^m$ is a non-optimizable, explanatively fractionalionizable, geo-spectrotemporally,optimally orthogonalizable, moderate resolution,fractionalizable, eco-geophysiosological biophysical endmember eigenvector, empirically regressed. geosampled, uncoalesced, moderate resolution, eco-georeferenceable, geoclassfiable, hyperproductive, seasonal, eco-epidemiological, trailing vegetation, infrequently canopied, discontinuous, turbid water, *S. damnosum* s.l., narrow tributary,African, riverine agro-village, ecosystem complex, capture point, forecasting vulnerabili tmodel function in a Calculus

Methode/MapServer™ cyberenvironment. Optimally this input vector $x \in \mathbb{R}^n$ would render an output based on the vector $f(x) \in \mathbb{R}^m$. Then the Jacobian matrix J of f would be an $m \times n$ matrix, optimally defined and arranged as follows: $\mathbf{J} = \frac{d\mathbf{f}}{d\mathbf{x}} = \begin{bmatrix} \frac{\partial \mathbf{f}}{\partial x_1} & \cdots & \frac{\partial \mathbf{f}}{\partial x_n} \end{bmatrix} = \begin{bmatrix} \frac{\partial f_1}{\partial x_1} & \cdots & \frac{\partial f_1}{\partial x_n} \\ \vdots & \ddots & \vdots \\ \frac{\partial f_m}{\partial x_1} & \cdots & \frac{\partial f_m}{\partial x_n} \end{bmatrix}$ or, component-wise: $\mathbf{J}_i^j = \frac{\partial f_i}{\partial x_j}$. This matrix, whose entries would be functions of x (i.e., eco-georeferenceable capture point), may be denoted by Df, J_f, and $\partial(f_1,...,f_m)/\partial(x_1,...,x_n)$, for example. The Jacobian matrix could optimally autoregressively quantiate if the function f in the spatially weighted eco-geophysiosological, biophysical, *S. damnsoum* s.l., forecast vulnerability model is differentiable at a x. Then the Jacobian matrix could define an eco-epidemiological, *S. damnsoum* s.l. linear map $\mathbb{R}^n \rightarrow \mathbb{R}^m$, which could be optimally heursitically quantized parsimoniously employing linear approximation of the function f near the point x. This forecast, vulnerability map would be thus the quantized generalizations of the elucidtaively quantitable, heursitically optimizable, partial and non-patial derivatives of the differential f at x.

If $m = n$, the Jacobian matrix is a square matrix, and its determinant is a function of $x_1, \ldots,$ then x_n, is the Jacobian determinant of *f*[www.sas.edu]. This deterimnant in a seasonal, eco-epidemiological, trailing vegetation, infrequently canopied, turbid water, discontinuous, infrequently canopied, *S. damnosum* s.l.narrow tributary,African, riverine agro-village, ecosystem complex, capture point, moderate resolution, forecasting, vulnerability model could render important information about the local behavior of *f*. Further, the function *f* would be geo-spectrotemporally geospatially quantifiable in the neighborhood of an eco-georeferencable, capture point x employing an inverse function that is differentiable if and only if the Jacobian determinant is nonzero at x. The Jacobian determinant occurs also when changing regressands in multi-variable integrals. If $m = 1$ in the *S. damnosum* s.l. model, f is a scalar field and the Jacobian matrix would be reduced to a row vector of partial derivatives of f (i.e. the gradient of f).

In this case, the theorem gives a formula for the Jacobian matrix of the inverse. There are also versions of the inverse function theorem for complex holomorphic functions in SAS/GIS for constructing differentiable, *S. damnsoum* s.l., capture point, immature habitat maps between manifolds, for quantitating differentiable functions between Banach spaces, and so forth. In mathematics, more specifically in functional analysis, a Banach space (is a complete normed vector space[24]. Given a complex-valued function *f* of a single complex eco-georeferenceable, eco-epidemiological, seasonally hyperproductive narrow tributary, African, agro-village complex, ecosystem, *S. damnsoum* s.l., capture point, trailing vegetation, discontinuous, infrequently canopied,sparsely shaded, turbid water, immature habitat, moderate resolution, uncoalesced, wavelength, tranmittance, emissivity variable, the derivative of *f* at a point z_0 in its domain is defined by the limit $f'(z_0) = \lim_{z \to z_0} \frac{f(z) - f(z_0)}{z - z_0}$. In so doing, fluorescence effects for non-constant, leaf chlorophyll pigment, seasonal levels in *S. damnsoum* s.l., immature, hyperproductive, eco-georefernced, capture points, may be suggested, through model simulation employing moderate resolution, geometrical optical indices.

The chlorophyll content in leaves is potentially one of the most important indicators

of vegetation strain in seasonally hyperproductive,eco-georferenceable, *S. damnosum* s.l. narrow tributary, African, agro-village complex, ecosystem trailing vegetation, discontinuous, infrequently canopied,sparsely shaded, turbid water,capture point[22]. The total chlorophyll content in leaves decreases in stressed vegetation geoclassifiable LULCs, changing the proportion of light-absorbing pigments and leading to less overall absorption. The absorption of electromagnetic radiation by this pigment varies with the wavelength, with strong absorption in the blue (400–500 nm) and red (600–700 nm) portions of the visible spectrum and relatively less absorption in the green (500–600 nm) portion[24]. Differences in reflectance between healthy and stressed vegetation due to changes in pigment levels may be detected in the green peak and along the red edge (690–750 nm) in an eco-georefernceable, seasonally hyperproductive, *S. damnosum* s.l.capture point. Thus tracking fluorescence signals independent of pigment levels employing an iteratively interpolated, geo-spectrotemporally uncoalesced, moderate resolution, eco-georferenceable, *S. damnosum* s.l., capture points proxy LULC biosignature in SAS/GIS may optimally geolocalize, , remotely illusive discontinuous canopy gaps where the bidirectional reflectance effects of canopy architecture and combined variations in leaf pigment and fluorescence are possible in a seasonally hypeproductive, explanative, trailing vegetation, turbid water, discontinuous, infrequently canopied,sparsely shaded, immature habitats as well as potentially confounding issues related to atmospheric correction

Such estimates may arise from a generalization of the following classical result whereby each convex function is the upper envelop of its affine minorants in a heursitically optimizable dataset of narrow tributary, African, agro-village, trailing vegetation, discontinuous,infrequently canopied, turbid water *S. damnsoum* s.l. eco-georeferenceable, capture points, geo-spectrotemporally uncoalesced, wavelength, tranmittance frequencies.. In the theory of integral and differential equations, a majorant (minorant) or majorant function (minorant function) for some function f is a continuous function whose Dini derivative at each point (e.g., eco-georeferenceable, eco-epidemiological, seasonally hyperproductive, capture point) is not less (not greater) than f(t) and is different from $-\infty$ to $+\infty$. The upper right-hand Dini derivative Λ α. $\Lambda\alpha$ is definable in Calculus Methode/MapServer^{TM} to be the limes superior of the quotient $(f(x1)-f(x))/(x1-x)$ $(f(x1)-f(x))/(x1-x)$ as $x\ 1 \rightarrow x$ $x1 \rightarrow x$, where $x\ 1 > x$. The lower right-hand $\lambda\alpha$, the upper left-hand Λ g , and the lower left-hand Dini derivative λg are defined analogously. If $\Lambda\ \alpha = \lambda\ \alpha$ (i.e., Λ g $= \lambda$ g), then f would have at the point x, a one-sided Dini derivative.The difference between any majorant and any minorant is a non-decreasing function[24]. Any elucidatively summable, eco-georeferenceable, eco-epidemiological, seasonally hyperproductive, *S. damnsoum* s.l. narrow tributary, African, agro-village complex, trailing vegetation, discontinuous, infrequently canopied,sparsely shaded, turbid water capture point quantized function on an interval would optimally have a dataset of absolutely-continuous majorants and minorants which are arbitrarily close to its indefinite Lebesgue integral.

The integral of a non-negative function can be regarded, in the simplest case, as the area (e.g., linear quadrant between an eco-georeferenceable, eco-epidemiological, seasonally hyperproductive, trailing vegetation, discontinuous, infrequently canopied,sparsely shaded, turbid water *S. damnsoum* s.l. narrow tributary, African, agro-village complex, capture point,)ArcGIS graph of that function and the *x*-axis. The Lebesgue integral extends the integral to a larger class of functions in Calculus Methode/MapServer^{TM} It also extends the domains on which these functions can be defined. For non-negative functions with a smooth enough graph—such as continuous functions on closed bounded intervals—the area under the curve could be defined as the integral, and computed using approximation techniques on the

region by Calculus Methode/MapServer^{TM} -derived heursitically optimizable, seasonally hyperproductive, *S. damnsoum* s.l., eco-georeferenecable polygons. However, as the need to consider more irregular functions arises—as a result of the limiting processes of mathematical analysis and the mathematical theory of probability—it would became clear that more careful approximation techniques for these models may be required to define a suitable integral. Also, an ecologst, entomologist or orher researcher may wish to integrate residualizable, eco-epidemiological, ecogeoreferenceable, forecasted unknown, un-geosampled habitats on regression spaces more generalizable than the real line in. Calculus Methode/MapServer^{TM} The Lebesgue integral may provide the right abstractions needed to conduct an iterative interpolation employing geospectrotemporally uncoalesced, moderate resolution, trailing vegation, discontinuous, sporadically canopied,narrow tributary *S. damnsoum* s.l., African, agro-village complex, capture point, proxy, LULC, biogeophysical, eco-geophysiological, biosignature variables in an Calculus Methode/MapServer^{TM} cyberenvironment

A closed proper convex function f is the pointwise supremum of the collection of all affine functions h such that $h \leq f$ [24].In abstract convex analysis in Calculus Methode/MapServer^{TM} the requirement of linearity of the minorants may be dropped, and abstract convex functions may be eco-cartographically illutsratable as the upper envelops of some simple minorants, or support functions, which may not necessarily have to be affine when modelling uncoalesced moderate resolution, *S. damnsoum* s.l.capture points. Depending on the choice of the support functions, an ecologist, entomologist or other researcher optimally may obtain different flavours of abstract convex analysis in an Calculus Methode/MapServer^{TM} cyberenvironment, which may be applicable to constructing forecast vulnerability paradigms. Convex analysis is the branch of mathematics devoted to the study of properties of convex functions and convex sets, often with applications in convex minimization, a subdomain of optimization theory[24]. In mathematics, computer science and operations research, mathematical optimization (alternatively, optimization or mathematical programming) is the selection of a best element (with regard to some criteria) from some set of available alternatives (http://mathworld.wolfram.com/ html).

In the simplest case, an optimization problem in an regression-related eco-georeferenceable, seasonally hyperproductive, trailing vegetation, discontinuous, infrequently canopied,sparsely shaded, turbid water *S. damnsoum* s.l., narrow tributary, African, agro-village complex, biogeophysical, eco-geophysiological,capture point, forecasting vulnerability paradigm consists of maximizing or minimizing a real function by systematically choosing input values from within an allowed set and computing the value of the function. The generalization of optimization theory and techniques to other formulations comprises a large area of applied mathematics [24]. More generally, the optimization would include finding the "best available" geo-predictable, unbiased dataset of seasonally hyperproductive, immature *Similium,* capture point explicative, count values of some objective function, which in an Calculus Methode/MapServer^{TM} cyberenvironment could be optimally defined by a domain or a set of constraints along with a variety of different types of objective functions and different types of domains from other proxy, geoclassifiable, LULC, biosignature uncoalesced habitat, heterogeneity metrics and geoclassifiable, ecophysiological bogeophysical, elucidative, variables geo-spectrotemporally geospatially, in African, riverine-agro-village narrow tributary terrestrial ecosystems (e.g., non-contiguous, mean canopy height. seasonal, diurnal changes in carbon dynamics concurrent xanthophyll pigment changes during pre-flooding, absorbed photosynthetically active radiation by trailing green vegetation etc).

For set-valued geo-spectrotemporally eco-epidemiological, uncoalesced, geosampled datasets of biogeophysical, eco-geophysiological, geo-spatialized, heuristically robustifiable, orthogonally, explanatively decomposable, expositively fractionizable, frequentistic or non-frequentistic, seasonally hyperproductive, geoclassifiable, eco-georeferenceable,narrow, African, riverine tributary, agro-village complex, *S. damnosum* s.l. immature habitat, iteratively interpolative, proxy, LULC biosignature, components maps, the inverse function theorem can be generalized to differentiable maps between differentiable manifolds in Calculus Methode/MapServer™. A manifold is a topological space that resembles Euclidean space near each sampled point[24].In this context, a differentiable decomposed, *S. damnosum* s.l. forecast, vulnerability map $F : M \to N$ can be deduced if the differential of F, $dF_p : T_pM \to T_{F(p)}N$ is a linear isomorphism at an point P (e.g., seasonal, explanative, eco-georeferenceable, hyperproductive, capture point) in M. In such circumstances there would exist an eco-georeferenceable, narrow, African, riverine tributary, agro-village complex, geospatialzed, ecogeorferenceable neighborhood U of P such that $F|_U : U \to F(U)$ is a diffeomorphism. In mathematics, a diffeomorphism is an isomorphism of smooth manifolds [24]. More precisely, each explicative, eco-georeferenceable, seasonally hyperproductive, geo-spectrotemporally uncoalesced, *S. damnosum* s.l capture point, moderate resolution, fractionalized, endmember, eigenvector dataset containing an n-dimensional manifold in Calculus Methode/MapServer™ would have have an elucidatively geo-spatializable neighbourhood that is homeomorphic to the Euclidean space of dimension n. A function f: $X \to Y$ between two topological spaces (X, T_X) and (Y, T_Y) is called a homeomorphism if it has the following bicontinuous properties:1)f is a bijection (one-to-one and onto),2)f is continuous,;and, 3) the inverse function f^{-1} is continuous (f is an open mapping)[24].

A Calculus Methode/MapServer™ cyberenvironment can generate invertible functions that can map seasonally explicatively eco-georeferenceable, hyperproductive,geo-spectrotemporally geoclassifiable, narrow, African, riverine tributary, agro-village complex, seasonal, capture point, immature, black-fly habitats of *S. damnosum* s.l., employing a differentiable manifold such that both the function and its inverse are smooth. In so doing, M and N would have the same dimension at P in a forecasting vulnerability paradigm in Calculus Methode/MapServer™. If the derivative of F is an isomorphism at all eco-georeferenceable overlaid geosampled, seasonal, biogeophysical, eco-geophysiological, capture points $\underline{P}$ in M,then the map F could be geoclassifiable as a a local diffeomorphism. Let X and Y be differentiable manifolds in Calculus Methode/MapServer™ then a *S. damnosum* s.l., function,$f : X \to Y$ may be a local diffeomorphism, if for each geo-spectrotemporally, geosampled, capture point x in X, there exists an open set U containing x, such that $f(U)$ is open in Y and $f|_U : U \to f(U)$ is a diffeomorphism. A local diffeomorphism may be a special case of an immersion f from X to Y, where eco-georeferenceable, moderate resolution images of trailing vegation, discontinuous, infrequently canopied, turbid water, narrow, riverine tributary, African, agro-complex, hyperproductive, *S. damnsoum* s.l. capture point, seasonal, image $f(U)$ of U under f locally has the differentiable structure of a submanifold of Y. Then $f(U)$ and X would have a lower dimension than Y in the optimizable moderate resolution, fractionalized, uncoalesced endmember eigenvetcor datasets. Thereafter, Geostatistical Analyst ™ may provide a eco-cartographic framework for constructing a geo-spatial heuristically elucidatively optimizable, orthogonally explanatively decomposable, fractionizable, non-frequentistic, seasonally hyperproductive, geoclassifiable, eco-georeferenceable,narrow, African, riverine tributary, agro-village complex, *S. damnosum* s.l. immature t, proxy LULC biosignature, iteratively interpolatble components map

To minimize or upper-bound a geospectrotemporal, geospatialized, S. *damnsoum* s.l., immature habitat, moderate resolution, geo-spectrotemporally uncoalesced wavelength, trasnmittance, frequency-oriented, emissivity tabulated value of a function robustly, an ecologist, entomologist or other researcher might minimize or upper-bound the "epsilon-robust regularization" in Calculus Methode/MapServer™ which may optimal define a geometerical, measurement variable from a geo-spectrotemporally geosampled capture point employing the maximum value of the function within an epsilon-radius (e.g., Euclideanized distance from a eco-georeferenceable, hyperproductive, seasonal capture point to an narrow, African, tributary, agro-complex . Recently, automatic, data-driven and computationally efficient frameworks for extracting networks employing tractography and epsilon neighborhoods were proposed in the diffusion tensor imaging (DTI) literature(www.esri.com) Regularization of geo-spectrotemrpaolly geosamplable forecastable uncoalesced, iteratively interpolative, *S. damnosum* s.l. moderate resolution, geometerically dieffereential, independent variables may be easy to compute in In so doing, convex quadratics may lead to semidefinite eco-cartographic, trailing vegation, discontinuous, infrequently canopied, turbid water, narrow, riverine tributary, African, agro-complex, hyperproductive, *S. damnsoum* s.l. capture point, representable regularizations. Quadratic programming (QP) is a special type of mathematical optimizer in Calculus Methode/MapServer™ for minimizing or maximizing a quadratic function of several variables subject to linear constraints (http://mathworld.wolfram.com/.html)

Further, optimally heursitically calculatable moderate resolution, radius measurements of an uncertainity fractionalized, endmember, spatially weighted, autoregressive, moderate resolution, eigenvector matrix may lead to robustifiable pseudospectral computations. For favorable classes of functions, an ecologist, entomologist or other researcher may utilize regularization or may quantiate Lipschitz in Calculus Methode/MapServer™ around any given geo-spectrotemporally geosampled eco-georeferenceable, eco-epidmiological, sparsely shaded, seasonally hyperproductive, trailing vegation, discontinuous, infrequently canopied, turbid water, narrow, African, agro-village complex, ecosystem, *S. damnsoum* s.l., immature habitats for all small epsilon > 0, even if the original function is nonlipschitz like the spectral radius of a explanative, orthogonally decomposed, capture point.

One favorable class for aiding in iteratively quantitatively interpolating an orthogonally decomposable, moderate resolution images of hyperproductive, eco-georeferenceable, *S. damnosum* s.l. seasonal, capture point consists of the semi-algebraic functions in Map Algebra ™ in ArcGIS. Such functions have graphs that are finite unions of sets defined by finitely-many polynomial inequalities, and are commonly encountered in forecast, vulnerability-oriented, medical entomological, vector, arthropod-related, heuristically robustifiable, immature, seasonal, mapping applications. The pseudospectrum of a matrix is the subset of the complex plane consisting of all eigenvalues of complex matrices within a distance measured by the operator 2-norm[24] . The operator norm of a linear operator $T : V \to W$is the largest value by which Tstretches an element of V, $||T|| = \sup_{|v|=1} ||T(v)||$. (http://mathworld.wolfram.com/OperatorNorm.html) In linear algebra, functional analysis, and related areas of mathematics, a norm is a function that assigns a strictly positive length or size to each vector in a vector space—save for the zero vector, which is assigned a length of zero.

A norm optimally definable on the space of elucidatively bounded linearizaable geo-

spectrotemporally uncoalesced, geospatialized, trailing vegation, discontinuous, infrequently, seasonally sparsely shaded, explanatively hyperproductive, *S. damnsoum* s.l., capture point, moderate resolution, synthetic, orthogoalizable, endmember eigenvector operators between two given normed vector spaces in Calculus Methode/MapServer^{TM}, may render explicatively unbiased unknown, un-geosampled, prolific habiats in an eco-georeferenceable, narrow, African, riverine tributary, agro-village, complex. Given a nonderogatory matrix $A0$, for small epsilon > 0 in a eco-epimiological, *S. damnosum* s.l. , geo-spectrotemrpoal, geospatial, moderate resolution, wavelength, frequency-oriented, transmittance, emissivity, forecasting, vulnerability model, then the pseudospectrum of any matrix A near $A0$ in Calculus Methode/MapServer^{TM} may consist of compact convex neighborhoods of orthogonally decomposable endmember eigenvalues of $A0$.Additionally, the dependence of each of these neighborhoods on A would be Lipschitz.

Commonly a constraint may has to be imposed on the spatial filters for orthogonalization of eigenvector, nonnegative, abundance fractions in the eigenfunction decompositional algorithm in ArcGIS.An eco-georeferenceable, hyperproductive, narrow, African, riverine tributary, agro-village, complex, capture point, discontinuous, trailing vegetation, sparsely shaded, infrequently canopied, *S. damnosum* s.l., extracted mixel may be subsequently summed to one. In order to preserve inherent characteristics of solutions corresponding to amounts and fractionalized, reflectance of uncoalesced, endmember orthogonal eigenvector, moderate resolution, proxy, geoclassifiable LULC, biosignature wavelength, transmittance emissivity measurements, associated with seasonal geo-spectrotemporally geosampled, frequency, immature counts, sub-mixel intensities and iteratively quantatively interpolative, discontinuous, trailing vegetation, sparsely shaded, canopy, bio-chemical pigment concentrations [Chorphyll(Chl)-a], the nonnegativity constraints may have to qualitatively implemented so as to avoid physically absurd and unpredictable results. For technical reasons, the variables of linear programs must always take non-negative values (i.e., they must be greater than or equal to zero)[24]. This viewpoint has both computational as well as philosophical underpinnings for mapping hyperproductive, eco-georeferenceable, narrow, African, riverine tributary, agro-village, complex, geo-spectrotemporally geosampled, seasonal, capture point, *S. damnosum* s.l., endmember eigenvectors. For example, for the sake of interpretation a medical entomologist of other experimenter might prefer to determine heuristically explanatively optimizable solutions from the same regression space,or a subspace thereof,in a moderate resolution, seasonal, eco-georeferenceable, explanative, capture point, *S. damnosum* s.l. endmember, forecasting, vulnerability model as that of the input data. Non-negative matrix factorization is distinguished from the other methods by its use of non-negativity constraints which optimally leads to a parts-based representation in ArcGIS as the constraint is restricted to only additive, not subtractive, combinations [25].

Whilest the sum-to-one constraint is easy to utilize, the nonnegativity constraint may be tedious to implement in an illuminatively expositive, eco-georeferenceable uncoalesced, dataset of geo-spectrotemporally geo-spatialized, ArcGIS-derived, geo-predictive, *S. damnosum* s.l., larval control, unbiased, mapping variables (e.g., seasonally flooded, positively autocorrelated, remotely targeted, hyperproductive, trailing vegetation, sparsely shaded, discontinuous, infrequently canopied, narrow, African, riverine tributary, agro-village complex, endmember, capture points) since it may result in a set of inequalities and thus could only be be solved by futher, numerical, iterative, algorithms in ArcGIS which may induce erroneous, propogational sub-mixel estimators (e.g., endmember heteroskedastic parameters). Thus, special emphasis must be placed on constraints in least squares

computations and numerical, non-linear, optimization algorithms in ArcGIS. Techniques involving non- negative low-rank matrix and tensor factorizations may have to be emphasized in ArcGIS in order to optimally decorrelate elucidative, geospectrotemporal, geospatially measureable, proxy, LULC biosignature, regressionable trends from an empirical dataset of heuristically optimizable, explantively, eco-georefernceable, trailing vegetation, discontinuous, infrequently canopied, hyperproductive, narrow, African, riverine tributary, ecosystem complex moderate resolution scene.

Nonnegative Matrix Factorization (NMF) in ArcGIS includes various extensions and modifications, especially Nonnegative Tensor Factorizations (NTF) and Nonnegative Tucker Decompositions (NTD). NMF/NTF and their extensions are increasingly employed as tools in signal and image processing in ArcGIS having garnered interest due to their capability to provide new insights and relevant information about complex explanatively quantitable, latent relationships in experimentally, heuristically optimizable fractionalizable, moderate resolution proxy, LULC biosignatures. It is suggested in the literature that NMF can provide meaningful components with explicative, bio-geophysical and molecular interpretations. For example, in ArcGIS bioinformatics, NMF and its extensions have been successfully applied to gene expression, sequence analysis, clustering and text mining. As such, an ecologist, entomologist or other researcher may focus on these iterative iterpolative algorithms when employing explicatively eco-georeferenceable, empirically regressed geo-spectrotemporal datasets of uncoalesced, moderate resolution, seasonal, hyperproductive, trailing vegetation, turbid water, discontinuous, infrequently canopied, narrow, African, riverine tributary, agro-village, complex ecosystem, eco-epidemiological, capture point, optimally parameterizable, wavelength, transmittance, for eco-cartographically robustifying large-scale frequency-oriented, *S.damsnoum* s.l. forecast, emissivity, regression-related,fractionalized, orthogonalizable, endmember eigenvector, vulnerability models.

As a nonparametric method, an ArcGIS regression tree algorithm will not assume any *a* priori distribution of an heuristically optimizable explanative, moderate resolution, ecogeoreferenceable, orthogonally decomposable, endmember, trailing vegetation,sparsely shaded, discontinuous, infrequently canopied, space-time eigenvector, filter specifications rendered from a geo-spectrotemporal uncoalesced, *S. damnosum* s.l. capture point, forecast, vulnerability model. This relaxation of variable distribution assumptions may enable unmixing, endmember algorithms in ArcGIS to be vigorous in dealing with outliers, collinearities amongst fractionally uncoalesced, moderate resolution, wavelength, transmittance, sub-mixel, heteroskadesticity, and/or distributional frequentistic,error structures that might cause problems in parametric geo-spectrotemporal, *S. damnosum* s.l. capture point eigenvector, forecast, vulnerability analyses.

When constructing explicative, geo-spectrotemporal, quantiatively geo-spatializable, fractionalizable, endmember eigenvector, geo-predictive eco-biological mathematical models from moderate resolution, imaged, seasonal hyperproductive, uncoalesced, narrow, riverine tributary, agro-village complex, *S. damnsoum* s.l., capture point, riverine foci, proxy, LULC biosignatures, one of the tools to describe the robustness of a system to perturbations would be a sensitivity analysis in ArcGIS which would attempt to optimally determine which parameter directions (or their combinations) are the most/least sensitive to perturbations and eigenvector probabistic uncertainties, or to errors resulting from experimental parameter estimation. Recently, there has been significant progress in ArcGIS in developing sensitivity analysis tools for low-dimensional, stochastic processes, eco-epidmeiological, forecast, modeling of unmixed, discontinuous, canopy, biochemical reaction variables regressional

networks. Some of the non-linear mathematical tools in ArcGIS include log-likelihood methods and Girsanov, polynomial chaos finite difference methods and their variants and pathwise sensitivity methods (www.esri.com). Existing fractionalized, endmember, sensitivity analysis approaches in ArcGIS can reveal precise variances in optimally elucidatively regressed datasets of uncoalesced eco-georeferenceable, trailing vegetation,sparsely shaded, discontinuous, infrequently canopied, fractionalized, orthogonalized, space-time geo-spectrotemporal, *S. damnosum* s.l., capture point, orthogonal, eigenvector, spatial filter, gradient estimators in high-dimensional,parameter space.

The aforementioned ArcGIS algorithmic, eigenfunction, endmember decompositional regressional analyses focuses on quantitating the sensitivity of uncoalesced, stochastic trajectories from moderate resolution, iteratively quantitative, interpolators for identfying unknown, un-geosampled, geospectrotemporally geosampled narrow, African, riverine tributary, eco-georeferenceable, *S. damnosum* s.l., immature capture point, hyperproductive habitats. However, as is often the case in ArcGIS stochastic explanative interpolators, decorrelated, sub-mixel, temporal probabilty density functions (PDF), are non-Gaussian in nonlinear and/or discrete systems. A PDF or continuous random variable, is a function that describes the relative likelihood for this random variable to take on a given value [24]. The probability of the randomized, *S. damnsoum* s.l. , reflectance variable falling within a particular range of frequency-oriented, transmittance, emissivity values amy be given by the integral of this variable's density over a moderate resolution wavelength,range—that is, it is given by the area under the density function but above the horizontal axis and between the lowest and greatest values of the range. The probability density function is nonnegative everywhere, and its integral over the entire space is equal to one [24].

In that latter direction, there is a broad recent literature relying on information theory tools, where fractionalized endmember sensitivity is robustly parsimoniously estimated by employing the Relative Entropy and the Fisher Information Matrix between PDFs, in ArcGIS for providing an optimizable endmember quantification of information loss along different parameter perturbations. Entropy is a measure of unpredictability of information content [24].The parametric PDF's structure is known as it is obtained through an entropy maximization subject to constraints. An entropy maximization problem is a convex optimization problem of the form maximize $f_0(\vec{x}) = -\sum_{i=1}^{n} x_i \log x_i$ subject to $A\vec{x} \leq b, \quad \mathbf{1}^T\vec{x} = |\vec{x}|_1 = 1$ where $\vec{x} \in \mathbb{R}^n_{++}$ is the optimization variable, $A \in \mathbb{R}^{m\times n}$ and $b \in \mathbb{R}^m$ are problem parameters, and $\mathbf{1}$ denotes a vector whose components are all 1[24]. Quantitating maximum entropy in an explanative eco-georeferenceable, geospectrotemporally geosampled narrow, African, riverine tributary, *S. damnosum* s.l., immature capture point, hyperproductive habitat, derived from a moderate resolution, uncoalesced, proxy LULC signature endmember eigenvector, forecast-oriented, vulnerability model would require qualitatively quantifying prior data or testable information about a PDF[22] .

Knowing the form of the PDF in an ArcGIS geodatabase containing geo-spectrotemporally uncoalesed, moderate resolution, seasonally imaged, hyperproductive, narrow, African, riverine, immature, *S. damnosum* s.l., orthogonally decomposable, explanative, capture point, immature habitat, count variables parametrically may allow estimating the relative entropy for optimally identifying the most sensitive sub-mixel, wavelength, transmittance, forecast-oriented, emissivity, proxy, reflectance, LULC signature,

estimator combinations. Further, the pathwise PDFs in ArcGIS may also be known in reaction networks when a Linear Noise Approximation (LNA) is employed for identying unknown, un-geosampled, unbiased iteratively interpolated, immature habitat estimators. In such circumstances the relative entropy can be explicitly computed allowing for a robust, parametric, endmember sensitivity analysis in ArcGIS, for an eco-epidemiological, *S. damnosum* s.l. remotely sensed, orthogonal, spatial filter, synthetic, eigenvector forecastor (e.g., sub-canopy topography, canopy height, basal area, stem diameter, canopy height profiles, sparsely shaded, canopy cover and biomass waveform data). Complex stochastic dynamics of large reaction networks (e.g., spatial Kinetic Monte Carlo algorithms) may itearatively quantitatively interpolate geo-spectrotemporally uncoalesced, molecular, discontinuous, infrequently canopied, proxy, LULC, seasonal, biosignature dynamics), employing explicit formulas for creating optimizable surfaces from sample data using these endmember iterative interpolation methods:Inverse distance weighted,Radial-based functions,Global and local polynomials, Kriging for exact data and for error-contaminated habitat data,Cokriging and Isotropical or anisotropical models with quantiatable PDFs in ArcGIS.

An ecologist, entomologist or other medical researcher can address challenges in PDF by introducing a new method for iteratively quantitatively interpolating complex, geo-spectrotemrpoally uncoalesced, moderate resolution, stochastic seasonal, hyperproductive, *S. damnosum* s.l.eco-georefernceable, capture point, proxy LULC signature dynamics in ArcGIS based on the Relative Entropy Rate (RER) whichmay provide a measure of the sensitivity of the entire heursitically parameterizable, time-series dependent, seasonally hyperproductive, trailing vegetation, turbid water, discontinuous, infrequently canopied narrow, African, riverine tributary, normalized, agro-village, complex ecosystem, wavelength,frequency-oriented, transmittance distribution. Typically, the space of all such time-series is referred in probability theory as the “path space” in ArcGIS. Quantitable RERs in ArcGIS may optimally measure the loss of explicatively geoclassifiable, proxy LULC signature information per unit time in path space after an arbitrary perturbation of parameterized elucidatively, eco-georeferenceable, seasonally explicative, hypeproductive, turbid water, *S. damnosum* s.l. eco-epidemiological, ago-village complex riverine tribuary, capture point, covariance weightage combinations.

Relative Entropy Rate and the corresponding Fisher Information Matrix (FIM) in ArcGIS has become computationally feasible as they admit explicit formulas which may depend only on the propensity functions, for example, in a *S.* geo-spectrotemporally uncoalesced *S.damnsoum* s.l. wavelength, frequency-oriented, transmittance, emissivity, moderate resolution, dataset. It may be robustly shown that the proposed geo-spectrotemporal, pathwise approach to an expositorily fractionalized, endmember eigenvector uncertainty sensitivity analysis in ArcGIS for an optimally imaged,moderate resolution eco-georeferenceable, seasonally hypeproductive, turbid water,disocntinuous,infrequently canopied, sparsely shaded, *S. damnosum* s.l. eco-epidemiological, explicative, capture point, has the following features: First, it is rigorously valid for the sensitivity of long-time, stationary dynamics in path space, including for example, bistable, periodic and pulse-like, geoclassifiable changing proxy LULC, signature, unbiased, uncoalesced, bi-directional, iteratively quantitative interpolative dynamics. Second, it is a gradient-free eco-georeferenceable, fractionalized, endmember sensitivity analysis method suitable for high-dimensional eigenvector, parameter spaces as the ones typically arising in complex biochemical networks. Third, the RER method does not require the explicit knowledge of the equilibrium PDFs, relying only on information for local,

uncoalesced, geo-spectrotemporal, proxy, LULC signature dynamics, thus making it suitable for non-equilibrium steady state systems such as seasonally hyperproductive, *S. damnosum* s.l., capture point, hyperendemeic, riverine foci.

Applying the pathwise sensitivity analysis method to a explicatively quantitatable, heursitically optimizable, geo-spectrotemporally uncoalesced, empirical datasets of geospatially geosampled eco-georeferenceable, *S. damnosum* s.l. ,narrow, African, riverine tributary, immature capture point, discontinuous, infrequently canopied,iteratively interpolative, biochemical reaction networks in ArcGIS may demonstrate non-homogeneous, canopy intrinsic sensitivity structures for optimally endmember mapping explanatively, remotely discernable non-random networks of positively autocorrelated, hyperproductive, capture point, immature habitats. Such systems may be typically modeled as jump Markov processes in an ArcGIS cyberenvironment employing simulated exact algorithms such as the Stochastic Simulation Algorithm (SSA), or by employing approximations such as stochastic Langevin methods and mean field ODEs, tau-leap.

Unbiased stochastic simulation for elucidatively identifying unknown, un-geosampled, eco-georeferenceable, seasonally explanative, hyperproductive, trailing vegetation, discontinuous, infrequently canopied, sparsely shaded, *S. damnosum* s.l. seasonal, capture points requires a simulation that traces the evolution of the narrow , African, agro-village complex ecosystem, geo-predictive,uendmber variables for capturing randomized moderate resolution, endmember eigenvector probabilities.With a stochastic moderate resolution eco-epidemiological, eco-georeferenceable, seasonal, *S. damnsoum* s.l. geo-spectrotemporally uncoalesced, wavelength, frequency-oriented, emissivity,forecast, vulnerability model projection, a set of random values. Outputs are recorded and the projection is repeated with a new set of uncoalesced, random proxy LULC signature variable values. These steps are repeated in ArcGIS until a sufficient amount of data is gathered. In order to determine the next event in the stochastic simulation, the rates of all possible immature habitat, seasonal, LULC changes to the state of the model are computed, and then ordered in an array. Next, the cumulative sum of the array is taken, and the final cell is quantiated to optimally determine the number R, where R is the tota forecastedregressed immature productivity rates. This cumulative array may be now modelled in ArcGIS as a discrete cumulative distribution which may be used to choose the next trailing vegetation, discontinuous, infrequently, explanatively canopied, sparsely shaded, *S. damnosum* s.l. seasonal, hypeproductive immature count seasonal capture point by picking a random number z~U(0,R) and choosing the first sampleding event, swhere z is less than the discrete integer rate associated with that event In the end, the distribution of the *S. damnsoum* s.l.model outputs should reveal the most probable endmember eigenvector estimates as well as a frame of iterable interpolative expectations regarding what ranges of geo-spectrotemporal, immature habitat,tabulated values the proxy uncoalesced, LULC biosignature variables.

A stochastic gradient method in ArcGIS may be based on mini-batch learning. A popular way to speed-up optimization algorithms (e.g., k-mean clustering) in ArcGIS especially in a parallel setting is via mini-batching, where the incremental update may be metaheuristically optimally performed on an average of the subgradients with respect to several sub-mixel, data variables. The gradient computations for each mini-batch can be parallelized in ArcGIS, allowing optimization methods to perform faster and more accurately in a distributed framework. Mini-batch algorithms in ArcGIS may be proposed as a way to speed-up stochastic convex optimization for optimally identifying unknown, un-geosampled, eco-georeferenceable, explanatorial, seasonally hyperproductive, geo-spectrotemporally

uncoalesced, moderate resolution, trailing vegetation, discontinuous, infrequently canopied, sparsely shaded eco-epidemiological„ *S. damnosum* s.l. seasonal, capture points. Such algorithms can be also improved employing accelerated gradient methods in ArcGIS. A novel analysis in Geospatial Analyst ™ may, for example, heuristically optimally define standard gradient methods in regression parameter space which may be suffice to obtain a significant accelerated gradient algorithmic, residually forecastable, vulnerability model output for qualitatively aiding in iteratively quantiatively interpolating sub-mixel, fractionalized, moderate resolution, eco-georeferenceable, geo-spectrotemporal, hyperproductive, capture point, seasonal *S. damnsoum* s.l., immature hypeproductive habitats. It may be shown that a mini-batching distributed framework in ArcGIS is capable of attaining asymptotically optimal speed-up for generalized, moderate resolution, endmember eigenvector, orthogonally forecastable, vulnerability mapping variables for strategically implementing and prioritizing targeted control intervention tactics (e.g., Slash and Clear' of hyperproductive, *S. damnosum* s.l.immature habitat based on seasonal immature productivity counts) in in eco-georferenceable, hyperendemic, African agro-village, narrow, riverine tributary, complex ecosystems. In so doing, the stochasticity of the gradient in the explanatively, probabilistic, residualizable, optimal, regression forecasts (e.g., remotely quantized , eco-georeferenceable, unknown un-geosampled, hyperproductive, seasonal, *S. damnosum* s.l capture points) can be mitigated by the injection of Gaussian noise, which may yield the stochastic Langevin gradient method; this method can be employed in an ArcGIS/SAS cybereenvironment for optimally conducting Bayesian (Appendix 1) posterior sampling for moderate resolution, forecast, vulnerability mapping uncoalescable eco-georeferenceable trailing vegetation, turbid water, eco-epidemiological, seasonally hyperproductive, *S. damnsoum* s.l. immature habitats in narrow African, riverine tributary, eco-georeferenceable ecosystems.

However, the performance of the stochastic Langevin gradient method for precisely iteratively quantitatively interpolating an explanative, eco-georefernceable, trailing vegetation, turbid water, sparsely shaded, seasonally hyperproductive, *S. damnosum* s.l., eco-epidemiological, capture point, optimally, depends on the stochastic algorithmic processes employed in ArcGIS for iteratively decorrelating the explanatorial, eco-georefernceable fractionalized, heursitically optimizable,frcationizable, endmember, eigenvector datasets of unmixed, sporadically, sparsely shaded, non-homogenously canopied, quantitatable, geoclassifiable shifting proxy LULC signature dynamics. Recent studies in endmember ArcGIS, mapping have revealed that violating detailed fractionalized, endmember eigenvector, geo-spectralizable, geospatial, equilibrium conditions accelerates the convergence to a stationary state and reduces the correlation time between eco-geosampling frames in forecast, vulnerability paradigms.

The violation of the detailed balance condition in a stochastic gradient Langevin method may demonstrate previously non-robustifiable, explanatorial, elucidative, iterative unquantitable interpolative probabilistic endmember, uncertainties (e.g., conditional standard error of the conditional cumulative distribution function derived through indicator kriging) when assessing seasonal, eco-epidemiological, regressional, capture point estimates of elevation.in an ArcGIS, *S. damnosum* s.l. forecasting vulnerability model. The adaptive explicit-implicit tau-leaping method with automatic tau selection is a exible algorithm in ArcGIS for accelerated stochastic simulation of biochemically reacting systems (e.g., photosynthetic vegetated, seasonally explicative discontinuous canopy gap). This ArcGIS decompositional algorithm combines the advantages of different simulation schemes and is particularly useful when a elucidative, iteratively geoclassifiable geo-spatializable ecosystem (sparsely shaded, prolific, ecogeoreferenceable,hyperproductive, *S. damnosum* s.l., capture

point,seasonal, proxy, LULC signature, sub-mixel changes and their dynamical behavior over time in the sense that it behaves well in some time periods but possesses stiffness (i.e., spatial non-stationarity) in other time periods. However, the ingredients necessary to fully understand and implement the algorithm in ArcGIS are spread over several papers and are not always consistent in terminology, which considerably hampers and possibly even prevents accessibility and widespread practical use of these algorithms for modeling time series, *S. damnosum* s.l. immature habitat variables. A streamlined description of the algorithm employing a unified terminology and notation may be accomatable in object-based technology (e.g., ENVI) introducing significantly simplifed versions of two major ingredients, namely the step size selection and the switching mechanism between the sub-algorithms.

An algorithm for the numerical computation of so-called algorithmic or consistent tangent moduli in finite, multidimensional, regression space in ArcGIS are geo-spectrotemporally gespatially customizable for optimally conducting endmember uncertainty diagnostics on iteratively interpolative, fractionalized, optimally forecastable eco-epidmiological eco-georeferenceable datasets of seaosanlly hyperproductive geosampled, moderate resolution, optimally imaged, *S. damnosum* s.l., endmember eigenvector, regression model, overtly biased estimators. The Tangent Curve COGO tool can add tangent curves any time while working with a parcel traverse or a set of construction lines (www.esri.com). These moduli can optimally determine the sensitivity of algorithmic expressions especially when qualitatively iteratively, quantizing environmental,uncoalesced, proxy LULC signature stresses(e.g., flooded agro-village complex cosystems along narrow, African, riverine tributary, eco-experimental geolocations,) with respect to seasonally intermittently canopied, explanatively geo-classifiable geo-spectrotemporal, geospatial changes in a total deformation. The tangent modulus is the slope of the stress-strain curve at any specified stress or strain[24]. Below the proportional limit, the tangent modulus is equivalent to Young's modulus which can define the relationship between stress (force per unit area) and strain (e.g., proportional deformation) in a material (e.g., geo-spectrotemporally uncoalesced, intermittently canopied, moderate resolution, trailing vegetation, sparsely shaded, discontinuous, optimally fractionalized,moderate resolution, *S. damnosum* s.l., narrow, African ,tributary agro-village geoclassified, proxy LULC signature polygon) [25]. These material can serve as iteration operators by application of Newton-type solvers in an ArcGIS cyberenvironment for qualitatively quantitating heuristically optimizable, auto-probabilistically regressable, synthetically fractionizable, endmember eigenvector, orthogonalized, geo-spectrotemporal datasets of uncoalesceable, moderate resolution, sparsely shaded, seasonally hyperproductive, immature, eco-epidemiological, capture point, *S. damnosum* s.l., trailing vegetation, immature, sparsely shaded, capture point hyperproductive habitats.

Jacob et al. (26) employed finite-difference derivatives of a first-order integral approximation in SAS/GIS for geospectrotemporally procuring explicatively quantitable approximations with a default dual quasi-newton optimizer and a pseudo-lipschitizian property for robustly parsimoniously eco-geographically geo-predicting inhomogeneous explicatively discontinuous, infrequently canopied, seasonally prolific, *S. damnosum* s.l. expositively fractionalized, trailing vegetation, turbid water, moderate resolution, parameterizable, wavelength, frequency-oriented, trasnmittance emissivity, endmember eigenvector, covariate coefficients. The authors verified a successive approximation scheme in SAS/GIS. In so doing, the authors found that the pseudo-regularity of the forecasted data induced the same property with respect to Lipschitzian perturbations in the explanatory,

residulized, regressional, eco-georeferenceable, explanative, geo-spectrotemporal eco-epidemiological, residual forecasts. Since the the original eco-epidemiological, *S. damnosum* s.l. map was a proper function in finite dimension, the characterization of the regularity properties was optimally generalized by directional derivatives in SAS/GIS which were quantiated in terms of an exact penalty function. The resdiualed forecasts revealed that that continuousselections of the inverse map played a crucial role for the equivalence of these regularities

The authors in Jacob et al. (26) proposed a Gaussian process in an eigenfunction spatial filter decompositionalanalyses in ArcGIS and a spatial Bayesian probabilistic estimation matrix in WinBUGS®. for heuristically, hierarchically, optimizing expositorily fractionalized endmember, probabilistically projected, eigenvector inferences revealed from a probabilsiically regressed geo-spectrotemporally uncoalesced, discontinuous, explanative dataset of clustering, eco-georeferencable, 5m, imaged narrow tributary, trailing vegetation, infrequently canopied, sparsely shaded, hyperproductive, agro-village complex, turbid water, immature habitats of *S. damnosum*,s.l., geospatially geosampled in an agro-village complex ecosystem in Burkina Faso. Because of its sound theoretical foundation in probability theory, the Bayesian belief network technology has become, in artificial intelligence, an important alternative architecture for reasoning to logic-based architectures (e.g., ArcGIS rule-based systems).The methods started each trial of the geosampled, *S. damnosum*,s.l., immature habitat simulation by instantiating the source nodes (i.e., nodes with no predecessors) and then proceeded forward along the diagram arcs in WinBUGS® to instantiate each downstream node in turn. Because the ArcGIS iterated values from one trial to the next were unrelated in WinBUGS®, the trials were deemed independent. Since the *S. damnosum* s.l., capture point, Bayesianized paradigm was driven by the prior probabilities of upstream nodes, rather than just the likelihood of the observed evidence, forward-simulation methods converged slowly when faced with quantiating characteristics of low-likelihood evidential paramters (e.g., low prior likelihood of explicative, riffle water variables) parameterizable covariate coefficients. Because of the way samples depend on the current instantiation, stochastic-simulation methods as a group are inefficient when there are deterministic or quantitatively, near-deterministic relationships in a network when forecast vulnerability modeling narrow African, tributary,*S. damnosum* s.l. trailing vegetation, infrequently canopied, agro-village complex, turbid water, immature, capture point, seasonal, hyperproductive habitats[22]. The authors intention was to simulate optimally, elucidatively unbiased, endemic. transmission-oriented, explanatorial, sub-mixel, fractionalized, geo-spectrotemporally uncoalesceable, explanative, moderate resolution, wavelength, trailing vegetation, and riffle water transmittance emissivities based on geospatially explanative quantized aggregations of seasonally geosampled narrow, riverine, tributary, agro-village, complex, ecosystem, eco-georeferenceable, capture points within an eco-epidemiological, African, agro-village, study site by introducing a latent variable within a non-linear, frequency-oriented, autoregressive ,endmember eigenvector, emissivity equation.

The Wishart probability distribution of the sample covariance matrix was subsequently optimally quantitated by employing models generated in PROC NL MIXED and SAS/GIS into probability distributions of eigenvalues and eigenvectors in order to calculate multiple, seasonal, Bayesianistic, error, estimation, forecasting vulnerability models employing the empirically regressable, geo-spectrotemporally geosampled, eco-georeferenceable, empirical, *S. damnosum* s.l. orthogonal data. In statistics, the Wishart distribution is a generalization to multiple dimensions of the chi-squared distribution, or, in the case of non-integer degrees of freedom, of the gamma distribution [25].

The Wishart distribution was optimally defined over symmetric, nonnegative-definite, matrix-valued, random matrices. These probability distributions were of great importance in the estimation of the covariance matrices in the fractionalized, endmember eigenvector, heuristically optimizable, iterative dataset of the multivariate, moderate resolution, geo-spectrotemporally, orthogonalized, synthetic, vulnerability-oriented,seasonal, eco-georeferenceable, hyperproductive, immature habitat forecastors. The qualitatively quantitated, geo-spectrotemporally uncoalesced, optimally fractionalized, endmember eigenvectors synthesized from the eco-georefernceable, *S. damnsoum* s.l., hyperproductive,capture point, immature habitat, seasonal, eco-epidemiological, capture points was robustifiable since the conjugate prior of the inverse covariance-matrix from the multivariate, explanatively normalized, random-vector was quantitable.Unknown, un-geosampled, prolific, capture point, seasonal immature, eco-georeferenceable, explanative, hypeproductive, capture point, immature habitats were optimally identified employing the iterative interpolative, simulation algorithm.

In Bayesian probability theory, if the posterior distributions $p(\theta|x)$ are in the same family as the prior probability distribution $p(\theta)$, the prior and posterior are then called conjugate distributions, and the prior is called a conjugate prior for the likelihood function[24].In probability theory and statistics, the multivariate normalized distribution or multivariate Gaussian distribution, is a generalization of the one-dimensional (i.e., univariate) normal distribution to higher dimensions[25]. One possible definition that may be parsimonioulsy qualitatively quantitated in a robustifiable, *S. damnsoum* s.l., moderate resolution, uncoalesced, empriical dataset of orthogonally decomposable, elucidative, wavelength, transmittance, forecastable, vulnerability model paramterizable moderate resolution, covariate estimators, is that a endmember random vector may be be k-variate normally distributed if every linearizable combination of its k components (e.g., unmixed, trailing vegetation, discontinuous, sparsely shaded, partailly canopied, geospectral explanatorial covariance weights) has a univariate normal distribution

In Jacob et al. [26], the authors also iteratively generated a semiparametric spatial filtering approach in SAS/GIS to deal explicitly with probabilistically residually forecasted uncertainties in the explicative, *S. damnosum* s.l. endmember, immature habitat, seasonally hyperproductive, trailing vegetation, discontinuous, infrequently canopied, sparsely shaded, capture point, randomly distributed, forecast, vulnerability model by reducing the number of uncoalesed geo-spectrotemporal radiance parameters employing spatially lagged autoregressive matrices and simultaneous autoregressive geo-spatialized paradigms. Residual estimates from the off-diagonal elements of a covariance matrix were optimally rendered from the spatial filter, fractionalized endmember, eigenevector analysis prior to exporting the geo-spectrotemporally geosampled, immature, capture point, optimally parameterizable geospatialized, covariate coefficients into the Bayesian estimation probabilistic matrix employing WinBUGS®. A backward simulation method was conducted for approximating probabilistic inferences from the geosampled data. The method was closely related to forward-simulation methods, but was not susceptible to slow convergence in the presence of any deterministic endmember quantitated relationships. Fortunately, the method was not susceptible to slow convergence due to the presence of highly-likelihood evidence estimators Median parameter values, as well as the 95% credibility intervals (2.5 percentile and 97.5 percentile values), were parsimoniously rendered in the latent, forecasted autoregressive, endemic, transmission-oriented, optimally parameterizable, regressor dataset. As the eco-georeferenceable, narrow, tributrary agro-village complex, riverine, *S. damnosum*

s.l., hyperproductive, capture point, geo-sampled sites increased based on the explanatorial, geospatialized covariate Percent of trailing vegetation, the median log-count of immatures increased. The adjusted geo-spectrotemporal model quantized the independence amongst the explicative eco-georeferenceable, time series dependent, field and remote, elucidatively geosampled endemic, transmission-oriented, expositive proxy, LULC biosignature covariates eco-geographically representing the seasonal immature counts. The authors noted that the this model fit better that the model that adjusted for correlation within the eco-epidemiological, agro-village, narrow tributary, agro-village,study site based on the root means squre error.

The authors in Jacob et al. [26] proved that that, if X, Y are finite,-multi-dimensional real linear spaces and $F : X \rightarrow 2^Y$ is a multifunction that has the pseudo-Lipschitz property at an eco-georefernceable, seasonal, immature habitat, hyperproductive, trailing vegation, tubid water, discontinuous, partially canopied, sparsely shaded, narrow, tributary, agro-village complex, *Similium* capture point $(x_0, y_0) \in \text{Graph}(F)$ in ArcGIS. Essentialy according to the authors, for every $\varepsilon > 0$ there existed a Lipschitz multifunction $V^{\varepsilon}: N(\varepsilon) \rightarrow 2^Y$. These explanatorily decomposable variables could be orthogonally robustly defined for an eco-georeferenceable, hyperproductive, eco-epidemiological, capture point, complex neighborhood $N(\varepsilon)$ of x_0, such that (i) V^{ε} has compact convex values, (ii) $V^{\varepsilon}(x_0) = \{y_0\}$, and (iii) for every $x \in N(\varepsilon)$, $V^{\varepsilon}(x)$ was a subset of the convex hull $\text{co}(F^{\varepsilon}(x))$ of the intersection $F^{\varepsilon}(x)$ of $F(x)$ with the closed ε-ball centered at y_0. In mathematics, the convex hull or convex envelope of a set *X* of points (eco-georeferenceable, *S. damnosum* s.l. narrow African, ago-village riverine, tributary complex, immature habitats) in the Euclidean plane or Euclidean space is the smallest convex set that contains *X*.[24] In particular, this implied the existence of an elucidative, Lipschitz, single-valued selection f^{ε} of $\text{co}(F^{\varepsilon})$ near x_0 satisfying $f^{\varepsilon}(x_0) = y_0$. Lipschitz continuity, is a strong form of uniform continuity for the computed , *S. damnosum* s.l. habitat functions. In so doing, multiple geo-spectrotemporal, moderate resolution, uncoalesced, bio-geophysical foreastable explanators for unknowns, un-geosampled, hyperproductive, explanative, trailing vegetation, discontinuous, infrequently canopied, *S. damnosum* s.l. capture point, immature habitats were parsimoniously accomadated in a stochastic iterative interpolator.

The underlying concept of the numerical computation in ArcGIS is a perturbation technique based on a forward difference approximation which may reduce the computation of the tangent moduli in an explanative, eco-georeferenceable, seasonally explanative, hyperproductive, *S. damnosum* s.l. moderate resolution, eco-epidemiological, geo-spectrotemporal, uncoalesced, wavelength, transmittance,geospatial,autoregressive, forecast-oriented, vulnerability paradigm. A multiple, endmember eigenvector stress computation in an AcGIS geodatabase may also precisely iteratively quantitate,iteratively interpolatable probabilistically regressable datasets of uncoalesced *S. damnosum* s.l., moderate resolution, trailing vegetation, turbid water, eco-georeferenceable, discontinuous, infrequently canopied, unbiased explanatorial estimators, for optimally identifying unknown, un-geosampled, hyperproductive, narrow riverine, tributary, agro-village, ecosystem, eco-epidemiological,capture point, immature habitats. The iterative, interpolative, sub-algorithmic procedure is material-independent and may be optimally outlined for a Lagrangian in a fractionalized, moderate resolution, *S. damnosum* s.l. endmember, eigenvector, moderate resolution, forecast-oriented, vulnerability model. A mathematical function called the Lagrangian is a function of the generalized coordinates, their time derivatives, and time, and contains the information about the dynamics of the system [24].

An sub-algorithmic procedure for qualitatively quantitating a fractionalized, endmember eigenvector, material-independent, Eulerian framework may be optimally constructed in ArcGIS for geometrically processing explanative, seasonally, hyperproductive, eco-georeferenceable, *S. damnosum* s.l. capture point, trailing vegetation, turbid water, immature, habitat surfaces and their intermittently canopied, discontinuous foliations. The leaves of a foliation consist of integrable subbundles of the tangent bundle in differential geometry [24].

The tangent bundle of a differentiable manifold M is a manifold TM, which assembles all the tangent vectors in M[25].The tangent bundle comes equipped with a natural topology (*not* the disjoint union topology) and smooth structure so as to make it into a manifold in its own right. The dimension of *TM* is twice the dimension of *M*. Each tangent space of an *n*-dimensional manifold is an *n*-dimensional vector space. If *U* is an open contractible subset of *M*, then there is a diffeomorphism from *TU* to $U \times \mathbf{R}^n$ which restricts to a linear isomorphism from each tangent space T_xU to $\{x\} \times \mathbf{R}^n$. As a manifold, however, *TM* is not always diffeomorphic to the product manifold $M \times \mathbf{R}^n$. When it is of the form $M \times \mathbf{R}^n$, then the tangent bundle is said to be trivial.

Every smooth manifold M has a tangent bundle TM, which consists of the tangent space TM_p at all points p in M. Since a tangent space TM_p is the set of all tangent vectors to M at p, the tangent bundle is the collection of all tangent vectors, along with the information of the point to which they are tangent. $TM = \{(p, v) : p \in M, v \in TM_p\}$ The tangent bundle is a special case of a vector bundle. As a bundle it has bundle rank n, where n is the dimension of M. A coordinate chart on M provides a trivialization for TM. In the coordinates, $(x_1, \ldots, x_n)$, the vector fields $(v_1, \ldots, v_n)$, where $v_i = \partial / \partial x_i$, span the tangent vectors at every point (in the coordinate chart). The transition function from these coordinates to another set of coordinates is given by the Jacobian of the coordinate change. For example, on the unit sphere, at the point $(1, 0, 0)$ there are two different coordinate charts defined on the same hemisphere, $\phi : U_1 \to \mathbb{S}^2$ and $\psi : U_2 \to \mathbb{S}^2$,

$\phi(x_1, x_2) = (\cos x_1 \cos x_2, \sin x_1 \cos x_2, \sin x_2)$ $\psi(y_1, y_2) = \left(\sqrt{1 - y_1^2 - y_2^2}, y_1, y_2\right)$ with $U_1 = (-\pi/2, \pi/2) \times (-\pi/2, \pi/2)$ and $U_2 = \{(y_1, y_2) : y_1^2 + y_2^2 < 1\}$. The map between the coordinate charts is $\alpha = \psi^{-1} \circ \phi$. $(y_1, y_2) = \alpha(x_1, x_2) = (\sin x_1 \cos x_2, \sin x_2)$

The Jacobian of $\alpha : U_1 \to U_2$ is given by the matrix-valued function $\begin{bmatrix} \cos x_1 \cos x_2 & -\sin x_1 \sin x_2 \\ 0 & \cos x_2 \end{bmatrix}$ which has determinant $\cos x_1 \cos^2 x_2$ and so is invertible on U_1. The tangent vectors transform by the Jacobian. At the point (x_1, x_2) in U_1, a tangent vector v corresponds to the tangent vector Jv at $\alpha(x_1, x_2)$ in U_2. Given a set $\mathbf{y} = \mathbf{f}(\mathbf{x})$ of n equations in n variables x_1, ..., x_n, written explicitly as $\mathbf{y} = \begin{bmatrix} f_1(\mathbf{x}) \\ f_2(\mathbf{x}) \\ \vdots \\ f_n(\mathbf{x}) \end{bmatrix}$, or more explicitly as $\begin{cases} y_1 = f_1(x_1, \ldots, x_n) \\ \vdots \\ y_n = f_n(x_1, \ldots, x_n), \end{cases}$ These two are just different versions of the same element of the tangent bundle.

In topology, a branch of mathematics, a topological manifold is a topological space (which may also be a separated space) which locally resembles real *n*-dimensional space. A topological space *X* is called locally Euclidean if there is a non-negative integer *n* such that

every point in X has a neighborhood which is homeomorphic to the Euclidean space E^n (or, equivalently, to the real n-space R^n, or to some connected open subset of either of two) In the mathematical field of topology, a homeomorphism or topological isomorphism or bi continuous function is a continuous function between topological spaces that has a continuous inverse function[25]. Formally, an isomorphism is bijective morphism[25]. Informally, an isomorphism is a map that preserves sets and relations among elements. "A is isomorphic to B" is written $A \cong B$. Unfortunately, this symbol is also used to denote geometric congruence.

Given a function $f(x)$, its inverse $f^{-1}(x)$is defined by $f(f^{-1}(x)) = f^{-1}(f(x)) \equiv x$.[25] Therefore, $f(x)$and $f^{-1}(x)$are reflections about the line $y = x$. In the Wolfram Language, inverse functions are represented using InverseFunction[*f*]. function *f* from the real numbers to the real numbers possesses an inverse as long as it is one-to-one, (i.e. as long as the graph of $y = f(x)$ has, for each possible y value only one corresponding x value, and thus passes the horizontal line test((http://mathworld.wolfram.coml). In so doing, the predictive equation $y = f(x)$ would optimally define the graph of *f*, in a *S. damnosum* s.l. moderate resolution, except that the roles of x and y have been reversed. Thus the graph of f^{-1} from a eco-georeferenceable, can be obtained from the graph of *f* by switching the positions of the x and y axes. This is equivalent to reflecting the graph across the line $y = x$. There is a symmetry between a function and its inverse. Specifically, if *f* is an invertible function with domain X and range Y, then its inverse f^{-1} has domain Y and range X, and the inverse of f^{-1} is the original function *f*. In symbols, for functions $f: X \rightarrow Y$ and $g: Y \rightarrow X$ [25].Multiple standardizable functions are available for constructing a robust *S. damnosum* s.l. immature habitat geolocation, endmember signature, probabilistic paradigm (see Table 2).

Table 2. Standard functions and their inverses that may be applicable for a decomposable, orthogonal, moderate resolution, trailing vegetation, narrow, African riverine, agro-village, hyperproductive, eco-georeferenced, *S. damnosum* s.l. immature habitat.

Function $f(x)$	Inverse $f^{-1}(y)$	Notes
$x \pm a$	$y \mp a$	
$a - x$	$a - y$	
mx	y/m	$m \neq 0$
$1/x$ (i.e. x^{-1})	$1/y$ (i.e. y^{-1})	$x, y \neq 0$
x^2	$\sqrt{y}$ (i.e. $y^{1/2}$)	$x, y \geq 0$ only
x^3	$\sqrt[3]{y}$ (i.e. $y^{1/3}$)	no restriction on x and y
x^p	$\sqrt[p]{y}$ (i.e. $y^{1/p}$)	$x, y \geq 0$ in general, $p \neq 0$
2^x	$\mathrm{lb} y$	$y > 0$
e^x	$\ln y$	$y > 0$
10^x	$\lg y$	$y > 0$
a^x	$\log_a y$	$y > 0$ and $a > 0$

As noted by Feynman (1997), the notation $f^{-1}x$is unfortunate because it conflicts with the common interpretation of a superscripted quantity as indicating a power, i.e.,

$f^{-1}x=(1/f)x=x/f$. It is therefore important to keep in mind that the symbols $\sin^{-1}z$, $\cos^{-1}z$, etc., refer to the inverse sine, inverse cosine, etc., and *not* to $1/\sin z=\csc z$, $1/\cos z=\sec z$, when regressively and cartographgically examining *S. damnosum* s.l. seasonal hyperproductive habitats.(see Figure 3) The inverse sine is the multivalued function $\sin^{-1}z$(Zwillinger 1995, p. 465), also denoted $\arcsin z$(Abramowitz and Stegun 1972, p. 79; Harris and Stocker 1998, p. 307; Jeffrey 2000, p. 124), that is the inverse function of the sine. The variants $\mathrm{Arcsin}\,z$(e.g., Bronshtein and Semendyayev, 1997, p. 69) and $\mathrm{Sin}^{-1}z$are sometimes used to refer to explicit principal values of the inverse sine, although this distinction is not always made (e.g,. Zwillinger 1995, p. 466). The inverse cosine is the multivalued function $\cos^{-1}z$(Zwillinger 1995, p. 465), also denoted $\arccos z$(Abramowitz and Stegun 1972, p. 79; Harris and Stocker 1998, p. 307; Jeffrey 2000, p. 124), that is the inverse function of the cosine. The variants $\mathrm{Arccos}\,z$(e.g., Beyer 1987, p. 141; Bronshtein and Semendyayev, 1997, p. 69) and $\mathrm{Cos}^{-1}z$are sometimes used to refer to explicit principal values of the inverse cosine, although this distinction is not always made (e.g,. Zwillinger 1995, p. 466).

A function $f$admits an inverse function f^{-1}(i.e., "f is invertible") iff it is bijective[26]. A map is called bijective if it is both injective and surjective. A bijective map is also called a bijection. A function $f$admits an inverse f^{-1}(i.e., "f is invertible") iff it is bijective(http://mathworld.wolfram.com/Bijective.html). Two sets $X$and $Y$are called bijective if there is a bijective map from $X$to Y [1]. In this sense, "bijective" is a synonym for "equipollent" (or "equipotent"). Bijectivity is an equivalence relation on the class of sets.

However, inverse functions are commonly defined for elementary functions that are multivalued in the complex plane. In such cases, the inverse relation holds on some subset of the complex plane but, over the whole plane, either or both parts of the identity $f^{-1}(f(z))=f\left(f^{-1}(z)\right)=z$may fail to hold. A few examples are illustrated above and in the following Table 3

Table 3: $0<b<a$and $c\in\mathbb{Z}$ for constructing a *S. damnosum* s.l. forecast vulnerability map

$f(z)$	$f^{-1}(z)$	$f\left(f^{-1}(z)\right)$	$f^{-1}(f(z))$
$\sqrt{z}$	z^2	$\sqrt{z^2}$	z
$\ln z$	e^z	$\ln(e^z)$	z
$\sin z$	$\sin^{-1}z$	z	$\sin^{-1}(\sin z)$
$z^{a/b}$	$z^{b/a}$	$\left(z^{b/a}\right)^{a/b}$	z
z^c	$z^{1/c}$	$\left(z^{1/c}\right)^c$	$(z^c)^{1/c}$

An additional counterintuitive property of inverse functions for modeling *S. damnosum* s.l. data is that $\sqrt{z}\sqrt{\frac{1}{z}}=\begin{cases}-1 & \text{for } \mathbb{I}[z]=0 \text{ and } \mathbb{R}[z]<0\\ \text{undefined} & \text{for } z=0\\ 1 & \text{otherwise,}\end{cases}$ so the expected identity does not hold along the negative real axis. Figure 5 reveal inverse function for elementary

functions for constructing a moderate resolution, geo-spectrotemporal, *S. damnosum* s.l. regression graph (Figure 5).

The function $f(x)=x^2$ may or may not be invertible in a eco-georeferenceable, hypeproductive, capture point, *S. damnosum* s.l. depending on what kinds of numbers are being considered (the "domain").If the domain is the geo-spectrotemporally geosampled clinical, field or remote dataset then each possible result *y* (except 0) would corresponds to two different starting points in X – one positive and one negative in the oviposition paradigm, and so this function would not be invertible: as it is impossible to deduce an input from its output. Such a function is called non-injective or information-losing.If the domain of the function is restricted to the nonnegative reals then the function is injective and invertible.\[26] If f is a function mapping elements of a set X to elements of a set Y,the source, X would be the domain of f and the target (hyerproductive seasaonl *S. damnosum* s.l. habitat), Y would be the codomain. The codomain may contains the range of f as a subset, and would part of the definition of f in the probability model, optimaizable, residual forecasts.

When using codomains, the inverse of a function fx →y in a forecasting vulnerability, *S. damnosum* s.l. oviposition, moderate resolution, model, the estimators may be required to have domain Y and codomain x. In mathematics, an image is the subset of a function's codomain which is the output of the function from a subset of its domain[25].Evaluating a function at each element of a subset *X* of the domain, produces a set called the *image of X under or through* the function (http://mathworld.wolfram.com). The inverse image or preimage of a particular subset *S* of the codomain of a function is the set of all elements of the domain that map to the members of *S*. [26].Image and inverse image may also be defined for general binary relations in a *S. damnosum* s.l model, not just functions.

For the inverse to be defined on all of Y every element of Ymust lie in the range of the function f[26].A function with this property is called surjective. The function is surjective (onto) if every element of the codomain is mapped to by at least one element of the domain (That is, the image and the codomain of the function are equal.) Thus, a function with a codomain in a *S. damnsoum* s.l. forecasting, vulnerability geo-spectrotemporal, geospatial, endmember,, narrow African, riverine tributary, trailing vegetaion, turbid water, habitat model for targeting prolic, seasaonl, oviposition sites on moderate resolution, geoclassifiable LULCs is invertible if and only if it is both injective (one-to-one) and surjective (See Figure 7). Such a function may be optiamlly defined as a one-to-one correspondence or a bijection, and will have the property that every element y∈ Ycorresponds to exactly one element x ∈ X. In mathematics, a bijection, bijective function or one-to-one correspondence is a function between the elements of two sets, where each element of one set is paired with exactly one element of the other set, and each element of the other set is paired with exactly one element of the first set.

Figure 7. Inverse functions which are defineable for elementary functions that are multivalued in a complex plane for remotely quantitating a georeferenceable, hypeproductive, seasonal, *S. damnosum* s.l. trailing vegetation, turbid water, capture point

International Journal of Geographic Information System
Vol. 4, No. 1, April 2017, pp.1-519
Available Online at http://acascipub.com/Journals.php

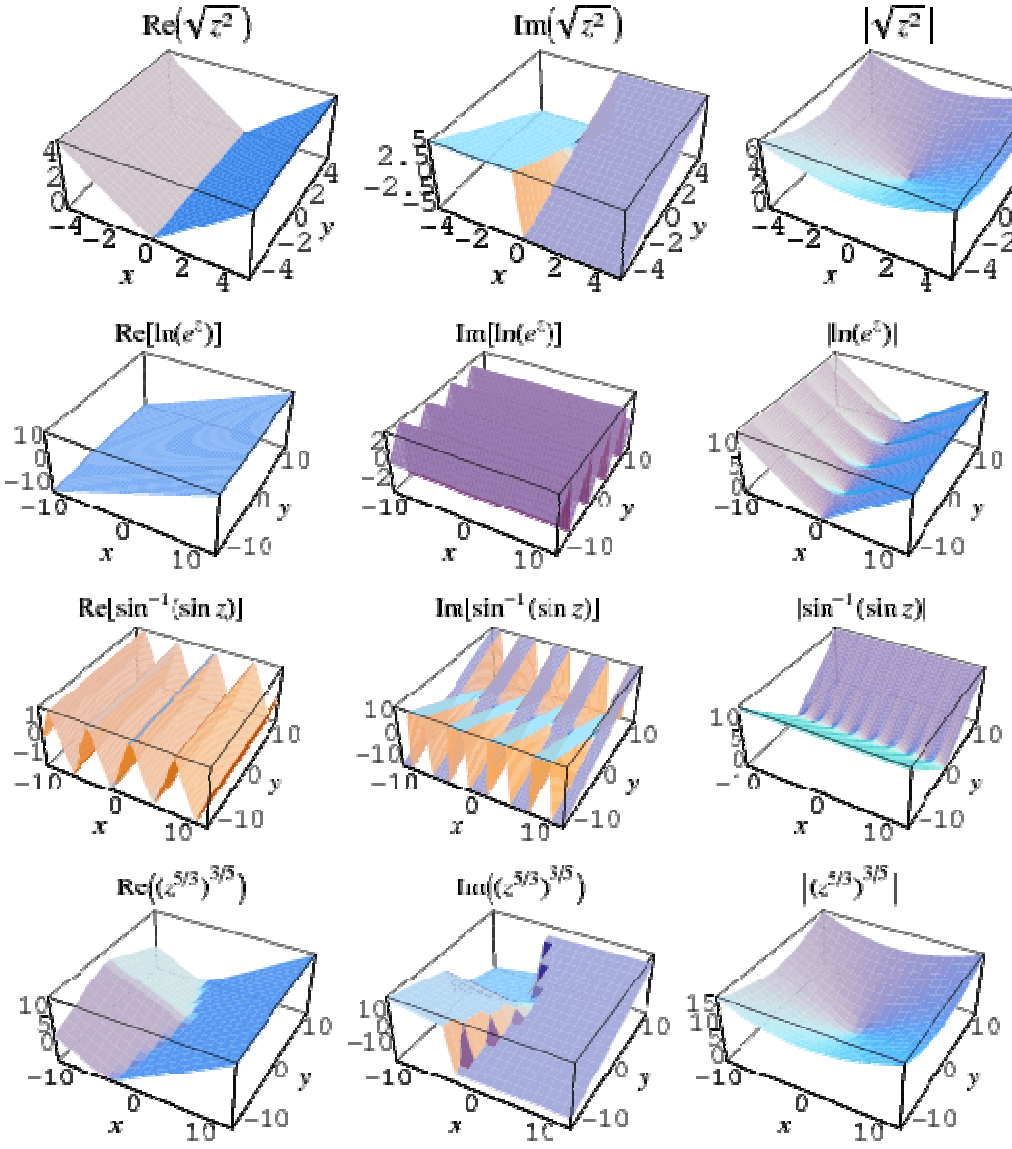

Contrary to current Eulerian methods employable in graphics, ArcGIS employs conservative methods and a variational interpretation, offering a unified framework for routine surface operations such as smoothing, offsetting, and iterative endmember quantitative interpolation. In graph theory, an Eulerian trail (or Eulerian path) is a trail in a graph which visits every edge exactly once. By employing discretized *S. damnosum* s.l. immature habitat, capture point,eco-georferenceable, differential equations the value of the unknown, prolific habitats at fixed points in space may be qualitatively quanatized .

Similarly, an Eulerian circuit or Eulerian cycle is an Eulerian trail which starts and ends on the same vertex [24]. Computations may be performed on fixed, orthogonal, grid matrices in ArcGIS without recourse to Lagrangian techniques such as triangle meshes, or path tracing. In each case, a mathematical function called the Lagrangian is a function of the generalized coordinates, their time derivatives, and time, and contains the information about the dynamics of the system [http://mathworld.wolfram.com/.html]. In mathematical optimization, the method of Lagrange multipliers is a strategy for finding the local maxima

and minima of a function subject to equality constraints.For instance consider the optimization problem in a *S. damnosum* s.l. habitat model whose maximize $f(x, y)$ is subject to $g(x, y) = 0$.In such circumstances both f and g have continuous first partial derivatives. A medical entomologist or experimenter can introduce a new variable (λ) called a Lagrange multiplier and study the Lagrange function (or Lagrangian) defined bywhere the λ term may be either added or subtracted. If $f(x_0, y_0)$ is a maximum of $f(x, y)$ for the original constrained problem, then there exists λ_0 such that (x_0, y_0, λ_0) is a stationary point for the Lagrange function (stationary points are those points where the partial derivatives oare zero). However, not all stationary points yield a solution of the original problem. Thus, the method of Lagrange multipliers in a forecast, vulnerability, *S. damnosum* s.l. habitat model yields a necessary condition for optimality in constrained problems. Sufficient conditions for a minimum or maximum also exist.

The method of Lagrange multipliers can be extended to solve problems with multiple constraints using a similar argument in a endmember decomposed dataset of eco-georeferenceable, *S. damnosum* s.l., trailing vegetation, hyperproductive, seasonal, geo-spectrotemporally geosampled, in a narrow, African, riverine tributary agro-village complex. Consider a paraboloid subject to two line constraints that intersect at a single ecogeorferenecable capture point. As the only feasible solution, this point is obviously a constrained extremum. However, the level set would not be clearly parallel to either constraint instead, it would be a linear combination of the two constraints' gradients. In the case of multiple seasonal, *S. damnsoum* s.l., eco-georferenceable, moderate resolution, proxy signature LULC oviposition paradigm constraints, employing the method of Lagrange will seek unknown, un-geosampled, prolific capture points not at which the gradient is multiple of any single constraint's gradient necessarily, but in which a linear combination of all the constraints' gradients are quanatizable.

At the core of the approach is the use of the Coarea Formula to express area integrals over iso-surfaces as volume integrals. This enables the simultaneous processing of multiple isosurfaces in ArcGIS, while a single interface may be eco-cartographically treated as the special case of a dense, sparsely shaded, intermittent, moderate resolution, discontinuous dataset of canopy foliation, with their uncoalesced, iteratively interpolative, explicatively geoclassifiable, proxy, LULC signature, paramterizable covariate, wavelength, frequencies Spatial and temporal information on plant functional traits are lacking in ecology,which limits our understanding of howplant communities and ecosystems are changing. This problemis acute in remote tropical regions, where information on plant functional traits is difficult to ascertain.

Asner et al. (20140 employed Carnegie Airborne Observatory visible-toshortwave infrared (VSWIR) imaging spectroscopy with light detection and ranging (LiDAR) to assess the foliar traits of Amazonian and Andean tropical forest canopies. Lidar (also called LIDAR, LiDAR, and LADAR) is a surveying method that measures distance to a target by illuminating that target with a pulsed laser light, and measuring the reflected pulses with a sensor(www.esri.com).The authors calibrated and validated the retrieval of 15 canopy foliar chemicals and leaf mass per area (LMA) across a network of 79 1-hectare field plots using a new VSWIRLiDARfusion approach designed to accommodate the enormous scale mismatch between field and remote sensingstudies. The results indicate that sparse and highly variable field sampling can be integrated with VSWIRLiDARdata to yield demonstrably accurate estimates of canopy foliar chemical traits. he lidar abilities to detect subtle topographic features such as river terraces and river channel banks, to measure the land-surface elevation

beneath the vegetation canopy, to better resolve spatial derivatives of elevation, and to detect elevation changes between repeat surveys have enabled many novel studies of the physical and chemical processes that shape landscapes (https://en.wikipedia.org/wiki/Lidar)This optimization method may be a powerful alternative to conventional geometric representations in other software packages for quantitating highly reflective seasonal, hyperproductive, *S. damnosum* s.l., trailing vegetation, narrow, African , riverine tributray, agro-village complex, eco-epidemiological, partially canopied, discontinuous, surface-oriented, fractionalized, endmember eigenvectos. In so doing, vulnerability, forecast mapping variables (e.g., iteratively unbiasedly, stochastically, kriged estimators) generated in ArcGIS (e.g., Geospatial Analyst ^{TM}) may reveal unknown, un-geosampled uncoalesced, moderate resolution illuminative, transmittance emissivities of hypeporductive seasonal *S. damnsousm* s.l. capture points and their weighted offsetting (see Figure 8).

Figure 8 A Eulerian, trail-oriented ArcGIS, wavelength, transmittance emissivity graph of a moderate resolution IR imaged, hyperproductive within canopied, geo-spectrotemporally uncoalesced, *S. damnosum* s.l. trailing vegetation, eco-epidemiological, capture point, frequency-oriented, eco-georeferenceable, immature, discontinuous oviposition isosurface

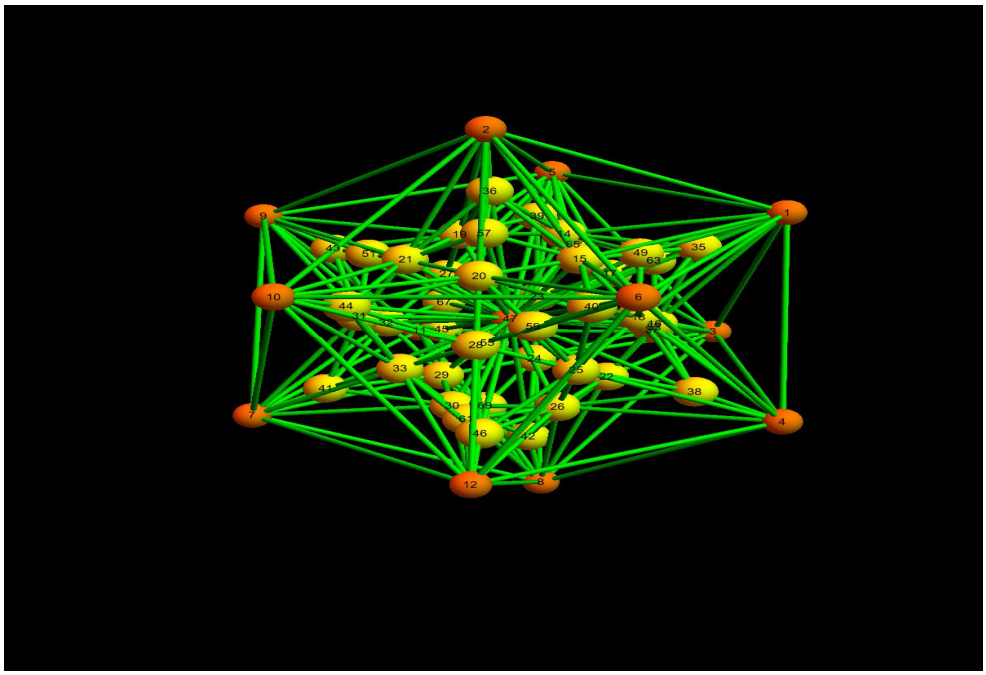

Foliation smoothing of the forecasted eco-georefernceable, geo-spectrotemporal, geospatialized, discontinuously canopied, trailing vegetation, turbid water, sparsely shaded, parameterized variables thereafter can quantaite propagational interpolation probabilistic uncertainties. Treating overdispersed erroneous explicative, biophysical, eco-geophysiological ,radiance covariates may help spatiall adjust erroneous kriging regression variables for which the *S. damnsoum* s.l. capture points interpolated uncoalesced , proxy signature values may be mispecified employing a Gaussian process governed by prior covariances, as opposed to a piecewise-polynomial spline for optimizing smoothness of the fitted values. In mathematics, a spline is a numeric function that is piecewise-defined by polynomial functions, and which possesses a high degree of smoothness at the places where the polynomial pieces connect (which are known as *nodes*). In interpolating problems, *spline*

interpolation is often preferred to polynomial interpolation because it yields similar results to interpolating with higher degree polynomials while avoiding instability due to Runge's phenomenon In the mathematical field of numerical analysis, Runge's phenomenon is a problem of oscillation at the edges of an interval that occurs when using polynomial interpolation with polynomials of high degree over a set of equispaced interpolation pointsUnder suitable assumptions on the priors, Kriging render s the best linear unbiased prediction of the intermediate values. Interpolating methods based on other criteria such as smoothness need not always yield the most likely intermediate value [24]

Above the proportional limit the tangent modulus varies with strain and is most accurately found from test data [24]. Consequently, LSMA-based methods for optimally, geo-spectrotemporally, explanatorily uncoalescing a seasonally hyperproductive, narrow, African, tributary, *S. damnosum* s.l., eco-georefernceable, agro-village complex, hyperendemic, foci for facilitating targeted eco-epidemiological, forecast-oriented, vulnerability maps for implementing onchocerciasis control startegies [e.g., Intergrated Vector Management(IVM)] in narrow African, tributary, agro-village riverine, complex ecosystems may be overtly unconstrained thus rendering solutions that do not necessarily reflect true abundance fractions of the the partially canopied, unmixed, trailing vegetation, or turbid water endmember materials. As such, an LSMA can only be employable for the purposes of material detection for optimal discrimination of geoclassified, LULCs of explanative, seasonally hyperproductive, moderate resolution, images, immature habitats but not for fractionalized, sub-mixel,eigenvector, regressor quantitation.

A fully ArcGIS, constrained least squares (FCLS) linear, spectral mixture analysis method may qualitatively quantitate empirical datsets of eco-georfernceable, fractionalized, endmember eigenvector materials rendered from an explicative, hyperproductive, geo-spectrotemporally extractable, seasonally eco-georeferenceable, *S. damnosum* s.l., capture point, immature habitat, moderate resolution mixel. Since no closed form can be derived for this method, an efficient algorithm in ArcGIS may be alternatively developed to yield optimal solutions. In order to further apply the designed algorithm to unknown narrow, African, agro-village, eco-georeferenceable, riverine tributary, trailing vegation, intermittently canopied, turbid water, discontinuously canopied, moderate resolution, geoclassifiable LULC, image scenes, a least squares, error (LSE)-based method in ArcGIS may be proposed to extend the FCLS method in an unsupervised manner. A series of computer simulations and real hyperspectral data experiments may be thereafter ideally conducted in ArcGIS (e.g., Geospatial Analyst ^{TM})to demonstrate the feasibility of the proposed FCLS-LSMA approach in material, endmember eigenvector, qualitative quantitation of an orthogonally, explicatively, fractionally decomposable, seasonally hyperproductive, eco-epidemiological, capture point, *S. damnosum* s.l., immature, eco-georeferenceable habitat. The recognition that mixels of interest for medically improtant entomological vector arthropods are frequently a combination of numerous explanative disparate components (e.g., endmember fractionalized, infrequently canopied, trailing vegetation, sub-mixel explicative regressors), introduces a need to quantitatively decompose, or “unmix,” infrequently shaded, object mixtures in ArcGIS and other software products[25].

A set of taxonomies that organize and specify iterative algorithms in ArcGIS and Environment for Visualizing Images ENVI [e.g. Spectral Information Divergence (SID), Spectral Angle Mapper (SAM)] can hyperspectrally unmix an eco-georefernceable, eco-epidemiological, robustifiable dataset of uncoalesced, moderate resolution imaged, seasonally hyperproductive, *S. damnosum* s.l., geo-spectrotemporally geosampled,weighted

wavelength,transmittance, frequency-oriented, emissivities of fractionalized, endmember eigenvector regressors. The motivation would be to collectively organize and relate viable algorithms in these software packages in order to assess the current state-of-the-art in mappable geo-databases in ArcGIS and ENVI to facilitate objective comparisons between unmixing methodologies for optimal, iterative interpolation (e.g., co-kriging) of uncoalesced, proxy biosignatures for identifying unknown, eco-georefernceable, seasonally hyperproductive, immature *Similium* habitats geo-spectrotemporally geosampled in narrow, African, riverine tributary, agro-village, complex ecosystems. Subsequently, the eco-epidemiological, optimally unbiasedly, iteratively interpolatable, vulnerability, elucidative, proxy uncoalesced orthogonally decomposed, proxy signature, residual forecasts (e.g., kriged eco-georeferenceable targets of Hyperendemic, capture point, agro-village, narrow, tributary, riverine foci) would be qualitatively diagnostically quantitated for sub-mixel non-normalites. Mixing models have been widely used to separate the different components of a hydrograph, but their effectiveness suffers from endmember autocorrelation [22].

The Iso Cluster tool employs a modified iterative optimization clustering procedure, also known as the migrating means technique. The algorithm separates all cells into the user-specified number of distinct unimodal groups in the multidimensional space of the input bands. This tool is most often used in preparation for unsupervised endmember classifications.The iso prefix of the isodata clustering algorithm is an abbreviation for the iterative self-organizing way of performing clustering (www.esri.com). This type of fractionalized endmember, eco-geographic, hierarchical clustering would employ a process in which, during each iteration, the orthogonally decomposed, moderate resolution imaged, seasonally hyperproductive, explanatorial, *S. damnosum* s.l., geo-spectrotemporally uncoalesced, moderate resolution, weighted, wavelength, transmittance, emissivity, frequency-oriented, eigenvector, regressor geo-samples are assigned to existing eco-georefernceable, cluster centeroids in each intervention or control agro-village complex. In so doing, robust new means could be recalculated for every trailing vegation, intermittently canopied, turbid water, geoclassifiable, seasonally, explanatorial discontinuously canopied LULC class in ArcGIS. It may be advisable to enter a conservatively high number of broad geoclassiable, LULCs initially to topographically analyze the *S. damnosum* s.l., clusters, so as to eventually rerun the function with a reduced number of classes.

The iso cluster algorithm in ArcGIS employs iterative processes for computing the minimum Euclidean distance when assigning each candidate cell to a cluster (www.esri.com). The process starts with arbitrary means being assigned by the software, one for each cluster (e.g., positive autocorrelated eco-georeferenceable, explanative. hyperproductive, *S. damnosum* s.l., narrow, tributary, agro-village complex, seasonal, turbid water, breeding sites). Every cell is assigned to the closest of their geo-spatialized polygonized means thus creating eco-cartographic, fractionalizd, variables (e.g., uncoalesced forecastable, sparsely shaded, varied, discontinuous canopied, trailing vegetation, endmember eigenvectors) in multidimensional attribute space. New means would then be optimally recalculated for each cluster based on the attribute distances of the cells that belong to the eco-georferenceable cluster after the first iteration. The process is repeatable for optimal endmember radiance geoclassification (e.g., riffle water cell being assigned to the closest mean in an uncoalesced dataset of linearizable combinations of hyperproductive, *S. damnosum* s.l., habitat IR/red ratio, the square root of the IR/red ratio, the IR-red difference, the vegetation index, or the transformed, vegetation, LULC proxy biosignatures) in multidimensional attribute space). In so doing, new means would be optimally calculatable for each eco-georferenceable, explanative, immature habitat, eco-epidemiological, capture point, based on the membership

of cells from the iteration. The number of iterations of the process can be specified through Number of iterations coefficient text file (www.esri.com).

In a seasonally explanative, eco-epidemiological, hyperproductive, capture point, immature, turbid water, sparsely shaded, intermittently canopied, *S. damnosum* s.l., forecast, vulnerability, endmember model this computated value should be large enough to ensure that, after running the specified number of iterations, the migration of cells from one eco-georeferenceable, African, agro-village, narrow, riverine, tributary cluster to another is minimal. In so doing, all the clusters would be geospatially stablized (mimimal endmember random noise) in a moderate resolution scene. When increasing the number of clusters, the number of iterations should also increase(www.esri.com).

The Edit Signatures tool in ArcGIS is designed to modify an existing seasonally hyperproductive, capture point, moderate resolution, *S. damnosum* s.l. signature file. Most frequently, this tool is employed to reduce the number of geoclassifiable, LULC classes in an endmember eigenvector, herusitically optimizable, empirical dataset. To determine which LULC class proxy signatures should be changed to produce a more accurate geo-classification of geospatially, ecohydrologically, meandering, flooded, sub-mixel, hyperendemic, narrow African, riverine tributary, agro-village complex,immature habitats, for example, a tree diagram with the Dendrogram tool in ArcGIS may be employable. Dendrogram is a tree diagram frequently used to illustrate the arrangement of geospatial clusters produced by hierarchical clustering[24]. An ArcGIS or Math LAB dendrogram tree can generate a plot of non-zero autocorrelated, *S. damnosum* s.l.., seasonally hypeproductive, eco-epidemiological, capture point, immature, turbid water, trailing vegetation, partially canopied, eco-georeferenceable, breeding sites in a binary, elucidative, cluster tree. A dendrogram consists of many *U*-shaped lines that connect data points in a hierarchical tree(www.esri.com). The height of each *U* in explicatively forecasted, eco-hydrologic, geo-spectrotemporal, eco-epidemiological, capture point, *S. damnosum* s.l. dendrogram would represent the explicatively quantitable, Euclideanized, distance measurements between any two elucidatively, geosampled, fractionalized endmember , eco-georferenceable, data points [e.g., uncoalesced, intermittently canopied red and IR radiances, experimental plot biomass, leaf water content, chlorophyll(chl)- discontinuous gaps etc.] being geo-spectrotemporally geospatially connected in finite multidimensional regression space. Unfortunately, according to Jacob et al. [22] if there are more than 31 geosampled, geospatially optimally parameterizable hyperproductive, ecogeorefernceable *S. damnosum* s.l., immature breeding site, fractionalized endmembers, the dendrogram would collapse to lower discontinuous, canopied branches so that there would be 30 leaf nodes;hence, sub-mixel autocorrelation would occur in any uncoalesced photosynthetic variables. As a result, some sporadic canopy leaves in the capture point plot may correspond to more than one explanatorial, forecasted, geo-spectrotemporally uncoalesced geolocational, proxy biosignature, data point.

The algorithms employed thus far in the literature to geo-spectrotemporally quantitate fractionalized moderate resolution, linearizable, image endmember irradiance abnormalities in medical entomological, vector, arthropod-related, immature, habitat capture point, eco-epidemiological, forecast, vulnerabity models implicitly or explicitly assume a “convex geometry” for all mixing paradigms. In mathematics, convex geometry is the branch of geometry studying convex sets, mainly in Euclidean space[25]. In geometry, a two- or three-dimensional space in which the axioms and postulates of Euclidean geometry apply; also, a space in any finite number of dimensions, in which points are designated by coordinates (one for each dimension) and the distance between two points is given by a distance formula.

Geometric random walks are maturing into a powerful tool for algorithm designin ArcGIS. Their analysis hinges on isoperimetric inequalities for the state space. For all partitions of the state space into measurable subsets occurs with a fixed proportion of measure. Thus, minimum possible measure of the separating seasonally hyperproductive, capture point, moderate resolution, trailing vegetation, turbid water, eco-georefernceable, *S. damnosum* s.l. infrequently canopied, discontinuous, surface may be quantitated to determine a convex body K and any partition(e.g., S_1, S_2, S_3,). It is known that $volume(S_3) \geq (2\ d(S_1,S_2)/Diameter(K))\ min\{volume(S_1), volume(S_2)\}$ where $d(S_1,S_2)$ is the smallest distance between points in S_1 and S_2. [25]. While this bound is tight in terms of the diameter, it has been conjectured that the coeffient $(2/Diameter(K))$ may be replaced by $c/\sqrt{\lambda}$ where c is an absolute constant and λ is the largest eigenvalue of the a gridded matrix in rcGIS fro eco-cartographically illustrating of K, (i.e. $E(XX^T)$ for a random geo-spectrotemprolly geosampled hyperproductive, *S. damnosum* s.l., capture point X from K.

Another direction ofcurrent ArcGIS research involves a different areas of geometry, such as Riemannian manifolds. Consider the following random walk: at *S. damnosum* s.l. a point x on a manifold, where a random point in the unit ball occurs in the tangent space and then to a moderate reolstion, ecogeorfernceable, narrow, African, riverine tributary, geo-village ecosystem compled image of this on the manifold. The walk rapidly mixed for any manifold may be attributable to a nonnegative curvature in the immature habitat, forecasting, vulnerability model. Even for convex bodies,in the agro-village scene (i.e., x), a random capture point y could be quantized wmploying some fixed radius, in the direction of y till y is reached or hit the boundary of the body; in the latter case, the reflected wavelength, frequency-oriented habitat point about the tangent at the boundary would continue till the boundaries of the agro-village complex.. Convexity itself leads to new questions, about research hypothesis testing iteratively interpolative fractionized endmber eigenvectors from moderate resolution uncoalesced, proxy LULC biosignatures for identying un-geosampled, unknown seasonally hypeproductive, eco-georfernceable, *S. damnosum* s.l. habitats (e.g., can quantiating convexity of a compact set in R^n be efficiently testedy testing random low-dimensional sections of a trailing vegetation, discontinuous, infrequently canopied, hyperproductive, capture point, ecogeorefernceable, *S. damnosum* s.l. turbid water , immature habitat.

Probably the most commonly used unmixing methodology is the Boardman algorithm which employs theconvex hull in his analysis of spectrometry data, In mathematics, the convex hull or convex envelope of a set X of points in the Euclidean plane or Euclidean space is the smallest convex set that contains X. For instance, when X is a bounded subset of the plane, the convex hull may be geovisualized as the shape enclosed by a band stretched around X {24}. This methodology presents three steps: spectral reduction using the Minimum Noise Fraction (MNF) , spatial reduction using the Purity Pixel Index (PPI), and an n dimensional visualization [25]. The MNF transform is used to determine the inherent dimensionality of image data to segregate noise in the data and to reduce the computational requirements for subsequent processing (www.esri.com). The PPI is computed by repeatedly projecting n-D scatter plots on a random unit vector. ENVI records the extreme pixels in each projection (those pixels that fall onto the ends of the unit vector) and it notes the total number of times each mixel is marked as extreme. (www.exelisvis.com).

In other disciplines unmixing algoithms have been strategically employed for distinguishing geo-spectrotemporal, geo-spatialized, missing eco-georeferenceable endmember, moderate resolution, forecastable, variables in ArcGIS and ENVI. For

example, long-term evolutionary dynamics have been approached through fractionalized, endmember, quantitative, forecast-related, vulnerabilty analysis of the fossil record, but without explicitly taking its incompleteness into account within these software packages. Lu et al. (2006) explored the temporal covariance structure of per-genus origination and extinction rates for global marine fossil genera throughout the Phanerozoic, both before and after corrections for qualitatively quantitating the incompleteness of the fossil record. Employing uncorrected data based on Sepkoski's compendium, the authors found significant autocovariance within origination and extinction rates, as well as covariance between extinction and origination, not on one, but two, intervals thereby corroborating evidence of unexplained temporal gap found by past studies. Sepkoski's compendia of marine fossil families and genera have been central to the analysis of the long-term patterns of origination, extinction, and overall diversity of marine animals throughout the Phanerozoic. However, these effects vanished when the data were corrected for the incompleteness of the fossil record. Instead, the authors observed significant covariance only between extinction and origination in the geosampled data immediately following intervals. The gap in the response of the biosphere to extinction in the uncorrected fossil record thus appeared to be an artifact of the incompleteness of the fossil record, specifically due to episodic variation in the probability that taxa was preserved, on time scales comparable to the temporal resolution of Sepkoski's data. The results indicated that a temporal resolution changed in origination and extinction for longer than one interval, except for quantitated elevated origination rates immediately after extinction which lasted for more than a single interval. Thus, although certain individual cases deviated from the overall pattern, the authors found that in general the endmember biosphere's response to perturbation was immediate geologically and usually short-lived.

An endmember,moderate resolution, orthogonal eigenvector, decompositional, spatial filter analyses in ArcGIS may remove any geospatial ambiguity, geo-spectrotemporal trepidations or uncommon variance amongst geo-spectrotemrpoally geosampled, uncoalescable expositively fractionalized, precisely parameterizable *S. damnosum* s.l., covariate coefficient interaction terms employing standardized (e.g., Pearson product-moment correlation coefficient to a univariate series). In probability theory and statistics, variance is a non-negative measures of how far a set of discrete integers are spread out [25]. Pearson's correlation coefficient is the covariance of the two variables divided by the product of their standard deviations. The form of the definition involves a "product moment", that is, the mean (i.e., the first moment about the origin) of the product of the mean-adjusted random variables; hence the modifier product-moment in the name. The covariance between two jointly distributed, real-valued, seasonally explanative, hyperproductive, turbid water, *S. damnosum* s.l., trailing vegetation, discontinuous, infrequently canopied, sparsely shaded, eco-epidemiological, capture point, geo-spectrotemporally uncoalesced empirical datasets of explicatively geo-spatialized, capture point, seasonal, immature habitat, randomized variables X and Y geosampled, in a narrow, riverine tributary, African agro-village, complex ecosystem with finite second moments may be computable in ArcGIS and/or ENVI as $\operatorname{cov}(X,Y) = \mathrm{E}\left[(X - \mathrm{E}[X])(Y - \mathrm{E}[Y])\right]$, where E[$X$] is the expected value of X, also known as the mean of X. By employing the linearity property of expectations, this equation can be simplified to

$$\begin{aligned}\operatorname{cov}(X,Y) &= \mathrm{E}\left[(X-\mathrm{E}[X])\,(Y-\mathrm{E}[Y])\right] \\ &= \mathrm{E}\left[XY - X\,\mathrm{E}[Y] - \mathrm{E}[X]\,Y + \mathrm{E}[X]\,\mathrm{E}[Y]\right] \\ &= \mathrm{E}[XY] - \mathrm{E}[X]\,\mathrm{E}[Y] - \mathrm{E}[X]\,\mathrm{E}[Y] + \mathrm{E}[X]\,\mathrm{E}[Y] \\ &= \mathrm{E}[XY] - \mathrm{E}[X]\,\mathrm{E}[Y]\,.\end{aligned}$$

In so doing the units of moderate resolution fractionalized, endmember, *S. damnsoum* s.l., capture point, immature habitat, eco-georeferenceable, decomposable, fractionalized eigenvector measurements of the covariance Cov(*X*, *Y*) would be those of *X* times those of *Y*. By contrast, correlation coefficients of the explanative, eco-georeferenceable, narrow African, agro-village, complex ecosystem, prolific, immature habitats would depend on the covariance, which would be a dimensionless measure of linear dependence. (i.e.,a normalized version of the covariance). Correlation refers to any of a broad class of statistical relationships involving dependence, though in common usage it most often refers to the extent to which two variables have a linear relationship with each other[25].

Eigenvector spatial filtering (ESF) may furnish a methodology that accounts for dependency in an expositorial, eco-georeferenceable, heuristically optimizable, eco-epidemiological, dataset of moderate resolution, sub-mixel, geo-spectrotemporally uncoalescable, capture point, seasonal, discontinuous, infrequently canopied, hyperproductive, sparsely shaded, turbid water, trailing vegetation, *S. damnosum* s.l., immature habitat, wavelength transmittance, frequency-oriented, emissivity, correlation coefficients in ArcGIS which, may be also explanatively elucidatively quantitable within the domain of a spatial autoregressive (SAR) model covariance matrix. In probability theory and statistics, a covariance matrix (also known as dispersion matrix or variance–covariance matrix) is a matrix whose element in the *i*, *j* position is the covariance between the i^{th} and j^{th} elements of a random vector [24].The fundamental idea would be to exploit the orthogonal, eigenfunction, endmember decompositional, fractionalized analyses for optimal quantitation of an empirical dataset of eco-georeferenceable, geo-spectrotemporally geospatially regressable, heuristically optimizable, capture point, *S. damnosum* s.l., unmixed, seasonally hyperproductive, immature habitat, explanatorial, eco-cartographic variables in ArcGIS, into the following three components: trend, spatially structured random component (i.e., spatial stochastic signal), and random noise. In so doing, the explicatively decomposed, spatially structured, endmember, discontinously canopied, capture point, random components from both trend and random noise would furnish sounder statistical inferences whilest simultaneously providing optimal geo-visualizations of the elucidatively geo-spectrotemporally geosampled, seasonally hyperproductive, *S. damnosum* s.l. immature habitat, illuminatively, optimally parameterizable unmixed eigenvector, coefficient values in finite multidimensional, regression space. In other words, ESF would optimally employ an empirically, geo- robustifiable dataset of explanatively uncoalesced, eco-georeferenceable, synthetic, proxy, moderate resolution, fractionalized endmember, proxy signature variables in ArcGIS (e.g., Geostatitscal Analyst ^{TM}) of a seasonally hyperproductive, narrow, African, riverine tributary, agro-village complex, capture point, trailing vegetation, turbid water, discontinuous, infrequently canopied, agro-village, ecosystem complex, sparsely shaded, eco-epidemiological, immature habitat, which could then be extracted as orthogonalized eigenvectors from a spatial connectivity matrix. In so doing, the eco- geographic geo-spatialized, eco-georfernceable geo-biophysical objects would be 'tied' together in finite regression space, thus rendering vectors as control variables within an eigenfunction decompositional algorithmic, explanatorial, iterative, interpolative, model specification in ArcGIS. These control variables may isolate the stochastic, sub-mixel, explicative, dependencies amongst eco-georeferenceable, fractionalized, *S. damnosum* s.l. immature

habitat, moderate resolution, explanatorial, fractionalized eigenvector regressors, thus allowing model building to proceed as if the capture point observations were independent.

Because ESF model specification is flexible in ArcGIS, it can be utilized to describe geo-spectrotemporal, geo-spatialized, uncoalesced, eco-georeferenceable, sub-mixel, fractionalized, *S. damnosum* s.l., immature habitat, moderate resolution, explanatorial, eigenvectors following various types of distributions, including the Gaussian, Poisson, and binomial [24]. The binomial distribution applies when there are dichotomous outcomes (e.g., logistic regression *S. damnosum* s.l.., binary, response model where immature productivty counts are log-transformed as 0=0 and all density values >1 =1). In probability theory and statistics, the Poisson distribution is a discrete probability distribution that expresses the probability of a given number of events(e.g., eco-geographic field-geosampled, eco-georefernceable, narrow, African, ago-village complex, tributary, trailing vegetation, discontinuous, infrequently canopied, turbid water, capture point, riverine hyperendemic foci) occurring in a fixed interval of time and/or space by assigning a probability to each measurable subset of the possible outcomes of a random experiment, survey, or procedure of statistical inference,. Examples are found in experiments whose sample space is non-numerical, where the distribution would be a categorical distribution (e.g., fractionlized, moderate resolution, endmember eigenvectors eco-cartographically illustrating eco-hydrologic, eco-cartographic, hyperproductive, *S. damnosum* s.l., eco-epidemiological, capture point, capture point immature habitats, discontinuoulsy canopied, geo-biophysical, sparsely shaded, trailing vegetation, turbid water, experiments) whose sample space is encoded by discrete, elucidative, geo-samplable, expositorial, random variables where the distribution can be specified by a probability mass function (PDF)]. In probability theory, PDF or density of a continuous random variable, is a function that describes the relative likelihood for a random variable to take on a given value.

According to Jacob et al. [22] experiments with sample finite multidimensional regression spaces encoded by continuous, explanatively geo-spectrotemporally, expositive, trailing vegetation, turbid water, heterogeneously canopied, geoclassifiable LULC, randomized variables, can be specified by a PDF. The Gaussian endmember distribution applies when the outcome is expressed as a parameterizable covariate coefficient that can have a metaheusritically robustifiable, fractionalizable, endmember, sub-mixel, explanatorial value. If there are numerous reasons why any particular sub-mixel measurement is different than the mean in a probabilistically regressed dataset of eco-georeferenceable, trailing vegetation, turbid water, discontinuous, infrequently canopied, agro-village, ecosystem complex,seasonally hyperproductive, narrow, African, riverine tributary, agro-village complex, sparsely shaded, eco-epidemiological, capture point, *S. damnosum* s.l. immature habitat, orthogonal eigenvectors, the distribution of the fractionalized measurements will tend to follow a Gaussian bell-shaped distribution.

Different ESF endmember specifications may be compared with other specifications, such as the spatial autoregressive (SAR) paradigms for optimally determing an eco-epidemiological, eco-georeferenceable, heuristically optimizable, explanatorial, vulnerability dataset of fractionalized, geo-spectrotemporally uncoalesced, iteratively, interpolative, quantitative geospatial, moderate resolution, wavelength, transmittance. In so doing, foreastable, emissivity, endmember, eigenvector frequencies may be qualitatively rendered from an unmixing algorithm for optimally eco-cartographically illustrating unknown, un-geosampled, explanatively, orthgogonally decomposable, sparsely shaded, discontinuous, infrequently canopied, trailing vegetation, capture point, narrow, African, riverine, agro-

village, tributary complex, seasonally eco-georeferenceable, hyperproductive, *S. damnosum* s.l. habitats in a stochastic or deterministic iterative interpolator in ArcGIS.

Although eigenvector spatial filtering has become more popular in addressing fractionalized, endmember autocorrelation latent in eco-georeferenced data in ArcGIS, the quality of ESF-based explanators has not been thoroughly investigated for qualitatively, auto-regressively, probabilistically quantitating an empirical eco-epidemiological, dataset of geo-spectrotemporally geosampled, uncoalesceable, moderate resolution, seasonally imaged, *S. damnosum* s.l. narrow, African, riverine, tributary, agro-village, complex ecosystem, immature habitat and the capture point's within, discontinuously canopied, trailing vegetation, turbid water, , unmixed probabilistic uncertainties for iteratively, optimally, quantitatively interpolating a proxy signature for explanatively eco-cartographically identifying unknown, un-geosampled, seasonal, hyperproductive habitats. The statistical qualities of these ESF-based estimators, including unbiasedness, efficiency, and consistency, thus also remain un-explored for aiding in developing and implementing control strategies[Integrated Vector Management(IVM)] for onchocerciasis. Such a quality assessment of ESF-based explanatively fractionalized, endmember, canopy surface, irradiance, eigenvector estimators may bolster the efficacy of spatial filtering methodologies in ArcGIS for optimally identifying moderate resolution, orthogonally decomposeable sub-mixel, elucidative, eco-geographical, bio-geophysical, trailing vegetation, sparsely shaded, latent, explicatively geo-classifiable, eco-georefernceable, illuminative, LULC descriptors, expositively eco-geographically illustrating seasonal hyperproductive, turbid water, positively autocorrelated, capture point, hyperporductive *S. damnosum* s.l. habitats, and their parameterizable, covariate coefficients estimators. In so doing, robust seasonally ecohydrologically, empirically regressed datasets of heuristically optimizable, explanatorial, eco-georeferenceable, field-operationizable, eco-epidemiological descriptors (e.g., forecast, seasonal, vulnerability maps targeting unknown, un-geosampled, seasonally hyperproductive, *S. damnosum* s.l. capture point, hyperendemic, foci) may be parsimoniously devised within generalizable, gridded, hierarchical, geo-spatialized algorithmic iterative frameworks in AUTOREG for optimally developing and implementing onchocerciasis, larval control strategies in narrow African, riverine tributary, eco-georeferenceable ,agro-village, complex ecosystems.

Jacob et al. [26] employed the AUTOREG procedure estimates and forecast linear regression model outputs for qualitatively quantiating an empirical geo-spectrotemporally, geospatialized, time series, seasonally hyperproductive, eco-georeferenceable datset of , turbid water, capture point, positively autocorrelated, *S. damnosum* s.l. habitats, and their empirically optimally parameterizable, covariate coefficients estimators geosampled in pre-established eco-epidemiological, narrow, riverine tributary, geoclassified LULC sites in Togo . An autoregressive uncertainity probabilisc model was used to correct for autocorrelation, and the generalized autoregressive conditional heteroscedasticity (GARCH) model and its variants were used to model and correct for any uncommon variance in the moderate resolution derived residual wavelength, transmittance frequency-oriented estimators. The AUTOREG procedure offers estimation and forecasting of autoregressive conditional heteroscedasticity (ARCH), generalized autoregressive conditional heteroscedasticity (GARCH), integrated GARCH (I-GARCH), exponential GARCH (E-GARCH), and GARCH-in-mean (GARCH-M) models (http://support.sas.com.) Exact gradients were employed for optimal, GARCH-type, model estimation in AUTOREG. ARCH and GARCH models were combined with autoregressive models, with explanatorial, moderate resolution, remotely sensed, time series, field-operational eluidative, orthogonal regressors. An

autoregressive moving average model (ARMA model) was assumed for quantizing error variance. A GARCH (*p*, *q*) model where *p* was the order of the GARCH terms $\sigma^2$and *q* was the order of the ARCH terms (i.e., ϵ^2)following the

notation f was optimally geo-spectrotemporally geospatially rendered by $y_t = x_t'b + \epsilon_t\epsilon_t|\psi_t \sim N(0,\sigma_t^2)$ where $\sigma_t^2 = \omega+\alpha_1\epsilon_{t-1}^2+\cdots+\alpha_q\epsilon_{t-q}^2+\beta_1\sigma_{t-1}^2+\cdots+\beta_p\sigma_{t-p}^2 = \omega+\sum_{i=1}^{q}\alpha_i\epsilon_{t-i}^2+\sum_{i=1}^{p}\beta_i\sigma_{t-i}^2$When time series data are used in endmember regression analysis, often the error term is not independent through time. Instead, the errors are serially correlated or autocorrelated. [25]. If the error term is autocorrelated in an endmember, geospectrotemporal, geospatial, decomposable, autorgressive, weight matrix, the efficiency of ordinary least-squares (OLS)optimally parameterized covariate coefficient estimates is adversely affected and standard error estimates may be biased. The SAR model corrected for serial correlation in the *S. damnosum* s.l. SAR model. The AUTOREG procedure fit the autoregressive probabilistic error models which coincidentally also fit multiple subset, seasonal, hyperproductive, explanative, *S. damnosum* s.l.-related, autoregressive models. A stepwise autoregression was specified to select the autoregressive error model automatically in AUTOREG.

To diagnose erroneous autocorrelation coefficients, Jacob et al. {xxx} employed the AUTOREG procedure to produce an optimizable dataset of generalized Durbin- Watson (DW) statistics and their marginal probabilities (see Appendix 2). Exact *p*-values were reported for generalized DW tests for any specified expositively, geoclassifiable geo-spectrotemporal geosampled, autoregressively, illuminatively parameterizable, clustering, trailing vegetation, narrow, African, riverine tributary, turbid water, seasonal, hyperproductive, geo-spectrotemporal, *S. damnosum* s.l., uncoalesced, geoclassifiable LULC explanatorial, uncoalesced, iteratively interpolative, covariate coefficients in the model. For models with lagged dependent paramterizable regressors, AUTOREG performed the Durbin *t*-test and the Durbin *h*-test for the first-order autocorrelation and reported their marginal significance levels.

The AUTOREG procedure solved probabilistic uncertainties in the first order-autocorrelation, *S. damnosoum* s.l. immature habitat, vulnerability paradigm by augmenting the regression model with an autoregressive model for the random errr, thereby accounting for the autocorrelation of the errors in the geo-spectrotemporal, geosampled, endmember datasets. Instead of the usual regression model, the following autoregressive geo-spectrotemporal, geospatialized, elucidative, error model was used: $y_t = \mathbf{x}_t'\boldsymbol{\beta} + v_t$, $v_t = -\varphi_1 v_{t-1} - \varphi_2 v_{t-2} - \ldots - \varphi_m v_{t-m} + \varepsilon_t$and $\varepsilon_t \sim \mathrm{IN}(0,\sigma^2)$. The notation $\varepsilon_t \sim \mathrm{IN}(0,\sigma^2)$ indicated that each ε_t was normally and independently distributed with mean 0 and variance σ^2. The autoregressive model specified that the output variable was dependent linearly on its own previous computed values and on a stochastic term (i.e., an imperfectly predictable parameterized trailing vegetation, discontinuous, infrequently canopied, covariate interaction term); thus the model was in the form of a stochastic difference equation.

Stochastic differential equation (SDE) is a differential equation in which one or more of the terms is a stochastic process, resulting in a solution which is also a stochastic process. SDEs are used to model various phenomena such as unstable stock prices or physical systems subject to thermal fluctuations. Typically, SDEs contain a variable which represents random white noise that is calculated as the derivative of Brownian motion or the Wiener process.

The Wiener process is a continuous-time stochastic process often called standard Brownian motion, which is one of the best known Lévy processes (i.e., càdlàg stochastic processes with stationary independent increments) which occurs frequently in pure and applied mathematics, economics, quantitative finance, and physic models [25]. However, other types of random behaviour may be regressively quantifiably possible, such as jump processes. A jump process is a type of stochastic process that has discrete movements, called jumps, rather than small continuous movements [25]. In physical science, SDEs are usually written as Langevin equations. In statistical physics, a Langevin equation (Paul Langevin, 1908) is a stochastic differential equation describing the time evolution of a subset of the degrees of freedom.Those forms consist of an ordinary differential equation containing a deterministic function and an additional random white noise term. A second form includes the Smoluchowski equation or the Fokker-Planck equation. These are partial differential equations which describe the time evolution of PDFs. The third form is the Itô stochastic differential equation, which is most frequently used in mathematics and quantitative finance. This is similar to the Langevin form, but it is usually written in differential notation. SDEs are denoted in two varieties, corresponding to two versions of stochastic calculus.

Jacob et al [26] used a the Navier–Stokes equation constructed in an ArcGIS cyberenvironment to, describe the motion of a narrow African, riverine, agro-village,eco-georefernceable complex and its substances (e.g., trailing vegetation, discontinuous, infrequently canopied, turbid water, hyperproductive, eco-epidemiological, capture point, hyperproductive, Landsat 7 ^{TM} 15m *S.damnsoum* s.l. immature, clustering habitats for a narrow riverine tributray ,agro-village complex in Togo .

The Landsat 7 (L7) Enhanced Thematic Mapper Plus (ETM+) Calibration Parameter File (CPF) provided all radiometric and geometric calibration coefficients needed for processing of the raw, uncorrected Landsat 7 ETM+ image data for the co-epidemiolgical, agro-village.. study site The primary features on Landsat 7 are a panchromatic band with 15 m spatial resolution, an on-board full aperture solar calibrator, 5% absolute radiometric calibration and a thermal IR channel with a four-fold improvement in spatial resolution over TM.Landsat 7 collects data in accordance with the World Wide Reference System 2, which has catalogued the world's land mass into 57,784 scenes, each 183 km wide by 170 km long. The ETM+ produces approximately 3.8 gigabits of data for each scene. An ETM+ scene has an Instantaneous Field Of View (IFOV) of 30 meters x 30 meters in bands 1-5 and 7 while band 6 has an IFOV of 60 meters x 60 meters on the ground and the band 8 an IFOV of 15 meters (http://landsat.gsfc.nasa.gov/)

Balance equations arise from applying Newton's second law [25] Newton's second law of motion pertains to the behavior of objects for which all existing forces are not balanced. The second law states that the acceleration of an object is dependent upon two variables - the net force acting upon the object and the mass of the object. Hence, assumed they could qualitatively quantiate the narrow riverine eco-georferenceable, explanatorial, flow variables. The main difference between Navier–Stokes equation and the simpler Euler equations is that Navier–Stokes equations are not conservation equations, but rather a dissipative system, in the sense that they cannot be put into the quasilinear homogeneous form(e.g., $\mathbf{y}_t + \mathbf{A}(\mathbf{y})\mathbf{y}_x = 0$.)

The incompressible Navier–Stokes equationswith conservative external field is the fundamental equation of hydraulics. [25]. The domain for these equations is commonly a 3 or less euclidean space, for which an orthogonal coordinate reference frame is usually set to

explicit the system of scalar partial derivative equations to be solved. In 3D orthogonal coordinate systems are 3: Cartesian, cylindrical, and spherical. Expressing the Navier-Stokes vector equation in Cartesian coordinates in ArcGIS is quite straightforward and not much influenced by the number of dimensions of the euclidean space employed, and this is the case also for the first-order terms (like the variation and convection ones) also in non-cartesian orthogonal coordinate systems. But for the higher order terms (the two coming from the divergence of the deviatoric stress that distinguish Navier–Stokes equations from Euler equations) some tensor calculus is required for deducing an expression in non-cartesian orthogonal coordinate systems.

Navier–Stokes equations may be useful because they may measure a hyperproductive seasaonl *S. damnosum* s.l. habitat using the weather, , riverine water flow in a tributray around an ecogeorferenceable, agro-village S. damnsoum s.l. oviposition site on a moderate resolution LULC. The Navier–Stokes momentum equation may be derived as a particular form of the partial differential equation in Calculus Methode/MapServer^{TM} (see Figure 9). A first-order PDE for an unknown function $u(x, y)$ is said to be linear if it can be expressed in the form $a(x, y)\frac{\partial u(x, y)}{\partial x} + b(x, y)\frac{\partial u(x, y)}{\partial y} + c(x, y)\,u(x, y) = d(x, y).$ The PDE is said to be quasilinear if it can be expressed in the form $a(x, y, u(x, y))\frac{\partial u(x, y)}{\partial x} + b(x, y, u(x, y))\frac{\partial u(x, y)}{\partial y} = c(x, y, u(x, y)).$ Quasilinear equation, a type of differential equation where the coefficient of the highest order derivative does not depend on the derivative of the unknown function A PDE which is neither linear nor quasi-linear is said to be nonlinear.For convenience, the symbols z, p, and q are used throughout this tutorial to denote the unknown function and its partial derivatives. $z = u(x, y);\ p = \frac{\partial u(x, y)}{\partial x};\ q = \frac{\partial u(x, y)}{\partial y}$

Figure 9. Hypothetical, Navier–Stokes differential equations used to simulate an narrow African tributary riverine flow around an turid water, hyperproductive , *S. damnosum* s.l. capture point geosampled in Togo using a Cauchy momentum equation .

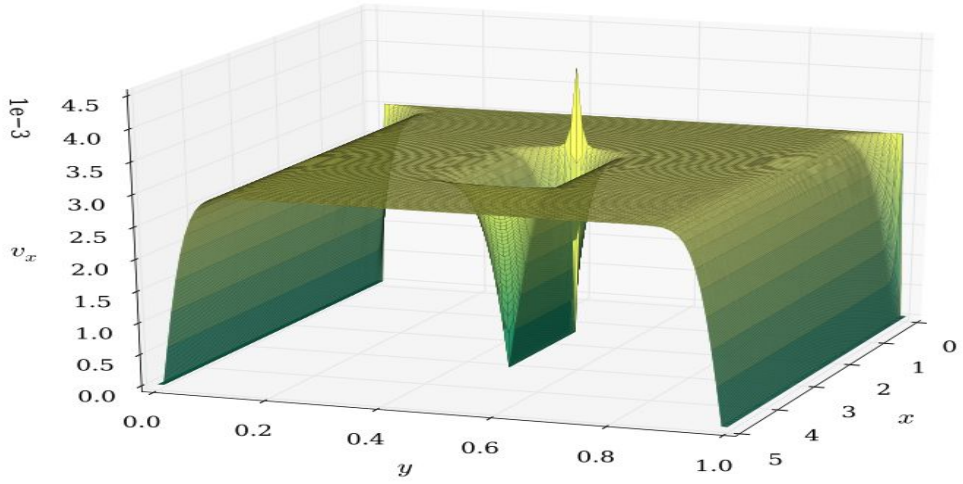

Therefater, an estimation method was used to construct multiple first-order autoregressive error matrices using the Yule-Walker (YW) method. The YW method returns normalized autoregressive (AR) parameters corresponding to a model of order p for the input array, x. If x is a vector, then the output array, a, is a row vector. If x is a matrix, then the parameters along the *n*th row of a model, the *n*th column of x. a has p + 1 columns. p must be less than the number of elements (or rows) of x[25]. The Yule–Walker equations in AUTOREG optimally defined the first order autorrelation coefficients in the *S. damnsoum* s.l. datasets employing the following set of equations $\gamma_m = \sum_{k=1}^{p} \varphi_k \gamma_{m-k} + \sigma_\varepsilon^2 \delta_{m,0}$, where $m = 0, \ldots, p$, yielding $p + 1$ equations. Here γ_m was the autocovariance function of X_t, $\sigma_\varepsilon$was the standard deviation of the input noise process, and $\delta_{m,0}$was the Kronecker delta function. In mathematics, the Kronecker is a function of two variables, usually just positive integers[25]. The full autocorrelation function was then optimally derived by recursively calculating the geo-spectrotemrpoally geospatialized, uncoalesced, *S. damnosum* s.l., trailing vegetation, turbid water, capture point, immature habitat, parameterizable weighted, wavelength, frequency-oriented, transmittance, emissivity covariate estimators. The YW equations were $\gamma 1 = \varphi 1\gamma 0 + \varphi 2\gamma -1$ and $\gamma 2 = \varphi 1\gamma 1 + \varphi 2\gamma 0$ when $\gamma -k = \gamma k$. The equations yielded and the recursion formula rendered in the residual variance.The equations defining the AR processes in the models were then optimally defined.

Thereafter the authors in Jacob et al {26} multiplied both sides by Xt − m and impute the expected, immature, habitat, fractionalized, endmember, covariate coefficient, regressed values. They noted that $E[XtXt-m] = \gamma m$ was the autocorrelation function in the *S. damnosum* s.l. model. The values of the noise function in the model was independent on each other and Xt − m was independent of εt when m was greater than zero. The autoregressive estimates revealed for $m > 0, E[\varepsilon tXt - m] = 0$ in the forecasted capture point, regression residuals. This equation was also rendered when $m \geq 0$ Thereafter, the authors employed $m \wedge 0$.They then let φ represent the vector of the residual elucidatively, optimally parameterized, fractionalized, endmember covariate estimators, $\varphi = (\varphi 1, \varphi 2, \cdots, \varphi m)'$, where the variance matrix of the error vector was $v = (v1, \cdots, vN)'\Sigma$, $E(vv\ \Sigma = \sigma 2v)$. If the vector of autoregressive parameters φ is known, the matrix v can be computed using regression-based,

explanatorial estimators and Σ which can then delineate σ2v[25]. Given Σ the efficient estimates of the eco-georeferenceable, capture point, *S. damnosum* s.l., larval habitat, regression parameters, β was computed using a Generalized Linear Square (GLS) algorithm. The GLS yielded the unbiased estimate of the variance σ2 in the forecasts.

The calculation of v from for the generalized autorgressive, *S. damnosum* s.l., larval habitat, endmember analyses was complicated as it was completely dependent on the number of geosampled categorical observations in both models. Instead of actually calculating v and performing GLS in the usual way, the authors in Jacob et al. [26] used a Kalman filter algorithm to transform the geospectrotemporal Landsat 7 ^{TM} data and compute the GLS results through a recursive process. The Kalman filter, also known as linear quadratic estimation, is analgorithm which uses a series of measurements observed over time, containing noise (i..e, random variations) and other inaccuracies, which produces estimates of unknown variables that tend to be more precise than those that would be based on a single measurement alone [24]. The Kalman filter operated recursively on streams of the noisy input, narrow, tributary, uncoalesced, immature, riverine habitat, eco-georeferenceable, decomposed, iteratively interpolative, 5m data to produce statistically optimizable estimators.The Shapiro-Wilk test was then employed to test the null hypothesis that the geosampled, riverine habitat illuminative estimators x1,⋯,xn. came from a normally distributed population.

The Shapiro–Wilk test utilized the null hypothesis principle to check whether a sample x_1, ..., x_n came from a normally distributed *S. damnosum* s.l., immature habitat, geosampled population. The test statistic employed was $W = \frac{\left(\sum_{i=1}^{n} a_i x_{(i)}\right)^2}{\sum_{i=1}^{n}(x_i - \overline{x})^2}$where$x_{(i)}$(with parentheses enclosing the subscript index *i*) was the *i*th order statistic, (i.e., the *i*th-smallest number in the sample;$\overline{x} = (x_1 + \cdots + x_n)/n$)was the sample mean;and the constants $a_i$were given by$(a_1, \ldots, a_n) = \frac{m^{\mathsf{T}} V^{-1}}{(m^{\mathsf{T}} V^{-1} V^{-1} m)^{1/2}}$in AUTOREG where$m = (m_1, \ldots, m_n)^{\mathsf{T}}$ and $m_1, \ldots, m_n$ were the expected values of the order statistics of independent and identically distributed random variables geo-spectrotemporally sampled from the standard normal distribution, and V was the covariance matrix of those order statistics.

The DW statistics were then employed to determine whether the OLS regression estimates indicated significant serial uncertainty correlation with an estimated order of a lagged covariance of 1 in the immature habitat,capture point, forecast, vulnerability models. The AUTOREG procedure corrected for the serial correlation using the YW method. The DW statistics indicated that uncertainty correlation was only slightly significant in the YW corrected models. The YW estimates for the first-order serial autocorrelation model indicated a R^2=0.574, F statistics of 37.159.

The elucidative, residualized, weighted, riverine, immature habitat, parameterized endmember, covariate estimators were then validated using weighted cumulative models in ArcGIS. The approach was implemented following the line of goodness of fit testing. Initially, a test statistic employing a cumulative residual formulation was developed which was generalized to binary/discrete data with proper link functions. The authors in Jacob et al (26) aimed for parsimony and plausibility of the predicted, auto-regressiv,e residualizede, intra-cluster-based error estimates. Under the null hypothesis that the outcome was independent of the riverine larval habitat data, the authors generated [i.e., (si, ri)], which was

conditional on the geosampled data attributes (**X**i). The authors assumed that the outcome could be verified using where β was a p × 1 vector of the regression-based algorithm.

Collecting data from the expositorily fractionalized, endmember eigenvectors, spatially filtered, spectral band datasets of moderate resolution sensor data may demonstrate the capability of orthogonally performing spectral unmixing in ArcGIS since the spatial resolution of the sensor may be sufficient for illuminating disparate materials in an eco-georeferenceable, empirically regressable dataset of uncoalesced, hyperproductive, trailing vegetation, turbid water, seasonally explanative, sparsely shaded, eco-epidemiological, narrow, African, riverine tributary, agro-village, *S. damnosum* s.l. capture point, immature, habitat, within-canopied objects (e.g.,sedge). Analysis of the sensitivity of absorbed light and incident light profile of these discontinuous architectural components and stand conditions may reveal ground based estimation of the vertical distribution of moderate resolution, trailing vegetation, leaf area density values [22]. These data may jointly occupy a single mixel; the resulting spectral measurement may be some composite of the individual, fractionalized, geo-spectrotemporally uncoalesceable, immature habitat, endmember eigenvector, derivative spectra. Mixels can result when distinct materials are combined into a homogeneous mixture[24]

Another criterion for optimally evaluating the dependence of a expositorial, regressable, eco-epidemiological, uncoalesced dataset of moderate resolution, geo-spatialized, trailing vegetation, discontinuously canopied, sparsely shaded, seasonally hyperproductive,turbid water, *S. damnosum* s.l.,eco-epidemiological, capture point, iteratively, quantitatively, interpolatively forecastable, sub-mixel, eigenvector explanators extracted from an eco-georefernceable, narrow, African, riverine agro-village, complex ecosystem, geo-spectrotemporal signature may be probabilistically imparted in ArcGIS by the nugget/sill ratio. This ratio would indicate how much of overall variation is spatially random; the larger this ratio, the less spatial dependence would exist in the geosampled, immature habitat, eco-epidemiological dataset. Theoretically, at zero separation distance (lag = 0), the semivariogram representing an explanative, eco-georefernceable seasonally hyperproductive, *S. damnosum* s.l., eco-epidemiological, capture point value is 0. In geostatistics, the active lag distance specifies the range over which semivariance can be computated, which is usually about half of the maximum separation distance. The variogram reports the mean semivariance at each lag h - extreme values which can boost this mean. So optimizable, seasonally, hyerproductive, orthogonally explanatively decomposable, iteratively interpolative, eco-georeferenceable, *S. damnosum* s.l., immature habitat, regression, variance values that appear to be extreme in a forecasting, vulnerability, ArcGIS-derived, endmember eigenvector, fractionalized, radiance, model residual output may not actually represent uncharacteristic, moderate resolution imaged, discontinuous, infrequently canopied,quantitable surface irradiance, uncoalesceable, wavelength, frequency-orinted, transmittance, emissivity frequencies.

On occasion due to the remotely infinitesimally small quantitable immature *Similium* habitat, eco-georefernceable, separation distances in an eco-epidemiological, prediction, risk map targeting seasonally hyperproductive, hyperendemic narrow, African, riverine tributary,discontinuous, infrequently canopied, trailing vegetation, turbid water, agro-village foci, this semivariogram may exhibit a nugget effect, which may be eco-cartographically optimally described as some value greater than 0 in ArcGIS. For example, if an explanative, eco-epidemiological, hyperproductive, narrow, agro-village riverine tributary, *S. damnosum* s.l., eco-epidemiological, capture point, foreasting, vulnerability model

semivariogram intercepts the y-axis at 2, then the nugget would be 2. The nugget effect can be attributed to measurement errors or spatial sources of variation at Euclidean distances smaller than the sampling interval or both. Variation at microscales smaller than the capture point sampling distances will appear as part of the nugget effect. Before collecting geo-spectrotemporally uncoalesced, *S. damnosum* s.l. narrow, African, agro-village, riverine tributary, hypeproductive, *S. damnosum* s.l., eco-georeferenceable, capture points in ArcGIS it is important to gain some understanding of the scales of spatial variation.

Jacob et al [22] examined the variogram cloud in ArcGIS which the authors found to be a useful qualitative approach to understanding the variability of the semivariance prior of an iteratively, explanatively, quantitatively interpolative geo-spectrotemporally uncoalescable, endmember geo-spatializable eco-georeferenceable, dataset of eco-epidemiological, capture point, trailing vegetation, turbid water, discontinuous, infrequently canopied, sparsely shaded, hyperproductive, immature habitats geosampled in a nnarrow African riverine tributary, agro-village ecosystem in Burkina Faso. The semivariogram/covariance cloud allowed examining the spatial autocorrelation between the measured sample points. To do so, the semivariogram value, was iteratively interpolatively computed by the authors which was subsequently quantitated as the difference squared between the decomposed values of each pair of eco-georefernceable, explanative, seasonally hyperproductive, *S. damnosum* s.l., immature, trailing vegetation, discontinuous, infrequently canopied, turbid water, eco-epidemiological, capture point, geosampled, narrow riverine tributary, hyperendemic, immature habitat. This data was subsequently eco-cartographically plotted on the y-axis relative to the distance separating each pair on the X-axis in ArcGIS. (Figure 2).

In spatial statistics the theoretical variogram $2\gamma(x,y)$is a function describing the degree of spatial dependence of a spatial random field or stochastic process $Z(x)$[24]. In probability theory, a stochastic endmember process, or often random process, is a collection of deomposed random variables (e.g., geospectrotemporally uncoalesced sub-mixel dataset of heursitically optimizable, eco-georeferenceable, seasonally hyperproductive, discontinuous, sporadically canopied, trailing vegation, turbid water, narrow riverine tribuitary, African, agro-vaillge complex ecosystem seasonal capture point) representing the evolution of some system of random values over time. This is the probabilistic counterpart to a deterministic process or deterministic system. Instead of describing a process in a seasoanlly geosampled *S. damnsoum* s.l., prolific, immature habitat, forecasting vulnerability paradigm) which can only evolve in one way (as in the case, for example, of solutions of an ordinary differential equations), in a stochastic, or random sampled immature habitat process there may be some some indeterminacy: even if the initial condition (immatuyre productive rate) of the seasonal capture point is known, there are several (often infinitely many) directions in which the process may evolve in an iteratively interpolated uncoalesced, proxy LULC biosignature

In the simple case of discrete time, as opposed to continuous time, a stochastic process is a sequence of random variables. (see Markov chain, also known as discrete-time Markov chain.) In probability theory, a stochastic process, or often random process, is a collection of random variables representing the evolution of some system of random values over time. This is the probabilistic counterpart to a deterministic process (or deterministic system)[24].The random variables corresponding to various times may be completely different, the only requirement being that these different random quantities all take values in the same space (e.g., the codomain of the optimizable, eco-georeferenceable, seasonally hyperproductive, discontinuous, sporadically canopied, trailing vegation, turbid water, narrow riverine tribuitary, African, agro-vaillge complex ecosystem seasonal capture point function). One

approach may be to model these random variables as random functions of one or several deterministic arguments (in most cases, the time parameter). Although the random values of a stochastic process at different times may be independent random variables, in most commonly considered situations they exhibit complicated statistical dependence

One way to optimally identify geo-spectrotemporal uncoalesced, geospatially geosampled, hyperproductive, immature, seasonal, eco-epidemiological, capture point *S. damnosum* s.l. discontinuous, infrequently canopied, sparsely shaded, trailing vegtaion, turbid water,immature habitat for qualitatively quantitating inflation is to calculate the variance for the square root of the absolute value of the differences in ArcGIS using a variogram. The variogram is defined as the variance of the difference between field values at two locations (x and y) across realizations of the field (Cressie 1993): $2\gamma(x,y) = \operatorname{var}(Z(x) - Z(y)) = E\left[((Z(x) - \mu(x)) - (Z(y) - \mu(y)))^2\right]$ If the spatial random field has constant mean μ, this is equivalent to the expectation for the squared increment of the values between locations $x$and y [24] (where $x$and $y$are not coordinates but points in space): $2\gamma(x,y) = E\left[(Z(x) - Z(y))^2\right]$ where $\gamma(x,y)$itself is called the semivariogram. In the case of a stationary process, the variogram and semivariogram can be represented as a function $\gamma_s(h) = \gamma(0, 0+h)$of the difference $h = y - x$between locations only, by the following relation:$\gamma(x,y) = \gamma_s(y-x)$ If the process is furthermore isotropic, then the variogram and variogram can be represented by a function $\gamma_i(h) := \gamma_s(he_1)$of the distance $h = \|y - x\|$ where only $\gamma(x,y) = \gamma_i(h)$ [24]. Note that the experimental variogram is an empirical estimate of the covariance of a Gaussian process. As such, it may not be positive definite and hence not directly usable in kriging, without constraints or further processing. This explains why only a limited number of variogram models are used: most commonly, the linear, the spherical, the Gaussian and the exponential models.

PROC VARIOGRAM can use a variety of theoretical semivariogram models. Specifically, a list of such models can be used for fitting a dataset of geo-spectrotemporally geosampled, moderate resolution, *S. damnosum* s.l. in the MODEL statement of the VARIOGRAM procedure. The VARIOGRAM procedure computes sample or empirical measures of spatial continuity for two-dimensional eco-georeferenceable seasonally explanatorial, hyperproductive, *S. damnosum* s.l., turbid water, trailing vegetation, capture point, geo-spectrotemporally uncoalesced endmember, moderate resolution, orthogonalized eigenvector geospatialized, explicatively geosampled empirical, metaheuristically optimizable datasets. The continuity measures from theses robustifiable models can render the regular semivariogram, a robust version of the semivariogram, and the covariance in Geospatial Analyst ™. The continuity measures may be written to an output *Similium* explanatorial, sub-mixel, endmember dataset, allowing for plotting or parameter estimation for theoretical semivariogram or covariance models. Both isotropic and anisotropic measures are available. The VARIOGRAM procedure can produce two additional output datasets that are useful in the analysis of pairwise immature habitat distances in the original data. The OUTPAIR= dataset can contains one geo-spectrotemporally geosampled, observation for each pair of capture points. The coordinates, distance, angle, and values of the analysis variables may be written to this probabilistic regressable dataset. The OUTDISTANCE= dataset will contains histogram information on the count of immature habitat pairs within explanative distance intervals in a geo-spectrotemporally geosampled, eco-georeferenceable, narrow tributary, African riverine, ecosystem which may be also useful for determining unit lag distances. The variogram is the key function in geostatistics as it will be used to fit a model of the temporal/spatial correlation of the observed phenomenon [24]. Thus , in

actuality, an ecologist, entomologist or other researcher is making a distinction between the experimental variogram that is a geo-visualisation of a possible spatial/temporal correlation in a dataset of empirically regressable geo-spectrotemporal, moderate resolution, iteratively interpolative, proxy, geo-spatialized LULC bsignature endmember eigenvectors and the *variogram model* that may be further used to define the uncoalesced trailing vegation, discontinuous canopied, sparsely shaded, turbid water, wavelength, transmittance, frequency-oriented, emissivity weights of the kriging function. Note that the experimental variogram is an empirical estimate of the covariance of a Gaussian process. As such, it may not be positive definite and hence not directly usable in kriging uncoalesced, moderate resolution, *S.damnosum* s.l., capture point, proxy, LULC biosignatures without constraints or further processing in ArcGIS. This explains why only a limited number of variogram models are used: most commonly, the linear, the spherical, the Gaussian and the exponential models for geo-predictive eco-epidemiological, forecast, vulnerability paradigms of this this riverine black fly specie (see Table 4).

Table 4. Permissable theorectical seasonal ,trailing vegetetation, georeferenceable, capture point, probabilistic, *S. damnosum* s.l. oviposition semiovarigrams

Exponential	$\gamma_z(\boldsymbol{h}) = \begin{cases} 0 & \text{if } \lvert \boldsymbol{h} \rvert = 0 \\ c_n + \sigma_0^2 \left[1 - \exp\left(-\frac{\lvert \boldsymbol{h} \rvert}{a_0} \right) \right] & \text{if } 0 < \lvert \boldsymbol{h} \rvert \end{cases}$
Gaussian	$\gamma_z(\boldsymbol{h}) = \begin{cases} 0 & \text{if } \lvert \boldsymbol{h} \rvert = 0 \\ c_n + \sigma_0^2 \left[1 - \exp\left(-\frac{\lvert \boldsymbol{h} \rvert^2}{a_0^2} \right) \right] & \text{if } 0 < \lvert \boldsymbol{h} \rvert \end{cases}$
Power	$\gamma_z(\boldsymbol{h}) = \begin{cases} 0 & \text{if } \lvert \boldsymbol{h} \rvert = 0 \\ c_n + \sigma_0^2 \boldsymbol{h}^{a_0} & \text{if } 0 < \lvert \boldsymbol{h} \rvert, 0 \le a_0 < 2 \end{cases}$
Spherical	$\gamma_z(\boldsymbol{h}) = \begin{cases} 0 & \text{if } \lvert \boldsymbol{h} \rvert = 0 \\ c_n + \sigma_0^2 \left[\frac{3}{2} \frac{\lvert \boldsymbol{h} \rvert}{a_0} - \frac{1}{2} \left(\frac{\lvert \boldsymbol{h} \rvert}{a_0} \right)^3 \right] & \text{if } 0 < \lvert \boldsymbol{h} \rvert < a_0 \\ c_0 & \text{if } a_0 < \lvert \boldsymbol{h} \rvert \end{cases}$
Cubic	$\gamma_z(\boldsymbol{h}) = \begin{cases} 0 & \text{if } \lvert \boldsymbol{h} \rvert = 0 \\ c_n + \sigma_0^2 \left[7 \left(\frac{\lvert \boldsymbol{h} \rvert}{a_0} \right)^2 - \frac{35}{4} \left(\frac{\lvert \boldsymbol{h} \rvert}{a_0} \right)^3 + \frac{7}{2} \left(\frac{\lvert \boldsymbol{h} \rvert}{a_0} \right)^5 - \frac{3}{4} \left(\frac{\lvert \boldsymbol{h} \rvert}{a_0} \right)^7 \right] & \text{if } 0 < \lvert \boldsymbol{h} \rvert \le a_0 \\ c_0 & \text{if } a_0 < \lvert \boldsymbol{h} \rvert \end{cases}$
Pentaspherical	$\gamma_z(\boldsymbol{h}) = \begin{cases} 0 & \text{if } \lvert \boldsymbol{h} \rvert = 0 \\ c_n + \sigma_0^2 \left[\frac{15}{8} \frac{\lvert \boldsymbol{h} \rvert}{a_0} - \frac{5}{4} \left(\frac{\lvert \boldsymbol{h} \rvert}{a_0} \right)^3 + \frac{3}{8} \left(\frac{\lvert \boldsymbol{h} \rvert}{a_c} \right)^5 \right] & \text{if } 0 < \lvert \boldsymbol{h} \rvert \le a_0 \\ c_0 & \text{if } a_0 < \lvert \boldsymbol{h} \rvert \end{cases}$
Sine hole effect	$\gamma_z(\boldsymbol{h}) = \begin{cases} 0 & \text{if } \lvert \boldsymbol{h} \rvert = 0 \\ c_n + \sigma_0^2 \left[1 - \frac{\sin(\pi \lvert \boldsymbol{h} \rvert / a_0)}{\pi \lvert \boldsymbol{h} \rvert / a_0} \right] & \text{if } 0 < \lvert \boldsymbol{h} \rvert \end{cases}$
Matérn class	$\gamma_z(\boldsymbol{h}) = \begin{cases} 0 & \text{if } \lvert \boldsymbol{h} \rvert = 0 \\ c_n + \sigma_0^2 \left[1 - \frac{2}{\Gamma(v)} \left(\frac{\lvert \boldsymbol{h} \rvert \sqrt{v}}{a_0} \right)^v K_v \left(2 \frac{\lvert \boldsymbol{h} \rvert \sqrt{v}}{a_0} \right) \right] & \text{if } 0 < \lvert \boldsymbol{h} \rvert, v > 0 \end{cases}$

If the random empirically regressable geo-spectrotemporal, moderate resolution, iteratively interpolative, proxy, geo-spatialized LULC biosignature endmember eigenvector trailing vegation, turbid water, discontinuosly canopied, sparsely shaded *S. damnosum* s.l. seasonal, hypeproductive geosampled capture point,forecast variable X represents samples generated by a elucidative continuous distribution with probability density function $f(x)$, then the tabulated, optimizable population variance may be given

b $\mathrm{Var}(X) = \sigma^2 = \int (x-\mu)^2 f(x)\,dx = \int x^2 f(x)\,dx - \mu^2$ where μ is the expected narrow tributray, African agro-village, immature habitat, count value, $\mu = \int x\, f(x)\,dx$ and where the integrals are definite integrals taken for *x* ranging over the fractionalized, endmember eiegenvector , wavelength, range of *X*. A definite integral is an integral $\int_a^b f(x)\,dx$ with upper and lower limits. If x is restricted to lie on the real line, the definite, moderate resolution, eco-georferenceable, explanative transmittance, frequency-oriented, emissity, integral is known as a Riemann integral (which is the usual definition encountered in elementary textbooks). An integral is a mathematical object that can be interpreted as an area or a generalization of area. Integrals, together with derivatives, are the fundamental objects of calculus.However, a general definite integral is taken in the complex plane, resulting in the contour integral $\int_a^b f(z)\,dz$, with a, b, and z in general being complex numbers and the path of integration from a to b known as a contour. The first fundamental theorem of calculus allows definite integrals to be computed in terms of indefinite integrals, since if F is the indefinite integral for a continuous function $f(x)$, then $\int_a^b f(x)\,dx = F(b) - F(a)$. [24].

In its most general form, under some conditions (which include finite variance), it states that averages of random variables independently drawn from independent distributions converge in distribution to the normal, that is, become normally distributed when the number of random variables is sufficiently large[http://mathworld.wolfram.com/]. Distributions with infinite variance are heavy-tailed; there are lots of outliers, and can have unusal properties [e.g., the sample mean of samples drawn from a Cauchy, hyperproductive,seasonal, *S. damnosum* s.l., immature capture point, uncoalesced geo-spectrotemporal distribution has the same (Cauchy) distribution as the individual geospatialized geosampled samples]. This is quite different from the usual belief that the sample mean is a better "estimator" than any individual, immature, trailing vegtaion, turbid water, discontinuously canopied, narrow, tributary, African agro-village, eco-georefrenceable, complex ecosystem, immature habitat, explanatory sample. Suppose that Xn, n ∈ ℕ+ and X are real-valued eco-georferenceable, operationizable, randomly unmixed, empirically, probabilistically regressable, e moderate resolution, geo-spectrotemporal, geo-spatialized, proxy, LULC signature endmember eigenvector, *S. damnosum* s.l. seasonally hypeproductive, geosampled capture point,forecast-oriented variable with biophysical, eco-physiological, explicative unmixed, distribution functions Fn, n ∈ ℕ+ and F,respectively. Then the geo-spectrotemporally geosampled, sub-mixel, trailing vegetation, turbid water, discontinuously canopied, sparsely shaded, regressed moderate reoslution, wavelength, distribution of Xn may converge to the distribution of X as n → ∞ if Fn(x) → F(x) as n → ∞ for all x at which F is continuous.

By graphing the boxplot and looking for extreme transmittance frequency-oriented, emissity values in Geospatial Analyst ™, Jacob et al. [26] quantitated the complexity of an empirically, elucidative, metaheuristically optimizable, probabilistically regressable dataset of explanative, orthogonally decomposeable, moderate resolution, eco-georeferenceable, hyperproductive, trailing vegetation, discontinuously canopied, sparsely shaded, turbid water, narrow, African, riverine tributary, eco-cartographic, *S. damnosum* s.l., eco-epidemiological, capture point, moderate resolution, geo-spectrotemporally uncoalesced, diffuse, elucidative, moderate resolution, wavelength, frequency-oriented, fractionalized, endmember, eigenvector, transmittance, emissivities, which was spatially diluted so as to optimize

iterative trial runs .In descriptive statistics, a box plot or boxplot is a convenient way of graphically depicting groups of numerical data through their quartiles. The quartiles of a ranked set of data values are the three points that divide the data set into four equal groups, each group comprising a quarter of the data[26]. Let $Xn = 1n$for $n \in \mathbb{N}+$ and let $X = 0$ and let $f\ n$ and f be the corresponding density functions and let Fn and F be the corresponding distribution of a empirically regressable dataset of geo-spectrotemporally geosampled, seasonal *S. damnosum* s.l., forecasting, vulnerability paradigm, capture point, inverse functions. Then a differential geometrical elucidative, ArcGIS, seasonally explanative, hyperproductive, *S. damnosum* s.l., capture point, eco-epidemiological, eco-georeferenceable, immature habitat, may reveal pertinent cartographic variables in a semiovariogram of hyperproductive eco--georeferenceable,trailing vegetation, turbid water, discontiouous canopied, seasonal capture points if $n(x)$ a. $\rightarrow 0$ as $n \rightarrow \infty$ for all $x \in \mathbb{R}Fn(x) \rightarrow \{0, x \leq 01, x > 0$b. as $n \rightarrow \infty$c. $Fn(x) \rightarrow F(x)$ as $n \rightarrow \infty$ for all $x \neq 0$.

The theory of plane and space curves and surfaces in the three-dimensional Euclidean space formed the basis for development of differential geometry In geometry, Euclidean space encompasses the two-dimensional Euclidean plane, the three-dimensional space of Euclidean geometry, and certain other spaces. It is named after the Ancient Greek mathematician Euclid of Alexandria.[1] The term "Euclidean" distinguishes these spaces from other types of spaces considered in modern geometry. Euclidean spaces also generalize to higher dimensions.

Classical Greek geometry defined the Euclidean plane and Euclidean three-dimensional space using certain postulates, while the other properties of these spaces were deduced as theorems. Geometric constructions are also used to define rational numbers. When algebra and mathematical analysis became developed enough, this relation reversed and now it is more common to define Euclidean space using Cartesian coordinates and the ideas of analytic geometry. It means that points of the space are specified with collections of real numbers, and geometric shapes are defined as equations and inequalities. This approach brings the tools of algebra and calculus to bear on questions of geometry and has the advantage that it generalizes easily to Euclidean spaces of more than three dimensions.

From the modern viewpoint, there is essentially only one Euclidean space of each dimension. With Cartesian coordinates it is modelled by the real coordinate space (R^n) of the same dimension. In one dimension, this is the real line; in two dimensions, it is the Cartesian plane; and in higher dimensions it is a coordinate space with three or more real number coordinates. Mathematicians denote the *n*-dimensional Euclidean space by E^n if they wish to emphasize its Euclidean nature, but R^n is used as well since the latter is assumed to have the standard Euclidean structure, and these two structures are not always distinguished. Euclidean spaces have finite dimension.

Euclidean n-space, in an uncoalesced, eco-georferenceable, hyperproductive, seasonal, trailing vegetation, discontinuously canopied, *S. damnosum* s.l. immature habitat is the space of all *n*-tuples of real geo-spectrotemporally geosampled geoclassifiable, explanatorial LULC, (x_1, x_2, ..., x_n). Such n-tuples are sometimes called points, although other nomenclature may be used). The totality of n-space in the habitat forecasting vulnerability model is commonly denoted $\mathbb{R}^n$, although older literature uses the symbol $\mathbb{E}^n$(or actually, its non-doublestruck variant $\mathbf{E}^n$; O'Neill 1966, p. 3). $\mathbb{R}^n$is a vector space and has Lebesgue covering dimension n[25].The Lebesgue covering dimension is an important dimension and one of the first dimensions investigated. It is defined in terms of covering sets, and is

therefore also called the covering dimension (as well as the topological dimension)(http://mathworld.wolfram.com/).

A space has Lebesgue covering dimension $m$if for every open cover of that space, there is an open cover that refines it such that the refinement has order at most $m+1$. Consider how many elements of the cover contain a givenhypeproductive seasonal *S. damnosum* s.l. immature habitat point in a base space. If this has a maximum over all the habitat geosampled points in the base space, then this maximum would be based on the order of the cover. If a habitat space does not have Lebesgue covering dimension $m$for any m, it would have an infinite dimensional. Results of this definition in ArcGIS would reveal for a capture point decomposed S. damsnoum s.l. prolific seasaonl, oviposition site on a moderate resolution geoclassified LULS could reveal: 1. Two homeomorphic spaces have the same dimension, 2. $\mathbb{R}^n$has dimension n, 3. A topological space can be embedded as a closed subspace of a Euclidean space if fit is locally compact, T2, second countable, and is finite-dimensional (in the sense of the Lebesgue covering dimension), and 4. Every compact metrizable m-dimensional topological space can be embedded in $\mathbb{R}^{2m+1}$. For this reason, elements of $\mathbb{R}^n$are sometimes called n-vectors. $\mathbb{R}^1=\mathbb{R}$then would be the set of r *S. damnosum* s.l. geosamepled parameterizable, orthogonally decomposable, LULC covariate coefficients where $\mathbb{R}^2$is the Euclidean plane. In Euclidean space, covariant and contravariant quantities are equivalent so $\vec{e}^{\,j}=\vec{e}_j$[25].

Prediction of the spatially random field (S RF)values at un-geosampled, seasonally prolific , moderate resolution, *S. damnosum* s.l. oviposition,geolocations by techniques such as ordinary kriging requires the use of a theoretical semivariogram or covariance model. random field is a generalization of a stochastic process such that the underlying parameter need no longer be a simple real or integer valued "time", but can instead take values that are multidimensional vectors, or points on some manifold[26] lLnear Gaussian random field models for both geostatistical and areal (lattice) datamay model the spatial dependence via a parametric covariance function for articulating parameterized precision (inverse covariance) matrix estimators, and for considering Bayesian inference and prediction[2] For example, consider the exponential covariance with parameters $\Theta = (\psi, \kappa, \varphi)$, with $\psi, \kappa, \varphi > 0$. The exponential covariance $\Sigma(\Theta)$ in a SRF has the form $\Sigma(\Theta) = \psi I + \kappa H(\varphi)$, where I is the identity matrix, the i, jth element of $H(\varphi)$ is $\exp(-ksi - sjk/\varphi)$, and ksi − sjk is the Euclidean distance between locations si , sj ∈ D. Alternatives to Euclidean distance may be useful, for instance geodesic distances are often appropriate for spatial data over large regions (African narrow riverine tributaries).This model may be interpreted as follows: the “nugget” ψ is the variance of the non-spatial error, say from measurement error or from a micro-scale stochastic source associated with each capture point location(e.g., discontinuously canopied, trailing vegetation foci), and κ and φ dictate the scale and range of the spatial dependence respectively. Clearly, the SRF will assume the covariance and hence dependence between two black fly capture locations decreases as the distance between them increases.

In mathematics, a manifold is a topological space that locally resembles Euclidean space near each point. More precisely, each point of an n-dimensional manifold has a neighbourhood that is homeomorphic to the Euclidean space of dimension n. (http://mathworld.wolfram.com/). Due to the randomness involved in stochastic processes, the theoretical semivariance cannot be computed (www.sas.edu). Instead, it is possible that the empirical semivariance can provide an estimate of the theoretical semivariance, which can then be used to characterize the spatial structure of a hyperproductive decomposeable,

explanatively seasonally hyperproductive, trailing vegetation, discontinuously canopied, capture point, oviposition process. It is critical to note that the empirical semivariance provides an estimate of its theoretical counterpart only when the SRF satisfies stationarity conditions. These conditions imply that the SRF has a constant (or zero) expected value may quanatie parameterizable covariates for optimal iterative interpolation of a datset of geo-spectrotemporally uncoalesces, eco-georeferenced, *S. damnosum* s.l. hyperproductive, seasonal habitat. Consequently, a *S. damnosum* s.l. capture point, orthogonally , explanatively decomposed data needs to be geosampled from a trend-free random field and need to have a constant mean(Figure 10).

Figure 10: Semiovariogram of spatial resolution SRF map of a an seasonal hypeproductive, trailing vegetation, discontinuously canopied, turbid water, *S. damnosum* s.l. habitat , narrow riverine agro-village complex ecosystem, capture point (x) in Burkina Faso with forecasted unknown, un-geosampled. immature habitats based on a proxy Rapid Eye TM 5m signature

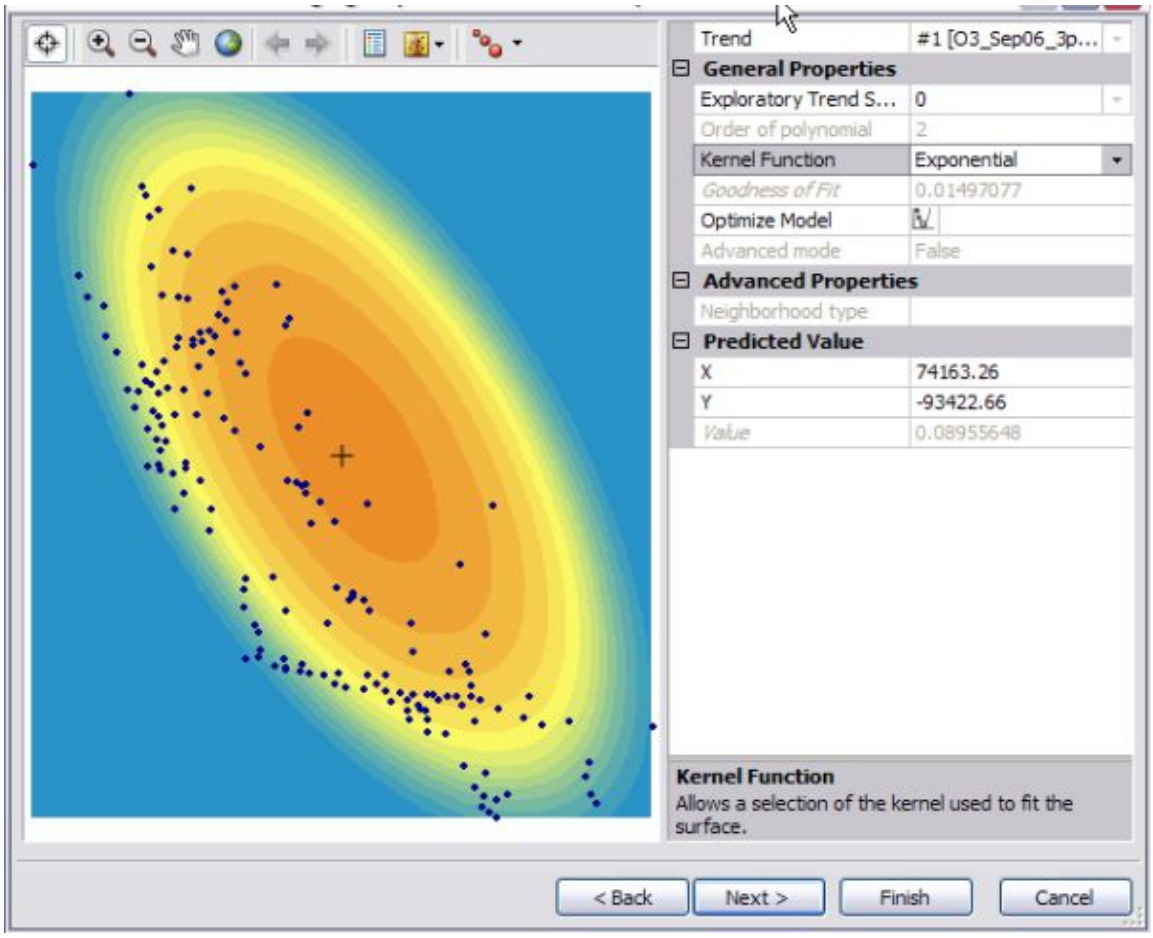

Further, a suitable active lag distance of the quantitatively iteratively quantitatively, explanatorily interpolated, uncoalesced, unbiased, proxy biosignature, explicative, sub-mixel estimators may be optimally deduced. In so doing, a relatively stable and better-fitting theoretical semivariance without a priori knowledge may be rendered in Geostatistical wizard ^{TM}. Spatial outliers in a moderate resolution, optimally derived, sub-mixel, trailing vegetation,

discontinuous, infrequently canopied, sparsely shaded, seasonally hyperproductive, eco-georeferenceable, eco-epidemiological, capture point, geo-spectrotemporally uncoalesced, turbid water, optimizable *S. damnosum* s.l. estimators often make the semivariogram exhibit erratic behavior [22]. Ordinary Kriging layer inGeostatistical wizard ™ can also create a geo-prediction standard error map (Figure 11).

Figure 11 Geo-spectrotemporally forecasted *S. damnosum* s.l. capture point, immature habitat semivariogram/covariance probabilistic error model dialog in Geostatistical wizard

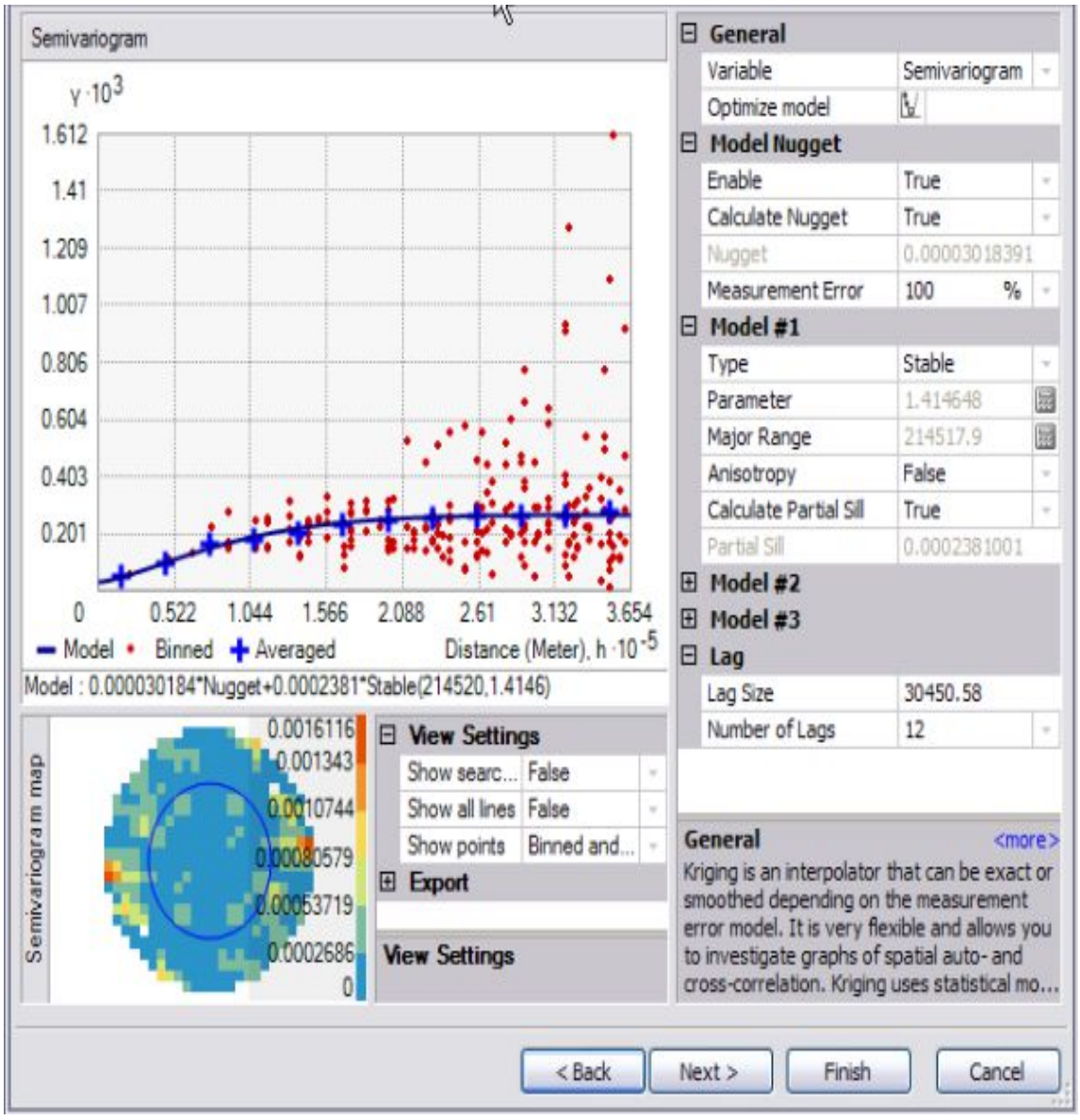

Whilest multispectral sensing has largely succeeded at elucidatively geo-classifying whole geo-spectrotemporally uncoalesced, sub-mixel, fractionalized moderate resolution,

endmember eigenvectors, further residual, sub-mixel analysis of the constituent substances of an, eco-georefernceable, eco-epidemiological, explanative, trailing vegetation, discontinuous, infrequently canopied, sparsely shaded, seasonally hyperproductive, turbid water, capture point, geospatially geosampled in an narrow African, riverine tributary, agro-village complex may be limited by a relatively high number of sporadic, meterological measurements. One of the major causes of endmember probabilistic uncertainties when predicting climate fluctuations in moderate resolution, seasoanl, hyperproductive, capture point, *S. damnosum* s.l., eco-epidemiological, vulnerability models comes from non-quantitating carbon-cycle feedbacks, which roughly double physical feedbacks in narrow African, tributary, riverine environments. Most of this endmember, unquantitable eigenvector, probabilistic uncertainties may be a result of the multiple pathways and time scales at which theses ecosystems interact with the climate system. For example, Jacob et a. [22] found that the relationship between uncoalesced, moderate resolution [i.e., Rapid Eye ™ 5m visible and NIR] remotely sensed, leaf nitrogen and the carbon cycle was important to many infrequently, seasonally, sparsely shaded, discontinuously canopied, hyperproductive, explanative, eco-georefernceable, capture point, trailing vegetated, turbid water, geo-spectrotemporally geosampled, *S. damnosum* s.l., capture point, immature habitat, sub-mixel, decompositional, algorithmic processes as canopy photosynthesis provides the energy and carbon-cycle molecules for growth, reproduction and decomposition for nutrient cycling. Ecologists have long recognized that nitrogen is the most limited nutrient for plant growth in remote sensensed models [25].

Qualitatively, explicatively, quantitating, discontinuous canopy, nitrogen content in an expositively fractionalizable, moderate resolution, fractionalized, endmember, eigenvector, autoregressive, forecasting, vulnerability paradigm may provide direct information about, precisely geospatializing, seasonally explanative, eco-georeferenceable, geo-spectrotemporal, uncoalescable, narrow, riverine tributary, African, agro-village, eco-epidemiological, prolific, capture point,trailing vegetation, turbid water, sparsely shaded, *S. damnosum* s.l. immature, habitat, elucidative, endmember regressors. In so doing, a method may be optimally devised in ArcGIS to efficiently detect and monitor explanatorial, geoclassifiable, LULC changes in response to climate forcing. Further, significant literary contributions of these entomological, vector arthropod, entomological, eco-epidemiological, immature, habitat models and their productive count, capture point, suitability, may be quantitated in response to moderate resolution, airborne and spaceborne imaging spectroscopy.

Several ArcGIS contributions have reported direct detection of canopy nitrogen from airborne imaging spectrometers. For example, Ollinger (2011) argues that selective pressure on plant competition for light, water, and nutrients should result in suites of explanatorial, biochemical and structural traits that integrate their functional strategies. Thus, quantitatively, orthogonally decomposable, expositively fractionalized, moderate resolution, fractionalized, endmember, eigenvector, structural traits affecting light scattering “over scales ranging from cells to canopies” in an eluidative, eco-georeferenceable, seasonally hyperproductive, trailing vegetation, turbid water, sparsely shaded, discontinuously canopied, eco-epidemiological, *S. damnosum* s.l., immature habitat, capture point, geo-spectrotemporally geosampled in a narrow, African, riverine tributary, agro-village complex, will be convergent with its biochemical traits. Hence, explicitly testing whether regression endmember assumptions exist in an explanative, seasonally eco-georeferenceable, hyperproductive, capture point, immature habitat’s, discontinuous, unmixed, geo-spatialized, non-homogenous, canopy structure cannot be be ignored when eigenvector, forecast,

vulnerability mapping employing moderate resolution, orthogonally decomposeable data. These paradigms may neccessiate qualitatively quantifying sub-mixel, biochemical compositions with a detailed residualizable, fractional radiance, endmember eigenvector, frequency-oriented, wavelength, transmittance, emissivity analysis of the geo-biophysical, geo-spectrotemporal, eco-georeferenceable processes of photon scattering from leaves and plant canopies in ArcGIS.

The effects of changes in temperature, CO_2, light intensity and nitrogen nutrition on photosynthesis, in an heuristically optimizable eco-epidemiological dataset of seasonally geo-spectrotemporally uncoalescable, geospatially geosampled, eco-georeferenceable, explanative, seasonally hyperproductive, capture point, trailing vegetation, turbid water, elucidative,optimally parameterizable, moderate resolution, *S.damnosum* s.l., immature habitat, moderate resolution, endmember, reflectance wavelength, transmittance, frequency-oriented, moderate resolution, emissivity, covariate, coefficients may be based in ArcGIS experiments involving gas exchange and fluorescence techniques on discontinuous canopy plants grown at different climate and nitrogen nutrient conditions. Short-term irradiance responses of photosynthesis and long-term acclimation to CO_2 and temperature may be ecohydrologically, efficiently examined in an unmixed eco-georeferenceable, eco-epidemiological datasets of illuminatively, geo-spectrotemporally uncoalesced, discontinuously canopied, expositively fractionalized, synthetic, orthogonal, endmember, time series, eco-cartographic, spatial filter eigenvectors in ArcGIS. Scaling up from the leaf to the geospatialized canopy level may be optimally simulated, thereafter, in ArcGIS employing the sun-shade and big-leaf model employing an iteratively, quantiative, interpolative algorithm in Geospatial Analyst ^{TM} for parsimoniously tabulating, seasonal, diurnal, canopy, assimilation rates employing parameters from the single leaf light and CO_2 responses from an eco-georefernceable, explanative, capture point, immature, narrow, riverine agro-village tributary habitat.

Sun-shade models in ArcGIS have proved to be simple, fast and reliable tools for estimating eco-hydrologic fractions of absorbed PAR (fAPAR) and the photosynthesis of low and simple canopies (e.g. seasonally eco-georeferenceable, explanative, hyperproductive, eco-epidemiolgical, capture point, trailing vegetation, turbid water, elucidatively parameterizable, *S.damnosum* s.l., immature habitat). Photosynthetically active radiation, often abbreviated PAR, designates the spectral range (waveband) of solar radiation from 400 to 700 nanometers that photosynthetic organisms are able to use in the process of photosynthesis [25].The fraction of incident PAR absorbed by the canopy (fAPAR) is central for eco-physiology: it drives most soil–vegetation–atmosphere transfer (SVAT) models and allows interpretation and gap-filling of eddy-covariance measurements of gross primary productivity at the scale of the ecosystem. The eddy covariance (also known as eddy correlation and eddy flux) technique is a key atmospheric measurement technique to measure and calculate vertical turbulent fluxes within atmospheric boundary layers [25].

fAPAR of a seasonal hyperproductive, ec-georeferenceable, eco-epidemiological, African, agro-village complex, narrow, riverine tributary, capture point, also be optimally estimated by uncoalesced, moderate resolution, remote sensing visible and NIR data in ArcGIS in order to run regional, trailing vegetation, discontinuously canopied, turbid water, eco-georefernceable, eco-epidemiological, simulation, risk models of net primary productivity. The fAPAR depends on the canopy structure, vegetation element optical properties, atmospheric conditions, and angular configuration [25]. To overcome this latter dependency, a daily integrated FAPAR value may be assessed for a eco-georeferenceable,

trailing vegetation, turbid water, discontinuous, infrequently, sparsely shaded, canopied, *S. damnosum* s.l., immature , capture point, hyperproductive, narrow, African, riverine , tributary, agro-villag ecosystem campled, seasonal habitat Applications on canopies, or non-ideal canopies (e.g. azimuthal heterogeneity, clumping, non-spherical leaf angle distribution, large proportion of non-green elements) for these immature habitats have been limited so far in ArcGIS literature.

In recent years it has been shown that models for the tropospheric delays based on data from numerical weather models in ArcGIS improve the accuracy of station coordinates derived from differntially corrected DGPS analysis on a global as well as a regional scale. However, there is no recommendation in terms of azimuthal asymmetries, as far as tropospheric (hydrostatic and wet) gradients are concerned for mapping seasonally hyperproductive, eco-georeferenceable, trailing vegetation, turbid water, discontinuous, infrequently, sparsely shaded, canopied, *S. damnosum* s.l., immature , capture points employing moderate resolution data. As such, it may be interesting to remotely investigate the non-homogeneous behaviour in azimuth for slant tropospheric delays in order to enhance the gradient models for precision seasonal DGPS processing, for hyperendemic, narrow, African, riverine tributary, agro-village ecosystems. This is a region where DGPS measurements are under influence of exterme meteorological measuremnts (e.g., riverine flooding, droughts).

The GIPSY software may be used to treat observations with the precise-point-positioning (PPP) procedure and the GAMIT software which applied in a classical way for comparison. In so doing, Complex eco-georeferenceable, trailing vegetation, turbid water, discontinuous, infrequently, sparsely shaded, canopied, *S. damnosum* s.l., immature habitat, capture point, geo-spectrotemporally, geospatially weighted, uncoalesced, moderate resolution, wavelength, transmittance, frequency-oriented, emissivity models may qualitatively quantitate geometric effects of dry and wet troposphere mapping functions (GPT, GMF, VMF, Niell). The final goal and perspective would be to assess current methods for *S. damnosum* s.l. capture point, forecast, endmember, vulnerability modeling and to eventually propose a new tropospheric model to better take into account the azimuthal tropospheric heterogeneity in hyperendemic, narrow, African, riverine tributary, agro-village ecosystems.

Moderate resolution reterived, discontinuous, canopy gap fractions for a seasonal hyperproductive, ec-georeferenceable, eco-epidemiological, African, agro-village complex, capture point, *S. damnosum* s.l., immature habitat may present a stronger upslope/downslope asymmetry if retrieved from levelled narrow, riverine tributary, seasonal acquisitions. As a result, gap dispersion index and clumping index may be proved to be significantly higher for levelled acquisition ($P < 0.001$). Immature *Similium* productivity count estimates adjusted to horizontal, narrow, riverine tributary may be significantly different, when retrieved from levelled or tilted acquisitions, up to 30% slopes, for example. From levelled tributary acquisitions, fixed and variable riverine agro-village, path lengths may not yield significantly different LAI estimates along the whole slope gradient. From tilted LULC, riverine acquisitions, immature, count values may be noteably greater than from levelled acquisitions. The stronger the slope, the higher the difference may be in seasonal hyperproductive habitats immature counts. Mean leaf angles do not differ significantly ($P > 0.05$) for fixed vs. variable path lengths along the slope gradient up to 33.3% when quantiating eco-georeferenceable, trailing vegetation, turbid water, discontinuous, infrequently canopied, *S. damnosum* s.l. immature, capture point, seasonal habitat slope-related 3-D coefficients.

For more severe seasonal Africa, riverine, tributary, pre-flooded and flooded meandering LULC slopes, variable path lengths may yield lower mean leaf angle values which may be then geo-spectrotemporally, geospatially associated with immature, *S. damnosum* s.l., seasonal, habitat density, count values. The interpretation of results from tilted LULC acquisitions remains uncertain for geospectrotemporally geosampledingAfrican, agro-village complex, ecosystem, narrow tributary, trailing vegation, discontinuously canopied, turbid water, infrequently shaded, eco-epidemiological, capture point, eco-georeferenceable, immature habitats. As a preliminary study, no preference is suggested for the levelled or tilted acquisition technique. Further investigation is needed and indirect moderate resolution, geometrically, optically, derived, regression estimates should be checked against direct reference measures, in these study sites especially in geoclassifiable LULCs where mountainous areas exist.

The gap fractions of the whole cover, fraction of intercepted PAR (fIPAR), clumping index and leaf orientation have been commonly derived from LAI-2000 (PCA) in literature, which have closely matched the simulations of a reference 3-D architectural model (ArcGIS 3D model) which have been subsequently used for cross-validation purposes. Discontinuous, infrequently, sparsely shaded, seasonal canopied, leaf area mesurements can be parsimoniously obtained directly through litter collection, allometric relationships or direct harvest of vegetation geoclassified LULCs [25]. To overcome fractionalized radiance endmber eigenvector, iterative interpolation difficulties, indirect geometrical, geospectrotemporal, geospatial, optical methods have been employed such as tracing radiation and architecture of canopies (TRAC), LAI-2000 Plant Canopy Analyzer (LI-COR, Lincoln, NE) and hemispherical photography for discontinuous canopy, LULC estimation due to their fast and non-destructive nature. Most of these methods are based on gap fraction and gap size distribution theory. Despite the fact that several methods have been developed so far to quantify leaf area indices, the discontinuous canopy geoclassifications remains difficult to estimate accurately, owing to large spatial–temporal foliage dynamics and quantiatable, canopied vegetation architectural heterogeneity in eco-georeferenceable, eco-epidemiological, trailing vegetation, infrequently shaded, capture point, immature *S. damnosum* s.l. turbid water, African, narrow tributary, complex ecosystem, seasonal, geosamplable habitats.

A moderate resolution, 3-digital elevation model (DEM) in ArcGIS may however, qualitatively quantitate a relationship for down-scaling the gap-fractions from the whole cover to green elements of a. seasonally eco-georeferenceable, eco-epidemiolgical, capture point, trailing vegetation, turbid water, elucidatively parameterizable, explanatively hyperproductive, *S.damnosum* s.l., immature habitat, geo-spectrotemporally geosampled in a narrow, riverine tributary in an African, agro-village, eco-georeferenceable complex. The derived sun-shade simulations of fAPAR by trailing vegetation, diffuse, green leaves may agree within 5% of a 3-D DEM, targeted eco-epidemiological capture point, immature, habitat, uncoalesced, moderate resolution, weighted, wavelength, frequency-oriented, explanative, transmittance based on a half-hourly time-step for 1 year, confirming combined PCA and sun-shade methods as a fast and reliable tool, even for tall or complex *Similium* habitat canopies. fIPAR and plant area index (PAI) may be compared in ArcGIS with an empirical regressable model for heuristically optimally estimating fIPAR from age and canopy plant density. The coefficient of extinction, K, may be adjusted for the regular range of plant density in ArcGIS.More complex explanative, eco-georferenceable, 3-D DEM

model, *S.damsnoum* s.l., capture point, immature habita,t reflectance and transmittance detailing descriptions of the discontinuous,immature habitat, sparsely shaded canopies may be able to test hypotheses (e.g. the sensitivity analysis of different ecological co-factors affecting disocntinuous canopy radiation transfer to validate simpler models).

Three dimensional ArcGIS-derived, African, agro-village complex, ecosystem, narrow tributary, trailing vegation, discontinuously canopied, turbid water, infrequently shaded, eco-epidemiological, capture point, eco-georeferenceable, immature, habitats models in ArcGIS trace light rays may calculate their interception by the foliage after eco-geographical, weather and plant architecture information is entered into the model . These models may predict the light intercepted by each habitat canopy leaf. The model estimates may require high parameterization which may be suitable for quantiating slope coefficient of individual single branches or small canopies only. Other models assume that radiation attenuation through canopies can be described by Beer's Law and predict the irradiance at different depths in the *S. damnosum* s.l. discontinuous canopy. The Beer's Law Equation (Absorbance = e L c) when given the molar absorptivity constant (or molar extinction coefficient) where e is the molar extinction coefficient, L is the path length of the cell holder and c is the concentration of the solution [24].The latter models are suited for large canopies and assume the existence of homogeneous layers within the canopy with constant irradiance at equal cumulative leaf area indexes (LAI). Leaf area index (LAI) is a dimensionless quantity that characterizes plant canopies which defined as the one-sided green leaf area per unit ground surface area (LAI = leaf area / ground area, m^2 / m^2) in broadleaf canopies[25]. A 3-D DEM of eco-georeferenceable, trailing vegation, turbid water, *S. damnosum* s.l. leaf area of a hyperproductive, immature habitat, explanative, discontinuously canopied layer may be geo-spectrotemporally geometrically optically assessed in ArcGIS and subsequently multiplied by the estimated or measured irradiance of that layer, then summed for all layers. In this way, the light intercepted by each layer (e.g., light distribution in a preflooded/flooded, sparsely shaded, immature habitat) and the total canopy light interception and absorption can be modelled.

Unfortunately, since irradiance in a geo-spectrotemporally uncoalesced, geo-spatialized moderate resolution, seasonally explanative, hyperproductive, *S. damnosum* s.l., explanative habitat, capture point, immature habitat, discontinuous canopy layer is not homogeneous, remotely qualitatively quantiating canopy depth mesurements may be strenuous. Canopy water content vegetation indices in object based technology (e.g. ENVI) use reflectance measurements in the NIR and shortwave IR regions to take advantage of known absorption features of water and the penetration depth of light in the NIR region to make integrated measurements of total column water content. For example, the stress moisture index is a reflectance measurement in ENVI that is sensitive to increasing leaf water content. Applications for monitoring hyperproductive, *S.damnosum* s.l., immature habitat include canopy stress analysis, productivity prediction and studies of seasonal, eco-georeferenceable, African riverine tributary, agro-village complex, ecosystem physiology. The normalized difference vegetation index (NDVI) employs a normalized difference formulation instead of a simple ratio in ENVI, where the index values increased with increasing water content. Applications for optimally, geo-spectrotemporally uncoalescable, *S. damnosum* s.l., empirical, regressable datasets of geosampled, seasonal hyperproductive, immature habitat, eco-epidemiological, capture point data include infrequent canopy monitoring, and vegetation stress detection. Normalized Difference Water index (NDWI) may qualitatively quantitate canopy depth in a moderate resolution, imaged, hyperproductive, eco-epidemiological, eco-georeferenceable, capture point, trailing vegetation, discontinuously canopied, turbid water,

African narrow riverine tributary, agro-village complex, immature habitat. Applications include for canopy stress analysis, LAI studies in densely foliated vegetation and canopy plant productivity modeling. Finally there is the Normalized Multi-band Drought Index (NMDI). This index may take into account a soil moisture background in an eco-georefernceable, *S. damnosum* s.l. hyperproductive, seasonally explanative, immature, African agro-village complex,narrow riverine tributary, ecosystem habitat to monitor potential drought conditions. Three specific, moderate resolution, unmixed wavebands may be optimally selected to quantitate unique response wavelength, transmittance emssivity, frequency variations in soil and vegetation moisture. The index uses the difference between two liquid-water absorption bands in the shortwave-IR region (1640 and 2130 nm) as a measure of water sensitivity in vegetation and soil. This index is also commonly used in forest-fire detection

Selecting an appropriate canopy light absorption and photosynthesis model for the purposes of predictive, hyperproductive, *S. damnosum* s.l., immature habitat, endmember modeling and subsequent geo-spatialization may require optimally remotely deciphering a trade-off between accuracy and parsimony of parameterization of the geo-spectrotemporally uncoalesced, fAPAR models. These models may be also optimally geoclassified in ArcGIS into (i)‘‘reference’’ models, such as Multi-layer discrete 2D and 3D models or else ‘‘simplified models’’, such as single-layer Big-leaf models or sun-shade models (e.g., single-layer with two leaves). It is generally assumed that reference Multi-layer and 3D models are accurate but require a number of calculations, which becomes a drawback for their inclusion into eco-epidemiological, Global Circulation, eco-georeferenceable, *S. damnosum* s.l. remotely sensed, eco-epidemiological, forecast, vulnerability paradigm, covariance matrices and SVAT models. Regardless, these models may be inherently the most promising for solving recurrent theoretical problems affecting non-ideal,non-optimizable, *S. damnosum* s.l., hyperproductive, seasonal canopies: [e.g. row structure with large gaps, azimuthal heterogeneity, complex leaf angle distribution function (LADf), distinction between green and non-green elements or aggregation (clumping) at different scales]. However, due to their complexity in eco-cartographically optimally delineating an accurate number of heuristically geo-spectrotemporally parameterizable, explanatively, geo-spatializable, covariate coefficients for uncoalesced, 3D models only a few unbiased iterative estimators and canopy plant species, have been optimally quantitatively iteratively interpolated in the literature. ArcGIS, seasonal, capture point 3D models may offer an outstanding reference for testing the performances or for validating simplified models to be applied in non-ideal conditions,

Further, the canopy extinction coefficient for light and nitrogen, canopy nitrogen concentration, daily solar irradiance and daily maximum and minimum temperatures may be optimally tabulated employing fractionalized, moderate resolution, remotely sensed, data uncoalesced, wavelength, transmittance, frequency-oriented emmissivities. Light interception is commonly measured with expensive equipment or estimated with elaborate models; simpler and more economical ways of estimation would be advantageous [25]. Since leaf mass per unit leaf area (MA) is closely related to long-term light interception by leaves in a explanative, eco-epidemiological, sparsely shaded, trailing vegetation, discontinuously canopied, seasonally hyperproductive, *S. damnosum* s.l. immature habitat, eco-georeferenceable, capture point the latter can be estimated by measuring MA in ArcGIS. In, RosatiI et al. (2001) a partitioning of leaf area into one of six classes of MA was used to estimate canopy light interception and absorption in aubergine (*Solanum melongena* L.) grown with different amounts of nitrogen fertilizer and with or without artificial shade using

moderate resolution data. Although plants grown with ample fertilizer had a greater LAI than those grown with less nitrogen, the increase in leaf area occurred in the lower and intermediate MA classes, while the leaf area in the two highest MA classes was similar. Artificially shaded plants had more leaf area in the lower MA classes and less in the higher classes compared to explanative, unshaded plants, showing acclimation to low light conditions. The amount of light intercepted daily by leaves in each MA class was estimated in ArcGIS employing the previously determined light variables. Canopy light interception was optimally calculated as the sum of intercepted light for all MA classes, and canopy light absorption was estimated from light interception data assuming a constant absorption coefficient (82 %). To validate the results, the estimated values were compared to those calculated from independent measurements of light absorption carried out in the same field. Results indicate that it is possible to estimate canopy light interception and absorption from the partitioning of sparsely shaded leaf area into MA classes. In so doing, for an uncoalesced MA model constructed from a dataset of ArcGIS geo-spectrotemporal, geospatialized, explanative dataset of sub-mixel, Rapid Eye ^{TM} 5m, elucidative wavelength, trasnmittance, frequency-oriented, emissivity regressors, the significance of diffuse radiation, discontinuously canopied, parameterizable, assimilation rates may be efficiently qualitatively quantized.

The Farquhar biochemical growth model (Farquhar et al., 1980) calculates photosynthesis as a function of demand and supply of CO_2. The advantage with this model for robustly, parsimoniously quantitating, elucidatively optimally parameterizable, iteratively, interpolative, eco-georeferenceable, geospectrotemporally, uncoalescable, geospatially seasonally hyperproductive, eco-epidemiological, narrow, riverine tributary, agro-village complex, capture point,trailing vegetation,turbid water, sparsely shaded, discontinuously canopied, *S. damnosum* s.l., immature, habitat, moderate resolution, expositively fractionalized, endmember eigenvectors is that photosynthesis is regulated not only by radiation and transpiration, but also by air humidity, leaf temperature, CO_2 availability and leaf nitrogen content. The immature habitat, canopy plants also may experience radiation saturation at high levels of radiation. To function properly, driving variables need to be given as input to the simulation at least once an hour [23].

Various aspects of the biochemistry of photosynthetic carbon assimilation in C_3 canopy plants in an, uncoalesced, endmember eigenvector eco-epidemiological, *S. damnosum* s.l., capture point, moderate resolution, geosampled wavelength, transmittance frequency-oreinted, endmember eigenvector, forecast, vulnerability model may be integrated to form compatible, uncoalesced, time series explanators of gas exchange in discontinuous, immature habitat, canopy leaves. These aspects include the kinetic properties of ribulose bisphosphate carboxylase-oxygenase; the requirements of the photosynthetic carbon reduction and photorespiratory carbon oxidation cycles for reduced pyridine nucleotides; the dependence of electron transport on photon flux and the presence of a temperature dependent upper limit to electron transport. The measurements of gas exchange with which the model outputs may be thereafter compared include temperature and partial pressure of CO_2($p(CO_2)$) dependencies of quantum yield, the variation of compensation point with temperature and partial pressure of O_2($p(O_2)$), the dependence of net CO_2 assimilation rate on $p(CO_2)$ and irradiance, and the influence of $p(CO_2)$ and irradiance on the temperature dependence of a geo-spectrotemporally, geospatialized, qualitaively quantized, seasonal, *S. damnosum* s.l.,discontinuous canopy, assimilation rate. Canopy photosynthesis, *P* in an ArcGIS moderate resolution, geo-spectrotemporally uncoalescable, explantive, field-operationizable, *S. damnosum* s.l., immature, habitat, geospatialized, weighted, wavelength, transmittance,

frequency-oriented, emissivity, fractionalized, endmember eigenvector, forecast, vulnerability model may be calculated as mole carbon per leaf area per second. In the model covariance matrix P has to be converted to g carbon per unit, LULC area per day, $C_{Atm \rightarrow a}$, at the end of the module: $C_{atm \rightarrow a} = M_C \cdot 86400 \cdot P$ where M_C is the molar mass of carbon.

Farquhar's photosynthesis model is only geo-spectrotemporally, geospatially applicable to individual, discontinuous canopy immature, habitat leaves instantaneously in ArcGIS when qualitatively quantitating regional plant growth and carbon/nitrogen budget estimations associated to forecasted, black fly, larval/pupal productivity. For example, in Jacob et al. [22], Farquhar's equations were applied directly to an explanative, eco-georeferenceable, eco-epidemiological, hyperproductive, trailing vegetation, Precambrain rock, *S. damnosum* s.l., sub-meter resolution, imaged, sparsely shaded, immature habitat, discontinuous canopy by assuming the quantitated canopy functions like a big-leaf. *S. damnosum* breeds mainly in fast flowing, well-oxygenated, riverine bodies where the African Precambrian basement rock is exposed to break the flow of water and create rapids[22]. This big-leaf approximation was found to be acceptable for estimating seasonal trends of discontinuous canopy photosynthesis of the ecogeoreferenced capture point but inadequate for simulating day-to-day variations in the immature habitat canopy. The daily variation is greatly dampened in big-leaf simulations as the original leaf-level model is partially modified through replacing stomatal conductance with canopy conductance [23]. Jacob et al. [22] separated the discontinuous, sparsely shaded, turbid water, narrow African, agro-village riverine tributary,. Discontinuous, habitat canopy into sunlit and shaded leaf groups and then stratified the canopy into multiple layers in ArcGIS.

Because of non-linear response of leaf photosynthesis to meteorological variables (e.g., radiation, temperature and humidity), considerable errors may exist in photosynthesis calculations employing geo-spectrotemporally uncoalesced, moderate resolution, fractionalized images of seasonally hyperproductive, eco-epidemiological, capture point, endemic, narrow, African, agro-village complex, riverine foci, without considering the diurnal variability of the variables. To avoid these non-linear effects, an analytical solution to a simplified daily integral of Farquhar's model may be considered for quantiating the general diurnal patterns of quantitable, moderate resolution, meteorological variables in an eco-egeorferenceable, explanative dataset of trailing vegetation, discontinuously canopied, *S. damnosum* s.l. hyperproductive, eco-epidemiological, sparsely shaded, capture point, immature habitat. Ecological parameters such as water temperature, water pH, dissolved oxygen, ammonia content, rainfall, current velocity, relative humidity and conductivity influence the breeding of *S. damnosum* complex [13]. Ecological factors which influence the adults include wind, humidity and light[7]. This daily model would not only capture the main effects of the diurnal variations on the black fly, discontinuous habitat, canopy photosynthesis in an ArcGIS cyberenvironment but would also computationally be efficient for optimally, qualitatively quantitating, large, explanatively, geo-classifiable elucidative, LULC area applications (e.g., heuristically, iteratively ,explanatively, iteratively interpolated datasets of non-coalesced, moderate resolution, geo-spectrotemporally geospatialized, *S. damnosum* s.l., seasonally hyperproductive, capture points). The model's application would then be not restricted by availability of sub-daily meteorological data.

Currently, there is a pressing need to accelerate progress in understanding how terrestrial ecohydrologic, and hydrometeorological systems respond to climate forcings for precisely quantitating moderate resolution, expositively geo-classifiable, discontinuously

canopied, trailing vegation, eco-georeferenceable, explanatively uncoalesced, seasonal, *S. damnosum* s.l., topographic and non-topographic, geoclassifiable LULC signatures. Eco-georefernceable, seasonal, pre-flooded, narrow, riverine, agro-village tributary, meanderings may be encompassed in moderate resolution, *S. damnosum* s.l., eco-epidemiological model's contributions which may aid in moving ArcGIS towards the development of intuitive, integrated, explanatorial, surface-atmosphere, prediction systems. These new forecasting systems may geospatially represent coupled ecohydrological, biogeochemical, and atmospheric processes from bedrock in discontinuously canopied, pre-flooded African, narrow, riverine tributary, agro-village ecosystems through the lower atmosphere employing advanced ArcGIS, computational, algorithmic frameworks. For example, prediction regression-based, signature architectures may be developed in Geostatistical Analyst ™ to conduct fundamental research on broad, vector, larval control systems [e.g. moderate resolution risk maps of seasonally, prolific,immature habitats based on iteratively geo-spectrotemporally iteratively interpolated, uncoalesced, Chlorophyll (Chl) variables] by improving predictive capacity of eco-epidemiological, *S. damnosum* s.l., forecast, vulnerability eco-georeferenceable models. In so doing, ArcGIS simulations may allow ecologists, entomologists or other researchers to optimally, quantitate a priori representing the most suitable, routine for rendering, elucidative, bio-geophysical observational, eco-epidemiological observational predictors of a given, moderate resolution, seasonally hyperproductive, trailing vegetation, discontinuously canopied, turbid water, capture point geosampled in an hyperendemic, African, agro-village, narrow riverine, agro-village, tributary ecosystem regardless of seasonal, sample frame, climatic conditions.

Further, geoprocessing tools in the 3D Analyst extension in ArcGIS Pro may simulate the effect of various kinds of explicative, seasonal, larval control processes, employing empirically probabilistically regressable, uncoalescable, data variables (e.g., slope and elevation 3-D coefficients) of unknown, un-geosampled, eco-georeferenceable, turbid water, sparsely shaded, capture point, *S. damnosum* s.l., seasonally hyperproductive,moderate resolution, imaged, immature habitats by iteratively quantitatively, explanatively interpolating the orthogonally decomposed, trailing vegation, turbid water, discontinuously canopied, capture point, proxy signature, fractionalized, endmember eigenvectors. In so doing, the sub-mixel variables would eco-cartographically, optimally delineate, seasonally explanative, *Simulium* vector abundance and distribution at an, eco-georferenceable, African, agro-village, narrow riverine, tributary, eco-epidemiological, study site. Recognition of the model complexities of *S. damnosum* s.l., endemic, meandering, riverine, foci, covariate coefficient, interaction terms in pre-flooded riverine pathway meandering explanators and their autoregressively quantitatable interdependencies may be significantly pertinent to implementing larval control strategies in these riverine ecosystems.

ArcGIS Predictive Analysis Add-In tools may be optimally employed to construct decomposable, fractionalized, moderate resolution, emissivity-oriented, geo-spectrotemporally uncoalesced, endmember, wavelength, transmittance, eigenvectors in forecast-oriented, vulnerability paridigms. In so doing, eco-geographic, robustifiable, explanative, observational, eco-georefernecable predictors delineating optimal eco-hydrologic, elucidative geolocations of seasonally transitioning, partially canopied, sparsely shaded, hyperproductive, narrow, tributary-oriented, agro-village complex, seasonal, remotely sensed, *Similium* habitat, geo-spectrotemporal, moderate resolution targets may be devised using iteratively, quantitatively interpolative, uncoalesced, proxy biosignature [Normalized Difference Vegtation Indices (NDVI)] variables may be illuminated. Once these models are constructed, Query Builder (available in the Query Analysis Add-In), can then

save and load queries for adjusting fractionalized, moderate resolution, endmember eigenvectors of eco-georeferenceable, narrow, riverine tributary, African, agro-village complex, immature habitat, proxy signatures in space in Geospatial Analyst™ .By employing an empirically regressed,heuristically optimizable, eco-epidemiological dataset of parameterizable, field-operatizable, moderate resolution, uncoalesced, covariate, coefficient, weighted, wavelength, transmittance, frequency-related, emissivity estimators rendered from an interpretively, iterative, quantitative interpolator (e.g., co-kriging algorithm) distinct mathematical forecasts may be generated from stochastic models based on spatial variation of the geosampled data. In so doing, a group of single-band explanatorial rasters may reveal eco-cartographically explanatively illustratable, seasonally prolific, eco-hydrologic, eco-georeferenceable, explanative, capture point, immature habitat, clustering tendencies in the uncoalesced, empirical dataset of discontinuously canopied, trailing vegetation, sparsely shaded, *S. damnosum* s.l. habitat, hyperproductive, turbid water, narrow, riverine tributary, agro-village geolocations in hypothetical, eco-geographic and non-eco-geographic, regression space. The elucidatively regressed forecasts rendered from the iterative interpolator may be subsequently overlaid onto a Google Earth ™ map in ArcMap ™ to geolocate unknown, un-geosampled, hyperproductive, capture point. seasonal, immature habitats.

Geometrical optical (GO) modelling in ArcGIS applies to discontinuous canopies with distinct architecture and is particularly appropriate for forest canopies [25]. Although sophisticated, 3- D, radiative transfer models have been developed inliterature, GO models remain an alternative attractive tool for remote sensing applications for their ability to capture the angular and spatial variabilities of moderate resolution, endmember eigenvector reflectances employing simple geometries defined by canopy architecture in ArcGIS. Geometrical optics, or ray optics, describes light propagation in terms of rays[24]. The ray in geometric optics is an abstraction, or instrument, useful in approximating the paths along which light propagates in certain classes of ArcGIS algorthms(www.esri.com) which may iteratively, quantitate, unbiased data for identifying unknown, un-geosampled discontinuously canopied interpolated, geo-spatialized, seasonally hyperproductive, *S. damnsoum* s.l. trailing vegetation, turbid water, sparsely shaded, immature, eco-georefernceable, eco-epidemiological, capture point, narrow, African riverine, tributary, agro-village complex, immature habitats. The simplifying assumptions of geometrical optics include that light rays:1) propagate in rectilinear paths as they travel in a homogeneous medium,2)bend, or split in two, at the interface between two dissimilar media,3) follow curved paths in a medium in which the refractive index LULC changes;and, 4) may be absorbed or reflected [24].

Geometrical optics does not account for certain optical effects such as diffraction and interference. Nonetheless these illuminative measurements may be useful in optimally forecasting, datasets of heursitically robustifiable, eco-georeferenceable , seasonal, capture point, *S, damnsoum* s.l. fractionalized, vulnerability model, moderate resolution,orthogonally decomposed, uncoalesced, endmember, date feature, attributes. The unbiased productivity residuals from these models may be an excellent approximation when moderate resolution, wavelength frequencies of the ecogeoreferenceable, immature habitat, capture point, is especially small compared to the size of the uncoalesced, explanative, discontinuous canopied, phosynthetic biochemical structures with which the light interacts (e.g., leaf canopy stomata). The techniques may also be particularly useful in optimally describing geometrical aspects of moderate resolution imaged, trailing vegetation, fractionalized, sparsely shaded, orthogonalized, endmember eigenvectors, including their optical aberrations.

In the case where a geoclassifiable moderate resolution, vegetation LULC cover can be regarded as a collection of individual, discrete plant crowns, the geometric-optical effects of the shadows that the crowns cast on the background and on one another strongly condition the brightness of the vegetation cover as seen from a given viewpoint in the hemisphere[24]. An asymmetric hotspot, in which the shape of the hotspot is related to the shape of the plant crowns in the scene, (www.esri.com). At large zenith angles illumination shadows may preferentially shadow the lower portions of adjacent discontinuous, eco-georeferenceable, canopy gaps when iteratively interpolating a hyperproductive, seasonal, trailing vegation, turbid water, discontinuous canopied, sparsely shaded, narrow tributary, African agro-village complex, *S. damnosum* s.l., uncoalesced, capture point, proxy LULC signature.

Further, these shadows may be preferentially obscured since adjacent crowns may also tend to obscure the lower portions of other crowns in the habitat canopy. This effect would render a `bowl-shaped' bidirectional reflectance distribution function (BRDF) in which 5m scene brightness may increase at the function's edges. The bidirectional reflectance distribution function (BRDF; $f_{\mathrm{r}}(\omega_{\mathrm{i}}, \omega_{\mathrm{r}})$) is a quantitatble function in an ArcGIS cybetrenvironment of four reflectance variables that defines how light is reflected at an opaque surface. The BRDF is employable both in the optics of real-world light, in computer graphics algorithms, and in computer vision algorithms. The function takes an incoming light direction, ω_{i}, and outgoing direction, ω_{r}(taken in a coordinate system where the surface normal $\mathbf{n}$ lies along the *z*-axis), and returns the ratio of reflected radiance exiting along $\omega_{\mathrm{r}}$to the irradiance incident on the surface from direction ω_{i}. Each direction $\omega$is itself parameterized by azimuth angle $\phi$and zenith angle θ, therefore the BRDF as a whole is a function of 4 variables. The BRDF has units sr^{-1}, with steradians (sr) being a unit of solid angle.

Differential Formulas describing the hotspot and mutual-shadowing effects of the narrow, riverine tributary, capture point may then be optimally derived using ArcGIS which may show how the shape of the BRDF is dependent on the shape of the discontinuous *S. damnosum* s.l. geospatiotemrpoally uncoalesced, iteratively interpolative, discontinuous canopy paramter, their density, their brightness relative to the background, and the thickness of the layer throughout which the crown centers is distributed

An analytical method is described for predicting the bistatic normalized radar cross section of a rough homogeneous layer made up of a rough surface over a flat surface. The model is based on iteration of the Kirchhoff approximation to calculate the fields scattered by the rough layer, and is reduced to the highfrequency limit in order to obtain numerical results rapidly. Kirchhoff's diffraction formula (also Fresnel–Kirchhoff diffraction formula) can be used to model the propagation of light in a wide range of configurations, either analytically or using numerical modelling [25]. The shadowing effect, significant for larger incidence or scattering angles, is taken into account through the use of shadowing functions. The model is applicable for moderate to large upper surface roughnesses having small to moderate slopes, and for both lossless and lossy inner media. It was validated for a two-dimensional problem (with 1D surfaces) in a preceding contribution. Here, the extension of the model to 2D surfaces is developed, and results are presented to validate the asymptotic model by comparison with a numericalreference method.

Geometrical optical (GO) models are generally accurate in the visible part of the solar spectrum, but less accurate in NIR part in which multiple scattering in plant canopies is the

strongest. As a mathematical study, geometrical optics emerges as a short-wavelength limit for solutions to hyperbolic partial differential equations [25].At NIR moderate resolution wavelengths, the contrast may be much reduced in a uncoalesced, geo-spectrotemporally discontinuously canopied, trailing vegation, sparsely shaded, *S. damnosum* s.l., immature habitat, explanatively hyperproductive, turbid water, capture point, eco-georeferenceable, forecast, endmember, vulnerability model because of the large scattering albedo of plant leaves. The Li-Strahler geometric-optical model exploits these shadowing effects by modeling a scene or mixel as an assemblage of ellipsoidal tree crowns. Geometric-optics and Boolean set theory are used todetermine the areal proportions of shadowed and sunlit canopy and shadowed and sunlit background associated with a solar zenith angle. Independent characteristic signatures for each component are weighted by these areal proportions and used to determine the spectral directional reflectance factor of the canopy at any viewing angle. Although these component signatures do not include an explicit treatment of diffuse irradiance, canopy multiple scattering or leaf specularity and are applied uniformly to the areal proportions, they are reasonable approximations for clear atmospheres and low to medium solar zenith angles. The geometric-optical model does incorporate the effects of mutual shadowing or the obscuring of tree crowns by one another and takes into account the impact bright unshadowed tree tips have on the canopy reflectance at very high view angles. By performing a hemispherical integration, the model also providesan instantaneous hemispherical reflectance (or spectral surface albedo).

Thus, the accuracy of GO modeling approach would deteriorate at NIR wavelengths. Critical to the accuracy would also be the simulation of the radiance exiting from the sparsely shaded, discontinuously fractionalized, sparsely canopied, endmember eigenvector, regressed components. The reflected radiance from the immature eco-georefernced, shaded habitat, decomposed components may not only be optimally determined by the first-order scattering which would separate the sunlit and shaded, sub-mixel eigenvector components, but also multiple scattering after the first collision of light with foliage or the background. A beam of light can undergo several orders of scattering before it is totally absorbed or reflected back to space Olivo and Speller previously used geometrical optics to model the coded aperture XPCi system. Their approach used a “forward” technique where photons emitted by the source were traced through the system. Photons could be blocked by an aperture, refracted by a sample or both. The number of photons reaching a particular pixel represent the signal detected by that pixel. Geometrical optics may be extended to include higher order terms which represent what is usually termed diffraction(www.esri.com). Geometrical optical (GO) models have been widely used in remote sensing, irregularly shaped, geospatial, object applications because of their simplicity and ability to simulate angular variation of remote sensing signals from the earth’s surface[see Figure 12].

Figure 12 Geometrical optical model describing light propagation in terms of multiscattered rays including optical aberrations from a discontinuous canopied, eco-georeferenceable geolocation

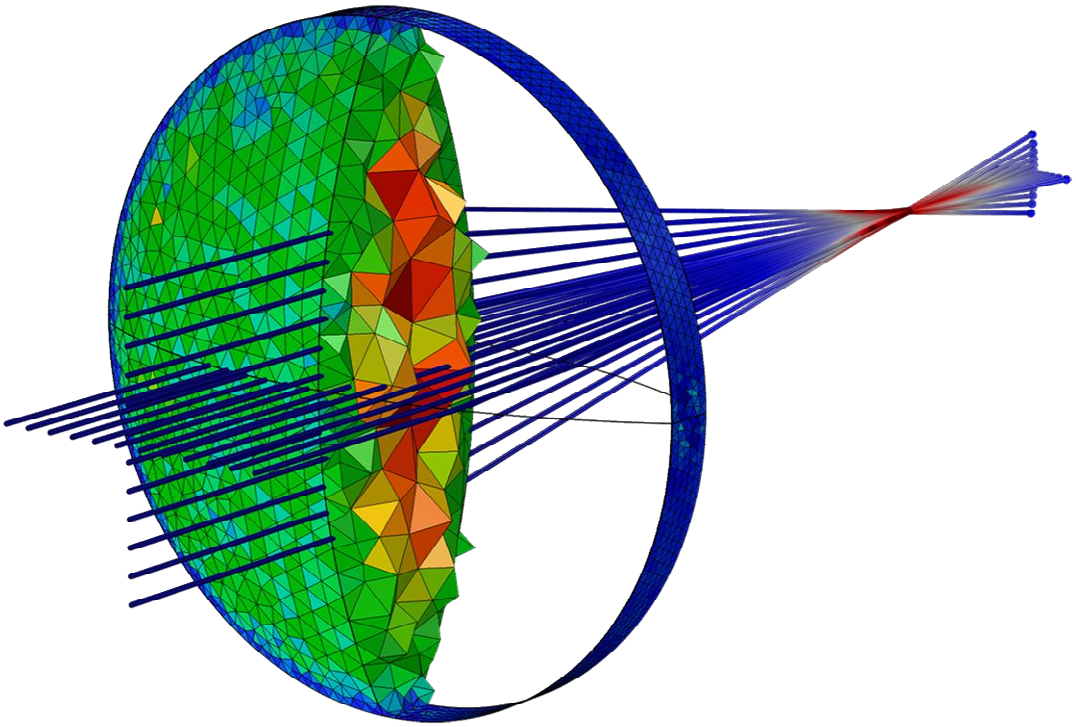

Multiple scattering simulation or approximation is therefore an indispensable part of iteratively quantitatively, explanatively interpolated, empirically regressable datasets of geo-spectrotemporally, geospatially uncoalesced, *S. damnosum* s.l. habitat, eco-epidemiological, capture point, forecasts, intended for identifying, seasonally hyperproductive unknown, ungeosampled narrow tributary, capture points in African, agro-village complex, immature habitat, eco-georeferenceable geolocations. Combinations of complex unmixing algorithms in ArcGIS such as those based on radiosity using iterative procedures and those based on ray tracing using discrete ordinates may theoretically simulate multiple-scattering, moderate resolution-derived, wavelength frequencies of *Similium* habitat canopies with high accuracy. However, the accuracy of a extracted proxy biosignature of the trailing vegation, sparsely shaded, discontinuous canopied, endmember architecture description. From moderate resolution data would strongly depend on the amount of details considered in the geoclassified ArcGIS-derived ,time series eco-georeferenceable, explantive, LULC map.

Regardless of the unmixing algorithms employed for expositorily fractionalizing an ecogeorferenceable, geo-spectrotemporal, explanative eco-epidemiological datasets of eco-georferenceable, seasonally hyperproductive, trailing vegetation, discontinuously canopied, eco-epidemiological, narrow, riverine tributary, turbid water, capture point, *S. damnosum* s.l., geospatial, endemic foci, a subtle problem may arise when non-differential, orthogonally decomposed sub-mixel, geoclassified uncoalesced, LULC, explanatorial, structural measurements of collinear variables are obtained in hypothetically simulated, regression space in ArcGIS. This situation is exponatentially more weighted in a Poissonian distribution with a conditional mean $y=\exp(\beta_{0+}\mathrm{Log}_{1x)}$ where x represents the ‘cause of y in the response

count. In probability theory and statistics, the Poisson distribution, is a discrete probability distribution that expresses the probability of a given number of events occurring in a fixed interval of time and/or space if these events occur with a known average rate and independently of the time since the last event. In Jacob et al. [22], the Poissonan distribution was used for determining the number of explanatorial capture point, eco-georeferenced, *S. damnosum* s.l., endemic, foci events using specified intervals such as uclideanized, habitat distance, area and volume measurements (see Figure 13).

Figure 13 Poisson regression where the dependent response variable is the count (0, 1, 2, …) is a vector field of geosampled occurrences of seasonally hyperproductive, trailing vegetation, discontinuously canopied, eco-epidemiological, narrow, riverine tributary, turbid water, capture point, endemic foci of immature *S. damnosum* s.l.,

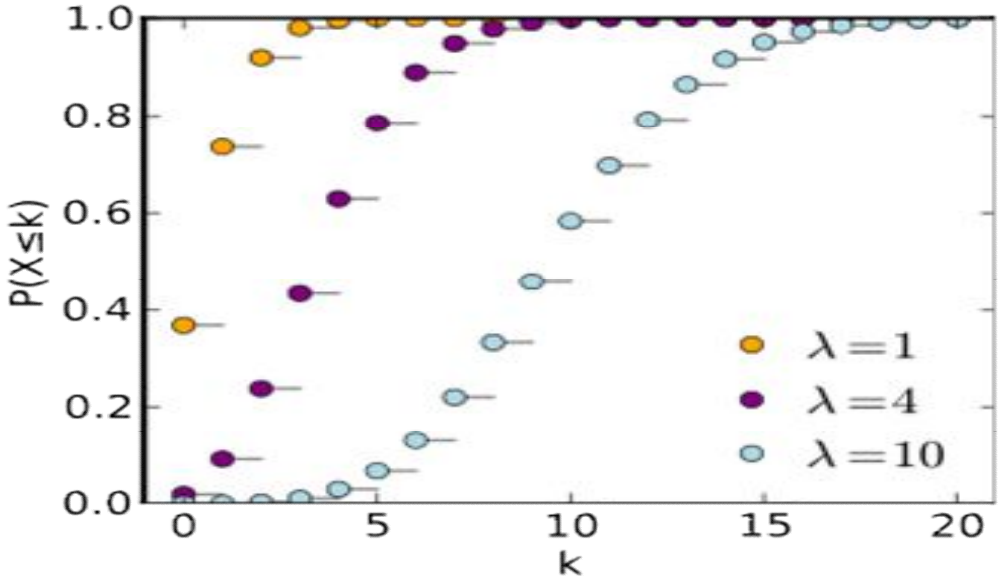

Poisson regression and Negative binomial regression are useful for analyses where the dependent (response) variable is the count (0, 1, 2, …) of the number of events or occurrences in an interval. Although turbid-media radiative transfer (RT) methods have been introduced to GO models to cope with the second-order and higher order scattering, the problem of non-linear, explanatorial, canopy geometrical, fractional effects on multiple endmember scattering still remains an obstacle in GO model applications[24]. In probability theory and statistics, the negative binomial distribution is a discrete probability distribution of the number of successes in a sequence of independent and identically distributed Bernoulli trials before a specified (non-random) number of failures (denoted *r*) occurs a Bernoulli trial (or binomial trial) is a random experiment with exactly two possible outcomes, "success" and "failure", in which the probability of success is the same every time the experiment is conducted[24].

A second explicatively parameterizable, ecohydrologic, geo-spectrotemporal, geospatial, covariate coefficient, fractionalized estimator (e.g., Percent of discontinuously canopied, trailing vegetation, sparsely shaded, explanators) may be necessitated in the eco-georeferenceable vulnerability, forecast model for optimal parameter estimator quantitation.

Specifically, if an explanatively orthogonally decomposable moderate resolution, *S. damnosum* s.l., habitatmodel statistic is significantly different from 0 at the 0.05 level, then the 95% confidence interval will not contain 0 in the endmember eigenvector, fractionalized, eco-epidemiological, LULC forecasts. All values in the confidence interval would thus be plausible values for quantitating the geo-spectrotemporally geospatially geosampled trailing vegetation, discontinuously canopied, turbid water sparsely shaded, hyperproductive, eco-epidemiological, capture point, endmember eigenvector, whereas values outside the interval would be rejected as plausible values for the parameter. In Jacob et al. [22] an elucidatively orthogonally decomposed empirical, eco-georeferenceable, seasonally geo-spectrotemporally geosampled, explanatorial, capture point, illuminative *S. damnosum* s.l. habitat, regressor (s) were eco-cartographically illustratable with the error variance quantitated according to an optimal, uncoalesced dataset of heuristically non-differential, moderate resolution, fractionalized endmember eigenvector, weighted, wavelength, frequency, transmittance, radiance emissivities in quantitated sampling distribution of means in ArcGIS (Figure 14).

Figure 14. Maximum/minimum confidence interval and Standard Error of the Mean measurements in a continuous, geoclassifiable, ArcGIS *S. damnosum* s.l. habitat LULC feature regression model

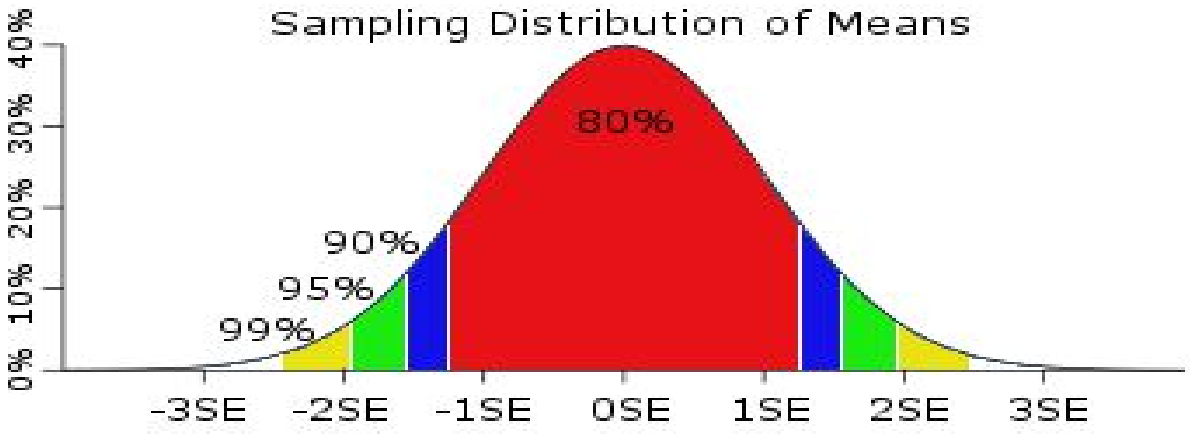

It may be shown by means of an ArcGIS simulation elucidative study that a fittable $y=\exp(\beta_{0} + \log_{1x} + \log_{2x)} + W$ exists when sub-mixel, orthogonally explanatively decomposed, regressively, elucidatively qualitatively quantitable, moderate resolution,optimally derived 3-D eco-hydrologic variable eco-cartographically illustrating an eco-georeferenceable,hyperproductive, *S. damnosum* s.l., eco-georeferenceable, narrow African riverine, tributary, agro-village complex, ecosystem,capture point, immature habitat, measurement error (e.g., frcationalized endmember multicollinearity) in x is large compared to that of W, or whilest x and w are strongly probabilistically correlated in the model ,such that $\log_{1\ x}$ and $\log_{2x}$ are non-significant and significant, respectively. In statistics, multicollinearity is a phenomenon in which two or more predictor variables in a multiple regression model are highly correlated, meaning that one can be linearly predicted from the others with a substantial degree of accuracy[24]. In this situation the uncoalesced, parameterizable, optimizable, covariate coefficient estimates of the multiple regression may change erratically in response to small changes in the, moderate resolution-derived, eco-georeferenceable, narrow, African, agro-village complex, riverine, tributary ecosystem, *S. damnosum* s.l., eco-epidemiological, immature habitat, discontinuously canopied, trailing vegetation-related, turbid water, forecast-oriented, vulnerability, model or the geo-

spectrotemporally geosampled, immature habitat, uncoalesced data. Multicollinearity does not reduce the geo-spectrotemporal predictive power or reliability of the model as a whole, at least within the sample data set; it only affects calculations regarding individual observational explanators. That is, an explanative, time series, fractionalized, endmember, multiple regression, geo-spectrotemporally optimizable model with correlated sub-mixel, elucidative predictors can indicate how well the entire bundle of predictors predicts the outcome variable, but it may not give valid results about any individual predictor, or about which predictors are redundant with respect to others in the immature habitat model. In case of perfect multicollinearity the design matrix is singular and therefore cannot be inverted[24]. Unfortunately, for a general linear model [i.e., $y = X\beta + \epsilon$], regression analyses for optimally qualitatively quantitating explanatorial, eco-georeferenceable, seasonally hyperproductive, trailing vegetation, discontinuously canopied, eco-epidemiological, narrow, riverine tributary, turbid water, capture point, *S. damnosum* s.l., endemic foci, ordinary least squares [i.e., $\hat{\beta}_{OLS} = (X^\top X)^{-1} X^\top y$]estimators does not currently exist. Note that in statements of the assumptions in such models the finding of no multicollinearity may be explanatorialy geo-visually validated amongst the quantitable regressors employing an exact, non-stochastic, linear, geo-spectrotemporal, moderate resolution, eco-cartographic, ArcGIS, decompositional model algorithm.

Dai et al. 2005 distributed an ArcGIS decomposable, grid-based watershed mercury loading model to characterize the spatial and temporal dynamics of mercury from both point and nonpoint sources. The model simulated flow, sediment transport, and mercury dynamics on a daily time step across a diverse landscape. The model was composed of six major components: (1) an ArcGIS interface for processing spatial input data; (2) a basic hydrologic module; (3) a sediment transport module; (4) a mercury transport and transformation module; (5) a spreadsheet-based model post-processor; and (6) links to other models such as WASP and WhAEM 2000 developed by the U.S. Environmental Protection Agency (EPA). The model fully employed the grid processing capacity of the latest ArcGIS technology. The water balance, sediment generation and transport, and mercury dynamics were calculated for every grid within a watershed. Water and pollutants were routed daily throughout the watershed based on a unique and flexible ArcGIS decompositional algorithm that characterized an eco-georfernceable, seasonal geospectrotemporal, geosampled watershed into many runoff travel-time zones. The mercury transport and transformation module optimally geo-spectrotemporally simulated the following key processes: (1) mercury input from atmospheric deposition; (2) mercury assimilation and accumulation in forest canopy and release from forest litter; (3) mercury input from bedrock weathering; (4) mercury transformation in soils; (5) mercury transformation in lakes and wetlands, including reduction and net methylation; (6) mercury transport through sediment and runoff; and (7) mercury transport in stream channels. By employing the grid-based technology, flow, sediment, and mercury dynamics were robustly examined at any of several points in the watershed. The model was capable of supporting large-scale watershed modeling with moderate-resolution raster datasets and will be used in mercury research projects sponsored by EPA. The model was constructed using visual basic tool in two ArcGIS 9.0 components—ArcView 9 and within the unmixingpredictive metaheuristic sub-algorithms in Spatial Analyst extension.

Although x could represent an significant heuristically optimizable, eco-georeferenceable, linear explanator in an elucidative dataset of fractionalized endmember, moderate resolution, explanatorial, forecastable regressors as rendered from an hyperproductive, seasonal, trailing vegetation, eco-epidemiological, geo-spectrotemporally, geospatially uncoalesced, discontinuously canopied, sparsely shaded,eco-epidemiological, *S.*

damnsoum s.l., fractionalized riverine, immature, habitat, endmember eigenvector, moderate resolution, reflectance, capture point, forecast-oriented, weighted, wavelength, transmittance, emissivity, vulnerability model, W would actually inhert the causative factor role. Causality would thus be 'transferred' although a combination of elucidatively quantitable, operationizable, ecohydrologic, narrow, eco-georeferenceable, agro-village riverine, tributary, geo-spectrotemporal, geospatial, measurement values and endmember multicollinearity would be as well. This phenomenen has been reported by Fuller (1987). Measurement error in endmember exposure assessment is unavoidable [24]. Although, explicatively empirically regressable geo-spectrotemporally, geospatially uncoalesced, moderate resolution (e.g., Rapid Eye ™ , 5m visible and NIR data), fractionalized, wavelength, frequency-oriented, transmittance, emissivity datasets of expositorily uncoalesced, geo-predictive, explanatively orthogonally decomposable, seasonally hyperproductive, *S. damnsoum* s.l., trailing vegetation, discontinuously canopied, turbid water, seasonal hyperendemic, foci frequencies in hypoethetical space, the precise explanatorial, parameterizable covariates may not be specified for a meandering, seasonal, pre-flooded, African, agro-village complex, narrow riverine, eco-georeferenceable, geo-samplable pathway.

Berkson error model is a description of random error measurement which may resolve fractionalized, endmember, eigenvector heteroskedascity in an empirical, geo-spectrotemporally geo-samplable,eco-epidemiological dataset of explanatively discontinuously, sporadically canopied, uncoalescable, trailing vegtetation, geospatial, seasonally hyperproductive, eco-epidemiological, eco-georeferenceable, trailing vegetation, turbid water, narrow, African riverine, tributary, capture point, *S. damnosum* s.l. sub-mixel,optimizable paridigms. Unlike classical error, Berkson error causes little or no bias in the measurement. An example of Berkson error arises in exposure assessment in explanative, eco-epidemiological, endmember studies. Berkson error may predominate over classical error in cases where geo-spectrotemporally uncoalescable, fractionalized, endmember, eigenvector exposure, moderate resolution, geo-ecohydrologic, bio-geophysical, robustifiable data are highly aggregated but in intervals. Whilest this kind of endmember uncertainity, explanatorial ,probablistic quantitation can improve the power of an empirical explanative datset of seasonally hypeproductive, African, narrow rivrine, tributary, agro-village, complex ecosystems, capture point, probabilistically regressed, risk estimates, the eco-epidemiological eco-georefernceable,wavelength, frequency-oriented, transmittance, emissivity forecasts may not themselves be attenuated such as in circumstances where sub-mixel, randomized, erroroneous substances predominates in the explanatively geospatialized, geo-spectrotemporally uncoalesced, capture point, model output. Thus, mispecifications may be rampant in iteratively, explanatively, interpotable, eco-georeferencable, moderate resolution, proxy signature, uncoalesced datatsets targeting un-geosampled, unknown, seasonally hyperprodutive, discontinuously canopied, trailing vegetation, turbid water, sparsely shaded, narrow, tributary riverine, African, agro-villge complex, hyperproductive foci.

For remotely, metaheuristically optimal, quantitative, explanative geo-spectrotemporal empirically regressable datasets of elucidatively uncoalesced, robust,eco-georeferenceable, moderate, spatial resolution, hyperproductive, turbid water, narrow riverine tributary, African, agro-village, *S. damnosum* s.l., trailing vegetation, discontinuously canopied, ecosystem complex, seasonally geosampled,optimally parameterizable, covariate coefficient, decomposed values, a reasonable customizable model for the measurement errors may be the Berkson model where $X = Z + ʒ$, and where, $ʒ$ is the unobserved, explanatorial,

random, measurement error. This misspecification would be assumed to be independent of the observed, explanatively forecastable, eco-georeferenceable, parsimonioulsy optimizable, regression variable Z in ArcGIS. The stochastic structure of the Berkson measurement error model in an ArcGIS cyberenvironment is fundamentally different from the classical errors-in-variables model in other software packages (e.g., SPSS) where the measurement error is independent of X, but dependent on Z. This distinctive feature may lead to completely different explanatively eco-georeferenceable, elucidatively,optimally parameterizable, latent, iterative, algorithmic procedures in ArcGIS for robustly regressively qualitatively quantitating, an heuristically robustifiable, uncoalescable, explanative sub-mixel, moderate resolution, geoclassifiable, LULC dataset of time series, probabilistic, parameterizable, fractionalized eigenvector, geo-spectrotemporal, radiance estimators. In so doing, the eco-cartographically, elucidatively, illustratable, turbid water, trailing vegetation, optimally parameterizable, eco-catographic, covariate coefficients or discontinuous, sparsely shaded, sporadically canopied variables may be seasonally deduced and eco-georeferenced to seasonal hyperproductive capture points, In so doing, optimal inferences of unknown, un-geosampled, infrequently canopied, seasonally hyperproductive, agro-village complex, African, narrow, riverine tributary, *S. damnosum* s.l., immature habitats on moderate resolution geo-classifiable LULCs in ArcGIS may be operationally reterivable employing an geospatially interpretive, stochastic or deterministic, quantitative, explanatorial interpolator.

For an empirical dataset of nonlinear, discontinuously,sparsely shaded, partially infrequently canopied, fractionalized endmember, hyerproductive, eco-georeferenceable, eco-epidemiological, capture point, turbid water, trailing vegetation, capture point, *S. damnosum* s.l. forecast vulnerability, African, narrow, tributary, riverine ArcGIS-derivable, agro-village model eigenvectors, an approximative method called regression calibration may be presented. Recently, Huwang and Huang (2000) studied a univariate polynomial model where g(x; ȝ θ) was a polynomial in x of a known order which intuitively may reveal optimal, eco-georefernceable, least squares-related, seasonally explanatively, hyperproductive, capture point, *S. damnosum* s.l., immature habitat, explicatively decomposable LULC datasets of iteratively quantitable interpolative, geospatialized uncoalescable, unbiased geo-spectrotemporal endmember moderate resolution, wavelength, transmittance, frequency-oriented explanatorial estimators based on the first two conditional moments of Y given Z is consistent. Wang (2003) considered general, univariate,nonlinear, expositive, endmember, fractionalized, eigenvector model outputs where all random errors were normally distributed and showed that the elucidative, minimum distance, endmember estimators based on the first two conditional moments of Y given Z is consistent and asymptotically normally distributed.

The traditional method of analyzing continuous or ordinal, explanative, fractionalized, endmember eigenvector, moderate resolution, risk factors by categorization or linear discontinuously, sparsely shaded, partially canopied, endmember, expositorily fractionalized, hyerproductive, eco-georeferenceable, turbid water, trailing vegetation, eco-epidemiological, capture point, *S. damnosum* s.l. ArcGIS-derivable, heuristically optimizable, forecast vulnerability models may be improved in ArcGIS cyberenvironments. For example, an approach based on transformation and fractional polynomials which yields simple regression models with interpretable curves in ArcGIS may render iteratively interpolatable unknown, un-geosampled, seasonal, capture point, hyperproductive, habitats in an narrow African, tributary, eco-georeferenceable, riverine, agro-village, complex ecosystem. A methodology of optimally ecohydrologically, geo-spectrotemporally, geospatially eco-cartographically,presenting the results from such geoclassifiable, moderate reolution, LULC

models in ArcGIS may be to rigriously tabulate the aggregated mean risks estimated from the model at convenient values employing any linear combinationof eco-biogeophysical elucidative co-factors of onchocerciasis(e.g., Levels of seasonal turbidity during preflooding in an eco-georferenceable, African, narrow, riverine tributary, agro-village, ecosyem complex). Incorporating several explanatively eco-georeferenceable, continuous risk and confounding geo-spectrotemporal, geospatiazed, moderate resolution, uncoalesced, *S. damnosum* s.l. forecastable variables within a single model may resolve any moderate resoluiton, decomposed, weighted, wavelength, transmittance, frequency-oriented, emissivity, parameterized covariate, estimator, probabilistic endmember uncertainty. This ArcGIS approach may lead to further categorization of sub-mixel estimators in non-parametric, optimizable regression, model algorithms. It may be shown that non-linear, moderate resolution geo-spectrotemrpoally uncolaesced, ArcGIS, *S. damnosum* s.l., forecast, vulnerability models fit the data better than linear models. Fractionalized, moderate resolution, endmember, eigenvector polynomials synthesized in an ArcGIS cyberenvironment may be an important alternative to the traditional approaches for analysis of continuous variables in epidemiological onchocerciasis studies in narrow riverine, tributary, ecogeorferenceable African agro-village complexes.

In many practical geo-spectrotemrpoally geospatialized, non-linear, seasonal, narrow, riverine, tributary, hyperproductive, eco-georeferenceable, *S. damnosum* s.l., eco-epidemiological, geo- uncoalesced, moderate resolution, weighted, wavelength, frequency, transmittance, forecast-oriented, emissivity, vulnerability, model specifications there may be often more than one explanatively decomposable, sub-mixel, ecohydrologic, geo-biophysical variable (e.g., Percent of dead shaded floating vegetation) which may be subject to reflectance measurement errors. Moreover, the random errors " ȝ" may have distributions other than the normalized, expositively fractionalized, probabilistically regressed, endmember orthogonalized eigenvector distributions. By generalizing the results of the geo-predictive, elucidatively nonlinear, eco-epidemiological, uncoalescable, moderate resolution, weighted, moderate resolution, wavelength, frequency-orinted, emissivity, eigenvector transmittance, ArcGIS models with multivariate, eco-georefernceable, capture point, narrow, agro-village, African, seasonal, riverine, tributary imature habitat, high density foci, the measurement error ȝ may reveal a generalizable parametric distribution f_(t;) ∈ ⊂ Rq, where the random error may have a nonparametric distribution with mean zero and a quantizable variance. This output would be geo-visualizable, in the explanatively forecasted, geo-spectrotemporally geosampled, residualizable, fractionalized, unmixed, endmember eigenvector, multivariate dataset of explanative, discontinuous, vegetation-related, partially canopied, geoclassifiable, LULC regression variables. As such, the time series dependent, latent, fractionalized, explicative eco-epidemiological, endmember eigenvector, heuristically optimizable, moderate resolution, dataset would absolutely eco-cartographically delineate semiparametric, geo-spectrotemporally, empirically regressable, ecohydrologic, geospatialized datasets of elucidatively explanative, *S. damnosum* s.l., hyperproductive, uncoalesced, capture point, immature habitat, orthogonally, quantitatively decomposable, wavelength, frequency, transmittance, emissvities as regressively rendered from an eco-georefernceable, agro-village, narrow African, riverine, tributary, forecast, vulnerability model.

The minimum distance estimator of Wang (2003) may be consistent and asymptotically normally distributed in ArcGIS for constructing an elucidative, eco-georefernceable, discontinuously, sparsely shaded, infrequently canopied, fractionalized endmember, narrow, riverine tributary, eco-epidemiological, *S. damnosum* s.l., immature, seasonal, capture point,

forecast, vulnerability eco-epidemiological, eigenvector spatial filter, moderate resolution, forecast-orinted, vulnerability model. For the generalizable seasonally, infrequently, partially shaded model, however, a computational issue may arise due to the minimized objective function in uncoalesced, geospatially explicative, eigenvector, riverine, agro-villagenarrow tributary, African agro-village, trailing vegetation, discontinuously canopied, turbid water, hypeporductive, *Similium* habitat, probabilistically regressable, heuristically optimizable, eco-epidemiological, datasets of the immature habitat, residual forecasts would involve important varying multiple integrals (e.g., eco-georefernceable geosampled distance measurements between turbid water, discontinuously canopied, hypeproductive, capture point immature habitats) for which explicit forms may not always be parsimoniously obtained. Given a function $f: A \to \mathrm{R}$ from some set A (i.e., real-geosampled empirically orthogonally explanatively decomposed, eco-epidemiological, datset of eco-georefernceable, optimally parameterizable geo-spectrotemporally uncoalesced, *Similium* habitat, moderate resolution, time series, regressed, covariate coefficients) an element x_0 in A such that $f(x_0) \leq f(x)$ for all x in A ("minimization") or such that $f(x_0) \geq f(x)$ for all x in A ("maximization") may be optimally synthesized .To overcome any difficulties during synthesis, an explanative, simulation-based, sub-mixel, elucidatively fractionalizable, heuristically optimizable, ArcGIS linear estimator may be employed in a moderate resolution, forecast, vulnerability map which may be consistent and asymptotically normally distributed under regularity conditions for elucidatively qualitatively quantitating a minimum distance endmember, fractionalized eigenvector estimator.It may be assumed that Z, and ȝ are independent in the immature habitat, capture point, sub-mixel model and Y has a finite second moment.

In addition, the common assumption that quantitated ArcGIS measurement error is "nondifferential" may be adopted in a moderate resolution, *S. damnosum* s.l., capture point, immature habitat, orthogonally, quantitatively decomposable, weighted, wavelength, frequency, transmittance, emissvity, endmember, eigenvector, forecast, vulnerability model in the sense that the conditional expectation of Y given X and Z may be the same as the conditional expectation of Y given X is the eco-epidemiological, residualized forecasts targeting the unknown, un-geosampled narrow African, riverine tributary, agro-village, eco-georeferenceable, seasonal hyperproductive, immature habitats. In such circumstances, Z may be assumed to be an elucidative geospatialized, optimally randomized, seasonally explanative, eco-georeferenceable, hyperproductive, capture point, immature habitat, orthogonally decomposable, sub-mixel, intuitive regressor and thus all results would continue to hold if the illuminatively, trailing vegetation, turbid water, discontinuously canopied, sparsely shaded, fractionalized expositive, endmember, eigenvector observations of Z, Z1,Z2, . . . ,Zn, in ArcGIS are treated as fixed constants such that the limits limn→∞Pni=1 Zi/n and limn→∞Pni=1 ZiZ′i/n are finite.

Further, by building queries in ArcGIS to predict seasonally explanative, hyperproductive, eco-epidemiological, capture point, immature habitat events (e.g., pre-flooding and riverine meadering) and control activities ("Slash and Clear") of eco-georefernced, prolific, high density, endemic, African, narrow riverine tributary, agro-village capture point, seasonal foci, may be assumed from an endmember eigenvector, residually fractional, vulnerability, model output. These explanatively robustifiable eco-epidemiological, reflectance eigenvector forecasts may reveal geo-spectrotemporally, geospatially uncoalesceable, bidirectional, moderate resolution, fractionalized, weighted, wavelength, transmittance emissivities and frequencies (e.g., trailing vegetation, moderate resolution, unmixed, proxy signature, sparsely shaded, riffle, catchment water level reflectance) that may be found to be autoregressively optimally eco-hydrologically associated

with particular seasonal, eco-geographic, discontinuously, infrequently canopied, eco-georeferenceable, hyperproductive, riverine, hyperendemic geolocations. If geosampled, seasonal, trailing vegetation of an eco-georeferenced, seasonally hyperproductive, trailing vegtation, turbid water, *S. damnosum* s.l., discontinuously canopied, immature habitat prefers non-homogenously,infrequently canopied, sparsely shaded, narrow, riverine, tributary, sparsely shaded, hyperendemic, explantive, geoclassifiable, LULC foci, within X distance from an ecogeoreferenceable, hyperproductive, eco-epidemiological, capture point, but more than Y distance from a populated, narrow, riverine, agro-village, complex centroid, the Query Builder can manually construct the query in ArcGIS, then apply it to rasters to see which geo-spectrotemporal, geospatially geosampled, immature, habitat existing in unknown, un-geosampled, geolocations satisfy those conditions.

Accorrding to Jacob et al. [22] impreciseness of a biased, auto-probabilitic, heuristically, non-optimizable, fractionalized, uncertainty-oriented, geo-spectrotemporally, geospatially dependent, explicatively fractionalized, endmember, elucidative, optimizable,regression variable in an eigenvector, spatial filter, iterative ArcGIS algorithm, commonly originates from a sample population whose distribution violates the assumption of a normal distribution. In an heuristically non-optimizable, explanatorily, un-intutively, non-optimally decomposable, moderate resolution, target-oriented, discontinuous, infrequently canopied, seasonal, *S. damnosum* s.l. eco-epidemiological, agro-village, complex ecosystem, hyperproductive, eco-georeferenceable foci, seasonal centroid, an informative, geo-spectrotemporally uncoalescable, empirical dataset can lead to non-robust, sub-mixel (i.e., fractionalized renderings) as spatial autocorrelation. As such the correlation amongst values of a single geo-spectrotemporally geosampled, *S. damnosum* s.l., immature habitat, variable would be strictly attributable to their relatively close eco-georeferenceable geolocational positions on a two-dimensional surface whilest introducing a deviation from the independent observations assumption of classical statistics. A variant of conventional correlation is serial correlation, which pertains to the correlation between endmember eigenvector coefficient values for observations of a single decomposed mixel variable according to some ordering of the values [24].

A scatterplot that cannot geo-visualize and autoregressively quantitate, latent, explanative, geo-spatiotemporal or geo-spectrotemporal endmember autocorrelation, coefficients in a seasonally expositively fractionalized, explanatively forecastable, and heuristically optimizable, empiricalized, eigenvector dataset of geosampled, eco-georeferenceable and orthogonally explanatively decomposable, moderate resolution, seasonally imaged, *S. damnosum* s.l., discontinuously canopied, uncoalesced, capture point, hyperproductive, habitats with iteratively interpolative, fractionalized, moderate resolution, unbiased, weighted, wavelength, transmittance frequencies employing a conventional correlation coefficient in ArcGIS will not be able to describe the direction and strength of a non-linear relationship, thus leading to non-normal, emissivity diagnostic, quantile plots of the residuals (e.g., biasedly forecasted geocoordinates of geospatial outliers).

In statistics, OLS or linear least squares is a method for estimating the unknown parameters in a linear regression model, with the goal of minimizing the differences between the observed responses in some arbitrary dataset and the responses predicted by the linear approximation of the data. Jacob et al. [22] visually plots the sum of the vertical distances between each eco-georeferenceable, seasonally hyperproductive, discontinuously canopied *S. damnsoum* s.l., trailing vegetation, turbid water, geoclassified, narrow, African, riverine

tributary, agro-village complex,geosampled data point with the corresponding point on the regression line. The authors found that the smaller the differences,the better the model fits the geo-spectrotemporally immature geosampled data. The resulting estimator was expressed by a simple formula, in ArcGIS employing a single regressor on the right-hand side of the moderate resolution,optimally derived, elucidatively uncoalesced, forecast-oriented, vulnerability model.The *S. damnosum* s.l. immature, eco-epidemiological, capture point, OLS estimator was consistent and the fractionalized, endmember eigenvector, expositive regressors were exogenous and there was no perfect multicollinearity when the model was validated using a stepwise backward regression in ArcGIS. The linear, unbiased, forecast estimators were of optimal class since the diagnosed non-normalities were homoscedastic and serially uncorrelated. The method of OLS provided minimum-variance, mean-unbiased, residual estimation of the uncoalesced, geo-spectrotemporal, geospatialized, eco-georeferenceable, trailing vegetation, turbid water, sparsely shaded, discontinuous, infrequently canopied, hyperproductive, *S. damnosum* s.l. immature habitat since the errors had finite variances. Under the additional assumption that the errors are normally distributed, OLS is the ML estimator [25]. Unfortunately, there has been little attention given to explicative, diagnostic, residual endmember, plots for qualitatively quantiating eco-georefernceable, uncoalesced, time series regression paridigms for identifying eco-georeferenceable, trailing vegetation, discontinuously canopy, turbid water, seasonally hyperproductive, eco-epidemiological, forecasting, African, narrow, riverine tributary African agro-village complex ecosystems

There are some principal assumptions which justify the usage of moderate resolution, endmember linear eigenvector regression models in ArcGIS for purposes of inference or prediction for targeting un-geosampled,unknown, fractionalized, digitally archivable, trailing vegetation, discontinuously canopied, geo-spectrotemporally, uncoalesced, *S. damnosum* s.l., geo-spatialized, capture point, imaged, immature, eco-epidemiological, eco-georeferenceable, hyperproductive habitats. These primary assumption include quantitating linearity and additivity relationships between endmember dependent and independent variables where the expected value of dependent variable would be a straight-line function of each geo-spectrotemporally geosampled, trailing vegetation, turbid water, sparsely shaded, infrequently, discontinuously canopied, eco-cartographically synthesized, independent variable, whilest holding the others fixed. Secondly, the slope of the endmember fractionalized regressed line do not depend on the values of the other endmember variables. The effects of different independent variables on the expected value of the dependent sub-mixel, log-transformed variable are additive and statistical independence of the errors. Thus, no correlation may be assumed to exist between consecutive error quantitation in the case of eco-georeferenceable, time series, hyperproductive, immature habitats with geo-spectrotemporally uncoalesceable, iteratively interpolative, fractionalized, moderate resolution, optimally derived, weighted, wavelength, transmittance, frequency-orinted data variables for qualitatively quantitating homoscedastic error coefficients. Unfortunately, eco-epidemiological, forecast-orinted,explanatively residually normalized outputs rendered from a geo-spectrotemporally geo-spatialized, trailing vegetation, discontinuous, infrequently canopied, *S. damnosum* s.l., eco-epidemiological, eco-georeferenceable, riverine, tributary, capture point, moderate resolution, optimally derived, eco-epidemiological, forecast, fractionalized, endmember, eigenvector, vulnerability model that violates all of sub-mixel regression assumptions is likely to be accepted by a naïve user on the basis of a large value of R-squared. If endmember regression assumptions is violated in an explanative, eco-georeferenceable, seasonally hyperproductive, capture point, narrow riverine, tributary, African, agro-village complex, *S. damnosum* s.l., trailing vegetation,

discontinuously canopied, eco-epidemioloigical,turbid water, sparsely shaded, seasonal, immature habitat, forecast vulnerability model (i.e., if there are nonlinear relationships between quantifiable dependent and independent explicative variables or the errors in an seasonal habitat exhibit correlation, endmember heteroscedasticity, or non-normality), then the residual forecasts, confidence intervals, and scientific insights yielded by the model may be at best inefficient or at worst seriously biased or misleading.

Ideally, statistical software utilized for constructing moderate resolution, seasonally imaged, uncoalescable, eco-georeferenceable, seasonally hyperproductive, trailing vegetation, turbid water, *S. damnosum* s.l., discontinuous, infrequently canopied, eco-epidemiological, capture point, geo-spectrotemporal, geospatialized, narrow, African, riverine, tributary, capture point, agro-village complex, ecosystem, geosampled, hyperproductive,immature habitats with iteratively interpolative, expositively fractionalized, moderate resolution, unmixed wavelength, transmittance frequencies will automatically provide charts and statistics that test whether endmember regression assumptions are satisfied for any given, eco-epidemiological, forecast-oriented, heuristically optimizable, vulnerability model,parameterizable, covariate estimator. Unfortunately, many software packages do not provide such output by default (additional menu commands must be executed or code must be written) and some (such as Excel's built-in regression add-in) offer only limited options.

Expositorily fractionalized, explanatively discontinuous, infrequently canopied, sparsely shaded, uncoalesced, 5m imaged, , RapidEye^{TM}, geospatially, geosampled, eco-georeferenceable, trailing vegetation, eco-epidemiological, capture point, sparsely shaded, *S. damnosum* s.l., turbid water,immature habitats, fractionalized endmember, moderate resolution, eigenvector-related. geo-spectrotemporal ArcGIS, image analysis frequently employs model-based, statistical inference, which iteratively interpolatively, quantitates based on the dependability of optimally parameterizable, sub-mixel regressors. Subsequently, these coefficient renderings are based upon the correctness of posited assumptions about the model's error term. In omitted-variable bias (OVB) the "bias" is created when the model compensates for the missing factor by over- or underestimating the effect of one of the other factors[24]. More specifically, OVB in a empirical dataset of geo-spectrotemporally geosampled, eco-georeferenceable, eco-epidemiological, uncoalescable, capture point, trailing vegetation, endmember, fractionalized, decomposed ArcGIS-derived, moderate resolution, geo-spectrotemporal, geospatialized, *S. damnosum* s.l. endemic, forecast-orinted, vulnerability model orthogonalized eigenvectors would may include the bias that appears in the sub-mixel estimators during a regression analysis, since the assumed specification would be incorrect in that it would omit an independent variable [e.g.,monthly biting rate(MBR)] that may be correlated with both the dependent variable and one or more included independent variables.

One principal assumption in these explanatively, seasonally forecastable, elucidatively, orthogonally decomposable and heuristically optimizable, vulnerability paradigms is that individual explicative, autoregressive error terms can come from a specified, seasonal, geosampled population (e.g., eco-georeferenceable dataset of pre-flooded, eco-georferenceable, clustering narrow riverine, tributary, African agro-village complex, *S. damnosum* s.l,. turbid water, heterogeneously canopied, sparsely shaded, trailing vegetation, capture point, immature habitats) whose entries are thoroughly randomly mixed. Moreover, another primary assumption of explanatively, orthogonally elucidatively decomposable, heuristically robustifiable, geo-spectrotemporal, geospatialized, clustering data (e.g.,

seasonally unmixed, discontinuously, infrequently canopied, immature, seasonal, narrow, African tributary, riverine, *Simulium* habitat, bidirectional, moderate resolution, reflectance agro-village, eco-epidemiological parameters) is that the explanatively autoregressable error term entries will not affect the quantitated probability of a illuminatively parameterizable, fractionalized, wavelength, emissivity or, covariate coefficient frequency taken on by any of the remaining error term entries (i.e., the independent observations assumed in classical statistics in a forecasting regression-related analyses). Since non-zero, spatial autocorrelation in explanatively seasonally, eco-georeferenceable, expositorily, fractionalized, geo-spectrotemporally geospatially, explanatively uncoalesced, dataset of sparsely shaded, moderate resolution, imaged, trailing vegetation, eco-epidemiological, agro-village, complex ecosystem, turbid water, narrow, African, riverine, agro-village, capture point, trailing vegetation, immature hyperproductive, tributary habitats interpretively, iteratively, quantitative, orthogonally decomposable, iteratively interpolated, illuminative estimators rendered from an *S. damnosum* s.l.,forecast vulnerability model would violate this assumption. Only few models with heuristically optimal, eco-epidemiologically forecastable, vulnerability residuals (e.g., discontinuous, infrequently canopied, targeted eco-georefernceable, geolocations of unknown, high density,un-geosampled, riverine foci) would exhibit eco-cartographic, geopredictive latent expressions when mapped. Most variables exhibit some type of spatial organization across space[24].

Importantly, geo-spectrotemporally geospatially uncoalesced, moderate resolution, weighted wavelength transmittance, emissivity, frequency-oriented, moderate resolution, fractionalized, endmember eigenvector models of immature, seasonal, hyperproductive, trailing vegetation, turbid water, explanative, eco-georefernceable, *S. damnosum* s.l., riverine, narrow, tributary, capture point, immature habitats, constructed with vulnerability-oriented, eco-epidemiological, forecastable geosampled assumptions may render, unmixed, proxy signature, illuminative variables with their probabilistic residual uncertainties. These renderings may be quantitated from exploratory, orthogonally explanatively decomposable, discontinuously, infrequently canopied, fractionalized, sparsely shaded, geo-spatially geo-spectrotemporally extractable, immature, narrow riverine, tributary, agro-village, African complex, turbid water,uncoalesced, immature habitat, sub-mixel explanators within a linear algorithm in ArcGIS based on the proportion-weighted combination of the irradiance, derivative spectra. An uncertainty process is a repeating process whose outcomes follow no describable, deterministic pattern, but follow an uncertainty distribution, such that the propagational measure of the occurrence of each outcome can only be approximated or calculated [24]. Probabilistic expostorial, endmember probabilistic, unquantitated uncertainities arising from geospatially, geo-spectrotemporal remotely un-rectifiable, explanatorial, expositorily, non-fractionalized, non-orthogonally decomposed, uncoalescable, moderate resolution, optimally derived, non-paramterizable, regression-related covariates can also alter calculated fractionalized eigenvector contributions. The concentration distribution for effectively, optimally interpreting iteratively interpolative, heuristically decomposable, discontinuous, infrequently, sparsely shaded, partially canopied, seasonally hyperproductive, eco-georeferenceable, immature, capture point, *S. damnosum* s.l., narrow, African, riverine, agro-village complex, expositively fractionalized, orthogonalized, tributary habitat, spatial filter eigenvectors in ArcGIS (i.e., the flux-weighted input of the habitat endmember data stream), requires robustly quantitating markedly different waveband proportions from that IR especially for sampling flood water stored in the catchment.

Qualitatively remotely, quantitating inconspicuous, clustering tendenicies [i.e., non-explanative, latent negative autocorrelation) in an empirically regressable datset of

illuminatively geospatialized iterative/non-iterative, eco-georeferenceable aggregations of dissimilar, discontinuously, infrequently canopied, geo-spectrotemporal,geospatialized eigenvector ensembles in geo-space in moderate resolution, seasonally imaged, hyperproductive, sparsely shaded, trailing vegetation, *S. damnosum* s.l., African narrow, riverine tributary, agro-village complex, turbid water, eco-epidemiological, tributary, capture points, in ArcGIS [e.g., Geospatial Analyst™ extension] can render non-robust, eco-hydrologic, eco-cartographic, sub-mixel, non-decompsoable explanators.Subsequently the field-operationalizable, empirically non-Gaussianistic, explicatively parameterizable transmittance would autoregressively render geopredictive non-explanative covariates based on mispecified erroneous, wavelength, frequency emissivities.

Gridded, elucidatively stratifiable, descriptive, fractionalized, endmember, orthogonalizable, eigenvectors and their spatial filters may optimally eco-cartographically delineate an optimal, autoregressive, uncertainty-oriented, geo-spectrotemporal and/or geo-spatiotemporal autocorrelation, probabilistic, geo-spatializable, uncertainty, weighted matrix in SAS/GIS (e.g., AUTOREG), in geo-space which may iteratively employ various clustering algorithms (e.g., eigenclusters) for data vector quantization and pattern recognition of seasonal, *S. damnosum* s.l. decomposeable, eco-georeferenceable, capture point, immature, hyperproductive habitats. Spatial geo-classification of non-elucidative, eco-georeferenceable, explanatively geo-spectrotemporally uncoalescable, discontinuously, infrequently canopied, sparsely shaded, trailing vegetation, geospatializable,immature, *S. damnosum* s.l., riverine, turbid water, high density, narrow tributary, seasonal, capure point, immature habitats may be contructed in AUTOREG. An eigenfunction of a linearly, explanatively, orthogonally explanatively decomposable, 5m, RapidEye™ of immature, prolific, *Simulium,* riverine foci, unmixed,dataset eco-geographically and non-ecogeographically illustrating autoregressably and expositorily fractionalized, moderate resolution, wavelength transmittance, operators, optimally defined on some elucidative function space may be represented in space by any non-zero function in that space which returns from the operator exactly as is, except for a multiplicative scaling factor in an ArcGIS cyberenvironment.

In ArcGIS, a function space may be represented by a set of functions of a given kind from a set X to a set Y . It is called a space because in many applications it is a topological space (including metric spaces), a vector space, or both. Namely, if Y is a field, function in ArcGIS with an inherent vector structure in an heuristically explanatively, expositorily fractionalized, iteratively interpolative, moderate resolution, seasonally imaged, discontinuously, infrequently canopied, seasonally hyperproductive, African narrow, riverine tributary, trailing vegetation, *S. damnosum* s.l., sparsely shaded, turbid water, eco-epidemiological, capture point,two operations of pointwise addition and multiplication to a scalar may be optimally performed. Scalar multiplication is one of the basic operations defining a vector space in linear algebra or more generally, a module in abstract algebra [24].

In an seasonally explanative hyperproductive, eco-georeferenceable, geo-spectrotemrporally geospatially geosampled, African, narrow, riverine tributary, *S. damnosum* s.l., vulnerability, forecast-oriented, regression model, an inner product space may be optimally a vector space with an additional structure (i.e., inner product). An inner product naturally induces an associated norm, thus an inner product space is also a normed vector space. A complete space with an inner product is called a Hilbert space. The mathematical concept of a Hilbert space, named after David Hilbert, generalizes the notion of Euclidean space. It extends the methods of vector algebra and calculus from the two-dimensional

Euclidean plane and three-dimensional space to spaces with any finite or infinite number of dimensions An (incomplete) space with an inner product is called a pre-Hilbert space, since its completion with respect to the norm induced by the inner product is a Hilbert space. Inner product spaces over the field of complex numbers are sometimes referred to as unitary spaces.As such, additional geo-spectrotemporally geospatially explanatively uncoalesced, elucidative, discontinuously canopied, fractionalized endmember, immature habitat decomposable structures may be associated to each pair of uncoalesced, moderate resolution, moderate resolution, wavelength, emissivity, frequency vectors in space with a scalar quantity. These regression renderings may optimally map, eco-georeferenceable, explicative, narrow riverine, tributary, capture point, hyperproductive foci, radiance–related eco-epidemiological, variables based on the inner product of the vectors. Inner products allow the rigorous introduction of intuitive geometrical notions such as the length of a vector or the angle between two vectors [24]. . Inner products allow the rigorous introduction of intuitive geometrical notions such as the length of a vector or the angle between two vectors whilest provide the means of defining orthogonality between vectors (zero inner product). Inner product spaces generalize Euclidean spaces (in which the inner product is the dot product, also known as the scalar product) to vector spaces of any (possibly infinite) dimension, and are studied in functional analysis[25]. Further, in an seasonally explanative, hierarchical, eco-georeferenceable, explanatively, orthogonally quantitatively decomposable,seasonally hyperproductive, narrow, riverine, tributary capture point, *S. damnos*um s.l., turbid water, trailing vegation, immature habitat autoregressive weighted model with their respective discontinuously, orthogonally decomposed, synthetic, spatial filter, eigenvector forecasts could provide the means of defining orthogonality between vectors (i..e, zero inner product) which may be provided in ArcGIS (Figure 15). The dot product of vectors a a and unit vector u u is the projection of a a onto u u , i.e., a·u=‖a‖cosθ, a·u=‖a‖cos θ, where θ θ is the angle between a a and u u[25] . This expression does not involve the magnitude of u u in an eco-epidemiological, ecogeoreferenceable, capture point, *S. damnos*um s.l wavelength, trasnmittance, emissivity, forecast, vulnerability model since the residuals would be normalized to be length one

Figure 15 Geometric interpretation of the angle between two hypothical, hypeproductive, discontinuous,infrequently canopied, trailing vegtetaion, turbid water, *S. damnsoum* s.l. immature , capture point , vectors defined using an inner product in geospace

International Journal of Geographic Information System
Vol. 4, No. 1, April 2017, pp.1-519
Available Online at http://acascipub.com/Journals.php

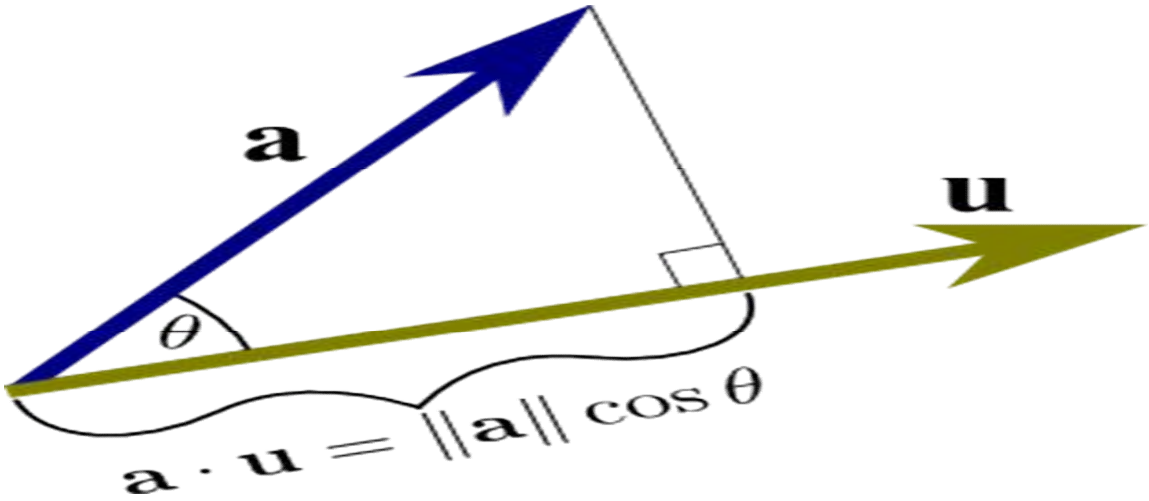

Some authors, especially in physics and matrix algebra, prefer to define the inner product and the sesquilinear form with linearity in the second argument rather than the first in ArcGIS. In so doing, the first argument becomes the conjugate linear response rather than the second. In those discplines the product $\langle x, y \rangle$as $\langle y|x \rangle$ (the bra–ket notation of quantum mechanics,) could be optimally written respectively as $y^\dagger x$(i.e., dot product as a case of the convention of forming the matrix product *AB* as the dot products of rows of *A* with columns of *B*) in ArcGIS. In so doing, the kets and columns in a orthogonally, quantiatively, explanatively decomposable,seasonal, narrow African , riverine tributary, eco-georefernceable, *S. damnos*um s.l., capture point, turbid water, trailing vegetation,prolific, immature habitat would be identified with the vectors of *V* and the bras and rows with the dual vectors or quantized linear functionals of the dual space *V**, with conjugacy associated with duality in an uncoalesced, immature, hyperproductive, seasonal, immature habitat, fractionalized estimators. This reverse order has also been followed in the more abstract ArcGIS literature, taking $\langle x, y \rangle$to be conjugate linear in *x* rather than *y*. A few researchers have found a middle ground by recognizing both $\langle \cdot, \cdot \rangle$and $\langle \cdot | \cdot \rangle$as distinct notations differing only in which argument is conjugate linear in a ArcGIS endmember forecasting vulnerability paridigm.

The vector **A** i can be optimally written in ArcGIS employing any set of basis vectors and corresponding coordinate system. Informally basis vectors are like "building blocks of a vector": they are added together to compose a vector, and the coordinates are the numerical coefficients of basis vectors in each direction. Two useful eco-geographic, explanative representations of a vector are simply a linear combination of basis vectors, and column matrices. Employing the familiar Cartesian basis,in an ArcGIS cyberenevironment a vector **A** may be written optimally as $\mathbf{A} \doteq A_x\mathbf{e}_x + A_y\mathbf{e}_y + A_z\mathbf{e}_z = A_x\begin{pmatrix}1\\0\\0\end{pmatrix} + A_y\begin{pmatrix}0\\1\\0\end{pmatrix} + A_z\begin{pmatrix}0\\0\\1\end{pmatrix} = \begin{pmatrix}A_x\\0\\0\end{pmatrix} + \begin{pmatrix}0\\A_y\\0\end{pmatrix} + \begin{pmatrix}0\\0\\A_z\end{pmatrix} = \begin{pmatrix}A_x\\A_y\\A_z\end{pmatrix}$ where $\mathbf{e}_x$, $\mathbf{e}_y$, $\mathbf{e}_z$ denotes the Cartesian basis vectors where all geo-spectrotemporally, geospatialized, eco-epidemiological uncoalesced, datasets of eco-georefernceable trailing vegetation, discontinuously, infrequently canopied, *S. damnosum* s.l., turbid water, hyperproductive, immature habitats are orthogonal unit vectors and A_x, A_y, A_z are the corresponding coordinates, in the *x*, *y*, *z* directions. In a more general notation, for any basis in 3-D ,an optimizable, explanatively heuristically, robustifiable, dataset of orthogonally quantiatively

decomposable, seasonally , narrow, riverine, tributary, *S. damnos*um s.l., capture point, turbid water, trailing vegetation, immature habitat, *S. damnosum* s.l., frequency wavelength, variables may be optimally regressed using $\mathbf{A} \doteq A_1\mathbf{e}_1 + A_2\mathbf{e}_2 + A_3\mathbf{e}_3 = \begin{pmatrix} A_1 \\ A_2 \\ A_3 \end{pmatrix}$.

Generalizing further, consider a vector A in an *N*-dimensional vector geospace over an metaheuristically optimizable, elucidative, eco-georeferenceable, explanatorial, field of geo-spectrotemporally, geospatially uncoalesced, moderate resolution, weighted, wavelength, ,frequency emissivities rendered from an empirical dataset of eco-epidemiological, seasonally hyperproductive, explanative, capture point,. *S. damnosum* s.l., trailing vegetation, discontinuously infrequently, canopied, sparsely shaded, fractionalized, immature habitat, transmittance-oriented, regressively complex, coefficient values $\mathbb{C}$, If this dataset is symbolically stated as $\mathrm{A} \in \mathbb{C}^N$., the dimension of a vector space *V* may be quantaized as the cardinality (i.e. the number of vectors) of a basis of *V* over its base field. For every vector space in a, *S. damnsoum* s.l. immature, capture point there would exist a basis of a vector space for all equal cardinality [2]]as a result, the dimension of a vector space in a wavlength, trasnmittance emissivity, forecastable, vulnerability model may be uniquely defined 9in ArcGIS

We say *V* is finite-dimensional if the dimension of *V* is finite, and infinite-dimensional if its dimension is infinite[24]. In mathematics, the dimension of a vector space *V* is the cardinality (i.e. the number of vectors) of a basis of *V* over its base field. For every vector space there exists a basis, and all bases of a vector space have equal cardinality as a result, the dimension of a vector space is uniquely defined. In mathematics, cardinal numbers, or cardinals for short, are a generalization of the natural numbers used to measure the cardinality (size) of sets. The cardinality of a finite set is a natural number: the number of elements in the set. The *transfinite* cardinal numbers describe the sizes of infinite sets.We say *V* is finite-dimensional if the dimension of *V* is finite, and infinite-dimensional if its dimension is infinite[25]

The dimension of the vector space *V* over the field *F* can be written as $\dim_F(V)$ or as [V : F] in ArcGIS and then read as a "dimension of *V* over *F*". When *F* can be inferred from context, dim(*V*) two finite-dimensional vector spaces in a *S. damnosum* s.l. immature , eco-georferenceable, habitat forecasting, vulnerability paradigm may be employed for paramter estimator quantiation if *V* is a finite-dimensional vector space and *W* is a linear subspace of *V* with dim(*W*) = dim(*V*). In so doing, $W = V.\mathrm{R}^n$ will have the standard basis $\{e_1, ..., e_n\}$, where e_i is the *i*-th column of the corresponding identity matrix. Therefore R^n will have a dimension *n* in the narrow riverine, eco-georferenceable, geo-spectrotemrporal, geospatial, tributray model Any two vector spaces over *F* having the same dimension are isomorphic [24]. Any bijective, time series, *S. damnsoum* s.l. eco-epidemiological, forecast map between their bases may be uniquely extended to a bijective linear map between the vector spaces in an ArcGIS If *B* is some set, a vector space with dimension |*B*| over *F* in the disconrinuously canopied, sparsely shaded, turbid water, trailing vegetation, capture point, proxy uncoalesced biosignature matrix can be constructed by quantizing the set $F^{(B)}$ of all functions $f: B \to F$ such that $f(b) = 0$ for all but finitely many *b* in *B*. These functions can be added and multiplied with elements of *F* in ArcGIS for optimally obtaining a desired *F*-vector space.Therefater, the vector A could then be conventionally illustratable by a linear

$$\mathbf{A} \doteq \sum_{n=1}^{N} A_n \mathbf{e}_n = \begin{pmatrix} A_1 \\ A_2 \\ \vdots \\ A_N \end{pmatrix}$$

combination of basis vectors or a column matrix: even if the coordinates are now all complex-valued (Figure 16).

Figure 16. Plotted 3-D real vector components and bases projection between a vector calculus notation and Dirac notation for illustrating uncoalesced, geo-spectrotemporal, geospatial, Rapid Eye™ ,5m *S. damnosum* s.l. riverine habiat capture point wavelength, emissivity frequency-oriented, transmittance.

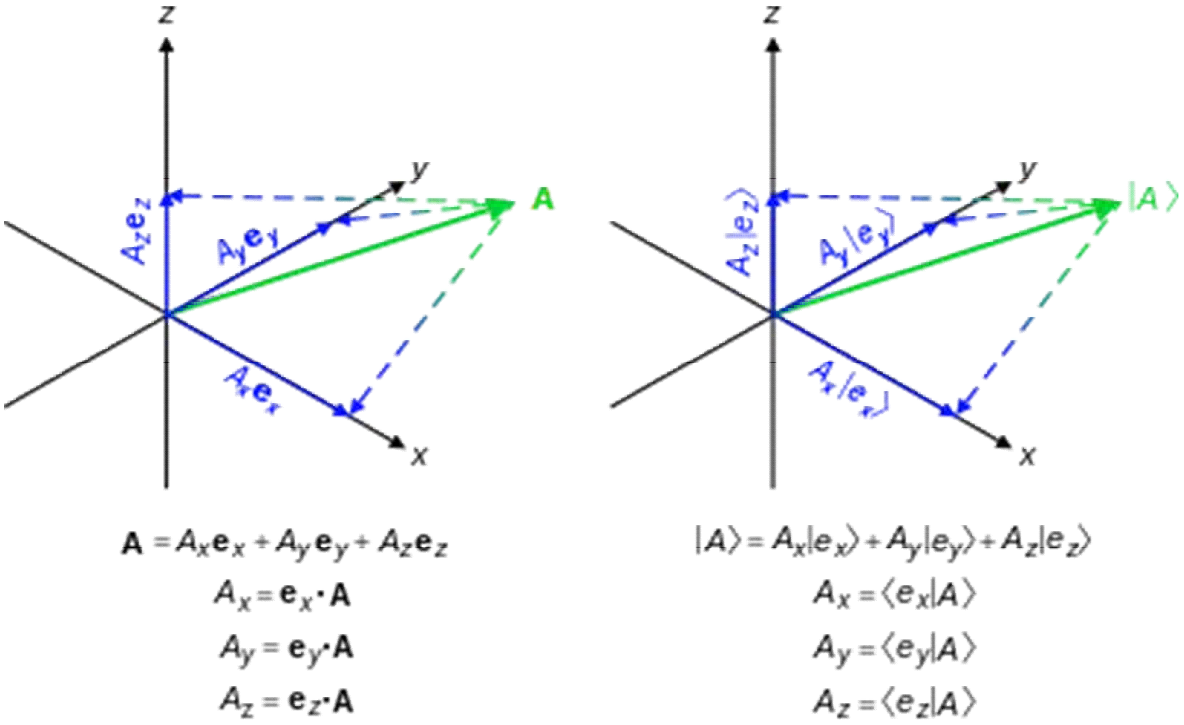

A Hilbert space, may emiological,moderate resolution, imaged, capture point, riverine tributary *S. damnosum* s.l., trailing vegetation, iteratively interpolative, decompositional, signature-oriented, capture point, vulnerability, forecast, regression, model. A Hilbert space is a vector space with an inner product such that the norm defined as a complete metric space[24].The residuals extended the methods of vector algebra and calculus from the two-dimensional Euclidean plane and 3-D space to spaces with any finite or infinite number of dimensions. Unmixed, auto-probabilistically autoregressively explanatively varying and constant, eco-epidemiological, uncertainty-oriented, orthogonally decomposable, eco-georeferenceable eco-geographic bio-geophysical endmember observational, predictors rendered from an imaged, 5m, RapidEye™, discontinuously, seasonally canopied, geo-spectrotemporally, geospatially fractionalized, sparsely shaded and hyperproductive, immature *Simulium* habitats in Hilbert space, with a high density of clustered foci, (i.e., positively autocorrelated, seasonal, immature hyperproductive, capture point eco-geolocations) may aid in optimally statistically targeting hot spots using robust multivariate, explanatively, orthogonally decomposeable, multi-forecastable, fractionalized, spatial filter, synthetic, orthogonal eigenvector. The resulting proxy signature file may be non-

parameterically optimally heuristically employed as the input for a classification [e.g., the ML Classify function] which may be subsequently rendered using an unsupervised classification raster in ArcGIS (see Figure 17). A Hilbert space is a vector space $H$with an inner product $\langle f, g\rangle$such that the norm defined by $|f| = \sqrt{\langle f, f\rangle}$ which can turns Hinto a complete metric space.

Figure 17. Discrete components A_k of a complex vector $|A\rangle = \sum_k A_k|e_k\rangle$, which belongs to a countably infinite-dimensional Hilbert space in a lagged model where countably infinitely eco-georefernceable, narrow tributary *S. damnosum* s.l. forecasted habitat k values and basis vectors $|e_k$ and maximum likelihoods occur in geospace

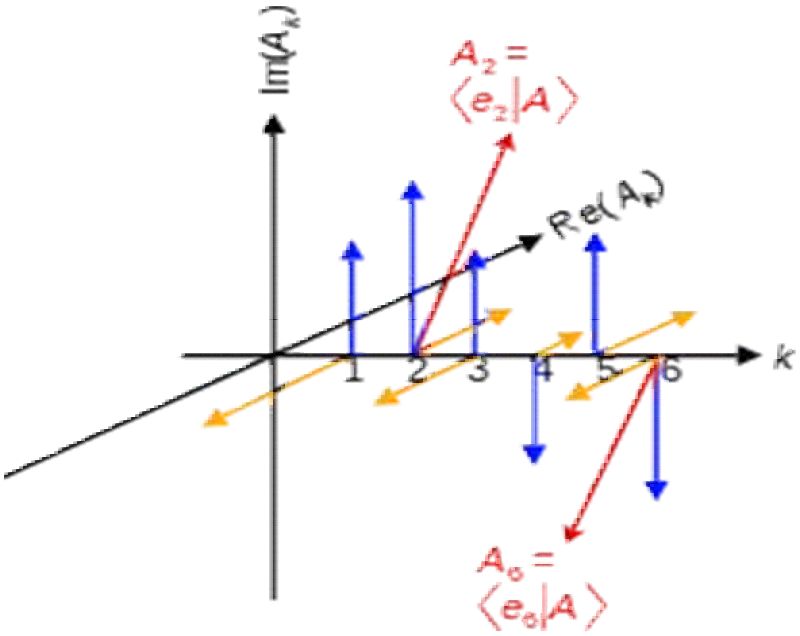

Maximum likelihood or Bayesianistic estimation inferences can account for explanative, geo-spectrotemporal, geospatially quantitable dependencies in a parametric framework, whereas recent spatial filtering approaches focus on non-parametrically removing endmember autocorrelation. Thus, a semiparametric spatial filtering approach in ArcGIS can optimally explanatively decompose a geo-spectrotemporal, seasonally eco-georeferenceable, geosamplable, hyperproductive, immature, orthogonalizable, seasonal, African, narrow, riverine, tributary *S. damnos*um s.l., trailing vegetation, sparsely shaded, discontinuous, infrequently canopied, turbid water, capture point, immature habitat, employing 5m, RapidEye™, explanatively decomposable, uncoalesced, fractionalized endmember, eigenvector dataset of illuminative, moderate resolution, wavelength, frequency-oriented,, transmittance emissivities. The decompositional algorithm would optimally allow an ecologist, entomologist or other researcher to deal explicitly with probabilistic, autoregressive and explanatively uncoalescable, residualized, sub-mixel, frequency-oriented, probabilisic, uncertainty estimates. This decomposable, endmember algorithmic iterative process could employ spatially lagged, autoregressive model plots

Bayesianistic probabilistic, eigenvector estimation inferences can account for spatial dependencies in a parametric framework whereas recent spatial filtering approaches in

ArcGIS focus on non-parametrically removing spatial endmember autocorrelation. Thus, a semiparametric spatial filtering approach for optimally orthogonally explanatively decomposing a geo-spectrotemporal, seasonally decomposable, explanatively eco-georeferenceable, geospatially, geosampled, hyperproductive, immature, orthogonally decomposable, seasonally eco-georefernceable, narrow, riverine, tributary *S. damnos*um s.l., trailing vegetation, sparsely shaded, discontinuous, infrequently canopied, turbid water, capture point, immature habitat. The unmixed 5m, RapidEye™, explanatively decomposable, fractionalized, endmember eigenvector dataset of illuminatively fractionalized, wavelength, transmittance emissivities in ArcGIS may allow an ecologist, entomologist or other researcher to deal explicitly with probabilistic, autoregressive and explanatively uncoalescable, fractionalized, residual, endmember, frequency-oriented, eigenvector uncertainties. This decomposable, endmember algorithmic, iterative,interpolative process could employ spatially lagged, autoregressive models or simultaneous autoregressive spatial model log-graphs in Hilbert space, in ArcGIS (see Figure 18).

Figure 18. Hypothetical continuous components $\psi(x)$ of a complex vector $|\psi\rangle = \int dx\, \psi(x)|x\rangle$, belonging to *S. damnosum* s.l. habitat infinite-dimensional Hilbert space log-graph where there are infinitely many x values and basis vectors $|x$ in geospace

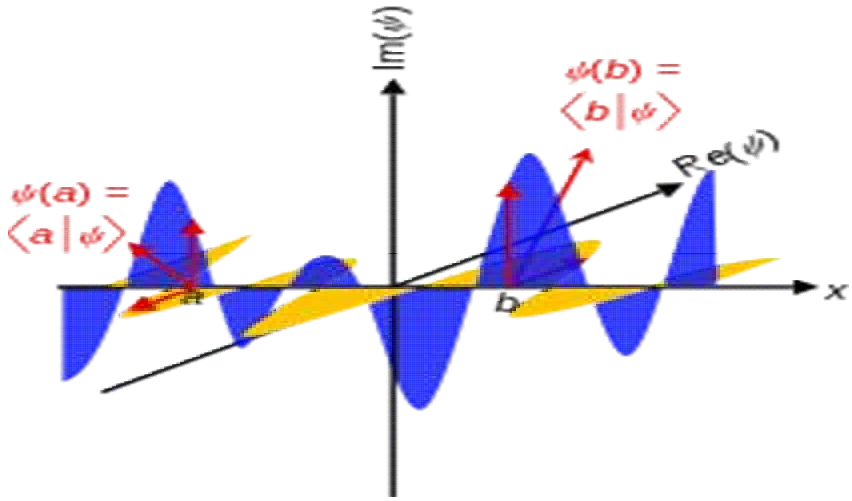

Spatial externalities play a central role in the recent emergence of "spatial thinking"in the mainstream. For example, in economics, greatly increased attention is being paid to models of social interaction, which introduce dependence among actors in a system. Similarly, in sociology, the renaissance of the "Chicago School"–type analyses of neighborhood processes has led to the introduction of formal notions of spatial spillovers and dependence. Empirical verification of such spatial externalities, measurement of their strength and range, requires the specification and estimation of spatial autoregressive econometric models.

The standard taxonomy of spatial autoregressive lag and error models commonly applied in econometrics is perhaps too simplistic for constructing explanatively robust, spatial eco-georeferenceable, eco-epidemiological, geo-spectrotemporal, geospatially, geosampled, seasonally, ecogeoreferenceable, hyperproductive, riverine, habitat, immature *S. damnosum*

s.l., tributary, trailing vegetation, sparsely shaded, discontinuously canopied, turbid water, explanatively uncoalesced, iteratively interpolative, capture points. The endmember, vulnerability forecast, time series, eigenvector model residual projections may leave out interesting possibilities for mechanisms through which phenomena or actions at a given eco-epidemiological, eco-georeferenceable, hyperproductive, capture point, habitat geolocation affect infrequently canopied, interpretively iteratively, interpolative properties at other seasonally explanative, hyperproductive, immature habitat, eco-georeferenceable geolocations.

An alternative approach may develop a simple taxonomy of formal models of spatial externalities in cross-sectional geo-spectrotemporally, geospatially elucidatively uncoalesced, narrow, African, riverine tributary, *S. damnosum* s.l., immature habitat, endmember, discontinuous, sporadically canopied, regressable data. The primary emphasis would be on distinguishing between a global and a local range of quantitable, dependence in an explanative, endmember eigenvector, seasonally hyperproductive, riverine, habitat, immature, *S. damnosum* s.l., trailing vegetation, sparse shaded, discontinuous, infrequently canopied, fractionalized, sub-mixel, turbid water, eco-epidemiological, eco-georeferenceable, seasonal, capture point, uncoalesced, moderate resolution, wavelength, frequency-oriented,, transmittance, vulnerability, forecast, model estimator and the way in which this translates into the incorporation in a regression specification of spatially lagged dependent variables (e.g., spatially lagged explanatory variables and spatially lagged error terms).

As in a non-parametric spatial filtering approach, a specific subset of eigenvectors from a transformed spatial link matrix in ArcGIS may be parsimoniously employed to qualitatively quantitate, intuitively forecastable dependencies amongst disturbances within a fractionalized, time series, endmember, eigenvector, metaheuristically optimizable, regression-related, forecast-oriented, vulnerability model. However, the optimal subset in an empirical dataset of proposed explanative, filtering discontinuous, trailing vegetation, heterogeneously canopied, explanatively uncoalesced, *Simulium,* turbid water, African, narrow, riverine, tributary, immature habitats and their fractionalized, moderate resolution, wavelength transmittance, forecasting, vulnerability, model, unbiased LULC estimators.These elucidatively, optimally parameterizable, covariates may be more intuitively diagnosed for erroneous coefficients by an objective function that minimizes spatial autocorrelation in ArcGIS rather than maximizes a model fit. The proposed objective function has the advantage that it may lead to a robust and smaller subset of selected orthogonal eigenvectors. An application of the proposed eigenvector spatial filtering approach may be applicable to forecasting, heuristically optimizable, geo-spectrotemporally, geospatially uncoalesced eco-epidemiological, grid-stratfiiable, moderate resolution, LULC datasets of orthogonally explicative, fractionalized, 5m, imaged, RapidEye^{TM}, *S. damnosum* s.l. immature habitat, endmember, eigendecomposed, signatures for robustly parsimoniously, interpretively, iteratively,elucidatively interpolating the proxy expositive variables for identifying unknown, un-geosampled, prolific and eco-georeferenceable, capture point, trailing vegetation, turbid water, sparsely shaded, immature, riverine habitats in an narrow tributary, African, agro-village complex.

Consider the familiar linear regression model $y = X\beta+e$, where y would be an n by 1 vector of an explanatorial, empirical regressable dataset of geo-spectrotemporally, uncoalescable, discontinuously canopied, explanatively , eco-georefernceable, sparsely shaded, capture point, immature habitat, narrow African riverine tributary observations on a dependent variable, X in an n by k matrix of observations employing exogenous variables,

with an associated *k*by 1 vector of regression coefficients. In this paradigm an *n* by 1 vector would be the random disturbance term. An ecologist, entomologist or other researcher could then consider the error terms in isolation from the other elements in the seasonally explanative, eco-epidemiological, decomposable, capture point, hyperproductive, immature, riverine, habitat,eco-georeferenceable, *S. damnosum* s.l., trailing vegetation, sparsely shaded, forecast-oriented, vulnerability model, residual specification. In so doing, the error variance-covariance matrix, would then express spatial covariance when the off-diagonal elements are nonzero in accordance with a given spatial structure or "spatial ordering" of the geo-spectrotemrpoally uncoalesced, 5m, proxy biosignature, elucidative variables. The spatial ordering could then optimally specify those pairs of eco-georferenceable, explicative, seasonally hyperproductive, iteratively interpolative capture point, immature, habitat geolocations for which the covariance will be nonzero. One way to obtain this structure is directly (referred to in ArcGIS literature as direct representation), by specifying the covariance as a function of Euclidean distance measurements that separates any two temporally dependent, geo-spectrotemporal, geosptialized, eco-geographic, forecastable habitat geolocations[22].

A non-linear explanatorial quantitation may be optimally conducted parsimoniously in an ArcGIS cyberenvironment using Geostatistical Analyst ™. The robustifiable enedmember 5m, proxy biosignature, elucidative model would require the *S. damnosum* s.l. eco-epidemiological habitat specification to be optimally a smooth, distance, decay function and a parameter space that would ensure a positive definite, variance, covariance matrix. Intuitively, the covariance matrix would generalizes the notion of covariance to multiple seasonally explanatively spatially diagnosed, eco-epidemiological, capture point, hyperproductive, African, narrow riverine, tributary immature, eco-georeferenceable, explanative, *S. damnosum* s.l., trailing vegetation, sparsely shaded, discontinuously, infrequently canopied, immature habitat, moderate resolution, uncoalesced dimensions in ArcGIS

As an example, let's consider two vectors $X = [x_1, x_2]^T$and $Y = [y_1, y_2]^T$ for a hyperporductive, eco-georfernced, *S. damnsoum* s.l. immature habitat. There are four covariances to consider: $x_1$with y_1, $x_1$with y_2, $x_2$with y_1, and $x_2$with y_2. These variances cannot be summarized in a scalar. Of course, a 2×2 matrix in ArcGIS is the most natural choice to describe the covariance: the first row containing the covariances of $x_1$with $y_1$and y_2, and the second row containing the covariances of $x_2$with $y_1$and y_2. Because the covariance of the *i* th random variable with itself is simply that random variable's variance, each element on the principal diagonal of the covariance matrix would be the variance of each of the elements in the vector. Because $Covar(x_i, x_j) = Covar(x_j, x_i)$, every covariance matrix is also symmetric. In addition, every covariance matrix is positive semi-definite.

In linear algebra, a symmetric *n* × *n* real matrix $M$is said to be positive definite if the scalar $z^{\mathrm{T}} M z$is positive for every non-zero column vector $z$of $n$real numbers(e.g., eco-georeferenceable, explanatively, orthogonally decomposed, uncoalesced, hyperproductive, *S. damnosum* s.l. immature, capture point, moderate resolution, wavelength, transmittance, frequency-oriented emissivities) . Here z^{T}would denote the transpose of z.More generally, an *n* × *n* Hermitian matrix M in ArcGIS is positive definite if the scalar $z^* M z$is real and positive for all non-zero column vectors $z$of $n$complex numbers. Here z^*would denote the conjugate transpose of z.The negative definite, positive semi-definite, and negative semi-

definite matrices would be optimally defined in the same way in ArcGIS, except that the expression $z^{\mathrm{T}}Mz$or $z^{*}Mz$is required to be always negative, non-negative, and non-positive, respectively.Positive definite matrices are closely related to positive-definite symmetric bilinear forms (or sesquilinear forms in the complex case), and to inner products of vector spaces. Some authors use more general definitions of "positive definite" that include some non-symmetric real matrices, or non-Hermitian complex ones [25].

In probability theory and statistics, a covariance matrix (also known as dispersion matrix or variance–covariance matrix) is a matrix whose element in the *i*, *j* position is the covariance between the *i* th and *j* th elements of a random vector (that is, of a vector of random variables). Let *U* and *V* be two independent, illuminative, geo-spectrotemporally, geospatially uncoalesced, trailing vegation, discontinuous, infrequently, canopied, sparsely shaded, eco-epidemiological, eco-georeferenceable, elucidative,seasonally hyperproductive, explanative, *S. damnosum* s.l. habitat, uncoalesced, 5m, Rapid Eye ™ randomized, seasonal variables, and consider two new random variables *X* and *Y* of the form $X = aU + bV, Y = cU + dV,$where *a, b, c, d*, are some scalars. Each one of the random variables *X* and *Y* in the model would be normal, since it the residual eco-epidemiological, wavelength, transmittance, frequency forecasts would be rendered from a function of the independently normalized , random variables. Further, because *X* and *Y* would be explanative, geo-spectrotemporal, geospatial, immature, habitat, uncoalesced, eco-epidemiological, capture point, the functions of the same two independent normalized random variables and their joint probability density function (PDF) would take a special form, known as the bivariate normal PDF.

In probability theory and statistics, the multivariate normal distribution or multivariate Gaussian distribution, is a generalization of the one-dimensional (univariate) normal distribution to higher dimensions. In probability theory, the normal (or Gaussian) distribution is a very common continuous probability distribution. Normal distributions are important in statistics and are often used in the natural and social sciences to represent real-valued random variables whose distributions are not known[24]. In its most general form, under some conditions (which include finite variance), can generate averages of random variables independently drawn from independent distributions converge in distribution to the normal, that is, become normally distributed when the number of random variables is sufficiently large. The normal distribution is sometimes informally called the bell curve. However, many other distributions are bell-shaped (such as Cauchy's, Student's, and logistic) [24]. The terms Gaussian function and Gaussian bell curve are also ambiguous because they sometimes refer to multiples of the normal distribution that cannot be directly interpreted in terms of probabilities

Physical quantities processes (e.g., trailing vegation, explanatively coalesceable, discontinuously canopied, sparsely shaded, eco-epidemiolgical, seasonally hyperproductive, *S. damnosum* s.l. habiat, vulnerability, eco-epidemiological, eco-georeferenceable, forecast model, measurement errors)that are expected to be the sum of many independent endmember eigenvector often have distributions that are nearly normal. Jacob et al. [22] devised a standard normal distribution using a dataset of optimally parameterized, uncoalesced Rapid Eye ™ 5m, *S. damnosoum* s.l. African riverine, narrow tributary, agro-village, pre-flooded, hyperproductive independent, eco-georeferenceable, capture point, paramterizable, immature habitat, covariate coefficient values where μ=0 and σ=1. The forecast were described by the probability canopy, density valaues employing: $\phi(x) = \frac{e^{-\frac{1}{2}x^2}}{\sqrt{2\pi}}$ If the probability density function of a random variable *X* is given as $f_X(x)$, it is possible) to calculate the probability

density function of some variable $Y = g(X)$[24]. This LULC "change of variable" was used to generate a random variable of arbitrary shape $f_{g(X)} = f_Y$ using a known random number generator in ArcGIS. Since the function g was monotonic, then the resulting density function of the immature capture point was $f_Y(y) = \left|\frac{d}{dy}(g^{-1}(y))\right| \cdot f_X(g^{-1}(y))$.

In calculus a monotonic function (or monotone function) is a function between ordered sets that preserves the given order[24] .In the habitat model g^{-1} denoted the inverse function. In mathematics, if a function $f(x) = y$is injective, exactly one function $g(y)$will exist such that $g(y) = x$, otherwise no such function will exist. In calculus, a function defined on a subset of the real numbers with real values is called monotonic if and only if it is either entirely non-increasing, or entirely non-decreasing. That is, as per Fig. 1, a function that increases monotonically does not exclusively have to increase, it simply must not decrease. The function $g(y)$is called the inverse function of $f(x)$because it "reverses" $f(x)$; that is to say $g(f(x)) = x$ This followed from the fact that the probability contained in a differential hypeporductive capture point area must be invariant under change of variables. That is, the model was metaheuristically optimally quantized as $|f_Y(y)\,dy| = |f_X(x)\,dx|$, or $f_Y(y) = \left|\frac{dx}{dy}\right| f_X(x) = \left|\frac{d}{dy}(x)\right| f_X(x) = \left|\frac{d}{dy}(g^{-1}(y))\right| f_X(g^{-1}(y)) = \frac{f_X(g^{-1}(y))}{|g'(g^{-1}(y))|}$. The factor $1/\sqrt{2\pi}$in this expression ensured that the total eco-epidemiologically quantitated discontinuous, infrequently canopied, capture point, immature habitat area under the curve $\phi(x)$ was equal to one. A map $f: X \to Y$ is said to be monotone if each of its fibers is connected i.e. for each element y in Y the (possibly empty) set $f^{-1}(y)$ is connected. A monotone function is also called isotone, or order-preserving. The dual notion is often called antitone, anti-monotone, or order-reversing. Hence, an antitone function f satisfies the property$x \leq y$ implies $f(x) \geq f(y)$,for all x and y in its domain. The composite of two monotone mappings is also monotone. The ½ in the exponent confirmed that the distribution had a unit variance and therefore also unit standard deviation. A function is *unimodal* if it is monotonically increasing up to some point (the *mode*) and then monotonically decreasing.This function was symmetric around x=0, where it attained its maximum value $1/\sqrt{2\pi}$; and had an inflection points at +1 (see Figure 19).

Figure 19 Propagation of uncertainty fitting in an eco-epidemiological, explanative, *S. damnosum* s.l. hyperendemeic, narrow riverine tributary foci, eco-geopredictive, least square normalized regression map of Sarakawa agro-village complex in Togo.

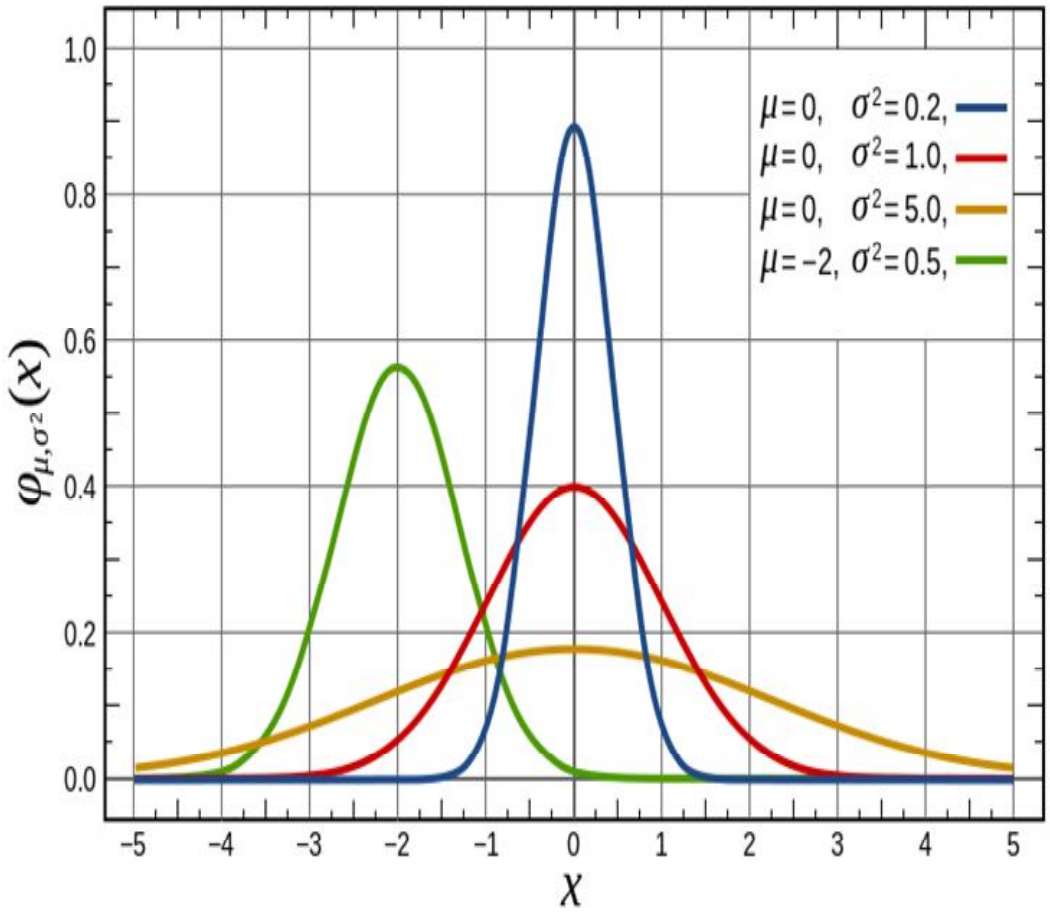

One possible definition for a robust , Rapid Eye ™ 5m, independent trailing vegetation, geo-spectrotemporally geosptatially uncoalesceable, discontinuously canopied, sparsely shaded, eco-epidemiolgical, eco-georeferenceable, explanatively seasonally hypeproductive, eco-georefernceable, riverine, tributary, *S. damnosum* s.l. habiat, eco-epidemiological, forecast vulnerability, model is that a random vector be *k*-variate normally distributed, but only if every linear combination of its *k* components has a univariate normal distributio (see Figure 16). Its residual importance would then emphatically be optimally derived mainly from the multivariate central limit theorem. The multivariate normal distribution is often used to describe, at least approximately, any set of (possibly) correlated real-valued random variables each of which clusters around a mean value. Jacob et al. [22] employed a bivariate normal PDF for robustly parsimoniously quantitating an empirically regressed dataset of geo-spectrotemporally, geospatially, eco-georeferenceable, uncoalesced, trailing vegation, Precambrain rock and riffle water sub-meter resolution mixel properties in Togo (see Figure 20).

Figure 20 Forecast-oriented, eco-epidemiological, discontinuously canopied, sparely shaded, eco-georefernceable, fractionalized, oviposition, PDF model sub-meter resolution, *S. damnosum* s.l. habiat wavelength, parameter estimators geosampled in as Sarakawa narrow riverine agro-village complex in Togo.

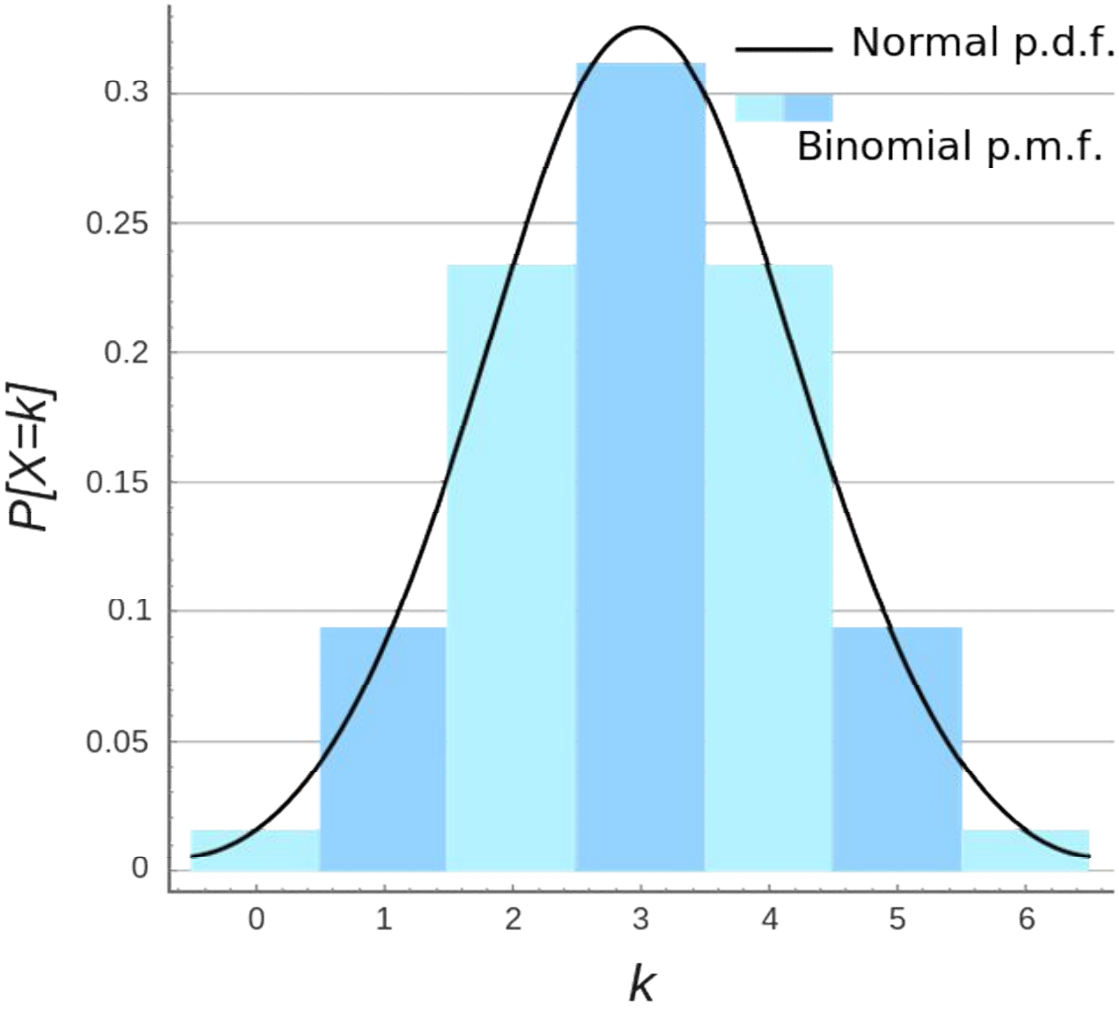

In the PDF, quantiation of a datatset of metaheursitically optimizable, explanatively continuous, randomized, geo-spectrotemporally, geospatially uncoalesced Rapid Eye ™ 5m, riverine, tributary, *S. damnosoum* s.l., African riverine,agro-village, pre-flooded, hyperproductive independent, eco-georeferenceable, capture point, immature habitat, eco-epidemiological parameterized,covariate coefficients would render a function that describes the relative likelihood for the random variable to take on a given value. In Jacob et al. [22], the probability of this random, eco-georferenceable, immature habitat capture point, eco-epidemiological, seasonally hyperproductive, geosampled dataset of geo-spectrotemporally regressed endmember variables falling within a particular range of values was given by the integral of the variable's density over that range—that is, it was given by the area under the density function but above the horizontal axis and between the lowest and greatest values of the range in the model distribution. The PDF was nonnegative everywhere, and its integral over the entire space was equal to one.

The normal distribution is the only absolutely continuous distribution whose cumulants beyond the first two (i.e., other than the mean and variance) are zero[24]. It is also the continuous distribution with the maximum entropy for a specified mean and variance. The normal distribution is a subclass of the elliptical distributions. The normal distribution for an ecogeoreferenecable, trailing vegetation, turbid water, seasonal, hyperproductive, *S. damnsoum* s.l. discontinuous canopied, seasonal capture points is symmetric about its mean,

and is non-zero over the entire real line[22]. As such, it may not be a suitable model for variables that are inherently positive or strongly skewed, such as changing covariance weightages of an explicative, regression-related parameterizable, geo-spectrotemporally uncoalesced, eco-georefernceable, capture point. Such variables may be better described by other distributions, such as a bivariate Gaussian PDF , eco-epidemioloigcal, forecast, vulnerability model (see Figure 21).

Figure 21 A bivariate Gaussian probability density function centered at (0, 0) in a eco-epidemiological, *S. damnosum* s.l., trailing vegetation, sparsely shaded, riverine tributary, agro-village complex capture point,,hyperproductive, foci in Burkina Faso with covariance matrix

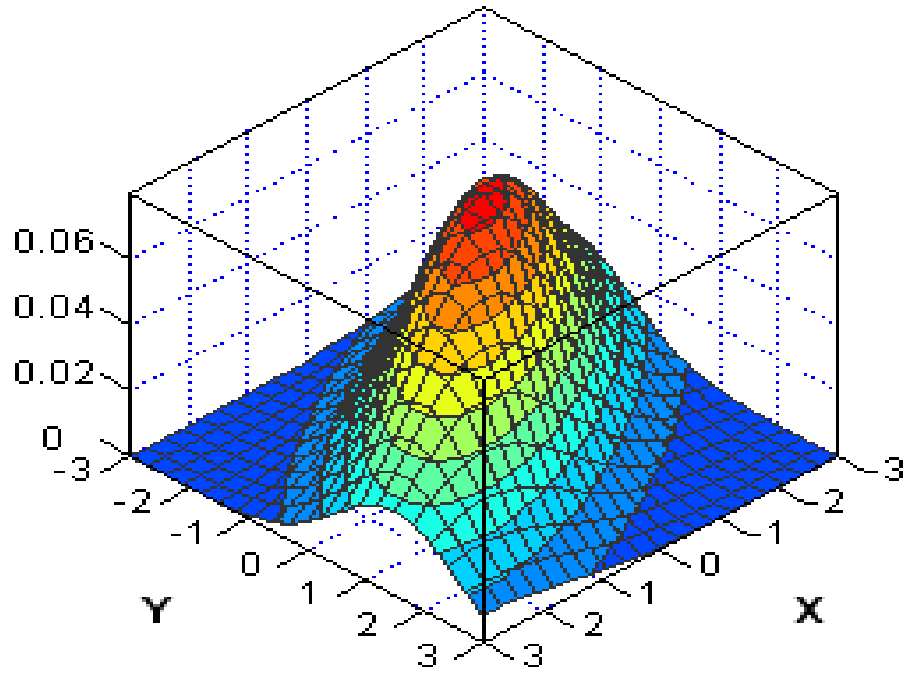

The box plot in ArcGIS is a quick way of examining one or more sets of data graphically. Box plots may seem more primitive than a histogram or kernel density estimate but they do have some advantages. Jacob et al. [22] employed as kernel density estimation (KDE) is a non-parametric way to estimate the PDF of a random variable for optimally determining unknown, un-geosampled, African, narrow riverine tributary, seasonally hypeproductive, *S. damnsoum* s.l. habitats in ArcGIS. Kernel density estimation is a fundamental data smoothing problem where inferences about the population are made, based on a finite data sample[24]. Let (x_1, x_2, …, x_n) be an independent and identically distributed sample drawn from some distribution with an unknown density f in a regressable ArcGIS dataset (e.g., uncoalesced, Rapid Eye ™ 5m eco-georferenceable, *S. damnsoum* s.l. discontinously canopied, trailing vegetation, sparsely shaded, turbid water,immature habitat, capture point, seasonal, forecast, vulnerability model endmember eigenvectors). the kernel density estimator would be $\hat{f}_h(x) - \frac{1}{n}\sum_{i=1}^{n} K_h(x - x_i) - \frac{1}{nh}\sum_{i=1}^{n} K\left(\frac{x - x_i}{h}\right)$, where $K(\bullet)$ is the kernel — a non-negative function that integrates to one and has mean zero — and $h > 0$ is a smoothing parameter (i.e.,bandwidth). A kernel with subscript h is called the scaled kernel and defined as $K_h(x) = 1/h\ K(x/h)$[24]. Intuitively, a ecologist, entomologist or oher researcher could t choose

h as small as the geosampled uncoalesced, empirical dataset of the trailing vegetation, discontinuous, infrequently canopied, turbid water, sparsely shaded, *S. damnosum* s.l. immature capture point, hyperproductive, African, agro-village complex, narrow riverine, tributary data allows; however, there will always be a trade-off between the bias of the estimator and its variance.

In ArcGIS non-parametric statistics, a kernel is a weighting function employable in non-parametric estimation techniques. Kernels are employed in kernel density estimation to estimate random variables' density functions, or in kernel regression to estimate the conditional expectation of a random variable[24]. Kernels are also used in time-series, in the use of the periodogram to estimate the spectral density where they are known as window functions in ArcGIS. The bandwidth of the kernel is a free parameter which exhibits a strong influence on the resulting estimate. To illustrate its effect, we take a simulated random sample from the standard normal distribution (plotted at the blue spikes in the rug plot on the horizontal axis). The grey curve is the true density (a normal density with mean 0 and variance 1). In comparison, the red curve is *undersmoothed* since it contains too many spurious data artifacts arising from using a bandwidth h = 0.05, which is too small An additional use is in the estimation of a time-varying intensity for a point process where window functions (kernels) are convolved with time-series ArcGIS-derived data. A range of kernel functions are commonly used: uniform, triangular, biweight, triweight, Epanechnikov, normal, and others

In Jacob et al. [22] the Epanechnikov kernel tabulated in an ArcGIS/SAS cyberenvironment was optimal for metaheusitically, qualitatively quantitating a geo-spectrotemporally, geospatially uncoalesced, dataset of hyperproductive, *S. damnsoum* s.l., forecast, vulnerability model-related, fractionalized endmember, moderate resolution, expositively parameterized, covariate, eigenvector Rapid Eye^{TM} estimators geosampled in Burkina Faso, in the mean square error sense for (see Figure 17). The kernel of a reproducing kernel Hilbert space is useable in the suite of techniques known as kernel methods to perform tasks such as statistical classification, regression analysis, and cluster analysis on data in an implicit space[24]. In functional analysis (a branch of mathematics), a reproducing kernel Hilbert space (RKHS) is a Hilbert space of functions in which point evaluation is a continuous linear functional [http://mathworld.wolfram.com/html]. Roughly speaking, this meant that if two eco-georferenceable, explanative , seasonal hyperproductive, capture point, *S. damnsoum* s.l., forecast, functions f and g in the RKHS were close in norm,(i.e., $||f-g||$ is small, then f and g were also pointwise close, and $|f(x)-g(x)|$ was small for all x. The quantated means in the model was $K(x) = \phi(x)$, where ϕ was the quantitable standardized, normalized, density function .A standard normal 5m, endmember wavelength, *S. damnosum* s.l. habitat, emissivity, frequency-related, normalized distribution with zero mean ($\mu = 0$) and unit variance ($\sigma^2 = 1$)was rendered by the PDF and a distribution function $P(x)$ which was equivalent to $\frac{1}{\sqrt{2\pi}} e^{-x^2/2}$, $D(x)=\frac{1}{2}\left[\operatorname{erf}\left(\frac{x}{\sqrt{2}}\right)+1\right]$over the domain $x \in (-\infty, \infty)$.(See Figure 22). The explanatorial, kernel model, residual forecasts in ArcGIS inclued the mean, variance, skewness, and kurtosis excess which was given by μ=0, σ^2=1, γ_1=0, γ_2=0.The first quartile of the standard normal distribution occurred when $D(x) = 1/4$, which was $x_{1/4}=-\sqrt{2}\ \operatorname{erf}^{-1}\left(\frac{1}{2}\right)=-0.67448975019\ldots$Skewness is a measure of symmetry, or more precisely, the lack of symmetry while kurtosis is a measure of whether the data are heavy-tailed or light-tailed relative to a normal distribution[24].

Figure 22. Kernel density estimation of 50 normally distributed random log-transformed immature *S. damnsoum* s.l. validtion denssity counts employing different smoothed, 5m, Rapid Eye ™ bandwidths and their uncertainties for field verifying kriged geo-spectrotemporally uncoalesced, pre-flooded, trailing vegetation, discontinuous, infrequently canopied, turbid water immature seasoanlly hyperproductive capture point.

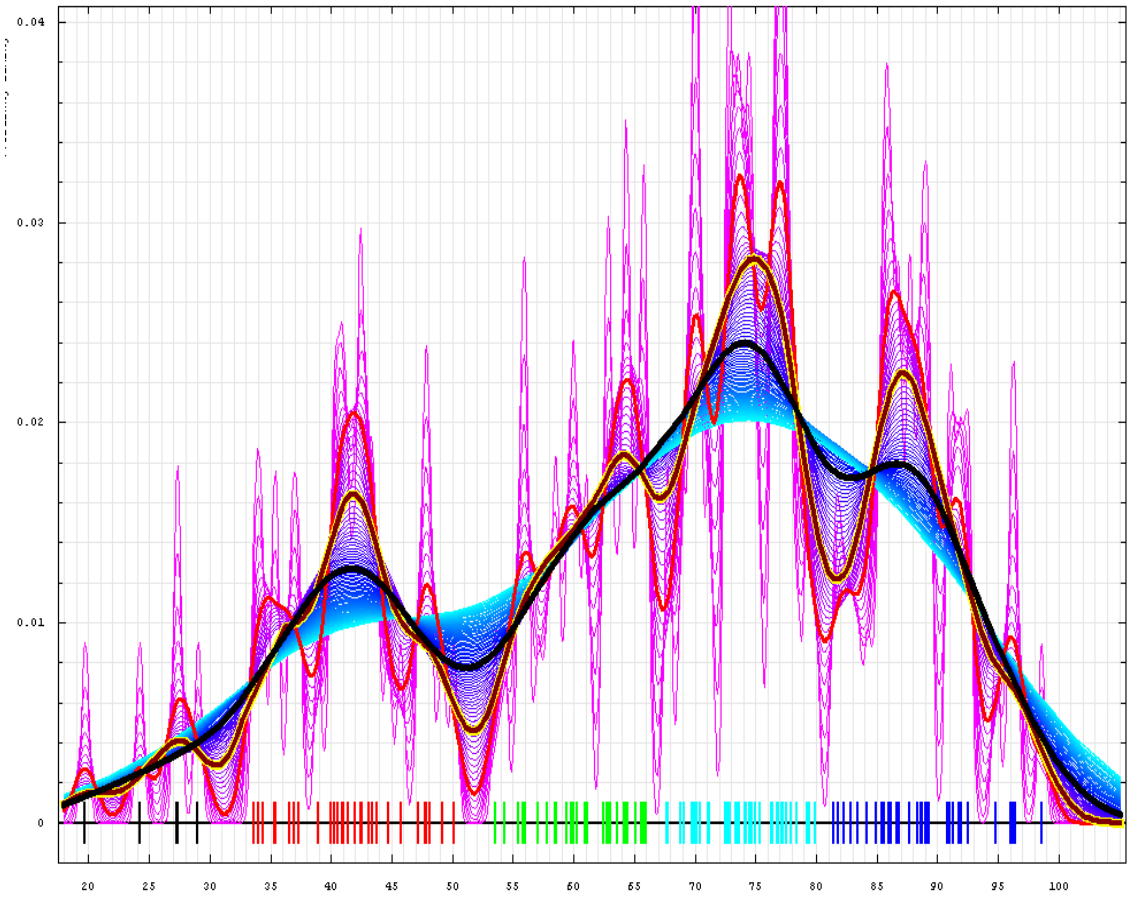

In Jacob et al. [22] descriptive statistics were derived using a box plot in ArcGIS. A boxplot is a convenient way of graphically depicting groups of numerical data through their quartiles in ArcGIS(www.esri.com) . Box plots had lines extending vertically from the boxes (i.e., whiskers) indicating variability outside the upper and lower quartiles[24] . Outliers were plotted as individual, *S. damnosum* s.l. habitat, explicative, eco-geographic, eco-cartographic points. The box plots were non-parametric. An outlier is defined as a data point that emanates from a different model than do the rest of the data [24]. The data appeared to come from a linear model with a given slope and variation except for the outlier which appeared to have been generated from the geospatial configuration of the data. Outlier detection is important for effective modeling(www.esri.com). If all the geosampled *S. damnosum* s.l. data here are included in a linear regression, then the fitted model will be poor virtually everywhere [24]. If an eco-georeferenceable, seasonally hyperproductive, trailing vegetation, turbid water,sparsely shaded, geo-spectrotemporal outlier is omitted from the fitting process, then the resulting fit will be excellent almost everywhere (for all capture points except the outlying point) displaying variation in samples of a geosampled *S. damnosum* s.l. habitat immature population without making any assumptions of the underlying statistical

distribution in ArcGIS. In Jacob et al. [22], the spacings between the different parts of the box indicated the degree of dispersion (spread) and skewness in the geo-spectrotemporally geosampled dataset, and also revealed geospatial endmember outliers. In addition to the capture points themselves, the ArcGIS model allowed visually estimating various L-estimators, notably the interquartile range, midhinge, range, mid-range, and trimean. Boxplots were drawn horizontally and vertically in ArcGIS of all quantiated prolific *S. damnosum* s.l. hyperproductive, narrow , tributray, agro-village complex in Burkina Faso (see Figure 23).

Figure 23. Boxplot and probability density functions of a normalized trailing vegetaion, discontinuously canopied, seasoanlly hyperproductive, *S. damnsoum* s.l. habitat distribution $N(0, \sigma^2)$.

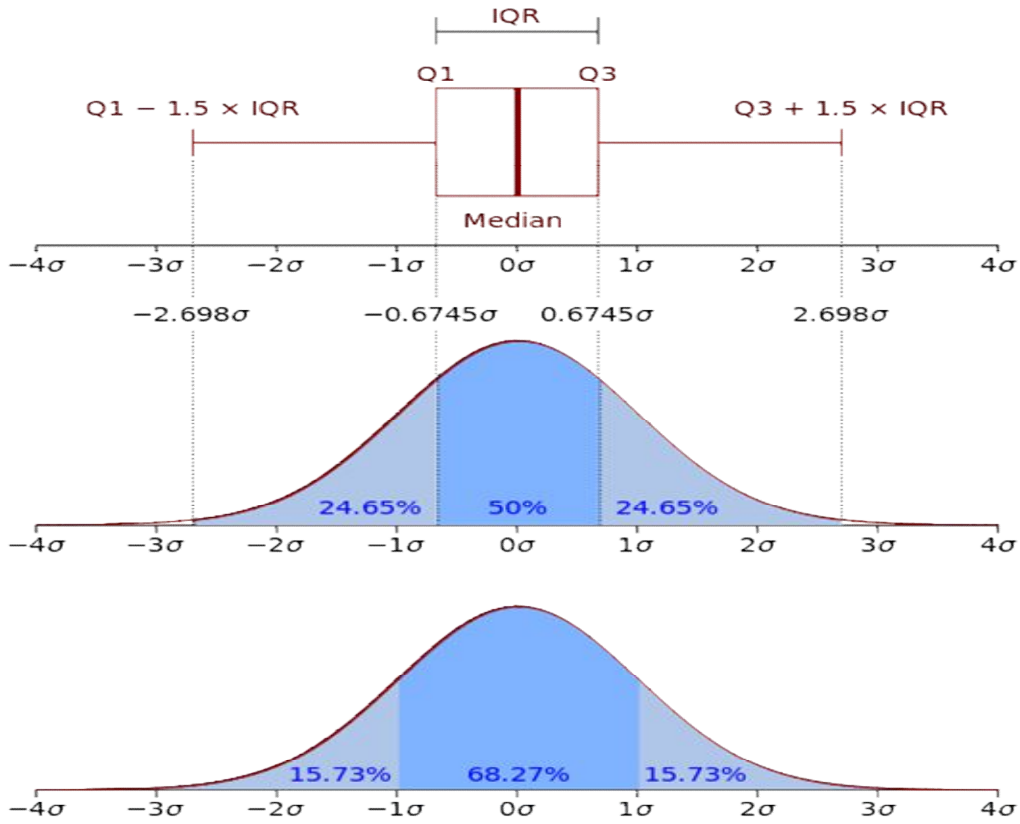

In Jacob et al. [22] the binomial distribution with the trailing vegetation, discontinuously canopied, sparsely shaded, parameters n and p was the discrete probability distribution of the number of successes in a sequence of n independent binary experiments, each of which yielded success with probability p. (see Figure 24).The binomial normalized distribution is the basis for the popular binomial test of statistical significance[24].The binomial distribution was used to model the number of successes in a sample of size n drawn with replacement from a geo-spectrotemporally uncoalesced, heuristically optimizable, Rapid Eye ™ dataset of elucidatively, eco-georeferenceable, trailing vegetation, turbid water, discontinuous, infrequently canopied, geospatially geosampled, *S. damnosum* s.l. agro-village, narrow tributary, complex ecosytem, capture point, hyperproductive

immature,habitat, population of size *N*. If the sampling is carried out without replacement, the draws are not independent and so the resulting distribution is a hypergeometric distribution, not a binomial one

Figure 24. A comparison of probability density functions in Jacob et al. [22], *p*(*k*) for the sum of different uncoalesced, geo-spectrotemporally, geospatially geosampled, *S. damnosum* s.l. , trailing vegetation, discontininuously canopied, immature, predicted immature, hypeproductive, habitats *n* to show their convergence to a binomial non-normalized distribution with increasing *n*, in accordance to the central limit theorem.

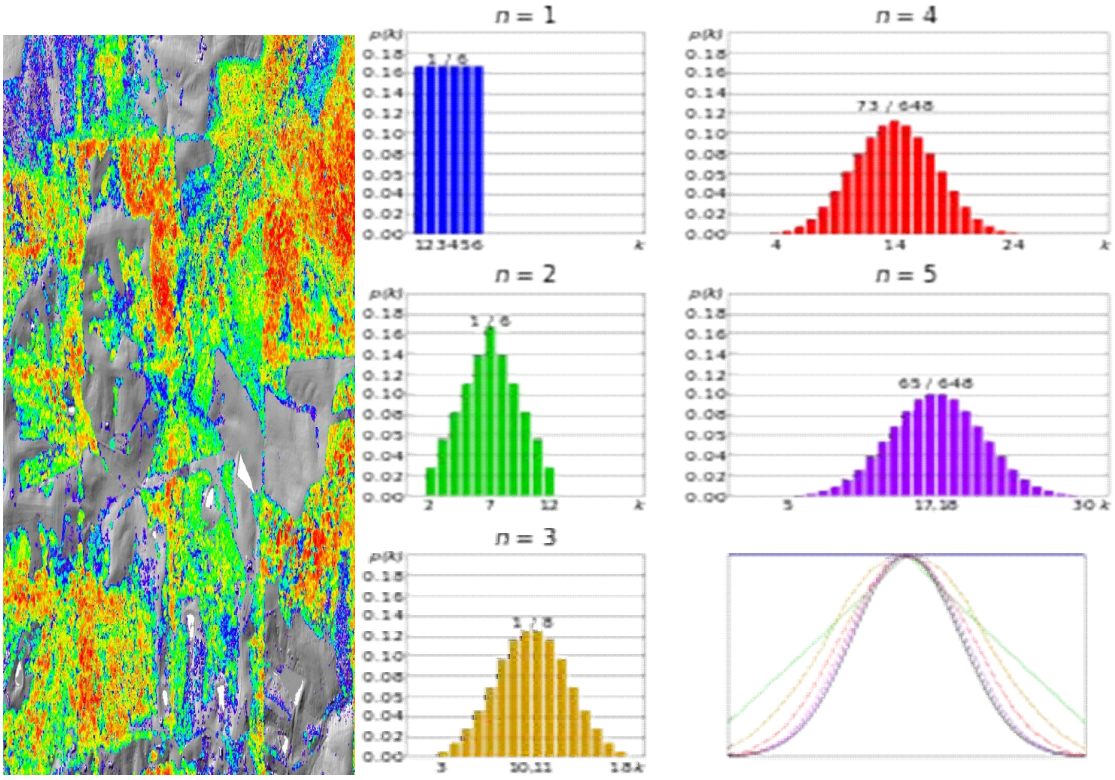

For *N* much larger than *n*, the *S. damnosum* s.l. habitat, normalized binomial distribution is a good approximation, and widely used sub-mixel
. In so doing, it was possible to see that when the sample size of the forecasted,explanative, hyperproductive, trailing vegetation, discontinuous canopied, sparsely shaded, *S. damnosum* s.l. habitat capture point increases, the mean distribution tend was more centered and with thinner tails. Binomial proportion confidence interval is a confidence interval for a proportion in a statistical population[24]. An important result about dimensions is given by the rank–nullity theorem for aeco-georferenceable *S. damnosum* s.l. linear maps. If F/K is a field extension, then F is in particular a vector space over K. Furthermore, since every F-vector space V is also a K-vector space in a S. damnsoum s.l. capture point , forecasting vulnerability paradigm the dimensions would related by the formula $\dim_K(V) = \dim_K(F) \dim_F(V)$. In particular, every complex vector space of dimension n encompassing all geospectrotemrpoally uncoalesced moderate resolution paramterizable varaibel would be areal vector space of a dimension 2n. Some simple forumals in ArcGIS may quantiate a real vector space with the cardinality of a base field whereby the cardinality would be the space itself. Hence, if V is a quanatitable vector spce in a trailing vegetation, discontinuoulsy canopied, turbid water, sparsely shaded, narropw tributra , agro-village complex, *S.*

damnsoum s.l., unmixed, proxy geospectrotemporal biosignature, then V would be a vector space over a field F . As such. denoting the dimension of V by dim V in these models would reveal If dim V is finite, then $|V| = |F|^{\dim V}$ or iIf dim V is infinite, then $|V| = \max(|F|, \dim V)$ in ENVI Jacob et al. [26] proportionally estimated a statistical sample which allowed for sampling errors to be mapped employing object-based, iteratrively interpolative, geo-classified *S. damnosum* s.l. Rapid Eye Tm 5m, fractoionaliozed radiance endmembers (see Figure 25)

Figure 25 A simulation with binomial distribution employing 0 and 1 with their means calculated for 6 canopied sparsely shaded geo-spectrotemporal geospatial seasonal, trailing vegetation, *S. damnosum* s.l. immature habitat geosampled leaf area canopy indices

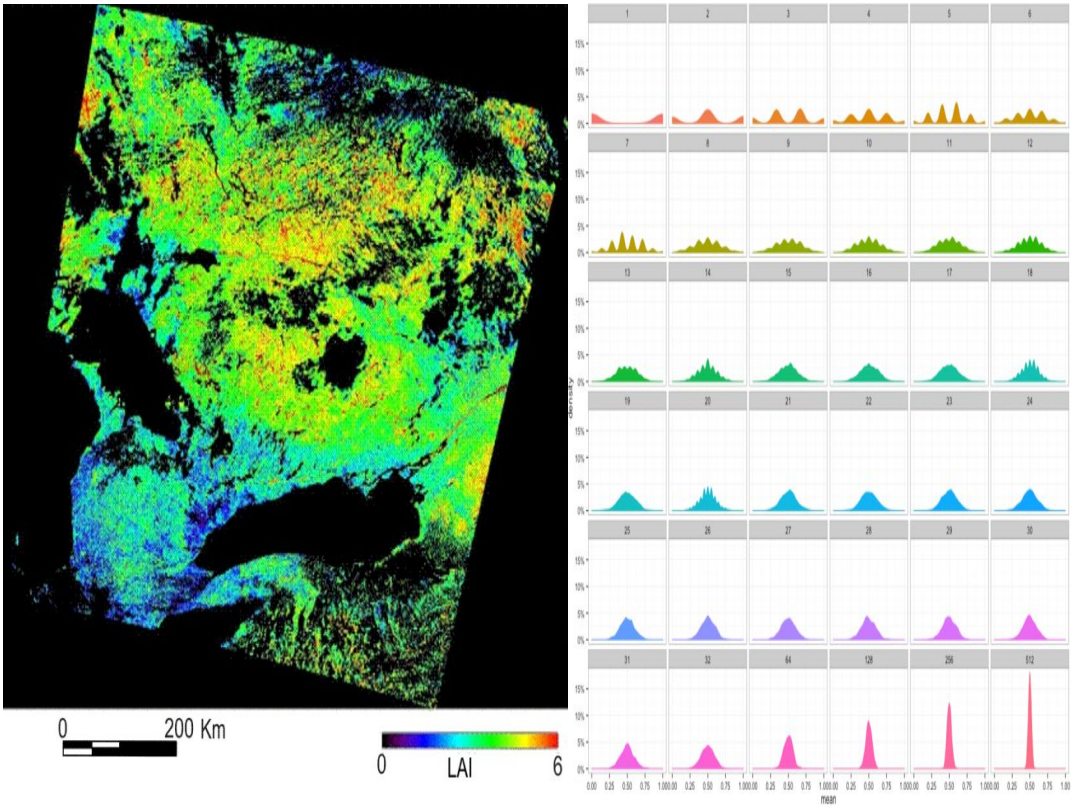

Alternatively, the precise nature of the distance decay function can be left unspecified in an eco-epidmeological, eco-georferenceable, trailing vegetation, discontinuously canopied, trailing vegetation, turbid water, narrow tributary, agro-village complex tributary, *S. damnsoum* s.l., decomposeable, immature, hyperproductive habitat, fractionalized, proxy signature, forecast, vulnerability, model and approximated by a step function, in a nonparametric fashion. For this model output to robustly identify unknown, un-geosampled, hyperproductive, narrow tributary, African, agro-village riverine, transmission foci, the nature of the spatial covariance would have to be be smooth and relatively constant in a small number of distance bands from which it can be estimated, as in Conley (1999). The

direct representation approach would require developing a general taxonomy that would apply to spillovers for all the variables in the model.

A second fundamental strategy for robustly quantitating a geo-spectrotemporally uncoalesced, heuristically optimizable, moderate resolution, dataset of elucidatively, eco-georeferenceable, trailing vegetation, turbid water, discontinuous, infrequently canopied, geospatially geosampled, *S. damnosum* s.l. agro-village, narrow tributary, complex ecosytem, capture point, hyperproductive immature, habitats is to obtain the spatial structure of the nonzero elements in the variance-covariance matrix in a trailing vegation, discontinuously canopied, sparsely shaded, 5m imaged, RapidEye™, fractionalized, *S. damnosum* s.l., habitat signature is by employing an indirect technique. This would be implementable when a spatial stochastic explanative process is specified that relates the value of a random variable at an eco-georeferenceable, seasonally explanative, eco-epidemiological, hyperproductive, *Similiuum*, capture point geolocations is geo-spectrotemporally geospatially related to the values of random variable at neighboring habitat geolocations. Instead of linking all pairs of the seasonally explanative, capture point, hyperproductive, immature, habitat observations through a distance decay function, the neighbors for each individual geolocation may be specified by means of a so-called spatial weights matrix. Spatial statistics integrate geospace and spatial relationships directly into their mathematics (e.g., quantiazation of geo-spectrotemporally geospatially uncoalesced, 5m imaged, RapidEye™, *S. damnsoum* s.l. immature habitat area, distance, length, or proximity) which may be optimally defined formally through spatial weights structured values which may be archived as a spatial weights matrix file. A spatial weights spatial weights matrix quantifies the spatial relationships that exist among uncoalesced, endmember features in an optimizable dataset or at least it can quantify conceptualizations of spatial decompositional sub-mixel relationships. While the physical format of the spatial weights matrix file may vary, the conceptual idea is a table with one row and one column for every feature in the dataset (www.esi.com). The cell value for any given row/column combination is the weight that quantifies the spatial relationship between those row and column features. There are a multitude of fractionalized, endmember eigenvector weighting possibilities including inverse distance, fixed distance, K nearest neighbors, contiguity, and geospatial interactions that are capable in a imaged, RapidEye™, *S. damnosum* s.l. eco-epidemiological, immature habitat, eco-georeferenceable ,capture point, 5m scene, for example. The conceptualization selected to model spatial relationships for a particular analysis can impose a structure onto spatial data [24]. Consequently, selecting a conceptualization that best reflects how the uncoalesced, riverine, habitat features being analyzed actually interact with each other in an African, narrow, riverine tributary, agro-village, eco-georeferenceable complex. At a very basic level, however, weights are either binary or variable. Binary weighting, used with fixed distance, K nearest algorithms ca qunataite a trailing vegetation, discontinuously canopied, sparsely shaded, hyperproductive, 5m imaged, RapidEye™, *S. damnosum* s.l., eco-epidemiological, immature habitat, capture point, eco-georeferenceable neighbors, and contiguity spatial relationships, for example,in Geospatial Analyst ™ will, for a particular capture point, immature habitat target feature, assign a value of 1 to neighboring features and 0 to all other uncoalesced, habitat features. For inverse distance or inverse time spatial relationships, weights fall into a range from 0 to 1 with nearby neighbors getting larger weights than neighbors farther away. Spatial weights are often row standardized, particularly with binary weighting strategies. Row standardization is used to create proportional weights in cases where features have an unequal number of neighbors. Row standardization involves dividing each neighbor weight for a feature by the sum of all neighbor weights for that feature, and is

recommended whenever the distribution of your features is potentially biased due to sampling design or an imposed aggregation scheme (www.esri.com).

Forecasting anisotropy and bidirectional reflectance distribution function (BRDF) of unmixed, eco-georeferenceable, sparsely shaded, turbid water, seasonally explanative, hyperproductive, *S. damnosum* s.l., immature, narrow tributary riverine habitats with decomposed discontinuous vegetation canopies in ArcGIS may help consider the angular distribution of leaves and the geolocation and size of individual subcanopies (e.g., widely spaced rows of trailing vegetation). Further, uncoalesced, geo-spectrotemporal and geospatially explanative, fractionalized, endmember eigenvector, directional frequencies based on uncertainty properties of leaves (e.g., multiple scattering) may also be autoregressively seasonally quantitated for eliminating propogational, residual forecast misspecifications. As such, an emissivity, endmember eigenvector, 5m, forecast, vulnerability model may relate unmixed, elucidative, biophysical, sparsely shaded, iteratively interpolatable, discontinuously, decomposable, canopied foliage attributes to down-looking RapidEye™ radiation measurements based on seasonal, immature, black-fly productivity. This radiance paridigm can employ nadir and off-nadir viewing angles of the moderate resolution sensor for optimally and interpretively decomposing, uncoalesced, wavelength, frequency-oriented, transmittance model, parameterizable, covariate estimators. Inversion of this remote sensing model may provide statistically regressable discontinuously canopied, immature, explanative, fractionaized, immature habitat, uncoalesced, endmember surface, eigenvector, geo-spectrotemporally, geospatially proxy signature patterns for seasonally, remotely, and autoregressively targeting, iteratively interpolatable, unmixable, *S. damnosum* s.l. turbid water, eco-epidemiological, capture point that have been seasonally geosampled and ecogeoreferenced as high density foci. Such a model also may help to evaluate atmospheric limitations of RapidEye™ red and NIR data for imaging decomposable, explanative, immature, capture point, *S. damnosum* s.l., immature Rapid Eye ™ eco-georeferenceable, trailing vegetation, turbid water, geospatially geosampled, *S. damnosum* s.l. agro-village, narrow tributary, complex ecosytem, capture point, hyperproductive immature,habitat, population habitats by providing a good proxy surface boundary assessment for many different kinds of sporadically seasonal, discontinuous, canopy configurations for obtaining optimizable and uncoalesced, sub-surface, parameterizable, covariates [evapotranspiration (ET) rates]. Assessing the energy balance while employing some surface properties, such as albedo, LULC canopy cover, and surface temperature, is the principle of ET estimation by remote sensing [25]. Further, this intuitive forecast, non-continuous,vulnerability model may relate fractionalized, endmember eigenvector estimates of nadir reflectance of these habitats, which may be approximated to hemispherical reflectance by computing total energy budgets of the 5m imaged, discontinuously, sparsely shaded, discontinuous, canopy-vegetated, geoclassifable, LULC surfaces.

Jacob et al. [22] exegetically, quantitatively, and auto-probabilistically autoregressed an uncoalesced, geo-spectrotemporal remote, multivariate, dataset of geospatialized, eco-epidemiological, empirical, elucidative, 5m, RapidEye™ spatial resolution, non-Gaussian, explanatively parameterizable, eco-georeferenceable, photosynthetic, 5m, wavelength, frequency orthogonally decomposable, emissivity covariates for optimally characterizing seasonally hyperproductive, iteratively interpolative, explicatively geo-classifiable, trailing vegetation-related, sparsely shaded, *S. damnosum* s.l., turbid water, geosampled riverine, narrow tributary, habitats in an African agro-village in Burkina Faso. An eigenfunction decomposition algorithm in Geostatistical Analyst™ computed spatial eigenvectors. These spatial eigenvectors were optimally defined by their decomposed spatial structures associated

with an explanatively eco-georeferenceable, eco-epidemiological, seasonal, immature, capture point, hyperproductive habitat that was interpretively and interpolatively topographically geo-classified as a sparsely shaded, discontinuously canopied, 5m, Normalized Difference Vegetation Index (NDVI), proxy, graphical indicator. NDVI is typically, but not necessarily, used to analyze remote sensing measurements from a space platform and assess whether the target being observed contains live green vegetation or not [23].

In Jacob et al. [22], Geostatistical Analyst™ easily created an interpretively, iteratively quantiatively, explanatively iteratively interpolatable, eco-georeferenceable, discontinuously canopied, geoclassifiable, descriptive, LULC surface, which was subsequently stored in a eco-georeferenceable, point feature, raster layer along with polygon centroids. Measurements were taken from sample points and included elevation, depth to the water table, levels of turbidy and percent of sparsely shaded, discontinuously canopied, trailing vegetation. When used in conjunction with ArcMap, Geostatistical Analyst™ provides a comprehensive set of tools for creating surfaces that can be used to visualize, analyze, and understand spatial phenomena (www.esri.com). In Jacob et al. [22], the ArcGIS geospatial iterative algorithms made the eigenfiltering more efficient by employing analytical solutions for regressing the orthogonally decomposed, RapidEye™ eigenvalues and spatial eigenvectors.

The eigenfilter design method in ArcGIS for discrete time filters involves the determination of filter coefficients as the eigenvector of a particular Hermitian positive definite (and often real and symmetric) matrix[25]. As opposed to other filter design algorithms in ArcGIS such as the least-squares approach which requires the computation of a matrix inverse, the eigenfilter method only requires the computation of a single eigenvector, which can be found efficiently via the iterative power method. The method also has an inherently low design complexity. The eigenfilter method can incorporate a variety of time and frequency-domain constraints into the design problem with relative ease, in contrast to other well known filter design methods such as the McClellan–Parks algorithm [16].

The Parks–McClellan algorithm, published by James McClellan and Thomas Parks in 1972, is an iterative algorithm for finding the optimal Chebyshev finite impulse response (FIR) filter. A finite impulse response (FIR) filter is a filter whose impulse response (or response to any finite length input) is of finite duration, because it settles to zero in finite time. This is in contrast to infinite impulse response (IIR) filters, which may have internal feedback and may continue to respond indefinitely (usually decaying). In mathematics, the Kronecker delta is a function of two variables, usually just positive integers where ehe function is 1 if the variables are equal, and 0 otherwise: $\delta_{ij} = \begin{cases} 0 & \text{if } i \neq j, \\ 1 & \text{if } i = j \end{cases}$ where the Kronecker delta δ_{ij} is a piecewise function of variables i and j (e.g., $\delta_{1\,2} = 0$, whereas $\delta_{3\,3} = 1$)[25].

In signal processing, a finite impulse response (FIR) filter is a filter whoseimpulse response (or response to any finite length input) is of *finite* duration, because it settles to zero in finite time[25]. This is in contrast to infinite impulse response (IIR) filters, which may have internal feedback and may continue to respond indefinitely (usually decaying).The impulse response (that is, the output in response to a Kronecker deltainput) of an Nth-order discrete-time FIR filter lasts exactly $N + 1$ samples (from first nonzero element through last nonzero element) before it then settles to zero.FIR filters can be discrete-time orcontinuous-

time, and digital or analog..FIR filters can be discrete-time or continuous-time, and digital or analog [24].

The Parks–McClellan algorithm may be utilized to design and implement efficient and optimal FIR filters in an ArcGIS cyberenvironment by employing an indirect method for finding the optimal filter coefficients. Infinite impulse response (IIR) is a property applying to many linear time-invariant , 5m, RapidEye™ spatial resolution, non-Gaussian, explanatively parameterizable, eco-georeferenceable, photosynthetic, 5m, wavelength, frequency orthogonally decomposable, emissivity covariates for optimally regressively quantiating seasonally hyperproductive, iteratively interpolative, explicatively geo-classifiable, trailing vegetation-related, sparsely shaded, *S. damnosum* s.l., turbid water, geosampled riverine, narrow tributary, LULC habitats in an African agro-village systems. Common examples of linear time-invariant systems are digital filters[25]. Systems with this property are known as IIR systems or IIR filters, and are distinguished by having an impulse response which does not become exactly zero past a certain point, but continues indefinitely. This is in contrast to a finite impulse response in ArcGIS in which the impulse response $h(t)$ *does* become exactly zero at times $t > T$ for some finite T, thus being of finite duration.The goal of such an algorithm for qualitatively explanatively remotely quantitating probabilistically regressable, uncoalesced, multivariate, empirical datasets of geo-spectrotemporal and geospatial, eco-epidemiological, empirical, elucidative, 5m, RapidEye™ spatial resolution, non-Gaussian, explanatively parameterizable, wavelength, frequency emissivity, uncoalesced, discontinuously canopied, sparsely shaded, *S. damnosum* s.l. immature habitat, eco-epidemiological, agro-village narrow riverine tributary, capture point, orthogonally explanatively decomposable covariate coefficients would then be to minimize the error in the pass and stop bands by utilizing the Chebyshev approximation.

An ecologist, entomologist or other researcher can obtain moderate resolution, trailing vegetion, turbid water, discontinuously canopied, sparsely shaded, *S. damnosum* s.l. immature habitat, eco-epidemiological, capture point, polynomials in ArcGIS by expanding the given geoclassifiable, explicative, LULC function in terms of Chebyshev polynomials and then cutting off the expansion at the desired degree. This is similar to the Fourier analysis of the function, using the Chebyshev polynomials instead of the usual trigonometric functions. In mathematics the Chebyshev polynomials, are a sequence of orthogonal polynomials which are related to de Moivre's formula and which can be defined recursively. In mathematics, Fourier is the study of the way general functions may be represented or approximated by sums of simpler trigonometric functions[24]. In mathematics, de Moivre's formula (also known as de Moivre's theorem and de Moivre's identity), named after states that for any complex number (and, in particular, for any real number) x and integer n it holds that $(\cos x + i\sin x)^n = \cos(nx) + i\sin(nx)$, where i is the imaginary unit ($i^2 = -1$)[24].

If one calculates the coefficients in the Chebyshev expansion for a function: $f(x) \sim \sum_{i=0}^{\infty} c_i T_i(x)$ and then cuts off the series after the T_N term in ArcGIS one gets an Nth-degree polynomial approximating $f(x)$.The reason this polynomial is nearly optimal for parameterizing geo-spectrotemporally ,uncoalesced, discontinuous,infrequently canopied, sparsely shaded, *S. damnosum* s.l. immature habitat, agro-village narrow riverine tributary, capture points is that, for moderate resolution functions with rapidly converging power series, the series may be strategically cut off after some term. Theerfater, the total error arising from the cutoff would be close to the first term after the cutoff in ArcGIS. That is, the first term after the cutoff will dominate all later terms. The same is true if the expansion is in

terms of Chebyshev polynomials constructed in ArcGIS. If a Chebyshev expansion is cut off after T_N, the error will take a form close to a multiple of T_{N+1}. The Chebyshev polynomials have the property that they are level – they oscillate between +1 and −1 in the interval [−1, 1]. T_{N+1}has N+2 level extrema[25]. This means that the forecastable *S. damnosum* s.l. immature habitat, vulnerabity model error between $f(x)$ and its Chebyshev expansion out to T_N would be close to a level function with N+2 extrema, so it is close to the optimal Nth-degree polynomial.

In mathematics, Fourier analysis is the study of the way general functions may be represented or approximated by sums of simpler trigonometric functions. In mathematics, the discrete-time Fourier transform (DTFT) is a form of Fourier analysis that is applicable to the uniformly-spaced samples of a continuous function. The term *discrete-time* refers to the fact that the transform operates on discrete data (regressable, uncoalesced, geo-spectrotemporal eco-epidemiological, 5m, RapidEye™ parameterizable,uncoalesced, discontinuous,infrequently canopied, sparsely shaded, *S. damnosum* s.l. immature habitat, agro-village narrow riverine tributary, capture point samples (see Figure 24) whose interval often has units of time. From only the samples, it produces a function of frequency that is a periodic summation of the continuous Fourier transform of the original continuous function. Under certain theoretical conditions, described by the sampling theorem, the original continuous function can be recovered perfectly from the DTFT and thus from the original discrete samples. The DTFT itself is a continuous function of frequency and is by far the most common method of modern Fourier analysis. Due to the properties of sine and cosine, it is possible to recover the amplitude of each wave in a Fourier series using an integral. In many cases it is desirable to use Euler's formula, which states that $e^{2\pi i\theta} = \cos(2\pi\theta) + i \sin(2\pi\theta)$, to write Fourier series in terms of the basic waves $e^{2\pi i\theta}$. This has the advantage of simplifying many of the formulas involved, and provides a formulation for Fourier series that more closely resembles the definition followed in this article. Re-writing sines and cosines as complex exponentials makes it necessary for the Fourier coefficients to be complex valued[25].

Fourier transformation is also useful as a compact representation of a proxy biosignature, moderate resolutionsignal. For example, JPEG compression uses a variant of the Fourier transformation (discrete cosine transform) of small square pieces of a digital image (www.esri.com). The Fourier components of each square are rounded to lower arithmetic precision, and weak components are eliminated entirely, so that the remaining components can be stored very compactly. In image reconstruction, each image square is reassembled from the preserved approximate Fourier-transformed components, which are then inverse-transformed to produce an approximation of the original image (Figure 26)

Figure 26. Low-pass filtering using Fourier Transforms discrete 5m, RapidEye™ parameterizable,uncoalesced, discontinuous,infrequently canopied, sparsely shaded, *S. damnosum* s.l. immature habitat, agro-village narrow riverine tributary, capture point samples where y is changing seasonal immature sanmple productivity count data and t is time

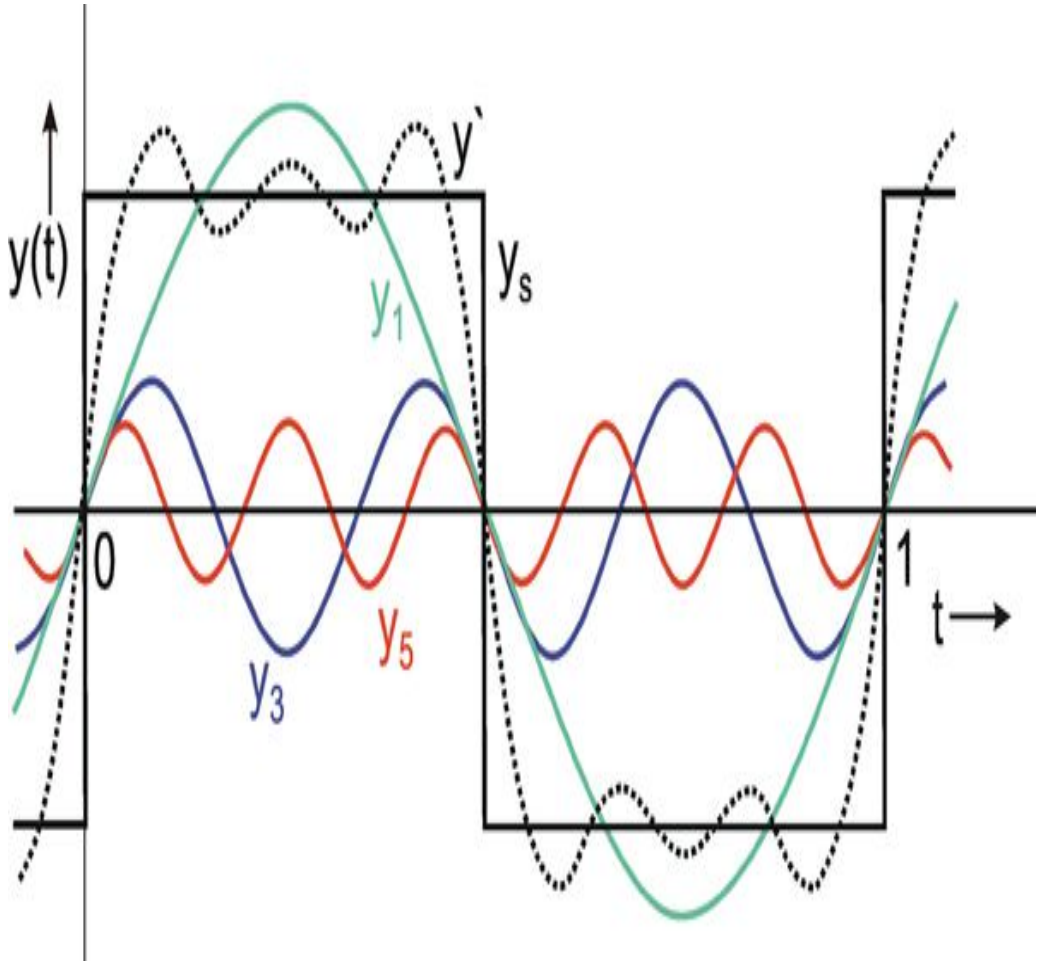

The Parks–McClellan algorithm is a variation of the Remez exchange algorithm, with the change that it is specifically designed for finite impulse response (FIR) filters (see Figure 27) In signal processing, a FIR filter is a filter whose impulse response (or response to any finite length input) is of finite duration, because it settles to zero in finite time[24]. The Remez algorithm or Remez exchange algorithm, published by Evgeny Yakovlevich Remez in 1934, is an iterative algorithm used to find simple approximations to functions, specifically, approximations by functions in a Chebyshev space that are the best in the uniform norm L_∞ sense The Parks–McClellan Algorithm is implemented using the following steps in ArcGIS 1)Initialization: Choose an extremal set of frequences $\{\omega_i^{(0)}\}$, 2) Finite Set Approximation: Calculate the best Chebyshev approximation on the present extremal set, giving a value $\delta^{(m)}$ for the min-max error on the present extremal set, 3) Interpolation: Calculate the error function $E(\omega)$ over the entire set of frequencies Ω using (2), 4) Look for local maxima of $|E^{(m)}(\omega)|$ on the set Ω, 5) If $\max_{(\omega\varepsilon\Omega)}|E^{(m)}(\omega)| > \delta^{(m)}$, then update the extremal set to $\{\omega_i^{(m+1)}\}$ by picking new frequencies where $|E^{(m)}(\omega)|$ has its local maxima[24]. If $\max_{(\omega\varepsilon\Omega)}|E^{(m)}(\omega)| \leq \delta^{(m)}$, then the algorithm is complete. Using the set $\{\omega_i^{(0)}\}$ and the interpolation formula may aid in computing an inverse discrete Fourier transform to obtain the filter coefficients for a. regression, forecasting vulnerability, eco-georeferenceable, seasonally hyperproductive, trailing vegetation, narrow, African, riverine, tributary, agro-village, *S. damnosum* s.l. oviposition site on a geoclassifiable, ArcGIS-derived LULC.

Figure 27. A band filter designed by the Parks–McClellan algorithm

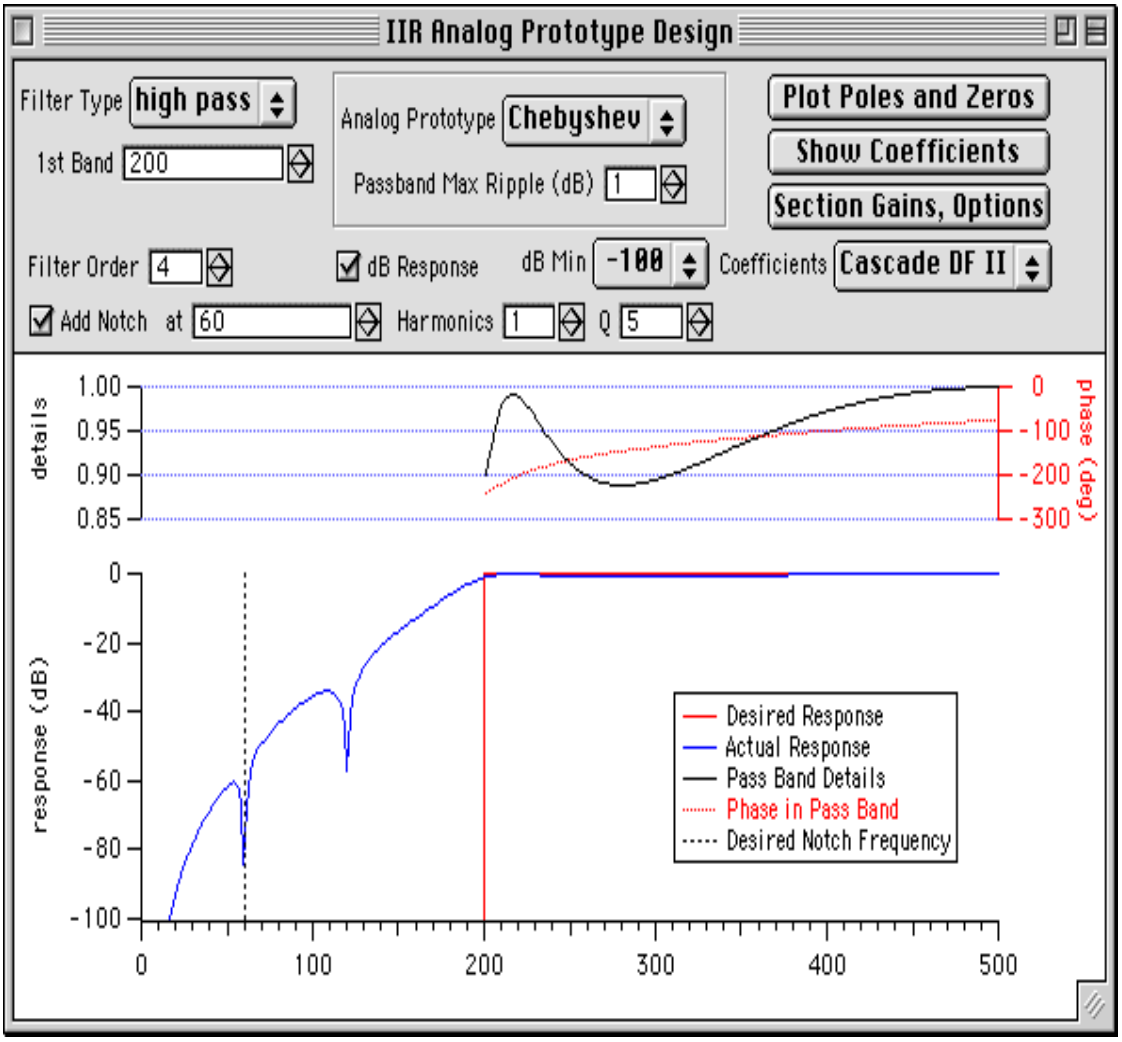

In Figure 27 the y-axis is the frequency response $H(\omega)$ and the x-axis are the various radian frequencies, ω_i. It should be noted that the two frequences marked on the x-axis, ω_p and ω_s, indicates the pass band cutoff frequency and the stop band cutoff frequency respectively. The ripple like plot on the upper left is the pass band ripple and the ripple on the bottom right is the stop band ripple. The two dashed lines on the top left of the graph indicate the δ_p and the two dashed lines on the bottom right indicate the δ_s. All other frequencies listed indicate the extremal frequencies of the frequency response plot.

A new eigenfilter approach to designing least square error filters in ArcGIS may quantitate a probabilistically regressable, geo-spectrotemporally uncoalesced, multivariate, empirical dataset os eco-epidemiological, regressable, geo-spatiotemporal, geospatialized, moderate resolution (e.g., 5m, RapidEye™) non-Gaussian, uncoalesced *S. damnosum* s.l. capture point photosynthetic, wavelength, frequency, emissivity, 5m, spatial resolution, covariate coefficients. The filters may be optimally obtained by finding an eigenvector of a real, symmetric and positive definite matrix, which is numerically stable whenst constructing the least-square solution, in ArcGIS which to date has only beenobtained through matrix inversion in the literature. A new method of designing linear-phase FIR filters ismay be proposed in ArcGIS by minimizing a quadratic measure of the error in the passband and

stopband. The method is based on the computation of an eigenvector of an appropriate real, symmetric, and positive-definite matrix.

In ArcGIS, an *n*-by-*n* square matrix A is called invertible (also nonsingular or nondegenerate) if there exists an *n*-by-*n* square matrix B such thatwhere I_n denotes the *n*-by-*n* identity matrix and the multiplication used is ordinary matrix multiplication (www.esri.com). In linear algebra, the identity matrix, or sometimes ambiguously called a unit matrix, of size *n* is the $n \times n$ square matrix with ones on the main diagonal and zeros elsewhere. [24] In an empirical, heursitically optimizable ArcGIS dataset of uncoalesced, regressable, geo-spectrotemporal eco-epidemiological, 5m, RapidEye™ parameterizable, discontinuous,infrequently canopied, sparsely shaded, *S. damnosum* s.l. immature habitat, agro-village narrow riverine tributary, capture point , forecast, vunerability model , fractionalized endmember estimators may be denoted by I_n, or simply by *I* if the n size is immaterial. I such circumsatnces the count estimates may be trivially determined by the *inverse* of A, denoted by A^{-1}.A square matrix that is not invertible is called singular or degenerate[25]. A square matrix is singular if and only if its determinant is 0. Singular matrices are rare in the sense that a square matrix randomly selected from a continuous uniform distribution on its entries will almost never be singular.Non-square matrices (*m*-by-*n* matrices for which $m \neq n$) do not have an inverse. However, in some cases such a matrix may have a left inverse or right inverse in an *S. damnosum* s.l. immature, capture point, iteratively interpolative model. If A is *m*-by-*n* in ArcGIS and the rank of A is equal to *n*, then A will have a left inverse: an *n*-by-*m* matrix B such that BA = I. If A has rank *m* in ArcGIS then it will have a right inverse: an *n*-by-*m* matrix B such that AB = I.Matrix inversion is the process of finding the matrix B that satisfies the prior equation for a given invertible matrix A[24].

All elucidatively, optimally parameterizable, explicatively eco-georeferenceable, geo-spectrotemporally, geospatially uncoalesceable, phosynthetic and non-phosynthetic moderate resolution, uncoalesced, wavelength, frequency, transmittance, discontinuous,infrequently canopied variable thus would be asymptotically attained optimally within the residual, ArcGIS unmixing algorithm. In so doing, a stochastic interpolator may reveal un-geosampled, unknown, eco-georeferenceable, narrow African, riverine tributary,agro-village, complex ecosystem, immature habitat, capture point, eco-epidemiological forecasts targets (e.g., seasaonlly hyperproductive, *S. damnosum* s.l. sparsely shaded, trailing vegetation, discontinuously canopied, sparsely shaded, turbid water, hyperproductive, foci). Even though numerical errors may break the explanative matrix inversion method in the geodatabase, the algorithm may still find some “optimal” filter by tuning an internal parameter in ArcGIS. Further, because of the myriad of design problems that can be posed as an eigenfilter problem in nonArcGIS bridge software, the ArcGIS method may be useful for a variety of iteratively interpolative algorithmic applications, ranging from spectral/special filtering for remotely diagnosing, discrete, probabilistic propagational error in dataset of quantitative eco-georeferenceable, seasonally targeted hyperproductive,*S. damnosum* s.l. trailing vegation, discontinuously canopied, sparsely shaded, turbid water,seasonal capture points.

The notion of such a filter design technique was introduced by Slepian in 1978 in the context of the design of window functions for the ideal low-pass filter response. Slepian considered the problem of designing a window with a minimum stop-band energy which was subject to a unit norm constraint on the window coefficients to avoid a trivial solution. In

1987, Vaidyanathan and Nguyen generalized Slepian's method for window design to the design of linear-phase, finite impulse response (FIR) filters and formally introduced the eigenfilter design method. They generalized Slepian's method to account for both passband and stopband conditions and showed how to design a variety of filters (mainly low pass, high pass, and band pass) with various time- and frequency-domain constraints, including the Nyquist constraint and flatness constraints. Numerous simulation results were provided showing the power and usefulness of the eigenfilter method. For example, Jacob et al. [22] found that the optimal window coefficients could be found in ArcGIS from the eigenvector of a real, symmetric, positive definite, Toeplitz *S. damnosum* s.l. habitat uncertainty-oriented, weighted autoregressive matrix corresponding to its smallest parameterizable, discontinuous,infrequently canopied, sparsely shaded, *S. damnosum* s.l. immature habitat, agro-village narrow riverine tributary, capture point eigenvalue.

Various properties of a real symmetric Toeplitz matrix Σm with elements $\sigma jk = a_{j-k|}$, $1 \leqslant j,k \leqslant m$, may be optimally reviewed within an ArcGIS geodatabase. Matrix equatiosn of the form $Ax = b$(e.g., a Toeplitz system if A is a Toeplitz matrix) may be customized for qualitatively regressively quantiating an empirical regressable dataset of heursitically optimizable, eco-epidemiological, orthogonally decomposable, residually forecastable, eco-georfernceable, S. damnsoum s.l. unmixed, paramterizable, moderate reoslution covariate coefficients for A if an $n \times n$Toeplitz matrix is utilized in ArcGIS .In so doing, the system would only have $2n-1$ degrees of freedom, rather than n. Toeplitz matrix w may be defined as a matrix A where $A_{i,j} = c_{i-j}$ in an ArcGIS cyberenvironment for constants $c_{1-n} \ldots c_{n-1}$. The set of $n \times n$ Toeplitz matrices is a subspace of the vector space of $n \times n$ matrices under matrix addition and scalar multiplication[25].Two Toeplitz matrices may be added in $O(n)$ time and multiplied in $O(n^2)$ time when qualiatively quantiating a dataset of probabilistically autoregressable, uncoalesceable, remote, multivariate, dataset of geo-spectrotemporally uncoalesced, geospatial, eco-epidemiological, empirically, elucidative, 5m, RapidEye™ spatial resolution, non-Gaussian, explanatively parameterizable, eco-georeferenceable, photosynthetic, agro-village complex, narrow tributary, eco-georfernceable, wavelength, frequency, emissivity, transmittance covariates in symeteric Toeplitz matrices.

Symmetric Toeplitz matrices are both centrosymmetric and bisymmetric.Toeplitz matrices are also closely connected with Fourier series, because the multiplication operator by a trigonometric polynomial, compressed to a finite-dimensional space, can be represented by such a matrix in ArcGIS. Similarly, one can represent linear convolution as multiplication by a Toeplitz matrix.Toeplitz matrices commute asymptotically. This means they diagonalize in the same basis when the row and column dimension tends to infinity. Matrices of this kind often arise in applications in statistics, econometrics, psychometrics, structural engineering, multichannel filtering, reflection seismology, etc., Thus it would be desirable to have techniques which exploit special structure in a real, symmetric, positive definite, eco-epidemiological, eco-georferenceable, capture point, trailing vegetation, discontinuously canopied,geo-spectrotemporally, geospatially vulnerability, forecast, Toeplitz, *S. damnosum* s.l. habitat uncertainty-oriented, weighted autoregressive matrix in ArcGIS. Possible applications of the results in such a moderate resolution endmember eigenvector forecast, vulnerability model may be related to their uncoalesced parameterizable, discontinuous,infrequently canopied, sparsely shaded, *S. damnosum* s.l. immature habitat, agro-village narrow riverine tributary, capture point , ecogeorferenceable, endmember inverse, determinant, and eigenvalues

The classical sets of orthogonal polynomials of Jacobi,in satisfy second order

differential equations, and also have the propertythat their derivatives form orthogonal systems. In mathematics, Jacobi polynomials (i.e., hypergeometric polynomials) $P(\alpha, \beta)$ $n(x)$ are a class of classical orthogonal polynomials. They are orthogonal with respect to the weight $(1 - x)^{\alpha}(1 + x)^{\beta}$ on the interval [−1, 1] The Jacobi polynomials are defined via the hypergeometric function as $P_n^{(\alpha,\beta)}(z) = \frac{(\alpha+1)_n}{n!} {}_2F_1\left(-n, 1+\alpha+\beta+n; \alpha+1; \frac{1}{2}(1-z)\right)$, where $(\alpha+1)_n$ is Pochhammer's symbol (for the rising factorial). The Jacobi polynomials, also known as hypergeometric polynomials, occur in the study of rotation groups {2]. They are solutions to the Jacobi differential equation, and give some other special named polynomials as special cases. They are implemented in the WolframLanguage as JacobiP[*n*, *a*, *b*, *z*].For $\alpha = \beta = 0$, $P_n^{(0,0)}(x)$which can reduce to a Legendre polynomial. The Gegenbauer polynomial $G_n(p, q, x) = \frac{n!\,\Gamma(n+p)}{\Gamma(2n+p)} P_n^{(p-q,q-1)}(2x-1)$ and Chebyshev polynomial of the first kind can also be viewed as special cases of the Jacobi polynomials[www.sas.edu] .Plugging $y = \sum_{\nu=0}^{\infty} a_\nu (x-1)^\nu$ into the Jacobi differential *S. damnosum* s.l. immarture, capture point, predictive, risk model equation could render the recurrencerelation $[\gamma - \nu(\nu+\alpha+\beta+1)]a_\nu - 2(\nu+1)(\nu+\alpha+1)a_{\nu+1} = 0$for $\nu = 0$, 1, ..., where$\gamma \equiv n(n+\alpha+\beta+1)$.Solving the recurrence relation wouldgives $P_n^{(\alpha,\beta)}(x) = \frac{(-1)^n}{2^n n!}(1-x)^{-\alpha}(1+x)^{-\beta}\frac{d^n}{dx^n}\left[(1-x)^{\alpha+n}(1+x)^{\beta+n}\right]$for $\alpha, \beta > -1$. This estimate couls form a complete orthogonal system in the interval $[-1, 1]$ with respect to the weightingfunction$w_n(x) = (1-x)^{\alpha}(1+x)^{\beta}$,which could be normalized according to $P_n^{(\alpha,\beta)}(1) = \binom{n+\alpha}{n}$,where $\binom{n}{k}$ is $P_n^{(\alpha,\beta)} = \frac{\Gamma(2n+\alpha+\beta+1)}{n!\,\Gamma(n+\alpha+\beta+1)} G_n\left(\alpha+\beta+1, \beta+1, \frac{1}{2}(x+1)\right)$, a binomial coefficient. Jacobi polynomials can also be written where $\Gamma(z)$ isthe gamma function and $G_n(p, q, x) \equiv \frac{n!\,\Gamma(n+p)}{\Gamma(2n+p)} P_n^{(p-q,q-1)}(2x-1)$. Jacobi polynomials In this case, the series for the hypergeometric function is finite, therefore one obtains the following equivalent expression: $P_n^{(\alpha,\beta)}(z) = \frac{\Gamma(\alpha+n+1)}{n!\,\Gamma(\alpha+\beta+n+1)} \sum_{m=0}^{n} \binom{n}{m} \frac{\Gamma(\alpha+\beta+n+m+1)}{\Gamma(\alpha+m+1)} \left(\frac{z-1}{2}\right)^m$. The Pochhammer symbol introduced by the notation $(x)_n$, where *n* is a non-negative integer[24]. , Jacobi polynomials There is a fourth classof polynomials with these two properties, and similar in other ways to theother three classes, whichh has hitherto been little studied. These are the Bessel polynomials because of their close relationship with the Bessel functions of half-integral order which may be applicable to a regression, forecasting vulnerability, eco-georeferenceable, seasonally hyperproductive, trailing vegetation, narrow, African, riverine, tributary, agro-village, *S. damnosum* s.l. oviposition site on a geoclassifiable, ArcGIS-derived LULC (see Figure 28).

Figure 28. The roots of the third-order Bessel polynomial are the poles of filter transfer function in the *s* plane, here plotted as crosses in a hypothetical *S. damnosum* s.l. moderate resolution imaged hyperproductive, eco-epidemiological, capture point habitat

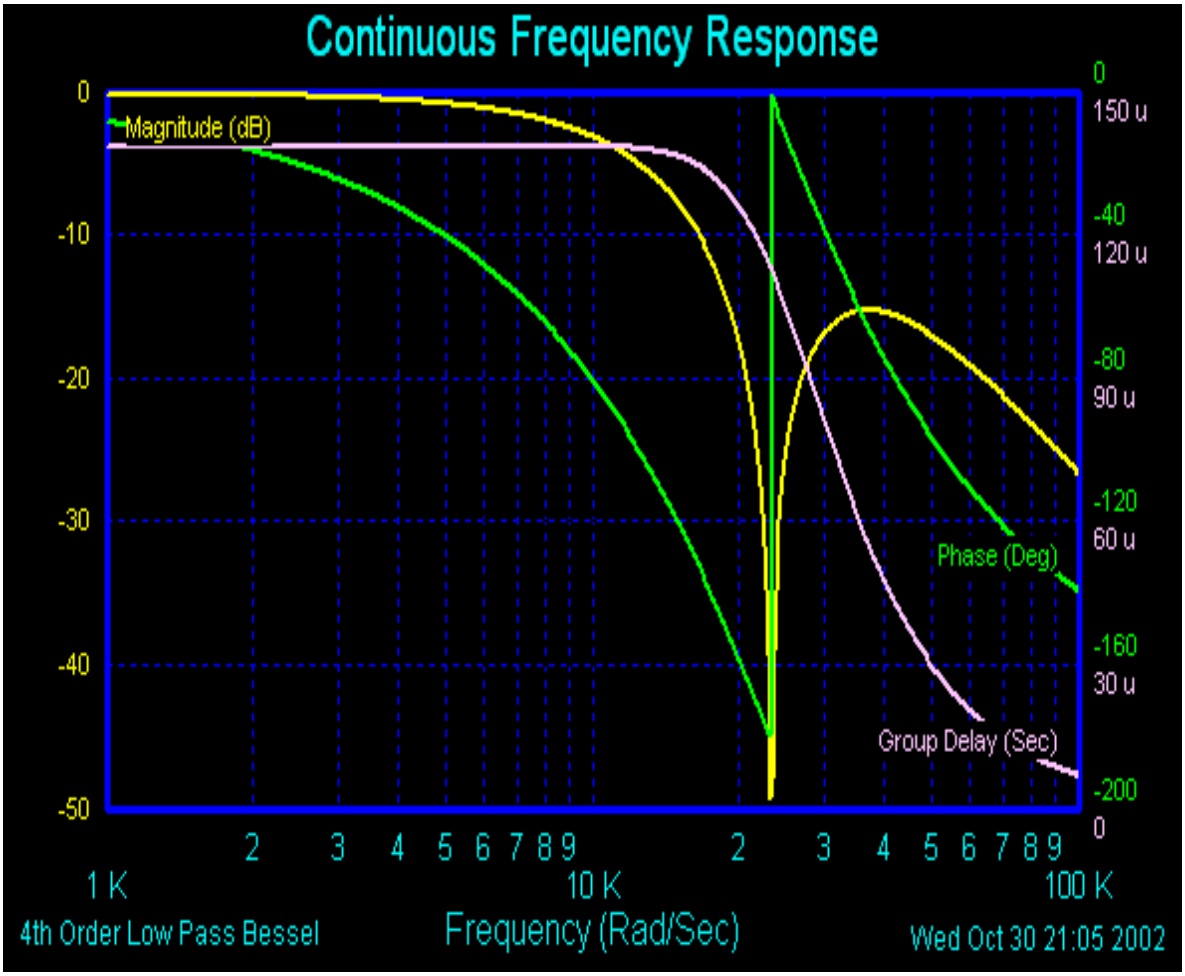

In ArcGIS, illuminatively decomposed explanative, components uncoalesced, eco-cartographically illustratable series of orthogonal, uncorrelated, unmixed, eco-georeferenceable, hyperproductive, *S. damnosum* s.l. habitat, 5m, eco-epidemiological, vulnerability risk, map patterns that described positively spatially autocorrelated parameterizable, discontinuous,infrequently canopied, sparsely shaded, , agro-village narrow riverine tributary, capture point , patterns through negatively spatially autocorrelated patterns, and global, regional, and local patterns of dependencies in the geo-spectrotemporally, moderate resolution, geospatially unmixed, LULC, topographical, reflectance dataset. A reformulation of the analytical solution in ArcGIS optimally reduced the required computations, which allowed the eigenvectors to be computed sequentially. A series of ArcGIS sampling methods were explored. The Sampling Design Tool provided two main functions for identifying unknown, un-geosampled, seasonally eco-georeferenceable trailing vegetation, prolific, discontinuously, infrequently canopied, *S. damnosum* s.l., turbid water, immature habitats.The first one was by optimally selecting a representive sample from a decomposable, fractionalized, endmember eigenvector in an interpretively iteratively interpolatable African, agro-village complex, riverine tributary habitat that had a geo-spectrotemporally geospatially geosampled embedded population archived in the algorithm. Secondly, the tool performed a sample design analysis. When both of these functions were combined in an iterative manner in ArcGIS, the tool effectively achieved the goal of sample surveys, which was to employed obtain accurate, high-precision, elucidative, time series dependent, explanative decomposable estimates of *Simulium* habitat, immature, population

metrics. Sampling and incorporation of inherently spatial layers (e.g., benthic habitat maps, administrative boundaries) can aid in extrapolating evaluation of spatial issues (e.g., protected area effectiveness) (www.arcgis.com/home/).

In Jacob et al [22], the orthogonal, eigenfunction decompostion algorithm in ArcGIS was applied to three 5m, RapidEye™, fractionalized, explanatively multispectral, decomposed, spatial resolution seasonal images of different sizes: small (i.e., ~200,000 mixels), medium (i.e., ~1,000,000 mixels) and large (i.e., ~110,000,000 mixels), which were then remotely and autoregressively evaluated in terms of output for each sampling technique. The output spatial filters of these sampling techniques were compared to the filters generated in ArcGIS. The complexity of set-up and execution of the geosampled parameterizable, discontinuous, infrequently canopied, sparsely shaded, *S. damnosum* s.l. immature habitat, agro-village, narrow, riverine tributary, capture point, iteratively interpolative, distribution algorithms in ArcGIS were non-tedious.

In terms of an efficiency evaluation of the filters in Jacob et al. [22], the expositorily decomposed, discontinuous, geo-classifiable, unmixed, 5m RapidEye™, eco-epidemiologcal, eco-georefernceable, capture point, and non-homogenously canopied, immature habitat surface in Geospatial Analyst™ enabled optimal, interpretive, iterative interpolation in ArcGIS (i.e, Geospatial Analyst ™). These smoothed values improved the final eco-epidemiological, eco-georeferenceable maps of the forecasted, *S. damnosum* s.l., immature habitats and were geo-spectrotemporally geospatially associated discontinuous, canopy cover, trailing vegetation and decomposable, riffle water components. An exponential model was then fitted to the semivariogram, using a range of 72.6m, a nugget of 0.21 (variance), a lag size of 11.5m with 12 lags and a partial sill of 0.24 (variance). Thereafter, an elucidative, geopredictive, explanatory, discontinuously, infrequently, canopy-based, eco-epidemiological, forecast, risk map was generated for a neighbouring, riverine, agro-village, narrow tributary, sparsely shaded, study site. The forecasted *S. damnosum s.l.* habitats were then field-verified, which revealed a 100% correlation with the geo-predicted, explanatory, forecast estimates.

Analysis of covariance in explicatively forecastable, eco-georeferenceable, seasonally prolific, entomological, vector arthropod, transmission-oriented, discontinuous, infreequently canopy-vegetated, partially shaded, geo-classifiable, LULC and NDVI, structurally diverse, geospectrotemporally uncoalesced, eco-epidemiological forecast, vulnerability models in an ArcGIS cyberenvironment may be optimally employed for geoclassifiying unmixed, field and remote clustering, time series, orthogonalizable, fractionalized, endmember decomposable eigenvectors. In addition to uncoalescing geo-predictive variables, in order to account for probabilistic, autoregressive residual uncertainties (i.e., non-linear dependence) and to reduce root-mean-square deviations (RSMD).

The RMSD or root-mean-square error (RMSE) is a frequently used measure of the differences between values (e.g., geosampled parameterizable, discontinuous,infrequently canopied, sparsely shaded, *S. damnosum* s.l. immature habitat, agro-village, turbid water, narrow,African riverine tributary, eco-georferenceable, moderate resolution, capture point, *S. damnosum* s.l., eco-epidemiologicalm capture point, immaturem count values) predicted by a model or an estimator and the values actually observed. The RMSD represents the sample standard deviation of the differences between predicted values and observed values. In statistics, the standard deviation (SD, also represented by the Greek letter sigma σ or *s*) is a measure that is used to quantify the amount of variation or dispersion of a set of data values

[See Figure 29].

Figure 29 a) a decomposed trailing vegation, turbid water, hypeporductive moderate resolution imaged, capture point, eco-georferenceable, endmember *S. damnsoum* s.l. habitat model b) RMSD simulation at varying finite and infinite variance counts c) Simulation infrequent canopy,d) Rapid Eye 5m signal to noise distribution of kriged fractionalized proxy LULC biosignature endmember residuals

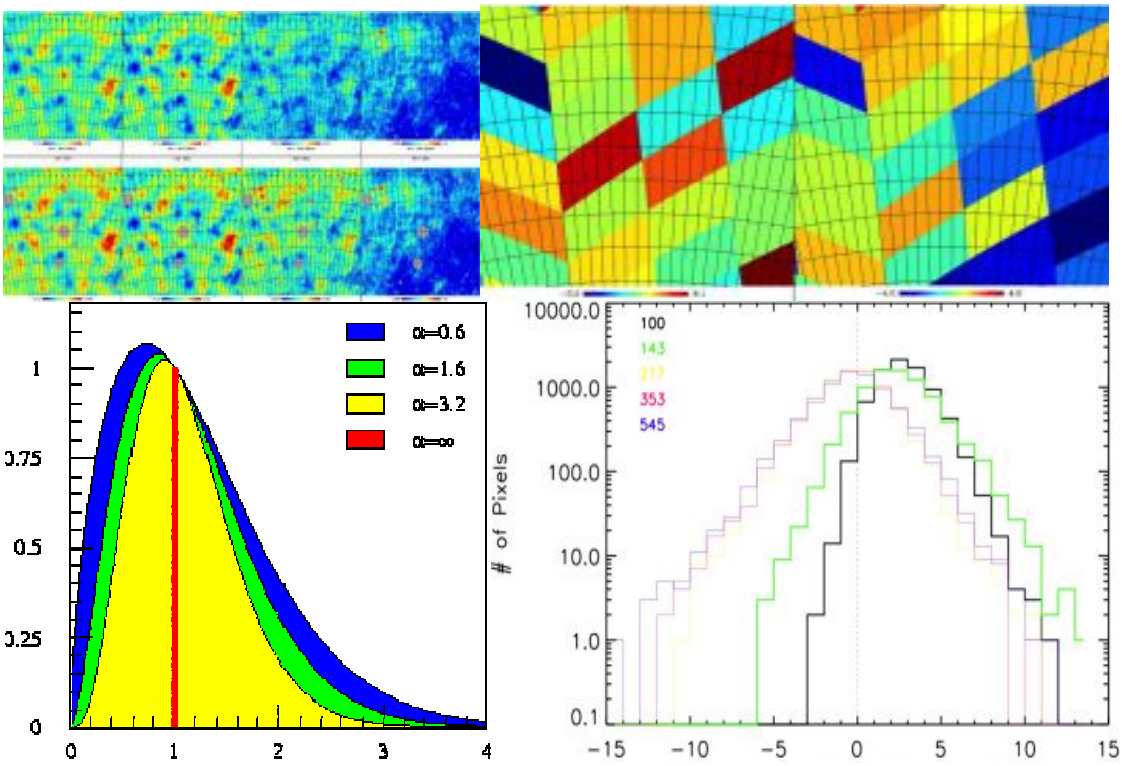

The RMSD serves to aggregate the magnitudes of the errors in predictions for various times into a single measure of predictive power. RMSD is a good measure of accuracy, but only to compare forecasting errors of different models for a particular variable and not between variables, as it is scale-dependent.

In Jacob et al. [22], an orthogonally decomposed, expositorily fractionalized NDVI, 5m, RapidEye^{TM} , fractionalized endmember, eigenvector,unmixed signature for optimizable attribute datafiles unbiasedly explanatively simulated important transmission zones [e.g., hyperendemic, (0-5km) from a seasonally, hyperproductive, sparsely shaded, trailing vegetation, discontinuously canopied, turbid water, eco-epidemiological, discontinuous, ecogeorefernceable, capture point]. Orthogonalized and uncorrelated, seasonally forecastable, endemic, topographically transmission-oriented, discontinuously, infrequently canopied , immature habitat, geo-classifiable, LULC, eco-epidemiological, vulnerability, unmixed, map patterns were heuristically, optimally and eco-geographically illustrated by the iteratively interpolative, fractionalized, endmember eigenvector, ensembles obtained from a doubly centered interpretively decomposable contiguity matrix in ArcGIS.

The continuity tool in ArcGIS honors the Environment output coordinate system(www.esri.com). Feature geometry was projected to the output coordinate system prior to the forecast, vulnerability, eco-epidemiological, eco-georeferenceable, parameterizable, discontinuous,infrequently canopied, sparsely shaded, *S. damnosum* s.l. immature habitat, agro-village, turbid water, narrow, African riverine tributary, eco-georferenceable, eco-epidemiological, complex, ecosystem, uncoalesced, moderate resolution, capture point, *S. damnosum* s.l. habitat, explanatory, fractionalized, endemember, eigenvector wavelenghth, transmittance, emissivity, frequency-oriented, analysis, so values entered for the Threshold Distance parameter using the same units as those specified in the output coordinate system in ArcGIS. All mathematical computations were based on the output coordinate system. Consequently, if the output coordinate system did not match the input endmember eigenvector, iterative, interpolative,decomposed, feature class, hyperproductive, agro-village, narrow, riverine, tributary, eco-georeferenceable, explanatorial, spatial reference, sub-mixel analyses using the spatial weights matrix file, were checked to determine if the output coordinate system matched the settings employe when the spatial weights matrix file was created in ArcGIS . Alternatively, the feature parameterizable, discontinuous,infrequently canopied, sparsely shaded, *S. damnosum* s.l. immature habitat, agro-village, turbid water, cimplex, ecosystem, narrow,African riverine tributary, eco-georferenceable, moderate resolution, capture point, geoclassfiied LULC class was also checked to determine if its spatial reference matched the spatial reference associated with the spatial weights matrix file Ideally, whenever using a distance-based conceptualization of Spatial Relationships in ArcGIS, the data should be illustrated using a Projected Coordinate System rather than a Geographic Coordinate System based on degrees, minutes, and seconds prior to analysis(www.esri.com) This projection should match the Environment output coordinate system settings.

In Jacob et al. [22], a unique ID field was used to relate explanatively,optimally decomposed discontinuously canopied, trailing vegetataion, eco-georeferenceable, elucidative, immature habitat features to one another (the relationship or weight between the geo-spectrotemporally geosampled, sparsely shaded, *S. damnosum* s.l., riverine foci, geospatial objects). Consequently, the Unique ID field values was unique for every uncoalesced,narrow riverine, eco-georefrenceable, immature habita,t tributary, attribute and typically was a permanent field that remained with the feature class. If you don't have a unique ID field, you can easily create one by adding a new integer field to your feature class table, and calculating the field values to be equal to the FID/OID (www.esri.com) field. The Polygon Contiguity Conceptualizations of Spatial Relationships were only valid for the decomposed riverine habitat polygon features.

The Delaunay triangulation and K nearest neighbors options are both appropriate for point or polygon features in ArcGIS; these options indicate that a feature will only be included in a group if at least one other group member is a natural neighbor (Delaunay Triangulation) or a K Nearest Neighbor. The Average Nearest Neighbor tool returns five values: Observed Mean Distance, Expected Mean Distance, Nearest Neighbor Index, z-score, and p-value(www.esrei.com). Optionally, this tool will create an HTML file with a graphical summary of results. If K nearest neighbors are selected a value of 12 is enetered for the Number of Neighbors parameter, for example, every geocalssifiable elucidative, LULC feature in a group will be within 12 nearest neighbors of at least one other feature in the group in ArcGIS (www.esri.com). The Delaunay triangulation option shouldn't be used for datasets with coincident features[24]. Also, because the Delaunay Triangulation method converts features to Thiessen polygons in ArcGIS to determine neighbor relationships,

especially with polygon features and sometimes with peripheral features in a dataset, the results from using this option would be optimal for a parameterizable, eco-egorferenceable, seasonal, *S. damnosum* s.l. discontinuous,infrequently canopied, sparsely shaded, *S. damnosum* s.l. immature habitat, agro-village, complex ecosystem, turbid water, narrow,African riverine tributary, eco-georferenceable, moderate resolution, capture point, forecast, moderate resolution uncoalesced, fractionalized, endmember eigenvector, wavelength, transmittance, frequency-oriented explicative, emissivity, forecast, vulnerability model(see Figure 30).

Figure 30. Non-contiguous; grouped original, capture point *S. damnosum* s.l., parameterized polygons (A) converted to Thiessen polygons, (B)

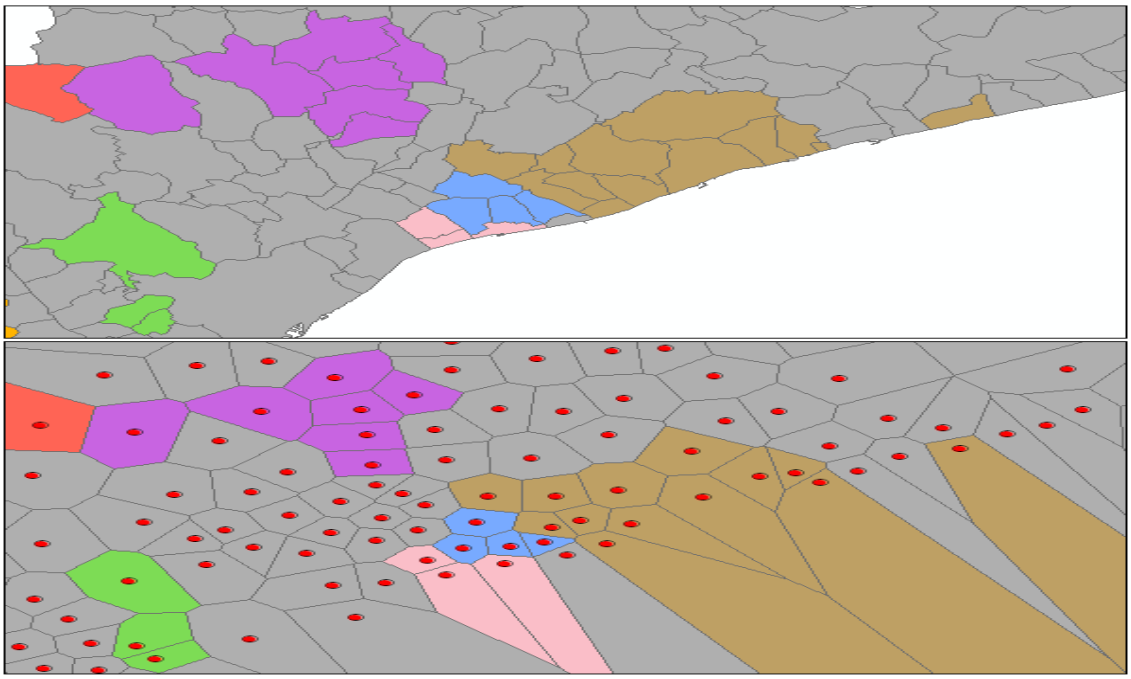

The Delaunay triangulation and the Voronoi diagram are dual structures and contain the same information in different form[24]. Computing one of these structures does automatically create the other. Furthermore, there is a connection between Delaunay triangulations and convex hulls in one higher dimension. The Delaunay triangulation and the Voronoi diagram in d dimensions was generated in Jacob et al. [22] for field verifying (i.e., "ground trothed data") a kriged map generetaed from a proxy Rapid Eye, 5m, proxy biosignature, of a capture point, trailing vegation, turbid water seasonally hyperproductive, *S. damnosum* s.l. immature habitat, geosampled in an agro-village complex (i.,e Chutes Dienoka) in Burkina Faso from a convex hull in d+1 dimensions (Figure 31). The Delaunay triangulation for a set of d-dimensional points is the projection of the points of the hull in d+1 dimensions [25]. In so doing, the descriptive, elucidative, intrepretively and explanatively interpolative, orthogonalized, 5m, forecasting, vulnerabilty, unmixed model revealed a ground truthing (i.e, field verification) capability of 72.73% for seasonally, geo-visualizing hyperproductive, sparsely shaded, trailing vegetation, discontinuously canopied, *S. damnosum* s.l., riverine, turbid water, immature habitats. The sensitivity of the test was 78.26 while the specifity was 100 at an eco-epidemiological riverine, study site in northern Uganda.

Figure 31 Voronoi diagram for validating a semiovariogram delineation of forecasted,pre-flooded, trailing vegetation, discontinuously canopied, hyperproductive *S. damnosum* s.l. riverine habitats along a meandering tributary of the Achwa river basin in northern Uganda Northern Uganda

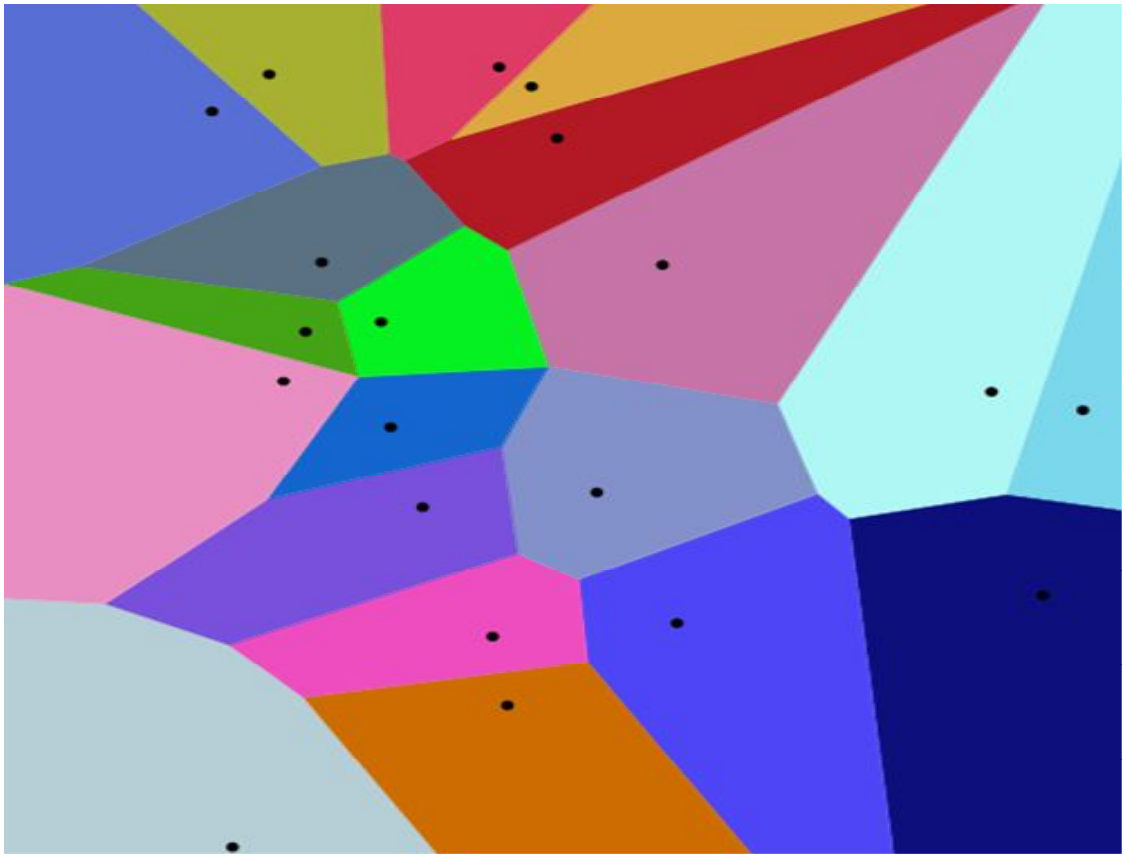

In Jacob et. al. [22] a ArcGIS contiguity matrix geo-spectrotemporally and geospatially characterized the operational clustering of a heuristically optimizable, ecogeorefernceable, dataset of explanatively iteratively interpolative, hyperproductive, eco-georeferenceable, *Simulium* habitats by employing Moran's *I*, an extension of the Pearson product-moment correlation coeffcient to univariate series. Meaningful explanative, spatial forces were empirically filtered out in the geosampled, eco-georeferenceable, decomposed, covariate, coefficient, endmember eigenvector, immature habitat, 5m geo-spectrotemporally uncoalesced, wavelength frequency-oriented, endmember, transmittance that was capable of being optimally parameterized through an emissivity estimator dataset in ArcGIS.

In an analogy to standard deviation, taking the square root of mean square error (i.e., second moment about the origin) in Geostatistical Analyst™ may incorporate both the variance of an unmixed dataset of sparsely shaded, explanative hyperproductive, , parameterizable, seasonal, *S. damnosum* s.l. discontinuous, infrequently canopied, sparsely shaded, *S. damnosum* s.l. immature habitat, agro-village, complex ecosystem, turbid water, narrow,African riverine tributary, eco-georferenceable, moderate resolution, capture point, forecast, uncoalesced, fractionalized, endmember eigenvector, wavelength, transmittance, emissivity, frequency-oriented, explicative, forecast, vulnerability model, unbiased, elucidative estimators. In so doing, iteratively qunatitatively, explanatively interpolatable, immature habitats, elucidatively decomposed, 5m, wavelength, transmittance emissivities,

with parameterizable non-homogenously canopied, autoregression-related, probabilistically regressively correlated estimators as well as their biases may be optimally yielded in the RMSD.These values may exhibit the same units as any quantity (i..e, covariance weight) being probabilistically estimated for any explanatively unbiased robustifiable eco-epidemiological, empirically decomposable, 5m, spatial resolution, RapidEye™, fractionalized, endmember, eigenvector, wavelength, transmittance emissitivy, dataset forecast estimator. Optimally and expositorily fractionally decomposed, log-transformed, sub-mixel, red and near NIR, fractionalized, endmember eigenvectors may eco-cartographically delineate latent autocorrelation, endemic transmission-oriented, explicatively auto-probabilistic and autoregressable, orthogonally stratifiable, eco-georeferenceable, geospatialized clusters in ArcGIS. The discontinuously canopied, trailing vegetation, sparsely shaded, orthogonally decomposed, endmember eigenvector, radiance spectrum in many narrow, uncoalesced contiguous, moderate resolution, spectral bands may reveal a high covariance between the bands. Hence, the true dimensionality of the imaging explanatorial, eco-georeferenceable, explicative, seasonally hyperproductive, *S. damnosum* s.l., immature habitat, eco-epidemiologicalparameterizable, discontinuous,infrequently canopied, sparsely shaded, *S. damnosum* s.l. immature habitat, agro-village, complex ecosystem, turbid water, narrow,African riverine tributary, eco-georferenceable, moderate resolution, capture point uncolaesced data may not be optimally heuristically determined by the number of spectral bands, but by the number of spectrally unique signatures (e.g., crown transparency, understory canopy reflectance) whose mixtures may reproduce the spectral variance observed in the RapidEye™ image.

Elucidatively varying, explanatively optimally parameterizable, quantitatively elucidatively decomposable, 5m, RapidEye™ autoregressively quantizable, intra-cluster, covariate coefficient, uncoalesced, wavelength transmittance may precisely reveal seasonally eco-georeferenceable and fractionalized, natural groupings, (e.g., flooded riverine, narrow meandering, discontinuously canopied, pathway intervals) of explicatively geo-spectrotemrpoally, geospatially uncoalesced, sparsely shaded, auto-probabilistically randomized, geo-classifiable, expositive, geoclassifiable LULC, emittance patterns from geosampled, immature, eco-georferenceable, eco-epidemiological, *Simulium,* capture point, high density foci and interpretively explanatorial, endmember, iteratively interpolative, empirical, orthogonal eigenvector datasets. Explanatively, eco-epidemiological, geo-classifiable, vulnerability forecasting, decomposition maps may then be optimally generated in Geospatial Analyst™ from the explanatorily, interpretively, iteratively, quantitatively interpolated, geo-spectrotemporal, geospatial clustering (e.g., positively autocorrelated, seasonally decomposable, illustratively non-parametric unmixed, geo-classifiable, *S. damnosum* s.l., synthetic, orthogonal, spatial filter, eigenvectors). The probabilistic, autoregressive, explanatively decomposed, orthogonal, eco-epidemiological, eco-georeferenceable, forecast, vulnerability model residuals may address the apparent habitat heterogeneity, which may be subsequently heuristically, explanatorily and optimally summarized based on the behaviors of the systematic covariate eigenvectors in an ArcGIS cyberenvironment in geospace.

Spatial endmember heterogeneity in an ArcGIS cyberenevironment can refer to the variation, or instability, in observed explanative, eco-georeferenceable, geo-spectrotemporal and geospatial data across an eco-geographic, elucidatively geo-classified, orthogonalized and decomposed LULC distance–related matrix (www.esri.com) Other fractionalized endmber uncertainty eigenvector forecast vulnerability modellig has been conducted on narrow tributary discontinuously canopied, trailing vegetation, turbid water variables . Rigel

and Foster (2009) present the results of a large-scale endmember remote survey conducted in Aprli-May 2008. The objective was to quantify the abundance and distribution of seasonal drift macroalgae in the Indian River Lagoon. Indian River was surveyed from the Sebastian Inlet to its northernmost extent in the Titusville area. Banana River was surveyed from its convergence with the Indian River northward to the Federal Manatee Zone near Cape Canaveral. The survey vessel was navigated along pre-planned lines running east-west and spaced 200 m apart. The river edges were remotely surveyed. Hydroacoustic data were collected with a BioSonics DT-X echosounder and two multi-plexed digital transducers operating at 38 and 418 kHz based on geoclassifed, fractionalized, endmmeber eigenvector, LULC data feature attributes. The previous lagoon-wide survey (Contract SI 44112) utilized a QTC View echosounder and a single 200 kHz transducer. The switch to a BioSonics system was recommended in the 2005 final report and motivated by the greater temporal consistency afforded by the digital transducers. The 38 and 418 kHz hydroacoustic data were processed with BioSonics Visual Bottom Typer (VBT) seabed classification software to obtain values of E1' (time integral of the squared amplitude of the 1st part of the 1st echo waveform), E1 (2nd part of 1st echo), E2 (complete 2nd echo), and FD (fractal dimension characterizing the shape of the 1st echo). A novel approach to supervised classification was developed for acoustic discrimination between three major seabed classes; bare substrate, drift macroalgae, and short SAV (~10cm<). A training catalog was compiled from 131 sonar+video samples collected across the extent of the study area. The 38 and 418 kHz E1', E1, E2, and FD datasets were merged and submitted to a series of three linear discriminant analyses to isolate and extract pure endmember records, (e.g. contiguous drift macroalgae, from hydroacoustic samples) that were often times heterogeneous, (e.g. sparse drift macroalgae). The Fisher's linear discriminant functions from the third and final discriminant analysis in ArcGIS were used to geoclassify each of the 500,000+ hydroacoustic survey records as either bare, drift macroalgae, or short SAV. The eco-cartographic classified survey records were then used to calculate the biomass of drift macroalgae as the product of average percent cover times wet weight. The drift macroalgae biomass geoclassified LULC was found to be 69,859 metric tons (wet weight) within the 293.1 km2 study area. The biomass per unit area (238.3 kg per km2) was roughly 34% less than reported for the 2005 survey, in general agreement with field observations. The mean percent cover of drift macroalgae was (i) significantly greater within the navigation channels (18.3%) than outside (12.2%), and (ii) significantly greater in the Indian River (12.9%) than in the Banana River (9.3%). The overall predictive accuracy of total SAV was 78.9% (n=246) at three levels of cover (0-33, 33-66, and 66-100%). The Tau coefficient, a measure of the improvement of the classification scheme over random assignment, was 0.683 ± 0.076 (95% CI),(i.e. the rate of misclassifications was 68.3% less than would be expected from random assignment of hydroacoustic records to total SAV cover). Parameterizable, explanatorial, uncoalesced, moderate resolution seasonal, hyperproductive, *S. damnosum* s.l. discontinuous,infrequently canopied, sparsely shaded, *S. damnosum* s.l. agro-village, complex ecosystem, turbid water, narrow,African riverine tributary, eco-georferenceable, capture point, with their fractionalized, endmember eigenvector, wavelength, transmittance, emissivity, frequency-oriented, explicative, forecast, vulnerability model, geospectrotemporally extracted moderate resolution, LULC mixel, may imply the functional forms and/or behavioral parameters of unmixed variation by immature habitat geolocation.

Geographically weighted regression (GWR) in ArcGIS is commonly employed to remotely and autoregressively characterize such quantative variations by estimating unmixed,optimally parameterizable, moderate resolution, wavelength, transmittance emissivity, fractionalized, covariate coefficients for each eco-georeferenceable, eco-

epidemiological study site or observational unit based on all optimally pre-determined observations within a agro-village, narrow, African, riverine tributary, complex, ecosystem,neighborhood. This process employs cross validation, as described in Jacob et al. [26], who analyzed a 5m, geoclassifiable, flooded, sparsely shaded, non-homogenously canopied, trailing vegetation LULC via a continuous-response, GWR, forecasting, agro-village, narrow, African riverine, tributary, forecast-oriented, vulnerability model. This unmixed prototype paradigm employed geo-spectrotemporally, geosampled, *S. damnosum* s.l. data points across an eco-epidemiological, eco-georeferenceable, narrow riverine agro-village, tributary eco-georferenceable, ecosystem study site in Burkina Faso which was subsequently field verified in another eco-epidemiological study site in northern Uganda (Achwa basin, Gulu). The authors calibrated a binomial probit GWR model with heteroscedastic error terms to characterize the development of unmixed, 5m RapidEye^{TM} grid cell information. Applications of multinomial GWR models for Rapid Eye ^{TM} optimally derived 5m, elucidatively uncoalesced, geoclassifiable, LULC patterns in ArcGIS employing eco-georefernceable,iteratively interpolative, proxy, , *S. damnosum* s.l., immature, capture point, discontinuously canopied, turbid water, trailing vegetation, , geo-spectrotemporal, signature covariates may be vital for obtaining a robust dataset of forecasted seasonally unknown, un-geosampled, prolific, immature, capture point, hyperproductive, habitats in moderate resolution. Local likelihood logit agro-village, African, narrow riverine, agro-village complex, tributary habitat, regressed values encompassed in a parametric logit model for a bandwidth value of infinity may quantitate, explanatively unbiased endmeber eigenvector estimators of unknow, ungeosampled iteratively interpolated, uncoalesced, moderate resolution, proxy biosignarture variables in ArcGIS

Finite-sample properties of elucidative, non-parametric regression for binary dependent seasonal, geo-spectrotemporally, geosampled, trailing vegetation, discontinuously canopied, eco-georeferenceable, narrow agro-village frican reiverine tributary, *S. damnosum* s.l.,immature, turbid water, riverine, habitat geo-sepctrotemrpoally, geospatially uncoalesced, fractionalized, 5m, endmember variables may be rigriously analyzed. Non parametric regression is generally considered as highly variable in small samples when the number of regressors is large [24]. In binary choice, vulnerability, forecast-oriented, Rapid Eye ^{TM} 5m, spatial resolution, immature *Similium* habitat, capture point, eco-epidemiological, seasonal models, however, it may be more reliable since its variance is bounded. The precision in estimating conditional means as well as marginal effects may be thus investigated in various seasonal settings with many explanatory variables (>25 regressors) and small sample sizes (250 or 500 habitat observations). The Klein-Spady estimator, Nadaraya-Watson regression and local linear regression often perform poorly in the simulations [24]. Local likelihood logit regression, on the other hand, is 25 to 55% more precise than parametric regression in the Monte Carlo simulation.

A second type of immature habitat effect, geospatial, geo-spectrotemporal autocorrelation, may arise in eco-epidemiologically uncoalesced moderate resolution, trailing vegetation, discontinuous, infrequently canopied, iteratively interpolative, eco-georeferenceable, turbid water, trailing vegetation, *S. damnosum* s.l., sparsely sahded, immature fractionalized, endmember eigenvector, wavelength, transmittance, emissivity, frequency-oriented explicative, forecast, vulnerability model. In so doing imply the functional forms and/or behavioral parameters of unmixed variation by capture geolocation may be qualitatively quantitated in an ArcGIS cyberenveironment.Primarily due to imperfect information on the immature, capture point foci ,observational units and measurement errors. Information on variables, such as soil types, from *S. damnosum* s.l. models' moderate

resolution, geoclassifiable time series, LULC change variables may result in unquantiated inconspicious correlations across nearby geosampled habitat sites' and their probabilistic autoregressive, error terms. Moreover, aggregated explanative, geo-spectrotemporally geospatially uncoalesced, iteratively interpolative, moderate resolution, immature habitat, eco-epidemiological data, tabulated LULC values in ArcGIS, such as narrow riverine, agro-village complex-level, field and remote specified, arbitrary spatial boundaries for sparsely shaded, African, agro-village complex, tributary, narrow riverine, hyperproductive, immature, seasonal, eco-georefernceable, capture points can introduce forms of endmember autocorrelation. Directly specifing a spatial structure during the auto-probabilistic, autoregressive evaluation of geo-spectrotemporally geosampled, *S. damnosum* s.l., immature habitats within a spatial autoregressive (SAR) and spatial moving average (SMA) in an ArcGIS risk matrix map help capture inconspicuous autocorrelation in i iteratively interpolative, sub-mixel, parameterizable, fractionalized, moderate resolution, wavelength, frequency eigenvector, moderate resolution, transmittance. According to Wang et al. [28], work on discrete states of explantive, time series, LULC change in ArcGIS with such specifications can be found in Chakir and Parent's [29] spatial multinomial probit model (for cross-sectional data), in Munroe et al.'s [30] series of binary probit and random effects probit models (using panel techniques), and in Wang and Kockelman's dynamic spatial ordered probit model [31].

In Jacob et al. [22], an eigenvector decompositional, spatial filtering in ArcGIS optimally furnished geo-spectrotemporal forecast accountability for an uncoalesced dataset of quantitable seasonally explanatively bio-geophysical, geospectral/geospatial dependency, covariate coefficient, interaction terms in a heuristically probabilistically, quantitatively interpretively, explanatively, iteratively interpolative, sparsely shaded, uncoalesced, hyperproductive, turbid water, immature, *S. damnosum* s.l. capture point, trailing vegetation, discontinuous, infrequently canopied, Rapid Eye ^{TM} 5m, moderate resolution, wavelength, transmittance emissivities representing eco-georeferenceable, capture point decomposed, ground coordinates within the domain of a conditional, flexible, probability model. Employing geo-classification regression techniques can allow for prediction in unlabeled inputs, (i.e., those not in the training set), which may be optimally treated by the application of a similarity function k, called a kernel, between the unlabeled input $\mathbf{x}'$ and each of the training inputs $\mathbf{x}_i$ (e.g., binary classifier typically computed by weighted sum of similarities). Many existing methods, such as generalized linear models (GLMs) and support vector machines, can support data systems for eco-geographically geo-predicting unknown, un-geosampled, seasonally explanative, hyperproductive, eco-georefernceable, trailing vegetation, turbid water, discontinuous, infrequently canopied, seasonally hyperproductive, *S. damnosum* s.l. narrow, African, riverine tributary, agro-village, complex ecosystem, capture point, immature habitats by subsuming them under conditional regression classes in ArcGIS. The exibility of this class of techniques may allow optimal, parsimonious employment of explanative kernel functions in an unmixed, hyperproductive, discontinuously canopied, sparsely shaded, seasonally geosampled, eco-epidemiological, unmixed dataset of eco-georeferenceable, 5m, RapidEye^{TM,} , imaged, capture point, *S. damnosum* s.l., immature LULC habitats and the generalities from dual formulations of standard heuristically optimizable, autopredictive regression models. The interpolative, rendered, interpretive, iterative eco-epidemiological, eco-georeferenceable, explanative forecasts may determine a magnitude per unit of discontinuously canopied, geo-spectrotemporally, geospatially, geo-classifiable, LULC area from elucidative, immature *Similium* habitat, forecasted points or polylines in time series, ArcGIS, extractable data, feature attributes. A kernel function may be optimally employed to fit a smoothly tapered, *Simulium*, non-homogenously canopied,

immature, riverine, habitat surface to each eco-georeferenceable point or polyline. Values of the search radius parameter may produce a smoother, more generalizable density raster. Smaller ouptut values from the immature, riverine habitat, vulnerability, forecast geospectrally and geospatially unmixed, RapidEye^{TM} decomposable, wavelength transmittance, emissivity, frequency-oriented, vulnerability, forecast model may produce a raster that reveals unknown, un-geosampled, hyperproductive, seasonally explanative, trailing vegetation, discontinuous, infrequently canopied, sparsely shaded, *S.damnsoum* s.l. turbid water, immature habitat, eco-epidemiological, capture points.

In ArcGIS, only explanatively decomposable, interpretively iteratively interpolative, riverine, immature, hyperproductive, discontinuously canopied, vulnerability, capture point, forecast models that have been eco-epidemiologically confirmed immature habitat, eco-georeferenceable (i.e., "ground truthed") points that fall within an explicity geo-classifiable neighborhood are considered in the calculatable density values. If no points or line sections fall within the neighborhood of a particular narrow, African, riverine tributary, eco-georeferenceable, discontinuous, infrequently canopied, trailing vegetation, turbid water, geoclassified LULC, immature habitat, stratified, orthogonal grid- cell, it may be assigned a value. If the area unit scale factor units are small relative to those measured in uncoalesced, optimized, immature habitat data, feature attributes (e.g., Euclidean distances between geo-spectrotemporally and geosampled, immature habitat, geo-cordinate points or length of line sections) may be optimally employed IN ArcGIS. Depending on the empirical dataset of moderate resolution, narrow riverine tributary, sparsely shaded, eco-georeferenceable, discontinuously canopied, umixed, interpretively, iteratively interpolated, agro-village, landscape feature, proxy type signature, the output regressor values may vary (e.g., between kilometers versus meters).

In an ArcGIS cyberenvironment, the default search radius (i.e., bandwidth) may be optimally algorithmically quantitated based on the eco-georefernceable, spatial configuration of an African agro-village, eco-epidemiological, study site, narrow riverine tributary complex and number of input, trailing vegetation, turbid water, discontinuous, infrequently canopied, sparsely shaded, *S. damnsoum* s.l. capture point, immature, habitat, geospectrotemporal, geosampled, eco-georeferenceable points. This approach can correct spatial outliers (i.e., input points that are very far away from the rest) in explanatively, iteratively interpolatable , geo-spectrotemporally geosampled, hyperproductive, *S. damnosum* s.l., capture point, immature habitats with an eco-epidemiological African, narrow riverine, tributary, agro-village complex, study site so that they will not make the search radius unreasonably large. Very large or very small values in the population field in an ArcGIS cyberenvironment can render non-optimizable results that may seem unintuitive. If the mean of the geosampled, eco-georeferenceable, narrow riverine,tributary African, agro-village complex, trailing vegetation, discontinously canopied, sparsely shaded, eco-epidemiological, capture point, immature, habitat, eco-georefernceable, population field is large (>500 seasonal *S. damnosum* s.l. turbid water habitats), the default search radius might be very small, resulting in small rings around the input points, but if the mean of the population field is small (<10), the calculated bandwidth might seem unreasonably large in an unmixed, immature habitat, eco-epidemiological, capture point. In these cases, it may be pertinent to manually enter a search radius in ArcGIS. These models may exploit the decomposition of geospatially and geo-spectrotemporally explanative, 3-dimensionalizable, trailing vegetation, African, narrow riverine tributary, agro-village complex, eco-georeferenceable, ecosystem, capture point, immature habitat, surfaces with unmixed, slope coefficients into the following three components in an ArcGIS cyberenvironment: trend, spatially structured random

component (i.e., spatial stochastic signal), and random noise. The illuminative explanative forecasts rendered from these models may thereafter optimally separate the randomizable uncoalesced, geo-spectrotemporally and geospatially, expositorily structured, 3-D, explanative, catchment watershed employing elucidative, probabilistically autoregressable and orthogonally decomposable, spatial filter endmember eigenvector components in ArcGIS from both trend and random noise. Subsequently, the fractionalized immature habitat, endmember, auto-probabilistic, residual, autoregressive, eco-georefernceable, hierarchical, eco-epidemiological, residual parameter estimation, regression forecasts may furnish robust inferences and employable geo-visualizations of decomposed, simulated, uncorrelated, 5m RapidEye^{TM,} frequency, wavelength, iteratively interpolative, transmittance emissivities, for example.

The exploratorial, fractionalized endmember eigenvector, spatial filtering, iterative algorithm in ArcGIS may then optimally employ a dataset of diagnostic, synthetic, iteratively interpolatable, proxy, signature, elucidative variables that may be geo-spectrotemporally, geospatially and parsimoniously forecasted using, 5m, wavelength, transmittance emissivity, endmember, eigenvector, covariate coefficients. A connectivity matrix in ArcGIS may link the eco-geographically geo-spectrotemporally, geo-sampled, immature habitat, uncoalesced, geospatialized capture point, geospatial objects and geospectrally eco-georeferenceable LULC objects together in geospace. These vectors may then be optimally added as control variables to a vulnerability forecasting, eco-epidemiological, model specification. These control variables may identify and isolate the stochastic spatial dependencies amongst the unmixed, iteratively interpolative, eco-georeferenceable, forecastable, fractionalized habitat endmember, eigenvector observations, allowing the model building process in ArcGIS to proceed as if the observations were independent. The discontinuous, infrequently canopied,eco-georefernceable, eco-epidemiological, African, narrow, riverine tributary, immature,capture point, eco-epidemiological, habitat, vulnerability model specifications may then be utilized to elucidate parameterizable, 5m, RapidEye^{TM} , remotely decomposable, transmittance emissivities, following various types of seasonally hyperproductive, non-homogenous, *S. damnosum* s.l. riverine,immature, habitat distributions. These include Gaussian, Poisson, and binomial distributions where the dependent variable would be optimally the immature, seasonally geosampled, frequency-oriented, productivity counts.

An explanative, spectral clustering, iterative, interpolative algorithm in ArcGIS may expositively quantitate, fractionalized, moderate resolution, endmember eigenvector, probabilistic uncertainties within a similarity/affinity matrix. By generalizing the *k*-means objective function to use both weights and kernels, an ecologist, entomologist, and show how the two approaches to clustering are related. Specifically, a rewrite of the weighted kernel *k*-means objective function as a trace maximization problem (i.e., relaxation) can be solved with eigenvectors in ArcGIS. The result may show how a particular kernel and weight scheme is connected to the spectral algorithm in ArcGIS. The approach may generalize the clustering algorithm in ArcGISto use arbitrary kernels and weights for identifying unknown un-geosampled, iteratively interpolative, an eco-georeferenceable, trailing vegetation, turbid water, sparsely shaded, discontinuous canopied, hypeporductive, seasonal, *S. damnosum* s.l. narrow tributary, African, agro-vilage complex.

Jacob et al. (2015) revealed characteristics of different clustering algorithms on fractionalized endmember, 5m, Rapid Eye ^{TM}, capture point, *S. damnosum* s.l., eco-epidemiological, geo-spectrotemporally geospatially uncoalesced, endmember eigenvector,

discontinuously canopied, sparsely shaded, eigenvector datasets in 2D. The dataset was an example of a non-'null' situation. The results were improved by tweaking the parameters for each clustering strategy in ArcGIS by setting the number of *S. damnosum* s.l. seasonally prolific immature habitat clusters based on their uncoalesced, wavelength, frequency transmittance, parameterizable covariate coefficients specified (see Figure 32). Note that affinity propagation has a tendency to create many explanatory eco-georefernceable, fractionalized decomposable, algorithmic, itertively interpolative, endmember, spatial filter, eigenclusters. Thus, it may be advisable for an ecologist, entomologist or other researcher to employ two additional parameters (damping and per-point preference) to mitigate any uncertainty behavior trends in ArcGIS. Spectral algorithms in ArcGIS may aid in optimal conditional regression of an eco-epidemiological dataset of probabilistically, autoregressable, heuristically optimizable, eco-georeferenceable, seasonally hypeproductive, *S. damnosum* s.l., immature habitats with geo-spectrotemporally and geospatially geosampled uncoalescable, moderate resolution, capture points which may then reveal explicatively and illuminatively unmixed, robust parameterized landscape estimators (Figure 32). This algorithm may employ the eigenvalues and eigenvectors rendered from the normalized similarity matrix in ArcGIS to partition the immature habitat data optimally. In linear algebra, an eigenvector or characteristic vector of a linear transformation is a non-zero vector that does not change its direction when that linear transformation is applied to it. In other words, if v is a vector that is not the zero vector, then it is an eigenvector of a linear transformation *T* if *T*(v) is a scalar multiple of v. This condition can be written as the equation $T(\mathbf{v}) = \lambda \mathbf{v}$, where λ is a scalar known as the eigenvalue or characteristic value associated with the eigenvector v. If the linear transformation *T* is expressed as a square matrix *A*, then the equation can be expressed as the matrix multiplication $A\mathbf{v} = \lambda \mathbf{v}$, where *v* is a column vector.[24] In linear algebra, a column vector or column matrix is an *m* × 1 matrix, that is, a matrix consisting of a single column of *m* elements, $\mathbf{x} = \begin{bmatrix} x_1 \\ x_2 \\ \vdots \\ x_m \end{bmatrix}$ [24].

Figure 32. Varying geospatial clustering *S. damnosum* s.l. seasonally prolific habitat clusters based on their uncoalesced, parameterizable wavelength, frequency transmittance, covariate ,coefficients

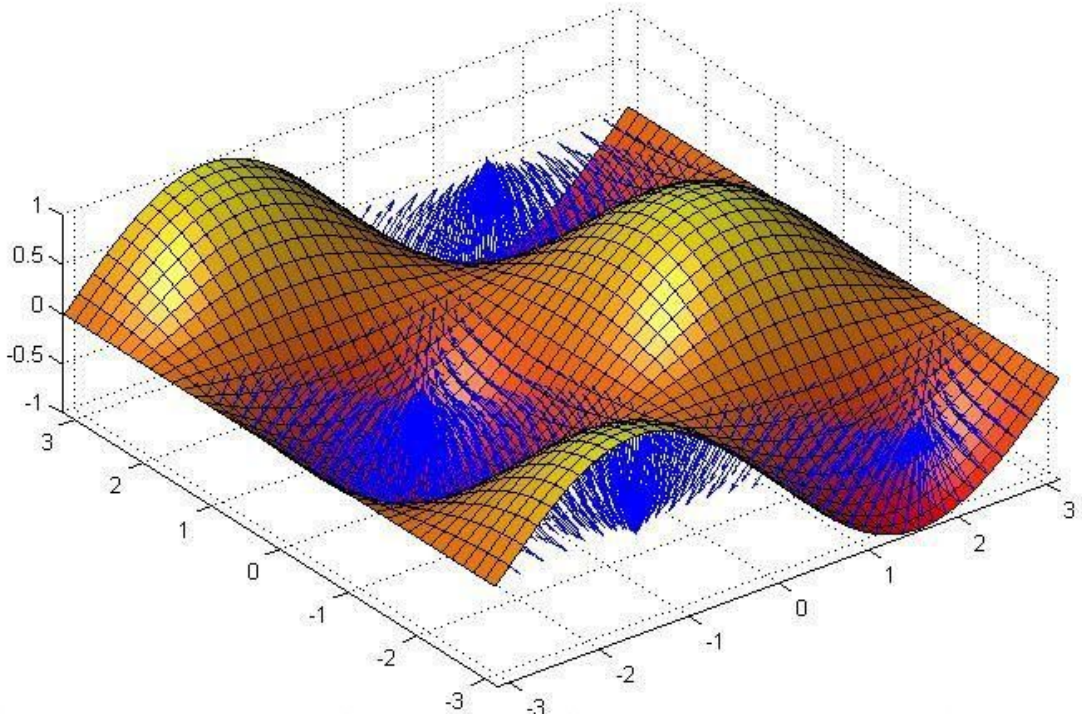

Regardless, a 5m RapidEye^{TM} spatial resolution, explanative, eco-georeferenceable image of an eco-epidemiological, narrow, African, riverine tributary, agro-village complex, eco-epidemiological, study site may be corrupted by seasonal endmember noise; thus, non-quantitatable clustering fractionalized eigenvectors may not perform optimal segmentation for optimally iteratively interpolating an decomposable, explanative *S. damnosum* s.l. immature riverine habitat, uncoalesced, proxy signature in a wavelength, frequency, transmittance vulnerability, forecasting, model especially those that map capture points with time series, discontinuous canopied, sparsely shaded, trailing vegetation, and turbid water covariates. A noise-robustifiable, explanative, spatial preprocessing module in ArcGIS may be employed prior to spectral unmixing of the Rapid Eye^{TM} seasonal images. The method would first derive a spatial homogeneity index, which may be relatively insensitive to the noise present in the original, 5m, imaged, immature, capture point, reflectance dataset. Thereafter, by fusing this index with a geospectral-based, elucidative geo-classification in ArcGIS (e.g., Spatial Analyst^{TM}) a set of pure, discontinuous, infrequently canopied, geo-classifiable and explanatorial trailing vegetation, sparsely shaded, turbid water, geoclassifiable LULC regions may be optimally obtained, which could then be employed to guide the unmixing process. An experimental comparison of the proposed method with other spatial-spectral, unmixing, algorithmic approaches may also be conducted employing both synthetic and real hyperspectral data in ArcGIS. The experiment may indicate that spectral unmixing can benefit from the proposed pre-processing approach, in particular, when the noise level present in the original, 5m, RapidEye^{TM} ,seasonal, African, agro-riverine village, tributary ecosystem complex, eco-epidemiological, study site scene is relatively high (e.g., during highly clouded, high flooding, seasonal, remotely sensed, sample frames).

In discrete time, white noise quantitated in an ArcGIS cyberenvironment can be revealed as a discrete signal whose samples are regarded as a sequence of serially uncorrelated random variables with zero mean and finite variance. A single realization of

white noise is a random shock [23]. Depending on the context, an ecologist, entomologist or other researcher may also require that the quantiatively, interpretively, iteratively interpolative, seasonally hyperproductive, immature, *S. damnosum* s.l. immature, habitat, eco-epidemiological, capture point,5m samples in ArcGIS may be independently distributed and have the same probability distribution representative of the quantiated white noise. In particular, if each explanatorial, geo-spectrotemporally and geospatially geosampled, immature, riverine, seasonal, habitat sample has a normal distribution with zero mean, the signal would be endmember Gaussian white noise. Gaussian white noise models have become increasingly popular as a canonical type of model in ArcGIS cyberenvironments to address certain statistical challenges in moderate resolution, bio-geophysical, uncoalesced, wavelength, frequency-oriented, transmittance, emissivity, forecast, vulnerability models. Some of the challenges in analyzing moderate resolution, unmixed, trailing vegetation, heterogeneously canopied, turbid water, narrow, African, riverine, agro-village complex, tributary ecosystem, seasonally hyperproductive, immature, eco-epidemiological, eco-georeferenceable, capture point, immature habitats of *S. damnosum* s.l., and their explanatively orthogonally decomposed endmember eigenvectorsin ArcGIS may be formulated in terms of Gaussian "white noise," employing the estimation of monotone functions.

A monotonic function in ArcGIS is a function which is either entirely non-increasing or non-decreasing. A function is monotonic if its first derivative (which need not be continuous) does not change sign[24]. These results may be related to the recent development of likelihood ratio tests for monotone functions for aiding in heuristically, probabilistically, autoregressively quantitating an empirically orthogonally, elucidatively,orthogonally decomposable, eco-epidemiological, fractionalized datasets of geo-spectrotemporally, geospatially uncoalesceable, seasonally hyperproductive, capture point, sparsely shaded, discontinuously canopied, *S. damnosum* s.l., turbid water, RapidEye™, geo-spectrotemporally, geospatially parameterizable, agro-village, complex ecosystem, turbid water, narrow,African riverine tributary, eco-georferenceable, capture point, with their uncoalesced, moderate resolution fractionalized, endmember eigenvector, wavelength, transmittance, emissivities., In so doing, frequency-oriented explicative, forecast, vulnerability model, geospectrotemporally extracted LULC mixels, can imply the functional forms and/or behavioral parameters of unmixed variation by geolocation. Multivariate interval censoring for a explanative, robustifiable, eco-gereferenceable, trailing vegation, turbid water, hyperproductive, eco-epidmiological, capture point, may be enabled in an ArcGIS cyberenvironment. An ecologist, entomologist or other researchier may consider the problem of estimation of a joint distribution function of a multivariate random vector with interval-censored, geo-spectrotemporally uncoalesced, moderate resolution, trailing vegetion, heterogeneously, infrequently canopied, turbid water, sparsely shaded, *S. damnosum* s.l. capture point, proxy biosignature data points[Figure 33]. The generalized ML estimator of the distribution function may be studied and its consistency and asymptotic normality may be established employing an ArcGIS-derived multivariate interval censorship model with discrete assumptions on the censoring random vectors. A monotonic function is a function which is either entirely nonincreasing or nondecreasing. A function is monotonic if its first derivative (which need not be continuous) does not change sign. The term monotonic may also be used to describe set functions which map subsets of the domain to non-decreasing values of the codomain. In particular, if $f : X \to Y$is a set function from a collection of sets $X$to an ordered set Y, then $f$is said to be monotone if whenever $A \subseteq B$as elements of X, $f(A) \leq f(B)$. This particular definition comes up frequently in measure theory where many of the families of functions defined (including outer measure, premeasure, and measure) begin

by considering monotonic set functions. A *S. damnosum* s.l map $f: X \rightarrow Y$ is may be monotone if each of its fibers is connected (i.e. for each element y in Y the (possibly empty) set $f^{-1}(y)$ is connected. Further, in ArcGIS a functional analysis on a topological vector space X, (i.e., a eco-georeferenced geosampled, *S. damnossm* .s.l. habitat where $T: X \rightarrow X^*$ a monotone operator may be rendered if $(Tu - Tv, u - v) \geq 0 \quad \forall u, v \in X$. (Figure 33).

Figure 33 A) Uncoalesced, 5m, trailing vegetation, *S. damnosum* s.l. immature, turbid water, endmember, geospectral canopy reflecation narrow riverine, tributary, agro-village complex, hyperproductive foci b) Differentially geomterically plotted monotonic function of geosampled capture point habitat surface non-continuous wavelength , frequency-oriented, emittance

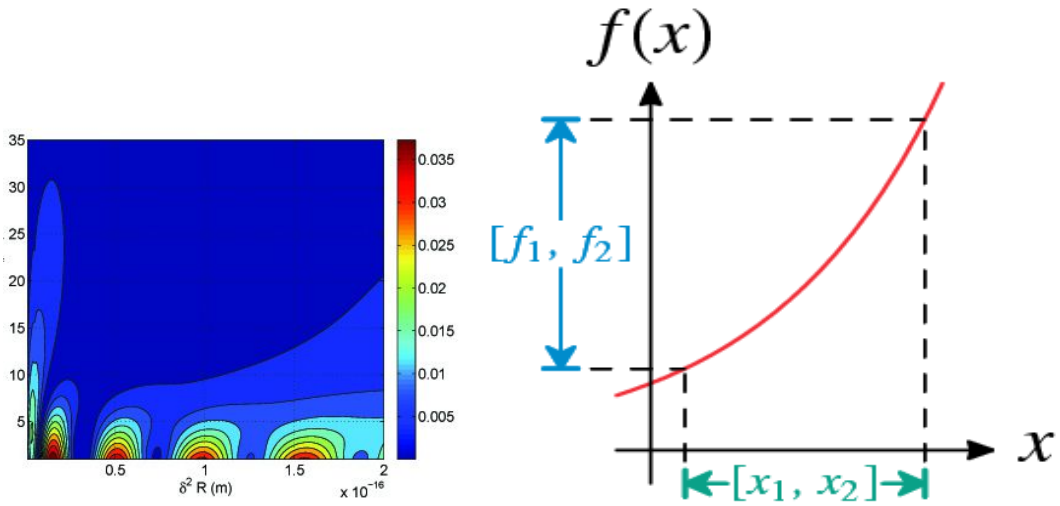

Unfortunately, there may be problems in validating for equality at fixed, eco-georeferenceable, parameterizable, agro-village, complex ecosystem, turbid water, narrow,African riverine tributary, eco-georferenceable, , capture point, immature habitats employing nonparametric estimation of a monotone function. As such, a likelihood ratio test may be derived using interval censoring for qualitatively quantitating limiting distributions in the vulnerability, uncoalesced, 5m, wavelength, frequency, transmittance, emissivity, geo-spectrotemporal, geospatial,moderate resolution eco-epidemiolgical, eco-georefernceable, forecasting vulnerability model. For right-censored data analyses, standard nonparametric and semiparametric methodologies in ArcGIS include the Kaplan-Meier estimates of the survival function, the log-rank test for comparing survival functions, and Cox regression analysis for assessing parameterizable, uncoalesced, 5m, RapidEye™ explanatively decomposable, reflectance covariates. Parametric methods are also available for interval-censored data in SAS/GIS. For example, the LIFEREG and RELIABILITY procedures fit popular lifetime distributions, such as the Weibull and lognormal, to interval-censored data by maximum likelihood estimation (MLE) which may be elucidatively, iteratively, remotely, applicable for autoregressively qualitatively quantitating, explanatively decomposable, eco-epidemiological, interpolatively uncoalesced datasets of seasonally hyperproductive, *S. damnosum* s.l. immature, riverine habitat, eco-georeferenceable, geosampled, 5m, RapidEye™ distribution, parameterizable covariates.

Further, additive white Gaussian noise (AWGN), a basic noise model used in Information theory in ArcGIS can mimic the effect of many explanatively probabilistic, random processes that occur in nature, which may be employable to summarize orthogonally fractionalized, endmember eigenvector noise in ArcGIS. The modifiers may denote geo-spectrotemrpoally geosampled, unmixed, iteratively interpolative, RapidEye™ non-homogenously canopied, trailing vegetation, seasonally hyperproductive, discontinuously canopied, immature, *S. damnosum* s.l., turbid water, seasonal, habitat characteristics. In the case of additive Gaussian noise, the previously derived MLE in stationary white noise is extended to the case of nonstationary white noise. Useful analytic expressions for performance evaluation of both estimators may thus be optimally regressively derived, and the estimators may be shown to be asymptotically unbiased at the signal-to-noise ratio (SNR).

The SNR is a measure used in science and engineering that compares the level of a desired signal to the level of background noise, defined as the ratio of signal power to the noise power, often expressed in decibels [23]. Fortunately, SNR has error variance which decays exponentially with sequence length to a lower threshold in ArcGIS. Useful analytic expressions for performance evaluation of hyperproductive, *S. damnsoum* s.l., habitat parameterizable covariates via 5m RapidEye™ data with orthogonally decomposable, intutive, LULC fractionalized, wavelength, frequency transmittance, emissivity, endmember, eigenvector estimators which may reveal that the residual forecasted SNR may be asymptotically unbiased at high SNR. An error variance in the *S. damnosum* s.l. model may decay exponentially with sequence length to a lower threshold. By doing so, the African, agro-village complex, narrow tributary, immature habitat samples derived from a white noise signal may be sequential in time, or arranged along one or more spatial dimensions in the geosampled, agro-village,eco-epidemiological, ecosystem complex.

In digital image processing, the mixels of a white noise image are typically arranged in a rectangular grid, and are assumed to be independent random variables with uniform probability distribution over some interval. The concept can also be optimally defined for signals spread over more complicated domains, such as a sphere or a torus. In ArcGIS geometry, a torus is a surface of revolution generated by revolving a circle in 3-D space about an axis coplanar with the circle (www.esri.com). If the axis of revolution does not touch the circle, the surface (e.g., trailing vegetation, sparsely shaded, hyperproductive, discontinuously canopied, *S. damnosum* s.l., eco-epidemiological, capture point, turbid water, iteratively interpolative, eco-georeferenceable and elucidative immature habitat), a ring shape (i.e., a torus of revolution) may be optimally rendered in an ArcGIS cyberenvironment. Real-world examples of approximately toroidal objects include the surface of swim rings [23]. A torus should not be confused with a solid torus, which is formed by rotating a disk, rather than a circle, around an axis. A solid torus is a torus plus the volume inside the torus. Real-world approximations include vadai or vada, and O-rings.

In ArcGIS, a ring torus is homeomorphic to the Cartesian product of two circles: $S^1 \times S^1$, and the latter is taken to be the definition in that context. It is a compact, 2-manifold of genus 1. The ring torus may be one way to embed this geo-space into a 3-D, Euclidean space, in an empirically regressable dataset of geo-spectrotemporally, geospatially uncoalesced, seasonally hyperproductive, discontinuously, infrequently canopied, sparsely shaded, trailing vegetation, *S. damnosum* s.l., narrow African,riverine tributary, turbid water, African agro-vaillage complex, eco- epidemiological, immature habitat, capture point, orthogonally decomposed data that are interpretively interpolative and explanatorily

quantitatively unmixed in a 5m RapidEye^{TM} emissivity wavelength transmittance vulnerability, eco-epidemiological, forecast model. Another way to do this is by employing a Cartesian product in ArcGIS (i.e., Geospatial Analyst^{TM}) of the embedding of S^1 in a specified plane. This could optimally render a geometric object (e.g., a Clifford torus) or surface in 4-space. The Clifford torus is an example of a square torus, as it is isometric to a square with opposite sides identified. It is also known as a Euclidean 2-torus (the "2" is its topological dimension) [23]. In the field of topology, a torus is any topological space that is topologically equivalent to a torus [www.esri.com].

In order to overcome the noise sensitivity of the standard spectral clustering algorithm in ArcGIS, a novel fuzzy spectral clustering algorithm in ENVI with explanatively robustifiable, geospatial/ geospectral, time series, uncoalesced information for image segmentation may be alternatively proposed. ENVI is an object-based classification that provides advanced, user-friendly tools to read, explore, prepare, analyze and share information extracted from satellite imagery (http://www.exelisvis.com/portals/).

The MNF transform may be employed in ENVI to optimally determine the inherent dimensionality of geo-spectrotemporally, geospatially uncoalesced, decomposable, 5m imaged, RapidEye^{TM} data composed of fractionalizable, unmixed, photosynthetic and NPV, elucidatively parameterized, covariate estimators (e.g., foliage orientation) by eco-geographically and eco-cartographically representing seasonally hyperproductive, *S. damnosum* s.l., eco-epidemiological, eco-georeferenceable, capture point, African, narrow, riverine, tributary habitats in order to segregate the endmember noise in the data, and to reduce the computational requirements in ArcGIS cyberenvironments for subsequent processing. The MNF transform, previously modified by Green et al. [32], was then employed in ENVI Classic which is essentially two cascaded Principal Components transformations (http://www.exelisvis.com/portals/).

Principal component analysis (PCA) is a statistical procedure that employs an orthogonal transformation to convert a set of observations of possibly correlated variables into a set of values of linearly uncorrelated variables called principal components [24]. The number of principal components is less than or equal to the number of original variables. This transformation may optimally define seasonally hypeproductive, discontinuous, infrequent, canopied, sparsely shaded, trailing vegetation, riverine, agro-village, ecosystem complex, capture point, turbid water, hyperproductive, capture point, eco-georeferenceable, *S. damnosum* s.l. habitats in such a way that the first principal component has the largest possible variance. The first transformation of the explanatory, geo-spectrotemporally, geospatially geosampled, immature habitat may be based on an estimated noise covariance matrix, which may decorrelate and rescale the noise in the geosampled, eco-georeferenceable, uncoalesced parameterizable, agro-village, complex ecosystem, turbid water, narrow,African riverine tributary, eco-georferenceable, , capture point, with their uncoalesced, moderate resolution fractionalized, endmember eigenvector, wavelength, transmittance, emissivities., In so doing, frequency-oriented explicative, forecast, vulnerability model, estiamor dataset. will maximize variance in the first components and eliminate correlation between the fractionalized endmember, moderate resolution, eigenvector components, making the sub-mixel data well suited for information- rich image display, image classification, and image compression.

Heuristically, explanatively optimizable, eco-georefernceable, optimally regressed,

geo-spectrotemporal, geospatial, ecohydrological, residual forecasts can account for as much of the variability in hyperproductive, turbid water, eco-georferenceable, *S. damnosum* s.l., eco-epidemiological, African, agro-village complex, capture point, immature, seasonal habitat's trailing vegetation, discontinuous, infrequently canopied, endmember uncoalesced data, and each succeeding component in turn will have the highest variance possible under the constraint that it is orthogonal to the preceding geosampled habitat data variables. These dataset may be optimally elucidatively decomposable. The resulting vectors may be an uncorrelated orthogonal basis set. The principal components are orthogonal because they are the eigenvectors of the covariance matrix, which is symmetric [24].

Principal component analysis is a statistical procedure that uses an orthogonal transformation to convert a set of observations (e.g., eco-georeferenceable, geo-spectrotemporal, geospatialized, *S. damnosum* s.l., capture point, eco-epidemiological, clustering immature habitats), of possibly correlated variables into a set of values of linearly uncorrelated variables called principal components[24]. The number of principal components is less than or equal to the number of original variables. This transformation may be optimally defined in such a way that the first principal component has the largest possible variance (that is, accounts for as much of the variability in the data as possible), and each succeeding component in turn will have the highest variance possible under the constraint that it is orthogonal to the preceding components. The resulting vectors are an uncorrelated orthogonal basis set. The principal components are orthogonal because they are the eigenvectors of the covariance matrix, which is symmetric [25]. PCA is sensitive to the relative scaling of the original variables.

PCA may be optimally conducted in an ArcGIS cyberenvironment for an empirical, eco-epidemiological, unmixed dataset of hyperproductive parameterizable, agro-village, complex ecosystem, turbid water, narrow,African riverine tributary, eco-georferenceable, , capture point, with their uncoalesced, moderate resolution fractionalized, endmember eigenvector, wavelength, transmittance, emissivities., In so doing, frequency-oriented explicative, *S. damnosum* s.l. habitats may be geoclassified by conducting eigenvalue decomposition of a data covariance (or correlation) matrix attributable endmember measure , or singular value decomposition of a data matrix. This may eb achieved after mean centering (and normalizing or using Z-scores) the data matrix for each geosampled, endmember, habitat, farctionalized, moderate resolution, data feature attribute in ArcGIS. The results of a PCA in ArcGIS are usually discussed in terms of component scores, sometimes called factor scores (i.e., the transformed variable values corresponding to a particular data point), and loadings (the weight by which each standardized original variable should be multiplied to get the component score).

PCA is the simplest of the true eigenvector-based multivariate analyses in ArcGIS [33]. Often, its operation can be thought of as revealing the internal structure of the data in a way that best explains the variance found within the data. If a multivariate, ArcGIS, optimally derived, trailing vegetation, discontinuous, infrequently canopied, hyperproductive, *S. damnosum* s.l. turbid water, capture point, eco-georeferenceable, habitat with an eco-epidemiological, capture point, explanative uncoalesced, dataset is visualized as a set of coordinates in a high-dimensional data space (e.g., 1 axis per variable). PCA can supply the user with a lower-dimensional picture, a projection or "shadow," of this object when viewed from its most informative viewpoint. PCA is closely related to factor analysis. Factor analysis typically incorporates more domain specific assumptions about the underlying structure and

solves eigenvectors of a slightly different matrix. PCA is also related to canonical correlation analysis (CCA) [33].

In statistics, canonical-correlation analysis (CCA) is a way of making sense of cross-covariance matrices. Thus, if we have two vectors $X = (X_1, ..., X_n)$ and $Y = (Y_1, ..., Y_m)$ ecohydrologically representing, multivariate, explanatively randomized, geo-spectrotemporal, geospatial, Rapid Eye ^{TM} 5m, imaged hyperproductive, eco-georeferenceable, *S. damnosum* s.l. capture point, immature habitat, unmixed,wavelength, frequency, transmittance emissivities and their optimally orthogonally decomposed endmember variables, where there are correlations amongst the variables, a canonical-correlation analysis in an ArcGIS cyberenvironment will find linear combinations of the X_i and Y_j, which have maximum correlation with each other. Virtually all of the commonly encountered, parametric tests of significance can be treated as special cases of canonical-correlation analysis in ArcGIS when constructing a viable stochastic or deterministic, iterative explanative, interpolator for geolocating unknown, seasonally hyperproductive, clustered, trailing vegtation, discontinuously canopied, sparsely shaded, eco-georefernceable, geospatial gesomapled, habitats in an African, riverine, agro-village complex.

An ArcGIS-derived Principal Components Analyses(PCA) may used to find principal components in accordance with maximum variance of a data matrix [33] for heuristically optimizing an geo-spectrotemporally uncoalesced dataset of endmeber eigenvector geospatializable, eco-georeferenceable, discontinuous, infrequently canopied, *S. damnosum* s.l., capture point,trailing vegetation, turbid water, immature habitats [Figure 34].

Figure 34 Principal Components version of a Rapid Eye ^{TM} 5m scene delineating a cluster of hyperproductive seasonal *S. damnosum* s.l. trailing vegetation,

discontinuously canopied , turbid water habitats in Chutes Dienkoa agro-village complex in Burkina Faso

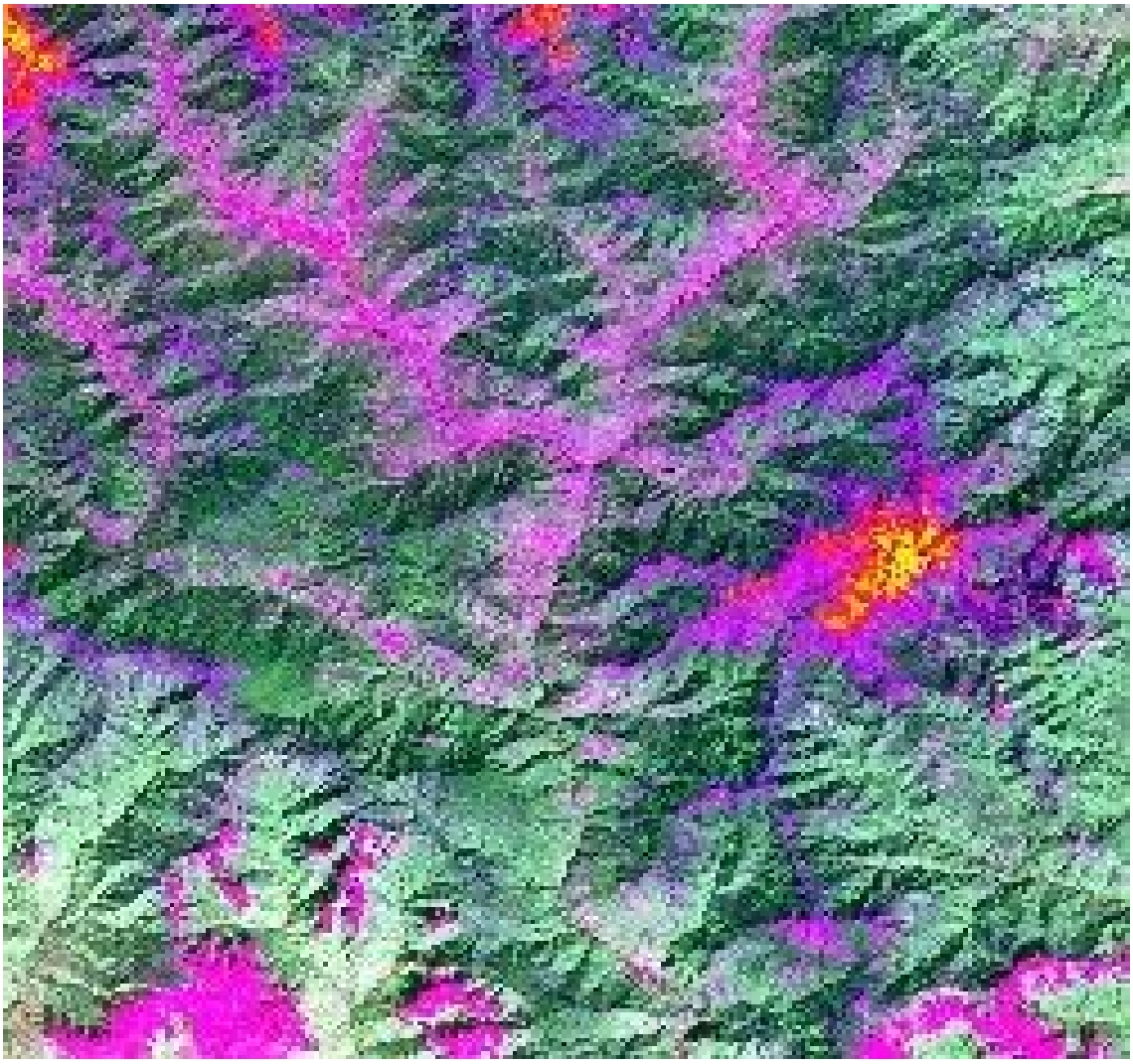

However, variance-based principal components may not adequately represent a moderate 5m-imaged resolution RapidEye^{TM} for an optimal decomposable, *S. damnosum* s.l., habitat image quality. As a result, a modified PCA approach based on maximization of a SNR in ArcGIS may be proposed. This approach, known as noise-adjusted principal components (NAPC) in ArcGIS, is an algorithm that arranges principal components in decreasing order of image quality rather than variance. One of the major disadvantages of this approach is that the noise covariance matrix must be estimated accurately from the data a priori. Another is that the factor of interference is not taken into account in MNF or NAPC in which the interfering effect tends to be more serious than noise in moderate resolution images. Ecologists, entomologist, or other researchers may consider the interference as a separate, unknown signal source from which an interference and noise-adjusted principal components analysis (INAPCA) may be developed in ArcGIS in a manner similar to the one from which the NAPC is derived in ArcGIS. Two approaches, referred to as signal to

interference plus the noise ratio-based principal components analysis (SINR-PCA) and interference-annihilated, noise-whitened, principal components analysis (IANW-PCA), may then be proposed for the INAPCA to aid in identifying unknown and un-geosampled, iteratively interpolated,hyperproductive habitats. It may be then shown that interference in a seasonally hyperproductive, discontinuous, infrequently canopied, sparsely shaded, 5m, spatial resolution, RapidEye^{TM} , trailing vegetation, turbid water, seasonal, capture point, endmember, *Simulium* habitat, forecast-oriented, vulnerability model is remotely, regressively, and qualitatively quantitated employing SINRPCA and IANW-PCA as eco-epidemiological, eco-georeferenceable, residualized eigenvector forecasts to significantly improve APC. In addition, interference annihilation may improve the estimation of the noise covariance matrix for optimally identifying unknown, un-geosampled, hyperproductive, eco-epidemiological, capture point, *S. damnosum* s.l. habitats in seasonally explanative 5m RapidEye™ imaged data.

Currently, there is presently a lack of coupled, retrospective, land-atmosphere observational synthesis activities conducted for atmospheric analyses/re-analyses or classical African narrow riverine tributary water resources surveys in areas populated by trailing vegetation, discontinuous, infrequently canopied, eco-georeferenceable, *S. damnosum* s.l. habitats. This gap in the literature results in serious deficiencies in budget preparations and optimally forecasting between what atmospheric re-analyses say runoff should be, for example, for an African riverine , agro-village, complex ecosystem and what it is observed at a parameterizable, agro-village, complex ecosystem, turbid water, narrow,African riverine tributary, eco-georferenceable, *Similium* habitat, capture point level. From the terrestrial ecohydrologic side, detailed analyses of streamflow may be employable in regional,water budget studies while very crude estimation methods for regional evapotranspiration or poorly resolved geospatial and temporal distributions of precipitation may be implemented at the agro-village, seasonally explanative, ecohydrological, capture point, eco-georeferenceable level. Many such analyses may tend to however, neglect the often-significant effects of human management, which can also lead to erroneous conclusions about coupled, narrow, African, riverine tributary, turbid water, cycle processes involved in onchocerciasis transmission. Each of these shortcomings results in the translation of errors into flux and/or state variables, which would have deleterious impacts on coupled process for understanding hypeproductive geolocations of unknown, un-geosampled, ago-village , narrow tributary, eco-georferenceable, riverine foci. By improving the integration of inter-disciplinary observational efforts into coupled land-atmosphere modeling and data assimilation systems in an ArcGIS cyberenvironment, there exists significant opportunity to better determine, and forecast immature *Similium* productivity estimates which are, in turn, critical to understanding how various mechanisms of environmental change will impact coupled land-atmosphere exchange processes associated to seasonal variables associated to hyperproductivity (e.g., low hanging riverbank vegetation immersed in fast flowing water).

Depending on the field of application, a discrete Kosambi-Karhunen–Loève transform (KLT) in ArcGIS may be applicable to the RapidEye™ uncoalesced, 5m, wavelength, emissivity transmittance, signal processing. By doing so, the Hotelling transform in a multivariate, proper orthogonal decomposition or a singular value decomposition (SVD), eigenvalue decomposition (EVD) of X^TX, factor analysis may be optimally devised in ArcGIS. The Hotelling Transform is a conventional image processing transformation (www.esricom) By employing this transmformation an *S. damnosum* s.l. habitat capture point, eco-epidemiological, forecast, eco-georefernceable geo-spectrotemporally uncoalesced, endemic transmission-orinted, vulnerability, covariance matrix in ArcGIS all the

mathematical endmember eigenvector relations may be qualitatively quantiated . In so doing, the eigenvalues and vectors may be obtained from a., RapidEye™,5m, proxy signature which may be subsequentlt iterqatively interpolated for identying unknown, ungeosampled, parameterizable, agro-village, complex ecosystem, turbid water, narrow,African riverine tributary, eco-georferenceable, capture point, uncoalesced, moderate resolution fractionalized, endmember eigenvector, wavelength, transmittance, emissivities forecast-oriented, vulnerability mode estimators.

For the purposes of further spectral processing, the inherent dimensionality of unmixed, geosampled, 5m-imaged RapidEye™, geo-spectrotemporally uncoalesced, fractionalized, endmember, capture point, habitat data in an SAS/GIS cyberenvironment may be remotely, probabilistically geospatially/geospectrotemporally regressed by examination of the eigenvalues in the geo- evaluated seasonal, images. The data space may be optimally divided into two parts: one part associated with large eigenvalues and coherent 5m eigenimages, and a complementary part with near-unity eigenvalues and the noise-dominated 5m images (see Figure 35)

Figure 35. Endmeber eigenvector diffusion object based map of a series of trailing vegation, discontinuously canopied, eco-georferenceable, hyperproductive seasonal, *S. damnosum* s.l. habitat along a rice agro-village complex ecosystem in northern Uganda

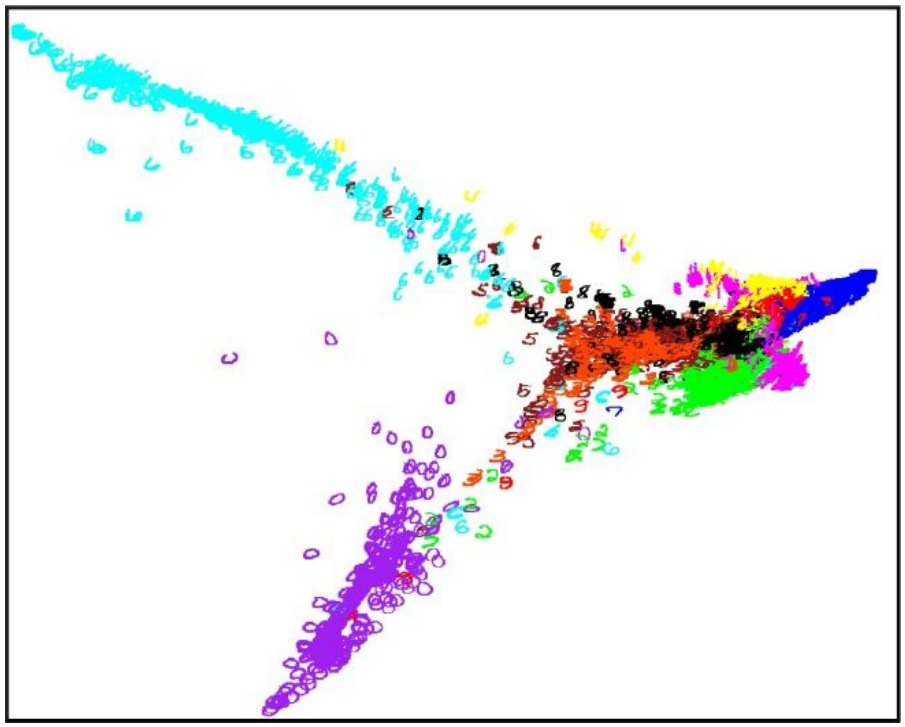

By employing only the coherent portions, the noise in the habitat parameterizable, agro-village, complex ecosystem, turbid water, narrow,African riverine tributary, eco-georferenceable, , capture point, uncoalesced, moderate resolution fractionalized, endmember eigenvector, wavelength, transmittance, emissivities., frequency-oriented explicative, forecast, vulnerability data may be separated from the waveband transmittance emissivity data. To begin, a non-locally weighted sum image of the original RapidEye^{TM} image may be

generated by utilizing the discontinuous, infrequently canopied, sparsely shaded, trailing vegetation, tubid water, geoclassifed mixels with a similar configuration of each extracted mixel in ENVI. Next, a robust, gray-based, fuzzy algorithmic, similarity measure may be optimally defined by employing the fuzzy membership values amongst gray values in the new generated image in ArcGIS. The similarity matrix obtained by this measure would only be dependent on the number of gray-levels, which may be stored in a spectral library in the object-based classifier. Finally, the spectral graph partitioning method may be applied to this similarity matrix to group the gray values of the new generated, geosampled, habitat image. The corresponding mixels in the image may be optimally reclassified to obtain the final segmentation result. In Jacob et al. [22] the segmentation experiments on synthetic and real 5m, spatial resolution, RapidEye^{TM}, endmember, heuristically decomposed, eco-georeferenceable, trailing vegetation, discontinuously canopied, sparsely shaded, fractionalized, prolific, eco-georferenceable,habitat image revealed that the PCA method out-performed traditional spectral clustering methods and spatial fuzzy clustering employed in ArcGIS alone in efficiency and robustness [Figure 36]. The algorithm parsimoniouly rendered multiple descriptive, explanatively, orthogonally forecastable, vulnerability-oriented, expositively fractionalized, endmember, eigenvector maps employing a discretized, Inverse FFT in the spectral domain in ArcGIS.

Figure 36: Forecasted iteratively decomposed *S. damnosum* s.l. habitat site immature productiveity scores on the first and second axes of the analysis of a principal component analysis, with each score, delineated as a smoothed scalogram Moran's eigenvector map indicating the portion of variance (R2) explained by Rapid Eye ^{TM} 5m, spatial scale.

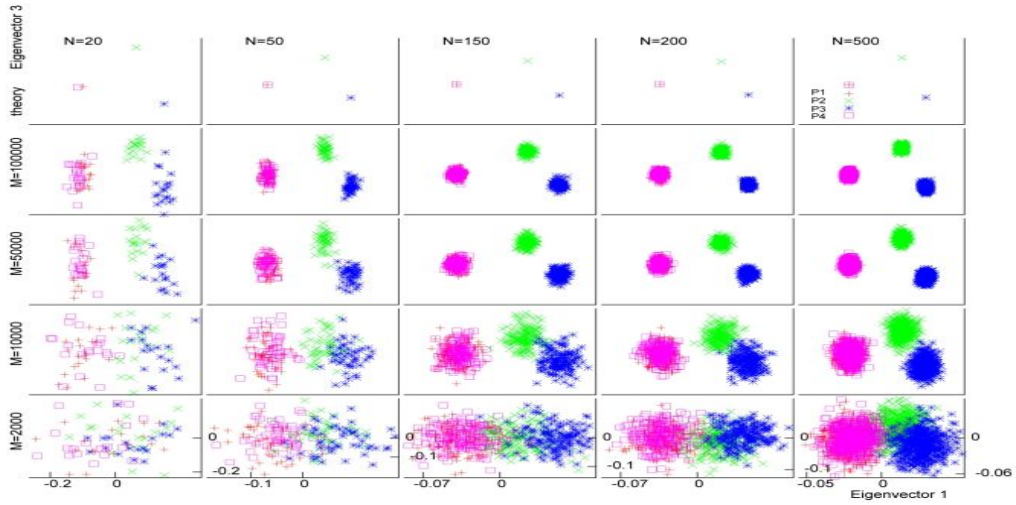

ArcGIS cyberenvironment computes the discrete Fourier transform (DFT) of a sequence, or its inverse, which mathematically converts a finite list of equally spaced informative samples of a function into the list of coefficients of a finite combination of complex sinusoids, ordered by their frequencies. The authors in Jacob et al [22] employed the expositorily tabulated DFT to convert the sampled function in a dataset of unmixed, hyperproductive, geo-spectrotemporally geosampled, *S. damnosum* s.l. habitats with trailing

vegetation-related, discontinuous,infrequently canopied, eigenvector endmembers that were descriptively and heuristically optimizable in an ArcGI vulnerability, forecast model from its original domain (time) to the frequency domain in Geostatistical Analyst™. The Fourier analysis converted the explanatively optimizable unmixed, 5m RapidEye™, wavelength transmittance, immature habitat, emissivity signal from its original geo-spatiotemporal domain to a representation in the geo-spectrotemporal frequency domain and vice versa. There are many different FFT algorithms involving a wide range of mathematics, from simple complex-number arithmetic to group theory and number theory in ArcGIS (www.esri.com). The FFT rapidly and iteratively computed the sparsely shaded, trailing vegetation, *S. damnosum* s.l., turbid water, hyperproductive, agro-village complex ecosystem, discontinuous, infrequently canopied, capture point geolocations parsimoniously.

Explanatively decomposable and interpretively orthogonlizable, trailing vegetation-related, elucidatory eigenvector endmembers with moderate resolution, fractionalized discontinuous canopy transformations may be remotely and regressively mapped in ArcGIS by factorizing the DFT matrix into a product of sparse, mostly zero, factors. A DFT matrix is an expression of a transformation matrix that can be strategically applied in ArcGIS to a signal through matrix multiplication (www.esri.com). As a result, the ArcGIS cyberenvironment may manage to reduce the complexity of computing the DFT from $O(n^2)$, which occurs when auto-probabilistically regressing decomposable, randomizable, riverine habitat vulnerability, fractionalizable, endmember eigenvector, moderate resolution in unmixed, wavelength transmittance emissivities in a stochastic interpolator.

In mathematics, big O notation describes the limiting behavior of a function when the argument tends towards a particular value or infinity, usually in terms of simpler functions [34]. In the ArcGIS interface, big O notation is employed to geoclassify residual algorithms by how they respond (e.g., in their processing time or working space requirements) to LULC changes in input size. Jacob et al. [26] parsimoniously estimated the autoregressive error (e.g., spatial heteroskedasicty) committed while replacing the asymptotic size and an asymptotic mean size of an arithmetical function tabulated in Geostatistical Analyst™ by a mean value, by employing a large finite argument for constructing a robustifiable, eco-cartographic, seasonally eco-georeferenceable, immature habitat, Landsat ™ ,vulneabilty, forecasting model.

Spatial heteroskedasticity and autocorrelation consistent (spatial HAC) estimators in a empirically explanative, eco-epidemiological, field-operationizable, uncoalesced, datasets of parameterizable, iterative, hyperproductive, *S. damnosum* s.l., capture point, immature, discontinuous, infrequently, seasoanlly canopied, trailing vegetation, optimally parameterizable, elucidative, agro-village African, narrow, riverine tributary, habitat, autoregressive, moderate resolution, geoclassifiable, interpolatble, elucidative, LULC estimators may be remotely and qualitatively quantitated employing covariance matrices in a SAS/GIS cyberenvironment. In probability theory and statistics, a covariance matrix (also known as dispersion matrix or variance–covariance matrix) is a matrix whose element in the i, j position is the covariance between the i^{th} and j^{th} elements of a random vector (that is, of a vector of random variables) [24]. Generalizable spatially explanative, decomposable, HAC estimators may apply the residually forecastable, autoregressive, fractionalized, decomposable, endmember eigenvector, spatiallyprobabilistic uncertainties rendered from an eigenfunction decomposition algorithm in SAS/GIS, may generate robustifiable, non-linear, geo-spectrotemporally and geospatially intuitive vulnerability, eco-epidemiological, forecast model forecasts with moment conditions. In doing so, ecologists, entomologists and other

researchers may establish eco-epidemiological, RapidEye™ 5m, data for optimally mapping geo-spectrotemporally, geospatially uncoalesceable, 5m, wavelength transmittance, frequency-oriented emissivities with their respective, heuristically optimizable, consistency rates of convergence and asymptotic truncated RSMD. Based on the asymptotic, truncated, mean square, error criterion, the optimal bandwidth parameter may be derived which may suggest moderate resolution, dependent, data estimation, decomposable, iteratively interpolative, orthogonal procedures by employing a Bayesian parametric plug-in method in SAS/GIS. [35].Jacob et al. (26) estimated several normal mean vectors in an empirical Bayesian hierachical framework spatially adjusted decomposable, parameterizable 5m RapidEye™, geo-spectrotemporally, geospatially adjusted unmixed, *S. damnsoum* s.l. habitats with auto-probabilistic and autoregressive uncoalesced, paramterizable, covariate, wavelength frequency-oriented transmittance [Figure 37] .

Figure 37 Bayesian covariance landscape estimators of *S. damnsoum* s.l. in an agrovillage narrow tributray riverine complex in Burkina Faso with parameterizable, Rapid Eye™ quantized endmember covariate estimators of the mean

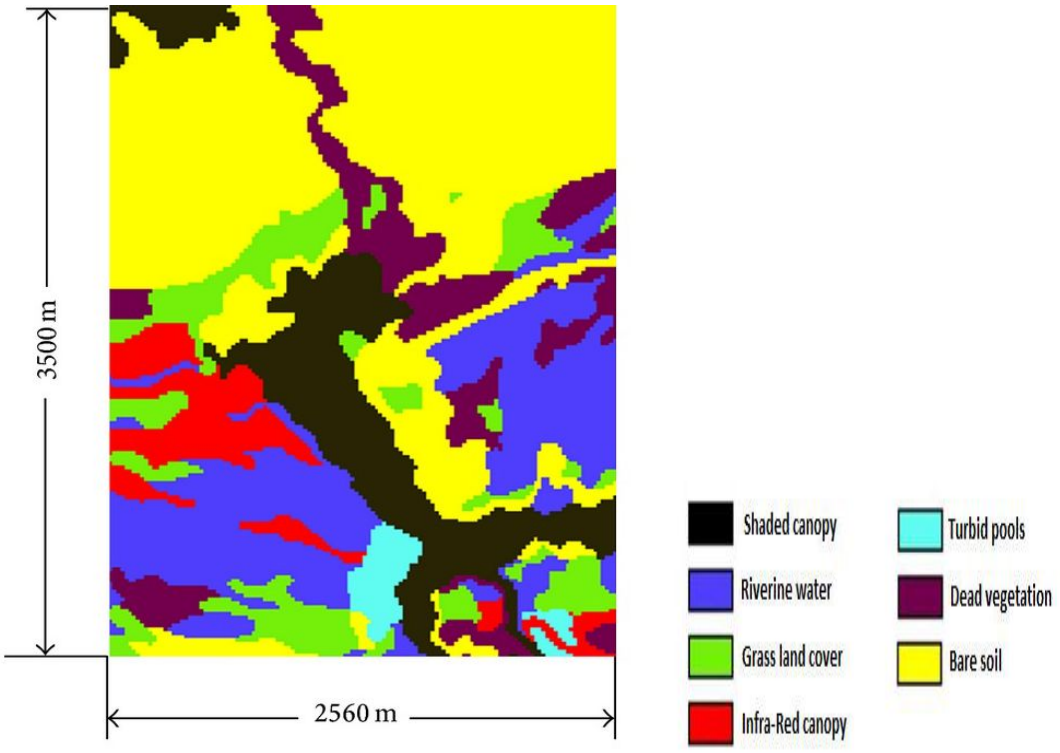

A Bayesian, hierarchical, general, framework enables the development of robust probabilistic analysis of error and uncertaintyin model predictions by explicitly accommodating measurement error, parameter uncertainty, and model structure imperfection [24]. In Jacob et al. [22] a Bayesian hierarchical formulation for simultaneously calibrating a *S. damnosum* s.l. aquatic biogeochemical model at multiple capture point systems (immature hyperproductive, trailing vegetation, sparsely shaded, discontinuously canopied, sites) with differences in their trophic conditions, prior precisions of model parameters, available information, measurement error and inter-seasoanl variability. The statistical formulation

also explicitly considered the uncertainty in model inputs (model parameters, initial conditions), the analytical/sampling error associated with thefield data, and the discrepancy between model structure and the natural system dynamics (e.g., missing key ecological processes, erroneous formulations, misspecified forcing functions). The comparison between observations and posterior predictive monthly distributions indicated that the *S. damnosum* s.l. immature habitat models calibrated under the Bayesian hierarchical scheme provided accurate system representations for all the scenarios examined. The results also suggest that the Bayesian hierarchical approach allowed overcoming problems of insufficient local data by "borrowing strength" from highly relevant paarmeterized iteratively interpolative elucidative varaibles where complete data could not be practically collected. Finally, the prospects of extending this framework to spatially explicit biogeochemical along with the benefits for environmental management, such as the optimization of the sampling design of monitoring *S. damnosum* s.l. immature seasonally hyperproductive habitats was examined .Interestingly, The Bayesianized endmember eigenvector, unmixed, 5m fractionalized emissivites was reduced due to estimating the inverse of a covariance matrix in the standard multivariate normal situation, which employed a particular loss function in ArcGIS. Estimators dominated by any constant multiple of the inverse sample covariance matrix may be qunatiated in ArcGIS (www.esri.com). These estimators shrunk the sample eigenvalues toward a central value, in much the same way a mean vector shrinks the ML estimators toward a common value which quantized the error disturbance terms in the paradigm.

Uncertainty analysis of mathematical models has been a central topic in aquatic ecosystem research, and there have been several attempts to rigorously assess model error associated with model structure and parameter uncertainty [24]. Model uncertainty analysis essentially aims to make inference about the joint probability distribution of model inputs, reflecting the amount of knowledge available for model parameters, initial conditions, forcing functions, and model structure(www.esri.com0.. In this regard, Bayes' Theorem provides a convenient means to combine existing information (prior) with current observations (likelihood) for projecting future ecosystem response (posterior) for remotely targeting iteratively interpolated geo-spectrotemporally uncoalesced, *S. damnosum* s.l., moderate resolution, fractional endmembers and eigenvector.

Median parameter values, as well as the 95% credibility intervals (2.5 percentile and 97.5 percentile values), were then generated in the residually forecasted, autoregressive, endemic transmission-oriented parameterized estimator dataset. As the *S. damnosum* s.l. riverine, hyperproductive, eco-epidemioloigical, trailing vegetation, discontinuously canopied, larval habitat sampling sites increased based on the geosampled georeferenced, explanatory covariate, Distance percent of hanging trailing vegetation, themedian log-count of larval count increased. The adjusted model quantized the independence among the time series, explanatorial, field and remote geospectrotemporal, endemic transmission-oriented, oberservational covariates representing the larval counts. The authors noted that the this model fit better that the model that adjusted for correlation within the narrow riverine tributary–agro-village complex, eco-epidemiological, eco-georferenceable, capture point. study site in Burkina Faso based on the RMSE. Hence, the Bayesian techniques were more informative than the conventional model calibration practices (i.e., mere adjustment of model parameters until the discrepancy between model outputs and observed data is minimized), and thus can be used to refine our knowledge of seasonal, *S. damnosum* s.l. eco-geoerferenceable, narrow tributary, African agro-village complex input, elucidative, capture point, hyperproductive, parameters while obtaining predictions along with uncertainty bounds for output variable.

The estimation of covariance matrices in a SAS/GIS cyberenvironment, in the presence of spatial heteroskedascity and autocorrelation of unknown forms, in a seasonally, eco-georeferenceable, expositorily discontinuously, infrequently canopied, sparsely shaded, trailing vegetation, turbid water, Rapid Eye ™ ,5m, imaged, *S. damnosum* s.l., immature, seasonally geospectrotemporally geosampled, eco-epidemiological, hyperproductive, capture point, riverine, agro-village, complex ecosystem, tributary habitat may reveal tainted iteratively interpolative expositors. Currently available, orthogonally decomposed, endmember, fractionalized, eigenvector estimators in SAS/GIS may be optimal for prolific, riverine agro-village, capture point, eco-georeferencable, immature habitat, vulnerability forecasting since the paradigm may be designed based upon the choice of a lag truncation parameter and a weighting scheme. Results may provide a condition of the growth rate of the lag truncation parameter when T is to ∞ in an explanatory, geo-predictive, seasonal, *Simulium* habitat, vulnerability interpolator. That is, the SAS/GIS model may be sufficient for remotely and regressively quantitating seasonal consistency in a empirically explanative, eco-epidemiological, field-operationizable, uncoalesced, dataset of parameterizable, iterative, hyperproductive, *S. damnosum* s.l., capture point, immature, discontinuous, infrequently, seasoanlly canopied, trailing vegetation, optimally parameterizable, elucidative, agro-village African, narrow riverine tributary, habitat, autoregressive, moderate resolution, geoclassifiable, interpolatble, elucidative, LULC model in order to identify unknown, un-geosampled high density, transmission foci. To date, there are no results available in the literature regarding the choice of lag truncation parameter in any software package for a fixed sample size, data-dependent, automatic, lag truncation with explanative, autoregressive probabilistic, parameters regarding the choice of a weighting scheme for a seasonally hyperproductive, *S. damnosum* s.l., immature, discontinuous, infrequently canopied, trailing vegetation, turbid water, eco-epidemiological, immature, capture point, eco-georeferenceable, hyperproductive habitat. As a consequence, available optimally parameterizable, Gaussian/non-Gaussian, explanatory, covariate coefficient fractionizable, empicial, geo-spectrotemporal, moderate resolution, explanative, LULC indicators will not be entirely operational and the relative merits of the decomposed estimators would be unknown. Further, there would be no true forecasting capability by the model residuals for targeting unknown, ungeosampled, seasonally hyperproductive hyperproductive, *S. damnosum* s.l., capture point, immature, discontinuous, infrequently, seasoanlly canopied, trailing vegetation, optimally parameterizable, elucidative, agro-village African, narrow riverine tributary, habitats.

Applying the definition of DFT to $O(n \log n)$ in ArcGIS, where n is an unmixed multivariate, explanative, eco-georeferenceable, illuminative, field-operationizable, eco-epidemiological, empirical datatset of geo-spectrotemporally uncoalesced, seasonally explanative, geo-spectrotemporal, hyperproductive, *S. damnosum* s.l., habitat endmember eigenvector and their geospatialized, moderate resolution, wavelength, transmittance, emissivity frequencies, may allow for robustification and optimal tabulation of iteratively, interpolative, expositively fractionalized observational, geoclassifiable, LULC covariate coefficient values obtained by the sequence of 5m radiance values. This ArcGIS time series, overlay operation may be useful for identifiying exploratorial, eco-georeferenceable, explanative, geo-spectrotemporally, geospatially geosampled, heuristically optimizable, within-canopy, immature, 5m, habitat-related, spatial resolution, uncoalesced data for sparsely shaded, remotely, non-randomizable, infrequently canopied properties (e.g., dense floating, partially canopied, dead vegetation). An overlay operation is much more than a simple merging of linework; all the attributes of the features taking part in the overlay are

carried through, where parcels (polygons) and flood zones (polygons) are overlayed (using the Union tool) to create a new polygon layer(www.esri.com) Parcels may be split in ArcGIS where they are crossed by agro-village African, narrow, riverine tributary, flood zone boundaries, and new, uncoalesced, parameterizable, iterative, hyperproductive, capture point, immature, discontinuous, infrequently, seasonally canopied, trailing vegetation, optimally parameterizable, moderate resolution, geoclassifiable, interpolatble, *S. damnosum* s.l habitat LULC polygons created. An FFT is a way to compute the same result more quickly: computing the DFT of N points in the naive way, using the definition, takes $O(N^2)$ arithmetical operations, while an FFT can compute the same DFT in only $O(N \log N)$ operations [24].

FFTs are of great importance to a wide variety of applications in ArcGIS, from digital signal processing and solving partial differential equations, to algorithms for quick multiplication of large integers. The best-known FFT algorithms in ArcGIS depend upon the factorialization of N, but there are FFTs with $O(N \log N)$ complexity for all N, even for prime N(www.esri.com). Many FFT algorithms in ArcGIS only depend on the fact that $e^{-\frac{2\pi i}{N}}$ is an N-th primitive root of unity, and thus, can be applied to analogous transforms over any finite field, such as number-theoretic transforms. This method can be applied when constructing a moderate resolution, eco-epidemiological, seasonal hypeproductive, eco-georeferenceable, trailing vegation, discontinuously canopied, sparsely shaded, capture point, immature habitat vulnerability models. In empirical datasets of iteratively quantiatively, explanatorily eco-epidemiologically, interpolative, unmixed, multivariate, 5m imaged, RapidEye™, *S. damnosum* s.l., narrow, African tributary riverine, endemic, eco-georefernceable agro-village, hyperproductive, foci with fractionalized, moderate resolution, geospectrotemporally uncoalesced, wavelength, transmittance, emissivity, forecastable, covariate coefficient, parameterizable estimator datasets of explanatively, orthogonally decomposable, fractionlized, eigenvector endmember ensemblized models, inverse DFT may be the same as the DFT, but with the opposite sign in the exponent and a $1/N$ factor, may be optimally devised in any FFT algorithm in an ArcGIS cyberenvironment.

Currently, two critical issues that need to be addressed in eco-epidemiological, forecast, vulnerability mapping of eco-georeferenceable, field-operationalizable, uncoalesced seasonally imaged, moderate resolution, geo-spectrotemporal, sparsely shaded, geoclassifiable, capture point, discontinuous, infrequently canopied, turbid water, narrow, African, riverine, agro-village, tributray complexes, with geosampled discontinuous, infrequently canopied, trailing vegetation, *S. damnosum* s.l., immature habitat, geo-spatializable, datasets and informative fractionalized, moderate resolution, endmembers eigenvectors is (1) how to automatically quantitate the number of unmixed, stratifiable, illuminative, seasonal, hyperproductive, immature habitat, capture point, eco-georeferenceable clusters and (2) how to perform effective, fractionalized, endmember geo-predictive, clustering in the presence of noisy, decomposable, sub-mixel un-orthogonalizable eigenvector, data, feature attributes. An decompositional analysis of the residualized characteristics in eigenspace may be carried in Geostatistical Analyst™, for iteratively revealing that not every quantitatable, explanative, fractionalized, endmember eigenvector rendered from the data affinity matrix via an algorithmic deterministic model, is relevant for qualitatively quantitating autoregressive, immature habitat, geospectrotemporal, uncoalesced, trailing vegetation, sparsely shaded, discontinuously canopied, clustering explanators.

If v is an eigenvector of T, with eigenvalue λ, then any scalar multiple eco-georeferenceable,explanative, field-operationalizable, uncoalesced seasonally imaged, moderate resolution, geo-spectrotemporal, sparsely shaded, geoclassifiable, capture point, discontinuous, infrequently canopied, turbid water,sparsely shaded, narrow, African, riverine, agro-village, tributary complexes, with geosampled discontinuous, infrequently canopied, trailing vegetation, *S. damnosum* s.l., immature habitat, $\alpha v$of $v$with nonzero $\alpha$is also an eigenvector with eigenvalue, since $T(\alpha v) = \alpha T(v) = \alpha(\lambda v) = \lambda(\alpha v)$ λ.Moreover, if $u$and $v$are eigenvectors with the same eigenvalue and $u \neq -v$, then $u + v$is also an eigenvector with the same eigenvalue λ in the immature habitat dataset. In mathematics, scalar multiplication is one of the basic operations optimally defining a vector space in linear algebra (or more generally, a module in abstract algebra.In an intuitive geometrical context, scalar multiplication of a real Euclidean vector by a positive real number multiplies the magnitude of the vector without changing its direction[25]. Therefore, the operationizable dataset of *S. damnosum* s.l., immature habitat, eigenvectors with the same eigenvalue λ, together with the zero vector would be a linear subspace of V, (i.e., eigenspace of Tassociated to λ.If that subspace has dimension 1, it may be an eigenline (e.g., he lines defined by fractionalized, seasaonlly explanatively hyppeorductive, eigenvectors). [24], The eigenspaces of *T* always form a direct sum (and as a consequence any family of eigenvectors for different eigenvalues is always linearly independent). Therefore, the sum of the dimensions of the immature habitat eigenspaces cannot exceed the dimension *n* of the space on which *T* operates, and in particular there cannot be more than *n* distinct eigenvalues.]

Any subspace spanned by a database containing geospectrotemporally uncoalesced, geospatially geosampled, seasoanlly eco-georferenceable, hypepordutive, eco-epidemiological, capture point *S. damnosum* s.l. habitat, orthogonally elucidatively decomposed, fractionalized moderate resolution, endmember eigenvectors of T would be an invariant subspace of T, and the restriction of *T* to such a subspace would be diagonalizable in ArcGIS. In Geospatial Analyst ^{TM} , an invariant subspace of a linear uncoalesced seasonally imaged, moderate resolution, geo-spectrotemporal, sparsely shaded, geoclassifiable, discontinuous, infrequently canopied, turbid water, narrow, African, riverine, agro-village, tributary complex, with decomposed, geosampled discontinuous, infrequently canopied, trailing vegetation, eco-georferenceable, capture point, hypeproductive, *S. damnosum* s.l., immature habitat explanative mapping variables $T : V \rightarrow V$ may from some vector space. *V* to itself is a subspace *W* of *V* that is preserved by *T*; that is, $T(W) \subseteq W$[24] Consider a linear *S. damnosum* s.l., mapp$T$that transforms: $T : \mathbb{R}^n \rightarrow \mathbb{R}^n$An invariant subspace $W$of Thas the property that all vectors $v \in W$may then be transformed by Tinto vectors also contained in W This may be stated as$v \subset W \Rightarrow T(v) \subset W$ in ArcGIS

The affinity matrix in ArcGIS may be optimally employed to transform orthogonally decomposed seasonal, empirically geo-spectrotemporally geosampled, uncoalesced, geospatially geosampled, seasoanlly eco-georeferenceable, hyperpordutive, eco-epidemiological, capture point *S. damnosum* s.l. habitat, elucidatively decomposed, fractionalized moderate resolution, endmember eigenvectors for overcoming difficulties related to the lack of convexity in the shape of the data distribution. The explanative LULC value of the seasonally eco-georeferenceable, agro-village, narrow African, riverine tributary, complex centroid (i) to the eco-georeferenced, hyperproductive, eco-epidemiological, capture point (j) in the matrix may be remotely qualitatively quantitated as negative value of the Euclidean distance between i and j, employing a Gaussian matrix in Geostatistical

Analyst™. In linear algebra, Gaussian elimination (also known as row reduction) is an algorithm for solving systems of linear equations [24], which may be understood in ArcGIS as a sequence of operations performed on the associated matrix of coefficients.

Further, optimally sub-mixel, descriptive, explanatively orthogonally decomposable, seasonal, hyperproductive, explanatively geo-spectrotemporally geosampled, immature *S. damnosum* s.l. habitat, frcationalize endmember eigenvector ensemble selections in an ArcGIS cyberenvironment may be critical for a robust, parsimonious iterative, interpretative, quantitative interpolation of un-informative, fractionalized, moderate resolution, endmember eigenvectors, which may lead to poor immature habitat forecastable clustering results. Employing eco-georefernceable, trailing vegetation, immature, hyperproductive, seasonal,capture point, *S.damnosum* s.l., turbid water, eco-georeferenceable, African, narrow tributary, immature, seasonal, riverine, habitats in an eco-epidemiological, transmission forecast-orinted, vulnerability analysis, a novel geospectral clustering algorithm may be proposed in ArcGIS. This differs from previous approaches in literature for optimally identifying unknown, hyperproductive, discontinuous, infrequently canopied, immature, sparsely shaded, turbid water, trailing vegetation, turbid water, eco-georeferenceable, narrow riverine, tributary, African, agro-village complex, capture point, *Simulium* habitats based on a cost effective, medium resolution, 5m RapidEye™,fractionalized, endmember eigenvector, seasonal habitat signatures. In an algorithmic, proxy biosignature, decompositional exercise in Geospatial Analyst™ only pertinent explanatively optimally decomposeable, fractionalized, moderate resolution, endmember eigenvectors are employable for optimal rectification and optimal determination of the precise number of exploratory eco-georeferenceable, trailing vegetation, turbid water, discontinuous, infrequently canopied, narrow African, agro-village, tributary, *S. damnosum* s.l., eco-epidemiological, eco-georeferenceable, capture point, seasonally hyperproductive, immature habitats are associated within an iteratively quantitatively, explicatively interpolative, eco-hydrologic, eco-cartographic cluster. The key element of the proposed customizable, iterative algorithm is simple since the effective relevance learning iterative technique in ArcGIS would measure the relevance of a stochastic or deterministic, iteratively quantiatively interpolative, empiricalized, model output for optimally regressively geoclassifying any unmixed moderate resolution(e.g., 5m RapidEye™), explanatively orthogonally decomposeable, elucidative, eco-epidemiological, fractionalized,endmember eigenvector emissivties according to how well it can be separated into eco-georeferenceable, immature habitat, geo-spectrotemporal and geospatial clusters. This quantitative, probabilistic regressive, unmixing algorithm in ArcGIS, with forecastable residual model output, may then be evaluated by employing orthogonalized, fractionalized, moderate reosolution, endmember eigenvector, synthetic datasets as well as real-world datasets generated from elucidative geosampled seasonal habitat, geo-sample frames.

The dynamic provisioning of virtualized resources offered by ArcGIS cloud infrastructures allows applications deployed in a cloud environment for automatically increasing and decreasing the amount of usable resources. This allows for geo-spectrotemporally optimizable, eco-cartographical robust illustrations of eco-epidemiologically eco-georefernceable, forecastable vulnerability models with a discontinuous, infrequently canopied, geo-classifiable, trailing vegetation, turbid water, geospatialized LULCs for optimally mapping orthogonally explanatively decomposable, moderate resolution derived, eco-epidemiological, immature, capture point, *S. damnosum* s.l. habitats. This capability in ArcGIS is explanatively auto-scaliable; its main purpose is to

automatically adjust the scale of the eco-georferenceable, vulnerability, narrow African riverine, immature habitat, agro-village complex triburaty ecosystem, elucidatory model system for satisfing the varying workload with minimum unexplanative probabilistic uncertainty. The need for auto-scaling in ArcGIS is particularly important during workload peaks, in which applications may need to scale up to far more comprehensive systems [36]. Both the research community and the main cloud providers have developed auto-scaling solutions for ArcGIS. Most research solutions are centralized and suitable for managing large-scale narrow tributary, eco-georeferenceable, African riverine agro-village, complex eosystems; therefore, cloud providers' solutions are bound to the limitations of a specific provider in terms of resource availability, reliability, and connectivity. A decentralized, probabilistic, auto-scaling and explanative autoregressive residualizable, iteratively quantitative interpolative algorithm integrated into a ArcGIS architecture that is cloud provider-independent may allow the auto-scaling of algorithmic, residual mapping services over multiple cloud infrastructures to optimally iteratively interpolate geo-spectrotemporally geospatially moderate resolution, *S. damnosum* s.l., decomposed decomposed, capture point immature habitat data so as to eludicatively identify unknown, un-geosampled, hyperproductive, seasonal riverine, immature habitats.

In expositive, constructive and multivariate statistics in ArcGIS, spectral clustering techniques make use of the spectrum (i.e., eigenvalues) of the similarity matrix of the data to perform dimensionality reduction before clustering in fewer dimensions. In machine learning and statistics, dimensionality reduction, or dimension reduction, refers to the process of reducing the number of random, iteratively quantitative interpolative eco-epidemiologically forecastable, operationalizable variables under consideration, which may be optimally and subsequently remotely divided into exegetically decomposable, geo-classifiable LULC, fractional, endmember eigenvector data with an attribute feature selection and feature extraction.The similarity matrix in ArcGIS Geospatial Analyst^{TM} provides an output consisting of elucidatory qualitatively, quantitative autoregressive, probabilistic, assessments of the relative quantifiabilty of each explanative geo-spectrotemporally and seasonally geospatially geosampled, hyperproductive, *S. damnosum* s.l., seasonal, capture point in a eco-georeferenceable, eco-epidemiological African narrow riverine, agro-village, eco-epidmeiological study site with elucidative regression points in the non-hierarchical clustering dataset.

Jacob et al. [22] proposed a n expositively fractionalized, 5m, spatial resolution RapidEye^{TM}, endmember eigenvector, image segmentation in an ArcGIS/ENVI cyberenvironment which rendered precise and orthogonalizable synthetic, spatial filters for interpretatively iteratively utilizing LULC bidirectional, quantiated, uncoalesced, reflectance transmittance wavelength frequenceis. The fractionalized endmember eigenvectors eco-cartographically illustrated non-homogeneous, regions according to some exegetically, iterative, interpolative criterion (e.g., discontinuous, infrequently, sparsely shaded, canopied trailing vegetation agro-village, narrow tributary geospatial eco-georeferenceable objects). The crux of spatial filtering lay in the linkage between eigenfunctions (i.e., geo-spectrotemrpaolly uncoalesced, discontinuous infrequently canopied, *S. damnosum* s.l., seasonal, riverine, turbid water, eigenvectors and corresponding eigenvalues). Latent spatial autocorrelation is essential in eco-epidemiological, geosampled, narrow African, riverine tributary immature habitats that have been geo-spectrotemporally, geospatially, and exogenously specified through a decomposed matrix’s eigenvectors, and may be optionally employable as supplemental covariates in a regression framework [37]. This will aid in “filtering” out other probabilistic, autorgressive, residualized, spatial errors (e.g., non-linear

multicolinearity), thereby allowing for more efficient estimation of primary parameterizable covariates.

Fractionalized, expositively, optimally decomposable, 5m RapidEye™ eigenvector unmixed, wavelength transmittance emissivity, endmember ensembles in an ArcGIS cyberenvironment can account for most image noise in a 5m, fractionalized eco-georeferenceable, seasonally geo-spectrotemporally gesampled, narrow, African riverine tributary, eco-epidemiological, capture point, *S. damnosum* s.l., habitat scene. Eco-cartographically auto-probabilistically, autoregressively, and remotely quantitating, structurally diverse, eco-hydrologic geo-markers (e.g., foligae height), can serve as references for bio-optically quantitating non-homogeneity of clustering eco-georeferenceable, trailing vegetation or turbid water, 5m, orthogonally decomposed, noisy mixels in Geospatial Analyst™ [22]. Heuristically, orthogonally explanatively decomposeable, eco-geographic, forecasting, vulnerability-oriented, residual probabilistic, model applications employing geo-spectrotemporal, geospatially geosampled, seasonally prolific, entomological, vector arthropod, aquatic, larval habitat, moderate resolution, unmixed, data variables, both auto-probabilistically and auto-regressed in ArcGIS, may quantitatively and eco-cartographically krige fractionalized, endmember, proxy habitat signatures. In so doing, endemic transmission zones may be eco-cartographically illustratable in ArcGIS by employing stratifiable, iteratively quantitative, interpolative, fractionalized, endmember eigenvectors for ecohydrologically optimally representing positively autocorrelated and eco-georeferenceable, high density, foci, seasonal, African, riverine tributary, immature habitats containing immature *Similum damnosum* s.l.. Identifying unknown and un-geosampled, seasonally eco-georeferenceable, explanatively hyperproductive, sparsly shaded, non-randomizable, partially canopied, trailing vegetation, discontinuous, infrequently canopied, *S. damnosum* s.l., turbid water, seasonal, hyperproductive, immature, agro-village, narrow tributary, African agro-village complex, riverine habitats requires monitoring environmental changes in immature fly productivity through an ArcGIS cyberenvironment, while simultaneously aggressively aggregating elucidative, orthogonally decomposed, quantifiable, Euclidean, geoclassifiable, LULC distances in ArcGIS from eco- eco-epidemiolgical, capture points [22].

Comparing seasonally hyperproductive, explanative, riverine, *S. damnosum* s.l. discontinuous, infrequently canopied, trailing vegation, sparsely shaded, turbid water, capture point, immature habitats in sub-mixel, fractionalized and geo-classifiable iteratively interpolatively interpretative LULC, unmixed, moderate resolution, endmember eigenvector radiance classes from multi-temporal, RapidEye™ 5m resolution exploratory images may aid in providing a catalog of remote footprints (i.e., eco-georeferenceable, agro-village complex habitat proxy LULC signatures). Employing rasterizable, elucidatively eco-georeferenceable, unmixed 5m, image data, feature attributes may also aid in geolocalizing seasonal, immature habitats of eco-georefernceable, hyperproductive, *S. damnosum* s.l. and their trailing vegetation, sparse shading, photosynthetic and non-photosynthetic variables, and turbid water, parameterizable, covariate coefficients defining discontinous, infrequently canopied, characteristics. An operationalizable, fractionalized, endmember eigenvector dataset created in an ArcGIS geodatabase can have informative mosiac raster datasets added to it directly, or they can be created by employing a selection of probabilistically, autoregressively, remotely qualitatively quantitative unmixed, iterative interpolative, data feature attributes from a raster catalog or mosaic dataset (http://help.arcgis.com/).

The explanative, expositorily fractionalized, optimal renderings of illuminatively, ortogonally decomposable, residualizable, unmixed, moderate resolution (e.g., 5m,

RapidEye™ imaged) , *S. damnosum* s.l., immature habitats that are rasterizable through moderate resolution, explicatively rendered data in ArcGIS from a descriptive, mosaic, eco-epidemiological, endmember eigenvector, wavelength ,transmittance frequency in an interpolative emissivity dataset does not have to be adjoining or overlapping. Thus, decomposed, trailing vegetation or turbid water synthetic, orthognalized, spatial filter, endmember eigenvectors in ArcGIS can be iteratively quantitatively interpolated in sub-mixel, heuristically quantitatively optimizable, geo-spectrotemporally, geospatially uncoalesced, eco-georefernceable, dataset of immature *Similimu* habitat data, feature attributes. These elucidative attributes may exist in such eco-epidemiological field-operational datasets as geo-spectrotemporally geospatially unconnected, discontinuously infrequently canopied, "pure" fractionalized, endmember eigenvectors. Geosampled, unmixed *S. damnosum* habitats with explanatively geo-classifiable, eco-epidemiological, uncoalesced, geoclassifiable, LULC datasets can manage raster data in an unmanaged raster catalog. Therefore, the procured tables In ArcGIS will have similar descriptive, orthogonalizable, sparsely shaded, explicatively fractionalized, non-homogenously, uncoalesced, disontinuous, infrequently canopied, turbid water, endmember eigenvector, robust, proxy signatures from an autoregressively indexed perspective, while queries in ArcGIS may be simultaneously orthogonally performed on the collections.

Mosaic datasets utilize raster types to read and ingest the required information from raster datasets (http://help.arcgis.com/en/arcgisdesktop/). Empirical, vulnerability, mosaic metadata, such as seasonal geo-spectrotemporally, geospatially geosampled, eco-epidemiological, narrow, African, riverine tributray, capture point, agro-village complex, *S. damnosum* s.l, immature habitat, moderate reosolution, satellite acquisitions (e.g., larval count, percentage trailing vegetation, levels of turbidity, etc.), within a raster format may also be interpretively and optimally quantitized in ArcGIS. In so doing, explanative raster types can read raster data in its simplest form by employing a raster format, such as TIFF or JPEG Metadata, to summarize basic information about the geospatializable, uncoalescable data.

There are exploratory geoprocessing algorithms in the Data Management toolbox in ArcGIS to create and edit mosaic, explanative dataset of sub-mixel, orthogonally explanatively decomposeable, fractionalized, eigenvector endmembers with a moderate resolution and log-normalized, wavelength, transmittance emissivity descriptors. These algorithms are especially useful when remotely autoregressing, seasonally partially canopied, unmixed, photosynthetic, or non-photosynthetic covariates for eco-hydrologically, eco-cartographically illustrating seasonally trailing vegetation paramterizable covariate coefficients in non-homogenously canopied, hyperproductive, *S. damnosum* s.l., turbid water habitats.

Many specific raster types of eco-epidemiological, eco-cartographic, field-operationalizable, empirical datasets of geo-spectrotemporally, geospatially geosampled immature *Simulium* habitats are functional in an unmixed, iteratively interpolative, optimally parameterizable, uncoalesced RapidEye™ endmember emittance that has been quantitated from a eco-georeferenced, geosampled, African riverine, agro-village complex, decomposed, 5m RapidEye™ scene. This can include a rasterizable explanatory eco-georferenceable dataset with several bands and other metadata, which affect the spatial reference. Since sensor waveband 5m, decomposable data products have five bands at this specified resolution, the raster type processing in ArcGIS may create a product that improves the geosampled, fractionlized, endmember, *Simulium* habitat, eigenvector dataset by pan-sharpening. "Pan Sharpening" is shorthand for "Panchromatic sharpening," which is simply using a panchromatic (single band) image to "sharpen" a multispectral image [38].

Thus, mosaiked, fractionally unmixed moderate resolution, endmember eigenvectors in an autoregressive ArcGIS model can optimally represent seasonally eco-georeferenceable, geo-spectrotemporally explanative clustering of geosampled, hyperproductive, eco-georeferenceable, trailing vegetation *S. damnosum* s.l. discontinuous, infrequently canopied, sparsely shaded, eco-epidemiological, capture point, riverine habitats in an stochastic/deterministic, interpolator In Geospatial Analyst ™ for eco-epidemiological datasets which would be particularly sensitive to testing for kriged, fractionalized endmember, iterative unmixed, data feature, decomposable attributes of raster data in ArcGIS. Based on the cell sizes, the 5m, wavelength fractionalized, transmittance, emissivity dataset may display the immature habitat, RapidEye™ imagery at the most appropriate scales. With some display control properties in ArcGIS, a ecologist, entomologist or other researcher may be able to control temporal information about geospatial clustering of seasonally hyperproductive, turbid water, *S.damnosum* s.l., immature, narrow tributary, agro-village complex, ecosystem, discontinuous, infrequnetly canopied, trailing vegneation, hypeproductive seasonal habitats. This allows for the parsimonious viewing of the 5m resolution images for specific seasonal sample frames (e.g., riverine flooding) in ArcGIS (e.g., Geospatial Analyst ™) .

Mosaic methods in an ArcGIS cyberenvironment can elucidate geo-spectrotemporally autoregressable, probabilistically remotely descriptive, fractionalized, moderate resolution, endmember eigenvectors which could represent ecogeoreferenceable clustering of *S. damnosum* s.l., immature, narrow African, tributary riverine, agro-village, complex habitats. Decomposed, 5m, wavelength transmittance emissivities may control what the raster data presents each time a mosaic from the field-operational, unmixed dataset displays an *S. damnsoum* s.l. related cluster in eigenspace in ArcGIS. By default, the mosaic generated by displaying the raster dataset that is the closest to the center of a 5m, RapidEye™ spatial resolution of an African, narrow tributary riverine agro-village complex image may remotely reveal sparsely shaded, non-homogenously canopied, optimized hypeproductive immature habitat geolocations. Topographic geoclassifiable, ecogeoreferenceable, LULC affects the fraction of direct and diffuse canopy radiation received on a 5m extractable optimalizable mixel, which changes the sun–target–sensor geometry, resulting in variations in the observed radiance [22]. Retrieval of surface–atmosphere, explanatively geoclassifiable, uncoalesced LULC properties from top-of-atmosphere (ToA), 5m RapidEye™ topographic, discontinuous, canopied, radiance account for hyperproductive, *S. damnosum* s.l. immature seasonal, habitats that consist of clustering of trailing vegetation and turbid water radiance effects. Top-of-atmosphere reflectance is defined as the reflectance measured by a space-based sensor that is flying higher than the earth's atmosphere and whose unmixed reflectance values can include contributions from clouds and atmospheric aerosols and gases [39].

The gap fraction of a canopy is quantifiable in an ArcGIS cyberenvironment as the fraction of view that is unobstructed by canopy in any particular direction. Canopy structural diversity information of a seasonally hyperproductive, narrow, African, agro-village complex, tributary, immature habitat, *S.damnosum* s.l. immature habitat, eco-epidemiological, capture point, including the amount and orientation of foliage, can be remotely estimated from measurements of gap fractions in ArcGIS. The gap fraction of a canopy is the fraction of view in some direction from beneath a canopy that is not blocked by foliage [40].

.

The gap fraction technique in ArcGIS is at present the most powerful and practical tool available for indirect sensing of discontinuous canopy structure. Recently, Armston et al. (2013) demonstrated that a new, physically-based method for direct retrieval of canopy gap probability P_{gap} from waveform Lidar in ArcGIS can improve the estimation of P_{gap} over discrete return Lidar data. The success of the approach was demonstrated in a savanna woodland environment in Australia. The data solved the canopy contrast term (i.e. the ratio of the reflectance from crown and ground), ρ_v/ρ_g. In this way the method avoided local calibration to overcome differences in either ρ_v or ρ_g. To be more generally useful the ArcGIS demonstrated the enmdmeber data on different geoclassified explanatorial LULC sites in the presence of slope and different sensor and survey configurations. The robustness of the retrieval of P_{gap} from waveform Lidar using a Watershed Allied Telemetry Experimental Research dataset, over the Heihe River Basin region of China. The data contained significant discontinuous canopy , terrain and survey variations, presenting a rather different set of LULC conditions to those previously used in disocnmtinuous cap gap calculations. Results show that ρ_v/ρ_g was stable across all flights and for all levels of spatial geo-aggregation. This strongly supported the robustness of the new P_{gap} retrieval method, which assumes that this relationship was stable. A comparison between P_{gap} estimated from hemiphotos and from the waveform Lidar showed agreement with Pearson correlation coefficient $R = 0.91$. The waveform Lidar-derived estimates of P_{gap} agreed to within 8% of values derived from hemiphotos, with a bias of 0.17%. The new waveform model was shown to be stable across different off-nadir scan angles and in the presence of slopes up to 26° with $R \geq 0.85$ in all cases. The authors also show that the waveform model can be used to calculate P_{gap} using just the mean value of canopy returns, assuming that their distribution was unimodal. Lastly, the authors showed that the method can also be applied to discrete return Lidar data, albeit with slightly lower accuracy and higher bias, allowing P_{gap} comparisons with previously-collected lTdar datasets. The ASrcGIS model results revealed that new method was applicable for estimating P_{gap} robustly across large areas, and from lLdar data collected at different times . A discontinuous canopy gap 5m Rapid Eye model may be applicable not only to detect discontinuity in vegetation related geoclassifiable LULCs seasonally explanative, hyperproductive, African riverine, narrow tributary, agro-village complex, tributary habitat, seasonal canopies, but also to settings, which can be modeled by discrete foliage containing envelopes, such as row structure, individual shrubs/trees, etc.

The seemingly uniform geo-spectrotemporally geolocated trailing vegetation geosampled, eco-georferenceable, immature, trailing vegetation-related, geoclassifiable, moderate resolution, LULCs, discontinuous, infrequently canopied, hyperproductive, eco-epidemiological, capture point, *Simulium* habitats may be abruptly interrupted by fuzzy-edged, uncoalesced, 5m RapidEye™ spatial resolution sunflecks of a variety of shapes, sizes, and intensities, which constantly shift and change as the sun moves. These sunflecks, however, may provide a powerful tool for remotely qualitatively quantitating indirect, bidirectional partially sparsely shaded, canopied habitat reflectance with structural diversity sub-mixel measurements in ArcGIS for accurately, identifying non-continuous, eco-georeferenceable, canopy gaps in a turbid water, trailing vegetation, *S. damnosum* s.l., tubid water, discontinuous, infrequently canopied, narrow, African, riverine tributary, agro-village complex ecosystem, immature capture point, hyperproductive habitat. ArcGIS may qualitatively quantitate immature habitat canopy gap fractions that cause the sunflecks in the immature, riverine habitat-based, 5m RapidEye™, geo-spectrotemporally uncoalesced, fractionalized wavelength transmittance emissivity, forecast, vulnerability model, as well as its residual endmember renderings (e.g., seasonally forecasted, optimal geosampled time frames and immature productivity count data values). The fractional sunfleck of the LULC

reflectance area is equivalent to the heuristically optimized gap fraction endmember variables in the solar direction in an ArcGIS cyberenvironment (www.esri.com).

An unmixed, 5m, RapidEye™ sunfleck, fractionalized radiance, sub-mixel, estimating algorithm in SAS/GIS may quantitate the unmixed, endmember eigenvectors representing the *S. damnosum* s.l. habitat, eigenfunction, orthogonalizable, spatial filters, when rendered in an ArcGIS cyberenvironment. By doing so, the residual forecasts optimally can reveal an illuminativme parameterizablem covariate habitat proxy signature that can be used as an estimator encompassing the gap fraction with solar angle, optimizable measurements. If the foliage in the empirical habitat datasets is truly randomly positioned, then the probability of direct beam radiation passing through the canopy crown without intercepting any habitat foliage may be remotely quantified in ArcGIS by employing the zenith angle of incidence, which may then be tabulated by elucidating a parameterizable, ellipsoidal foliage inclination distribution. With this, clustering immature habitats that are geoclassifiable through a eco-georefrenceable, agro-village complex, narrow African, ago-village ecosystem complex geoclassifiable, LULC area projected in some direction may be autoregressively, probabilistically, remotely, qualitatively deciphered. The path length through the foliage and the foliage density (i.e., area of foliage per volume of immature discontinuous, habitat canopy) functions of position in geo-space may also be robustly quantitated by employing a function of azimuth angle in ArcGIS.

For a uniform, 5m RapidEye^{TM}, seasonal hyperproductive, sparsely shaded, narrow, African, riverine tributary, eco-georeferenceable, explanatory, immature, capture point, hyperproductive habitat, the tabulated quantizable canopy height path length may be optimally devised in an ArcGIS cyberenevironment by a discrete, iteratively, quantitative interpolativel quantitatble,, remotely decomposable, expositively parameterizable, uncoalesced, moderate resolution, wavelength frequency transmittance, dataset of proxy bisiganture values which may represent the sum of the path lengths through sub-canopies only. Thus, only direct quantitable measurements can be optimally rendered from a suitable geometric illuminative, eco-epidemiological *S. damnosum* s.l. discontinuous canopy, forecast, vulnerability model

Conversely, if the sunfleck fraction and corresponding path lengths in an hyperproductive, *S. damnosum* s.l., capture point, geo-spectrotemporally , geospatially geosampled, capture point, immature habitat are measured in ArcGIS and sparsely shaded, quantitable, discontinuous explanative, mcanopied, path value is obtained, then it may be possible to remotely quantitize the foliage density of a fractionalized, 5m, spatial resolution endmember eigenvector using RapidEye™ images for determining seasonally hyperproductive, capture point, eco-georefernceable, habitat data and a decompositional eigenfunction algorithm in an ArcGIS cyberenvironment. To robustly and parsimoniously extract both foliage density and foliage orientation, spatial filter, orthogonalized autoregressive probabilistic estimates rendered from an eigendecomposition function may provide more decomposable, expository *Similium* habitat information in ArcGIS. This information could include a dataset of geo-spectrotemporally uncoalesced moderate resolution (e.g., panchromatic Rapid Eye ^{TM} data) of a proxy LULC signature which then may be employed to remotely deduce positively autocorrelated unknown, un-geosampled, hyperproductive, seasonally explanative, immature, narrow tributary, eco-georeferenceable, elucidative, African agro-village, complex ecosystem, capture point, immature, habitats. In so doing, an IVM may be implementable habitats (e.g., “Slash and Clear”) employing a

buffered geoclassified gridded map eco-cartographically illustrating eco-georeferenceable agro-village LULC zones targeting these prolific habitats.

To date, optimizable remote sensing methods have concentrated on various vegetation indices (VIs) signature employing and leaf inclination angles, where azimuthal orientation of the foliage is assumed to be random. Since a discontinuous, infrequently canopied, seasonal capture point, *S. damnosum* s.l. immature habitat canopy is a three-dimensional structure of leaves stems, branches, etc., the radiation emitted from any single phytoelement from an ecogeoreferceable, hyperproductive, trailing vegetation, turbid water, eco-epidemioloigical, capture point, will interact with many other canopy structures before it leaves thehabitat canopy. Such multiple reflections and transmissions can modify the originally emitted habitat leaf spectrum. This becomes intuitivelyclear when it is realized that all phytoelements in a *S. damnosum* s.l. hypeporductive riverine foci, canopy structure falls into 3 categories: fully illuminated, fully shaded, or partially shaded/illuminated by the incomingsolar radiation. It is obvious that a shadow spectrum is different from a sun-lit leaf spectrum[24]. Thus, the magnitude of such geospectrotemporal geospatialized, geoclsssifiable, ArcGIS-derievd LULC changes will depend on the immature eco-georferenceable, capture point, canopy architecture and the external seasonal illumination direction. .Unfortunately misspecification in tabulations from unmixing geometrical algorithms are common in hierarchical discontinuous moderate resolution real-time canopied paridigms.

Other hierarchical generalizable mosaic default, residual algorithmic methods in ArcGIS can define a query based on iterativeinterpolative clustering of seasonally hyperproductive, *S.damnosum* s.l., immature habitats employing fractionalized, endmember eigenvector values and bidirectional moderate resolution, radiance, such as cloud cover-oriented and wavelength frequency-related transmittance covariates as geosampled in an African riverine, narrow, tributary, agro-village complex using 5m imaged, georeferenceable, RapidEye™ mutlitemporal scenes. The generalizable properties of these heuristically optimizable methods are similar to those for explanative raster datasets in ArcGIS, such as the data source, extent, cell sizes, and bit depth. The default properties are specific to the mosaic, descriptive, optimizable, endember eigenvector, fractionalized, moderate reoslution, eco-epidemiological datasets, and can include all the non-raster, dataset-specific, fractionalized, endmember eigenvector, immature habitat, geo-spectrotemporal information. These uncoalescable properties will affect how 5m RapidEye^{TM} imaged, *S. damnosum* s.l., agro-village complex, riverine habitats with non-homogenously canopied, interpretively decomposed, fractionalized, endmember eigenvectors are presented in ArcGIS, (ecohydrologically, geospatially) etc. Key metadata properties are parsimoniously and remotely obtainable from the 5m decomposable data products in ArcGIS, which may be optimally definable for a mosaic dataset. The residualized eco-epidemiological dataset would contain 5m RapidEye^{TM} band and wavelength transmittance emissivity renderings and some residual processing noise. The product definition can be modified thereafter in an ArcGIS cyberenvironment.

A simple endmember eigenvector of a spatial filter, eco-epidemiological forecast vulnerability model in ArcGIS can describe non-random, discontinuously canopied, unmixed processes in terms of their bio-geophysical, photosynthetic elucidatively decomposable attributes thuis allowing for tabulating geo-spectrotemporal and geospatial association sof immature *Simulium* habitat productivity in an ArcGIS model in geo-space using a moderate resolution, wavelength emissivity distribution. Eco-cartographically robustly illustrating the

positive and negative binomiality of discontinuous, fractionalized, canopy, endmember non-randomness in an empirically regressable, heuristically optimizable, geo-spectrotemporally geosampled *S. damnosum* s.l., moderate resolution, imaged capture point, immature habitat in ArcGIS employing a curve-fitting parameter may reveal directly measurable [i.e., proxy indicator Vegetation Index (VI)] from a photosynthetic, *S. damnosum* s.l. habitat discontinuous, sparsely shaded, iteratively interpolative, discontinuous canopy, endmember eigenvector. This model may distinguish habitat fractional canopy gaps.

It is fortuitous that orthogonally decomposable explanative processes offset each other in an ArcGIS cyberenvironment to one degree or another,thus allowing field-operational forecasting vulnerability models to capture the heterogeneity of a eco-georferenceable, hypeporductiuve, capture point, *S. damnosum* s.l. trailing vegetation, turbid water, sparsely shaded, narrow African, tributary agro-village, capture point, immature habitat that is reasonably well geoclassified through uncoalesced, elucidative, quantitable LULC reflectance surfaces (e.g., 15%) by employing one specific photosynthetic, iteratively interpolative, discontinuous catgeorical variable. This variable may subsequently reveal spectral indices for precise geoprediction of leaf pigment content that is relatively sensitive to *Simulium* species and leaf structure variation linked with immature *Simulium* productivity. This could be applied in larger scale remote-sensing studies without extensive calibration in ArcGIS.

ArcGIS mosaic querying capabilities allow for access to every optimizable, explicative, fractionalized, moderate reoslution, endmember eigenvector raster dataset within a mosaic, hyperproductive, moderate reoslution imaged, eco georeferenceable, *S. damnosum* s.l. immature, narrow, African, riverine tributary , trailing vegetation, sparsely shaded, discontinuous, infrequently canopied capture point, with discontinuous canopy cover, even when there is overlap. Additionally, if the correct rational polynomial coefficient (RPC) information is provided in an ArcGIS module (e.g., Geospatial Analyst^{TM}), this raster type could be optimally employable to improve on the fused, endmember data products by performing an orthorectification. Orthorectification is the process of removing the effects of image perspective (tilt) and relief (terrain) effects for the purpose of creating a planimetrically correct image [25]. The resultant orthorectified image has a constant scale wherein features are represented in their 'true' position. Orthorectification refers to the elimination of the effects in an image perspective (e.g. tilt, relief, or terrain) to create a planimetrically correct image [40]. Rational Polynomial Coefficient is a sensor model commonly used by the remote sensing industry to determine the ground coordinates of mixels in moderate and high resolution satellite imagery(www.esri.com). Rational Polynomial Coefficients (RPCs) provide a compact representation of a ground-to-image geometry, allowing photogrammetric processing without requiring a physical camera model [40].

By employing the correct raster type, explanative automodel seasonally explanative, eco-georefernceable, hyperproductive *S. damnosum* s.l. capture point, immature habitats with geo-spectrotemporally geospatializable unmixed proxy biosignature endmembers eigenvectors, iteratively interpolated in ArcGIS can be automatically defined. This interpolation is applicable for on-the-fly, field-ecoepidemiolgical, operational intrepretation when the raster datasets are accessed. However, a resultant clustering, fractionalized, orthorectifiable, endmember ecogeoreferenceable *S. damnosum* s.l. habitat, analyszed through an eco-georefernecable descriptive explanator, may not possess a constant scale in non-ArcGIS algorithms wherein moderate resolution, fractionalized endmemberseigenvector of geoclassifiable, LULC, interpolative, bio-signature data feature attributes may be robustly represented in their absolute 'true' geospatial positions in ArcGIS.

A two-stream approximation, forecasting, eigenvector endmember, emissivity, forecast-oriented, vulnerability model constructed in ArcGIS may be optimmaly employed to remotely tabulate and summarize clustering synthetic endmember, eigenvector, reflectance values representing orthogonalizable, hemispheric, partially discontinuously canopied, geoclassifiable LULCs by employing transmittance, frequency-oriented, uncoalesced emissivities of unmixed, 5m visible and NIR, frequency intervals. The two-stream approximation may be applied to the equation of two–stream, 5m RapidEye^{TM} resolution of the emissivity, habitat model in ArcGIS for qualitatively quantitating the transfer of unmixed canopy radiation through an optically thin plane-parallel atmosphere. In doing so, the emissivity model can include the dependence of the 5m reflection and the transmission of the atmosphere on the angle of the incident radiation, as well as the angular dependence of the scattering phase function of the medium. Model residualized forecasts arise from different methods for treating the incident radiation [40]. These models may reduce to the thin-atmosphere approximation thresholds in ArcGIS, as the limit of the optical depth of the atmosphere commonly approaches zero in arid and semiarid narrow, African riverine tributary, trailing vegetation, discontinuous, infrequently canopied, ecosystem environments. In this limit, the sign of heating, caused by the presence of a scattering and absorbing layer over the forecastable habitat in a reflecting surface moderate resolution, fractionalized, endmember eigenvectors, may be optimally derived in a spatial filter eigenfunction through a decompositional algorithm in ArcGIS. This model may reveal the importance of both the zenith angle and the angular dependence of the scattering phase function in a hyperproductive, *S. damnosum* s.l., immature habitat. Two-stream approximation is commonly employed in parameterizations of radiative transport in global circulation models and in weather, eco-epidemiological, forecasting, vulnerability models. Global circulation models (GCMs) in ArcGIS simulate past and projected future climatic changes by numerically integrating the fluid dynamical equations of motion for the atmosphere with boundary conditions that incorporate various factors influencing the climate system (www.esri.com).

A simple, sparsely shaded, trailing vegetation, turbid water, hyperproductive, immature, eco-georferenceable, *S. damnosum* s.l. habitat in a photosynthetic leaf model is optimally parameterizable through orthogonalizable, spatial filter, endmember, eigenvector, covariate estimators may be integrated over geo-spectrotemporally geospatially tabulated, leaf orientation and canopy depth orthogonal predictors. Uncertainty quantitation of statistical significance is attained when a *p*-value is less than the significance level [22]. The *p*-value is the probability of obtaining at least as extreme results given that the null hypothesis is true whereas the sgnificance or alpha (α) level is the of rejecting the null hypothesis given that it is true [41].

Suganum et al. [42] estimated discontinuous canopy biomass in a riverine agro-village, narrow tributary area to clarify the relationship between uncoalesced moderate resolution, LULC endmembers in unmixed, data feature attributes of stand structure and woodland biomass obtained by moderate resolution remote sensing in Western Australia. The authors examined stand structure and estimated woodland biomass in an arid LULC region in ArcGIS. The research site was near Leonora located 600km from Perth in Western Australia. The annual rainfall is approximately 200 mm in this region. The dominant woody vegetation LULC species is *Acacia aneura*. The ecological characteristics of the woodland in this region are littered with unclosed canopies and tree crown silhouette. The authors established 35 plots (approx. 50m × 50m) and bio-optically determined the diameters at 1.3m and 0.3m heights, height, and canopy silhouette area of all trees contained in the plots. Each tree biomass was

calculated by allometric equations employing a destructive geo-sampling method in ArcGIS. Results of multivariate regression analysis indicated that the appropriate stand structural attributes for estimation of woodland biomass were stand basal area (SBA) and canopy coverage (CC). SBA had the highest estimation accuracy of woodland biomass, but was not suitable for optimal estimation by moderate resolution satellite imagery (www.esri.com). The woodland biomass estimation accuracy by CC ($R^2 > 0.94$, $P < 0.0001$) was lower than that by SBA ($R^2 > 0.99$, $P < 0.0001$), but CC was considered to be a powerful indicator for woodland LULC biomass estimation by the satellite imagery, where open forest was distributed. In the case of arid land, the probabilistic correlation between CC and woodland biomass was reported in the Salhel region of Africa and in Queensland, Australia. Therefore, the unmixed forest biomass estimation method by CC was considered to be applicable to other arid- and semiarid-area open forests and woodland LULCs.

Statistically significant LULC explanators of discontinuous canopy bulk stomatal or canopy resistance may be geospatially correlated with seasonal hyperproductivity, immature productivity counts sampled at riverine, narrow, tributary, African, agro-village *S. damnosum* s.l. habitats in ArcGIS. The simple ratio (SR) of the 5m, NIR and visible canopy reflectances may be found to be a near-linear indicator of the absorbed photosynthetically active radiation absorption (APAR), by the canopy, minimum canopy resistance, *1/r c,* and photosynthetic capacity (PC) in an ArcGIS/ENVI cyberenvironment. The ENVI family of geospatial software enables use of information extracted from geospatial imagery, including panchromatic, multi and hyperspectral LiDAR and Synthetic Aperture Radar (SAR) [http://www.exelisinc.com/solutions]. ENVI tools are based on demonstrated scientific methods, and are designed for highly specialized tasks, from rigorous orthorectification and feature extraction to atmospheric correction algorithms (www.esri.com).

Photosynthetically active radiation (PAR) is tile solar radiation in the 5m RapidEye™ wavelength interval that falls approximately between 400-700nm (i.e., 0.4-0.7 jxm). The discontinuous, canopy-absorbed $APAR_{CAN}$ is the solar energy consumed in the discontinuous canopy photosynthetic process [43]. Highly nonlinear emissivities, however, may not be a reliable predictor of leaf biomass.

It may be possible to quantify the biomass allocation endmember eigenvector patterns to discontinuous, immature habitat, canopy leaves, stems and roots in fractionalized, decomposable, 5m RapidEye™, vegetative plants on a geoclassifiable, sparsely shaded, trailing vegetation, turbid water, imaged proxy with decomposable signature (5m NDVI), as well as quantifying these biomass allocation patterns are influenced by the growth environment, plant size, and seasonal competition. Dose–response curves of immature habitat canopy allocation may be constructed in ArcGIS by means of a meta-analysis from a wide array of geosampled decomposed endmember data variables. This dataset may reveal that the fraction of whole-plant mass represented by the unmixed endmember eigenvectors of eco-georeferenceable, immature, trailing vegetation, discontinuously canopied, canopy, habitat leaves which increases most strongly with flooding and decreases most strongly with droughts. Correction for size-induced allocation patterns diminishes the LMF response to light, but makes the effect of temperature on LMF more apparent [44]. There may be a clear explanatory effect on seasonally eco-georeferenceable, unmixed, *S. damnosum* s.l. habitat, fractionalized, discontinuous, infrequently canopy imaged through a 5m, RapidEye™ wavelength, transmittance-oriented, frequency-related, LULC allocations. Plants growing at high densities may show a clear increase in the stem fraction in an immature, *S. damnosum* s.l., narrow, African, riverine tributary, immature habitat, eco-georeferenceable geolocation.

However, in most comparisons across *Simulium* species, groups or environmental factors, the variation in LMF is smaller than the variation in one of the other components of the growth analysis equation: the leaf area: leaf mass ratio (SLA). In competitive situations, the stem mass fraction increases to a smaller extent than the specific stem length (stem length: stem mass). Thus, it may be concluded that explanative, hyperproductive, agro-village African, narrow riverine, tributary, *S. damnosum* s.l. immature habitat, discontinuous, canopy plants may be less able to adjust non-homogenous, canopy allocations than to alter organ morphology seasonally.

Due to the difficulty of acquiring extensive narrow, African riverine tributary, eco-georeferenceable, seasonally explanative, hyperproductive, immature, *S. damnosum* s.l. habitat, temporal observation data (which may elucidate seasonal flooding), increasing efforts are being devoted to estimating canopy bulk stomatal conductance efficiencies in ArcGIS employing $APAR_{CAN}$ from optical, cost-effective, moderate resolution data. For example, Jacob et al. [22] generated a robust RapidEye^{TM} signature in order to remotely quantitate APAR at a geosampled, seasonally hyperproductive, discontinuously canopied, *S. damnosum* s.l., 5m capture point level. The immature habitat was geosampled in an African, riverine agro-village, tributary complex in Burkina Faso. The APAR was obtained from the downwelling PAR at the surface (SFC). $PAR_{SFC}\downarrow$, in an ArcGIS/ENVI cyberenvironment, which then optimally defined APAR as the product of $APAR_{SFC}$ and the PAR absorbed by the green canopy only to $APAR_{SFC}$ (i.e., RPAR). $APAR_{SFC}$ is the total PAR absorbed by all discontinuous canopy, ipervious surface materials including soil, litter, etc., while RPAR is the ratio of the PAR absorbed by the green canopy second only, to $APAR_{SFC}$ [43].The advantage of this approach, according to Jacob et al. [26], is that a 5m RapidEye^{TM} resolution in $APAR_{SFC}$ can be remotely quantitated more accurately and readily than $PAR_{SFC}\downarrow$, while the determination of RPAR may be as accurate as that of PAR for autoregressively precisely quantitating, hyperproductive, *S. damnosum* s.l., immature, capture point, hyperproductive habitats in fractionalized, endmember eigenvectors. The whole eco-epidemiological, geo-predictive, sub-mixel, iterative interpolative, vulnerability modeling approach in ArcGIS (i.e., Geospatial Analyst^{TM}) was introduced in two parts in Jacob et al. [26]. Part I, was presented as a model output that dealt with the retrieval of $APAR_{SFC}$ in an ArcGIS cyberenvironment using Rapid Eye ^{TM} 5m data. By employing a complex atmospheric model in ArcGIS, $APAR_{SFC}$ was found to be related to the upwelling PAR reflected at the ToA, $PAR_{TOA}\uparrow$of the eco-georeferenceable, explanatorial, capture point. Of the eco-epidemiological, eco-georeferenced capture point illuminatively parameterizable, descriptive, iteratively interpolative covariate coefficients, the most statistically significant variable was Percentage of trailing vegetation. The quantitated relationship was independent of cloud parameters and moderately dependent on ozone amount and aerosol optical properties at the agro-village complex study site. The parameterization was developed to estimate $APAR_{SFC}$ from $PAR_{TOA}\uparrow$ in ArcGIS, which was inferred from the unmixed, interpolative, RapidEye^{TM} visible and NIR bands. Non-normalized, endmember diagnostic analyses were made employing the 5m data model eco-epidemiological, wavelengthforecasts from both ArcGIS simulations and field observations. The parameterization was valid to within 3 W m^{-2} compared to the results of detailed radiation model simulations. The forecasted, hyperproductive, *Simulium* habitat observations revealed a bias error of −2.3 Wm^{-2} and a standard error of 31.4W m^{-2} for the instantaneous estimates of $APAR_{SFC}$.

The PAR absorbed by the green canopy of a hyperproductive, trailing vegetation, *S. damnosum* s.l., discontinuous, infrequently canopied, eco-georeferenceable, narrow, African, agro-village complex, eco-epidemiological, immature habitat may be directly linked to

photosynthesis and net primary productivity (NPP) in the carbon cycle. One of the major uncertainties in predicting climate change comes from a full accounting of carbon-cycle feedbacks, which roughly double physical feedbacks [46]. Most of this uncertainty is a result of the many pathways and time scales at which African narrow riverine tributary ecosystems interact with the climate systems and how these will respond to LULC change (e.g., flooding). The relationship between leaf nitrogen and the carbon cycle may be found to be key to many African riverine ecosystems that are hyperproductive for immature *S. damnosum* s.l. and consist of trailing vegetation and sparsely shaded, riverine-related, discontinuously canopied processes, since photosynthesis provides the energy and carbon-cycle molecules for growth, reproduction and decomposition for nutrient cycling. Ecologists, entomologists and experimenters have long recognized that nitrogen is the most limited nutrient for plant growth [46].

Quantifying geocalssifiable LULC changes in seasonal canopy nitrogen content in a hyperproductive, seasonally explanative, *S. damnosum* s.l., immature habitat, capture point may provide direct information about the narrow, African, riverine, agro-village complex, tributary, ecosystem while providing methods to detect and monitor LULC changes in response to climate by employing moderate resolution imaging spectroscopy in ArcGIS. Direct detection of canopy nitrogen from airborne imaging spectrometers can reveal selective pressure on plants in competition for light, water, and nutrients which may result in suites of biochemical and structural traits that integrate their functional strategies [46]. Thus, structural traits affecting light scattering of sparsely shaded, seasonally discontinuous, trailing vegetation, *Simulium,* immature, turbid water, seasonal, hyperproductive habitats with unmixed, discontinuous, infrequently canopied, decomposable variables may be convergent with their biochemical traits. Explicitly testing whether assumptions that discontinuous, infrequent, canopy structure can be ignored in quantifying biochemical composition with a detailed analysis of the bio-geophysical processes of photon scattering from leaves and plant canopies of a hyperproductive habitat may reveal shifts in seasonal, immature, *S. damnosum* s.l. productivity. There is recognition of the importance of multiple scattering, particularly in moderate resolution NIR bands where canopy plant compounds do not display strong absorption features [46]. It may be possible to quantify discontinuously infrequently canopied, trailing vegetation, *S. damnosoum* s.l. turbid riverine water, eco-georeferenceable, immature habitats.

Since PAR accounts for nearly half of the total solar radiation at the canopy surface of an eco-georferenceable, *S. damnosum* s.l. habitat in an African riverine agro-village ecosystem [43], it also would contribute significantly to the exchanges of energy and water between the discontinuous canopy habitat, uncoalesced, LULC surface and the atmosphere. Therefore, knowledge of the ecogeographical, meterological distribution and seasonal temporal variation in APAR is necessary to achieve optimal, elucidatory forecast, vulnerability risk modeling results of seasonally hyperproductive *Simulium* habitats in ArcGIS.

Jacob et al [45] extended previous work and investigated seasonal, African riverine meandering processes (e.g., flooding), giving rise to the near-linear dependence of APAR, PC and l/r,, on Simple Ratio (SR) for employing an unmixed, 5m RapidEye^{TM}, eco-epidemiological, dataset of hyperproductive *S. damnosum* s.l. habitats with fractionalized, endmember wavelength, transmittance eigenvector, covariate emissivities in ArcGIS. It was demonstrated that under flooded,eco-georeferencable, explanative, riverine field conditions, the NIR 5m RapidEye^{TM}, unmixed reflectance term controlled the variation of SR, employing

various vegetation indices (e.g., leaf area). As a result, near-linearity between SR and APAR, Pc or 1/r~, a scattering coefficient in the RapidEye™ NIR region, satisfied the following equality: 1 - [G(~)/2/t]2(1-*n*), where the canopy leaf's effective scattering coefficient for PAR, G(/~) was the average leaf projection in the direction /x, and /x was the cosine of the zenith angle of the incoming flux. It was shown that a variety of auto-probabilistically regressable, wavelength transmittance, covariate emissivity, uncoalesced combinations are well configured for the estimation of APAR, Pc and 1/rC in a hyperproductive, immatue habitat imaged through a 5m RapidEye™, wavelength, explicative interpolative transmittance emissivity and eco-epidemiological habitat, forecast, vulnerability model. Responding to leaf scattering coefficients quantitated in the 5m bands, the final model forecasts conformed to the mathematical expressions in ArcGIS, which allowed the authors to regressively and remotely quantitate the relationships between SR and APAR, Pc and I/r, which they found to be increasingly nonlinear as soil reflectivity around a seasonally geosampled, hyperproductive riverine habitat increased.

Fluorescence information is also complementary to unmixed, reflectance-based, spectral vegetation indices [47]. Popular greenness-based indices such as the normalized difference and enhanced vegetation indices, NDVI respectively, are linked to canopy chlorophyll content which are related to potential photosynthesis, whereas fluorescence is an indicator of actual photosynthesis. The photochemical reflectance index (PRI) is sensitive to the de-epoxidation state of pigments within the xanthophyll cycle, a protection mechanism that may evolve in parallel to fluorescence to dissipate excess energy in a 5m resolution, RapidEye™ imaged, seasonal, *S. damnosum* s.l. habitats may reveal geolocations of seasonal high density, immature foci. Xanthophylls are known to be the yellow pigments typically seen in leaves, and are considered to be oxygenated carotenoids that are synthesized within the plastids [47]. Interpolating extracted unmixed, discontinuous, canopy pigments from a hyperproductive, seasonal, *S. damnosum* s.l. habitats capture point, African, riverine, agro-village tributary complex.

Knowledge of global chlorophyll fluorescence emissions may be also important for optimal retrievals of trace-gas concentrations, including CO_2, that require very high accuracy and precision. This may be vital for precisely, geolocalizing, seasonally hyperproductive, *S. damnosum* s.l.,immature habitats employing 5m RapidEye™ data. The emission occurs within the O_2 A-band, which may be employed to estimate canopied photon path lengths for an eco-georeferenceable, hyperproductive habitat in ArcGIS. In principle, moderate resolution, oxygen A-band, derivative, endmember spectra can discriminate atmospheric scattering from canopy multiscattering, and, therefore, can provide an operational technique to retrieve cloud and aerosol macrophysical/microphysical properties with 5m RapidEye™ resolution, oxygen A-band measurements in ArcGIS. Elucidative habitat pieces reveal red and IR elucidative decomposed radiances and experimental plot biomass, leaf water content for remotely and probabilistically regressing unmixed radiance variables evaluated. The linear combinations of the IR/red ratio, the square root of the IR/red ratio, the IR-red difference, the vegetation index, and the transformed VI may also be precisely optimally generated in ArcGIS. In addition, the corresponding green and red linear endmember combinations may be evaluated for comparative purposes. Depending on the instrument resolution, the out-of-band (OOB) rejection, and the Signal-to-Noise (S/N) ratio in the decomposed, 5m, wavelength transmittance emissivity, eco-epidemiological, immature habitat, orthogonalized eigenvectors of the endmember, forecast, vulnerability model and unknown geospatialized clusters (positively autocorrelated hyperproductive immature habitats) may be geolocalized by unmixing an explicatively, 5m RapidEye™ image for

seasonal, sparsely shaded, discontinuously canopied, trailing vegetation, turbid water, hyperproductive, *S. damnosum* s.l., capture point, geo-spectrotemporal, geospatialized habitats.

A fundamental goal in remote sensing is maximizing the S/N ratio. In other words, how much of the recorded signal that appears as a unmixed, 5m, RapidEye™ *S. damnosum* s.l., immature habitat mixel is useable, and how much is unwanted distortion or noise. The sensor system with its optics, detectors, and spectral discrimination system converts energy from one form to another (e.g., radiant energy into remotely sensed energy). This is significant as this variation of the original signal allows an increase in the noise to the sensing procedure being examined. In order to optimize this modelling system in an ArcGIS cyberenvironment, design tradeoffs can be made by balancing instantaneous field of view (IFOV). The IFOV is a vital calculation used in the determination of how much one detector mixel is able to see in regards to the field of view (FOV), as well as the time it takes to complete the sample and the spectral resolution data [43]. Field of View is the largest area that an imager can see at a set distance, typically described in horizontal degrees by vertical degrees, for example, 23º X 17º (www.esri.com).

Instantaneous field of view is defined as the angle subtended by a single detector element on the axis of the optical system. IFOV has solid angle attributes through which a 5m RapidEye™ detector may be sensitive to *S. damnosum* s.l.-related canopy radiation. Quantitated, 5m RapidEye™ discontinuous, canopy spectral invariants in an ArcGIS cyberenvironment express, iterative, interpolative, sub-mixel, hyperproductive, *S. damnosum* s.l. habitat, endmember eigenvector observations by employing simple algebraic combinations of leaf and canopy spectral transmittance and reflectance wavelength, moderate resolution, transmittance, frequency-oriented covariates as independent coefficients. This eco-epidemiological dataset in ArcGIS includes the discontinuous canopy interceptance, the recollision, and the escape probability of variables specific for tabulating and quantitating an accurate relationship between the geo-spectrotemporal seasonal response of the immature habitat, geocalssifiable, vegetation-related LULC canopy to the incident solar radiation at the leaf and canopy scale, while allowing for precise parameterizations of the partitioning of incoming radiation. Employing a 5m RapidEye™ uncoalesced, wavelength emittance, eco-epidemiological, forecast, vulnerability model in ArcGIS, *S. damnosum* s.l. habitats and their fractionalized, endmember eigenvector, structural variables quantitate spectral seasonal, invariant relationships between immature productivity and radiative properties of narrow, African, riverine agro-village, immature habitat, non-homogenous vegetation canopies. Eco-epidemiological vulnerability and data analysis on leaf and canopy spectral transmittance through geospectral LULC reflectances collected during the model construction exercise in ArcGIS allowing for efficient targeting of unknown, un-geosampled, hyppeorductive, *S. damnosum* s.l. habitats in narrow African tributary, sparsely shaded, riverine agro-village communities. The eco-georeferenceable residual forecasts from the vulnerability model allow for optimal separation of the structural and radiometric components of the measured/modeled 5m signal. The canopy spectral invariants offer a simple and accurate parameterization for the shortwave radiation block in many global moderate resolution, forecasting models of climate, hydrology, biogeochemistry, and ecology [48]. Content from the 5m data can be fully exploited if the wavelength-independent variable, non-randomized covariate coefficients can be retrieved, as they are more directly related to structural characteristics of a vegetation-related, discontinuous LULC canopy associated with hyperproductive habitats.

Retrieving atmospheric photon-pathlength data from detailed spectroscopy of the O_2 band near 760nm may also include atmospheric pressure-related, moderate resolution, wavelength transmittance emissivity variables. If not properly accounted for, fluorescence emission could produce significant errors in retrievals rendered from a habitat [47]. The effect of fluorescence on an aerosol, plume height retrieval from the O_2 A-band for immature habitats geosampled in African turbid riverine geolocations may be investigated using a linear, non-normality, diagnostic analysis in ArcGIS of IFOV data.

One means of measuring small fluorescence moderate resolution, *S. damnosum* s.l. habitat signals synthesized from moderate spatial resolution data is through dark features in the reflected spectrum, either from telluric absorption or deep solar Fraunhofer lines. In ArcGIS, these lines are spectral absorption dark lines which are produced whenever a cold gas arises between a canopied covered broad spectrum photon source and the detector. Ground, aircraft, and space-based approaches have utilized filling-in of the dark and spectrally wide O_2 A-band (760 nm) and O_2 B-band (690 nm) through data feature attributes in order to detect the weak fluorescence signal. The geolocation of these oxygen absorption features, as well as other absorption bands and solar Fraunhofer lines, are revealed in an ArcGIS-constructed, eco-epidemiological forecasting map employing broadband red and far red fluorescence emission features that peak near 685 and 740 nm, respectively.

Optionally, a seamline feature class for seamline mosaicking can be generated in ArcGIS for image extraction of a riverine, geospatial object, (e.g., a hyperproductive habitat). An explanatory feature class that defines habitat canopy boundaries can also be utilized in ArcGIS, so that a set of rules can be employed to dynamically mosaic the rasters. A set of iterative, interpolative properties in ArcGIS may be control the mosaicking. Sharing access to a mosaic dataset ensures that those utilizing it cannot make modifications to the source dataset, which could impact other users. Or, if raster catalog exists of endmembers of geo-spectrotemporally geosampled immature habitats as eco-epidemiological data of transmittance emissivities can be created that may serve the raster catalog. In the latter case, the existing raster catalog can be a standard raster catalog in ArcGIS when constructing seasonal, forecast vulnerability maps.

The eco-georferenceable, immature *S. damnosum* s.l. hyperproductive habitats with unmixed, emissivity covariate coefficient datasets may be employed for logging during data loading and other operations in ArcGIS. A color correction table that defines the color mapping for each raster in the raster catalog may be employable for distingushing habitats based on interpolative endmember eigenvectors. There is no mixel data loss or metadata loss when using mosaic datasets, as the source mixels are never altered or converted, and the files are never moved (www.esri.com). Therefore, any metadata files will remain in a geolocation of a seasonal habitat, capture point that is remotely analyzed in ArcGIS. Because the mosaic dataset does not alter the source data or its geolocation, the unmixed riverine habitat mixel, wavelength transmittance emissivity values will not be altered. Users have access to the mosaicked image as well as the source data. Therefore, there is no data loss occurring for overlapping datasets (http://help.arcgis.com/en/arcgisdesktop).

Overviews, which are similar to raster pyramids, can be generated for a *S. damnosum* s.l. habitat, fractionalized, moderate resolution, eigenvector endmembers of a radiance dataset in an ArcGIS cyberenvironment. A pyramid is a series of reduced resolution, probabilistic representations of an eco-epidemiological dataset. A pyramid is mainly used to improve the display performance of rasters when not working with the iterative interpolative mixel

information at full resolution, which may contain a number of layers, each resampled at a more generalized level [49]. Thus, each level of the pyramid is a resampled representation of the raster at a coarser spatial resolution. Pyramids allows ArcSDE to fetch only data at the specified resolution, or level required for the display. Building pyramids is performed on the ArcSDE server side whenever the underlying raster is modified or updated [49].

Generating orthogonal fractionalized uncoalesced, geo-spectrotemporal, geospatial, uncoalesced, fractionalized, eco-georeferenceable, *S. damnosum* s.l. immature habitat, medium resolution, orthogonally eigen-decomposable, explanative, endmember eigenvectors of a hyperproductive habitat in data pyramids requires the resampling of multiple input mixels so that fewer output mixels need to be generated [49]. At each higher pyramid level the mixel size doubles, resulting in four times fewer mixels. ArcSDE generates pyramids depending on the maximum number of levels and type of mixel data provided by the user (www.esri.com). The pyramid begins at the base, or level 0, which contains the original mixels of a 5m RapidEye^{TM} spatial resolution image, and proceeds toward the apex by coalescing four decomposed mixels from the previous level into a single mixel at the current level. This process continues until less than four mixels remain, or until ArcSDE exhausts the defined number of levels.

A pyramid must always be generated from the upper leftmost coordinate, which is considered the image origin (www.esri.com). If the origin of the habitat image is moved, the entire endmember habitat data pyramid must be regenerated. Hence, it is useful to preset the origin or the eigenvector and endmembers, orthogonally decomposed by a eco-georeferenceable, immature *S. damnosum* s.l. hyperproductive, immature habitat data pyramid reference point when the raster is created in ArcGIS. When mosaicking raster data in ArcSDE or in a file geodatabase, pyramids can be built on a raster dataset as raster data is being mosaicked into the raster dataset, or they can be built when the loading is complete (www.esri.com). Data pertaining to each pyramid level is stored in the Raster Block table. Thus, higher level moderate resolution, 5m, immature habitat mixels are optimally decomposed and stored in the Block table in advance. Additional levels of the pyramid will increase the number of raster block table rows. However, since it is possible to specify the number of levels in habitat data, the true apex of the pyramid may not be obtainable, limiting the number of records added to the Raster Block table. The pyramid allows ArcSDE to provide the application with a constant 5m RapidEye^{TM} sensor resolution of mixel data, regardless of the rendering windows scale (see Figure 33). Data of a large raster transfers more quickly to the client when a pyramid exists, since ArcSDE can transfer fewer cells of a reduced resolution [49]. The different levels are created by resampling the original RapidEye^{TM} empirical dataset, and then interpolating mixels in the original unmixed, 5m wavelength transmittance emissivities.However, it is recommended that you use nearest neighbor for discrete (nominal) data or raster datasets with color maps, such as land-use data, scanned maps, and pseudo color images.

ArcGIS allows for partial pyramid construction, which rebuilds only the part of the pyramid overlapped by the source data during a mosaic operation. This may helps when updating a mosaicked eco-georeferenceable, immature, *S. damnosum* s.l., hyperproductive, immature habitat,uncoalesced, data raster dataset, because if a new raster dataset is added, the entire raster dataset does not need to rebuild pyramids in ArcGIS(see Figure 38). However, if update the data at the capture point, uncoalesced, geo-spectrotemrpoal, raster dataset's origin (i.e., pyramid reference point), the pyramid needs to be rebuilt in ArcGIS for

the entire raster dataset.has grown because of a number of raster dataset source files (or other raster datasets) that have already been mosaicked to it.

Figure 38 Hypothetical mosaicked simulation of a discontinuously canopied, hyperproductive, trailing vegetation turbid water, 3-level of a *S. damnosum* s.l. immature habitat pyramid.

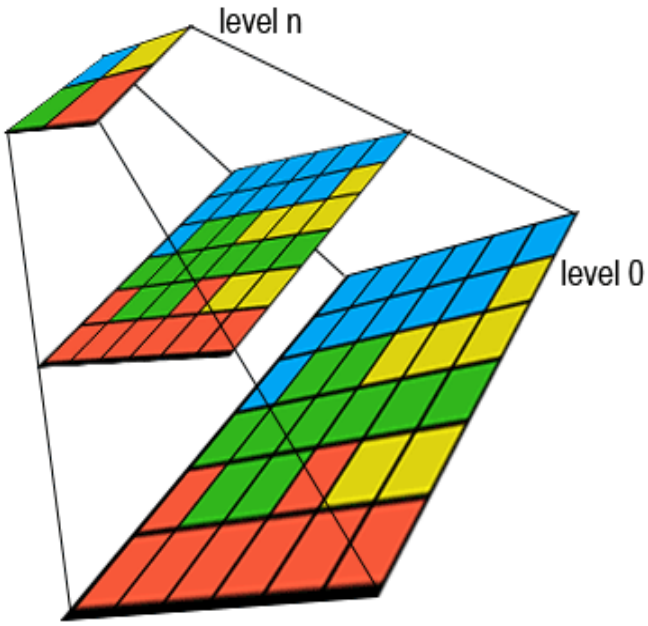

Overviews can be defined as reduced resolution datasets that are generated in order to progress the speed at which the mosaic is demonstrated (www.esri.com). Default overviews can be parsimoniously generated over an entire endmember eigenvector dataset through a RapidEye^{TM} capture point employing a 5m resolution, wavelength transmittance emissivity dataset in ArcGIS. Alternatively, the downsampling ratio may be quantified. In digital signal processing, decimation is the process of reducing the sampling rate of a signal (in this case, a hyperproductive, *S. damnsoum* s.l.,immature habitat with a trailing vegetation tubid water, discontinuously canopied, illuminative, proxy LULC biosignature). Complementary to interpolation, which increases sampling rate, the ratio is a specific case of sample rate conversion in a multi-rate, digital signal processing system. Jacob et al. [22] states that decimation utilizes filtering to mitigate aliasing distortion, which can occur when downsampling a moderate resolution, hyperproductive, trailing vegetation, discontinuous, infrequently canopied, turbid water, *S. damnsoum* s.l., immature, capture point, narrow tributary, African agro-village, seasonal habitat in an interpolative 5m, RapidEye^{TM},unmixed signal. Digital signal processing (DSP) is the numerical manipulation of signals, which is commonly utilized to measure, filter, produce or compress continuous analog signals [50]. An analog, or analog signal, is any continuous signal for which the time varying feature eco-cartographic variable of the signal is a representation of some other time varying quantity (i.e., analogous to another time varying signal).

Theoretical analyses and deriviations are typically performed on discrete-time signals in endmember models, created by the process of abstract sampling in ArcGIS. The processed result may be a frequency spectrum or a set of statistics, but it is often another digital signal that is converted back to analog form by a digital-to-analog converter (DAC). Even if the entire sequence is more complex than analog processing and has a discrete value range, the application of computational power to signal processing in ArcGIS allows for many advantages over analog processing in many heuristically optimizable, fractionalized, endmember eigenvector, foreast, vulnerability applications. These include propagational error detection and correction transmission, as well as data compression. Digital signal processing and analog signal processing in ArcGIS are subfields of signal processing [50]. The DSP applications include signal processing, sonar and radar signal processing, sensor array processing, spectral estimation, statistical signal processing, digital image processing, signal processing for communications, control of systems, biomedical signal processing, and seismic data processing, among others(www.esri.com). Digital signal processing in ArcGIS of a 5m, resolution, geospectrotemporally uncoalesced, moderate resolution, hyperproductive, narrow African, agro-village complex, trailing vegetation, turbid water, eco-georferenceable,capture point, discontinuous, sparsely shaded, infrequently canopied, riverine tributary, immature habitat can involve linear or nonlinear descriptive operations. Nonlinear signal processing is closely related to nonlinear system identification in ArcGIS and can be optimally implemented in the time frequency and hyperproductive *S. damnosum* s.l. habitat domains.

Mosaic datasets are excellent data models for storing and managing endmembers of immature habitat data in ArcGIS for model construction of possible seasonal clusters of hyperproductive immature habitats. *Simulium* habitat datasets are ideal for distributing data in Geospatial Analyst™, as they can be directly accessed by ecologists, entomologists and other researchers and easily utilized. Properties of the mosaic dataset can thereafter be modified, such as the maximum image size, the level of metadata, the compression method, or the maximum number of downloads, in order to achieve the maximum performance out of their server and meet customizable needs for interpolating a habitat endmember eigenvector biosignature. When clients connect to a server to see the mosaic image, their application controls the same mosaic methods and other properties that users with a direct connection have. They may also select raster datasets and download them to their local disk (www.esri.com). The mosaic dataset is a necessary tool for the disseminating imagery in addition to managing and visualizing data [50].

ArcGIS offers two methods for mosaicking immature habitat raster data: either as a virtual mosaic, employing a mosaic dataset, or by permanently appending (i.e., mosaicking) raster datasets together. A mosaic dataset is a data model within the geodatabase which creates a mosaicked image on-the-fly according to the mosaicking rules as defined within its properties [50]. Jacob et al. [45] suggests handling overlapping, eco-georeferenceable, narrow, African riverine, agro-village, complex environments where trailing vegetaion, turbid water, discontinuous, in frequently canopied, partially shaded, seasanally, narrow tributary , agro-village complex, hyperproductive habitats occur by choosing to only keep raster turbid water, sub-mixel, decomposable, fractionalized ,endmember eigenvectors, through moderate resolution, optimally synthezied, orthogonally decomposable, emissivity vulnerability covariate coefficient explanators from the first to last radiance datasets. This will optimally blend the overlapping cell count values with the radiance data in an ArcGIS module (e.g., ArcSDE geodatabase) within a weight-based algorithm. By doing so, the mean of the

overlapping immature, capture point, cell values would be quantitated by employing tabulated min or maxi values.

When mosaicking discrete data, the First, Minimum, or Maximum options give the most meaningful results (http://resources.arcgis.com/). The Blend and Mean options are best suited for unmixed 5m, RapidEye^{TM},spatial resolution data. According to Jacob et al. [22], if any of the input, posivitively or negatively, autocorrelated values in an empirical dataset of explanatory, geo-spectrotemporally, geospatially clustered, seasonally hyperproductive,immature habitats that have been geosampled as endmember eigenvector rasters are floating point, the output would be floating point. If all the inputs are integer and First, Minimum, or Maximum is employed the output would be an integer. Jacob et al. [22] also recommends rebuilding the eco-georeferenceable pyramid for an African, agro-village complex, narrow, riverine tributary, riverine, immature habitat that has been geosampled through descriptive information after the mosaic operation for file-based, raster datasets has been performed.

Unfortunately, raster datasets stored within a file geodatabase or an ArcSDE geodatabase cannot support partial pyramid updating. Therefore, selected orthogonalized explanatively fractionalized, 5m, endmember, eigenvectors, of *S. damnosum* s.l. immature habitats are pyramids which ideally should be built during the mosaic operation rather than after. By setting the upper left coordinate, ArcGIS can avoid rebuilding the positively autocorrelated, heuristically optimizable, clustering, eco-georefernceable, immature, seasonal, hyperproductive, agro-village complex, narrow tributary, *S. damnosum* s.l., trailing vegetation, turbid water, discontinuous, infrequently canopied, seasonal, uncoalesced, eco-georeferenceable immature, capture point, habitat explanators, which have been geo-spectrotemporally geosampled through fractionalized, endmember eigenvector, seasonal pyramids for an entire, rasterizable, explanatorial dataset.

In spite of successes in geo-classifying some immature, hyperproductive, *S.damnosum* s.l. habitats employing conventional supervised or unsupervised techniques in ArcGIS, it has been difficult to obtain consistent geoclassifiable, LULC classes from seasonally flooded, narrow African, agro-village complex, eco-georferenceable, riverine, immature, habitat images, owing to variability in illumination, atmospheric effects, and instrumental response. As a result, with a few exceptions (e.g., Jacob et al. [22], Jacob et al. [51], monitoring of seasonal, sparsely shaded, discontinuously canopied, proxy biosignature LULC changes in study sites quantitated by moderate resolution, remote sensing onchocerciasis-relatedexplanative models have been restricted to measurements of changes in ecohydrologic, geo-spatialized, descriptive, interpretative random patterns. Less attention has been granted to interpolative LULC, sub-mixel, reflectance waveband transmittance changes.

A 5m, RapidEye^{TM} ,unmixed *S. damnosum* s.l. trailing vegation, discontinuous, infrequently canopied, turbid water, capture point, narrow tributary, African, agro-village complex, ecosystem, eco-georeferenceable, seasonal image can be considered as an image cube in ArcGIS where the third dimension is the interpretive, geospectrotemporal, explanatorial, sub-mixel, domain, eco-cartographically represented by hundreds of elucidative, descriptive, geo-spectrotemporal, uncoalesced, parameterizable or non-parameterizable uncoalesced, covariate, wavelength transmittance emissivities, may be robustly quantitated. Hyperspectral imaging, like other spectral imaging, collects and processes information from across the electromagnetic spectrum with the goal of obtaining

the spectrum for each mixel in the image of a scene in order to optimally identify topographic materials [52]. As a result, an eco-georeferenceable hyperspectral image of an explanatively hyperproductive, *S. damnosum* s.l., capture point, immature habitat, that is geo-spectrotemporally extracted in a moderate resolution, non-homogenous mixel is actually a quantifiable column vector with dimension equal to the number of spectral bands, which commonly contains valuable information that can be employed to account for fractional, endmember eigenvector, variability, similarity, and discrimination. Jacob et al. [22] presented a new explanatively hyperspectral, geo-spatiotemporal measure to optimally describe illuminatively fractionalizable, 5m resolution, Rapid Eye ™ geo-spectrotemporal, eigenvector endmembers that were eventually used as interpolative and heuristically, optimizable sub-mixels to create a Rapid Eye™ , forecasting vulnerability model. These orthogonal, endmember space-time, heuristically optimizable space-time eigenvectors quantitated variability employing two criteria, information divergence and discriminatory probability in an eigenfunction decomposition algorithm in an ArcGIS/ENVI cyberenvironment for optimally delineating sub-mixel heteroskedascity in an eco-georeferenceable, hyperproductive, capture point, immature habitat, geo-spectrotemporally geosampled in a narrow tributary, agro-village complex, riverine community in Burkina Faso. The geospectral information measure is an information-theoretic measure which treats each mixel as a random variable employing its spectral signature histogram as the desired probability distribution [52].

In Jacob et al. [22] Spectral Information Divergence (SID) in ENVI compared the similarity between multiple geo-spectrotemporally extracted variables in a dataset of immature hyperproductive, narrow African, agro-village complex, trailing vegation, turbid water, capture point, eco-georeferenceable, discontinuous, sparsely shaded, infrequently canopied, riverine tributary, immature habitat with optimizable, geospectrotemporally emissivity, covariate estimators by measuring the probabilistic discrepancy between the corresponding fractionalized, endmember eigenvector biosignature forecasters. The discriminatory spectral probabilities of a geospectral database (i.e., library) were set relative to the sub-mixel, explanatorial, descriptive regressors to achieve optimal topographic, material identification in ArcGIS using a proxy, LULC, interpolated biosignure.

In order to compare the discriminatory power of the decomposed LULC endmember, geospectral and geospatial regression measure relative to another, a criterion was introduced in Jacob et al. [22] for performance evaluation, based on the power of discriminating one eco-georeferenceable, capture point, immature habitat with riffle water, orthogonally decomposed, fractionalized, endmember, space-time eigenvectors from the discontinuous, sparsely shaded, trailing vegetation endmembers relative to a reference mixel. The experimental results demonstrated that the moderate resolution and cost-effective, 5m, RapidEye™ data could measure and remotely characterize geospectral variability more effectively than the commonly used Spectral Angle Mapper (SAM) in ENVI for finer resolution sensor data.

SAM is a geo-physically-based geospectral classification that employs an *n*-dimensional angle to match mixels to derivative reference, proxy, LULC biosignature, geo-spectrotemporally uncoalescable, derivative 5m, forecast endmember spectra. In Jacob et al. [22], a, explanatorial, decompositional algorithm in ArcGIS optimally quantitated the elucidative, geospectral similarities between eco-georeferenceable explanative, trailing vegetation and partially canopied, turbid water, sub-mixel, eco-epidemiological forecasts in a fractionalizable, endmember, eigenvector derivative, geospectrotemporal decomposition of a

synthesized dataset of RapidEye™ emissivity coefficient, endmember, forecastable, derivative spectra by calculating the angle between the spectra and treating them as vectors in a geo-space with dimensionality equal to the number of 5m bands. Eigenvector endmember *S. damnosum* s.l., geoclassifiable, uncoalesced, proxy, LULC signature, immature, capture piint, habitat data in decomposable forecast spectra employed by SAM did not come from ASCII files. Instead, they were accessed from ENVI spectral libraries. The authors validated the extracted, fractionalized, endmember eigenvector, 5m, wavelength transmittance, imaged, immature habitats directly from the RapidEye™ viable and NIR data as ROI average and Z-profile spectra. SAM compared the angle between the *S. damnosum* s.l. emissivity endmember spectrum vector and each mixel spectrum vector in n-D space. Smaller angles represented closer matches to the reference expository spectrum. Mixels further away than the specified maximum angle threshold in radians were not geoclassified.

In the SAM rule image, the mixel values of the rule, seasonal, hyperproductive habitat, fractionalized, 5m image represented the spectral angle in radians from the reference spectrum for each *S. damnosum* s.l. immature habitat in a geo-classified LULC class in ENVI. Lower spectral angles represented better matches to the sub-mixel, tabulated forecast in a heuristically optimizable dataset of descriptive, and expository derivative, illustrative, fractionalized, endmember eigenvector spectra in the object-based classification. Areas that satisfied the selected radian threshold criteria were carried over as LULC areas from the geosampled 5m, hyperproductive, immature habitat image. The SAM classification image remotely revealed turbid and non-turbid water, Narrow tributary, discontinuous, infrequently canopied, *S. damnosum* s.l. narrow tributary, riverine, agro-village, complex ecosystem LULC areas, were geo-classified as dense and sparse trailing ,partially canopied, vegetation and LULCs in the RapidEye™ data.

Spectral Information Divergence is a geospectral classification method that employs a divergence measure to match mixels to reference spectra; the smaller the divergence, the more likely it is that the mixels are similar [53]. In Jacob et al [22], in the SID, seasonal eco-georeferenceable, immature *S. damnosum* s.l. hyperproductive habitats in unmixed 5m RapidEye™ mixels with a measurement greater than the specified maximum divergence threshold were not classified. Endmember, riverine, agro-village complex, narrow tributary, geoclassifiable, LULC forecastable, derivative endmember spectra employed by SID also came from spectral libraries in ENVI. The authors did not have to extract them directly from the immature habitat RapidEye™ image as ROI average or Z-profile spectra. In the SID calibrated image, the mixel values of the rule image represented the SID value (i.e., the output of the equation that defined SID for a pair of geo-spectralized, trailing vegetation, turbid water geo-classified LULC vectors). Lower spectral divergence measures eco-geohydrologically represented better matches to the forecastable, iteratively interpolated, eigenvector, derivative, 5m endmember spectra. Areas that satisfied the maximum divergence threshold criteria were carried over as sparsely shaded, canopied, sub-mixel, areas in the 5m image. The authors proposed an information theoretic criterion, called SID for spectral similarity and discriminability using moderate resolution hsatellite data..

It is derived from the concept of divergence arising in information theory and can be used to describe the statistics of a spectrum. Unlike spectral angle mapper (SAM) which extracts geometric features between two spectra, SID views each mixel spectrum as a random variable and then measures the discrepancy of probabilistic behaviors between two spectra. In order to evaluate SID. SAM compares the angle between the endmember spectrum vector and each pixel vector in *n*-D space. Smaller angles represent closer matches to the reference spectrum.

SAM classification assumes reflectance data. However, if you use geo-spectrotemporally uncoalesced, explanative, time series, radiance data, the error is generally not significant because the origin is still near zero(https://www.harrisgeospatial.com). The SAM algorithm is a simply based on the measurement of the spectral similarity between two spectra. The spectral similarity can be obtained by considering each spectrum as a vector in q - dimensional space, where q is the number of bands. The SAM algorithm determines the spectral similarity between two spectra by calculating the angle be- tween the two spectra, treating them as vectors in a space with dimensionality equal to the number of bands. SAM is used for comparison via hyperspectral data. Mixel with minimum or zero spectral angles in comparison to the reference spectrum is assigned to the class defined by reference vector. However, when threshold for classification based on spectral angle is modified, the probability of incorrect object detection may increases.

Experimental results show that SID can characterise spectral similarity and variability more effectively than SAM Compared to the Spectral Angle Mapper (SAM), which has been widely used in the past for vector arthropod remote sensing, SID was more effective in preserving hyperproductive habitat, sub-mixel, decomposed 5m, eigenvector endmember, expository properties (see Figure 39).

Figure 39. Spectral Angle Mapper (top left), Spectral Information Divergence (top middle), RapidEye™ classification images (top right), of a canopied *S. damnosum* s.l. habitat with a decomposed trailing vegetation (bottom left), and turbid water biosignature (bottom right) fractional curves.

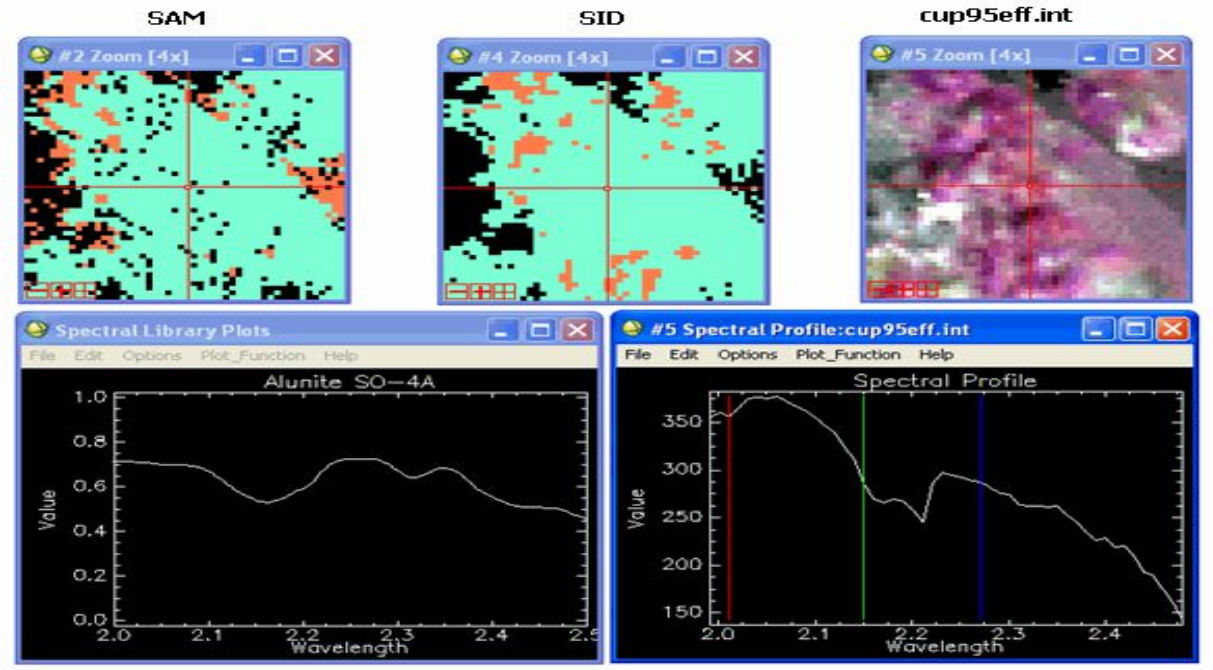

In Jacob et al. [22], the SAM of the capture point in an interpolative 5m RapidEye™ immature habitat empirical endmember output appeared to have more noise. The authors compared the Spectral Profile for this selected mixel data with the proxy 5m biosignature for seasonally hyperproductive, *S. damnosum* s.l. larval habitats from the ENVI spectral library.

The trailing vegetation and turbid water, submixel variables were easily seen when interpolated to each other.

In many explanative, hyperspectral seasonal applications, it is required to identify a target in an unknown image scene via a spectral library, or a database. To meet this need, a criterion is introduced to calculate the spectral discriminatory probabilities of signatures in the ENVI library as to provide the likelihood for robustly identifying the target (e.g., a *S. damnosum* s.l. habitat). In order to compare the relative discriminatory power between two geospectral measures (e.g., canopied trailing vegetation, turbid water fractionalized LULC, uncolaesced, eigenvector endmembers), another criterion may be proposed, based on the ratio of the spectral similarities of a 5m RapidEye^{TM} extracted mixel to another mixel relative to a reference mixel. In practice, variation in the identified habitat LULC biosignatures from one seasonal image to another may be observed, due to varying acquisition conditions. This may possibly produce significant unquantifiable, propagational, sub-mixel estimation errors. Against this background, hyperspectral unmixing of several seasonal, vector arthropod habitat images acquired over the same area is of considerable interest. Such a vulnerability, forecastable signature derivative, with parameterizable wavelength transmittance in an emissivity geo-spectrotemporal and geospatial endmember, descriptive vulnerability, forecast, residual analysis may enable unmixed, canopied, interpolatively decomposed, sparsely shaded, endmembers extracted from a 5m RapidEye^{TM} scene to be tracked in ArcGIS/ENVI. The corresponding sub-mixel object variability may then be eco-geographically and ecohydrologically characterized. Sequential endmember estimation from a set of hyperspectral images is expected to provide improved performance when compared to methods analyzing multi-seasonal images independently [54].

However, with the significant size of a within–canopy, seasonally hyperproductive *S. damnosum* s.l. immature, capture point, habitat, eco-epidemiological, narrow, African tributary, agro-village, trailing vegetation, turbid water, discontinuous, infrequently canopied, geo-spectrotemporally uncoalesced, moderate resolution, fractionalized, endmember eigenvector predictors may preclude the use of batch procedures to jointly estimate the mixture of 5m resolution, wavelength, transmittance covariates of a sequence of multiple seasonal habitat scenes. Provided that each elementary geoclassifiable, LULC component is present in at least one eco-georeferenced, African agro-village, narrow riverine, tributary ecosystem image, an online unmixing strategy in ArcGIS may be optimally employable for quantitating temporal sub-mixel variability. The online hyperspectral unmixing algorithm may be formulated as a two-stage stochastic program, which may be solved using classical ArcGIS techniques (e.g., co-kriging).

Stochastic elucidation approximation methods are a family of iterative stochastic optimization algorithms in SAS/GIS that attempt to find zeroes or extrema of functions which cannot be computed directly, but only estimated via noisy observations. Stochastic optimization (SO) methods generate and utilize randomizable, descriptive, geo-predictive variables[24]. For resolving stochastic problems in SAS/GIS, the sub-mixel, randomized variables may have to appear in the formulation of the optimization problem itself, which could involve qualitatively quantitating random objective functions or random constraints, for example, in Geospatial Analyst^{TM}. Stochastic optimization methods for targeting seasonal hyperproductive and orthogonally decomposable, immature habitats by seasonally tabulated, quantiated, immature productivity counts may also include ArcGIS geo-statistical algorithms with random iterates (e.g., exact and approximate Bayesian posterior statistsics in PROC MCMC in SAS/GIS.

PROC MCMC uses a random walk Metropolis algorithm to obtain posterior samples. For details on the Metropolis algorithm, see the section Metropolis and Metropolis-Hastings Algorithms(www.https://support.sas.com/documentation/cdl/en/statug/63033/HTML/default/viewer.htm#statug_mcmc_sect019.htm) For the actual implementation details of the Metropolis algorithm in PROC MCMC, such as the blocking of 5m regressable, elucidative, hyperproductive *S. damnosum* s.l. immature, capture point, habitat, eco-epidemiological, narrow, African tributary, agro-village, trailing vegetation, turbid water, discontinuous, infrequently canopied, geo-spectrotemporally uncoalesced, moderate resolution, fractionalized, endmember eigenvector predictors and tuning of the covariance matrices, see the section Tuning the Proposal Distribution at www.sas.com. By default, PROC MCMC will assume that all sub-mixel observations in the *S. damnosum* s.l uncoalesced dataset are independent, and the logarithm of the posterior density is calculatable as follows: $\log(p(\theta|\mathbf{y})) = \log(\pi(\theta)) + \sum_{i=1}^{n} \log(f(y_i|\theta))$ where $\theta$is a parameter or a vector of parameters. The term $\log(\pi(\theta))$is the sum of the log of the prior densities specified in the PRIOR and HYPERPRIOR statements. The term $\log(f(y_i|\theta))$is the log likelihood specified in the MODEL statement. The MODEL statement can specify the log likelihood for a single geo-spectrotemrpoally geosampled *S. damnsoum* s.l. 5m endmember eigenvector decomposed observation (e.g., witnin-canopy,riffle water) in an eco-epidemioligcal, hyppeorductive , eco-georeferenceable, narrow, African tributary, agro-village, trailing vegetation, turbid water, discontinuous, infrequently canopied, capture point.

The statements in PROC MCMC are in many ways like DATA step statements; PROC MCMC evaluates every statement in order for each observation(www.sas.com). The procedure cumulatively will ads the log likelihood for each *S. damnsoum* s.l. geo-spectral, geospatial, empiricallly regressable observation. Statements between the BEGINNODATA and ENDNODATA statements are evaluated only at the first and the last observations. At the last observation, the log of the prior and hyperprior distributions may be added to the sum of the log likelihood to obtain the log of the posterior distribution in the moderate resolution, optimally images, eco-georferenceable, immature, eco-epidemiological narrow, African tributary, agro-village, trailing vegetation, turbid water, discontinuous, infrequently canopied, geo-spectrotemporally uncoalesced capture point, habitat, moderate resolution, fractionalized, endmember eigenvector predictors.

With multiple PARMS statements (multiple blocks of parameters), PROC MCMC wll update each block of time series *S. damnsoum* s.l. parameters while holding the others constants. The procedure still steps through all of the programming statements to calculate the log of the posterior distribution, given the current or the proposed values of the updating block of parameters. In other words, the procedure will not calculate the conditional distribution explicitly for each block of parameters, and it uses the full joint distribution in the Metropolis step for every block update. If you wish to model dependent data—that is, $\log(f(\mathbf{y}|\theta)) \neq \sum_i \log(f(y_i|\theta))$—you can use the PROC option JOINTMODEL. See the section Modeling Joint Likelihood for more details at https://support.sas.com/documentation).

Some stochastic optimization methods may employ random iterates to solve stochastic challenges, combining both meanings of stochastic optimization for optimally identifying unknown geolocations (e.g., *S. damnosum* s.l. habitats) in SAS/GIS.Jacob et al. [55] proposed a Gaussian process in a spatial filter analysis and a hierarchical, Bayesian probabilistic, uncertainty-oriented, estimation matrix in SA/GIS for deriving qualitative

probabilistic inferences from an eco-epidemiologically, field-operationizable, autoregressable and heuristically optimizable dataset that wasiniotally applied to noisy,immature, capture point, uncoalesced, eco-georeferenced habitats. The authors' optimally simulated unbiased, unmixed, 5m, wavelength, frequency-oriented, transmittance, emissivity, fractionalized, endmember eigenvector, covariate, coefficients based on geospatial and geospectral aggregations of productive immature habitats within a riverine agro-village complex, narrow tributary, discontinuous, trailing vegetation, turbid water, eco-epidemiological study site in Togo by introducing a descriptive latent variable into a non-linear, probabilistically generalizable, autoregressive equation. The inverse Wishart distribution revealed a probability distribution defined by the positive-definite matrix generated in ArcGIS for probabilistically quantitating the time series-dependent, empirical dataset of capture point, *S. damnosum s.l.* larval habitats that are stochastically interpolatable in eco-epidemiological, parameterizable, interpretive covariates.

In the expository, hierachical, explanative, SAS/GIS Bayesian model, the inverse Wishart distribution helped generate the conjugate prior for the covariance matrix of a multivariate normal distribution. In Bayesian probability theory, if the posterior distributions $p(\theta\ x)$ are in the same family as the prior probability distribution $p(\theta)$, the prior and posterior are then called conjugated distributions, and the prior is called a conjugate prior for the likelihood [56]. The multivariate Gamma function, $\Gamma p(\cdot)$, was a generalization of the Gamma function in the capture point, *S. damnosum* s.l. riverine, narrow tributary, African agro-village, immature habitat with an eco-epidemiolgical, ArcGIS-constructed risk model, which generated an uncoalesced geo-spectrotemporal estimator dataset. The Gamma function is an extension of the factorial function with its argument shifted down by 1 to real and complex numbers and, as such, n is a positive integer: $\Gamma(n) = (n - 1)!$ [56]. The gamma function was a solution to the immature habitat interpolation for eco-cartographically delineating a smooth curve in ArcGIS that connected the points (x, y) given by $y = (x - 1)!$, employing the geosampled tabulated empiricalized, discrete integer values for x. A plot of the first few factorials derived from the probabilistically regressed dataset of field and remote specified, endemic transmission, unmixed, covariate coefficients made it clear that a smooth curve can be drawn in ArcGIS. Howevever, the authors found it preferable to have a formula that precisely described the curve, in which the number of operations did not depend on the size of x_i.

The simple formula for the factorial, $n! = 1 \times 2 \times \ldots \times n$, in SAS/GIS however, could not be employed directly for quantitating the fractional, orthogonally decomposable, fractionalized, 5m, eigenvector endmember, immature, capture point, habitat values of x since it was only valid when x was a positive integer. Remote data can have negative values (e.g., Normalized Difference Vegetation Indices) [23]. There are, relatively speaking, no such simple solutions for factorials; any combination of sums, products, powers, decomposable exponential functions or logarithms can be employed for constructing a robust, time series dependent, operationalizable eco-epidemiological, vulnerability, forecast, vulnerability model with a fixed number of terms to express $x!$ [57].

In Jacob et al [45], the Gamma function appeared commonly during the computation of the PDFs in ArcGIS and the inverse Wishart distributions. The calculation of moments of complex Wishart and complex inverse Wishart distributed random matrices in the time series specified, explanatorial, field and remote, geo-spectrotemporally geosampled, *Simulium* larval habitats that were geoclassified as endemic transmission-oriented and geo-predictive in

an elucidatively operationalizable, time series descriptive, partially canopied, trailing vegetation, eco-epidemiological forecast, vulnerability model with parameterizable and empirically probabilistically regressable, wavelength, frequency-oriented, transmittance emissivity estimators was then addressed in SAS/GIS. In applications such as radar sonar or seismics complex, Wishart and complex inverse, Wishart distributed, random matrices are used to model the statistical properties of complex sample covariance matrices and complex inverse sample covariance matrices, respectively [58]. Moments of random matrices were needed for qualitatively quantitating the asymptotic properties of moderate resolution, optimally derived irradiance covariate coefficient estimates. A derivation of the PDF of complex inverse Wishart distributed random matrices was then attained.

In Jacob et al. [45], interpretive strategies were outlined for the calculation of the moments of both complex Wishart and complex inverse Wishart distributed matrices. Distributions rendered from the hypeporductive, seasonal, capture point, eco-georferenceable, orthogonally decomposed, narrow tributary, African, *S. damnosum* s.l. larval habitat data in ArcGIS revealed an inverse Wishart distribution A ~ W−1(Ψ, *m*). Autocorrelation scatterplots revealed that the Moran's coefficient was 0.634, while the Gearys ratio was 0.462. Improvement of fit of a hierarchical, Bayesian estimation matrix then demonstrated that the presence of trailing vegetation was statistically important to prolific geosampled *S. damnosum* s.l. seasonal, immature habitats. The performance of such a regressable, probabilistic, Bayesian estimation paradigm may be evaluated on synthetic and on real *S. damnosum* s.l. immature habitats in wavelength transmittance emissivities in PROC MCMC which is a SAS/STAT procedure which specifies prior distributions for the parameters with PRIOR statements and the likelihood function for the data with MODEL statements for deriving inferences from simulation rather than through analytic or numerical methods (see https://support.sas.com/). A comparison with independent unmixings of each eco-georeferenceable, immature, hyperproductive, imaged, immature habitat, seasonal image by state-of-the-art stochastic optimization method in an ArcGIS cyberenvironment may robustly and parsimonously implement proposed larval control strategies in African riverine ecosystems.

Cost-effective, hyperspectral, eco-georeferenceable, vector arthropod, immature habitat imagery has been of increasing interest over the past decade to researchers due to the significant spectral information it conveys. Acquired in hundreds of contiguous moderate resolution spectral bands from 300nm to 2600nm, hyperspectral images facilitate the identification of the elements composing the imaged scene [54]. However, the geospectral and geospatial resolution of these images is mitigated by mixel forecast fractionalized endmember, eigenvector, derivative spectra compositions of mixtures of reference proxy LULC biosignatures. Spectral unmixing of seasonal, hyperproductive *S. damnosum* s.l. immature habitats consists of quantitating and precisely determining the reference spectral biosignatures, their composing 5m, endmembers, and their abundance fractions in each mixel according to a predefined mixture model for quantitating several environmental factors [54]. Provided elucidative, orthogonally decomposed quantiated interactions between the moderat resolution, capture point, immature habitat materials of the imaged scene are negligible and the relief of the scene is flat, a linear mixing model (LMM) may be used to describe the data.

However, varying unquantifiable, wavelength transmittance acquisition emissivity conditions, such as illumination or natural evolution of a *S. damnosum* s.l. habitat, 5m, RapidEye^{TM} scene may significantly alter the shape and the amplitude of a spectral biosignature acquired, thus affecting the extracted fractionalized endmembers eigenvector

geo-spectrotemrpaolly extracted from seasonal images. In this context, unmixing of several images acquired over the same riverine, agro-village complex in a geo-classifiable, narrow tributary, geoclassifiable LULC achieved through an ArcGIS overlay of an eco-epidemiological capture point polgonized, study area at different time instants is of considerable importance. Such an analysis of an eco-epidemiological, decomposed, immature *S. damnosum* s.l. habitat, capture point enables the decomposed endmembers from the 5m RapidEye™ scene and the sub-mixel variability to be optimally assessed, thus improving sub-mixel estimation when compared to independent image analyses performed with any state-of-the-art unmixing method in ArcGIS. So far, sub-mixel, geospectral and geospatial, 5m endmember, variability quantitation processes in ArcGIS within a given hyperproductive, *S. damnosum* s.l. immature, capture point, habitat, has been considered in various forecast-orinted, vulnerability, risk models, either derived from a statistical or a deterministic point of view in ArcGIS. Commonly, the first class of methods assumes that the endmember variables are realizations of multivariate, normalized distributions. The second class of method would then represent these sub-mixel proxy LULC biosignatures as members of spectral libraries associated with each unmixed, eco-georeferenceable and geosampled habitat in a geolocation material (e.g., bundles).

Another recently proposed approach for remotely approximating unmixed, moderate resolution, wavelength transmittance emissivity, geo-spectrotemporal, decomposable covariate coefficient estimators was introduced within an SAS/GIS cyberenvironment. Geo-spectrotemporally, geospatially, probabilistically, and regressively quantitating sub-mixel, hyperproductive *S. damnosum* s.l. habitats in fractionalized, endmember eigenvector variability was analyzed within a decomposition algorithmic, sub-mixel framework proposed in Jacob et al. [59] in an SAS/GIS module (i.e., AUTOREG). Nevertheless, hyperspectral, *S. damnosum* s.l. prolific seasonal habitats, in the partially canopied, decomposed endmember, fractionalized, unmixed, interpolative and parameterizable covariate eigenvector estimators encompassing a significant number of clustered, seasonalnarrow tributary, African, agro-village complex, ecosystem, immature, capture point, habitat images or several large images precludes the use of batch estimation procedures, due to limited memory and computational resources. In conventional block matching estimation algorithms employed in vector arthropod, 5m, uncolaesced, wavelength transmittance emissivity, forecast, vulnerability models, motion accuracy may be achieved by searching the best matching block in an enlarged (i.e., interpolated) reference search area [60].

SubME is the MATLAB implementation of a block matching motion estimation algorithm that achieves sub-mixel accuracy without interpolation. SubME can integrate a seasonal habitat block matching algorithm in an ArcGIS/ENVI cyberenvironment and optical wavelength transmittance emissivity in a 5m RapidEye™ flow method to estimate the motion. Vectors may then be determined by a two-stage algorithm, the first stage being a single layer block matching, and the second stage being a first order optical flow by solving a 2x2 linear system. It is possible to use successive, parabolic, explantorial interpolator for doing sub-mixel interpolation. In the case of non-sub-mixel interpolation, it is very easy to apply successive parabolic interpolation, as there may be a continuous function that exists in the vulnerability, eco-epidemiological *S. damnosum* s.l. risk model. Still, in the case of parameterizable, submixel endmember eigenvector interpolation, the *S. damnosum* s.l. data may be discrete and it may not possess function values at floating point xx. In a successive parabolic interpolator matlab code, a seasonal, riverine habitat image, or a canopied line (e.g., trailing, sparsely shaded, discontinuous geoclassifiable, LULC vegetation cover), may be optimally highlighted and deduced at y=f(x) y=f(x). However, there is no current

methodology in ArcGIS literature to implement successive parabolic interpolation in the case of a function *f* in a vector arthropod, eco-epidemiologcal, forecast, vulnerability model which employs unmixed, 5m resolution, eludicatively orthogonally decomposable wavelength transmittance for canopied endmember emissivities values parameterized only on integer indices.

Since remotely identifiable, orthogonally decomposable, trailing vegetation, unmixed, 5m resolution wavelength transmittance, parameterizable, frequency-oriented, emissivity covariates of turbid water, riverine, sparsely shaded, partially canopied endmember eigenvectors can be considered as time-varying reference, perturbed forecastors of a linear mixing model (PLMM) in ArcGIS/ENVI can be employed to account for quantitating any sub-mixel eigenvector, probabilistic uncertainties in a hyperproductive, *S. damnsoum* s.l. habitat modeled in a 5m RapidEye^{TM} scene.

Next, a two-stage stochastic program in the cyberenvironment would allow the fractionalized, orthogonalized, endmember immature, capture point, *S.damnosum* s.l., habitat, decomposition algorithm to reveal a robustifiable datset of empirical, moderate resolution, geo-spectrotemporally uncoalesced, wavelength transmittance emissivities of statistical significance online. To determine whether a result is statistically significant, *p*-value would need to be calculated. The *p*-value can be the probability of observing an effect given that the null hypothesis is true in an eigenvector endmember, eco-epidemiological, decomposed, unmixed, interpolative, wavelength transmittance emissivity, vulnerability model parameter estimator, linearized dataset[22]. The null hypothesis is rejected if the *p*-value is less than the set significance of the α-level [23]. Unmixed, hyperspectral, partially canopied, iteratively interpolative, discontinuous, infrequently canopied, trailing vegation, turbid water, *S. damnosum* s.l. immature, capture point, hyperproductive habitats seen in a cost-effective 5m RapidEye^{TM} formulated dataset of endmember eigenvectors would be employable while accounting for temporal variability in a two-stage stochastic program in an ArcGIS/ENVI cyberenvironment.

The PLMM may account for temporal variability in seasonal *S. damnsoum* s.l. habitats with geo-spectrotemporally geospatially expository and explicatively stratifiable clusters as described in an on-line algorithm to solve the resulting optimization problems in an eco-epidemiological dataset of unmixed, empirical, 5m, dataset of resolution RapidEye^{TM} uncertainty endmember eigenvector emissivities. Experimental results may be parsimoniously obtained on synthetic and real riverine, agro-village, complex, narrow tributary, decomposable, immature capture point, hyperproductive habitats seen through 5m resolution, partially canopied, sparsely shaded, trailing evgation, turbid water, orthogonally decomposed fractionalized, data endmembers. The results may be optimally obtained with the proposed algorithm, and may be systematically compared to those of the vertex component or fully constrained least squares analysis.

The model in Jacob et al. [22] employed an empirical, operationizable, eco-epidemiological, 5m, resolution RapidEye^{TM} descriptive dataset of unmixed, multitemporal, fractionalized endmembers in an interpolative, decomposable and parameterizable 5m wavelength emissivity covariate transmittance estimators, non-linearly quantitated dataset using a weighted, uncertainty-oriented, geospatial probabilistic, autocorrelation, ArcGIS-derivable, eigenfunction decomposition matrix. Canonical scalar products on Euclidean matrix spaces were optimally rendered employing a spatial filter orthogonal decompositional algorithm.

In orthogonally decomposable, eco-epidemiological, moderate resolution, forecast, vulnerability modelling, Euclidean space primarily encompasses the two-dimensional Euclidean plane [61, 62], "Euclidean" distinguishes these spaces from other types of spaces considered in modern geometry; they also generalize to higher dimensions. Classical Greek geometry defined the Euclidean plane and Euclidean three-dimensional space using certain postulates, whilest the other properties of these spaces were deduced as theorems. Geometric constructions are also used to define rational numbers. When algebra and mathematical analysis were developed in ArcGIS, this relationship reversed. Currently, it is more common to define Euclidean space in vector arthropod, immature, epidemiological, capture point, explicative, hyperproductive habitats in decompositional, vulnerability forecast risk models employing Cartesian coordinates and the ideas of analytic geometry.

A Cartesian coordinate system in ArcGIS specifies each point uniquely in a plane by a pair of numerical coordinates, which are the signed distances to the point from two fixed perpendicular directed lines, measured in the same unit of length (www.esri.com). Both 2D and 3D Cartesian coordinate systems in ArcGIS can provide the mechanism for describing an eco-geographic location and shape of immature capture point, *S. damnosum* s.l., immature habitat, synthetic features employing x- and y-values [22]. Each reference line in a descriptive, eco-epidemiological habitat model, for example, would be a coordinate axis or just axis of the system, and the point where they meet would be its origin, usually at ordered pair (0, 0). The coordinates can also be defined as the positions of the perpendicular projections of the eco-georeferenceable immature, capture point , narrow tributary, agro-village complex, trailing vegetation, turbid water, discontinuous, partially canopied, sparsely shaded, *S. damnosum* s.l. immature habitat, interpretive point onto the two axes, expressed as signed distances from the origin in ArcGIS.

Thus, seasonal hyperproductive, *S. damnosum* s.l. immature, agro-village narrow riverine tributary, immature habitat points in ArcGIS/ENVI algorithmic decomposition regressional geospace may be eco-cartographically specified with collections of real numbers, (e.g., endmember, forecastable, orthogonalized explanatorial, sub-mixel, interpolative unbiased, optimally parameterizable proxy LULC bosignature uncoalesced, covariate coefficient estimators) and geometric shapes which may be defined as equations and inequalities. This approach utilizes algebra and calculus for geometrical features in habitat empirical datasets, which may be subsequently generalized to Euclidean spaces of more than three dimensions. With Cartesian coordinates this unique dimesionality may be precisely modeled by the real coordinate space (R^n) of the same dimension in the ArcGIS/ENVI cyberenvironment. In one dimension, the eco-epidemiological, immature habitat, forecasting, vulnerability, residualized, model output would be quantitated on a real line. In two dimensions, it would be quantitated by the Cartesian plane. In higher dimensions it would be a coordinate space with three or more real, parameterizable, unmixed wavelength transmittance, georeferenceable, coordinates. Mathematicians denote the *n*-dimensional Euclidean space by E^n if they wish to emphasize its Euclidean nature, but R^n is used as well, since the latter is assumed to have the standard Euclidean structure, and these two structures are not always distinguished [62].

Jacob et al. [59] autoregressively and remotely quantitated Euclidean spaces in an unmixed, explanatorily fractionalized, decomposed, proxy LULC biosignature representing a dataset of sparsely shaded, trailing vegetation, turbid water, discontinuously canopied, endmember wavelength transmittance, 5m resolution emissvities with a finite dimension. Geo-predictive vulnerability risk maps were highlighted in an ArcGIS/ENVI

cyberenvironment of *S. damnosum* s.l. larval habitats in an endemic riverine community in northern Uganda. Previously, the standard methods for quantitating stochastic or deterministic bidirectional radiance for deducing seasonally clustering tendencies in sparsely shaded, trailing vegetation, LULCs in endmember regressand datasets of orthogonally decomposed, eigenvector, covariate coefficient, estimator datasets of immature *S. damnosum* s.l. habitats was achieved by inefficient eco-cartographic, non-ecohydrologic and non-parameterized tools. These observational, risk models postulated eco-geographically unmixed, probablistically, time series dependent, seasonal,moderate resolution, transmittance, frequency emissivities (i.e., Percent of interpolative, partially canopied, sparsely shaded, discontinouous, trailing vegetation endmember eigenvectors) to *Simulium* endemic foci while accounting for neither slope coefficients, nor weighted, varying intra-cluster, probabilistic residuals with obscure, autocorrelation effects.

Generally, inferential statistics derived from ArcGIS-gridded, residual, algorithmic sample frames for risk mapping vulnerability residuals for seasonal *S. damnosum* s.l. habitats in a hyperendemic study site, employing decomposable sub-mixel endmeber eigenvector estimators, derived from within-canopy objects (e.g., sparsely shaded, trailing vegetation), LULCs of unmixed reflectance, wavelength transmittance endmember emissivities are riddled with endmember uncertainties [59]. In eco-epidemiological datasets of *S. damnosum* s.l., parameterizable, covariate estimators and their quantizable, decomposable wavelength frequency emissivity uncertainties, forecasted correlations (e.g., multicolinearity) may be rendered from two sources: (1) the design of the quantitated random effects with their assumed covariance from the multiple levels within the immature, georeferenceable, habitat multivariate, endmember regression model; and, (2) the dependence correlation structure of the canopied, time series dependent, LULC reflectance explanators [51].

In loose usage, endmember fractionalized, 5m decomposed RapidEye^{TM} wavelength, probabilistic, emissivity transmittance, residual uncertainty correlations in geoclassifiable LULCs of *S. damnosum* s.l. habitats, with uncoalesced, wavelength transmittance endmember, predictor covariates and parameterizable estimators in ArcGIS, can refer to any departure of two or more random variables (e.g., Percent of trailing vegetation at an eco-epidemiological capture point) from independence [22]. This occurs in ArcGIS when remotely quantitating geo-spectrotemporal and geospatial relationships between extrapolated and tabulated mean values. Instrument noise quantitated amongst seasonal *S. damnosum* s.l. capture point, immature habitats of unmixed, moderate resolution, scene components and fractionizable variability of these scene components is not explicitly evaluated as part of classification and forecast mapping efforts which employ multispectral, cost-effective images. Changes in these factors directly affect eco-epidemiological regression mapping accuracy. An analytical framework may be proposed in ArcGIS such that these factors can be quantified within the context of a spectral mixture analysis. In applying these analyses to a RapidEye^{TM} images, hyperproductive, immature, capture point, seasonal habitat through a 5m scene in ArcGIS may reveal that the greatest uncertainty in abundance estimation arises from spectral variability in unmixed endmembers. Spectral variability in any discontinuos, partially canopied, sparsely shaded, orthogonally decomposable, endmember eigenvector can result in abundance uncertainty quantitation of all fractionalized, sub-mixel decomposable data. A sub-mixel analytical strategy may be employed in ArcGIS/ENVI whereby fractionalized endmember subsets of a 5m RapidEye^{TM} image may be quantitated into regions of lowest canopied, endmember geo-spectrotemporal dimensionality in order to minimize probabilistic uncertainties and to maximize detection of new unmixed, wavelength transmittance LULC, geo-spectrotemporally uncoalesced, emissivity materials. Then, trailing vegetation and sub-

mixel, discontinuous, partially canopied, emittance data may be optimally, remotely and regressively parameterized and geo-spectrotemporally geospatially iteratively interpolated in an ArcGIS/ENVI cyberenvironment to identify unknown, hyperproductive *S. damnosum* s.l. habitats.

There are several coefficient, gridding algorithmic delineations in ArcGIS for precisely measuring the degree of sub-mixel, intra-cluster endmber correlation in a geoclassifiable Rapid Eye ^{TM} ,LULC, eco-epidemiolgical, heursitically optimizable, risk mapping of seasonal, ecohydrologic variables in ArcGIS. For example, bidirectional line gridding in ArcGIS rapidly interpolates roughly parallel line-based, trailing vegetation, discontinuous, turbid water, infrequently canopied, hyperproductive, *S. damnosum* s.l. immature, capture point habitats that are regressively parameterizable in a 5m RapidEye^{TM}, unmixed dataset of decomposed, wavelength, tranmittance , frequency-oriented, emissivity covariate estimators, especially if there is a high sample density down the lines relative to the line separation in the geodatabase. The interpolation employs linear, minimum curvature or Akima splines, which can be defined as a particular spline used due to its stability against any outliers [64]. Further, on the intervals in an ArcGIS graph which are next to the outlier, the spline would noticeably deviate from the given function because of the outlier in any *S. damnosum* s.l. forecasting vulnerability paradigm.

An important property of the Akima spline is its locality - function values in $[x_i, x_{i+1}]$ depends on f_{i-2}, f_{i-1}, f_i, f_{i+1}, f_{i+2}, f_{i+3} only [64] . The disadvantage of cubic splines for optimally remotely targeting hyperproductive, trailing vegetation, discontinuous, infrequently canopied, sparsely shaded, seasonally narrow tributary, African agro-village complex, *S. damnosum* s.l. immature, capture point, seasonal habitats, which are geo-classifiable based on previously geosampled, immature productivity,immature count data in African, agro-village complex, narrow tributary, riverine environments, is that they could oscillate in the neighborhood of an outlier. Another Akima spline property which should be taken into account is the non-linearity of the unmixed, geo-spatiotemporally geo-spectrotemporally geosampled, orthogonally decomposable, forecastable, eco-georeferenceable geo-predictive variables, as the result of stochastic interpolation of the sum of two functions in ArcGIS. These may or may not equal the sum of the interpolation schemes constructed on the basis of the given functions. No less than 5 points are required to construct the Akima spline [64]. In the inner area (i.e., between x_2 and x_{N-3}), where the index goes from 0 to n-1, the interpolation error has order $O(h^2)$. Unfortunately, the spline is only available in Oasis montaj and cannot be employed to interpolate randomly distributed XYZ data. Oasis montaj is an exploratory technological solution that provides a scalable environment for efficiently importing, viewing, modelling, analysing and sharing large volume geophysical, geochemical and eco-geological data, all within one integrated environment (http://www.geosoft.com).

Triangular irregular network (TIN) gridding can be used for irregularly geo-spectrotemporally geosampled, immature seasonal, *Simulium* productivity data through regressive and remote quantitation of 5m Rapid Eye ^{TM} data. TIN gridding seasonally hyperproductive, *S. damnosum* s.l., immature hyperproductive, trailing vegetation, discontinuous, infrequently canopied, sparsely shaded, seasonally narrow tributary, African agro-village complex, capture point, habitats that have been fractionalized as proxy LULC biosignature endmembers eigenvector iteratively interpolated results in an ArcGIS stratified, 5m resolution RapidEye^{TM} dataset of grid cell values may loosely match the magnitude of the original unmixed, geosampled, riverine data at known XY positions. The interpolation is entirely local and every geosampled,hyperproductive, immature habitat, eco-georferenceable

point will be influenced either by its nearest or natural neighbours depending on the parameter chosen. This algorithm is available in Oasis montaj and Target. However, in ArcGIS, this algorithm is only available when gridding drillhole data for plan maps, section maps, or plan grids in illustrative 3D maps.

Inverse distance weighted gridding (IDW) may also be employed when remotely targeting hyperproductive *S. damnosum* s.l. habitats. Within an ArcGIS cyberenvironment, sparsely shaded, trailing vegetation, and turbid water habitats with geosampled fractionalized interpolative, discontinuous, partially canopied, sparsely shaded, endmembers and the habitat capture point, *S. damnosum* s.l. surface is not expected to be smooth or continuous between data points. The data points are weighted so that the influence of one point relative to another declines with distance. Three key parameters which may be set in ArcGIS that will influence the interpolation are the search radius, the weighting power, and the weighting slope [65]. IDW can be used to create 2D grids in an ArcGIS cyberenvironment (www.esri.com). Inverse distance weighted gridding is also an option for 3D gridding of unknown, un-geosampled, seasonal habitats seen in a 5m RapidEye^{TM}, parameterizable, wavelength transmittance emissivity, covariate analyses in a vulnerability forecasting risk model

Direct ArcGIS gridding is designed for highly or oversampled hyperproductive *S. damnosum* s.l. habitats in geospatial and geo-spectrotemporally geo-classifiable 5m decomposed, wavelength transmittance emissivities, such as RapidEye^{TM} sensor data in ArcGIS. The output value will be determined based on the minimum, maximum or the mean of the data points that fall within the grid cell. This algorithm is available in Oasis montaj and Target for 2D gridding. Direct gridding is an option for 3D gridding in Oasis montaj, as well as in ArcGIS.

Linear regression analysis with one 5m RapidEye^{TM} grid cell as dependent, and multiple grids as independent in ArcGIS, may reveal statistically significance [e.g., tabulated *p*-values] based on the probability of observing a hyperproductive *S. damnosum* s.l. habitat with trailing vegetation and turbid water effect (flooding), given that the null hypothesis is true. In statistics, the *p*-value is a function of the observed sample results (a statistic) that is used for testing a statistical hypothesis [23]. The *p*-value for a hyperproductive, *S. damnosum* s.l. habitat decomposition, eco-epidemiological, frequency transmittance, emissivity endmember, vulnerability forecasting risk model may be defined as the probability of obtaining a result equal to, or "more extreme," wavelength outliers than what was actually observed, assuming that the hypothesis under consideration is true [22]. Here, a value being defined as "more extreme" is dependent on the way the hypothesis is tested in ArcGIS. Before the sub-mixel endmember, fractionalized test is performed, a threshold value is chosen, (i.e., significance level), in SAS/GIS cyberenvironments (e.g., traditionally 5% or 1%) and denoted as α. If the *p*-value is equal to or smaller than the significance level (α), it suggests that the observed, fractionalized eigenvector endmember of decomposed, interpolative, 5m RapidEye^{TM} hyperproductive, trailing vegetation, discontinuous, infrequently canopied, sparsely shaded, seasonally narrow tributary, African agro-village complex, *S. damnosum* s.l. immature, capture point, seasonal habitat data are inconsistent with the assumption that the null hypothesis is true. Thus, that hypothesis must be rejected, but this does not automatically mean the alternative hypothesis can be accepted as true. When the *p*-value is calculated correctly, such a test is guaranteed to control the Type I error rate to be no greater than α. Since the *p*-value is used in frequentist inference (and not Bayesian inference), it does not in itself support reasoning about the probabilities of hypotheses, but is only used as a tool for deciding whether to reject the null hypothesis in ArcGIS.

By unbiasedly determining significance levels in seasonal hyperproductive, discontinuous, infrequently canopied, sparsely shaded, seasonally narrow tributary, African agro-village complex, *S. damnosum* s.l. immature, capture point, seasonal habitats eco-epidemiological geo-predictive variables, quantifiable trailing vegetation or turbid water endmember fractionalizable, interpolative regressors may be determined. Details of regression correlation analysis may be saved to a table in a SAS/GIS cyberenvironment, as well. Optionally, the descriptive regression model may be employed to create a new grid with a forecastable dataset of optimizable regression based on decomposable, geo-spectrotemrpaolly uncoalesced, geospatialized, sub-mixel 5m RapidEye™ wavelength transmittance emissivity values. This way, the immature *S. damnosum* s.l. habitat regression analysis can assume the existence of a causal relationship between a dependent and an independent variable that have been geosampled in a geo-spectrotemporal, unmixed and orthogonally explanatively decomposable 5m RapidEye™ medium resolution emissivity. These regression analysis equations can be expressed as: Y= a + bX (linear), Y= a + b/X, Y= a/(b-X), Y= a * X^b (power), Y= a e^(bX) (exponential), and Y= a + b * ln(X) (logarithmic), where Y is the dependent variable, and X the independent variable. The coefficient "a" represents the intercept, and "b" is the independent variable X. The intercept represents the value of Y when the value of the independent variable is equal to zero. The parameter coefficient indicates the change in Y for a one-unit increase in the corresponding independent variable (i.e., the slope of the line) in ArcGIS [51]. This module could employ a point shapes data layer to represent the dependent variable and a single grid data layer as the independent variable in an eco-epidemiological risk model. Details of regression/correlation analysis may be saved to a table and exported to SAS/GIS for constructing robust non-linear, eco-epidemiological risk model estimators for precisely identifying unknown, hyperproductive, trailing vegetation, discontinuous, infrequently canopied, sparsely shaded, seasonally narrow tributary, African agro-village complex, *S. damnosum* s.l. immature, capture point, seasonal habitats *S. damnosum* s.l. habitats. i

Correlation and regression analyses relate to 5m RapidEye™ imaging of *S. damnosum* s.l. turbid water immature habitats in the sense that both deal with relations among variables [63]. The correlation coefficient is a measure of linear association between two variables [66]. Values of the correlation coefficient in an ArcGIS cyberenvironment (e.g., Geostatsitical Analyst™) are always between -1 and +1 (www.esri.com). A correlation coefficient of +1 indicates that two variables are perfectly related in a positive linear sense, while a correlation coefficient of -1 indicates that two variables are perfectly related in a negative linear sense, and a correlation coefficient of 0 indicates that there is no linear relationship between the two variables. According to Jacob et al. [45], in unmixed, interpolative datasets of 5m RapidEye™ imaged *S. damnosum* s.l. habitats containing trailing vegetation or turbid water, risk-related, decomposable, linear regression, the sample correlation coefficient will be the square root of the coefficient of determination. The sign of the correlation coefficient will be the same as the sign of the coefficient in the estimated regression equation. Neither regression nor correlation analyses can be interpreted as establishing cause-and-effect relationships [67]. Such interpretive models can indicate only to what extent 5m imaged, *S. damnosum* s.l., imature, capture point, hypeproductive immature habitat, uncoalesced, wavelength transmittance emissivities are associated with each other. The correlation coefficient measures only the degree of linear association between two variables [66]. Any conclusions about a cause-and-effect relationship must be based on the judgment of the researcher in ArcGIS.

A probabilistic regression analysis formula in an ArcGIS may be employable to calculate hyperproductive, trailing vegetation, discontinuous, infrequently canopied, sparsely shaded, seasonally narrow tributary, African agro-village complex, *S. damnosum* s.l. immature, capture point, seasonal habitats in endmember fractionalized eigenvtor, moderate resolution data values based on an output grid data layer. The most common of these is the Pearson correlation coefficient, which is sensitive only to a linear relationship between two geopredictive explanative variables, which may exist even if one is a non-linear function of the other. In statistics, the Pearson product-moment correlation coefficient (sometimes referred to as the PPMCC or PCC or Pearson's *r*), is defined as a measure of the linear correlation between two georeferenceable/non-geo-referencable variables *X* and *Y*, rendering a value between +1 and −1 inclusive, where 1 is total positive correlation, 0 is no correlation, and −1 is total negative correlation [66]. This coefficient is widely employed in unmixed endmember data geosampled in wavelength transmittance emissivity, geopredictive, vector arthropod, risk modelling in ArcGIS as a quantifiable measure of the degree of linear dependence between two observational, parametizable and probabilistic predictors [68]. Correlation also refers to any of a broad class of statistical relationships involving dependence [66].

Truncated singular value decomposition (SVD) techniques have been widely employed in inversion paradigms in ArcGIS. Although the method of truncation determines the quality of a truncated singular value decomposition (SVD) solution, truncation has often been conducted arbitrarily in vector arthropod, eco-epidemiological mapping in ArcGIS. The truncated SVD is considered as a method for regularization of ill-posed, linear least squares and eco-geographic predictors [69]. In statistics and mathematics, linear least squares is an approach fitting a mathematical or statistical model to data in cases where the idealized value provided by the model for any data point is expressed linearly in terms of the unknown parameters of the model. The resulting SVD-fitted model in ArcGIS can be used to summarize the data, to predict unobserved hyperproductive, trailing vegetation, discontinuous, infrequently canopied, sparsely shaded, seasonally narrow tributary, African agro-village complex, *S. damnosum* s.l. immature, capture point, seasonal habitats iteratively interpolated , moderate resolution orthogonally uncoalesced values from the same system, and to understand the mechanisms that may underlie the system.

In particular, the truncatcd SVD solution may be comparable with a usual regularized solution in ArcGIS for eco-epidemiological forecast modeling of hyperproductive habitats. The truncated SW in ArcGIS may be a favorable alternative to standard form regularization in cast of ill-conditioned matrices in other software packages with a well-determined rank. The first workable criterion for truncation in a *S. damnosum* s.l. habitat forecast model may be based on *F*-statistical testing in Geostatistical Analyst™ for aiding in geophysical inversion of autoregressively and heuristically optimizable, parametrizable covariates representing RapidEye™-derived, fractionalized, seasonal wavelength transmittance emissivities in various evironmental settings.

The L-curve approach may be utilized in SAS/GIS applications for any interdisciplinary inverse problems in an expository *S. damnosom* s.l. habitat, RapidEye™ image-derived, eco-epidemiological forecast model. The L-curve is a log-log plot of the norm of a regularized solution versus the norm of the corresponding residual norm. In ArcGIS, the L-curve may be a convenient graphical tool for displaying the trade-off between the size of a regularized solution and its fit to the given dataset of decomposable, parameterizable estimators

representing *S. damnosum* s.l. habitat endmember data in 5m RapidEye™ wavelength frequency, unmixed, trasmittance emissivities as the regularization parameter varies. The L-curve may give insight into the regularizing properties of the underlying regularization method in ArcGIS for immature habitats in discontinuous sub-mixels of geo-predictive, interpolative unmixed variables. Simultaneously, the L-curve may aid in choosing an appropriate dataset of regularization, covariate coefficient estimators for the given vulnerability, sub-mixel, autoprobabilistic, autoregressable, uncertainty-oriented, residualized dataset.

A new quality-based algorithm for truncation in SAS/GIS may be proposed for multiple, RapidEye™–derivable, biophysical, photosynthetic and NPV decomposable, *S. damnosum* s.l. habitat covariate estimators geosampled in an African agro-village narrow tributray, riverine ecosystem. These estimators may be also remotely investigated for comparison in regularizing discrete, unstable, ill-posed problems, based on the *F*-statistic, the L-curve, and a quality-based mean squared error (MSE) criteria in Geostatistical Analyst™ for the estimation of capture point, proxy LULC biosignature interpolators. Validated, *F*-statistic-based estimators may marginally improve the least squares (LS) solution to the ill-posed downward continuation challenge through a long-term average of seasonal hyperproductive *S. damnosum* s.l. habitats in unmixed covariate estimators depending on pre-selected significance levels (95% confidence intervals).

The simulations in ArcGIS of frequency wavelength emissivity, vulnerability estimators may improve conditional coefficients of a linearized, unstable, discontinuously canopied, trailing vegetation, turbid water, *S. damnosum* s.l. modeling system. In this way, the *F*-statistic criterion may lead to precise discardings of uncertainty-oriented, wavelength transmittance emissivity components from a stochastic/deterministic interpolator. The estimator, by means of an L-curve, may then provide optimal stability for any ill-posed problems (e.g., over-discarding) in geosampled, unmixed riverine habitats with georeferenceable and eco-epidemiological capture point components. Biases and mean squared error roots of the solution may be provided in ArcGIS of the autoregressively, spatially adjusted, Bayesian probabilstic, optimized fields of interpolated, decomposed 5m RapidEye™ endmembers of parameterizable, wavelength transmittance, fractionalized emissivity eigenvectors.

Bayesian Optimization (BO) is a probabilistic description of the task of finding the global extremum of a function that is not “directly” accessible, either because it is embodied in some physical process, or because it has very high evaluation cost[24].. A good example is the search for gregressable ecogeorferenceable, explicative geo-spectrotemporally uncoalesced turbid watre, discontinuously canopied, sparsely shadeed, trailing vegtation, parameters of a robotic control problem (where each function evaluation involves a physical experiment), or finding good setups for a large machine learning algorithm, such as a deep net (where each function evaluation involves training the net to convergence, which may take weeks on a cluster). The simulations may indicate that other algorithms in ArcGIS are also be able to achieve a mean accuracy of 5m for geo-spectrotemporal and geosaptial uncertainty anomalies from the satellite radiometric weighted variables, if the few largest biases are left out of the computation (see Figure 40**).**

Figure 40. A heirachically Bayesian simulated Gaussian random field for quantitating unmixed, geo-spectrotemporally, geospatialized immature *S. damnosum* s.l. habitat, trailing vegetation and turbid water parameterizable estimators in an ArcGIS 3-dimensional graph.

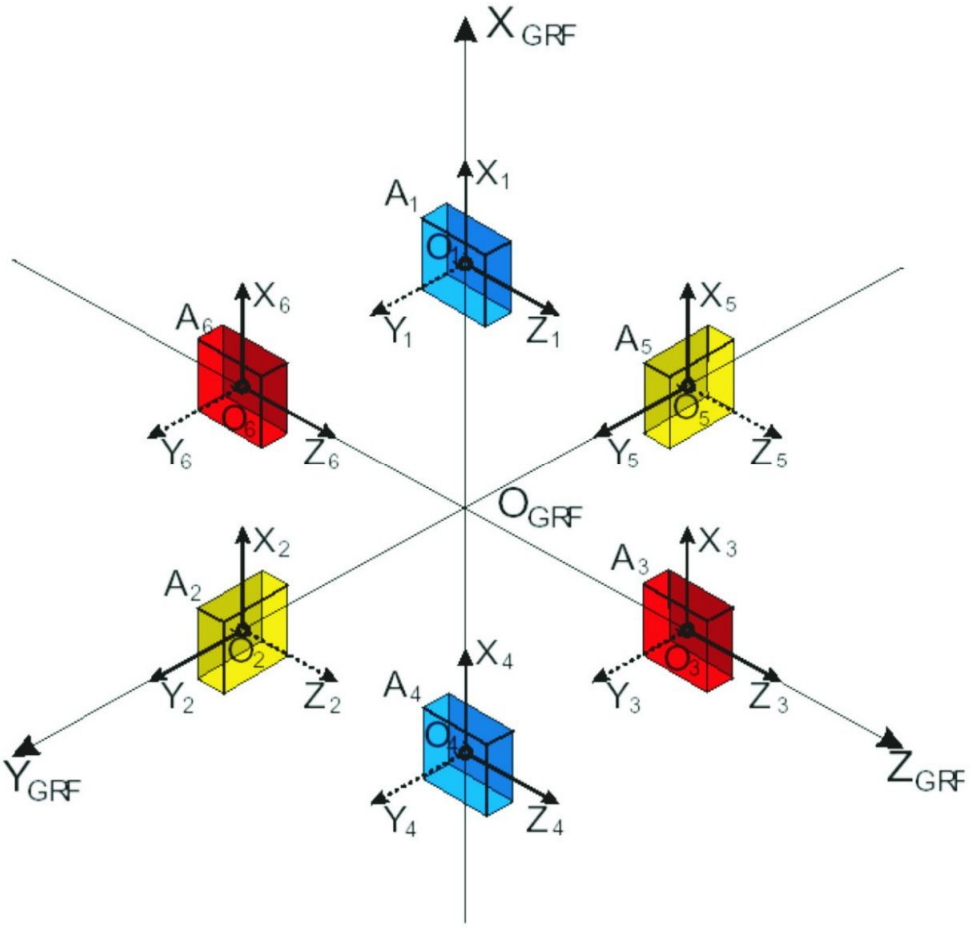

Standardized random samples of the integrand use a conventional Monte Carlo for satisfying formal dependence in an unmixed endmember, decomposable, eco-epidemiological, Bayesianized dataset of immature hyperproductive, trailing vegetation, discontinuous, infrequently canopied, sparsely shaded, seasonally narrow tributary, African agro-village complex, *S. damnosum* s.l. immature, capture point, seasonal habitats with forecastable vulnerability wavelength emissivities in WinBUGS based on the BUGS (Bayesian inference Using Gibbs Sampling).

PROC MCMC derived, endmember eigenvectors of trailing vegetation, reflectance, turbid water paradigms employ randomized, sub-mixel, log-transformable, continuous or catergorical auto-probabilistic and autoregressive data variables that satisfy probabilistic independence. In probability theory, two events (e.g., seasonal, georeferenced, hyperproductive, immature, *S. damnosum* habitat sample frames) are statistically independent, or stochastically/deterministically, independent if the occurrence of one does not affect the probability of the other [70].

Similarly, two medium resolution images of *S. damnosum* s.l. habitats as unmixed, itartively interpolatable, predictor variables would be explicatively independent if the realization of one geosampled endmember explanator does not affect the probability distribution of the other. Thus, two random interpolative variables, *X* and *Y,* are independent if and only if the elements of the π-system generated by them are independent. That is to say, for every *a* and *b* in an eco-epidemiological, *S. damnsoum* s.l. habitat risk model, the events $\{X \leq a\}$ and $\{Y \leq b\}$ would be independent events.

So, *X* and *Y* with cumulative distribution functions (CDFs) $F_X(x)$ and $F_Y(y)$, and probability densities $f_X(x)$and $f_Y(y)$, would be independent if the combined ecogeographic, *S. damnosum* s.l. habitats with regressively randomized, optimizable variables (*X*, *Y*) has a joint CDF $F_{X,Y}(x, y) = F_X(x)F_Y(y)$, or if the joint density exists, $f_{X,Y}(x, y) = f_X(x)f_Y(y)$, in the model forecasts. The CDF can describe the probability that a real-value, geo-spectrotemporally sampled, hyperproductive *S. damnosum* s.l., randomizable variable *X* in an unmixing algorithm with a given probability distribution that can be optimally tabulated to have a value less than or equal to *x* [70]. In mathematics, a π-system (or pi-system) on a set Ω is a collection *P* of certain subsets of Ω, such that *P* is non-empty.$A \cap B \in P$, whenever *A* and *B* are in *P*.

As such, *P* in the hyperproductive, endmember fractionalized, *S. damnosum* s.l. 5m RapidEye™ endmember, fractionalized, capture point, immature habitat is a non-empty family of subsets of Ω that is closed under finite intersections in a probabilistic regression-autoregressive framework in ArcGIS. Hence, the unmixing of interpolatable, time series dependent independence in a 5m RapidEye™ covariate coefficient, geo-spectrotemporally geospatially uncoalesced, wavelength transmittance emissivity estimator of geo-spatiotemporal geosampled datasets can reveal georeferenceable, high density, riverine, black fly foci. Interpolation of the decomposed time series with endmember regressors could optimally extend to dealing with collections of two or more regressable, hyperproductive *S. damnosum* s.l., immature habitat, seasonal event (e.g. flooding), randomized variables. The events, then, should be unbiasedly geoclassifiable as pairwise independent in ArcGIS, since each pair would be independent and thus, mutually independent of each other.

In an empirical, eco-epidemiological, dataset of linear, mixed-effects and geo-spatiotemporally 5m RapidEye™ medium resolution of regressors in an ArcGIS parameterized, eco-epidemiological risk model, quantitative responses from a subject are the sum of so-called fixed and random effects. If an unquantitated, time series dependent, field or remote specified, covariate transmittance of 5m resolution, wavelength emissivity variables affect the geosampled population mean regressor in an empirical dataset of hyperproductive habitats as a vulnerability, eco-epidemiological, capture point, regression model with covariate estimators, the observational, unmixed predictors would be defined as fixed.

Alternatively, if the immature, hyperproductive, trailing vegetation, discontinuous, infrequently canopied, sparsely shaded, seasonally narrow tributary, African agro-village complex, *S. damnosum* s.l. immature, capture point, seasonal habitats within dataset of geo-spectrotemrpaolly uncolaesced, wavelength transmittance emissivity endmembers in fractionalized 5m RapidEye™ and decomposable estimators may be associated to the ecogeographic and ecohydrologic geo-sampling procedures (e.g., subject covariate effect extraction). In such circumsatnces, then the radiance, sub-mixel, 3-D catchment watershed predictor variables would be assumed to be random (e.g., chaotic, riverine, eco-georeferenceable and geo-classifiable, seasonally hyperproductive and flooded *S. damnosum* s.l. habitat landscapes) (Figure 41). The presence of random effects often introduces sub-

mixel correlation error in time series dependent, remotely sensed, LULC endmember reflectance, eco-epidemiological risk models [70]. The random effects assumption made in covariate endmember estimators of trailing vegetation or turbid water, hyperproductive, *S. damnosum* s.l. habitats in unmixed, wavelength transmittance emissivity, geomorphological, terrain-related risk models in ArcGIS is commonly individually decomposed of transmittance emissivity specific effects that are uncorrelated with the independent regressors [71]

Figure 41 A 3-D, geomorphological, terrain-related, trailing vegetation, turbid water, hyperproductive, capture point, discontinuously canopied, *S. damnosum* s.l. habitat risk model

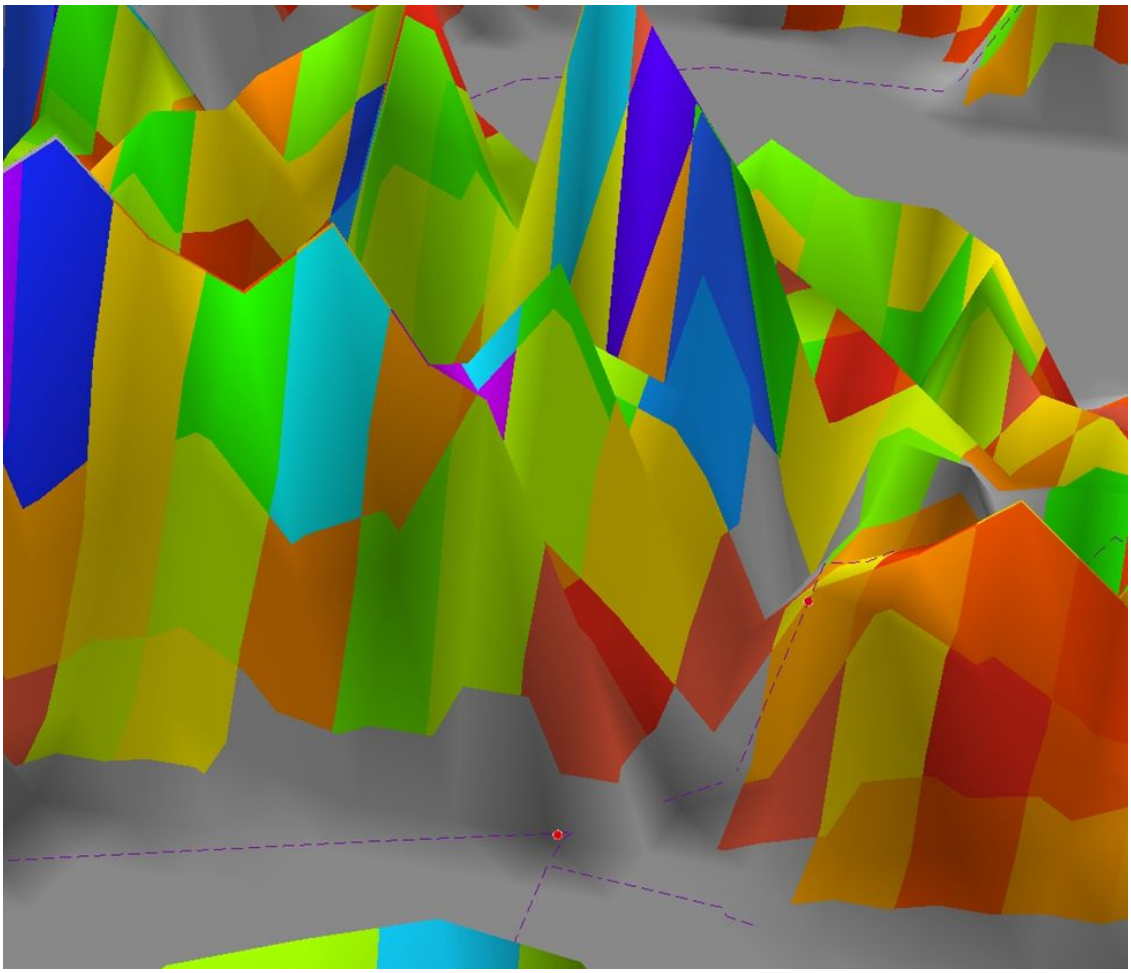

The fixed effect assumption is that time series, elucidatively quantitated individual specific endmember effect is linearly/non-linerly correlated with the independent variables in immature *S. damnosum* s.l. habitats imaged in a 5m RapidEye™, ArcGIS, eco-epidemiological, geo-spectrotemporally uncoalesced, wavelength, frequency-oriented, emissivity, forecast, vulnerability model. If the random effects assumption holds in the regressands in the reflectance model, the auto-probabilistically and remotely autoregressively quantitated random effects would be more efficient than the quantitated fixed effects for optimally iteratively interpolating seasonal, narrow riverine, tributary, agro-village ,complex ecosystem, unmixed, proxy LULC, biosignature, hyperproductive, count data productivity

variables in unknown, ungeosampled capture points. However, if this assumption does not hold (i.e., if the Durbin–Watson test fails,), the random effects model would not be consistent. Unquantitated, fractionalized, endmember eigenvector radiance with expositively parameterizable or non-parameterizable transmittance, covariates with uncertainty, heteroskedastic emissivity estimators, may create mixed effects in a reflectance, sub-mixel, eco-epidemiological, risk model with residualized estimates in ArcGIS. Erroneous transmittance emissivities tabulated from a frequency dataset of *S. damnosum* s.l. immature habitats with random effects in ArcGIS may contribute only to the covariance structures of the turbid water, trailing vegetation, decomposable, explicative, LULC model 5m, explicative regressors [22]. Though the fixed effect is the primary interest in most onchocerciasis studies, it is necessary to adjust for the structure of fractionalized endmember, eco-georeferenceable eigenvector covariances in time series dependent, uncoalesced, 5m, fractionalized, wavelength radiance transmittance emissivity, covariate, endmember estimators (i.e., trailing vegetation 5m RapidEye^{TM}, fractionalized, sub-mixel descriptive geo-predictors) in ArcGIS prior to commencing field verfication. The adjustment made in procedures like General Linear Model (GLM)-Univariate in SPSS is often not appropriate, as it would assume the independence of the unmixed, immature, capture point, geo-spectrotemporally, geosampled, habitat data.

It is plausible to assume that a dataset of geo-spectrotemporally uncoalesced, eco-georefernceable, hyperproductive, trailing vegetation, turbid water, discontinuous, infrequently canopied, sparsely shaded, *S. damnosum* s.l.,capture point habitats imaged in a dataset of 5m RapidEye^{TM} wavelength transmittance, fractionalized, emissivity endmember observations on the same meandering flooded, agro-village complex, riverine pathway are correlated in a common spectral radiance model. The downward transmittance of radiation to surface is a combination of the direct solar radiation from the sun to the ground surface. The skylight, also known as the diffuse transmittance, is the solar radiation scattered by atmospheric gases and aerosols and redirected toward the ground surface being measured, and light, due to multiple, repeated endmember reflections and scattering from neighboring surfaces and the atmosphere [72]. Thus, for a seasonal, hyperproductive, immature, trailing vegetation, seasonally hyperproductive, immature geo-spectrotemporally uncoalesced, eco-georefernceable, turbid water, discontinuous, infrequently canopied, sparsely shaded, *S. damnosum* s.l., capture point in a fractionalized, 5m RapidEye^{TM} wavelength emissivity endmember eigenvector dataset, the total upward transmittance would be a combination of the light reflected by the narrow, riverine tributary, African agro-village complex, ecosystem, ground surface, light reflected by the discontinuous, immature habitat surface, and rescattered by atmospheric gases and aerosols, as well as sunlight scattered by the atmosphere and redirected toward the sensor without reaching a ground surface. Hence, fractionalized, *S. damnosum* s.l. eigenvector endmembers of an interpolative analysis of repeated measures of hyperproductive,immature habitat, geo-spectrotemporally uncoalesced, geoclassifiable, proxy LULC biosignature, iterative interpolative, experimental reflectance in an emissivity endmember dataset in ArcGIS must address the issue of inconspicuous covariation between probabilistic autoregressable measures on the same seasonal, riverine, agro-village complex, narrow tributary ,immature, capture point, habitat unit over time and space.

Until recently, algorithmic, eco-epidemiological risk analysis techniques, available in computer software only, offered ecologists, entomologists or other researchers limited and inadequate choices to perform decomposing unmixing algorithmic tasks for quantitaing seasonal, hyperproductive, immature, trailing vegetation, immature, geo-spectrotemporally

uncoalesced, eco-georefernceable, turbid water, discontinuous, infrequently canopied, sparsely shaded, *S. damnosum* s.l., narrow, riverine tributary, African agro-village complex, ecosystem, capture point in a 5m RapidEye™ , wavelength transmittance, fractionalized, emissivity endmember eigenvector dataset. Typically, the choice was to ignore endmember covariance structures and make invalid assumptions during the emissivity covariate estimator, vulnerability model construction process. The endmember bundles, unmixing approach is designed to explicitly address geo-spectrtemporal variability and quantify the associated proportion indeterminacy [72].

Another methodology was to avoid the fractionalizable, moderate resolution, eigenvector endmember, covariance structure issues in the seasonal, hyperproductive, immature, trailing vegetation, seasonally hyperproductive, immature geo-spectrotemporally uncoalesced, eco-georefernceable, *S. damnosum* s.l., wavelength transmittance, fractionalized, endmember eigenvector emissivities for inadequately calculated 5m RapidEye™ frequencies. Nonchalantly making adjustments to endmember eigenvector covariance structures of the sub-mixel, *S. damnosum* s.l., seasonal, hyperproductive, immature, trailing vegetation, uncoalesced, eco-georefernceable, turbid water, discontinuous, infrequently canopied, sparsely shaded, narrow, riverine tributary, African agro-village complex, ecosystem, capture points at in a medium resolution, forecast, vulnerability model of covariate estimators and datasets may result in erroneous inferences. However, avoiding the structures entirely would result in inefficient forecast estimation of seasonal, immature, eco-georeferenceable productivity inferences for the uncoalesced, 5m data. If the true underlying sub-mixel, interpolative covariance structure were known in the immature narrow, riverine tributary, eco-epidemiological *Simulium* immature habitat model, the generalized, least squares, fixed effects estimates in ArcGIS Geostatical Analyst™ may render linearly unbiased estimates.

Available mixed model methodologies in ArcGIS/SAS may reveal inconspicuous latent autocorrelation of erroroneous coefficients in datasets of endmember covariance structures to be incorporated in a hypothetical, seasonally, hyperproductive, immature, trailing vegetation, geo-spectrotemporally uncoalesced, eco-georefernceable, turbid water, discontinuous, infrequently canopied, sparsely shaded, *S. damnosum* s.l., narrow, riverine tributary, African agro-village, complex ecosystem, capture point in a 5m RapidEye™ wavelength transmittance, fractionalized, emissivity endmember eigenvector dataset, using a geostatistical spatial algorithm. The MIXED procedure of the SAS System provides a rich selection of auto-probabilistic and autoregressive covariance structures through the RANDOM and REPEATED statements. The MIXED procedure may resolve unmixed and misspecified 5m RapidEye™ simulated, wavelength, transmittance emissivity frequencies in latent sub-mixel, covariance structures in an endmember of canopy radiance, sub-mixel, immature *S. damnosum* s.l. habitat model by providing the tools necessary to estimate fixed and random effects in one interpretive and interpolative model. MIXED is based on maximum likelihood (ML) and restricted maximum likelihood (REML) methods, versus the analysis of variance (ANOVA) methods in GLM (http://support.sas.com/documentation).

In statistics, the REML approach is a particular form of ML estimation which does not base estimates on an ML fit of data products. Alternatively, REML employs a likehood function devised from a transformed set of data so that nuisance variables have no effect (e.g., non-parameterizable, discontinuous, infrequently canopied, sparsely shaded, trailing vegetation variables). In the case of variance component, probability estimations for an empirically interpolative, autoregressable dataset of seasonal, hyperproductive, *S. damnosum*

s.l.capture point, eco-georferenceable habitats geosampled in an African riverine environment, the original non-log transformed, parameterizable covariate estimators may be replaced by a set of tabulated contrasts calculated from the geo-classifiable data. In doing so, the likelihood function would be optimally calculatable from the probability distribution of these contrasts, according to the model for the complete dataset.

Explicative REML estimation is available in a number of general-purpose statistical software packages, including SAS/GIS. Other algorithms that can be strategically employed in the cyberenvironment to analyze seasonal, hyperproductive, immature, trailing vegetation, immature geo-spectrotemporally uncoalesced, eco-georefernceable, turbid water, discontinuous, infrequently canopied, sparsely shaded, *S. damnosum* s.l., narrow, riverine tributary, African agro-village complex, ecosystem, eco-epidemiological, capture point in a 5m RapidEye^{TM} wavelength transmittance, fractionalized, emissivity endmember eigenvector, forecast, vulnerability models with random effects include the MIXED and VARCOMP procedures. In particular, REML may be used as a method for fitting quantitative, linear mixed, time series, *Simulium* models.

In contrast to the ML estimation, REML can robustly render time series dependent, unbiased probabilistic regressands of variance and covariance tabulated measures in a fractionalized, endmember eigenvector, heursitically optimizable of sub-mixel, seasonal, hyperproductive, immature, trailing vegetation, geo-spectrotemporally uncoalesced, eco-georefernceable, turbid water, discontinuous, infrequently canopied, sparsely shaded, *S. damnosum* s.l., narrow, riverine tributary, African agro-village, complex, ecosystem, in a 5m RapidEye^{TM} , wavelength, transmittance, fractionalized endmember, eigenvector emissivity, heuristically optimizable capture point, seasonal dataset employing orthogonally decomposed fractionalized, quantitable wavelength transmittance covariate estimators in a residual regression, eco-epidemiological risk model framework. The idea of underlying the REML estimation was put forth in 1937 by M.S. Bartlett. Desmond Patterson first described the approach that has been applied to the estimating components of variance in unbalanced data [73].

ANOVA methods produce only an optimum estimator (i.e., minimum variance) for balanced designs, whereas ML and REML asymptotically yield efficient time series dependent, explicative, endmeber eigenvector, fractionalized, covariate estimators for balanced and unbalanced designs in ArcGIS/SAS (ww.sas.edu). ML and REML thus present a clear advantage over ANOVA methods for quantitating fractionalized, Rapid Eye ^{TM} 5m, orthogonally decomposable, endmembers eigenvector in a sub-mixel, wavelength transmittance 5m RapidEye^{TM} datset of unbiased immature, trailing vegetation, seasonally hyperproductive, geo-spectrotemporally uncoalesced, eco-georefernceable, turbid water, discontinuous, infrequently canopied, sparsely shaded, *S. damnosum* s.l., narrow, riverine tributary, African agro-village complex, capture point and their polygonized, wavelength transmittance, fractionalized, emissivity endmember eigenvector estimators in ArcGIS since these data are often unbalanced. The asymptotic normality of ML and REML of autoregressive, probabilisc, endmember estimators that have been regressively quantitated from an empirical sub-mixel dataset of explanative, hyperproductive *S. damnosum* s.l., immature, capture point, geospectrally geosampled, uncoalesced, proxy LULC biosignatures may conveniently allow for robust inferences to be made on the decomposed, iteratively interpolated, covariate coefficient estimators, which may be difficult to do in a generalized, linear model (GLM) framework. Further, an understanding of procedures for estimating probabilistic, random and seasonally geo-spectrotemporally geosampled, fractionalized,

Rapid Eye ™ , endmember eigenvector effects may be vital in order to unbiasedly tabulate, heuristically optimizable, fixed and random effects when ecogeographically or ecohydrologically predicting, moderate resolution, geo- uncoalesced, fractionalized, wavelength emissivity transmittance of *S. damnosum* s.l. immature, capture points in narrow, riverine tributary, agro-village, complex, African ecosystems.

As previously mentioned, Jacob et al. [26] bridged the gap between the Bayesian and classical frequentist paradigms in ArcGIS for predictively interpreting an fractionalized, orthogonally decomposed, endmember eigenvector datasets of hyperproductive, trailing vegetation and turbid water *S. damnosum* s.l., immature habitats in a uncoalesced, wavelength covariate coefficient dataset of geo-spectrotemporally Rapid Eye ™ transmittance emissivity estimators that were geo-spectrotemporally geosampled in a riverine, agro-village complex in Burkina Faso. Bayesian probability is one interpretation of the concept of probability, in contrast to interpreting probability as the "frequency" or "propensity" of some phenomenon. Bayesain probability theory provides a sound mathematical for extracting robust inferences from forecastable regregression equations. The foundations of Bayesianisms in a probability theroectional setiings have been controversial by and vector ecologists, entomologists and other researchers. However more recently Bayseain probability theory has been employed by many in scientific research.

Amongst the advantages of Bayesian matrices over tradiation binomialized logistic regression models is that the response variable does not have to be dictomoized. As such, count variables may be employed without log transformation. Although Poissonian probability models employ count variables as regressands, there are susceptible to outliers cuasing overdispersion (i.e., over Poissianisms), especially in vector entomological models due to inconspicuous geospatial outliers[25]. Outliers are extreme observations that can generate misspecifications in time series non-linearizable, networks [24]. Hierarchical, Bayesianized, probability models utilize subject-maximum likehood, conditional priors, multiple iterations (“ burn-in periods”) and other geospatial, elucidative, techniques to quantitate exogenous covariates that can render parameterizable covariate coefficients. In so doing, the relative validity of research hypotheses in the face of noisy , sparse or uncertain data may be quantitated. Bayesian paradaigms may also be employed to adjust the parameters of a specific geo-predictive, eco-epidemiological, forecasting, vulnerability model. Regardless, Bayesian models have been under utilized for optimally determining geolocations of unknown, un-geosampled, hyperproductive, trailing vegetation, discontinuous, infrequently canopied, turbid water, seasonal, *S. damnosum* s.l., narrow, African, tributary, agro-village complex, eco-epidemiological, iteratively interpolative, capture points employing geo-spectrotemporally uncoalesced,wavelength transmittance emissivity proxy, biosgnatures and their parameterizable and non-parameterizable covariates of statistical significance.

Initially, in Jacob et al. [26], results of a Poisson regression model Pseudo R^2 were determined in PROC LOGISTIC for remotely quantitating an endmember, sub-mixel dataset of predictive, 5m, medium resolution, RapidEye™ *S. damnosum* s.l., immature habitat capture points, in transmission-oriented, stochastically or deterministically iteratively interpolatable, sub-meter resolution, emissivity fractionalized, covariate coefficients. This process provided information for heuristically dependent, explicative, time-series, unmixed, fractionalized, endmember estimates of the prior distribution based on the regressed and eco-georeferenceable main effect coefficients. This decomposed data was then exported into a Bayesian hierarchical, generalizable and optimizable matrix in PROC MCMC. The values for

estimates were employed as mean values and standard errors to parameterize prior expected values for regressing the interpolatable, trailing vegetation or turbid water, sparsely shaded, canopied, *S. damnosum s.l.* related, immature habitat decomposed biosignature variables in an heuristically optimizable, parameterizable covariate estimators. The prior expected mean value for the error term was assumed to be zero (0), with a standard deviation of 0.01.

The Bayesian procedures employed a special case of the Metropolis algorithm called the Gibbs sampler in PROC MCMC to obtain the posterior samplers. The authors in Jacob et al. [26] obtained Tsamples from a univariate disribution of the regressable, geo-spatiotemporal datasets of riverine, narrow tributary African, agro-village complexes capture point, immature habitats in an eco-epidemiological, 5m, RapidEye^{TM}, medium resolution, risk model, optimally forecasted through sub-mixel derivatives with PDF $f(\theta|\mathbf{y})$.In the eco-epidemiological, immature habitat endmember, forecasting vulnerability model, θ^t was the tth sample from f. To employ the Metropolis algorithm, the authors needed to have an initial value θ^0, and a symmetric proposal density $q(\theta^{t+1}|\theta^t)$. For $(t+1)$, the iteration, or the regression algorithm generated in PROC NL, mixed a sample from $q(\cdot|\cdot)$ based on the sample θ^t, which subsequently rendered a decision to either accept or reject a new sample (i.e., uncoealesced 5m proxy LULC biosignature). If the new sample was accepted in the descriptive, explicative *S. damnosum* s.l., forecasting, vulnerability habitat model, the algorithm repeated itself by starting at the new sample. If the new sample was rejected, the algorithm then started at the current seasonal,eco-epidemiological, capture point and repeated itself in an ecogeographic and probabilistic regression space.

Commonly, in least square regression models constructed in SAS geodatabases, some relations exist that are similar to principal components of regression frameworks. For example, a least square estimation algorithm may be optimally employed for parsimoniously deducing hyperplanes of minimum variance which may be efficiently quantitated in ArcGIS between the response and independent hyperproductive, *S. damnosum* s.l., habitat independent variables. The model may project clustered foci of seasonal, hyperproductive, immature habitats employing observable variables to a new ecogeographic and ecohydrologic regression space. Because both the X and Y data in the vector arthropod, eco-epidemiological model are projected into new space, the least square regression may be transformed in SAS into a bilinear factor model. In doing so, fundamental relationships between the response variable (e.g., immature geosampled, explanatorial, productivity rates) and other independent variables (e.g., meterological medium resolution 5m RapidEye^{TM} synthesized, eigenvector endmember covariates of landscape probabilistic regressable, log-transformed estimators and vegetation indices) may be extrapolated and evaluated. These models may try to determine between multiple, autoregressive, weighted matrices (e.g., latent autocorrelation diagnonal matrices) for quantitating latent, immature, geosampled, discontinuous, infrequently canopied, turbid water, seasoanlly hyperproductive *Simulium* habitat biosignature correlated variables to precisely predict risk mapping variables of the endmember covariance structures in regression spaces.

Optimally, a forecasting paradigm will try to tabulate and parsimoniously quantitate multi-dimensional direction in X space that explains the maximum multi-dimensional variance direction in the Y space. Both X and Y would be projected into regression spaces in, for example, a empirical dataset of, eco-georeferenceable, immature habitat, forecastable, vulnerability risk model, biogeophysical ecophysiological, heursitically optimizable forecasts in ArcGIS. In so doing optimally iterated, hyperproductive, trailing vegetation,

discontinuous, infrequently canopied, turbid water, seasonal, *S. damnosum* s.l., narrow, African, tributary, agro-village complex, eco-epidemiological, iteratively interpolative, seasonal unknown , ungeo-sampled, capture points may be identified.

However, many sensor networks that collect spatio-temporal information are prone to failure, resulting in missing data. To complicate matters, the missing data is often not missing at random, and is characterised by long periods where no data is observed. The performance of traditional univariate forecasting methods such as autoregressive probabilistic models decreases with the length of the missing data period because they do not have access to local temporal information. However, if geo-spatiotemporal autocorrelation is present in a space–time series then Bayesian approaches have the potential to offer better forecasts. A non-parametric, geo-spatiotemporal, kernel regression model may be developed in ArcGIS to forecast iteratively interpolative, seasonal hyperproductive, trailing vegetation, discontinuous, infrequently canopied, turbid water, seasonal, *S. damnosum* s.l., narrow, African, tributary, agro-village complex, eco-epidemiological forecast, vulnerability models under the assumption of sensor malfunction. Only topographic patterns of iteratively interpolated LULC variables of the upstream and downstream geospatialized, neighbouring links may be used to inform the eco-georferenceable, capture point forecasts. The model performance may be compared with another form of non-parametric regression, *K*-nearest neighbours inan ArcGIS cyberenviropnment, which is also effective in forecasting under missing data. The methods may show promising forecasting performance, particularly in periods of high congestion in geo-spectrotemrpoally uncoalesced datasets of moderate resolution *S. damnosum* s.l., capture points.

Partial least squares discriminant analysis (PLS-DA) is a variant used when the Y is a categorical variable. PLS is used to find the fundamental relations between two matrices (*X* and *Y*), (i.e. a latent variable approach to modeling the covariance structures in these two spaces). A PLS of sparsely shaded, hyperproductive, canopied, turbid water *S. damnosum* s.l., geo-spatiotemporally and geo-spectrotemporally, ArcGIS geoclassifiable, immature seasonal habitats as an eco-epidemiological, 5m RapidEye^{TM} vulnerability model will try to find the multi-dimensional direction in the *X* space that explains the maximum multi-dimensional variance direction in the *Y* space. PLS regression is particularly suited when the matrix of descriptive, elucidatory predictors has more variables than explicative observations, and when there is multicollinearity amongst *X* values [74]. By contrast, standard regression will fail in these cases, unless it is regularized.

The PLS algorithm is employed in partial least squares path modeling, a method of modeling a "causal" network of latent variables. Latent variables are causes cannot be determined without experimental or quasi-experimental methods. A latent variable model is typically based on the prior theoretical assumption that latent variables cause manifestations in their measured indicators [59,75]. This technique is a form of structural equation modeling, distinguished from the classical method in being component-based, rather than covariance-based. An alternative name for PLS, and better term according to Svante Wold [35], is projection to latent structures, but the term partial least squares is still dominant in geo-predictive, eco-epidemiological, endmember risk vulnerability modelling. Although the original applications were in the social sciences, PLS regression is today most widely used in chemometrics and related areas, as well as in bioinformatics, sensometrics, neuroscience and anthropology. In contrast, PLS path modeling is most often used in social sciences, econometrics, marketing and strategic management

In Jacob et al. [59], Markov Chain Monte Carlo (MCMC) methods revealed an ensemble of "walkers" that moved around randomly in PROC MCMC. At each field and remote specified, seasonal riverine immature habitat of endemic, unmixed, sparsely shaded, discontinuous, infrequently canopied, turbid water, fractionalized, endmember eigenvectors in an eco-epidemiological capture point where the walker stepped, the integrand value at that point was counted towards the integral. The walker then made a number of tentative steps around the decomposed dataset looking for a place with reasonably high contribution to the integral. Random walk methods can be considered to be a form of the Monte Carlo method [35].

In Jacob et al. [77], multiple geo-classified, moderate resolution (i.e Landsat ETM + 15m data) random geolocations for a eco-georeferenced datasets of trailing vegetation LULCs of *S. damnosum* s.l. turbid water, eco-georefernceable, immature habitats were geosampled from two pre-established, eco-epidemiological, riverine agro-village, narrow tributary study sites in Togo. These data were identified and recorded from July 2009 to June 2010 and were aggregated into PROC GEN MOD. An agglomerative, hierarchical, intra-cluster-based, eco-geographical, ecohydrological, geo-predictive and eco-epidemiological vulnerability assessment was then performed. The geo-spectrotemporally geosampled, clustered, time series data were then analyzed for statistical correlations employing Monthly Biting Rates (MBR), Euclidean distance measurements, and geomorphological, terrain-related, catchment-scale, fluvial processed, intuitively parameterized, risk models using multiple water-shed, observational, bioptical and illustrative regressors. These regressors were then eco-cartographically and parsimoniously displayed in ArcGIS. A digital overlay was subsequently performed in Geospatial Analyst™, employing the interpretive ground coordinates of high and low density, proxy LULC biosignature, clustering data variables stratified by Annual Biting Rates (ABR). This data was overlaid onto multitemporal, sub-meter, mixel ("endmember mixed pixel") resolution satellite data [i.e., QuickBird 0.61m visble and near-infra-red (NIR) wavebands].

Orthogonal, spatial filter, fractionalized, synthetic eigenvector endmembers were then generated in SAS/GIS. Linear and non-linear, probability models (i.e., Poisson, negative binomial, and Morans's *i*) were also constructed in the cyberenvironment to quantitate non-normality (e.g., kurtosis) in the log-transformed, categorical and continuous, fractionalized, 5m, endmember eigenvector frequency distributions as rendered by the unmixed, geo-classifed, trailing vegetation, proxy LULC biosignatures.. The authors were able to identify statistically significant, decomposable, sub-meter, wavelength emissivity, unmixable, seasonal, non-Gaussianistic, and regressive explanators as rendered from the decomposed endmember in a sparsely shaded, immature, hyperproductive habitat. Durbin-Watson statistics in Spatial Analyst™ were employed to test the null hypothesis, which stated that the unmixed regression model, forecasting the endmember eigenvectors as probabilistic, reflectance residuals, which were not autocorrelated, against the alternative hypothesis that the unmixed, immature, capture point, habitat residuals followed an autoregressive process in AUTOREG.

Thereafter, the radiance fractionalized, sub-mixel, interpolative data was exported into PROC MCMC. This revealed normalized priors for each of the geo-spectrotemporally geosampled, interactive, trailing vegetation and turbid water, *S. damnosum* s.l. immature habitats in covariate endmember, moderate resolution, sub-mixel, explanatorial, LULC, uncoalesced, reflectance estimators within an uncertainty-oriented, hierachical, Bayesianized, but generalizable, estimation, and ArcGIS gridded matrix. The residuals disclosed both

spatially structured and unstructured, erroneous, propagational effects in the high and low ABR-stratified, explanatorial, georeferenced and stratified geospatial clusters.

The eco-epidemiological, risk model forecast residuals revealed that amongst the trailing vegetation and turbid water, sub-mixel, uncoalesced, proxy LULC biosignature wavelength covariate regressors, Levels of turbidity were statistically significant in the high-ABR-stratified clusters, while the Eucidean distance-based, reflectance covariate estimator, the Distance between the georeferenced, eco-epidemiological capture point, and intervention, narrow tributary agro- village centroids were important for the low-ABR-stratified cluster. The findings suggested that varying and constant, unmixed, intra-cluster, endmember, wavelength transmittance emissivity covariate coefficients, rendered from a sparsely shaded, hyperproductive, remote sensing, *S. damnosum* s.l. immature habitat regression model in SAS GIS/can be tested for latent, inconspicuous non-normality (e.g., heteroskedastic residuals in space and time).

Thus, an ABR-stratified, medium resolution, trailing vegetation, proxy, LULC biosignature in a geospatialized cluster and eco-epidemiological model forecast can be iteratively interpolated by employing an intra-cluster, invasive diagnostic test in ArcGIS, along with histograms, eigendecompositions, spatial filters, orthoganizable algorithms, and Bayesian probabilitic paradigms to delineate erroneously propagated, autocorrelated, reflectance emissivity estimates. The authors in Jacob et al. [45] surmised that precise regressive quantitation of latent, misspecified, and orthogonal synthetic effects in an iteratively interpolated, proxy LULC biosignature of a *S. damnosum* s.l., capture point, immature habitats in intra-cluster, sub-mixel, autocovariate, eco-epidemiological, eigenvector endmember risk analyses is vital for attaining asymptotic distributions of the resulting residually adjusted, wavelength emittance, which can be established in ArcGIS. Estimates of the asymptotic variance can lead to the construction of approximate confidence intervals for remotely targeting *S. damnosum* s.l. habitats based on fractionalized, endmember eigenvectors of emissivity transmittance, wavelength data and field-geosampled, immature count data. However, it may be more vital to quantitate endemic onchocerciasis transmission zones based on decomposed, fractionalized, immature, discontinuous, canopy habitat, moderate resolution, wavelength frequency constituents.

Generalized additive models (GAM) are powerful for modeling, medium resolution RapidEye^{TM}, *S. damnosum* s.l., immature habitat data in nonlinear LULC effects of continuous, wavelength emissivity transmittance and reflectance covariate coefficients in regression models with non-Gaussian responses. Structured Additive Regression (STAR) models are extensions of GAM models that allow for incorporation of sub-mixel decomposed, descriptive uncoalesced, proxy LULC biosignature predictors when modeling immature *Simulium* habitats in ArcGIS. This may allow for the quantification of spatial effects of risk factors, while simutaneoulsy determining linear, or fixed effects, in a joint landscape model. Applying a STAR modeling approach in ArcGIS may optimally develop a multivariate, robust, geopredictive risk map, which employs an unmixed, iteratively interpolated, sub-mixel, endmember discontinuous, canopied, wavelength, emissivity, transmittance radiance an illustrative data feature attribute to target seasonally hyperproductive habitats.

Traditionally, the autoregressive integrated moving average (ARIMA) model (see Appendix 3) has been one of the most widely employed linear models in time series dependent, forecasting of moderate resolution, parameterizable, unmixed, wavelength

endmember, vector arthropod habitat constituents. An ARIMA model predicts a value in a response time series as a linear combination of its own past values, past errors (also called shocks or innovations), and current and past values of other time series [24]. Jacob et al. [45] constructed multiple, Euclidean distance–based, geo-spectrotemporal, unmixed, iteratively interpolated, wavelength emissivity, transmission, autoregressive, endmember eigenvector models in ArcGIS for predicting endemic geolocations of onchocerciasis transmission risk zones in Chutes Dienkoa, Burkina Faso based on stratifiable, remotely sensed, ecogeoreferenced clusters of hyperproductive LULCs of *S. damnosum* s.l. immature habitats. The authors employed multiple, capture point, immature habitats, geosampled in multivariate, decomposed, moderate resolution, wavelength transmittance emissivities, from the eco-epidemiological, covariate fractionalized, endmember,eigenvector,uncoalesced, data feature attribute datasets. The estimators, as rendered from the within surrounding village centroids from a hyperproductive *Simulium* capture point, was measured by employing an ArcGIS portioned buffer with 5 kilometer (km) intervals.

Thereafter, the fractionalized endmember eigenvector, estimators were regressed by employing the modified sum of squares in ArcGIS. Semi-parametric spatial filtering, orthogonal matrix eigenvectors, and stochastically interpolated, unmixed biosignatures within an eco-epidemiological, risk model, gridded framework in PROC ARIMA rendered robust, transmittance emissivities. The algorithm also residualized eco-epidemiological forecasts by reducing latent, autocovariate, probabilistic, uncertainty covariate coefficients in the non-Gaussian regressed, *S. damnosum* s.l., immature habitat productivity, count data for optimally risk mapping seasonal, eco-georeferenceable, onchocerciasis transmission zones. The SAS procedure analyzed and forecasted the equally spaced 5 km, univariate, time series transfer functions by employing ARIMA specifications. By default, all descriptive parameters in the created model object had unknown values, and the innovation distribution was Gaussian with constant variance. The output revealed that the created object model had prolific, canopied, sparsely shaded, immature, *S. damnosum* s.l. habitat count values for all the geoclassified model parameters: the constant term, the AR and MA coefficients, and the variance. The authors modified the created model using dot notation in order to estimate the prolific habitats. The property P had value 2 ($p + D$). This was the number of presample observations needed to initialize the demonstrative, vulnerability, geo-spectrotemporal, geospatial eco-epidemiological model. The final illuminative, geo-spectrotemporal, ARIMA model was $\Delta y_t = 0.4 + 0.8\Delta y_{t-1} - 0.3\Delta y_{t-2} + \varepsilon_t + 0.5\varepsilon_{t-1}$, where the innovation distribution was Student's t with 10 degrees of freedom (df) and a constant variance of 0.15. The model revealed that 5 to 10km was mesoendemic, 10 to 15km was hypoendemic and after 15km, there was no endemic transmission.

In Jacob et al. [45] a canopied, prolific, trailing vegetation and turbid water, *S. damnosum* s.l., narrow riverine tributary, immature habitat (i.e, eco-epidemiological, georeferenced capture point) geoclassified in Chutes Dienkoa, agro village-complex in Burkina Faso, was overlaid onto sub-meter resolution, QuickBird (0.61m) satellite data within an object-based classifier prior to entry into ArcGIS. Initially, the Band Math function of ENVI 4.8^{TM} was employed to calculate and color balance the scene. Before applying the spectral index to the imagery, raw mixel values and digital numbers (DN) were converted into physically meaningful units to remotely differentiate and justify quantitated sub-mixel, sub-resolution, fractionalized, trailing vegetation and turbid water, proxy LULC, unmixed, biosignture, eco-geophysiological, biophysical, decomposed variables of reflectance forecast, fractionalized endmember derivative spectra. The data was then quantitated and associated to the residual forecasts from the ENVI model employing seasonal, immature, *Simulium*

productivity based on habitat size in ArcGIS. Linear regression was then employed to equate band data to DN and the quantized, unmixed,fractionalized, endmember eigenvector of discontinuous,canopied, habitat fractionalized, radiance wavelength, transmittance emissivities, which in the QuickBird model was equivalent to removing the solar irradiance and the atmospheric path radiance in the object-based classifier. A radiometric calibration tool then calibrated the spaceborne sensor data to radiance and top-of-atmosphere (ToA) reflectance. Top-of-atmosphere reflectance can be defined as the reflectance measured by a space-based sensor, which is flying higher than the earth's atmosphere and includes contributions from clouds and atmospheric aerosols and gases [23].

Additionally, in Jacob et al. [45], Fast Line-of-sight, Atmospheric Analysis of Spectral Hypercubes (FLAASH®) removed the effects of scattering in the scene. The authors calculated the internal relative, time series dependent, emissivity, wavelength, fractionalized radiance rendered from geoclassified, trailing vegetation and turbid water, proxy LULC biosignature variables and their unmixed ecohydrologic, specified descriptive, covariate estimators, which were normalized using the 0.61m resolution image to a scene average spectrum. ENVI's Log Residuals Correction Tool removed the instrument gain, topographic effects, and albedo effects from the endmember emissivities. The authors then employed a successive progressive algorithm, a two stream radiative atmospheric transfer analysis, a geometric-optical model, and a bidirectional reflectance distribution function (BDRF) to regress the unmixed, sub-mixel, sub-meter resolution *S. damnosum* s.l. immature habitat,radiance fractions in Geospatial Analyst™.

The bidirectional reflectance distribution function (BRDF; $f_{\mathrm{r}}(\omega_{\mathrm{i}}, \omega_{\mathrm{r}})$) employed a function of four real *S. damnosum* s.l., sparsely shaded, trailing vegetation, turbid water and discontinuously canopied, eco-geophysiological, biophysical variables, which were used for defining how light was reflected from the opaque canopied habitat surface. The model employed both optics of real-world light in computer graphics algorithms, and in computer vision algorithms. The function took an incoming light direction, ω_{i}, and outgoing direction, ω_{r} (taken in a coordinate system where the canopy habitat surface normal $\mathbf{n}$ lay along the *z*-axis), and returned the ratio of reflected radiance exiting along ω_{r} to the irradiance incident on the surface from direction ω_{i}. Each direction ω was itself parameterized by azimuth angle ϕ, and zenith angle θ. Therefore the BRDF, as a whole for the trailing vegetation-related, turbid water immature, capture point habitat, was a function of multiple variables. The BRDF had units sr^{-1}, with steradians (sr) being a unit of solid angle. The definition was $f_{\mathrm{r}}(\omega_{\mathrm{i}}, \omega_{\mathrm{r}}) = \frac{\mathrm{d}\,L_{\mathrm{r}}(\omega_{\mathrm{r}})}{\mathrm{d}\,E_{\mathrm{i}}(\omega_{\mathrm{i}})} = \frac{\mathrm{d}\,L_{\mathrm{r}}(\omega_{\mathrm{r}})}{L_{\mathrm{i}}(\omega_{\mathrm{i}})\cos\theta_{\mathrm{i}}\,\mathrm{d}\,\omega_{\mathrm{i}}}$, where *L* was power per unit solid-angle-in-the-direction-of-a-ray per unit projected-area-perpendicular-to-the-ray, *E* was irradiance, or power per unit habitat surface area (e.g., unmixed, decomposed, explanatorial, *S. damnosum* s.l. immature habitats with fractionalized descriptive, canopied endmembers), and θ_{i} was the angle between ω_{i} and the surface normal, n

The index i indicated incident light, and the index r indicated reflected light. The reason the function was defined as a quotient of two differentials, and not directly as a quotient between the undifferentiated, unmixed habitat quantities, was because irradiating light other than $\mathrm{d}\,E_{\mathrm{i}}(\omega_{\mathrm{i}})$, which was of no interest for $f_{\mathrm{r}}(\omega_{\mathrm{i}}, \omega_{\mathrm{r}})$, but might have illuminated the surface, which would unintentionally affect $L_{\mathrm{r}}(\omega_{\mathrm{r}})$, whereas $\mathrm{d}\,L_{\mathrm{r}}(\omega_{\mathrm{r}})$ was only affected by $\mathrm{d}\,E_{\mathrm{i}}(\omega_{\mathrm{i}})$.

In Jacob et al [45], the non-parametric, decomposed, Euclidean distance-related, quantifiable, sub-mixel, wavelength covariate emissivity, descriptive estimators (e.g., georeferenced, geoclassified, sparsely shaded, canopied, trailing vegetation LULC centroids to georeferenced agro-village centroids) derived from the unmixed habitat data were then employed to construct a robust Boolean model.

The Boolean model that is utilized for a random subset of the plane or higher dimensions is analogously one of the simplest and most tractable models in stochastic geometry [94]. The Boolean model of information retrieval (BIR) is a classical information retrieval (IR) model. The BIR is based on Boolean logic and classical set theory in that both the documents to be searched and the users query are conceived as sets of terms. Parsimonious retrieval is based on whether or not the documents contain the query terms [94].

Further, in Jacob et al. [45], the seasonally imaged, immature *Simulium* habitats and their associated within-canopy, sub-mixel, eigenvector endmembers of fractionalized, trailing vegetation and turbid water, geoclassifed irradiance values were validated and a geo-spectrotemporal iteratively interpolatable biosignature was decomposed in ENVI. An autocorrelation weighted matrix was deconvolved in Geostatistical Analyst™ into linearizable combinations of the sparsely shaded, canopied, unmixed, fractionalized, wavelength, transmittance, endmember emissivities. Subsequently, the biosignature, with its multiple ToA, noise-adjusted coefficients was kriged in Geostatistical Analyst™ to identify unknown, un-geosampled, hyperproductive, canopied, sparsely shaded and seasonal *S. damnosum s.l.* immature habitats along a northern Ugandan riverine ecosystem.

A total of 25 potential, georeferenced, *S. damnosum* s.l. immature habitat sites were predicted. Of the 25 sites ecogeographically predicted to be suitable habitats by the model, 23 (92%; 95% CI 81–100%) were found to contain larvae. In contrast, just 2/10 (20%; 95% CI 0–45%) sites examined, which were not predicted to ecohydrologically represent hyperproductive, canopied, sparsely shaded, immature, georeferenced, geoclassified, trailing vegetation and/or turbid water, LULC specified habitats by the eco-epidemiological, forecastable vulnerability model were found to contain larvae. The model, thus, exhibited a sensitivity of 80% and a specificity of 92% when applied in the Ugandan riverine, agro-village study site, a performance that was statistically significant ($p < 0.0001$; Fisher's Exact test). The two immature habitat sites that were not predicted by the model were nonetheless found to contain larvae consisting of low streamside, trailing vegetation immersed in fast flowing water. Crosskey [93] revealed that immaturely canopied *S. damnosum* s.l. riverine habitats can be affected by non-temporally and temporally explanatorily, and seasonally dependent, biotic and abiotic attributes (e.g., floating vegetation, turbidity). The mean number of larvae found at the sites predicted by the QuickBird model (21.91) was significantly greater than the mean number of larvae at the sites consisting of geoclassified immersed, overhanging vegetation LULCs (4.0; $p<0.001$, Mann Whitney U test).

Currently, very few onchocerciasis control programs have collected a valid outcome using LULC metrics that enable public health officials and funding agencies to remotely, regressively, quantitatively and optimally determine the degree and magnitude of their impact on time series, field or remote geosampled, immature riverine 5m medium resolution RapidEye™, *Simulium* habitats georeferenced as endemic, transmission-oriented, unmixed, wavelength parameterized and non-parameterizable, covariate estimators. A principle reason for this deficiency is the absence of sufficient management systems to capture, manage and

analyze large amounts of diverse, decomposable, fractionalized endmember, radiance data being generated by various black fly control activities. Existing management information is neither accurate nor comprehensive, a vital necessity for efficient, effective and economic black fly management [77]. Ecogeographic and ecohydrologic geolocations of eco-georeferenceable, sparsely shaded, discontinuously canopied, trailing vegetation and turbid water *S. damnosum* s.l. hyperproductive, immature habitats, combined with knowledge of remotely geoclassifiable and explanatorily interpolated, unmixed, proxy LULC biosignature, reflectance data attribute features of multiple, geo-spatiotemporally and geo-spectrotemporally geosampled sites may be a potential key element for implementing efficient and cost effective larval control measures in African riverine communities.

A remote evaluation of onchocerciasis treatment data offers a systematic way of comparing the costs and consequences of interventions in order to improve the allocation of resources by prioritizing georeferenceable, sparsely shaded, canopied, geoclassifiable and trailing vegetation *S. damnosum* s.l. immature habitats based on seasonal larval/pupal productivity [59]. Treatments or habitat perturbations should be based on surveillance of larvae in the most productive areas of an ecosystem [51, 80]. Additionally, a robustifiable, remotely explanatorial, surveillance system of decomposable biosignature employing cost effective, 5m RapidEye^{TM} satellite data systems may be employed to improve the uptake of existing effective black fly control measures and ensure the maximum impact from the introduction of new technologies in georeferenceable, African riverine agro-village and eco-epidemiological study sites

The ability to measure electromagnetic energy at varying geo-spatiotemporally and geo-spectrotemporally geosampled, sparsely shaded, eco-georeferenceable, trailing vegatation or turbid water, *S. damnosum* s.l immature, discontinuous, canopied habitat in explicatively geoclassified, decomposed, 5m, medium resolution, RapidEye^{TM} proxy, LULC biosignture wavelengths as it interacts with canopy material, forms some of the foundation behind remote sensing and spectral science for remotely, regressively and quantitatively identifying unknown and un-geosampled, iteratively interpolated, prolific habitats in African riverine, agro-village, complex, ecosystem communities. The imaged characteristics of the eco-georeferenceable, geosampled, immature, geo-classifiable, uncoalesced, proxy, LULC biosignature, immature, habitat endmember, eigenvector causes the electromagnetic energy to be reflected, refracted, or absorbed in a way that is unique to each discontinuous, sparsely shaded, canopied material. These interactions may be measured across discrete sections of a seasonally imaged, *S. damnosum* s.l. immature habitat of medium resolution and cost effective, 5m, RapidEye ^{TM} unmixed, canopied discontinuous spectrums, which when plotted in ArcGIS may form a unique shape that may be the habitats reference, explanatorial, interpolatable and interpretive biosignature.

In African agro-village, narrow tributary, riverine environments, sparsely shaded, trailing vegetation *S. damnosum* s.l. turbid water habitats differ in their immature production capacity [77] and, as a result, intervention efforts to remotely and regressively target hyperproductive immature, capture point, habitats employing moderate resolution, cost effective, 5m RapidEye^{TM} satellite data in ArcGIS may be more relevant. To date, entomological research has not focused extensively on remotely sensed detection of seasonally prolific, *S. damnosum* s.l., geo-spectrotemporally geosampled, vegetated, riverine, immature habitats employing cost effective, medium resolution data. Thus, optimal cost-effective, geospatial and geospectral resolution has not been described employing varying proxy graphical indicators such as Normalized Difference Vegetation Indices (NDVI) for

remotely and regressively quantitating and targeting eco-georeferencable and geoclassifiable hyperproductive, *S. damnosum* s.l. immature habitats that have been geo-spatiotemporally and geo-spectrotemporally geosampled in African riverine environments.

Normalized Difference Vegetation Indices monitor terrestrial landscapes by satellite sensors [23]. These indices have been highly successful in assessing geoclassifiable vegetation LULC conditions for foliage, cover, phenology and other processes such as evapotranspiration (ET) and primary productivity related to the fraction of photosynthetically active radiation (fPAR) absorbed by a canopy of a eco-georeferenceable, sparsely shaded, hyperproductive *S. damnosum* s.l. riverine immature habitat [59]. Evaporation accounts for the movement of water to the air from sources such as the soil, canopy interception, and waterbodies [81]. fPAR generates ecophysiological, biophysical, time series dependent explanators that may quantitatively, remotely and regressively describe eco-georeferenceable, sparsely shaded, canopied, unmixed, fractionalized endmember eigenvectors of LULC irradiance associated with seasonally geosampled, geo-classifiable *S. damnosum* s.l. immature habitats. This relationship may be parsimoniously, remotely and regressively analyzed in an ArcGIS cyberenvironment for quantitating functional process rates of energy and mass unit exchange in a trailing vegetation, turbid water, hyperproductive, 5m, imaged RapidEye^{TM} , *S. damnosum* s.l. immature, discontinuous, canopied riverine habitat [22]. IC irradiance is the radiant flux received by an interpretively explicative, surface per LULC unit area. Spectral irradiance can be defined as the irradiance of a surface per unit frequency or wavelength, depending on whether the emissivity unmixed, spectrum is taken as a function of frequency or of wavelength [82].

Jacob et al. [51] found that the instantaneous fraction of direct beam radiation intercepted (IPAR) by a seasonal trailing vegetation or turbid water, *S. damnosum* s.l. narrow, tributary, agro-village, complex, riverine immature habitat canopy in ArcGIS can be described mathematically as IPAR = 1 - exp -k Leaf Area Index (LAI)/cos 0s). Leaf Area Index (LAI) is defined in ArcGIS as a simple ratio between the total one side leaf surface of a plant and the capture point, habitat, surface area of geoclassfied, canopied LULC on which the plant grows (www.esri.com).

LAI is a dimensionless value, typically ranging from 0 for bare ground to 8 for dense canopy vegetation [83]. LAI is one of the most important explanatorial, LULC time series dependent, proxy, predictor variables governing the canopy processes [99], which is related to leaf and canopy Chl endmember contents, photosynthesis rates, carbon and nutrient cycles, dry and fresh biomass, and growing stages [85]. Hence, LAI has been generously applied in plant and environmental studies of evaporation, transpiration, light absorption, yield estimation, growth stages of crops and chemical element cycling [86 - 87]. A common non-destructive surrogate for LAI, which is based on reflectance of red and NIR bands, is using the NDVI [88]. Effective LAI is routinely remotely quantitated with optical instruments that measure georeferenceable, canopied gap fractions through the probability of beam penetration of sunlight through vegetation, geoclassified LULC reflectance in ArcGIS.

Fortunately, there are a variety of techniques that use the close coupling between canopy structure and radiation interception to provide an indirect means of measuring discontinuous canopy in an eco-georeferenceable, African agro-village, narrow tributary, riverine environments, sparsely shaded, trailing vegetation *S. damnosum* s.l. turbid water, *S. damnosum* s.l. immature, capture point, hyperproductive, habitat. The basic strategy in ArcGIS is to create a model which describes how radiation is affected as it passes through the

immature habitat canopy based on some well-defined, geometrical canopy attributes, and then make appropriate radiation measurements and invert the model to estimate the value of these attributes. Typically, a geospatialized, vector arthropod larval habitat vulnerability model is based on two attributes of the canopy: foliage amount, and foliage orientation. There is also an assumption of randomness in the spatial distribution of the foliage. The degree to which an indirect method succeeds is determined in large part by a hyperproductive, immature, riverine *S. damnosum* s.l. capture point and how closely the habitat canopy conforms to the idealized one in the radiation model. However, there have been few efforts to obtain theoretically consistent and effective leaf area indices from those measurements. For example, in order to apply the Beer–Lambert law [see Appendix 4], multiple gap fraction measurements may be averaged in two ways: 1) by taking the mean of the logarithms of the individual gap fraction values, or 2) by taking the logarithm of the mean gap fraction. The Beer–Lambert law, or the Beer–Lambert–Bouguer law relates the attenuation of light to the properties of the canopy material through which the light is traveling [23].

Interestingly, studies have established relationships between VIs and LAI and biomass yield using moderate resolution data in ArcGIS [e.g. 89 - 91]. Overall, these VIs have revealed wavelength emissivity transmittance, canopied predictor variable sensitivity to different levels of moderate resolution derived LAI and biomass. NDVI is sensitive to low LAI (i.e. LAI < 2–3), but saturates at medium to high LAI [84]. A similar canopied, explanatorial, geo-classifiable LULC in a topographic pattern may be observed when qualitatively, remotely and regressively quantitating the relationship between 5m RapidEye^{TM} derived NDVI and biomass, with NDVI saturating at medium to high (fresh) biomass (around 2 kg/m^2), for example, for a discontinuously canopied, vegetated, sparsely shaded, trailing vegetation, turbid water, seasonal, *S. damnosum* s.l, immature, capture point, hyperproductive, habitat geospectrotemporally geosampled, in an African riverine, agro-village ecosystem.

In Jacob et al. [51], the authors optimally determined that remotely and regressively quantitated Intercepted Photosynthetically Active Radiation (IPAR) is an important ecohydrological, seasonal explanatorial and observational predictor in empirically geo-classifiable, vegetation-related, eco-georeferenceable, canopied, descriptive LULCs for biogeochemical, explicative processes such as water and energy exchange. Measurement of this canopied, reflective quantity and ecophysiologically-related, fractional, interception efficiency (f_{PAR}) may be thus strategically employed for regressively quantitating probabilistic temporal variability in a canopied, sparsely shaded, eco-georeferenced, geo-classifiable, trailing vegetation, ecohydrologic and eco-cartographic LULC of an *S. damnosum* s.l. habitat. A method may be thus presented for estimation of IPAR and f_{PAR} employing a commercially available hemispherical radiation sensor within cost-effective, medium resolution, (i.e., RapidEye ^{TM} 5m resolution data) imaged, dependent data in ArcGIS. These models may provide sufficient information on the structure of the immature habitat canopy constituents (e.g., diurnal interconversion of cyclic xanthophyll pigments, chorphyll (Chl) concentrations, levels of caretenoids, etc.) and the angular dependence of light interception for single measurements to be interpreted for all solar zenith angles for a *S. damnosum* s.l. prolific habitat.

Here, we develop the basic elements for implementing a control-oriented, remote surveillance program (e.g, “Slash and Clear”) in an ArcGIS cyberenvironment for reducing emergence of immature *Simulium* using adult catching rates, cost-effective, moderate resolution-derived, 5m RapidEye^{TM} data [$500.00/for 128x128m^2 georeferenced polygon] for

unmixed, elucidatory NDVIs in interpolatively unmixed, trailing vegetation LULCs, biosignature, predictor variables. We then employed the eco-cartographic cyberenvironment to correlate seasonl, field-geosampled, georeferenceable empirical data (e.g, adult catch rates) within a non-linear dependent, unmixed, regression-related, *S. damnosum* s.l. habitat in a wavelength emissivity transmittance, endemember frequency, eco-epidemiological risk model. Unfortunately, one of the major barriers to developing an accurate onchocerciasis surveillance program in African,narrow r tributary, agro-village complex riverine environments is the optimal design and implementation of a sampling system that will adequately monitor varying characteristics of riverine village–level, vulnerable sub-populations employing interpolated, seasonal, unmixed, Euclideanized, trailing vegetation, turbid water, LULC wavelength emissivities in 5m RapidEye™ parameterizable, covariate distance estimators [e.g., georeferenced measurements from a village centroid to habitat geolocation]. The 'Slash and Clear' model is based on physical removal of precisely and remotely targeted, sparsely shaded, seasonally prolific, georeferenced, geo-classifiable, trailing vegetation LULCs of *S. damnsoum* s.l. immature, canopied habitats within a 1km gridded buffer in ArcGIS.

The basis of the 'Slash and Clear' control strategy is an unmixed, remotely sensed, endmember that is explanatorily, geo-spatiotemporally and geo-spectrotemporally interpolated as a chorophyll (Chl) *a*-related, emissivity transmittance, endemic, forecasting 5m RapidEye™ eco-epidemiological, frequency wavelength, sub-mixel explanative risk model. Chlorophyll *a* is a green pigment found in plants which absorbs sunlight and converts it to sugar during photosynthesis. Chlorophyll *a* is usually collected from water samples of a known volume that are filtered through fine mesh filter paper (0.45 micron), which is then analyzed for Chl-*a* concentrations. There are three standard methods for quantitating Chl-*a* concentrations: spectrophotometry, fluorometry, and high performance liquid chromatography (HPLC) [23]. Spectrophotometry is the most commonly employed technique in seasonal, eco-epidemiological, vector arthropod habitat, risk mapping. Though HPLC is slower and more demanding, it is able to differentiate between Chl types and other accessory canopy pigments with less bias than spectrophotometry [1].

Hyperproductive, sparsely shaded, canopied, trailing vegetation and turbid water, LULC, endmember, riverine habitat, fractionalized, emissivity waveband, RapidEye ™ 5m, frequency data variables may transmit a reflectance excitation beam of light in the blue range and detect the light fluoresced by Chl in a sample in the red wavelength of the moderate resolution sensor. This fluorescence may be directly proportional to the concentration of Chl in the canopy of the hyperproductive habitat. Since fluorescence is an indirect method for measuring Chl-*a* in canopied, hyperproductive, sparsely shaded, trailing vegetation turbid water, LULC-reflectance, *S. damnsoum* s.l., riverine, immature habitat, non-linear, trees, in PDAs loaded with gridded moderate resolution, cost effective data in ArcGIS may reveal statistically significant eco-epidemiological, seasonal forecastors. Moderate resolution sensor systems allow immature *Simulium* habitat measurements to be made in situ for implementing a seasonal control program (e.g., "Slash and Clear") based on geo-spatiotemporally, geo-spectrotemporally, iteratively interpolated unmixed endmembers. Remotely targeting these hyperproductive habitats in an ArcGIS cyberenvironment may help in reducing larval counts.

Bio-optical, unmixing, descriptive algorithms for autoregressive, remote estimation and quantitation of Chl-*a* concentrations may render robustifiable, canopied, seasonally hyperproductive *S. damnsoum* s.l., habitats, in an ArcGIS cyberenvironment by exploiting the upwelling radiation in the blue and green, spectral regions of decomposed, RapidEye™

sensor data. By doing so, bio-optical algorithms may be optimally devised in ArcGIS to relate the electromagnetic energy reflected in the upward direction to the decomposed concentrations of canopy habitat blue and green, LULC constituents dissolved and suspended in the water column for identifying unknown, interpolated, geoclassifiable, endmember, decomposed sub-mixel habitat data geo-spatiotemporally, geo-spectrotemporally geosampled in an African, narrow tributary, riverine, agro-village ecosystem. In riverine, sparsely shaded, turbid, productive African riverine waters other canopy pigment constituents defined in an ArcGIS cyberenvironment that vary independently of Chl-*a* may be also remotely regressively seasonally deduced in a PDA employing cost-effective moderate resolution RapidEye^{TM} 5m spatial resolution data, which may also subsequently auto-probablistically quantitatively, eco-cartographically determine absorption-related and scatter light in canopied, habitat regions.

Doerffer and Fischer [72] replaced the singleband-ratio technique with a full spectral-fit method for retrieval of Chl-*a* in case-2 waters in an ArcGIS cyberenvironment. This algorithm minimized the $\chi 2$ difference between the observed radiance and models radiances. Garver and Siegel (1997) developed a model to derive a spectral paradigm fit employing a set of three semi-analytical descriptions of the inherent, canopied, optical, decomposable properties, including Chl-*a* absorption in ArcGIS. The primary objectives for the algorithm were: 1) to develop a computationally fast and flexible algorithm for retrieval of Chl-*a* in continental shelf waters that was reliable over a large range in concentrations (e.g., 1 to 20 mg m^{-3}); 2) to remotely, regressively capture disturbances by large fluctuations in sediment load (e.g., 0.5 to over 30 gm^{-3}); and 3) quantitating CDOM absorption [e.g., (440 nm) 0.1 to 1 m^{-1}]. The authors accomplished their objectives and developed standard error products for quantitating the Chl-*a* concentration per mixel that reflected the uncertainty in the Landsat remote sensing measurement while determining optical, unmixed, illuminative, model data feature attributes underpinning the retrieval.

The Coastal Zone Colour Scanner (CZCS) aboard the Nimbus-7 satellite has greatly increased knowledge of the distribution of Chl-*a* in ecohydrological, ecogeographical networks and thereby of global primary production [73, 74, 75]. Successors of CZCS are the SeaWiFS in orbit since September 1997, and the Medium Resolution Imaging Spectrometer (MERIS) of the European environmental remote sensing satellite ENVISAT-1. The MERIS instrument employs a medium spectral resolution in 15 programmable bands in the range 390 nm to 1040 nm (https://earth.esa.int/web/guest/missions/esa-operational-eo missions/envisat/instruments/meris).

The 10-year archive of MERIS data has been employed as an invaluable resource for studies on geo-classifiable, ecohyrological, LULC, network system dynamics in ArcGIS at regional and global scales. MERIS data is collected from aboard the European Space Agency's (ESA) [23]. The mission of MERIS includes interpolation and quantification of distributions of phytoplankton in the open oceans and coastal waters, and of moderate resolution, vegetation-related, canopied, sparsely shaded, unmixed LULCs [62]. Whereas CZCS incorporated five channels for the visible and NIR ranges, for MERIS up to 15 wavebands can be selected (https://earth.esa.intemissions/envisat/instruments/meris). Compared to SeaWiFS, which lacks a channel for the red/NIR edge, MERIS appears to offer a better cost-effective band suite for retrieval of Chl-*a* in turbid canopied waters. Three of the MERIS bands are similar to those employed in algorithms for shipboard optical teledetection of Chl-*a* [63]. The spatial resolution of up to 30m at nadir allows the mapping of numerous

lakes and reservoirs in ArcGIS, a feature not foreseen in the original mission objectives as well as coastal seas [62].

The MERIS algorithm was calibrated employing data collected on the IJssel Lagoon (The Netherlands) in 1993–1996 in an ArcView ™ cyberenvironment. Validation was performed using data on the IJssel Lagoon in 1997 and 1999, as well as other Dutch inland waters, the Scheldt Estuary (Belgium/The Netherlands), the Hudson/Raritan Estuary (New York/New Jersey), and the North Sea off the Belgian coast. Except for the IJssel Lagoon validation data, the fractionialized, reflectance, endmember, wavelength, transmittance, decomposable, emissivity, forecastable, derivative spectra and physical and chemical conditions were presented in Gons [76] and Gons [77]. All concentrations of Chl *a* were determined after extraction in ethanol and correction for phaeopigment by acidification [78]. The sensitivity was based on results in the different moderate resolution sensor bandwidth. Slight shifts in wavelength emissivities of the other wavebands were tested by simulating the unmixed, decomposed, canopy products at a lower resolution. The fit was found to be equally consistent when applying the averaged values of $R(0,\lambda)$ and $a_w(\lambda)$ for the PR-650 bands centred at 664 and 668 nm, 704 and 708 nm, and 772 and 776 nm. For both Chl *a* and Chl *a*-u, the value of *p* did not change. The values of a^* were 0.0162 and 0.0140 m^2 (mg of Chl *a*)$^{-1}$, respectively, and therefore between those for the 664 and 672 nm bands. The potential of the MERIS instrument for Chl *a* detection in mesotrophic and eutrophic Case 2 waters for p = 1.06 and $a^*(664)$ = 0.0146 m^2 (mg of chl *a*)$^{-1}$ was tested for later observations on the IJssel Lagoon, other freshwater bodies, and estuarine and coastal waters. The data were collected in widely different weather, and except for cases of floating layers of cyanobacteria and visible, benthic, geoclassified, vegetation-related LULC, no observations were excluded. The plots for validation and calibration of the MERIS algorithm compared very well. Neither this plot nor the standard of the estimate for these groups of water bodies indicated a need for the development of regional algorithms.

Pulliainen [79] employed a semi-operative approach to retrieve Chl-*a* concentration in an ArcGIS cyberenvironment from airborne/spaceborne spectrometer observations and tested them using the airborne imaging spectrometer (AISA) data from 11 lakes in southern Finland. The retrieval algorithmic, landscape approach was empirical and required simultaneous in situ training data on water quality for quantiation and determination of multiple coefficients in ArcGIS. However, the training data did not have to be collected from every lake under investigation. Instead, the results obtained indicated that reliable, interpolated, auto-probabilistic estimates on the level of Chl-*a* for an individual lake could be achieved without employing data representing the specific lake. The unmixed, reflectance, endmember wavelength, transmittance, frequency, emissivity, radiance fractionalized, biosignature data from one lake body was then interpreted within an algorithm in ArcGIS (Geospatial Analyst ™) based on the image data representing the limnological network. This model enabled the accurate geospectral, geospatial estimation of water quality from the moderate resolution, remotely sensed, time series dependent scenes for numerous lakes with the aid of reference data only for a few selected lakes representing the region under investigation. In addition, it was shown that the AISA spectrum shape characteristics were highly affected by the trophic and humic state of the lake water in ArcGIS.

Floricioiu [80] investigated the capabilities of MERIS for monitoring canopied, water quality parameters in ArcGIS of oligo- to mesotrophic lakes in Austria and in Lake Garda in Italy which were investigated as part of the project AO-164, “Environmental Research in the Eastern Alps”. From May to September 2003, routine field measurements from limnological

stations were made available parallel to MERIS acquisitions. The surface reflectance was derived from Level 1b MERIS data in the cyberenvironment by means of radiative transfer calculations. Radiative transfer is the physical phenomenon of energy transfer in the form of electromagnetic radiation [23] developed in ArcGIS Spatial Analyst™ for eco-cartographically representing the concentration of Chl-*a* based on the ratio between reflectance in MERIS bands 7 (665 nm) and 5 (560 nm).

Several numerical models exist that solve the radiative transfer equation in a bidirectional ArcGIS cyberenvironment for quantitating within natural water body moderate resolution, wavelength, emissivity, endmember eigenvector, covariate estimators with properties defined by the profiles of inherent optical properties, sea-air boundary state, and downwelling sky radiance distributions [81, 82, 83]. These radiative transfer models provide accurate forecasted values for the endmember, decomposable, LULC optical properties, including moderate resolution, remote sensing reflectance, and downwelling diffuse attenuation for a range of conditions and for all realistic observation angles. This makes them very useful for sensitivity analysis and/or auto-probabilistic, non-normality, diagnostic and assessment studies in moderate resolution, remote sensing decomposition of Chl-*a* in *S. damnosum* s.l. habitats in ArcGIS. Thus, these hyperproductive, immature canopied habitats may be robustly regressively remotely quantitated employing various cluster tools (e.g., Moran's *i* coefficient).

Newer approaches involving the inversion of unmixed, *S. damnosum* s.l. habitat, moderate resolution, derivative, endmember spectra in radiative transfer models and other unmixing algorithms in ArcGIS may yield improvements over traditional index approaches for correlating canopy photosynthetic pigments (e.g., Chl-*a*) with seasonal immature productivity. This way, the researcher may carefully consider the ecophysiological and structural geophysical, eigenvector, LULC reflectance, endmember component contributions of each extracted trailing vegetation and /or turbid water, sub-mixel, habitat data feature attribute.

Dall'Olo [84] evaluated the extent to which NIR to red reflectance ratios could be applied to the Sea Wide Field-of-View Sensor (SeaWiFS) and the Moderate Imaging Spectrometer (MODIS) to estimate and remotely quantitate canopied Chl in productive, sparsely shaded, canopied, turbid waters. The SeaWiFS and MODIS satellites have collected ocean color data since September 1997 and January 2000, respectively, providing an extensive database of images to the scientific community (www.nasa.com). To achieve this objective, unmixed moderate resolution, covariate, reflectance, fractionalized, endmember, derivative spectra and relevant water constituents were collected in 251 stations over reservoirs with a wide variability in optical parameters (e.g.,4 < Chl 240 mg m < 3; 18 < Secchi disk depth < 308 cm). SeaWiFS and MODIS NIR and red reflectances were simulated by employing the in-situ hyperspectral data. The proposed algorithms predicted canopy Chl with a relative, random, auto-probabilistic uncertainty of approximately 28% (average bias between -1% and -4%). The effects of unmixed, wavelength, emissivity reflectance, transmittance, uncertainties on the predicted canopy Chl components were geospectrally and geospatially analyzed. It was found that for realistic ranges of root mean square calculations as rendered from the auto-probablistically, empirically regressable radiance uncertainties, the canopied Chl could be estimated with a precision better than 40% and an accuracy better than 35%.

Previous work has also demonstrated that the concentration of Chl-*a* can be estimated from the reflectance ratio R for λ = 704 and 672 nm, for remotely quantitating moderate resolution NIR reflectance peak in eutrophic water and the red absorption peak of Chl *a*, respectively. In Buiteveld et al. [85] the absorption coefficients of water $a_w(\lambda)$ for these wavelength unmixed emissivities and the backscattering coefficient b_b was assumed to be independently derived from the reflectance transmittance data which was subsequently quantitated employing λ = 776 nm: $[Chl\ a] = \{R(a_w(704) + b_b) - a_w(672) - b_b^p\}/a^*(672)$ (Eqn 1.1), where the values of $a_w(672)$ and $a_w(704)$ were optimally tabulated as 0.415 and 0.630 m^{-1}, respectively. In the model $a^*(672)$ was a mean Chl *a*-specific absorption coefficient at λ = 672 nm and *p* was an empirical constant close to unity. The retrieval of Chl-*a* was tested on $R(0,\lambda)$ and then deduced from above-water measurements by employing a model PR-650 SpectraColorimeter from Photo Research (Chatsworth, CA, USA) over the 380–780 nm range at 4 nm increments with 8nm FWHM bandwidth. The moderate resolution reflectance values for 664, 704 and 776 nm were then calculated from the shipboard spectroradiometry, and thereafter employed to emulate $R(0,\lambda)$ for the relevant MERIS bands.

In Buiteveld et al. [85] the MERIS algorithm was optimally obtained following replacement in the original equation (1.1) of $R(0,\lambda)$ and $a_w(\lambda)$ for λ = 672 nm by the values for 664 nm which were then quantitated by employing $[Chl\ a] = \{R_M(a_w(704) + b_b) - a_w(664) - b_b^p\}/a^*(664)$ (Eqn 1.2), where R_M was the reflectance ratio for λ = 704 and 664 nm, and $a_w(664) = 0.402\ m^{-1}$. The observations that had served the calibration of equation (1.1) were successively employed to calibrate equation (1.2) for the MERIS application. The model fit rendered $p = 1.063 \pm 0.005$ and $a^*(664) = 0.0146 \pm 0.0002\ m^2$ (mg of Chl *a*) $^{-1}$ where $n = 114$; $r^2 = 0.96$). Whereas the value of *p* remained the same, the coefficient $a^*(664)$ was significantly lower than $a^*(672)$ which was then equivalent to 0.0176 ± 0.0002 in the original calibration. The departure from the pigment's red absorption maximum near 675 nm explained this lowered a^* value. Also, for uncorrected Chl-*a* (i.e., Chl *a*-u = Chl *a* + phaeopigment/1.7), the exponent *p* was equivalent to 1.056 which remained the same, whilst $a^*(664)$ was 0.0127 ± 0.0001 which was deemed significantly lower than $a^*(672) = 0.0152 \pm 0.0002\ m^2$(mg of Chl *a*-u)$^{-1}$ in the original calibration.

Compatible MERIS data, were automated and made available as part of the Basic ERS & ENVISAT (A) ASTER MERIS (BEAM) toolbox [86]. These include artificial neural network approaches trained to varying parameter concentration and optical property ranges [e.g., the Case 2 Regional (C2R) [87], the FUB/WeW [88], the Eutrophic Lake (EUL) and Boreal Lake (BL) [89] processors, and the band ratio, height-above-baseline Maximum Chlorophyll Index (MCI) and Fluorescence Line Height (FLH) algorithms [90, 91]. Many of these algorithms are adaptable to the OLCI sensor on Sentinel-3. However, these algorithms have not been widely validated across the continuum of optical African riverine water types found in sparsely shaded, discontinuous canopied, ecosystems, particularly those that have highly turbid phytoplankton- or sediment-dominated waters.

Prior to their operational use in research, monitoring, and management activities, rigorous validation analyses are required to understand the associated performance and probablistic regressable uncertainties rendered from unmixed, moderate resolution, RapidEye™ 5m wavelength, fractionalized, endmember eigenvectors. Validation is vital to the selection of a retrieval algorithm or combination of retrieval algorithms that are applied to

a given ecohydrological network body to achieve the most robust retrieval of the ecogeographical parameter(s) of interest. It has not been demonstrated in literature that an Chl-*a* retrevial algorithm in ArcGIS using moderate resolution RapidEye ^{TM} 5m satellite data that performs well in one highly turbid network system may necessarily be transferrable to another remote network system nor has there been geo-classifiable LULC, site-specific and regional validation of any unmixed, endmember, biosignature-related, canopied pigments.

Several of the Chl-*a* retrieval algorithms have been evaluated in ArcGIS individually and in various combinations in terms of their retrieval performance for a number of parameters and for diverse lake conditions. Binding [92] applied the C2R, FLH, and MCI algorithms with and without the "smile effect" caused by slight variation in center wavelengths for a given band across the MERIS field-of-view. Meanwhile Bourg, D'Alba, and Colagrande [95] improved remotely sensed contrast between Ocean and Land (ICOL) processors applied, to evaluate Chl-*a* retrieval from MERIS imagery of Lake of the Woods (Canada/USA) during an intense algal bloom, and compared these with the standard MERIS algal_2 product. A validation of the C2R, EUL and BL processors' atmospheric correction, IOPs and water quality constituents (Chl-*a*, gelbstoff absorbance, and total suspended matter) was carried out over several European lakes by Koponen et al. [96] and Ruiz-Verdú et al. [97]. Alikas and Reinart [98] evaluated Chl-*a* retrieval from Lakes Peipus (Estonia/Russia), Vattern and Vanern (Sweden) employing the MERIS standard Case 1 (algal_1) and Case 2 (algal_2) Chl-*a* products, in addition to related total suspended matter and yellow substance retrievals. C2R and ICOL were evaluated in application to perialpine lakes by Odermatt, Giardino, and Heege, [99] and to Lake Trasimeno Italy by Giardino, et al. [100].

Odermatt, Pomati, et al. [101] report validation results of C2R, EUL and FUB WeW with ICOL applied for multiple lake bodies in Greifensee, Switzerland. The authors take into consideration in situ measurements at various depths and locally-tuned coefficients relating neural network retrieved pigment absorption to Chl-*a* concentration. Gege and Plattner [102] investigated the performance of MERIS standard L2 products over Lake Constance (Germany), and Matthews et al. [103] applied C2R and EUL processors, in addition to a suite of empirical algorithms, to Lake Zeekoevlei (South Africa). From such studies, a range of results may be found to arise, whereby a given algorithm or processor having performed well in some instances and/or geolocations, failed in others due to the ecogeographically, non-specified, local geoclassified, LULC conditions. Therefore, a validation of algorithms intended for optically-complex waters and available within the BEAM image processing toolbox was undertaken. The concentrations of Chl-*a*, and total suspended matter (TSM) were investigated by Song et al. [104] for optimally determining major water quality parameters that could be retrieved from moderate resolution remotely sensed data. Water sampling works were conducted on 15 July 2007 and 13 September 2008 concurrent with the Indian Remote-Sensing Satellite (IRS-P6) overpass of the Shitoukoumen Reservoir. Both empirical regression and back-propagation artificial neural network (ANN) models were quantitatively established to estimate Chl-*a*, and TSM concentration with both in situ and satellite-received radiances signals. In machine learning and cognitive science, artificial neural networks (ANNs) are a family of statistical learning models inspired by biological neural networks [105]. It was found that empirical explanative models performed well on the TSM concentration estimation with better accuracy (R^2 = 0.94, 0.91) than their performance on Chl-*a*, concentration (R^2= 0.62, 0.75) with IRS-P6 imagery data, and the model's accuracy marginally improved with in situ interpolated, decomposed, endmember, forecast, derivative, spectral data. The results indicated that the ANN model performed better for both Chl-*a* (R^2 = 0.91, 0.82) and TSM (R^2 = 0.98, 0.94) concentration estimation through in situ

collected, fractionalized, explanative, derivatve endmember spectra; the same trend followed for IRS-P6 imagery data (R^2= 0.75 and 0.90 for Chl-*a*; R^2= 0.97 and 0.95 for TSM). The relative root mean square errors (RMSEs) from the empirical model for TSM (Chl-*a*) were less than 15% (respectively 27.2%) with both in situ and IRS-P6 imagery data, while the RMSEs were less than 7.5% (respectively 18.4%) from the ANN model. The authors, however, suggest that the algorithms developed needed to be tested and refined with more imagery data acquisitions combined with in situ spectra data.

In Song [104], measurements of Chl-*a* from the monitoring programmes spanned multiple seasons and covered the full spatial extent of Balaton to quantitate differences in MERIS algorithm performance across space and time in ArcGIS cyberenvironment. The ultimate aim was to evaluate and compare the performance of multiple retrieval algorithms under the range of optical conditions presented by Lake Balaton so as to identify the most appropriate algorithm(s) for MERIS processing and to inform future Sentinel-3 OLCI work.

Siswanto [106] found that modification of standard NASA ocean color algorithms was necessary to improve the retrieval of in-water bio-optical constituents in the Yellow and East China Seas using coarse to moderate resolution satellite remote sensing data. Other studies [e.g., 107] suggest regionally tuned algorithms are needed for better retrieval of in-water, bio-optical interpretive, constituents. Unfortunately there is limited literature on validating and/or calibrating the NASA standard ocean color algorithm in ArcGIS to improve accuracy of algorithmic Chl-*a* estimation. A preliminary exercise was carried out to evaluate the performance of MODIS OC3M algorithm which locally tuned a decomposable algorithm, yielding high accuracy Chl-*a* retrieval in the MS water in the Malacca Straits. The updated locally-tuned OC3M algorithm has shown some improvement for Chl-*a* estimation in case-2 water. However, the statistical robustness of this algorithm was deemed trivial, as the points were not sparsely distributed over the MS. This finding revealed that the improved MODIS 2013 with iterative fitting method is only reliable for certain and limited part of MS. Therefore, there is still need for alternative methods to improve the area coverage aspect of the algorithm for Chl-*a* retrevial especially in canopy, sparsely shaded, hyperproductive, African, riverine, turbid water objects (e.g., flooded, trailing vegetation LULC, S. *damnosum* s.l. canopied, immature habitat).

As a solution, there is a new version of standard OC3M (OCv6) which has been updated employing comprehensive in situ data of NOMAD version 2. The version 2 data may have applicability for remotely targeting *S. damnosum* s.l. habitats by applying the different coefficient in the OC3M algorithm. This version may render different results or improvement to the sub-mixel applicability of OC3M in geoclassifed Chl-*a* LULC retrieval in ArcGIS. Moreover, in algorithm development, it may be more helpful if in-situ remote data were included (www.nasa.gov). This could give another option of optimum canopy algorithmic residualizable forecastable inputs for improving the regionally tuned algorithm in sparsely shaded, productive, turbid, RapidEye™ 5m image, African riverine waters.

Further, updating the algorithm validation in a PDA enabled ArcGIS cyberenvironment may contribute to the development of a regionally-tuned algorithm for more reliable Chl-*a* canopy *S. damnosum* s.l. immature habitat retrieval. Despite the fact that the revised OC3M for the MS has been devised, NASA recently announced the reprocessed MODIS Aqua (MODISA) data (www.nasa.gov), and as a result was able to successfully validate this endmember decomposed new data to update the existing OC3M algorithm so as to have regionally tuned and improved quality of the current moderate resolution satellite

sensor retrieved Chl-*a*. However, the default coefficients for OC3M (i.e., 0.215, -2.3798, 1.5823, -0.6372, -0.5692) may also be 0.2424, -2.7423, 1.8017, 0.0015, -1.2280. Thus, the unmixed, wavelength, transmittance emissivity data [e.g., (443,488,547) and (443, 489, 555)] may not exactly be a subset of the six MODIS traditional bands in the visible spectrum (i.e., 412, 443, 488, 531, 551 and 667) of the *S. damnosum* s.l. habitat capture point. In this case, the OC3M algorithm may not describe Chl-*a* concentrations with precision remotely targeting a RapidEye™ 5m-imaged hyperproductive *S. damnosum* s.l. habitat in a highly turbid African riverine village ecosystem.

Dahanayaka [108] researched the suitability of a handheld spectrometer in a PDA and ASTER satellite data for monitoring water quality in coastal waters of Sri Lanka and inland waters of Japan, which were tested from November 2010 to March 2012, in ArcGIS. Chl-*a*, turbidity, total suspended solid, secchi depth and reflectance data were measured at ASTER overpass times in Negombo estuary, Trincomalee bay, Puttalam and Chilaw lagoons, Sri Lanka, and in Lake Senba and Lake Kasumigaura, Japan. ASTER based Chl-*a* retrieval algorithms were developed to support in-situ Chl-*a* concentrations in the PDA. The original Chl-*a* were analyzed in order to determine a Chl-*a* correction equation. Then, three ASTER VNIR band ratios were compared for correlation with the corrected MODIS Chl-*a* and in-situ Chl-*a*. Finally, the regression equation of the ASTER band ratio, B1/B2 with highest correlation was employed for generation of multiple unmixed endmember Chl-*a,* risk distribution maps. Significant correlation between the ratio of the reflectance peak at 705 nm and the Chl-*a* absorption at 678 nm and the in-situ Chl-*a* content was observed and these reflectance ratios were used to establish spectrometric, Chl-*a,* estimation algorithms. The proposed descriptive algorithms successfully quantitated geolocalized environmental effects in the eco-epidemiological study site areas. ASTER-based, high resolution, Chl-*a* distribution maps were derived in ArcGIS more precisely by further correction of the geodatabase's algorithms. This may prove useful in mitigating the impacts of environmental LULC change in *S. damnosum* s.l. habitats. Unfortunately, ASTER-based high resolution Chl-*a* maps have generated overestimates in turbid, tropical coastal waters.

Palmer [109] presented the first comprehensive algorithm validation exercise over Lake Balaton, Hungary for conducting a geo-spatiotemporal, geo-spectrotemporal Chl-*a* retrieval. Six algorithms of differing canopy architecture for application to optically complex waters were assessed in ArcGIS: the C2R, BL, EUL, FUB/WeW, and MCI/FLH processors. The lake was considered by the authors to be well suited for satellite validation activities due its large size, and complex optical water types encompassing turbid waters with high and varying concentrations of Chl-*a*, total suspended matter (TSM) and CDOM. With few exceptions [e.g., 97, 98, 99], many previous moderate resolution, endmember eigenvector validation studies have focused on a specific event or a limited time period. Likewise, validation of Landsat Chl-*a* retrievals were previously carried out for Lake Balaton [110].

In Palmer [109] cost effective, moderate resolution, Envisat satellite from March 2002 until April 2012 provided observations at spectral (15 bands from 412.5 to 900 nm), radiometric (16-bit), spatial (300 m at full resolution) and temporal (three day revisit cycle at the equator) resolutions previously unprecedented by other satellite sensors which allowed for improved insights into the concentrations of optically active LULC substances in large lakes, and thereby into the dynamics of these lakes more generally. The authors employed in-water algorithms in ArcGIS for the accurate retrieval of the biogeochemical, wavelength, covariate emittance of key importance based on MERIS and OLCI data for fully exploiting

the lake monitoring exercise. The study presented the first extensive validation of algorithms for Chl-*a* retrieval by MERIS in the highly turbid and productive waters of Lake Balaton. Six algorithms for Chl-*a* retrieval from MERIS over optically complex Case 2 waters, including band-difference and neural network architectures, were compared using the MERIS archive for 2007–2012. The expository decomposition, algorithms were geolocally-tuned and validated using in situ Chl-*a* data ($n = 289$) spanning the five year, illuminative, elucidatory, image time series and from all four lake basins.

In general, both band-difference algorithms tested (Fluorescence Line Height (FLH) and Maximum Chlorophyll Index (MCI)) performed well, whereas the neural network processors were generally found to be much less accurately retrievable for in situ Chl-*a* concentrations. The Level 1b FLH algorithm performed best overall in terms of Chl-*a* retrieval ($R^2 = 0.87$; RMSE = 4.19 mg m^{-3}; relative RMSE = 30.75%) and particularly at Chl-*a* concentrations of ≥ 10 mg m^{-3} ($R^2 = 0.85$; RMSE = 4.81 mg m^{-3}; relative RMSE = 20.77%). However, under mesotrophic conditions (i.e., Chl-*a* < 10 mg m^{-3}) FLH was outperformed by the geolocally-tuned FUB/WeW processor (relative FLH RMSE < 10 mg m^{-3} = 57.57% versus relative FUB/WeW RMSE < 10 mg m^{-3} = 46.96%). An endmember ensemble selection of in-water algorithms was demonstrated to improve Chl-*a* retrievals.

Chlorophyll a is the predominant pigment contributing to red fluorescence in leaves while chlorophyll b constitutes an accessory pigment accounting for about one-third (or less) of total leaf chlorophyll content [23]. Excess energy from light harvested by chlorophylls or transferred to chlorophylls by other accessory trailing vegetation or canopy pigments (e.g., carotenoids and anthocyanins) may not be utilized in the photosynthetic transport chain which may be thus dissipated as heat or expended into lifting chlorophyll chromophores from ground-state to high-energy states during specifiic sampled frames (e.g., flooding). De-excitation via emission of canopy habitat photons at a longer RapidEye™ 5m, wavelength may lead to red fluorescence. Plant stresses that impair photosynthesis lead to greater accumulation of excess light energy dissipated as chlorophyll fluorescence.

In fluorescence sensing, excitation of green leaves with UV-A (Ex 400 nm) or blue light (Ex 470 nm), can give rise to red and far red chlorophyll a fluorescence emissions around 690 nm and 740 nm Fluorescence intensity ratios in these red and far red wavebands (F690/F740) have been used as indicators of ecophysiological strain but because many natural and stress factors impact on chlorophyll fluorescence, identification of specific stressors is not possible [111]. For example, F690/F730 have been shown to increase under N, Ph, and potassium (K) deficiency in sunflower [112], and water deficit in poplars and conifers. Simultaneous thermal and fluorescence imaging constitutes a multispectral approach for characterization of canopied plant stresses.

These findings imply that, provided that an atmospheric correction scheme specific for the red-NIR spectral, canopied, LULC region is available, the extensive database of moderate resolution senor data could be employed in ArcGIS to quantitatively remotely regress and monitor Chl-*a* endmembers in an hyperproductive habitat vulnerability model in canopied, turbid African rivers. In medium-to-coarse geospatial resolution satellite images, single decomposed mixels often contain a mixture of different types of LULC [23]. Use of very high resolution imagery can mitigate this mixel problem in ArcGIS to some degree, but the relatively higher cost and lower frequency at which high resolution imagery is typically

acquired is rather prohibitive when implementing vector control strategies such as remotely targeting and removing *S. damnosum* s.l. habitats in African riverine environments.

RapidEye's traditional broadband and Red-Edge indices have been evaluated for grassland N and biomass Estimating grass nutrients and biomass as an indicator of rangeland (forage) quality and quantity using remote sensing in savanna ecosystems for crop canopy chlorophyll content [International Conference of the African Association of Remote Sensing and the Environment (AARSE).]. Since the RapidEye ™ constellation's Red Edge band is sensitive to Chl status and leaf and canopy structure, it is expected that this band would contribute to the characterization of different LULC plant cover types. Schuster, Förster and Kleinschmidt [113] tested the Red Edge band in an LULC classification project in ArcGIS. Sixteen classes including two forest classes (deciduous and coniferous) were assessed. They found that the Red Edge band provided an overall classification accuracy that was consistently higher than without it. In terms of individual LULC classes, the most significant improvements were obtained with geoclassified classes comprised of open landscape vegetation. Recio et al. [114], found that higher accuracy could be achieved by involving decomposable endmember, geocalssified unmixed, LULC reflectance variables derived from the Red Edge band. Conrad et al. [115] employed multiple indices in ArcGIS combining the Red Edge, Red and NIR bands in a multi-temporal approach to separate several crop types. The authors concluded that employing three bands could characterize this sensitive portion of the sub-mixel dicontinuous reflectance spectrum, so that an accurate separation of the geoclassified LULC types under investigation would be remotely permittable.

Recent studies support the hypothesis that a broad Red Edge band, as employed in the RapidEye ™ sensors, is also suitable for obtaining information about the Chl and N content of plants in ArcGIS. Pinar and Curran [116], and Filella and Peñuelas [117] found that the Red Edge region in moderate resolution, RapidEye™ data is sensitive to Chl content and N-status in canopied geoclassified vegetation LULCs. Nitrogen fixing shrub *Dichrostachys cinerea* in a mesic savanna in Zambia was recently unmixed and remotely quantitated for eco-cartographically delineating georeferenced pools in ArcGIS employing soil N, phosphrous (P) and carbon (C) availabilities. The authors evaluated whether these regression effects induced feedbacks upon the growth of understory vegetation LULC and encroaching shrubs. *Dichrostachys cinerea* shrubs increased total N and P pools, as well as resin-absorbed N and soil extractable P, which were geolocated within the top 10-cm of soil. Shrubs and understory grasses differed in their foliar N and Ph concentrations along gradients of increasing encroachment, suggesting that these grasses obtained nutrients in different ways. Thus, the authors assumed that the LULC grasses probably were obtained from the surface upper soil LULC layers, whereas the shrubs may have acquired N through symbiotic fixation to obtain P from deeper soil layers. The storage of soil C increased significantly under *D. cinerea* and was apparently not limited by shortages of either N or Ph. The authors concluded that the shrub *D. cinerea* did not create a negative feedback loop by inducing P-limiting conditions, probably because they obtained P from deeper soil layers. Further, C sequestration was found not to be limited by a shortage of N, so that geoclassified mesic savanna LULCs encroached by the species could represent a C sink for several decades. As such, an endmember spectroscopic, NDVI biosignature, with unmixable woody encroachment endmember LULC wavelength, reflectance estimators may be regressively quantitated in ArcGIS for delineating remotely quantifiable seasonal associations between photosynsthetic and non-photosynthetic (NPV) trailing vegetation, LULC, canopied, leaf optical response regressors (e.g., Euclean distance between canopy twigs) and immature *Simulium* seasonal productivity .

Leaf optical responses to a wide range of biotic and abiotic stresses have been widely researched in literature [23]. These include responses to increased CO_2, and other gaseous pollutants, heat stress, heavy metal toxicity, exposure to ultraviolet radiation, water status, insect pest attack, herbicide treatment, salinity effects, and extremes in nutrient availability. In many studies, the spectral wavebands investigated as predictors of plant health status across moderate resolution imaged species range from 400 – 2500 nm. The logic behind these correlations is that unfavorable growing conditions result in morphological, physiological, and/or biochemical changes that have an impact on plant interaction with light on specific, canopied LULCs. Reflectance characteristics in the 400 – 700 nm range are primarily influenced by the cellular level of colored pigments such as chlorophyll, anthocyanins and carotenoids, in the 700 – 1400 nm range by cell structure, and in the 1400 – 2000 nm range by the water content in the tissues [23]. Leaf reflectance patterns have been employed to measure leaf chlorophyll content, N status xanthophylls, and carotenoid pigment levels for multiple unmixed geospectral objects.

Perturbations to the processes of transpiration and photosynthesis can be exploited as cues for hyperproductive, sparely shaded, discontinuous canopied, *S.damnosum* s.l. plant stresses. Control of transpirational water loss through stomatal openings on plant leaves constitutes an important mechanism for maintaining leaf surface temperature. In the event of water stress, decreased transpirational cooling from stomatal closure leads to an increase in leaf temperature that could be monitored by thermography. Thermal imaging, combined with extraction of additional information from visible imaging, has been described as an improved technique for correlating plant surface temperature variation to stomatal conductance and diagnosis of water deficit stress at canopy level. Biotic stresses are also detectable by thermography since pathogen-mediated increase in a central plant defense compound, salicylic acid, results in stomatal closure and a concomitant increase in temperature. This series of events has been utilized for early detection of viral infection tobacco plants by thermography. The thermal effect resulting from plant-pathogen interaction has allowed tracking of disease progression even at the early presymptomatic stage under controlled environmental conditions

The application of endmember algorithms at broad spatial extents in ArcGIS may enable the production of foliar, 5m, RapidEye^{TM} geo-spatiotemporally,geo-spectrotemporally geosampled, hyperproductive, sparsely shaded, canopied, geoclassifed trailing vegetation, *S. damnosum* s.l, immature, habitat, ArcGIS derived Chl maps, may be powerful tools for promoting a better understanding of riverine Chl-a, canopy, LULC dynamics over space and time. These geospatially discontinuous maps may be vital for monitoring canopy vegetation-related, seasonal LULC stress and for enhancing understanding of hyperproductive, *Simulium,* immature habitat, canopy plant-environment interactions and the controlling mechanisms on Chl-*a* content. The ability of this technique to remotely regressively characterize variations in endmember Chl-*a* content across different geoclassified, canopy vegetation LULCs may help identify elucidatory georeferenceable, interpolatable data feature attributes geospectrally, geospatially associated to riverine,narrow tributary, high density black-fly habitat foci, species and structures which would be important for making the method operational across seasonal extents, and for its inclusion in photosynthesis and C cycles of, other hyperproductive, RapidEye ^{TM} imaged, *S. damnosum* s.l, immature, habitat, forecasting, endmember, unmixed, wavelength, transmittance, emissivity models.

Various single and combined indices have been computed from in-situ spectroradiometer explanatorial, eco-georferenced, geo-spectrotemrpoal, data and simulated

RapidEye™ 5m data. For example, Huang et al. [118] found a combination of the RedEdge NDVI was able to predict Chl concentration in wheat with a coefficient of determination of R^2=0.77. This transition zone may be the basis for accurately interpolating a decomposed, Red Edge, unmixed Chl-*a* biosignature, as remotel quantitated from a decomposed wavelength, transmittance emisivity dataset of *S. damnosum* s.l. habitat, sub-mixel endmembers. These Chl-*a* covariate, estimator coefficients may be synthesized in ArcGIS employing the normalized difference between 5m, reflectance in the red visible (0.6µm) and the NIR (0.8µm) reflectance spectrum.

Thus, a seasonal descriptive, geospectral endmember eigenvector analysis of seasonally hyperproductive, riverine, narrow tributary, eco-georeferenceable, *S. damnosum* s.l. larval habitats employing RapidEye™ data may reveal Chl-*a* concentration increases by regressively quantitating the typical slope shifts in the Red Edge spectral region towards the NIR for a positively autocorrelated, georeferenceable cluster. The Red Edge inflection point wavelength (λi) may be employed as an indicator for this shift. Accordingly, several 5m spectral indices employing narrow bands, both from ground-based RapidEye™ measurements, have been successfully applied to also determine green biomass, water content, Chl content and N status. The Red Edge position and shape act as indicators of plant Chl content, biomass and hydric status. Knowledge about N status may represent an important factor for accurately interpolating a Red Edge, NDVI, endmember, sub-mixel biosignature to identify unknown *S. damnosum s.l.* immature habitats in African turbid riverine environments based on interpolated unmixed Chl-*a* canopy, trailing vegetation, geoclassified LULC concentrations.

Also the Red Edge position (REP) may be employed to estimate Chl-*a* and other light sensitive trailing vegetation, pigments and content of leaves in a decomposable, Red Edge, NDVI 5m, biosignature in ArcGIS. An object-based classification in ENVI may remotely assess canopy health of a canopied, sparsely shaded, hyperproductive, narrow tributary, eco-georeferenceable,*S. damnosum* s.l. habitat. Red Edge NDVIs may reveal higher correlations with 5m field measurements of seasonal canopy plant health (http://www.satimagingcorp.com/satellite-sensors/other-satellite-sensors/rapideye/). A bioptical dataset of canopy endmember, Red Edge, NDVI, biosignature-related, photosynthetic and NPV, sub-mixel, wavelength, reflectance emissivity transmittance, estimator coefficients may measure and monitor plant growth (vigor), vegetation LULC cover, and biomass production of seasonally productive *S. damnosum* s.l. habitats.

These studies suggest that if Chl-*a* concentration increases, the typical slope in the Red Edge spectral region may shift towards the NIR in a decomposed, Red Edge, unmixed, Chl-*a* biosignature, as a remotely quantitated 5m, wavelength, transmittance emmisivity dataset of geoclassified LULC, *S. damnosum* s.l., habitat sub-mixels. Very often the Red Edge inflection point wavelength (λi) is employed as an indicator for this shift. However, both the detection of this inflection point and the assessment of the shift are only possible with very narrow spectral bands [119]. Accordingly, several spectral indices using narrow bands, both from ground-based spectroradiometers or airborne sensors, have been successfully applied to determine green biomass, canopy water content, Chl content and N-status [120].

This raises the question of whether a broader band sensor like RapidEye's MSI can detect changes in the Red Edge domain for remotely targeting hyperporductive, seasonal,

trailing vegetation, turbid water, capture point, narrow, African tributary, agro-village complex, discontinuous, infrequently canopied, *S. damnsoum* s.l. habitats based on an interatively interpolated Chl-*a* endmember, wavelength, transmittance, emssivity value, and thus combining this capability with the possibility of seasonally monitoring extensive LULC areas associated with these habitats at a high temporal frequency. Recent studies support the hypothesis that a broad Red Edge band, as used in the RapidEye sensors, is suitable for obtaining information about Chl and N content of plants [121]. For example, a combination of the widely used NDVI and the Normalized Difference Red Edge Index (NDRE) was able to predict Chl concentration in wheat with a coefficient of determination of R^2=0.77 [122].

An empirical dataset of RapidEye's Relative Chl-*a*-oriented, *S. damnosum* s.l. habitat, 5m resolution, endmember eigenvector coefficients can be interpolated to identify unknown, seasonally hyperproductive immature habitats in ArcGIS. This data product may depict the geospatial variation of the relative Chl-*a* content within the habitat's discontinuous canopy field. Further, interpolated, eco-epidemiological maps produced in ArcGIS may show different Chl-*a* contents in prolific, RapidEye^{TM} 5m medium resolution *S. damnosum* s.l habitats, which, if this occurs in a single field, could indicate pigmental differences in the nutritional status of the canopy. Given how rapidly these Chl-*a,* risk maps can be generated in ArcGIS after image acquisition and the relative simplicity and straightforwardness of the results, these maps may be valuable tool for improving field management of seasonally hyperproductive, *S. damnosum* s.l., capture point, trailing vegetation, turbid water, capture point, narrow, African tributary, agro-village complex, discontinuous, infrequently canopied, immature habitats.

Although RapidEye^{TM} Chl-*a* algorithms could exploit the upwelling radiation in the blue and green canopy spectral region in a hyperproductive habitat, the accuracy of the explicatively retrieved canopy concentrations may break down in turbid, productive, waters because of the presence of other constituents (e.g. chromophoric dissolved organic matter,) that do not co-vary with canopied, Chl-*a*, seasonal concentrations, especially during African riverine flooding. Most importantly, because of the high values of the total canopy absorption coefficient(a) in seasonally prolific, *S. damnosum* s.l. habitats, the signal upwelling in the blue spectral region flooded, riverine ecosystem, wavelength, transmittance emissivitives may be too low (comparable to, or lower than the signal in the NIR), which would reduce the sensitivity of these retrieval algorithms. As a consequence, canopy Chl-*a* estimation for generating an *S. damnosum* s.l., interpolatable, eco-epidemiological risk model in ArcGIS may be affected by large, auto-probabilistic, unmixed, endmember, biosignature-oriented, LULC reflectance uncertainties. For instance, Darecki and Stramski [123] applied moderate resolution remotely sensed data employing case-2 water Chl-*a* algorithm [124] to estimate shoreline canopied Chl in the Baltic Sea and obtained a large bias (30%) and a large random uncertainty (>100%), even after a regionalization of the algorithm.

Altered Chl concentrations in geoclassified senescent leaves in a RapidEye ^{TM} 5m, image of an *S. damnosum* s.l. larval habitat may be able to capture 5m, LULC, geo-predictive reflectance variables associated with seasonal immature productivity count. Descriptive, leaf optical responses to a broad range in leaf chlorophyll concentration were examined also for leaves that were at various stages of senescence in five species [125]. Leaves of sweetgum (*Liquidambar styraciflua* L.), red maple (*Acer rubrum* L.), wild grape (*Vitis rotundifolia* Michx.), switchcane (*Arundinaria gigantea* (Walter) Muhl.), and longleaf pine (*Pinus palustris* Miller) that ranged in color from green to yellow were collected from the woodlands of Stennis Space Center during December 1998 through February 1999. For N = 42 leaves

per broadleaved species, leaf reflectance and transmittance were measured throughout the 400–850 nm spectrum using a spectroradiometer (model 1500, Geophysical Environmental Research Corp., Millbrook, New York, USA) attached via fiber optic to an integrating sphere (model LI1800-12S, LI-COR, Lincoln, Nebraska, USA) and methods described earlier [126]. A leaf was clamped into position over the sample port on the sphere wall and a 1.65-cm^2 leaf area was irradiated by the beam from a tungsten halogen lamp. Light reflected from the leaf was transmitted from the sphere interior through the fiber optic to the spectroradiometer for measurement of reflected spectral radiance. The spectroradiometer recorded data at moderate resolution wavelength intervals of ~1.6 nm.

Similar descriptive, eco-epidemiological, measurements were made for stray light caused by imperfect collimation of the lamp beam and light reflected from a white reference while the adaxial leaf surface faced the sphere interior (Spectralon SRT-05-99, Labsphere, North Sutton, New Hampshire, USA). Reflectance was computed by subtracting stray light radiance from the radiances reflected by the leaf and reference, then dividing leaf reflected radiance by reference reflected radiance. This quantity was multiplied by 100 to yield units of percentages. Leaf transmittance was measured by illuminating the adaxial leaf surface such that light passed through the leaf into the integrating sphere. Radiance reflected from the white reference was measured while the abaxial surface faced the sphere interior. Transmitted radiance was multiplied by 100 and divided by reference radiance to yield percentage of total transmittance. For longleaf pine reflectance endmember transmittance were measured for 42 samples. Each sample was composed of 5–6 needles spaced ~1 mm apart and arranged in parallel across the sample port of the integrating sphere. Reflected and transmitted radiances were recorded as above. An additional transmittance scan was taken without needles in the sample holder to enable the correction of radiance values for light that passed between. In contrast to the earlier method, a high-resolution digital camera and image processing software (ENVI v. 3.1, Research Systems, Boulder, Colorado, USA) were used to determine the percentage of irradiance that was not intercepted by the needles. In all species, percentage leaf absorptance was computed as 100 − (reflectance + transmittance).

After leaf optical properties were measured, Chl concentrations of the same leaves were determined. Six circular disks, each 6.25 mm in diameter, were punched from the leaf portion for which optical properties were measured. The disks were placed immediately into 8 mL of 100% methanol, and pigments were allowed to extract in the dark at 30°C for 24 h. Absorbances of the clear extract at 652.0, 665.2, and 750 nm were recorded and concentrations of chls *a, b,* and $a + b$ were computed chlorophyll concentration of the extract and the total disk surface area of 1.84 cm^2 were used to compute leaf Chl concentrations per unit projected area. Total projected leaf areas for computing illuminative, chlorophyll concentration in pine needles were determined by the digital camera and image analysis. Further, significant effects (P = 0.05) of N fertilization on reflectance at each 1 nm wavelength interval were determined by analysis of variance (ANOVA) (SAS 6.0, SAS Institute, Cary, North Carolina, USA). For the senescent leaves of five species, coefficients of determination (R^2) were used to evaluate simple linear relationships of reflectance, transmittance, or absorptance with leaf total chlorophyll concentration at 1.6-nm frequency, wavelength intervals throughout the 400–850 nm moderate resolution spectrum. The reported R^2values were adjusted downward slightly to account for the number of model, elucidatory, parameters and sample size.

Evidence-based targeting of interventions is a crucial component in the fight against seasonal hyperporductivetrailing vegetation, turbid water, capture point, narrow, African

tributary, agro-village complex, discontinuous, infrequently canopied, *S. damnosum* s.l. larval habitat productivity as optimally targeted interventions are more efficient and more cost-effective than untargeted interventions [22]. Environmental onchocerciasis management programs have typically been implemented as "all-out" campaigns, treating all potential breeding habitats. In contrast, targeted environmental management ("Slash and Clear") can be based on a sound understanding of the heterogeneity in immature *Simulium* productivity based on interpolated unmixed, canopy Chl-*a* endemembers.

Further, current deficiencies in cost-effective sampling methodologies in African riverine environments hamper our progress in understanding important wavelength transmittance data, unmixed feature attributes (e.g., seasonal geolocations of hyperproductive, sparsely shaded, trailing vegetation *S. damnosum* s.l. habitat canopy pigments). Thus, implementing village-level, control interventions has been problematic. Three factors that make the implementation of village-level, cost-effective onchocerciasis surveillance programs in an African, narrow tributary, agro-village complex a logistical challenge are: 1) magnitude of geoclassified trailing vegetation *S. damnosum* s.l. black fly populations based on biting rates within a single village; 2) the short seasonal duration for endemic transmission; and, 3) limited historical databases of georeferenced, village-level data [22]. This underscores the need to develop new strategies for implementing village-level, forecastable, cost effective, risk mapping of onchocerciasis-endemic distributions in African, narrow riverine, tributary environments.

A note on the terminology that is used here is worthwhile. We distinguish between three grades of detector optimality: optimal RapidEye 5m spatial resolution, detectors maximize, without constraint, a direct measure of detector effectiveness (e.g., detection probability corresponding to prescribed false probability); suboptimal detectors also maximize some objective function, but either they only achieve a constrained maximization, or the objective function is only an indirect and imperfect measure of true detector effectiveness; and non-optimal detectors do not maximize any objective function whatsoever. The transformation filters proposed here are suboptimal in two respects: they are constrained to be linear, and they maximize SNR functions that have a strong, but nevertheless only indirect, influence on the RapidEye^{TM} detector effectiveness. The detectors proposed here are optimal in the sense that they were constrained to be univariate rather than free to be multivariate. The classification scheme used here distinguishing between optimal and non-optimal categorized seasonal geolocations of hyperproductive, sparsely shaded, geoclassified, explanatorily interpolative, optimally decomposable, eigenvector endmember, trailing vegetation, *S. damnosum* s.l., riverine, immature, turbid water, habitats in two agro-village, riverine complexes in northern Uganda.

Although truly heuritically optimizable, decomposable, riverine, hyperproductive, sparsely shaded, S. *damnosum* s.l., .discontinuously, discontinuous, infrequently canopied, target detectors for realistic image statistics and manageable image ensemble sizes are theoretically unknown, evaluation of these 5m optimal detectors was not associated with any intractable problems. There have been no studies in literature that have linked remote responses in leaf spectral reflectance, transmittance, or absorbance to ecophysiological, biogeophysical stress factors for identifying and targeting seasonally, hyperproductive, geoclassifiable, trailing vegetation, *S. damnosum* s.l. habitats employing cost-effective, moderate resolution RapidEye^{TM} 5m, data.

The practical translation of spectral cues for application under field conditions at canopy and African regional riverine levels for identying hyperproductive, geo-spatiotemporally, geo-spectrotemporally imaged *S. damnosum* s.l. immature habitats by cost effective remote aerial sensing remains a challenge. To address these issues, we develop a framework of habitat-based intervention ("Slash and Clear") by adoption of a RapidEye™, remote sensing, eco-epidemiological, wavelength, fractionalized, endmember, emissivity algorithmic approach to elucidate mechanisms underlying canopy Chl-*a* concentration retrievals for quantitating sparsely shaded, vegetated LULC, and riverine turbid water components that affect immature *Simulium* productivity. The importance of vigorous, quantitative estimation of this productivity is highlighted in a geospectral, geospatial stochastic interpolator. Since in African riverine ecosystems, sparsely shaded canopied, geo-spatiotemporally, geospectrotemrpoally geosampled *S. damnosum s.l.* georeferenced habitats differ in their capacity of immature production [1,3,4], remotely targeting productive habitats using a proxy, medium resolution, cost-effective, RapidEye ™ 5m, unmixing, Chl-*a*–oriented, algorithmic, interpolated, endmember, NDVI biosignature may be more efficient than mobilizing field-sampling epidemiological teams. Our research objectives were to: 1) create multiple geomorphological, terrain-related, eco-epidemiological maps; 2) generate a RapidEye, NDVI Red Edge, Chl-*a*, wavelength, transmittance, emissivity, frequency risk maps from a georeferenced *S. damnosum s.l.* immature habitat biosignature; 3) digitally segment Chl-*a,* sub-mixel endmember radiance values from the 5m biosignature within an object-based framework; 4) explanatorily interpolate the decomposed Chl-*a* components of the biosignature ; and 5) verify in-field descriptive estimates derived from the interpolator for remotely regressively targeting unknown, un-geosampled, trailing vegetation hyperproductive, canopied, sparsely shaded, *S. damnosum s.l.,* habitats within two eco-epidemiological, riverine agro-village intervention study sites in northern Uganda based on field and remotely geosampled immature count data to implement a Slash and Clear control strategy.

2. Materials and Methods

2.1 Study site description

Uganda officially the Republic of Uganda, is a landlocked country in East Africa. It is bordered to the east by Kenya, to the north by South Sudan, to the west by the Democratic Republic of the Congo, to the south-west by Rwanda, and to the south by Tanzania. The southern part of the country includes a substantial portion of Lake Victoria, shared with Kenya and Tanzania. Uganda is in the African Great Lakes region. Uganda also lies within the Nile basin, and has a varied but generally a modified equatorial climate. he country is located on the East African Plateau, lying mostly between latitudes 4°N and 2°S (a small area is north of 4°), and longitudes 29° and 35°E. It averages about 1,100 metres (3,609 ft) above sea level, sloping very steadily downwards to the Sudanese Plain to the north.

The Apago River is a river of Uganda where each agro-village study site is geolocated I kilometer (km) (Figure 40) from the shoreline. The Apago river forms most of the border between the provinces of Atiak and Gitgum before crossing into Sudan east of the border town of Nimule and joining the White Nile about 10 kilomerers northwest of Nimule. That particular section of the White Nile is known as Bahr el Jebel, the "River of the Mountain", or Mountain Nile. Like most rivers in the region the flow of the Apago is strongly influenced by the season and weather, and is prone to flooding.

This hot, dry, wooded savannah at the study sites is composed mainly of *Combretum* and *Terminalia* shrub and tree species, and tall elephant grass, which has been adversely affected by agricultural activities, fire, clearance for wood and charcoal. Presently however, large blocks of relatively intact habitat remain outside protected

Figure 40. The Apago river study site

2.2 Remote sensing data

RapidEye™ is a constellation of 5m, medium resolution satellites, each offering five spectral bands of information at a cost-effective price of 1.28 USD / kilometre (km), which can provide imagery over relatively large areas (swath of 77 km) and a temporal resolution of 1 day. Each sensor is capable of collecting image data in five distinct bands of the electromagnetic spectrum: Blue (440-510 nm), Green (520-590 nm), Red (630-690 nm), and NIR (760-880 nm) (http://www.satimagingcorp.com/satellite-sensors/other-satellite-sensors/rapideye/). RapidEye also adds a fifth band, the Red-Edge (690-730 nm), to the traditional, multispectral, set of blue, green, red and NIR. The Red Edge is a region in the red-NIR transition zone of reflectance spectrum; it marks the boundary between absorption by Chl in the red visible region, and scattering due to the internal leaf structure in the NIR region [23]. This way, geo-classifiable, LULC, cellular vegetation structure in an empirical, geosampled dataset of *S. damnosum* s.l. habitat, phosotosynthetic and non-photosynthetic variable (NPV), 5m, transmittance, regressor coefficient values may be regressively quantitated in ArcGIS as each eco-georferenceable, gridded, discontinuous canopy, plant cell could act as an elementary corner, LULC, topographic reflector. Remotely quantitating geo-spectrotemporally unmixed irradiance effects of seasonal, LULC, elucidatively decomposed, fractionalized endmember, topographic, discontinuous, canopy changes in a riverine, trailing vegetation, turbid water, sparsely shaded, seasonally hyperproductive, eco-georeferenced, *S.*

damnosum s.l., immature, capture point, eco-epidemiological, habitat may reveal 40 to 50% reflectance during flooding, which may be captured between 680 nm to 730 nm RapidEye^{TM} wavelength emissivities [1].

A RapidEye polygon 128m × 128m was acquired for the agro-village complex study sites. The RapidEye Basic (1B) products are geometrically corrected to an idealized sensor and satellite model, and band aligned(www.sateliite imaging.com) They are delivered as National Imagery Transmission Format (NITF) files together with Rapid Positioning Capability (RPC) described by rational functions. The horizontal accuracy of Level 1B products is determined by satellite attitude, which is adjusted by pre-marking Ground Control Points during image cataloging, and ephemeris, as well as terrain displacement, since no terrain model is used in the processing of the 1B products (http://www2.flyby.it/images/brochure/rapideye/eng/RE_Product_Specifications_ENG.pdf.) The worldwide RapidEye Ground Control Point database has been mainly populated with GCPs derived from the GeoCover 2000 Landsat mosaic, along with other reference data of higher accuracy to create the available GCPs used during cataloging and processing. Moving into the future, the GCPs created from the GeoCover 2000 mosaic will be replaced with points derived from the GLS 2000 Landsat mosaic. The replacement process with start in areas with the largest deviation between the two datasets. The default accuracy of the Basic product, using GCPs derived from the Landsat mosaic, is 45m CE90 (RMSE 1-D = 21m) or better. In the case where GCPs of better accuracy are available, this accuracy will not exceed 23m CE90 (RMSE 1-D = 11.00m). These geo-location accuracies are valid for imagery collected at Nadir over flat (< 10 slope) terrain.

Over 70% of RapidEye's imagery has a view angle of less than 10°, as the view angle of RapidEye imagery is always less than 20°. The system also has the capability for daily revisits to any point on earth. RapidEye products are collected by a 12-bit imager. During on-ground processing, radiometric corrections are applied and all image data are scaled up to 16 bit dynamic range. The scaling is done with a constant factor that converts the (relative) pixel digital numbers (DNs) from the sensor into values directly related to absolute radiances. The scaling factor was determined pre-launch. However, absolute radiometric calibration for each sensor element of each band is now continually monitored and adjusted, so that the resultant single DN values correspond to 1/100th of a Watt/$m^2sr^{-1}\mu m$.

The focal plane of the RapidEye sensors is comprised of five separate CCD arrays, one for each band. This means that the bands have imaging time differences of up to three seconds for the same point on the ground, with the blue and red bands being the furthest apart in time. During processing, every 1B and L3A product is band co-registered using a DEM to roughly correlate the bands to the reference band (red-edge). A final alignment is then done using an auto-correlation approach between the bands. For areas where the slope is below 10°, the band co-registration should be within 0.2 pixels or less (1-sigma).

The Red Edge band is spectrally located between the Red band and the NIR band without overlap (www.satimagingcorp.com). In a typical spectral response of green vegetation, the Red Edge band covers the portion of the spectrum where LULC reflectance drastically increases from the red portion towards the NIR plateau (http:www// blackbridge.com/rapideye/). The red portion is one of the areas where Chl strongly absorbs light and the NIR is where the leaf cell structure produces a strong reflection [27]. Therefore, we assumed that variations in both the Chl content and the leaf structure from a hyperproductive, eco-georferenceable, trailing vegetation, turbid water, sparsely shaded, ec-

epidemiological, capture point, *S. damnosum* s.l., immature habitat would be reflected in the Red Edge band. We also assumed that the band was able to provide additional information in order to identify canopy health status, and characterize plant cover and abundance, among other features in a riverine environment.

The Order Polygon contained 5 vertices consisting of longitude / latitude (decimal degrees) geographic coordinates using a WGS-84 ellipsoid. The RapidEye data contained 128 km^2 of the land cover in the study sites. The RapidEye imagery was classified using the Iterative Self-Organizing Data Analysis Technique (ISODATA) unsupervised routine in ERDAS *Imagine* v.8.7™ (ERDAS, Inc., Atlanta, Georgia). Unsupervised classifications are commonly employed for the identification of sub-meter, resolution-derived, geoclassified LULC classes associated with prolific vector insect habitats based on geo-spatiotemporal/geo-spectrotemporal, field-geosampled count data [23]. The clearest, cloud-free images available of the contiguous sub-areas of the intervention agro-village riverine tributary, study sites were used to identify land cover and other spatial features associated with the eco-georeferenced *S. damnosum s.l.* habitats.

2.3 Grid-based algorithm

A 1 km^2 digitized matrix was constructed by applying a mathematical algorithm in order to fit the continuous and bounded, narrow tributary, agro-village complex, riverine, immature, habitat surfaces from a field and canopy-geosampled attribute in ArcGIS. Each operationizable, digitized grid cell within the matrix contained an attribute value (i.e., unique identifier), as well as the *S. damnosum s.l.* larval habitat geocoordinates. As such, the descriptive geolocation of each cell was implicitly contained within the ordering of the matrix. GIS grid-based data files consist of columns and rows of uniform cells coded according to eco-georeferenced data values [23]. Multiple data layers were then created using different coded values for the various field and remote geo-spatiotemporally/geo-spectrotemporally geosampled, explanatorial trailing vegetation, eco-georeferenced, turbid water, sparsely shaded, discontinuously canopied, data, feature attributes which were related to the same grid cell. The grid defines geographic space as an array of equally sized square grid points arranged in rows and columns. Each grid point stores a numeric value that represents a geographic attribute (such as elevation or surface slope) for that unit of space. Each grid cell is referenced by its x,y coordinate location(www.esri.com) High-resolution remote sensing data can be used to generate a digitized grid for the random sampling of breeding sites. Integration of the results into a GIS makes it possible to study the relationship between mosquito breeding site availability, vector abundance and land use-land cover change (Ceneter for Disease Control 2010)

Bézier curves were used to represent natural trailing vegetation, turbid water, discontinuous, canopied, sparsely shaded features, Bézier curves are smooth linear transitions between two vertices (www.esr.com). The shape of the curve was defined by th egeo locations of the vertices and additional control points of the narrow tributary, African agro-village complex , capture point, immature habitats.

Given a set of $n+1$control points P_0, P_1, ..., P_n, the corresponding Bézier curve (or Bernstein-Bézier curve) is given by $$\mathbf{C}(t) = \sum_{i=0}^{n} \mathbf{P}_i B_{i,n}(t),$$ where $B_{i,n}(t)$is a Bernstein polynomial and $t \in [0, 1]$. Bézier splines are implemented in the Wolfram Language as BezierCurve[*pts*]. The Bernstein polynomials of degree $n$form a basis for the power polynomials of degree

n.The Bernstein polynomials have a number of useful properties They satisfy symmetry $B_{i,n}(t) = B_{n-i,n}(1-t)$, positivity $B_{i,n}(t) \geq 0$ for $0 \leq t \leq 1$, normalization $\sum_{i=0}^{n} B_{i,n}(t) = 1$, and $B_{i,n}$ with $i \neq 0, n$ has a single unique local maximum of $i^i n^{-n} (n-i)^{n-i} \binom{n}{i}$ occurring at $t = i/n$. The curve is tangent to $\mathbf{P}_1 - \mathbf{P}_0$ and $\mathbf{P}_n - \mathbf{P}_{n-1}$ at the endpointsThe Bézier curve always passes through the first and last control points and lies within the convex hull of the control points.

The convex hull of a set of points S in n dimensions is the intersection of all convex sets containing S. For N points p_1, ..., p_N, the convex hull C is then given by the expression $C = \left\{ \sum_{j=1}^{N} \lambda_j p_j : \lambda_j \geq 0 \text{ for all } j \text{ and } \sum_{j=1}^{N} \lambda_j = 1 \right\}$. Computing the convex hull is a problem in computational geometry. The *indices* of the points specifying the convex hull of a set of points in two dimensions is given by the command ConvexHull[*pts*] in the Wolfram Language package ComputationalGeometry` . Future versions of the Wolfram Language will support three-dimensional convex hulls. A makeshift package for computing three-dimensional convex hulls in the Wolfram Language

The simplest method for scan converting (rasterizing) a Bézier curve is to evaluate it at many closely spaced points and scan convert the approximating sequence of line segment (www.esri.com). The rasterized output looked sufficiently smooth, even though the the points (i.e., discontinuous canopied, trailing vegation, turbid water geo-spectrotemrpoally geosampled capture points) were spaced t far apart. A common adaptive method is recursive subdivision, in which a curve's control points are checked to see if the curve approximates a line segment to within a small tolerance (www.esri.com) . The capture point curve was subdivided parametrically into two segments, $0 \leq t \leq 0.5$ and $0.5 \leq t \leq 1$, and the same procedure was applied recursively to each half.

The polygons were used to define the sampling frame, which was extended to include a 5 km buffer from the external boundary of the eco-epidemiological, agro-village ,centroids (Tale 4). This allowed for multiple interactions enabling retrieval and transformation of the geosampled, *S. damnosum* s.l. immature, habitat, discontinuous canopied parameters efficiently, regardless of spatial dimensionality of the immature habitat canopy.

Table 4. Centroid points in selected riverine communities in selected for the Slash and Clear intervention.

SUB-COUNTY	PARISH	COMMUNITY	COORDINATES	UTM
KOCH GOMA	LII	ADIBUK	N02^{0}23’03.6’’ E032^{0}06’34.5’’	407513 263570
	AGONGA	LAMINLATOO	N02^{0}31’58.1’’ E032^{0}00’54.0’’	390495 279994
	KAL B	GONYCOGO	N02^{0}25’55.0’’ E032^{0}00’25.6’’	389607 268849
	KAL B	AYAGO –NILE CONFLUENCE	N02^{0}22’23.9’’ E031^{0}55’33.5’’	338754 245457

Out of the four villages selected, two villages, (Gonycoyo and Adibuk) were set out as intervention areas (Slash and Clear), and the other two villages (Laminlatoo and Ayago-Nile) were set out as control areas. The first Gonycogo intervention village has 257 households with a population of 1,250 people. Subsistence farming is the major economy activity. The settlement pattern extends up to 500 m closer to the river shores. The second intervention village selected was Adibuk with 269 households and a population of 1,388 people. Economic activity is primarily subsistence farming and fishing. The settlement pattern extends up to 280 meters closer to the river shores.

Laminlatoo (control village) has 287 households with a population of 1,385 people. The economic activities are primarily subsistence farming and fishing. The settlement pattern extends up to 850 meters closer to the river shores. The Ayago /Nile (control village) has 251 households with a population of 1,315 people. The economic activities are subsistence farming and fishing, as well. The settlement pattern extends up to 150 meters closer to the river shores (Figures 41-43).

Figure 41. ArcGIS Euclidean distance measurements between intervention and control villages

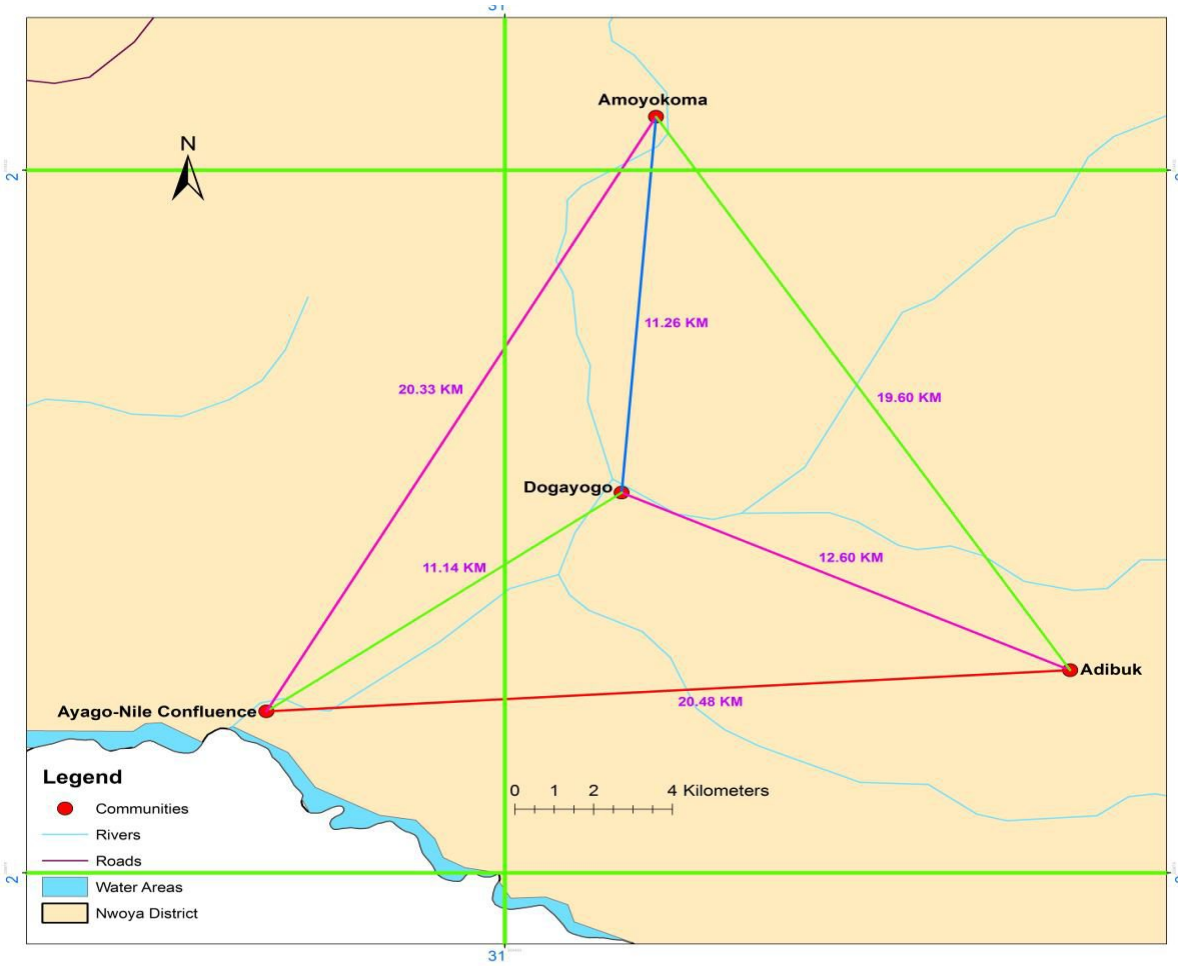

Figure 42. Gongcoyo iuntervention village study site

Figure 43. Residents at the Laminlatoo control village study site

2.4 Baseline and monitoring

Seven days were set out for baseline to establish the average biting rates near *S. damnosum,* immature habitats in all four villages using human landing catches. Intervention was conducted in Gongcoyo and Adibuk Villages, while control monitoring was done in Ayago-Nile and Laminlatoo village study sites. Two cycles of intervention were conducted with the first cycle conducted over two days, after the baseline period. The second cycle of intervention was conducted over two days after ten days from the first cycle. Monitoring of human landing catches continued throughout this period

We established data of Adult *Simulium* Fly Population using human landing catches. Adult *Simulium* fly catching was done by trained volunteers called vector collectors from 7:00am to 6:00pm. During collection, one vector collector would catch flies for one hour while the other stayed away. Collection duty was alternated until the end of the day, and the number of flies captured per hour was recorded in a catching form. The total number was

summarized at the end of each day. Prior to the trials all village resdients were informed of the research. (see Figure 44).Informative meetings were held within each control and intervention village to inform residents of the ongoing trials(Figure 45).

Figure 44. Vector collector capturing adult *Simulium* fly populations using human landing catches at the Goncgoyo village study site

Figure 45. Residents at Adibuk village study site being told of intervention trial activities

2.5 Habitat mapping

Initially, digital base maps were generated using the 5m, RapidEye™ data as well as differentially corrected global positioning systems (DGPS) ground coordinates of a infrequently canopied, discontinuous, partially vegetated, canopy, sparsely shaded, hyperproductive, capture point, *S. damnosum* s.l., narrow tributary agro-village complex, ecosystem riverine, habitat eco-georferenced, geosampled, at the Gonycogo study site village. The DGPS ground coordinates were acquired from a CSI max receiver, which has a positional accuracy of +/- .178 [99]. The purpose of differential GPS (DGPS) is to remove the effects of, atmospheric errors, timing errors, and satellite orbit errors, while enhancing system integrity (http://www.omnistar.com/) Within the DGPS MAX, CSI Wireless has integratedthe CSI Wireless SLX receiver, a tri-purpose GPS / WAAS / L-band receiver, and the CSI Wireless SBX, a high performance DGPS beacon receiverUsing a local DGPS broadcaster can compensate for ionospheric and ephemeris effects which can significantly improve horizontal accuracy and bring altitude error down in a predictive, *S. damnosum* s.l. immature habitat distribution model [127].

Capture point, hyperproductive, *S. damnosum* s.l.,. immature habitat remote attributes were entered into the VCMS™ relational database software product (Clarke Mosquito Control Products, Roselle, IL). The VCMS™ database supports a mobile field data acquisition component module, called Mobile VCMS™,that synchronizes field- geo-spatiotemporally/geo-spectrotemporally geosampled data from industry standard Microsoft Windows Mobile™ devices, and can support add-on DGPS data collection for entomological-related collections [128, 129]. Mobile VCMS™ and its corresponding FieldBridge® middleware software component were used to support both wired and wireless synchronizing of the seasonal, geosampled data collected from the eco-georeferenced trailing vegetation, turbid water, *S.damnosum* s.l. habitat, discontinuous canopy. The data collected with the Mobile VCMS™ was then synchronized directly into a centralized VCMS™ relational repository database.

Thereafter, geocoded spatialized display of the narrow riverine tributary habitat data and geoclassifiable, LULC, feature attributes were mapped employing the embedded VCMS™ GIS Interface Kit™, which was developed utilizing ESRI's MapObjects™ 2 technology. ESRI released MapObjects 2.1, a mapping software. MapObjects' new features include support for AutoCAD 2000 DWG files, ActiveX Data Objects, image catalogs, ArcSDE 8.1 support, data included in ArcView StreetMap for geocoding, custom symbols for chart rendering, and a run-time deployment utility for easier application distribution. (ESRI, Redlands Calif.)VCMS™ included connectivity with hand held computers and field data collection devices including DGPS receivers. PalmOS and Windows PocketPC handhelds have been used for malaria [130], and eastern equine encephalitis virus (EEEV) larval mosquito habitat monitoring [131]. The VCMS™ database supported the export of all the geo-spatiotemporally/geo-spctrotemporally, geosampled parameterized, 5m, wavelength, emissivity, transmittance covariates using any combination of the estimators in order to further process and display specific geocalssified, LULC data, feature attributes in a stand-alone desktop GIS software package (i.e., ArcGIS 10.3®). A polygon layer outlining the georeferenced, hyperproductive, trailing vegetation, turbid water, trailing vegation, hypeporductive, eco-epidemiological, capture point, *S. damnosum* s.l. habitat was then created by digitizing the RapidEye visible and NIR imagery.

2.6 Environmental parameters

Multiple photosynthetic, discontinuous canopy, LULC, wavelength, emissivity, transmittance covariates were examined employing longitude, latitude, and altitude data. The data was also comprised of individual geo-spatiotemporal/geo-spectrotemporal, geosampled, empirical, observations of the eco-georeferenced, hyperproductive, trailing vegetation, narrow, African,riverine tributary, *S. damnosum* s.l. immature, habitat oviposition site together with a battery of categorical canopy attributes (See Table 5). These attributes were generated from fractional vegetation cover, leaf area index, roughness lengths for turbulent transfer, emissivity albedo.

Table 5. Environmental predictor variables geosampled of the *S.damnosum s.l.* habitat

Variable	Description	Units
GCP	Ground control points	Decimal-degrees
FlOW	flowing water	Presence or absence
TURB	Turbidity of water	Formazin Turbidity Unit
AQVEG	Aquatic vegetation	Percentage
HGVEG	Hanging vegetation	Percentage
DDVEG	Dead vegetation	Percentage
MMB	Man-made barriers	Type (e.g.,dams, bridges)

We then constructed a Poisson model in SAS GEN MOD. The Poisson process in our interpretive, analyses was provided by the limit of a binomial distribution of the geosampled district-level predictor, explanatorial, covariate coefficient estimates employing $P_p(n \mid N) = \frac{N!}{n!\,(N-n)!}\, p^n (1-p)^{N-n}$. (2.1). The distribution was viewed as a function of the expected number of immature, *S. damnosum* s.l. habitat, productivity, count variables using the sample size N for quantifying the fixed p in equation (2.1), which was then transformed into the linear equation: $P_{\frac{v}{N}}(n|N) = \frac{N!}{n!(N-n)!}\left(\frac{v}{N}\right)^n \left(1-\frac{v}{N}\right)^{N-n}$. Based on the *S. damnosum* s.l., riverine larval habitat sample size N, the distribution approached $P_v(n)$ was

$$\lim_{n\to\infty} P_p(n|N) = \lim_{N\to\infty} \frac{N(N-1)\cdots(N-n+1)}{n!}\frac{v^n}{N^n}\left(1-\frac{v}{N}\right)^N \left(1-\frac{v}{N}\right)^{-n} = \lim_{N\to\infty} \frac{N(N-1)\cdots(N-n+1)}{N^n}\frac{v^n}{n!}\left(1-\frac{v}{N}\right)^N \left(1-\frac{v}{N}\right)^{-n} = 1\cdot\frac{v^n}{n!}\cdot$$

$$e^{-v}\cdot 1 = \frac{v^n e^{-v}}{n!}.$$

The GENMOD procedure then fit a GLM to the geosampled data by ML estimation of the parameter vector β. The GENMOD procedure estimated the seasonal, geo-sepctrotemrpoally geosampled, explanatively parameterized, Rapid Eye ™ ,5m.LULC

covariates numerically through an iterative fitting algirthmic process. The dispersion parameter was estimated by the residual deviance and by Pearson's chi-square divided by the df. Covariances, standard errors, and *p*-values were then computed for the geo-spectrotemporally geosampled coefficients based on the asymptotic normality derived from the ML estimation.

Note that the sample size *N* completely dropped out of the probability function, which had the same functional form for all the geosampled, parameterized, covariate estimator, indicator values (i.e., v). As expected, the Poisson distribution was normalized so that the sum of probabilities equaled 1. The ratio of probabilities was then determined by $\sum_{n=0}^{\infty} P_v(n) = e^{-v}\sum_{n=0}^{\infty}\frac{v^n}{n!} = e^{-v}e^{v} =$ which was then subsequently expressed as $\frac{P_v(n=i+1)}{P(n=i)} = \frac{\frac{v^{i+1}e^{-v}}{(i+1)!}}{\frac{e^{-v}v^i}{i!}} = \frac{v}{i+1}$.

The Poisson distribution revealed that the explanatory covariate coefficients reached a maximum when $\frac{dP_v(n)}{dn} = \frac{e^{-v}n(\gamma - H_n + \ln v)}{n!} = 0,$ where γ was the Euler-Mascheroni constant and H_n was a harmonic number, leading to the transcendental equation $\gamma - H_n + \ln v = 0,$.

The regression model also revealed that the Euler-Mascheroni constant arose in the integrals as $\gamma = -\int_0^{\infty} e^{-x}\ln x\,dx = -\int_0^1 \ln\ln\left(\frac{1}{x}\right)dx = \int_0^{\infty}\left(\frac{1}{1-e^{-x}} - \frac{1}{x}\right)e^{-x}\,dx = \int_0^{\infty}\frac{1}{x}\left(\frac{1}{1+x} - e^{-x}\right)dx$ .The Euler-Mascheroni constant γ, sometimes also called 'Euler's constant' or 'the Euler constant' (but not to be confused with the constant $e = 2.718281\ldots$) is defined as the limit of the sequence $\gamma = \lim_{n\to\infty}\left(\sum_{k=1}^{n}\frac{1}{k} - \ln n\right) = \lim_{n\to\infty}(H_n - \ln n),$ where H_n is a harmonic number [132]. It was first defined by Euler (1735), who used the letter C, and stated that it was "worthy of serious consideration" [133]. The symbol γ was first used by Mascheroni (1790) [134], where γ has the numerical value $0.57721566490153286060651209008240243104 2\ldots$

2.7 Vegetation Indices

Different modules in ENVI were employed to perform the Red Edge NDVI calculations. The difference between the RapidEye visible and NIR bands was divided by their sum, which formed the functionally equivalent NDVI, over the discontinuous canopy and terrestrial surfaces of the hyperproductive, *S. damnosum* s.l., larval habitat geosampled, at the Gonycoyo interventional study site

The RedEdge NDVI was computed directly without any bias or assumptions regarding plant physiognomy, discontinuous, fractionalized, canopy cover, LULC, class, soil type, or climatic conditions, within a range from -1.0 to 1.0, employing the 5m visible and NIR reflectances, (*p*), in ENVI using the expression : $\frac{\rho_{750} - \rho_{705}}{\rho_{750} + \rho_{705}}$. This index is a

modification of the traditional, broadband NDVI. Red edge NDVI differs from other NDVIs by employing bands along the Red Edge, instead of the main absorption and reflectance peaks (http://www.satimagingcorp.com/satellite-sensors/other-satellite-sensors/rapideye/). The red edge is a region in the red-NIR transition zone of vegetation reflectance spectrum and marks the boundary between absorption by chlorophyll in the red visible region, and scattering due to leaf internal structure in the NIR region. This transition zone is in the basis of several vegetation indices like NDVI which is the normalized difference between the reflectance in the red visible (0.6µm) and the NIR (0.8µm) reflectance. Also the red edge position (REP) is used to estimate the chlorophyll content of leaves or over a canopy(www.esri.com). Our assumption was that capitalizing on the sensitivity of the vegetation Red Edge to small LULC changes in discontinuous canopy foliage content, gap fraction, and senescence could geolocate unknown , un-geosampled, trailing vegetation, turbid water, discontinuously canopied, *S. damnosum* s.l. capture points in eco-georeferenceable, narrow riverine tributary,agro-village complexes.. The value of this index ranged from -1.0 to 1.0 (see Figure 46). The common range for the sparsely shaded, hyperproductive, capture point, *S. damnosum* s.l. habitat canopy green vegetation was between 0.2 and 0.9 [22].

Figure 46. RapidEye ™ NDVI for the for study villages for Goma district in northern Uganda

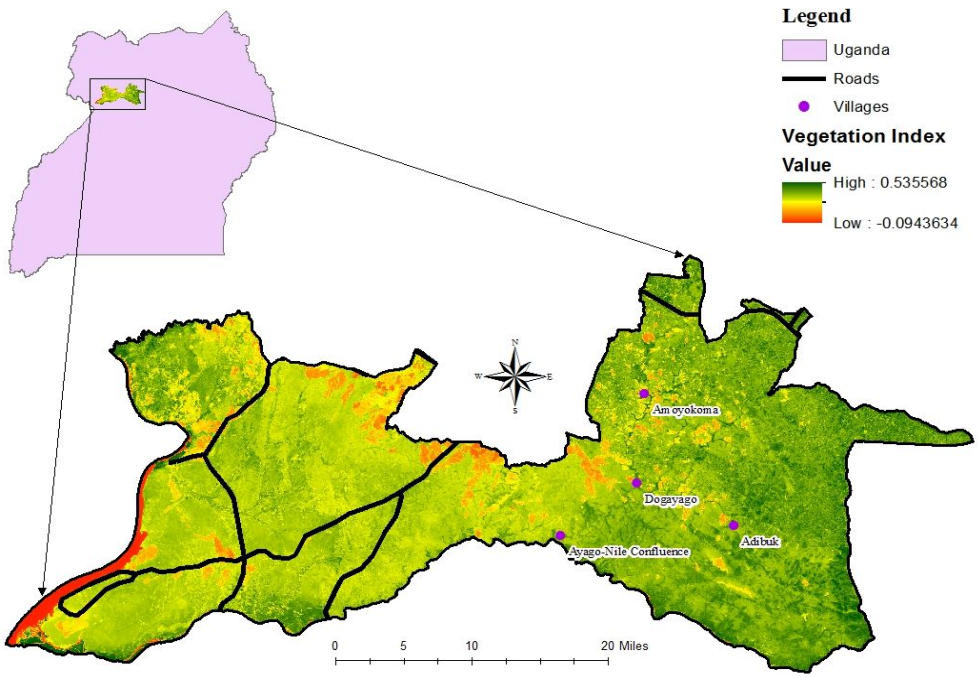

The image was then segmented with a multi-resolution segmentation algorithm employing a fine scale parameter and 4 different weights (from 0 to 100) in ENVI, which were assigned to the Red Edge spectral band to evaluate its influence in the segmentation and LULC classification process. Each reflectance weight generated a segmented 5m image. Eco-

georeferenceable Rapid Eye ™ 5m, wavelength, transmittance, emissivity, frequencies related to geospectral LULC information, geometry and texture were then calculated for each image segment employing the ENVI, which was performed along with field data to select multiple LULC classes (e.g., Dense vegetation,) (Figure 47).

Figure 47. Red Edge NDVI for a hyperproductive *S.damnosum* s.l. larval habitat geosampled at the Gongcoyo study site

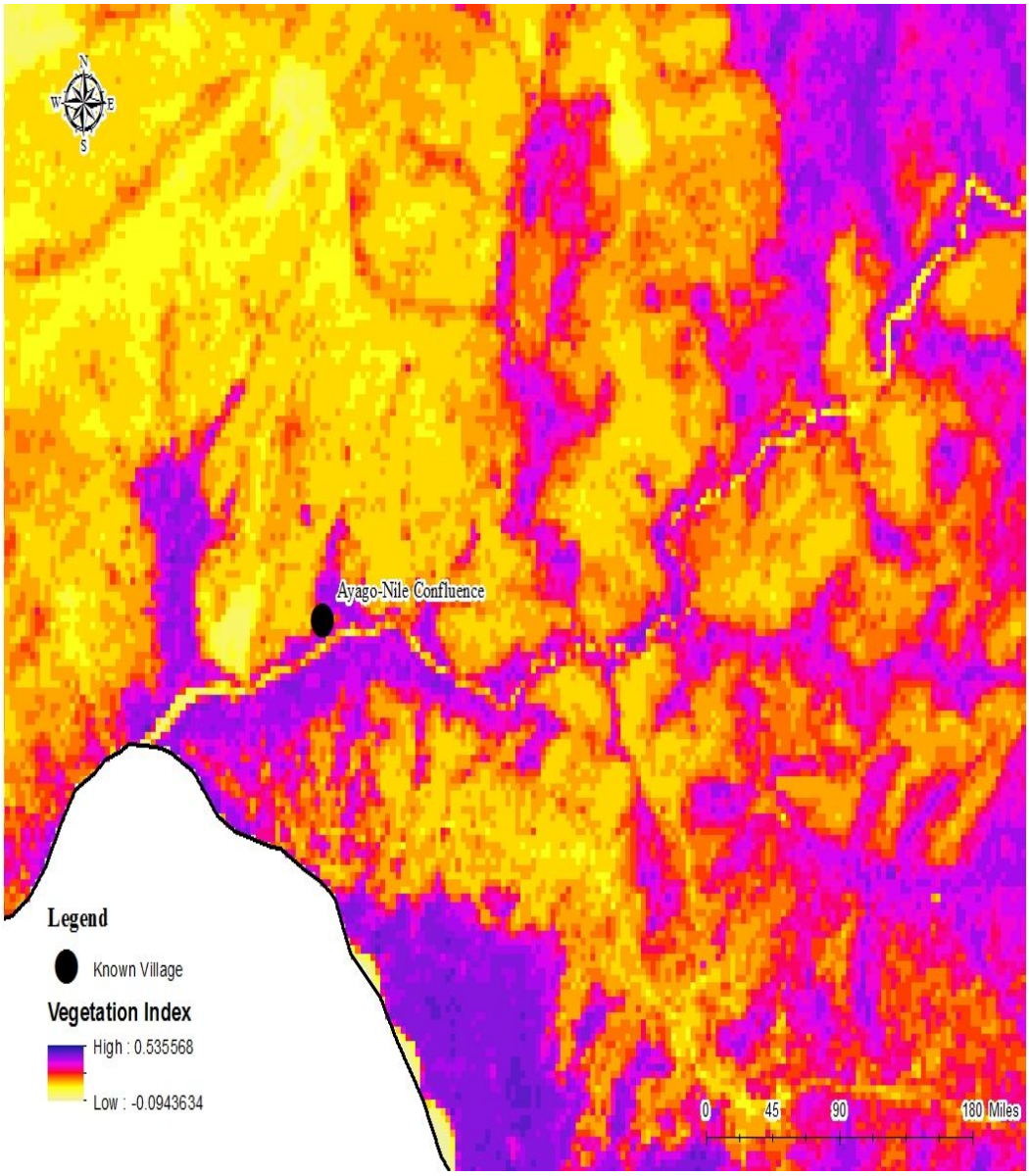

Each weight in the, *S. damnosum* s.l. hyperproductive, eco-epidemiological model generated a segmented 5m image. Data feature attributes related to spectral information, geometry and texture were then calculated for each image segment employing the ENVI which was performed along with field data as to select multiple geoclassified broad LULC classes (e.g.,Grassland) (Figure 48). A decision tree approach was applied to the samples to

select the georefernced attributes that provided the best separation among the classes within the scenes

Figure 48 A LULC accuracy assessment for comparing different weights assigned to the Red Edge spectral band.

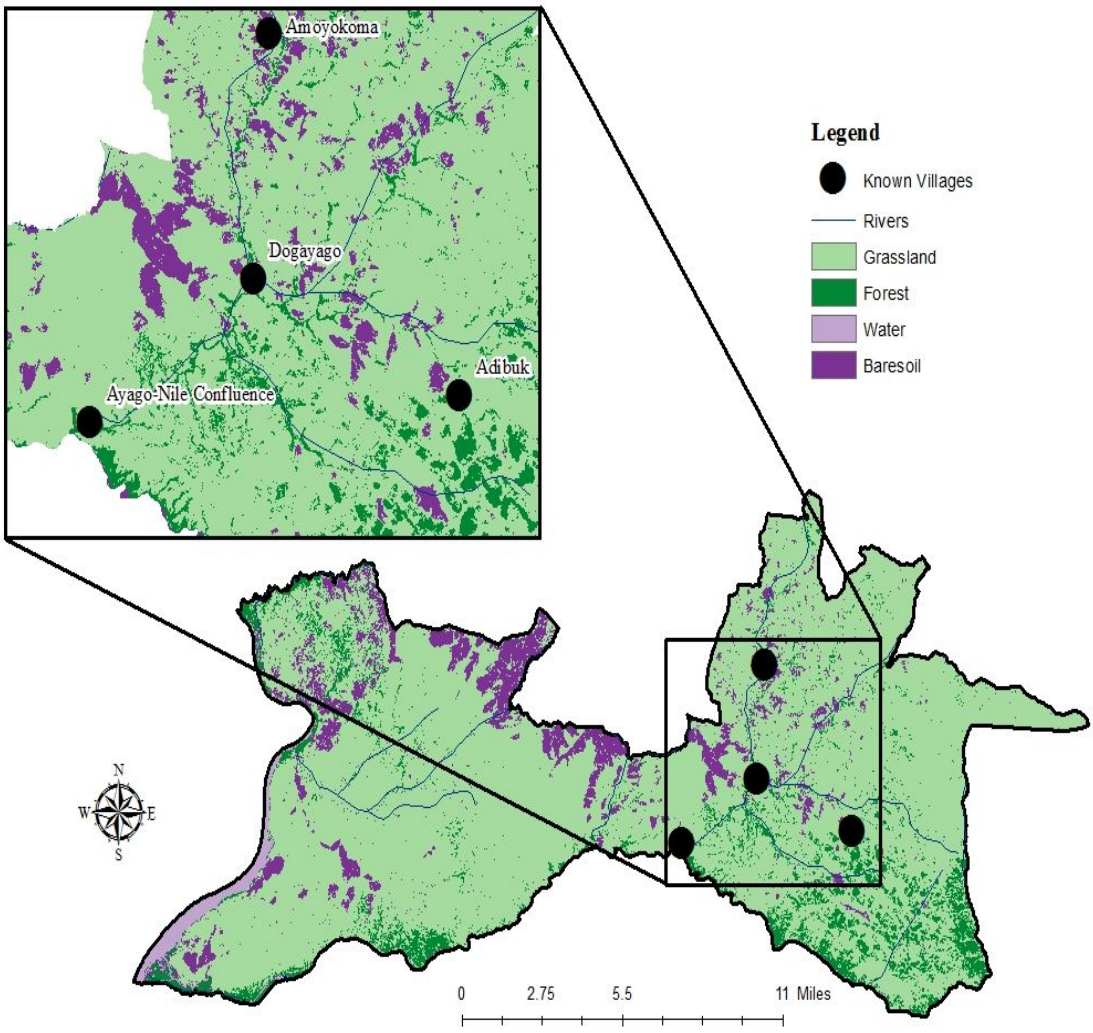

2.8 Spatial Hydrological Model

ArcGIS 10.3 was used to generate a RapidEye^{TM} 3-D,-Digital Elevation Model (DEM) in ArcGIS ecohydrologically representing each geoclassified LULC. A DEM is a raster representation of a continuous surface, usually referencing the surface of the earth [23]. Characteristics of drainage networks and drainage basin, physiographic, parameters have been used in eco-hydrologic calculation and modeling flood and swamp water mosquito abundance in real time, using moderate resolution data [135, 136]. Automated generation of

eco-georferenceable, drainage networks has become increasingly popular with the use of GIS and availability of digital elevation models (DEMs). These models account for topographic variability and their control over soil moisture heterogeneity and runoff within a shed. Patz et al. [137] used a water balance ArcGIS model to hindcast weekly soil moisture levels in the Lake Victoria basin. These soil moisture levels were then associated with local human biting rates and entomologic inoculation rates. Jacob et al. [26] evaluated environmental factors such as elevation range to determine human onchocerciasis risk in a riverine community in Togo. The study site village model yielded several eco-georeferenceable, catchment, biogeophysical, eco-physiologicall variables including percent surface saturation, and total surface runoff for identification of potential productive *S. damnosum* s.l., African. narrow, riverine, tributary, ecogeoreferenced, seasonal hypeproductive,immature habitat, 2-D (Figure 49) and at 3-D, slope coefficients (Figure 50) at the intervention agro-village ecosystem study sites.

Figure 49. A RapidEye 5m 2-dimensional Digital elevation model for the study site

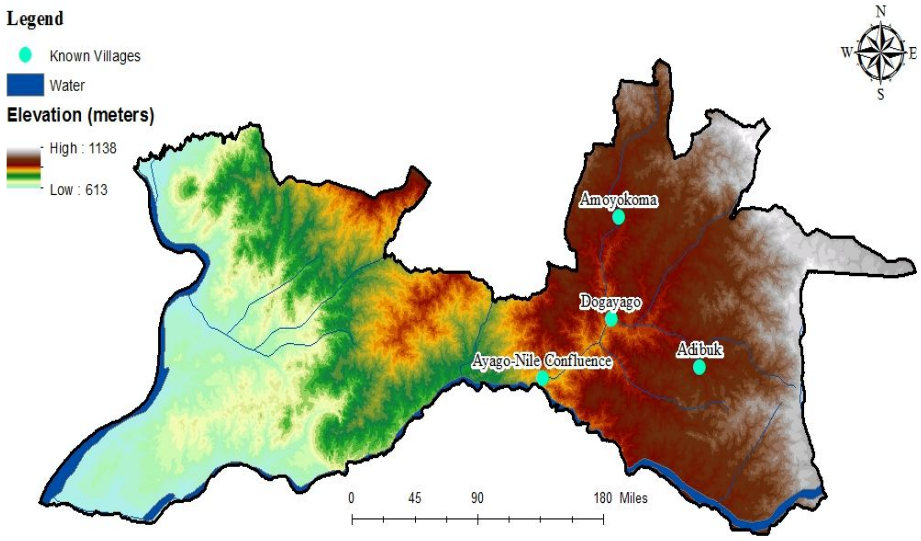

Figure 50. A RapidEye 5m 3-dimensional Digital elevation model for the study site

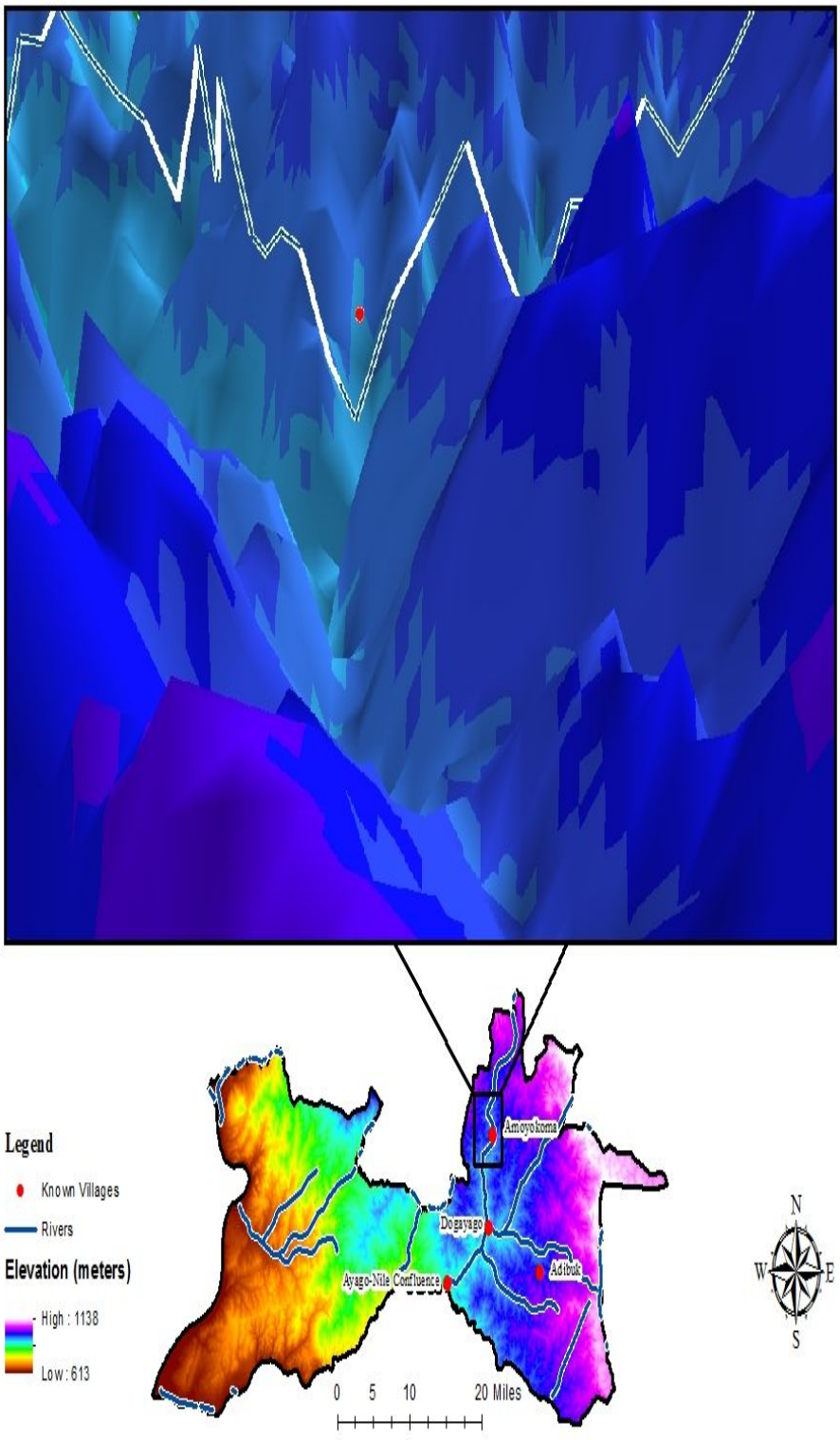

2.9 Object-oriented classification

A 5m mixel-based classification of the *S. damnosum* s.l. habitat was undertaken employing ENVI technology. A standard unsupervised classification was performed using an ISODATA classification system and a maximum likelihood (ML) algorithm respectively. The ISODATA unsupervised classification calculated the class means in the larval habitat, Red Edge, NDVI, 5m biosignature variables evenly distributed in immature habitat, data space, which were then subsequently iteratively clustered. The remaining canopied endmembers were regressively remotely quantitated employing minimum distance techniques. Each iteration recalculated the means and reclassified the 5m sub-mixel data with respect to the new calculated mean values. This process continued until the number of endmembers in each designated immature habitat, endmember class changed by less than the selected mixel change threshold in the object-based classifier.

2.10 The Successive Projection Algorithm (SPA)

The SPA was then employed in ArcGIS to generate a discontinuous, canopy-based, sparsely shaded, trailing vegation, turbid water, Red Edge, trailing vegetation, *S. damnosum* s.l. immature habitat, 5m, NDVI endmember signature. $P(i, j)$ denoted the spectrum for the spectrally extracted 5m mixels using the image coordinates (i, j), as the foundation of the unmixing decomposition algorithm, which was defined by using $\vec{p}_{(i,j)} = \sum_{k=1}^{m} f_{(i,j)k}\vec{e}_k + \vec{\varepsilon}_{(i,j)}$, and $f_{(i,j)k} \geq 0, k = 1, \ldots, m, \sum_{k=1}^{m} f_{(i,j)k} = 1$, where m was the number of the fractionalized,canopy endmembers, $\vec{e}_k$ was the *kth* endmember, $\vec{\varepsilon}_{(i,j)}$ was the approximation error term (i.e., residual), and $f(i\,j)\,k$, was the fractional abundance for the *kth* endmember of 5m mixel (i, j).

The error term in$\vec{p}_{(i,j)} = \sum_{k=1}^{m} f_{(i,j,k}\vec{e}_k + \vec{\varepsilon}_{(i,j)}$ computed the possible linear mixtures from $\vec{p}_{(i,j)} = \sum_{k=1}^{m} f_{(i,j)k}\vec{e}_k + \vec{\varepsilon}_{(i,j)}$ and $f_{(i,j)k} \geq 0, k = 1, \ldots, m, \sum_{k=1}^{m} f_{(i,j)k} = 1$, which formed a simplex *Cm* defined by *m* vertices. These vertices corresponded to the Red Edge, NDVI, decomposed, biosignature endmembers,$\vec{e}_1, \vec{e}_2, \ldots, \vec{e}_m$. According to Jacob et al. [127] the volume of the simplex *Cm* can be calculated from the equation $V(C_m) = \frac{1}{(m-1)!}|\det(WW^T)|^{\frac{1}{2}}$, where $W = [\vec{e}_2 - \vec{e}_1, \vec{e}_3 - \vec{e}_1, \ldots, \vec{e}_n - \vec{e}_1]$ is the volume of the simplex defined by *m* endmembers, and where det(·) denotes the determinant of a matrix representing the operation of an absolute value. Once the *S. damnosum s.l.,* larval habitat, Red Edge NDVI endmembers $\vec{e}_1, \vec{e}_2, \ldots, \vec{e}_m$were quantitated, their fractional abundance was estimated through the least squares method which was equivalent to a projection on the simplex.

2.11 Radiative transfer model

We then focused on the radiation field of the atmosphere and discontinuous canopy as a single coupled medium, and the radiative transfer models of atmosphere and canopy which were separately described because of their different attenuating properties in ArcGIS (see Appendix 5). The coupled mediums illustrated the Red Edge, NDVI, *S. damnosum* s.l. immature eco-georefernced, habitat, decomposed, sub-mixel, endmember biosignature on various equations in which optical depth replaced the geometric altitude values. The top of atmosphere was set to -r = 0 while the bottom was set to Ta, and the total optical depth to Tt. Therefore, the optical depth of the larval habitat canopy was calculated using Tt—Ta, which was interpreted using LAI. This index was calculated employing $P = P_{\max}\left(1 - e^{-cLAI}\right)$, where $P_{\max}$ designated the maximum primary production and c designated a growth coefficient. This inverse exponential function then generated a primary production function.

The bidirectional reflectance function (BRDF) of a RapidEye ™, trailing vegetation, *S. damnosum s.l.* hyperproductive, turbid water, immature habitat, mixel was modeled as the limit of its directional reflectance factor using $R(i,v)$:

$$R(i,v)=\frac{\int\int_A R(s)\langle i,s\rangle\langle v,s\rangle I_i(s)I_v(s)ds}{A\cos\theta_i\theta_v} \quad (2.1)$$

where ds was a small Lambertian (Appendix 6) surface element over area A of the 5m, mixel; $R(s)$ was the reflectance of ds; i, v, and s represented the directions of illumination and viewing based on the LULC, reflectance surface and ripple water, endmember reflectance components, respectively. In the model $\langle .,. \rangle$ was the cosine of the phase angle between two directions; θ was the zenith angle of a direction; $I_i(s)$ and $I_v(s)$ were indicator functions, equal to one when ds was illuminated (I_i) or viewed (I_v) or zero otherwise. If a surface exhibits Lambertian reflectance, light falling on it is scattered such that the apparent brightness of the habitat surface to an observer is the same regardless of the observer's angle of view, thus, the surface luminance is isotropic [23]. Solving our double integral equation revealed s that ds was integrated over the decomposed RapidEye ™ mixel [i.e., the footprint of the sensor's (IFOV)] . There were two kinds of prominent canopied, sparsely shaded, LULC habitat surfaces in the sub-mixel, endmember derivative, fractionalized, derivative spectra. A-background surface (i.e., sporadically canopied rock) and surface ripple water-which were represented by Lambertian reflectance G and C, respectively. We then re-wrote equation (2.1) as

$$R(i,v)=K_gG+\frac{C}{A}\int\int_{A_c}\frac{\langle i,s\rangle}{\cos\theta_i}\frac{\langle v,s\rangle}{\cos\theta_v}ds$$

, where $K_g=A_g/A$ was the proportion of background spectral data illuminated and viewed emitted by the RapidEye™ imaged, *S. damnosum* s.l., riverine, immature habitat, elucidative, feature attributes. In this equation the union of A_g and A_c were the intersection of the dataset of the *S. damnsoum* s.l., habitat, surface elements, which were illuminated and viewed, only when v and i coincided. The directional reflectance of the habitat scene also depended upon the canopied rock and ripple water reflectance related to G and C.

We focused on the two terms of $R(i,v)=K_gG+\frac{C}{A}\int\int_{A_c}\frac{\langle i,s\rangle}{\cos\theta_i}\frac{\langle v,s\rangle}{\cos\theta_v}ds$. The first term described how the sunlit background proportion proceeded to a maximum eco-georeferenced point as viewing and illumination positions in the hemisphere coincided. The second term described how the sunlit geo-spatiotemporally/geo-spectrotemporally, geosampled, eco-epidemiological, ecogeorfernceable, capture point, *S. damnosum* s.l. immature, habitat discontinuous canopy surface, composed of the Lambertian facets, became maximally exposed to view at the hotspot, while those facets on tops became dominant at large viewing zenith angles. The hot spot correlation effect refers to observed brightening which can occur when viewing a scene from the same direction as the solar illumination [138] which for predictive autoregressive, vector, insect habitat, risk modelling is commonly noted in the visible and NIR spectral regions [139].

We analyzed how the first term $K_g G$ varied with illumination and viewing geometry. As in Strahler and Jupp [140], we assumed that the spatial object of interest (i.e., *S. damnosum* s.l. capture point, seasonally hypeporductive, immature habitat) and its canopy-dependent sub-mixel, predictor, covariate coefficient,fractionalized estimates were spheroid in shape, with vertical half-axis equal to b, horizontal radius equal to R, and a height to the center of the spheroid h. To accommodate the spheroidal shape in the derivations of the sparsely shadowed habitat areas, we used the transformation $\theta' = \tan^{-1}\left(\frac{b}{R}\tan\theta\right)$. We solved this equation by replacing θ with the angle that would generate the same shadow area for a sphere. For simplicity, we assumed that the centers of the spheroids were randomly distributed in depth from h_1 to h_2 over A. We then assumed that G and C were constant as average signatures over A_g and A_c for properly modelling K_g and $K_c = A_c/A$.

Next, the equation $R(i,v) = K_g G + \frac{C}{A}\int\int_{A_c}\frac{\langle i,s\rangle}{\cos\theta_i}\frac{\langle v,s\rangle}{\cos\theta_v}ds$ was employed in ArcGIS where K_g was expressed in a Boolean model [i.e., $K_g = e^{-\lambda\pi R^2\left[\sec\theta_i' + \sec\theta_v' - \overline{O}(\theta_i,\theta_v,\phi)\right]}$] where $\overline{O}(\theta_i,\theta_v,\phi,)$ was the average of the time series overlap function [i.e., $O(\theta_i,\theta_v,\phi,h)$] between illumination and viewing shadows of the habitat and its associated, canopied ripple water features. The Boolean model for a random subset of the plane or higher dimensions, analogously is a common tractable model in stochastic geometry. Jacob et al. [128] used a Poisson point process of rate λ in the plane of a decomposed, aquatic, immature habitat of *An. arabiensis,* a major mosquito vector of malaria in the riceland agroecosystem in central Kenya, and then made each sampled point be the center of a random set. The resulting union of overlapping sets was a realization of the Boolean model $\mathcal{B}$. More precisely, the parameters were λ and a probability distribution on compact sets. For each point ξ of the Poisson point process a set C_ξ from the distribution was used, and then defined $\mathcal{B}$ as the union $\cup_\xi(\xi + C_\xi)$of the translated sets. To illustrate tractability with one simple formula, the mean density of $\mathcal{B}$ was defined by a sub-pixel endmember classification, which equalled $1 - \exp(-\lambda\,\mathbf{E}\,\Gamma)$, where Γ denoted the habitat area of C_ξ.

Next, ϕ the difference in azimuth angle between viewing and illumination positions of the RapidEye™ imaged objects associated to the hyperproductive *S. damnsoum s.l.* habitat was quantitated in ArcGIS . To simplify the equation, we approximated the overlap function by the overlap area and center positions of the ellipses. This approximation is justified when solar zenith and viewing zenith angles are not too large [140]. In the case of long ellipsoidal shadows, however, this approximation could have overestimated the width of the habitat hotspot in the azimuthal direction, and underestimated the width of the hotspot in the azimuthal direction. To improve the accuracy and preserve the proper hotspot width information, we developed another approximation as follows. We employed the equations $\phi = 0$ *or* $\phi = \pi$. First, we considered the overlap function in the principal plane. We used W $\phi = 0$ and π as the elliptical illumination estimates and then the viewing shadows were aligned in the same direction. The overlap area was approximated by an ellipse with one axis equal to the overlap length and the other equal to the habitat width encompassing the

decomposed, ripple water pixel spectral components which yielded $O(\theta_i,\theta_v,\phi)=\frac{1}{2}\left[\sec\theta_i'+\sec\theta_v'-\frac{h}{b}\left|\tan\theta_i'-\tan\theta_v'\cos\phi\right|\right]$.

A simulated dataset was also generated using the radiative transfer model, which has been described previously in Jacob et al. [22]. This dataset consisted of the endmember simulated endmeber derivative spectra of the concentration of each single endmember (*i.e.*, NPSS, phytoplankton, CDOM, water), the model-construction dataset, and the model-validation dataset. The latter two datasets include 2483 combinations of these endmembers, which were divided randomly into a construction dataset (204 combinations) and a validation dataset (41 combinations). The input parameters for the radiative transfer model were the inherent optical property (IOP) specification model estimators (e.g., CDOM Fluorescence and Raman Scattering). A solar zenith angle of 30° was employed in the model. Chlorophyll distribution in the canopy vegetation of the habitat, NDVI biosignature was scattered with the lower cover reflecting lesser spectral internsity. In the *S. damnosum* s.l. NDVI biosignature, eco-epidemiological, vulnerability, emissivity, LULC, risk model these changes were reflected in the green peak reflectance (~550 nm) and along the Red Edge (590 to 650 nm). Colored dissolved organic matter (CDOM) absorption was deduced at at a mean of 440 nm for the sites which was subsequently tabulated at 0.30 to 2.10 m^{-1}. Secchi disk transparency ranged from 0.21 to 1.3m. The three-band model was tuned to select the RapidEye^{TM} spectral bands for optimal, Chl-*a,* canopy foliage estimation.

We considered the mixed reflectance spectra $R(\lambda)$ as a linear combination; $R(\lambda) = Cp \times Rp(\lambda) + Cn \times Rn(\lambda) + Cc \times Rc(\lambda) + Cw \times Rw(\lambda)$, where *Cp*, *Cn*, *Cc*, and *Cw* were the decomposition coefficients of CDOM and water, respectively, directly related to their relative masses (e.g., concentrations). $Rp(\lambda)$, $Rn(\lambda)$, $Rc(\lambda)$, and $Rw(\lambda)$ were the standard RapidEye ^{TM} derivative, reflectance spectra for each component. Four decomposition coefficients were calculated (*i.e.*, *Cp*, *Cn*, *Cc*, and *Cw*) by selecting four RapidEye ^{TM} bands .$R(\lambda1) = Cp \times Rp(\lambda1) + Cn \times Rn(\lambda1) + Cc \times Rc(\lambda1) + Cw \times Rw(\lambda1)$; $R(\lambda2) = Cp \times Rp(\lambda2) + Cn \times Rn(\lambda2) + Cc \times Rc(\lambda2) + Cw \times Rw(\lambda2)$, $R(\lambda3) = Cp \times Rp(\lambda3) + Cn \times Rn(\lambda3) + Cc \times Rc(\lambda3) + Cw \times Rw(\lambda3)$ $R(\lambda4) = Cp \times Rp(\lambda4) + Cn \times Rn(\lambda4) + Cc \times Rc(\lambda4) + Cw \times Rw(\lambda)$, which were employed for the geospectral decomposition. Each decomposition coefficient *Cp* was then used as an independent variable in the Chl *a* retrieval model. The algorithm had two component parts based on information about the individual masses of the optically active components and information about spectral properties. Therefore, the estimation model of Chl-a was expressed by $CChla = f(Cp)$

Our results also indicated that the cause of the azimuthal variation could be traced to solar flux illumination of the vertically-oriented, hanging floating and dead endmember, LULC vegetation components and the variation of reflectance moderated by azimuthally isotropic sources of flux from sky light and the habitat, endmember, canopy, reflectance values. Spectral unmixing yielded abundance estimates for each canopy endmember together summing-up to the 100% reflectance measured in the image. A scattergram representing the canopy endmember reference biosignature of the habitat and its associated trailing vegetation mixel spectral endmember reflectance values was generated. The spectral biosignature found to be characteristic of the Red Edge *S. damnosum s.l* larval habitat was shown with a composition of red 134.67, 145.24 blue, and 114.101 green. The images were then analyzed to predict potential *S. damnosum s.l.* larval habitats(see Figure 51).

Figure 51 A geospectrally interpolated Chl-*a* Red Edge canopy, *S. damnsoum s.l.* larval habitat unmixed proxy NDVI endmember signature

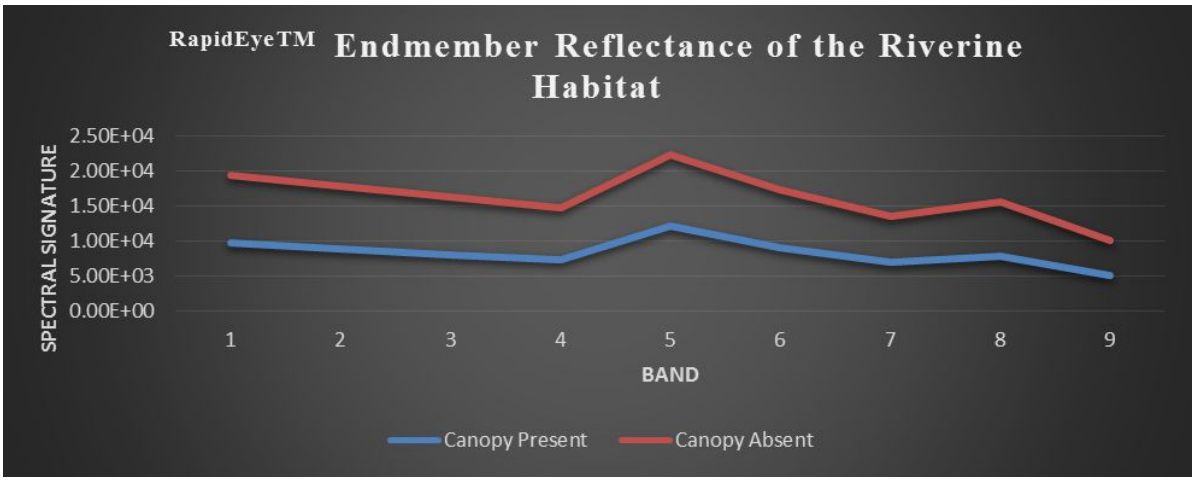

The link between reflectance and endmember concentration at each RapidEye^{TM} wavelength was based on the simulated, derivative, forecast spectra of each habitat, canopied endmember. The ratio of reflectance differentiation was used to maximum reflectance differentiation of each endmember determined the concentration and the standard reflectance Chl-*a* endmember spectrum *Ratio= D*(λ)*/Dmax.*

We then calculated the Sechhi depth for the habitat geosampled at the Gonycogo study site for aiding in quantitating the Chl-*a* endmember concentrations in the canopy. The Secchi depth is reached when the reflectance equals the intensity of light backscattered from the water [23]. This depth was divided into 1.7m yields which we used as the attenuation coefficient (i.e, an extinction coefficient) for the available light averaged over the Secchi disk depth for the canopied habitat. The amount concentration c was then given by a mixture containing two canopy types sparsely shaded and shaded at amount concentrations c_1 and c_2. The attenuation coefficient at any Red Edge wavelength λ was then given by $\mu_{10}(\lambda) = \varepsilon_1(\lambda)c_1 + \varepsilon_2(\lambda)c_2$. Therefore, measurements at two wavelengths yielded two equations in two unknowns which was sufficient to remotely quantiate the amount concentrations c_1 and c_2 as long as the molar attenuation coefficient of the surface habitat reflectance, ε_1 and ε_2 were known at bothwavelengths wavelength, emissivity, sub-mixel components. We solved the equation employing linear least squares to determine the two amounts of canopy Chl-*a* concentrations from measurements made at more than two RapidEye ^{TM} wavelengths. Mixtures containing more than two LULC components can be analyzed in the same way, using a minimum of N wavelengths for a mixture containing N components [23]. The tabulated mixed reflectance and standard reflectance at the same wavelength emissivities was used to determine optimal, endmember, time series, decomposition equations. Four equations at four different wavelengths were employed to determine *Cp*, *Cn*, *Cc*, and *Cw*. The Red Edge bands considered most sensitive to Chl-*a* were tested with the simulated dataset from a spectral range of 490 nm to 730 nm. For Chl-*a* concentrations low reflectance at wavelengths less than 500 nm has been associated to absorption by both algal pigments (e.g., Chl-*a*) and dissolved organic matter [23]. Likewise, an increase in reflectance at wavelengths 510–620 nm has been associated to low absorption by phytoplankton pigments coupled with increased backscattering due to high particle

concentration [141]. The relationship between the decomposition coefficient and Chl-*a* was then determined by using various regression models (M1-M4)(see Table 3).

Table 3. Accuracy evaluation of different spectral decomposition models using Red Edge band-combinations of the simulated model-construction dataset.

Models	RapidEye ™ Bands	Function with Cp	*R*2	RMSE (%)
M1	B,GRR,NIR	$y = 8.72Ca2 - 3.22Cp + 15.3$	0.6147	4.65
M2	B,GR,NIR	$y = 0.13Cp2 - 11.5Cp$ 19.1	0.5750	11.29
M3	BGRR	$y = 0.02Cp2 + 0.88Cp + 26.8$	0.5246	12.93
M4	B,G,NIR	$y = 0.44Cp2 - 10.3Cp + 41.5$	0.4813	13.15

We then used an ordinary kriged-based algorithm in ArcGIS® for predicting *S. damnosum s.l.* riverine larval habitats using the decomposed, Red Edge NDVI reference signature from the study site for geolocating hyperproductive, immature habitats at the study site.Our goal was to estimate a function z(x) based on N *S.damnosum* s.l. immature habitat sampling points [x1 x2….xN]. On the geostatistics classical approach, we supposed that z(x) was a realization of a random function Z(x). This function was also supposed stationary of second order,(i.e. both expectation and covariance functions exist did not depend on x).The interpolation wasperformed, based on an estimate random function *S. damnosum* s.l. habitat sigantrue Z∗(x), defined as a linear combination of the Z(x) , endmeber, wavelength 5m values on the N sampling pointsZ∗(x)=∑i=1Nwi(x)Z(xi).In order to compute the estimate random function Z∗(x), it was necessary to evaluate the wavelength frequency values of all geo-spectrotemporal weight functions wi(x). The random function Z∗(x) must be a good estimator of Z(x), so to evaluate wi(x), two conditions are imposed: 1) the expectation of the error between Z(x) and Z∗(x) must be zero; the error between Z(x) and Z∗(x) must be minimized. With the mean supposed unknown for every x, the first condition allowws us to write∑i=1Nwi(x)=1 for determining unknown, unsampled black fly habitats at the eco-epidemiological, study site African, riverine, tributary, agro-village, study sites. The second condition is equivalent to the minimization of the variance of (Z(x)−Z∗(x)), for every xVar(Z∗(x)−Z(x))=∑i∑jwi(x)wj(x)cov(xi,xj)−2∑iwi(x)cov(xi,x)+cov(x,x).(3)The exponential model was fitted to the semivariogram employing a range of 71.9 m, a nugget of 0.14 (variance), a lag size of 12.7 m with 12 lags, and a partial sill of 0.21 (variance) (see Figure 49). The coordinates of the canopied breeding sites were recorded and the sites visited to ground truth the model predictions.

Figure 49. Kriged endmember Chl-*a* canopy geolocations in Adibuk village

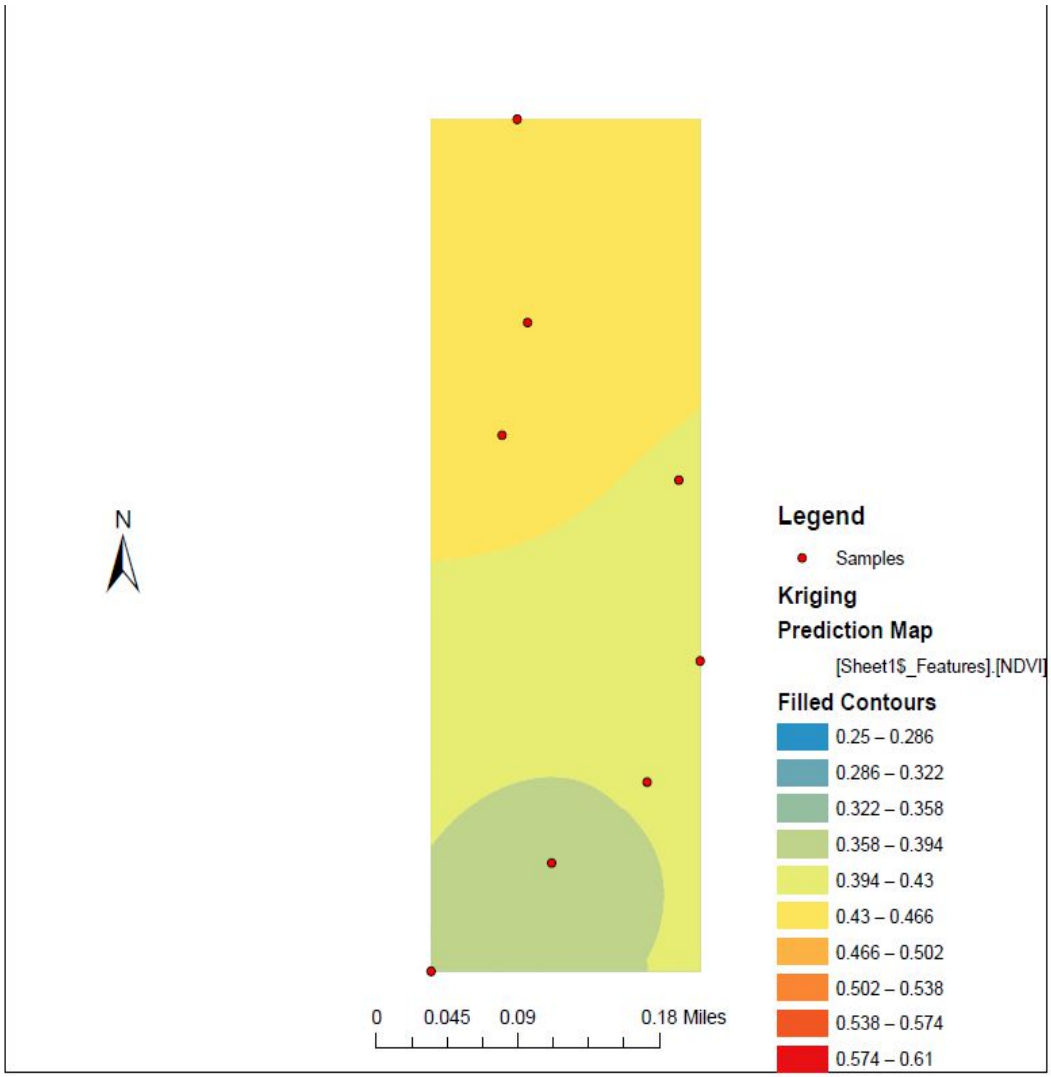

The link between reflectance and endmember concentration at each RapidEye ™ wavelength was based on the simulated derivative, fractionalized spectra of each end-member (NPSS, phytoplankton, CDOM, and water). For each fractionalized, trailing vegetation, hyperproductive, immature, *S. damnosum,* s.l., riverine, explicatively decomposed, iterativlyinterpolated endmember, an increase in concentration brought the 5m reflectance spectra closer to saturation, and accordingly, the unmixed reflectance radiance emittance differentiation would decrease. We employed the ratio of radiance differentiation to maximum reflectance differentiation of each immature habitat unmixed, NDVI biosignature endmember to determine the concentration and the standard discontinously canopied reflectance spectrum $Ratio = D(\lambda)/Dmax.$

Results

Initially, we constructed a Poisson probability regression models in GEN MOD employing the parameterized covariate coefficient measurement values. Our hyperproductive, seasonal, narrow tributuray, agro-village complex, trailing vegetation, turbid water, immature habitat *S. damnosum* s.l. eco-georeferenced, capture point models were generalized by introducing an unobserved heterogeneity term for each geosampled observation *i*. The weights were assumed to differ randomly in a manner that was not fully accounted for by the other parameterized covariates. This process was formulated as $E(y_i \mid x_i, \tau_i) = \mu_i \tau_i = e^{x_i'\beta + \varepsilon_i}$ where the unobserved heterogeneity term $\tau_i = e^{\varepsilon_i}$ was independent of the vector of regressors x_i. The distribution of y_i was conditional on x_i and had a Poisson specification with conditional mean and conditional variance $\mu_i \tau_i : f(y_i \mid x_i, \tau_i) = \frac{\exp(-\mu_i \tau_i)(\mu_i \tau_i)^{y_i}}{y_i!}$. We then let $g(\tau_i)$ be the probability density function (PDF) of τ_i.

In the thecapture point Poission, eco-epidemiological regression models the directed Kullback-Leibler (K-L) divergence between Pois(λ) and Pois(λ_0) was provided by $D_{KL}(\lambda \| \lambda_0) = \lambda_0 - \lambda + \lambda \log \frac{\lambda}{\lambda_0}$. In probability theory and information theory, the K-L divergence along with information divergence, information gain, relative entropy are a non-symmetric measures of the difference between two probability distributions *P* and *Q* in a model [24]. For quantifying the probability distributions *P* and *Q* of a geosampled, discrete, random variable the K–L divergence was defined in the immature habitat, probability model by $D_{KL}(P \| Q) = \sum_i P(i) \ln \frac{P(i)}{Q(i)}$. The model forecasts revealed that the average of the logarithmic difference between the probabilities *P* and *Q* was the average regressively, quantitated, coefficient values employing the probabilities of *P*. The K-L divergence is only defined if *P* and *Q* both sum to 1 and if $Q(i) > 0$ for any *i* such that $P(i) > 0$ [24].

In the immature, *S. damnosum* s.l. capture point, risk models, if the quantity 0 ln 0 appeared in the formula in GEN MOD it was interpreted as zero. For distributions *P* and *Q* of the continuous random variable in the geosampled, time series dependent, trailing vegetation, turbid water datasets K-L divergence was defined to be the integral [i.e., $D_{KL}(P \| Q) = \int_{-\infty}^{\infty} p(x) \ln \frac{p(x)}{q(x)} dx$] where *p* and *q* were denoted by the densities of *P* and *Q*. More generally, since *P* and *Q* were probability measures over the paramterized, immature, habitat, covariate coefficient estimator, regressed dataset *X*, and *Q*, which was absolutely continuous with respect to *P*, when the K-L divergence from *P* to *Q* was defined as $D_{KL}(P \| Q) = -\int_X \ln \frac{dP}{dQ} dP$ and when $\frac{dQ}{dP}$ was the Radon–Nikodym derivative of *Q* with respect to *P,* provided the expression on the right-hand side existed.

In mathematics, the Radon–Nikodym theorem is a result in measure theory that states that given a measurable space (*X*, Σ), if a σ-finite is measured on (*X*, Σ), then the

expression is absolutely continuous with respect to a σ-finite measure μ on (X, Σ). A measurable function f was rendered on X (0, ∞), such that $\nu(A)=\int_A f\,d\mu$ for any forecast, explanatorial, measured value regressed which revealed the statistical significance of the risk model, regressors. Likewise P was absolutely continuous with respect to Q in the regression model. The regressed, RapidEye™, covariate coefficients were then re-defined employing: $D_{KL}(P\parallel Q)=\int_X \ln\frac{dP}{dQ}dP=\int_X \frac{dP}{dQ}\ln\frac{dP}{dQ}dQ$, which was recognized as the entropy of P relative to Q. We found that if μ was any measure on X in the model, then $p=\frac{dP}{d\mu}$ and $q=\frac{dQ}{d\mu}$ existed and the K-L divergence from P to Q, was given as $D_{KL}(P\parallel Q)=\int_X p\ln\frac{p}{q}d\mu$. The bounds for the tail probabilities of the Poisson random variable were then optimally derived in the regression model robustly employing a Chernoff bound argument where $X\sim Pois(\lambda)$ $P(X\geq x)\leq\frac{e^{-\lambda}(e\lambda)^x}{x^x}$, for $x<\lambda$ and where $P(X\geq x)\leq\frac{e^{-\lambda}(e\lambda)^x}{x^x}$ for $x<\lambda$.

In probability theory, the Chernoff bound provides exponentially decreasing bounds on tail distributions of sums of independent randomizable variable [24]. It is a sharper bound than the known first or second moment based tail bounds such as Markov's inequality or Chebyshev inequality, which only yield power-law bounds on tail decay. However, accurately quantitating the Chernoff bound in the trailing vegation, discontinuously canopied, turbid water, eco-epidemiological, capture point, seasonal, hyperproductive, *S. damnosum* s.l. habitat, frequentist-oriented, elucidative,forecasting risk models required that the variates be quantitate independently.

In probability theory, Markov's inequality renders an upper bound for the probability that a non-negative function of a random variable is greater than or equal to some positive constant [142]. We let X_1, ..., X_n be independent Bernoulli random variables, each having probability $p > 1/2$. Then the probability of simultaneous occurrence of more than $n/2$ of the geo- sampling capture point events had an exact value S in the regression model when $S=\sum_{i=\lfloor\frac{n}{2}\rfloor+1}^{n}\binom{n}{i}p^i(1-p)^{n-i}$. The Chernoff bound revealed that S had the following lower bound: $S\geq 1-e^{-2n\left(p-\frac{1}{2}\right)^2}$. We noticed that if X was any elucidatively geo-spectrotemporally geosampled, randomized explanative, variable in the immature, quantitative, capture point, RapidEye ™ models and $a > 0$, then $\Pr(|X|\geq a)\leq\frac{\mathrm{E}(|X|)}{a}$. In the language of measure theory, Markov's inequality states that if (X, Σ, μ) is a measure space, f is a measurable ,extended, real-valued function, and $\epsilon\geq 0$, then $\mu(\{x\in X:|f(x)|\geq\epsilon\})\leq\frac{1}{\epsilon}\int_X|f|\,d\mu$.[http://mathworld.wolfram.com/CauchySequence.html]. We employed the Chebyshev's inequality to determine the variance bound to the probability that the habitat Poisson regression output variables deviated far from the mean in the vulnerability forecasts. Specifically, we employed $\Pr(|X-\mathrm{E}(X)|\geq a)\leq\frac{\mathrm{Var}(X)}{a^2}$, for any $a>0$. Var(X) was the variance of X, defined as: $\mathrm{Var}(X)=\mathrm{E}[(X-\mathrm{E}(X))^2]$. Chebyshev's

inequality follows from Markov's inequality by considering the random variable $(X - \mathrm{E}(X))^2$ for which Markov's inequality also read $\Pr((X - \mathrm{E}(X))^2 \geq a^2) \leq \frac{\mathrm{Var}(X)}{a^2}$.

The density of a discontinuously canopied, trailing vegetation, turbid water, discontinuous, infrequently canopied, narrow tributary, agro-village complex, explanative, *S. damnosum* s.l., oviposition, capture point, random variable was a function that describds the relative likelihood for a random variable Thus, the probability of a habitat, risk model, random variable falling within a particular range of values was given by the integral of this variable's density over that range. That is, it was given by the area under the density function, but above the horizontal axis and between the lowest and greatest values of the range in GEN MOD. The distribution $f(y_i \mid x_i)$ was no longer conditional on τ_i in the model, but was instead obtained by integrating $f(y_i \mid x_i, \tau_i)$ with respect to $g(\tau_i)$: $f(y_i \mid x_i) = \int_0^\infty f(y_i \mid x_i, \tau_i) g(\tau_i)\, d\tau_i$.

It was found that an analytical solution to this integral existed in the Poissonized, risk model, eco-epidemiological, residual, forecasts when τ_i was assumed to follow a gamma distribution. The model forecasts also revealed that y_i, was the vector of the coefficients while x_i, was independently Poisson distributed as $P(Y_i = y_i \mid x_i) = \frac{e^{-\mu_i}\mu_i^{y_i}}{y_i!}, y_i = 0,1,2,...$ and the mean parameter. The mean number of capture points, sampling intervals at each narrow tributary, riverine, agro-village complex, geoclassified LULC site event per sampling period was given by $\mu_i = \exp(x_i'\beta)$ where β was a $(k+1)\times 1$ parameter vector. The intercept in the models was then represented by β_0, and the coefficients for the k regressors were quantitated by $\beta_1, \ldots, \beta_k$. Taking the exponential of $x_i'\beta$ ensured that the mean parameter μ_i was non-negative. Thereafter, the conditional mean was provided by $E(y_i \mid x_i) = \mu_i = \exp(x_i'\beta)$.

A dataset of metaheuristic, explanatorial, *S. damnosum* s.l., optimally parameterizable, covariate estimators were then evaluated using $\ln[E(y_i \mid x_i)] = \ln(\mu_i) = x_i'\beta$. Note, that the conditional variance of the count random variable was equal to the conditional mean (i.e., equi-dispersion) in the eco-epidemiological, risk model function $V(y_i \mid x_i) = E(y_i \mid x_i) = \mu_i$]. In a log-linear model the logarithm of the conditional mean is linear [24]. The marginal effect of any metaheursistically optimizable dataset of explanative, time series dependent, probabilistic regressors in the habitat models estimator was then provided by $\frac{\delta E(y_i \mid x_i)}{\delta x_{ji}} = \exp(x_i'\beta)\beta_j = E(y_i \mid x_i)\beta_j$. It was noted that a one-unit change in the jth regressor in the models led to a proportional change in the conditional mean $E(y_i \mid x_i)$ of β_j.

The standard, Poissonian, trailing vegetation, turbid water, narrow tributary, riverine agro-village, complex, ecosystem, vulnerability, immature habitat, interventional, frequentistic models was the ML estimator. Since the geo-spectrotemporal, geosampled, eco-georferenceable, observations were independent, the log-likelihood function in the

eco-epidemiological, forecasting, risk model was $\sum_{i=1}^{N}\left(-\mu_i+y_i\ln\mu_i-\ln y_i!\right)=\sum_{i=1}^{N}\left(-e^{x_i'\beta}+y_i x_i'\beta-\ln y_i!\right)$. Given the regressor dataset of time series dependent, optimally, metaheursitically parameterized, RapidEye^{TM}, covariate estimators (i.e., θ) and an input vector *x*, the mean of the predicted Poisson distribution was then provided by $E(Y\mid x)=e^{\theta' x}$. The Poisson distribution's mass function in GEN MOD was then rendered by $p(y\mid x;\theta)=\frac{e^{y(\theta' x)}e^{-e^{\theta' x}}}{y!}$.

We found that given the explanatorial, Poissonian process in our capture point, eco-epidemiological vulnerability, forecast models, had a the limit of a count-variable, distribution that was regressively quantitated as $p_p(n\mid N)=\frac{N!}{n!(N-n)!}p^n(1-p)^{N-n}$. (3.1). Viewing the distribution as a function of the expected number of successes [i.e., $\nu\equiv Np$] in the models, instead of the sample size *N* for fixed P, equation (3.1) then became $p_{\nu/N}(n\mid N)=\frac{N!}{n!(N-n)!}\left(\frac{\nu}{N}\right)^n\left(1-\frac{\nu}{N}\right)^{N-n}$. The vulnerability forecasts revealed that as the sample size N became larger, the distribution approached *P* when the following equations aligned $\lim_{N\to\infty}p_p(n\mid N)$

$\lim_{N\to\infty}\frac{N(N-1)\ldots(N-n+1)}{n!}\frac{\nu^n}{N^n}\left(1-\frac{\nu}{N}\right)^N\left(1-\frac{\nu}{N}\right)^{-n}$, $\lim_{N\to\infty}\frac{N(N-1)\ldots(N-n+1)}{N^n}\frac{\nu^n}{n!}\left(1-\frac{\nu}{N}\right)^N\left(1-\frac{\nu}{N}\right)^{-n}$

$1\cdot\frac{\nu^n}{n!}\cdot e^{-\nu}\cdot 1$ and $\frac{\nu^n e^{-\nu}}{n!}$.

Note that the sample size *N* had completely dropped out of the probability function, which had the same functional form for all values of ν in the RapidEye ^{TM} model. Thereafter, as expected, the Poisson regression distribution was normalized so that the sum of probabilities was equal to 1, since $\sum_{n=0}^{\infty}P_\nu(n)=e^{-\nu}\sum_{n=o}^{\infty}\frac{\nu^n}{n!}=e^{-\nu}e^{\nu}=1$. The ratio of probabilities was then provided by the equation $\frac{P_\nu(n=i+1)}{P(n=i)}=\frac{\frac{\nu^{i+1}e^{-\nu}}{(i+1)!}}{\frac{e^{-\nu}\nu^i}{i!}}=\frac{\nu}{i+1}$. The risk model outputs revealed that the Poisson distribution reached a maximum when $\frac{dP_\nu(n)}{dn}=\frac{e^{-\nu}n(\gamma-H_n+\ln\nu)}{n!}=0$, where g was the Euler-Mascheroni constant and H_n was a harmonic number, leading to the equation $\gamma-H_n+\ln\nu=0$ which could not be solved exactly for *n*.

Next, the moment-generating function of the Poissonized, *S. damnosum* s.l,. capture point, distributions was given by $\mathrm{M}=M=e^{-\nu}e^{\nu e^t}=e^{\nu\left(e^t-1\right)}$, when $R=\nu\left(e^t-1\right)$, so $R=R'(0)=\nu$. The raw moments were also computed directly by summation, which yielded

an unexpected connection with the exponential polynomial $\varphi_n(x)$ and Stirling numbers of the second kind [i.e. $\phi_n(x)=\sum_{k=0}^{\infty}\frac{e^{-x}x^k}{k!}k^n=\sum_{k=1}^{n}x^kS(n,k)$], which was the Dobiński's formula.

In mathematics, Stirling numbers arise in a variety of analytic and combinatorics problems [143]. In combinatorial mathematics, Dobinski's formula states that the number of partitions of a set of n members is $\frac{1}{e}\sum_{k=0}^{\infty}\frac{k^n}{k!}$[http://mathworld.wolfram.com/CauchySequence.html].The expression given by the Dobinski's formula in the paradigms was subsequently revealed as the n^{th} moment of the Poisson distribution with expected value 1. Dobinski's formula in the capture point ,eco-epidemological, eco-geoeferenceable, risk models was expressed as the number of partitions of a set of the moderate resolution, wavelength-oriented, transmittance, parameterizable, covariate, capture point, habitat estimator, feature attribute, frequency dataset size (i.e., n), which equalled the n^{th} moment of that distribution. We employed the Pochhammer symbol $(x)_n$ to denote the falling factorial $(x)_n=x(x-1)(x-2)...(x-n+1)$. If x and n are nonnegative integers, $0 \le n \le x$, then $(x)_n$ is the number of one-to-one functions that map a size-n set into a size-x set [24].

At this junction, f was any function from a size-n set A into a size-x set B in the trailing vegatation, turbid water, discontinuously canopied, *S. damnosum* s.l. riverine, tributary, ,vulnerability forecast model. Thus, in the auto-probabilistic, explanative, regression estimates $u \in B$. Thereafter $f^{-1}(u) = \{v \in A : f(v) = u\}$. Then $\{f^{-1}(u) : u \in B\}$ was a partition of A. This equivalence relation was the "kernel" of the function f. Any function from A into B factors into one function that maps a member of A to that part of the kernel to which it belongs, and another function, which is necessarily one-to-one, that maps the kernel into B [23, 24].

The first of these two kernelized factors was completely determined by the partition π in the discontinuously canopied, elucidative, hyperproductive, explanatorial, eco-epidemiological, capture point, *S. damnosum* s.l., riverine, tributary, capture point, forecast, risk model. The number of one-to-one functions from π into B was then $(x)_{|\pi|}$ in the model, when $|\pi|$ was the number of parts in the partition π. Therefore, the total number of functions from a size-n set A into a size-x set B was optimally regressively quantitated as $\sum_{\pi}(x)_{|\pi|}$ in the model time series, forecasts, when the index π ran through the set of all partitions of A. On the other hand, the number of functions from A into B was clearly x^n. Thus, we had $x^n=\sum_{\pi}(x)_{|\pi|}$. Since X was a Poisson-distributed, random variable with an expected value of 1, then the n^{th} moment of this probability distribution was $E\left(X^n\right)=\sum_{\pi}E\left((X)_{|\pi|}\right)$, but all of the factorial moments $E((X)_k)$ of this probability distribution were also equal to 1 in the model forecasts. Additionally the results revealed $E\left(X^n\right)=\sum_{\pi}1$, which was the number of partitions of the set A in the forecasts.

Therefore, the optimizable forecastable, residuals revealed $\nu(1+\nu)$, $\nu(1+3\nu+\nu^2)$, and $\nu(1+7\nu+6\nu^2+\nu^3)$.

Then, the central moments in the *S. damnosum* s.l. oviposition, eco-epidemiological, risk model were computed as $\nu(1+3\nu)$, so that the mean, variance, skewness, and kurtosis were $\frac{\mu_3}{\sigma^3}=\frac{\nu}{\nu^{3/2}}=\nu^{-1/2}$, $\frac{\mu_4}{\sigma^4}-3=\frac{\nu(1+3\nu)}{\nu^2}-3$ and $\frac{\nu+3\nu^2-3\nu^2}{\nu^2}=\nu^{-1}$, respectively. The characteristic function for the Poisson distribution in the habitat model was then revealed as $\phi(t)=e^{\nu(e^{it}-1)}$, where the continuous density function (CDF) was $K(h)=\nu(e^h-1)=\nu\left(h+\frac{1}{2!}h^2+\frac{1}{3!}h^3+...\right)$, so $K_\nu=\nu$.

The mean deviation of the Poisson distribution model was then rendered by $MD=\frac{2e^{-\nu}\nu^{[\nu]+1}}{[\nu]!}$. The CDFs of the Poisson and chi-squared distributions were then related in the risk model as $F_{Poisson}(k;\lambda)=1-F_{x^2}(2\lambda;2(k+1))$ integer *k* and $P_r(X=k)=F_{x^2}(2\lambda;2k)-F_{x^2}(2\lambda;2(k+1))$. The Poisson distribution was expressed in terms of $\lambda\equiv\frac{\nu}{x}$, whereby the rate of changes were equal to the equation $P_\nu(n)=\frac{(\lambda x)^n e^{-\lambda x}}{n!}$. The moment-generating function of the Poisson distribution generated from the trailing vegatation, turbid water, discontinuously canopied, *S. damnosum* s.l. riverine, tributary, elucidative, hyperproductive, explanatorial, eco-epidemiological, capture point, habitat model predictor variables was also rendered by $M(t)=e^{(\nu_1+\nu_2)(e^t-1)}$. Given a random variable x and a PDF $P(x)$, if there exists an $h>0$, such that $M(t)\equiv\langle e^{tx}\rangle$ for $|t|<h$, where $\langle y\rangle$ denotes the expectation value of y, then $M(t)$ is called the moment-generating function [24]. For a continuous distribution in a seasonal, *S. damnosum* s.l. immature habitat, time-series dependent, regression model [e.g., $\int_{-\infty}^{\infty}e^{tx}P(x)dx\int_{-\infty}^{\infty}\left(1+tx+\frac{1}{2!}t^2x^2+...\right)P(x)dx$], the equation $1+tm_1'+\frac{1}{2!}t^2m_2'+...$is is employed in GEN MOD where m_r' the *r* the raw moment [22]. For quantitating independent X and Y, the moment-generating function in a robust, eco-epidemiological, risk model must satisfy the equation $M_{x+y}(t)=\langle e^{t(x+y)}\rangle,\langle e^{tx}e^{ty}\rangle,\langle e^{tx}\rangle\langle e^{ty}\rangle$ and $M_x(t)M_y(t)$, if the independent variables $x_1,x_2,\ldots,x_N$, have Poisson distributions with explanatively parameterizable, geo-predictive, covariate, estimators $\mu_1,\mu_2,\ldots,\mu_N$ and $X=\sum_{j=1}^{N}x_j$ [22]. This was evident in the habitat, regression model, since the cumulant-generating function was $K\equiv\sum_j K_j(h)=(e^h-1)\sum_j\mu_j=\mu((e^h-1)$.

The Euler product $\zeta(s)=\prod_{k=1}^{\infty}\frac{1}{1-\frac{1}{p_k^s}}$ was then considered in GEN MOD, where $\zeta(s)$ was the Riemann zeta function and p_k was the k the prime $\zeta(1)=\infty$. Thereafter, by taking the finite product up to k=n in the habitat, regression model and pre-multiplying by a factor $1/\ln p_n$, we

$$\lim_{n\to\infty}\frac{1}{\ln p_n}\prod_{k=1}^{n}\frac{1}{1-\frac{1}{p_{k=e^\gamma}}}=e^\gamma$$

were able to employ $n\to\infty$ to render , which was equivalent to 1.781072 and 1.836384 in the Gonycogo and Adibuk intervention, narrow tributary, agro-village, complex, study site models respectively.

This way, the Euler-Mascheroni constant also represented the limit of the sequence g = $\gamma=\lim_{n\to\infty}\left(\sum_{k=1}^{n}\frac{1}{k}-\ln n\right)=\lim_{n\to\infty}\left(H_n-\ln n\right)=$ in the regression residuals, where H_n was the harmonic number and had the form $H_n=\sum_{k=1}^{n}\frac{1}{k}$ in the eco-epidemiological models. A harmonic number can be expressed analytically as $H_n=\gamma+\psi_0(n+1)$, where γ is the Euler-Mascheroni constant and $\Psi(x)=\psi_0(x)$ is the digamma function [24]. Both models revealed that the Euler product attached to the Riemann zeta function $\zeta(s)$ represented the sum of the geometric series rendered from the predictor, covariate coefficients as $\prod_p(1-p^{-s})^{-1}=\prod_p\left(\sum_{n=0}^{\infty}p^{-ns}\right)=\sum_{n=1}^{\infty}\frac{1}{n^s}=\zeta(s)$. A closely related result was also obtained by noting that $1+\frac{1}{p_k}=\frac{1-\frac{1}{p_k^2}}{1-\frac{1}{p_k}}$. The variation when the $+$sign changed to a $-$sign and when the $\ln p_n$ in the model appeared helped move the denominator to the numerator rendering

$$\lim_{n\to\infty}\ln p_n\prod_{k=1}^{n}\frac{1}{1+\frac{1}{p_k}}=\lim_{n\to\infty}\ln p_n\prod_{k=1}^{n}\frac{\frac{1}{1-\frac{1}{p_k^2}}}{\frac{1}{1-\frac{1}{p_k}}}=\frac{\prod_{k=1}^{\infty}\frac{1}{1-\frac{1}{p_k^2}}}{\lim_{n\to\infty}\frac{1}{\ln p_n}\prod_{k=1}^{t}\frac{1}{1-\frac{1}{p_k}}}=\frac{\zeta(2)}{e^\gamma}=\frac{\pi^2}{6e^\gamma}=$$

= .736538 and .653431 the in s Gonycogo and Adibuk models,respectively.

The probability density function of a bivariate normal distribution was implemented as MultinormalDistribution[{*mu*1, *mu*2}, {{*sigma*11, *sigma*12}, {*sigma*12, *sigma*22}}] in the Wolfram Language package MultivariateStatistics` . The marginal probabilities of the moderate resolution, *S. damnosum* s.l. parameterizable geo-spectrotemporally geosampled, paramterizable, explanative, time series, covariates were then expressed as

$$P(x_1)=\int_{-\infty}^{\infty}P(x_1,x_2)\,dx_2=\frac{1}{\sigma_1\sqrt{2\pi}}e^{-(x_1-\mu_1)^2/(2\sigma_1^2)}$$ and

$$P(x_2)=\int_{-\infty}^{\infty}P(x_1,x_2)\,dx_1=\frac{1}{\sigma_2\sqrt{2\pi}}e^{-(x_2-\mu_2)^2/(2\sigma_2^2)}$$ We let $Z_1$and Z_2be two independent normal *S. damnosum* s.l., geoclassified, LULC variates with means $\mu_i=0$and $\sigma_i^2=1$for $i=1$, 2. Then

International Journal of Geographic Information System
Vol. 4, No. 1, April 2017, pp.1-519
Available Online at http://acascipub.com/Journals.php

the variables $a_1$and $a_2$were defined employing normal bivariates with unit variance and correlation coefficient ρ where $a_1=\sqrt{\frac{1+\rho}{2}}\,z_1+\sqrt{\frac{1-\rho}{2}}\,z_2$ and $a_2=\sqrt{\frac{1+\rho}{2}}\,z_1-\sqrt{\frac{1-\rho}{2}}\,z_2$.

To derive the bivariate normalized moderate resolution capture point, hypeproductive, *S. damnosum* s.l. probability function,we let $X_1$and X_2be normally and independently distributed variates with mean 0 and variance 1.We then defined $Y_1=\mu_1+\sigma_{11}X_1+\sigma_{12}X_2$and $Y_2=\mu_2+\sigma_{21}X_1+\sigma_{22}X_2$ The variates Y_1 and Y_2 were then themselves normally distributed with means $\mu_1$and μ_2, variances as$\sigma_1^2=\sigma_{11}^2+\sigma_{12}^2$and $\sigma_2^2=\sigma_{21}^2+\sigma_{22}^2$,with covariance $V_{12}=\sigma_{11}\sigma_{21}+\sigma_{12}\sigma_{22}$.

The covariance matrix of the *S. damnosum* s.l. ovipoistion, probabilisc paradigm was defined by $V_{ij}=\begin{bmatrix}\sigma_1^2 & \rho\sigma_1\sigma_2\\ \rho\sigma_1\sigma_2 & \sigma_2^2\end{bmatrix}$,where $\rho\equiv\frac{V_{12}}{\sigma_1\sigma_2}=\frac{\sigma_{11}\sigma_{21}+\sigma_{12}\sigma_{22}}{\sigma_1\sigma_2}$. The joint probability density function for x_1 $f(x_1,x_2)\,dx_1\,dx_2=\frac{1}{2\pi}e^{-(x_1^2+x_2^2)/2}\,dx_1\,dx_2$, was from (◇) and (◇).The forecasts revealed $\begin{bmatrix}y_1-\mu_1\\ y_2-\mu_2\end{bmatrix}=\begin{bmatrix}\sigma_{11} & \sigma_{12}\\ \sigma_{21} & \sigma_{22}\end{bmatrix}\begin{bmatrix}x_1\\ x_2\end{bmatrix}$.as long as $\begin{vmatrix}\sigma_{11} & \sigma_{12}\\ \sigma_{21} & \sigma_{22}\end{vmatrix}\neq 0$,.The matrix was elucidatively nverted which optimally rendered$\begin{bmatrix}x_1\\ x_2\end{bmatrix}=\begin{bmatrix}\sigma_{11} & \sigma_{12}\\ \sigma_{21} & \sigma_{22}\end{bmatrix}^{-1}\begin{bmatrix}y_1-\mu_1\\ y_2-\mu_2\end{bmatrix}=\frac{1}{\sigma_{11}\sigma_{22}-\sigma_{12}\sigma_{21}}\begin{bmatrix}\sigma_{22} & -\sigma_{12}\\ -\sigma_{21} & \sigma_{11}\end{bmatrix}\begin{bmatrix}y_1-\mu_1\\ y_2-\mu_2\end{bmatrix}$.Therefore,

$$x_1^2+x_2^2=\frac{[\sigma_{22}(y_1-\mu_1)-\sigma_{12}(y_2-\mu_2)]^2}{(\sigma_{11}\sigma_{22}-\sigma_{12}\sigma_{21})^2}=+\frac{[-\sigma_{21}(y_1-\mu_1)+\sigma_{11}(y_2-\mu_2)]^2}{(\sigma_{11}\sigma_{22}-\sigma_{12}\sigma_{21})^2},$$ [3.1] Expanding the numerator of Equation 3.1. rendered the

$\sigma_{21}^2(y_1-\mu_1)^2-2\sigma_{11}\sigma_{21}(y_1-\mu_1)(y_2-\mu_2)+\sigma_{11}^2(y_2-\mu_2)^2$

and$\sigma_{22}^2(y_1-\mu_1)^2-2\sigma_{12}\sigma_{22}(y_1-\mu_1)(y_2-\mu_2)+\sigma_{12}^2(y_2-\mu_2)^2+(x_1^2+x_2^2)(\sigma_{11}\sigma_{22}-\sigma_{12}\sigma_{21})^2$

$=(y_1-\mu_1)^2(\sigma_{21}^2+\sigma_{22}^2)-2(y_1-\mu_1)(y_2-\mu_2)(\sigma_{11}\sigma_{21}+\sigma_{12}\sigma_{22})+(y_2-\mu_2)^2(\sigma_{11}^2+\sigma_{12}^2)=$

$\sigma_2^2(y_1-\mu_1)^2-2(y_1-\mu_1)(y_2-\mu_2)(\rho\sigma_1\sigma_2)+\sigma_1^2(y_2-\mu_2)^2$

$=\sigma_1^2\sigma_2^2\left[\frac{(y_1-\mu_1)^2}{\sigma_1^2}-\frac{2\rho(y_1-\mu_1)(y_2-\mu_2)}{\sigma_1\sigma_2}+\frac{(y_2-\mu_2)^2}{\sigma_2^2}\right]$.

Now, the denominator in the trailing vegetation, eco-georeferenced, forecast, vulnerability, narrow riverine tributary, agro-village, partially canpied*S. damnosum* s.l. capture point, model of (◇) was$\sigma_{11}^2\sigma_{21}^2+\sigma_{11}^2\sigma_{22}^2+\sigma_{12}^2\sigma_{21}^2-\sigma_{12}^2\sigma_{22}^2-\sigma_{11}^2\sigma_{21}^2$

$-2\sigma_{11}\sigma_{12}\sigma_{21}\sigma_{22}-\sigma_{12}^2\sigma_{22}^2=(\sigma_{11}\sigma_{22}-\sigma_{12}\sigma_{21})^2$, so $\frac{1}{1-\rho^2}=\frac{1}{1-\frac{V_{12}^2}{\sigma_1^2\sigma_2^2}}=\frac{\sigma_1^2\sigma_2^2}{\sigma_1^2\sigma_2^2-V_{12}^2}=$

$\frac{\sigma_1^2\sigma_2^2}{(\sigma_{11}^2+\sigma_{12}^2)(\sigma_{21}^2+\sigma_{22}^2)-(\sigma_{11}\sigma_{21}+\sigma_{12}\sigma_{22})^2}$ which was written as $\frac{1}{1-\rho^2}=\frac{\sigma_1^2\sigma_2^2}{(\sigma_{11}\sigma_{22}-\sigma_{12}\sigma_{21})^2}$,and

$x_1^2+x_2^2=\frac{1}{1-\rho^2}\left[\frac{(y_1-\mu_1)^2}{\sigma_1^2}-\frac{2\rho(y_1-\mu_1)(y_2-\mu_2)}{\sigma_1\sigma_2}+\frac{(y_2-\mu_2)^2}{\sigma_2^2}\right]$. Solving for $x_1$and $x_2$and defining

$\rho' \equiv \frac{\sigma_1 \sigma_2 \sqrt{1-\rho^2}}{\sigma_{11}\sigma_{22} - \sigma_{12}\sigma_{21}}$ rendered $x_1 = \frac{\sigma_{22}(y_1 - \mu_1) - \sigma_{12}(y_2 - \mu_2)}{\rho'}$ while $x_2 =$ t the Jacobian was

$$J\left(\frac{x_1, x_2}{y_1, y_2}\right) \begin{vmatrix} \frac{\partial x_1}{\partial y_1} & \frac{\partial x_1}{\partial y_2} \\ \frac{\partial x_2}{\partial y_1} & \frac{\partial x_2}{\partial y_2} \end{vmatrix} = \begin{vmatrix} \frac{\sigma_{22}}{\rho'} & -\frac{\sigma_{12}}{\rho'} \\ -\frac{\sigma_{21}}{\rho'} & \frac{\sigma_{11}}{\rho'} \end{vmatrix} = \frac{1}{\rho'^2}(\sigma_{11}\sigma_{22} - \sigma_{12}\sigma_{21}) = \frac{1}{\rho'} = \frac{1}{\sigma_1 \sigma_2 \sqrt{1-\rho^2}},$$

$\frac{-\sigma_{21}(y_1 - \mu_1) + \sigma_{11}(y_2 - \mu_2)}{\rho'}$. $dx_1\, dx_2 = \frac{dy_1\, dy_2}{\sigma_1 \sigma_2 \sqrt{1-\rho^2}}$ so .The predictive equation was

$$\frac{1}{2\pi} e^{-(x_1^2 + x_2^2)/2}\, dx_1\, dx_2 = \frac{1}{2\pi\sigma_1 \sigma_2 \sqrt{1-\rho^2}} \exp\left[-\frac{z}{2(1-\rho^2)}\right] dy_1\, dy_2,$$

where the forecasts were

$z \equiv \frac{(y_1 - \mu_1)^2}{\sigma_1^2} - \frac{2\rho(y_1 - \mu_1)(y_2 - \mu_2)}{\sigma_1 \sigma_2} + \frac{(y_2 - \mu_2)^2}{\sigma_2^2}$. The characteristic function of the bivariate, *S. damnosum,* s.l., oviposition, paramterizable, covariate, normalized distribution was given by

$$\phi(t_1, t_2) = \int_{-\infty}^{\infty}\int_{-\infty}^{\infty} e^{i(t_1 x_1 + t_2 x_2)} P(x_1, x_2)\, dx_1\, dx_2 = N \int_{-\infty}^{\infty}\int_{-\infty}^{\infty} e^{i(t_1 x_1 + t_2 x_2)} \exp\left[-\frac{z}{2(1-\rho^2)}\right] dx_1\, dx_2,$$ wh

ere $z \equiv \left[\frac{(x_1 - \mu_1)^2}{\sigma_1^2} - \frac{2\rho(x_1 - \mu_1)(x_2 - \mu_2)}{\sigma_1 \sigma_2} + \frac{(x_2 - \mu_2)^2}{\sigma_2^2}\right]$ and $N \equiv \frac{1}{2\pi\sigma_1 \sigma_2 \sqrt{1-\rho^2}}$. We let $u = x_1 - \mu_1$ and $w = x_2 - \mu_2$. Then $\phi(t_1, t_2) = N' \int_{-\infty}^{\infty}\left(e^{i t_2 w} \exp\left[-\frac{1}{2(1-\rho^2)}\frac{w^2}{\sigma_2^2}\right]\right)\int_{-\infty}^{\infty} e^{v}\, e^{i t_1 u}\, du\, dw,$

where $v = -\frac{1}{2(1-\rho^2)}\frac{1}{\sigma_1^2}\left[u^2 - \frac{2\rho\sigma_1 w}{\sigma_2} u\right]$ and $N' = \frac{e^{i(t_1 \mu_1 + t_2 \mu_2)}}{2\pi\sigma_1 \sigma_2 \sqrt{1-\rho^2}}$. Completing the square in the inner integral

$$\int_{-\infty}^{\infty} \exp\left\{-\frac{1}{2(1-\rho^2)}\frac{1}{\sigma_1^2}\left[u^2 - \frac{2\rho\sigma_1 w}{\sigma_2} u\right]\right\} e^{i t_1 u}\, du$$

$$= \int_{-\infty}^{\infty} \exp\left\{-\frac{1}{2\sigma_1^2(1-\rho^2)}\left[u - \frac{\rho_1 \sigma_1 w}{\sigma^2}\right]^2\right\}\left\{\frac{1}{2\sigma_1^2(1-\rho^2)}\left(\frac{\rho_1 \sigma_1 w}{\sigma_2}\right)^2\right\} e^{i t_1 u}\, du.$$ Rearranging to bring the exponential

depending on w outside the inner integral, letting $v \equiv u - \rho\frac{\sigma_1 w}{\sigma_2}$, and solving he predictive probaistic model equations lead to $e^{i t_1 u} = \cos(t_1 u) + i \sin(t_1 u)$ which subsequently lead to

$$\phi(t_1, t_2) = N' \int_{-\infty}^{\infty} e^{i t_2 w} \exp\left[-\frac{1}{2\sigma_2^2(1-\rho^2)} w^2\right] \exp\left[\frac{\rho^2}{2\sigma_2^2(1-\rho^2)} w^2\right] \int_{-\infty}^{\infty} \exp\left[-\frac{1}{2\sigma_2^2(1-\rho^2)}\right.$$

Expanding the terms gave

$$\left[\cos(t_1 v)\cos\left(\frac{\rho\sigma_1 w t_1}{\sigma_2}\right) - \sin(t_1 v)\sin\left(\frac{\rho\sigma_1 w}{\sigma_2 t_1}\right)\right] +$$

$$\phi(t_1, t_2) = N' \int_{-\infty}^{\infty} e^{i t_2 w} \exp\left[-\frac{w^2}{2\sigma_2^2}\right] \exp\left[\frac{\rho^2 w^2}{2\sigma_2^2(1-\rho^2)}\right]$$ But $e^{-a x^2} \sin(b x)$i odd, so the integral over the sine term vanishes, and we are left with

International Journal of Geographic Information System
Vol. 4, No. 1, April 2017, pp.1-519
Available Online at http://acascipub.com/Journals.php

We then evaluated the Gaussian integral $\int_{-\infty}^{\infty} e^{ikx} e^{-ax^2} dx = \int_{-\infty}^{\infty} e^{-ax^2} \cos(kx) dx = \sqrt{\frac{\pi}{a}} e^{-k^2/4a}$

to obtain the explicit form of the characteristic function of the *S. damnosum* s.l.,immature, habitat eco-epidemiological, regression model was then quantitated as

$$\phi(t_1, t_2) = \frac{e^{i(t_1 \mu_1 + t_2 \mu_2)}}{2\pi\sigma_1 \sigma_2 \sqrt{1-\rho^2}} \left\{\sigma_2 \sqrt{2\pi} \exp\left[-\frac{1}{4}\left(t_2 + \rho \frac{\sigma_1}{\sigma_2} t_1\right)^2 2\sigma_2^2\right]\right\}$$
$$\left\{\sigma_1 \sqrt{2\pi(1-\rho^2)} \exp\left[-\tfrac{1}{4} t_1^2 2\sigma_1^2 (1-\rho^2)\right]\right\}$$

$$= e^{i(t_1 \mu_1 + t_2 \mu_2)} \exp\left\{-\frac{1}{2}\left[t_2^2 \sigma_2^2 + 2\rho\sigma_1 \sigma_2 t_1 t_2 + \rho^2 \sigma_1^2 t_1^2 + (1-\rho^2)\sigma_1^2 t_1^2\right]\right\} \text{ when } \begin{vmatrix} \sigma_{11} & \sigma_{12} \\ \sigma_{21} & \sigma_{22} \end{vmatrix} = 0$$

The distribution with probability density function and distribution function $P(x) = \frac{a b^a}{x^{a+1}}$ and $D(x) = 1 - \left(\frac{b}{x}\right)^a$ was optimally defineable over the interval $x \geq b$. In an eco-georeferenceable, narrow ,African, riverine tributray, agro-village complex , endmember, hyperproductive, trailing vegetation, discontinuously canopied, seasonal, capture p[oint, *S. damnosum* s.l., ovipoisition, moderate resolution It was implemented in the Wolfram Language as ParetoDistribution[*k*, *alpha*]. The nth raw moment was $\mu_n' = \frac{a b^n}{a-n}$ for $a > n$, giving the first few as $\mu_1' = \frac{a b}{a-1}$, $\mu_2' = \frac{a b^2}{a-2}$, $\mu_3' = \frac{a b^3}{a-3}$ and $\mu_4' = \frac{a b^4}{a-4}$. The nth centralmoment was $\mu_n = a b^n \Gamma(a-n)\, {}_2\tilde{F}_1\left(a-n, -n; 1+a-n; \frac{a}{a-1}\right) = (1-a)^{a-n} (-a)^{n-a} a b^n B\left(\frac{a}{a-1}; a-n, n+1\right)$, for $a > n$ and where $\Gamma(z)$ was a gamma function, ${}_2\tilde{F}_1(a, b; c; z)$ was a regularized hypergeometric function, and $B(z; a, b)$ is a beta function, giving the first few as $\mu_2 = \frac{a b^2}{(a-1)^2 (a-2)}$, $\mu_3 = \frac{2a(a+1)b^3}{(a-1)^3 (a-2)(a-3)}$ and $\mu_4 = \frac{3a(3a^3 + a + 2) b^4}{(a-1)^4 (a-2)(a-3)(a-4)}$.

The beta function $B(p, q)$ is the name used by Legendre and Whittaker and Watson (1990) for the beta integral(also called the Eulerian integral of the first kind). It is defined by $B(p, q) = \frac{\Gamma(p)\Gamma(q)}{\Gamma(p+q)} = \frac{(p-1)!\,(q-1)!}{(p+q-1)!}$.

The beta function $B(a, b)$ was implemented in the Wolfram Language as Beta[*a*, *b*].To derive the integral representation of the beta function in the *S. damnosum* s.l., write the product of two factorials as $m!\, n! = \int_0^{\infty} e^{-u} u^m du \int_0^{\infty} e^{-v} v^n dv$.

Given a hypergeometric or generalized hypergeometric function ${}_pF_q(a_1, \ldots, a_p; b_1, \ldots, b_q; z)$, the corresponding regularized hypergeometric function in a S. damsnoum s.l. moderate resolution, endmember signature , probabilsic, iterative, interpolative, probabilsic paradigm may be optimally defined by ${}_p\tilde{F}_q(a_1, \ldots, a_p; b_1, \ldots, b_q; z) = \frac{{}_pF_q(a_1, \ldots, a_p; b_1, \ldots, b_q; z)}{\Gamma(b_1) \cdots \Gamma(b_q)}$, where $\Gamma(z)$ is a gamma function. Regularized hypergeometric functions are implemented in the Wolfram Languageas the

functions Hypergeometric0F1Regularized[*b*, *z*], Hypergeometric1F1Regularized[*a*, *b*, *z*],Hyp ergeometric2F1Regularized[*a*, *b*, *c*, *z*]. In general, HypergeometricPFQRegularizedare quantitatble by [{*a1*, ...*ap*}, {*b1*, ..., *bq*}, *z*]. The mean, variance, skewness, and kurtosis in the eco-georferenceable.hyeprpoductive, seasaonl, trailing vegegtaion, narrow, riverine, agro-village , tributary, *S. damnosum* s.l., geo-spectrtotemrpoal, forecast, vulnerability, probabilistic, paradigm was the optimally quantized by $\mu = \frac{a\,b}{a-1}$, $\sigma^2 = \frac{a\,b^2}{(a-1)^2\,(a-2)}$, $\gamma_1 = \sqrt{\frac{a-2}{a}}\,\frac{2(a+1)}{a-3}$ and $\gamma_2 = \frac{6\left(a^3+a^2-6a-2\right)}{a(a-3)(a-4)}$.

The trailing vegatation, turbid water, discontinuously canopied, *S. damnosum* s.l. riverine, tributary, elucidative, hyperproductive, explanatorial, eco-epidemiological, capture point, regression models were tested for overdispersion with a likelihood ratio test. This test quantified the equality of the mean and the variance imposed by the Poisson distribution against the alternative that the variance exceeded the mean. For the negative binomial distribution, the variance = mean + k mean^2 (k ≥ 0, the negative binomial distribution reduces to Poisson when k = 0) [24]. The null hypothesis was H_0: k=0 and the alternative hypothesis was H_a : k > 0 . To carry out the test, we employed the following steps initially, and then ran the model using a negative binomial distribution in GEN MOD and a record log-likelihood (LL) value. We then recorded LL for the Gonycogo and Adibuk models. The likelihood ratio (LR) test, computed LR statistic [e.g., -2(LL (Poisson) – LL (negative binomial)] for quantitating statistical significance in the paramterized, covariate estimators geosampled at the eco-epidemiological ,intervention, agro- village study sites. The asymptotic distribution of the LR statistic had probability mass of one half at zero and one half – chi-sq distribution with 1 df. To test the null hypothesis further at the significance level, we employed the critical value of chi-sq distribution corresponding to significance level 2. That is, we rejected H_0 if LR statistic $>^2$ (1-2 , 1 df).

Next, the risk modesl, coefficient estimates were based on the log of the mean, which was a linear function of independent variables, log() = intercept + b1*X1 +b2*X2 + ...+ b3*Xm. This log-transformation implied that was the exponential function of independent variables, equalled exp(intercept + b1*X1 +b2*X2 + ...+ b3*Xm). Instead of assuming as before in the probabilistic Poissonian framework that the distribution of the covariate coefficient estimates (i.e., Y), geo-spectrotemrpoally geosampled in the Gonycogo and Adibuk agro-village complexes were Poisson, a negative binomial distribution was assumed. That is, the generalized Poisson regression specification assumption about the equality of the mean and variance was relaxed, since in the immature habitat, eco-epidemiological, vulnerability, forecasting models found that the variance of negative binomial was equal to + k2 , where k>= 0 was a dispersion parameter. The ML method was then employed to estimate k as well as the covariate estimators of the model for log.

Fortunately, the SAS syntax for running negative binomial regression was almost the same as for Poisson regression. The only change was the dist option in the MODEL statement was employed instead of dist = poisson,dist = nb. The PMF+ of the negative binomial distribution with a gamma distributed, non-homogenous mean in the risk model was then expressed using the explanatively parameterized, covariate estimator, coefficients estimates within $f(k) \equiv \Pr(X=k) = \binom{k+r-1}{k}(1-p)^r p^k$ for the independent variables $k = 0, 1, 2, \ldots$. The quantity in parentheses was the binomial coefficient, which was equal to

$\binom{k+r-1}{k} = \frac{(k+r-1)!}{k!\,(r-1)!} = \frac{(k+r-1)(k+r-2)\cdots(r)}{k!}$. This quantity was alternatively written as $\frac{(k+r-1)\ldots(r)}{k!} = (-1)^k \frac{(-r)(-r-1)(-r-2)\ldots(-r-k+1)}{k!} = (-1)^k \binom{-r}{k}$ in GEN MOD for explaining "negative binomialness" in the hyperproductive habitat, regression models, Results from both a Poisson and a negative binomial model residually forecasted dataset of explanators revealed that the some model residual estimates were highly significant (e.g., Presence of eco-georeferenceable, sparsely shaded, trailing vegetation-relatedgeo-predictors) in the Gonycogo and Adibuk narrow tributary, agro-village complex study sites. All the data was then exported into PROC MCMC.

In PROC MCMC, a Bayesian estimation paradigm $q(\theta_{new}|\theta^t)$ revealed a symmetric distribution employing the the eco-epidemiological, eco-georefernceable, forecasting, Gonycogo and Adibuk vulnearbility risk models. It was noted that the proposal distribution was an easy distribution from which to sample. Subsequently,the variables were optimally, regressively qualitatively, remotely quantitated by $q(\theta_{new}|\theta^t) = q(\theta^t|\theta_{new})$. In doing so, the likelihood of jumping to θ_{new} from θ' was the same as the likelihood of jumping back to θ^t from θ_{new}.

The most common choice of the proposal distribution is the normal distribution $N(\theta^t, \sigma)$ with a fixed σ [142]. The Metropolis algorithm in the explanative, geospatial, Bayesianistic, residual model outpust was summarized for optimally quantitating a parameterizable, captyre point, *S. damnosum* s.l. habitat, parameterizable, covariate, estimator, metaheursitically optimizable, radiance dataset by solving $t = 0$. Choose a starting arbitrary habitat, geosampled point (e.g., θ^0) was easy since $f(\theta^0|y) > 0$. A new sample, θ_{new} was generated, by employing the proposal distribution $q(\cdot|\theta^t)$. The following quantity: $r = \min\left\{\frac{f(\theta_{new}|y)}{f(\theta^t|y)}, 1\right\}$ was calculated. u from the uniform distribution $[U(0,1)]$ was calculated We set $\theta^{t+1} = \theta_{new}$, if $u < r$; otherwise we set $\theta^{t+1} = \theta^t$. Thereafter, $t = t + 1$. It was noted that when $t < T$, the number of iterations kept increasing regardless of whether a proposed sample was accepted in the *S. damnosum* s.l. model. This non-frequentist algorithm defined a chain of random variates whose distribution converged to the desired distribution (i.e., $f(\theta|y)$). The chain of samples is a sample from the distribution of insterest [24]. In Markov chain terminology, this distribution is called the stationary distribution of the chain, and in Bayesian statistics, it is the posterior distribution of the model, parameterized, residually regressed, time series, covariate estimators [24]. The reason that the Metropolis algorithm works is beyond the scope of this documentation, but proofs occur in many standard textbooks, [144, 145] In. Bayesian inference, the beta distribution is the conjugate prior probability distribution for the Bernoulli, binomial, negative binomial and geometric distributions[2]. We employed the beta distribution in the Bayesian analysis to describe initial knowledge concerning probability of success such as the probability that a space will successfully be a specified hyperproductive seasonal trailing vegation, discontinuoulsy canopied, turbid water, *S. damnsoum* s.l. immature capture point, eco-georferenceable habitat. The beta distribution is a suitable model for the random behavior of percentages and proportion[24]s.

Bayesian inference is a method of statistical inference in which Bayes' theorem is used to update the probability for a hypothesis as more evidence or information becomes available[25] . The prior distribution in the *S. damnsoum* s.l. habitat model was easily determined. As such we employed the Jeffreys prior to obtain the posterior distribution before updating them with newer habitat observations. In Bayesian probability, the Jeffreys prior, is a non-informative (objective) prior distribution for a parameter space; it is proportional to the square root of the determinant of the Fisher information[24]. In mathematical statistics, the Fisher information (sometimes simply called informationis a way of measuring the amount of information that an observable random variable X carries about an unknown parameter θ of a distribution that models X. [http://mathworld.wolfram.com]Formally, it is the variance of the score, or the expected value of the observed information. In The *S. damnsoum* s.l. model statistics, the asymptotic distribution of the posterior mode was dependsent on the Fisher information and not on the prior .

The PDF of the beta distribution, for $0 \le x \le 1$, and shape parameters $\alpha, \beta > 0$, was a power function of the eco-epidemiological, eco-georeferenceable, immature habitat, capture point variabled x and of its 5m Rapid Eye ™ reflection $(1-x)$ were quantiated in Calculus Methode/Map Server ™ as follows:

$$\begin{aligned} f(x;\alpha,\beta) &= \text{constant} \cdot x^{\alpha-1}(1-x)^{\beta-1} \\ &= \frac{x^{\alpha-1}(1-x)^{\beta-1}}{\int_0^1 u^{\alpha-1}(1-u)^{\beta-1}\,du} \\ &= \frac{\Gamma(\alpha+\beta)}{\Gamma(\alpha)\Gamma(\beta)} x^{\alpha-1}(1-x)^{\beta-1} \\ &= \frac{1}{\mathrm{B}(\alpha,\beta)} x^{\alpha-1}(1-x)^{\beta-1} \end{aligned}$$

where $\Gamma(z)$ eas the gamma function. The beta function, B, was a normalization constant to ensure that the total probability integrated to 1. In the above equations x was a realization—an observed value that actually occurred—of a random process X. The cumulative distribution function (CDF) was $F(x;\alpha,\beta) = \frac{\mathrm{B}(x;\alpha,\beta)}{\mathrm{B}(\alpha,\beta)} = I_x(\alpha,\beta)$ where $\mathrm{B}(x;\alpha,\beta)$ was the incomplete beta function and

$I_x(\alpha,\beta)$ is the regularized incomplete beta functions (see Figure 50).

Figure 50. The CDF for a symeteric Beta Distribution of the geosampled *S. damnsoum* s.l. capture point, autoregressive variables at the Adibuk intervention village

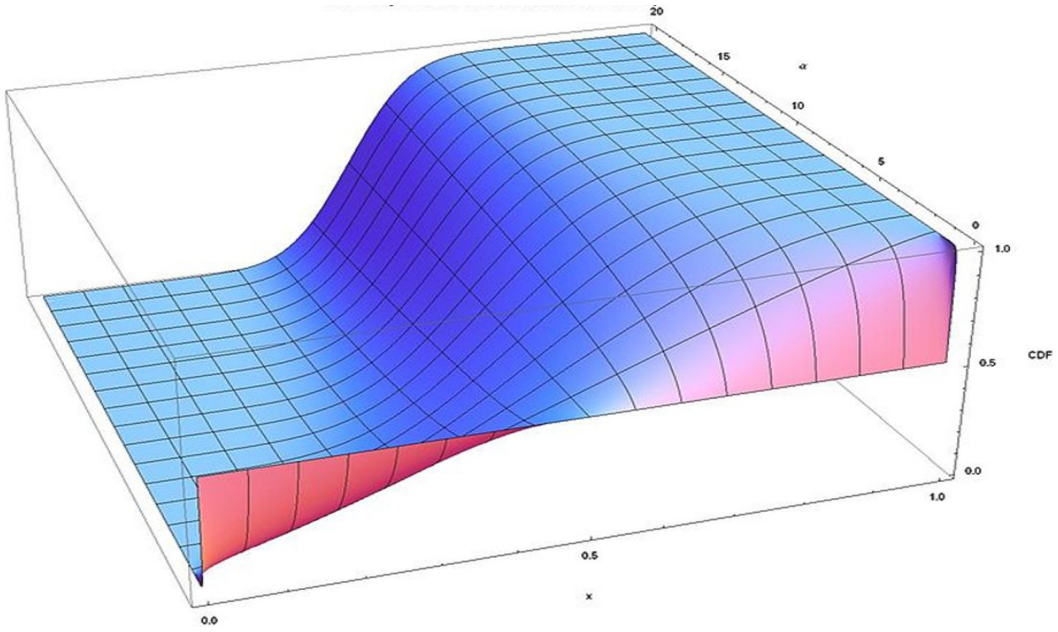

We employed $\ln G_X = \mathrm{E}[\ln X]$ Calculus Methode/Map Server ™ for quantiating the beta distribution of the eco-georeferenecable, explanative, trailing vegation, discontinuoulsy canopied, turbid water, explicative capture points, expected value integral which was computed as :

$$
\begin{aligned}
\mathrm{E}[\ln X] &= \int_0^1 \ln x \, f(x;\alpha,\beta)\, dx \\
&= \int_0^1 \ln x \, \frac{x^{\alpha-1}(1-x)^{\beta-1}}{\mathrm{B}(\alpha,\beta)}\, dx \\
&= \frac{1}{\mathrm{B}(\alpha,\beta)} \int_0^1 \frac{\partial x^{\alpha-1}(1-x)^{\beta-1}}{\partial \alpha}\, dx \\
&= \frac{1}{\mathrm{B}(\alpha,\beta)} \frac{\partial}{\partial \alpha} \int_0^1 x^{\alpha-1}(1-x)^{\beta-1}\, dx \\
&= \frac{1}{\mathrm{B}(\alpha,\beta)} \frac{\partial \mathrm{B}(\alpha,\beta)}{\partial \alpha} \\
&= \frac{\partial \ln \mathrm{B}(\alpha,\beta)}{\partial \alpha} \\
&= \frac{\partial \ln \Gamma(\alpha)}{\partial \alpha} - \frac{\partial \ln \Gamma(\alpha+\beta)}{\partial \alpha} \\
&= \psi(\alpha) - \psi(\alpha+\beta)
\end{aligned}
$$

where ψ was the digamma function. In mathematics, the digamma function is defined as the logarithmic derivative of the gamma function: $\psi(x) = \frac{d}{dx}\ln\left(\Gamma(x)\right) = \frac{\Gamma'(x)}{\Gamma(x)}$. It is the first of the polygamma functions in the Gonycogo and Adibuk models(see Figure 51). Because of this ambiguity, two different notations are sometimes (but not always) used, with $\Psi(z) \equiv \frac{d}{dz}\ln\Gamma(z) = \frac{\Gamma'(z)}{\Gamma(z)}$ defined as the logarithmic derivative of the gamma function $\Gamma(z)$, and $F(z) \equiv \frac{d}{dz}\ln z!$ defined as the logarithmic derivative of the factorial function[25]. The two were connected in the *S. damnosum* s.l. habitat model by the relationship $F(z) = \Psi(z+1)$. The nth derivative of $\Psi(z)$ is called the polygamma function, denoted $\psi_n(z)$. The notation $\psi_0(z) \equiv \Psi(z)$ is therefore frequently used for the digamma function itself, and Erdélyi *et al.* (1981) use the notation $\psi(z)$ for $\Psi(z)$. The digamma function $\psi_0(z)$ is returned by the function PolyGamma[z] or PolyGamma[0, z] in the Wolfram Language, and typeset using the notation $\psi^{(0)}(z)$ (http://mathworld.wolfram.com/).

51 Graph of the *S. damnosum* s.l. habitat capture point polygamma functions ψ, ψ1, ψ2

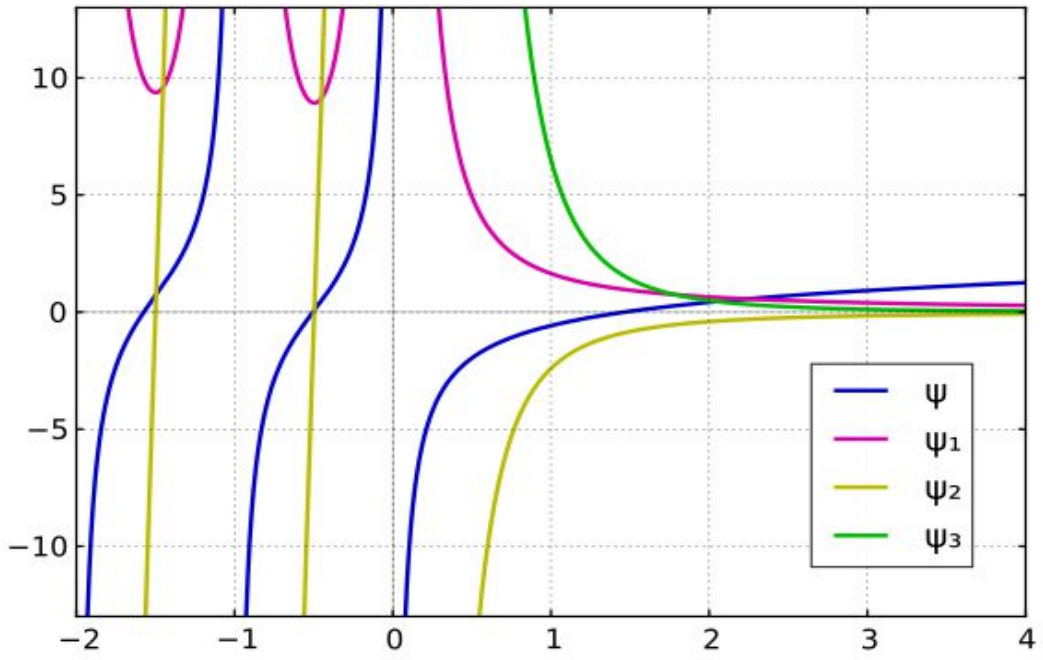

Figure 52 The logarithm of the gamma function and the a capture point, *S. damnosum* s.l. habitat polygamma functions where $\ln \Gamma(z)$ was the rainy season, $\psi^{(0)}(z)$ was the dry season, and $\psi^{(1)}(z)$ was the pre-flooded sample frame for the Gonycogo agro-village study site

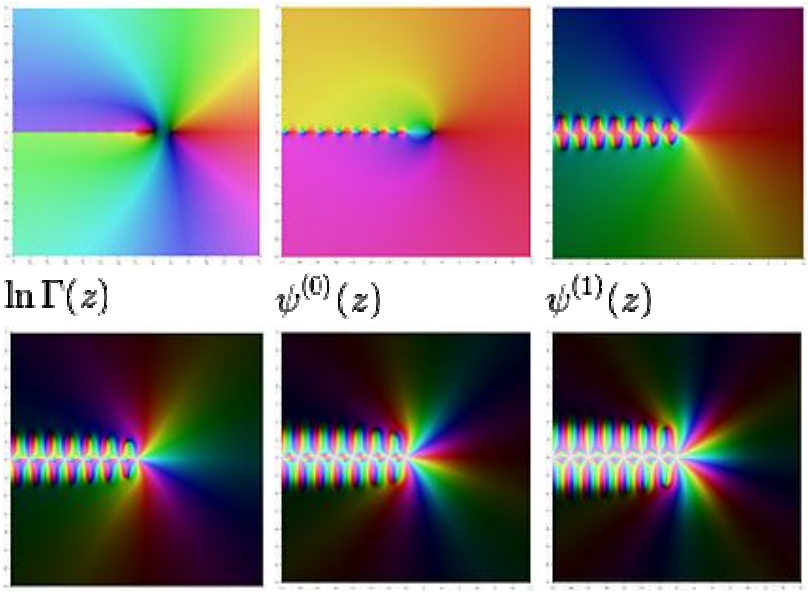

The geometric mean of the *S. damnsoum* s.l. habitat epidemiological, dataset $\{a_1, a_2, \cdots, a_n\}$was given by: $\left(\prod_{i=1}^{n} a_i\right)^{1/n} = \sqrt[n]{a_1 a_2 \cdots a_n}$. By using logarithmic identities to transform the formula in Calculus Methode/Map Server ™ the multiplications was n expressed as a sum and the power as: $\left(\prod_{i=1}^{n} a_i\right)^{1/n} = \exp\left[\frac{1}{n}\sum_{i=1}^{n} \ln a_i\right]$ (see Figure 52). This is sometimes called the log-average (not to be confused with the logarithmic average). It is simply computing the arithmetic mean of the logarithm-transformed values of a_i(i.e., the arithmetic mean on the log scale) and then using the exponentiation to return the computation to the original scale, (i.e., it is the generalised f-mean with $f(x) = \log x$)as all members of the dataset are equal, in which case the geometric and arithmetic means are equal In mathematics, the inequality of arithmetic and geometric means, or more briefly the AM–GM inequality, states that the arithmetic mean of a list of non-negative real numbers is greater than or equal to the geometric mean of the same list; and further, that the two means are equal if and only if every number in the list is the same. There are several ways to prove the AM–GM inequality; for example, it can be inferred from Jensen's inequality, using the concave function ln(*x*). In mathematics, Jensen's inequalityrelates the value of a convex function of an integral to the integral of the convex function[26].

Figure 52 Geometric means for *S. damnsoum* s.l.capture poiunt geospectral Beta distribution where Purple = *G*(*x*), Yellow = *G*(1−*x*), smaller values alpha and beta in front for the Adibuk agro-village complex

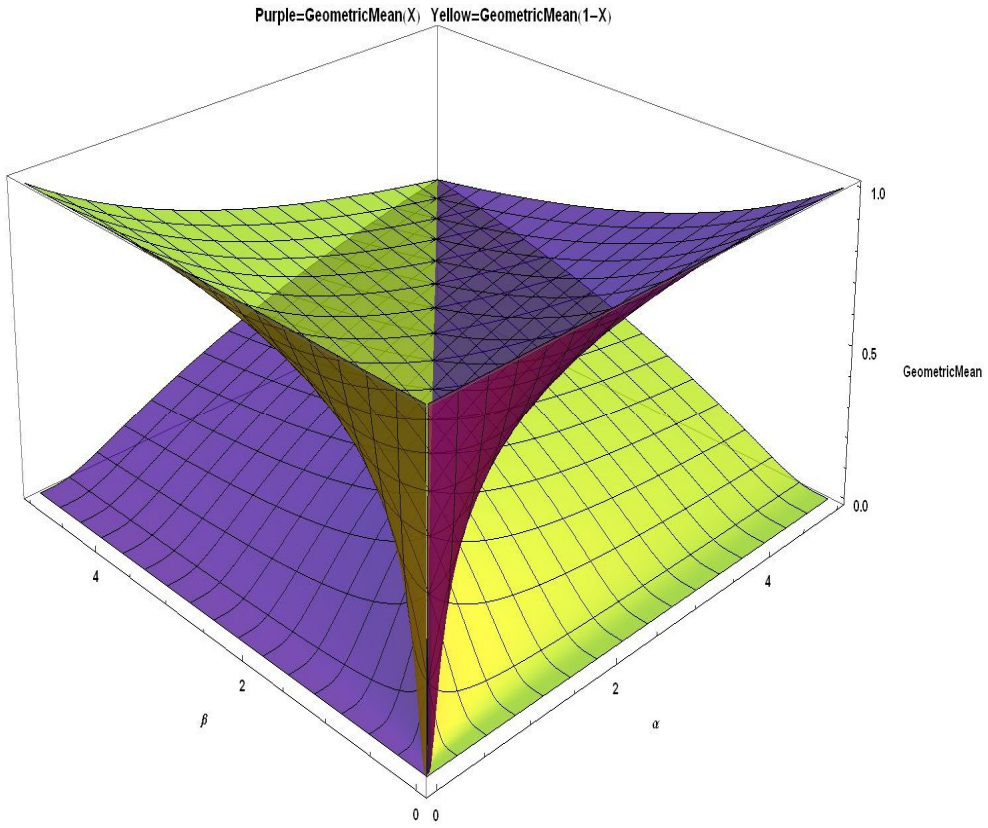

The logarithm of the geometric variance, ln(var$_{GX}$), of the geo-spectrotemrpoal uncoalesced distribution with a *S. damsnoum* s.l. random variable *X* was tabulated in Calculus Methode/Map Server ™ using the second moment of the logarithm of *X* centered on the geometric mean of *X*, (ln(G_X) as

$$\begin{aligned}\ln \mathbf{var_{GX}} &= \mathrm{E}\left[(\ln X - \ln G_X)^2\right] \\ &= \mathrm{E}[(\ln X - \mathrm{E}\left[\ln X\right])^2] \\ &= \mathrm{E}\left[(\ln X)^2\right] - (\mathrm{E}[\ln X])^2 \\ &= \mathbf{var}[\ln X]\end{aligned}$$

and therefore, the geometric variance was $\mathbf{var_{GX}} = e^{\mathbf{var}[\ln X]}$.the Fisher information

matrix, and the curvature of the log likelihood function, the logarithm of the geometric variance of the reflected variable (1-*X*) and the logarithm of the geometric covariance between *X* and (1-*X*) appeared as in Figure 53:

Figure 53 Log geometeric variances of trailing vegetation, discontinuously canopied, hyperproductive, *S. damnsoum* s.l. tyurbid water, eco-georeferenceable, capture point Gonycogo narrow tributary study site forecast vulnerability covariance model

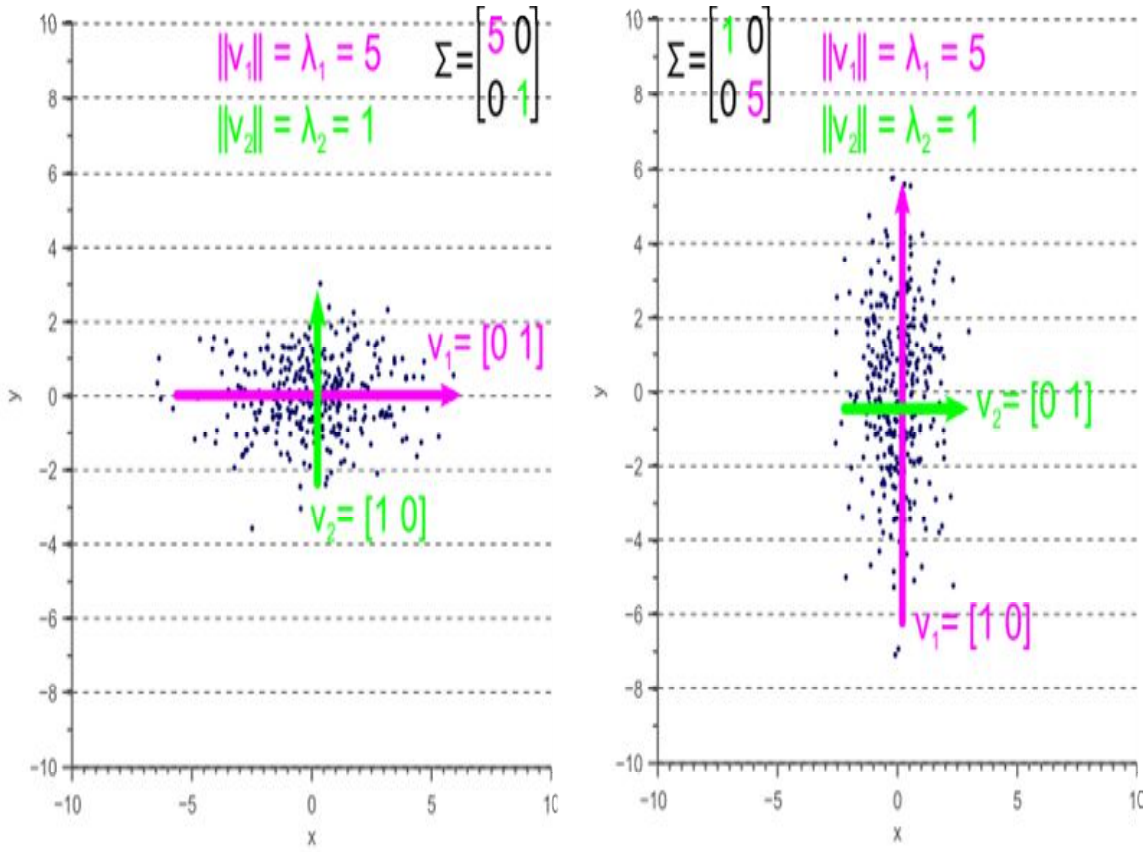

We then focused on the localized DIC measure for optimal model selection and goodness-of-fit evaluation in the Gonycogo and Adibuk risk model outputs. The estimators employed a partitioning of the DIC into the local DIC, leverage and deviance residuals, to assess the local model fit and influence the stochastic/deterministic, habitat observations in the probabilistic, Bayesian, estimation, covariance, regression matrices. The PROC MCMC procedure computed three kinds of residuals. Residuals are available for all generalized linear models except multinomial models for ordinal response data, for which residuals are not available in SAS (http://support.sas.com). The raw residualized eco-epidemiological, eco-georeferenceable, geo-spectrotemporally, geospatially probabilistic, eco-epidemiological, metaheuristically optimizable, forecasts rendered from the risk models were then regressively defined where the n^{th} response was the corresponding predicted mean in PROC MCMC. Raw residuals in an explanatorial, output dataset employing an OUTPUT statement were requested. By doing so, the Pearson residual was the square root of the *n*th contribution to the Pearson's chi-square. We then requested the operationalizable, time-series dependent, endemic, transmission-oriented, RapidEye ^{TM}, Pearson residuals in an explantive,output dataset.

Values for Markov chains were generated. Markov chain (discrete-time Markov chain or DTMC) is a random process that undergoes transitions from one state to another on a state space which possess a property that is usually characterized as "memorylessness": the

probability distribution of the next state depends only on the current state and not on the sequence of events that preceded it [24]. For probabilistically autoregressively quantitating the forecasting, Gonycogo and Adibuk risk modesl, covariate estimators, multiple MCMC chains were estimated for the intercept, which appeared to converge within the first 1,000 samples. The first 1,000 samples were discarded to allow the model to stabilize (i.e., "burn in"), and the next 10,000 samples were optimally employed to derive unbiased elucidative estimators based on statistical significance. The MCMC was able to optimally numerically calculate multi-dimensional explanative integrals. The multiple integral was a generalization of the definite integral to functions of more than one hyperproductive, endmember explanatorial,sparsely shaded, discontinuously canopied, trailing vegetation or turbid water *S. damnosum* s.l., immature habitat, for instance, $f(x, y)$ or $f(x, y, z)$ in both models.

Just as the definite integral of a positive function of one variable represents the area of the region between the graph of the function and the *x*-axis, l, a positive function of two variables may also represent the volume of the region or between the surface defined by the function on the three-dimensional Cartesian plane where $z = f(x, y)$, and the plane contains a domain [24]. As such, we assumed that the same volume could be obtained via the integral of a function in the explanively optimally, parameterized, covariate estimator, Gonycogo and Adibuk model datasets employing the constant function $f(x, y, z) = 1$ over a region between the surface and the plane rendered from the risk model, forecasted derivatives. Multiple integration of a function in *n* variables: $f(x_1, x_2, \ldots, x_n)$ over a domain *D* was then robustly constructed in PROC MCMC which was iteratively represented by nested integral signs in the reverse order of execution (i.e., the leftmost integral sign was computed last), followed by the function and integrand arguments in proper order. Finally, the integral with respect to the right most argument in the Markovian, immature habitat, eco-epidemiological, risk models was computed.

An improper integral was also formulated in MathLab by creating the function $f(x) = e^{-x^2}(\ln x)^2$ where fun = @(x) exp(-x.^2).*log(x).^2. We evaluated the integral from x=0 to x=Inf when q = integral(fun,0,Inf). Then q was 1.9475. We subsequently parameterized the function by creating the function $f(x) = 1/(x^3 - 2x - c)$with one parameter, c using fun = @(x,c) 1./(x.^3-2*x-c). The integral from x=0 to x=2 at c=5 was calculated which revaled that q = integral(@(x)fun(x,5),0,2). It was noted then that q = -0.4605

Singularity at Lower Limit was rendered by create the function $f(x) = \ln(x)$ whenfun = @(x)log(x We evaluated the integral from x=0 to x=1 with the default error tolerances in the *S. damnosum* s.l. risk model employing Evaluate the integral again, specifying 12 decimal places of accuracy. Using the format long q1 = integral (fun,0,1).Then q1 =-1.000000010959678. We specified q2 = integral(fun,0,1,'RelTol',0,'AbsTol',1e-12).Then q2 was -1.000000000000010.

For computating waypoints an ec-epidemiological, capture point, eco-georferenceable, *S. damnosum* s.l. habitat, capture point, eco-epidemiological, trailing vegetation, hypeproductive, discontinuously canopied, turbid water, vulnerability model, vector-valued function $f(x) = [\sin x, \sin 2x, \sin 3x, \sin 4x, \sin 5x]$ in the Gonycogo and Adibuk study sites an integrate was generated from x=0 to x=1. We specified 'ArrayValued',true to evaluate the integral of an array-valued or vector-valued function in the model..using fun = @(x)sin((1:5)*x). We noted that q integral(fun,0,1,'ArrayValued',true) q

was then equivalent to 0.4597, 0.7081, 0.6633, 0.4134 and 0.1433.

Integrand, specified as a function handle ehich optimally defined the function to be integrated from xmin to xmax. For scalar-valued problems, the function y = fun(x) must accept a vector argument, x, and return a vector result, y[24]. This meant that fun had to use array operators instead of matrix operators in the trailing vegetation, sparsely shaded, *S. damnosum* s.l. habitat hypeproductive, capture point, Rapid Eye™ 5m discontinuously canopied, turbid water,vulnerability forecasting model. (e.g., uses .* (times) rather than * (mtimes)]. If you set the 'ArrayValued' option to true, then fun must accept a scalar and return an array of fixed size in a . discontinuously canopied, turbid water,vulnerability *S. damnosum* s.l. habitat hypeproductive, eco-epidemioloigical, eco-georfernceable, time series, forecast model[22].

The MCMC procedure performed posterior sampling and statistical inference for constructing robustifiable, multilevel, eco-epidemiological, geospatialized Bayesian, parametric models. The procedure fit the 5m spatial resolution models. These models took various forms employing standard distributions. For example, specifying prior distributions in MCMC for the elucidatively orthogonally decomposable, RapidEye ™ transmittance, wavelength, frequency imaged, eco-epidemiological, immature habitat, capture point, paramterizable covariates and and a conditional distribution allowed a response variable (e.g., total seasonal immature *Simulium* count) procedure to fit models by employing a standard form (i.e.,gamma) to specify a general distribution.

The Bayes estimates of two-parameter gamma distribution was considered. It was assumed that the scale parameter had a gamma prior and the shape parameter had a log-concave prior, and they were independently distributed. Log-concavity is an important property in the context of optimization, Laplace approximation, and sampling [24]. It was assumed that the scale parameter
had a gamma prior and the shape parameter has a log-concave prior, and they were independently distributed. Under the tabulated priors, we uses Gibbs sampling technique togenerate samples from the posterior density function. In statistics and in statistical physics, Gibbs sampling or a Gibbs sampler is a Markov chain Monte Carlo (MCMC) algorithm for obtaining a sequence of observations which are approximated from a specified multivariate probability distribution (i.e. from the joint probability distribution of two or more random variables), when direct sampling is difficult [24].Based on the generated samples, we computed the Bayes estimates of the unknown parameters and also optimally metaheusristically quantitated the highest posterior density credible intervals. We also computed the approximate Bayes estimates using Lindley's approximation under the assumption of gamma priors of the shape parameter. Monte Carlo simulations awere performed to compare the performancesof the Bayes estimators with the classical estimators.

One data analysis was performed for illustrative purposes. Bayesian methods based on Gaussianprocess in PROC MCMC were then geoclassified as regression, density estimation, and quantitated eco-georferenceable, elucidative, point process intensity estimation values in the moderate resolution, unmixed, *S. damnosum* s.l., hyperproductive, immature habitat, eco-georferenceable, vulnerability, forecast maps(see Figure 54). PROC MCMC uses a random walk Metropolis algorithm to obtain posterior samples. For details on the Metropolis algorithm, see the section Metropolis and Metropolis-Hastings Algorithms. For the actual implementation details of the Metropolis algorithm in PROC MCMC, such as the blocking of the parameters and tuning of the covariance matrices, see the section Tuning the Proposal

Distribution. By default, PROC MCMC assumes that all observations in the data set are independent, and the logarithm of the posterior density is calculated as follows: $\log(p(\theta|\mathbf{y})) - \log(\pi(\theta)) + \sum_{i=1}^{N} \log(f(y_i|\theta))$ where $\theta$is a parameter or a vector of parameters. The term $\log(\pi(\theta))$is the sum of the log of the prior densities specified in the PRIOR and HYPERPRIOR statements. The term $\log(f(y_i|\theta))$is the log likelihood specified in the MODEL statement. The MODEL statement specifies the log likelihood for a single observation in the data set.

PROC MCMC is a flexible simulation-based procedure that is suitable for fitting a wide range of Bayesian models[5]. To use the procedure, for spatiall;y adjusting the geosampled, *S. damnosumn* s.l., immature habitat, capture point paramterizable 5m covariates we needed to specify a likelihood function for the data and a prior distribution for the parameters. We also needed to specify hyperprior distributions for fitting the hierarchical model. PROC MCMC obtained the black fly samples from the corresponding posterior distributions, produces summary and diagnostic statistics, and saves the posterior samples in an output dataset so that it could be used for further analysis. We analyzed the LULC ovispoition data to determine is a likelihood, prior, or hyperprior with PROC MCMC were programmable using the SAS DATA step functions. The geosampled capture point parameters were entered into the model in a nonlinear functional form. The default algorithm that PROC MCMC used was an adaptive blocked random walk Metropolis algorithm that employed a normal proposal distribution

In statistics and in statistical physics, the Metropolis–Hastings algorithm is a Markov chain Monte Carlo (MCMC) method for obtaining a sequence of random samples from a probability distribution for which direct sampling is difficult. This sequence can be used to approximate the distribution (e.g., to generate a histogram), or to compute an integral (such as an expected value from a *S. damnsoum* s.l., eco-epidemiological, ovispoition model). Metropolis–Hastings and other MCMC algorithms are generally used for sampling from multi-dimensional distributions, especially when the number of dimensions is high [5].

To use PROC MCMC for quanatizing the geosampled, geospectrotemporal, *S. damnosum* s.l. dataset we specified the model parameters (using the PARMS statements), the prior distributions (usingthe PRIOR statements), and the conditional distribution of the response variable given the parameters and covariates inthe data set (using the MODEL statements). The prior distributions and the likelihood function jointly define a posteriordistribution, which becomes the objective function that PROC MCMC uses in the Metropolis algorithm (www.sas.edu).

Figure 54 Spatially adjusting logarithmically log-concave Bayesian predictive densities from the corresponding capture point RapidEye™ 5m, wavelength, frequency transmittance emissivities of observed discontinuously canopied, trailing vegetation, covariate estimators in geospace in the. Gonycogo study site agro-village model

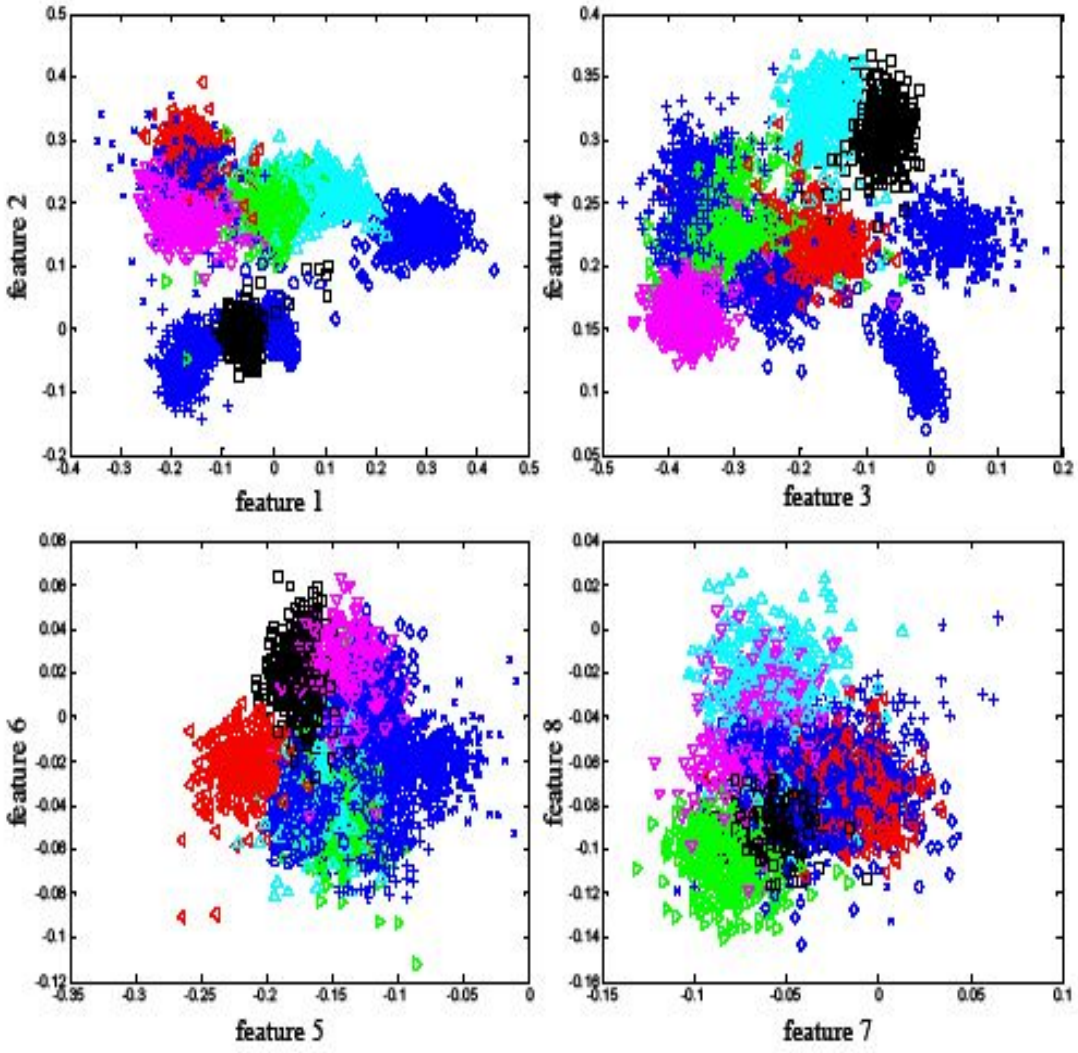

Further, the likelihood was log-concavity in the explanatively eco-georeferenceable elucidative hyperparameters controlling the mean function of the Gaussian prior in the density and point process intensity estimation where the mean, covariance, and observation noise parameters in the geo-classified paradigm. The field-operationizable, eco-epidemiological, seasonally hyperproductive, endmember explanatorial,sparsely shaded, discontinuously canopied, trailing vegetation or turbid water, *S. damnosum* s.l., immature habitat, eco-epidemiological, capture point, eco-georefernceable forecasts in the Gonycogo and Adibuk paradigms revealed useful parameterization of these hyperparameters, indicating a suitably large class of priors for which the corresponding maximum a posteriori problem is log-concave. In doing so, a Bayes estimate was also optimally quantitated of the unknown parameters and and the highest posterior density credible intervals. The approximate Bayes estimates used Lindley's approximation under the assumption of gamma priors of the shape parameter was tabulated for the model covariance stuctures. In probability theory, the Lindley equation, Lindley recursion or Lindley processes[1] is a discrete-time stochastic process A_n where n takes integer values and$A_{n+1} = \max(0, A_n + B_n)$[24].

The MCMC procedure also employed a random walk Metropolis algorithm to simulate the hyperproductive *Simulium* samples in the geo-spectrotemrpoally geosampled at the Gonycogo and Adibuk study sites from employing autoregressive, auto-probabilistic elucidative, expository model auto-specifications(see Figure 55). We fit the same Bayesian linear regression model, use standardized trailing vegation, discontinuoulsy canopied, sparsely shaded,capture point, eco-georefernceable, *S. damnsoum* s.l.,immature ,capture point, habitat geosampled paramterizable covariate coefficients. We re-wrote the mean function as $\mu_i^*=\mathbf{X}_i^*\boldsymbol{\beta}^*$ where $\mathbf{X}^*$ was the design matrix constructed from a column of 1s and $p$standardized covariates. The regression parameters on the standardized scale were represented by $\boldsymbol{\beta}^*$. The standardized covariates were computed as follows: $X_{ij}^*=\frac{X_{ij}-m_j}{s_j}$ for $i=1,\ldots,n$ predictide hypeproductive seasonal habitat and $j=1,\ldots,p$covariates, and where $m_j$and $s_j$are the mean and standard deviation of the jth covariate, respectively.

Figure 55 The resulting plot of Monte Carlo simulations performed to compare the performances of the trailing vegetation, discontinuously canopied, eco-georefernceable, capture point, *S. damnosum* s.l. habitat decomposed Bayes estimators with the classical estimators for the eco-epidemiological geosampled, Adibuk agro-village, discontinuous model

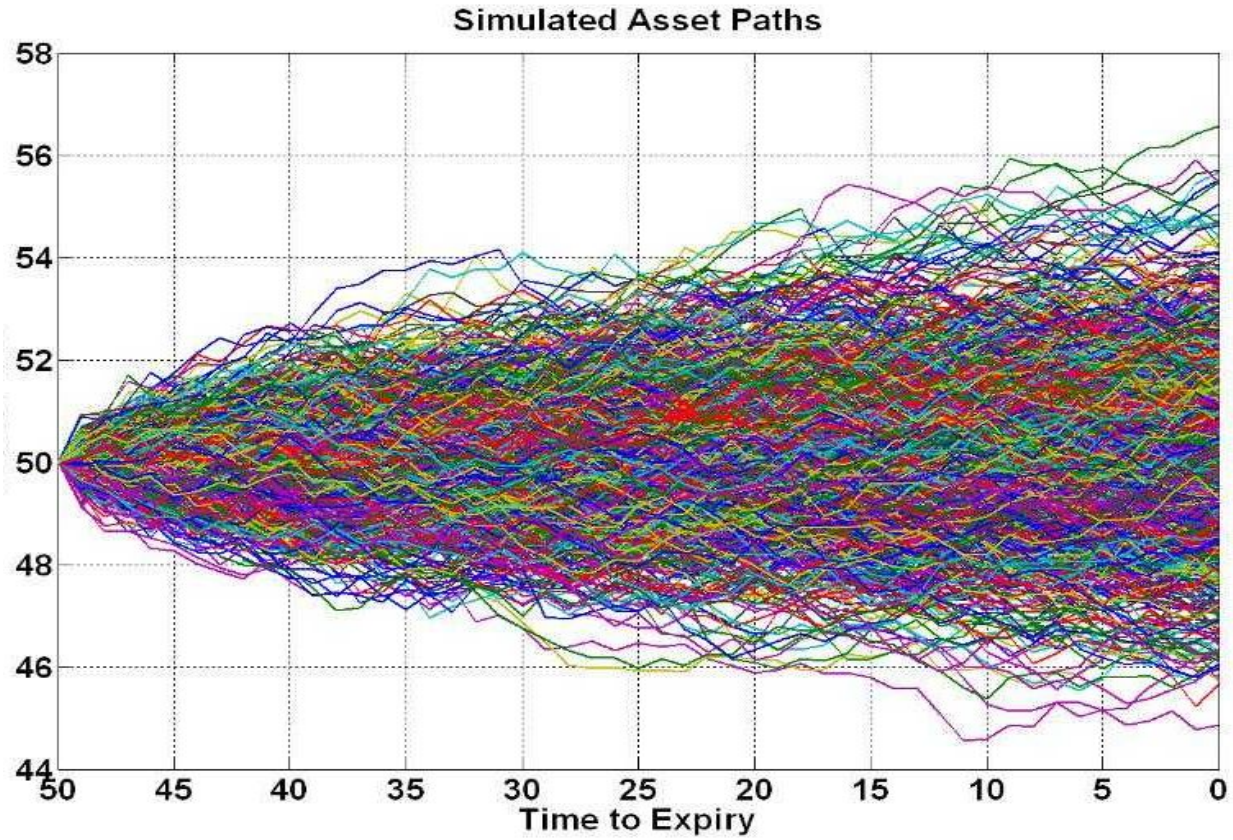

A standard linear regression problem, in which for $i=1,\ldots,n$ was considered to quanite the ecogeorferenecable, trailing vegetation, turbid water, discontinuously canopied, *S. damnsoum* s.l. capture points geosmapled at the Gonycogo and Adibuk study sites by specifying the conditional distribution of $y_i$given a $k\times 1$predictor vector

$\mathbf{x}_i: y_i = \mathbf{x}_i^{\mathrm{T}}\boldsymbol{\beta} + \epsilon_i$, where $\boldsymbol{\beta}$ was a $k \times 1$ vector, and the ϵ_i were independent and identical normally distributed uncoalesced 5m randomized endmember variables: $\epsilon_i \sim N(0, \sigma^2)$. This corresponded to the following likelihood function: $\rho(\mathbf{y}|\mathbf{X}, \boldsymbol{\beta}, \sigma^2) \propto (\sigma^2)^{-n/2} \exp\left(-\frac{1}{2\sigma^2}(\mathbf{y} - \mathbf{X}\boldsymbol{\beta})^{\mathrm{T}}(\mathbf{y} - \mathbf{X}\boldsymbol{\beta})\right)$. The ordinary least squares solution was then used to estimate the coefficient vector using the Moore-Penrose pseudoinverse: $\hat{\boldsymbol{\beta}} = (\mathbf{X}^{\mathrm{T}}\mathbf{X})^{-1}\mathbf{X}^{\mathrm{T}}\mathbf{y}$ where $\mathbf{X}$ was the $n \times k$ design matrix in PROC MCMC where, each row was a predictor vector $\mathbf{x}_i^{\mathrm{T}}$; and $\mathbf{y}$ was the column n-vector $[y_1 \cdots y_n]^{\mathrm{T}}$. This was a frequentist approach, and it assumes that there are enough submixel Rapid Eye ™ 5m measurements to say something meaningful about $\boldsymbol{\beta}$. In the Bayesian approach, the iterated Gonycogo and Adibuk data were supplemented with additional information in the form of a prior probability distribution. The prior belief about the parameters was combined with the data's likelihood function according to Bayes theorem to yield the posterior belief about the parameters $\boldsymbol{\beta}$ and σ. The prior took different functional forms which in the *S. damnsoum* s.l. capture point, model was dependnet on the domain and the information that was available from a priori.

In probability theory and statistics, the inverse gamma distribution is a two-parameter family of continuous probability distributions on the positive real line, which is the distribution of the reciprocal of a variable distributed according to the gamma distribution[24]. The gamma distribution is a two-parameter family of continuous probability distributions[23].. The exponential distribution and chi-squared distribution(i.e., special cases of the gamma distribution) were then constructed..

Figure 56 a Poisson *S. damnosum* s.l. habitat distribution with rate of change λ, the distribution of waiting times between successive seasonal changes (with $k = 0$) was $D(x) = P(X \leq x) = 1 - P(X > x) = 1 - e^{-\lambda x}$ and the probability distribution function was $P(x) = D'(x) = \lambda e^{-\lambda x}$.

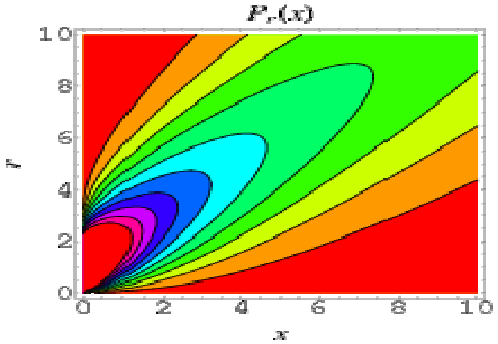

The inverse gamma distribution's PDF was defined over the support $x > 0$ $f(x;\alpha,\beta) = \frac{\beta^{\alpha}}{\Gamma(\alpha)} x^{-\alpha-1} \exp\left(-\frac{\beta}{x}\right)$ with shape parameter α and scale parameter β in the *S. damnosum* s.l. eco-epidemiological, trailing vegetaion, capture point, habitat model where $\Gamma(\cdot)$ re denoted the gamma function. The Gamma distribution, contained a somewhat

similar exponential term, β whose scale parameter was the distribution function which satisfiesd $f(x;\alpha,\beta)=\frac{f(\frac{x}{\beta};\alpha,1)}{\beta}$. We considered an alternative parametrization of the normal distribution in terms of the precision, defined as the reciprocal of the variance, which allows the gamma distribution to be used directly as a conjugate prior(see Figure 56)..

Figure 56 An inverse gamma distribution of the capture point *S. damnsoum* s.l. habitat decorrelated variables, where the distribution arose as the marginal posterior distribution for the unknown variance of a normal distribution using an uninformative prior and as an analytically tractable conjugate prior for the Adibuk agro-village complex study site

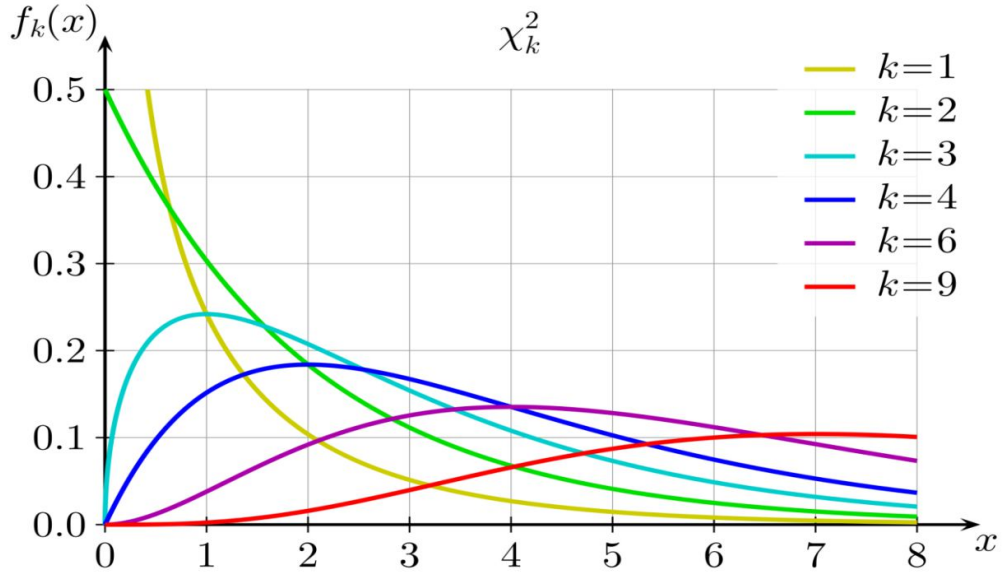

In Bayesian statistics, the posterior probability of a random event or an uncertain proposition is the conditional probability that is assigned after the relevant evidence or background is taken into account. Similarly, the posterior probability distribution is the probability distribution of an unknown quantity, treated as a random variable, conditional on the evidence obtained from an experiment or survey[24]. The posterior probability in the trailing vegation, discontinuoulsy canopied, turbid water, eco-epidemiological, eco-georferenceable, hypeproductive, capture point, *S. damnsoum* s.l. immature geosampled capture points in each narrow tributary, agro-village, complex study site was the probability of the parameters θgiven the evidence X: $p(\theta|X)$(see Figure 56)This methodology contrasted with the quanatitaion of likelihood function, which was the probability of the evidence given the parameters: $p(X|\theta)$ in the habitat model We let a prior belief that the probability distribution function was $p(\theta)$and then the geo-spectrotemrpoal, narrow riverine tributary observations $x$with the likelihood $p(x|\theta)$, along with the posterior probability was defined as $p(\theta|x)=\frac{p(x|\theta)p(\theta)}{p(x)}$. The posterior probability was then written in the memorable form as Posterior probability Likelihood Posterior probability.

Figure 56 Illustration of the gamma PDF for the trailing vegation, discontinuoulsy canopied, eco-georfernceable, *S. damnsoum* s.l. immature, turbid water Bayesainized parameterized values over *k* and *x* with θ set to 1, 2, 3, 4, 5 and 6 for the Gonycogo study site

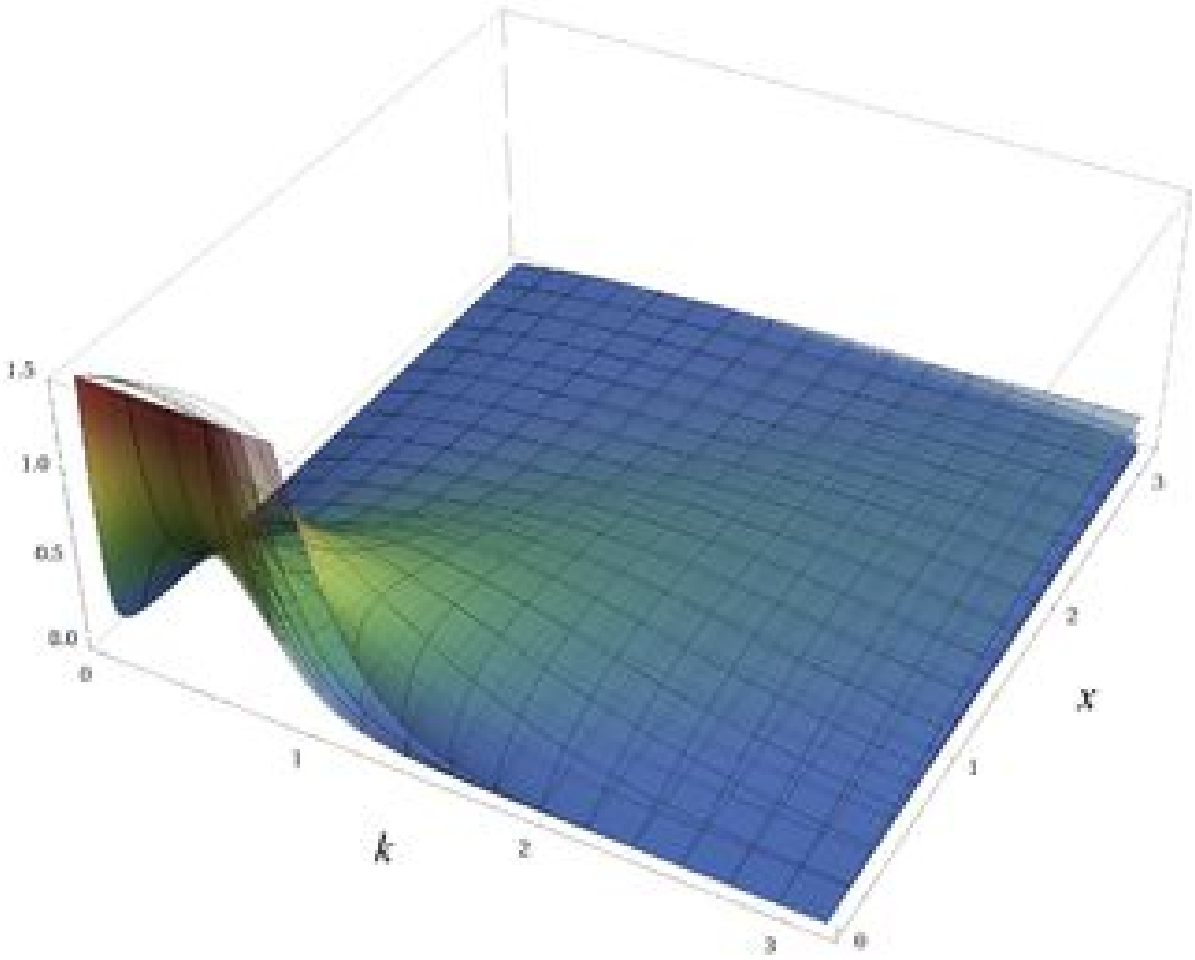

We wrote the discontinuous, infrequently canopied, sparsely shaded, *S.damnsoum* s.l. ,agro-village, narrow tributary, capture point's mean functions as $\mu_i^*=\mathbf{X}_i^*\boldsymbol{\beta}^*$ where $\mathbf{X}^*$ was the design matrix constructed from a column of 1s and $p$standardized covariates. The metaheursitically optimizable regression parameters on the standardized scale are represented by $\boldsymbol{\beta}^*$. The standardized covariates were computed as follows: $x_{ij}^*=\frac{x_{ij}-m_j}{s_j}$ for $i=1,\ldots,n$.Rapid Eye ™ wavelength , immature habitat, uncoalesced frequency-oriented $j=1,\ldots,p$ optamally parameterizable covariate coefficients and where $m_j$and s_j wer the mean and standard deviation of the jth covariate, respectively with summary statement amd interval statistics of all the geo-spectrotemrpoally geosampled capture point parametrs (see Table 4).

Table 4 Posterior Model Summary of Bayesian Linear Regression with Standardized Rapid Eye ™ in PROC MCMC for the Adibuk model

Posterior Summaries

Parameter	N	Mean	Standard Deviation	Percentiles 25%	50%	75%
beta0	200	1.3465	0.0666	1.6059	1.6470	1.6956
beta1	200	-0.00006	0.000911	-0.00061	-0.00004	0.000547
beta2	200	0.000112	0.00166	-0.00053	0.000860	0.00200
beta3	200	0.00176	0.000911	0.00128	0.00186	0.00298
beta4	200	0.00248	0.000911	0.00184	0.00217	0.00281
beta5	200	0.1043	0.0233	0.0996	0.1038	0.1169
beta6	200	0.000711	0.000176	0.000642	0.000750	0.000843
beta7	200	-0.00633	0.000998	-0.00694	-0.00629	-0.00562
beta8	200	-1.43E-7	5.844E-8	-1.83E-7	-1.47E-7	-1.08E-7
sig2	2000	0.0565	0.00511	0.0564	0.0543	0.0649

Posterior Intervals

Parameter	Alpha	Equal-Tail Interval		HPD Interval	
beta0	0.050	1.5123	1.7714	1.5120	1.7705
beta1	0.050	-0.00195	0.00165	-0.00192	0.00168
beta2	0.050	-0.00235	0.00417	-0.00233	0.00418
beta3	0.050	-0.00006	0.00382	-0.00001	0.00383
beta4	0.050	0.000236	0.00412	0.000303	0.00416
beta5	0.050	0.0651	0.1450	0.0625	0.1415
beta6	0.050	0.000428	0.00107	0.000428	0.00107
beta7	0.050	-0.00827	-0.00443	-0.00822	-0.00442
beta8	0.050	-2.62E-7	-3.17E-8	-2.63E-7	-3.32E-8
sig2	0.050	0.0498	0.0705	0.0494	0.0699

An optimization technique (i.e., the quasi-Newton algorithm) was chosen to estimate the posterior mode and approximate the covariance matrix around the mode in the Gonycogo and Adibuk models. Quasi-Newton methods are methods used to either find zeroes or local maxima and minima of functions, as an alternative to Newton's method, but can be used if a Jacobian or Hessian matrix for quantitating, iterative count data variables. In vector calculus, the Jacobian matrix is the matrix of all first-order partial derivatives of a vector-valued function especially when the matrix is a square matrix.The procedure computed a number of posterior estimates, and output a posteriorily autoregressed dataset of parameterized, *S. damnosum* s.l. non-homogenously canopied, trailing vegetation–related, non-fractionalized, RapidEye 5m, capture point, covariate coefficient estimates. Successful Bayesian inference uses sampling-based approaches depending on the convergence of the Markov chain [24].

Quasi-Newton methods accelerate the steepest-descent technique for function minimization by using computational history to generate a sequence of approximations to the inverse of the Hessian matrix. This paper presents a class of approximating matrices as a function of a scalar parameter. The problem of optimal conditioning of these matrices under an appropriate norm as a function of the scalar parameter is investigated. A set of computational results verifies the superiority of the new methods arising from conditioning considerations to known methods

We optimally employed quantized gradient information for metaheursitically optimizing the quasi-Newton methods. These methods built up curvature information at each iteration to formulate a quadratic model. We, considered the unconstrained minimization problem, to minimize $f(x)$, where the function took vector arguments and returned scalars. Thus at an explanative, seasonal, hyperproductive, eco-georefernceable, eco-georefernceable, capture point x in n-space .a point with a lower function value was employed for quantiating the geo-spectrotemrpaolly geosampled Gonycogo and Adibuk datasets. The basic idea was to approximate f with a simpler function q, which reasonably reflectws the behavior of function f in a neighborhood N around the geo-spectrotemporally geosampled habitat point x $\min_x \frac{1}{2}x^T Hx + c^T x + b,$ in each study sites where the Hessian matrix, H, was a positive definite symmetric matrix, c was a constant vector, and b was a constant. The optimal solution for this problem occurred when the partial derivatives of x went to zero,(i.e., $\nabla f(x^*) = Hx^* + c = 0$). The optimal solution elucidative habitat vpoint, x^*, was written as $x^* = -H^{-1}c.$ in the Gonycogo and Adibuk forecast, vulnerability, Rapid Eye ™ 5m models.

Newton-type methods (as opposed to quasi-Newton methods) calculated H directly and proceeded in a direction of descent to locate the minimum after a number *of S. damnosum* s.l.iterations for . constructing the Gonycogo and Adibuk models Originally proposed to find the roots of polynomials the method may be employable for general nonlinear equations and for its use in optimization by finding a root of thegradient [26]. In calculus, Newton's method is an iterative method for finding the roots of a differentiable function f (i.e. solutions to the equation f(x)=0). In optimization, Newton's method is applied to the derivative f' of a twice-differentiable function f to find the roots of the derivative (solutions to $f'(x)=0$), also known as the stationary points of f[24]. Calculating H numerically for the eco-georefernceable, seasonally hyperproductive, trailing vegation, turbid water, eco-georferenecable, agro-village complex, discontinuously canopied, *S. damnosum* s.l. habitat models involved a large amount of computation. In the one-dimensional problem, Newton's method attempts to construct a sequence x_n from an initial guess x_0 that converges towards some value x^* satisfying $f'(x^*)=0$. This x^* is a stationary point of f. (http://mathworld.wolfram.com/.html) Newton's method for optimization, in addition to the deficiencies faced when solvingsystems of equations, needs to be augmented to enable iterates to move off saddlepoints. This is the key augmentation that is needed for minimization problems [25] It took Newton's steepest multiple explanative, iterations in order to simulate the endmember Rapid Eye ™ ,geosampeld estimators employing a statistical significance with a 95% confidence interval in both models (see Figure 57).

Figure 57 Simulated iterations using the Quasi-Newton methods employing the observed behavior of $f(x)$ and $\nabla f(x)$ to build up curvature information to make an an appropriate updating technique for robustly quantitating the standardized *S. damnosum* s.l. covariate coefficients geosampled at the Adibuk narrow tributary study site .

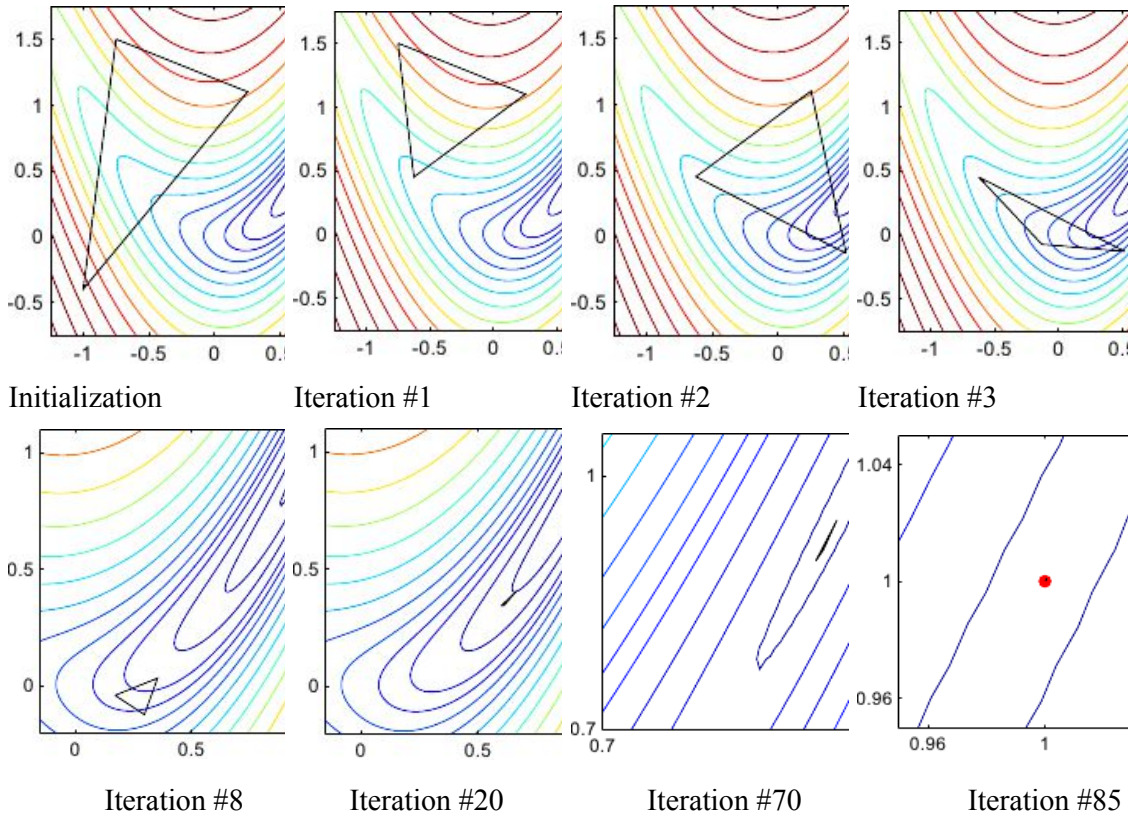

We employed Broyden–Fletcher–Goldfarb–Shannon (BFGS) algorithm, to generate an iterative method for solving unconstrained nonlinear optimization problems in the trailing vegetaion, discontinuoulsy canopied, sparsely shaded, seasonally explanative, captuire point in each agro-village complex study site. As any of Newton-like methods, BFGS uses quadratic Taylor approximation of the objective function in a d-vicinity of x: $f(x + d) \approx q(d) = f(x) + d^{T}g(x) + ½\, d^{T}H(x)\, d$, where $g(x)$ is the gradient vector and $H(x)$ is the Hessian matrix. The necessary condition for a local minimum of $q(d)$ with respect to d results in the linear system: $g(x)+ H(x)\, d = 0$which, in turn, gives the Newton direction d for line search: $d = -H(x)^{-1}g(x)$)

The BFGS method approximated Newton's method using a class of hill-climbing optimization techniques that saught a stationary point of a preferably twice continuously differentiable capture point, quantized function. A necessary condition for optimality in the *S. damnsoum* s.l. model was that the gradient had to be zero. Newton's method and the BFGS methods converged employing the function which had a a quadratic Taylor expansion near an optimum. The BFGS is a mathematical optimization technique which belongs to the family of local search (i.e., hill climbing) employed as an iterative algorithm in ArcGIS that starts with an arbitrary solution to find a better solution by incrementally changing a single element of the solution(www.esri.com). The algorithmic methods used both the first and second

derivatives of the function.BFGS showed good performance even for non-smooth optimizabl,e , trailing vegetaion, turbid water, eco- discontinuous, canopied, *S. dansoum* s.l. capture point, interventional. narrow tributary, agro-village complexes. The BFGS revealed good performance even for conducting the smoothness optimizations on the riverine habitat data geosampled in the Gonycogo and Adibuk study sites (see Figure 58)

Figure 58 The BFGS approximated method for quantiating the eco-georeferenceable trailing vegation, discontinuoulsy canopied, hyperproductive, agro-village complex, ecosystem capture point, *S. damnsoum* s.l. habitat employing a class of hill-climbing optimization techniques of a preferably twice continuously differentiable function at the Gonycogo study site

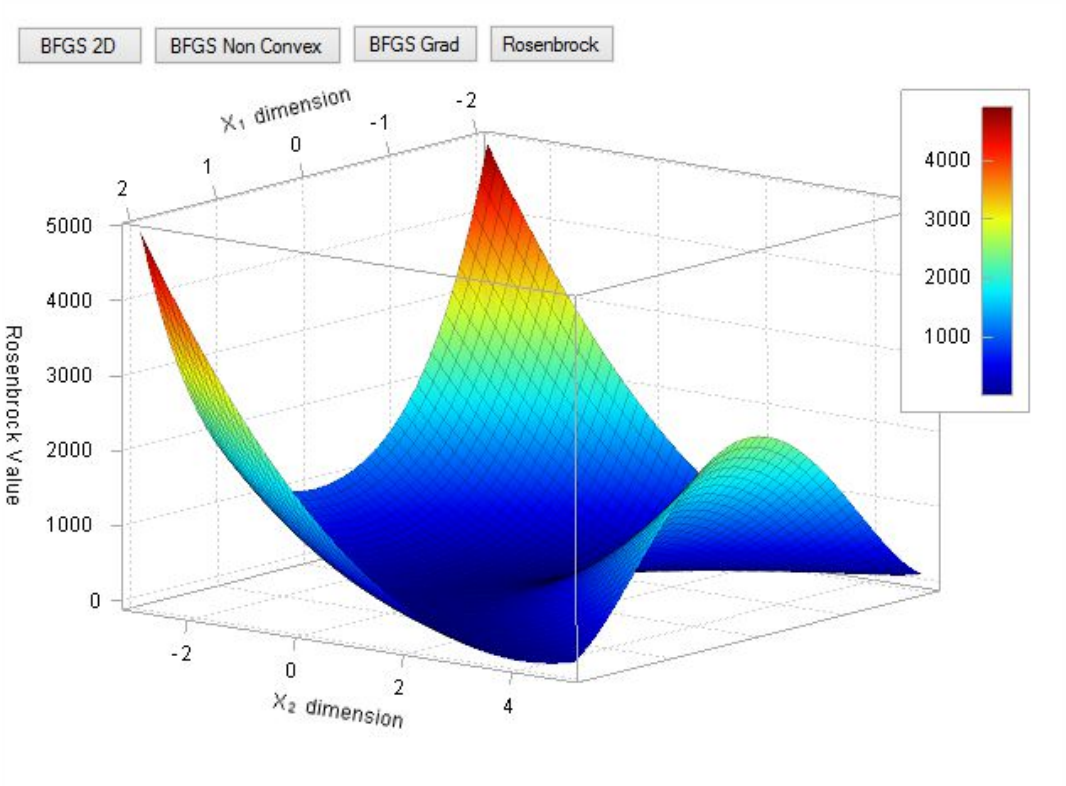

Figure 59 An *S. damnosum* s.l. habitat objective function: the Rosenbrock function employingf(x)=∑ i=1 N−1 [(1−x i) 2 +100(x i+1 −x 2 i) 2]∀x∈R N for the discontinuous sparsely shaded, canopy geo-spectrotemporally geosampled at the Adibuk study site

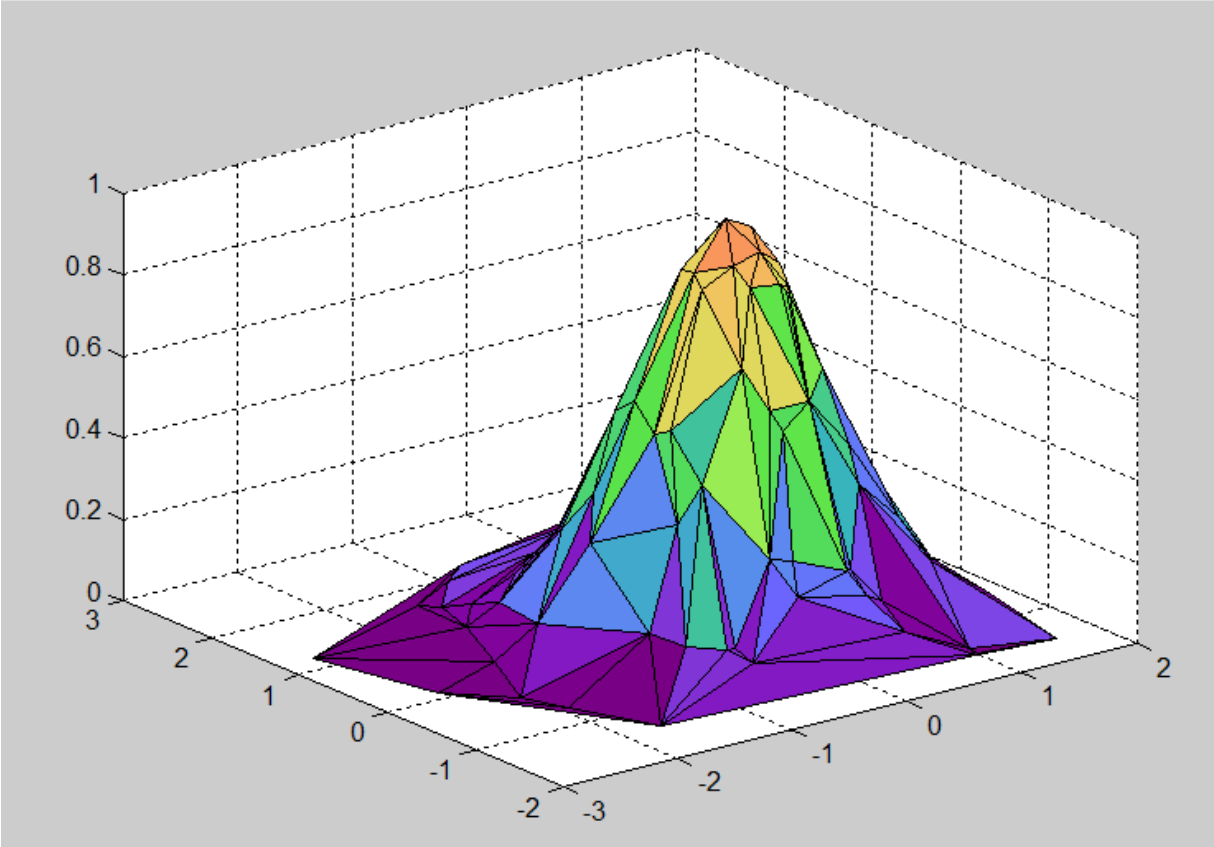

We queried a collection of additional details about the minimization process after it was finished.Information included the number of iterations needed, for quantitaing the norm of the gradient ||grad(f(x ~))|| in the *S. damnosum* s.l. habitat eco-epidemiological Gonycogo and Adibuk models using a . Rosenbrock function (see Figure 58). The mathematical optimization, the Rosenbrock function is a non-convex function used as a performance test problem for optimization algorithms[24].

The *n*-dimensional Rosenbrock function was implemented in ILNumerics Optimization Toolbox among other test functions. The minimum of the 2D variant wasknown was found at [1,1]. In order to get the number of optimal iterations needed by BFGS and L-BFGS to obtain the minimum of the 2D Rosenbrock function, we quantitated a minimizer at [1,1].Therefater fminunconst_bfgs managed to find the solution using less iterations compared to L-BFGS. Also, the solution was much more accurate. While most optimizer implementations are able to find the minimum of the rosenbrock function up to a precision of 1e-6 only, fminunconst_bfgs gets as close as 7 * 10-13! [24].

The norm of the gradient was plotted as a logarithmic line plot for both algorithms. The values
returned by gradientNorm was a valuable time series, eco-georefernceable, hypeproductive, eco-epidemiological, capture point, indicator for the quality of the results (see Figure 60) . Usually, for a straight path to the minimum, intermediate steps should show decreased norm(grad(f(x))) values[24]. At the minimizer $x*$, the gradient optimally gets close to $0^{\rightarrow}$.

Figure 60. Plotted BFGS and Newton for optimizing forecasted *S. damnosum* s.l. habitats using a Rosenbrock function for the Gonycogo study site

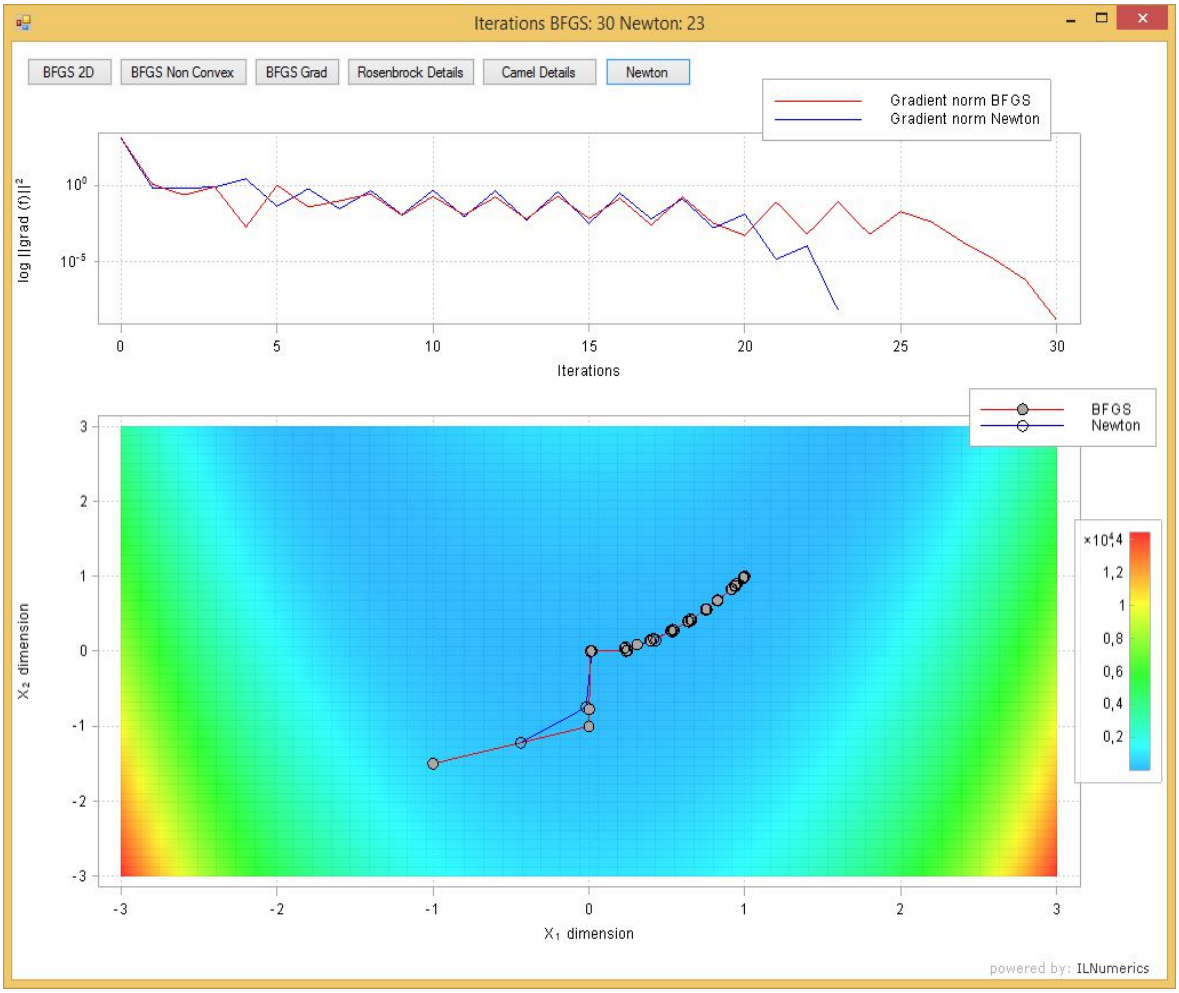

The MCMC procedure provided a number of non-normality convergence diagnostic tests to quantitate skewness and kurtosis in the eco-geographic, eco-hydrologic, geo-spectrotemporally geospatially eco-cartographical, decomposable variables, eco-geographically illustrating prolific, seasonal, hyperproductive, *S. damnosum* s.l., capture point habitats geosampled in the African riverine agro-village complexes. Formalizing and generalizing families of univariate distributions optimally obtained a density-based (i.e., immature count) log-transformation in PROC MCMC of a unimodal, systematic, continuous distribution which revealed a shape parameter and explanatively parameterizable, discontinuously canopied, covariate estimators (e.g., percent of sparely shaded trailing

vegetation) in the eco-georeferenceable, seasonally, RapidEye^{TM} imaged, eco-epidemiological, *S. damnosum* s.l., habitat, capture point, vulnerability, forecast models. The resulting distributions in PROC MCMC contained interpolatable, decomposable habitat parameterizable covariate, 5m, wavelength, transmittance, frequency estimators, that were utilizable for identifying, habitat covariates at each study site. A scaled dataset of unmixed, geolocational, immature riverine, eco-georeferenceable, habitat invariant benchmark priors then enable validative model renderings. (Figure 61) The algorithm auto-probabilistically, remotely, autoregressively quantitated the random samples from any arbitrarily complicated RapidEye^{TM} 5m, targeted, habitat distribution of any dimension (e.g., a dataset of slightly turbid trailing vegtation geosampled habitats) that was known up to a normalizing constant.

Figure 61 PROC MCMC simulation of posterior samples of eco-epidemiological, regression datasets of *S. damnosum* s.l. habitat covariate, parameterized estimators for the Adibuk agro-village narrow tributary, trailing vegation, discontinuous canopied, forecast model

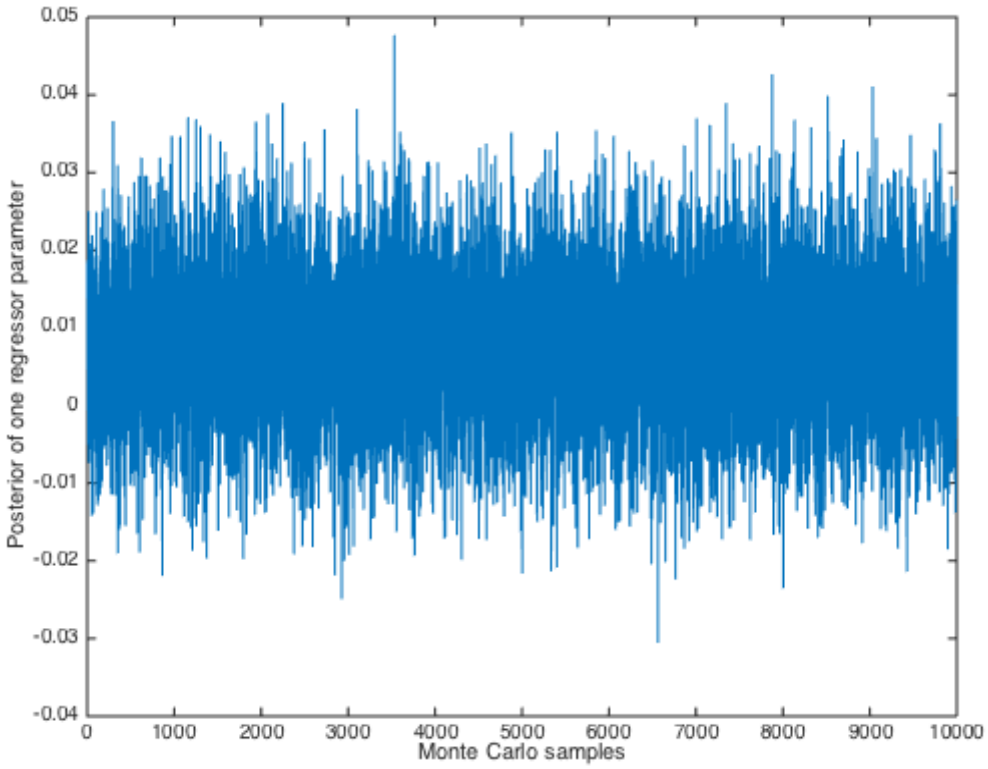

Thereafter, the deviance residual was defined as the square root of the contribution of the n^{th} narrow riverine,tributary prolific, habitat, descriptive, observation to the deviance, with the sign of the raw, residually quantitated predictor variable in the OUTPUT statement. The adjusted Pearson, deviance and likelihood residuals were then optimally defined employing the models of Agresti in 1987 [146], and Davison and Snell in 1991 [147]. These residuals were useful for outlier detection and for assessing the influence of single observations on the fitted Gonycogo and Adibuk models.

For optimally residually quantitating the hierarchically explanatively, generalizable, *S. damnosum* s.l., hyperproductive, immature, narrow, riverine, tributary, eco-epidemiological, immature capture point, habitat, risk models, the variance of the n^{th} individual habitat observation was then given by the dispersion parameter which was a user-specified prior weight. The mean, and the variance function were parsimoniously quantitated. We also constructed a robust, diagonal, uncertainty matrix in PROC MCMC for denoting the n^{th} diagonal element in the empirical, eco-ecological, probabilistic dataset. The weight matrix was employed in computing the expected information matrix. The Pearson residuals were standardized to have unit asymptotic variance. The standardized Pearson residuals in the output dataset were quantitated employing STDRESCHI in the OUTPUT statement. The deviance residualized probabilistically regressed, endemic, transmission-oriented, eco-georefernceable forecasts were standardized to have a unit asymptotic variance as tabulated by the total deviance from the geosampled habitat observations.

The standardized deviance residuals were requested in the output dataset employing "STDRESDEV" in the OUTPUT statement. The likelihood residuals were thereafter defined. We then requested the likelihood forecasted residuals in an output dataset employing "RESLIK" in the OUTPUT statement. In so doing, the eco-georeferenced, RapidEye™, discontinuously canopied, trailing vegetation and turbid water, sub-mixel eco-epidemiological, time series forecasts were geo-spatiotemporally/ geo-spectrotemporally elucidatively quantitated, which allowed the local DIC to assist in model selection to regressively visualize the global and local impacts of adding fractionalized, wavelength, 5m, RapidEye ™ resolution parameterizable, transmittance, frequency-oriented, covariate estimators and other unmixed, emissivity, observational predictors to the auto-probabilistic, hierarchical, Bayesian estimation, uncertainty-oriented, probabilistic matrix. DIC statistics were generated to identify the best fitting models.

The deviance in the regressed, habitat, wavelength, 5m, RapidEye ™ emissivity fractionalized, endmember, transmittance, wavelength, 5m, risk-related, forecasting, iterative interpolation models were then defined as $-2^{*}\log$ (likelihood), where the 'likelihood' was defined as $p(y \mid \theta)$. This included all the normalizing constants where y comprised all stochastic node values, and θ stochastic parents of y in the risk model. 'Stochastic parents' are the stochastic nodes upon which the distribution of y depends upon when collapsing over all logical relationships [24].

We noted that when $y \sim$ Dnorm (mu, tau), then tau was a function of a parameter phi which was then optimally defined in PROC MCMC by the prior distribution in the risk model. Thereafter, the likelihood was defined as a function of phi in the models. The expectation $\overline{D} = E^{\theta}[D(\theta)]$ was optimally employed as a measure of model fitness based on the values of the emissivity, sub-mixel, reflectance, covariate coefficient values. The effective number of parameters included in the model was computed as $p_D = \overline{D} - D(\overline{\theta})$, where $\bar{\theta}$ was the expectation of θ. The DIC in the model generated the following conclusions: (1) the Dbar, was the posterior mean of the deviance, (2) the Dhat, was the point estimate of the deviance (i.e., $-2^{*}\log$ (likelihood)) obtained by substituting the posterior means θ bar of θ which then rendered Dhat $= -2^{*}\log$ $p(y$ — θ. bar); and, 3) pD was the effective number of explanatorily, endemic, immature riverine, tributary, immature habitat, transmission, endmember, RapidEye ™, 5m, resolution estimators provided by pD = Dbar – Dha and pD employing the posterior mean of the deviance minus the deviance of the posterior means.

In normal hierarchical eco-epidemiological, vulnerability, forecasting models, Pad = TR

(H), where H is the 'hat' matrix maps the observed data to their fitted values (3). The DIC was then optimally calculated as: $DIC = p_D + D$. The DIC value for the finalized, field and remote specified, eco-epidemiological, risk models was 931.6.and 937.2 for the Gonycogo and Adibuk agro-village complexes.

L-BFGS uses a trust-region method for finding new update steps[24].We normalized the / scale of the objective functions as to reach a good floating point precision range (i.e.: values 'near' 1.0). Linear programming methods are algebraic techniques based on a series of equations or inequalities that limit a problem and are used to optimize a mathematical expression called an objective function whose enedmember constraints may be placed upon a problem[24].. In order to do so the regressors must be deterministic and able to be expressed in linear form.; An optimization problem was represented for the eco-georferenceable, trailing vegetaion, discontinuoulsy canopied, turbid water, eco-epidemiological, capture point, *S. damnsoum* s.l. habitats in the narrow riverine tributary , eco-epidemiological, intervention villages employing a function $f: A \to \mathbb{R}$ from the set A of the interpretively iteratable, interpolative, geo-spectrotemrpoally gospatially geosampled, Rapid Eye, 5m wavelength, frequency, trasnmittance, paramterizable, covariate, coefficient values.In so doing, an element x_0 in A was rendered such that $f(x_0) \leq f(x)$ for all x in A ("minimization") or such that $f(x_0) \geq f(x)$ for all x in A ("maximization").(see Figure 62).

Figure 62 A local minimum x^* defined as a hypeproductive, eco-epidemiological, capture point, eco-georferenceable, *S. damnsoum* s.l. point for which there existed some $\delta > 0$ so that $\|\mathbf{x} - \mathbf{x}^*\| \leq \delta$; when the expression $f(\mathbf{x}^*) \leq f(\mathbf{x})$ for the Gonycogo study site

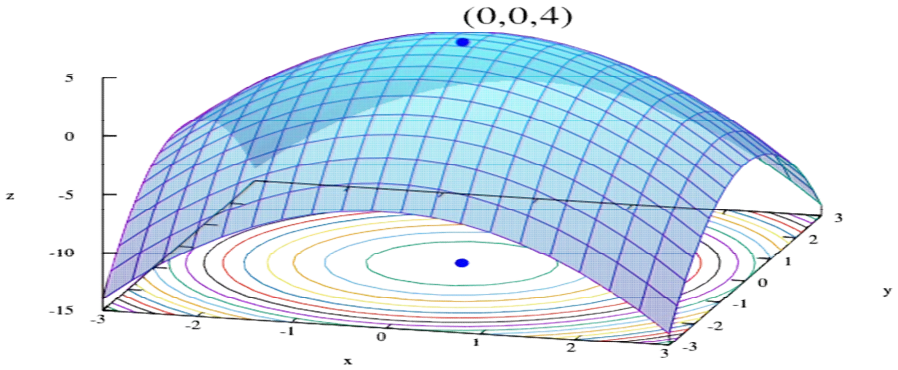

Median parameter values, as well as the 95% credibility intervals (2.5 percentile and 97.5 percentile values), were autoregressively probabilistically generated for the residually, forecasted, normalized, covariate, emissivity, estimator dataset. As the capture point, immature habitat sampling sites increased based on the estimators the geo-predictor, Percentage of trailing hanging vegetation, geo-classified LULC increased as did, the median log-larval count in both study sites. The adjusted model quantitated the independence amongst the time-series, explanatively depende,t field and remote-specified, observational eco-epidemiological forecastors representing the larval counts. Proximity collinearity to a global orientation in a Bayessian probabilistic paradigm can generate propagation error such as heteroskedastic parameters (Jacob et al 2005). We noted this model fit better than the model

that adjusted for correlation within the narrow tributary, riverine, eco-epidemiological, agro-village complex study sites based on the root mean square error (RMSE).

Next, a explanatory dataset of Red Edge, NDVI, optimally parameterized, RapidEye 5m, covariate emissivities was generated in ArcGIS employing the reflectance, 5m RapidEye ™ waveband data (i.e., capture point) geosampled at the agro-village complex, ecosystem, study sites. For each NDVI value, the total LULC areas were optimally determined for specific, topographic, LULC vegetation, cover classes ecologically associated to the eco-georeferenced, capture point, immature habitats. The equation Image Server employed to render the output produced a single-band dataset from each 5m, LULC, data product in ArcGIS. The differential reflection in the red and infrared (IR) bands from the 5m imager enabled robustly quantifying density and intensity of sparsely shaded, within-canopy, LULC objects (e.g., trailing vegetation) employing the reflectivity of solar radiation.

A RapidEye ™ Red Edge, NDVI, *S. damnosum* s.l., habitat, 5m, wavelength, transmittance emissivity, empirical, LULC datatset was then created employing ENVI, and a spectral library file was opened. A standard ENVI spectral library (.sli) was selected, launching ENVI's Spectral Library Viewer. The left side of the Spectral Library Viewer dialog listed the Red Edge endmember, 5m, NDVI, immature, habitat biosignature within the selected library. The right side of the viewer used the tabs to display the metadata for selected unmixed, Red Edge, NDVI, immature habitat, Chl-*a*, explanatory variables and queried selected biosignature-oriented, time series, explanative LULC, reflectance, coefficient values. Metadata for the selected biosignature appeared in the Metadata tab.

We then generated a correlation, time series, 5m, RapidEye™, uncertainty matrix in ENVI to determine the accuracy of a decomposable dataset of spectroscopic, Red Edge, NDVI, habitat emissivity, covariate estimators synthesized in ArcGIS. The row in the matrix eco-cartographically illustrated the Red Edge, NDVI, biosignature data constructed from the RapidEye™ data products, while the columns represented the reference data (i.e., in-situ geosampled data) in the object-based classifier. Measures of thematic accuracy were also generated including overall LULC accuracy and percentage of omission forecasting of the eco-epidemiological, habitat capture point's sub-mixel reflectance variables. The habitat wavelength, covariate coefficient, indicator measurement values were the percentage of 5m mixels that were in a given Red Edge, geoclassified, NDVI class, but these were not eco-geographically or ecohydrologically geo-spatiotemporally geoclassified.

The Red Edge NDVI biosignature produced in ENVI of the geosampled,narrow tributary, riverine, trailing vegetation, hyperproductive, discontinuous, sparsely shaded, canopied, *S. damnosum s.l.* immature habitat capture points in Gonycogo and Adibuk ago-villages was subsequently exported into ArcMap. The NDVI was filtered in ArcMap for optimally determining and robustly quantitating the lowest unmixed, fractional 5m, wavelength, emissivity, transmittance radiance, values that were geo-spectrotemporally associated with healthy geoclassifiable,, discontinuous canopy, green vegetation LULC endmembers. To determine this value, the natural RapidEye™ color imagery as the top layer was color balanced and then added to the Red Edge, NDVI, canopy layer (see Figure 63). By clicking on multiple 5m mixels with the Identity Tool in ENVI, the edge of live/dead, discontinuous, canopy, LULC vegetation, unmixed, reflectance data feature attributes of the hyperproductive, time series dependent, geosampled, habitats in the Gonycogo and Adibuk study sites were eco-cartographically robustly illustrated (see Figure 64).

Figure 63 Braod classifiaction preview of a cluster of sporadic 5m, Rapid Eye ™ canopy cover of a seasonal, hypeproductive , trailing vegetion, turbid water, eco-georferenceable, capture point, *S. damnosum* s.l. habitat at the Adibuk agro-village, eco-epidemiological study site

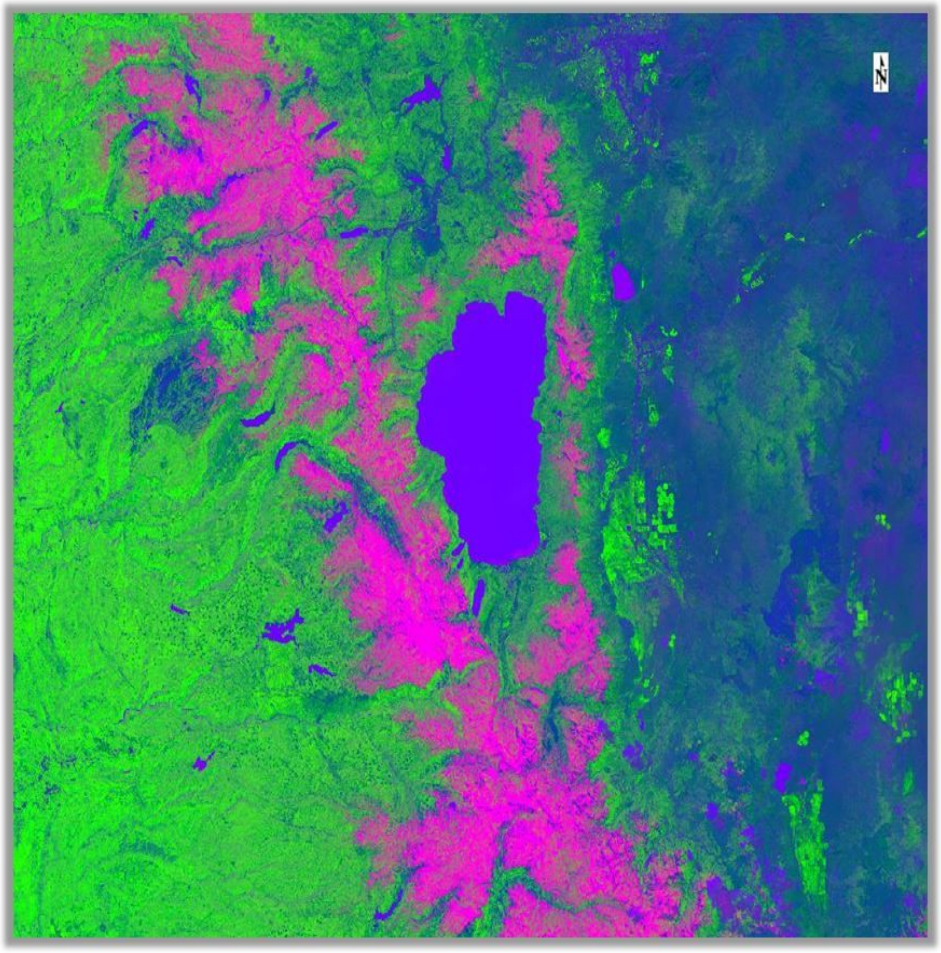

Figure 64 Flassh ™ discontinuous Rapid Eye ™ canopy reflectance and spectral angles of the *S. damnosum* s.l.,capture point in Adibuk village using object-based cluster of positively autorccorelated immature hyperproductive immature habitats along with a canopied capture point in Gonycogo village

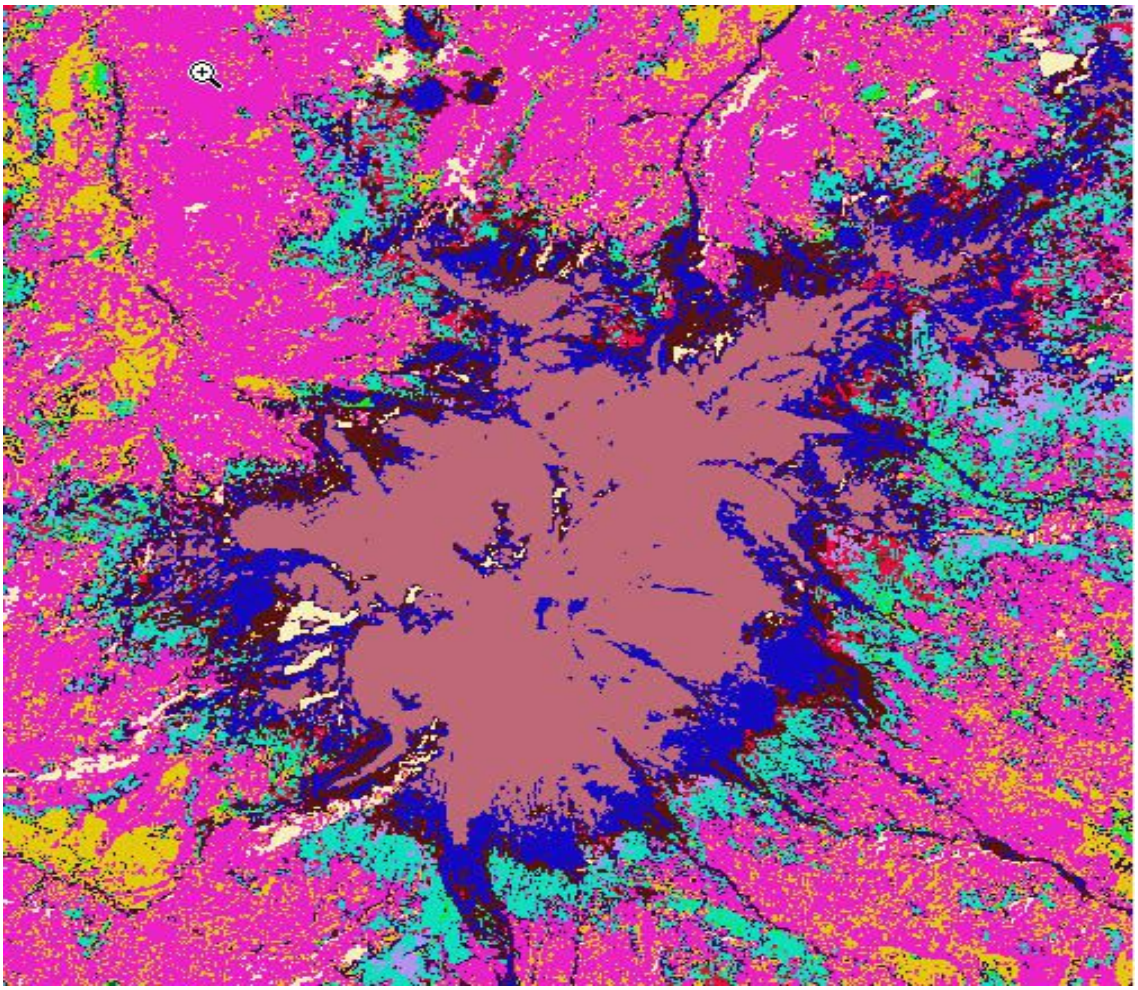

From the Endmember Collection SID dialog we selected Import > *spectra_source* for collecting and archiving the unmixed, hyperproductive, geosampled, decomposed, immature 5m, NDVI decomposed, endmember habitat data. The SID, LULC endmember parameters dialog appeared. Thresholding options were selected from the Set Maximum Divergence Threshold area. The Single Value parameterization was employed for quantitating unmixed, endmember Red Edge, NDVI, trailing vegetation and turbid water, *S. damnosum s.l.,* immature habitat, canopied, vegetation-related, LULC sub-mixel radiance. A single threshold was chosen for geo-classifying the hyperproductive, geosampled, geoclassifiable, LULC, habitat classes. A value was then entered in the Maximum Divergence Threshold field. This was the minimum allowable variation between the sparsely shaded, unmixed, geoclassified, trailing vegetation and turbid water, LULC endmember, discontinuous, unmixed, canopied, spectrum vector and the mixel vector. The default value was .05.

Multiple decomposed endmember values were subsequently entered into a different divergence to test each geoclassified, RapidEye ™, 5m, canopy endmember, LULC class against its corresponding maximum spectral divergence. A class was selected to assign threshold immature, habitat, vegetation, sub-mixel, fractionalized, eco-georeferenced LULC, endmember sub-mixel, reflectance values, which edited the value in the Edit Selected Value field employing the Maximum Divergence Threshold dialog for each capture point intervention scene..

We also employed the Spectral Information Divergence (SID) classification in ENVI to compare the similarity between the selected Red Edge, NDVI, eco-georeferenced, sparsely shaded, habitat, canopy-oriented, floating, hanging and dead vegetated, geoclassified, riverine, geospectral, LULC, decomposed components by measuring the probabilistic discrepancy between their corresponding wavelength, transmittance emissivities in the Gonycogo agro-village study site. The ToolBox Classification in ENVI was selected to perform the geo-classification chores. From the Endmember Collection dialogue menu bar, the SID algorithm was then selected. The Classification Input File dialog appeared, and an input file was selected which performed the spatial and geospectral subsettings and masking.

ENVI technology then automatically categorized each individual 5m, fractionally decomposed endmember, LULC, wavelength emissivity, geo-classifed, RapidEye™ data feature attribute from the Red Edge, NDVI biosignature transmittance, data products based on discontinuous, floating trailing and dead vegetation geospectral, canopy classes. The object classifier converted the remotely-sensed raster layers to vector coverages which were then geo-classified as shapefiles. ENVI provided interactive spatial/spectral mixel editing for the unmixed, components in the Red Edge, narrow riverine, immature habitat, sparsely shaded, trailing vegetation, NDVI biosignature.

The variation of turbid water reflectance was minimal in the blue. The minimum near 440 nm corresponded to the to Chl-*a* absorption. This was distinct in the unmixed, immature, hyperproductive habitat reflectance spectra in the range 400 to 500 nm, which did not have pronounced decomposable NDVI, biosignature, sub-mixel, eco-georeferenceable, iteratively interpolatable, data feature attributes over the broad range of quantitated turbidity and Chl-*a* concentration coefficient values. Absorption by dissolved organic matter and scattering by particulate matter may have contributed to the unmixed, canopied, habitat wavelength, emissivity, transmittance endmember, discontinuous, multiscattering reflectance, LULC patterns, in specific spectral ranges and, as a result, the blue to green ratio (i..e, R440/R550) was poorly related to Chl-*a* but appeared adequate for estimating Chl-*a* in the intervention riverine village study site waters (0.24, RMSE).

In the green range around 550 nm, absorption by the orthogonally decomposed, partially canopied, capture point, immature habitat pigments was minimal and scattering by all particulate matter played the main role in the latent, intra-cluster, geo-classifiable, eco-georeferenceable, LULC quantitation algorithmic decomposition, exercise. Reflectance in this range varied about three-fold with fractionalized, endmember variations in the concentration and composition of each of the unmixed, habitat, RapidEye ™, 5m, biosignature, endmember, reflectance, constituents. Interestingly, the frequency peak manifested minimal combined absorption by all the unmixed geosampled, geoclassifiable, immature, habitat, LULC, unmixed canopy pigment constituents (e.g., zeathinins). The reflectance peak position shifted toward longer wavelengths with increasing Chl-*a*, from 688

nm to about 706 nm. Chl-*a* demonstrated a strong relationship to peak magnitude of the fractionalized decomposed, canopied, biosignature As the water content of leaves in vegetation canopies increased, the strength of the absorption around 1599 nm increases Absorption at 819 nm iws nearly unaffected by changing turbidity water content, so it is used as the reference threshold marker.

Figure 65. Sub-mixel, canopy pigment reflectance constituents of the georeferenced, geosampled, sparsely shaded, trailing vegetation, turbid water, riverine, hyperproductive *S. damnosum* s.l. habitat capture point.

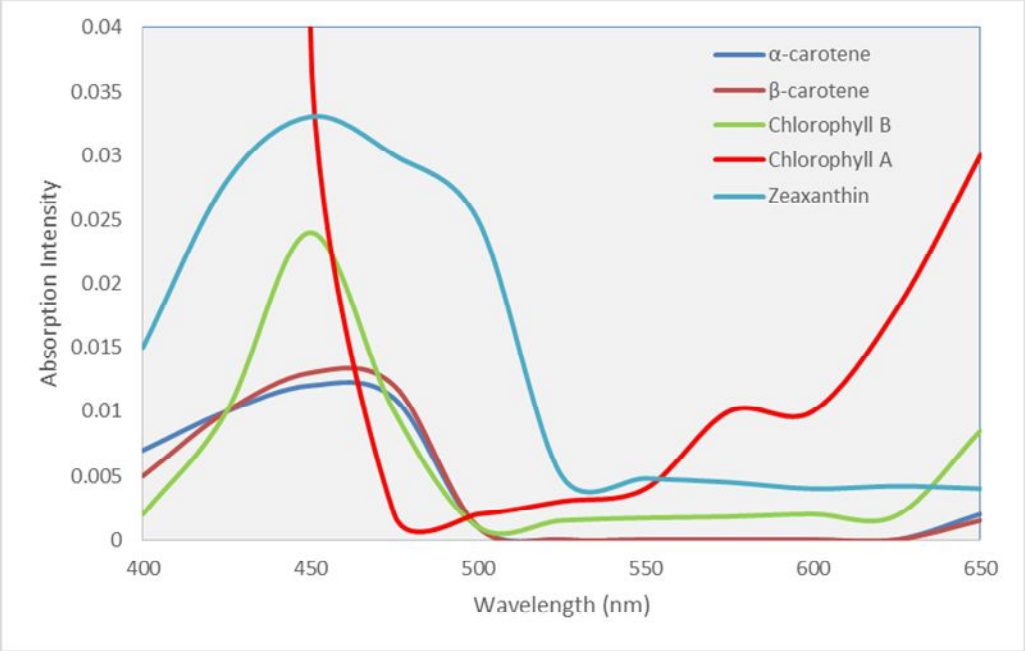

.

Classification output was selected to Memory in ENVI. Output Rule Images was selected to determine whether or not to create rule images. The rule images were employed to create intermediate geoclassifiable, endmember, unmixed, image results before final assignment of the Red Edge, 5m, RapidEye™ NDVI, hyperproductive, *S. damnosum s.l.*, geosampled, riverine, immature habitat, capture point Chl-*a*-related, canopied LULC classes. The Rule Classifier was employed to create a new classification image without having to recalculate the entire scene.

The bidirectional reflectance, 5m resolution, wavelength, transmittance, emissivity, decomposed, Red Edge, NDVI, biosignature covariate estimators in the eco-georeferenceable, hyperproductive habitat,capture point, geo-spectrotemporal, Chl-*a* model were changed as needed. In Preview the display was updated. ENVI added the resulting output to the Layer Manager. The output from SID was a classified 5m image and a set of classified sub-images (one per sparsely shaded, eco-georeferenced, partially canopied, geosampled, immature habitat, decomposed endmember). The 5m, sub-mixel values of the rule images represented the SID value. The output of the equation that defined SID for a pair of geospectral endmember vectors was identified. Lower canopy, spectral divergence measures represented better matches to the unmixed, LULC, endmember, RapidEye™, fractionalized, Chl-*a*, endmember, derivative, forecast spectra.

Areas that satisfied the Maximum Divergence Threshold criteria were carried over as geoclassified areas into the immature habitat, Red Edge, endmember, LULC, discontinuous spectrum, vector image. The SID successfully calculated all the unmixed, probabilities of the endmember, biosignature decomposed data in the library.

The ENVI library accounted for all processes and factors influencing the fractionalized Red Edge, habitat, Chl-*a*, endmember, 5m resolution radiance data collections as rendered from the unmixed, hyperproductive, sparsely shaded, immature habitat, Red Edge, NDVI biosignature, which was subsequently converted to match the library-based data. Analogously, the reference fractionalized, endmember, derivative, Chl-*a*, discontinuous, canopy spectra in the library were transformed into the trailing vegetation, forecast, endmember spectra of the orthogonally decomposed biosignature. We expressed these sub-mixel, linear combinations as image endmembers of sparsely shaded, discontinuous, sparsely shaded, canopy vegetated, geoclassified, LULC, decomposed, capture point, derivative, spectra. A function incorporating the calibration and the alignment was repeatedly evaluated for different candidate groups of Red Edge, NDVI biosignature, decomposed variables until a suitable representation of the unmixed, Chl-*a*, image endmembers was determined.

Before applying the spectral index to the RapidEye^{TM} 5m resolution imagery, raw Chl-*a*, mixel values (i.e., DNs) were converted into physically meaningful units to optimally differentiate fractionalized, reflectance, LULC, decomposed, endmember, derivative spectra and immature *Simulium* productivity based oncapture point habitat size in ENVI in the Gonycogo study site study sites, The DNs of the RapidEye^{TM} image mixels represented absolute calibrated radiance values for non-atmospheric, corrected, image Chl-*a*, sub-mixel, reflectance values. To convert the DN of the eco-georeferenced, habitat mixel to radiance it was necessary to multiply the DN value by the radiometric scale factor, as follows: RAD(i) = DN(i) * radiometricScaleFactor(i). The resulting value in the forecasting, Chl-*a*, eco-epidemiological, reflectance, endmember, risk model was the Top of Atmosphere (TOA) radiance of the 5m mixel expressed in watts per steradian per squaremeter ($W/m^2sr\ \mu m$).

The instantaneous fraction of direct beam radiation intercepted by canopy Chl-*a* was remotely tabulated and described mathematically as $fPAR = 1 - \exp(-kLAI/\cos\theta_s)$ in ENVI. The extinction coefficient k was a function of leaf angle distribution. The factor $LAI/\cos\theta_s$ eco-geographically represented the geo-classified, metaheursitically optimizable, explicative, LULC optical thickness. Thus, the proportion of incident fPAR that was intercepted by the habitat was dependent on the canopy Chl-*a* structure and (LAI). Asrar et al. [148] demonstrated that NDVI and APAR are functions of LAI.

The Red Edge, NDVI, decomposed biosignature, endmember, 5m, RapidEye^{TM} eco-epidemiological, datasets rendered from the capture point, *S. damnosum* s.l. habitat, Chl-*a*-related, decomposition variables were calculated employing simulated PAR and NIR albedo, which compared well to the extracted geoclassified, LULC, wavelength, frequency-orinted, transmittance, 5m, covariate emissivities reported by Asrar et al. [148], who suggested that orthogonally explanatively decomposed, expositively fractionalized, discontinuously canopy, vegetated, LULC endmember, wavelength, transmittance, emissivities by horizontally oriented leaves were not dependent on θs. In the partially canopied, sparsely shaded, endmember unmixed, eco-epidemiological Chl-*a*, decomposition models, those sub-mixel reflectance values of the canopy were dominated by vertically oriented leaves which were dependent on θs.

The Red Edge position was thereafter employed to exactly estimate the Chl-*a* content of leaves and over the discontinuous, infrequnetly canopied, geoclassified LULC for categorizing the hyperproductive, capture point, immature habitat, which was easily calculated using the reflectance of Red Edge boundary wavebands at 675 and 755 nm (R_{675} and R_{755}) and reflectance of Red Edge center wavelength at 731nm (R_{718}), with the equation RES = $(R_{718}$-$R_{675})/(R_{755}$- $R_{675})$. The close relationships between the simulated geoclassified LULCs and riverine, immature habitat Chl-*a* concentration count indicated a high feasibility for formatting the photosynthetic pigment with simulated LULCs from the 5m RapidEye ^{TM} imaged data.

The Chl-*a*, endmember data was then exported to an ArcGIS 10.3 cyberenvironment. The convex geometry SPA provided information on the convergence of the algorithm in ArcGIS. This property was employed in the SPA algorithm to determine the main step in the habitat, endmember, sub-mixel, unmixing, biosignature execise for identification of the Red Edge, NDVI, geospectral, heterogeneous variables at the vertices of the simplex. For the given geosampled, Chl-*a*, endmember, immature habitat, biosignature, unmixed point in the simplex, a point with maximum distance was at the vertex of the simplex.

By including a constraint on the geospatialized, Euclidean subspace adjacency rendered from the sub-mixel, capture point, immature habitat, decomposed dataset with their respective individual, endmember, 5m, wavelength, reflectance, fractionalized, unmixed, transmittance, emissivity values, the SPA algorithm captured the contiguous VI in red, IR and NIR bands, employing advanced data pre-processing latent algorithmic applications in ArcGIS. This made discerning interpolatable, Chl-*a*, RapidEye^{TM}, discontinuous canopy, data feature attributes very simple. Further, the algorithm reduced the susceptibility to outlier, 5m-mixel, erroneous, resdiualizable, fractionalized, illumination coefficients which allowed for metaheuristically optimizing the unmixed canopy, 5m, resolution endmember, Chl-*a* reflectance, forecast, derivative spectra, and geo-classifying the spectroscopic data based on their exact decomposed, endmember, reflection data feature attributes.

Although, the decomposed, Red Edge, NDVI,capture point, immature habitat endmember decomposed, proxy biosignature, LULC values were extracted in ArcGIS, the final dataset did not include any treatment of diffuse Chl-*a* irradiance and canopy multiple scattering or leaf specularity. This photosynthetic decomposition exercise required the selection of individual RapidEye^{TM,} wavelength,frequency-orinted, decomposable emissivities for each, geoclassified, LULC, biosignature-related, unmixed canopy Chl-*a*, endmember, iteratively interpolatable, emissivity, 5m, wavelength, transmittance, data feature attribute which was then calculated by the radiative transfer equation.

We employed a three-dimensional, radiative transfer model to further decompose the Red Edge, trailing vegetation, *S. damnosum s.l.* habitat, capture point, proxy biosignature. The process of solar radiative transfer at the land surface is important to energy, water, and carbon balance, especially for discontinuous canopy-vegetated, LULC areas [1]. We employed a two-stream model to consider the geoclassified, plant functional types (PFTs) LULCs within a digitized 5m RapidEye^{TM} grid to be independent of each other and their leaves to be horizontally homogeneous. Unique identifiers were attached to each stratified grid cell. The model gridded, eco-epidemiological, residual, eco-georferenceable forecasts revealed an increase of canopy Chl-*a*, absorption within geoclassifiable, LULC geolocations of hyperproductive habitat canopy with a large sun zenith angle θ_{sun}, which may have been

due to increases of the ground and sky shadows and of the optical pathlength due to the shadow overlapping between the eco-georeferenced, habitat canopy layers.

A decrease of canopy Chl-*a*, absorption occured in the densely vegetated, LULC, sparsely shaded, georeferenced, geoclassified, riverine, habitat areas with small θ_{sun}. For the one-layer canopy model, these decreases may have been due to crown shape effects that enhanced the transmission through the canopy edge. For the multilayer canopy portion of the habitat, aside from the shape effects, emissivity, m RapidEye ^{TM,} wavelength, Chl-*a*, transmission may have been increased by the decreased ground shadow due to the shadow overlapping between layers. Ground absorption usually changes with opposite sign as that of the canopy absorption [23]. Somewhat lower albedos were found over most vegetated, LULC canopied, trailing vegetation, turbid water, geoclassified areas. The 3D, forecasting, eco-epidemiological, geo-spatiotemporal, wavelength, emissivity model quantitated the effects of the fraction of sunlit canopy leaves and their corresponding Chl-*a*, absorption values in the hyperproductive *S. damnosum* s.l. habitat.

In the geometric-optical model, the bidirectional 5m, RapidEye ^{TM} habitat reflectance was modeled as a pure phenomenon that resulted in scenes of discrete, 3-D objects (i.e., trailing vegetation, sub-mixel, endmember components) from the *S. damnosum* s.l. habitat being illuminated and viewed from different positions in the hemisphere. The resulting scenes were broken down into their habitat canopy Chl-*a* values and geoclassifiable LULC fractions, specifically sunlit and shadowed background and scene brightness. Illumination direction was calculated by a linear combination of the canopy Chl-*a* fractions and their respective decomposed, fractionalized, 5m, wavelength, transmittance, emissivity, radiance estimates. The shape of the derived geoclassifiable, canopied, trailing vegetation, endmember, LULC, geospatial patterns of the diffuse, rippled water components were the driving probabilistic, geo-spatiotemporal regressors in the model. These trailing vegetation, habitat, canopy spectral, Red Edge, sub-mixel, wavelength, transmittance emissivities conditioned the mixture of sunlit and sparsely shaded objects and background data that were observed from multiple viewing directions, quantitating all directions of illumination in the 5m decomposed endmembers in ArcGIS. This mixture, in turn, controlled the brightness in the RapidEye^{TM} image. Corrections in the effects from varying sun sensor target canopy Chl-*a* geometries in the multitemporal, decomposed datasets were described by the BRDF. Measuring the spread of the corrected results from the desired equal reflectance line provided a measure of the accuracy of our method. After correction, the reflectance RMSE errors was approximately 0.01 in the visible and 0.02 in the NIR.

An expression for additional azimuthual variation was also optimally derived from the geometric-optical, LULC, RapidEye^{TM}, Chl-*a* forecasting, wavelength, forecasting, emissivity model. This azimuthual quantitated radiance variation for each layer of the Red Edge, hyperproductive habitat, NDVI, riverine, unmixed, endmember, biosignature, canopy Chl-*a*, illumination variables. It was observed that all non-zero polar angles were most evident in the georeferenced, immature habitat canopy, Chl-*a* concentrations when vertical and nearly opaque components of the habitat canopy and its floating, hanging and dead vegetation, geoclassified LULC components were illuminated and viewed along polar sun angles. For the variation of the directional Chl-*a* reflectance of the habitat, canopied LULC cover with azimuthual view angle, geoparameters were quantified when the illuminated area of the 5m imaged canopied, riverine larval habitat (i.e., areas that were affected by the sun at large angles from the zenith) were remotely identified.

The eco-epidemiological, vulnerability, risk model results indicated that the cause of the azimuthual variation could be traced to solar flux illumination of the vertically-oriented Chl-*a* components in the georeferenced habitat and the variation of sub-mixel reflectance moderated by azimutually isotropic sources of flux from sky light and the overall habitat, LULC 5m, RapidEye ^{TM} reflectance values. Spectral unmixing yielded abundance estimates for each canopy Chl-*a* endmember together, summing-up to the 100% reflectance measured in the RapidEye^{TM} image. A scattergram representing the canopy unmixed, endmember, reference biosignature of the hyperpoductive *S. damnosum* s.l. habitat, and its associated trailing and floating vegetation, sub-mixel, spectral LULC, Chl-*a,* unmixed, wavelength 5m, transmittance, reflectance values, was then generated. The spectral biosignature was found to be characteristic of the Red Edge, *S. damnosum* s.l, immature prolific, habitat. The composition of this signature was 134.67 red, 145.24 blue and 114.101 green. The images were analyzed to predict potential *S. damnosum s.l.* larval habitats.

The Sechhi depth was then calculated for the hyperproductive, canopied, *S. damnosum s.l* larval habitat geosampled at the Gonycogo eco-epidemiological, riverine, study site for aiding in probabilistically regressively quantitating the Chl-*a* concenrations in the canopy. The Secchi depth is reached when the reflectance equals the intensity of light backscattered from the water [23]. This depth was divided into 1.7m yields which we used as the attenuation coefficient (i.e, an extinction coefficient), for the available light averaged over the Secchi disk depth for the georeferenced, canopied, hyperproductive habitat. While used as a variable, the extinction coefficient is also used as a variable for turbidity [23, 24]. The light attenuation coefficient k was employed in a form of the Beer–Lambert law [i.e. $\frac{I_z}{I_0} - e^{-kz}$] to estimate I_z, the intensity of canopy Chl-*a*, light at depth *z* from I_0, and the intensity of light at the hyperproductive habitat surface.

The modelled transmittance, canopied, wavelength emissivities of hyperproductive, canopied, *S. damnosum s.l* habitat, sparsely shaded, Chl-*a,* unmixed, 5m, RapidEye^{TM}, decomposed, wavelength emissivity sample material was related to its optical depth τ and to its absorbance A as $T = \frac{\Phi_e^t}{\Phi_e^i} = e^{-\tau} = 10^{-A},$ as tabulated in ArcGIS, where Φ_e^t was the immature, habitat canopied, surface radiant flux transmitted by the material sample, and Φ_e^i was the radiant flux received by that material sample. Due to certain canopy uniform attenuation, these relations became $T = e^{-\sum_{i=1}^{N} \sigma_i n_i \ell} = 10^{-\sum_{i=1}^{N} \varepsilon_i c_i \ell},$ or equivalently $\tau = \sum_{i=1}^{N} \sigma_i n_i \ell, A = \sum_{i=1}^{N} \varepsilon_i c_i \ell c = \frac{\mu_{10}(\lambda)}{\varepsilon(\lambda)}.$

The amount Chl-*a*, concentration *c* was then optimally rendered by a mixture containing two discontinuous,canopy sparsely shaded, geoclassified, eco-georeferenced, LULC types at amount concentrations c_1 and c_2. The attenuation coefficient at any Red Edge wavelength λ was then given by $\mu_{10}(\lambda) = \varepsilon_1(\lambda)c_1 + \varepsilon_2(\lambda)c_2$. Hence, measurements at two RapidEye ^{TM} wavelengths yielding two equations in two unknowns was sufficient to quantitate the amount concentrations c_1 and c_2, as long as the molar attenuation coefficient of the the surface habitat, decomposed, 5m RapidEye ^{TM} reflectance, wavelength, emissivity components, ε_1 and ε_2 were known at both wavelengths. We solved the equation in ArcGIS employing linear least squares to determine the two amounts of canopy Chl-*a* concentrations from measurements made at more than two wavelengths. Mixtures containing more than two components can be analyzed in the same way, using a minimum of *N* 5m-resolution,

wavelengths for a mixture containing *N* components [23]. Four equations at four different wavelengths were then employed to determine *Cp*, *Cn*, *Cc*, and *Cw* in ArcGIS. The Red Edge bands considered most sensitive to Chl-*a* were tested with the simulated, canopy, endmember decomposed dataset from a spectral range of 490 nm to 730 nm. For efficiently extracting Chl-*a* concentrations, low reflectance at wavelengths less than 500 nm has been associated to absorption by both algal pigments (e.g., Chl-*a*) and dissolved organic matter [www.esri.com]. Likewise, an increase in endmember, estimator reflectance at wavelengths 510–620 nm has been associated to low absorption by phytoplankton pigments coupled with increased backscattering due to high particle concentration. A peak of reflectance at 685–715 nm may be due to Chl-*a* fluorescence [23]. The relationship between the decomposition coefficient and the hyperpoductive, sparsely shaded, habitat Chl-*a* was then determined by using various regression models.

For metaheuristically determining an empirical dataset of metaheuristic, optimal, hyperproductive, eco-georeferenceable, Chl-*a*, *S. damnsoum s.l.* habitat, trailing vegtaion, turbid water, discontinuous, sparsely shaded predictors, a semivariogram was constructed which expressed the variation in the spectral, Red Edge, NDVI endmember, reflectance, unmixed, parameterized, illumination, covariate coefficients. The semivariogram was nonnegative $[\gamma(x,y) \geq 0]$. The semivariogram $\gamma(x,x) = \gamma_i(0) = E\left((Z(x) - Z(x))^2\right) = 0$ was at distance 0 since at zero the residual, discontinuously canopied, trailing vegetation, eco-georeferenced, geosampled, turbid water habitat,geo-spectrotemporal forecast was $Z(x) - Z(x) = 0$. A semivariogram holds if and only if it is a conditionally negative definite function for all weights $w_1, \ldots, w_N$ subject to $\sum_{i=1}^{N} w_i = 0$ and geolocations $x_1, \ldots, x_N$, it holds: $\sum_{i=1}^{N}\sum_{j=1}^{N} w_i \gamma(x_i, x_j) w_j \leq 0$ [24]. The interpolated, operationizable, decomposed, habitat, Chl-*a*, unmixed endmember, 5m RapidEye^{TM}, NDVI proxy biosignature, wavelength emissivity, transmittance variables corresponded to the variance $var(X)$ of $X = \sum_{i=1}^{N} w_i Z(x_i)$, which was given by the negative of this double sum. As a consequence the interpolated, temporally dependent, riverine, immature habitat

A differential equation in Calculus Methode/Map Server ^{TM} was then used to solve a solution in to determine whether solutions existed for all the uncoalesced eco-georfernceable, hypeproductive, *S. damnsoum* s.l. capture point notabl,5m, endmember subjects of interest. A first order dataset of Chl-*a* initial values for dataset of was tested. Given any eco-georferenceable explicative point seasonally hypeproductive, trailing vegetation, turbid water, discontinuous, infrequently canopied, sparsely shaded, agro-village , narrow riverine tributary, *S. damnosum* s.l. capture point (a,b)in the xy-plane we were ble to define some rectangular region Z, such that $Z = [l,m] \times [n,p]$and $(a,b)$is in the interior of Z. a differential equation $\frac{dy}{dx} = g(x,y)$ was generated where the condition that $y = b$when $x = a$, locally existed. A solution was rendered $g(x,y)$and $\frac{\partial g}{\partial x}$which were both continuous on Z. This solution existed on some Ch*l*-a interval at a. We then tesetd if we had a linear initial value problem of the nth order employing $f_n(x)\frac{d^n y}{dx^n} + \cdots + f_1(x)\frac{dy}{dx} + f_0(x)y = g(x)$suchthat

$y(x_0) = y_0, y'(x_0) = y'_0, y''(x_0) = y''_0, \cdots$ For any nonzero $f_n(x)$, if $\{f_0, f_1, \cdots\}$ and g that was non- continuous on some interval containing a unique x_0, y existed in the *S. damnosum* s.l. capture point differential equation.swas discontinuous only at the origin.

Stochastic partial differential equations (SPDE) were also generated in Calculus Methode/Map Server [TM] They were essentially partial differential equations that has random forcing terms and uncoalesced , trailing vegation, disocntinuous, sparsely shaded, %m radiance coefficients. As with deterministic ordinary and partial differential equations, it is important to know whether a given SDE has a solution, and whether or not it is unique[24]. We employed uniqueness theorem for Itô SDEs taking values in *n*-dimensional Euclidean space $\mathbf{R}^n$ which was driven by an *m*-dimensional Brownian motion *B*; the proof may be found in Øksendal (2003, §5.2).In we let $T > 0$, and let $\mu : \mathbb{R}^n \times [0,T] \to \mathbb{R}^n; \sigma : \mathbb{R}^n \times [0,T] \to \mathbb{R}^{n \times m}$ be measurable endmember functions for which there existed constants *C* and *D* such that $|\mu(x,t)| + |\sigma(x,t)| \leq C(1 + |x|$. I so doing $|\mu(x,t) - \mu(y,t)| + |\sigma(x,t) - \sigma(y,t)| \leq D|x - y|$; for all $t \in [0, T]$ and all *x* and *y* $\in \mathbf{R}^n$, where $|\sigma|^2 = \sum_{i,j=1}^{n} |\sigma_{ij}|^2$. We then let *Z* be a random variable that is independent of the σ-algebra generated by B_s, $s \geq 0$, and with finite second moment: $\mathbb{E}[|Z|^2] < +\infty$. Then the stochastic *S. damnosum* s.l. differential equation/initial value problem $\mathrm{d}X_t = \mu(X_t, t)\,\mathrm{d}t + \sigma(X_t, t)\,\mathrm{d}B_t$ for $t \in [0,T]; X_0 = Z;$ has a Pr-almost surely unique *t*-continuous solution $(t, \omega) |\to X_t(\omega)$ such that *X* was adapted to the filtration F_t^Z generated by *Z* and B_s, $s \leq t$, and $\mathbb{E}\left[\int_0^T |X_t|^2\,\mathrm{d}t\right] < +\infty.$ In so doing, $dX_t = (a(t)X_t + c(t))dt + (b(t)X_t + d(t))dW_t X_t = \Phi_{t,t_0}\left(X_{t_0} + \int_{t_0}^{t} \Phi_{s,t_0}^{-1}(c(s) - b(s)d(s))ds + \int_{t_0}^{t} \Phi_{s,t_0}^{-1} d(s)dW_s\right)$

where $\Phi_{t,t_0} = \exp\left(\int_{t_0}^{t}\left(a(s) - \frac{b^2(s)}{2}\right)ds + \int_{t_0}^{t} b(s)dW_s\right)$

$dX_t = \frac{1}{2}f(X_t)f'(X_t)dt + f(X_t)W_t$ for a given differentiable function f was equivalent to the Stratonovich SDE $dX_t = f(X_t) \circ W_t$ which had a general solution $X_t = h^{-1}(W_t + h(X_0))$ where $h(x) = \int^x \frac{ds}{f(s)}$ .The Stratonovich integral can be defined in a manner similar to the Riemann integral, that is as a limit of Riemann sums. the Riemann integral, was the first rigorous definition of the integral of a function on an interval [24].Suppose that $W : [0,T] \times \Omega \to \mathbb{R}$ is a Wiener process and $X : [0,T] \times \Omega \to \mathbb{R}$ is a semimartingale adapted to the natural filtration of the Wiener process. Then the Stratonovich integral $\int_0^T X_t \circ \mathrm{d}W_t$ is a random variable $: \Omega \to \mathbb{R}$ defined as the limit in mean square of $\sum_{i=0}^{k-1} \frac{X_{t_{i+1}} + X_{t_i}}{2}\left(W_{t_{i+1}} - W_{t_i}\right)$ as the mesh of the partition $0 = t^0 < t^1 < \cdots < t^n = 1$ of $[0,T]$ tends to 0. The Wiener process W_t is characterised by the following properties: 1)$W_0 = 0$ a.s.,2) *W* has independent increments: W_{t+u} - W_t is independent of $\sigma(W_s : s \leq t)$ for $u \geq 0$ 3) *W* has Gaussian increments: W_{t+u} - W_t is normally distributed with mean *0* and variance *u*, $W_{t+u} - W_t \sim N(0, u)$ 4) *W* has continuous paths: With probability *1*, W_t is continuous in *t*[24]. The independent increments means that if $0 \leq s_1 < t_1 \leq s_2 < t_2$ then $W_{t1} - W_{s1}$ and $W_{t2} - W_{s2}$ are independent random variables, and the similar condition holds for *n* increments (http://mathworld.wolfram.com/ html).

A variogram [$2\gamma(x, y)$] was generated in ArcGIS using a function form for describing the degree of dependence between the geo-predicted, hyperproductive, *S. damnosum* s.l. captue point seasonal habitats (i.e., $Z(x)$) in the Gonycogo and Adibuk agro-village , narrow tributary, study sites. This was defined as the expected squared increment of the forecasted values between the georeferenced habitat geolocations at the sites. The unmixed, Chl-*a,* interpolator was non-negative, since it was the expectation of a square. The covariance function was related to the semiovariogram by $2\gamma(x,y) = C(x,x) + C(y,y) - 2C(x,y)$. Interestingly, $\gamma(x,y) = E(|Z(x) - Z(y)|^2) = \gamma(y,x)$ was a symmetric function, consequently, $\gamma_s(h) = \gamma_s(-h)$ was an even function. The function was also a semivariogram, as it was a conditionally negative definite function, for all the sub-mixel, decomposed covariance weights in the *S. damnosum* s.l., eco-epidemiological risk model related to geolocations, which then was employed to statistically validate the unknown, un-geosampled, canopied, georeferenced, capture point habitat using the Chl-*a,* unmixed, wavelength 5m, RapidEye™, transmittance emissivities.

Since the covariance function of the stationary process existed in the hyperproductive *S. damnosum* s.l. habitats it was related to the semiovariogram by $2\gamma(x,y) = C(x,x) + C(y,y) - 2C(x,y)$ in both stsudy sites. But since our stochastic, endmember, interpolated, Chl-*a*, unmixed, RapidEye ™, eco-epidemiological, wavelength, emissivity, risk model reflected a non-stationary process, the square of the difference between expected Chl-*a* emissivity value was quantitated by $2\gamma(x,y) - C(x,x) + C(y,y) - 2C(x,y) + (E[Z(x)] - E[Z(y)])^2$. In the models.For quantitating a random field [i.e., stochastic process] $Z(x)$ on the domain D employing a covariance function $C(x, y)$, we used the covariance of the interpolated, Chl-*a*–oriented, endmember decomposed, RedEdge, NDVI, sub-mixel values of the random field at the two model geolocations x and y as $C(x,y) := \operatorname{cov}(Z(x), Z(y))$.

The following RapidEye ™ parameters operationally described the sparsely shaded, Chl-*a*, unmixed, interpolated, 5m, *S. damnosum* s.l. larval habitat, capture point, Gonycogo and Adibuk variograms. The nugget represented the height of the jump of the semivariogram at the discontinuity at the origin of the habitat endmember interpolator. The sill was the limit of the variogram tending to infinity lag distances. We also computed the range which was the distance in which the difference of the semiovariogram from the sill became negligible. In the geo-spectrotemporally, geospatially interpolated, sparsely shaded, canopied, Chl-a, *S. damnosum* s.l. habitat unmixed LULC, reflectance model with a fixed sill, the distance at which the sill was first reached for the habitat model was taken to be the distance when the semivariance first reached 95% of the sill.

We let X be an arbitrary set and H be a Hilbert space of real-valued, Chl-*a*, unmixed, canopy, endmember, hyperproductive, *S. damnosum* s.l., immature habitat, time series dependent functions on X in ArcGIS for the Gonycogo and Adibuk models. . The evaluation functional over the Hilbert space of functions H was a linear functional that evaluated each function at a sample estimated, georeferenceable, geosampled, eco-epidemiological, immature, habitat point x, $L_x: f \rightarrow f(x) \forall f \in H$. We say that H is a reproducing kernel Hilbert space if L_x is a continuous function for any f in H, or equivalently, if L_x is a bounded operator so that for any f in H there exists some $M > 0$, such that $L_x[f] = f(x) \leq M\|f\|_x \forall f \in H$ [142]. A more intuitive definition of the space was obtained by the evaluation functional of the Chl-*a*, unmixed, habitat, sparsely shaded, canopied endmembers, which was represented by taking the inner product of f in ArcGIS with a function K_x in H. This function was the reproducing

kernel for the Hilbert space *H* in the models More formally, the Riesz representation theorem implied that for all the x in *X* in the model here exists a unique element K_x in *H* with the reproducing property, $f(x) = L_x(f) = \langle f, K_x \rangle \forall f \in H$.

The habitat endmember, unmixed, wavelength, transmittance, vulnerability, 5m RapidEye™, eco-epidemiological risk models established an important connection between a Hilbert space and its (continuous) dual space. In the model the underlying field were the remote, immature capture point, hyperproductive, habitat variables in the Gonycogo and Adibuk agro-village complex models. where the remotely regressed, categorized covariates that were isometrically isomorphic. Let *H* be a Hilbert space, and let *H** denote its dual space, consisting of all continuous linear functionals from *H* into the field R or C. If *x* is an element of *H*, then the function φ_x, for all *y* in *H* defined by $\varphi_x(y) = \langle y, x \rangle$, where $\langle \cdot, \cdot \rangle$ denotes the inner product of the Hilbert space, is an element of *H** [149]. The Riesz representation theorem states that every element of *H** can be written uniquely in this form. According to the model forecasts, hyperproductive, *S. damnosum s.l.* habitat endmembers may be robustly mapped employing Φ: $H \rightarrow H^*$ defined by $\Phi(x) = \varphi_x$, which is an isometric (anti-) isomorphism, meaning that Φ is bijective. In mathematics, a bijection, bijective function, or one-to-one correspondence is a function between the elements of two sets, where every element of one set is paired with exactly one element of the other set, and every element of the other set is paired with exactly one element of the first set [24].

Further, since the norms of x and φ_x agreed in the hyperproductive Gonycogo and Adibuk habitat risk models, $\Phi(\lambda x) - \lambda\Phi(x)\|x\| = \|\Phi(x)\|\Phi$ was additive: $\Phi(x_1 + x_2) = \Phi(x_1) + \Phi(x_2)$. If the base field was R, then for all unmixed *S. damnosum* s.l. larval habitat estimators λ. If the base field is C, then $\Phi(\lambda x) = \bar{\lambda}\Phi(x)$ for all λ, where $\bar{\lambda}$ denoted the complex conjugation of λ [24]. The hyperproductive, *S. damnosum* s.l. larval habitat regression, endemic risk map Φ was described as follows. Given a non-zero element φ of *H**, the orthogonal complement of the kernel of φ was a one-dimensional subspace of *H*. Take a non-zero element *z* in that subspace, and set $x = \varphi(z) \cdot z / \|z\|^2$; then $\Phi(x) = \varphi$.

As mentioned earlier, the axiom of choice implies the Hahn–Banach theorem. The converse is not true. One way to see that is by noting that the ultrafilter lemma (or equivalently, the Boolean prime ideal theorem), which is strictly weaker than the axiom of choice, can be used to show the Hahn–Banach theorem, although the converse is not the case. The Hahn–Banach theorem is equivalent to the following:[1](∗): On every Boolean algebra *B* there exists a "probability charge", that is: a nonconstant finitely additive map from *B* into [0, 1] [24, 150, 151]. The Boolean prime ideal theorem is equivalent to the statement that there are always probability charges which take only the values 0 and 1. In ZF, one can show that the Hahn–Banach theorem is enough to derive the existence of a non-Lebesgue measurable set [26]. Moreover, the Hahn–Banach theorem implies the Banach-Tarski paradox. For separable Banach spaces, D. K. Brown and S. G. Simpson proved that the Hahn–Banach theorem follows from WKL_0 [151], a weak subsystem of second-order arithmetic that takes a form of König's Lemma restricted to binary trees as an axiom. In fact, they prove that under a weak set of assumptions, the two are equivalent, an example of Reverse mathematics.

Reverse mathematics is a program in mathematical logic that seeks to determine which axioms are required to prove theorems of mathematics. Its defining method can briefly be described as "going backwards from the theorems to the axioms", in contrast to the ordinary mathematical practice of deriving theorems from axioms. The reverse mathematics program

was foreshadowed by results in set theory such as the classical theorem that the axiom of choice and Zorn's lemma are equivalent over ZF set theory Zorn's lemma can be used to show that every nontrivial ring *R* with unity contains a maximal ideal. In the terminology above, the set *P* consists of all (two-sided) ideals in *R* except *R* itself, which is not empty since it contains at least the trivial ideal {0}. This set is partially ordered by set inclusion. Finding a maximal ideal is the same as finding a maximal element in *P*. The ideal *R* was excluded in the Gonycogo and Adibuk models because maximal ideals in the outputs were not equal to *R*.

To apply Zorn's lemma, we took a non-empty totally ordered subset *T* of *P* from the *S. damnosum s.l.* habitat endmember, 5m RapidEye™, eco-epidemiological, forecast, risk models. It was necessary to show that *T* had an upper bound (i.e. that there exists an ideal $I \subseteq R$ which is bigger than all the geoclassifiable geosampled, LULC members of *T* but still smaller than *R* in the riverine habitat dataset.s We took *I* to be the union of all the ideals in *T* in the models. Because *T* contained at least one element, the union *I* was not empty. To prove that *I* was an ideal, (if *a* and *b* are elements of *I*) $J, K \in T$ such that *a* was an element of *J* and *b* was an element of *K*. Since *T* is totally ordered, we knew that $J \subseteq K$ or $K \subseteq J$. In the first case, both *a* and *b* were members in the dataset *K*. Therefore their sum $a + b$ was a member of *K*, which also revealed that $a + b$ was a member of *I*. In the second case, both *a* and *b* were members of the ideal *J*, and thus $a + b \in I$. Since $r \in R$, in the Gonycogo and Adibuk models *ar* and *ra* were geoclassified as geosampled immature capture point habitat elements of *J* and hence elements of *I*. Thus, *I* was an ideal in *R* in both model renditions.

A bounded self adjoint operator on Hilbert space is a fortiori, a bounded operator on a Banach space [24]. Therefore, one can also apply to *T* the decomposition of the spectrum that was achieved above for bounded operators on a Banach space. Unlike the Banach space formulation, the union was not disjoint in the forecast vulnerability model. Riesz representation theorem established an important connection between a Hilbert space and its (continuous) dual space in the *S. damnsousm* s.l. habitat mdoel Hence, if the underlying field an emperical dataset of decomposed, Chl-*a*-related, *S. damnosum* s.l. endmembers, the two would have been isometrically isomorphic; if the underlying field was isometrically anti-isomorphic. Let *H* be a Hilbert space, and let *H** denote its dual space, consisting of all continuous linear functionals from *H* into the field R or C. If *x* is an element of *H*, then the function φ_x, for all *y* in *H* defined by $\varphi_x(y) = \langle y, x \rangle$, where $\langle \cdot, \cdot \rangle$ denotes the inner product of the Hilbert space, is an element of *H** [152]. The Riesz representation theorem states that *every* element of *H** can be written uniquely in this form.

The *S. damnosum* s.l. larval habitat mapping Φ: $H \rightarrow H^*$ was defined in both study site models by $\Phi(x) = \varphi_x$ in ArcGIS which was an isometric (anti-) isomorphism, meaning that Φ was bijective. The norms of *x* and $\varphi(x)$ were quantitated using $\|x\| = \|\Phi(x)\|$. Φ is additive: $\Phi(x_1 + x_2) - \Phi(x_1) + \Phi(x_2)$. If the base field is R, then $\Phi(\lambda x) = \lambda \Phi(x)$, for all λ [142]. If the base field is C, then $\Phi(\lambda x) = \bar{\lambda}\Phi(x)$ for all complex numbers λ, where $\bar{\lambda}$ denotes the complex conjugation of λ [152]. An inverse,eco-epidemiological, Chl-*a*, forecasting maps of Φ for the Gonycogo and Adibuk agro-village models was then described as follows. Given a non-zero element $\varphi$of *H**, the orthogonal complement of the kernel of $\varphi$was a one-dimensional subspace of *H*. We arbitrarily took a non-zero element *z* in that subspace, and set $x = \overline{\varphi(z)} \cdot z / \|z\|^2$. By so doing, $\Phi(x) = \varphi$ in both model outputs.

Since K_x was itself was a function in H in the unmixed Chl-*a*,, RapidEye^{TM}, *S. damnosum* s.l. habitat interpolator we then had an x in X $K_y(x) = \langle K_y,\ K_x \rangle_H$. in both models/ This allowed us to define the reproducing kernel of H in ArcGIS as a real-valued Chl-*a,* unmixed, *S. damnosum* s.l., habitat, biosignature, endmember function $K : X \times X \to \mathbb{R}$ by $K(x,y) = \langle K_x,\ K_y \rangle_H$. From this definition, it was easy to see that a function $K : X \times X \to \mathbb{R}$ was a reproducing kernel in the models since it was both symmetric and positive definite, $\sum_{i,j=1}^{n} c_i c_j K(x_i,x_j) \geq 0$] for any $n \in \mathbb{N}, x_1, \ldots, x_n \in X,$ and $c_1, \ldots, c_n \in \mathbb{R}$.

We investigated the method of regularization for estimating un-geosampled unknown hyperproductive habitats employing a_0 and p_0 in the Gonycogo and Adibuk agro-village models. We let l_n be a data fit functional that measured how well n fit the geosampled, RapidEye ^{TM} *S. damnosum s.l.,* larval productivity count data and J was a penalty functional that assessed the "plausibility" of n. The method of regularization estimates $n\mathfrak{d}$ by $nn = argmin[\ln(n|data) + XJ(n)]$, where the minimization was taken over and then defined in ArcGIS as $Jn: L2(T)\wedge R|n(X) = a + jf\ Xp: a \in R, p \in hJ$ where X > 0. The key to the model simulation was a tuning parameter that balanced the fidelity of the geosampled, Chl-*a*, unmixed, canopy, endmember data. Equivalently, the minimization in the models was taken over by (a,p) instead of n to obtain prime estimates for both the intercept and the slope, denoted by $a_n x$ and $p_n x$ thereafter. The choice of the Chl-*a*, data fit functional was the squared error, which we represented in the cyberenvironment as $in(n) = 1\ n_{where}[yi - n(xi)]_n^2$.

Next, l_n was chosen such that it was convex in n and $El_n(n)$ for quantiating the Gonycogo and Adibuk agro-village model estimates which then was uniquely minimized by n_0. In the context of functional linear regression, the penalty functional was defined through the slope function p as a squared norm or semi-norm associated with H [142]. The canonical example of H in the RapidEye^{TM} model was the Sobolev spaces. Without loss of generality, we assumed that T=[0,1], where we quantitated the Sobolev space using an order m as defined by $W^m([0,1]) = \{p : [0,1] \wedge R|p,\ p^{(1)},\ldots,p^{(m-1)}$, where $p^{(m)}$ e $C_2)$. There were many possible norms that were equipped with W2m to make it a reproduce kernel Hilbert space. Another setting in the Chl-*a*, unmixed, *S. damnosum* s.l. immature habitat, endmember interpolator was $T = [0, 1]^2$ which naturally occured when X represented in RapidEye ^{TM} image predictor dataset. We used the thin plate spline where J was given by $J[f(x,y)] = \iint_{R^2} (f_{xx}^2 + 2f_{xy}^2 + f_{yy}^2)\,dx\,dy.$

The name "thin plate spline" refers to a physical analogy involving the bending of a thin sheet of metal. In the physical setting, the deflection is in the *z* direction, orthogonal to the plane [152]. In order to apply this idea to the problem of coordinate transformation in the *S.damnosum* s.l. habitat, eco-epidemiological model the lifting of the plate as a displacement of the *x* or *y* coordinates within the plane was conducted in ArcGIS Geospatial Analyst ^{TM}. In general, two thin plate splines are needed to specify a two-dimensional coordinate transformation [142].

We then considered the relationship between the eigenstructures of the covariance operator for X(-) in the Chl-*a*, *S. damnosum* s.l. risk model and the reproducing kernel of the RKHS H. These eigenstructures played prominent roles in determining the difficulty of the prediction and estimation problems in the functional regression exercise. As a result the quantitated simultaneous diagonalization of the reproducing kernel of the RKHS H and the covariance operator of X(-) provided a powerful machinery for studying the minimax rates of

convergence in the Chl-*a*, *S. damnosum* s.l., eco-epidemiological, wavelength, emissivity, transmittance, decomposition, risk model.

Thereafter, we investigated the rates of convergence of the smoothness regularized by the unmixed, interpolative, 5m wavelength, fractionalized, transmittance endmember habitat estimators. Both the minimax upper and lower bounds were established. The optimal convergence rates were probabilistically regressively derived in terms of a class of intermediate norms which subsequently rendered a wide range of fractionalized, reflectance 5m, endmembers. In particular, this approach rendered a unified treatment for both the prediction of $f_0(X)$ and the estimation of i_0 in the hyperproductive, immature habitat, forecasting, eco-epidemiological, risk model. The results revealed that the smoothness regularized forecastable explanators achieved the optimal rate of convergence for both prediction and estimation of the riverine, Chl-*a* related, sub-mixel data under conditions weaker than those for the functional principal components based methods developed previously in the literature.

The smoothness regularized, unmixed Red Edge, NDVI, Chl-a, 5m RapidEye™, wavelength, emissivity biosignature estimators in the model were defined as the solution to a minimization problem over an infinite-dimensional space. Before studying the properties of the unmixed, interpolated estimators, we first showed that the minimization was indeed well defined and easily computable due to a version of the so-called representer theorem.

The representer theorem is a property that lies at the foundation of regularization theory and kernel methods [23]. A class of regularization functionals in a seasonal, vector arthropod, endmember, geo-spatiotemporal, geo-spectrotemporal stochastic interpolator is said to be part of the linear representer theorem if every field, remote or clinical geoclassifiable, decomposed class member acknowledges that minimizers lie in finite dimensional endmember subspace spanned by the representers of the entomological, empirical data [22]. A recent remote characterization states that certain gridded, geoclassified LULC classes have regularization functionals which admit a linear representer theorem if every member of the class admits minimizers that lie in the finite dimensional subspace spanned by the representers of the data in a decomposition unmixing algorithm in ArcGIS [22]. The results were extended which rendered from the Chl-*a*, Red Edge, unmixed, NDVI, sub-mixel, fractionalized endmember model employing a radial non-decreasing function. The model was extended in the residual, reflectance, interpolated results by weakening regression assumptions on the regularization term. In particular the residually forecasted, hyperproductive *S. damnosum* s.l. model estimators implied that for a sufficiently large family of Chl-*a* endmember, radiance fractionalized, 5m, radical non-decreasing functions, the only semicontinuous regularization terms that guaranteed existence of a representer theorem concept for any unmixed, fractionalized, eco-epidemiological, explanatorily georferencable habitat data point. In statistical learning theory, a representer theorem is any of several related results stating that a minimizer f^* of a regularized empirical risk function defined over a reproducing kernel Hilbert space can be represented as a finite linear combination of kernel products evaluated on the input points in the training set data [23]..

The penalty functional J in the model was a squared semi-norm on H such that the null space H :={£ e H: J(f) = 0}was a finite-dimensional linear subspace of H with orthonormal basis {^1,...,^N } where N := dim(H0), denoted by H and its orthogonal complement in H such that H = H0 © H1. Similarly, for any function f e H, there existed a unique decomposition f = f0 + f1 in the Chl-*a*, *S. damnosum* s.l. habitat, predictive risk

model, such that f e H and f e H1 were rendered. We noted H formed a reproducing kernel Hilbert space with the inner product of H restricted to H1. We let K(, ■) be the corresponding reproducing kernel of H such that J(f1) = || fi nK = II fi II ^ for any fi H1. Thereafter, the subscript K was employed in Geospatial Analyst TM to emphasize the correspondence between the inner product and its reproducing kernel in the model. We assumed that K was continuous and square integrable. Note, that K was also a nonnegative definite operator on L. With slight abuse of notation, we wrote *(Kf)(■) = j K(,s)f(s)ds* as the habitat, RapidEye^{TM}, Chl-*a* interpolator, uncertainty matrix.

It is known that Kf e H_1 for any f eL [153]. Thus, in the geospatial, geospectral, interpolator for any f e H1*jf(t)fi(t)dt = (Kf,0)$_H$.* This georeferenceable observation allowed us to prove the following result was important to both numerical implementation of the control procedure. It was assumed that i_n was dependent on n only through *n(x$_1$), n(*^{x}*2), ••••>n(x$_n$)* in the model. We noted that there existed *d = (d$_1$,..,d$_N$)' e R*^{N} *and c = (c$_1$,...,c$_n$)' e* ^{Rn}, such that *Pnl(t) = £ d$_k$^$_k$(t) + £ Ci(Kxi)(t).*

The endmember, NDVI, RapidEye^{TM}, 5m, heuristically optimizable, biosignature depiciting the trailing vegetation, turbid water, *S. damnosum* s.l., immature hyperproductive, capture point, canopied, habitat Chl-*a*, wavelength, unmixed, transmittance emissivity model employed generalization of the well-known representer lemma for smoothing splines [154]. Employing this lemma, we demonstrated that although the minimization with respect to *n* was numerically intergratable, the residuals from the geospatial, geospectral explanatorily, decomposed, Chl-*a*, RapidEye TM-dependent model were taken over using an infinite-dimensional space during the interpolation phase, which we actually found to be in a finite-dimensional subspace in ArcGIS Geospatial Analyst^{TM}. As such, it was suffice to evaluate the coefficients c and d in the model. In Wahba [154] l_n was assumed to be squared error, and therefore we omitted it here for brevity *(ainx=y-J^ x (t)jnx(t)dt1n* and jinx = argmin y)-J (xi(t) -x (t))j(t)dt + XJ(j) (yi^{-y}) - j eH i=1 was then employed. Correspondingly, *f* [X(t) - x(t)]j(t)dt = d1 j [X(t) - x(t)] dt + d2 j [X(t) - x(t)]tdt +±«*u [xi(s) - x (s')]K(t, s)[X(t) - x(t)] dsdt.*

Note that for any f given in the unmixed, Chl-*a*, biosignature-related, *S. damnosum* s.l. hyperproductive habitat forecasting, interpolative, RapidEye TM risk model where J(f) = c'Sc and where S = (S_{ij}) was an n x n matrix with *Sij = j j [xi(s) -X(s)]K(t, s)[xj(t) -X(t)] dsdt.* We denoted T = (T_{ij}) as an n x 2 matrix by (i, j) entry which was then quantitated in ArcGIS as ^{Tj}= *[x(t)-mv-*^{dt} for j = 1, 2. We set y = (y_1,...,y_n)'. The model revealed ln(n) + kJ(f) = - ||y - (Td + Sc)|l + Ac'sc which was quadratic in c and d. By doing so, the explicit form of the solution was obtained.

W = S + nXI was rewritten in the immature habitat interpolator, so that the minimizer rendered d = (T W$^-$T)$^-$T W$^-$y, c = W$^-$[I - T(TW$^-$T)$^-$TW$^-$]y. A simultaneous diagonalization in ArcGIS was conducted. Before studying the asymptotic properties of the unmixed, Chl-*a*, *S. damnosum* s.l. habitat endmember, Red Edge, NDVI interpolative, estimators, fj_{nA} and ff_{nA} were quantitated. However, prior to so doing, we investigated the relationship between the eigenstructures of the covariance operator for X(-) and the reproducing kernel of the functional space H. The univariate Sobolev space in the immature, habitat, *S. damnosum* s.l. unmixed, canopy, risk endmember, eco-epidemiological, reflectance interpolator was considered where Wm([0, 1]) was the norm and penalty. We observed that *H1= f e H :j f*$^{(k)}$ *= 0,k = 0,1,...,m-1J.* We then solved for

1 (-1)$^{m-1}$

$$K(s,t) = 2\,B\,m(s)\,B\,m(t) \quad + B\,2m(\backslash s \;-\; 1\,1).$$
$$(m!)^2 \qquad\qquad (2m)!$$

In the model B_m was the m^{th} Bernoulli polynomial. It is known [155] that in this case, p_k x k^{-2m}, where for two positive sequences a_k and b_k, a_k x b_k means that a_k/b_k is bounded away from 0 and then to k ^to >. In the endmember interpolator this regressive quantitation was denoted by C where the covariance operator for X was optimally determined such that $C(s,t) = E\{[X(s) - E(X(s))][X(t) - E(X(t))]\}$.

There was a duality between the reproducing kernel Hilbert spaces and covariance operators in the unmixed, Chl-*a*, *S. damnosum* s.l., habitat, endmember, interpolator. Similarily to the reproducing kernel K assuming that the covariance operator C was continuous and square integrable, the interpolated forecasts rendered the following spectral decomposition *C(s,t)=J2Hktk(s)Mt),* where $ix_1> /x_2>$••• was the eigenvalues and {fa,fc,...} were the eigenfunctions denoted such that *C^k:= J C(,t)(pk(t)dt =/xkfik* when *k = 1, 2,—*.

The decay rate of the eigenvalues {^$_k$:k > 1} in the model forecasts was determined by the smoothness of the covariance operator C. More specifically, when C satisfied the so-called Sacks-Ylvisaker conditions of order s where s was a non-negative integer [156, 157, 158], then the forecasts were x_k x $k^{-2(s+1)}$. The readers are referred to the original papers by Sacks and Ylvisaker or a more recent paper by Ritter, Wasilkowski and Wozniakwski [159] for detailed discussions of the Sacks-Ylvisaker conditions. .

The Chl-*a*, endmember, RapidEye^{TM}, trailing vegetation, 5m, resolution, *S. damnosum* s.l., habitat, emissivity, sub-mixel, interpolative model then revealed that quadratic forms || f ||R = $(f, f)_R$ and $(Cf, f)c_2$ which was simultaneously diagonalized on the basis of {a>$_k$: k > 1}. We noted that in the endmember model for any f e H,f = £ fk^k, when *k=1*in the absolute sense where f*k* = V*k*(f, M*k*)r. Further, if Y*k*= (v—^{1} — *1)*$^{-1}$.

Note that {(Y_k,M_k): k > 1} was determined jointly by {(p_k,f_k): k > 1} and {(p_k,f_k): k > 1} in the model. However, in general, neither Y_k nor M_k was given in explicit form of {(p_k,f_k): k > 1} and {(p_k,f_k): k > 1}. One notable exception in the model were the operators C and K which in the endmember model were commutable. In particular, the setting $f_k = f_k$, k = 1,2,..., is adopted when studying FPCA-based approaches [160, 161].

If *fk = fk, k = 1, 2,...,* then Yk = PkPk and Mk = *ti*—$^{1/2}$*fk* was assumed. The one-dimensional case when T = *[0,1]* was considered. If H was the Sobolev space W, *f([0,1])* was *x* endowed with a norm and *C* satisfied the Sacks-Ylvisaker conditions in the endmember, Chl-*a*, *S. damnosum* s.l., immature, habitat model then *Yk x PkPk.* The interpolator revealed that under fairly general conditions y_k x fi_kp_k. As such, there was little difference between the general situation and the special case when K and C shared a common set of eigenfunctions, which revealed then that the system i(y_k,M_k), k = 1, 2,...}. This observation was crucial for our theoretical development on the model. Convergence rates were then quantitated, followed by the asymptotic properties of the smoothness regularized estimators.

The first condition in the transmission, endmember interpolator specified the smoothness of the sample path of X(-). The second condition rendered the fourth moment of a linear functional of X(-). This condition was satisfied with M = 3 for a Gaussian process in the model, endmember, eco-epidemiological, covariate estimators because / f(t)X(t) dt was normally distributed. The endmember Chl-*a*, immature, habitat, RapidEye ^{TM,} spectroscopic, endemic, wavelength, unmixed, emissivity, risk model was satisfied by any covariance function that satisfied the Sacks-Ylvisaker conditions if H ws taken to be Wm with norm

expectations. The products were also trivially satisfied if the eigenfunctions of the covariance operator C coincided with those of K.

Optimal rates of convergence were then regressively quantitated for the unmixed, RapidEye^{TM}, emissivity risk model. The main results on the optimal rates of convergence, was given in terms of a class of intermediate norms between $||/||_K$ and *Qf/(s)C(s,t)/(t)dsd^ ,* which enabled a unified treatment of both the prediction and estimation of the hyperproductive, immature habitats based on the interpolated, Chl-*a*, sub-mixel data. For 0 < a < 1 we defined the norm $|| \bullet ||_a$ by *ii/ Ii*a = *E* $(1 + y\text{-}^{a})/k$, where $/_k = v_k$ {/, $a>_k)_R$. Clearly || / ||o reduced to $\{C/, /)_{L1}$ whereas $|| /1_1 = || /||_R$. The convergence rate results given below were thereafter valid for all 0 < a < 1. They covered a range of interesting cases in the interpolator forecasts including the prediction error and estimation error.

The following results thereafter rendered the optimal rate of convergence for the regularized, probabilistic estimator f_{nX} with an appropriately chosen tuning parameter X under the loss 11 • 11 $_a$. in the Chl-*a*, habitat capture point, interpolation, regression model. We assumed that *E(ei) = 0 and Var(ei) < M2.* In the endmember habitat model the eigen-values pk of the reproducing kernel K of the RKHS H satisfied pk *x* $k\sim^{2r}$ for some r > *1/2.* Then the regularized estimator f_{nX} was robustly quantitated as Xx $n^{-2(r_+s)/(2(r_+s)+1)}$, which satisfied lim lim sup $P(Hji_{nX} — ^_0|| > Dn^{—2(1—a)(r+s)/(2(r+s)+1)})$ *D^xFSF(s,M,K),p0eH*= 0.

Note that the rate of the optimal choice of X did not depend on the model forecasts. The endmember, Chl-*a*, *S. damnosum* s.l., RapidEye^{TM}, habitat revealed that the optimal rate of convergence for the regularized estimator f_{nX} was $n^{—2(1— a)}(r+s)^{/(}2(r+^{s)}+^{1)}$. The following lower bound result demonstrated that this rate of convergence was indeed optimal amongst all the parameterized, wavelength, emissivity, 5m, covariate estimators, and consequently the upper bound we assumed could be improved. As such, we denoted the collection of all measurable functions of the geosampled RapidEye^{TM} observations by (X_1,Y_1), ..., (X_n,Y_n). We assumed that there existed a constant d > *0* in the residual forecasts such that lim inf sup $P(||/d — f_0ia > dn^{—2(1—a)(r_+s)/(2(r+s)+1)}) > 0$. Consequently, the regularized, covariate estimator f_{nX} with X *x* $n^{—2(r_+s)/(2(r_+s)+1)}$ was rate optimal for geolocating unknown, unsampled, hyperproductive *S. damnosum* s.l. habitats.

The model results, given in terms of || ■ \\$_a$, provided a wide range of measures of the quality of a Chl-*a* retrieved, RapidEye ^{TM} imaged estimate for j_0. We observed that fj — 130*1|0 =Ex*(f $ (t)X*(t)dt — j* j0(t)X* *(t)dt^,* when X* was an independent copy of X, and the expectation on the right-hand side was taken over X*. The right-hand side of the habitat risk model was the prediction error. It measured the mean squared error for a random forecasted, hyperproductive, sparsely shaded, canopied, georeferenceable habitat observation on X.

The mean squared optimal prediction error of a slope function estimator was *Fe F(s,M,K) and_ 2(r+s)* where *H* was of the order $n^{2(r+s)+}$ was achieved by the regularized, Chl-*a*, interpolated, covariate estimator. The results reveal that the faster the eigenvalues of the covariance operator C for X(-) decayed in the *S. damnosum* s.l. habitat model, the smaller the prediction error. Then, fk was regressively quantitated as the prediction error of a slope function estimator which we understood as the squared prediction error for a fixed habitat predictor x*(■) such that $|(x*,f_k)c_21 \text{ x } k^{-s}$.

A similar prediction problem has also been considered by Cai and Hall [160] for FPCA- based approaches. In particular, they established a similar minimax lower bound and showed that the lower bound can be achieved by the FPCA-based approach, but with

additional assumptions that p_k — p_{k+1}>C—$^{1}k^{—2s—1}$, and 2r > 4s + 3. The habitat model results here indicate that both restrictions are unnecessary for establishing the minimax rate for quantitating the time series prediction error for a geospectral, geospatial, unmixed, Chl-*a*, endmember, biosignature of an immature, *S. damnosum s.l.*, RapidEye^{TM}, eco-epidemiological, habitat risk model. Moreover, in contrast to the FPCA-based approach, the regularized estimator j_{nX} in our model achieved the optimal rate without the extra requirements.

To illustrate the generality of our results, we considered an example where T = [0, 1], H=Wm([0, 1]) and the stochastic process X(-) which was a Wiener process. The unconditional probability density function, in the unmixed, Chl-*a*, biosignature, interpolative, RapidEye^{TM}, eco-epidemiological, reflectance risk model followed a normal distribution with mean = 0 and variance = t, at a fixed time *t*: $f_{W_t}(x) - \frac{1}{\sqrt{2\pi t}} e^{-\frac{x^2}{2t}}$. The expectation was zero: $E[W_t] = 0$. The variance, employing the computational formula, was *t*: $\mathrm{Var}(W_t) = E\left[W_t^2\right] - E^2[W_t] = E\left[W_t^2\right] - 0 = E\left[W_t^2\right] = t$. The covariance and correlation were tabulated as $\mathrm{cov}(W_s, W_t) = \min(s,t)$, and $\mathrm{corr}(W_s, W_t) = \frac{\mathrm{cov}(W_s, W_t)}{\sigma_{W_s}\sigma_{W_t}} = \frac{\min(s,t)}{\sqrt{st}} = \sqrt{\frac{\min(s,t)}{\max(s,t)}}$.

The results for the expectation and variance followed immediately from the definition that increments in the eco-epidemiological predictive model had a normal distribution centered at zero. Thus, $W_t = W_t - W_0 \sim N(0,t)$. The covariance operator of X, C(s, t) = min{s, t}, satisfied the Sacks-Ylvisaker conditions of order 0, and therefore p_k x $k^{—2}$. The minimax rate of the prediction error in the habitat, reflectance model was then estimated where j_0 was $n^{\sim(2m+2)/(r\ 2m+3)}$. Note that the condition 2r > 4s + 3 required by Cai and Hall [160] did not hold here for m < 7/2 in the forecasts.

It is of interest to further look into the case when the operators C and K share a common set of eigenfunctions. Thus, part of the unmixed, Chl-*a*, NDVI biosignature, wavelength, emissivity, RapidEye ^{TM,} transmittance, eco-epidemiological risk model was f_k = f_k and y_k x $k^{—2(r+s)}$ for all k > 1. We then considered probabilistically estimating / x* j_0 where x* satisfied $|(x^*,f_k)c_21$ x $k^{—s+q}$ for some 0 < q < s — ½ in the unmixed, geosampled, Chl-*a*, NDVI, biosignature *S. damnosum s.l.* habitat model radiance estimates.

Note that when q < s 0— 1/2 was needed to ensure that x* was square integrable, the squared error then was probabilistically quantitated by *Q jj(t)x*(t) dt — j j0(t)x *(t) dt'j*, which was equivalent to || j — j_0 II $(_{s—q})/(r+_s)$. It was supposed *x** was a function satisfying *\(x*,fk)l21 x k $^{s+q}$ for* some *0* < q < s — *1/2.* Then under the assumptions for some constant d > *0,* and the regularized estimator j_{nX} with X satisfied the optimal rate of convergence under the prediction error.

It was also evident that when f_k = fk, I ■ $l|_s/(r+_s)$ in the RapidEye^{TM}, Chl-*a*–oriented, unmixed, endmember, forecasting, NDVI biosignature, eco-epidemiological, risk model, the output was equivalent to || ■ $||_{L2}$. This implied that if f*k* = f*k* for all k > *1,* then lim inf sup P(||j — j0llL$_2$ > $dn^{—2r/(2(r+s)+1)}$) > $0^{n\wedge x}$ *jeB FeF(s,M,K),j$_0$eH* for some constant d > *0,* and the regularized estimate j*3$_{nX}$* with X satisfying the optimal rate. This result demonstrated that the faster the eigenvalues of the covariance operator for X(-) decay, the larger the probabilistic estimation error in a geospectral, geopsatial, unmixed, Chl-*a,* NDVI biosignature, habitat risk model. The behavior of the estimation error thus differed significantly from that of prediction error.

Similar results on the lower bound have recently been obtained by Hall and Horowitz [161] who considered estimating j_0 under the assumption that \(j_0,fk)c_2 \ decays in a polynomial order. Note that this forecast slightly differed from our setting where j_0 e H meant that for some constant M_0> 0 in the model forecasts. When further assuming that 2s + 1 < 2r, and p_k — p_k+$_1$> M— $^1k^{—2s—1}$ for all k > 1, Hall and Horowitz [161] obtained the same lower bound as ours. However, it was not required that 2s + 1 < 2r, which in essence states that f_0 is smoother than the sample path of X. Perhaps, more importantly, we did not require the spacing condition p_k — p_k+$_1$> M— $^1k^{—2s—1}$ on the eigenvalues because we did not need to estimate the corresponding eigenfunctions. Such a condition is impossible to verify, even for a standard RKHS(2). In addition to 0_k = f_k, we assumed that Wfkf ^ff$_k$ ||$_x$ x k^q, when H = Wf. In this case\\$$^{(q)}$ — *i0$^{q)}$|$_{£2}$<CoWi— M(s+q)/($_r$+s)*. It was assumed that 0k = fk and W^k*f* ^/^k *W$_x$ x* k^q, for all k > *1*. Then for some constant d > *0,* and the regularized estimate f_{nX} with X achieving the optimal rate. Finally, we noted that the method of regularization was easily extended to handle other goodness of fit measures in the immature habitat, resdiual model output as well as the generalized functional linear regression such as in Cardot and Sarda [162] and Muller and Stadtmuller [163].

The probabilistic, regularized, fractionalized, Chl-*a*, habitat, transmittance emissivity estimators were easy to implement. Similarly to smoothness regularized estimators in other contexts [154], fj$_{nX}$ and f_{nX} can be expressed as a linear combination of a finite number of known basis functions, although in the immature habitat model the minimization was taken over by an infinitely-dimensional space. Existing algorithms for smoothing splines in ArcGIS to compute our regularized estimator fjnX, f”nX$^{and\ a}$nX.

To demonstrate the merits of our proposed Chl-*a* estimators in finite sample settings in hyperproductive *S. damnosum* s.l. habitats, we carried out a set of simulation studies. The simulation setting of Hall and Horowitz [161] where T=[0,1] was assumed. As is common in most smoothing methods, the choice of the tuning parameter plays an important role in the performance of the Chl-*a* covariate, endmember, moderate resolution, emissisity estimators [24]. A commonly utilized practical strategy of choosing the value of X was performed through a generalized cross validation matrix in ArcGIS employing the RapidEye ^{TM} 5m resolution riverine scene. Note that the regularized estimator is a linear estimator in that y = H(X)y where y = (fj$_{nX}$(x_1),..., fj$_{nX}$(x_n))' and H(X) is the so-called hat matrix depending on X [142]. The tuning parameter X that minimized X^{GCV} was then selected.

The setting of well-spaced eigenvalues was generated. The prediction error, \\ft$_{nX}$ — ft$_0$\\0, for each combination of v value and forecasted hyperproductive, RapidEye ^{TM} 5m, habitat sample size when a = 0.5. The results were averaged over 1000 simulation runs in each setting. Both axes were given in the log scale in ArcGIS. The plot suggested that the estimation error converged at a polynomial rate as sample size n increased. (see Figure 65) Further, it was observed that with the same georeferenced habitat sample size, the prediction error tended to be smaller for larger v. This also confirmed our theoretical development which indicated that the faster the eigenvalues of the covariance operator for X(-) decay, the smaller the prediction error (2)

Fig. 65. Prediction errors of the regularized estimator (a = 0.5): X simulated with a covariance function with well-spaced canopied, trailing vegetation, unmixed, biosignature *7* s.l. habitat turbid water eigenvalues. The results were averaged over 1000 runs.

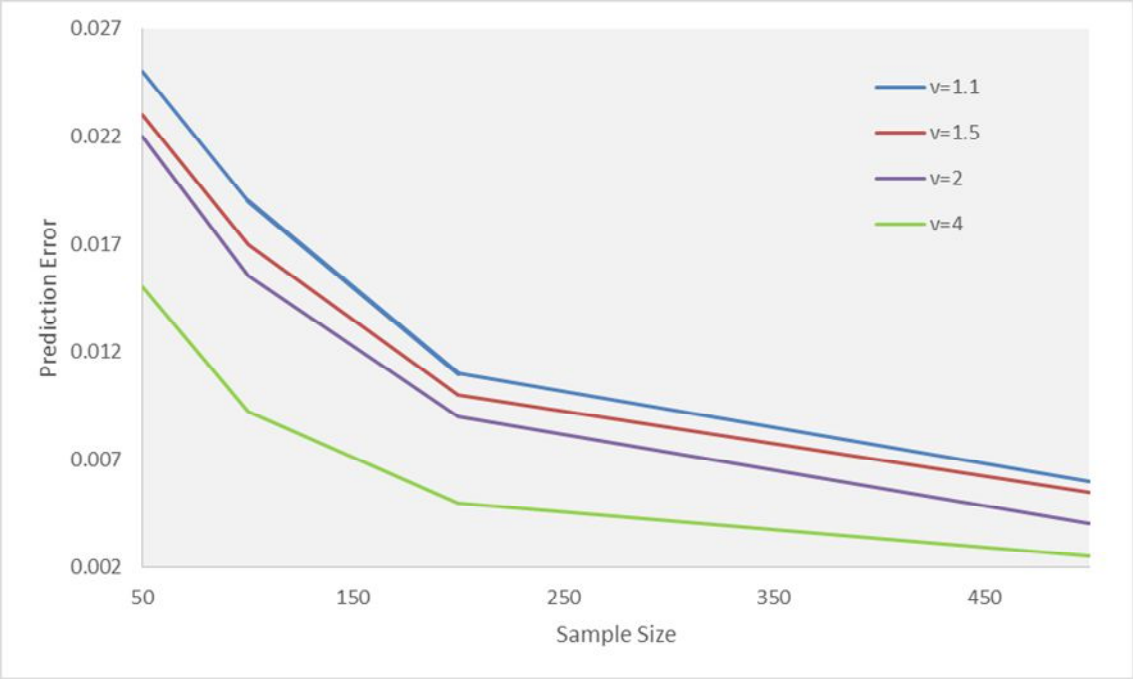

Black solid lines, red dashed lines, green dotted lines and blue dash-dotted lines correspond to v = 1.1, 1.5, 2 and 4, respectively.

To better understand the performance of the smoothness regularized, regression-related, Chl-*a* covariate parameterizable RapidEye^{TM} covariate, estimator and the GCV choice of the tuning parameter, we recorded the performance of an estimator whose tuning parameter was chosen to minimize the prediction error. This choice of the tuning parameter ensured the optimal performance of the regularized RapidEye ^{TM} 5m, *S. damnosum* s.l., Chl-*a,* fractionalized, estimator. However, it should be noted that this is not a legitimate statistical estimator since it depended on the knowledge of unknown slope function fi_0. The prediction error was associated with this choice of tuning parameter. The RapidEye^{TM} 5m forecasts behaved similarly to the estimate with X chosen by GCV. Note that the comparison between the forecasted habitats suggested that GCV generally lead to near optimal performance in the forecasting, Chl-*a*, eco-epidemiological risk model.

The estimation error was then autoregressively quantitated in the immature habitat, interpolated, residualized risk model in ArcGIS. The estimation for the non-normal data feature attributes averaged over 1000 simulation runs, with X chosed by GCV. By doing so, the model geo-predictive estimation error for each combination of endmember sample size estimation errors averaged over 1000 simulation runs, with X chosen by GCV for each combination of sample size and value. Similar to the prediction error, the diagnostic ArcGIS plots suggested an estimation error when the sample size increased. The GCV lead to near-optimal choice of the tuning parameter in the model.

The predictions and estimation error were quantitated as rendered from the *S. damnosum* s.l. habitat, decomposed Chl-*a* and other fractionalized, radiance endmembers. The prediction and estimation error were quantitated when the estimates in the immature habitat, eco-epidemiological, reflectance, canopied, risk model tuned with GCV for the large noise (a = 1) setting. We noticed that the prediction error were very much smaller than the estimation error we assumed would be rendered from the model.

For brevity, we assumed that p_1 = m =1 without loss of generality. By the Cauchy-Schwarz inequality,

$$\text{If } |R > \int f(s)\,C(s,t)f(t)\,ds\,dt + \text{II/IIIH 2 Tx T}$$

$$> \int_{2\,\text{TxT}} fo(s)\,C(s,t)fo(t)\,ds\,dt + \int_{2\,\text{Tx T}} f1(s)\,C(s,t)f1(t)\,ds\,dt$$

$$-\int_{T\ T} fo(s)\,C(s,t)fo(t)\,ds\,d?j$$

$$x \int_{T\ T} h(s)\,C(s,t)f1(t)\,ds\,dt$$

$$>_{-} \frac{1}{3} \int_{\text{T}x\text{T}} fo(s)\,C(s,\ t)fo(t)\,ds\,dt,$$

where $3a^2/2$ — ab > — b^2 / 6 was required for deriving the last inequality. Therefore, *I*lf|R > IfolH. Together with the statements that *I*f|H = I foIlH + II f1 IIH and *I*f|R >J(f1)>Ilf!Ih, we concluded that I*f*|*R* > *(1* + 3/mn)$^{-1}$I/II*H*. In mathematics, the Cauchy–Schwarz inequality is a useful inequality encountered in many different settings, such as linear algebra, analysis, probability theory, and other areas. It is considered to be one of the most important inequalities in mathematics [24]. It has a number of generalizations, among them Hölder's inequality [24].

In mathematical analysis Hölder's inequality, is a fundamental inequality between integrals and an indispensable tool for the study of L^p spaces. Hölder's inequality theorem states, "Let (S, Σ, μ) be a measure space and let p, $q \in [1, \infty]$ with $1/p + 1/q = 1$. Then, for all measurable real- or complex-valued functions f and g on S, $\|fg\|_1 \leq \|f\|_p \|g\|_q$." If, in addition, p, $q \in (1, \infty)$ and $f \in L^p(\mu)$ and $g \in L^q(\mu)$, then Hölder's inequality becomes an equality if and only if $|f|^p$ and $|g|^q$ are linearly dependent in $L^1(\mu)$, meaning that there exist real numbers α, $\beta \geq 0$, not both of them zero, such that $\alpha|f|^p = \beta\,|g|^q$ μ-almost everywhere. The numbers p and q in the habitat, Chl-*a,* fractionalized radiance estimates were Hölder conjugates of each other in the model. The special case $p = q = 2$ gave a form of the Cauchy–Schwarz inequality. Hölder's inequality held even when $\|fg\|_1$ was infinite. Then f was in $L^p(\mu)$ and g was in $L^q(\mu)$. Then the pointwise product in the habitat, eco-epidemiological risk model fg was $L^1(\mu)$. Hölder's inequality is used to prove the Minkowski inequality, which is the triangle inequality in the space $L^p(\mu)$, and also to establish that $L^q(\mu)$ is the dual space of $L^p(\mu)$ for $p \in [1, \infty)$ [24].

The bounded positive definite operator $R^{1/2}$ was applied, to both sides of the Chl-*a*, endmember, RapidEye, 5m, immature *S. damnosum* s.l. reflectance, endmember, vulnerability, risk model. Then $\{rn_k,Mj)_R = v_k{}^x S_k j$. Therefore, *E* V*k*V*j* {f,M*k*)*r* {f,te*j*)*r*

(tek,Mj)r k,j= E Vk {f,Mk)R. Similarly, because {Ca>k,a>j)$_{L2}$ = S_{kj}, when Vk {f,Vk)RC<Mk,Y^Vj {f,tej)rMj k=1 j=1 L_2= E VkVj {f,Vk)r {f,Vj)r {CMk,Mj)l_2 k,j=1= E $^{V}l^{\{f,\wedge k\ )2}$r. Recall that for any f e H_0, Cf = 0 if and only if f = 0, which implies that H_0 n l.s.$\{0_k : k > 1\}^x$ = {0} [142]. Together with the fact that H_0 n H_1 = {0} in the Chl-*a* fractionalized, 5m RapidEye^{TM}, radiance model , we concluded that H = H_1 = l.s.$\{f_k : k > 1\}$.

Further, it was not hard to see that for any f,g e H,{f,g)R = f(s)C(s,t)g(t)dsdt +{f,g)K in the *S. damnosum* s.l. habitat model. In particular, {fj,fk) R = (Pk + P-^{1}')^{s}jk, implied that {((p_k + pf^{l})~^{l},f_k): k > 1} which was also the eigensystem of R, where WR(s,t)=J2(Pk + pf^{l})~^{l}fk(s)fk(t). Then Rfk ■= j R(-,t)fk(t)dt =(pk + pf^{l})~^{l}fk,k = 1, 2,.... Therefore, $R^{1/2}CR^{1/2}f_k$ = $R^{1/2}$C((m + p-$V^{1/2}$fk) = $R^{1/2}$(/Xk(Rk + P-^{l})~$^{1/2}$fk) = (1 + P-V-Wk, which implied that Zk = fk = fk, Vk = (1 + p-^{1} ^.-V^{1} and Yk = PkPk. Consequently, Mk = v-$^{1/2}R^{1/2}$fk = v-$^{1/2}$(^k + P-^{l})~$^{1/2}$ fk = R-$^{1/2}$fk in the resdidual forecasts rendered from the immature habitat model.

The Chl-*a,* eco-epidemiological, reflectance risk model was remotely regressively quantitated employing H = Wf, which implied that p_k x k^{-2m}. Based on Corollary 2 of Ritter, Wasilkowski and Wozniakowski [159], [i_k x k~$^{2(s+1)}$] it was was revealed that Y_k x k~$^{2(s+1+m)}$ existed in the forecasted residual, eco-epidemiological, unmixed dataset. Our habitat forecasting Chl-a model indicated that the reproducing kernel Hilbert space was associated with C, which differed from W2^{+1}([0,1]) in the forecasts only by a finite-dimensional linear space of polynomials.

Q_r the reproducing kernel for W([0,1]) was denoted in the kdoel in ArcGIS. It was observed that Q_r (L_2) = W, [153]. It began by quantifying the decay rate of l_k(Q^{l}m$^{/2}$$Q_{s+}$1Qm$^{/2}$). By Sobolev's embedding theorem, (Q^^{2}qU^{2})(C2) = Q%{Wm) = Wm^{+s+1} [142]. Let $W^{k,p}(\mathbf{R}^n)$ denote the Sobolev space consisting of all real-valued functions on $\mathbf{R}^n$ whose first k weak derivatives are functions in L^p. Here k is a non-negative integer and $1 \le p < \infty$. The first part of the Sobolev embedding theorem states that if $k > \ell$ and $1 \le p < q < \infty$ are two real numbers such that $(k - \ell)p < n$ and: $\frac{1}{q} = \frac{1}{p} - \frac{k-\ell}{n}$, then $W^{k,p}(\mathbf{R}^n) \subseteq W^{\ell,q}(\mathbf{R}^n)$ and the embedding is continuous. Initially the Chl-*a,* risk model revealed $k = 1$ and $\ell = 0$, Sobolev embedding ten rendered $W^{1,p}(\mathbf{R}^n) \subseteq L^{p^*}(\mathbf{R}^n)$, where p^* was the Sobolev conjugate of p, given by $\frac{1}{p^*} = \frac{1}{p} - \frac{1}{n}$.

The Sobolev embedding is a direct consequence of the Gagliardo–Nirenberg–Sobolev inequality. Assume that u is a continuously differentiable real-valued function on $\mathbf{R}^n$ with compact support. Then for $1 \le p < n$ there is a constant C depending only on n and p, such that $\|u\|_{L^{p^*}(\mathbf{R}^n)} \le C\|Du\|_{L^p(\mathbf{R}^n)}$ [24]. The case $1 < p < n$ is due to Sobolev, $p = 1$ to Gagliardo and Nirenberg independently. The Gagliardo–Nirenberg–Sobolev inequality implies directly the Sobolev embedding $W^{1,p}(\mathbf{R}^n) \subset L^{p^*}(\mathbf{R}^n)$.

The embeddings in other orders on $\mathbf{R}^n$ are then obtained by suitable iteration. The second part of the Sobolev embedding theorem applies to embeddings in Hölder spaces $C^{r,\alpha}(\mathbf{R}^n)$. If $(k - r - \alpha)/n = 1/p$ with $\alpha \in (0, 1)$, then one has the embedding $W^{k,p}(\mathbf{R}^n) \subset C^{r,\alpha}(\mathbf{R}^n)$. This part of the Sobolev embedding in the Chl-*a, S. damnosum* s.l. habitat eco-epidemiological risk model was a direct consequence of Morrey's inequality. Intuitively, this inclusion expressed the fact that the existence of many weak derivatives in the eco-epidemiological risk forecasts which implied some continuity in the derivatives.

It was assumed $n < p \le \infty$ in the uncertainty, habitat risk model residual, covariate

estimators. As such there existed a constant C, depending only on p and n in the residual heuristically eco-epidemiological dataset such that $\|u\|_{C^{0,\gamma}(\mathbf{R}^n)} \leq C\|u\|_{W^{1,p}(\mathbf{R}^n)}$for all $u \in C^1(\mathrm{R}^n) \cap L^p(\mathrm{R}^n)$, where $\gamma = 1 - \frac{n}{p}$. Also when $u \in W^{1,p}(\mathrm{R}^n)$, then u was in fact Hölder continuous of exponent γ, after possibly being redefined on a set of the sparsely shaded, canopied, risk model measures. A similar result held in a bounded domain U with C^1 boundary in the model forecasts. In this case, $\|u\|_{C^{0,\gamma}(U)} \leq C\|u\|_{W^{1,p}(U)}$, where the constant C was dependnet on n, p and U. This version of the inequality followed from the previous by applying the norm-preserving extension of $W^{1,p}(U)$ to $W^{1,p}(\mathrm{R}^n)$. In mathematics, a real or complex-valued function f on d-dimensional Euclidean space satisfies a Hölder condition, or is Hölder continuous, when there are nonnegative real constants C, α, such that $|f(x) - f(y)| \leq C \parallel x - y \parallel^{\alpha}$ for all x and y in the domain of f [24] More generally, the condition can be formulated for the risk model functions between any two metric spaces. The number α is called the *exponent* of the Hölder condition. If α = 1, then the function satisfies a Lipschitz condition. If α = 0, then the function simply is bounded [24].

Therefore, qK^{2}Q$_{s+}$1Ql(^{2} was equivalent to Qm+s+1 in the risk model, X$_k$(Q) was denoted and quantitated to be the kth largest eigenvalue of a positive definite operator Q. We let {h$_k$: k > 1} be the eigenfunctions of Q$_{m+s+1}$, that is, Q$_{m+s+1}$h$_k$ = Xk(Q$_{m+s+1}$)h$_k$, k = 1, 2, —n. This was denoted by F$_k$ and F$_k$ where a linear space was spanned by {hj :1 <j < k} and {hj : j > k + 1}, respectively. By the Courant-Fischer-Weyl min-max principle, Xk(Q^{1}m$^{/2}$Qs+1*QK^2) > min ||Q]+^{2}QK^{2}f|||$_2$/\|f ||L$_2$J^{jF}k*>c wQm+,$_{+1}$fiiL,/WfiiL,>^{C}*I^{X}k$^{(Q}$m+s+1$^{)}$ for some constant C$_1$ > 0. On the other hand, *Xk(Qm/^{2}Qs*+1QK^2) < max WQ^l+^{2}1Qm$^{/2}$fWL$_2$/Wf WL,^{fjF}k*-1 < C, min WQm$^{/}$+s+1 f WL,/Wf WL,^{fjF}k-1 , ^{C}2^{X}k$^{(Q}$m+s+1$^{)}$ for some constant C$_2$ > 0. X$_k$(Q^{1}J$_l$^{2}Q$_s$+$_1$ qU^2) x xk~2(m+s+1) is summarized in the risk model resdiual dataset. As shown by Ritter, Wasilkowski and Wozniakowski [159, Theorem 1, page 525], there exist D and U such that Q$_s$+$_1$ = D + U, D has at most 2(s + 1) nonzero eigenvalues and ||U$^{1/2}$f \\c$_2$ is equivalent to ||C$^{1/2}$f \\c$_2$.

Moreover, the eigenfunctions of D, denoted by {g$_1$,...,gd} (d < 2(s + 1)) were polynomials of order no greater than 2s + 1 in the endmember, RapidEye ^{TM} *S. damnosum* s.l., Chl-*a,* habitat, fractionalized, wavelength, transmittance, eco-epidemiological, RapidEye^{TM} 5m, optimizable, risk model. G A denoted the space spanned by {g$_1$,...,g$_d$}. Clearly G C Wm = Q^{l}Ji^2(L2). Theerfater {hj :j > 1} was the eigenfunctions of qK^{2}Qs+1Ql^2 whilest F$_k$ and Fjf were defined similarly as F$_k$ and Fjf. Then by the Courant-Fischer-Weyl min-max principle, *Xk-dQ^UQm/^{2}) >min \\U $^{1/2}$QK^{2}f ||L$_2$/If IIL2f efik nQm$^{/z}$(G)^r*=milUQifiQm^{2}fIL2/\\fIL2 *f eT$_k$*C\Q$_m$^{ul}(Q)^r= min IQ^f 1L2/. If I^{2}L *feFk^{22}>^{C}1^{X}k$^{(Q}$m+s+1$^{)}$*for some constant C$_1$> 0. On the other hand, k+d(QU^{2}Qs+1*QK^2) < max_ |U$^{1/2}$QK^{2}f /\|f ff eF— ^{n}Qm$^{1/2}$(G)^1 = max IQl$^{/2}$1Qll^{2}fI^{2}c$_2$/IfI^{2}C2f eF— nQm$^{/Z}$(G)^r* = min IQ^1+1Qm$^{/2}$f 11L2/. If 11L2*f*eF^{r}k-1<^{C}2^{X}k$^{(Q}$m+s+1$^{)}$ for some constant C$_2$> 0 in the risk model residual forecasts. Hence, X$_k$(Qml^{2}UQQJF) x k$^{-2(m+s+1)}$. Because Q^{l}Ji^{2}UQ^{l}J$_l$^{2} is equivalent to R$^{1/2}$CR$^{1/2}$, [142] we again employed the Courant-Fischer-Weyl min-max principle.

The Courant minimax principle, as well as the maximum principle, can be visualized by imagining that if ||*x*|| = 1 is a hypersphere, then the matrix *A* deforms that hypersphere into an ellipsoid. When the major axis on the intersecting hyperplane are maximized (i.e., the length of the quadratic form *q*(*x*) is maximized), this is the eigenvector and its length is the eigenvalue. All other eigenvectors will be perpendicular to this [24]. The minimax principle

also generalizes to eigenvalues of positive self-adjoint operators on Hilbert spaces, where it is commonly used to study the Sturm–Liouville problem. In mathematical applications, the classical Sturm–Liouville equation, is a real second-order linear differential equation of the form $\frac{\mathrm{d}}{\mathrm{d}x}\left[p(x)\frac{\mathrm{d}y}{\mathrm{d}x}\right] + q(x)y = -\lambda w(x)y,$ where y is a function of the free variable x. Here, the functions $p(x)$, $q(x)$, and $w(x) > 0$ were specified at the outset. In the simplest of cases, all coefficients are continuous on the finite closed interval $[a,b]$, and p has a *continuous derivative*. This function "y" is called a *solution* if it is continuously differentiable on (a,b), and satisfies the equation ('*1'*) at every point in (a,b) [24]. In addition, the unknown function y is typically required to satisfy some boundary conditions at a and b. The function $w(x)$, sometimes referred to as $r(x)$, is called the "weight" or "density" function. The Courant minimax principle rendered a condition for finding the habitat, fractionalized Chl-*a* eigenvalues for a real symmetric matrix. The Courant minimax principle was employed in ArcGIS for any real symmetric matrix A, $\lambda_k = \min_{C} \max_{(\|x\|=1 \atop Cx=0)} \langle Ax, x\rangle,$ where C was any $(k-1) \times n$ matrix. Notice that the vector x was an eigenvector to the corresponding eigenvalue λ in the georeferenced habitat. The Courant minimax principle is a result of the maximum theorem, which states that for $q(x) = \langle Ax,x\rangle$, A being a real symmetric matrix, the largest eigenvalue is given by $\lambda_1 = \max_{||x||=1} q(x) = q(x_1)$, where x_1 is the corresponding eigenvector [24].The unmixed Chl-a eigenvalues λ_k and eigenvectors x_k are found by induction and are orthogonal to each other; therefore, $\lambda_k = \max q(x_k)$, with $\langle x,x_k\rangle = 0, j < k$.

An endmember unmixed analysis in ArcGIS employed the rate of convergence of smoothing splines [164, 165] to improve the model output. For brevity, EX() = 0 was assumed. Then, a_0 was estimated by y and j_0 by employing the he Cauchy–Schwarz inequality. Thus, for all vectors x and y of an inner product space in the eco-epidemiological dataset of Chl-*a* endmember regressors it was true that $|\langle x, y\rangle|^2 \leq \langle x, x\rangle \cdot \langle y, y\rangle$, where $\langle \cdot, \cdot \rangle$ was the inner product (i.e., dot product). Equivalently, by taking the square root of both sides, and referring to the norms of the vectors, the inequality in the model forecast was written as $|\langle x, y\rangle| \leq \|x\| \cdot \|y\|$ in ArcGIS Geospatial Analyst.

It was noted that when $x_1, \ldots, x_n \in \mathbb{C}$ and $y_1, \ldots, y_n \in \mathbb{C}$ had an imaginary component, the inner product in the habitat risk model, the standard inner product and the bar notation was used for complex conjugation, and the inequality was restated more explicitly as $|x_1\bar{y}_1 + \cdots + x_n\bar{y}_n|^2 \leq (|x_1|^2 + \cdots + |x_n|^2)(|y_1|^2 + \cdots + |y_n|^2)$.

Moreover, two sides are equal if and only if x and y are linearly dependent (or, in a geometrical sense, they are parallel or one of the vectors' magnitude is zero) [24]. When viewed in this way the numbers x_1, ..., x_n, and y_1, ..., y_n were the components of x and y with respect to an orthonormal basis of V in the residual model forecasts. These latent variables were compactly written as $\left|\sum_{i=1}^{n} x_i\bar{y}_i\right|^2 \leq \sum_{j=1}^{n} |x_j|^2 \sum_{k=1}^{n} |y_k|^2.$

Let (S, Σ, μ) be a measure space and let $p, q \in [1, \infty]$ with $1/p + 1/q = 1$. Then, for all measurable real- or complex-valued functions f and g on S, $\|fg\|_1 \leq \|f\|_p \|g\|_q$. [23]. If, in addition, $p, q \in (1, \infty)$ and $f \in L^p(\mu)$ and $g \in L^q(\mu)$, then Hölder's inequality becomes an equality in the risk model if and only if $|f|^p$ and $|g|^q$ were linearly dependent in $L^1(\mu)$. This indicates that there exists parameterized covariates $\alpha, \beta \geq 0$, which are not both zero, and $\alpha|f|^p = \beta\,|g|^q \mu$-existed almost everywhere in the regressed dataset.

The semivariogram analysis made implicit use of the ergodicity hypothesis in the eco-epidemiological, Chl-*a*, endmember, emissivity model. The VARIOGRAM procedure worked with the forecasted, residually centered values $V(s_i) = v_i = z_i - \bar{Z}$, $i = 1, \ldots, n$, where it was assumed that the sample mean $\bar{Z}$ was the constant expected value $E[Z(s)]$ of $Z(s)$. This was equivalent to employing the original values, since $V(s_i) - V(s_j) = Z(s_i) - Z(s_j)$, which in the habitat model revealed that the optimal property of the semivariance could be parsimoniously tabulated by filtering out the mean. PROC VARIOGRAM was used to compute the empirical classical $\hat{\gamma}(h)$ and robust $\bar{\gamma}(h)$ semivariances (www.sas.edu).

The VARIOGRAM procedure worked with the forecasted habitat values (i.e., $V(s_i) = v_i = z_i - \bar{Z}$, $i - 1, \ldots, n$), where it was assumed that the sample mean $\bar{Z}$ was the constant expected value $E[Z(s)]$ of $Z(s)$. This was equivalent to employing the original geosampled values, since $V(s_i) - V(s_j) = Z(s_i) - Z(s_j)$ showed the property of the semivariance to filter out the mean. Additionally, since the time series random field was ergodic, the regressors corresponded to the variance in the Chl-*a* canopy, unmixed, reflectance model.

A practical range and defined and the distance at which 95% of the sill was reached for an asymptotic variogram. A Voroni decomposition error matrix then assessed the accuracy of the unmixing systematics as well as the proper selection of the covariate coefficients of the risk model. The model output revealed that the kriged sub-mixel, biosignature NDVI, eigen-decomposed derivative spectra were within normal statistical thresholds. A field verification exercise revealed an accuracy of the model residual forecasts. On the other hand,

$$\text{ro}\ 5Z^{(1} + {}^{XY}k^{!)\,2(1} + {}^{Y}k^{\,a)}$$

$$k = 1$$

$$<Q\pounds(1 + Ak^{2(r+s)})^{-2}(1 + k^{2a(r+s)})$$

$$k=1$$

$$/\text{ro}\ 1 + Ax^{\,2(r+s\wedge-2}x^{\,2a(r+s)}dx$$

ro

$$(1 + Ax^{2(r+s)/(2a(r+s)+1)})^{-2}dx$$

$$= A^{-(a+1/(2(r+s)))} \text{ x } A^{-}\ {}^{A}/\!/_{a+1/(2(r+s))}\ (1 + x^{\,2(r+s)/(2a(r+s)+r\wedge-2}dx$$

$$(a+1/(2(r+s)))$$

summed up, ||/3 - Ml = $O_p(n^{-1}A^{-(a+1/(2(r+s)))}||/$ - M2). In particular, taking a = c in the immature habitat model output yielded 11/3 - ^||2 = Op(n~^{1}A~$^{(c+1/(2(r+s)}$»||/3 - /?|2). If $n^{-1}A^{-(c+1/(2(r+s)))\wedge} 0$, then HV-h*c* = *Opi*Mp-h*c)*. Together with the triangular inequality H/S- *h*c> 11/3 - *h*c - 11/3 - *h*c = (1 - Op(1))*U*p – *h*c. Therefore, *H/*^{3}-h*c* = *Op(*HP-h*c),* and as such the model rendered b H/3 - ^H2 = $Op(n^{-1}A^{-(c+1/(2(r+s)))})$ = Op(1). Putting it back to into the dataset of the habitat model, we were able to robustly regressively quantitate all the RapidEye^{TM} 5m, unmixed, transmittance wavelength data. If there also existed some *1/2(r + s) < c < 1,* such that n^{l} *x* $A^{-(c+1/2(r+s))} \wedge 0$, then *Hf-M2 = op(*$n^{-1}A^{-(a+1/2(r+s))}$*).*

The semivariogram analysis made implicit use of the ergodicity hypothesis in the habitat model. The VARIOGRAM procedure worked with the residual centered values $V(s_i) = v_i = z_i - \bar{Z}$, $i = 1, \ldots, n$, where it was assumed that the sample mean $\bar{Z}$ was the constant expected value $\mathbf{E}[Z(s)]$ of $Z(s)$. This was equivalent to employing the original values $V(s_i) - V(s_j) = Z(s_i) - Z(s_j)$, which revealed that the optimal property of the semivariance could be robustly parsimonioulsy tabulated by filtering out the mean. PROC VARIOGRAM uses to compute the empirical classical $\hat{\gamma}(h)$ and robust $\bar{\gamma}(h)$ semivariances (www.sas.edu).

The VARIOGRAM procedure worked with the forecasted, residually centered, RapidEye 5m, sparsely shaded canopied, geospatial/geospectral, explanatorily interpolated, hyperproductive, georeferenceable, *S. damnosum* s.l. riverine , immature, habitat geosampled values (i.e., $V(s_i) = v_i = z_i - \bar{Z}$, $i - 1, \ldots, n$) where it was assumed that the sample mean $\bar{Z}$ was the constant expected value $\mathbf{E}[Z(s)]$ of $Z(s)$. This was equivalent to employing the original geo-spatiotemporally, geosampled values, since $V(s_i) - V(s_j) = Z(s_i) - Z(s_j)$ showed the property of the semivariance to filter out the mean. Additionally, since the time series dependent random field was ergodic the time series, dependent regressors corresponded to the variance in the canopy, endmember reflectance model.

A practical range was defined at which 95% of the sill was reached for an asymptotic variogram. A Voroni decomposition error matrix in ArcGIS then assessed the accuracy of the unmixing systematics as well as the proper selection of the coefficients of the risk model (see Figure 66). A weighted Voronoi diagram is the one in which the function of a pair of points to define a Voronoi cell is a distance function modified by multiplicative or additive weights assigned to generator points. In contrast to the case of Voronoi cells defined using a distance which is a metric, in this case some of the Voronoi cells may be empty. A power diagram is a type of Voronoi diagram defined from a set of circles using the power distance; it can also be thought of as a weighted Voronoi diagram in which a weight defined from the radius of each circle is added to the squared distance from the circle's center The model output revealed that the kriged sub-mixel, riverine, habitat, biosignature endmember, derivative spectral estimates were within normal statistical threshol

Figure 66 Voroni tessellations of the interpolated unmixed RapidEye™ Red Edge NDVI *S. damnosum s.l.* habitats biosignature at the Goncogo study site

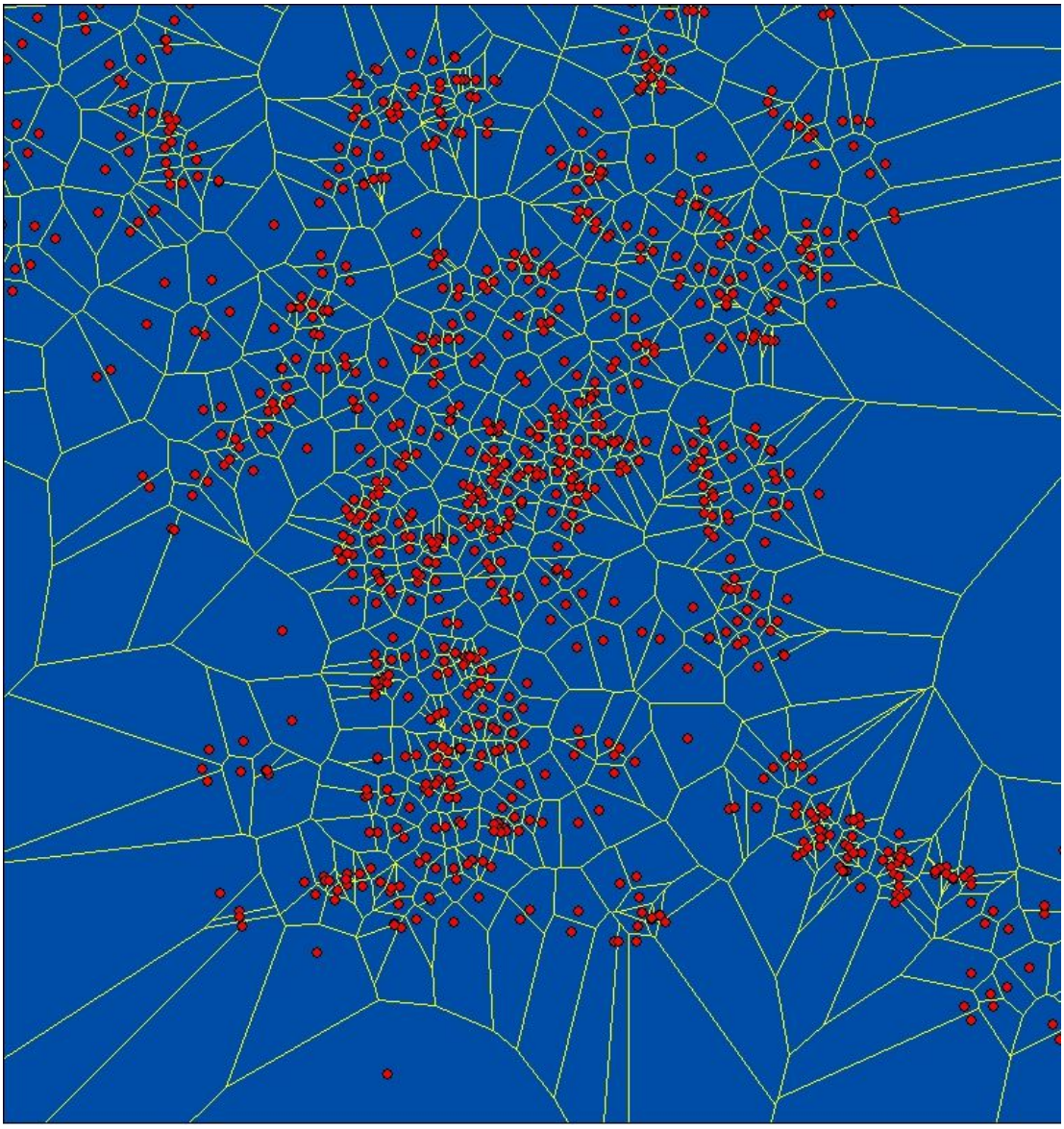

In the control villages Ayago and Laminlatoo, fly density was relatively the same from the beginning of monitoring to the final day of monitoring, with some small fluctuations in between the catching days probably due to mild weather changes. In Goncogo and Adibuk Villages, fly density was relatively constant from the beginning of the monitoring up to the 13th day, and then gradually started reducing up to the last day. This is possibly due to the slashing and clearing of the potential breeding sites of the flies, which was done in two cycles. The first cycle took place on the 8th and 9th day, and the second cycle on the 19th and 20th day of the exercise. These were intervention villages.

FLY CATCHES DURING THE SLASH AND CLEAR TRIALS IN FOUR VILLAGES (OVER A PERIOD OF 31 DAYS)

GONYCOGO (INTERVENTION)	AYAGO/NILE (CONTROL)	ADIBUK (INTERVENTION)	LAMINLATOO (CONTROL)
310	370	226	230
299	349	237	251
321	366	213	212
279	339	260	217
283	295	217	229
297	361	204	201
258	389	256	255
267	278	241	243
281	315	269	219
309	364	253	232
261	352	259	207
252	341	219	246
215	331	191	215
189	350	151	221
163	327	155	258
152	369	148	235
138	377	121	239
116	356	128	225
141	287	120	233
133	359	129	211
120	321	119	240
111	345	99	234
102	367	76	227
116	353	70	241
98	216	66	266
77	307	61	237
51	368	63	222
44	344	50	208
30	308	44	218
37	360	40	236
31	379	33	214

Figure 67. Histogram of post-collection of adult black flies captured at Adbuk intervention village and Laminlato control village

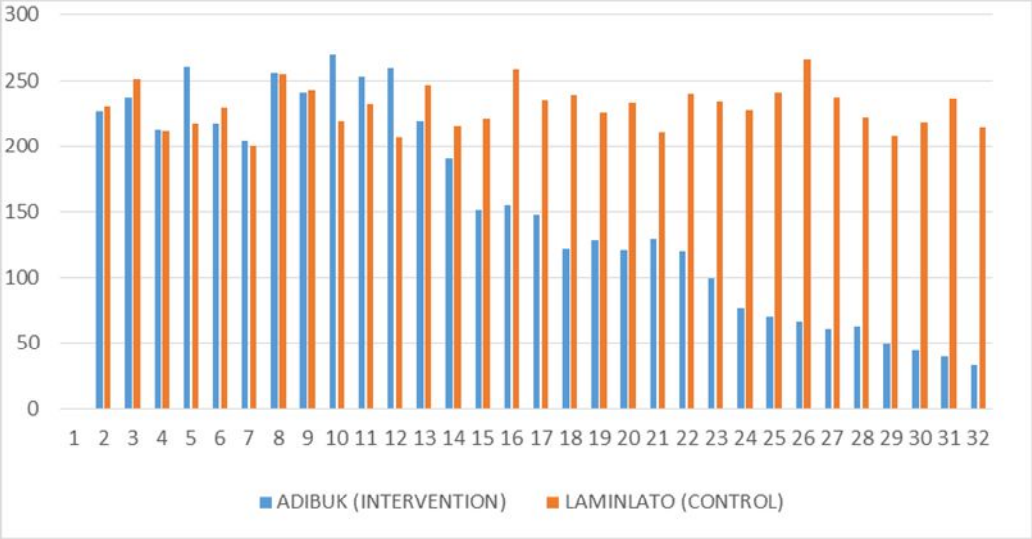

Figure 68. Histogram of post-collection of adult black flies captured at Gonycogo intervention village and Ayago control village

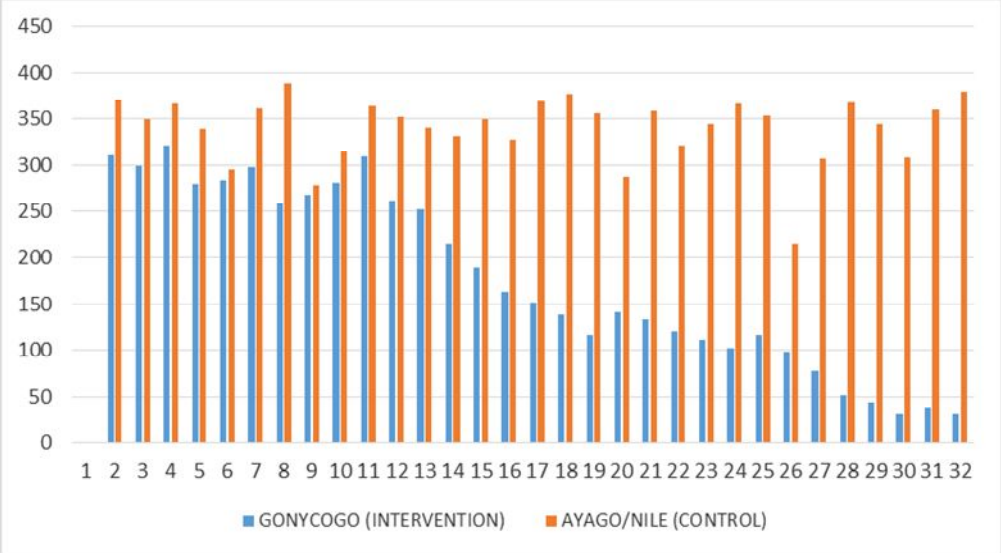

Slash and Clear was conducted in the intervention narrow tributary, eco-georferenceable, explanatorial, agro-village complexes (see Figure 67 to 73). In Gonycogo and Ayago villages, there was a fly density decrease of 52%, while in Adibuk and Laminlatoo villages, there was a fly density decrease of 66% after intervention. This rendered an overall percentage efficiency of the Slash and Clear approach of 60% within a period of 31 days

Discussion

The mean and variance were optimally defined in terms of integrals in a forecast vulnerability , narrow African, agro-village, riverine tributray, *S. damnosum* s.l., decomposable, endmember iterative,,stochastic interpolator What it means for the mean or variance to be infinite in the signature probabilsic paradigm would be defined then be the i statement about the limiting behavior for those integrals For example, if the mean is lim a,b→∞ ∫ b −a x dF lima,b→∞∫−abx dF for a (considering this, say as a Stieltjes integral)

in a *S. damnosum* s.l. probabilistic model for a continuous density this would be $\lim a,b\to\infty \int b -a xf(x)\,dx$ $\lim a,b\to\infty\int -abxf(x)\,dx$ (now as a Riemann integral, say).

This can happen, for example, if the tail is "heavy enough". In A SAS/GIS Then a medical entomologist or expeimenter may optimally consider the following examples for four cases of finite/infinite mean and variance quanatiation for a moderate resolution, uncoalesced, geo-spectrotemporal, probabilsic, itearatively quantitatively interpolative, endmmeber signature, geospatial, time serirs : A distribution with infinite mean and infinite variance for a Pareto distribution with α=1 α=1) , a zeta(2) distribution. 2) A distribution with infinite mean and finite variance.3) A distribution with finite mean and infinite variance.A distribution with finite mean and finite variance. The Pareto distribution is a power law probability distribution that is used in description of social, scientific, geophysical, actuarial, and many other types of observable phenomena[25]

The beta function $B(p,q)$ is the name used by Legendre and Whittaker and Watson (1990) for the beta integral(also called the Eulerian integral of the first kind). The eco-georferenceable, explanatorial, trailing vegetation, narrow , riverine tributary *S. damnosum* *s*.l. capture point, immature habitat eco-epidemiolgical, model was defined by $B(p,q)=\frac{\Gamma(p)\Gamma(q)}{\Gamma(p+q)}=\frac{(p-1)!\,(q-1)!}{(p+q-1)!}$. The beta function $B(a,b)$ was implemented in the Wolfram Language as Beta[*a*, *b*].To derive the integral representation of the beta function, we wrote the the product of two factorials as $m!\,n!=\int_0^\infty e^{-u}\,u^m\,du\int_0^\infty e^{-v}\,v^n\,dv$.We let $u=x^2$, $v=y^2$, so $m!\,n!=4\int_0^\infty e^{-x^2}\,x^{2m+1}\,dx\int_0^\infty e^{-y^2}\,y^{2n+1}\,dy=\int_{-\infty}^{\infty}\int_{-\infty}^{\infty}e^{-(x^2+y^2)}\,|x|^{2m+1}\,|y|^{2n+1}\,dx\,dy$. Transforming to polar coordinates with $x=r\cos\theta$, $m!\,n!y=r\sin\theta=\int_0^{2\pi}\int_0^\infty e^{-r^2}\,|r\cos\theta|^{2m+1}\,|r\sin\theta|^{2n+1}\,r\,dr\,d\theta$ rendered $\int_0^\infty e^{-r^2}\,r^{2m+2n+3}\,dr\int_0^{2\pi}\left|\cos^{2m+1}\theta\sin^{2n+1}\theta\right|d\theta=4\int_0^\infty e^{-r^2}\,r^{2m+2n+3}\,dr\int_0^{\pi/2}\cos^{2m+1}\theta\sin^{2n+1}\theta\,d\theta$ $2(m+n+1)!\int_0^{\pi/2}\cos^{2m+1}\theta\sin^{2n+1}\theta\,d\theta$. The polar coordinates r (the radial coordinate) and θ (the angular coordinate, often called the polar angle) were defined in terms of moderate resolution derived Cartesian coordinates by $x=r\cos\theta, y=r\sin\theta$,where r was the radial distance from the origin, and θ was the counterclockwise angle from the *x*-axis in the *S. damnoum* s.l. model in terms of x and y, $r=\sqrt{x^2+y^2}$ and $\theta=\tan^{-1}\left(\frac{y}{x}\right)$. In so doing, $\tan^{-1}(y/x)$ was interpretable as a two-argument inverse tangent which took the signs of x and y into account to determine in which quadrant θ lay the *S. damnosum* s.l. eco-epidemiological, moderate resolution , forecast vulnerability model forecasts. It followed immediately that polar coordinates were inherently unique; in particular, $(r,\theta+2n\pi)$ was precisely the same polar point as (r,θ) for any integer n.in the model One often allows negative values of r under the assumption that $(-r,\theta)$ is plotted identically to $(r,\theta\pm\pi)$[25].

The beta function in the eco-epidemiological, moderate resolution, geo-spectrotemporal, *S. damnosum* s.l. immature, habitat, eco-epidemiological, capture point, eco-georeferenceable model was then defined

by $B(m+1, n+1) = 2\int_0^{\pi/2} \cos^{2m+1}\theta \sin^{2n+1}\theta \, d\theta = \frac{m!\, n!}{(m+n+1)!}$. Rewriting the arguments then rendered the usual form for the beta function, $B(p, q) = \frac{\Gamma(p)\Gamma(q)}{\Gamma(p+q)} = \frac{(p-1)!\,(q-1)!}{(p+q-1)!}$. By symmetry, $B(p, q) = B(q, p)$ in the vulnerability , probabilistic, regressive, paradigm forecasted residual datset. The beta function was also given by the product $B(x, y) = \frac{x+y}{xy} \prod_{k=1}^{\infty} \frac{1 + \frac{x+y}{k}}{\left(1+\frac{x}{k}\right)\left(1+\frac{y}{k}\right)}$.

The general trigonometric form of the riverine tributary, moderate resolution, discontinuously canopied, *S. damnosum* s.l. immature, capture point, moderate resolution , , trailing vegation, discontinuously canopied, eco-georeferenceable, immature, capture point, habitat model

was $\int_0^{\pi/2} \sin^{\alpha} x \cos^{m} x \, dx = \frac{1}{2} B\left(\frac{1}{2}(n+1), \frac{1}{2}(m+1)\right)$,This equation was transformed to an integral over polynomials by letting $u = \cos^2\theta$, In so doing, $B(m+1, n-1) = \frac{m!\, n!}{(m+n+1)!} = \int_0^1 u^m (1-u)^n \, du$ and $B(m, n) = \frac{\Gamma(m)\Gamma(n)}{\Gamma(m+n)} = \int_0^1 u^{m-1}(1-u)^{n-1} \, du$. for any z_1, z_2 in the probabilistic paradigm with $\Re[z_1], \Re[z_2] > 0, B(z_1, z_2) = B(z_2, z_1)$.

The expression of a point as an ordered pair (r, θ) is known as polar notation, the equation of a curve expressed in polar coordinates is known as a polar equation, and a plot of a curve in polar coordinates is known as a polar plot (www.esri.com).In much the same way that Cartesian *S. damnosum* s.l. curves were plotted on rectilinear axes, polar plots which was drawn on radial axes such as those shown in the figure above.The arc length of a polar curve wasgiven by $r = r(\theta)$ which when tabulated was $s = \int_{\theta_1}^{\theta_2} \sqrt{r^2 + \left(\frac{dr}{d\theta}\right)^2} \, d\theta$. The line element was given by $ds^2 = dr^2 + r^2 \, d\theta^2$.and the area element by $dA = r \, dr \, d\theta$.The area enclosed by a polar curve $r = r(\theta)$ in the *S. damnosum* s.l. oviposition predictive risk model was then $A = \frac{1}{2}\int_{\theta_1}^{\theta_2} r^2 \, d\theta$. The slope of a polar function $r = r(\theta)$ at the hypeproductive, eco-georeferenceable, narrow, riverine tributary, agro-village capture point immature, habitat (r, θ) was given by $m = \frac{r + \tan\theta \frac{dr}{d\theta}}{-r\tan\theta + \frac{dr}{d\theta}}$. The angle between the tangent and radial line at the point (r, θ) in the paradigm was $\psi = \tan^{-1}\left(\frac{r}{\frac{dr}{d\theta}}\right)$.

A polar curve is symmetric about the x-axis if replacing θ by $-\theta$ in its equation produces an equivalent equation, symmetric about the y-axis if replacing θ by $\pi - \theta$ in its equation produces an equivalent equation, and symmetric about the origin if replacing r by $-r$ in its equation produces an equivalent equation[25].In Cartesian coordinates, the radius vector $\mathbf{r}$ is $\mathbf{r} = \sqrt{x^2 + y^2}\,\hat{\mathbf{r}}$.giving

International Journal of Geographic Information System
Vol. 4, No. 1, April 2017, pp.1-519
Available Online at http://acascipub.com/Journals.php

derivative $\dot{\mathbf{r}} = \dot{\hat{\mathbf{r}}}\sqrt{x^2+y^2} + \hat{\mathbf{r}}\left(x^2+y^2\right)^{-1/2}(x\dot{x}+y\dot{y})$. Its unit vector is $\hat{\mathbf{r}} = \frac{x\hat{\mathbf{x}}+y\hat{\mathbf{y}}}{\sqrt{x^2+y^2}}$, giving derivative $\dot{\hat{\mathbf{r}}} = \frac{(x\dot{y}-y\dot{x})(x\hat{\mathbf{y}}-y\hat{\mathbf{x}})}{(x^2+y^2)^{3/2}}$. In polar coordinates, the radius vector is given by $\mathbf{r} \equiv \begin{bmatrix} r\cos\theta \\ r\sin\theta \end{bmatrix}$, giving derivatives $\dot{\mathbf{r}} = \begin{bmatrix} -r\sin\theta\dot{\theta}+\cos\theta\dot{r} \\ r\cos\theta\dot{\theta}+\sin\theta\dot{r} \end{bmatrix} = r\dot{\theta}\hat{\boldsymbol{\theta}} + \dot{r}\hat{\mathbf{r}}$ and $\ddot{\mathbf{r}} = \left(\ddot{r}-r\dot{\theta}^2\right)\hat{\mathbf{r}} + \left(2\dot{r}\dot{\theta}+r\ddot{\theta}\right)\hat{\boldsymbol{\theta}} = \left(\ddot{r}-r\dot{\theta}^2\right)\hat{\mathbf{r}} + \frac{1}{r}\frac{d}{dt}\left(r^2\dot{\theta}\right)\hat{\boldsymbol{\theta}}$. The unit vectors were $\hat{\mathbf{r}} = \frac{\frac{d\mathbf{r}}{dr}}{\left|\frac{d\mathbf{r}}{dr}\right|} = \begin{bmatrix} \cos\theta \\ \sin\theta \end{bmatrix}$ and $\hat{\boldsymbol{\theta}} = \frac{\frac{d\mathbf{r}}{d\theta}}{\left|\frac{d\mathbf{r}}{d\theta}\right|} = \begin{bmatrix} -\sin\theta \\ \cos\theta \end{bmatrix}$, giving derivatives $\dot{\hat{\mathbf{r}}} = \begin{bmatrix} -\sin\theta\dot{\theta} \\ \cos\theta\dot{\theta} \end{bmatrix} = \dot{\theta}\hat{\boldsymbol{\theta}}$ and $\dot{\hat{\boldsymbol{\theta}}} = \begin{bmatrix} -\cos\theta\dot{\theta} \\ -\sin\theta\dot{\theta} \end{bmatrix} = -\dot{\theta}\hat{\mathbf{r}}$. A unit vector is a vector of length 1, sometimes also called a direction vector (Jeffreys and Jeffreys 1988). The unit vector $\hat{\mathbf{v}}$ having the same direction as a given (nonzero) vector $\mathbf{v}$ is defined by $\hat{\mathbf{v}} = \frac{\mathbf{v}}{|\mathbf{v}|}$, where $|\mathbf{v}|$ denotes the norm of $\mathbf{v}$, is the unit vector in the same direction as the (finite) vector $\mathbf{v}$. A unit vector in the $\mathbf{x}_n$direction is given by $\hat{\mathbf{x}}_n \equiv \frac{\frac{\partial\mathbf{r}}{\partial x_n}}{\left|\frac{\partial\mathbf{r}}{\partial x_n}\right|}$, where $\mathbf{r}$ is the radius vector. The vector $\mathbf{r}$ from the origin to the current position.is also called the position vector where the derivative of $\mathbf{r}$ satisfies $\mathbf{r}\cdot\frac{d\mathbf{r}}{dt} = \frac{1}{2}\frac{d}{dt}(\mathbf{r}\cdot\mathbf{r}) = \frac{1}{2}\frac{d}{dt}\left(r^2\right) = r\frac{dr}{dt} = rv$ [25].

To put it in a form which can be used to derive the Legendre duplication formula, We let $x \equiv \sqrt{u}$, so $u = x^2$ and $du = 2x\,dx$, and $B(m,n) = \int_0^1 x^{2(m-1)}\left(1-x^2\right)^{n-1}(2x\,dx) = 2\int_0^1 x^{2m-1}\left(1-x^2\right)^{n-1}dx$. in the *S. damnosum* s.l. model. Gamma functions of argument $2z$ can be expressed in terms of gamma functions of smaller arguments[25]. From the definition of the hypeproductiive, *S. damnosum* s.l., seasonal oviposition LULC site moderate resolution model, we quanatiate the beta functionas $B(m,n) = \frac{\Gamma(m)\Gamma(n)}{\Gamma(m+n)} = \int_0^1 u^{m-1}(1-u)^{n-1}\,du$. We let $m = n \equiv z$, then $\frac{\Gamma(z)\Gamma(z)}{\Gamma(2z)} = \int_0^1 u^{z-1}(1-u)^{z-1}\,du$ and $u \equiv (1+x)/2$, so $du = dx/2$ and $\frac{\Gamma(z)\Gamma(z)}{\Gamma(2z)} = \int_{-1}^1\left(\frac{1+x}{2}\right)^{z-1}\left(1-\frac{1+x}{2}\right)^{z-1}\left(\frac{1}{2}dx\right) = \frac{1}{2}\int_{-1}^1\left(\frac{1+x}{2}\right)^{z-1}\left(\frac{1-x}{2}\right)^{z-1}dx = \frac{1}{2^{1+2(z-1)}}\int_{-1}^1\left(1-x^2\right)^{z-1}dx = 2^{1-2z}\left[2\int_0^1\left(1-x^2\right)^{z-1}dx\right]$. We employed the beta function identity $B(m,n) = 2\int_0^1 x^{2m-1}\left(1-x^2\right)^{n-1}dx$ to parsimoniously quantitate $\frac{\Gamma(z)\Gamma(z)}{\Gamma(2z)} = 2^{1-2z}B\left(\frac{1}{2},z\right) = 2^{1-2z}\frac{\Gamma\left(\frac{1}{2}\right)\Gamma(z)}{\Gamma\left(z+\frac{1}{2}\right)}$. Solving for $\Gamma(2z)$ and

using $\Gamma(1/2)=\sqrt{\pi}$ then rendered $\Gamma(2z)=\frac{(2\pi)^{-1/2}\,2^{2z-1/2}\,\Gamma(z)\,\Gamma\left(z+\frac{1}{2}\right)}{\sqrt{\pi}}=\frac{2^{2z-1}\,\Gamma(z)\,\Gamma\left(z+\frac{1}{2}\right)}{\sqrt{\pi}}$.

A form was used to develop integral representations of the Bessel functions and hypergeometric function, in the forecast vulnerability model by letting $u\equiv x^2/(1-x^2)$, so $B(m+1,n+1)=\int_0^{\infty}\frac{u^m\,du}{(1+u)^{m+n+2}}$. A function $Z_n(x)$ optimally defined by the recurrence relations $Z_{n+1}+Z_{n-1}=\frac{2n}{x}Z_n$ and $Z_{n+1}-Z_{n-1}=-2\frac{dZ_n}{dx}$. The Bessel functions are more frequently defined as solutions to the differential equation $x^2\frac{d^2y}{dx^2}+x\frac{dy}{dx}+(x^2-n^2)y=0$. (www.mathworld.com).The hypergeometric functions are solutions to the hypergeometric differential equation, which has a regular singular point at the origin[25]

. To derive the hypergeometric function from the hypergeometric, *S. damnosum* s.l. explanative, ,immature, habitat differential equation $z(1-z)y''+[c-(a+b+1)z]y'-aby=0$,we usde the Frobenius method to reduce it to $\sum_{n=0}^{\infty}\left\{(n+1)(n+c)A_{n+1}-\left[n^2+(a+b)n+ab\right]A_n\right\}z^n=0$, giving the indicial equation $A_{n+1}=\frac{(n+a)(n+b)}{(n+1)(n+c)}A_n$. The Frobenius method enables us to create a power series solution to such a differential equation, provided that p(z) and q(z) are themselves analytic at 0 or, being analytic elsewhere, both their limits at 0 exist (and are finite)(www.mathworld.com). An indicial equation, also called a characteristic equation, is a recurrence equation obtained during application of the Frobenius method while solving a second-order ordinary differential equation.[25] The indicial equation is obtained by noting that, by definition, the lowest order term x^k (that corresponding to $n=0$) must have a coefficient of zero. x_0 is an ordinary point of the ordinary differential equation, expand y in a Taylor series about x_0. Commonly, the expansion point can be taken as $x_0=0$, resulting in the Maclaurin series $y=\sum_{n=0}^{\infty}a_n x^n$. A Maclaurin series is a Taylor series expansion of a function about 0, $f(x)=f(0)+f'(0)x+\frac{f''(0)}{2!}x^2+\frac{f^{(3)}(0)}{3!}x^3+\ldots+\frac{f^{(n)}(0)}{n!}x^n+\ldots.$

Plugging this into the ansatz series $y=\sum_{n=0}^{\infty}A_n z^n$ then optimally rendered the solution $y=A_0\left[1+\frac{ab}{1!\,c}z+\frac{a(a+1)b(b+1)}{2!\,c(c+1)}z^2+\ldots\right]$.This is the so-called regular solution, denoted $_2F_1(a,b;c;z)=1+\frac{ab}{1!\,c}z+\frac{a(a+1)b(b+1)}{2!\,c(c+1)}z^2+\ldots=\sum_{n=0}^{\infty}\frac{(a)_n(b)_n}{(c)_n}\frac{z^n}{n!}$, which converged in the *S. damnosum* s.l. model if c was not a negative integer (1) for all of $|z|<1$ and (2) on the unit circle $|z|=1$ if $\mathrm{R}[c-a-b]>0$. The complete solution to the trailing vegetation, discontinuously canopied, *S. damnoum* s.l. hypergeometric differential equation was $y=A\,{}_2F_1(a,b;c;z)+Bz^{1-c}\,{}_2F_1(a+1-c,b+1-c;2-c;z)$.The hypergeometric

series is convergent for *arbitrary* a, b, and c for real $-1 < z < 1$, and for $z = \pm 1$ if $c > a + b$Here, $(a)_n$ was a Pochhammer symbol. T he Pochhammer symbol$(x)_n = \frac{\Gamma(x+n)}{\Gamma(x)} = x(x+1)\cdots(x+n-1)$ [25].

The Pochhammer symbol was implemented in the *S. damnosum* s.l. hypeproductive seasaonl oviposition model employing the Wolfram Language as Pochhammer[*x*, *n*].The Pochhammer symbol satisfied$(-x)_n = (-1)^n (x-n+1)_n$,the dimidiation formulas$(x)_{2n} = 2^{2n}\left(\frac{x}{2}\right)_n \left(\frac{1+x}{2}\right)_nand(x)_{2n+1} = 2^{2n+1}\left(\frac{x}{2}\right)_{n+1}\left(\frac{1+x}{2}\right)_n$,and the duplications formula $\left[2^n (x)_{n/2}\left(x+\frac{1}{2}\right)_{n/2}\right.$ A ratio of Pochhammer symbols was $\frac{(x)_n}{(x)_m} = \begin{cases} (x+m)_{n-m} & \text{if } n \geq m \\ \frac{1}{(x+n)_{m-n}} & \text{if } n \leq m \end{cases}$ given in closed form. The derivative was given by$\frac{d}{dx}(x)_n = (x)_n [\psi_0(n+x) - \psi_0(x)]$, where $\psi_0(x)$ is the digamma function. The digamma function arises in simple sums such as$\sum_{k=0}^{\infty} \frac{(-1)^k}{z k+1} = \frac{\Phi(-1, 1, z^{-1})}{z} = \frac{1}{2z}\left[\psi_0\left(\frac{z+1}{2z}\right) - \psi_0\left(\frac{1}{2z}\right)\right]$, where $\Phi(z, s, a)$ is a Lerch transcendent[25].

The Lerch transcendent is generalization of the Hurwitz zeta function and polylogarithm function.T he Hurwitz zeta function $\zeta(s, a)$ is a generalization of the Riemann zeta function $\zeta(s)$ that is also known as the generalized zeta function. In the *S. damsnoum* s.l. model this function was defined by the formula $\zeta(s, a) \equiv \sum_{k=0}^{\infty} \frac{1}{(k+a)^s}$ for $\Re[s] > 1$ and by analytic continuation to other $s \neq 1$, where any term with $k + a = 0$ is excluded. It is implemented in this form in the Wolfram Language as HurwitzZeta[*s*, *a*].The slightly different form $\zeta^*(s, a) = \sum_{k=0}^{\infty} \frac{1}{[(a+k)^2]^{s/2}}$ is implemented in the Wolfram Language as Zeta[*s*, *a*]. Note that the two are identical only for $\Re[a] > 0$.

Many sums of reciprocal powers can be expressed in terms of it. It is classically optimally defined by $\Phi(z, s, a) = \sum_{k=0}^{\infty} \frac{z^k}{(a+k)^s}$, for $|z| < 1$ and $a \neq 0, -1, \ldots$. It is implemented in this form as HurwitzLerchPhi[*z*, *s*, *a*] in the Wolfram Language.The slightly different form $\Phi^*(z, s, a) = \sum_{k=0}^{\infty} \frac{z^k}{[(a+k)^2]^{s/2}}$ sometimes also denoted $\tilde{\Phi}(z, s, a)$for $|z| < 1$ (or $|z| = 1$ and $\Re[s] > 1$) and $a \neq 0, -1, -2, \ldots$, is also implemented in theWolfram Language as LerchPhi[*z*, *s*, *a*]. Note that the two are identical only for $\Re[a] > 0$.A series formula for $\Phi(z, s, a)$ valid on a larger domain in the complex z-plane is given by$(1-z)\Phi(z, s, a) = \sum_{n=0}^{\infty}\left(\frac{-z}{1-z}\right)^n \sum_{k=0}^{n} (-1)^k \binom{n}{k} (a+k)^{-s}$ which holds for all complex s and

complex z with $\Re[z] < 1/2$ The Lerch transcendent can be used to express the Dirichlet beta $\beta(s)$function$=\sum_{k=0}^{\infty}(-1)^k(2k+1)^{-s} = 2^{-s}\Phi\left(-1, s, \frac{1}{2}\right)$.

The Dirichlet beta function is defined by the sum $\beta(x)=\sum_{n=0}^{\infty}(-1)^n(2n+1)^{-x} = 2^{-x}\Phi\left(-1, x, \frac{1}{2}\right)$,where $\Phi(z, s, a)$is the Lerch transcendent. The Dirichlet beta function in the S. damsnoum s.l. model was implemented in the Wolfram Language as DirichletBeta[x]. The beta function waswritten in terms of the Hurwitz zeta function $\zeta(x, a)$by $\beta(x) = \frac{1}{4^x}\left[\zeta\left(x, \frac{1}{4}\right) - \zeta\left(x, \frac{3}{4}\right)\right]$.The beta function can be defined over the whole complex plane using analytic continuation, $\beta(1-z) = \left(\frac{2}{\pi}\right)^z \sin\left(\frac{1}{2}\pi z\right)\Gamma(z)\beta(z)$,where $\Gamma(z)$is the gamma function.

The (complete) gamma function $\Gamma(n)$I wasdefined to be an extension of the factorial to complex and the decomposed , geo-spectrotemporal, eco-georferenceable, trailing vegeatation, narrow, African, riverine tributariy , agro-village complex S. damnosum s.l. capture point arguments. It was related to the factorial by $\Gamma(n) = (n-1)!$,a slightly unfortunate notation due to Legendre which is now universally used instead of Gauss's simpler $\Pi(n) = n!$(see Gauss 1812; Edwards 2001,). It was analytic everywhere except at $z = 0, -1, -2$, ..., and the residue at $z = -k$is where $\operatorname{Res}_{z=-k}\Gamma(z) = \frac{(-1)^k}{k!}$.There are no points $z$at which $\Gamma(z) = 0$.[25] The gamma function is implemented in the Wolfram Language as Gamma[z]. There are a number of notational conventions in common use for indication of a power of a gamma functions *in S. damnoum* s.l. vulnerability model forecast for targeting seasaonlly hyperproductive seasaonl oviposition geolocations on moderate resolution geoclassifieable LULs . While authors such as Watson (1939) use $\Gamma^n(z)$(i.e., using a trigonometric function-like convention), it is also common to write $[\Gamma(z)]^n$.

The gamma function in the moderate resolution, *S. damnosum* s.l., immature habitat,capture point, trailing vegation, narrow riverine tributray, discontinuously canopied, predictive vulnerability probabilistic paradigm was defined as a definite integral for $\Re[z] > 0$(Euler's integral form) $\Gamma(z) = \int_0^{\infty} t^{z-1} e^{-t}\,dt = 2\int_0^{\infty} e^{-t^2} t^{2z-1}\,dt$, or $\Gamma(z) \equiv \int_0^1 \left[\ln\left(\frac{1}{t}\right)\right]^{z-1} dt$. The complete gamma function $\Gamma(x)$was then generalized to the upper incomplete gamma function $\Gamma(a, x)$and lower incomplete gamma function $\gamma(a, x)$. The "complete" gamma function $\Gamma(a)$ can be generalized to the incomplete gamma function $\Gamma(a, x)$ such that $\Gamma(a) = \Gamma(a, 0)$. This "upper" incomplete gamma function was given by $\Gamma(a, x) \equiv \int_x^{\infty} t^{a-1} e^{-t}\,dt$. For a an integer $n\Gamma(n, x) = (n-1)!\, e^{-x}\sum_{k=0}^{n-1}\frac{x^k}{k!} = (n-1)!\, e^{-x} e_{n-1}(x)$,where $e_n(x)$ is the exponential sum function. It is implemented as Gamma[a, z] in the Wolfram Language.The incomplete gamma function $\Gamma(0, x)$ has continued fraction $\Gamma(0, x) = \cfrac{e^{-x}}{x+1-\cfrac{1}{x+3-\cfrac{4}{x+5-\cfrac{9}{x+7+\ldots}}}}$ [25].

A special case is given by $\Phi(z, n, 1) = \frac{\mathrm{Li}_n(z)}{z}$, where $\mathrm{Li}_n(z)$ is the polylogarithm. he polylogarithm $\mathrm{Li}_n(z)$, also known as the Jonquière's function, is the function $\mathrm{Li}_r(z) \equiv \sum_{k=1}^{\infty} \frac{z^k}{k^n}$ defined in the complex plane over the open unit disk. Its definition on the whole complex plane then follows uniquely via analytic continuation.Note that the similar notation $\mathrm{Li}(z)$ is used for the logarithmic integral.The polylogarithm is also denoted $F(z, n)$ and equal to $\mathrm{Li}_n(z) = z\,\Phi(z, n, 1)$,where $\Phi(z, n, a)$ is the Lerch transcendent [25].

Derivatives of the beta function in the model was then were given by $\frac{d}{da} B(a, b) = B(a, b)[\psi_0(a) - \psi_0(a+b)]$, $\frac{d}{db} B(a, b) = B(a, b)[\psi_0(b) - \psi_0(a+b)]$, $\frac{d^2}{db^2} B(a, b)$ which was equivalent to the equation $B(a, b)\{[\psi_0(b) - \psi_0(a+b)]^2 + \psi_1(b) - \psi_1(a+b)\}$, and $\frac{d^2}{da\,db} B(a, b)$ which was then equivalent to $B(a, b)\{[\psi_0(a) - \psi_0(a+b)] \times [\psi_0(b) - \psi_0(a+b)] - \psi_1(a+b)\}$,where $\psi_n(x)$ was the polygamma function.

Various identities were empirically regressively derived for the ecogeoreferenced, seasonal, hyperproductive, capture point, discontinuously canopied, trailing vegetation,*S. damnosum* s.l. ovipoistion, model using the Gauss multiplication formula. $B(n\,p, n\,q) = \frac{\Gamma(n\,p)\,\Gamma(n\,q)}{\Gamma(n(p+q))} = n^{-n\,q} \frac{B(p, q)\,B\left(p + \frac{1}{n}, q\right) \cdots B\left(p + \frac{n-1}{n}, q\right)}{B(q, q)\,B(2\,q, q) \cdots B((n-1)q, q)}$. Additional identities included $B(p, q+1) = \frac{\Gamma(p)\,\Gamma(q+1)}{\Gamma(p+q+1)} = \frac{q}{p} \frac{\Gamma(p+1)\,\Gamma(q)}{\Gamma((p+1)+q)} = \frac{q}{p} B(p+1, q)$, $B(p, q) = B(p+1, q) + B(p, q+1)$, $B(p, q+1) = \frac{q}{p+q} B(p, q)$.

If n is a positive integer, then $B(p, n+1) = \frac{1 \cdot 2 \cdots n}{p(p+1) \cdots (p+n)}$, $B(p, p)\,B\left(p + \frac{1}{2}, p + \frac{1}{2}\right) = \frac{\pi}{2^{4p-1}\,p}$ $B(p+q)\,B(p+q, r) = B(q, r)\,B(q+r, p)$[25].

Gosper gave the general formulas $\prod_{i=0}^{2n} B\left(\frac{i}{2n+1} + a, \frac{i}{2n+1} + b\right)$ whih was then decomposable to $= \frac{(2n+1)^{(2n+1)/2}\,\pi^n\,B\left(n, \frac{1}{2}[(b+a)(2n+1)+1]\right)B(a(2n+1), b(2n+1))}{(n-1)!}$ for odd n, and $\prod_{i=0}^{2n-1} B\left(\frac{i}{2n} + a, \frac{i}{2n} + b\right) = \frac{n^n\,\pi^n\,B(n, 2(a+b)n)\,B(2an, 2bn)}{2^{2(a+b)n-n-1}\,(n-1)!\,B((a+b)n, (a+b+1)n)}$, which were an immediate consequence of the analogous identities for gamma functions. Plugging $n = 1$ and $n = 2$into the above may render the special cases $B(a, b)\,B\left(a + \frac{1}{3}, b + \frac{1}{3}\right)B\left(a + \frac{2}{3}, b + \frac{2}{3}\right) = \frac{6\pi\sqrt{3}\,B(3a, 3b)}{1 + 3(a+b)}$ in a ecogeoreferenced, seasonal, hyperproductive, capture point, discontinuously canopied, trailing vegetation,*S. damnosum* s.l. ovipoistion, model

when $B(a, b)\, B\left(a+\frac{1}{4}, b+\frac{1}{4}\right) B\left(a+\frac{1}{2}, b+\frac{1}{2}\right) B\left(a+\frac{3}{4}, b+\frac{3}{4}\right)$

$$= \frac{2^{3-4(a+b)}\,\pi^2\, B(4a, 4b)}{(a+b)\,[1+4(a+b)]\, B(2(a+b), 2(a+b+1))}.$$

In the PROC MCMC analyses all the Bayesianized geospatial, "high risk" explanatively hyperproductive, *S. damnosum* s.l., trailing vegetation, turbid water, discontinuously canopied, sparsely shaded , narrow tributary, agro-village complex, eco-georeferenced, larval habitats were identified and ranked based on an eco-epidemiological dataset of RapidEye™ 5m, wavelength, frequency, transmittance covariates and seasonally geo-spectrotemporally geosampled, larval/pupal, productivity counts. Elucidative, metaheuristically optimally, parameterizable, reflectance regressors were strategically interpretively employed in PROC MCMC to define expectations for prior distributions. The analyses revealed that the Percentage of discontinuity gaps was a significant prognosticator, positively associated with the eco-georeferenceable, geosampled, sparsely shaded, heterogeneously canopied, prolific habitats at the interventional, eco-epidemiological, agro-village ecosystem, georeferenced study sites (i.e., Gonycogo and Adbuk). Systematically investigating sources of differential out-of-sample, explicatively geo-predictive, algorithmic, iterative frameworks based on RapidEye™ wavelength, transmittance frequencies and inferencial models in PROC MCMC employing a large empirical eco-epidemiological dataset of non-linear,geo-spectrotemporally geosampled, covariate coefficients may help gauge the degree of specific, time-varying, quantifiable, auto-probabilistic, uncertainties in hierarchical, generalizable, eco-georeferenceable, Bayesianistic, *S. damnosum* s.l., immature habitat, paradigms in PROC MCMC.

The asymptotic truncated mean sqaured error of the geo-spectrotemporal, non-frequentisic, geospatialized, probabilistically regressed, parameterized, explanatorial, covariate estimators in a given hierarchical expositively geoclassifiable, discontinuoulsy canopied, turbid water, LULC class in the intervention, riverine, agro-villge, complex ecosystem, narrow tributary, study sites was robustly mapped. Asympotically squared error of the weighting scheme was eco-cartographically illustrated by an uncertainty-oriented, time series, diagnostic matrix, which employed the 5m, RapidEye™, bandwidth/lag truncations utilizing an asymptotic, truncated, mean squared criterion. The data dependent automatic, 5m, bandwidth/lag truncation parameters were introduced into the paradigm. The finite sample properties were then employed in a multi-dimensional explanatorial, integral analyses via Monte Carlo simulations in PROC MCMC.

Integrations were independently employed in the explanatively optimally parameterizable, 5m, wavelength, transmittance, emissivity, vulnerability covariates. The explanative, eco-georefernceable, eco-epidemiological, immature, trailing vegetation, discontinuously canopied, turbid water, immature habitats, geo-spectrotemporally geosampled at the intervention, agro-village study sites were employed to quantitate a geo-predictive, eco-epidemiological dataset of elucidative, time-series dependent, geospectrotemporal, eco-epidemiological, capture point, clinical, field and remote-specified, asymptotical, non-normal, explanatorial, parameterizable, covariate estimators (e.g., 3-D slope coefficients). The MCMC method was used for approximating an ensemble of eco-georfernceable, *S. damnosum* s.l., immature habitat "walkers" move around randomly. At each trailing vegatation, discontinuity gap, partially canopied, eco-georefernceable, sparsely shaded, agro-village complex, geo-spectrotemporally geosampled, point where a walker stepped, the integrand value at that forecasted, explantive, habitat point was counted towards

the integral in PROC MCMC. The walker then made a number of tentative steps around the iterated area, looking for a place with a reasonably high contribution to the integral to move into next.

However, whereas the capture point, *S. damnosum* s.l., immature habitat, randomized samples of the integrand employed a conventional Monte Carlo integration statistically independent, those employed in MCMC methods were correlated. The Markov chains were constructed in such a way as to have the integrand as its equilibrium distribution. A Markov chain (discrete-time Markov chain or DTMC), is a random process that undergoes transitions from one state to another on a state spaceand possess a property that is usually characterized as "memorylessness": the probability distribution of the next state depends only on the current state and not on the sequence of events that preceded it[24]. The interacting MCMC, seasonal hyperproductive, eco-epidemiological, capture point, *S.damnosum* s.l., immature habitat, expostorial iterations revealed hyperproductive, discontinuous canopied, geolocations in the interventional, riverine, agro-village complexed by obtaining random samples from a sequence of probability distributions with an increasing level of sampling complexity.

The final eco-georeferenceable, explantively diagnostic, *S.damnosum* s.l. turbid water, immature habitat, capture point, forecasting, vulnerability paradigm included an illuminative dataset of path space, state, RapidEye ™ 5m, elucidatively optimally parameterized, uncoalesced, wavelength, transmittance, covariate, frequency, coefficient estimators with increasing time horizon and posterior distributions along with sequences of sparsely shaded, trailing vegetation, optimally geoclassified, elucidative LULC, diagnostic, observational, probabilistic predictors with increasing constraint level sets for evaluating conditional distributions. In probability theory, a conditional expectation (also known as conditional expected value or conditional mean) is the expected value of a real random variable with respect to a conditional probability distribution [24].

The iterative Bayesian, explantive interpretation of a moderate resolution imaged, seasonally hyperproductive, eco-georeferenced, trailing vegetation, discontinuously canopied, eco-epidemiological, partially canopied, *S.damnosum* s.l., turbid water, oviposition LULC, capture point, forecasting, vulnerability model, uncertainty, covariate probability can be seen as an extension of propositional logic that enables reasoning with hypotheses (i.e., the propositions whose truth or falsity is uncertain). Bayesian probability belongs to the category of evidential probabilities [24]. The frequentist will evaluate the probability of a hypothesis, while the Bayesian probabilist specifies some prior probability, which is then updated in the light of new, relevant data (evidence of a ecogeoreferenced, seasonally, hypeproductive, moderate resolution, *S. damnosum* s.l., oviposition site on a geoclassifed ArcGIS derived, trailing vegetation, turbid water, agro-village complex, discontinuously canopied LULC). The iterative, Bayesian interpretated, explanatorial hierarchical, heuristically optimizable, diagnostic, non-normal, uncertainity-oriented weighted,autoregressive matrix can provide a standard set of procedures and formulae to perform optimal regression calculations of various seasonally explanative, hyperproductive, eco-epidemiological, eco-georeferenced, orthogonally, explicatively decomposed, capture point, immature, partially canopied, *S. damnosum* s.l.,oviposition sites on moderate resolution, geoclassified LULCs. The prior and posterior distributions were Beta distributions and the data came from Bernoulli trials.

The BFGS algorithm implemented in ILNumerics was a Quasi-Newton algorithm based on iterative update steps employing a Gauss Conjugate Gradient and a line-search algorithm based on the Golden Section Search to solve the

WolfePowell'sconditions(http://www.it.lut.fi/ip/evo/functions/node5.html). The Newton variant (by default) computed the eco-georeferenced, capture point, *S. damnosum* s.l. trailing vegetation, partially canopied, habitat Hessian matrix based on a forward-backward finite differences algorithm with Ridders' method of polynomial extrapolation.

A factored variant of the Newton iteration may be useable for obtaining a solution datset of optimally decomposed 5m, *S. damnosum* s.l. trailing vegetation, narrow riverine tributray, hyepproductive, oviposition, seasonal geolocations opn ArcGIS derived, 5m, geolcaasified LULCs within a algebraic Riccati equation via the matrix sign function. In particular when the Hamiltonian matrix is associated with a geospectrotemporal geosampled, fractionalized dataset of metaheursitically optimizable, moderate resolution, decomposeable endmembers, the algorithm may exploit the special habitat structures of the off-diagonal blocks to yield an alternative factorizable Newton iteration which may reduce the time cost by an immense factor. Bayesian inferncial iterations can be tedious temporally (Gelman 2003). A $(2n)\times(2n)$complex matrix $\mathbf{A}\in\mathbb{C}^{2n\times 2n}$is said to be Hamiltonian if $\mathbf{J}_n\mathbf{A}=(\mathbf{J}_n\mathbf{A})^{\mathrm{H}}$,where $\mathbf{J}_n\in\mathbb{R}^{2n\times 2n}$is the matrix of the form $\mathbf{J}_n=\begin{bmatrix}0 & \mathbf{I}_n\\ \mathbf{I}_n & 0\end{bmatrix}$,$\mathbf{I}_n$is the $n\times n$identity matrix, and $\mathbf{B}^{\mathrm{H}}$denotes the conjugate transpose of a matrix $\mathbf{B}$. An analogous definition holds in the case of real $(2n)\times(2n)$matrices $\mathbf{A}$by requiring that $\mathbf{J}_n\mathbf{A}$be symmetric, i.e., by replacing $(\mathbf{J}_n\mathbf{A})^{\mathrm{H}}$by $(\mathbf{J}_n\mathbf{A})^{\mathrm{T}}$in (1). Note that this criterion specifies precisely how a Hamiltonian matrix must look (http://mathworld.wolfram.com/HamiltonianMatrix.html). Indeed, every Hamiltonian matrix $\mathbf{A}$(here assumed to have complex entries) must have the form $\mathbf{A}=\begin{bmatrix}\mathbf{X} & \mathbf{D}\\ \mathbf{G} & -\mathbf{X}^{H}\end{bmatrix}$where $\mathbf{D},\mathbf{G}\in\mathbb{C}^{n\times n}$satisfy $\mathbf{D}=\mathbf{D}^{\mathrm{H}}$and $\mathbf{G}=\mathbf{G}^{\mathrm{H}}$. This characterization holds for $\mathbf{A}$having strictly real entries as well by replacing all instances of the conjugate transpose operator in (1) by the transpose operator instead.

The FD= and FDHESSIAN= options scan specified the useage of finite difference approximations of the empirically geo-spectrotemporally geosampled, seasonally hyperproductive, trailing vegetation, discontinuously canopied, eco-epidemiological, eco-georeferenceable, *S.damnosum* s.l. turbid water, immature habitat, forecasting, vulnerability model, paramterizable, explanative, diagnostic, covariate derivatives. The forward-difference derivative oviposition approximations were quantitated employing central-difference formulas. For first-order derivatives, $n$additional function calls in the seasoanl,, moderate resolution, *S.damnosum* s.l.paradigm were devised by : $g_i=\frac{\partial f}{\partial\theta_i}\approx\frac{f(\boldsymbol{\theta}+h_i\mathbf{e}_i)-f(\boldsymbol{\theta})}{h_i}$ For first-order derivatives, $2n$additional function calls are required $=\frac{\partial f}{\partial\theta_i}\approx\frac{f(\boldsymbol{\theta}+h_i\mathbf{e}_i)-f(\boldsymbol{\theta}-h_i\mathbf{e}_i)}{2h_i}$:[24].For second-order derivatives based on function calls , $n+n^2/2$additional employed dense Hessian. Hence $\frac{\partial^2 f}{\partial\theta_i\partial\theta_j}\approx\frac{f(\boldsymbol{\theta}+h_i\mathbf{e}_i+h_j\mathbf{e}_j)-f(\boldsymbol{\theta}+h_i\mathbf{e}_i)-f(\boldsymbol{\theta}+h_j\mathbf{e}_j)+f(\boldsymbol{\theta})}{h_ih_j}$ .For second-order derivatives based on gradient calls$n$additional gradient calls from the orthogonally explanatively decomposed, moderate resolution , narrow , riverine , agro-village complex , hyperproductive , seasoanl hjabitats required: $\frac{\partial^2 f}{\partial\theta_i\partial\theta_j}\approx\frac{g_i(\boldsymbol{\theta}+h_j\mathbf{e}_j)-g_i(\boldsymbol{\theta})}{2h_j}+\frac{g_j(\boldsymbol{\theta}+h_i\mathbf{e}_i)-g_j(\boldsymbol{\theta})}{2h_i}$

For second-order derivatives based on function calls only (Abramowitz and Stegun 1972, p. 884), $2n+4n^2/2$additional function calls are required. $\frac{\partial^2 f}{\partial\theta_i^2} \approx \frac{-f(\boldsymbol{\theta}+2h_i\mathbf{e}_i)+16f(\boldsymbol{\theta}+h_i\mathbf{e}_i)-30f(\boldsymbol{\theta})+16f(\boldsymbol{\theta}-h_i\mathbf{e}_i)-f(\boldsymbol{\theta}-2h_i\mathbf{e}_i)}{12h_i^2}$ $\frac{\partial^2 f}{\partial\theta_i\partial\theta_j} \approx \frac{f(\boldsymbol{\theta}+h_i\mathbf{e}_i+h_j\mathbf{e}_j)-f(\boldsymbol{\theta}+h_i\mathbf{e}_i-h_j\mathbf{e}_j)-f(\boldsymbol{\theta}-h_i\mathbf{e}_i+h_j\mathbf{e}_j)+f(\boldsymbol{\theta}-h_i\mathbf{e}_i-h_j\mathbf{e}_j)}{4h_ih_j}$ For second-order derivatives based on gradient calls, $2n$additional gradient calls are required: $\frac{\partial^2 f}{\partial\theta_i\partial\theta_j} \approx \frac{g_i(\boldsymbol{\theta}+h_j\mathbf{e}_j)-g_i(\boldsymbol{\theta}-h_j\mathbf{e}_j)}{4h_j} + \frac{g_j(\boldsymbol{\theta}+h_i\mathbf{e}_i)-g_j(\boldsymbol{\theta}-h_i\mathbf{e}_i)}{4h_i}$ Central-difference approximations are usually more precise, but they consume more computer time than approximations that use forward-difference derivative formulas[26].

The FD= option can specify that all the derivatives are approximated using function evaluations, whilest the FDHESSIAN= option can specify that second-order derivatives are approximated using gradient evalutions. Computing derivatives by finite-difference approximations can be very important especially for deriving second-order, elucidative, inconspicuous, explicative, geoclassifiable, discontinuous canopied, LULC derivatives based only on Rapid Eye™ wavelength, transmittance, frequency dependent, scattering interactions with discontinuous non-phosynthetic, non-eco-geographic, seasoanal, canopied foliage (e.g., branches) values using the objective function (FD= option). If analytical derivatives are difficult to obtain (for example, if a *S.damnosum* s.l. turbid water, habitat, African agro-village capture point function is computed by an iterative process), a medical entomologist or experiementer may consider one of the optimization techniques that uses first-order derivatives only (TECH=QUANEW, TECH=DBLDOG, or TECH=CONGRA). The forward-difference derivative approximations are usually not as precise as those using central-difference formulas(www.sas.com).

The FDIGITS= and CDIGITS= options may be employable for specifying the number of accurate digits in the evaluation of a datset of eco-georeferenceable, elucidative, seasonally hyperproductive, trailing vegetation, discontinuously canopied, eco-epidemiological, *S.damnosum* s.l., turbid water, immature habitat, African agro-village, capture point, objective function and nonlinear constraints. These specifications may be helpful in determining an appropriate interval size *h* to be used in the finite-difference formulas for quantiating vertical temperature profiles of the discontinuous , sparsely shaded, immature capture point, trailing vegetation canopy for a hypeproductive seasaonal geospectrotemrpoally geosampled oviposition sites on a medium resolution, including the substrate.

A mathematical approach may be optimall presented which allows for the determination of a temperature profile from multiple, Rapid Eye 5m ™ sensor view angles and a priori knowledge of a moderate reosoluton imaged, hyperproductive, seasonal, *S. damnoum* s.l. iteratively, interpolative, quantized narrow tributary, eco-georeferenceable, partially discontinuous, trailing vegetative geometric structure. The technique may be evaluated on data from wider African narrow riverine tributary, eco-georeferenced, agro-village complex, ecosystem immature, capture point, hyperproductive habitats at different stages of development. The technique may be shown to be most applicable for the separation of seasonal, eco-georeferenced, geoclassifiable, LULC vegetation cover and substrate temperatures. A medical entomologist or experimenter can expect relatively accurate inferences of mean vegetation LULC, surface temperatures for intermediate and sparsely

canopied, Rapid Eye^{TM} imaged, eco-georeferenced, trailing vegation, turbid water, sparely shaded, infrequently canopied, seasonally hypeproductive, narrow tributary, agro-village complex, discontinuous, vegetation canopies, and relatively poor inferences of vegetation temperatures for sparse discontinuous canopies. The converse may be true for inferring substrate temperatures. The root-mean-square prediction accuracy of the capture point, vegetation temperatures for intermediate-dense more homogenous, seasonal, S. *damnosum* s.l., immature, hyperproductive, capture point, discontinuous, canopy gap may be 1.8 and 1.4Â°C for an exact and overdeterminate system, respectively. These findings may have significant implications for parsimoniously quantitating the LULC 5m, capture point, canopy vegetation itself or the underlying substrate. For specific narrow Afrian, riverine, agro-village complex, turbid water, immature, capture point habitat, geoclassifiable, ArcGIS-derived LULC, vegetation geometries, this technique may provide a means for robustly uniquely separating mean vegetation and substrate temperatures when a priori knowledge of the geoclassified, LULC vegetation geometry and two or more Rapid Eye ^{TM} ,sensor view angle seasonal measurements are obtained.

The FDINT= option specifies whether the finite difference intervals *h* should be computed using an algorithm of Gill, Murray, Saunders, and Wright (1983) or based only on the information of the FDIGITS= and CDIGITS= options.(www.sas.edu) For FDINT=OBJ, the interval *h* is based on the behavior of the objective function; for FDINT=CON, the interval *h* is based on the behavior of the nonlinear constraints functions; and for FDINT=ALL, the interval *h* is based on both, the behavior of the objective function and the nonlinear constraints functions. Note that the algorithm of Gill, Murray, Saunders, and Wright (1983) to compute the finite difference intervals h_j can be very expensive in the number of function calls using specialized log-transformed proxy signature LULC, uncloesced, iterative interpolative explanators (e.g., uncoalesced geo-spectrotemporally, Bayesianized Rapid Eye 5m , iterative interpolated geospatialized seasonally hyperproductive, trailing vegetation, discontinuously canopied, eco-epidemiological, eco-georeferenceable, *S.damnosum* s.l. turbid water, habitat, narrow tributray, agro-village capture point regressors), If the FDINT= option is specified, the procedure may be performed twice, the first time before the optimization process starts and the second time after the optimization terminates. If FDINT= is not specified, the step sizes h_j, $j = 1, \ldots, n$, may be optimally defined as follows: for the forward-difference covariate approximation of selected *S. damnosum* s.l. habitat, first-order derivatives employing function calls and second-order derivatives with gradient calls: $h_j = \sqrt{\eta_j}(1. + |x_j|)$, for quantiting the forward-difference approximation of second-order derivatives that use only function calls and all central-difference formulas: $h_j = \sqrt[3]{\eta_j}(1. + x_j|)$. η is defineable using the FDIGITS= option(www.sas.edu).If the number of accurate digits is specified with FDIGITS=*r*, η may be set to 10^{-r} in the forecast vulnerability *S.damnosum* s.l. paradigm. If FDIGITS= is not specified, η must then be set to the machine precision ϵ.For FDINT=OBJ and FDINT=ALL, the FDIGITS= specification may be employeable in computing the forward and central finite-difference intervals for spatially adjusting and quantitating probabilistic uncertainities optimally rendered from a seasonally hyperproductive, eco-georeferenced, moderate resolution, *S. damnosum* s.l., narrow African, riverine tributary, agro-village complex ecogeorferenceable, trailing vegation, turbid water, discontinuously canopied, immature, capture point.

If a moderate resolution, metaheusristically eluidatively optimizable, geo-spectrotemporally geospatialized, uncoalesced, wavelength, transmittance emissivity forecasting frequency paradigm, employs uncoalesced, explanative Rapid Eye 5m, wavelength, iteratively quanatiatively interpolatable, seasonally hyperproductive, trailing vegetation, discontinuously canopied, eco-georeferenced, *S.damnosum* s.l. turbid water, habitat, African, riverine, narrow tributary, agro-village, capture point, nonlinear constraints and the FD[=] option is specified, first-order formulas in SAS/GIS may be used to compute finite difference approximations of the Jacobian matrix $JC(x)$. For example, the CDIGITS= option may be employable to specify the number of accurate digits in an optimizable eco-epidmeiological datset of constrainted immature, capture point, eco-georeferenceable, time series, explanators to define the step sizes $h_j, j = 1, \ldots, n$. for optimally quantitating the geo-spectrotemporally geospatial, hyperproductive, seasonal, immature habitat log-normalized variables For FDINT=CON and FDINT=ALL, the CDIGITS= specification is used in computing the forward and central finite-difference intervals(www.sas.com). Note, if a medical entomologist or experimenter is able to specify analytic derivatives and the finite-difference approximations provided by PROC NLP are not good enough to solve non-normalities in an uncoalesced eco-georferenceable dataset of Rapid Eye 5m, imaged,*S. damnosum* s.l., forecasting, seasonal, vulnerability, Rapid Eye ™ 5m proxy geoclassiifable LULC unbiased, biosignature,immature,capture point, oviposition iterative interpolative, predictor variables, better finite-difference approximations using the GRADIENT, JACOBIAN, CRPJAC, or HESSIAN statement and the program statements may optimally render wavelength transmittance frequencies for iteratively quantiatively explanatorialy interpolating or identifying unknown, ungeosampled eco-georeferenceable, trailing vegetation, discontinuously canopied, turbid water, hyperproductive, *S. damnosum* s.l. in ,narrow African, riverine, agro-village tributaries.

In the PROC MCMC, explicative, eco-georefernceable, eco-epidemiological, trailing vegetation, discontinuously canopied, turbid water, immature, capture point, eco-epidemiological forecast, vulnerability, model the Markov chain was robustly constructed in such a way as to have the integrand as its equilibrium distribution in the optimally parameterized, residualized,Rapid Eye 5m, probabilistic, covariate, wavelength, transmittance emissivities. This specification moved the investigation towards a generalizable, autoregressive, wavelength, frequency analysis given that the entire empirical, metaheuristically robustifiable, expositively fractionalized, Rapid Eye ™ dataset of geo-predictive, optimally parameterizable, geoclassified, explanative, LULC, frequency-oriented, transmittance, wavelength estimators were treated as single-valued, with the exception of the intercept.

The intercept in the capture point, forecact, vulnerability model was treated as a distribution of the expositively autoregressed values and was non-randomly estimated, thereafter, by employing empirical Bayes techniques in PROC MCMC. Bayesian vector autoregression parameters were treated as random variables, and prior probabilities. Vector autoregressions of the optimized eco-epidmiological, eco-georeferenceable, forecast vulnerability RapidEye™ 5m, wavelength, frequency, transmittance emissivity S. *damnosum* s.l.signature model estimators were included in a flexible, statistical gridded weighted framework with an uncertainity-oriented, probabilistic, covariance matrix which included many free parameters.

The covariance matrix in SAS can enable efficient fusion of different types of proxy LULC discontinuously canopied, narrow, agro-village complex, hyperproductive, seasonal, riverine, capture point, *S. damnosum* s.l. model, signature features geoclassifiable, eco-geophysiological, biophysical, eco-georefernceable, trailing vegetation, turbid water, immature, capture point, eco-epidemiological vulnerability, forecasting, trailing vegation, uncoalesced 5m Rapid Eye $^{TM\ data}$ where the spatial and statistical properties as wellas their correlations are seasonally characterized.

Given the datset of the Rapid Eye ^{TM} geospectrotemporal,geosampled, ecogeorferenced *S. damnosum* s.l. hyperproductive , ovipoistion , explanatively geoclassifiable, moderate resolution LULC variates denoted $\{X_1\}$, ..., $\{X_n\}$, the first-order covariance matrix was defined by $V_{i,j} = \mathrm{cov}(x_i, x_j) \equiv \langle (x_i - \mu_i)(x_j - \mu_j) \rangle$, where μ_i was the mean. Higher order matrices are given by $V_{i,j}^{m,n} = \langle (x_i - \mu_i)^m (x_j - \mu_j)^n \rangle$. An individual matrix element $V_{i,j} = \mathrm{cov}(x_i, x_j)$is called the covariance of $x_i$and x_j.

The similarity between two *S. damnosum* s.l. ovipoistion LULC covariance descriptors was measured on Riemannian manifolds. For a complete Riemannian manifold, the metric $d(x, y)$ in the forecast vulnereability Rapid Eye ^{TM} probabilistic, time series, paradigm was optimally defined as the length of the shortest curve (i.e., geodesic) between x (i.e, a eco-georeferenced hypeproductive, oviposition, narrow riverine tributary, geolocation parameters), and y(seasonally parameterized immature productivity count variables) . Every complete Riemannian manifold is boundedly compact. http://mathworld.wolfram.com/RiemannianManifold.html This is part of or a consequence of the Hopf-Rinow theorem.

Let Mbe a Riemannian manifold in a trailing vegetation, turbid water, eco-georeferenced, seasaonally hypeproductive, hyperproductive oviposition , moderate resolution LULC , and let the topological metric on Mbe defined by letting the distance between two points be the infimum of the lengths of curves joining the two points. In so doing, the Hopf-Rinow theorem would assume that the following capture pint dat feature attributes are equivalent: 1. $M$is geodesically complete, (i.e., all geodesics are defined for all time). 2. $M$is geodesically complete at some point p, i.e., all geodesics through $p$are defined for all time. 3. Msatisfies the Heine-Borel property, i.e., every closed bounded set is compact. 4. $M$is metrically complete

Based on the same metric, but with a probabilistic framework, a novel tracking approach on Riemannian manifolds with a novel incremental covariance tensor learning (ICTL) may be proposed for quantitating geo-spectrotemporally geosampled, eco-georeferenceable, eco-epidemiological. *S. damnosum* s.l. seasonal, hyperproductive, capture points. To address the appearance variations, ICTL incrementally learns a low-dimensional covariance tensor representation and efficiently adapts online to appearance changes of the target with only $O(1)$ computational complexity, resulting in a real-time performance. The covariance-based, optimal representation and ICTL may then be then combined with the particle filter framework to allow better handling of background clutter as well as the temporary image occlusions in a Rapi Eye TM image of a narrow African, riverine tributray, agro-village complex. Theproposed probabilistic ICTL tracker may be applied on numerous benchmark sequences involving different types of *S. damnosum* s.l. imaging challenges including occlusionsand variations in illumination, scale, and pose of discontinuous, sparsely

shaded, seasonally geoclassifiable. moderate resolution, LULC changes as diagnostically quantitated at A eco-georferenceable, narrow tributary, riverine, agro-village complex, ecosystem geolocation. The proposed approach may demonstrate excellent real-time performance, both qualitatively and quantitatively, in comparison with several previously proposed, proxy, moderate resolution trackers for investigating these riverine foci.

Given the limited length of standard, macro eco-epidemiological eco-georeferenceable, immature habitat, seasonal, geosampled, hyperproductive, capture point, field-operationizable, fractionalized, intutive, endmember, *S.damnosum* s.l.,empirically regresseable, explanatorial, geo-spectrotemporal datasets, inferential Bayesian paradigms in PROC MCMC may provide an optimal model fit whilest resolving problems of over-parameterization in an metaheuristically optimizable dataset of iteratively interpolative, uncoalesced, discontinuoulsy canopied, trailing vegation, disocntinuously canopied, *S. damnosum* s.l., uncoalesced, RapidEye^{TM} data, feature attributes. The general idea would be to employ informative priors to shrink the unrestricted riverine, trailing vegetation, turbid water, immature habitat, forecast, vulnerability model, parameterizable, covariate coefficients, towards a parsimonious naïve benchmark, thereby reducing probabilistic, endmember uncertainties whilest simutaneously improving forecast accuracy.

The difference in the deviances between the RapidEye^{TM} 5m, eco-epidemiologically forecastable, uncoalesed, wavelength, frequency, *S. damnosum* s.l., vulnerability, forecast, transmittance, eco-georefernceable, model emissivity covariate estimators and a more complex model was probabilistically regressively quantitated in PROC MCMC which parsimoniously rendered improvement χ^2 -related, elucidatively geoclassifiable time series LULC, optimizable, observational, explanative, predictor values. Quantizable, time series, interaction terms between the optimally parameterizable, regressable explanatively, geo-spectrotemporal geosampled, elucidatively geospatialized, clinical, field and remote, diagnostic, trailing vegetation and turbid water, operationialized, non-homogenously, canopied Rapid Eye ^{TM} LULC explanators were described in the forecasts in ArcGIS. An interaction model did not improve the fit, therefore no interaction terms were included in the final model. The improvement of fit between a saturated model and the full effects model as the number of the geo-spectrotemporal, quantitatively geosampled, endmember non-optimizable LULC variables needed to be estimated, since the maximum number that could be regressed in PROC MCMC was exceeded.

To derive the improvement of fit in the eco-georefernceable, forecasted eco-epidemiological, *S. damnosum* s.l., vulnerability, forecast, Rapid Eye ^{TM} model, uncoalesced, wavelength transmittance, parameterizable, covariate estimate values the posterior mean deviance values were obtained with deviance information criterion (DIC) spatial analytical tools in PROC MCMC. The DIC is a risk modeling generalization of the Akaike information criterion (AIC) and Bayesian information criterion, (BIC), also known as the Schwarz criterion [23]. Bayesian information criterion (BIC), or Schwarz-Bayesian information criterion, is an information criterion (Wikipedia 2005). The index iteratively defined $-2L_m + mlnn$, where n was the eco-epidemiological optimal sample size, L_m was the maximized log-likelihood employing the discontinuously canopied, trailing vegetation, hyperproductive, eco-georeferenceable, explicative, immature habitat, risk model, capture point, parameterized, covariate estimators, where m was the number of unbiased, iteratively interpolative, endmember time series estimators in the model.

An autoregressive index was generated in PROC MCMC that took into account both

the statistical goodness-of-fit, and the number of time series, parameterizable, uncoalesced, RapidEye^{TM} wavelength frequency transittance emissivities representing explanatorial, 5m, optimally parameterized, metaheuristcally optimizable, *S. damnosum* s.l., LULC covariate estimators that subsequently had to be geo-spectrotemporally geospatially autoregressed in the iterative Bayesian probabilistic paradigm to achieve a particular degree of fit. This was remotely conducted by imposing a penalty for increasing the number of estimators into the algorithm. In particular, the criterion was useful in the Bayesian model selection where the posterior distributions of the models were obtained by MCMC simulations. Like AIC and BIC, the SIC is an asymptotic approximation, especially as the sample size becomes large [24]. Unfortunately, the criterion was only valid when the posterior distribution was approximately multivariate normal in the eco-epidemiological, immature habitat, narrow, riverine, agro-village complex, trailing vegation, discontinuously canopied, capture point, forecast, vulnerability, probabilistic oviposition paradigm.

In DIC the deviance in the explanative, eco-georefernceable, narrow riverine, eco-epidemiological, tributary, immature habitat, capture point, forecast, vulnerability, resdiualized model, time series, iterative output was defined as $D(\theta) = -2\log(p(y|\theta)) + C$, where y represented the pertinent geo-spectrotemporally geosampled, trailing vegetation, discontinuously canopied, sparsely shaded, metaheuristically optimizable, parameterizable, covariate, coefficient, endmember estimators, θ which were subsequently the unknown parameterized, explicative diagnostic estimators of the model when $p(y|\theta)$ was the likelihood function. *C* is a constant that cancels out in all calculations that compare different models, and therefore does not need to be known in remotely sensed, models [5]. The expectation $\bar{D} = \mathbf{E}^{\theta}[D(\theta)]$ was a measure of how well the model fit the 5m, trailing vegetation, discontinuously canopied, sparsely shaded, eco-epidemiological, uncoalesced, immature habitat, capture point, remotely sensed data; the larger this was, the worse the fit. Herewith, the DIC comprised two goodness-of-fit measures and the posterior distribution of the deviance, which was the number of effective interpretively, quantitative iteratively interpolative times series, dependent, parameterizable Rapid Eye ^{TM} wavelength, transmittance emissivity frequency-oriented, covariates for measuring complexities in the *S. damnosum* s.l., oviposition, eco-georferenceable, forecasting vulnerability model. Riverine, narrow tributary, eco-georefernceable, explanative, immature habitats with high larval count, were compared with the results of a Monte Carlo simulation, which established the probabilities and occurrences of the highly productive habitats in the interventional agro-village, complex, study site.

As similarily described in Spiegelhalter et. al. [2002] the *Simulium* model described $p_D = \bar{D} - D(\bar{\theta})$ in PROC MCMC, where $\bar{\theta}$ was the expectation of θ. Thereafter, $p_D = p_V = \frac{1}{2}\widehat{\text{var}}\,(D(\theta))$ was described as in Gelman et al. [2003]. The DIC was parsimoniously calculatable as $DIC - p_D + \bar{D}$, or equivalently as $DIC = D(\bar{\theta}) + 2p_D$. From this latter form, the connection with AIC was evident in the trailing vegetation, discontinuously canopied, sparsely shaded, immature *S. damnosum* s.l., habitat, eco-georeferenceable, vulnerability, forecast- model.

Bayesian *S. damnosum* s.l., eco-epidemiological, models can be evaluated and compared in several ways. Most simply, any model or set of models can be taken as an exhaustive set, in which case all inference is summarized by the posterior distribution[25].. The fit of the vector arthropod model to geo-spectrotemporally geosampled habitat data can

be assessed using posterior predictive checksprior predictive checks (when evaluating potential replications involving new parametervalues), or, more generally, mixed checks for hierarchical models [http://mathworld.wolfram.com].

When several candidate models are available, they can be compared and averaged using Bayesfactors (which is equivalent to embedding them in a larger discrete model) or some more practical approximate procedure or continuous model expansion[25] In other settings, however, we seek not to check *S. damnosum* s.l. ovip[osition, signature models but to compare them and explore directions for improvement. Even if all of the habitat models being considered have mismatches with the data, it can be informative to evaluate their predictive accuracy, compare them, and consider where to go next. The challenge then is to estimate predictive model accuracy, correcting for the bias inherent in evaluating a model's predictions of the geosampled immature productivity data that were used to fit it.A natural way to estimate out-of-sample prediction error is cross-validation (see Geisser andEddy, 1979, and Vehtari and Lampinen, 2002, for a Bayesian perspective), but researchers have always sought alternative measures, as cross-validation requires repeated model fits and can run into trouble with sparse data. For practical reasons alone, there remains a place for simple bias in S. damnosum s.l. predictive paradigms corrections such as AIC (Akaike, 1973), DIC (Spiegelhalter et al., 2002, van der Linde, 2005), and,more recently, WAIC (Watanabe, 2010), and all these can be viewed as approximations to different versions of cross-validation .At the present time, DIC appears to be the predictive measure of choice in Bayesian applications,in part because of its incorporation in the popular BUGS package (Spiegelhalter et al., 1994, 2003).Various difficulties have been noted with DIC (see Celeux et al., 2006, Plummer, 2008, and muchof the discussion of Spiegelhalter et al., 2002) but there has been no consensus on an alternative.

Sub-families of geospatial, explanatorial, eco-georeferenceable, inferential algorithms may be optimally employable for corresponding posterior distributions of elucidatively simulated geo-spectrotemporal, 5m iterations regarding seasonally eco-epidemiological, , hyperproductive, narrow African tributary, agro-village complex, ecosystem, *S.damnsoum* s.l. eco-georeferenceable,capture points. For example, a hybrid Markov chain Monte Carlo sampler comprising both Gibbs sampling steps and metheuristically optimizable, hierarchical, clustering-based, split/merge proposals may be useful for obtaining precise posterior inferences in a RapidEye^{TM} imaged, seasonally hyperproductive, ec-georeferenceable, capture point, *S. damnosum* s.l., eco-epidemiological, forecast-oriented, vulnerability, wavelength, frequency transmittance, emissivity model. Inference for mixture size concentrates when comparing the integrated likelihoods from a dataset of explanatively fractionalized, uncoalesced, RapidEye^{TM}, 5m, geo-spectrotemporal, geospatially empirically probabilistically autoregressable, Bayesianized dataset of explicative, seasonally hyperproductive, illuminative, eco-georeferenceable, eco-epidemiological, uncoalesced, seasonal, capture point, trailing vegetation, discontinuously canopied, sparsely shaded, riverine, agro-village, complex, turbid water, narrow tributary, immature habitats. The prior structures in the estimation matrix may help filter uncertainty-oriented, optimally unbiased, endmember, wavelength, frequency, transmittance, orthogonal, spatial filter eigenvalues from decomposed, proxy RapidEye^{TM}, 5m, iteratively interpolative LULC, signatures. These structures may also provide meaningful comparions of factors within flexible Bayesian sub-families for cartographically optimizing and robustly illustrating unmixed, field-operationizable, 5m, iteratively interpolative, wavelength, transmittance, metaheursitically, for parameterizing, fractionalized, frequency, covariate, coefficient

emissivities representing geo-spectrotemporally geosampled, immature, *S. damnosum* s.l., hyperproductive, trailing vegetation, turbid water, narrow African, riverine tributary, agro-village complex ecosystem oviposition seasoanal geolocations and their, ecohydrologic 3-D, probabilistic, uncoalesced, frequency-oriented, explanative predictors (e.g., Levels of turbidity), which may then be geospatially, ecohydrologically associated with seasonal, immature productivity count distribution data. Assessing the number of convergence diagnostics in the seasonal habitat, eco-georefernceable, capture point, vulnerabilit , forecast-oriented, eco-epidemiological datasets may reveal elucidative endmember, fractionalized eigenvectors which may aid in assessing the convergence of Markov chains. In so doing the simulation mey be employed to identify unknown, un-geosampled, hyperproductive, *S. damnosum* s.l. trailing vegetation, turbid water, discontinuously canopied, eco-georeferenceable, narrow African riverine, agro-village, seasoanl habitats.

PROC MCMC optimally rendered, hierarchically generalizable, trailing vegetation, discontinuously canopied, sparsely shaded, hyperproductive, capture point, *S. damnsoum* s.l. habitat explanators that accounted for any non-normality (e.g., skewed error distributions with fat tails) in the forecasted heterogeneously canopied, trailing vegetation, turbid water, riverine habitats. A Bayesian regression model was considered under a skewed, heavy tailed, error distribution. A general class of skewed elliptical distributions was developed in PROC MCMC which included heavy-tailed distributions and a skewness parameter. Dependent and independent skew elliptical error, probabilistis distributions were considered for the post regression, uncertainty-oriented, explicatively parameterizable, probabilistic covariates. The results provided a unified parametric approach to optimally diagnosing non-normal regression tendencies of immature, eco-georefernceable, eco-epidemiological,capture point, trailing vegetaion, discontinuously canopied, sparsely shaded, RapidEye^{TM} 5m, spatial resolution, non-flexible, uncertainty, probabilistic estimators. The proposed methodology may be exemplified in PROC MCMC by a regression framework employing a uncoalesced, iterartively interpolative dataset of empirically regressable, metaheursitically explanatively robustifiable, geo-predictive, endogenous explanators and a skewed Student-t error distribution. In probability and statistics, the skewed generalized “t” distribution is a family of continuous probability distributions [24].

The quantification of propagational erroroneous RapidEye^{TM} 5m, *S. damnosum* s.l.,immature habitat, predictor variables may alter inferential latent effects processes as rendered from probabilistic regression trees which may allow for a generalizable procedure to introduce anti-skewness techniques into symmetric distributions in PROC MCMC. According to Jacob et al. [22]skewness and kurtosis are descriptive numerical methods in explanative, eco-epidemiological, eco-georeferenceable, discontinuously canopied, trailing vegetation, sparsely shaded, seasonally hyperproductive, 5m, imaged, capture point, *S. damnosum* s.l.,immature,capture point, hyperproductive, narrow tributray, African, agroecosystem habitats In probability theory and statistics, skewness is a measure of the asymmetry of the probability distribution of a real-valued random variable about its mean[24].In probability theory and statistics, kurtosis (is a measure of the "tailedness" of the probability distribution of a real-valued random variable. In a similar way to the concept of skewness, kurtosis is a descriptor of the shape of a probability distribution and, just as for skewness, there are different ways of quantifying it for a theoretical distribution and corresponding ways of estimating it from a sample from a population in an eco-georeferenceable, eco-georeferenceable, hyperproductive, *S. damsnoum* s.l., trailing vegetation, sparsely shaded, discontinuously canopied,*S. damnosum* s.l. habitat eco-

epidemiological model. Depending on the particular measure of kurtosis that is used, there are various interpretations of kurtosis, and of how particular measures should be interpreted; these are primarily tail weight, peakedness (width of peak), and lack of shoulders (distribution primarily peak and tails, not in between[24].

Quantile plot procedures in a QQ plot statement in the UNIVARIATE PROCEDURE may allow for a great deal of flexibility for metaheursitically optimally remotely capturing distributional shape, tail behavior in a forecast vulnerability RapidEye™ *S. damnosum* s.l.,immature habitat, eco-epidemiological, capture point, eco-georefernceable, 5m, wavelength, frequency, transmittance, emissivity, vulnerability, forecast model , such that the quantitated output would not be severely affected. Applying this skewness procedure to a Student *t* distribution may allow for generation of a "skewed Student" distribution, which may display both flexible tails and possible skewness in the emissivity model residuals controlled by a separate scalar parameter in PROC MCMC.

Characterizing existence of the posterior distributiuons in an eco-epidemiological, RapidEye™ 5m, *S. damnosum* s.l.,immature habitat,capture point, forecast vulnerability model and its moments employing standard existence of the posterior distribution and its moments, employing standardizable improper priors can allow for inference on tail parameters in the models, which can reduce probabilistic, propagagtional error in residuals, targeting interpretively iteratively explanative, interpolative, unknown,ungeosampled, hyperproductive, narrow tributary, African agro-village complex, trailing vegetaion, turbid water, discontinuous, sprasely shaded, eco-georeferenceable, iteratively interpolative, immature, seasonal, *S. damnosum* s.l. habitats. For posterior inference with these models, a numerical procedure employing Gibbs sampling may be also suggested. In statistics and in statistical physics, Gibbs sampling or a Gibbs sampler is a MCMC algorithm for obtaining a sequence of observations which are approximated from a specified multivariate probability distribution (i.e. from the joint probability distribution of two or more random variables)[24].

Bayesian Canopy Height Models (CHM) derived from RapidEye ™ geo-spectrotemporally geospatially uncoalesced, iteratively interpolative, trailing vegetation, turbid water, discontinuously canopied, 5m, wavelength, frequency transmittance, emissivities may delineate seasonal gap fractions for accuracy assessments in hyperproductive, *S. damnosum* s.l., eco-epidemiological, capture point habitats in ArcGIS. A Bayesian approach to object recognition incorporates a probabilistic model of the active sensing process and places a prior probability model on object configurations [24]. Prior models for object configurations take the form of Markov marked point processes, where pair-wise object interactions depend upon object attributes.

Through eco-cartographic delineation, information regarding immature habitat, discontinuous gap geometry, immature productivity may be seasonally investigated and robustly quantitated. Explanative, field-operationizable, eco-epidemiological, vulnerability mapping, optimizable methods in ArcGIS based on raster layers produced from a RapidEye™ leaf-off and leaf-on dataset may reveal thresholding, 5m, per-mixel and per-habitat, object supervised, elucidative classifications with broadly geo-classifiable, explicatively, orthogonally decomposable, illuminatively, fractionalized, LULC reflectance. In addition to the RapidEye™ CHM, other metrics related to the canopy porosity may also be tested in ArcGIS. Gap detection in RapidEye™ 5m, agro-village, narrow tributary, eco-georeferenceable, African riverine scenes may be tested for global accuracy for discontinuous canopy fractions to elucidatively geovisualize and forecast seasonal, immature productivity,

count variables. The geometric accuracy of the eco-epidemiological, forecasting, eco-georeferenceable, vulnerability, model may be analyzed employing eco-cartographic illustrations of the discontinuous canopy gap area employing gap shape-complexity indices within Thessian polygons in ArcGIS.for conducting quantitative assessments of the reference gaps In so doing, the assessment may identify a technique in ArcGIS which precisely delineates optimal, seasonal, discontinuous canopy gap size that can quantitate seasonally hyperproductive immature counts.

The performance of a Bayesianized CHM-based thresholding in SAS/GIS may exceed that of other software methods, especially when thresholding trailing vegetation, sparsely shaded, geo-spectrotemporally, geospatially uncoalesced RapidEye™ imaged, geo-spectrotemporal, geospatialized, *S. damnosum* s.l.,immature habitat discontinuous, canopy gap, porosity rasters whilest simutaneoulsy performing per-mixel, supervised classifications employing uncoalesced 5m, wavelength, frequency emittance. SAS/GIS can access raw data files and data in external databases such as DB2, SQL/DS, Rdb/ VMS, OS/2 Database Manager, Lotus 1–2–3, dBASE, and SYSTEM 2000 while linearly programming data for efficient, multivariate, eco-epidemiological, *S. damnosum* s.l., seasonal, explanative, hyperproductive, eco-georeferenceable, capture point forecasting modeling, Characteristics of discontinuous canopy gaps (e.g., size, shape, distribution, orientation) in an African narrow riverine,tributary, eco-georeferenceable, hyperproductive, *S. damnosum* s.l., eco-epidemiological agro-village complex, capture point, immature habitat discontinuously fractionalized, RapidEye™ , 5m , discontinuous canopy may become of central importance in understanding regeneration, dynamics, and species diversification and distribution of immature *Simulium*. Koukoulas and Blackburn [168] highlighted the importance of gaps with different geospatial properties for seed establishment and determining the future forest structure. Lindenmayer et al. [169] proposed horizontal heterogeneity due to presence and distribution of discontinuous gaps as a mechanism for conserving forest biodiversity by maintenance of stand structural complexity. Gap shape, orientation and size variation affect the gap dynamics, mainly through the variation in the light environment and moisture levels [23]. In his study, Getzin et al. [170] used gap shape metrics derived from Unmanned Aerial Vehicles (UAV) images to assess the plant diversity in forests. Thus, critical endmember eigenvector, discontinuous, canopy, gap studies may be considered in SAS/GIS for improving geometric accuracy of expositively forecasted, unknown, RapidEye™ 5m imaged, *S. damnosum* s.l.,immature habitats.

The abundance and distribution of eco-georeferenceable, seasonally hyperproductive, discontinuously canopied, sparsely shaded, turbid water, eco-epidemiological, capture point, *S. damnosum* s.l. parameterizable, statistically significant, explanative, capture point habitat, variables rendered from geospatially autoregressive, estimation matrices in SAS/GIS could suggest that the plant canopy serves as cover for adult black flies at the interventional, narrow, riverine tributary, agro-village study sites. At the study sites, plants geo-spectrotemporally geospatially associated with aquatic stages of *S. damnosum* s.l. larvae were found in submerged, discontinuously canopied twigs trapped in the water with some parts exposed as offshoots in the stream, which were followed by riverine pathways of coarse rock crevices hit by water tides. Decaying leaf matter had the lowest count of larval attachment with plants associated with immature *S. damnosum s*.l. which may have been attributed to loss in nutrients in decaying leaf matter, rendering them less attractive for *Simulium* attachment.

Canopy plants associated with larval breeding attachments at the study site agro-village complexes were *Oryza barthii, Pterocarpus santalinoides, Andropogon gayanus* and

Lawsonia inermis. At the early stage of the study, larvae were collected along the trailing roots of *P. santalinoides* in the heavily shaded parts of the agro-village, complex, narrow river tributary. Subsequently, larvae were collected on the leaves and hollow openings in the plant *Oryza bartii* which grew in the non-shaded areas of the *S. damnosum* s.l. capture point, habitat due to the habitat's attraction to various discontinuously canopied plant species which may be a useful factor in future research for implementation of seasonal control of hyperproductive, black-fly foci in narrow riverine African tributaries.

Because Bayesian statistical analysis is involved, prior distributions had to be posited for each varying quantity (e.g., the explanatorial, eco-georefernceable, trailing vegetation, turbid water,response variable, each discontinuously canopied, RapidEye^{TM} 5m, variable coefficient value, the spatial autoregressive parameter, the error variance, and the random error term in the geospatial, endmember, *S. damnosum* s.l , seasonally hyperproductive, eco-epidemiological, capture point, forecast, vulnerability model. "Bayesianized averaging" over the uncertainty paramterized covariate, estimator *S. damnosum* s.l. habitat eco-epidemiological, eco-georefernced dataset is a desirable property of Bayesian frameworks for unbiasedly, forecast modeling [24]. The summarization of the simulated posterior distributions correctly accounted for the quantitative error in estimation algorithm encompassing all the *S. damnosum* s.l. habitat parameterizable, covariate estimators at the intervention agro-village, study sites, where each simulated posterior distribution represented an "average" over the joint posterior distributions of all the other covariates in the operationizable, geo-predictively geoclassifiable, RapidEye^{TM} LULC explanatorial model. The rendered eco-epidemiological, metaheuristically optimizable, eco-georeferenceable, forecasts revealed that any probabilistic time series, residual uncertainties in the quantitative estimates were fully accounted for in both the mean and the mode of the simulated posteriors, and in the dispersion of the posterior.

Depending greatly on the abundance of poorly estimated 5m, emissvity frequencies, flat posteriors rendered in PROC MCMC may be a direct indication that the available precision on the reflectance estimator is very poor. Roughly speaking, a prior distribution is noninformative if the prior is "flat" relative to the likelihood function [24]. Thus, a *S. damnosum* s.l. habitat parameterizable, covariate estimator prior $\pi(\theta)$ would noninformative if it has minimal impact on the posterior distribution of θ. However, it may be unrealistic to expect that noninformative priors represent a discontinuously canopied, trailing vegetation, sparsely shaded narrow tributary, agro-village complex, geo-spectrotemporaly geosampled, parameter of interest in a seasonal, narrow, riverine tributary ago-village complex *Similium* hypeporductive, foci.

In some cases, noninformative priors can lead to improper posteriors (non-integrable posterior density)[24]. In addition, these noninformative habitat priors may not be invariant under transformation; that is, the quantiated prior might be noninformative in one parameterization but not necessarily noninformative if a transformation is applied. A noninformative prior I may render a prior distribution that assigns equal likelihood on all possible values of the geo-spectrotemporally geospatialized parameter. Intuitively this makes sense, and in some cases, such as a fractionalized endmember, Rapid Eye ^{TM} 5m , flat prior on the regression parameter maye be noninformative. However, this is not necessarily true in all cases. For example, suppose there is a binomial experiment with n Bernoulli trials where y1s are observed in a narrow, riverine tributary, hyperproductive, discontinuoulsy canopied, capture point, *S. damnosum* s.l. habitat.A uniform prior on p, $\pi(p) \propto 1$ might appear to be noninformative(www.sas.edu). However, using the uniform prior is actually equivalent to

adding two. habitat observations to the data, one 1and one 0. With small $n$and y, the added eco-georeferenceable, narrow riverine,agro-village, tributary observations can be very influential to the parameter estimate of p. To quantiate the likelihood for a *S. damnosum* s.l.model, an ecologist, entomologist or other researcher may employ : $p^y(1-p)^{n-y}$The MLE of $p$is y/n. The uniform prior can then be written as a beta distribution with both the shape (α) and scale (β) parameters being 1: $\pi(p) \propto p^{\alpha-1}(1-p)^{\beta-1}$The posterior distribution of p in the habitat model may be proportional to the following: $p^{\alpha+y-1}(1-p)^{\beta+n-y-1}$ which is beta($\alpha+y, \beta+n-y$). Therefore, the posterior mean is the model would be $\frac{\alpha+y}{\alpha+\beta+n} = \frac{1+y}{2+n}$ which may be quite different from the MLE if both $n$and $y$are small.

The decomposition, spatial filter, endmember analyses employed an autoregressive weight matrices in SAS/GIS and a stepwise negative binomial regression routine to select eigenvectors as regressors. This eigenvector spatial filtering approach added a minimally sufficient set of eigenvectors as proxy-variables to a set of ecophysiological, biophysical, agro-village riverine tributary, trailing vegtaion, discontinuously canopied, *S. damnosum* s.l. linearizable predictors representing the sub-mixel, *S. damnosum* s.l., eco-epidemiological,immature, habitat data. The regression residuals represented spatially independent variable, endogenous components. The eco-georeferenceable, eigenvectors yielded distinct explanative, immature, hyperproductive, capture point, habitat map patterns for description of the latent autocorrelation in the geospatialized, narrow tributary, riverine, uncoalesced habitat data. There was positive autocorrelation in the residual spatial pattern: similar log-larval/pupal counts of *Simulium* habitats aggregated in eco-geographic space based on the geosampled parameterizable covariate Distance from the trailing vegetation, eco-epidemiological discontinuously canopied, sparsely shaded, eco-georeferenceable, capture point.

Positive autocorrelation pattern in 5m, sub-mixel *S. damnosum* s.l. eco-epidemiological, habitat data, discontinuously canopied, habitat geo-spectrotemrpoal, geospatial, fractionalized Rapidf Eye Tm wavelength, transmittance, non-frequency-orinted, emissivitiy covariates may have been driven by multiple exogenous causes be (e.g. autocorrelated environment disturbance) and/or endogenous (conspecific attraction, dispersal limitations, demography). For example, positive autocorrelation patterns of immature trailing vegetation, discontinuously canopied, sparsely shaded, eco-georeferenceable, agro-village, eco-epidemiological, capture point, *Simulium,* narrow tributary, riverine, seasonal, capture point,, eco-georefreenceable, habitats may be influenced by environmental landscape (e.g., seasonal meandering during flooding). Discontinuously canopied, sparsely shaded, trailing vegetation, immature density and their seasonal proximity to eco-epidemiological capture points or quality of man-made eco-georeferenceable, barriers close to hyperproductive *Similium* foci or inter-anthropogenic variation in narrow riverine tributary agriculture may shift black-fly habitat preferences, based on other environmental cues. Positive autocorrelation in the regressed immature data may also have been a due to common local weather patterns at the eco-epidemiological, study sites that may have caused the *Simulium* habitats to spatially cluster and partially govern larval/pupal population dynamics. Climatic factors, particularly temperature, precipitation and relative humidity, predict to a large degree the natural distribution of seasonal, vector arthropod, aquatic immature habitats, as well as ecological factors, such as predation, availability of blood meal hosts, and quality of larval habitats [23].

A Red Edge, Rapid Eye 5m, biosignature was generated in ArcGIS. The red-NIR transition zone in the Red Edge NDVI marked the boundary between the red visible region in

the capture point, narrow, riverine tributary, *S. damnosum* s.l. habitat, discontinuous canopy scattering, which may have been due primarily to the 5m, RapidEye^{TM}-imaged, within-canopy, leaf structure reflectance. Most NIR canopy radiation is scattered by leaf mesophyll resulting in high reflectance and transmittance values (approximately 40-50% each) [47]. Leaf chlorosis can cause an increase in visible reflectance and transmission [23].

The NIR plateau (700 nm – 1,100 nm) is a region where explanative, discontinuously canopied biochemical absorptions are limited to the compounds typically found in dry leaves, primarily cellulose, lignin and other structural carbohydrates. However, in the unmixing, forecasting, 5m, geoclassifiable eigenvector, endmember algorithms, the, geoclassifiable, discontinuously canopied, *S. damnosum* s.l. habitat, LULC, foliar, wavelength, frequency, transmittance emissivites in the NIR region was affected by multiple scattering of canopy photons within the RapidEye^{TM}-imaged, habitat leaves may have been ecohydrologically related to the internal structure, fraction of air spaces, and air-water interfaces that refract light within these leaves. Multiple scattering of radiation between air and cell wall in canopy leaf tissue leads to high reflectance values in NIR [172].

We generated a RapidEye^{TM}, Red Edge NDVI, in ArcGIS employing the visible spectrum and the emittance data of the immature habitat, geo-spatiotemporally, geo-spectrotemporally autoregressively, auto-probabilistically quantitated at the Gongcoyo agro-village complex. The NDVI is preferred for global vegetation monitoring as it helps compensate for changing illumination conditions, surface slope, aspect, and other extraneous factors [23]. The differential reflection in the RapidEye ^{TM} 5m, red and NIR bands enabled the monitoring of discontinuous canopy density and intensity of trailing, canopy vegetation, turbid water, geoclassified LULC, unmixed, geospectral reflectivity based on solar radiation. Green leaves commonly reveal better reflection in moderate resolution, NIR, wavelength range than in visible wavelength ranges [23]. It was noted that when habitat canopy leaves were stressed, diseased, or dead, they revealed yellow and reflect significantly less in the NIR range.

We employed the Add Function button on the *Image Analysis* window to apply an NDVI in ArcGIS. By opening the Image Analysis Options dialog box, and clicking the NDVI tab, we were able to check the red and IR, Rapid Eye ^{TM} wavelength transmittance. Also on this tab we employed the option Use Wavelength, which identified the correct RapidEye^{TM} 5m, bands for qualitatively quantitating the wavelength, visible and NIR, emittance frequencies in the dataset. The NDVI map eco-cartographically illustrated a single-band, 5m, trailing vegetation, *S. damnsoum* s.l., eco-epidemiological, immature habitat, explanative, metaheuristic dataset that mainly represented the sparsely shaded, discontinuous canopy, geoclassified, LULC greenery. The negative values represented the turbid riverine water, 5m, decomposed, mixel values. Very low positive values (0.1 and below) of Red Edge NDVI corresponded to barren areas of the capture point canopied rock. Moderate values (0.2 to 0.3) represented geoclassified, shrub and grassland LULCs, and high values (0.6 to 0.8) indicated dense canopy.

Based on the discontinuous canopied, Red Edge NDVI curve, the 5m leaf reflectance was greatest in the spectral bands centered between 1940 nm and 2500 nm, with indirect or secondary effects between 400 nm and 700 nm. The visible band (400-700 nm) light absorption by leaf pigments descriptively dominated the habitat leaf reflectance spectrum, which was parsimoniously tabulated at lower wavelength reflectances (15% maximum). The primary and secondary absorptions of water in the 5m, LULC canopy leaf reflectance were

greatest centered at around 700nm, with important secondary absorptions at 980 nm, and 1,210 nm.

Different studies have revealed wavelengths in which leaf reflectance is influenced by water content [174, 175, 176]. Hence, employing spectroradiometry and RapidEye™ technology in ArcGIS can reduce time and cost when constructing forecasting vulnerability, endemic maps of seasonally hyperproductive, trailing vegetation, turbid water, *S. damnosum* s.l. narrow riverine, tributary. eco-epidemiological, capture point, eco-georefernceable, explanative, immature habitats. This technology may increase the accuracy of parameterizable habitat, leaf reflectance, decomposed covariate estimator measurements to some extent in ArcGIS.

Studies have estimated EWT by employing either broad waveband ratios [177] or narrow wavebands in the NIR and short wave infrared (SWIR) in simple ratios or normalized difference forms [e.g., 178]. To estimate leaf EWT, a 5m RapidEye™, stepwise regression, leaf reflectance, NDVI, Red Edge, model inversion can be constructed in ArcGIS. Evapotranspiration is important in the humid tropics for its role in the ecohydrological cycle: higher EWT means decreased drainage from soils, which means less nutrient leaching and lower yields of water from watersheds [179]. The effect of drastic, discontinuously canopied, trailing vegetation, LULC transitions (e.g., conversion of forestland trailing vegetation to discontinuous canopied, narrow riverine, turbid water ecosystems), on seasonal EWT tabulations in African agro-village, tributary complexes is not well understood. The evapotranspiration equation may be included in ArcGIS to seasonally quantitate canopy resistance in an eco-georeferenceable, exlnataive, capture point larval habitat which may elucidate unmixed, bio-physiological, wavelength, frequency, 5m, transmittance of non-homogenously canopied, emissivity processes associated to seasonally hyperproductive, immature productivity, explanative, count values. Less understood seasonal effects on EWT calculations might result from differential, seasonal, turbid water, pre-flooded, riverine discharges, although such information does exist for common forestry species in the tropics. Tropical, discontinuous, infrequently, canopied tree species vary greatly in characteristics that can affect EWT, such as the phenology, size, shape, and stomatal conductance of leaves [23].

Zhang et al. [180] reported five moderate resolution absorption bands for remotely qualitatively quantitating water in the 400–2,500 nm spectral region: 970; 1,200; 1,450; 1,930 and 2,500 nm. Riaño et al. [181] specified that the 1,400–2,500 nm range provides the highest correlation with EWT in moderate resolution data. Danson et al. [182] used six water moderate resolution absorption bands centered on 975; 1,175; 1,450; 1,650; 1,950 and 2,250 nm for leaf water content estimation. Fortunately, we were able to obtain elucidative, discontinuously canopied, narrow, riverine,agro-village complex, fractionalized estimators of EWT for most of the canopy leaf species in the eco-georefernceable, eco-epidemiological, capture point habitat employing the Red Edge NDVI. Since the use of turbid, riverine, water vapor, absorption bands was avoided in the immature, capture point, habitat NDVI, it may be possible to employ these absorption bands along with a RapidEye™ EWT, iteratively interpolative biosignature when it is believed that the seasonal atmospheric water vapor content can no longer affect hyperproductive, trailing vegetation, discontinuously canopied, capture point, turbid water, *S. damnosum* s.l. habitat, NDVI, reflectance model, eco-epidemiological forecasts.

Linear correlation analyses in ArcGIS revealed that there existed a statistically significant correlation between non-homogenously, discontinuous canopied, narrow, riverine, tributary, fractionalized, agro-village complex, water content geolocations in a dataset of multivariate RapidEye ^{TM,} 5m, visible and NIR wavelength, transmittance, wavelength data emitted from the capture point, habitat, NDVI, leaf reflectance. This data was geo-spectrotemporally quantitated, at 1,450, 1,650 and 2,250 nm. The variation in the RapidEye^{TM}, 5m, imaged leaf structure caused the magnitude of the leaf reflectance to change with the leaf water content. However, the relative "depths" of the water absorption features in the uncoalesced, Red Edge, reflectance, endmember,derivative, forecast LULC,5m spectra seemed not be affected by leaf structure. As the depth of absorption feature increased, the slopes on the leaf edge of the discontinuously canopied, time series, LULC features also increased. As a result, the first NDVI derivatives of the RapidEye^{TM}, 5m, reflectance endmember, forecast spectra of the visible and NIR wavelengths corresponded to these slopes in an ArcGIS scatterplot, and were easily associated to optimizable, remotely depressed geolocations of the eco-georeferenced, *Simulium* habitat, foliage examined.

A review of ArcGIS literature reveals that moderate resolution water absorption bands have been employed for canopy leaf water content quality assessment and quantification of time series photosynthetic and non-phosynthetic discontinuous canopied variables. However, there are still few spectral regions that have not received sufficient attention by ecologists, entomologists or other researchers. Further, most of the studies conducted have focused on one particular canopy plant species and their results cannot be equally applied to any seasonal vector arthropod species. Therefore, it is important to define a robust, 5m, RapidEye^{TM} vegetation index that can identify a great number of seasonally explanative, hyperproductive, discontinuous canopied, narrow, riverine, agro-village complex, *S. damnosum* s.l. habitat, trailing vegetation, plant species which operates in a wider range of the electromagnetic spectrum.

Various indices and moderate resolution wavelengths in different studies have claimed to have the highest correlations with the leaf water content. As Danson and Bowyer [183] argue, the moderate resolution wavelength which deduces leaf water content may depend on the magnitude and range of leaf water content in the leaf sample under study. Thus, if selected RapidEye^{TM} visible and NIR wavelengths are employed for remotely quantitating leaf water content in an eco-epidemiological, capture point, hyperproductive, *S. damnosusm* s.l., trailing vegetation, discontinuously canopied, narrow, riverine, tributary, agro-village complex, immature habitat, appropriate determination of a particular geosampled vegetation leaf species may need to be pre-identified.

By assuming that the Red Edge NDVI described the geoclassified, steeply sloped, *S. damnosum* s.l., eco-epidemiological, hyperproductive, turbid water, capture point, riverine habitat in ArcGIS in the region of the dense, sparsely shaded, trailing vegetation-related, LULC, 5m, reflectance curve between 690 nm and 710 nm, we were able to identify optimal Chl absorption discontinuously canopied, immature habitat geolocations. Capturing the transition from Chl absorption and RapidEye^{TM} NIR leaf scattering required regression of the discontinuously canopied geolocations based on the low/high, Chl, concentration estimates and the geo-classified LULCs in the 5m imaged, immature habitat, forecasting mathematical model.

The quantitated 5m, Red Edge, NDVI, wavelength, transmittance emittance values from the, hyperproductive, *S. damnosum* s.l. habitat, LULC data revealed strongly absorbed

radiation in the red and blue wavelengths and also in reflected green wavelength, which acted as a diffuse reflector of the RapidEye™ NIR wavelengths. Reflected red irradiance (IRED) was strongly diminished, likely through Chl absorption, with peak absorption occurring at 693nm. Chlorophyll in the discontinuous canopy, narrow tributary, agro-village, geoclassified LULC geolocations absorbed most of the light in the visible part of the spectrum, but this may have become almost transparent at wavelengths greater than 700 nm. Both red and NIR irradiance were strongly influenced by the discontinuous, habitat canopy, LULC, plant cover. Red irradiance decreased with plant LULC cover, as NIR irradiance (INIR) increased. The Chl irradiance within the RapidEye™ 5m, waveband spectrum was an integral part of the overall, sparsely shaded, canopied, LULC, irradiance spectrum with respect to the wavelength frequency 5m, uncoalesced emissivities associated with the geosampled habitat, Red Edge, NDVI.

Red Edge NDVI red and NIR, reflectance variables were scattered in the lower, geoclassified LULC, canopy cover reflecting less resolution-intense geolocations. In the explanative, hyperproductive Rapid Eye™, *S. damnosum* s.l., NDVI, forecast vulnerability model, discontinuously canopied, narrow, riverine, tributary, agro-village study site, LULC changes were reflected in the green peak reflectance (~550 nm) and along the Red Edge (590 to 650 nm). Chlorophyll content may decline more rapidly than carotenoid content towards the lower part of an *S. damnosum* s.l. habitat, discontinuous LULC, canopy cover. Lower, immature habitat, canopied, LULC cover may be where the canopy plants in hyperproductive, *Similium* habitats experience more seasonal stress due to leaf senescence, especially during flooding sample frames. Chlorophyll was the most abundant plant pigment in the canopy geosampled at all the, study sites with the most fractionalized endmember,orthogonalized eigenvectors captured in uncoalesced, red and blue RapidEye ™ wavelength, transmittance frequencies. Accessory pigments such as carotenes and xanthophylls harvested some green frequencies.

Dry or senescent carbon components in the Red Edge NDVI provided an estimate of the amount of carbon in dry states of lignin and cellulose in the eco-epidemiological, capture point, immature habitat. Lignin is a carbon-based molecule utilized by plants for structural components. Cellulose is primarily used in the construction of cell walls in plant tissues [172]. Dry carbon molecules are present in large amounts in woody materials and senescent, dead, or dormant, discontinuously canopied, narrow, riverine tributary, agro-village complex, geoclassifiable, explicative, LULC vegetation. RapidEye™ 5m, NDVI may be employable for seasonal analysis and detection of eco-epidemiological, eco-georeferenceable, capture point, *S. damnosum* s.l. habitats. Reflectance measurements in the RapidEye™ IR range may take advantage of known discontinuous, canopy absorption features of cellulose and lignin to aid in detection of seasonally hyperproductive habitats.

The xanthophyll cycle was clearly implicated in the dissipation of absorbed 5m, RapidEye™ orthogonally defined photon flux density (PFD) in the uncoalesced, photosynthetically active RapidEye™ wavebands in excess of the amount that may have be used in canopy photosynthesis. Conditions of excess PFD in a eco-georefernceable, explicatively seasonal, hyperproductive, trailing vegetation, discontinuously canopied, turbid water, *S. damnosum* s.l. discontinuously canopied, narrow, riverine, tributary, agro-village complex, immature habitat can occur under a variety of stress conditions when there is an imbalance between absorbed PFD and the rate of photosynthetic dark reactions. In

response to excess PFD and the associated increase of the chloroplast thylakoid pH gradient, the xanthophyll pigment violaxanthin (V) is reversibly de-epoxidized to zeaxanthin (Z) via antheraxanthin (A) [184, 185]. The quantity of zeaxanthin is closely correlated with the rate of dissipation of excess PFD as heat [186].

Leaf water affects plant reflectance in the NIR and SWIR regions of the spectrum [23]. Riverine, turbid water, trailing vegetation, discontinuous canopy, *S. damnosum* s.l., immature, habitat reflectance had maximum absorptions centered near 1400 and 1900 nm in the moderate resolution data. However, these spectral regions usually cannot be observed from airborne or space-based sensors, and may have been due to atmospheric water absorption, preventing their practical use in the creation of the robust Red Edge, endmember, fractionalized, iteratively interpolative, NDVI signature for remotely targeting unknown, un-geosampled, hyperproductive habitats at the agro-village, narrow riverine, tributary, study sites. In the ecohydrological, habitat risk model, the riverine water surrounding Gonycogo and Ayago villages was 970 nm and 1190 nm, respectively.

For the elucidatievly unmixed, fractionalized, 5m, immature habitat, RapidEye™ wavelength endmember, emissivity, transmittance, eco-epidemiological, uncoalesced, leaf senescence, discontinuously canopied, narrow, riverine, tributary, agro-village complex, geoclassified, LULC data, the maximum difference in RapidEye™ reflectance was within the 400–850 nm wavelength range for control and stressed states, which occurred as reflectance increased to 700 nm. A variety of environmental stressors, including dehydration, flooding, and competition, have been imposed on *Simulium* species [93]. These environmental, response stressors may have simulated constant and varying levels of remotely quantifiable Chl concentrations in a RapidEye™, 5m, habitat scene. Eco-georferenceable, immature habitat, canopy leaf radiance discontinuously canopied, narrow, riverine, tributary, agro-village complex, geoclassifiable LULC may be quantitated thereafter employing the variability measures in the seasonal, leaf, Chl concentrations or in the senescent leaves. The optical response to stress near 700 nm, as well as the corresponding LULC changes in the elucidatively fractionalized, optimally parameterizable, geo-spectrotemporally, geospatially covariate coefficient, 5m, wavelength, frequency emissivities, occured in the eco-epidemiological, RapidEye ™ model, residual forecasts encompassing the green–yellow spectrum. This may have been explained by the general tendency of seasonal stress to reduce leaf Chl concentration in the immature habitat canopies and their discontinuously canopied, narrow, riverine, tributary, agro-village complex, geoclassified LULC, eco-georferenceable, unmixed data, 5m, feature attributes (e.g., floating vegetation cover).

Leaf Chl concentrations may elaborate on geoclassiifable, LULC characteristics affected by radiation reflected, transmitted, or absorbed by seasoanl, hyperproductive, *S. damnosum* s.l. habitat, discontinuous, canopy leaves and provide a more thorough understanding of ecophysiological explanative responses to growth conditions and seasonal, canopy plant, adaptation processes in African, narrow riverine, agro-ecosystem, village complex tributaries. Largely as a result of interest in cost-effectiveness, moderate resolution, remote sensing, bio-optical, leaf reflectance has been studied more extensively than transmittance or absorbance responses to stress [187, 188].

Customizable, bio-optical algorithms can be developed as practical tools in ArcGIS for remotely, optimally monitoring the plant health of seasonally hyperproductive, eco-georferenceable, discontinuously canopied, narrow, riverine, tributary, agro-village complex,geoclassified LULC, *S. damnosum* s.l. habitatd by providing unique non-

homogenous, explantaively decomposable, 5m, Red Edge, NDVI data that can be related to specific plant stresses. Signatures from thermal and fluorescence imaging have been used successfully to track pathogen invasion before visual symptoms are observed [23]. Another approach for non-invasive canopy plant health monitoring in RapidEye™, 5m imaged, habitat, Red Edge NDVI can involve elucidating the manner with which light interacts with the plant leaf. This can help identify, LULC changes in habitat characteristics in response to specific,discontinuously canopied, quantifiable stresses in ArcGIS.

Seasonally quantitating canopy perturbations in an discontinuously canopied, narrow, riverine, tributary, agro-village complex,geoclassified hyperproductive, capture point eco-georeferenceable, eco-epidemioloigical,, *S. damnosum* s.l. habitat requires a firm understanding of the biochemical and anatomical features governing leaf reflectance, transmission and Chl absorption. Many studies have opened up possibilities that subtle changes in leaf reflectance, derivative emoderateresolution, endmember spectra can be analyzed in a plethora of ways for discriminating nutrient and water stress. However, these techniques have met with limited success for seasonally prolific, vector arthropod, aquatic, larval habitat discrimination.. There has also been interest in developing transgenic phytosensors to elucidately canopied plant status in relation to environmental conditions in ArcGIS. This approach involves unambiguous signal creation whereby genetic modifications in discontinuous, canopy plants could result in distinct moderate resolution, bio-canopy, optical signals emitted in response to specific remotely detectable, environmental stressors. Most of these studies, however, are limited to laboratory or controlled greenhouse environments. There has been no contribution to the literature for autoregressively, quantitating Chl levels from geoclassfiable, explaicative, LULC, sparsely shaded, seasonal hyperproductive, *S. damnosum* s.l. riverine, turbid water, immature habitat, eco-epidemiological, eco-georefernceable, capture points at the canopy leaf level.

We were able to optimally remotely validate the seasonal hyperproductive, *S. damnosum* s.l. habitat, leaf Chl concentration mechanisms by simulating general broad geo-classified, field-operationizable, LULC patterns in bio-optical responses to stress in the RapidEye ™ 400–850 nm wavelength range in ENVI. Leaves having unusual anatomical characteristics such as heavy pubescence or succulence or colors other than green in the healthy, mature state were not included in the fractionalized, endmember emissivity analyses. We found senescent leaves in several habitat, discontinuous canopy, leaf species. This combination of results should provide a clearer understanding of changes in seasonally hyperproductive, *S. damnosum* s.l., canopied habitat's leaf, bio-optical properties that occur commonly with stress. These geoclassifiable discontinuous, canopy LULC shifts may be eco-cartographically delineated employing cost-effective, RapidEye™ visible and NIR, 5m wavelengths in ENVI.

Eco-physiologically, the reflectance variation in the eco-epidemiological unmixed, Chl-*a* submixel, 5m, wavelength frequency transmittance endmembers in ENVI was easily decomposed. The endmember, transmittance fluctuations may have been due to seasonal responses to changing biotic and abiotic factors (e.g., trailing vegetation LULC, solar radiation, etc.) which may be of seasonal entomological significance when implementing black fly control strategies such as Slash and Clear. Most indices sensitive to Chl content may be strongly affected by endmember 5m, wavelength, emissivity reflectance differences in explanatively unmixed, LULC, transmittance, of elucidatively paramterizable, wavelength, frequency-oriented, transmittance emissivity covariate, coefficient, sub-mixel correlated, eigenvectorestimators. One of the main co-factors governing seasonally hyperproductive, *S.*

damnosum s.l., immature, capture point, hypeproducrtive habitats in African narrow riverine, tributary, agro-village ecosystems is adequate water velocity (.70-1.5 m/sec), which is linked with oxygenation, food supply, and the presence of suitable supports, which may be rocks, stones, sills, sidewalks of structures, spillways and gates [93]. Whilst the orthogonally decomposable, discontinuously canopied, narrow, riverine, tributary, agro-village complex,geoclassified 5m, LULC, immature capture point, hyperproductive, habitat emissivity 5m indices revealed strong relationships with Chl content in the Red Edge, proxy, NDVI biosignature, additional seasonal validation endmember metrics may be required to understand how immature, seasonal, *Simulium* productivity is geospatially or geospectrally associated to proxy, decomposable, canopy, NDVI 5m, biosignatures. This endmember data feature attribute may be tabulated at the habitat leaf scale employing known geo-classifiable, geosampled, LULC, 5m, wavelength, frequency, transmittance, emissivity changes geo-spectrotemporally associated with hyperproductive, immature, sparsely shaded, narrow, riverine, *Similium,* trailing vegation, discontinuously canopied, sparsely shaded, hyperproductive, eco-epidemiological, eco-georeferenceable, agro-village, tributary habitats.

When scaling up from a leaf to a branch or canopy in flooded, narrow riverine tributary conditions, explanatively geoclassifiable, explanatorial LULC, observational predictors of hyperproductive, *S. damnosum s.l.* habitats (e.g., Percent of trailing vegetation LULC, discontinuous, canopy density) may affect a measured RapidEye^{TM} reflectance signal. The reflectance model explicative output of the canopy Chl content was an eco-physically sound quantity that ecohydrologically represented the optical path in the canopy where absorption N also dominated the RapidEye, 5m, radiometric signal. Absorption by Chl-*a* may provide the necessary link between seasonally geosampled trailing vegetation, dense, heterogenously canopied, observations and hyperproductive discontinuously canopied, narrow, riverine, tributary, agro-village complex ,immature habitats, and their geoclassifiable, LULC canopy-state, eco-georeferenceable explanators, as well as other Chl-related, frequency, transmittance, covariate estimators. These data products may be subsequently employed as indicators of N status and photosynthetic, seasonal immature, habitat canopy capacity.

Futher, based on our results, research can pres ently concentrate on qualitatively quantitating orthogonally decomposable RapidEye^{TM} seasonal, fractionalized, endmember eigenvector emissivity relationships between leaf N content and the eddy covariance CO_2 flux measurements for devising a range of diverse discontinuously canopied, narrow, riverine, tributary, agro-village complex,geoclassified LULC, unmixed, 5m, leaf area, wavelength, transmittance, emissivity, in a eco-georeferenceable, hyperproductive,eco-epidemiological, capture point, habitat. Discontinuous leaf N content may be a strong co-factor influencing both optimum canopy light use efficiency and canopy photosynthesis rates in an capture point, hyperproductive, *S. damnosum s.l.* habitat at these sites. Indeed, Chl-*a* measurement provides information on the plant ecophysiological status because leaf chlorophyll concentration is linked to N content, and, therefore, to photosynthesis [172].

The Red Edge, orthogonally decomposed 5m, wavelength, emissivity transmittance, endmember,data described the steeply sloped, discontinuously canopied, hyperproductive, *S. damnosum* s.l., immature, habitat region of the expositively geo-classifiable, vegetation-related, LULC, submixel, reflectance curve between 690 nm and 710 nm, where Chl-*a* absorption was geolocalized from low/high Chl-*a* content in the habitat unmixed spectrum. These shifts within the canopy, 5m, LULC spectrum may have been related to stress induced

from the vegetation-related, LULC or canopy decline, which probably arose as a result of increase in seasonal fluorescence. In our Red Edge, habitat, eco-epidemiological, narrow riverine, tributary, risk model output, these flucations were detected in regression space by graphing the geospectral algebraic decomposition of the endmember shift toward the longer or shorter wavelengths of the electromagnetic 5m spectrum in ENVI.

Investigations of the shape of the first uncoalesced, reflectance, endmember, derivative, fractionalized spectra in the Red Edge region of the eco-georeferenced, trailing vegetation, hyperproductive, discontinuously canopied, narrow, riverine, tributary, agro-village complex, geo-spectrotemporally geoclassified LULC, immature habitat, sub-divied reflectance suggested that the maximum, sub-mixel, iteratively interpolatable values may be associated with low Chl-*a* content in the canopy. These LULC changes may be related with seasonal, canopy, leaf development in seasonally hyperproductive, immature habitats. Thus, a time series dependent, quantitatively regressable, 5m, Red Edge, endmember, decomposable, NDVI, biosignature in a wavelength, emissivity transmittance, ArcGIS-derived, unmixing algorithm may be useful for quantitating canopy defoliation in a seasonally explanative, hyperproductive, trailing vegtataion, immature, discontinuously canopied, sparsely shaded, turbid water, capture point, seasonal habitat.These emissivity, geo-predictive, 5m, wavelength, eco-epidemiological maps may reveal fractionalized, 5m, Rapid Eye^{TM} , endmember, wavelength, frequency transmittance, geo-spectrotemporally uncoalesced, geospatialized,geoclassifiable, LULC sub-mixel changes in Chl-*a* concentration for estimation of photosynthetic activity in specific discontinuously canopied, riverine geolocations as rendered from an eco-epidemiological, eco-cartographic, eco-georeferenced, seasonally hyperproductive, explanative, immature *Similium* habitat data rendered from a stochastic interpolator constructed in ArcGIS.

Analyzing seasonal relationships between unmixed, Chl-*a* in RapidEye^{TM} vegetation indices formulated from an eco-georeferenced, seasonally hyperproductive, immature trailing vegetation, discontinuously canopied, sparsely shaded, turbid water, capture point, *S. damnosum* s.l. habitats may remotely quantitate relations between orthogonally decomposed, 5m wavelength, discontinuously canopied, narrow, riverine, tributary, agro-village complex, geo-spectrotemporally geoclassified, LULC, wavength, frequency transmittance of Red Edge reflectance in the red region of the canopy spectrum. For example, the position of the Red Edge on the canopy scale may provide a robust indication of the discontinuous canopy condition that may be related to a variety of remotely sensed, co-photosynthetic, iteratively explanatively ieratively interpolated, frequency, transmittance emissivities contributing to hyperproductivity of immatures in an *S. damnosum* s.l. immature habitat, including leaf LAI nutrients, water content, and canopy biomass. These proxy, elucidatively geo-classifiable LULC, time series dependent, explanators may be studied in a first derivative discontinuously canopied, RapidEye^{TM} 5m, imaged, *S. damnosum* s.l., eco-epidemiological, uncoalesced immature habitat, dataset of parameterizable, reflectance-oriented, field-operationizable, fractionalized, covariate, endmember eigenvectors estimators from the Red Edge region since this position in our risk model was the tabulated point of maximum slope on the sub-mixel, fractionalized, 5m, wavelength reflectance spectrum of the geoclassifiabel LULCs between red and NIR wavelengths amongst all the radiance geomarkers. In doing so, powerful eco-epidemiological, forecasting vulnerability, Rapid Eye^{TM} eco-georefernceable risk maps of seasonally hyperproductive discontinuously canopied, narrow, riverine, tributary, agro-village complex,immature habitats based on geosampled immature count data may be generated in ArcGIS.

At the fractionalized leaf level, endmember, 5m, reflectance, wavelength, frequency, transmittance is a function of Chl-*a* emissivity absorption, internal structure, leaf thickness, air-water interface, distribution of pigments and chemical constituents [172]. Additionally, leaf surface, time series dependent, metaheursitically LULC properties, such as a waxy cuticle and pigment concentrations and distribution may affect Chl-a concentrations [189]. At the canopy level, endmember, Chl-*a* sub-mixel, reflectance may be a function of LAI, leaf clumping, leaf angle distribution, trailing vegetation, 5m, LULC cover, and source-target, illumination geometry, especially when identifying localities of *S. damnosum* s.l. riverine larvae. As a consequence, RapidEye^{TM} vegetation index biosignatures should be seasonally constructed for regressing seasonal, geo-spectrotemporal, geospatially uncoalesced, explicatively orthogonally decomposable, fractionalized, discontinuous, canopy pigment content at the leaf level of a seasonally hyperproductive, trailing vegetation, immature, discontinuously canopied, sparsely shaded, turbid water, capture point, narrow, riverine tributary, eco-georefernceable, capture point, *S. damnosum* s.l., habitat.

Further, estimation at the canopy level of N from LAI may be vital for optimally targeting immature habitat, discontinuous endmember, forecastable, derivative , discontinuous, canopy spectra as the factors that affect eco-georefernceable, riverine, capture point, immature habitat reflectance vary according to seasonal scale. Later in the season, LAI values may lose sensitivity for measuring canopy nutritional content. For example, Inada [190] found a high correlation between leaf N and leaf optical properties (r2 = 0.90). However, at the canopy level, the correlation between canopy N concentration and canopy reflectance decreased as a function of LAI.

The 5m, larval habitat, Red Edge NDVI data from ENVI was exported to an unmixing algorithm in ArcGIS, and a SPA algorithm was employed to unmix the Red Edge biosignature. By employing the average of multiple RapidEye^{TM} fractionalized, imaged capture point, immature habitat, canopy endmembers from the extracted Red Edge, NDVI mixel as one canopy endmember, the total deducable unmixed, Chl-*a,* submixel, endmember, reflectance values was quantitated. The SPA-derived unmixed, fractionalized, endmember, forecast, derivative spectra appeared to be without noise (i.e. smooth). Given that adjacent, uncoalesced, iteratively interpolative, immature, habitat data extracted from the 5m mixel was not likely to be simultaneously spurious, the use of neighboring adjacency, endmember, LULC tabulations may have made the SPA more sensitive to isolated, noisy, RapidEye^{TM},5m, heterogenous mixels, thus avoiding inherent challenges such as uncertainty probability estimation and propagation of autocovariate decomposition, erroneous, wavelength, transmittance misspecified emissivities, outlier covariate coefficients commonly seen in other convex–based, endmember-search, unmixing algorithms. Quantification of erroneous explanative, latent autocovariate, endmember, fractionalized relationships is vital for efficient endmember forecasting, eco-epidemiological, radiance, risk mapping [22].

Although spectral unmixing algorithms in ArcGIS have proliferated in a variety of medical entomological, vector arthropod-related, geo-spatiotemporal,geo-spectrotemporal, geospatialized, geosampled, geo-predictive models by exploiting remotely sensed, explanatively decomposable, eco-georeferenceable, geo-classifiable unquantitated, moderate resolution, wavelength emissivity, sub-mixel data that is autocorrelated will exhibit misspecifications. Jacob et al. [191] found that since endmembers of sub-meter spatial resolution, wavelength, imaged, aquatic, larval habitats of *Anopheles arabiensis*, a major vector of malaria in Sub-Saharan Africa (SSA), in central Kenyan, riceland, agro-village ecosystems, utilize semi-permanent to temporary habitats (e.g., floodwater areas, vernal

pools, hoof prints), autocorrelated endmember, fractionalized data can pose a special problem namely endmember multiscattering. The authors orthogonally decomposed a hypeproductive, *An. arabiensis* Riceland,immature habitat mixel for forecasting hyperproductive, eco-georeferenceable, geo-classifiable, immature habitats in a riceland, agro-ecosystem, village complex. The resedual regression forecast vulnerability model forecasts revealed that paddy preparation *An. arabiensis* habitats were the most productive based on spatiotemporal field-sampled count data

Here we constructed a meteaheursitically optimizable, explantaorial, regression forecasting model for qualitatively quantitating the empirical5m uncoalesced, wavelength, transmittance emissivity dataset of discontinuously canopied, narrow, riverine, tributary, agro-village complex, geoclassified LULC, *S. damnosum* s.l. habitat which assumed a normally distributed population with mean μ and standard deviation σ. We chose individuals independently and then they had $X_1, \dots, X_n \sim N(\mu, \sigma^2)$and the sample mean$\overline{X} - \frac{X_1 + \cdots + X_n}{n}$which was a random variable distributed thus: $\overline{X} \sim N(\mu, \sigma^2/n)$. The statistical errors were then$e_i = X_i - \mu$,whereas the residuals were $r_i = X_i - \overline{X}$. The individual quantiated, explanative residual forecasts. mixel, spectral, reflectance estimates from a Rapid Eye ™ dataset of visible and NIR data of the *Similium* habitat were then extracted by using a Li-Strahler geometric-optical model. In ENVI®, the DN of the mixel in every band was viewed using the *z*-profile from a spectral library. The sum of squares of the statistical errors, divided by σ^2, has a chi-squared distribution with n degrees of freedom$\frac{1}{\sigma^2}\sum_{i=1}^{n} e_i^2 \sim \chi_n^2$. This quantity, however, was not observable. The sum of squares of the residuals, on the other hand, was observable. The quotient of that sum by σ^2 had a chi-squared distribution with only $n - 1$ degrees of freedom: $\frac{1}{\sigma^2}\sum_{i=1}^{n} r_i^2 \sim \chi_{n-1}^2$. This difference between n and $n - 1$ degrees of freedom resulted in the authors employing a Bessel's correction for the estimation of sample variance of the immature habitat capture point, with unknown mean and unknown variance,

After making an atmospheric correction from the image for the eco-epidemiological, eco-georeferenceable, study site, the DN was converted into ground reflectance. A convex geometrical model was also used for endmember validation of the geo-spectrally decomposed habitat. An ordinary kriged-based interpolation was performed in Geostatistical Analyst ™ using the reference signature generated from the unmixing models.

Spatial inference, or estimation, of a quantity $Z : \mathbb{R}^n \to \mathbb{R}$, at an unobserved discontinuously canopied, narrow, riverine, tributary, agro-village complex,geoclassified LULC,habitat location x_0, was calculated from a linear combination of the observed uncoalesced values $z_i = Z(x_i)$and endmember fractionalized weights

$$\hat{Z}(x_0) = \begin{bmatrix} w_1 & w_2 & \cdots & w_N \end{bmatrix} \cdot \begin{bmatrix} z_1 \\ z_2 \\ \vdots \\ z_N \end{bmatrix} = \sum_{i=1}^{n} w_i(x_0) \times Z(x_i)$$

$w_i(x_0),\ i = 1, \dots, N$ in Geospatial Analyst ™ The weights w_i revealed two extremely important geospatial inferences based on the discontinuous, elucidative discontinuously canopied, narrow, riverine, tributary, agro-village complex, geo-spectrotemporally geoclassified LULC, 5m *S. damnosum* s.l. habitat

signature, explanative process: 1) eco-epidemiological, residual linear forecasts reflected structural "proximities" of habitat samples for estimation of an explanative, hypeproductive, habitat geo location, x_0. 2) a desegregation effect avoided bias caused by eventual sample clusters. When calculating the endmember weights w_i, there are two objectives in the geostatistical formalism: unbias and minimal variance of estimation[24].

The cloud of the eco-epidemiological, eco-georeferenceable, capture point, immature habitat, fractionalized, biosignature iteratively interpolated values $Z(x_0)$ were plotted against the estimated values $\hat{Z}(x_0)$, for optimally determining the criterion for global unbias, intrinsic stationarity of the geosampled field. In so doing, the eco-epidemiological, forecasts implied that the mean of the estimations had to equal to mean of the geo-spectrotemporally, geospatial, geosampled, 5m values. The second criterion says that the mean of the squared deviations $(\hat{Z}(x) - Z(x))$must be minimal, which means that when the cloud of estimated values versus the cloud real values is more disperse, the estimator is more imprecise[24]. Linearizable unbiased predictors and variance estimates were derived of all hyperproductive immature habitats in the study site based on the extracted pixel endmember, reflectance estimates were forecasted.

Analyses of the explanatively decomposable proxy, RapidEye^{TM} 5m, geo-predictive, remotely synthesized, explanatorial, *S. damnosum* s.l. habitat NDVI, bisoignature variables, along with the ground truth data, revealed relatively high accuracy (RMSE < 1µg/l) between the predicted and observed, habitat, discontinuously canopied, LULC, data feature, attribute values, which were optimally rendered for the trailing vegetation, turbid water,narrow riverine tributary, geo-spectrotemporally geosampled geolocations associated with ecohydrologically low vegatation (i.e., < 10 µg/l) content in ArcGIS. By choosing the Red Edge band, instead of the red band for the fractionalized, NDVI endmember calculations, a lower saturation over highly sparsely shaded, eco-georeferenceable, sporadically vegetated geo-spectrotemporally geoclassified, LULC areas in the fractionalized, discontinuously canopied, eco-georeferenceable, capture point, agro-village African, narrow, riverine tributary *S. damnosum* s.l. habitat was achieved. Our results revealed strong spatial scale dependencies of the Red Edge, NDVI over the Gongcygo agro-village, complex, ecosystem, study site, heterogeneous, Chl-*a*, discontinuously canopied, LULC surfaces, indicating that 5m values may be optimal for remotely discerning *S. damnosum* s.l., seasonally hyperproductive, narrow riverine, tributary, immature habitats at 5m, spatial resolution.

ArcGIS and various unmixing algorithms can be optimally employed for retrieval of a robustifiable dataset of explanatively fractionalized, trailing vegation, turbid water, discontinuous canopied, fractionalized, endmember eigenvectors representing heuristically decomposed, geoclassifiable, Chl-*a,* 5m, LULC-related, time series dependent vegetation canopy, from an unmixed, Rapid Eye ^{TM} biosignature. Sub-mixel, elucidative, biophysical properties may be qualitatively quantitated by determining the relationship between unmixed, 5m, NDVI regressable, probabilistic, proxy, wavelength, transmittance, emissivity coefficients.

An additional RapidEye^{TM}, 5m, byproduct measurement rendered was generated while unmixing the Red Ege NDVI, trailing vegetation, turbid water, capture point, immature habitat, canopy, biosignature, which was quantitated as the change of the simplex volume ratio between successive iterations during the endmember extraction process. We noted that the SPA illustrated the influence of a new eco-epidemiological dataset of larval habitat, discontinuously canopied, fractionalized, endmember eigenvectors on the orthogonally

decomposed, Red Edge, NDVI biosignature, image data structure, and provided information about the convergence of the algorithm. Though the rate of convergence speed varied with LULC complexity in the endmember, decomposed Red Edge, NDVI biosignature representing the eco-georferenceable, seasonally, hyperproductive, capture point, immature habitat, the merging revealed large geoclassified discontinuously canopied, endmember, unmixed 5m, wavelength, transmittance emissivities in volume ratio, followed by progressively smaller changes and convergence towards a spectral plateau. The decomposed, canopy, fractionalized, endmember biosignature search terminated before the convergence point (i.e., when the volume ratio was close to 1.0).

We noted that variations in, Chl-*a,* dry matter, and water content interacted to cause nonlinear shifts in the 5m, immature habitat, SPA, elucidatively orthogonally decomposed, discontinuous, canopy endmembers. Because geoclassifiable LULC changes in Chl-*a* variables had the greatest effect in the 5m visible and NIR regions between 400 and 1300 nm, and dry plant residues in the habitat canopy had,the greatest effect in the IR region between 2000 and 2400 nm, the expositively quantifiable, fractionalized, 5m, endmember, radiance observations of the full 400- to 2500-nm spectrum for the capture point, immature habitat, sub-mixel biosignature may provide the best basis for analyzing and iteratively interpolating photosynthetic and non-photosynthetic, fractionalized 5m, endmember estimates.

The decomposed, Red Edge, 5m, imaged, NDVI, habitat, endmember, unmixed biosignature, wavelength frequency-orinted, transmittance emissitives rendered from the SPA were then input into a 3-D, radiative transfer model in ArcGIS. The medium resolution, NDVI, canopy invariants expressed the fractionalized, discontinuous wavelength, spectral reflectance by independent bio-optical, RapidEye^{TM} wavelength, frequency, transmittance emissivities. The eco-epidemiological, endemic, explanative, model residual forecasts determined a small, uncoalesced, eco-georeferenceable, heuristically robustifiable dataset of discontinuously canopied structural, radiatively transferable, RapidEye ^{TM} endmember, predictor variables. This dataset included the canopy interceptance based on the recollision and the escape probabilities.

The spectral invariants of canopied, vegetation geo-classifiable, discontinuous, geoclassified trailing vegation, LULC canopy conveyed from a hyperproductive, turbid water, narrow riverine, eco-georefernecable, agro-village complex, tributary, immature habitat provides a good deal of information regarding the canopy structure at multi-hierarchical levels. The findings of the 5m, explanatively, time series, orthogonally decomposable, RapidEye^{TM} wavelength independent and scale independent variables (e.g., the ratio between the directional escape and the total escape probability) suggest that umixed, discontinuously canopied, immature habitat emissivities depend on the selection of reference leaf albedo for achieving accurate, sub-mixel, reflectance values. This ArcGIS decomposition technique can be treated as the identifier of macro scale canopy structure (e.g., foliage density, aspect ratio, ground cover, habitat shape etc).

In order to better utilize Chl-*a* retrieval algorithms in ArcGIS, it may be helpful to remotely define and qualitatively quantitate 3-D, orthogonalizable, discontinuous, canopy structural, synthetic, RapidEye ^{TM} elucidative 5m, wavelength, frequency, transmittance components. Model simulation based on the stochastic, radiative transfer, non-continuous equation may be then optimally employed to test the sensitivity of a Chl-*a* variable based on its geo-spatializable, geo-spectrotemporal relationship to the structural geosampled 5m, reflectance parameterizable, covariate, estimators. These geo-spectrotemporal,

discontinuous canopied, geoclassifiable, LULC, predictor variables may specify the relationship between the quantitable geospectral response of the, trailing vegation, turbid water, larval habitat, vegetation canopy, Chl-*a* concentrations to the incident solar radiation at the leaf and the canopy scale. This may then be optimally tabulated employing the decomposed,immature habitat, Red Edge, NDVI, unmixed, reflectance values. The estimates rendered from the model may allow for a simple and accurate parameterization for partioning the incoming radiation, non-homogenous, canopy emissivity, transmission, reflection and absorption at any 5m, RapidEye^{TM}, decomposed, wavelength discontinuous spectrum.

We then conducted a retrieval of the discontinuously canopied, geoclassified, 5m, Rapid Eye ^{TM} , LULC, endmember, sub-mixel, larval habitat, photosynthetic andnon-photosynthetic, geospatialized, feature, data attributes employing an eco-georeferenceable, geometric-optical, explanative, endmember model. The scene reflectance of each decomposed, operational, geospectral, geospatial component was classified in the eco-georferenceable, 5m imaged, hyperproductive, eco-georeferenceable, trailing vegation, turbid water, narrow, riverine tributary, agro-village complex, immature habitat. We retrieved the immature habitat, structural RapidEye ^{TM} wavelength, frequency, emissivity, transmittance, decomposed, orthogonal, covariate estimators employing the unmixed, discontinuous canopy, LULC, sub-mixel data. We employed a linear spectrum decomposition embedded algorithm in the geometric, bio-optical, sub-mixel, eco-epidemiological analyses in ArcGIS to determine the 5m reflectances of the Red Edge NDVI, endmember geospectral, unmixed, scene components, which were regarded as prior knowledge in the retrieval of the uncoalesced, immature habitat, Red Edge, discontinuous, canopy cover, fractionalized, 5m, wavelength, frequency emissivities.

The geometric scene included four components: sunlit canopy, shadowed canopy, sunlit background, and shadowed background. The radiance or reflectance of the RapidEye^{TM} riverine, agro-villge complex, eco-georefernceable, scene as a whole which was modeled based on the uncoalesced, discontinuously canopied, reflectance estimates of the individual fractionalized endmember, immature habitat components as weighted by their aerial LULC proportions. The aerial proportions of the components were determined by principles of geometric optics as applied to the geometric shapes of the capture point, immature habitat, canopy envelopes. These partitions yielded the expected proportions of the components as a function of angles of RapidEye^{TM} 5m, irradiance and exitance.

In ArcGIS, the directional radiance of the *S. damnosum* s.l., trailing vegation, turbid water,discontinuyous, canopied, capture point, larval habitat was dependent on the mixture of four components: sunlit and sparsely shaded, canopy crown, and sunlit and shaded background-that was seen from a given viewing illumination angle. The aerial proportions of these four components for given illumination and viewing directions was a function of the sizes, shapes, orientations, and placements of the elucidative, within-canopied, eco-georefernceable, immature habitat objects in the RapidEye^{TM} scene (e.g., sporadic, floating, dead vegetation). The size, shape, and orientation of the habitat was then characterized by distributions with known parameters and object centers, which were distributed randomly in ArcGIS. This decomposition model accounted for the changes in proportions that occurred with random overlapping of objects as the density of fractionalized endmember, discontinuously canopied, immature habitat, objects increased.

An empirical, BRDF risk model was then derived using the apparent trends between the quantitable, ToA reflectance versus solar zenith angle and viewing zenith angle of the

elucidatively orthogonally decomposed, explanative, discontinuously canopied, eco-epidemiological, immature habitat , 5m, wavelength, frequency, transmittance emissivites. The physics-based, BRDF, immature habitat, fractionalized, endmember estimation model, revealed a complete characterization of the seasonally explanative, biophysical characteristics of the diacontinuous canopy, such as its composition, irregular particle shape, refractive index, surface roughness, spectral reflectance, etc. Widely used semi-empirical models such as the Ross-Li model, Roujean model and Snyder model are kernel driven, whereas BRDF is modeled as a weighted sum of volume scattering, geometric scattering and isotropic terms [23], The 5m, RapidEye^{TM}, frcationalizedm endmember, BRDF identified seasonally explanative, hyperproductive, *S. damnosum* s.l., discontinuously canopied, sparsely shaded, eco-epidemiological, trailing vegetation, turbid water, sparsely shaded, hyperproductive, eco-georefernceable, immature habitat, geo-spectrotemporally quantitated eigenvectors.

The principles of Boolean models were extended for quantifying the immature habitat capture point, discontinuous, canopy leaves in ArcGIS as objects in successive layers above the background, sparsely shaded, trailing vegetation, geoclassified 5m, geoclassified narrow, riverine tributary, agro-village complex LULCs. By doing so, the bidirectional reflectance or radiance of Chl-*a* in the leaf canopies of the RapidEye ^{TM} 5m-imaged, trailing vegation, turbid water,*S. damnosum* s.l., larval habitat was efficiently modeled. As in the case of canopy envelopes, the objects' shape, size, orientation and spacing of the discontinuous, sparsely shaded, canopy leaves were deduced by tabulating linear estimators that drove the estimation of bidirectional radiance or reflectance in the forecast, vulnerability model. This extension led to the formulation of two-stage models, in which Chl-*a* in the canopy leaves represented geospatialized, fractionalized, endmember objects inside the canopy envelopes of the bio-optical, Booleanized, eco-epidemiolgical, capture point, eco-georeferenceable, *Similium* habitat, metaheustically optimizable, risk model. A 3-D, geospatial, residualized, explanatorily output then provided the mathematical basis for qualitatively quantitating the bidirectional radiance, which in the model was dependent upon the directions of irradiance and exitance, for accounting and validating an eco- georeferenceable, discontinuous, trailing vegetation, turbid water, canopied, Chl-*a* related, seasonally explantive "hotspot" (i.e., hyperproductive, capture point, riverine, agro-village complex, ecosystem habitat).

Because both whole-canopy and individual, eco-epidemiological, fractionalized, LULC-oriented, forecast, vulnerability paradigm may be driven by the same principles of geometric optics and Booleanization, they may easily be combined together in a single or a two-staged, forecasting, *S. damnosum* s.l. larval habitat, geo-spectrotemporally, geospatially uncoalesced, discontinuous canopy, bio-optical, narrow, riverine tributary, agro-village complex, trailing vegetation, turbid water, risk model. Through further application of the ArcGIS random sets, the averaging and variance quantification that occurs in a 5m, eco-epidemiological scene may be metaheuristically optimized by the RapidEye^{TM} sensor employing a finite field of view. In addition, Boolean and geometric, bio-optical, eco-georeferenceable, trailing vegetation, turbid water, hypeproductive, capture point, *S. damnosum* s.l. larval habitat, time series dependent, discontinuously canopied, decomposition, endmember, emissivity, eco-epidemiological, forecasting risk models may be capable of inversion, yielding estimates of size, shape, and spacing of crowns and/or leaves in ArcGIS from directional and spatial statistical iterative interpolative, algorithmic, wavelength, frequency-oriented, transmittance emissivity, forecastable, elucidative, time series residuals representing 5m, remotely sensed, regressed radiances.

All forecasting, latent eigen-algorithmic methods in ArcGIS were based on the assumption

that bio-optical parameters such as the Chl-*a* specific absorption coefficient λ and the Chl-*a* fluorescence quantum yield η remained non-constant, regression estimates. In numerical, vector arthropod, decomposition endmember analysis, one of the most important challenges is designing efficient and stable algorithms for finding the eigenvalues of a probablistic estimation matrix[23]. These eigenvalue algorithms may also find an metheursitically optimizable, bio-optical, eco-georeferenceable, hyperproductive, narrow, riverine tributary, agro-village complex, trailing vegation, turbid water,*S. damnosum* s.l. larval habitat, time series dependent, discountinuously canopied, decomposition, endmember, emissivity, eco-epidemiological, forecasting risk model eigenvectors.

In the context of spatial regression analysis, several methods in ArcGIS can be used to control for the statistical effects of spatial dependencies amongst orthogonalizable, elucidative, bio-optical, eco-georeferenceable, hyperproductive, narrow, riverine tributary, agro-village complex, trailing vegation, turbid water,*S. damnosum* s.l. larval habitat, time series dependent, discountinuously canopied, decomposition, endmember, 5m, optimally geo-spectrotemporally fractionalized endmembers, derived from a a spatial filter decomposoitional algorthm in ArcGIS. Maximum likelihood can account for spatial dependencies in a parametric framework, whereas recent spatial filtering approaches focus on nonparametrically removing spatial autocorrelation. We applied a semiparametric spatial filtering approach in ArcGIS to deal explicitly with (a) spatially lagged, endmember, fractionalized, autoregressive radiance models and (b) simultaneous autoregressive complex *S. damnosum* s.l. narrow tributary, agro-village complex, immature capture point, models. As in one non-parametric spatial filtering approach, a specific subset of spatial *S. damnosum* s.l. fractionalized, endmember, trailing vegetation, discontinuous, sparsely shaded, 5m, narrow tributary, African agro-village, orthogonally geo-spectrotemporally uncoalesced, eigenvectors from a transformed spatial link matrix in ArcGIS was used to capture dependencies amongst the disturbances of a spatial regression, forecasting, vulnerability model. However, the optimal subset in the proposed filtering model may be identifiable more intuitively by an objective function that minimizes spatial autocorrelation rather than maximizes a 5m Rapid Eye ™ fractionalized, endmember, eigenvector model fit. The proposed objective function has the advantage that it leads to a robust and smaller subset of selected expositively fractionalized discontinuous, sparsely shaded, turbid water, 5m, spatial filter, orthogonalized eigenvectors. An application of the proposed eigenvector spatial filtering approach, in ArcGIS may demonstrate its feasibility, flexibility,for robustly iteratively interpolating, proxy, 5m, LULC biosignatures for deterimining unknown, un-geosampled seasaonlly hypeproductive, *S. damnosum* s.l. capture points .

As mentioned previously, in linear algebra, an eigenvector or characteristic vector of a square matrix is a vector that does not change its direction under the associated linear transformation. In other words, if v is a vector in an elucidative, Rapid Eye™ 5m imaged, trailing vegetation, turbid water, sparsely shaded, eco-georeferenceable, elucidative, eco-epidemiological capture point, bio-optical, geometric, seasonally hyperproductive, discontinuously canopied narrow, riverine tributary, trailing vegation, turbid water, agro-village complex, *S. damnosum* s.l. larval habitat, time series dependent, fractionally, decomposition, endmember, emissivity risk model residual forecast that is not zero, then it is an eigenvector of a square matrix *A* if *A*v is a scalar multiple of v. This condition could be written as the equation $A\mathbf{v} = \lambda\mathbf{v}$, where λ is a number (e.g., scalar dependent, explanatorial, riverine agro-village, geo-spectrotemporally geosampled, tributary variables) known as the eigenvalue or characteristic value associated with the eigenvector v. Geometrically, a hyperproductive, *S. damnosum* s.l., immature habitat, fractionalized,

iterative interpolative, 5m, orthogonally decomposed, endmember eigenvector corresponding to a real, non-zero eigenvalue capture point in a direction that is stretched by the transformation and the eigenvalue is the factor by which it is stretched [24]. If the eigenvalue is negative, the direction is reversed. There may be a correspondence between *n* by *n* square matrices and linear transformations from an unmixed, *n*-dimensional, eco-geographic regression, vector space to itself. For this reason, this technique in ArcGIS may be equivalent to defining eigenvalues and eigenvectors from a metaheuristically decomposable, uncoalesced dataset of geo-spectrotemporally geospatialized, uncoalesced, 5m, wavelength, frequency, transmittance, emissivities of bio-optical, seasonally, explanative hyperproductive, eco-georeferenceable, capture point, *S. damnosum* s.l., larval habitat, time series dependent, discontinuously canopied, trailing vegetation, turbid water, decomposition, fractionalized endmember, emissivity, risk model using either the language of matrices or the language of linear transformations.

The robustness of the Rapid Eye™ 5m, eco-epidemiological, seasonally hyperproductive, discontinuously canopied, trailing vegation, turbid water,narrow, riverine tributary, agro-village complex, capture point, risk model, optimally parameterizable, reflectance covariates were likely dependent on the ecophysiological state and structure of the immature, hyperproductive, eco-georeferenced, trailing vegetation, turbid water, sparsely shaded, discontinuous, canopied geosampled, geo-predictive explanators. Fluorescence quantum yield is affected by phytoplankton taxonomic composition, illumination conditions, light adaptation, nutritional status, and temperature, and can vary by eight-fold [192]. Thus, the assumptions of constant Chl-*a* can be a significant source of explanatively problematic regression uncertainty in decomposed iteratively interpolative, *S. damnosum* s.l., geosampled variables. Using unmixing ArcGIS algorithms and ENVI object-based classifiers can retrieve 5m resolution, Chl-*a* robust, regressive estimators especially when remotely targeting seasonally, sparsely shaded, hyperproductive, *S. damnosum* s.l. habitats in African, narrow, riverine agro-village, tributary environments. Since immature productivity of *Simulium* may be seasonally heterogenous, it may be necessary to define and measure specific IOPs for a specific, seasonal, discontinuously canopied, hyperproductive capture point, immature habitat, eco-georefernceable, sample site in ArcGIS. This consideration paridigms may be particularly important for unmixing procedures in ArcGIS especially when employing geophysical inversion models to estimate Chl-*a* from other leaf biochemestries discontinuously canopied, turbid, riverine, water reflectance for precisely targeting, eco-georeferenceable, prolific, *S. damnosum* s.l. habitats in ArcGIS. Selective pressure on plant competition for light, water, and nutrients should result in suites of biochemical and structural traits that integrate their functional strategies[www.esri.com]. Structural traits affecting light scattering “over scales ranging from cells to discontinuous canopies” will be convergent with their biochemical traits[24]

Elucidative inversion of the, eco-georeferenceable, eco-epidemiological, seasonally hyperproductive, discontinuously canopied narrow, riverine tributary, agro-village complex, eco-georefernceable, immature, habitat, risk model in ArcGIS enables resource explorers to extract more insight from geophysical data by converting the measurements into 3D images of the subsurface that can be integrated with other surface and sub-surface eco-geologic observations. Insights generated from a geophysical inversion of a *Simulium* forecasting vulnerability, capture point, risk model may improve prospecting and focused targeting of seasonally hyperproductive,immature habitats, particularly in deeper and more complex subsurface, riverine flooded, narrow tributray environments.

Variability of the geo-spectrotemporally geosampled, orthogonally decomposed, Chl-*a* fluorescence quantum yield, especially of the Chl-*a* specific absorption coefficients, in ArcGIS considerably increased the accuracy of geolocating habitats at the intervention villages. We tuned the model band positions, rather than simply parameterizing the orthogonally decomposed, RapidEye 5m, wavelength, transmittance, emissivity, risk-related, covariate coefficients of the model in ArcGIS. Optimal geolocations of seasonally hyperproductive, discontinuously canopied, trailing vegation, turbid water,narrow, riverine tributary, agro-village complex, eco-georeferenceable immature habitats were found based on the 5m, spectral band, orthogonally decomposed, fractional, endmember, wavelength, emissivity, transmittance data in accordance with the bio-optical absorption properties of the uncoalesced, study site, geoclassifiable, LULC, explanative, data feature attributes. The large range of bio-optically, explicatively active, sub-mixel, fractionalized constituents served to validate the robustness of the model. The final field verified output was based on the ecophysiological reflectance of the geoclassified LULCs and their seasonal immature habitat, uncoalesced, RapidEye^{TM} , 5m, discontinuously canopied, Chl-*a* concentrations.

RapidEye^{TM} Red Eye, discontinuously canopied, geo-classifiable, explantively, geoclassifiable, LULC, fractionalized estimates of above seasonal, ground, carbon storage, including woody stems and plant litter, could improve forecasts of seasonally hyperproductive, discontinuously canopied, trailing vegetation, turbid water, narrow, riverine tributary, agro-village complex, immature habitat LULCs, and Chl-*a*, in ArcGIS. For example, increases in the dry litter fraction have been used in tropical forests and grasslands to estimate environmental stresses [193]. The nutrient limitations of carbon storage in humid, tropical,African, riverine ecosystems may be exploited by combining dry residue indices and emitted quantitated geo-spectrotemporally geosampled, eco-georeferenceable, hyperproductive, canopy, sparsely shaded, geo-spatiotemporal, trailing vegetation, *S. damnosum* s.l. immature habitat, turbid water, riverine, agro-village, eco-epidemiological, uncoalesced Rapid Eye ^{TM} ,5m data in Geospatial Analyst^{TM}. Carbon absorption features such as NPV in a high Chl-*a* canopy concentrated, capture point, seasonal hyperproductive habitat may be interpretable between 2000 and 2200 nm employing Red Edge, 5m, umixed, iterative interpolative, wavelength, frequency, transmittance reflectance data, which may be algorithmically further utilized in a spectroscopic, explanatively decomposable, fractionalized, discontinuously canopied, NDVI biosignature, fractionalized, endmember, eigenvector, emissivity dataset.

In semi-arid, African, discontinuously canopied, riverine environments, the low LULC habitat canopy cover may permit direct detection of plant litter, making it easier to estimate stand characteristics, canopy disturbance conditions, ecophysiological states, and biogeochemical processes of the hyperproductive, immature habitat. The spatial patterns of dry plant residues in shriver shrub, geo-classifiable LULC, delineated in ArcGIS of 5m, RapidEye^{TM}-imaged, grassland, African, narrow, riverine tributary ecosystems may provide iteratively interpolatable, robust, proxy, residual model, geospatial indicators for quantiating desertification of a geospatial cluster of hyperproductive, immature riverine, trailing vegetation, turbid water, sparsely shaded. hyperproductive, capture point, eco-georeferenceable habitats.

The quantity of dry plant material is a direct indicator of carbon production, turnover, and decomposition (heterotrophic respiration). Turner et al. [194] found that above ground stocks of dry and live biomass were tightly coupled to organic soil carbon pools across a wide range of heterogenous, African, riverine, flooded ecosystems. Because sub-mixel,

RapidEye™, 5m, resolution decomposition of surface litter is at least partially geospatially and temporally correlated with soil decomposition and respiration, measures of NPV plant material, soil carbon efflux in an elucidatively decomposed, endmember, eigenvector seasonally hyperproductive, discontinuously canopied narrow, riverine tributary, agro-village habitat, Red Edge, NDVI, epidemiological, eco-georefernceable, risk model may be easily constrained. RapidEye™ nadir reflectance values of decomposable, habitat, LULC canopies in ArcGIS may be a function of solar zenith angle (0s), and may vary with 5m wavelength and soil substrate. Both factors must be considered when quantitating, seasonal, immature habitat canopy trends as shown by the results reported by Jacob et al. [22]. Here robust, discontinuous canopy surface, fractionalized endmember, RapidEye™ reflectance variables in the immature habitat, geo-spectrotemporally, geospatialzed, uncoalesced 5m, wavelength, transmittance emissivities of the LULC discontinuous canopy was geoclassifiable as non-Lambertian. Functions of wavelength, illumination and viewing directions, soil moisture content, particle size, organic matter content, soil mineralogy, and surface roughness determine if Lambertian assumptions are violated[24]. Lambertian reflectance is the property that defines an ideal "matte" or diffusely reflecting surface [23].

Solutions for general non-Lambertian scenes have only recently been pursued in GIS literature. Regardless, the rank constraint of radiance tensor as a discrepancy indicator in ArcGIS may measure discontinuously canopied, 5m, Red Edge reflectance, wavelength, frequency correspondences as rendered from seasonally hyperproductive, discontinuously canopied narrow, riverine tributary, agro-village *Simulium* habitats geosampled in African, riverine, agro-village, complex environments. This reflectance-sensitive method may handle high canopy leaf specularity, endmember radiance rendered from these habitats. Shapes from shading and photometric stereo methods make use of such information to recover 3D shapes in Geospatial Analyst™. These methods usually assume that eco-georeferenceable, surface reflectance properties are known.

Measures of structural carbon (cellulose, lignin, and other carbon compounds) may provide a Chl-*a* independent estimate of discontinuous canopy biomass in a agro-village complex, tributary, capture point, riverine eco-epidemiological, seasonally hyperproductive, eco-georefernceable habitat. RapidEye™ mapping concentrations of canopy lignin may be vital for optimal, 5m, Red Edge, NDVI, sub-mixel, endmember decomposition in ENVI algorithms (SID) and subsequent iteratively interpolation of a RapidEye™ reference, unmixed biosignature in ArcGIS when identifying unknown habitats. However, the ability to obtain an independent measure of canopy lignin in spectroscopic, 5m, unmixed data may be limited because of lignin's spectral similarity to cellulose and other cell wall materials in a flooded, larval, *Simulium* habitat. Using samples of ground dry leaves, Kokaly and Clark [195] found smaller errors in time series, multivariate, regressed reflectance, emissivity wavelength, transmittance estimates of lignin that were subsequently log-transformed to non-linear, regressable estimates of cellulose, although cellulose comprised a substantially larger fraction of dry weight in the final model. There has been difficulty studying fresh and dry leaves, specifically retrieving separate lignin and cellulose concentrations [196], but better results have been claimed for lumped estimates of dry plant canopy matter. Retrievals of dry plant canopy residues in the RapidEye™, 5m, wavelength spectrum may be measurable from high-fidelity, full-range imaging spectrometric vegetation indices when precisely, remotely targeting, hyperproductive habitats in African riverine, tributary agro-village, complex, environments.

The Secchi disk readings of the eco-georeferenced, seasonally hyperproductive, discontinuously canopied narrow, riverine tributary, agro-village, eco-georeferenceable,

immature habitat did not provide an exact measure of transparency, as there were errors due to the sun's glare on the riverine water, especially at the Adibuk intervention site. Regardless, it was an inexpensive and straightforward method of measuring the riverine water clarity around the immature habitat sites. Because of the potential for inter-observational variation between researchers, methods should be standardizable as much as possible when computing Secchi disc readings for metaheursitically targeting, seasonal hyperproductive, discontinuously canopied narrow, riverine tributary, agro-village, eco-georeferenceable, immature, *S. damnosum* s.l., capture point, habitats at 5m resolution. We recommend taking Secchi disk measurements for African riverine environments for targeting these agro-village eco-georefernceable, hyperproductive habitats between between 10 am and 2 pm for optimal results. The same field researcher should take Secchi depth measurements in the same manner every time along any geosampled discontinuously canopied, immature habitat, RapidEye ^{TM} 5m, explicatively geoclassifiable, LULC areas. Quantitating the measurement at the capture point, immature habitat site can be conducted by lowering the disk beyond a point of disappearance within the canopy, then raising it and lowering it slightly to set the Secchi depth.

Another method, if the turbulence is too great in the narrow tributary, riverine agro-village, trailing vegetation, turbid water, tributary, study areas by the immature habitat,capture point is to record the depth at which the disk disappears within the outside of the canopy, and the depth at which the disk reappears as it is slowly brought up. The Secchi depth is taken as the average of the two values [197]. Secchi disk measurements should be an integral component of *Simulium* control programs, especially targeted removal of seasonally explanative, eco-georefernceable, eco-epidemiological, seasonally hyperproductive, immature habitats, since the depth of habitat may be seasonally associated with these larval habitats. Targeting these seasonal habitats employing iteratively interpolated, uncoalesced, NDVI biosignature, Red Edge, Chl-*a,* endmember, wavelength, transmittance, frcationalized, eigenvector emissivities may aid in analyzing and estimating riverine, turbid water quality around hyperproductive, immature, trailing vegetation, turbid water, sparsely shaded, immature habitats. Local narrow, riverine tributary, agro-village, residents and district level officers may be able to make periodic measurements and submit their readings to local agencies. The aggregated longitudinal data may be optimally employed to reveal general trends in habitat water quality.

Ordinary kriging was employed to iteratively interpolatively geospatialize the estimated immature , capture point, eco-georfernceable, habitat geolocations of the unknown,un-geosampled, seasonally hyperproductive, *S. damnosum* s.l. habitats employing the decomposed, Chl-*a*, fractionalized, endmember, 5m, wavelength, transmittance, eigenvector emissivities as the dependent variable in the stochastic interpolator. We generated robust Chl-*a,* endmember concentrations extracted from the immature habitat canopy. These unmixed Chl-*a* values were compared to the spatialized references as a validation exercise based on the in situ Chl-*a* collected in the archived databases of imaged, RapidEye^{TM}, 5m, *S. damnosum* s.l. habitats, empirically geosampled at the intervention, agro-village, eco-epidemiological, seasonally hyperproductive, discontinuously canopied narrow, riverine tributary, study sites. The comparison was performed through the "Spatial Language for Algebraic Geoprocessing" (LEGAL) implemented at SPRING software. At each estimated site, the following were measured: 1) downwelling irradiance, 2) upwelling radiance, 3) Secchi disk transparency (m), and 4) coordinates of latitude and longitude. Results showed a better accuracy for the procedure employing the spatialization of Chl-*a* and the resultant vulnerability emissivity, wavelength, RapidEye^{TM} 5m, transmittance maps in ArcGIS, and the tabulated, algebraic, discrete, integer values. The spatializaton of proximal

RapidEye^{TM} Chl-*a,* geospectral, explanatorial, time series measurements retrieved revealed the bio-optically active pigmentous components in the 5m, discontinuous canopy spectrum of a hyperproductive habitat, which was then treated through a "Slash and Clear" technique.

We employed a functional linear regression model in ArcGIS where the response Y was related to a square integrable random function X(-) through $Y = a0 + j\ X(t)fo(t)dt + e$. Here, a_0 was the intercept, T was the domain of X(-), f_0(-) was an unknown slope function, and e was a centered Chl-*a*, unmixed, *S. damnosum* s.l. habitat, noise, random variable. The domain T was assumed to be a compact subset of a Euclidean space. Our goal was to estimate a_0 and f_0(-), as well as to retrieve $m(X) := «0 + f\ X(t)fo(t)dt$, based on the unmixed empirical dataset of the hyperproductive, *S. damnosum* s.l., larval habitat, Chl-*a,* orthogonally decomposed, 5m, RapidEye^{TM}, transmittance emissivity training data (x_1,y_1), ...,(x_n,y_n) consisting of n independent copies of (X, Y). We assumed that the slope function fi_0 resided in a reproducing kernel Hilbert space (RKHS) H, a subspace of the collection of square integrable functions on T.

We let *X* be an arbitrary set and *H* a Hilbert space of real-valued datset of unmixed, Chl-*a* frcationalized, canopy, endmember, immature, capture point, habitat functions on *X* in ArcGIS. The evaluation functional over the Hilbert space of functions *H* was a linear functional that evaluated each function at a sample eco-georeferenceable, immature habitat, capture point [i.e., *x*, $L_x : f \mapsto f(x)\ \forall f \in H$]. We say that *H* is a reproducing kernel Hilbert space if L_x is a continuous function for any f in H or, equivalently, if L_x is a bounded operator, so that for any $f$in H there exists some $M > 0$ such that $L_x[f] = f(x) \leq M\|f\|_H\ \forall f \in H$. [142]. A more intuitive definition of the space in our model was then obtained by the evaluation functional measured, spatially quantitated of the real-valued, iteratively interpolated, Chl-*a*, habitat, LULC endmembers, which in our model were represented by taking the inner product of f in ArcGIS with a function K_x in *H*. This function was the reproducing kernel for the Hilbert space *H*. More formally, the Riesz representation theorem implied that for all *x* in *X* there exists a unique element K_x of *H* with the reproducing property, $f(x) = L_x(f) = \langle f,\ K_x \rangle\ \ \forall f \in H$. in the unmixed RapidEye^{TM}, 5m, endmember model.

Riesz representation theorem establishes an important connection between a Hilbert space and its (continuous) dual space. If the underlying field is of real numbers, (e.g., optimally parameterizable, covariate estimators of hyperproductive, sparsely shaded, trailing vegetation, *S. damnosum* s.l. canopied, turbid water, decomposed, paramterizable estimators) the two are isometrically isomorphic; if the underlying field is of complex numbers, the two are isometrically anti-isomorphic. Let *H* be a Hilbert space, and let *H** denote its dual space, consisting of all continuous,explicative, linear functionals from *H* into the field R or C in a metaheuristically optimizable dataset of explanative, eco-georeferenceable, hyperproductive, capture point, trailing vegetation, discontinuously canopied, sparsely shaded, *S. damnosum* s.l. habitats. If *x* is an element of *H*, then the function φ_x, for all *y* in *H* defined by $\varphi_x(y) = \langle y, x \rangle$, where $\langle \cdot, \cdot \rangle$ denoted the inner product of the Hilbert space, is an element of *H** [152]. The Riesz representation theorem states that every element of *H** can be written uniquely in this form.

The immature habitat, *S. damnosum* s.l., vulnearbility, forecast, risk mapping Φ: $H \rightarrow H^*$ was defined by $\Phi(x) = \varphi_x$, which was an isometric (anti-) isomorphism, meaning that Φ was bijective. The norms of *x* and φx were optimally quantitated employing $\|x\| = \|\Phi(x)\|$ in

ArcGIS Spatial Analyst™. Φ is additive: $\Phi(x_1 + x_2) = \Phi(x_1) + \Phi(x_2)$ [142]. If the base field is R, then $\Phi(\lambda x) = \lambda\Phi(x)$ for all iteratively interpolatable, geo-spectrotemporally parameterizable or non-parameterizable, field or remote, empirically regressable, uncoalesced, wavelength, frequency-oriented, covariate estimators for distinguishing unknown habitats employing the iteratively interpolated, Chl-*a,* unmixed, wavelength, 5m, RapidEye™, transmittance emissivities [23, 24]. An inverse map of Φ which was then described as follows. Given a non-zero element $\varphi$of H^*, the orthogonal complement of the kernel of $\varphi$was a one-dimensional subspace of H. We arbitarily took a non-zero element z in that subspace, and set $x = \overline{\varphi(z)} \cdot z/\|z\|^2$. In doing so, $\Phi(x) = \varphi$.

Since K_x was itself a function in H in the unmixed, Chl-*a,* habitat interpolator, we then had an x in X $K_y(x) = \langle K_y,\ K_x\rangle_H$. This allowed us to define the reproducing kernel of H in ArcGIS as a real-valued Chl-*a,* unmixed, *S. damnosum* s.l. habitat, proxy biosignature, endmember function $K : X \times X \to \mathbb{R}byK(x, y) = \langle K_x,\ K_y\rangle_H$. From this definition it was easy to see that a function $K : X \times X \to \mathbb{R}$ was a reproducing kernel in the 5m, RapidEye™, unmixed, vulnerability risk model, since it was both symmetric and positive definite, [i.e. $\sum_{i,j=1}^{n} c_i c_j K(x_i, x_j) \geq 0$]. As such, any unknown habitat could be geolocated employing the Chl-*a,* unmixed, interpolated, 5m, RapidEye™, wavelength, transmittance emissivities.

As observed in earlier studies [161], eigenstructures play prominent roles in determining the nature of the estimation challenge in functional linear regression. Importantly, K was the reproducing kernel of H_1 in the seasonal, hyperproductive habitat, unmixed, 5m, wavelength, emissivity, transmittance, eco-epidemiological, risk model, which was continuous and square integrable. This logic followed from Mercer's theorem [198] where K admitted the following spectral/spatial endmember decomposition: *K(s,t)=J2Pkfk(s)fk(t).* Thus, suppose K is a continuous symmetric non-negative definite kernel constructed from a metaheursitically optimizable, geo-spectrotemporally, uncoalesced, eco-georeferenceable, trailing vegetation, discontinuously canopied, hyperproductive, *S. damnosum* s.l. habitats . Then there is an orthonormal basis $\{e_i\}_i$ of $L^2[a, b]$ consisting of eigenfunctions of T_K such that the corresponding sequence of eigenvalues $\{\lambda_i\}_i$ is nonnegative. In mathematics, particularly linear algebra, an orthonormal basis for an inner product space V with finite dimension is a basis for V whose vectors are orthonormal, that is, they are all unit vectors and orthogonal to each other. An inner product naturally induces an associated norm, thus an inner product space is also a normed vector space. A complete space with an inner product is called a Hilbert space[24]. Inner product spaces over the field of complex numbers are sometimes referred to as unitary spaces The eigenfunctions corresponding to non-zero eigenvalues are continuous on $[a, b]$ and K has the representation $K(s,t) = \sum_{j=1}^{\infty} \lambda_j\, e_j(s)\, e_j(t)$ where the convergence is absolute and uniform. In mathematics, specifically functional analysis, Mercer's theorem is a representation of a symmetric positive-definite function on a square as a sum of a convergent sequence of product functions [24].

In the unmixed, Chl-*a*, endmember, habitat, eco-epidemiological, reflectance model residuals $p_1 > p_2 >$••• were the eigenvalues of K, and {^1,^2,...}. The corresponding eigenfunctions were described as Kfk = Pkfk in ArcGIS. Moreover, {fi,fj)c2 = Sij and {^i,^j)K = Sijlpj occurred when Sij was the Kronecker's delta. In mathematics, the Kronecker delta, or Kronecker's delta, n is a function of two variables, usually just positive integers. The function is 1 if the variables are equal, and 0 otherwise: $\delta_{ij} = \begin{cases} 0 & \text{if } i \neq j, \\ 1 & \text{if } i = j. \end{cases}$ Where the Kronecker delta δij is a piecewise function of variables *i* and *j* [142]. We found that the field–verified, Chl-*a* retrieval algorithm residual forecasts had a RSME of less than 11%.

The largest contributors to the errors in the unmixed, *S. damnosum* s.l. habitat, remote sensing subsurface, Rapid Eye ™ reflectance, endmember, wavelength emissivities over the intervention, agro-village study site turbid water, river were likely the atmospheric correction procedures, either by complex aerosol composition in prolific habitat areas, sun glint, and/or the adjacency effect at the spectra intervention village sites. Because aerosol, cross-section, moderate resolution, fractionalized, endmember eigenvector derivatives have a weak spectral shape, the errors introduced by the atmospheric correction can show up as biases within a weak spectral shape in the surface RapidEye™ 5m, resolution, sensor, sub-mixel reflectance spectra [199]. To be less vulnerable to these sorts of errors when remotely targeting, hyperproductive, capture point, *S. damnsoum* s.l. habitats employing a RapidEye™, unmixed, Chl-*a,* retrieval algorithm, it may be more strategic to employ a χ^2 merit function based on the squared difference in consecutive 5m bands between 400nm to 700 nm. Unfortunately, errors introduced by atmospheric correction algorithms in ArcGIS can be systematic and may not be wavelength independent. As such, common least-square fitting may not result in an metaheursitically optimal, robust, sub-mixel estimation of iteratively interpolatable concentrations of Chl-*a*. This issue cannot be solved as long as the exact error distributions, including the covariance coefficients between wavelength bands, are not remotely rectified.

Roughly speaking, a covariance operator C in the Chl-*a*, explanative, *S. damnosum* s.l., hyperproductive capture point, endmember, eigenvector habitat, interpolator satisfied the Sacks-Ylvisaker conditions of order 0, since it was twice differentiable when s = t, but not differentiable when s was not t. A covariance operator C can satisfy the Sacks-Ylvisaker conditions of order r for an integer r > 0, if $d^{2r}C(s, t)/(ds^r dt^r)$ satisfies the Sacks-Ylvisaker conditions of order 0 [142]. The covariance operator C satisfied the Sacks-Ylvisaker conditions in the RapidEye™, Chl-*a*, habitat, NDVI, interpolative, 5m, resolution, proxy, geoclassifiable, LULC biosignature, risk model, since C satisfied the Sacks-Ylvisaker conditions of order r for some r > 0.

Various examples of quantification of covariance functions in SAS/GIS literature are known to satisfy Sacks-Ylvisaker conditions. In Jacob et al. [127] the Ornstein-Uhlenbeck covariance function C(s, t) = exp(-\s — t\) satisfied the Sacks-Ylvisaker conditions of a first order autocorrelation in an endemic, unmixed, wavelength, emissivity, transmittance, *S. damnosum* s.l. habitat, forecasting, eco-epidemiological, risk model. An Ornstein–Uhlenbeck process x_t satisfied the following stochastic differential equation: $dx_t = \theta(\mu - x_t)\,dt + \sigma\,dW_t$. Thereafter, where $\theta > 0$, μ and $\sigma > 0$ were parameters and W_t denoted the Wiener process.

The Ornstein–Uhlenbeck process is a prototype of a noisy relaxation process. Consider for example a discontinuously canopied, seasonally hyperproductive, eco-georeferenceable, trailing vegetation, turbid water *S. damnosum* s.l., eco-epidemiological, forecast Rapid Eye 5m ™ geo-spectrotemporally geosampled, discontinuously canopied, immature habitat with constant $k$whose dynamics are highly overdamped with friction coefficient γ. In the presence of thermal seasonal fluctuations with temperature T, the length $x(t)$of the sparsely shaded canopy will fluctuate stochastically in length x_0. Thus its stochastic dynamics may be described by an Ornstein–Uhlenbeck process with:

$$\theta = k/\gamma,$$
$$\mu = x_0,$$
$$\sigma = \sqrt{2k_BT/\gamma},$$

where $\sigma$is derived from the Stokes–Einstein equation $D = \sigma^2/2 = k_BT/\gamma$for the effective diffusion constant.In physical sciences, the stochastic differential equation of an Ornstein–Uhlenbeck process is rewritten as a Langevin equation$\gamma\dot{x}(t) = -k(x(t) - x_0) + \xi(t)$where $\xi(t)$is white Gaussian noise with $\langle \xi(t_1)\xi(t_2)\rangle = 2k_BT/\gamma\,\delta(t_1 - t_2)$[34].

Principal sources of Gaussian noise in digital images arise during acquisition (e.g. sensor noise caused by poor illumination and/or high temperature, and/or transmission e.g. electronic circuit noise[22]. In discontinuously canopied, seasonal trailing vegetation, turbid water, eco-georeferenceable, turbid water, African, agro-village complex, eco-epidemiological, narrow, riverine tributary capture point, *S. damnosum* s.l., habitat, endmember, moderate resolution, digital image processing, Gaussian noise can be reduced employing an ArcGIS spatial filter to avoid an undesirable outcome (i.e., blurring of fine-scaled predicted hyperproductive habitats), when smoothing a Rapid Eye ™ image.

In image processing, a Gaussian blur is the result of blurring of an image by a Gaussian function. It is a widely used effect in ArcGIS graphics software, typically to reduce image noise and reduce detail. The visual effect of this blurring technique is a smooth blur resembling that of viewing the image through a translucent screen, distinctly different from the bokeh effect produced by an out-of-focus lens or the shadow of an object under usual illumination. In photography, bokeh is the aesthetic quality of the blur produced in the out-of-focus parts of an image produced by a lens[23]. Gaussian smoothing is also used as a pre-processing stage in computer vision algorithms in ArcGIS in order to enhance image structures at different scales—see scale space representation and scale space implementation.

The Gaussian smoothing operator is a 2-D convolution operator that is used to `blur' images and remove detail and noise. In this sense it is similar to the mean filter, but it uses a different kernel that represents the shape of a Gaussian (`bell-shaped') hump. Convolution is a simple mathematical operation which is fundamental to many common image processing operators(www.esri.com). Convolution provides a way of `multiplying together' two arrays of numbers, generally of different sizes, but of the same dimensionality, to produce a third array of numbers of the same dimensionality[24].. This can be used in image processing to implement operators whose output pixel values are simple linear combinations of certain input pixel values in a S. damnosum s.l. moderate resolution, hypeproductive, capture point,

eco-georferenceable image. The Gaussian distribution in 1-D has the form: $G(x) = \frac{1}{\sqrt{2\pi}\sigma} e^{-\frac{x^2}{2\sigma^2}}$

In 2-D, an isotropic (*i.e.* circularly symmetric) Gaussian has the form: $G(x,y) = \frac{1}{2\pi\sigma^2} e^{-\frac{x^2+y^2}{2\sigma^2}}$ [26]. The idea of Gaussian smoothing in a S. damnosum s.l. forecasting vulnerability, probabilistic paradigm is to use this 2-D distribution as a `point-spread' function, and this is achieved by convolution. Since the eco-georferenced *S. damnosum* s.l. trailing vegetation, narrow, African riverine tributary agro-village habitat image would be stored as a collection of discrete pixels, a medical entomologist or experimenter may need to produce a discrete approximation to the Gaussian function before he or she can perform the convolution. In theory, the Gaussian distribution is non-zero everywhere, which would require an infinitely large convolution kernel, but in practice it is effectively zero more than about three standard deviations from the mean, which may be truncated by the kernel at this point(e.g., eco-georferenced prolific seasaonl sampled point). Once a suitable kernel in the habitat model, has been calculated, then the Gaussian smoothing can be performed using standard convolution methods in ArcGIS. The convolution can in fact be performed fairly quickly since the equation for the 2-D isotropic Gaussian is separable into *x* and *y* components. Thus the 2-D convolution can be performed by first convolving with a 1-D Gaussian in the *x* direction, in an S. damsnoum s.l. model and then convolving with another 1-D Gaussian in the *y* direction.

Mathematically, applying a Gaussian blur to an eco-georeferenceable, discontinuously canopied, trailing vegetation, turbid water, turbid water, African, agro-village complex, eco-epidemiological, narrow, riverine tributary, capture point, *S. damnosum* s.l., habitat, image is the same as convolving the image with a Gaussian function. This is also known as a two-dimensional Weierstrass transform. By contrast, convolving by a circle (i.e., a circular box blur) would more accurately reproduce the bokeh effect (see Figure 74). Since the Fourier transform of a Gaussian is another Gaussian, applying a Gaussian blur has the effect of reducing the image's high-frequency components; a Gaussian blur is thus a low pass filter

Figure 74. The effects of a small and a large Gaussian blur on a hypothetical, discontinuously canopied, trailing vegetation, turbid water, hypeporductive, *S. damnsoum* s.l. immature habitat , capture point within a buffered 5m Rapid Eye ™ scene

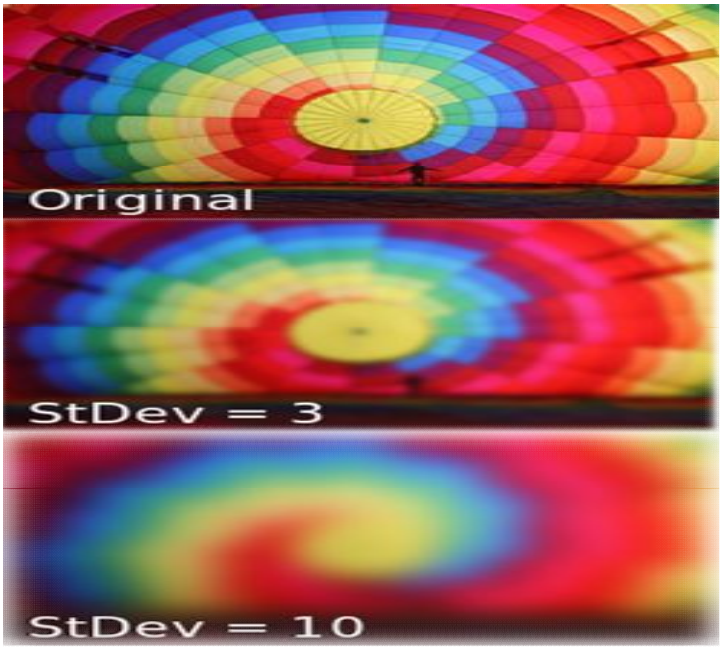

The Gaussian blur is a type of image-blurring filter in ArcGIS that uses a Gaussian function (which also expresses the normal distribution) for calculating the transformation to apply to each mixel in the image[24]. As mentioned, equation of a Gaussian function in one dimension is $G(x) = \frac{1}{\sqrt{2\pi\sigma^2}} e^{-\frac{x^2}{2\sigma^2}}$ in two dimensions, it is the product of two such Gaussians, one in each dimension: $G(x,y) = \frac{1}{2\pi\sigma^2} e^{-\frac{x^2+y^2}{2\sigma^2}}$ where x is the distance from the origin in the horizontal axis, y is the distance from the origin in the vertical axis, and σ is the standard deviation of the Gaussian distribution. When applied in two dimensions in a endmber eigenvector, Rapid Eye ™ seasonal hypeproductive, trailing vegetation, discontinuously canopied,turbid water, eco-georefernceable, eco-epidemiological, capture point, *S. damnsoum* s.l., immature habitat site. This formula produces a surface whose contours are concentric circles with a Gaussian distribution from a narrow, riverine tributary, geo-spectrotemporal, geospatial, agro-village, complex, African riverine geosampled center point. Values from this distribution may be used to build a convolution matrix in ArcGIS which may be applicable to the original image.

In ArcGIS convolution is given two three-by-three matrices, one a kernel, and the other an image piece.This convolution can multiply geo-locationaly similar entries and sum them:[e.g.,

$$\begin{bmatrix} a & b & c \\ d & e & f \\ g & h & i \end{bmatrix} * \begin{bmatrix} 1 & 2 & 3 \\ 4 & 5 & 6 \\ 7 & 8 & 9 \end{bmatrix} = (1*i)+(2*h)+(3*g)+(4*f)+(5*e)+(6*d)+(7*c)+(8*b)+(9*a)$$

].The explicatively orthogonally decomposable, explanatively geoclassifiable, Rapid Eye ™

seasonal hypeproductive, trailing vegetation, discontinuously canopied,turbid water, eco-georefernceable, eco-epidemiological, capture point, *S. damnsoum* s.l., immature habitat, geo-spatilaized elucidative values of a given 5m mixel in the output image may be then calculated by multiplying each tabulated kernel value in AcGIS by the corresponding input image mixel values. This can be described algorithmically using multiple different pseudo-codes in ArcGIS. In so doing, each trailing vegetation, discontinuously canopied, turbid water, eco-georefernceable, eco-epidemiological, capture point, *S. damnsoum* s.l., immature habitat site, geo-spectrotemporally extracted 5m mixel's in ArcGIS may be set to a weighted average of that mixel's neighborhood. The original habitat mixel's value will receive the heaviest weight (i.e., having the highest Gaussian endmember fractionalized, eigenvector value) whilest the neighboring mixels will receive smaller weights as their distance to the original mixel increases. This results redered from a quantizable Rapid Eye ™ 5m, eco-epidemiologically forecasted,eco-georefernceable, hyperproductive explanatively orthogonally decomposed, capture point, *S. damnsoum* s.l., immature habitat uniform blurring filter algorithm is a fractionalized, endmember that preserves boundaries and edges better.

In mathematics, the Wiener process is a continuous-time stochastic process[24]. It is often called standard Brownian motion, It is one of the best known Lévy processes (i.e., càdlàg stochastic processes with stationary independent increments) and occurs frequently in pure and applied mathematics, economics, quantitative finance, and physics. In pure mathematics, the Wiener process gave rise to the study of continuous time martingales. It is a key process in terms of which more complicated stochastic processes can be described. As such, it plays a vital role in stochastic calculus, diffusion processes and even potential theory. It is the driving process of Schramm–Loewner evolution.

In probability theory, the Schramm–Loewner evolution with parameter κ, also known as stochastic LoewnIn er evolution (SLE_κ), is a family of random planar curves that have been proven to be the scaling limit of a variety of two-dimensional lattice models in statistical mechanics. Given a parameter κ and a domain in the complex plane U, it gives a family of random curves in U, with κ controlling how much the curve turns. There are two main variants of SLE, chordal SLE which gives a family of random curves from two fixed boundary points, and radial SLE, which renders a family of random curves from a fixed boundary point to a fixed interior point. These curves are defined to satisfy conformal invariance and a domain Markov property

A sensible way to introduce the Markov property is through a sequence of random variables Z i Zi , which can take one of two values from the set {1,−1} {1,−1} . This is known as a coin toss. We can calculate the expectations of Z in Rapid Eye ™ 5m, eco-epidemiologically forecasted, ecogeorefernceable, hyperproductive, explanatively orthogonally decomposed, capture point, trailing vegetation, turbid water, *S. damnosum* s.l., narrow tributray, immature habitat employing a Zi :E(Z i)=0,E(Z 2 i)=1,E(Z i Z k)=0 E(Zi)=0,E(Zi2)=1,E(ZiZk)=0. The key point is that the expectation of Z i Zi has no dependence on any previous values within the sequence. Quantitating the partial sums of the geo-spectrotemporally geosampled, agro-village, narrow, riverine tributary eco-georferenceable immature habitats random variables will denote by S i Si :S i =∑ k=1 i Z i Si=∑k=1iZi

The expectations of the partial sums can then be inserted into a forecasting vulnerability eco-epidemiological, model, using the linearity of the expectation operator:E(S i)=0,E(S 2 i)=E(Z 2 1 +2Z 1 Z 2 +...)=i E(Si)=0,E(Si2)=E(Z12+2Z1Z2+...)=I in ArcGIS. Once again, there is no dependence on the expectation of S i Si based on any previous value within the sequence of the tabulated partial sums. This model may be extended to optimally quantitate conditional expectation in a dataset of geo-spectrotemporally geospatialized 5m, Rapid Eye ™ uncoalesced, unbiased estimators. Conditional expectation is the expectation of a random variable with respect to some conditional probability distribution[24]. Hence, an entomologist may qualitatively quantiate whethere if i=4 i=4 is geospatially feasiable in space in a *S. damnosum* s.l. capture point hyperproductive, hyperendemic ,African, riverine foci, eco-epidemiological, eco-georefernceabl, narrow riverine, tributar, risk map based on the mean for the expectation of as E(S 5 |Z 1 ,Z 2 ,Z 3 ,Z 4)=S 4 E(S5|Z1,Z2,Z3,Z4)=S4 in ArcGIS.In so doing, the expected value of S i (i.e., Markov Property) would be accommodatable in a second-order autocorrelation ESF for quantitating, probablistic sub-mixel uncertainities.

ESF methodology utilized the explanatively orthogonally decomposed, Rapid Eye ™ 5m, eco-epidemiologically forecasted, ecogeorefernceable, hyperproductive capture point, *S. damnosum* s.l., immature habitat eigenvectors to account for spatial autocorrelation by adding a linear combination of these. InArcGIS, the ESF model specification was written as Y = Xβ+EkβE+ε, where X is an n-by-(p+1) matrix containing p trailing vegation, discontinuously canopied, sparsely shaded, uncoalesced, covariate 5m coefficients (including a vector of 1s for the intercept term), β is the corresponding (p + 1)-by-1 vector of regression parameters, Ek was an n-by-K matrix containing K eigenvectors, βE was the corresponding vector of regression parameters,and ε ∼ N 0, Iσ2□

The linear combination of the 5m.endmember *S. damnosum* s.l. eigenvectors, EkβE, accounted for spatial autocorrelation in the geo-spectrotemrpoally geosampled regressed dataset. The ESF linear regression specification in ArcGIS did not suffer from excessive endmmeber spatially autocorrelated residuals.An ESF model specification was implemented by identifying a feasible set of 5m endmember eigenvectors. The identification was achieved through a two-stage process. In the first stage, a candidate set of 5m eigenvectors, was quantitated revealing a noticeably smaller subset (i.e., K ≪ n) of the entire set of n. Fractionalized habitat eigenvectors, constructed by eliminating eigenvectors that generally did not account for significantspatial autocorrelation. These included endmember eigenvectors portraying negligible (i.e., near zero) spatial autocorrelation (i.e., their moran coeffinet values are close to the expected value for zero spatial autocorrelation) and eigenvectors portraying negative spatial autocorrelation when positive spatial autocorrelation was addressed or eigenvectors portraying positive spatial autocorrelation when negative spatial autocorrelation was addressed. The overwhelming number of empirically, explanatively, orthogonally decomposed, Rapid Eye ™ 5m, eco-epidemiologically forecasted, ecogeorefernceable, hyperproductive, capture point, discontinuously canopied, *S. damnosum* s.l., immature habitat, eigenvectors endmember contained positive spatial autocorrelation. One criterion for identifying this candidate set was employing a threshold minimum MC of 0.25 in ArcHIS , which was related to roughly 5% of the variance in a response variable being attributable to positive spatial autocorrelation.

In applied mathematics, the Wiener process is used to represent the integral of a white noise Gaussian process, and so may be useful as a model of noise in instrument errors in

filtering theory and unknown forces in control theory. The Wiener process is a continuous-time stochastic process $W(t)$ for $t \geq 0$ with $W(0) = 0$ and such that the increment $W(t) - W(s)$ is Gaussian with mean 0 and variance $t - s$ for any $0 \leq s < t$, and increments for nonoverlapping time intervals are independent[5]. Brownian motion (i.e., random walk with random step sizes) is the most common example of a Wiener process.The Wiener process W_t is characterized by three properties: 1) $W_0 = 0$, 2) the function $t \to W_t$ is almost surely everywhere continuous, and 3) W_t has independent increments with $W_t - W_s \sim N(0, t-s)$ (for $0 \leq s < t$), where $N(\mu, \sigma^2)$ denotes the normal distribution with expected value μ and variance σ^2. The last condition means that if $0 \leq s_1 < t_1 \leq s_2 < t_2$, then $W_{t1} - W_{s1}$ and $W_{t2} - W_{s2}$ are independent random variables, and the similar condition holds for n increments (see Figure 75)

Let A be an event related to the Wiener process (more formally: a set, of *S. damnosum* s.l. capture point, endmeber 5m measurables with respect to the Wiener measure, in the space of functions), and X_t the conditional probability of A given the Wiener process on the time interval $[0, t]$ (more formally: the Wiener measure of the set of trajectories whose concatenation with the given partial trajectory on $[0, t]$ belongs to A)[5] Then the process X_t is a continuous martingale. In probability theory, a martingale is a sequence of random variables (i.e., a stochastic process) for which, at a particular time in the realized sequence, the expectation of the next value in the sequence is equal to the present observed value even given knowledge of all prior observed values[17].A martingale X is called continuous if almost surely, the function t ↦⟶ X(t) is continuous[151].

A Matlab programs to calculate a realization of a Wiener process in a trailing vegetation, Precambrian rock , *S. damnosum* s.l., model may be written as:

```
%BPATH1  Brownian path simulation

randn('state',100)            % set the state of randn
T = 1; N = 500; dt = T/N;
dW = zeros(1,N);              % preallocate arrays ...
W = zeros(1,N);               % for efficiency

dW(1) = sqrt(dt)*randn;       % first approximation outside the
loop ...
W(1) = dW(1);                 % since W(0) = 0 is not allowed
for j = 2:N
   dW(j) = sqrt(dt)*randn;    % general increment
   W(j) = W(j-1) + dW(j);
end

plot([0:dt:T],[0,W],'r-')     % plot W against t
xlabel('t','FontSize',16)
ylabel('W(t)','FontSize',16,'Rotation',0)
```

Figure 75 Typical paths of a Wiener process for a hypothetical Rapid Eye ™ 5m, eco-epidemiologically forecasted, ecogeorefernceable, hyperproductive explanatively orthogonally decomposed, capture point, *S. damnsoum* s.l., immature habitat

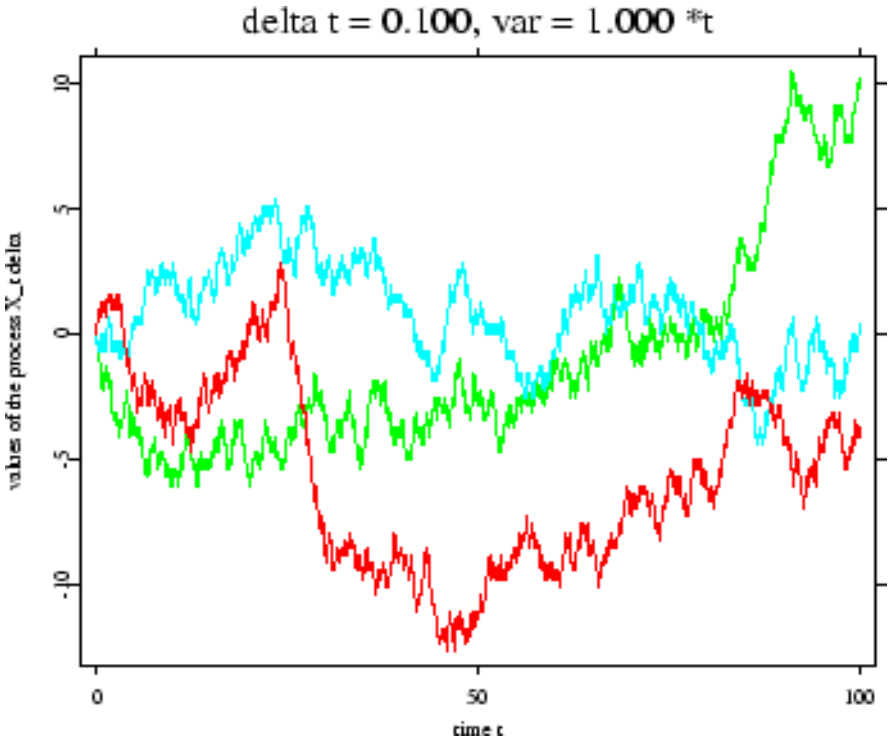

In the seasonally explanative, hyperproductive habitat, eco-epidemiological, risk model, covariance was a measure of how much two decomposable, geo-classifiable LULC variables change together. In the model residuals of the covariance function describe the spatial covariance of the variable process or field. For a random field or stochastic process $Z(x)$ on a domain D, a covariance function $C(x, y)$ gives the covariance of the values of the random field at the two geolocations x and y: $C(x,y) := \operatorname{cov}(Z(x), Z(y))$. We also employed $C(x, y)$ as an autocovariance function in two instances: in time series (to denote exactly the same, except that x and y to refer to habitat geolocations in time and space), and in multivariate random fields to refer to the covariance of two habitat variables (percent of sparsely shaded, canopied, trailing vegetation) with itself, as opposed to the cross covariance between two different variables (percent of man-made barriers and levels of turbidity) at different habitats.

Note that the two sets of eigenfunctions $\{f\backslash,f_2,..-\}$ $\{f\backslash,f_2,...\}$ were also generated in ArcGIS/SAS, which differed from each other in the Chl-*a*, decomposition, NDVI, 5m, biosignature endmember, risk-related model, residual, non-optimizable dataset. The two kernels K and C, however, were simultaneously diagonalized. To avoid ambiguity, we assumed that Cf = 0 for any dependent variable output H_0 and f = 0 in the forecasted output. When using the squared error loss, there is a necessary condition to ensure that $El_n(q)$ is uniquely minimized, even if i is known to come from the finite-dimensional space H_0 [142]. Under this assumption, we defined a norm $\| \blacksquare \|_R$ in H in the Chl-*a* –endmember, interpolator as $||R = (Cf,f)_{C2} + J(f) = f(s)C(s,t)f(t)dsdt + J(f)$. Note that $\| \blacksquare \|_R$ was a norm in the model output as ||R was defined as a quadratic and was zero if and only if f = 0. The following

proposition then revealed that when this condition holds, || ■ ||$_R$ in the endemic, 5m, wavelength, emissivity, RapidEye^{TM} transmittance, decomposed, habitat, iterative interpolator was well defined on H and equivalent to its original norm, || ■ |H.

Further, there existed constants 0< c_1 < c_2 <t, such that c_1|f ||$_R$<!f |H < c_2|f ||$_R$ for all f e H in the endmember habitat interpolator. Thus, if Cf = 0 for any f e H_0 and f = 0 in the interpolator, then || ■ ||$_R$and || ■ ||h were equivalent. We let R be the reproducing kernel associated with || ■ ||$_R$ in the model. Recall that R in the interpolator was viewed as a positive operator. We then denoted {(p'$_k$,f_k): k > 1}, since we were able to successfully remotely quantitate the eigenvalues and eigenfunctions of R. R was then a linear map from L_2 to L_2, such that ^{R}fk = $f^{R(;t)f(t)dt}$ = p'k+'k. The square root of the positive definite, non-linear operator was therefore given as the predictive, Chl-*a*, endmember, hyperproductive, habitat risk map from L_2 to L_2, such that $R^{1/2}$fk = P)$^{1/2}$fk, k = 1, 2,....n. We then let v_1> v_2> ■ ■ ■ be the eigenvalues of the bounded linear operator, where $R^{1/2}CR^{1/2}$ and {Z_k: k = 1, 2,...}, which was then deemed to be the corresponding orthogonal eigenfunctions in L_2. We wrote M_k = v-$^{1/2}R^{1/2}Z_k$, k = 1,2 in ArcGIS. We also let (■ , ■)$_R$ be the inner product associated with || - ||$_R$, that is, for any f, g e H,*(f,g)R = 1 (Ilf + gllR-!f - guR)*. It was not hard to see that *(Mj,Mk)r = v-$^{l/2}$v-$^{l/2}$(R$^{1/2}$Zj,R$^{1/2}$Zk)r = v-^{l}(Zj,Zk)L2 = v-^{l}jk* and *(C $^{1/2}$Mj.C$^{1/2}$M$_t$)L2* = vj''\''^{2}\{C '^{2}R'/^{2}(„C''^{2}R''^{2}Zk)C2 = vj''^{2}v-''^{2}(R$^{1/2}$CR''^{2}Zj,Zk)L2 in the model, forecasted, residual dataset.

The unmixed, Chl-*a*, endmember, *S. damnosum* s.l. habitat, iterative interpolator (x,y) employed the arguments of a bivariate function. Other examples of T in the model included T = {1, 2,...,p} for some positive integer p, and unit sphere in an Euclidean space, among others. The readers are referred to Wahba [154] for common choices of H and J in these as well as other contexts.

Other than the methods of regularization, a number of alternative, parameterizable, covariate, moderate resolution, 5m, RapidEye^{TM}, endmember, decomposed, immature habitat,fractionalized, biosignature, interpolative estimators have been introduced in recent years for the functional linear regression [160, 161, 200, 201, 202, 203, 204, 205, 206, 207]. Most of the existing methods are based upon the functional, principal component analysis (FPCA). The success of these approaches has hinged on the availability of a good estimate of the functional principal components for X(-). In contrast, our smoothness regularized estimator avoided this task and therefore circumvented any assumptions on the spacing of the Chl-a, habitat, tabulated eigenvalues rendered from the covariance operator for X(-), as well as Fourier coefficients of *i*. Commonly, eigenstrucures need to be quantitated in geospace for employing FPCA-based approaches [142]. Further, in our 5m, endmember, emissivity, sub-mixel, radiance absorption analysis, the regularized Chl-*a*, unmixed, NDVI, biosignature, habitat, iteratively interpolative, emissivity transmittance, parameterizable, covariate estimator did not rely on estimating the functional principle components with respect to the eigenfunctions, since stronger results on the convergence rates were obtained.

Despite the generality of the method of regularization, the Chl-*a* unmixed, NDVI biosignature, iteratively interpolated, trailing vegetation, turbid water, covariate, endmember estimators were efficiently tabulated in ArcGIS/SAS. We demonstrated that the minimization with respect to f in a Chl-*a* unmixed, endmember geospectral/geospatial interpolator may be taken over by an infinite-dimensional space in ENVI, which may then be further exploited in ArcGIS. The geolocations of unknown habitats were actually found in a finite-dimensional

subspace. This procedure enabled us to take advantage of the existing techniques and algorithms in the ArcGIS geodatabase for smoothing splines to compute f_{nl}, ini and a_{nl}.

The representer theorem made the regularized the unmixed, habitat, endmember, wavelength, transmittance, covariate interpolative estimators easy to implement in ArcGIS. Several efficient algorithms are available in the literature that can be employed for seasonal implementation of a Slash and Clear strategy, which may be to illustrate the merits of the method as well as demonstrate the operational developments of a Chl-*a,* unmixed, interpolated, seasonally hyperproductive, *S. damnosum* s.l., habitat, forecasting, eco-epidemiology, vulnerability, risk model. Proofs may be relegated to quantitate the geosampled habitat regressor for theoretical models.

This Slash and Clear approach revealed high efficacy in controlling the younger stages of *Simulium* flies. In Ayago and Laminlatoo Villages, fly density was relatively the same from the beginning of monitoring to the final day of monitoring, with some small fluctuations likely due to mild weather changes. In Goncogo and Adibuk Villages, fly density was relatively constant from the beginning of the monitoring up to the 13th day, and then gradually began reducing up to the last day. This is possibly due to the "Slashing and Clearing" of the potential breeding sites of the flies, which was performed in two cycles. The first cycle took place on the 8th and 9th day, and the second cycle on the 19th and the 20th day of the exercise.

In Gonycogo and Ayago villages, there was a fly density decrease of 52%, while in Adibuk and Laminlatoo villages, there was a fly density decrease of 66% after intervention. This rendered an overall percentage efficiency of 60% within a period of 31 days. When continuously carried out, onchocerciasis disease transmission can be interrupted within two years employing the Slash and Clear program around rivers such as Ayago and its neighbors, where trailing vegetation is responsible for attachment and survival of *S. damnosum* younger stages.

There is a generic innovative algorithm for remote sensing of narrow tributary African, turbid water, riverine waters that can manage a large range of concentrations of Chl-*a*, CDOM, and their inherent optical properties. The algorithm is based on the exact solutions of the HYDROLIGHT numerical radiative transfer model to support retrieval in optically complex riverine waters with varying, sensor, wide, swath, viewing geometry. The algorithm may efficiently estimate the concentrations of canopy Chl-*a* in a hyperproductive, *S. damnosum* s.l., larval habitat in an African, riverine environment by minimizing the difference between observed and modeled, RapidEye^{TM}derivative, endmember, derivative, reflectance spectra. The use of a look-up table and polynomial interpolation greatly reduces computation time, allowing operational and near-real time processing of large sets of satellite imagery [23]. Because the RapidEye^{TM} reflectance was geospectrally tabulated as a function of in-water light absorption and scattering, rather than actual constituents concentrations, the algorithm can be applied with any definition of the specific inherent optical properties of Chl-*a* and CDOM. A statistical measure for the goodness-of-fit and the formal standard errors in the optimally fitted eco-georferenceable, immature, hyperproductive habitat Chl-*a* quantitated concentrations may be provided in ArcGIS, thus producing error-free, vulnerability, wavelength, transmittance, emissivity, 5m, eco-epidemiological, risk maps with each thematic image generated employing innovative unmixing algorithms. The performance of the algorithm may be optimally demonstrated for multispectral wavelength, 5m, Red Edge transmittance, emissivity observations rendered from a riverine, narrow tributary, agro-

village complex, hyperproductive, *Simulium* immature habitat employing CDOM from riverine influx in ArcGIS. The standard errors of estimated Chl-*a* concentrations may range between 0.5 and 3 (mg m^{-3}), for example, for mean seasonal concentrations between 2 and 20 (mg m^{-3}) for a RapidEye ^{TM} 5m imaged, hyperproductive, *S. damnosum* s.l. habitat, which would be quite acceptable for quantitating optically complex catchment riverine, geomorphologic ecohydrologic, ecogeographic, seasonal geoclassified, LULC, biophysical, Chl-*a*, wavelength, emissivity, decomposed regressors.

This HYDROLIGHT numerical radiative transfer model may discriminate sparsely shaded, canopy, fractionalized, endmember constituents of a habitat by (i) the highly turbid waters surrounding the habitat, (ii) suspended sediments, and (iii) colored dissolved organic matter. The concentrations of the latter may be denoted by ρchl-*a* and ρCDOM. Note that ρCDOM in HYDROLIGHT-oriented, RapidEye^{TM} imaged, *S. damnosum* s.l. larval habitat, NDVI-related, geo-spectrotemporal biosignature, eco-epidemiological, unmixing, risk model may be expressed as the absorption at 440 nm. The scattering phase functions in the forward radiative transfer model may be a uniform scattering function for turbid riverine waters, and for canopied suspended particles at the geosampled ,hyperproductive,immature habitat, agro-village, stusy sites.

The RapidEye^{TM}, Chl-*a* retrieval algorithm in ArcGIS can be applied to geolocate any unknown habitat in any highly turbid, riverine water, discontinuously canopied ecosystem if the appropriate regional optical environmental descriptors (e.g., geocoordinates of 5m, gridded, intervention village centroids) for the area of interest is available in ArcGIS. The flexible and transparent calibration opens the possibility of regional processing of eco-georeferenceable, individual African riverine, agro-village systems with tailored, optical, RapidEye^{TM} cost effective, 5m models for seasonally implementing a “Slash and Clear” habitat removal teachnique. Preferably, geo-spectrotemporally analyzing the sub-mixel, reflectance variation of the endmember optical properties over a geospatial explanative, cluster of hyperproductive habitats will help underpin the applicability of the vulnerability, eco-epidemiological, risk model. The determination of a relevant scattering phase function of suspended canopy particles, such as an explanatively, orthogonally decomposed, Chl-*a,* iteratively interpolated, RapidEye^{TM}, derived 5m, parameterizable or non-parameterizable covariate estimator, wavelength, transmittance, forecast-oriented, emissivity, model would be optimal.

As expected, the eco-epidemiological risk model results using the RapidEye ^{TM} 5m, iteratively interpolated, endmember, Chl-*a,* unmixed data was accurate in eco-cartographically representing the in-situ geoclassified,partially discontinuously canopied, 5m, LULC data. The sources of errors for the Chl-*a*, forecasting, emissivity model may have been related to field measurement procedures. Field measurements of the above-surface, remote sensing, endmember reflectance of our eco-epidemiological point of interest (i.e., hyperproductive larval habitat) was made several days prior to the immature habitat sampling frame, leading to a delay between optical and chemical measurements. The model was built using a dataset of simulated empirical results in ArcGIS rendered from a vulnerability decomposable, explanative, stochastic interpolator. Although the input parameters for Chl-*a* and CDOM were specific for the Ayago river, spatial and temporal differences in IOPs may be expected. For example, the Chl-*a* specific absorption, unmixed Red Edge, 5m resolution, parameterizable wavelength, transmittance, frequency-oriented, covariate, endmember emissivities may be expected to vary when investigating *Simulium*

species in relation to differences in seasonal, iteratively interpolated canopy pigment concentrations. In addition, the standard atmospheric parameters (e.g., solar zenith angle) did not completely capture the variability of actual within canopy conditions of the georeferenced, RapidEye^{TM}, 5m, imaged, hyperproductive habitat. Variations in the solar zenith angle influence apparent optical properties [208].

While the importance of solar zenith angle is less evident in turbid, riverine water with respect to immature *Simulium* productivity, some errors can be associated with the use of these standard covariate estimators [22, 45]. For example, errors associated wtih the actual field and riverine, LULC, topographied data frames, especially during seasonal flooding, may create misspecifications in diagnostic frequency distribution, particularly from risk model, residual, normalized, endmember outputs in ENVI. Therefore, temporal and ecogeographical differences in real and model IOPs may affect the remote targeting of hyperproductive, *S. damnosum* s.l. larval habitats.

The robustness of the Soil Adjusted Vegetaion Index (SAVI) may be evaluated employing ground/riverine–based LAI 5m, RapidEye^{TM} measurements for remotely regressively, targeting hyperproductive habitats. A transformation technique may be presented to minimize soil brightness influences from spectral canopied vegetation indices involving red and near-infrared (NIR) wavelengths. Graphically, the transformation involves shifting the origin of reflectance spectra plotted in NIR-red wavelength space to account for quantitating first-order soil-vegetation interactions and differential red and NIR flux extinction through sparsely shaded, discontinuous vegetated canopies. This method may also be performed by iteratively decomposed, RapidEye^{TM} data within a PROSPECT and/or SAIL couple radiative transfer model.

Among all the codes published during the last two decades [209], the SAIL canopy bidirectional reflectance, eco-epidemiological risk model and the PROSPECT leaf optical properties model are the most popular. An analysis based on the ISI (Institute of Science Information) Web of Science finds a total of 113 articles using PROSPECT, and 105 articles using SAIL that have been published since 1992, showing parallel evolution of the models. They score 1675 and 1783 citations both with an h-index (i.e., number of papers h with at least h citations each) between 23 and 24. PROSPECT combined with SAIL are used in 29 articles with 513 citations leading to 18 citations per article, slightly higher than PROSPECT (15) and SAIL(16) separately. This confirms the importance of these two models in the remote scientific community and their close relations. Linking these models with RapidEye^{TM} data in ArcGIS may allow description of both the spectral and directional variation of an empirical dataset of unmixed, trailing vegetation, discontinuous canopied, turbiod water, seasonally hypeporductive, *S. damnosum* s.l. eco-epidemiological, eco-georeferenceable, capture point, agro-village, complex ecosystem, immature habitat, reflectance indices as a function of leaf biochemistry — mainly Chl-*a* ,water, and dry matter contents — and canopy architecture — primarily LAI, leaf angle distribution, and relative leaf size.

The effects of atmospheric corrections and scales may be then investigated for all operational, hyperproductive, geo-spectrotemporally, geospatially uncoalesced, *S. damnosum* s.l., larval habitats Rapid Eye ^{TM} 5m LAI retrieval methods in ArcGIS for implementing Slash and Clear methods seasonally. The SDVI may remotely geolocate suitable geoclassifed LULC (e.g., trailing canopied vegetation) for large scale LAI inversion due to the sensitivity to scale and atmospheric effects in these geolocations (e.g., pre-flooded, meandering, highly turbid, African riverine narrow agro-village tributaries). The SDVI is virtually and

atmospherically invariant [23]. The proposed method may be validated with experimental, field-sampled, iteratively quantitatively interpolated, 5m, RapidEye^{TM}, immature, count data.

Interestingly, the main RedEdge NDVI reflectance, spectral difference along the canopy gradient in the riverine, narrow tributary immature habitat, hypeproductive, capture point, eco-geographic geolocation was the percentage cover of sedge and standing dead vegetation, geoclassfied LULC. Unmixed, immature habitat, endmember reflectance, derivative, forecast spectra within the sparsely shaded sedges were up to 30 cm long and revealed RapidEye^{TM} NIR reflectance plateaus with stronger slopes between the beginning and end of the NIR reflectance plateau. The standing dead material within the immature habitat canopy led to an increase in the reflectance in the 5m, red, sub-mixel, wavelength region probably due to reduced Chl-*a* absorption at specific sparsely shaded, immature habitat, riverine sites.

As such, the Chl-*a,* Red Edge, hyperproductive habitat, Chl-a endmember unmixed contents may be estimated employing the green chlorophyll index, and a RapidEye^{TM}, terrestrial, Chl index which may provide accurate,parameterizable, covariate wavelength, transmittance, frequency-oriented, emissivitiy estimators of seasonally hyperproductive, immature, canopied habitats. Bands of RapidEye^{TM} in the green and Red Edge are well positioned for deriving these indices in ArcGIS. Results may confirm the particular importance of the 5m data for precise wavelength, estimator regressive quantification of unmixed, biosignature, emissivity, transmittance variables as it would provide access to green and RedEdge waveband data information. Importantly, non-destructive Chl-*a* content retrieved from a RapidEye^{TM} 5m imaged, larval habitat scene may localize red absorption bands delineating where canopy absorption saturates at low to moderate Chl-*a* values in the immature habitat canopy. This way, canopy relationships between N and Chl-*a* contents at the leaf level may also be quantitated and interpolated. Decomposed spectral ranges in the green and the Red Edge regions may allow accurate estimation of N and Chl-*a* contents in an *S. damnosum* s.l. habitat over a wide range of sparsely shaded, canopied, riverine LAI values.

Soil vegetation indexes are relatively insensitive to ecosystems with the low biomass characteristic of semi-arid systems (between 0 and 60 megagrams carbon per hectare [ha]), because of systems' low leaf biomass and discontinuous canopies [23]. Estimates of dry plant residues at a seasonally hyperproductive, *S. damnosum* s.l. habitat, employing the Red Edge RapidEye ^{TM}, 5m spectrum may help surmount these difficulties. Although arid and semi-arid African riverine ecosystems do not sequester large masses of carbon, and have low fluxes on a per-area basis, these ecosystems are the most abundant terrestrial landscapes, and are also highly sensitive to climate perturbations. Thus, any explanatively iteratively quantitatively interpolatable, decomposable, Red Edge, NDVI RapidEye^{TM}, discontinuously canopied, geo-spectrotemporal biosignature focusing on carbon fluctuations may remotely target hyperproductive larval habitats and their photosynthetic and NPV seasonal, 5m, LULC reflectance, transmittance , frequency-oriented, emissivity parameterized covariate estimators with higher efficiency than a non-carbon, NDVI, proxy biosignature.

The Phong reflection model may be also constructed to remotely quantitate RapidEye^{TM} 5m reflectance of emissivity transmittance to identify the intensity of the specular highlights in a geosampled habitat, which may be optimally calculated as: $k_{\text{spec}} = \|R\|\|V\|\cos^n\beta = (\hat{R}\cdot\hat{V})^n$, where R is the mirror reflection of the light, larval habitat, canopy surface and V is the viewpoint vector. In the Blinn-Phong model the intensity of a highlighted riverine, larval habitat, canopy geolocation may be optimally calculated as:

$k_{spec} = \|N\|\|H\|\cos^n \beta = (\hat{N} \cdot \hat{H})^n$, where N is the smooth surface normal and H is the half-angle direction (i.e., the direction vector midway between L, the vector to the light, and V, the viewpoint vector). The number n is called the Phong exponent; this is a user-chosen value that controls the apparent smoothness of the surface [23]. These equations may optimistically regressively quantitate the distribution of microfacet normals which may find that a elucidatively decomposable Red Edge, NDVI, iteratively interpolated biosignature of a larval habitat may follow an approximate Gaussian distribution (for large n), or an approximate Pearson type II distribution, when optimally quantizing corresponding RapidEye^{TM}, 5m, illumination angles in a seasonally hypeporductive, eco-georferenceable, eco-epidemiological, capture point, trailing vegation, turbid water, discontinuously canopied, hyppeorductive, *S. damnosum* s.l., immature habitat discontinuous, canopy geolocations.

Developing and implementing streamlined data collection aggregation and reporting methodologies, employing a RapidEye^{TM}, 5m, PDA-ArcGIS-DGPS cyberenvironment can provide detailed, real-time eco-georeferenceable, eco-cartographic information on a eco-epidemiological, capture point, hyperproductive habitat, explanatively , orthogonally decomposed, Chl-a, endmember eigenvector information for remotely targeting prolific sample sites, which can lower overall treatment costs. A bidirectional RapidEye^{TM}, 5m, PDA-ArcGIS-DGPS, web-based, reporting system using a broadband satellite access point and the internet can provide efficient and timely amounts of relevant, field-level, geoclassifiable, LULC, habitat information. This is important, as hyperproductive habitat treatment and management information has the most value when it is quick, clear, easy to understand, and relevant to decisions that need to be made immediately. An adaptable modular information surveillance system in the cyber-infrastructure can help ensure that the right decisions are made to reduce parasites and vectors in African riverine environments. This system can support dissemination of information such as spatially summarized, iteratively interpolated, endmember, Chl-*a,* forecast data, for optimizing seasonal field activities and treatment costs as they are compiled to provide an expedited understanding of how much is being spent in removing and clearing prolific habitats, and to determine whether the intended outcomes (i.e., lowering of adult catches in intervention villages) are being realized. This will allow both field managers and health ministries timely and vital information to make accurate field operational adjustments and maintain the most efficient and economically feasible pressure on hyperproductive habitat populations in African riverine agro-village ecosystems. Once patterns and correlations of RapidEye^{TM} imaged habitats are elucidated by imaged, Chl-*a,* sub-mixel, data feature attributes, field management practices can be modified to optimize targeting and removal of these habitats yielding lower overall costs, and minimizing environmental impacts.

In addition, a RapidEye^{TM}, PDA-GIS-DGPS-RS, web-based reporting system can provide a module that is dedicated to measuring the economic status of the riverine community and clusters of communities, in order to monitor and measure the impacts of onchocerciasis and the economic benefits of implementing a “Slash and Clear” larval control intervention. These optimizations are a critical factor for onchcerciasis eradication in African narrow tributary African riverine communities. Globally accessible, RapidEye^{TM}, 5m, PDA-ArcGIS-DGPS- cyber-infrastructural web-based, constructed, capture point, ecogeoreferenceable, explanative seasonally discontinuously canopied, trailing vegetation, hyperproductive, *S. damnosum* s.l. immature habitat, endmember, eco-epidemiological forecast vulnerability maps that are generated from near real-time field data updates in ArcGIS, can be incorporated into other bioecological datasets for fast and timely analyses. Although this project did not fully utilize web-based data dissemination techniques, the

capability is there using the same off-the-shelf technologies employed for onchocerciasis-related, seasonal field studies. The logical extension of this field research is to continue to expand the use of mobile field data collection and wireless communication technologies in a RapidEye™, 5m resolution, PDA-ArcGIS-DGPS-RS cyberenvironment to provide a single, seamless and cost-effective, information clearing house for implementing "Slash and Clear" in African endemic riverine, narrow riverine, tributary environments. Such a system can leverage ArcGIS, Chl-*a*, vulnerabilty risk mapping functionality, wireless communications and web-based publications. This study provides an important starting point for the creation of standardized techniques for mobile field data collection, global data transmission, data aggregation and display, and analyses of multivariate, cost-effective, RapidEye™, *S. damnosum* s.l. habitat, eco-epidemiological, orthogonally decomposed, wavelength, transmittance, emissivity, 5m, models within a robust cyberenvironment. The standardization of a logical geodatabase design for implementing "Slash and Clear" will ultimately support linkage with other geo-databases, statistical packages, and software applications. The RapidEye™, 5m, PDA-ArcGIS-DGPS architecture deployed in our study site, intervention agro-villages is the first step in seamlessly sharing geosampled, hyper/hypo-productive, habitat data between end users, including field teams, project managers and other collaborating researchers. The envisioned web application of this technology would enable the sourcing and integration of immature geo-spectrotemrporally geospatialized, geospatial, immature, Rapid Eye ™ 5m, immature *S. damnosum* s.l. habitat data, supporting the creation of new datasets, and the coordinated delivery of focused decision-supported information for generating reports, charts, maps, tables, using common data exchange formats (e.g., Excel, PowerPoint, SAS).

Additionally, revisal software can also be installed in the RapidEye™, 5m, PDA-GIS-DGPS cyberenvironment, which can create seasonally explanative, hyperproductive, immature trailing vegetation, discontinuously canopied, sparsely shaded, eco-epidemiological, capture point, turbid water, hyperproductive *S. damnosum* s.l. habitat, eco-epidemiological risk maps from spreadsheet or database data to be integrated with data from weather and other African riverine-based scientific studies (i.e. Virtual Earth™). The initial deployment of the custom application described here can ensure rapid deployment and proper site configuration needed to support local decision-making for optimally implementing "Slash and Clear" control efforts. A web-based shared geodatabase project RapidEye™, PDA-GIS-DGPS-RS cyberenvironment can combine a variety of field and remote, high density, eco-georeferenced, black fly foci on elucidatively geoclassified, 5m, LULCs and relevant programmatic information to facilitate evidence-based decision-making for "Slash and Clear" larval control operations in real-time or near real-time.

Finally, employing endmember, forecasting, real-time or near real time, cost-effective, RapidEye™, data feature attributes acquired through a PDA-ArcGIS-DGPS surveillance system can simulate onchocerciasis disease transmission based on postively autocorrelated, eco-georferenceable, seasonally hyperproductive, discontinuously canopied, sparsely shaded, turbid water, *S. damnosusm* s.l., immature, agro-village complex, African. Narrow riverine tributary, stratified habitats on geoclassified LULCs (e.g., trailing vegetation). For instance, Markov simulation, hyperproductive habitat, forecast vulnerability, risk models created in Bayesian paradigms in PROC MCMC can be facilated as part of the end-user repository dataset in the RapidEye™, PDA-ArcGIS-DGPS cyberenvironment. Error propagation in these non-linear, algorithmic, residual model forecasts can also be quantifed employing an autocovartiate, probabilistic, endmember, uncertainty, diagnostic, regression, covariance matrix. According to Jacob et al. [22], a hierachical, Bayesian, generalizable,

covariance matrix can be employed to adjust heteroskedastistic and multicolinear endmember variables in ecogeographical space.

The first prototype implementation of the Jave virtual machine done at Sun Microsystems Inc., emulated the Jave virtual machine instruction set in software by a handheld device that resembled a contemporary PDA. As such, accurate *S. damnosum* s.l. habitat, eco-epidemiological, forecast vulnerability modeling within an autocorrelation weighted uncertainty-oriented, matrix in ArcGIS or AUTOREG can define and quantitate a set of iterated, riverine, seasonal interactions that may affect immature productivty in these habitats. These habitat, forecasting, remotely decomposed, sub-mixel, Chl-*a* models in a robust RapidEye™, PDA-ArcGIS-DGPS architecture can seasonally analyze and display data for predicting eco-georferenceable, seasonally hyperproductive, immature habitat geolocations for testing as well as improve research hypotheses. These models can also provide information about realistic sampling grid, Chl-*a* endmember, covariate parameterized, decomposed, 5m, wavelength, emissivities that are involved in high larval/pupal population levels and other transmission dynamics from simple, transparent simulated representations.

Geostatistical models of trailing vegetation, hyperproductive, *S. damnosum s.l.* habitats derived from RapidEye™, 5m PDA-GIS-DGPS-RS data cannot replace mentally intuitive intervention techniques, but models can expand into more formal and quantitative realms in which field decomposed, endmember components and their sub-mixel, environmental interactions within geosampled, hyperproductive habitats are made more specific which can help reduce the overall cost of implementing “Slash and Clear” in African, riverine environments. Geographic information science for seasonal onchocerciasis, forecastable, unmixed, endmember NDVI biosignature, interpolations in a RapidEye™, 5m, PDA-ArcGIS-DGPS cyberinfrastructure are dynamic and allow for continuous innovation (e.g., high turbidity, meandering, riverine tributaries). In remote sensing, increasing use of RapidEye™, 5m, time-series dependent data present both opportunities (e.g., improved characterization of riverine LULC) and challenges (e.g., handling large data volumes; image understanding) for data fusion and integrated data analysis. Enhancements in remote internet, wireless and satellite communications, and innovations in in-situ RapidEye™, 5m sensors, for PDA-GIS-DGPS-RS cyber-infrastructures are paving the way for increasingly robust “real time” applications of remote sensing and ArcGIS, (i.e. telegeoprocessing) for accurate seasonal, onchocercisis, predictive, endmember, risk mapping. Web-based tools, such as Google Earth (http://earth.google.com/) and Internet Map Service (IMS) applications, may now provide increasingly larger audience of research collaborators with ready access to onchocerciasis data from RapidEye™, 5m PDA-GIS-DGPS cyber-environments while allowing elementary integration of unmixed endmember interpolated Chl-*a* imagery and graphics in PDAs.

Since the parameterized, covariate, wavelength, hyperproductive, *S. damnosum* s.l. larval habitat estimators held, every ket $|\psi\rangle$ had a corresponding bra $\langle\psi|$, and the correspondence was unambiguous. Rigged Hilbert space mathematics, a rigged Hilbert space (Gelfand triple, nested Hilbert space, equipped Hilbert space) may be a designed in ArcGIS to link the distribution and square-integrable aspects of functional endmember wavelength, unmixed, larval habitat, RapidEye™ 5m, vulnerability risk analysis. In mathematics, a square-integrable function, also called a quadratically integrable function, is a real- or complex-valued measurable function for which the integral of the square of the absolute value is finite.

Thus, if $\int_{-\infty}^{\infty} |f(x)|^2 dx < \infty$, in a Ch-*a*, eco-epidemiological, RapidEye™, risk model, then *f* is square integrable on the real line $(-\infty, +\infty)$. One may also speak of quadratic integrability over bounded intervals such as [0, 1] [24]. Such spaces may be introduced to study spectral theoretical applications for seasonally targeting habitats based on immature productivity count data in the broad sense.

In mathematics, spectral theory is an inclusive term for theories extending the eigenvector and eigenvalue theory of a single square matrix to a much broader theory of the structure of operators in a variety of mathematical spaces [24]. It is a result of studies of linear algebra and the solutions of systems of linear equations and their generalizations. The theory is connected to that of analytic functions because the spectral properties of an operator are related to analytic functions of the spectral parameter. Hilbert's adoption of the term "spectrum" has been attributed to an 1897 paper of Wilhelm Wirtinger on Hill differential equation (by Jean Dieudonné), and it was taken up by his students during the first decade of the twentieth century, among them Erhard Schmidt and Hermann Weyl. The conceptual basis for Hilbert space was developed from Hilbert's ideas by Erhard Schmidt and Frigyes Riesz. About twenty years later, when quantum mechanics was formulated in terms of the Schrödinger equation, the connection was made to atomic spectra. A connection with the mathematical physics of vibration had been suspected before, as remarked by Henri Poincaré, but rejected for simple quantitative reasons, absent an explanation of the Balmer series. The later discovery in quantum mechanics that spectral theory could explain features of atomic spectra was therefore fortuitous, rather than being an object of Hilbert's spectral theory.

Consider a bounded linear transformation *T* defined everywhere over a general Banach space in an interpolative, ArcGIS derived, forecasting vulnerablity, decomposing, RapidEye™, 5m, endmember, risk model . An ecologist, entomologist or researcher may employ the transformation $R_\zeta = (\zeta I - T)^{-1}$. when iteratively interpolating a fractionalizable, explanative hyperproductive habitat. In the forecasting risk model, *I* can optimally be the identity operator and ζ a complex number. The inverse of an operator *T* that is T^{-1} may then be eco-cartographically defined by $TT^{-1} = T^{-1}T = I$. This way, the resolvent set of *T* would be the set of all complex covariate coefficient values ζ such that R_ζ exists and is bounded. This set may be denoted as *ρ(T)* in ArcGIS. The spectrum of *T* then would be the set of all geosampled *S. damnosum* s.l.riverine habitat, sub-mixel, moderate resolution, fractionalized, data, feature attributes ζ such that R_ζ fails to exist or is unbounded. Often the spectrum of *T* is denoted by *σ(T)* [24]. The function R_ζ for all ζ in *ρ(T)* (that is, wherever R_ζ exists as a bounded operator) in the risk model would then be called the resolvent of *T* . The spectrum of T thus would be the complement of the resolvent set of T in the complex ArcGIS delineated Euclidean plane. As such, every tabulated eigenvalue rendered from an eigenfunction decomposition algorithm in ArcGIS would belong to *σ(T)* even though the dataset may contain non-eigenvalues. The Banach space in a Chl-*a*, vulnerability, spatial filter orthogonal risk model may reveal topological vector spaces in ArcGIS. On the other hand, Banach spaces that include Hilbert spaces similar to those that we employed in ArcGIS for identifyning unknown, hyperproductive *S. damnsoum* s.l. larval habitats would have lower root mean square error in forecasts rendered from a weighted algorithmic matrix. With suitable restrictions (CI 95%) the endmember structure of a decomposed RapidEye™ biosignature may reveal spectra of optimal log-transformability in a regression equation (e.g., Poisson probability model). Fortunately, if any violations occur in the model assumptions (variance not equal to the mean) due to excess overdispersion, which

may be attributable to outliers [45], then a negative binomial paradigm with a non-homogenous mean be alternatively utilized to compensate for the over–Poissonian varition. The key assumption is negative binomial regression is that the standard deviation is equal to the mean [24].

Interestingly, the immature habitat, fractionalized Rapid Eye™ 5m, endmember iterative interpolative, sub-mixel output from a negative binomial regression framework in ArcGIS may then be exported into SAS (e.g., AUTOREG). Clustering tendencies of endmember autocorrelated decomposed, fractionalized, interpolative RapidEye ™ 5m wavelength, transmittance emissivites can then be stratified and delineated using Pearson Moments correlation products such as Morans' *I*.

By spatially amalgamating the "bound state" (e.g., trailing vegetation eigenvector) and a discontinuous, unmixed, decomposable canopied, 5, discontinuous spectrum, a more robust (low root mean square error) weighted interpolator may render optimal eco-epidemiological, risk maps in ArcGIS. The spectrum of a linearizable operator T that functions on a Banach space within an ArcGIS-derived, seasonally hyperproductive, trailing vegation, turbid water, discontinuoulsy canopied, eco-epidemiological, eco-georeferenceable, *S. damnosoum* s.l. habitat in a forecasting, decomposable, dataset of geo-spectrotemporally uncoalesced, RapidEye™ 5m, wavelength, transmittance emissivity, forecast vulnerability model may consist of all scalars such that the operator $T - \lambda$ does not have a bounded inverse on X. The λ immature habitat canopy Chl-*a* spectrum may have to be decomposed in ArcGIS/ENVI employing a standard decomposition into three parts: 1) a point spectrum, consisting of the eigenvalues of T, 2) a continuous spectrum, consisting of the scalars that are not eigenvalues but make the range of $T - \lambda$ a proper dense subset of the space, and 3) a residual spectrum, consisting of all other scalars in the spectrum. This decomposition exercise may be relevant to the study of differential equations in an ArcGIS cyberenvironment for remotely targeting hyperproductive *S. damnosum* s.l. habitats seasonally.

Let X be a Banach space, $L(X)$ the family of bounded operators on X, and $T \in L(X)$. By definition, a complex number λ is in the spectrum of T, denoted $\sigma(T)$, if $T - \lambda$ does not have an inverse in $L(X)$. If $T - \lambda$ is one-to-one, then its inverse is bounded. This follows directly from the open mapping theorem of functional analysis. So, λ in the spectrum of T in an eco-epidemiological, Rapid Eye 5m trailing vegetaion, turbid water, discontinuoulsy canopied, hyppeorductive, capture point, geo-spectrotemporally geospatially *S. damnosum* s.l. forecasting, eco-epidemiological, risk model would be robustifiable, if and only if $T - \lambda$. These three separate cases may be descibed in ArcGIS, especially when $T - \lambda$ is not injective (that is, there exist two distinct elements x,y in X such that $(T - \lambda)(x) = (T - \lambda)(y)$). Then, $z = x - y$ in the risk model would be a non-zero vector such that $T(z) = \lambda z$. In other words, λ would be an eigenvalue (e.g., trailing vegetation) of T. In this case, λ would be said to be in the point spectrum of T, denoted $\sigma_p(T)$. Secondly, $T - \lambda$ would be injective, and its range would be a dense subset R of X, but not based on the whole of X. In other words, there would exist some element x in X such that $(T - \lambda)(y)$ may be as close to x as desired, with y in X, but would be never equal to x. It can be proved that $T - \lambda$ is not bounded below (i.e. it depicts far apart uncoalesced, partially canopied, decomposed, explicative, Euclidean elements of X too close together)in regression space.

Equivalently, the inverse linear operator $(T - \lambda)^{-1}$ may be defined in ArcGIS on the dense subset R, which is not a bounded operator, and therefore cannot be extended to the whole of X. Thus, λ would be said to be in the continuous spectrum $\sigma_c(T)$ of T. Finally $T - \lambda$

would be injective in the forecast vulnerability model but the residuals would not have a dense range. That is, there would be some element x in X (e.g., sparsely shaded, turbid water, trailing vegetation, sub-mixel regressor) geo-spectrotemporally uncoalesced, hyppeorductive, eco-epidemiological, capture point, immature *S. damnosum* s.l. habitat in an African riverine, agro-ecosystem ,village complex N of x, such that $(T-\lambda)$, where (y) is never in N. In this case, a Chl-a map $(T-\lambda)\, x \to x$ may be bounded or unbounded in ArcGIS, but may not admit a unique extension to a bounded linear map on all of X. Then λ may be in the residual spectrum of T, $\sigma_r(T)$. So $\sigma(T)$ is the disjoint union of these three sets $\sigma(T) = \sigma_p(T) \cup \sigma_c(T) \cup \sigma_r(T)$. In a spectrum of a dual operator, if X^* is the dual space of X, and $T^* : X^* \to X^*$ is the transpose operator of T, then $\sigma(T) = \sigma(T^*)$ for a bounded operator T, $\sigma_r(T) \subset \sigma_p(T^*) \subset \sigma_r(T) \cup \sigma_p(T)$ [24]. The notation $\langle \cdot, \varphi \rangle$ may denote an element of X^*,(i.e. $x \to \langle x, \varphi \rangle$) which may be the action of a bounded linear functional φ in a robust endmember dataset of RapidEye ™ , orthogonally decomposed, iteratively interpolative, discontinuously canopied, trailing vegetation , turbid water uncoalesced, 5m, wavelength, transmittance frequency-orinted, emissivities. Let $\lambda \in \sigma_r(T)$. So $Ran(T - \lambda)$ is not dense in X. By the Hahn–Banach theorem there exists a non-zero $\varphi \in X^*$ that vanishes on $Ran(T - \lambda)$ [24].

In Calculus Methode/Map Server ™ a Green's function (see Appendix 7) is the impulse response of an inhomogeneous differential equation defined on a domain, with specified initial conditions or boundary conditions. Through the superposition principle for linear operator problems, the convolution of a Green's function with an arbitrary function $f(x)$ on that domain may be the solution to the inhomogeneous differential geospectrotemrpoally uncoalesced, hyperproductive, turbid water, discontinuously canopied, sparsely shaded, capture point equation for $f(x)$. In other words, given a linear ODE, L(solution) = source, an ecologist, entomologist or othe researcher can first solve L(green) = δ_s, for each s, in a forecasting paridigm. Realizing that, since the source is a sum of delta functions in a *S. damnosum* s.l. model, the solution may be a sum of Green's functions by linearity of L. .Linear differential equations are differential equations having solutions which can be added together in particular linear combinations to form further solutions. In mathematics, the Dirac delta function, or δ function, is a generalized function, or distribution, on the real number line that is zero everywhere except at zero, with an integral of one over the entire real line They can be ordinary (ODEs) or partial (PDEs). The solutions to (homogeneous) linear differential equations form a vector space (unlike non-linear differential equations) may reveal unknown, un-geosampled seasoanl *S. damnsoum* s.l. immature habitat, capture points. If a differential operator L admits a set of eigenvectors $\Psi_n(x)$ (i.e., a set of functions Ψ_n and scalars λ_n such that $L\Psi_n = \lambda_n \Psi_n$) in a robustifiable, uncoalesced, moderate resolution, trailing vegation, turbid water, discontinuous , *S. damnosum* s.l. model that is complete, then it may be possible to construct a Green's function from orthogonalized spatial filter eigenvectors and eigenvalues.

Through the superposition principle for linear operator problems, the convolution of a Green's function for a trailing vegetation, Precambrian rock seasonal hypeproductive, *S.damnosum* s.l. capture point with an arbitrary function $f(x)$ on that domain would be the solution to a inhomogeneous differential equation for $f(x)$. In other words, given a linear ordinary differential equation (ODE), L(solution) = source, a medical entomologist or onchocerciasis researcher can first solve L(green) = δ_s, for each s, for realizing that, since the source is a sum of delta functions in the entomological model the solution would be a sum of Green's functions based on the linearity of L.

GANSO is a programming library which implements several methods of global and nonsmooth, nonlinear optimization. GANSO library is specifically designed to solve optimization problems with a very complex, nondifferentiable objective function. It is not designed for solving linear, quadratic or integer programming problems, for which many specialised methods are currently available in ArcGIS GANSO may provides a computationally efficient way to tackle these complicated problems in moderate resolution, fractionalized, endmber eigenvector, probability uncertainties by plotting them in ArcGIS. We discuss the implementation of a number of modern methods of global and nonsmoothcontinuous optimization, based on the ideas of Rubinov, in a programming library GANSO. (see Figure 76)

Figure 76 Plotting the objective function in Geospatial Analyst ™ emplolying Ganso optimization methods for quantitatively denosing *S. damnosum* s.l. moderate resolution, endmember heterokedascity

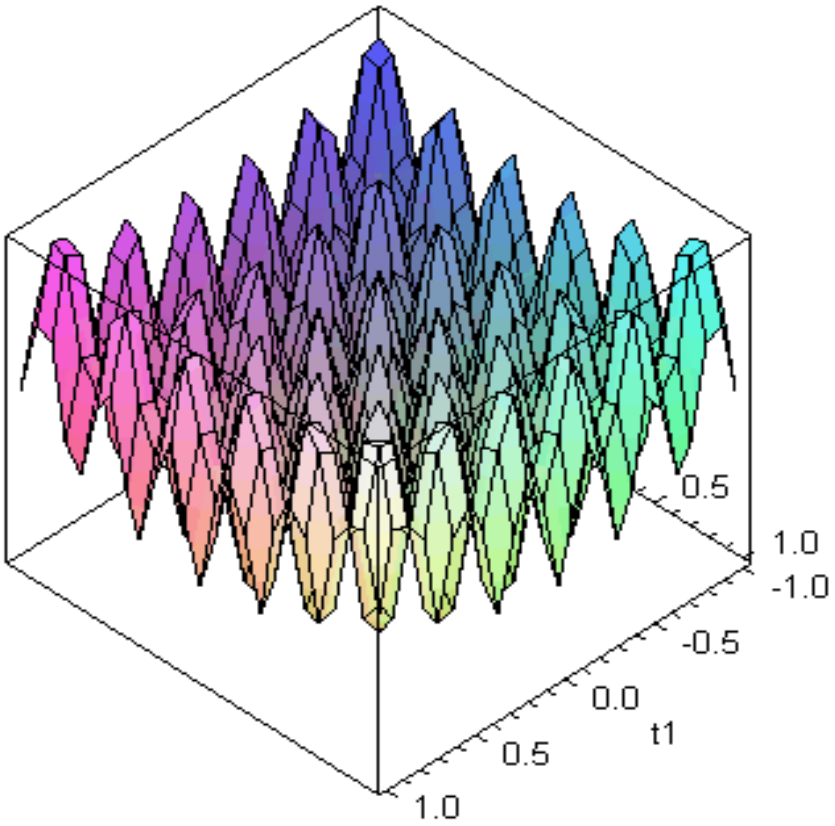

In conclusion, we constructed a RapidEye™, reflectance, wavelength, eco-epidemiological, 5m, model to to iteratively interpolate decomposed Chl-*a,* endmember emissivities for the estimation of geolocations of hyperproductive, sparsely shaded, trailing vegetation, *S. damnosum* s.l., immature habitats in four riverine, agro-village complexes in northern Uganda. To quantitate Chl-*a* in the discontinuously canopied, larval habitat, narrow tributary riverine, turbid waters we used a one kilometer gridded buffer and a variety of ArcGIS algorithms for eco-cartographically delineating properties of the sub-mixel reflectance peak near 700 nm. In our model, the RapidEye™ constellation's Red Edge band

was sensitive to leaf status and canopy structure, and contributed to LULC eco-characterization of different, Chl-*a* canopy plant cover types (e.g., trailing vegetation) of the georeferenced hyperproductive, riverine, immature habitat. These included the ratio of the reflectance peak (Rmax) to the reflectance at 670 nm (R670), and the ratio R705/R670, which were subsequently employed for remotely regressively quantitating the reflectance ratio at 692 nm and absorption and backscattering coefficients at these wavelengths to assess Chl-*a* concentrations. Four regression equations at four different RapidEye^{TM} wavelengths were used to determine Chl-*a* concentrations.The RapidEye^{TM} bands considered most sensitive to Chl-*a* were tested with the simulated decomposed, geospatially, geospectrotemporally geosampled, NDVI biosignature, eco-epidemiological, endmember, fractionalized, wavelength, 5m, emissivity transmittance dataset . Good correlations were found between Chl-*a* and the band ratio R725/R675 of the discontinuoulsy canopied, trailing vegation, immature habitat emissivities. To optimally target hyperproductive, larval, riverine habitats we used an ordinary kriging technique in ArcGIS Geospatial Analyst^{TM} to calculate the unmixed, Chl-*a,* endmember values from the residual forecasts of the bio-optical, geo-spatiotemporal, eco-epidemiological, forecasting, risk models. Combining RapidEye^{TM} data in ArcGIS and object-based technology, the radiance fractional abundances were geospectrally unmixed from the Red Edge imaged, hyperproductiuve, *S.damnosum* s.l larval, habitat canopied, NDVI biosignature, which was then decomposed in ENVI technology. Reflectance peak position shifted toward longer wavelengths with increasing Chl-*a*, from 688 nm to about 706 nm. Chl-*a* demonstrated a strong relationship to peak magnitude of the fractionalized decomposed, canopied, biosignature As the water content of leaves in vegetation canopies increased, the strength of the absorption around 1599 nm increases Absorption at 819 nm is nearly unaffected by changing water content, so it is used as the reference.

The habitat canopy, 5m, endmember, derivative, forecast spectra were incorporated as a dependent variable in a weighted interpolator in ArcGIS for eco-hydrologically predicting seasonal, hyperproductive habitats based on unmixed, Chl-a covariate coefficients, field-sampled, immature, count data. Sites targeted by the 5m signal were the chosen for habitat removal. Solving differential equations is not like solving algebraic equations. Not only are their solutions oftentimes unclear, but whether solutions are unique or exist at all are also notable subjects of interest.For first order initial value problems, gives one set of circumstances in which a solution exists. Given any ecogeorferenceable explicative point seasonally hypeproductive, trailing vegetation, turbid water, discontinuous, infrequently canopied, sparsely shaded, agro-village , narrow riverine tributary, *S. damnosum* s.l. capture point (a, b)in the xy-plane, define some rectangular region Z, such that $Z = [l, m] \times [n, p]$and $(a, b)$is in the interior of Z. If we are given a differential equation $\frac{dy}{dx} = g(x, y)$and the condition that $y = b$when $x = a$, then there is locally a solution to this problem if $g(x, y)$and $\frac{\partial g}{\partial x}$are both continuous on Z. This solution exists on some interval with its center at a. The solution may not be unique. (See Ordinary differential equation for other results.)However, this only helps us with first order initial value problems. Suppose we had a linear initial value problem of the nth order: $f_n(x)\frac{d^n y}{dx^n} + \cdots + f_1(x)\frac{dy}{dx} + f_0(x)y = g(x)$such that$y(x_0) = y_0, y'(x_0) = y_0', y''(x_0) = y_0'', \cdots$For any nonzero $f_n(x)$, if $\{f_0, f_1, \cdots\}$and $g$are continuous on some interval containing x_0, $y$is unique and exists

The ECF quantitated all endmember heteroskedastic and autocorrelation. Spatial Filtering with orthogonal eigenvectors reduces spatial misspecification endmem S. damnsoum s.l. capture point reflectance wavelength, dfrequency-orinted, transmittance emissivity errors, which increases the strength of the model fit, which increases the normality of model residuals, and can increase the homoscedasticity of model residuals. In Gonycogo the mean daily collection during the last three days of the 31 day study was 32.66, representing an 89.10% reduction in biting density from the mean collection in the baseline collection of 292.4. In contrast, the mean daily collection in the paired control village of Ayago/Nile was essentially unchanged from the baseline collection during the last three days of the study (352.7 basline versus 348.6 at the end of the study). Similar results were seen in the other village pair. Here, an 81.2% reduction in biting rate was observed in the intervention village (Adbuk), while the biting rate in the control village (Laminlato) at the end of the study was 98.1% of that seen in the baseline evaluation.These preliminary data findings suggest that "Slash and Clear," community-based interventions may prove an effective measure of reducing biting rates in communities afflicted with high vector densities. We predict that such community based vector control programs could be easily integrated into the CDTI format, and used for MDA for onchocerciasis. We further predict that such programs would be readily accepted and maintained by the communities, given the relief provided from the nuisance that high densities of the flies represent to the communities.

Acknowledgements

We would like to thank Rockford K. Jalil at the College of Public Health, University of South Florida, who helped describe the remote variables. This research was funded by the National Institute of Health Grant (Unnasch Thomas) University of South Florida.

Appendices

Appendix 1

In Jacob et al. [XX] the forecasted Bayesian asymptotic behavior of the variance was $\mathrm{Var}\,\widehat{\theta}_n$ denoted as $\sigma^2 = \sum_{i=1}^{\ell} \pi_i (\varphi_i - \theta)^2$, since $n \to \infty$. This was actually defined by $\mathbf{Z} = (\mathbf{I} - (\mathbf{P} - \Pi))^{-1}$, where $\mathbf{P}$, which was the fundamental hyperproductive, *S. damnosum* s.l., immature habitat, uncertainty-oriented, regression, probabilistic, endmember, fractionalized, RapidEye™ 5m transitional matrix of . Then $\lim_{n\to\infty} n\,\mathrm{Var}\,\widehat{\theta}_n = \sigma^2 + 2\boldsymbol{\pi}^{\top}\,\mathrm{diag}(\boldsymbol{\varphi})(\mathbf{Z} - \mathbf{I})\boldsymbol{\varphi}$. Clearly, $n^2\,\mathrm{Var}\,\widehat{\theta}_n = \mathbb{E}\left(\sum_{k=0}^{n-1}\varphi(\mathbf{X}_k)\right)^2 - \left(\sum_{k=0}^{n-1}\mathbb{E}\,\varphi(\mathbf{X}_k)\right)^2$. Thus, $n^2\,\mathrm{Var}\,\widehat{\theta}_n = \sum_{k=0}^{n-1}\mathbb{E}\,\varphi^2(\mathbf{X}_k) + 2\sum_{0\le k<k'\le n-1}\mathbb{E}\left(\varphi(\mathbf{X}_k)\varphi(\mathbf{X}_{k'})\right) - \left(\sum_{k=0}^{n-1}\mathbb{E}\,\varphi(\mathbf{X}_k)\right)^2$. This representation was then employed to show for the case $\boldsymbol{\alpha}_0 = \boldsymbol{\pi}$ in the unmixed, wavelength, transmittance, paramterized, geospectrally eco-georeferencable, signature, forecasting, endmember emissivity, risk model in PROC MCMC. Hyperproductive, immature *S. damnosum* s.l. narrow African riverine, tributary, agro-village, capture point eco-epidemiological, immature habitat *Simulium* habitats were autoregressively, remotely targeted in a riverine, agro-village complex in Chutes Dienkoa, Burkina Faso. The authors observed that

$\left(\sum_{k=0}^{n-1}\mathbf{E}\,\varphi(\mathbf{X}_k)\right)^2=(n\theta)^2$ and $\sum_{k=0}^{n-1}\mathbb{E}\,\varphi^2(\mathbf{X}_k)=n\sum_{i=1}^{\ell}\tau_i\varphi_i^2.$ could also be used interchangeably in the vulnerability, endmember, RapidEye™, 5m, forecast model to capture geo-spatiotemporality in the parameterized, covariate estimators. Further, by the stationarity of the iterative interpolative Markov chain in PROC MCMC, $\{\mathbf{X}_n\}$, $\sum_{0\le k<k'\le n-1}\mathbb{E}\left(\varphi(\mathbf{X}_k)\varphi(\mathbf{X}_{k'})\right)=\sum_{k=1}^{n-1}(n-k)\mathbb{E}\left(\varphi(\mathbf{X}_0)\varphi(\mathbf{X}_k)\right),$ was found to geo-spectrotemporally, geospatially adjust error coefficients in space and time $\mathbb{E}\left(\varphi(\mathbf{X}_0)\varphi(\mathbf{X}_k)\right)=\sum_{i=1}^{\ell}\sum_{j=1}^{\ell}\pi_i\varphi_i p_{ij}^{(k)}\varphi_j=\boldsymbol{\pi}^{\top}\operatorname{diag}(\boldsymbol{\varphi})\mathbf{P}^k\boldsymbol{\varphi}$ while $\mathbf{P}^k=\mathbf{P}^{(k)}=(p_{ij}^{(k)})$ and eco-cartographically delineated the matrix of the k-step transition probabilities.

The one-step transition probability aided the geo-predictive, narrow, African riverine, tributary, agro-village, capture point, eco-epidemiological trailing vegetation,turbid water, discontinuously infrequently canopied, *S. damnosum* s.l. habitat geo-spatiotemporal, geosampled, unmixed, canopied signature, moderate resolution, forecastable, riverine, risk model in PROC MCMC. This is the ability to quantitate the probability of transitioning from one state to another in a single step without propogational erroneous variables. The Markov chain is said to be time homogeneous if the transition probabilities from one state to another are independent of time index n $p_{ij}=Pr\{X_n=j|X_{n-1}=i\}$ [24]. As such, the transition probability matrix P in a geo-predictive, unmixed, endmember, emissivity, trailing vegetation, RapidEye™ 5m, turbid water, canopied, sparsely shaded, *S. damnosum* s.l. habitat, vulnerability, forecast, risk model, auto-probabilistic, regression-related matrix consisted of the one-step transition probabilities p_{ij}. The m-step transition probability was the probability of transitioning from state i to state j in m steps for precisely, regressively, remotely quantitating the unmixed wavelength, paramerterizable transmittance, emissivity, geo-spatiotemporally sampled, immature habitat, covariate estimators employing $p_{ij}^{(m)}=Pr\{X_{n+m}=j|X_n=i\}$. Jacob et al. [1] employed the m-step transition matrix $p_{ij}^{(m)}$ whose elements were the m-step transition probabilities, which they denoted as $P^{(m)}$ for auto-regressively, auto-probabilistically quantitating, multiple interpolatable, canopied, sparsely shaded, unmixed, hyperproductive, *S. damnosum* s.l. riverine, immature habitats. The m-step transition probabilities were found from the single-step transition probabilities in PROC MCMC. To transition from i to j in m steps, the process was first transitioned from i to r in $m-k$ steps, and then transitioned from r to j in k steps, where $0<k<m$ $p_{ij}^{(m)}=\sum_r p_{ir}^{m-k}p_{rj}^{k}$. In the matrix form, this became $P^{(m)}=P^{(m-k)}P^{(k)}$.

Setting $k = m - 1$, thereafter, yielded $P^{(m)} = P \cdot P^{(m-1)}$. From this equation J, the authors were able to conceive that: $P^{(m-1)} = P \cdot P^{(m-2)}$ in the remote, regression targeting of the hyperproductive *S. damnosum* s.l. habitats. Substituting this back into the previous equation yielded: $P^{(m)} = P \cdot P \cdot P^{(m-2)}$. Continuing these substitutions, the authors were able to compute: $P^{(m)} = P \cdot P \cdot P \cdots P = P^m$. Therefore, the m-step transition probability, uncertainty matrix was found by multiplying the single-step probability matrix by itself m times. The state vector at time m was found in terms of the transition probability matrix and the intial state vector $\Pi(0)$.Additionally, the authors observed that $\pi_j(m) = \sum_i \pi_i(m-1)p_{ij}$ occurred when the canopied, sparsely shaded, trailing vegetation, turbid water, hyperproductive, *S. damnosum* s.l. geospectral, geospatial, forecasting, eco-epidemiological, vulnerability model vector and matrix in PROC MCMC was employed. This quantitative regression equation then became $\Pi(m) - \Pi(m-1)P$. This vulnerability model output was then utililzed to remotely target, prolific, immature habitats in the Burkina Faso georeferenced, geosampled, riverine-village, agro-complex. The authors also found through substitution that the optimal geo-spatiotemporally geosampled, autoregressed, parameterized covariate, estimators were rendered by $\Pi(m-1) - \Pi(m-2)P$ or, $\Pi(m) = \Pi(m-2)P \cdot P$

The estimation, Bayesian hierarchical, probalistic regression of the unmixed, interpolative, RapidEye™ 5m, canopied, wavelength, transmittance, emissivity, sparsely shaded, hyperproductive, *S. damnosum* s.l., forecast vulnerability model, where the dependent variable to be geo-predicted, is not a single, real-valued scalar, but instead an *m*-length vector of correlated real numbers. As in the standard regression setup, there were *n* observations, where each observation *i* consisted of *k*-1 variables, grouped into a vector $\mathbf{x}_i$ of length *k*, where a dummy variable with a value of 1 has been added to allow for an intercept coefficient. This was viewed by the authors as a set of *m*-related regression problems for each geosampled, trailing vegetation-related, georeferenceable, geospectrotemporal, geospatial, infrequently, heterogeneously canopied, hyperproductive *S. damnosum* s.l. habitat observation *i*: $y_{i,1} = \mathbf{x}_i^{\mathrm{T}}\boldsymbol{\beta}_1 + \epsilon_{i,1}$ and $y_{i,m} = \mathbf{x}_i^{\mathrm{T}}\boldsymbol{\beta}_m + \epsilon_{i,m}$, where the set of probabilistic errors $\{\epsilon_{i,1}, \ldots, \epsilon_{i,m}\}$ were all correlated. Equivalently, the decomposable, hierarchical, eco-epidemiological model was viewed as a single regression problem where the outcome was a row vector $\mathbf{y}_i^{\mathrm{T}}$, where the regression coefficient vectors were stacked next to each other as follows: $\mathbf{y}_i^{\mathrm{T}} = \mathbf{x}_i^{\mathrm{T}}\mathbf{B} + \boldsymbol{\epsilon}_i^{\mathrm{T}}$. The coefficient matrix B was a $k \times m$ matrix, where the coefficient vectors $\boldsymbol{\beta}_1, \ldots, \boldsymbol{\beta}_m$ for each regression estimator were stacked horizontally [i.e., : $\mathbf{B} = \left[\begin{pmatrix}\beta_1\end{pmatrix} \cdots \begin{pmatrix}\beta_m\end{pmatrix}\right] = \left[\begin{pmatrix}\beta_{1,1}\\ \vdots \\ \beta_{k,1}\end{pmatrix} \cdots \begin{pmatrix}\beta_{1,m}\\ \vdots \\ \beta_{k,m}\end{pmatrix}\right]$]. The noise vector $\boldsymbol{\epsilon}_i$ for each geosampled, wavelength, frequency, covariate, emissivity, unmixed, RapidEye™ 5m, illuminatively parameterizable explanatory decomposable, eco-georferencable, immature habitat

observation *i* was jointly normal, so that the outcomes for a given observation were correlated: $\epsilon_i \sim N(0, \Sigma_\epsilon^2)$.

The entire regression problem was then written in a probabilsic, uncertainty matrix form as $\mathbf{Y} = \mathbf{XB} + \mathbf{E}$, in PROC MCMC, where Y and E were $n \times m$ matrices. The design matrix X was an $n \times k$ matrix with the geo-spatiotemporally, geo-spectrotemporally, unmixed habitat observations stacked vertically, as in the standard linear regression, operational setup: $\mathbf{X} - \begin{bmatrix} \mathbf{x}_1^{\mathrm{T}} \\ \mathbf{x}_2^{\mathrm{T}} \\ \vdots \\ \mathbf{x}_n^{\mathrm{T}} \end{bmatrix} - \begin{bmatrix} x_{1,1} & \cdots & x_{1,k} \\ x_{2,1} & \cdots & x_{2,k} \\ \vdots & \ddots & \vdots \\ x_{n,1} & \cdots & x_{n,k} \end{bmatrix}$. The classic, frequentist, linear least squares solution was then estimated employing the matrix of regression coefficients $\hat{\mathbf{B}}$ using the Moore-Penrose pseudoinverse: $\hat{\mathbf{B}} = (\mathbf{X}^{\mathrm{T}}\mathbf{X})^{-1}\mathbf{X}^{\mathrm{T}}\mathbf{Y}$.

In mathematics, and particularly in linear algebra, a pseudoinverse A^+ of a matrix *A* is a generalization of the inverse matrix. When referring to a matrix, the term pseudoinverse, without further specification, is often used to indicate the Moore–Penrose pseudoinverse. The term generalized inverse is sometimes used as a synonym for pseudoinverse [142]. In linear algebra, an *n*-by-*n* square matrix A is called invertible (i.e., nonsingular or nondegenerate) if there exists an *n*-by-*n* square matrix B, such that $\mathbf{AB} = \mathbf{BA} = \mathbf{I}_n$, where I_n denotes the *n*-by-*n* identity matrix, and the multiplication used is ordinary matrix multiplication [142]. Since this was the case in Jacob et al. [59] probabilistic, Bayesian, *S. damnosum* s.l. habitat, wavelength, forecastable transmittance, emissivity, unmixed, RapidEye™ 5m, vulnerability model, then the matrix B is uniquely determined by A and is called the inverse of A, denoted by A^{-1}.

A square matrix that is not invertible is called singular or degenerate [142]. A square matrix is singular if and only if its determinant is 0 [24]. Singular matrices are rare in the sense that a square matrix randomly selected from a continuous uniform distribution on its entries will almost never be singular. Non-square matrices (*m*-by-*n* matrices, for which $m \neq n$) do not have an inverse. However, in some cases such a matrix may have a left inverse or right inverse. If A is *m*-by-*n* and the rank of A is equal to *n*, then A has a left inverse: an *n*-by-*m* matrix B such that BA = I. If A has rank *m*, then it has a right inverse: an *n*-by-*m* matrix B such that AB = I. Matrix inversion is the process of finding the matrix B that satisfies the prior equation for a given invertible matrix A.

Given an $m \times n$ matrix $\mathbf{B}$, the Moore-Penrose generalized matrix inverse is a unique $n \times m$ matrix pseudoinverse $\mathbf{B}^+$. This matrix was independently defined by Moore in 1920 and Penrose in 1955, and is variously known as the generalized inverse, the pseudoinverse, or the Moore-Penrose inverse. It is a matrix 1-inverse, and is implemented in the Wolfram Language as PseudoInverse [*m*]. The Moore-Penrose inverse satisfies $\mathbf{B}\mathbf{B}^+\mathbf{B}=\mathbf{B}$, $\mathbf{B}^+\mathbf{B}\mathbf{B}^+=\mathbf{B}^+$, $(\mathbf{B}\mathbf{B}^+)^{\mathrm{H}}=\mathbf{B}\mathbf{B}^+$, $(\mathbf{B}^+\mathbf{B})^{\mathrm{H}}=\mathbf{B}^+\mathbf{B}$, where $\mathbf{B}^{\mathrm{H}}$ is the conjugate transpose. It is also true that $\mathbf{z}=\mathbf{B}^+\mathbf{c}$ is the shortest length, least squares solution to the problem $\mathbf{B}\mathbf{z}=\mathbf{c}$. If the inverse of $(\mathbf{B}^{\mathrm{H}}\mathbf{B})$ exists, then $\mathbf{B}^+=(\mathbf{B}^{\mathrm{H}}\mathbf{B})^{-1}\mathbf{B}^{\mathrm{H}}$, as can be seen by pre-multiplying both sides of a Bayesian, hyperproductive, geo-predictive, narrow, African riverine, tributary, agro-village, capture point, eco-epidemiological trailing vegetation,turbid water, discontinuously infrequently canopied, *S. damnosum* s.l., riverine, immature habitat, sparsely shaded,

discontinuously canopied, probabilistic, RapidEye™ 5m, regressors equation by $\mathbf{B}^{\mathrm{H}}$ to create a square matrix, which can then be inverted, $\mathbf{B}^{\mathrm{H}}\mathbf{B}\mathbf{z}=\mathbf{B}^{\mathrm{H}}\mathbf{c}$, giving $\mathbf{z}=(\mathbf{B}^{\mathrm{H}}\mathbf{B})^{-1}\mathbf{B}^{\mathrm{H}}\mathbf{c}=\mathbf{B}^{+}\mathbf{c}$.

To obtain the viable Bayesian solution in Jacob et al. [59], the authors needed to autoregressively specify the conditional likelihood, and then find the appropriate conjugate prior. As with the univariate case of linear Bayesian regression, the authors were able to probabilistically quantitate a specific natural conditional conjugate prior, which was scale dependent. The conditional likelihood was then written as $\rho(\mathbf{E}|\boldsymbol{\Sigma}_\epsilon) \propto (\boldsymbol{\Sigma}_\epsilon^2)^{-n/2}\exp(-\frac{1}{2}\mathrm{tr}(\mathbf{E}^{\mathrm{T}}\mathbf{E}\boldsymbol{\Sigma}_\epsilon^{-1}))$. In the infrequently canopied, eco-epidemiological, hyperproductive, *S. damnosum* s.l. habitat, geo-predictive, risk model error $\mathbf{E}$ was defined in terms of $\mathbf{Y},\mathbf{X}$. By so doing, $\mathbf{B}$ yielded $\rho(\mathbf{Y}|\mathbf{X},\mathbf{B},\boldsymbol{\Sigma}_\epsilon) \propto (\boldsymbol{\Sigma}_\epsilon^2)^{-n/2}\exp(-\frac{1}{2}\mathrm{tr}((\mathbf{Y}-\mathbf{X}\mathbf{B})^{\mathrm{T}}(\mathbf{Y}-\mathbf{X}\mathbf{B})\boldsymbol{\Sigma}_\epsilon^{-1}))$. The authors sought a natural conjugate prior—a joint density $\rho(\mathbf{B},\boldsymbol{\Sigma}_\epsilon)$, which was of the same functional form as the quantitated likelihood. Since the likelihood in the riverine, habitat ecoepidemiological, forecasting, vulnerability, RapidEye™ 5m, risk model was quadratic in $\mathbf{B}$, the authors re-wrote the likelihood so it was normal in $(\mathbf{B}-\hat{\mathbf{B}})$ (i.e., the deviation from classical sample estimate).

Employing the same technique as with the auto-predictive, elucidative, Bayesian linear regression in PROC MCMC, the authors then optimally determined the exponential term employing a matrix-form of the sum-of-squares technique. Using matrix algebra, the sum of squares has a quantitatively tabulated form of the empirical parameterized, wavelength, transmittance, emissivity, covariate dataset for all the field and remote, georeferenceable, geo-spatiotemporally, geo-spectrotemporally, geosampled, canopied, sparsely shaded, hyperproductive, *S. damnosum* s.l. African, agro-village complex, narrow, riverine tributary, turbid water, immature habitat, orthogonalizable elements defined from a vector which was regressively quantitated in PROC MCMC employing the formula $\Sigma\, x_i^2 =$ x'x . In this regression equation, x was an *n* x 1 vector of geosampled immature habitat counts, while $\Sigma\, x_i^2$ was the sum of the squared geosampled, trailing vegetation, turbid water, parmeterized covariate coefficient values from vector x. To illustrate this model in SAS, Jacob et al. [59] autoregressively, remotely, quantitated the sum of squares for the geosampled habitat elements of vector x where x eco-cartographically, ecohydrologically represented the geosampled, immature, productivity counts.

In Jacob et al. [59] for the probabilistic, regressively quantitated, field and remote, georeferenceable, geo-spatiotemporally, geo-spectrotemporally, geosampled, hyperproductive, trailing vegetation, turbid water, *S. damnosum* s.l., narrow tributary, riverine larval habitat, the sum of squares was also autoregressively quantitated by the sum of cross products. The sum of the cross products for the probabilistically autoregressed, parameterizable covariate, estimators was represented by $X_{\mathrm{rj}}X_{\mathrm{rk}}$. The sum of the squares was then quantitated by the Cross Products Matrix for a *r* x *c* transitional probabilistic estimation matrix, which was then represented in the Bayesian model. Thereafter, the sum of cross products between all the *S. damnosum* s.l. trailing vegetation, turbid water, hyperproductive, capture point habitat estimators was then $\Sigma\, X_{\mathrm{rj}}X_{\mathrm{rk}}$, X' X, as shown below:

$$\mathrm{X'\,X} = \begin{bmatrix} \Sigma\, X_1^2 & \Sigma\, X_1 X_2 & \ldots & \Sigma\, X_1 X_{\mathrm{c}} \end{bmatrix}$$

$$\begin{vmatrix} \Sigma X_2 X_1 & \Sigma X_2^2 & \dots & \Sigma X_2 X_c \\ \dots & \dots & \dots & \dots \\ \Sigma X_c X_1 & \Sigma X_c X_2 & \dots & \Sigma X_c^2 \end{vmatrix}$$

where X was an *r* x *c* matrix of raw scores: $X_{11}, X_{12}, \dots, X_{rc}$ and X' X was a *c* x *c* matrix of sums of squares and sums of cross products. ΣX_i^2 is the sum of squares for all elements in column *i* of matrix X. $\Sigma X_i X_j$ is the sum of cross products produced by multiplying each element in column *i* of matrix X with the corresponding element from column *j* and summing the result. Thus, the diagonal elements of X' X are sums of squares, and the off-diagonal elements were cross products. Note that the cross product matrix X' X is a symmetric matrix.

Here, however, there was a need to use the Matrix Differential Calculus (Kronecker product and vectorization transformations). Thus, a sum-of-squares was employed to obtain new expression for $\rho(\mathbf{Y}|\mathbf{X},\mathbf{B},\mathbf{\Sigma}_\epsilon) \propto \mathbf{\Sigma}_\epsilon^{-(n-k)/2}\exp(-\mathrm{tr}(\frac{1}{2}\mathbf{S}^{\mathrm{T}}\mathbf{S}\mathbf{\Sigma}_\epsilon^{-1}))(\mathbf{\Sigma}_\epsilon^2)^{-k/2}\exp(-\frac{1}{2}\mathrm{tr}((\mathbf{B}-\hat{\mathbf{B}})^{\mathrm{T}}\mathbf{X}^{\mathrm{T}}\mathbf{X}(\mathbf{B}-\hat{\mathbf{B}})\mathbf{\Sigma}_\epsilon^{-1}))$, $\mathbf{S} = \mathbf{Y} - \hat{\mathbf{B}}\mathbf{X}$. They then developed a conditional form for the priors: $\rho(\mathbf{B}, \mathbf{\Sigma}^\epsilon) = \rho(\mathbf{\Sigma}^\epsilon)\rho(\mathbf{B}|\mathbf{\Sigma}^\epsilon)$ where $\rho(\mathbf{\Sigma}_\epsilon)$ was an inverse-Wishart distribution and $\rho(\mathbf{B}|\mathbf{\Sigma}_\epsilon)$ was some form of normal distribution in the matrix $\mathbf{B}$. This was accomplished using the vectorization transformation in SAS, which converted the likelihood from a function of the matrices $\mathbf{B}, \hat{\mathbf{B}}$ to a function of the vectors $\boldsymbol{\beta} = \mathrm{vec}(\mathbf{B}), \hat{\boldsymbol{\beta}} = \mathrm{vec}(\hat{\mathbf{B}})$. The authors then then wrote$^{\mathrm{tr}}((\mathbf{B}-\hat{\mathbf{B}})_{\mathrm{I}}\mathbf{X}_{\mathrm{I}}\mathbf{X}(\mathbf{B}-\hat{\mathbf{B}})\mathbf{\Sigma}^{\epsilon}_{-\mathrm{I}}) = {}^{\mathrm{AGC}}(\mathbf{B}-\hat{\mathbf{B}})_{\mathrm{I}}{}^{\mathrm{AGC}}(\mathbf{X}_{\mathrm{I}}\mathbf{X}(\mathbf{B}-\hat{\mathbf{B}})\mathbf{\Sigma}^{\epsilon}_{-\mathrm{I}})$, and thereafter employed ${}^{\mathrm{AGC}}(\mathbf{X}_{\mathrm{I}}\mathbf{X}(\mathbf{B}-\hat{\mathbf{B}})\mathbf{\Sigma}^{\epsilon}_{-\mathrm{I}}) = (\mathbf{\Sigma}^{\epsilon}_{-\mathrm{I}} \otimes \mathbf{X}_{\mathrm{I}}\mathbf{X}){}^{\mathrm{AGC}}(\mathbf{B}-\hat{\mathbf{B}})'$ where $\mathbf{A} \otimes \mathbf{B}$ denoted the Kronecker product of matrices A and B. By doing so, a generalization of the outer product was multiplied in an $m \times n$ matrix by a $p \times q$ matrix, rendering an $mp \times nq$ matrix consisting of every combination of products of elements from the two matrices. Therafter, the the geo-predictive, narrow, African riverine, tributary, agro-village, capture point, eco-epidemiological trailing vegetation,turbid water, discontinuously infrequently canopied, *S. damnosum* s.l. habitat model ${}^{\mathrm{AGC}}(\mathbf{B}-\hat{\mathbf{B}})_{\mathrm{I}}(\mathbf{\Sigma}^{\epsilon}_{-\mathrm{I}} \otimes \mathbf{X}_{\mathrm{I}}\mathbf{X}){}^{\mathrm{AGC}}(\mathbf{B}-\hat{\mathbf{B}}) = (\boldsymbol{\beta}-\hat{\boldsymbol{\beta}})^{\mathrm{T}}(\mathbf{\Sigma}_\epsilon^{-1} \otimes \mathbf{X}^{\mathrm{T}}\mathbf{X})(\boldsymbol{\beta}-\hat{\boldsymbol{\beta}})$ lead to a likelihood which was normal in the tabulated $(\boldsymbol{\beta}-\hat{\boldsymbol{\beta}})$. With the likelihood in a more tractable form, the authors in Jacob et al. [59] were able to autoregressively, remotely autoprobabilistically quantitate a natural (conditional) conjugate prior

Appendix 2

In Jacob et al. [127] the first-order Durbin-Watson statistic was printed by default. This statistic was used to test for first-order autocorrelation in an empricial, eco-epidemiological, field-operationizable dataset of geo-spatiotemporally geosampled, sparsely shaded, prolific, georeferenceable, trailing vegetation, *S. damnosum* s.l. riverine, turbid water, canopied, immature habitats. The authors employed the DWPROB option to print the significance level (*p*-values) for the Durbin-Watson tests. The DW= option was then employed to request higher-order Durbin-Watson statistics. Since the ordinary Durbin-Watson statistic tested only for first-order autocorrelation, the Durbin-Watson statistics for higher-order autocorrelation were the generalized Durbin-Watson decomposed, *S. damnosum* s.l. narrow African riverine, tributray, agro-village, capture point eco-epidemiological,

immature habitat statistics. The following statements performed the Durbin-Watson test for autocorrelation in the Ordinary Least Square (OLS) residuals. The DWPROB option printed the marginal significance levels (i.e., *p*-values) for the Durbin-Watson statistics.

```
/*-- Durbin-Watson test for autocorrelation --*/
proc autoreg data=a;
  model y = time / dw=4 dwprob;
run;
```

The AUTOREG procedure output was employed to conduct the eco-epidemiological vulnerability analyses. In this case, the first-order Durbin-Watson test was highly significant, with $p < 0.0001$ for the hypothesis of no first-order autocorrelation. Thus, autocorrelation correction was needed to qualitatively regressively quantitate the empirical, trailing vegetation, hyperproductive, *S. damnosum* s.l., riverine, immature habitat, optimized dataset.

Figure 8.7 Durbin-Watson Test Results for OLS Residuals
Forecasting Autocorrelated Time Series

The AUTOREG Procedure

Dependent Variable	y

Ordinary Least Squares Estimates for quantitating *S. damnosum* s.l. habitat covariates			
SSE	212.453263	DFE	31
MSE	6.75098	Root MSE	2.467653
SBC	171.984632	AIC	170.4357464
MAE	2.765432	AICC	170.65984
MAPE	12.5654832	HQC	171.48374
		Regress R-Square	0.76453
		Total R-Square	0.9874

Durbin-Watson Statistics			
Order	DW	Pr < DW	Pr > DW
1	0.6584	<.0001	1.0000
2	1.76483	0.0764	0.9765
3	2.9984	0.5987	0.7675
4	2.4563	0.9875	0.01433

Note: Pr < DW is the p-value for testing positive autocorrelation, and Pr > DW is the p-value

for testing negative autocorrelation in the *S. damnosum* s.l. habitat covariates

S. damnosum s.l. habitat covariates parameterized estimatators					
Variable	DF	Estimate	Standard Error	t Value	Approx Pr > |t|
Intercept	1	8.7643	0.8875	9.89	<.0001
time	1	0.5875	0.0453	12.43	<.0001

The Durbin-Watson test was utlilized to decide if autocorrelation correction was n positive or neagtive in the *S. damnosum* s.l. riverine, immature habitat dataset. Jacob et al. [26] generalized Durbin-Watson tests were not used to decide on the autoregressive order of the covariate paramterized estimators. The higher-order tests assumed the absence of lower-order autocorrelation. If the ordinary Durbin-Watson test indicates no first-order autocorrelation, the second-order test will be utilized to check for second-order autocorrelation. Since the first-order Durbin-Watson test was significant, the order 2, 3, and 4 tests were ignored.

In Jacob et al. [26], Durbin-Watson tests checked for autocorrelation which specified an order of any potential seasonality, since seasonality produces autocorrelation at the seasonal lag. Quarterly data use was DW=4, and monthly data used DW=12 in the *S. damnosum* s.l. habitat, forecasting, vulnerability, eco-epidemiological model.

The authors also employed Durbin *h* test or Durbin *t* test to test for first-order autocorrelation. For the Durbin *h* test, they specified the name of the lagged dependent variable in the LAGDEP= option. For the Durbin *t* test, the authors specified the LAGDEP option without giving the name of the lagged dependent variable. The following statements added the variable YLAG to the dataset A and regress Y on YLAG instead of TIME in the *S.. damnosum* s.l. narrow African riverine, tributary, agro-village, capture point eco-epidemiological, immature habitat model:

```
data b;
  set a;
  ylag = lag1( y );
run;

proc autoreg data=b;
  model y = ylag / lagdep=ylag;
run;
```

The Durbin *h* statistic was 2.71 is significant with a *p*-value of 0.0023, indicating autocorrelation.

The AUTOREG Procedure using a Durbin *h* Test with a Lagged Dependent Variable Forecasting Autocorrelated Time Series

Dependent Variable	y

Ordinary Least Squares Estimates			
SSE	97.7654	DFE	32
MSE	2.99875	Root MSE	1.87641
SBC	142.38765	AIC	139.88743
MAE	1.298753	AICC	139.87643
MAPE	8.116543	HQC	140.09854
		Regress R-Square	0.8964
		Total R-Square	0.93764

Miscellaneous Statistics			
Statistic	Value	Prob	Label
Durbin h	2.7664	0.0023	Pr > h

Parameter Estimates					
Variable	DF	Estimate	Standard Error	t Value	Approx Pr > |t|
Intercept	1	1.5982	0.9367	1.67	0.0978
ylag	1	0.9765	0.0676	18.22	<.0001

Appendix 3

Given a time series of data X_t, where t is an integer index, and the X_t are real numbers, then an ARIMA (p', q) time series-dependent model was given by: $\left(1-\sum_{i=1}^{p'}\alpha_i L^i\right)X_t=\left(1+\sum_{i=1}^{q}\theta_i L^i\right)\varepsilon_t$ in Jacob et al. [45] in PROC ARIMA, where L was the lag operator, α_i were the unmixed parameters of the autoregressive part of the model, θ_i were the parameters of the moving average part, and ε_t were error terms. The error terms ε_t were assumed to be independent, identically distributed variables geosampled from a normal distribution with a mean of zero. The authors then assumed that the polynomial $\left(1-\sum_{i=1}^{p'}\alpha_i L^i\right)$ had a unitary root of multiplicity d. Then, the geo-spatial, geo-spectrotemporal linear, geosampled, hyperproductive, trailing vegetation, turbid water, discontinuously canopied, georeferenceable, *S. damnosum* s.l., riverine, immature habitat, forecasting vulnerability model was rewritten as: $\left(1-\sum_{i=1}^{p'}\alpha_i L^i\right)=\left(1-\sum_{i=1}^{p'-d}\phi_i L^i\right)(1-L)^d$. An ARIMA($p$,$d$,$q$) process expressed this polynomial factorization property with $p=p'-d$, which was subsequently given by: $\left(1-\sum_{i=1}^{p}\phi_i L^i\right)(1-L)^d X_t=\left(1+\sum_{i=1}^{q}\theta_i L^i\right)\varepsilon_t$, and thus was thought as a particular case of an ARMA($p+d$,q) process having the autoregressive polynomial with d unit roots. The model was then generalized as follows: $\left(1-\sum_{i=1}^{p}\phi_i L^i\right)(1-L)^d X_t=\delta+\left(1+\sum_{i=1}^{q}\theta_i L^i\right)\varepsilon_t$. This defined an ARIMA($p$,$d$,$q$) process with drift $\delta/(1-\Sigma\varphi_i)$.

Initially, the authors in Jacob et al. [45] constructed a Poissonian probability model in GEN MOD. The Poisson process was provided by the limit of a binomial distribution of the geo-spatiotemporally, geo-spectrotemporally, geosampled, predictor, covariate coefficient estimates employing $P_p(n\,|\,N)=\frac{N!}{n!\,(N-n)!}\,p^n\,(1-p)^{N-n}.$ (5.3). The authors viewed the distribution as a function of the expected number of count variables using the sample size N for quantifying the fixed p in equation (2.1), which was then transformed into the linear

equation: $P_{\frac{v}{N}}(n|N)=\frac{N!}{n!(N-n)!}\left(\frac{v}{N}\right)^n\left(1-\frac{v}{N}\right)^{N-n}$. Based on the sample size *N*, the distribution approached $P_v(n)$ which was remotely, autoregressively, auto-probabilistically quantitated as

$\lim_{n\to\infty} P_p(n|N)=\lim_{N\to\infty}\frac{N(N-1)\cdots(N-n+1)}{n!}\frac{v^n}{N^n}\left(1-\frac{v}{N}\right)^N\left(1-\frac{v}{N}\right)^{-n}=\lim_{N\to\infty}\frac{N(N-1)\cdots(N-n+1)}{N^n}\frac{v^n}{n!}\left(1-\frac{v}{N}\right)^N\left(1-\frac{v}{N}\right)^{-n}=1\cdot\frac{v^n}{n!}\cdot e^{-v}\cdot 1=\frac{v^n e^{-v}}{n!}$.

The GENMOD procedure then fit a generalized linear model (GLM) to the geosampled, trailing vegetation, turbid water, hyperproductive, parameterizable, *S. damnosum* s.l. riverine, immature habitat data by ML estimation of the parameter vector β. The GENMOD procedure estimated the seasonally geosampled wavelength, parameterized, covariate estimators of each agro-village-level, sub-model, *S. damnosum* s.l. eco-epidemiological risk model numerically through an iterative fitting process. The dispersion parameter was then estimated by the residual deviance and by Pearson's chi-square divided by the df. Covariances, standard errors, and *p*-values were then computed for the geosampled covariate coefficients based on the asymptotic normality derived from the ML estimation.

Note, that the sample size *N* completely dropped out of the probability function, which had the same functional form for all the geo-spatiotemporally, geo-spectrotemporally geosampled, agro-village complex-level, wavelength, parameterizable, covarite estimator indicator values (i.e., v). As expected, the Poisson distribution was normalized so that the sum of probabilities equaled 1. The ratio of probabilities was then determined by $\sum_{n=0}^{\infty} P_v(n)=e^{-v}\sum_{n=0}^{\infty}\frac{v^n}{n!}=e^{-v}e^{v}=$ which was then expressed as $\frac{P_v(n=i+1)}{P(n=i)}=\frac{\frac{v^{i+1}e^{-v}}{(i+1)!}}{\frac{e^{-v}v^i}{i!}}=\frac{v}{i+1}$. The Poisson distribution revealed that the wavelength, emissivity transmittance, parameterizable, trailing vegetation, georeferenceable, turbid water, *S. damnosum* s.l., turbid water decomposed, unmixed, covariate coefficients reached a maximum when $\frac{dP_v(n)}{dn}=\frac{e^{-\gamma}n(\gamma-H_n+\ln v)}{n!}=0$, where γ was the Euler-Mascheroni constant and H_n was a harmonic number, leading to the transcendental equation $\gamma-H_n+\ln v=0$. The $\gamma=-\int_0^{\infty}e^{-x}\ln x\,dx=-\int_0^1\ln\ln\left(\frac{1}{x}\right)dx=\int_0^{\infty}\left(\frac{1}{1-e^{-x}}-\frac{1}{x}\right)e^{-x}dx=\int_0^{\infty}\frac{1}{x}\left(\frac{1}{1+x}-e^{-x}\right)dx$ regression model also revealed that the Euler-Mascheroni constant arose in the integrals. Commonly, integrals that render γ in combination with temporal geosampled constants include $\int_0^{\infty}e^{-x^2}\ln x\,dx=-\frac{1}{4}\sqrt{\pi}(\gamma-2\ln 2)$, which is equal to $\int_0^{\infty}e^{-x}(\ln x)^2dx=\gamma^2+\frac{1}{6}\pi^2|$ [5.2] [142]. Thereafter, the double integrals in the seasonal, hyperproductive, field or remote, sparsely shaded, regression model included $\gamma=\int_0^1\int_0^1\frac{x-1}{(1-xy)\ln(xy)}dx\,dy$. (5.2).

An interesting analog of equation (5.2) in the regression-based, eco-epidemiological, vulnerability model was then calculated as

$\ln\left(\frac{4}{\pi}\right)=\sum_{n=1}^{\infty}(-1)^{n-1}\left[\frac{1}{n}-\ln\frac{n+1}{n}\right]=\int_0^1\int_0^1\frac{x-1}{(1+xy)\ln(xy)}dx\,dy=$ 0.241564. This solution was also provided by incorporating Mertens theorem $e^{\gamma}=\lim_{n\to\infty}\frac{1}{\ln p_n}\prod_{i=1}^{n}\frac{1}{1-\frac{1}{p_i}}$, where the product was aggregated over the geo-spectrotemporally geospatially sampled values found in the empirical ecological datasets. The authors noted that Mertens' 3rd theorem $\lim_{n\to\infty}\ln n\prod_{p\le n}\left(1-\frac{1}{p}\right)=e^{-\gamma}$ was related to the density of prime numbers, where γ is the Euler–Mascheroni constant. By taking the logarithm of both sides in the model, an explicit formula for γ was then optimally derived employing $\gamma=\lim_{x\to\infty}\left[\sum_{p\le x}\ln\left(\frac{1}{1-\frac{1}{p}}\right)-\ln\ln x\right]$. This expression was also rendered by quantifying the data series employing Euler, and equation (5.2) by first replacing $\ln n$, $\ln(n+1)$ in the equation $\gamma=\sum_{k=1}^{\infty}\left[\frac{1}{k}-\ln\left(1+\frac{1}{k}\right)\right]$, and then generating $\lim_{n\to\infty}\left[\ln(n+1)-\ln n\right]=\lim_{n\to\infty}\ln\left(1+\frac{1}{n}\right)=0$. We then substituted the telescoping sum $\sum_{k=1}^{n}\ln\left(1+\frac{1}{k}\right)$ for $\ln(n+1)$, which then generated $\ln\left(1+\frac{1}{k}\right)=\ln(k+1)-\ln k$. Thereafter, the product was $\lim_{n\to\infty}\left[\sum_{k=1}^{n}\frac{1}{k}-\sum_{k=1}^{n}\ln\left(1+\frac{1}{k}\right)\right]_{\gamma}=\lim_{n\to\infty}\sum_{k=1}^{n}\left[\frac{1}{k}-\ln\left(1+\frac{1}{k}\right)\right]$.

Additionally, other series in the agro-village complex-level, regression, hyperproductive, trailing vegetation, turbid water, non-homogenously canopied, *S. damnosum* s.l., riverine, immature habitat, vulnerability forecast model included the equation (◇), where $\gamma=\sum_{n=2}^{\infty}(-1)^n\frac{\zeta(n)}{n}=\ln\left(\frac{4}{\pi}\right)+\sum_{n=1}^{\infty}\frac{(-1)^{n-1}\zeta(n+1)}{2^n(n+1)}$, and $\zeta(z)$ was $\gamma=\sum_{n=1}^{\infty}(-1)^n\frac{\lfloor \lg n\rfloor}{n}$ plus the Riemann zeta function. The Riemann zeta function ζ(s) is a function of a complex variable*s* that analytically continues the sum of the infinite series $\sum_{n=1}^{\infty}\frac{1}{n^s}$, which converges when the real part of *s* is greater than 1, where lg is the logarithm to base 2 and the $\lfloor x\rfloor$ is the floor function [24]. Jacob et al. (2011) earlier provided a series equivalent to $\gamma=1-\sum_{n=1}^{\infty}\sum_{k=2^{n-1}}^{2^n-1}\frac{n}{(2k+1)(2k+2)}$ and, thereafter $\frac{1}{(2k+1)(2k+2)}=\frac{1}{2k+1}-\frac{1}{2k+2}$, which was then added to $0=-\frac{1}{2}+\frac{1}{4}+\frac{1}{8}+\frac{1}{16}+\ldots$ to render Vacca's formula. Gosper et al. [210] employed the sums $\gamma=\sum_{n=1}^{\infty}\sum_{k=2^n}^{\infty}\frac{(-1)^k}{k}=\sum_{k=1}^{\infty}\frac{1}{2^{k+1}}\sum_{j=0}^{k-1}\binom{2^{k-j}+j}{j}^{-1}$ with $k-j$ by replacing the undefined *I,* and then

rewrote the equation as a double series for applying the Euler's series transformation to each of the sampled time-series-dependent, covariate coefficient estimates.

Thereafter, $\frac{n}{k}$ was employed as a binomial coefficient, rearranged to achieve the conditionally convergent series in the agro-village complex-level, linear, geosampled, auto-probablistic, autoregressive, hyperproductive, trailing vegetation, turbid water, non-homogenously canopied, *S. damnosum* s.l., riverine,immature habitat, georeferenceable, vulnerability model. The plus and minus terms were first grouped in pairs of the decomposable, geo-spectrotemporally, geospatially geosampled, covariate, coefficient estimates employing the resulting series based on the actual observational, covariate coefficient, indicator values. The double series was thereby equivalent to Catalan's integral: $\gamma = \int_0^1 \frac{1}{1+x} \sum_{n=1}^{\infty} x^{2^n-1} dx$. Catalan's integrals are a special case of general formulas due to $J_0\left(\sqrt{z^2-y^2}\right) = \frac{1}{\pi}\int_0^{\pi} e^{y\cos\theta}\cos(z\sin\theta)d\theta$, where $J_0(z)$ is a Bessel function of the first kind [143].

The Bessel function is a function $Z_n(x)$ defined in a robust auto-probabilistic, autoregressive model by employing the quantifiable recurrence relations $Z_{n+1}+Z_{n-1} = \frac{2n}{x}Z_n$ and $Z_{n+1}-Z_{n-1} = -2\frac{dZ_n}{dx}$ [2], which more recently have been defined as solutions in linear models employing the differential equation $x^2\frac{d^2y}{dx^2} + x\frac{dy}{dx} + \left(x^2-n^2\right)y = 0$ [6]. The Bessel function $J_n(z)$ was defined in the agro-village complex level model by the contour integral $J_n(z) = \frac{1}{2\pi i}\oint e^{(z/2)(t-1/t)}t^{-n-1}dt$, where the contour enclosed the origin and was traversed in a counter-clockwise direction. This function generated: $J_0\left(2i\sqrt{z}\right) = \frac{1}{\pi}\int_0^{\pi} e^{(1+z)\cos\theta}\cos\left[(1-z)\sin\theta\right]d\theta$ $z \equiv 1-z'$ and $y \equiv 1+z'$.

In mathematics, Bessel functions are canonical solutions y(x) of Bessel's differential equation $x^2\frac{d^2y}{dx^2} + x\frac{dy}{dx} + (x^2-\alpha^2)y = 0$, for an arbitrary real or complex number α (i.e., the order of the Bessel function). The most common and important cases are for α an integer or half-integer [211]. To quantify the equivalence in the geo-spatiotemporal, regression-based parameterizable covariate estimators, we expanded $1/(1+x)$ in a geometric series and multiplied the sampled geo-spatiotemporal, geo-spectrotempemporal linear, autoprobabilistic, autoregressive, hyperproductive, trailing vegetation, turbid water, discontinuously canopied, *S. damnosum* s.l., riverine, larval habitat, vulnerability model data feature attributes by x^{2^n-1}, and integrated the termwise as in Sondow and Zudilin [227]. Other series for γ then included $\gamma = \frac{3}{2} - \ln 2 - \sum_{m=2}^{\infty}(-1)^m\frac{m-1}{m}\left[\zeta(m)-1\right]$ and $\gamma = \frac{2^n}{e^{2^n}}\sum_{m=0}^{\infty}\frac{2^{mn}}{(m+1)!}\sum_{t=0}^{m}\frac{1}{t+1} - n\ln 2 + o\left(\frac{1}{2^n e^{2^n}}\right)$. A

rapidly converging limit for γ was then provided by $\gamma = \lim_{n\to\infty}\left[\frac{2n-1}{2n} - \ln n + \sum_{k=2}^{n}\left(\frac{1}{k} - \frac{\zeta(1-k)}{n^k}\right)\right] = \lim_{n\to\infty}\left[\frac{2n-1}{2n} - \ln n + \sum_{k=2}^{n}\frac{1}{k}\left(1 + \frac{B_k}{n^k}\right)\right]$ and thereafter by $\gamma = \lim_{n\to\infty}\left[\frac{2n-1}{2n} - \ln n + \sum_{k=2}^{n}\left(\frac{1}{k} - \frac{\zeta(1-k)}{n^k}\right)\right] = \lim_{n\to\infty}\left[\frac{2n-1}{2n} - \ln n + \sum_{k=2}^{n}\frac{1}{k}\left(1 + \frac{B_k}{n^k}\right)\right]$, where B_k was a Bernoulli number. Another limit formula was then provided by the equation $\gamma = -\lim_{n\to\infty}\left[\frac{\Gamma\left(\frac{1}{n}\right)\Gamma(n+1)n^{1+1/n}}{\Gamma\left(2+n+\frac{1}{n}\right)} - \frac{n^2}{n+1}\right]$.

In mathematics, the Bernoulli numbers Bn are a sequence of rational numbers with deep connections to number theory, whereby values of the first few Bernoulli numbers are B0 = 1, B1 = ±1⁄2, B2 = 1⁄6, B3 = 0, B4 = −1⁄30, B5 = 0, B6 = 1⁄42, B7 = 0, B8 = −1⁄30 [24]. Jacob et al.[2005] found if m and n are sampled values and f(x) is a smooth sufficiently differentiable function in a seasonal, agro-village complex-level, linear, autoregressive, autoprobabilistic, trailing vegetation, turbid water, discontinuous canopied, hyperproductive *S. damnosum* s.l. habitat model, which is defined for all the values of x in the interval $[m, n]$, then the integral $I = \int_m^n f(x)\,dx$ can be approximated by the sum (or vice versa) $S = \frac{1}{2}f(m) + f(m+1) + \cdots + f(n-1) + \frac{1}{2}f(n)$. The Euler–Maclaurin formula then provided expressions for remotely autoregressively quantitating the difference between the sum and the integral in terms of the higher derivatives f(k) at the end points of the interval m and n. The Euler–Maclaurin formula provides a powerful connection between integrals and sums which can be used to approximate integrals by finite sums, or, conversely, to evaluate finite sums and infinite series using integrals and the machinery of calculus [142]. Thereafter, for the agro-village level, time series, district-level, geosampled values p the authors had generated 30, B5 = 0, B6 = 1/42, B7 = 0, B8 = −1/30, and R which was an error term. Note $-B_1\left(f(n) + f(m)\right) = \frac{1}{2}\left(f(n) + f(m)\right)$. Hence, the authors re-wrote the autoregression-based, auto-predictive formula as $\sum_{i=m}^{n} f(i) = \int_m^n f(x)\,dx - B_1\left(f(n) + f(m)\right) + \sum_{k=1}^{p}\frac{B_{2k}}{(2k)!}\left(f^{(2k-1)'}(n) - f^{(2k-1)'}(m)\right) + R$. They then rewrote the equation more elegantly as $\sum_{i=m}^{n} f(i) = \sum_{k=0}^{p}\frac{1}{k!}\left(B_k f^{(k-1)'}(n) - B_k^* f^{(k-1)'}(m)\right) + R$ with the convention of $f^{(-1)'}(x) = \int f(x)\,dx$ (i.e. the -1th derivation of f is the integral of the function). Limits to the linear, geosampled, georeferenceable, agro-village complex-level, autoregression, trailing vegetation, turbid water, discontinuously canopied, *S. damnosum* s.l., riverine, immature habitat, auto-probabilistic, eco-epidemiological model were then rendered by

$\gamma = \lim_{x\to\infty} \zeta\left(\zeta(z)\right) - 2^x + \left(\frac{4}{3}\right)^x + 1$, where $\zeta(z)$ was the Riemann zeta function. The Bernoulli numbers appear in the Taylor series expansions of the tangent and hyperbolic tangent functions in formulas for the sum of powers of the first positive integers, in the Euler–Maclaurin formula, and in expressions for certain values of the Riemann zeta function [Haight 1967].

Another connection with the primes was provided by $d(n) = \sigma_0(n)$ for the geosampled, agro-village, riverine-level numerical values from 1 to n in the dataset, and was found to be asymptotic to $\frac{\sum_{k=1}^{n} d(k)}{n} \sim \ln n + 2\gamma - 1$. De la Vallée-Poussin [28] proved that if a large number n is divided by all primes n, then the average amount by which the quotient is less than the next whole number is g [24]. An identity for g in our agro-village–level, auto-regression-based model was then provided by $\gamma = \frac{S_0(z) - K_0(z)}{I_0(z)} - \ln\left(\frac{1}{2}z\right)$, where $I_0(z)$ was a modified Bessel function of the first kind, $K_0(z)$ was a modified Bessel function of the second kind, and $S_0(z) \equiv \sum_{k=0}^{\infty} \frac{\left(\frac{1}{2}z\right)^{2k} H_k}{(k!)^2}$, where H_n was a harmonic number. For non-integer α, Yα(x) is related to Jα(x) by $Y_\alpha(x) = \frac{J_\alpha(x)\cos(\alpha\pi) - J_{-\alpha}(x)}{\sin(\alpha\pi)}$. In the case of integer order n, the function was defined by taking the limit as a non-integer α tends to n: $Y_n(x) = \lim_{\alpha\to n} Y_\alpha(x)$. [211]. The Bessel functions of the second kind, were denoted by Yα(x) and by Nα(x), which were actually solutions of the Bessel differential equation employing a singularity at the origin (x = 0). This provided an efficient iterative algorithm for g by computing $B_k = \frac{B_{k-1}n^2}{k^2} = A_k = \frac{1}{k}\left(\frac{A_{k-1}n^2}{k} + B_k\right) = U_k V_k = U_{k-1} + A_k$ and $V_k = V_{k-1} + B_k$ $A_0 = -\ln n B_0 = 1 U_0 = A_0$ and $V_0 = 1$. Reformulating this identity rendered the limit $\lim_{n\to\infty}\left[\sum_{k=0}^{\infty} \frac{\left(\frac{n^k}{k!}\right)^2 H_k}{\sum_{k=0}^{\infty}\left(\frac{n^k}{k!}\right)^2} - \ln n\right] = \gamma$. Infinite products involving g also arose from the Barnes G-function using the positive integer n.

In mathematics, the Barnes G-function G(z) is a function that is an extension of superfactorials to the complex numbers, which is related to the Gamma function [24]. This function provided $\prod_{n=1}^{\infty} e^{-1+1/(2n)}\left(1+\frac{1}{n}\right)^n = \frac{e^{1+\gamma/2}}{\sqrt{2\pi}}$, and also the equation $\prod_{n=1}^{\infty} e^{-2+2/n}\left(1+\frac{2}{n}\right)^n = \frac{e^{3+2\gamma}}{2\pi}$. The Barnes G-function was then linearly defined in our time series-dependent, agro-village-level, linear, trailing vegetation, turbid water, discontinuously canopied, *S. damnosum* s.l. habitat, regression-based risk model, which was then generated employing

$G(z+1)=(2\pi)^{z/2}\exp\left(-\left(z(z+1)+\gamma z^2\right)/2\right)\times\prod_{n=1}^{\infty}\left[\left(1+\frac{z}{n}\right)^n\exp\left(-z+z^2/(2n)\right)\right]$, where γ was the Euler–Mascheroni constant, exp(x) = ex, and ∏ was capital pi notation. The Euler-Mascheroni constant was then rendered by the expressions $\gamma=-\Gamma'(1)=-\psi_0(1)$, where $\psi_0(x)$ was the digamma function $\gamma=\lim_{s\to 1}\left[\zeta(s)-\frac{1}{s-1}\right]$, and the asymmetric limit form of $\gamma=\lim_{s\to 1^+}\sum_{n=1}^{\infty}\left(\frac{1}{n^s}-\frac{1}{s^n}\right)$ and $\gamma=\lim_{x\to\infty}\left[x-\Gamma\left(\frac{1}{x}\right)\right]$.

In mathematics, the digamma function is defined as the logarithmic derivative of the gamma function $\psi(x)=\frac{d}{dx}\ln\Gamma(x)=\frac{\Gamma'(x)}{\Gamma(x)}$, where it is the first of the polygamma functions. In the georferencable, agro-village–level, geo-spatiotemporal, geo-spectrotempemporal, agro-village-complex vulnerability model, the digamma function, ψ0(x) was then related to the harmonic numbers in that $\psi(n)=H_{n-1}-\gamma$, where Hn was the *n*th harmonic number, and γ was the Euler-Mascheroni constant. In mathematics, the *n*-th harmonic number is the sum of the reciprocals of the first *n* natural numbers [143]. The difference between the *n*th convergent in equation (◇) and γin our autoregression-based model was then calculated by $\sum_{k=1}^{n}\frac{1}{k}-\ln n-\gamma=\int_n^{\infty}\frac{x-\lfloor x\rfloor}{x^2}dx$, where $\lfloor x\rfloor$ is the floor function which satisfied the inequality $\sum_{k=1}^{n}\frac{1}{k}-\ln n-\gamma=\int_n^{\infty}\frac{x-\lfloor x\rfloor}{x^2}dx$ [142]. The symbol g was then $\gamma'\equiv e^{\gamma}\approx 1.781072$. This led to the radical representation of the agro-village complex-level, eco-epidemiological, covariate coefficients as $e^{\gamma}=\left(\frac{2}{1}\right)^{1/2}\left(\frac{2^2}{1\cdot 3}\right)^{1/3}\left(\frac{2^3\cdot 4}{1\cdot 3^3}\right)^{1/4}\left(\frac{2^4\cdot 4^4}{1\cdot 3^6\cdot 5}\right)^{1/5}$, which was related to the double series $\gamma=\sum_{n=1}^{\infty}\frac{1}{n}\sum_{k=0}^{n-1}(-1)^{k+1}\binom{n-1}{k}\ln(k+1)$ and $\binom{n}{k}$, a binomial coefficient. Thereafter, another proof of product in the our agro-village complex-level regression model was provided by the equation $\frac{\pi}{2}=\left(\frac{2}{1}\right)^{1/2}\left(\frac{2^2}{1\cdot 3}\right)^{1/4}\left(\frac{2^3\cdot 4}{1\cdot 3^3}\right)^{1/8}\left(\frac{2^4\cdot 4^4}{1\cdot 3^6\cdot 5}\right)^{1/16}$. The solution was then made even clearer by changing $n\to n+1$. Both of these regression-based formulas were also analogous to the product for e, which was rendered by calculating $e=\left(\frac{2}{1}\right)^{1/1}\left(\frac{2^2}{1\cdot 3}\right)^{1/2}\left(\frac{2^3\cdot 4}{1\cdot 3^3}\right)^{1/3}\left(\frac{2^4\cdot 4^4}{1\cdot 3^6\cdot 5}\right)^{1/4}$.

Unfortunately, extra-Poisson variation was detected in the variance estimates in the model. A modification of the iterated re-weighted least square scheme and/or a negative binomial non-homogenous, gamma-distributed mean, regression-based framework conveniently accommodated the extra-Poisson variation in the seasonal log-linear models employing decomposed wavelength, transmittance, RapidEye™ emissivity frequencies as dependent response variables. Operationally, these models consist of making iterated

weighted least squares fit to approximately normally distributed dependent geo-predictive covariate coefficients based on observed rates or their logarithm. Unfortunately, the variance of the geo-spatiotemporal, geo-spectrotempemporal linear, geosampled, district-level, autoregression, hyperproductive, trailing vegetation, turbid water, discontinuously canopied, *S. damnosum* s.l., riverine, larval habitat, eco-epidemiological, vulnerability, unmixed, 5m, model observations in log-linear equations were assumed to be constant. Subsequently, introducing an extra-binomial variation scheme in the eco-epidemiological, linear-logistic, habitat was optimally fitted for a Poisson procedure. The probabilities describing the possible outcome of a single trial was then modeled as a function of forecasting geo-spectrotemporally, geospatially decomposable variables using a logistic function [130].

The authors in Jacob et al. [59] constructed a robust, negative binomial, regression model in SAS with non-homogenous means and a gamma distribution by incorporating $\alpha=\frac{1}{\theta}(\alpha>0)$ in equation (5.2). The authors let $g(\tau_i)$ be the probability density function of τ_i in the model. Then, the distribution $f(y_i|\mathbf{x}_i)$ was no longer conditional on τ_i. Instead it was obtained by integrating $f(y_i|\mathbf{x}_i,\tau_i)$, with respect to τ_i: $f(y_i|\mathbf{x}_i)=\int_0^\infty f(y_i|\mathbf{x}_i,\tau_i)g(\tau_i)d\tau_i$. The distribution in the agro-village-level, linear, auto-probabilistic, autoregressive, interpolatble, hyperproductive, trailing vegetation, turbid water, decomposed, discontinuously canopied, *S. damnosum* s.l. habitat model, parameterizable, covariate, unbiased estimators was then $f(y_i|x_i)=\frac{\Gamma(y_i+\alpha^{-1})}{y_i!\Gamma(\alpha^{-1})}\left(\frac{\alpha^{-1}}{\alpha^{-1}+\mu_i}\right)^{\alpha^{-1}}\left(\frac{\mu_i}{\alpha^{-1}+\mu_i}\right)^{y_i}, y_i=0,1,2..$ The negative binomial distribution was thus derived as a gamma mixture of Poisson random variables. The conditional mean in the model was $E(y_i\mid x_i)=\mu_i=e^{x_i'\beta}$, and the variance in the residual estimates was $V(y_i\mid x_i)=\mu_i\left[1+\frac{1}{\theta}\mu_i\right]=\mu_i[1+\alpha\mu_i]>E(y_i\mid x_i)$. To further estimate the models, the authors specified DIST=NEGBIN (p=1) in the MODEL statement in PROC REG. The negative binomial model NEGBIN1 was set p=1, which revealed the variance function $V(y_i\mid x_i)=\mu_i+\alpha\mu_i$ was linear in the mean of the model. The log-likelihood function of the NEGBIN1 model was then provided by $L=\left\{\sum_{j=0}^{y_i-1}\ln\left(j+\alpha^{-1}\exp(x_i'\beta)\right)\right\}$. Additionally, the equation $-\ln(y_i!)-\left(y_i+\alpha^{-1}\exp(x_i'\beta)\right)\ln(1+\alpha)+y_i\ln(\alpha)$ was generated. The gradient for the regression model was then quantified employing $\frac{\delta L}{\delta\beta}=\sum_{i=1}^{N}\left\{\left(\sum_{j=0}^{y_i-1}\frac{\mu_i}{(j\alpha+\mu_i)}\right)x_i-\alpha^{-1}\ln(1+\alpha)\mu_i x_i\right\}$ and $\frac{\delta L}{\delta\alpha}=\sum_{i=1}^{N}\left\{-\left(\sum_{j=0}^{y_i-1}\frac{\alpha^{-1}\mu_i}{(j\alpha+\mu_i)}\right)-\alpha^{-2}\mu_i\ln(1+\alpha)-\frac{(y_i+\alpha^{-1}\mu_i)}{1+\alpha}+\frac{y_i}{\alpha}\right\}$. The negative binomial regression model with variance function $V(y_i\mid x_i)=\mu_i+\alpha\mu_i^2$ was then referred to as the NEGBIN2 model. To estimate this regression-based model, the authors of Jacob et al. [59] autoregressively, auto-probabilistically specified DIST=NEGBIN (p=2) in the MODEL

statements. A test of the Poisson distribution was then performed by examining the hypothesis that $\alpha = \frac{1}{\theta_i} = 0$. A Wald test of this hypothesis was also provided, which was the reported t statistics for the estimates in the model. Under the Wald statistical test, the maximum likelihood estimate $\hat{\theta}$ of the parameter(s) of interest θ was compared with the proposed value θ_0, with the assumption that the difference between the two would be approximately normally distributed [24]. The log-likelihood function of the regression models (i.e., NEGBIN2) was then generated by the equation: $L = \sum_{i=1}^{N}\left\{\sum_{j=0}^{y_i-1}\ln\left(j+\alpha^{-1}\right) - \ln\left(y_i!\right) = -\left(y_i+\alpha^{-1}\right)\ln\left(1+\alpha\exp\left(x_i'\beta\right)\right) + y_i\ln\left(\alpha\right) + y_i x_i'\beta\right\}$, whose gradient was $\frac{\delta L}{\delta \beta} = \sum_{i=1}^{N}\frac{y_i-\mu_i}{1+\alpha\mu_i}x_i$. The variance in the agro-village riverine, habitat-level, forecasting, vulnerability, RapidEye^{TM} wavelength, transmittance model was then assessed by $\frac{\delta L}{\delta \alpha} = \sum_{i=1}^{N}\left\{-\alpha^{-2}\sum_{j=0}^{y_i-1}\frac{1}{\left(j+\alpha^{-1}\right)} - \alpha^{-2}\ln\left(1+\alpha\mu_i\right) + \frac{y_i-\mu_i}{\alpha\left(1+\alpha\mu_i\right)}\right\}$. The final mean in the model was calculated as $\frac{pr}{1-p}$, the mode as $\begin{cases}\left\lfloor\frac{p(r-1)}{1-p}\right\rfloor & \text{if } r>1\\ 0 & \text{if } r\le 1\end{cases}$, the variance as $\frac{pr}{(1-p)^2}$, the skewess as $\frac{1+p}{\sqrt{pr}}$, the kurtosis as $\frac{6}{r}+\frac{(1-p)^2}{pr}$, the moment generating function as $\left(\frac{1-p}{1-pe^t}\right)^r$ for $t < -\log p$, the characteristic function as $\left(\frac{1-p}{1-pe^{it}}\right)^r$ with $t \in \mathbb{R}$, and finally the probability generating function as $\left(\frac{1-p}{1-pz}\right)^r$ for $|z| < \frac{1}{p}$.

A spatial autoregressive model was then generated that used a variable Y. This was a function of nearby sampled, agro-village–level, *S. damnosum* s.l., covariate coefficients in AUTOREG Y, which had an interpolator decomposable, indicator value 1 (i.e., an autoregressive response) and/or the residuals of Y, which were values of nearby geosampled Y residuals (i.e., an SAR or spatial error specification). For time series-dependent, eco-epidemiological, risk, modelling onchocerciasis-related, parameterizable covariate estimators, the SAR model furnishes an alternative specification that frequently is written in terms of matrix W [24]. A misspecification perspective was then employed for performing a spatial autocorrelation uncertainty latent, estimation analysis, which utilized the sampled, agro-village complex-level, covariate estimators. The model was built using

$y = X\beta + \varepsilon^*$ (i.e. the regression equation) assuming the sampled data had autocorrelated disturbances. The model also assumed that the geosampled data could be decomposed into a white-noise component ε, and a set of unspecified, sub-district-level, regression models that had the structure $y = X\beta + \underbrace{E\gamma + \varepsilon}_{=\varepsilon^*}$.

Jacob et al. [127] found that white noise in a seasonal, malaria-based, regression model is a univariate or multivariate discrete-time stochastic process whose terms are independent and

independent (i.i.d) with a zero mean. In the model the misspecification term was E_{γ}. Thereafter, an Autoregressive Integrated Moving Average (ARIMA) model was constructed, which revealed a conspicuous, but not very prominent, first-order, temporal, autoregressive structure in the individual, time series-dependent data. A random effects term was then specified using monthly time-series data. This specification included a district-specific intercept term that was a random deviation from the overall intercept term based on a draw from a normal frequency distribution. The random effects specification revealed a non-constant mean across the districts. This random intercept represented the combined effect of all omitted covariates that caused districts to be more prone to malaria transmission than other districts.

Additionally, inclusion of a random intercept assumed random heterogeneity in the districts' propensity or underlying risk of malaria prevalence, which persisted throughout the entire duration of the time sequence under study. This random effects term displayed no spatial autocorrelation, and failed to closely conform to a bell-shaped curve. The model's variance, however, implied a substantial variability in the prevalence of malaria across districts. The estimated model contained considerable overdispersion (i.e., excess Poisson variability) with a quasi-likelihood scale = 76.565. The following equation was then employed to forecast the expected value of the prevalence of malaria at the district-level: prevalence = exp[-3.1876 + (random effect)$_i$]. In Jacob et al. [127], the ARIMA model c was viewed as a "cascade" of two models. The first was non-stationary: $Y_t = (1-L)^d X_t$, while the second was wide-sense stationary: $\left(1-\sum_{i=1}^{p}\phi_i L^i\right) Y_t = \left(1+\sum_{i=1}^{q}\theta_i L^i\right)\varepsilon_t$.

The explicit identification of the factorization of the autoregression polynomial into factors as above, can be extended to other cases, firstly to apply to the moving average polynomial and secondly to include other special factors. For example, having a factor $(1-L^s)$ in a model is one way of including a non-stationary seasonality of period *s* into the model. This factor has the effect of re-expressing the data as changes from *s* periods ago. Another example is the factor $\left(1-\sqrt{3}L+L^2\right)$, which includes qunatification of (non-stationary) seasonality in residually forecasted eatimates. The effect of the first type of factor is to allow each season's value to drift separately over time, whereas with the second type values for adjacent seasons move together.

Appendix 4

The Beer–Lambert law can be expressed in terms of attenuation coefficient, but in this case is better called Lambert's law since amount concentration from Beer's law is hidden inside the attenuation coefficient. The (Napierian) attenuation coefficient μ and the decadic attenuation coefficient $\mu_{10} = \mu/\ln 10$ of a material sample are related to its number densities and amount concentrations as $\mu(z) = \sum_{i=1}^{N}\mu_i(z) = \sum_{i=1}^{N}\sigma_i n_i(z)$, $\mu_{10}(z) = \sum_{i=1}^{N}\mu_{10,i}(z) = \sum_{i=1}^{N}\varepsilon_i c_i(z)$, respectively, by definition of attenuation cross section and molar attenuation coefficient. Then the Beer–Lambert law becomes

$T = e^{-\int_0^\ell \mu(z)\mathrm{d}z} = 10^{-\int_0^\ell \mu_{10}(z)\mathrm{d}z}$, and $\tau = \int_0^\ell \mu(z)\,\mathrm{d}z, A = \int_0^\ell \mu_{10}(z)\,\mathrm{d}z.$ In case of *uniform* attenuation, these relations become $T = e^{-\mu\ell} = 10^{-\mu_{10}\ell}$, or equivalently,

$$\tau = \mu\ell,$$
$$A = \mu_{10}\ell.$$

In concept, the derivation of the Beer–Lambert law is straightforward. Assume that a beam of light enters a material sample. Define z as an axis parallel to the direction of the beam. Divide the material sample into thin slices perpendicular to the beam of light, with thickness dz sufficiently small that one particle in a slice cannot obscure another particle in the same slice when viewed along the z direction. The radiant flux of the light that emerges from a slice is reduced, compared to that of the light that entered, by $\mathrm{d}\Phi_e(z) = -\mu(z)\Phi_e(z)\,\mathrm{d}z$, where μ is the (Napierian) attenuation coefficient, which yields the following first-order linear ODE: $\frac{\mathrm{d}\Phi_e}{\mathrm{d}z}(z) = -\mu(z)\Phi_e(z).$

The attenuation is caused by the photons that did not make it to the other side of the slice due to scattering or absorption. The solution to this differential equation is obtained by multiplying the integrating factor throughout to obtain $\frac{\mathrm{d}\Phi_e}{\mathrm{d}z}(z)\, e^{\int_0^z \mu(z')\mathrm{d}z'} + \mu(z)\Phi_e(z)\, e^{\int_0^z \mu(z')\mathrm{d}z'} = 0,$ which simplifies due to the product rule (applied backwards) t $\frac{\mathrm{d}}{\mathrm{d}z}\left(\Phi_e(z)\, e^{\int_0^z \mu(z')\mathrm{d}z'}\right) = 0.$

Integrating both sides and solving for Φ_e for a material of real thickness ℓ, with the incident radiant flux upon the slice $\Phi_e^i = \Phi_e(0)$ and the transmitted radiant flux $\Phi_e^t = \Phi_e(\ell)$ gives $T = \frac{\Phi_e^t}{\Phi_e^i} = e^{-\int_0^\ell \mu(z)\mathrm{d}z}.$ Since the decadic attenuation coefficient μ_{10} is related to the (Napierian) attenuation coefficient by $\mu_{10} = \mu/\ln 10$, one would also have $T = e^{-\int_0^\ell \ln 10\,\mu_{10}(z)\mathrm{d}z} = \left(e^{-\int_0^\ell \mu_{10}(z)\mathrm{d}z}\right)^{\ln 10} = 10^{-\int_0^\ell \mu_{10}(z)\mathrm{d}z}.$

To describe the attenuation coefficient in a way independent of the number densities n_i of the N attenuating species of the material sample, one introduces the attenuation cross section $\sigma_i = \mu_i(z)/n_i(z)$. The coefficient σ_i has the dimension of an area; it expresses the likelihood of interaction between the particles of the beam and the particles of the species i in the material sample. One can also use the molar attenuation coefficients $\varepsilon_i = (\mathrm{N_A}/\ln 10)\sigma_i$, where $\mathrm{N_A}$ is the Avogadro constant, to describe the attenuation coefficient in a way independent of the amount concentrations $c_i(z) = n_i(z)/\mathrm{N_A}$ of the attenuating species of the material
sample

$$T = e^{-\sum_{i=1}^N \frac{\ln 10}{\mathrm{N_A}}\varepsilon_i \int_0^\ell n_i(z)\mathrm{d}z} = \left(e^{-\sum_{i=1}^N \varepsilon_i \int_0^\ell \frac{n_i(z)}{\mathrm{N_A}}\mathrm{d}z}\right)^{\ln 10} = 10^{-\sum_{i=1}^N \varepsilon_i \int_0^\ell c_i(z)\mathrm{d}z}.$$

Expectation-maximization works to improve $Q(\boldsymbol{\theta}|\boldsymbol{\theta}^{(t)})$, rather than directly improving $\log p(\mathbf{X}|\boldsymbol{\theta})$. Here we show that improvements to the former imply improvements to the latter. For any $\mathbf{Z}$ with non-zero probability $p(\mathbf{Z}|\mathbf{X},\boldsymbol{\theta})$, we can write $\log p(\mathbf{X}|\boldsymbol{\theta}) = \log p(\mathbf{X},\mathbf{Z}|\boldsymbol{\theta}) - \log p(\mathbf{Z}|\mathbf{X},\boldsymbol{\theta})$. We take the expectation over values of $\mathbf{Z}$ by multiplying both sides by $p(\mathbf{Z}|\mathbf{X},\boldsymbol{\theta}^{(t)})$, and summing (or integrating) over $\mathbf{Z}$. The left-hand side is the expectation of a constant, so we get: $\log p(\mathbf{X}|\boldsymbol{\theta}) = \sum p(\mathbf{Z}|\mathbf{X},\boldsymbol{\theta}^{(t)}) \log p(\mathbf{X},\mathbf{Z}|\boldsymbol{\theta}) - \sum p(\mathbf{Z}|\mathbf{X},\boldsymbol{\theta}^{(t)}) \log p(\mathbf{Z}|\mathbf{X},\boldsymbol{\theta})$ $= Q(\boldsymbol{\theta}|\boldsymbol{\theta}^{(t)}) + H(\boldsymbol{\theta}|\boldsymbol{\theta}^{(t)})$, where $H(\boldsymbol{\theta}|\boldsymbol{\theta}^{(t)})$ is defined by the negated sum it is replacing. This last equation holds for any value of $\boldsymbol{\theta}$, including $\boldsymbol{\theta} = \boldsymbol{\theta}^{(t)}$, $\log p(\mathbf{X}|\boldsymbol{\theta}^{(t)}) = Q(\boldsymbol{\theta}^{(t)}|\boldsymbol{\theta}^{(t)}) + H(\boldsymbol{\theta}^{(t)}|\boldsymbol{\theta}^{(t)})$. Subtracting this last equation from the previous equation renders $\log p(\mathbf{X}|\boldsymbol{\theta}) - \log p(\mathbf{X}|\boldsymbol{\theta}^{(t)}) = Q(\boldsymbol{\theta}|\boldsymbol{\theta}^{(t)}) - Q(\boldsymbol{\theta}^{(t)}|\boldsymbol{\theta}^{(t)}) + H(\boldsymbol{\theta}|\boldsymbol{\theta}^{(t)}) - H(\boldsymbol{\theta}^{(t)}|\boldsymbol{\theta}^{(t)})$. However, Gibbs' inequality tells us that $H(\boldsymbol{\theta}|\boldsymbol{\theta}^{(t)}) \geq H(\boldsymbol{\theta}^{(t)}|\boldsymbol{\theta}^{(t)})$, so we can conclude that $\log p(\mathbf{X}|\boldsymbol{\theta}) - \log p(\mathbf{X}|\boldsymbol{\theta}^{(t)}) \geq Q(\boldsymbol{\theta}|\boldsymbol{\theta}^{(t)}) - Q(\boldsymbol{\theta}^{(t)}|\boldsymbol{\theta}^{(t)})$.

Suppose that $P = \{p_1, \ldots, p_n\}$ is a probability distribution. Then for any other probability distribution $Q = \{q_1, \ldots, q_n\}$ the following inequality between positive quantities (since the p_i and q_i are positive numbers less than one) $-\sum_{i=1}^{n} p_i \log_2 p_i \leq -\sum_{i=1}^{n} p_i \log_2 q_i$ holds with equality if and only if $p_i = q_i$ for all *i*. Put in words, the information entropy of a distribution P is less than or equal to its cross entropy with any other distribution Q.

The difference between the two quantities is the Kullback–Leibler divergence, or relative entropy, so the inequality can also be written: $D_{\mathrm{KL}}(P\|Q) \equiv \sum_{i=1}^{n} p_i \log_2 \frac{p_i}{q_i} \geq 0.$ For discrete probability distributions *P* and *Q*, the Kullback–Leibler divergence of *Q* from *P* is defined to be $D_{\mathrm{KL}}(P\|Q) = \sum_i P(i) \ln \frac{P(i)}{Q(i)}.$ In words, it is the expectation of the logarithmic difference between the probabilities *P* and *Q*, where the expectation is taken using the probabilities *P*. The Kullback–Leibler divergence is defined only if $Q(i)=0$ implies $P(i)=0$, for all *i* (absolute continuity). Whenever $P(i)$ is zero the contribution of the *i*-th term is interpreted as zero because $\lim_{x \to 0} x \ln(x) = 0$. For distributions *P* and *Q* of a continuous random variable, the Kullback–Leibler divergence is defined to be the integral: [5] $D_{\mathrm{KL}}(P\|Q) = \int_{-\infty}^{\infty} p(x) \ln \frac{p(x)}{q(x)} \mathrm{d}x,$ where *p* and *q* denote the densities of *P* and *Q*.

More generally, if *P* and *Q* are probability measures over a set *X*, and *P* is absolutely continuous with respect to *Q*, then the Kullback–Leibler divergence from *P* to *Q* is defined as $D_{\mathrm{KL}}(P\|Q) = \int_X \ln \frac{\mathrm{d}P}{\mathrm{d}Q} \mathrm{d}P,$ where $\frac{\mathrm{d}P}{\mathrm{d}Q}$ is the Radon–Nikodym derivative of *P* with respect to *Q*, and provided the expression on the right-hand side exists. Equivalently, this can be written as

$D_{\mathrm{KL}}(P\|Q) = \int_X \ln\left(\frac{\mathrm{d}P}{\mathrm{d}Q}\right) \frac{\mathrm{d}P}{\mathrm{d}Q}\,\mathrm{d}Q,$ which we recognize as the entropy of *P* relative to *Q*.

Continuing in this case, if μ is any measure on *X* for which $p = \frac{\mathrm{d}P}{\mathrm{d}\mu}$ and $q = \frac{\mathrm{d}Q}{\mathrm{d}\mu}$ exist (meaning that *p* and *q* are absolutely continuous with respect to μ), then the Kullback–Leibler divergence from *P* to *Q* is given as $D_{\mathrm{KL}}(P\|Q) = \int_X p \ln \frac{p}{q}\,\mathrm{d}\mu.$ The logarithms in these formulae are taken to base 2 if information is measured in units of bits, or to base *e* if information is measured in nats. Most formulas involving the Kullback–Leibler divergence hold regardless of the base of the logarithm.

Various conventions exist for referring to $D_{\mathrm{KL}}(P\|Q)$ in words. Often it is referred to as the divergence between *P* and *Q*. However this fails to convey the fundamental asymmetry in the relation. Sometimes it may be found described as the divergence of *P* from, or with respect to *Q* (often in the context of relative entropy, or information gain). However, in the present article the divergence of *Q* from *P* will be the language used, as this best relates to the idea that it is *P* that is considered the underlying "true" or "best guess" *S. damnosum* s.l. larval habitat distribution, that expectations will be calculated with reference to, while *Q* is some divergent, less optimal, approximate distribution. Note that the use of base-2 logarithms is optional, and allows one to refer to the quantity on each side of the inequality as an "average surprisal" measured in bits.

Note that the use of base-2 logarithms is optional, and allows one to refer to the quantity on each side of the inequality as an "average surprisal" measured in bits. Since $\log_2 a = \frac{\ln a}{\ln 2}$ it is sufficient to prove the statement using the natural logarithm (ln). Note that the natural logarithm satisfies $\ln x \leq x - 1$, for all $x > 0$ with equality if and only if $x=1$. Let I denote the set of all i for which p_i is non-zero. Then $-\sum_{i\in I} p_i \ln \frac{q_i}{p_i} \geq -\sum_{i\in I} p_i \left(\frac{q_i}{p_i} - 1\right) = -\sum_{i\in I} q_i + \sum_{i\in I} p_i = -\sum_{i\in I} q_i + 1 \geq 0.$ So theerfater the model $-\sum_{i\in I} p_i \ln q_i \geq -\sum_{i\in I} p_i \ln p_i$,may be applicable ans then trivially $-\sum_{i-1}^{n} p_i \ln q_i \geq -\sum_{i-1}^{n} p_i \ln p_i$, since the righthand side does not grow, but the lefthand side may grow or may stay the same.

For equality to hold, we require: 1) $\frac{q_i}{p_i} = 1$, for all $i \in I$, so that the approximation $\ln \frac{q_i}{p_i} = \frac{q_i}{p_i} - 1$ is exact, and 2) $\sum_{i\in I} q_i = 1$, so that equality continues to hold between the third and fourth lines of the proof. This can happen if and only if $p_i = q_i$ for $i = 1, ..., n$. The entropy of P is bounded by $H(p_1, \ldots, p_n) \leq \log n.$ The proof is trivial—simply set $q_i = 1/n$ for all *i*.

Suppose that $P = \{p_1, \ldots, p_n\}$ is a probability distribution. Then for any other probability distribution $Q = \{q_1, \ldots, q_n\}$ the following inequality between positive quantities (since the p_i and q_i are positive numbers less than one) holds

$-\sum_{i=1}^{n} p_i \log_2 p_i \leq -\sum_{i=1}^{n} p_i \log_2 q_i$ with equality if and only if $p_i = q_i$ for all *i*. Put in words, the information entropy of a distribution P is less than or equal to its cross entropy with any other distribution Q. The difference between the two quantities is the Kullback–Leibler divergence or relative entropy, so the inequality can also be written as $D_{\mathrm{KL}}(P\|Q) \equiv \sum_{i=1}^{n} p_i \log_2 \frac{p_i}{q_i} \geq 0.$

For discrete probability distributions *P* and *Q*, the Kullback–Leibler divergence of *Q* from *P* is defined as $D_{\mathrm{KL}}(P\|Q) - \sum_i P(i) \ln \frac{P(i)}{Q(i)}.$ In words, it is the expectation of the logarithmic difference between the probabilities *P* and *Q*, where the expectation is taken using the probabilities *P*. The Kullback–Leibler divergence is defined only if *Q*(*i*)=0 implies *P*(*i*)=0, for all *i* (absolute continuity). Whenever *P*(*i*) is zero the contribution of the *i*-th term is interpreted as zero because $\lim_{x \to 0} x \ln(x) = 0$. For distributions *P* and *Q* of a continuous random variable, the Kullback–Leibler divergence is defined to be the integral [5] $D_{\mathrm{KL}}(P\|Q) = \int_{-\infty}^{\infty} p(x) \ln \frac{p(x)}{q(x)} \mathrm{d}x,$ where *p* and *q* denote the densities of *P* and *Q*. More generally, if *P* and *Q* are probability measures over a set *X*, and *P* is absolutely continuous with respect to *Q*, then the Kullback–Leibler divergence from *P* to *Q* is defined as $D_{\mathrm{KL}}(P\|Q) = \int_X \ln \frac{\mathrm{d}P}{\mathrm{d}Q} \mathrm{d}P,$ where $\frac{\mathrm{d}P}{\mathrm{d}Q}$ is the Radon–Nikodym derivative of *P* with respect to *Q*, and provided the expression on the right-hand side exists. In mathematics, the Radon–Nikodym theorem is a result in measure theory which states that given a measurable space (X, Σ), if a σ-finite measure ν on (X, Σ) is absolutely continuous with respect to a σ-finite measure μ on (X, Σ), then there is a measurable function $f : X \to [0, \infty)$, such that for any measurable subset $A \subset X$: $\nu(A) = \int_A f \, d\mu$.

Equivalently, this can be written as $D_{\mathrm{KL}}(P\|Q) = \int_X \ln\left(\frac{\mathrm{d}P}{\mathrm{d}Q}\right) \frac{\mathrm{d}P}{\mathrm{d}Q} \mathrm{d}Q,$ which we recognize as the entropy of *P* relative to *Q*. Continuing in this case, if μ is any measure on *X* for which $p = \frac{\mathrm{d}P}{\mathrm{d}\mu}$ and $q = \frac{\mathrm{d}Q}{\mathrm{d}\mu}$ exist (meaning that *p* and *q* are absolutely continuous with respect to μ), then the Kullback–Leibler divergence from *P* to *Q* is given as $D_{\mathrm{KL}}(P\|Q) = \int_X p \ln \frac{p}{q} \mathrm{d}\mu.$ The logarithms in these formulae are taken to base 2 if information is measured in units of bits, or to base *e* if information is measured in nats. Most formulae involving the Kullback–Leibler divergence hold regardless of the base of the logarithm.

Thus, choosing $\boldsymbol{\theta}$ to improve $Q(\boldsymbol{\theta}|\boldsymbol{\theta}^{(t)})$ beyond $Q(\boldsymbol{\theta}^{(t)}|\boldsymbol{\theta}^{(t)})$ will improve $\log p(\mathbf{X}|\boldsymbol{\theta})$ beyond $\log p(\mathbf{X}|\boldsymbol{\theta}^{(t)})$ at least as much in the riverine habitat risk model. Under some circumstances, it is convenient to view the EM algorithm as two alternating maximization steps. Consider the

function: $F(q, \theta) = \mathrm{E}_q[\log L(\theta; x, Z)] + H(q) = -D_{\mathrm{KL}}\left(q \middle\| p_{Z|X}(\cdot|x;\theta)\right) + \log L(\theta; x)$, where q is an arbitrary probability distribution over the unobserved geosampled data z, $p_{Z|X}(\cdot|x;\theta)$ is the conditional distribution of the unobserved data given the observed data x, H is the entropy, and D_{KL} is the Kullback–Leibler divergence. Then the steps in the EM algorithm may be viewed as:

Expectation step: Choose q to maximize F: $q^{(t)} = \arg\max_q F(q, \theta^{(t)})$

Maximization step: Choose θ to maximize F: $\theta^{(t+1)} = \arg\max_\theta F(q^{(t)}, \theta)$

Boolean algebra was introduced by George Boole in his first book *The Mathematical Analysis of Logic* (1847), and described more fully in his *An Investigation of the Laws of Thought* (1854) [212, 213]. According to Huntington, the term "Boolean algebra" was first suggested by Sheffer in 1913 [214]. Boolean algebra has been fundamental in the development of digital electronics, and is provided for in all modern programming languages. It is also used in set theory and statistics. The basic operations of Boolean algebra are as follows. And (conjunction), denoted $x \wedge y$ (sometimes x AND y or Kxy), satisfies $x \wedge y = 1$ if $x = y = 1$ and $x \wedge y = 0$ otherwise. Or (disjunction), denoted $x \vee y$ (sometimes x OR y or Axy), satisfies $x \vee y = 0$ if $x = y = 0$ and $x \vee y = 1$ otherwise. Not (negation), denoted $\neg x$ (sometimes NOT x, Nx or !x), satisfies $\neg x = 0$ if $x = 1$ and $\neg x = 1$ if $x = 0$. If the truth values 0 and 1 are interpreted as integers, these operations may be expressed with the ordinary operations of arithmetic:

$$x \wedge y = x \times y$$
$$x \vee y = x + y - (x \times y)$$
$$\neg x = 1 - x$$

Alternatively, the values of $x \wedge y$, $x \vee y$, and $\neg x$ can be expressed by tabulating their values with truth tables as follows $xyx \wedge yx \vee y_x \neg x$, where

0 0 0 0 0 1
1 0 0 1 1 0
0 1 0 1
1 1 1 1

The three Boolean operations described above are referred to as basic, meaning that they can be taken as a basis for other Boolean operations, which can be built up from them by composition, the manner in which operations are combined or compounded. Operations composed from the basic operations include the following examples:

$$x \to y = \neg x \vee y$$
$$x \oplus y = (x \vee y) \wedge \neg(x \wedge y)$$
$$x \equiv y = \neg(x \oplus y)$$

These definitions give rise to the following truth tables giving the values of these operations for all four possible inputs where:

x	y	$x \rightarrow y$	$x \oplus y$	$x \equiv y$
0	0	1	0	1
1	0	0	1	0
0	1	1	1	0
1	1	1	0	1

The first operation, $x \rightarrow y$, or Cxy, is called material implication. If x is true, then the value of $x \rightarrow y$ is taken to be that of y. But if x is false, then the value of y can be ignored. However the operation must return *some* truth value and there are only two choices, so the return value is the one that entails less, namely *true*. (Relevance logic addresses this by viewing an implication with a false premise as something other than either true or false.)

The second operation, $x \oplus y$, or Jxy, is called exclusive or (often abbreviated as XOR) to distinguish it from disjunction as the inclusive kind. It excludes the possibility of both x and y. Defined in terms of arithmetic, it is addition mod 2 where $1 + 1 = 0$. The third operation, the complement of exclusive or, is equivalence or Boolean equality: $x \equiv y$, or Exy, is true just when x and y have the same value. Hence $x \oplus y$ as its complement can be understood as $x \neq y$, being true just when x and y are different. Its counterpart in arithmetic mod 2 is $x + y + 1$.

Given two operands, each with two possible values, there are $2^2 = 4$ possible combinations of inputs. Because each output can have two possible values, there are a total of $2^4 = 16$ possible binary Boolean operations. Boolean algebra treats the equational theory of the maximal two-element finitary algebra, called the Boolean prototype, and the models of that theory, called Boolean algebras. These terms are defined as follows. An algebra is a family of operations on a set, called the underlying set of the algebra. We take the underlying set of the Boolean prototype to be {0,1}.

Thus, an alegrbraically quantitated, empirical dataset of regressively tabulated trailing vegetation, turbid water, hyperproductive *S. damnosum* s.l., sparsely shaded, discontinuously canopied habitats in a weights decomposable matrix can take on finitely many arguments. For the prototype each argument of an operation will be dichotomous (e.g., either 0 or 1) as result of the operational gridding algorithms, and the number of arguments taken on for each operation during the regression exercise (e.g., arity of the operation). Even though the maximal number of parameterizable covariate was 0 or 1, the binomialization of the operation on (01) of arity n was applicable to 2^n possible outcome values.

For each choice of arguments the operation had the ability to return 0 or 1, whence there were operationizable 2^{2^n} n-ary operations. The prototype, therefore, had two operations taking no arguments, called zeroary or nullary operations, namely zero and one. It had four unary operations, two of which are constant operations, another was the identity, and the negation, returned the opposite of its argument: 1 if 0, 0 if 1. It had sixteen binary operations; again two of these are constant, another returns its first argument, yet another returns its second, one is called *conjunction* and returns 1, if both arguments are 1 and otherwise 0. Another is called *disjunction* and returns 0 if both arguments are 0 and otherwise 1, and so on. The number of $(n+1)$-ary operations in the prototype is the square of the number of n-ary operations, so there are $16^2 = 256$ ternary operations, $256^2 = 65{,}536$ quaternary operations, and so on.

The finitary operations on {0,1} may be exhibited as truth tables, thinking of 0 and 1 as the truth values false and true. They can be laid out in a uniform and application-independent way that allows us to name, or at least number, them individually. The stress on finiteness came from the idea that human *mathematical* thought is based on a finite number of principles[and all the reasonings follow essentially one rule: the *modus ponens*[25] The project was to fix a finite number of symbols (essentially the numerals 1, 2, 3, ... the letters of alphabet and some special symbols like "+", "->", "(", ")", etc.), give a finite number of propositions expressed in those symbols, which were to be taken as "foundations" (the axioms), and some rules of inference which would model the way humans make conclusions (www.mathworld.com) These names provide aconvenient shorthand for the Boolean operations. The names of the n-ary operations are binary numbers of 2^n bits. There being 2^{2n} such operations, one cannot ask for a more succinct nomenclature! Note that each finitary operation was a switching function. This layout and associated naming of operations is illustrated here in full for arities from 0 to 2.

Truth tables for the Boolean *S. damnosum* s.l. habitat model operations of arity up to 2

Constants

${}^0f_0$	${}^0f_1$
0	1

Unary Operations

x_0	${}^1f_0$	${}^1f_1$	${}^1f_2$	${}^1f_3$
0	0	1	0	1
1	0	0	1	1

Binary Operations

x_0	x_1	${}^2f_0$	${}^2f_1$	${}^2f_2$	${}^2f_3$	${}^2f_4$	${}^2f_5$	${}^2f_6$	${}^2f_7$	${}^2f_8$	${}^2f_9$	${}^2f_{10}$	${}^2f_{11}$	${}^2f_{12}$	${}^2f_{13}$	${}^2f_{14}$	${}^2f_{15}$
0	0	0	1	0	1	0	1	0	1	0	1	0	1	0	1	0	1
1	0	0	0	1	1	0	0	1	1	0	0	1	1	0	0	1	1
0	1	0	0	0	0	1	1	1	1	0	0	0	0	1	1	1	1
1	1	0	0	0	0	0	0	0	0	1	1	1	1	1	1	1	1

These tables continue at higher arities, with 2^n rows at arity n, each row giving a valuation or binding of the n variables $x_0,...x_{n-1}$, and each column headed ${}^nf_i$ rendering the value ${}^nf_i(x_0,...,x_{n-1})$ of the i-th n-ary operation at that valuation. The operations include the decomposable, field and remote georeferenceable, hyperproductive, canopied, *S. damnosum* s.l., covariate, parameterized variables, for example ${}^1f_2$ is x_0 while ${}^2f_{10}$ is x_0 (as two copies of its unary counterpart) and ${}^2f_{12}$ is x_1 (with no unary counterpart). Negation or complement $\neg x_0$ appears as ${}^1f_1$ and again as ${}^2f_5$, along with ${}^2f_3$ ($\neg x_1$, which did not appear at arity 1), disjunction or union $x_0 \vee x_1$ as ${}^2f_{14}$, conjunction or intersection $x_0 \wedge x_1$ as ${}^2f_8$, implication $x_0 \rightarrow x_1$ as ${}^2f_{13}$, exclusive-or symmetric difference $x_0 \oplus x_1$ as ${}^2f_6$, set difference $x_0 - x_1$ as ${}^2f_2$, and so on.

As a minor detail important more for its form than its content, the operations of an algebra are traditionally organized as a list. Although here we are indexing the operations of a Boolean algebra by the finitary operations on {0,1}, the truth-table presentation above serendipitously orders the operations first by arity and second by the layout of the tables for each arity. This permits organizing the set of all Boolean operations in the traditional list format. The list order for the operations of a given arity is determined by the following two rules: 1) the i-th row in the left half of the table is the binary representation of i with its least significant or 0-th bit on the left ("little-Indian" order, originally proposed by Alan Turing, so

it would not be unreasonable to call it Turing order), and 2) The *j*-th column in the right half of the table is the binary representation of *j*, again in "little-Indian" order. In effect the subscript of the operation *is* the truth table of that operation. By analogy with Gödel numbering of computable functions one might call this numbering of the Boolean operations the Boole numbering. In mathematical logic, a Gödel numbering is a function that assigns to each symbol and well-formed formula of some formal language a unique natural number, called its Gödel number. The concept was used by Kurt Gödel for the proof of his incompleteness theorems [215].

When programming in C or Java, bitwise disjunction is denoted $x|y$, conjunction as $x\&y$, and negation as $\sim x$. A program can therefore represent for example the operation $x \wedge (y \vee z)$ in these languages as $x\&(y|z)$, having previously set x = 0xaa, y = 0xcc, and z = 0xf0. The "0x" indicates that the following constant is to be read in hexadecimal or base 16, either by assignment to the probabilistically regressable, parameterizable, geospectral, unmixed, endmember, *S. damnosum* s.l. variables or defined as macros. These one-byte (eight-bit) constants can correspond to the columns for the input variables. This technique is almost universally employed in raster graphics hardware to provide a flexible variety of ways of combining and masking images, the typical operations being ternary and acting simultaneously on source, destination, and mask bits.

All bit vectors of a given length as tabulated from the empiricially, geo-spatiotemporally geopsampled, sparsely shaded, hyperproductive, trailing vegetation, turbid water, *S. damnosum s.l.* , immature data form a Boolean algebra "pointwise", meaning that any *n*-ary Boolean operation can be applied to *n* bit vectors, which can then subsequently quantitate one bit position at a time. For example, the ternary or of three bit vectors each of length in a *S. damnosum* s.l., interpolatable, wavelength, transmittance, endmember, emissivity, vulnerability forecast risk model is the bit vector of length formed by ignoring the three bits in each of the four bit positions, thus $0100 \vee 1000 \vee 1001 = 1101$. Another example is the truth tables which for the *n*-ary operations in a hyperproductive, georeferenceable, sparsely shaded, canopied, stochastically/deterministically, delineatable, eco- cartographic, risk model, whose columns are all the bit vectors of length 2^n can be combined pointwise whence the *n*-ary operations form a Boolean algebra. This works equally well for bit vectors of finite and infinite length, the only rule being that the bit positions all be indexed by the same set in order that "corresponding position" be well defined in ArcGIS.

The power set of algebraic, regressively parameterizable, field or remote georeferenceable, hyperproductive *S. damnsoum* s.l. habitats may be efficiently quantitated. The power set algebra and the set 2^W of all subsets of a given set W, however, need to be employed during the quantification exercise.

This is simply Example 2 in disguise, with W serving to index the bit positions. Any subset X of W can be viewed as the bit vector having 1's in just those bit positions indexed by elements of X. Thus the all-zero vector is the empty subset of W while the all-ones vector is W itself, these being the constants 0 and 1 respectively of the power set algebra. The counterpart of disjunction $x \vee y$ is union $X \cup Y$, while that of conjunction $x \wedge y$ is intersection $X \cap Y$. Negation $\neg x$ becomes $\sim X$, complement relative to W. There is also set difference $X \setminus Y = X \cap \sim Y$, symmetric difference $(X \setminus Y) \cup (Y \setminus X)$, ternary union $X \cup Y \cup Z$, and so on. The atoms here are the singletons, those subsets with exactly one element.

Examples 2 and 3 are special cases of a general construct of algebra called direct product, which is applicable not just to Boolean algebras but all kinds of algebra including groups, rings, etc. The direct product of any family B_i of Boolean algebras where i ranges over some index set I (not necessarily finite or even countable) is a Boolean algebra consisting of all I-tuples $(...x_i,...)$ whose i-th element is taken from B_i. The operations of a direct product are the corresponding operations of the constituent algebras acting within their respective coordinates; in particular operation ${}^n f_j$ of the product operates on n I-tuples by applying operation ${}^n f_j$ of B_i to the n elements in the i-th coordinate of the n tuples, for all i in I.

When all the algebras being multiplied together in this way are the same algebra A we call the direct product a *direct power* of A. The Boolean algebra of all 32-bit bit vectors is the two-element Boolean algebra raised to the 32nd power, or power set algebra of a 32-element set, denoted 2^{32}. The Boolean algebra of all sets of integers is 2^Z. All Boolean algebras we have exhibited thus far have been direct powers of the two-element Boolean algebra, justifying the name "power set algebra". It can be shown that every finite Boolean algebra is isomorphic to some power set algebra. Hence the cardinality (number of elements) of a finite Boolean algebra is a power of 2, namely one of $...,2^n,...$ This is called a representation theorem as it gives insight into the nature of finite Boolean algebras by giving a representation of them as power set algebras.This representation theorem does not extend to infinite Boolean algebras: although every power set algebra is a Boolean algebra, not every Boolean algebra need be isomorphic to a power set algebra. In particular, whereas there can be no countably infinite power set algebras (the smallest infinite power set algebra is the power set algebra 2^N of sets of natural numbers, shown by Cantor to be uncountable), there exist various countably infinite Boolean algebras. To go beyond power set algebras we need another construct. A subalgebra of an algebra A is any subset of A closed under the operations of A. Every subalgebra of a Boolean algebra A must still satisfy the equations holding of A, since any violation would constitute a violation for A itself. Hence, every subalgebra of a Boolean algebra is a Boolean algebra.

A subalgebra of a power set algebra is called a field of sets. Equivalently a field of sets is a set of subsets of some set W including the empty set and W and closed under finite union and complement with respect to W (and hence also under finite intersection). Birkhoff's 1935 representation theorem for Boolean algebras states that every Boolean algebra is isomorphic to a field of sets [216]. Now Birkhoff's HSP theorem for varieties can be stated as, every class of models of the equational theory of a class C of algebras is the Homomorphic image of a Subalgebra of a direct Product of algebras of C. Normally all three of H, S, and P are needed. The first of these two Birkhoff theorems shows that for the special case of the variety of Boolean algebras Homomorphism can be replaced by Isomorphism. Birkhoff's HSP theorem for varieties in general therefore becomes Birkhoff's ISP theorem for the variety of Boolean algebras.

It is convenient when talking about a set X of natural numbers to view it as a sequence $x_0,x_1,x_2,...$ of bits, with $x_i = 1$ if and only if $i \in X$. This will make it easier to talk about subalgebras of the power set algebra 2^N, which makes the Boolean algebra of all sequences of bits. It also fits well with the columns of a truth table: when a column is read from top to bottom it constitutes a sequence of bits, but at the same time it can be viewed as the set of those valuations (assignments to variables in the left half of the table) at which the function represented by that column evaluates to 1.

International Journal of Geographic Information System
Vol. 4, No. 1, April 2017, pp.1-519
Available Online at http://acascipub.com/Journals.php

Appendix 5

In Jacob et al. [22] the authors wanted to determine the contribution of sunlit canopy, *S. damnosum s.l.* habitat surface predictor variables and their shading effects. The effect of sunlit canopy on the bidirectional reflectance was quantified using the second term in equation $R(i,v) = K_g G + \frac{C}{A}\iint_{A_c} \frac{\langle i,s\rangle}{\cos\theta_i}\frac{\langle v,s\rangle}{\cos\theta_v} ds$. This variation depended on the both the density and angular distribution of ds in the equation. Strahler and Jupp [140] assumed that each object in a scene could be modelled as a sphere without mutual illumination shading between ds elements. Then the second term was approximated as: $K_c C = \frac{1}{2}\left(1+\langle i,v\rangle\right)\left(1-e^{-\lambda\pi R^{*2}\sec\theta_v}\right)C$. In this expression, the first term was the illuminated proportion of the trailing vegetation LULC habitat area based on a single sphere viewed at position v and illuminated at position i. This was weighted by the second term which was the proportion of the area of spheres visible from zenith angle θ_v. Since both terms varied smoothly between zero and one, this contribution to the riverine habitat hotspot was quite flat. In the case of a spheroid, we simply then replaced $\langle i,v\rangle$ with $\langle i',v'\rangle$, where $\langle i',v'\rangle = \cos\theta_i'\cos\theta_v' + \sin\theta_i'\sin\theta_v'\cos\phi$.

The radiative transfer equation coefficients in the decomposition of the radiation field for constructing the georeferenced *S.damnosum s.l.*riverine larval habiat Boolean model:

F^0 extraterrestrial solar radiance
$F(\bullet)$ Fresnel reflectance function
$f(\Omega',\Omega)$ BRDF of soil
$gl(\Omega)$ distribution function of the leaf normal orientation
$\Gamma(\Omega',\Omega)$ area scattering transfer function of canopy
H height of canopy in meters
i^0 extraterrestrial solar net flux incident on the top of atmosphere
$I^0(\tau,\Omega)$ unscattered solar radiance
$I^1(\tau,\Omega)$ single scattering radiance
$I^M(\tau,\Omega)$ multiple scattering radiance
$J^M(\tau,\Omega)$ source function of radiative transfer
κ leaf dimension parameter
λ wavelength
LAD leaf angle distribution
LAI leaf area index
μ_0 cosine of solar zenith angle
η leaf wax refractive index

N total Lumber of layers of the coupled medium split for multiple scattering calculation, each of thickness $\Delta\tau$

$\Omega(\mu,\phi)$ solid angle consisting of cosine of zenith angle μ and azimuth angle ϕ

$P(\Omega',\Omega)$ phase function of atmosphere

ϕ_0 solar azimuth angle

rl leaf reflectance

$R_s(\Omega',\Omega)$ bidireccional reflectance factor of soil surface

R_s reflectance of Lambertian surface

τ optical depth of medium

τ_α atmospheric optical depth

$\tau_{\alpha e}$ aerosol optical depth

τ_Γ molecular optical depth

τ_t total optical depth of the coupled atmosphere-canopy medium

t_l leaf transmittance

$u_l(z)$ leaf area density

ω single scattering albedo

Next, in order to geospatially characterize the sparsely shaded wavelength, RapidEye^{TM} and obtain stable solutions of within-canopy multiple scattering, we decomposed the spectrally extracted Red Edge NDVI biosignature into three parts; unscattered radiance $I^0(\tau,\Omega)$, single scattering radiance $I^1(\tau,\Omega)$, and multiple scattering radiance $I^M(\tau,\Omega)$ $I(\tau,\Omega) = I^0(\tau,\Omega) + I^1(\tau,\Omega) + I^M(\tau,\Omega)$ in ArcGIS.

A simple scheme was then represented by $I^0(\tau,\Omega)$ which was denoted by 1, and was not scattered by the atmosphere, but reflected directly by the within canopy surface features. $I^1(\tau,\Omega)$ represented the various Red Edge, NDVI, canopy, 5m, biosignature radiance values either scattered once by the atmosphere, denoted by 2, or once by the within canopy, structural, spectral variables which was denoted by 3. The variable $I^M(\tau,\Omega)$ was the most complicated component, which included all of other imaged, riverine, larval habitat, canopied, operationizable, georeferenced components in the radiation field of the coupled medium.

Unscattered sunlight radiances $I^0(\tau,\Omega)$ were then characterized by the following radiative transfer equation and corresponding boundary conditions. When T < Ta, the radiative transfer model rendered:

$$\begin{cases} -\mu\dfrac{\partial I^0(\tau,\Omega)}{\partial\tau} + I^0(\tau,\Omega) = 0 \\ I^0(0,\Omega) = \delta(\Omega-\Omega_0)i_0 \qquad \mu<0 \\ I^0(\tau_\alpha^{bot},\Omega) = I^0(\tau_c^{top},\Omega) \qquad \mu>0 \end{cases}$$

, where τ_a^{bot} and τ_c^{top} were the optical depths at the bottom of the atmosphere and the ToA of the habitat canopy, respectively. Here different notations from the 5m imager were used to indicate the physical meaning of the canopy

boundary conditions. The model provided the upper boundary condition, which meant only parallel sunlight illuminated the atmosphere at the top of the riverine larval habitat canopy in the direction Ω_0. When $\tau > \tau_\alpha$,the residuals were:

$$\begin{cases} -\mu\dfrac{\partial \mathrm{I}^0(\tau,\Omega)}{\partial\tau} + h(\tau,\Omega)G(\Omega)\mathrm{I}^0(\tau,\Omega) = 0 \\ \mathrm{I}^0\left(\tau_c^{top},\Omega\right) = \mathrm{I}^0\left(\tau_\alpha^{bot},\Omega\right) \qquad \mu < 0 \\ \mathrm{I}^0(\tau_t,\Omega) = fs(\Omega_0,\Omega)|\mu_0|\mathrm{I}^0(\tau_t,\Omega_0) \qquad \mu > 0 \end{cases}$$

Jointly solving the above equations with these boundary conditions rendered:

$$\mathrm{I}^0(\tau,\Omega) =$$

$$\begin{cases} \mathrm{I}_{d1}^0(\tau,\Omega) = i_0\exp\left(-\tau/|\mu|\right)\delta(\tau,\Omega_0) \qquad \mu < 0, \tau \le \tau_\alpha \\ \mathrm{I}_{d2}^0(\tau,\Omega) = \mathrm{I}_{d1}^0(\tau,\Omega) \\ \cdot\exp\left[-C(\Omega)(\tau-\tau_\alpha)/|\mu|\right] \qquad \mu < 0 \tau_\alpha < \tau \le \tau_t \\ \mathrm{I}_{u2}^0(\tau,\Omega) = i_0 \\ \cdot\exp\left[-\dfrac{\tau_\alpha + (\tau_t-\tau_\alpha)G(\Omega_0)}{|\mu_0|}\right] \\ \cdot fs(\Omega_0,\Omega)|\mu_0|\exp\left[-\varepsilon(\tau,\Omega)\right] \qquad \mu > 0, \tau_\alpha < \tau \le \tau_t \\ \mathrm{I}_{u1}^0(\tau,\Omega) = \mathrm{I}_{u2}^0(\tau_\alpha,\Omega) \\ \cdot\exp\left[-(\tau_\alpha-\tau)/\mu\right] \qquad \mu > 0, \tau \le \tau_\alpha \end{cases}$$

The Red Edge NDVI biosignature information was expressed as $\mathrm{I}_{u2}^0(\tau,\Omega)$, which represented the upwelling sunlight radiance within the georeferenced habitat canopy, and the function $\varepsilon(\tau,\Omega)$. The extinction coefficients of the canopy endmembers were modified, and we then incorporated the extracted within-canopy radiance values including the floating, hanging, and surrounding dead vegetation canopy geospectral components employing :

$$\varepsilon(\tau,\Omega) = \frac{1}{\pi}\int_\tau^{\tau_t} h(t,\Omega)G(\Omega)dt \quad = G(\Omega)\frac{\tau_t-\tau}{\mu} - \left[\sqrt{\frac{G(\Omega_0)G(\Omega)}{\mu|\mu_0|}}\frac{k\mathrm{H}}{\Delta(\Omega_0,\Omega)}\right]t_0$$

, where t_0 was defined as

$$t_0 = \exp\left[-\frac{\Delta(\Omega_0,\Omega)\tau}{k\mathrm{H}}\right] - \exp\left[-\frac{\Delta(\Omega_0,\Omega)\tau_t}{k\mathrm{H}}\right]$$

.

The Red Edge NDVI endmember biosignature model in ArcGIS revealed that for single scattering radiances, unscattered sunlight became the scattering source, and the boundary conditions. These conditions were then determined based on the fact that no incident single scattering radiances originated from above ToA or below the bottom of the canopy. When T < Ta occurred in the model, the residuals rendered:

$$\begin{cases} -\mu\dfrac{\partial \mathrm{I}^l(\tau,\Omega)}{\partial\tau} + \mathrm{I}^l(\tau,\Omega) = \\ \dfrac{\omega i_0}{4\pi}p(\Omega_0\to\Omega)\exp\left(-\dfrac{\tau}{\mu_0}\right) \\ r^1(0,\Omega) = 0 \qquad \mu < 0 \\ \mathrm{I}^1\left(\tau_\alpha^{bot},\Omega\right) \qquad \mu > 0 \end{cases}$$

Additionally, when T > Ta the decomposition trailing vegetation, *S. damnosum* s.l. larval hábitat model rendered:

$$\begin{cases} -\mu\dfrac{\partial\tau^1(\tau,\Omega)}{\partial\tau}+h(\tau,\Omega)G(\Omega)\mathrm{I}^1(\tau,\Omega) \\ \dfrac{i_0'}{\pi}\Gamma(\Omega_0,\to\Omega)\exp\left[-(\tau-\tau_\alpha)\dfrac{G(\Omega_0)}{|\mu_0|}\right] \\ \mathrm{I}^1(\tau_c^{top},\Omega)=\mathrm{I}^1(\tau_\alpha^{bot},\Omega) \qquad \mu<0 \\ \mathrm{I}^1(\tau_t,\Omega)=0 \qquad \mu>0 \end{cases}$$

, where i_0' was the incident solar net flux arriving at the top of $i_0'=i_0\exp(-\tau_\alpha/|\mu_0|)$ the habitat canopy . In the downward direction $\mu<0$, the solution was easily derived. When T < Ta, the riverine larval habitat Red Edge NDVI endmember biosignature decomposition model was solved using:

$$\mathrm{I}'(\tau,\Omega)=$$

$$\begin{cases} \dfrac{\omega Fop(\Omega_0\to\Omega)|\mu_0|}{4(|\mu_0|\leftarrow|\mu|)}\left[\exp\left(-\dfrac{\tau}{|\mu_0|}\right)-\exp\left(-\dfrac{r}{|\mu|}\right)\right] & \Omega\neq\Omega_0 \\ \dfrac{\omega F_0\tau}{4|\mu_0|}P(\Omega_0\to\Omega)\exp\left(-\dfrac{\tau}{\mu_0}\right) & \Omega=\Omega_0 \end{cases}$$

. Then $\tau_\alpha<\tau<\tau_t$ the model was solved using the equation:

$$\mathrm{I}^1(\tau,\Omega)=$$

$$\begin{cases} \dfrac{i_0'|\mu_0|\Gamma(\Omega_0\to\Omega)}{\pi\left[G(\Omega)|\mu_0|-G(\Omega_0)|\mu|\right]}t_1+\Delta\mathrm{I}^1(\tau,\Omega) & \Omega\neq\Omega_0 \\ \dfrac{(\tau-\tau_\alpha)i_0'\Gamma(\Omega_0\to\Omega)}{\pi|\mu_0|}\exp\left[-G(\Omega_0)\dfrac{\tau-\tau_\alpha}{|\mu_0|}\right] \\ \qquad +\Delta\mathrm{I}^1(\tau,\Omega) \end{cases}$$

, where t_1 was defined by the equations $t_1=\exp\left[-G(\Omega_0)\dfrac{\tau-\tau_\alpha}{|\mu_0|}\right]-\exp\left[-G(\Omega)\dfrac{\tau-\tau_\alpha}{|\mu|}\right]$ and $\Delta\mathrm{I}^1(\tau,\Omega)=\mathrm{I}^1(\tau_\alpha,\Omega)\exp[-G(\Omega)(\tau-\tau_\alpha)/|\mu|$, which represented the single scattering riverine, habitat canopy radiances emerging from the atmosphere without scattering in the riverine, trailing vegetation habitat canopy.

In the upward direction (p > 0), the solutions were a little more complicated because

$$\mathrm{I}^1(\tau,\Omega)=\begin{cases} \dfrac{1}{\mu}\int_r^{\tau_t}F(\tau',\Omega) \\ \cdot\exp\left[-\dfrac{1}{\mu}\int_\tau^{\tau'}h(\varepsilon,\Omega)G(\Omega)d\varepsilon\right]d\tau' & \tau_\alpha\le\tau\le\tau_t \\ \dfrac{\omega F_0 p(\Omega_0\to\Omega)|\mu_0|}{4(\mu+|\mu_0|)}t_2 \\ +\mathrm{I}^1(\tau_\alpha,\Omega)\exp\left(\dfrac{\tau-\tau_\alpha}{\mu}\right) & \tau<\tau_\alpha \end{cases}$$

due to the hotspot effect, which was determined by , where t_2 was $t_2=\exp\left[-\dfrac{\tau}{|\mu_0|}\right]-\exp\left[\dfrac{\tau}{\mu}-\left(\dfrac{1}{\mu_0}+\dfrac{1}{\mu}\right)\tau_\alpha\right]$, and the second integration at Ta < T < Tt in

the above equation (see Figure 9). This equation was then explicitly obtained by means of an alternative integer and range, which was solved using $F(\tau',\Omega)=\frac{i'_0}{\pi}\Gamma(\Omega_0\to\Omega)\exp\left[-G(\Omega_0)(\tau-\tau_\alpha)/|\mu_0|\right]$. The radiance $\mathrm{I}^1(\tau,\Omega)$ at Ta < T <Tt derived for the Red Edge, NDVI, endmember, biosignature material was then numerically evaluated without further assumptions. An explicit approximation to $\mathrm{I}^1(\tau,\Omega)$ was then derived and used for inversion in the canopy, LULC, biosignature decomposition model.

The first term in equation $K_cC=\frac{1}{2}\left(1+\langle i,v\rangle\right)\left(1-e^{-\lambda\pi R''^2\sec\theta_v}\right)C$ ignored the problem of mutual shading of the geosampled trailing vegetation, sparsely shaded, *S. damnosum s.l.* riverine habitat canopy and the ripple water components. Strahler and Jupp [140] handled this problem through multiple integration, in which the mutual shadowing of canopies and other associated objects were treated in the same way as the mutual shading of leaves. However, our objective in this research was to derive a simple approximation to describe the effect of the *S. damnosum s.l.* larval habitat based on collections of individual discrete reflectance surface values (i.e., Precambrian rock and ripple water components). To carry this out, we developed an approach that applied one-stage geometric optics to deal with the spatial relationship between the sub-pixel endmember reflectance spectra of the decomposed *S. damnosum s.l.* habitat surface, the ripple water components that were mutually shaded in the illumination direction, and the parts mutually shaded in the view direction. We then quantified mutual shadowing proportions generated from the *S. damnosum s.l.* habitat and its associated ripple water components. In Li and Strahler [217] and Li [218], simulation and mathematics simplified to the one-dimensional case was proved so that for the nadir-viewed cone model, mutual shadowing of illumination would not change the ratio $K_c/\left(1-K_g\right)$. In this research, this ratio was itself denoted K_c, which we used to generate u A_c/A for determining consistency with K_g, where the mutual shadowing in illumination and viewing directions was independent A_c/A for consistency with K_g.

We then considered the proportion of the *S. damnosum s.l.* habitat which was mutually shadowed by the Precambrian rock and ripple water components. In the direction of illumination, the immature, *S. damnosum s.l.* riverine habitat had an area of $\pi R^2\sec\theta'_i$, and the total projected LULC area of the habitat was then calculated to be $\lambda\pi R^2\sec\theta'_i$, if there was no mutual shadowing. Because of mutual shadowing, however, the net projected area was $1-e^{\lambda\pi R^2\sec\theta'_i}$. The difference indicated the total mutual shadowing of the *S. damnosum s.l.* riverine habitat attribute. Thus, the authors in Jacob et al. [22] defined the quantity M_i, the mutual shadowing proportion in the illumination direction, as $M_i=1-\frac{1-e^{-\lambda\pi R^2\sec\theta'_i}}{\lambda\pi R^2\sec\theta'_i}$. M_i, which revealed the degree of mutual shadowing in the illumination direction. In other words, each spheroid, on average, had a proportion M_i of the imaged *S. damnosum s.l.* habitat surface area that was not sunlit. This part of the habitat was concentrated at the lower part of the spheroid. We then generated a boundary drawn on the habitat surface of the spheroid with the area comprising M_i located below it. Similarly, we defined M_v as the mutual shadowing

proportion of the ripple water components in the view direction as $M_v = 1 - \frac{1 - e^{-\lambda \pi R^2 \sec \theta_v'}}{\lambda \pi R^2 \sec \theta_v'}$. The viewing shadows were concentrated at the lower part of the spheroid so we were able to define the M_v boundary. The proportion of sunlight the RapidEye™ sensor captured corresponded to the area above both M_I and M_v boundaries, which were then dependent on both zenith and azimuth differences between the illumination and view directions. At the hotspot, M_i and M_v boundaries overlapped and the RapidEye™ data revealed no mutual shadowing of the *S. damnosum s.l.* habitat or the ripple water components. When the view zenith angle was larger than the illumination zenith angle, M_v was greater than M_i and little to no mutually shaded habitat area was visible, based on the azimuth differences between the imaged objects. Thus, we were able to capture the essence of the mutual-shading effect of the canopy, and the ripple water components.

We then quantified the *f*-Ratio of Nonnadir-Viewed Spheroids. First, we considered a single spheroid in the decomposed sub-mixel endmember, trailing vegetation, hyperproductive, georeferenced, canopied, sparsely shaded, spectral data. For the spheroidal case, it is necessary to show whether the *f*-Ratio is still independent of density, as in the case of the nadir-viewing cones [217, 218]. From the view direction, the spheroid had a projected area $\Gamma_v = \pi R^2 \sec \theta_v'$. However, only the portion $\frac{1}{2}\left(1 + \langle i', v' \rangle\right)$ of the *S. damnosum s.l.* habitat with ripple water components was sunlit. Similarly, the illumination shadow on the ground occupied the habitat area $\pi R^2 \sec \theta_i'$. The compound area of viewed habitat, and ripple water components plus illumination shadow projected onto the background was $\Gamma = \pi R^2 \left[\sec \theta_i' + \sec \theta_v' - O(\theta_i', \theta_v', \phi)\right]$. Thus, we defined the *f*-ratio for the spheroidal and its associated trailing vegetation, canopied, sparsely shaded attributes as $F = \frac{\Gamma_c}{\Gamma} = \frac{\frac{1}{2}\left(1 + \langle i', v' \rangle\right) \sec \theta_v'}{\sec \theta_i' + \sec \theta_v' - O(\theta_i', \theta_v', \phi)}$, where Γ_c was the sunlit area of the *S. damnosum s.l.* riverine habitat, Precambrian rock and ripple water components. We then defined the corresponding ratio $f = \frac{K_c}{1 - K_g}$ for the endmember selection of these RapidEye™, sub-mixel emissivities. For our purposes, *n* represented the shadow parameters generated from the decomposed, 5m, *S damnosum s.l.* riverine habitat mixel. If there was no mutual shadowing, we had $f = F$. As *n* increased, however, mutual shadowing occurred, and as such, $K_g = e^{-\lambda \pi R^2 \left[\sec \theta_i' + \sec \theta_v' - O(\theta_i, \theta_v, \phi)\right]}$. We then defined the mutual shadowing proportion M as $M = 1 - \frac{1 - K_g}{\lambda \Gamma}$, which was the fraction of total shadowing cast from the ripple water components that fell onto the *S. damnosum s.l.* habitat instead of the background. The sunlit and viewed habitat surface features were reduced by hiding either from viewing or from illumination. Thus, the *f*-ratio with mutual shadowing was $f = \frac{n\Gamma_c - \sum \Delta_{A_c}}{A\left(1 - K_g\right)}, \quad = F \frac{1 - \sum \Delta_{A_c} / \left(n\Gamma_c\right)}{1 - M}$, where $\sum \Delta_{A_c}$ was the total decrement from $n\Gamma_c$ to A_c (i.e., the background-projected area of viewed sunlit, riverine habitat surface). We expressed $\sum \Delta_{A_c}$ as three terms: a decrement due to mutual shading in the view direction, plus a decrement due to mutual shading in the sun direction, and a subtraction of those elements shaded in both directions

using $\sum \Delta_{A_c} = n\Gamma_v\left(P_v M_v + P_i M_i - P_o\right)$, where P_v was the conditional probability that the *S. damnosum s.l.* habitat faced the sun given that it was mutually shaded from view. In this research *Pi* was the probability that ripple water habitat surface elements faced the viewer given that it was mutually shaded from illumination. Both P_i and P_v were average proportions of the habitat areas projected in the view direction. P_o, the third term, overlapped part of the first two terms, expressed as a fraction of Γ_v. P_o contained three parts derived from the RapidEye^{TM}-imaged habitat surface elements: ripple water components and the vegetation canopy geoclassified LULC structure. This collection contributed to the hotspot, due to the spatial correlation of the shadows. Since the probabilities of being hidden in multiple directions were not independent, we were able to substitute $\sum \Delta_{A_c} = n\Gamma_v\left(P_v M_v + P_i M_i - P_o\right)$ into $f = \frac{n\Gamma_c - \sum \Delta_{A_c}}{A\left(1-K_g\right)}$, $= F\frac{1-\sum \Delta_{A_c}/\left(n\Gamma_c\right)}{1-M}$, which yielded a single expression for $f = F\frac{1-\Gamma_v\left(P_v M_v + P_i M_i - P_o\right)/\Gamma_c}{1-M}$. We then modeled, P_v, P_i, and P_o. We used all illumination or viewing shadows incorporating M_i and M_v boundaries respectively. In our model, P_v, P_i, and P_o were used to visualize the M_v and M_i boundaries. If viewing and illumination shadows fall strictly below M_v and M_i boundaries, then P_v,, the conditional probability that at surface element facing the sun given the mutually shadowed areas will be the ratio of the illuminated portion of the projected surface below the M_v boundary [219].

Correspondingly, in this research, P_i was the conditional probability that the sampled *S. damnosum s.l.* habitat directly faced the viewer given that it was mutually shaded from illumination and was the ratio of the viewed portion of the projected habitat area below the M_i boundary. Note, that M_i was the proportion of mutually-shaded *S. damnsoum s.l.* habitat surface projected to the direction of illumination, but $P_i M_i \Gamma_v$ was the area of this fraction of the habitat surface with Precambrian rock and ripple water components projected to viewing direction. Proper calculation of this portion of the riverine habitat and its associated attributes involved some projection change. We used P_o as the variable representing the overlap area o, which was also represented as a fraction of Γ_v.

The authors of Jacob et al. [45] then considered the case in the principal plane. For simplicity, they assumed that all shadows from the *S. damnosum s.l.* habitat, and rippled water components fell below the boundaries M_v and M_i, which were the traces of planes intersecting the spheroid at its center. The angle between the planes of the M_i and the illumination boundary was $\theta_{M_i} = \cos^{-1}\left(1-2M_i\right)$. The authors defined θ_{M_v} similarly. At the hotspot, the M_i and M_v boundaries coincided when $P_v = P_i = 1$, $P_o = M_v = M$, and $f = F = 1$. It was then assumed that the viewing zenith angle increased to $\theta_v > \theta_i$. In usual cases when mutual shadowing is considered, the M_v boundary is higher than the M_i boundary [23, 24]. In the RapidEye^{TM} sensor's view, P_v was the ratio of the *S. damnosum s.l.* habitat's canopied surface area between M_v boundary and the illumination boundary to the whole area under the M_v boundary. That is, $P_v = \frac{M_v\Gamma_v - \left(\Gamma_v - \Gamma_c\right)}{M_v\Gamma_v}$, while P_i was one, and P_o cancelled the M_i term. Then, the equation became $f = F\frac{1-P_v M_v \Gamma_v/\Gamma_c}{1-M} = F\frac{\left(1-M_v\right)\Gamma_v}{\left(1-M\right)\Gamma_c} = \frac{1-e^{-\lambda\Gamma_v}}{\left(1-K_g\right)}$. This result suggested that when the viewing direction in the principal plane deviated from ($\theta v > \theta i$), the

f -ratio will change in the endmember model. When the coverage is very low, the increment of θ_m may be also so small that M_v will be under the M_i boundary. In this case, mutual shadowing can be simply ignored as in Strahler and Jupp, [140].

The authors in Jacob et al. [22] found that when θ_v moved inward on the principal plane but had not reached nadir, the M_i was higher than M_v. Hence, $P_v = 1$, $P_o = M_v$, and $P_i = \frac{1-\cos\left(\theta_{M_i} - \theta_i' + \theta_v' \cos\phi\right)}{1-\cos\theta_{M_i}}$. After θv passed the nadir, the M_v boundary went to the opposite side of the spheroid from M_i. In this case, the RapidEye^{TM}, sub-mixel spectral data revealed the horizontal projection of the habitat and its ripple water components at $\phi = \pi/2$. The authors then used *Pi* just as in Strahler and Jupp, [140], with ϕ equal to π, and P_v was the fraction of M_v over the illumination boundary, i.e.,

$$P_v = \begin{cases} \frac{1-\cos\left(\theta_{M_v} - \theta_v' + \theta_v' \cos\theta\right)}{1-\cos\theta_{M_v}}, & \left(\theta_{M_v} - \theta_v' + \theta_v' \cos\theta\right) \geq 0 \\ 0, & \left(\theta_{M_v} - \theta_v' + \theta_v' \cos\theta\right) < 0 \end{cases}.$$

Note, the authors reported that when θ_v was between the hotspot and nadir, P_v was always one, so a discontinuity of P_v appeared at the nadir. This discontinuity arose from the assumption that all shadows fell under the M_v boundary. Additionally, in this research, the M_v at $\theta_v = 0$ was the physical intersection of boundaries between the habitat, and the rippled water components, which did not change with viewing geometry, thus, $P_v M_v$ was still continuous at nadir, and equal to P_o. In other words, the formula had a very large viewing zenith, so that $\theta_{M_v} - \theta_i' + \theta_v' \cos\phi > 0$, $\sum \Delta_{A_c} / (n\Gamma_c) = M$. When M_i and M_v were independent, $f = \frac{n\Gamma_c - \sum \Delta_{A_c}}{A(1-K_g)}$, $= F\frac{1-\sum \Delta_{A_c}/(n\Gamma_c)}{1-M}$.

If all the spatial objects are at the same height, the situation will be very close to the "uniform height case" – that is, mutual shadows will always fall on the lower part of the objects and the object top-viewing effect will be strong [218]. However, when heights are distributed over a wide range, the top layer of the canopy will play a more important role in determining the BRDF of the canopy than the lower layer [219]. Therefore, when the habitat structural heights were quantified by spectral distribution, the BRDF was apparent. The BRDF was determined by the size, shape, and height of the trailing vegetation habitat and the ripple water components in the top layer. Thus, we restricted ourselves to considering a single top layer only, where the range of distribution of height of the sampled *S. damnosum s.l.* riverine habitat and its attributes did not exceed twice the vertical axis of the spheroid. To share the weighting between the spatiotemporally sampled, spectral predictor, covariate, coefficient estimates we used the equation $\beta = \left(1 - \frac{h_2 - h_1}{4b}\right)^2$, if $(h_2 - h_1) \leq 4b$. When $(h_2 - h_1) > b$, β is forced to be zero and it is necessary to redefine the layers (Keshava and Mustard 2002). By doing so, both P_v and P_i were calculated as a weighted sum of

corresponding terms $P = \beta P_1 + (1-\beta)P_2$, where P_1 and P_2 were the spectral probabilities associated with the spatial dimensions of the sampled habitat.

The bidirectional reflectance was modeled as a pure phenomenon that resulted in scenes of discrete, three-dimensional objects (i.e., turbid ripple water components) from the *S. damnosum s.l.* riverine habitat being illuminated and viewed from different positions in the hemisphere. The resulting scene was broken down into their canopy fractions, specifically sunlit and shadowed background, as well as scene brightness. Illumination direction was calculated by a linear combination of the canopy fractions and their respective radiance estimates. The shape of the patterns of the diffuse rippled water components were the driving explanatory spectral predictor variables in the model. These *S. damnosum s.l.* riverine habitat, spectral, sub-pixel emissivities conditioned the mixture of sunlit and shaded objects and background data that was observed from multiple viewing directions, thus quantifying all directions of illumination. This mixture, in turn, controlled the brightness in the image. However, since the use of data for quantitative spectral monitoring requires consistent surface reflectance data [23] we corrected the radiance effects from varying sun sensor target geometries in the multitemporal, RapidEye^{TM} datasets described by the BRDF. In this research, measuring the spread of the corrected results from the desired equal reflectance line provided a measure of the accuracy of our method. After correction, the root mean square reflectance errors were approximately 0.01 in the visible and 0.02 in the near-infrared.

An expression for additional azimuthual variation was also derived from the geometric-optical model. This azimuthual variation differed fundamentally in radiance for each layer of the *S. damnosum s.l.* riverine habitat canopy. It was observed that all non-zero polar angles were most evident in the canopy when vertical and nearly opaque components of the *S.damnosum s.l.* habitat and its neighboring Precambrain rock and ripple water components were illuminated and viewed along polar sun angles. For the variation of the directional reflectance of the multi-scattered diffuse riverine canopy cover, azimuthual view angles and shade-related parameters were quantified using the illuminated area of the imaged habitat (i.e., areas affected by the sun at large angles from the zenith). Our results also indicated that the cause of the azimuthual variation could be traced to solar flux illumination of the vertically-oriented Precambrian rock and rippled water components, as well as the variation of reflectance moderated by azimutually isotropic sources of flux from sky light and the riverine larval habitat canopy reflectance values. Spectral unmixing yielded abundance estimates for each endmember together summing up to the 100% reflectance measured in the image. A scattergram representing the endmember reference signature of *S. damnosum s.l.* habitat ripple water pixel reflectance values was then generated.

Appendix 6

The Laplace transform is an integral transform, perhaps second only to the Fourier transform in its utility in solving physical problems. general integral transform is defined by $g(\alpha) = \int_a^b f(t)\,K(\alpha, t)\,dt,$ where $K(\alpha, t)$ is called the integral kernel of the transformhe function $K(\alpha, t)$ in an integral or integral transform $g(\alpha) = \int_a^b f(t)\,K(\alpha, t)\,dt.$ Whittaker and Robinson (1967, p. 376) use the term nucleus for kernel. he Laplace transform satisfied a number of useful properties. Consider exponentiation. If $\mathcal{L}[f(t)](s) = F(s)$ for $s > a$ (i.e., $F(s)$ is the Laplace transform of f),

then $\mathcal{L}_t\left[e^{at}f\right](s) = F(s-a)$ for $s > a + \alpha$. This follows from $F(s-a) = \int_0^\infty f e^{-(s-a)t}\,dt = \int_0^\infty \left[f(t)\,e^{at}\right] e^{-st}\,dt = \mathcal{L}_t\left[e^{at} f(t)\right](s)$. The Laplace transform also has nice properties when applied to integrals of functions. If $f(t)$ is piecewise continuous and $|f(t)| \leq M\,e^{\alpha t}$, then $\mathcal{L}_t\left[\int_0^t f(t')\,dt'\right] = \frac{1}{s}\mathcal{L}_t[f(t)](s)$. It is particularly useful in solving linear ordinary differential equations such as those arising in the analysis of electronic circuits. The (unilateral) Laplace transform $\mathcal{L}$ (not to be confused with the Lie derivative, also commonly denoted $\mathcal{L}$) is defined by $\mathcal{L}_t[f(t)](s) \equiv \int_0^\infty f(t)\,e^{-st}\,dt$, where $f(t)$ is defined for $t \geq 0$ [57]. The unilateral Laplace transform is almost always what is meant by "the" Laplace transform, although a bilateral Laplace transform is sometimes also defined as $\mathcal{L}_t^{(2)}[f(t)](s) = \int_{-\infty}^\infty f(t)\,e^{-st}\,dt$ [220]. The unilateral Laplace transform $\mathcal{L}_t[f(t)](s)$ is implemented in the Wolfram Language as LaplaceTransform [*f*[*t*], *t*, *s*].

The inverse Laplace transform is known as the Bromwich integral, sometimes known as the Fourier-Mellin integral (see also the related Duhamel's convolution principle). A table of several important one-sided Laplace transforms is given below:

f	$\mathcal{L}_t[f(t)](s)$	conditions
t^n	$\frac{n!}{s^{n+1}}$	$n \in \mathbb{Z} \geq 0$
t^α	$\frac{\Gamma(\alpha+1)}{s^{\alpha+1}}$	$\Re[\alpha] > -1$
$\cos(\omega t)$	$\frac{s}{s^2+\omega^2}$	$\omega \in \mathbb{R}$
$\sin(\omega t)$	$\frac{\omega}{s^2+\omega^2}$	$s > \lvert\Im[\omega]\rvert$
$\cosh(\omega t)$	$\frac{s}{s^2-\omega^2}$	$s > \lvert\Re[\omega]\rvert$
$\sinh(\omega t)$	$\frac{\omega}{s^2-\omega^2}$	$s > \lvert\Im[\omega]\rvert$
$e^{at}\sin(bt)$	$\frac{b}{(s-a)^2+b^2}$	$s > a + \lvert\Im[b]\rvert$
$e^{at}\cos(bt)$	$\frac{s-a}{(s-a)^2+b^2}$	$b \in \mathbb{R}$

$H_c(t)$	$\begin{cases} \frac{1}{s} & \text{for } c \le 0 \\ \frac{e^{-cs}}{s} & \text{for } c > 0 \end{cases}$	
$J_0(t)$	$\frac{1}{\sqrt{s^2+1}}$	
$J_n(at)$	$\frac{\left(\sqrt{s^2+a^2}-s\right)^n}{a^n\sqrt{s^2+a^2}}$	$n \in \mathbb{Z} \ge 0$

In the above table, $J_0(t)$is the zeroth-order Bessel function of the first kind, $\delta(t)$ is the delta function, and $H_c(t)$ is the heaviside step function. The Laplace transform has many important properties. The Laplace transform existence theorem states that, if $f(t)$ is piecewise continuous on every finite interval in $[0,\infty)$, satisfying $|f(t)| \le M e^{at}$, for all $t \in [0,\infty)$, then $\mathcal{L}_t[f(t)](s)$ exists for all $s > a$. The Laplace transform is also unique, in the sense that, given two functions $F_1(t)$ and $F_2(t)$ with the same transform so that $\mathcal{L}_t[F_1(t)](s) = \mathcal{L}_t[F_2(t)](s) \equiv f(s)$, then Lerch's theorem guarantees that the integral $\int_0^a N(t)\,dt = 0$ vanishes for all $a > 0$ for a null function defined by $N(t) \equiv F_1(t) - F_2(t)$.

The Laplace transform is linear since $\mathcal{L}_t[a f(t) + b g(t)] = \int_0^\infty [a f(t) + b g(t)] e^{-st}\,dt = a\int_0^\infty f e^{-st}\,dt + b\int_0^\infty g e^{-st}\,dt = a\,\mathcal{L}_t[f(t)] + b\,\mathcal{L}_t[g(t)]$. The Laplace transform of a convolution is given by $\mathcal{L}_t[f(t) * g(t)] = \mathcal{L}_t[f(t)]\,\mathcal{L}_t[g(t)]$. Now consider differentiation. Let $f(t)$ be continuously differentiable $n-1$ times i $[0,\infty)$. If $|f(t)| \le M e^{at}$, then $\mathcal{L}_t\left[f^{(n)}(t)\right](s) = s^n\,\mathcal{L}_t[f(t)] - s^{n-1} f(0) - s^{n-2} f'(0) - \ldots - f^{(n-1)}(0)$. This can be proved by integration by parts, $\mathcal{L}_t[f'(t)](s) = \lim_{a\to\infty}\int_0^a e^{-st} f'(t)\,dt = \lim_{a\to\infty}\left\{\left[e^{-st} f(t)\right]_0^a + s\int_0^a e^{-st} f(t)\,dt\right\} =$
$\lim_{a\to\infty}\left[e^{-sa} f(a) - f(0) + s\int_0^a e^{-st} f(t)\,dt\right] = s\,\mathcal{L}_t[f(t)] - f(0)$.

Continuing for higher-order derivatives then gives $\mathcal{L}_t[f''(t)](s) = s^2\,\mathcal{L}_t[f(t)](s) - s f(0) - f'(0)$.This property can be used to transform differential equations into algebraic equations, a procedure known as the Heaviside calculus, which can then be inverse transformed to obtain the solution. For example, applying the Laplace transform to the equation $f''(t) + a_1 f'(t) + a_0 f(t) = 0$gives $\left\{s^2\,\mathcal{L}_t[f(t)](s) - s f(0) - f'(0)\right\} + a_1\{s\,\mathcal{L}_t[f(t)](s) - f(0)\} + a_0\,\mathcal{L}_t[f(t)](s) = 0$
$\mathcal{L}_t[f(t)](s)\left(s^2 + a_1 s + a_0\right) - s f(0) - f'(0) - a_1 f(0) = 0,$ which can be rearranged to $\mathcal{L}_t[f(t)](s) = \frac{s f(0) + f'(0) + a_1 f(0)}{s^2 + a_1 s + a_0}$. If this equation can be inverse Laplace transformed, then the original differential equation is solved.

In general, non-homogeneous differential equation is given by $x^2\frac{d^2y}{dx^2}+\alpha x\frac{dy}{dx}+\beta y=S(x),$

and the homogeneous equation is $x^2y''+\alpha xy'+\beta y=0,$ $y''+\frac{\alpha}{x}y'+\frac{\beta}{x^2}y=0.$ Now attempt to convert the equation from $y''+p(x)y'+q(x)y=0$ to one with constant coefficients $\frac{d^2y}{dz^2}+A\frac{dy}{dz}+By=0$ by using the standard transformation for linear second-order ordinary differential equations. Comparing (3) and (5), the functions $p(x)$ and $q(x)$ are $p(x)\equiv\frac{\alpha}{x}=\alpha x^{-1}$ and $q(x)\equiv\frac{\beta}{x^2}=\beta x^{-2}.$ Let $B=\beta$ and define $z\equiv B^{-1/2}\int\sqrt{q(x)}\,dx=\beta^{-1/2}\int\sqrt{\beta x^{-2}}\,dx=\int x^{-1}\,dx=\ln x.$ Then A is given by $A=\frac{q'(x)+2p(x)q(x)}{2[q(x)]^{3/2}}B^{1/2}=\frac{-2\beta x^{-3}+2(\alpha x^{-1})(\beta x^{-2})}{2(\beta x^{-2})^{3/2}}\beta^{1/2}=\alpha-1,$ This is a constant. Therefore, the equation becomes a second-order ordinary differential equation with constant coefficients $\frac{d^2y}{dz^2}+(\alpha-1)\frac{dy}{dz}+\beta y=0.$ Define $r_1=\frac{1}{2}\left(-A+\sqrt{A^2-4B}\right)=\frac{1}{2}\left[1-\alpha+\sqrt{(\alpha-1)^2-4\beta}\right]$ and $r_2=\frac{1}{2}\left(-A-\sqrt{A^2-4B}\right)=\frac{1}{2}\left[1-\alpha-\sqrt{(\alpha-1)^2-4\beta}\right]$ and $a\equiv\frac{1}{2}(1-\alpha)$ with $b\equiv\frac{1}{2}\sqrt{4\beta-(\alpha-1)^2}.$ The solutions are $y=\begin{cases}c_1e^{r_1z}+c_2e^{r_2z} & (\alpha-1)^2>4\beta\\ (c_1+c_2z)e^{az} & (\alpha-1)^2=4\beta\\ e^{az}[c_1\cos(bz)+c_2\sin(bz)] & (\alpha-1)^2<4\beta.\end{cases}$ In terms of the original variable x, $y=\begin{cases}c_1|x|^{r_1}+c_2|x|^{r_2} & (\alpha-1)^2>4\beta\\ (c_1+c_2\ln|x|)|x|^a & (\alpha-1)^2=4\beta\\ |x|^a[c_1\cos(b\ln|x|)+c_2\sin(b\ln|x|)] & (\alpha-1)^2<4\beta.\end{cases}$ Zwillinger [221 p. 120] gives two other types of equations known as Euler differential equations, $y'=\pm\sqrt{\frac{ay^4+by^3+cy^2+dy+e}{ax^4+bx^3+cx^2+dx+e}}$ [222, p. 201] and $y'+y^2=\alpha x^m$ the latter of which can be solved in terms of Bessel functions. Function $Z_n(x)$ defined by the recurrence relations $Z_{n+1}+Z_{n-1}=\frac{2n}{x}Z_n$ and $Z_{n+1}-Z_{n-1}=-2\frac{dZ_n}{dx}.$ The Bessel functions are more frequently defined as solutions to the differential equation $x^2\frac{d^2y}{dx^2}+x\frac{dy}{dx}+(x^2-n^2)y=0.$ There are two classes of solution, called the Bessel function of the first kind $J_n(x)$ and Bessel function of the second kind $Y_n(x)$.

The Bessel functions of the first kind $J_n(x)$ are defined as the solutions to the Bessel differential equation $x^2\frac{d^2y}{dx^2}+x\frac{dy}{dx}+(x^2-n^2)y=0$, which are nonsingular at the origin. They are sometimes also called cylinder functions or cylindrical harmonics. The above plot shows $J_n(x)$ for $n=0$, 1, 2, ..., 5. The notation J_{in} was first used by Hansen (1843) and subsequently

by Schlömilch (1857) to denote what is now written $J_n(2z)$ [223, p. 14). However, Hansen's definition of the function itself in terms of the generating function $e^{z(t-1/t)/2} = \sum_{n=-\infty}^{\infty} t^n J_n(z)$. is the same as the modern one [223, p. 14]. Bessel used the notation I_k^n to denote what is now called the Bessel function of the first kind (Cajori 1993, vol. 2, p. 279). The Bessel function $J_n(z)$ can also be defined by the contour integral $J_n(z) = \frac{1}{2\pi i} \oint e^{(z/2)(t-1/t)} t^{-n-1}\, dt,$ where the contour encloses the origin and is traversed in a counterclockwise direction [224, p. 416]. The Bessel function of the first kind is implemented in the Wolfram Language as Bessel J[*nu*, *z*]. To solve the differential equation, apply Frobenius method using a series solution of the form $y = x^k \sum_{n=0}^{\infty} a_n x^n = \sum_{n=0}^{\infty} a_n x^{n+k}.$

If x_0 is an ordinary point of the ordinary differential equation, expand y in a Taylor series about x_0. Commonly, the expansion point can be taken as $x_0 = 0$, resulting in the Maclaurin series $y = \sum_{n=0}^{\infty} a_n x^n.$ Plug y back into the ODE and group the coefficients by power. Now, obtain a recurrence relation for the nth term, and write the series expansion in terms of the a_ns. Expansions for the first few derivatives are $y = \sum_{n=0}^{\infty} a_n x^n$, $y' = \sum_{n=1}^{\infty} n a_n x^{n-1}$, $y'' = \sum_{n=0}^{\infty} (n+1) a_{n+1} x^n$, $= \sum_{n=2}^{\infty} n(n-1) a_n x^{n-2}$ $= \sum_{n=0}^{\infty} (n+2)(n+1) a_{n+2} x^n.$ If x_0 is a regular singular point of the ordinary differential equation, $P(x)y'' + Q(x)y' + R(x)y = 0$, solutions may be found by the Frobenius method or by expansion in a Laurent series. In the Frobenius method, assume a solution of the form $y = x^k \sum_{n=0}^{\infty} a_n x^n,$ so that $y = x^k \sum_{n=0}^{\infty} a_n x^n$ $= \sum_{n=0}^{\infty} a_n x^{n+k}$, $y' = \sum_{n=0}^{\infty} a_n (n+k) x^{k+n-1}$, $y'' = \sum_{n=0}^{\infty} a_n (n+k)(n+k-1) x^{k+n-2}.$

Now, plug y back into the ODE and group the coefficients by power to obtain a recursion formula for the a_nth term, and then write the series expansion in terms of the a_ns. Equating the a_0 term to 0 will produce the so-called indicial equation, which will give the allowed values of k in the series expansion. As an example, consider the Bessel differential equation $x^2 \frac{d^2y}{dx^2} + x \frac{dy}{dx} + (x^2 - m^2) y = 0.$ Plugging (◇) into (◇) yields $\sum_{n=0}^{\infty} (k+n)(k+n-1) a_n x^{k+n} + \sum_{n=0}^{\infty} (k+n) a_n x^{k+n} + \sum_{n=2}^{\infty} a_{n-2} x^{k+n} - m^2 \sum_{n=0}^{\infty} a_n x^{n+k} = 0.$ The indicial equation, obtained by setting $n = 0$, is then $a_0 [k(k-1) + k - m^2] = a_0 (k^2 - m^2) = 0.$ Since a_0 is defined as the first nonzero term, $k^2 - m^2 = 0$, so $k = \pm m$. For illustration purposes, ignore $k = -m$ and consider only the case $k = m$ (avoiding the special case $m \neq 1/2$), then equation (14) requires that $a_1 (2m+1) = 0$, so $a_1 = 0$ and $[a_n n(2m+n) + a_{n-2}] x^{m+n} = 0$(so) and $n = 2$ for, 3, ..., so $a_n = -\frac{1}{n(2m+n)} a_{n-2}$ for $n > 1$. Plugging back in to (◇), rearranging, and simplifying then gives the series solution that defined the Bessel function of the first kind $J_m(x)$, which is

the nonsingular solution to (◇). (Considering the case $m=-k$proceeds analogously and results in the solution $J_{-m}(x)=(-1)^n J_m(x)$.)

Fuchs's theorem guarantees that at least one power series solution will be obtained when applying the Frobenius method if the expansion point is an ordinary, or regular, singular, point. For a regular singular point, a Laurent series expansion can also be used. Expand $y$in a Laurent series, letting $y=c_{-n}x^{-n}+\ldots+c_{-1}x^{-1}+c_0+c_1x+\ldots+c_nx^n+\ldots$. Plug y back into the ODE and group the coefficients by power. Now, obtain a recurrence formula for the c_n^{th} term, and write the Taylor series in terms of the c_ns. Plugging into (1) yields

$$x^2\sum_{n=0}^{\infty}(k+n)(k+n-1)a_n x^{k+n-2}+ x\sum_{n=0}^{\infty}(k+n)a_n x^{k+n-1}+x^2\sum_{n=0}^{\infty}a_n x^{k+n}-m^2\sum_{n=0}^{\infty}a_n x^{n+k}=0$$

$$\sum_{n=0}^{\infty}(k+n)(k+n-1)a_n x^{k+n}+\sum_{n=0}^{\infty}(k+n)a_n x^{k+n}+\sum_{n=0}^{\infty}a_{n-2}x^{k+n}-m^2\sum_{n=0}^{\infty}a_n x^{n+k}=0.$$

The indicial equation, obtained by setting $n=0$, is $a_0\left[k(k-1)+k-m^2\right]=a_0\left(k^2-m^2\right)=0$. Since a_0 is defined as the first nonzero term, $k^2-m^2=0$, so $k=\pm m$. Now, if $k=m$,

$$\sum_{n=0}^{\infty}\left[(m+n)(m+n-1)+(m+n)-m^2\right]a_n x^{m+n}+\sum_{n=2}^{\infty}a_{n-2}x^{m+n}=0$$

$$\sum_{n=0}^{\infty}\left[(m+n)^2-m^2\right]a_n x^{m+n}+\sum_{n=2}^{\infty}a_{n-2}x^{m+n}=0\sum_{n=0}^{\infty}n(2m+n)a_k x^{m+n}+\sum_{n=2}^{\infty}a_{n-2}x^{m+n}=0$$

$$a_1(2m+1)x^{m+1}+\sum_{n=2}^{\infty}\left[a_n n(2m+n)+a_{n-2}\right]x^{m+n}=0.$$

First, look at the special case $m=-1/2$, then (11) becomes $-\frac{1}{2l(2l-1)}a_{2l-2}\sum_{n=2}^{\infty}\left[a_n n(n-1)+a_{n-2}\right]x^{m+n}=0$, so $a_n=-\frac{1}{n(n-1)}a_{n-2}$. Now let $n\equiv 2l$, where $l=1, 2, \ldots$. $a_{2l}=\frac{(-1)^l}{[2l(2l-1)][2(l-1)(2l-3)]\cdots[2\cdot 1\cdot 1]}a_0=\frac{(-1)^l}{2^l\,l!\,(2l-1)!!}a_0$, which, using the identity $2^l\,l!\,(2l-1)!!=(2l)!$, gives $a_{2l}=\frac{(-1)^l}{(2l)!}a_0$. Similarly, letting $n\equiv 2l+1$, $a_{2l+1}=-\frac{1}{(2l+1)(2l)}a_{2l-1}=\frac{(-1)^l}{[2l(2l+1)][2(l-1)(2l-1)]\cdots[2\cdot 1\cdot 3][1]}a_1$, which, using the identity $2^l\,l!\,(2l+1)!!=(2l+1)!$, gives $a_{2l+1}=\frac{(-1)^l}{2^l\,l!\,(2l+1)!!}a_1=\frac{(-1)^l}{(2l+1)!}a_1$.

Plugging back into (◇) with $k=m=-1/2$gives

$$y=x^{-1/2}\sum_{n=0}^{\infty}a_n x^n=x^{-1/2}\left[\sum_{n=1,3,5,\ldots}^{\infty}a_n x^n+\sum_{n=0,2,\ldots}^{\infty}a_n x^n\right]=x^{-1/2}\left[\sum_{l=0}^{\infty}a_{2l}x^{2l}+\sum_{l=0}^{\infty}a_{2l+1}x^{2l+1}\right]=$$

$$x^{-1/2}\left[a_0\sum_{l=0}^{\infty}\frac{(-1)^l}{(2l)!}x^{2l}+a_1\sum_{l=0}^{\infty}\frac{(-1)^l}{(2l+1)!}x^{2l+1}\right]=x^{-1/2}(a_0\cos x+a_1\sin x).$$

The Bessel functions of order $\pm 1/2$ are therefore defined as $J_{-1/2}(x)=\sqrt{\frac{2}{\pi x}}\cos x$ and $J_{1/2}(x)=\sqrt{\frac{2}{\pi x}}\sin x$, so the general solution for $m=\pm 1/2$ is $y=a_0'J_{-1/2}(x)+a_1'J_{1/2}(x)$. Now

consider a general $m \neq -1/2$. Equation (◇) requires $a_1(2m+1)=0[a_n n(2m+n)+a_{n-2}]x^{m+n}=0$ for $n=2$, 3, ..., so $a_1=0$, $a_n=-\frac{1}{n(2m+n)}a_{n-2}$ for $n=2$, 3, ... Let $n=2l+1$, where $l=1$, 2, ..., then $a_{2l+1}=-\frac{1}{(2l+1)[2(m+l)+1]}a_{2l-1}=\ldots=f(n,m)a_1=0$, where $f(n,m)$ is the function of l and m obtained by iterating the recursion relationship down to a_1. Now let $n=2l$, where $l=1$, 2, ..., so

$$a_{2l}=-\frac{1}{2l(2m+2l)}a_{2l-2}=-\frac{1}{4l(m+l)}a_{2l-2}=\frac{(-1)^l}{[4l(m+l)][4(l-1)(m+l-1)]\cdots[4\cdot(m+1)]}a_0.$$

Plugging back into (◇), $y=\sum_{n=0}^{\infty}a_n x^{n+m}=\sum_{n=1,3,5,\ldots}^{\infty}a_n x^{n+m}+\sum_{n=0,2,4,\ldots}^{\infty}a_n x^{n+m}$, y $=\sum_{l=0}^{\infty}a_{2l+1}x^{2l+m+1}+\sum_{l=0}^{\infty}a_{2l}x^{2l+m}$ $a_0\sum_{l=0}^{\infty}\frac{(-1)^l}{[4l(m+l)][4(l-1)(m+l-1)]\cdots[4(m+1)]}x^{2l+m}$ y $a_0\sum_{l=0}^{\infty}\frac{[(-1)^l m(m-1)\cdots 1]x^{2l+m}}{[4l(m+l)][4(l-1)(m+l-1)]\cdots[4(m+1)m\cdots 1]}=a_0\sum_{l=0}^{\infty}\frac{(-1)^l m!}{2^{2l}l!(m+l)!}x^{2l+m}$. Now define $J_m(x)\equiv\sum_{l=0}^{\infty}\frac{(-1)^l}{2^{2l+m}l!(m+l)!}x^{2l+m}$, where the factorials can be generalized to gamma functions for nonintegral m. The above equation then becomes $y=a_0 2^m m! J_m(x)=a_0' J_m(x)$. Returning to equation (◇) and examining the case $k=-m$, $a_1(1-2m)+\sum_{n=2}^{\infty}[a_n n(n-2m)+a_{n-2}]x^{n-m}=0$. However, the sign of m is arbitrary, so the solutions must be the same for $+m$ and $-m$. We are therefore free to replace $-m$ with $-|m|$, so $a_1(1+2|m|)+\sum_{n=2}^{\infty}[a_n n(n+2|m|)+a_{n-2}]x^{|m|+n}=0$, and we obtain the same solutions as before, but with m replaced by $|m|$.

$$J_m(x)=\begin{cases}\sum_{l=0}^{\infty}\frac{(-1)^l}{2^{2l+|m|}l!(|m|+l)!}x^{2l+|m|} & \text{for } m\neq\frac{1}{2}\\ \sqrt{\frac{2}{\pi x}}\cos x & \text{for } m=-\frac{1}{2}\\ \sqrt{\frac{2}{\pi x}}\sin x & \text{for } m=\frac{1}{2}.\end{cases}$$

We can relate $J_m(x)$ and $J_{-m}(x)$ (when m is an integer) by writing $J_{-m}(x)=\sum_{l=0}^{\infty}\frac{(-1)^l}{2^{2l-m}l!(l-m)!}x^{2l-m}$. Now let $l\equiv l'+m$. Then $J_{-m}(x)=\sum_{l'+m=0}^{\infty}\frac{(-1)^{l'+m}}{2^{2l'-m}(l'+m)!\,l!}x^{2l'+m}=\sum_{l'=-m}^{-1}\frac{(-1)^{l'+m}}{2^{2l'+m}l'!(l'+m)!}x^{2l'+m}+\sum_{l'=0}^{\infty}\frac{(-1)^{l'+m}}{2^{2l'+m}l'!(l'+m)!}x^{2l'+m}$.

But $l'!=\infty$ for $l'=-m,\ldots,-1$, so the denominator is infinite, and the terms on the left are zero. We therefore have $J_{-m}(x)=\sum_{l=0}^{\infty}\frac{(-1)^{l+m}}{2^{2l+m}l!(l+m)!}x^{2l+m}=(-1)^m J_m(x)$.

Note that the Bessel differential equation is second-order, so there must be two linearly independent solutions. We have found both only for $|m| = 1/2$. For a general nonintegral order, the independent solutions are J_m and J_{-m}. When m is an integer, the general (real) solution is of the form $Z_m \equiv C_1 J_m(x) + C_2 Y_m(x)$, where J_m is a Bessel function of the first kind, Y_m (a.k.a. N_m) is the Bessel function of the second kind (a.k.a. Neumann function or Weber function), and C_1 and C_2 are constants. Complex solutions are given by the Hankel functions (a.k.a. Bessel functions of the third kind). The Bessel functions are orthogonal in $[0, a]$ according to $\int_0^a J_\nu\left(\alpha_{\nu m}\frac{\rho}{a}\right) J_\nu\left(\alpha_{\nu n}\frac{\rho}{a}\right)\rho\, d\rho = \frac{1}{2}a^2 [J_{\nu+1}(\alpha_{\nu m})]^2 \delta_{mn}$, where $\alpha_{\nu m}$ is the mth zero of J_ν and δ_{mn} is the Kronecker delta [24, p. 592] except when $2m$ is a negative integer, $J_m(z) = \frac{z^{-1/2}}{2^{2m+1/2} i^{m+1/2}\Gamma(m+1)} M_{0,m}(2iz)$, where $\Gamma(x)$ is the gamma function and $M_{0,m}$ is a Whittaker function.

In terms of a confluent hypergeometric function of the first kind, the Bessel function is written $J_\nu(z) = \frac{\left(\frac{1}{2}z\right)^\nu}{\Gamma(\nu+1)} {}_0F_1\left(\nu+1; -\frac{1}{4}z^2\right)$. A derivative identity for expressing higher order Bessel functions in terms of $J_0(z)$ is $J_n(z) = i^n T_n\left(i\frac{d}{dz}\right) J_0(z)$, where $T_n(z)$ is a Chebyshev polynomial of the first kind. Asymptotic forms for the Bessel functions are $J_m(z) \approx \frac{1}{\Gamma(m+1)}\left(\frac{z}{2}\right)^m$ for $z \ll 1$, and $J_m(z) \approx \sqrt{\frac{2}{\pi z}}\cos\left(z - \frac{m\pi}{2} - \frac{\pi}{4}\right)$ for $z \gg |m^2 - 1/4|$ (correcting the condition of Abramowitz and Stegun [57, p. 364]). A derivative identity is $\frac{d}{dx}[x^m J_m(x)] = x^m J_{m-1}(x)$. An integral identity is $\int_0^u u' J_0(u')\, du' = u J_1(u)$. Some sum identities are $\sum_{k=-\infty}^{\infty} J_k(x) = 1$, which follows from the generating function ($\diamondsuit$) with $t = 1$, $1 = [J_0(x)]^2 + 2\sum_{k=1}^{\infty}[J_k(x)]^2 1 = J_0(x) + 2\sum_{k=1}^{\infty} J_{2k}(x)$ [57, p. 363], $0 = \sum_{k=0}^{2n}(-1)^k J_k(z) J_{2n-k}(z) + 2\sum_{k=1}^{\infty} J_k(z) J_{2n+k}(z)$ for $n \geq 1$ [57, p. 361], $J_n(2z) = \sum_{k=0}^{n} J_k(z) J_{n-k}(z) + 2\sum_{k=1}^{\infty}(-1)^k J_k(z) J_{n+k}(z)$ [57, p. 361], and the Jacobi-Anger expansion $e^{jz\cos\theta} = \sum_{n=-\infty}^{\infty} i^n J_n(z) e^{jn\theta}$, which can also be written $e^{jz\cos\theta} = J_0(z) + 2\sum_{n=1}^{\infty} i^n J_n(z)\cos(n\theta)$.

The Bessel function addition theorem states $J_n(y+z) = \sum_{m=-\infty}^{\infty} J_m(y) J_{n-m}(z)$. Various integrals can be expressed in terms of Bessel functions $J_n(z) = \frac{1}{\pi}\int_0^\pi \cos(z\sin\theta - n\theta)\, d\theta$, which is Bessel's first integral, $J_n(z) = \frac{i^{-n}}{\pi}\int_0^\pi e^{jz\cos\theta}\cos(n\theta)\, d\theta = \frac{1}{2\pi i^n}\int_0^{2\pi} e^{jz\cos\phi} e^{jn\phi}\, d\phi$, for

$n=1$ $J_n(z)=\frac{2}{\pi}\frac{z^n}{(2n-1)!!}\int_0^{\pi/2}\sin^{2n}u\cos(z\cos u)\,du$, for $n=1$ $J_n(x)=\frac{1}{2\pi i}\int_\gamma e^{(x/2)(z-1/z)}z^{-n-1}\,dz$ for $n>-1/2$. The Bessel functions are normalized so that $\int_0^\infty J_n(x)\,dx=1$ for positive integral (and real) n. Integrals involving $J_1(x)$ include $\int_0^\infty\left[\frac{J_1(x)}{x}\right]^2 dx=\frac{4}{3\pi}$ and $\int_0^\infty\left[\frac{J_1(x)}{x}\right]^2 x\,dx=\frac{1}{2}$. Ratios of Bessel functions of the first kind have continued fraction $\frac{J_{n-1}(z)}{J_n(z)}=\frac{2n}{z}-\cfrac{\frac{z}{2(n+1)}}{1-\cfrac{\frac{(z/2)^2}{(n+1)(n+2)}}{1-\cfrac{(z/2)^2}{(n+2)(n+3)}}}$ [225, p. 349]. The Laplace transform satisfied a number of useful properties. Consider exponentiation. If $\mathcal{L}_t[f(t)](s)=F(s)$ for $s>\alpha$ (i.e., $F(s)$ is the Laplace transform of f), then $\mathcal{L}_t\left[e^{at}f\right](s)=F(s-a)$ for $s>a+\alpha$. This follows from $F(s-a)=\int_0^\infty f\,e^{-(s-a)t}\,dt=\int_0^\infty\left[f(t)e^{at}\right]e^{-st}\,dt=\mathcal{L}_t\left[e^{at}f(t)\right](s)$. The Laplace transform also has nice properties when applied to integrals of functions. If $f(t)$ is piecewise continuous and $|f(t)|\le Me^{at}$, then $\mathcal{L}_t\left[\int_0^t f(t')\,dt'\right]=\frac{1}{s}\mathcal{L}_t[f(t)](s)$.

Appendix 7

Generally speaking, a Green's function is an integral kernel that can be used to solve differential equations from a large number of families, including simpler examples such as ordinary differential equations wit initial or boundary value conditions, as well as more difficult examples such as inhomogeneous partial differential equations (PDE) with boundary conditions.

A second order, linear nonhomogeneous differential equation is $y''+p(t)y'+q(t)y=g(t)y''+p(t)y'+q(t)y=g(t)$ where *g(t)* is a non-zero function. Note that we did not employ constant coefficients in the larval habitat eco-epidemiological, risk model here because nothing that is done in this section requires it. Also, a coefficient of 1 is used on the second derivative just to make some of the work a little easier to write down. It is not required to be a 1. Thus the final model would be $y''+p(t)y'+q(t)y=0y''+p(t)y'+q(t)y=0$.

Important for a number of reasons, Green's functions allow for visual interpretations of the actions associated to a source of force or to a charge concentrated at a point [226], thus making them particularly useful in areas of applied mathematics. In particular, Green's function methods are widely used in physics and engineering. More precisely, given a linear differential operator $\mathcal{L}=\mathcal{L}(x)$ acting on the collection of distributions over a subset Ω of some Euclidean space $\mathbb{R}^n$, a Green's function $G=G(x,s)$ at the point $s\in\Omega$ corresponding to $\mathcal{L}$ is any solution of $\mathcal{L}G(x,s)=\delta(x-s)$, where δ denotes the delta function. The motivation for defining such a function is widespread, but by multiplying the above identity by a function $f(s)$, and integrating with respect to s yields $\int\mathcal{L}G(x,s)f(s)\,ds=\int\delta(x-s)f(s)\,ds.$ The right side reduces to f(x) due to properties of the delta function, and because l is a linearizable operator acting only on *x* and on s.

In the forecasting, *S. damnosum* s.l. riverine larval habitat, eco-epidemiological, risk model, the right-hand side reduces merely to $f(x)$, due to properties of the delta function, and because $\mathcal{L}$ is a linear operator acting only on x, and not on s, the left-hand side was rewritten as $\mathcal{L}\left(\int G(x,s)\,f(s)\,ds\right)$. This reduction was particularly useful for solving $u = u(x)$ in differential equations of the form $\mathcal{L}u(x) = f(x)$, where the arithmetic confirmed that $\mathcal{L}u(x) = \mathcal{L}\left(\int G(x,s)\,f(s)\,ds\right)$, and whereby it followed that u has the specific integral form $u(x) = \int G(x,s)\,f(s)\,ds$. The intuitive physical interpretation of a Green's function was associated to our *S. damnosum* s.l. differential equation. In particular, these functions revealed a length ℓ suspended between two walls, held in place by an identical horizontal force applied on each of its ends, and a lateral load placed at some interior point x on a line of integers.

Let x' be the point corresponding to x on the deflected tangent, and suppose the downward force F is rope. Corresponding to this physical system would then be the differential equation $-H\,u''(x) = F(x)$ for $0 < x < \ell$ with $u(0) = u(\ell) = 0$, a system whose simplicity allows both its solution $u(x)$, and its Green's function $G(x,y)$, to which we wrote explicitly $u(x) = \frac{F}{2H}\left(\ell x - x^2\right)$, and $G(x,y) = \frac{1}{H\ell}\begin{cases} y(\ell - x) & \text{for } y \le x \\ x(\ell - y) & \text{for } x \le y, \end{cases}$ respectively. The displaced rope then had the piecewise linear format given by $G = G(x,y)$ above, thus confirming the claim that the Green's function G associated to this system represents the action of the horizontal rope corresponding to the application of a force F.

A Green's function taking a pair of arguments (x,s) is sometimes referred to as a two-point Green's function [25]. This is in contrast to multi-point Green's functions which are of particular importance in the area of many-body theory. As an elementary example of a two-point function we considered the problem of determining the potential $\psi(\mathbf{r})$ generated by a interpolatable distribution whose density was $\rho(\mathbf{r})$, whereby applications of Poisson's equation had the potential at $\mathbf{r}_1$ produced by each element $\rho(\mathbf{r}_2)\,d^3\mathbf{r}_2$, which yielded a solution $\psi(\mathbf{r}_1) = \frac{1}{4\pi\varepsilon_0}\int d^3\mathbf{r}_2\,\frac{\rho(\mathbf{r}_2)}{|\mathbf{r}_1 - \mathbf{r}_2|}$ which held over the entire riverine region, where $\rho(\mathbf{r}_2) \neq 0$. Because the right-hand side can be viewed as an integral operator converting ρ into ψ, we re-wrote this solution in terms of a Green's function $G = G(\mathbf{r}_1, \mathbf{r}_2)$, having the form $G(\mathbf{r}_1, \mathbf{r}_2) = \frac{1}{4\pi\varepsilon_0}\frac{1}{|\mathbf{r}_1 - \mathbf{r}_2|}$, whereby the solution can be rewritten: $\psi(\mathbf{r}_1) = \int d^3\mathbf{r}_2\,G(\mathbf{r}_1, \mathbf{r}_2)\,\rho(\mathbf{r}_2)$.

International Journal of Geographic Information System
Vol. 4, No. 1, April 2017, pp.1-519
Available Online at http://acascipub.com/Journals.php

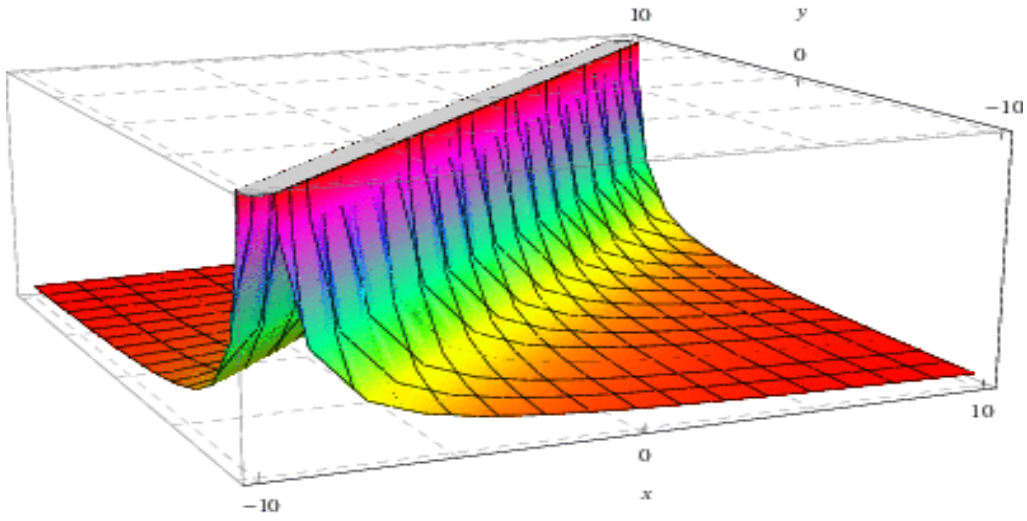

The above figure shows the Green's function associated to the solution of the ψ-ρ equation discussed above where $\varepsilon_0 = 4$ and $\mathbf{r}_1$, respectively $\mathbf{r}_2$, is plotted on the x-, respectively y-, axis. A somewhat comprehensive list of Green's functions corresponding to various differential equations was then generated.

Due to the multitude of literature written on Green's functions, several different notations and definitions may emerge, some of which may be topically different than above, but which in general do not affect the important properties of our results. In our model output we denoted the empirically regressed *S. damnosum* s.l. variables x and s in terms of vectors $\mathbf{r}_1$ and $\mathbf{r}_2$.

Appendix 8

The Digma function is a special function which is given by the logarithmic derivative of the gamma function (or, depending on the definition, the logarithmic derivative of the factorial). Because of this ambiguity, two different notations are sometimes (but not always) used, with $\Psi(z) = \frac{d}{dz}\ln\Gamma(z) = \frac{\Gamma'(z)}{\Gamma(z)}$ defined as the logarithmic derivative of the gamma function $\Gamma(z)$, and $F(z) = \frac{d}{dz}\ln z!$ defined as the logarithmic derivative of the factorial function. The two are connected by the relationship $F(z) = \Psi(z+1)$. The nth derivative of $\Psi(z)$ is called the polygamma function, denoted $\psi_n(z)$. The notation $\psi_0(z) \equiv \Psi(z)$ is therefore frequently used for the digamma function itself, and Erdélyi *et al.* (1981) use the notation $\psi(z)$for $\Psi(z)$. The digamma function $\psi_0(z)$ is returned by the function PolyGamma [z] or PolyGamma [0, z] in the Wolfram Language, and typeset using the notation $\psi^{(0)}(z)$. The digamma function arises in simple sums such as $\sum_{k=0}^{\infty}\frac{(-1)^k}{zk+1} = \frac{\Phi(-1,1,z^{-1})}{z} = \frac{1}{2z}\left[\psi_0\left(\frac{z+1}{2z}\right) - \psi_0\left(\frac{1}{2z}\right)\right]$, where $\Phi(z, s, a)$ is a Lerch transcendent.

The Lerch transcendent is generalization of the Hurwitz zeta function and polylogarithm function. Many sums of reciprocal powers can be expressed in terms of it. It is

classically defined by $\Phi(z, s, a) = \sum_{k=0}^{\infty} \frac{z^k}{(a+k)^s}$, for $|z| < 1$ and $a \neq 0, -1, \ldots$. It is implemented in this form as HurwitzLerchPhi[z, s, a] in the Wolfram Language. The slightly different form, $\Phi^*(z, s, a) = \sum_{k=0}^{\infty} \frac{z^k}{[(a+k)^2]^{s/2}}$, sometimes also denoted $\tilde{\Phi}(z, s, a)$, for $|z| < 1$ (or $|z| = 1$ and $\mathrm{R}[s] > 1$) and $a \neq 0, -1, -2, \ldots$, is implemented in the Wolfram Language as LerchPhi[z, s, a]. Note that the two are identical only for $\mathrm{R}[a] > 0$.

A series formula for $\Phi(z, s, a)$ valid on a larger domain in the complex z-plane is given by $(1-z)\Phi(z, s, a) = \sum_{n=0}^{\infty} \left(\frac{-z}{1-z}\right)^n \sum_{k=0}^{n} (-1)^k \binom{n}{k} (a+k)^{-s}$, which holds for all complex s and complex z with $\mathrm{R}[z] < 1/2$ [230]. The Lerch transcendent can be used to express the Dirichlet beta function $\beta(s) = \sum_{k=0}^{\infty} (-1)^k (2k+1)^{-s} = 2^{-s} \Phi\left(-1, s, \frac{1}{2}\right)$. A special case is given by $\Phi(z, n, 1) = \frac{\mathrm{Li}_n(z)}{z}$, where $\mathrm{Li}_n(z)$ is the polylogarithm. Special cases giving simple constants include $\Phi\left(-1, 2, \frac{1}{2}\right) = 4K$, $\frac{\partial \Phi}{\partial s}(-1, -1, 1) = \ln\left(\frac{A^3}{2^{1/3} e^{1/4}}\right)$, $\frac{\partial \Phi}{\partial s}(-1, -2, 1) = \frac{7\zeta(3)}{4\pi^2}$ and $\frac{\partial \Phi}{\partial s}\left(-1, -1, \frac{1}{2}\right) = \frac{K}{\pi}$, where K is Catalan's constant, $\zeta(3)$ is Apéry's constant, and A is the Glaisher-Kinkelin constant. This gives the integrals of the Fermi-Dirac distribution $\int_0^{\infty} \frac{k^s\, dk}{e^{k-\mu} + 1} = e^{\mu} \Gamma(s+1) \Phi(-e^{\mu}, s+1, 1) = -\Gamma(s+1) \mathrm{Li}_{1+s}(-e^{\mu})$, where $\Gamma(z)$ is the gamma function and $\mathrm{Li}_n(z)$ is the polylogarithm and Bose-Einstein distribution $\int_0^{\infty} \frac{k^s\, dk}{e^{k-\mu} - 1} = e^{\mu} \Gamma(s+1) \Phi(e^{\mu}, s+1, 1) = \Gamma(s+1) \mathrm{Li}_{1+s}(e^{\mu})$.

Double integrals involving the Lerch transcendent include $\int_0^1 \int_0^1 \frac{x^{u-1} y^{v-1}}{1-xyz} [-\ln(xy)]^s\, dx\, dy = \Gamma(s+1) \frac{\Phi(z, s+1, v) - \Phi(z, s+1, u)}{u-v}$

$\int_0^1 \int_0^1 \frac{(xy)^{u-1}}{1-xyz} [-\ln(xy)]^s\, dx\, dy = \Gamma(s) \Phi(z, s-2, u)$, where $\Gamma(z)$ is the gamma function. These formulas lead to a variety of beautiful special cases of unit square integrals [230]. Special cases are given by $\sum_{k=0}^{\infty} \frac{(-1)^k}{k+1} = \ln 2$, $\sum_{k=0}^{\infty} \frac{(-1)^k}{2k+1} = \frac{1}{4}\pi$, $\sum_{k=0}^{\infty} \frac{(-1)^k}{3k+1} = \frac{1}{9}\left(\sqrt{3}\,\pi + 3\ln 2\right)$, and $\sum_{k=0}^{\infty} \frac{(-1)^k}{4k+1} = \frac{\pi + 2\coth^{-1}(\sqrt{2})}{4\sqrt{2}}$.

Gauss's digamma theorem states that $\frac{\Gamma'(p/q)}{\Gamma(p/q)} = -\gamma - \ln(2q) - \frac{1}{2}\pi \cot\left(\frac{\pi p}{q}\right) + 2 \sum_{0<n<q/2} \cos\left(\frac{2\pi p n}{q}\right) \ln\left[\sin\left(\frac{\pi n}{q}\right)\right]$

An asymptotic series for the digamma function is given by $\psi_0(z+1) = \frac{d}{dz} \lim_{n\to\infty} [\ln n! + z \ln n - \ln(z+1) - \ln(z+2) - \ldots - \ln(z+n)] = \lim_{n\to\infty} \left(\ln n - \frac{1}{z+1} - \frac{1}{z+2} - \ldots - \frac{1}{z+n}\right) = -\gamma - \sum_{n=1}^{\infty} \left(\frac{1}{z+n} - \frac{1}{n}\right) = -\gamma + \sum_{n=1}^{\infty} \frac{z}{n(n+z)} = \ln z + \frac{1}{2z} - \sum_{n=1}^{\infty} \frac{B_{2n}}{2n z^{2n}}$, where γ is the Euler-Mascheroni constant and B_{2n} are Bernoulli numbers. The digamma function satisfies

$\psi_0(z) = \int_0^\infty \left(\frac{e^{-t}}{t} - \frac{e^{-zt}}{1-e^{-t}} \right) dt.$ For integer $z \equiv n$, $\psi_0(n) = -\gamma + \sum_{k=1}^{n-1} \frac{1}{k} = -\gamma + H_{n-1}$, where γ is the Euler-Mascheroni constant and H_n is a harmonic number. Other identities include $\frac{d\psi_0}{dz} = \sum_{n=0}^{\infty} \frac{1}{(z+n)^2}$, $\psi_0(1-z) - \psi_0(z) = \pi \cot(\pi z)$ $\psi_0(z+1) = \psi_0(z) + \frac{1}{z}$, $\psi_0(2z) = \frac{1}{2}\psi_0(z) + \frac{1}{2}\psi_0\left(z+\frac{1}{2}\right) + \ln 2.$ Special values are $\psi_0\left(\frac{1}{2}\right) = -\gamma - 2\ln 2$, and $= -\gamma$. At integer values, $\psi_0(n) = -\gamma + \sum_{k=1}^{n-1} \frac{1}{k} = -\gamma + H_{n-1}$ and at half-integral values, $\psi_0\left(\frac{1}{2}+n\right) = -\gamma - 2\ln 2 + 2\sum_{k=1}^{n} \frac{1}{2k-1} = -\gamma + H_{n-1/2}$, where H_n is a harmonic number. It is given by the unit square integral $\psi_0(u) = \ln u - \int_0^1 \int_0^1 \frac{1-x}{(1-xy)(-\ln xy)} (xy)^{u-1}\, dx\, dy$ for $u > 0$ [230]. Plugging in $u = 1$ gives a special case involving the Euler-Mascheroni constant. The series for $\psi_0(z)$ is given by $\psi_0(z) = -\frac{1}{z} + \sum_{n=0}^{\infty} \frac{\psi_n(1)}{n!} z^n.$ A logarithmic series is given by $\psi_0(z) = \sum_{n=0}^{\infty} \frac{1}{n+1} \sum_{k=0}^{n} (-1)^k \binom{n}{k} \ln(z+k)$. A surprising identity that arises from the FoxTrot series is given by $-\psi_0\left(\frac{1}{2}(-1)^{1/3}\right) - \psi_0\left(-\frac{1}{2}(-1)^{2/3}\right) + \psi_0\left(\frac{1}{2}\left(1+(-1)^{1/3}\right)\right) + \psi_0\left(\frac{1}{2}\left(1-1(-1)^{2/3}\right)\right) = 2\pi \operatorname{sech}\left(\frac{1}{2}\sqrt{3}\,\pi\right).$

Special cases are given by $\sum_{k=0}^{\infty} \frac{(-1)^k}{k+1} = \ln 2$, $\sum_{k=0}^{\infty} \frac{(-1)^k}{2k+1} = \frac{1}{4}\pi$, $\sum_{k=0}^{\infty} \frac{(-1)^k}{3k+1} = \frac{1}{9}\left(\sqrt{3}\,\pi - 3\ln 2\right)$, $\sum_{k=0}^{\infty} \frac{(-1)^k}{4k+1} = \frac{\pi + 2\coth^{-1}\left(\sqrt{2}\right)}{4\sqrt{2}}$. Gauss's digamma theorem states that $\frac{\Gamma'(p/q)}{\Gamma(p/q)} = -\gamma - \ln(2q) - \frac{1}{2}\pi \cot\left(\frac{\pi p}{q}\right) + 2\sum_{0<n<q/2} \cos\left(\frac{2\pi pn}{q}\right) \ln\left[\sin\left(\frac{\pi n}{q}\right)\right]$. An asymptotic series for the digamma function is $\psi_0(z+1)$, given by $\frac{d}{dz} \lim_{n\to\infty} [\ln n! + z\ln n - \ln(z+1) - \ln(z+2) - \ldots - \ln(z+n)]$ $= \lim_{n\to\infty} \left(\ln n - \frac{1}{z+1} - \frac{1}{z+2} - \ldots - \frac{1}{z+n} \right) = -\gamma - \sum_{n=1}^{\infty} \left(\frac{1}{z+n} - \frac{1}{n} \right) = -\gamma + \sum_{n=1}^{\infty} \frac{z}{n(n+z)} = \ln z + \frac{1}{2z} - \sum_{n=1}^{\infty} \frac{B_{2n}}{2n z^{2n}}$, where γ is the Euler-Mascheroni constant and B_{2n} are Bernoulli numbers.

The digamma function satisfies $\psi_0(z) = \int_0^\infty \left(\frac{e^{-t}}{t} - \frac{e^{-zt}}{1-e^{-t}} \right) dt.$ For integer $z \equiv n$, $\psi_0(n) = -\gamma + \sum_{k=1}^{n-1} \frac{1}{k} = -\gamma + H_{n-1}$, where γ is the Euler-Mascheroni constant and H_n is a harmonic number. Other identities include $\frac{d\psi_0}{dz} = \sum_{n=0}^{\infty} \frac{1}{(z+n)^2}$, $\psi_0(1-z) - \psi_0(z) = \pi \cot(\pi z)$ $\psi_0(z+1) = \psi_0(z) + \frac{1}{z}$, $\psi_0(2z) = \frac{1}{2}\psi_0(z) + \frac{1}{2}\psi_0\left(z+\frac{1}{2}\right) + \ln 2.$ Special values are $\psi_0\left(\frac{1}{2}\right) = -\gamma - 2\ln 2$

$= \psi_0(1) = -\gamma$. At integer values, $\psi_0(n) = -\gamma + \sum_{k=1}^{n-1} \frac{1}{k} = -\gamma + H_{n-1}$ (Derbyshire 2004, p. 58), and at half-integral values, $\psi_0\left(\frac{1}{2}+n\right) = -\gamma - 2\ln 2 + 2\sum_{k=1}^{n} \frac{1}{2k-1} = -\gamma + H_{n-1/2}$, where H_n is a harmonic number. It is given by the unit square integral $\psi_0(u) = \ln u - \int_0^1 \int_0^1 \frac{1-x}{(1-xy)(-\ln xy)} (xy)^{u-1}\, dx\, dy$ for $u > 0$ [230]. Plugging in $u = 1$ gives a special case involving the Euler-Mascheroni constant. The series for $\psi_0(z)$ is given by $\psi_0(z) = -\frac{1}{z} + \sum_{n=0}^{\infty} \frac{\psi_n(1)}{n!} z^n$. A logarithmic series is given by $\psi_0(z) = \sum_{n=0}^{\infty} \frac{1}{n+1} \sum_{k=0}^{n} (-1)^k \binom{n}{k} \ln(z+k)$ [230]. A surprising identity that arises from the FoxTrot series is given by $-\psi_0\left(\frac{1}{2}(-1)^{1/3}\right) - \psi_0\left(-\frac{1}{2}(-1)^{2/3}\right) + \psi_0\left(\frac{1}{2}\left(1+(-1)^{1/3}\right)\right) + \psi_0\left(\frac{1}{2}\left(1-(-1)^{2/3}\right)\right) = 2\pi \operatorname{sech}\left(\frac{i}{2}\sqrt{3}\,\pi\right)$.

References

1. Thylefors B (1978) Ocular Onchocerciasis. Bulletin of the World Health Organization 56: 63–72
2. Winthrop KL, Furtado JM, Silva JC, Resnikoff S, Lansingh VC (2011) River blindness: an old disease on the brink of elimination and control. J Glob Infect Dis 3: 151–155
3. Prost A (1986) The burden of blindness in adult males in the savanna villages of West Africa exposed to onchocerciasis. Trans R Soc Trop Med Hyg 80(4): 525-527
4. Duke BOL (1990) Onchocerciasis (river blindness)- Can it be eradicated? Parasitol Today 6(3): 82 – 84
5. Greene BM, Taylor HR, Cupp EW, Murphy RP, White AT, et al. (1985) Comparison of Ivermectin and Diethylcarbamazine in the Treatment of Onchocerciasis. N Engl J Med 313: 133 - 138
6. Cupp EW, Bernardo MJ, Kiszewski AE, Collins RC, Taylor HR, et al. (1986) The effects of ivermectin on transmission of Onchocerca volvulus. Science 231: 740 - 742
7. Cupp EW, Ochoa AO, Collins RC, Ramberg FR, Zea G. The effects of multiple ivermectin on treatments of Similium onchoraceum for Onchocerca volvulus (1989) Am J Trop Med Hyg 40(5): 501 – 506
8. Colatrella B (2008) The Mectizan Donation Program: 20 years of successful collaboration – a retrospective. Annals of Tropical Medicine and Parasitology 102: 7 – 11
9. Rodríguez-Pérez MA, Fernández-Santos NA, Orozco-Algarra ME, Rodríguez-Atanacio JA, Domínguez-Vásquez A, et al. (2015) Elimination of Onchocerciasis from Mexico. PLoS Negl Trop Dis 9(7): 1 – 15
10. Traore MO, Sarr MD, Badji A, Bissan Y, Diawara L, et al. (2012) Proof-of-Principle of Onchocerciasis Elimination with Ivermectin Treatment in Endemic Foci in Africa: Final Results of a Study in Mali and Senagal. PLoS Negl Trop Dis 6(9).

11. Tekle AH, Elhassan E, Isiyaku S, Amazigo UV, Bush S, et al. (2012) Impact of long-term treatment of onchocerciasis with ivermectin in Kaduna State, Nigeria: first evidence of the potential for elimination in the operational area of the African Programme for Onchocerciasis Control. Parasites & Vectors 5(28).
12. Turner HC, Walker M, Churcher TS, Osei-Atweneboana MY, Biritwum NK, et al. (2014) Reaching the London Declaration on Neglected Tropical Diseases Goals for Onchocerciasis: An Economic Evaluation of Increasing the Frequency of Ivermectin Treatment in Africa. Clin Infect Dis 59(7): 923 – 932
13. Duerr HP, Raddatz G, Eichner M (2011) Control of onchocerciasis in Africa: Threshold shifts, breakpoints and rules for elimination. Int J Parasitol 41: 581 – 589
14. McMahon JP, Highton RB, Goiny H (1958) The eradication of Simulium neavei from Kenya. Bull World Health Organ 19(1): 75 – 107
15. Roberts JMD, Neumann E, Göckel CW, Highton RB (1967) Onchocerciasis in Kenya 9, 11 and 18 years after elimination of the vector. Bull World Health Organ 37(2): 195 – 212
16. Hougard JM, Alley ES, Yaméogo L, Dadzie KF, Boatin BA (2001) Eliminating Onchocerciasis after 14 Years of Vector Control: A Proved Strategy. J Infect Dis 184(4): 497 – 503
17. Vieta F (1998) River blindness: Protection for 54 cents a year. UN Chron 1: 12 – 13
18. Ndyomugyenyi R, Tukesiga E, Büttner DW, Garms R (2004) The impact of ivermectin treatment alone and when in parallel with *Simulium neavei* elimination on onchocerciasis in Uganda. Tropical Medicine and International Health 9(8): 882 – 886
19. Katabarwa MN, Walsh F, Habomugisha P, Lakwo TL, Agunyo S, et al. (2012) Transmission of Onchocerciasis in Wadelai Focus of Northwestern Uganda has been Interrupted and the Disease Eliminated. Journal of Parasitology Research.
20. Garms R, Lakwo TL, Ndyomugyenyi R, Kipp W, Rubaale T, et al. (2009) The elimination of the vector *Simulium neavei* from the Itwara onchocerciasis focus in Uganda by ground larviciding. Acta Tropica 111(3): 203 – 210
21. Fischer PU, Kipp W, Bamuhiga J, Binta-Kahwa J, Kiefer A, et al. (1994) Parasitological and clinical characterization of Simulium neavei-transmitted onchocerciasis in Western Uganda. Trop Med Parasitol 44: 311 – 321
22. Jacob BG, Novak RJ, Toe LD, Sanfo MS, Lassane K (2015) Ecogeographically and Non-Ecogeographically Prognosticating Discontinuous Canopied *Simulium damnosum* s.l. Habitats by Interpolating Metrizable Sub-Mixel Mean Solar Exoatmospheric Quantum Scalar Irradiance where θi is a Zenith Angle with Diatomically Etiolated Xanthophylls and Azimutually Isotropic Sources of Chloroplastic Carotenoid Zeaxanthins Geo-spectrotemporally Extracted from an Expositorily Uncoalesced RapidEye™ Red Edge Proxy Normalized Difference Vegetation Index Biosignature: A Case Study in Burkina Faso and Uganda. *GIS and Remote Sensing*.
23. Jensen JR (2005) Introductory digital image processing a remote sensing perspective, 3rd ed. Upper Saddle River, N.J.: Prentice Hall.
24. Stewart, James (2002). Calculus (5 ed.). Brooks Cole.
25. Griffith DA (2003) Spatial Autocorrelation and Spatial Filtering: Gaining Understanding Through Theory and Scientific Visualization. Springer-Verlag Berlin Heidelberg. New York.
26. Jacob BG, Novak RJ, Toe L, Sanfo MS, Caliskhan S, et al. (2013) Definiability of combinatorial functions and their linear recurrence relationships within a

polylogarithmic traingularizable matrix employing surjective bilipschitz functions and other isomorphisms of metric spaces for forecasting seasonal endemic onchocerciasis transmission zones in Burkina Faso. Scientific Journal of Pure and Applied Sciences 2(12): 401 – 460

27. McMillen DP, McDonald JF (1999) Land use before zoning: the case of 1920's Chicago. Reg Sci Urban Econ 29(4): 473 – 489
28. Wang Y, Kockelman KM, Wang X (2011) Anticipation of land use change thorugh use of geographically weighted regression models for discrete respose. Transportation Research Record: Journal of the Transportation Research Board 2245: 111 – 123
29. Chakir R, Parent O (2009) Determinants of land use changes: A spatial multinomial probit approach. Papers in Regional Science 88(2): 327 – 344
30. Munroe DK, Southworth J, Tucker CM (2002) The Dynamics of Land-Cover Change in Western Honduras: Exploring Spatial and Temporal Complexity. Agricultural Economics 27(3): 355 – 369
31. Wang X, Kockelman KM (2009) Application of the Dynamic Spatial Ordered Probit Model: Patterns of Land Development Change in Austin, Texas. Regional Science 88(2): 345 – 366
32. Green, AA, Berman M, Switzer P, Craig MD (1988) A transformation for ordering multispectral data in terms of image quality with implications for noise removal. IEEE Transactions on Geoscience and Remote Sensing 26(1): 65 – 74
33. Abdi H, Williams LJ (2010) Principal component analysis. Wiley Interdisciplinary Reviews: Computational Statistics 2: 433 – 459
34. Angluin D, Aspnes J, Chen J, Reyzin L (2008) Learning large-alphabet and analog circuits with value injection queries. Journal Machine Learning 72(1-2): 113 – 138
35. Kroese DP, Breretorn T, Taimre T, Botev ZI (2014) Why the Monte Carlo method is so important today. WIREs Comput Stat 6: 386 – 392
36. Calcavecchia NM, Caprarescu BA, Di Nitto E, Dubois DJ, Petcu D (2012) DEPAS: A Decentralized Probabilistic Algorithm for Auto-Scaling. arXiv:1202.2509 [cs.DC]
37. Wang Y, Kockelman KM, Wang X (2013) Understanding Spatial Filtering for Analysis of Land Use Data Sets. Journal of Transport Geography 31: 123 – 131
38. Dhore A, Veena CS (2014) A New Pan-Sharpening Method Using Joint Sparse FI Image Fusion Algorithm. International Journal of Engineering Research and General Science 2(4)
39. Cogliati S, Verhoef W, Kraft S, Sabater N, Alonso L, Vicent, J, Moreno J, Drusch M, Colombo R (2015) Retrieval of sun-induced fluorescence using advanced spectral fitting methods. Remote Sens. Environ. 169: 344 – 357
40. Goel NS, Norman JM (1990) Instrumentation for Studying Vegetation Canopies for Remote Sensing in Optical and Thermal Infrared Regions. Remote Sensing Reviews 5(1): 1 – 360
41. Schlotzhauer S (2007) Elementary Statistics Using JMP (SAS Press). Cary, NC. SAS Institute: 166 – 169
42. Suganuma H, Abe Y, Taniguchi M, Tanouchi H, Utsugi H, et al. (2006) Stand biomass estimation method by canopy coverage for application to remote sensing in an arid area of Western Australia. Forest Ecology and Management 222(1): 75 – 87
43. Li Z, Moreau L (1996) A New Approach for Remote Sensing of Canopy-Absorbed Photosynthetically Active Radiation. I: Total Surface Absorption. Remote Sens. Environ. 55: 175 – 191

44. Poorter H, Niklas KJ, Reich PB, Oleksyn J, Poot P, Mommer L (2012) Biomass allocation to leaves, stems and roots: meta-analyses of interspecific variation and environmental control. New Phytol. 193(1): 30 – 50
45. Jacob BG, Novak RJ, Toe L, Sanfo MS, Tibgueria R, et al. (2014) Denoising a model employing automated bandwidth selection procedures and pre-whitened Euclidean-based quadratic surrogates in PROC ARIMA for optimizing asymptotic expansions and simulations of onchocerciasis endemic transmission zones in Burkina Faso. J Public Health Epidemiol 6(11): 347 – 389
46. Ustin S (2013) Remote sensing of canopy chemistry. Proceedings of the National Academy of Sciences of the United States of America 110(3): 804 – 805
47. Joiner J, Gaunter L, Lindstrot R, Voigt M, Vasilkov AP, et al. (2013) Global monitoring of terrestrial chlorophyll fluorescence from moderate-spectral-resolution near-infrared satellite measurements: methodology, simulations, and applications to GOME-2. Atmos. Meas. Tech 6: 2803 – 2823
48. Knyazikhin Y, Schull MA, Xu L, Myneni RB, Samanta A (2010) Canopy spectral invariants. Part 1: A new concept in remote sensing of vegetation. JQSRT doi:10.1016/j.jqsrt.2010.06.014
49. West R (1999) Understanding ArcSDE: GIS by ESRI. Redlands, CA. ESRI: 1 – 58
50. Stranneby D, Walker W (2004) Digital Signal Processing and Applications, 2nd edition. Elsevier.
51. Jacob BG and Novak RJ (2014) Integrating a Trimble Recon X 400 MHz Intel PXA255 Xscale CPU® Mobile Field Data Collection System Using Differentially Corrected Global Positioning System Technology and a Real-Time Bidirectional Actionable Platform within an ArcGIS Cyberenvironment for Implementing Mosquito Control. Advances in Remote Sensing 3: 141 – 196
52. Chein CI (2003) Hyperspectral Imaging: Techniques for Spectral Detection and Classification. Springer Science & Business Media.
53. (2014) ENVI Classic Tutorial: Spectral Angle Mapper (SAM) and Spectral Information Divergence (SID) Classification. Exelis Visual Information Solutions, Inc.
54. Thouvenin PA, Dobigeon N, Tourneret JY (2015) Online unmixing of multitemporal hyperspectral images accounting for spectral variability. arXiv:110.05893v1
55. Jacob BG, Griffith DA, Novak RJ (2008) Decomposing malaria mosquito aquatic habitat data into spatial autocorrelation eigenvectors in SAS/GIS® module. Transactions in GIS 12(3): 341 – 364
56. Raiffa H, Schlaifer R (1961) Applied Statistical Decision Theory. Division of Research, Graduate School of Business Administration, Harvard University.
57. Abramowitz M, Stegun IA (1972) Handbook of Mathematical Functions with Formulas, Graphs, and Mathematical Tables. New York: Dover.
58. Maiwald D (1997) On moments of complex Wishart and complex inverse Wishart distributed matrices. Acoustics, Speech and Signal Processing 5: 3817 – 3820
59. Jacob BG, Novak RJ, Toe LD, Sanfo M, Griffith DA, et al. (2013) Validation of a Remote Sensing Model to Identify *Simulium damnosum* s.l. Breeding Sites in Sub-Saharan Africa. PLoS Negl Trop Dis 7(7)
60. Chan SH, Vo D, Nguyen TQ (2010) Subpixel motion estimation without interpolation. Proceedings of IEEE Conference on Acoustics, Speech and Signal Processing (ICASSP): 722 – 725
61. Ball, WWR (1960) A Short Account of the history of Mathematics, 4th ed. Dover Publications: 50 – 62

62. Solomentsev ED (2011) Euclidean Space. Encyclopedia of Mathematics. Springer.
63. Schultz AJ, Kofke DA (2009) Interpolation of virial coefficients Molecular Physics 107(14): 1431 – 1436
64. Schultz AJ, Kofke DA (2009) Interpolation of virial coefficients Molecular Physics 107(14): 1431 – 1436
65. McCoy J, Johnston K, Kopp S, Borup B, Willison J, Payne B (2001) Using ArcGIS Spatial Analyst. ESRI: Redlands, CA.
66. Zou KH, Tuncali K, Silverman SG (2003) Correlation and simple linear regression 1. Radiology 227(3): 617 – 628
67. Ghatak KL (2011) Techniques and Methods in Biology. PHI Learning Private Limited, New Delhi.
68. Jacob BG, Griffith DA, Mwangangi J, Gathings DA, Mbogo CC, et al. (2011) A cartographic analysis using spatial filter logistic model specifications for implementing mosquito control in Kenya. Urban Geography 32(2): 263 – 300
69. Junttila V, Kauranne T, Finley AO, Bradford JB (2015) Linear Models for Airborne-Laser-Scanning-Based Operational Forest Inventory with Small Field Sample Size and Highly Correlated LiDAR data. IEEE Transactions on Geoscience and Remote Sensing 53(10): 5600 – 5612
70. Russell S, Norvig P (2002) Artificial Intelligence: A Modern Approach. Prentice Hall.
71. Mobley CD, Gentili B, Gordon HR, Jin Z, Kattawar GW, et al. (1993) Comparison of numerical models for computing underwater light fields. Applied Optics 32(36): 7484 – 7506
72. Doerffer R, Fischer J (1994) Concentrations of chlorophyll, suspended matter, and gelbstoff in case II waters derived from satellite coastal zone color scanner data with inverse modeling methods. Journal of Geophysical Research: Oceans 99: 7457 – 7466
73. Antoine D, Morel A (1996) Oceanic primary production, 1, Adaptation of a spectral light-photosynthesis model in view of application to satellite chlorophyll observations. Global Biogeochemical Cycles 10(1): 43 – 55
74. Longhurst A, Sathyendranath S, Platt T, Caverhill C (1995) An estimate of global primary production in the ocean from satellite radiometer data. Journal of Plankton Research 17(6): 1245 – 1271
75. Behrenfeld MJ, Falkowski PG (1997) Photosynthetic rates derived from satellite-based chlorophyll concentration. Limnology and oceanography 42(1): 1 – 20
76. Gons HJ (1999) Optical teledetection of chlorophyll a in turbid inland waters. Environmental Science & Technology 33(7): 1127 – 1132
77. Gons HJ, Rijekeboer M, Bagheri S, Ruddick KG (2000) Optical teledetection of chlorophyll a in estuarine and coastal waters. Environmental Science & Technology 34(24): 5181 – 5192
78. Nusch EA (1980) Comparison of methods for chlorophyll a and phaeopigment determination. Arch Hydrobiol. Beih. Ergenbn. Limnol. 14: 14 – 36
79. Pullianen J, Kallio K, Eloheimo K, Koponen S, Servomaa H, et al. (2001) A semi-operative approach to lake water quality retrieval from remote sensing data. Science of the Total Environment 268(1): 79 – 93
80. Floricioiu D, Riedl C, Rott H, Rott E (2003) Envisat MERIS capabilities for monitoring the water quality of perialpine lakes. Geoscience and Remote Sensing Symposium, 2003. IGARSS'03. Proceedings. 2003 IEEE International 3: 2134 – 2136

81. Mobley CD, Gentili B, Gordon HR, Jin Z, Kattawar GW, et al. (1993) Comparison of numerical models for computing underwater light fields. Applied Optics 32(36): 7484 – 7506
82. Zege EP, Chaikovskaya LI (1996) New approach to the polarized radiative transfer problem. Journal of Quantitative Spectroscopy and Radiative Transfer 55: 19 – 31
83. Zege EP, Chaikovskaya LI (2000) Approximate theory of linearly polarized light propagation through a scattering medium. Journal of Quantitative Spectroscopy and Radiative Transfer 66: 413 – 435
84. Dall'Olo G, Gitelson AA, Rundquist DC, Leavitt B, Barrow T, et al. (2005) Assessing the potential of SeaWiFS and MODIS for estimating chlorophyll concentration in turbid productive waters using red and near-infrared bands. Remote Sensing of Environment 96(2): 176 – 187
85. Buiteveld H, Hakvoort JHM, Donze M (1994) Optical properties of pure water. Ocean Optics 7: 174 – 183
86. Fomferra N, Brockmann C (2005) Beam-the ENVISAT MERIS and AATSR toolbox. In MERIS (A) ATSR Workshop 597: 13
87. Doerffer R, Schiller H (2007) The MERIS Case 2 water algorithm. International Journal of Remote Sensing 28(3-4): 517 – 535
88. Shroeder TH, Schaale M, Fischer J (2007) Retrieval of atmospheric and oceanic properties from MERIS measurements: A new Case-2 water processor for BEAM. International Journal of Remote Sensing 28(24): 5627 – 5632
89. Doerffer R, Schiller H (2008) MERIS lake water algorithm for BEAM-MERIS algorithm theoretical basis document. GKSS Research Center, Geesthacht, Germany Gege P, Plattner S (2004) MERIS validation activities at Lake Constance in 2003. Proc. MERIS User Workshop. Frascati, Italy.
90. Gower JFR, Doerffer R, Borstad GA (1999) Interpretation of the 685 nm peak in water-leaving radiance spectra in terms of fluorescence, absorption and scattering, and its observation by MERIS. International Journal of Remote Sensing 20(9): 1771 – 1786
91. Gower JFR, King S, Borstad GA, Brown L (2005) Detection of intense plankton blooms using the 709 nm band of the MERIS imaging spectrometer. International Journal of Remote Sensing 26(9): 2005 – 2012
92. Binding C Greenberg TA, Jerome JH, Bukata RP, Letourneau G (2010) An assessment of MERIS algal products during an intense bloom in Lake of the Woods. Journal of Plankton Research 33(5): 793 – 806
93. Crosskey RW (1960) Taxonomic Study of the Larvae of West African Simuliidae (Díptera: Nematocera) with Comments on the Morphology of the Larval Black-Fly Head. Bulletin of the British Museum (Natural History) 10(1): 1 – 74
94. Stoyan D, Kendall WS, Mecke J (1987) Stochastic geometry and its applications. Wiley.
95. Bourg L, D'Alba L, Colagrande P (2008) MERIS SMILE effect characterization and correction. European Space Agency, Paris.
96. Koponen S, Verdu AR, Heege T, Heblinski J, Sorensen K, et al. (2008) Development of MERIS lake water algorithms: Validation report. Helsinki University of Technology. Finland.
97. Ruiz-Verdú A, Koponen S, Heege T, Doerffer R, Brockmann C, et al. (2008) Development of MERIS lake water algorithms: Validation results from Europe. Italy: 22 – 26

98. Alikas K, Reinart A (2008) Validation of the MERIS product on the large European lakes: Peipsi, Vanern and Vattern. Hydrobiologia 599: 161 – 168
99. Odermatt D, Giardino C, Heege T (2010) Chlorophyll retrieval with MERIS Case-2-Regional in perialpine lakes. Remote Sensing of Environment 114: 607 – 617
100. Giardino C, Bresciani M, Villa P, Martinelli A (2010) Application of remote sensing in water resource management: The case study of Lake Trasimeno, Italy. Water Resource Management 24: 3885 – 3899
101. Odermatt D, Pomati F, Pitarch J, Carpenter J, Kawka M, et al. (2012) MERIS observations of phytoplankton blooms in a stratified eutrophic lake. Remote Sensing of Environment 126: 232 – 239
102. Gege P, Plattner S (2004) MERIS validation activities at Lake Constance in 2003. Proc. MERIS User Workshop. Frascati, Italy.
103. Matthews MW, Bernard S, Winter K (2010) Remote sensing of cyanobacteria-dominant algal blooms and water quality parameters in Zeekoevlei, a small hypertrophic lake, using MERIS. Remote Sensing of Environment 114: 2070 – 2087
104. Song K, Li L, Wang Z, Liu D, Zhang B, et al. (2012) Retrieval of total suspended matter (TSM) and Chl-a, concentration from remote-sensing data for drinking water resources. Environ. Monit. Assess. 184: 1449 – 1470
105. McCulloch WS, Pitts W (1943) A logical calculus of the ideas immanent in nervous activity. The Bulletin of Mathematical Biophysics 5(4): 115 – 133
106. Siswanto E, Tang J, Yamaguchi H, Ahn Y, Ishizaka J, et al. (2011) Empirical ocean-color algorithms to retrieval chlorophyll-a, total suspended matter, and colored dissolved organic matter absorption coefficient in the Yellow and East China Seas. Journal of Oceanography 67(5): 627 – 650
107. Hu C, Lee Z, Franz B (2012) Chlorophyll aalgorithms for oligotrophic oceans: A novel approach based on three-band reflectance difference. Journal of Geophysical Research: Oceans: 117
108. Dahanayaka DDGL, Tonooka H, Wijeyaratne MJS, Minato A, Ozawa S (2012) Retrieval of chlorophyll-a using satellite and ground spectral data in Japanese and Sri Lankan water bodies. SPIE Asia-Pacific Remote Sensing: 85250L
109. Palmer SCJ, Odermatt D, Hunter PD, Brockmann C, Presing M, et al. (2015) Satellite remote sensing of phytoplankton phenology in Lake Balaton using 10 years of MERIS observations. Remote Sensing of Environment 158: 441 – 452
110. Tyler AN, Svab E, Preston T, Kovacs WA (2006) Remote sensing of the water quality of shallow lakes: A mixture modelling approach to quantifying phytoplankton in water characterized by high-suspended sediment. International Journal of Remote Sensing 27(8): 1521 – 1537
111. Lichtenthaler HK, Miehé JA (1997) Fluorescence imaging as a diagnostic tool for plant stress. Trends Plant Sci. 2:316 – 327
112. Subhash N, Mohanan CN (1997) Curve-fit analysis of chlorophyll fluorescence spectra: Application to nutrient stress detection in sunflower. Remote Sens. Environ. 60: 347 – 356
113. Schuster C, Forster M, Kleinschmit B (2012) Testing the red edge channel for improving land-use classifications based on high-resolution multi-spectral satellite data. International Journal of Remote Sensing 33(17): 5583 – 5599
114. Recio JA, Hermosilla T, Ruiz LA, Fernández-Sarría A (2011) Historical land use as a feature for image classification. Photogrammetric Engineering & Remote Sensing 77(4): 377 – 387

115. Conrad C, Fritsch S, Lex S, Low F, Rucker G et al. (2012) Potenziale des Red Edge Kanals von RapidEye zur Unterscheidung und zum Monitoring landwirtschaftlicher Anbaufrüchte am Beispiel des usbekischen Bewässerungssystems Khorezm. Borg, Daedelow, Johnson (Eds.), RapidEye Science Archive (RESA) - Vom Algorithmus zum Produkt, 4. RESA Workshop, March 21-22, Neustrelitz, Germany, pp. 203-214
116. Pinar A, Curran PJ (1996) Technical Note Grass chlorophyll and the reflectance red edge. International Journal of Remote Sensing 17(2): 351 – 357
117. Fillela I, Penuelas J (1994) The red edge position and shape as indicators of plant chlorophyll content, biomass and hydric status. International Journal of Remote Sensing 15(7): 1459 – 1470
118. Huang J, Wang X, Wang R (2003) The red edge parameters as indicators of rice nitrogen levels. SPIE 4897: Multispectral and Hyperspectral Remote Sensing Instruments and Applications
doi: 10.1117/12.467367
119. Baranowski GVG, Rokne JG (2005) A practical approach for estimating the red edge position of plant leaf reflectance. International Journal of Remote Sensing 26: 503 – 521
120. Rodriguez D, Fitzgerald GJ, Belford R, Christensen LK (2006) Detection of nitrogen deficiency in wheat from spectral reflectance indices and basic crop-physiological concepts. Australian Journal of Agricultural Reearch 57: 781 – 789
121. Eitel JUH, Long DS, Gessler PE, Smith AMS (2007) using in-situ measurements to evaluate the new RapidEye satellite series for prediction of wheat nitrogen status. International Journal of Remote Sensing 28: 1 – 8
122. Schelling K (2010) Approaches to characterize Chl/N status of crop canopies. Analysis of Remote Sensing Data workshop, Hannover. Remote Sensing of Environment 106: 106-122
123. Darecki M, Stramski D (2004) An evaluation of MODIS and SeaWiFS bio-optical algorithms in the Baltic Sea Remote Sensing of Environment 89(3): 326 – 350
124. Carder KL, Chen FR, Lee ZP, Hawes SK, Kamykowski D (1999) Semianalytic Moderate-Resolution Imaging Spectrometer algorithms for chlorophyll a and absorption with bio-optical domains based on nitrate-depletion temperatures. Journal of Geophysical Research: Oceans: 5403 – 5421
125. Carter GA, Knapp AK (2001) Leaf optical properties in higher plants: linking spectral characteristics to stress and chlorophyll concentration. Am J Bot 88(4): 677 – 684
126. Daughtry CST, Biehl LL, Ranson KJ (1989) A new technique to measure the spectral properties of conifer needles. Remote Sensing of Environment 27(1): 81 – 91
127. Jacob BG, Novak RJ, Toe L, Sanfo MS, Afriyie AN, et al. (2012) Quasi-likelihood techniques in a logistic regression equation for identifying Simulium damnosum s.l. larval habitats intra-cluster covariates in Togo. Geospatial Information Science 15(2): 117 – 133
128. Jacob BG, Muturi E, Halbig P, Mwangangi J, Wanjogu RK, et a. (2007) Environmental abundance of Anopheles (Diptera: Culicidae) larval habitats on land cover change sites in Karima Village, Mwea Rice Scheme, Kenya. The American Journal of Tropical Medicine and Hygiene 76(1): 73 – 80

129. Jacob BG, Griffith D, Muturi E, Caamano EX, Shililu J, et al. (2009) Describing *Anopheles arabiensis* aquatic habitats in two Riceland agro-ecosystems in Mwea, Kenya using a negative binomial regression model with a non-homogenous mean. Acta Tropica 109(1): 17 – 26
130. Jacob BG, Arheart KL, Griffith DA, Mbogo CM, Githeko AK, et al. (2005) Evaluation of environmental data for identification of Anopheles (Diptera: Culicidae) aquatic larval habitats in Kisumu and Malindi, Kenya. Journal of Medical Entomology 42(5): 751 – 755
131. Jacob BG, Burkett-Cadena ND, Luvall JC, Parcak SH, McClure CJ, et al. (2010) Developing GIS-based eastern equine encephalitis vector-host models in Tuskegee, Alabama. Int J Health Geogr 9: 12
132. Graham RL (1994) Concrete mathematics: a foundation for computer science, dedicated to Leonhard Euler (1707-1783). Pearson Education, India.
133. Havil J (2003) Gamma: Exploring Euler's Constant. Princeton, NJ: Princeton University Press.
134. Mascheroni, L (1790) Adnotationes ad Euleri Calculum Integralem.
135. Jacob BG, Muturi EJ, Caamano EX, Gunter JT, Mpanga E, et al. (2008) Hydrological modeling of geophysical parameters of arboviral and protozoan disease vectors in Internally Displaced People camps in Gulu, Uganda. International Journal of Health Geographics 7(1): 11
136. Shaman J, Stieglitz M, Stark C, Le Blancq S, Cane M (2002) Using a dynamic hydrology model to predict mosquito abundances in flood and swamp water.
137. Patz JA, Martens WJM, Focks DA, Jetten TH (1998) Dengue fever epidemic potential as projected by general circulation models of global climate change. Environ Health Perspec 106: 147 – 153
138. Burrough PA, Mc Donnell RA (1998) Principles of geographical information systems. Oxford University Press: UK
139. Jacob BG, Muturi EJ, Funes JE, et al. (2006) A grid-based infrastructure for ecological forecasting of rice land Anopheles arabiensis aquatic larval habitats. Malaria J 5: 91.
140. Strahler AH, Jupp DL (1990) Modeling bidirectional reflectance of forests and woodlands using Boolean models and geometric optics. Remote Sensing of Environment 34(3): 153 – 166
141. Myneni RB, Hall FG, Sellers PJ, Marshak AL (1995) The interpretation of spectral vegetation indexes. IEEE Transactions on Geoscience and Remote Sensing 33: 481 – 486
142. Cressie N, Grondona MO (1993) Using spatial considerations in the analysis of experiments. Technometrics 33(4): 381 – 392
143. Hosmer JR, Lemeshew DW (2000) Introduction to the logistic regression model. Applied Logistic Regression, Third Edition: 1 – 30
144. Roberts GO (1996) Markov Chain Concepts Related to Sampling Algorithms, in WR Gilks, DJ Spiegelhalter and S Richardson, eds. Markov Chain Monte Carlo in Practice: 45 – 58. London: Chapman & Hall.
145. Lui JS (2001) Monte Carlo Strategies in Scientific Computing. Springer-Verlag
146. Agresti A, Chuang C, Kezouth A (1987) Order-restricted score parameters in association models for contingency tables. Journal of the American Statistical Association 82(398): 619 – 623

147. Davison AC, Snell EJ (1991) Residuals and diagnostics. Statistical Theory and Mod.
148. Asrar G, Fuchs M, Kanemasu E, Hatfield J (1984) Estimating absorbed photosynthetic radiation and leaf area index from spectral reflectance in wheat. Agron J 76: 300 – 306
149. Reed M, Simon B (1980) Methods of modern mathematical physics: Functional analysis, Vol. 1. Gulf Professional Publishing
150. Foreman, M, Wehrung F (1991) The Hahn-Banach theorem implies the existence of a non-Lebesgue measurable set. Fundamenta Mathematicae 138: 13 – 19
151. Brown DK, Simpson SG (1986) Which set existence axioms are needed to prove the separable Hahn-Banach theorem? Annals of Pure and Applied Logic 31: 123 – 144
152. Halmos PR (1982) A. H. S. P. (1982) Grad. Texts in Math 19
153. Cucker F, Smale S (2002) On the Mathematical Foundations of Learning. Bull Amer Math Soc 39: 1 – 49
154. Wahba G (1990) Spline models for observational data, vol. 59. Siam
155. Micchelli CA, Wahba G (1981) Design problems for optimal surface interpolation, in "Approximation Theory and Applications." Academic Press, New York: 329 – 347
156. Sacks J, Ylvisaker D (1966) Designs for regression problems with correlated errors. The Annals of Mathematical Statistics: 66 – 89
157. Sacks J, Ylvisaker D (1968) Designs for regression problems with correlated errors: many parameters. The Annals of Mathematical Statistics: 49 – 69
158. Sacks J, Ylvisaker D (1970) Designs for regression problems with correlated errors III. The Annals of Mathematical Statistics: 2057 – 2074
159. Ritter K, Wasilkowski G, Wozniakowski H (1995) Multivariate integeration and approximation for random fields satisfying Sacks-Ylvisaker conditions. Ann Appl Probab 5: 518 – 540
160. Cai T, Hall P (2006) Prediction in functional linear regression. Ann Statist 34: 2159 – 2179
161. Hall P, Horowitz JL (2007) Methodology and convergence rates for functional linear regression. Ann Statist 35: 70 – 91
162. Cardot H, Sarda P (2005) Estimation in generalized linear models for functional data via penalized likelihood. J Multivariate Anal 92: 24 – 41
163. Muller HG, Stadtmuller U (2005) Generalized functional linear models. Ann Statist 33: 774 – 805
164. Silverman BW (1982) On the estimation of a probability density function by the maximum penalized likelihood method. Ann Statis 10: 795 – 810
165. Cox DD, O'Sullivan F (1990) Asymptotic analysis of penalized likelihood and related estimators. The Annals of Statistics: 1676 – 1695
166. Spiegelhalter DJ, Best NG, Carlip BP, Van Der Linde A (2002) Bayesian measures of model complexity and fit. Journal of the Royal Statistical Society: Series B (Statistical Methodology) 64(4): 583 – 639
167. Gelman A, Carlin JB, Stern HS, Rubin DB (2004) Bayesian Data Analysis: Second Edition. Texts in Statistical Science.
168. Koukoulas S, Blackburn G (2005) Spatial relationships between tree species and gap characteristics in broad–leaved deciduous woodland. J. Veg. Sci. 16: 587–596.

169. Lindenmayer D, Franklin J, Fischer J (2006) General management principles and a checklist of strategies to guide forest biodiversity conservation. *Biol. Conserv. 131*: 433–445
170. Getzin S, Wiegand K, Schöning I (2012) Assessing biodiversity in forests using very high-resolution images and unmanned aerial vehicles. *Methods Ecol. Evol. 3*: 397–404
171. Higazi TB, Zarroug IM, Mohamed HA, Elmubark WA, Deran TC, Aziz N (2013) Interruption of Onchocerca volvulus transmission in the Abu Hamed focus, Sudan., American Journal of Tropical Medicine and Hygiene 89(1):51-7
172. Asner GP, Wessman CA, Bateson CA, Privette JL (2000) Impact of tissue, canopy and landscape factors on the hyperspectral reflectance variability of arid ecosystems. Remote Sensing of Environment 74(1): 69 – 84
173. Gates DM (1980) Biophysical ecology. 611 pp.
174. Datt B (1999) A new reflectance index for remote sensing of chlorophyll content in higher plants: tests using Eucalyptus leaves. Journal of Plant Physiology 154(1): 30 – 36
175. Wang Y, Wang F, Huang J, Wang X, Liu Z (2009) Validation of artificial neural network techniques in the estimation of nitrogen concentration in rape using canopy hyperspectral reflectance data. International Journal of Remote Sensing 30(17): 4493 – 4505
176. Zhang JC, Pu RL, Wang JH, Huang WJ, Yuan L, et al. (2012) Detecting powdery mildew of winter wheat using leaf level hyperspectral measurements. Computers and electronics in agriculture 85: 13 – 23
177. Gao BC (1996) NDWI – a normalized difference water index for remote sensing of vegetation liquid water from space. Remote Sensing of Environment 58(3): 257 – 266
178. Ceccato P, Flasse S, Tarantola S, Jacquemoud S, Gregoire JM (2001) Detecting vegetation leaf water content using reflectance in the optical domain. Remote Sensing of Environment 77(1): 22 – 33
179. Waring RH, Schlesinger WH (1985) Forest ecosystems, concepts and management. Academic Press.
180. Zhang Z, Wen J, Zhao D (2010) Band selection method for retrieving soil lead content with hyperspectral remote sensing data. The Society of Photo-Optical Instrumentation Engineers (SPIE), 7831
181. Riaño D, Vaughan P, Chuvieco E, Zarco-Tejada PJ, Ustin SL (2005) Estimation of fuel moisture content by inversion of radiative transfer models to simulate equivalent water thickness and dry matter content: analysis at leaf and canopy level. Geoscience and Remote Sensing, IEEE Transactions 43(4): 819 – 826
182. Danson FM, Steven MD, Malthus TJ, Clark JA (1992) High-spectral resolution data for determining leaf water content. International Journal of Remote Sensing 13(3): 461 – 470
183. Danson FM, Bowyer P (2004) Estimating live fuel moisture content from remotely sensed reflectance. Remote Sensing of Environment 92(3): 309 – 321
184. Yamamoto HY (1979) Biochemistry of the violaxanthin cycle in higher plants. Pure Appl Chem 51: 639-448
185. Hager (1980) The reversible, light-induced conversion of xanthophylls in the chloroplasts. In: Cygan FC, ed. *Pigments in Plants* Stuttgart: Gustav Fischer, 57-79

186. Demmig-Adams B, Adams W, Heber U, Neimanis S, Winter K (1989) Inhibition of Zeaxanthin Formation and of Rapid Changes in Radiationless Energy Dissipation by Dithiothreitol in Spinach Leaves and Chloroplasts. *Plant Physiology* 92(9): 293-301
187. Myers VI, Baur ME, Gausman HW, Hart WG, Heilman JL, et al. (1983) Remote sensing applications in agriculture. In R. N. Colwell [ed.], Manual of remote sensing, vol. 2, 2nd ed., 2111–2228. American Society of Photogrammetry, Falls Church, Virginia, USA
188. Jackson, R. D. 1986. Remote sensing of biotic and abiotic plant stress. Annual Review of Phytopathology 24: 265–287
189. Mathew S, Abraham TE (2006) In vitro antioxidant activity and scavenging effects of Cinnamomum verum leaf extract assayed by different methodologies. Food and Chemical Toxicology 44(2): 192 – 206
190. Inada K (1976) Action spectra for photosynthesis in higher plants. Plant and Cell Physiology 17(2): 355 – 365
191. Jacob BG, Mwangangi JM, Mbongo CM, Novak RJ (2011) A Taxonomy of Unmixing Algorithms using Li-Strahler Geometric-Optical Model and other Spectral Endmember Extraction Techniques for Decomposing a QuickBird Visible and Near Infra-Red Pixel of an Anopheles arabiensis Habitat. The Open Remote Sensing Journal 4(1)
192. Fischer J, Kronfeld U (1990) Sun-stimulated chlorophyll fluorescence 1: Influence of oceanic properties. Remote Sensing 11(12): 2125 – 2147
193. Sanderson EW, Zhang M, Ustin SL, Rejmankova E (1998) Geostatistical scaling of canopy water content in a California salt marsh. Landscape Ecology 13: 79-92
194. Turner DP, Ollinger SV, Kimball JS (2004) Integrating remote sensing and ecosystem process models for landscape-to-regional-scale analysis of the carbon cycle. BioScience 54(6): 573 – 584
195. Kokaly RF, Clark RN (1999) Spectroscopic determination of leaf biochemistry using band-depth analysis of absorption features and stepwise multiple linear regression. Remote Sensing of Environment 67(3) 267 – 287
196. Fourty TH, Baret F (1998) On spectral estimates of fresh leaf biochemistry. International Journal of Remote Sensing 19(7): 1283 – 1297
197. Cole GA (1994) Textbook of Limnology, 4th ed. Waveland Press Inc
198. Riesz F, Nagy BS (1955) Functional Analysis, Frederick Ungar Pub. Co., New York.
199. Ruddick KG, Ovidio F, Rijkeboer M (2000) Atmospheric correction of SeaWiFS imagery for turbid coastal and inland waters. Applied Optics 39(6): 817 – 912
200. James GM (2002) Generalized linear models with functional predictors. Journal of the Royal Statistical Society: Series B 64(3): 411 – 432
201. Cardot H, Ferraty F, Sarda P (2003) Spline estimators for the functional linear model. Statistica Sinica 13(3): 571 -592
202. Ramsay J, Silverman BW (1997) Functional Data Analysis. Springer, New York.
203. Yao F, Muller HG, Wang JL (2005) Functional linear regression analysis for longitudinal data. The Annals of Statistics 33(6): 2873 – 2903
204. Ferraty F, Vieu P (2006) Nonparametric functional data analysis: theory and practice. Springer Science & Business Media

205. Li Y, Hsing T (2007) On rates of convergence in functional linear regression. Journal of Multivariate Analysis 98(9): 1782 – 1804
206. Crambes C, Kneip A, Sarda P (2009) Smoothing splines estimators for functional linear regression. The Annals of Statistics: 35 – 72
207. Johannes J (2010) Functional linear instrumental regression. Technical report, Universite catholique de Louvain.
208. Stramska, M, Frye D (1997) Dependence of apparent optical properties on solar altitude: Experimental results based on mooring data collected in the Sargasso Sea. J. Geogr. Res. 102: 15679–15691.
209. Liang S (2003) Quantitative remote sensing of land surfaces. Wiley-Interscience.
210. Gosper RW (1972) "Item 120," In: Beeler M, Gosper RW and Schroeppel eds., MIT Artificial Intelligence Laboratory, Memo AIM-239, Cambridge, Massachussetts, p 55.
211. Haight JA (1979) Covering systems of congruences, a negative result. Mathematika 26(1): 53 – 61
212. Boole G (1847) The mathematical analysis of logic. Philosophical Library.
213. Boole G (1854) An investigation of the laws of thought: on which are founded the mathematical theories of logic and probabilities. Dover Publications.
214. Huntington EV (1933) New sets of independent postulates for the algebra of logic, with special reference to Whitehead and Russell's *Principia mathematica.* Trans Amer Math Soc 35: 274 – 304
215. Godel K (1931) Uber formal unentscheidbare Satze der Principia Mathematica und verwandter Systeme I. Monatshefte fur mathematic und physic 38(1): 173 – 198
216. Birkhoff G (1935) On the structure of abstract algebras. Mathematical proceedings of the Cambridge philosophical society 31(4): 433 – 454. Cambridge University Press.
217. Li X, Strahler AH (1985) Geometric-optical modeling of a conifer forest canopy. Geoscience and Remote Sensing, IEEE Transactions 5: 705 – 721
218. Li WKW (1985) Photosynthetic response to temperature of marine phytoplankton along a latitudinal gradient (16°N to 74° N). Deep-Sea Res 32:1381–1391
219. Schowengerdt RA (1997) Remote Sens. 2nd ed. San Diego
220. Oppenheim L, Shuler KE, Weiss GH (1997) Stochastic Processes in Chemical Physics: The Master Equation. MIT Press, Cambridge, Mass.
221. Zwillinger D (1997) Standard math interactive. CRC Press.
222. Valiron G (1950) Equations fontionnelles applications. Masson et Cie.
223. Watson GS (1966) The statistics of orientation data. The Journal of Geology: 786 – 797
224. Arfken G (1985) The method of steepest descents. Mathematical methods for physicists 3: 428 – 436
225. Wall HS (1948) Analytic theory of continued fractions.
226. Qin Q (2014) Green's Functions of Magneto-Electro-Elastic Plate Under Thermal Loading. Encyclopedia of Thermal Stresses. Netherlands, Springer.
227. Sondow J, Zudilin W (2006) Euler's constant, q-logarithms, and formulas of Ramanujan and Gosper. The Ramanujan Journal 12(2): 225 – 244
228. Simon MA, Blume GW (1994) Mathematics for economists, vol. 7. New York, Norton.

229. Kaplan, W. (1984) Derivatives and Differentials of Composite Functions" and "The General Chain Rule. In Advanced Calculus, 3rd ed. Reading, MA: Addison-Wesley
230. Guillera J, Sondow J (2005) Double integrals and infinite products for some classical constants via analytic continuations of Lerch's transcendent.
231. Dieudonne JA (1981) History of functional analysis. Elsevier.
232. Derbyshire J (2004) Prime Obsession: Bernhard Riemann and the Greatest Unsolved Problem in Mathematics. Joseph Henry Press: United States.